

**10th International Meeting
on Lithium Batteries
"Lithium 2000"**

**Villa Erba Conference Center
Como, Italy**

May 28-June 2, 2000

IMLB

ALL INFORMATION CONTAINED
HEREIN IS UNCLASSIFIED
DATE 10/1/00 BY 60322
UNLIMITED

QUALITY INSPECTED
20000816 027

CHAIRMAN

Bruno Scrosati

Dipartimento di Chimica

Università "La Sapienza"

Piazzale A. Moro 5

00185 Rome, Italy

Phone: +39-6-49913530

Fax: +39-6-491769

Email: scrosati@axrma.uniroma1.it

CO-CHAIRMEN

Peter G. Bruce - University of St. Andrews, Scotland

Frank R. McLarnon - Lawrence Berkeley Laboratory, USA

Zempachi Ogumi - Kyoto University, Japan

INTERNATIONAL SCIENTIFIC COMMITTEE

K. M. Abraham - Covalent Associates, Inc, USA

M. Armand - Université de Montréal, Canada

R. Atanasoski - 3M Research Center, USA

D. Aurbach - Bar-Ilan University, Israel

J. O. Besenhard - Technische Universität Graz, Austria

M. Broussely - SAFT, Advanced Batteries, France

K. R. Bullock - C&D Technologies, Inc., USA

J. R. Dahn - Dalhousie University, Canada

G. C. Farrington - Lehigh University, USA

G. T-K. Fey - National Central University, Taiwan, ROC

R. Marassi - Università di Camerino, Italy

M. Mastragostino - Università di Bologna, Italy

R. Neat - AEA Technology, Harwell, UK

B. B. Owens - Research International, USA

T. Osaka - Waseda University, Tokyo, Japan

J. -K. Park - KAIST, Korea

E. Peled - Tel Aviv University, Israel

W. H. Smyrl - University of Minnesota, USA

E. Spila - Eldor Corporation, Italy

J. M. Tarascon - Université de Picardie Jules Verne, France

M. Thackeray - Argonne National Laboratory, USA

J. O. Thomas - Uppsala University, Sweden

R. Vellone - ENEA, Rome, Italy

C. A. Vincent - University of St. Andrews, Scotland

M. Wakihara - Tokyo Institute of Technology, Japan

K. West - Technical University of Denmark

O. Yamamoto - Mie University, Japan

LOCAL ORGANIZING COMMITTEE

Fausto Croce, Università di Roma, Italy

Roberto Marassi, Università di Camerino, Italy

Marina Mastragostino, Università di Bologna, Italy

Stefania Panero, Università di Roma, Italy

Francesca Schiatti, Villa Erba, S.p.A., Italy

Bruno Scrosati, Università di Roma, Italy

Eraldo Spila, Eldor Corp, S.p.A., Italy

MEETING ORGANIZATION

ADMINISTRATION

The Electrochemical Society, Inc.

65 South Main Street

Pennington, NJ 08534-2839, USA

Phone: 609.737.1902

Fax: 609.737.2743

E-mail: ecs@electrochem.org

Responsible Persons: Brian E. Rounsavill & Elizabeth Brennfleck

LOCAL ARRANGEMENTS

Centro Volta

Villa Olmo, Via Cantoni 1

22100 Como, Italy

Phone: 39-031-579-812

Fax: 39-031-573-395

E-mail: stefanetti@icil64.cilea.it

Responsible persons: Chiara Stefanetti & Nadia Tasini

SPONSORS



Comitato Nazionale per le Celebrazioni Voltiane

Comitato Comasco per le Manifestazioni Voltiane nel Bicentenario dell'Invenzione della Pila 1997-2000;



The Electrochemical Society, Inc., Battery Division;

The Electrochemical Society Inc; European Local Section;



Electrochemical Society of Japan, Committee of Battery Technology;

Electrochemical Society of Japan, Committee on Capacity Technology;

Università "La Sapienza" di Roma;

Elettrochimica ed Energia, Roma;

Divisione Elettrochimica della Società Chimica Italiana;



ENEA, Ente per le Nuove Tecnologie, l'Energia e l'Ambiente, Roma;



Lithium Battery Energy Storage Technology Research Association;



US Army European Research Office, London;



ARCOTRONICS ITALIA SpA;



AUSIMONT SpA;



ELDOR Corporation

THE CONFERENCE

The lithium battery field has tremendously expanded since 1982 when the first edition of IMLB (IMLB-1) was held in Rome. The rapidly expanding commercialization of rechargeable lithium batteries in the consumer electronics market, and the extension of their use for electric vehicle applications, has dramatically increased the academic and industrial interest in this exciting field. This can be seen in a continuously growing participation in the past IMLB meetings, which in the case of IMLB-9, exceeded 600. The scientific and technological innovations in lithium batteries are expected to progress and IMLB-10 appears to be the ideal forum for reporting and discussing them. Thus, this special edition, which comes to celebrate the 20th anniversary of IMLBs and the turn of the millennium, should not be missed by anyone in the field.

The organizing committee and the supporting scientific societies invite you to participate in IMLB-10 in Como in 2000. The established format of the meeting will be continued with plenary and invited speakers highlighting key advances in the field. Dedicated poster sessions with time for presentation and ample discussion will ensure that all the contributed papers are given their rightful prominence. There will also be an exhibit of the latest instrumentation by companies in the industry.

All presentations will be in English.

CONFERENCE PROGRAM

The Conference will begin on Sunday, May 28, 2000 with a reception at 18:30 hours. Registration will open on Sunday, as well as exhibit and poster set-up. In general, the Technical Sessions will begin at 08:45 on Monday, May 29, 2000 and continue until 18:15 on Friday, June 2, 2000, with the exception of having the afternoon off on Wednesday, May 31, 2000 to explore Como. Each day there will be a luncheon held from 13:00 to 14:30 as well as two coffee breaks, one at 10:30 and the other at 16:00, held in the exhibit and poster area. Poster sessions are scheduled from 16:30 to 19:00 on Monday, Tuesday, and Thursday. The conference banquet is scheduled at 20:30 on Thursday, June 1, 2000.

Following the tradition set by previous international meetings on lithium batteries, invited speakers will highlight the key developments in the field. There will be no parallel sessions. All contributed papers will be presented as posters. As a result, the poster sessions will be given special prominence with ample visibility and time available for discussion.

PROGRAM OUTLINE

The following sessions will be included in the conference program:

- General
- Anodes
- Cathodes
- Liquid Electrolytes
- Polymer, Gel, and Glass Electrolytes
- Batteries
- Battery Materials
- Medical Batteries
- Supercapacitors

INVITED SPEAKERS

- M. Armand**, University of Montreal, Canada
D. Aurbach, Bar-Ilan University, Israel
J. O. Besenhard, Graz University, Austria
P. Birke, Fraunhofer Institut Siliziumtechnologie, Germany
 M. Broussely, SAFT, France
P. G. Bruce, St. Andrews University, UK
F. Croce, University of Rome, Italy
J. R. Dahn, Dalhousie University, Canada
C. Delmas, CNRS Bordeaux, France
J. Desilvestro, Pacific Lithium, Ltd., New Zealand
 J. Drews, Litronik GmbH, Germany
M. Duclot, ENSEEG, S. Martin d'Heres, France
A. Du Pasquier, Telcordia Technologies, USA
G. T. Fey, National Center University, Taiwan
 S. Greenbaum, CUNY, USA
R. Hamlen, US Army - CECOM, USA
U. Heider, Merck KGaA, Germany
C. F. Holmes, Greatbatch-Hittman, Inc., USA
 M. Inaba, Kyoto University, Japan
P. Jacobsson, Chalmers University, Sweden
R. Marsh, Wright-Patterson AFB, USA
C. M. Martin, University of Florida, USA
C. Masquelier, Universite Paris-Sud, Orsay, France
M. Mastragostino, University of Bologna, Italy
F. R. McLarnon, Lawrence Berkeley National Laboratory, USA
 K. Nakajima, Sony Corporation, Japan
K. Naoi, Tokyo University of Agriculture & Technology, Japan
S. Narukawa, Sanyo Electric Co., Ltd., Japan
P. Novak, Paul Sherrer Institute, Switzerland
 T. Osaka, Waseda University, Japan
 J.-K. Park, KAIST, Taejon, Korea
 S. Passerini, ENEA, Italy
E. Peled, Tel Aviv University, Israel
J. Prakash, Illinois Institute of Technology, USA
 D. Sadoway, MIT, USA
 M. Salomon, Max-Power Inc., USA
D. A. Scherson, Case Western Reserve University, USA
 D. Schleich, University of Nantes, France
 C. Schmidt, Medtronic, USA
W. H. Smyrl, University of Minnesota, USA
S. Surampudi, Jet Propulsion Laboratory, USA
 K. Takada, NIRIM, Ibaraki, Japan
 Y. Takeda, Mie University, Japan
 T. Tanaka, CRIEPI, Japan
J. M. Tarascon, Université de Picardie, France
M. Thackeray, Argonne National Laboratories, USA
 J. O. Thomas, Uppsala University, Sweden
 S. Tsuda, Matsushita Electric Ind., Japan
I. Uchida, Tohoku Institute of Technology, Japan
 W. van Schalkwijk, Self Charge, Inc., USA
M. Wakihara, Tokyo Institute of Technology, Japan
 R. Yazami, LEPMI-INPG, Grenoble, France
A. Yoshida, Matsushita Electric Industry Company, Ltd., Japan
K.-S. Yun, Korea Institute of Science and Technology, Korea
 W. Weppner, Kiel University, Germany

PUBLICATION

All scheduled abstracts will be published in a Meeting Abstracts volume, copyrighted by The Electrochemical Society, Inc. The volume is published photo-offset directly from copy submitted by the author. The volume size is 7 X 10 in. (178 x 254 mm).

PROCEEDINGS

The Conference Proceedings will be a special issue of the *Journal of Power Sources* (JPS), which conference delegates will receive directly from the publisher approximately 9 months after the meeting. Acceptance of an abstract does not imply acceptance in the JPS. Only those papers presented at the meeting will be considered for publication in the JPS. Papers will be subject to the standard JPS review procedure. The full length manuscript should be submitted on the first day of the meeting in Como. Manuscripts need not be camera-ready, as they will be typeset by the publisher. The maximum number of published pages in the JPS including abstracts, figures, tables, and references are limited. Information on this will be sent to the authors, along with paper acceptance, at a later date. Please refer to the "Instructions for Authors" of the *Journal of Power Sources* when preparing your manuscript.

EXHIBITION

The IMLB10 Meeting is a terrific opportunity for equipment manufacturers to present, face-to-face, their products and services to a vital research market which is ordinarily difficult for sales people to reach. This Exhibition will be conveniently located adjacent to the Technical Program and Poster Sessions, and the meeting has been arranged to allow ample time for participants to visit the Technical Exhibits.

EXHIBITORS (as of presstime):

Arbin Instruments

3206 Longmire Drive
College Station, TX 77845 USA
Contact: Derek L. Smith

Arbin Instruments is a developer and manufacturer of equipment for testing and production of capacitors, batteries of all chemistries and electrochemistry applications. Features include multiple current range (up to three per independent channel) bipolar output for full current/voltage control through zero crossing, true potentiostat/galvanostat circuitry and redundant safety for lithium applications.

Bitrode Ltd.

H1 Draycott Business Park
Dursley, Glos. GL11 5DQ, UK
Contact: Michael Young

Specialists in battery testing and formation solutions, Bitrode provides computer controlled test equipment for R&D and QA applications - single cell cycling to bench testing complete power systems - micro-amps to kilowatts. Our specialized Lithium Formation System has modular design allowing pilot line applications to high volume fully automated formation systems.

Braun S.r.l.

Via Fontevivo,25
19100 La Spezia, Italy
Contact: Peter Novak

BRAUN has been designing, building and perfecting gloveboxes. Our experience has enabled us to enhance our system technology and to learn what our customers expect and deserve in a controlled environment. Like the pieces of a puzzle, BRAUN glove box systems can be "pieced together" to form the solution for countless applications.

Elf-Atochem

Cerdato, Route du Rilsan
Serquigny, 27470, France
Contact: Anissa Brahmi

Elf-Atochem is the world's leading producer of PVDF. Our particular brand of high purity, battery grade PVDF resins are KYNAR® and KYNAR FLEX® for anodes, cathodes and separators. Elf-Atochem has offered its long and successful track record in engineering polymer chemistry to help develop Lithium Batteries technology.

Elsevier Science

Molenwerf 1
1014 AG Amsterdam
The Netherlands
Contact: Bianca Lathouwers

For over 100 years, Elsevier Science has been dedicated to facilitating the exchange of information. Today, Elsevier Science remains more committed than ever to that mission and has grown into a publishing entity of truly global proportions with offices around the world. Elsevier Science has become a leader in the publication and dissemination of literature covering the broad spectrum of scientific endeavors.

FMC - Lithium Division

449 North Cox Road
Gastonia, NC 28054
Contact: Fernando Marin or Tracy Lee Anderson

FMC is the world's leading supplier of lithium-based products to the primary and secondary battery industry. We supply LECTRO® Plus-Cathode Materials, LECTRO® Max-Anode Materials and LECTRO® Lyte-Salts. Ask us about our latest product innovation, LECTRO® Plus 165-Lithium Cobalt Oxide.

Hohsen Corporation

10-4-601 Minamisenba 4-chome
Osaka, Chuo-ku, 542-601, Japan
Contact: Kazuo Tagawa

Hohsen Corporation initially focussed on the coordination of testing equipment and the sale of related raw materials and components. Hohsen is now working to develop revolutionary new testing and manufacturing equipment to meet the needs of our clients.

Limtech, Inc.

2600 Blvd. Laurier
Sainte-Foy, Quebec, G1V 4W2, Canada
Contact: Gilles Dupuis

LIMTECH is a producer of high purity lithium carbonate. Its products are used in several industries including the fabrication of lithium battery cathodes and electrolytes, and in the fabrication of SAW filters used in cellular telephones and VCR's. LIMTECH's patented process allows products to be tailored to client needs.

Merck KGaA

Frankfurter Str. 250
Darmstadt 64271, Germany
Contact: Winfried Geissler

Merck KGaA is a leading European pharmaceuticals, laboratory, and specialty chemical group. Merck is present in 46 countries with 170 owned companies and manufactures at 63 locations in 26 countries. The product range comprises more than 20,000 different chemical, laboratory, medical and technological products. The technical industry is one business unit of the specialty chemical group. This business unit markets among other things materials for lithium batteries. Merck has developed a program for the production of primary and secondary lithium batteries. The optimization of electrolytes and cathode powders as well as the system analysis of electrolyte-cathode interrelations is one of the main topics of the application laboratory.

OnPower Battery S.p.A.

Viale Cialdini, 4/E
50137 Firenze, Italy
Contact: Peter Novak

OnPower Battery is a leader in advanced, long life primary and rechargeable batteries for mobile applications. The company develops products for the cellular phone, laptop computer, electric vehicle and other markets requiring high performance and high reliability. OnPower emphasizes innovation through its continuous R&D process that provides customers with comprehensive, high performance turnkey battery solutions.

Solartron

Victoria Road, Farnborough
Hampshire GU1 7PW, UK
Contact: Andrew Hinton

Solartron, a Roxboro Group Company, designs and manufactures a range of electrochemical and materials measurement solutions. The product range includes frequency response analyzers, potentiostats/galvanostats, multiplexers and materials interfaces. Solartron has also released the 1470 multichannel battery test system. This is targeted at research/development for battery, fuel cell, and supercapacitor technologies.

Thermal Hazard Technology

1 North House, Bond Avenue
Bletchley MK1 1SW, England
Contact: Martyn Ottaway

Thermal Hazard Technology's No. 1 concern is SAFETY! THT is a world leader in battery safety testing. We offer instrumentation and sample testing services. Our Adiabatic Battery Calorimeter/Accelerating Rate Calorimeter with Battery Cycling Option uniquely allows a full range of safety and efficiency tests for batteries or components. NEW! THT launches the EV Calorimeter, allowing similar testing with EV or storage batteries.

THE VENUE

Como is one of the most beautiful Alpine lakes in Northern Italy and also the birthplace and working residence of Alessandro Volta, the inventor of the first battery. Villa Erba, in Cernobbio (Como), Italy, is a new exhibition and conference center located in a park with exceptional landscaping next to a villa of historical and artistic importance. Just half an hour from Milan, Lake Como is a jewel-like oasis of tranquillity, a magical combination of lush Mediterranean foliage and snowy alpine peaks. Of all the lakes of north Italy, Lake Como, lined with elegant 19th century villas, crowned by snow-capped mountains, and buzzing with ferries, is an outstanding venue for IMLB10.

ACCOMMODATIONS

The IMLB 10 conference will be held at the Villa Erba Conference Center in Como, Italy. The Centro Volta will be handling all hotel and tour accommodations. Therefore, should you have any questions or require additional information regarding your hotel or tour plans, please contact the Centro Volta directly via Phone: 39.031.579.812, Fax: 39.031.573.395, or E-mail: congress@icil64.cilea.it. The deadline for making hotel reservations is April 1, 2000. Written requests for refunds of deposits (by e-mail or fax) will be honored up until May 15, 2000. All reservations must be accompanied by a deposit equal to 100.000 It. Lit. per person to guarantee the hotel reservation.

Please specify your choice of hotel category on your reservation form. If your choice is not available, you will be confirmed in the next higher available category. The special convention hotel rates are:

★★★★★ (5 Star Luxury Hotel)
single room: IT. Lire 420.000
double room: IT. Lire 700.000

This luxury category is available only at VILLA d'ESTE, one of the most famous luxury hotels in all of Europe, well known as a shelter for VIPs, movie and rock stars, due to the privacy and seclusion of this place.

★★★★ (4 Star Luxury Hotel)
single room: IT. Lire 180.000
double room: IT. Lire 230.000

All rooms have direct dial phone, mini bar, satellite TV and air conditioning. For the most part, the 4 star hotel have sports facilities, lake views and excellent restaurants.

★★★ (3 Star Luxury Hotel)
single room: IT. Lire 130.000
double room: IT. Lire 170.000

Differing from the 4 star category, these hotels have no sports facilities and usually are not near the lake. Some of these hotels are air-conditioned and have restaurants inside.

★★ (2 Star Luxury Hotel)
single room: IT. Lire 90.000
double room: IT. Lire 130.000

The cheapest option for an informal and familiar accommodation. Some rooms have a bathroom in the corridor; none of them are air-conditioned or have a television.

IMPORTANT: All prices include breakfast. Prices indicated are 1999 prices—some increases may be possible.

ACCOMPANYING PERSON TOUR PROGRAM

The following tours have been arranged for individuals accompanying attendees of the IMLB 10 conference. The Centro Volta will be handling all tour arrangements. Therefore, should you have any questions or require additional information regarding your tour plans, please contact the Centro Volta directly via Phone: 39.031.579.812, Fax: 39.031.573.395, or E-mail: congress@icil64.cilea.it. The deadline for making tour reservations is April 1, 2000. Written requests for refunds of deposits (by e-mail or fax) will be honored up until May 15, 2000. Tour reservations will be taken at the meeting based on availability, subject to a surcharge.

Tour on Como Lake

(half-day tour)

Departure from Villa Erba pier (or Como pier) for a guided tour of Como lake by boat. The boat will pass Cernobbio and the famous luxury hotel Villa d'Este, Brienno, Argegno, Lenno and Isola Comacina. Arrival in Tremezzo and visit to Villa Carlotta, famous for its Italian gardens and Canova sculptures. Return to Como, coasting Menaggio and Bellagio.

Price: It. Lit. 50.000 per person

Tour of historical Como

(half-day tour)

Guided tour in the center of the city, visiting the Cathedral, Broletto and S. Fedele Roman Catholic Church.

Price It. Lit. 15.000 per person

Silk Shopping

(half-day tour)

Visit to the magnificent silk museum in Como to discover local main production. A shopping tour to the Mantero outlet will follow.

Price It. Lit. 30.000 per person

Tour of Milan

(all day tour)

Departure from hotels by bus. Arrival in Milan and meeting with local guides. Visit to the Cathedral (fourth largest church in the world with 135 spires and 3200 statues). Visit to La Scala Theatre and its museum. Stop for lunch and in the afternoon visit of the Castello Sforzesco and its museum. Return to Como.

Price It. Lit. 80.000 per person

GENERAL INFORMATION

Climate:

It is often sunny and warm in Como in May (average temp. 20-25°C), nevertheless there may be some rain as the weather is changeable. An umbrella and a light coat are recommended.

Banking:

Normal banking opening hours in Como are from:

08:30 to 13:20

15:00 to 16:00 (weekdays)

Closed: Saturday and Sunday.

TRAVEL TO COMO

Como is easily reached by plane, being close to both the Milano Airports of Malpensa and Linate. Como is also very well connected by trains to all of the major European cities. Frequent and fast train service connects Como to Milan or to Switzerland daily. Driving to Como is also very easy and pleasant, either by fast highways or by scenic mountain roads.

For visitors arriving by plane, Lugano airport is only a 20-minute drive from Villa Erba, and Malpensa, Bergamo, and Linate airports are roughly 30-45 minutes away. Motorists will find their journey just as easy; the Como Nord exit on the A9 motorway from Milan takes them virtually to the gates of Villa Erba, where there is ample parking for delegates and exhibitors for a charge. Villa Erba is served by two railway lines Ferrovie Nord Milano, with a station at Como Lago, and Italian State Railways, whose Como S. Giovanni station is on the international Milan-Chiasso line. Delegates can even arrive by boat if they wish; the regular Lake Como ferry service docks at Villa Erba's own landing stage on request.

Transportation

How to reach Como - Villa Erba

By Air:

From Milano—Linate Airport

A) **1 Bus STAM** from Milano - Linate airport to Central Railway Station (30 min. approx.; frequency: every 20 min. from 6.00 to 7.00, every 30 min. from 7.00 to 23.00; price one way Lit. 5.500 available on bus) or **Taxi** from Milano - Linate airport to Central Railway Station (30 min. approx.; price max. Lit. 30.000) 2. Trains from Central Station to Como S.G. Station (see time-table on page 12) 3 Buses from Como S.G. station to Villa Erba n. 1,6,11,14 (price Lit.1.600; tickets are not available on buses)

B) **Taxi** from Milano - Linate airport to Como (Lit. 170.000 maximum by motorway, approx. 1.30 h.; please ask the taxi-driver the fare before leaving!)

From Milano—Malpensa Airport

A) **Bus AIRPULMANN** from Milano-Malpensa airport to Como (1 hour approx.; frequency: every hour from 8.00 to 12.00, every 3 hours from 12.00 to 19.30; on Sunday only two runs at 9.25 and at 12.00)

2. **Malpensa EXPRESS** from Milano-Malpensa airport to Saronno station and change for Como Lago FNM Station (1 hour approx. - see time-table on page 12)

3. **Buses** from Como Lago FNM to Villa Erba n. 6 (price Lit. 1.600; tickets are not available on buses.)

B) **Taxi** from Milano - Malpensa airport to Como (Lit. 140.000 maximum; approx. 40/60 min.; please ask the taxi-driver the fare before leaving!)

By Train:

International railway line North Europe - Basel - Chiasso - Como or North Europe - Zurich - Chiasso - Como

By Car:

From Milano: motorway A9, exit Como Monte Olimpino or Como Nord

From Switzerland: motorway A9, exit Como Nord or Como Sud

How to reach Milano Linate Airport from Como

Train from Como S.G. station to Milano Centrale Railway Station (see time-table on page 12)

Bus from Milano Centrale Railway Station to Milano - Linate airport (every 20/30 min. from 5.40 to 21.00)

How to reach Milano Malpensa Airport from Como

Bus AIRPULMANN from Piazza Matteotti (Como) (1 hour approx.; frequency: 1st run at 5.50, from 7.20 to 17.50 every 2 hours, on Sunday only two runs at 7.20 and at 10.50)

Train to Saronno and change for Malpensa EXPRESS (1 hour approx. - see time-table on page 12)

How to reach the Villa Erba once in Como

Individuals who have accommodations in the hotels in Cernobbio can reach the Villa Erba conference center by a short walk of not more than 5 to 10 minutes. Individuals who have accommodations in the center of Como have two different options:

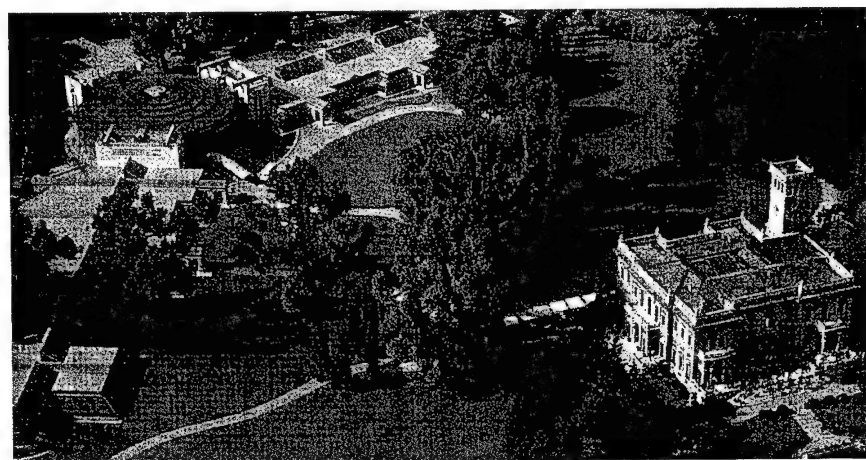
Travel by boat - from the main Piazza Cavour they can take a boat, every 30 minutes from 07.35 until 19.45. In 13 minutes they will be in Cernobbio and can reach Villa Erba by walking a short distance. The cost of the ticket is about 4.000 lire (approximately \$2.00 US Dollars);

Travel by bus - from the Bus Station in Piazza Matteotti in Como they can catch bus no. 6 and reach Villa Erba (bus stop "Tavernola Breggia", just in front of Villa Erba) in 10 minutes. Buses run from 06:00 until 23:00 and the cost of the ticket is about 3.000 lire (approximately \$1.50 US Dollars).

MEETING ORGANIZATION

The IMLB 10 meeting will be administratively managed by The Electrochemical Society, Inc. (Pennington, NJ, USA) and the local arrangements will be coordinated by the Volta Center (Como, Italy). For more information, contact the ECS Headquarters Office and the Chairman by sending an e-mail message to the following address: imlb10@electrochem.org.

VILLA ERBA CONFERENCE CENTER



TRAIN TIME-TABLE (to/from Linate Airport)

Milano C.	dep.	0:30	07:15	07:25	08:25	09:25	11:15	11:25	12:25	13:25	14:25
Como S.G.	arr.	1:37	07:47	08:05	09:05	10:05	11:50	12:05	13:05	14:05	15:05
Milano C.	dep.		15:25	16:25	17:30	18:15	18:25	19:15	19:25	20:25	21:25
Como S.G.	arr.		16:05	17:05	18:19	18:47	19:05	19:49	20:00	21:05	22:06
Como S.G.	dep.	07:02	07:55	08:02	08:55	10:13	11:49	12:09	12:56	13:56	14:56
Milano C.	arr.	07:45	08:35	08:55	09:35	10:45	12:35	12:45	13:35	14:35	15:35
Como S.G.	dep.	15:29	15:56	16:13	17:56	18:56	19:56	20:56	21:56	22:13	
Milano C.	arr.	16:30	16:35	16:45	18:35	19:35	20:35	21:35	22:35	22:45	

Time-tables and prices are referred to September 1999

TRAIN TIME-TABLE (to/from Malpensa Airport)

Malpensa	dep.	07:45	08:45	09:45	11:15	12:15	13:45	15:15	16:45	17:45	
Saronno	arr.	08:05	09:05	10:05	11:35	12:35	14:05	15:35	17:05	18:05	
Como	dep.	08:33	09:33	10:29	12:04	13:04	14:29	16:04	17:23	18:23	
Como	dep.	07:36	08:14	10:14	11:14	12:14	13:14	14:14	15:14	16:14	17:40
Saronno	dep.	08:09	09:09	11:09	12:09	13:09	13:39	15:09	16:09	17:09	18:09
Malpensa	arr.	08:30	09:30	11:30	12:30	13:30	14:00	15:30	16:30	17:30	18:30

Last train leaving Como is at 19:14, change in Saronno at 20:09, and arrive in Malpensa at 20:30.

TECHNICAL SESSIONS

SUNDAY, MAY 28, 2000

- 14:00-18:00 Registration in Ala Cernobbio
 14:00-18:00 Authors Presenting Posters during the week should set-up their posters in Ala Cernobbio
 18:30-20:00 Welcome Reception at Villa Erba

Time Abs. #

ORAL PRESENTATIONS MONDAY, MAY 29, 2000

Padiglione Centrale, Villa Erba Conference Center

General Session

Chair: Z. Ogumi

- 8:45 Opening Remarks by B. Scrosati
 9:00 **1** Year 2000 R&D Status of Large-Scale Lithium Secondary Batteries in the National Project of Japan - T. Tanaka (Central Research Institute of Electric Power Industry (CRIEPI)) and N. Arai (Lithium Battery Energy Storage Technology Research Association (LIBES))
 9:30 **2** From Gems to Lithium Battery Electrodes - M.M. Thackeray (Argonne National Laboratory) (Argonne National Laboratory)
 10:00 **3** Aging Mechanism in Li Ion Cells and Calendar Life Predictions - M. Broussely, S. Herreyre, P. Biensan, P. Kaszteljna, K. Nechev, and R.J. Staniewicz (SAFT)
 10:30 Coffee Break in Ala Lario

Chair: F. R. McLarnon

- 11:00 **4** The Status of Sony Li-Ion Polymer Battery - K. Nakajima, K. Kezuka, and T. Hatazawa (Sony Corporation, Energy Co.)
 11:30 **5** Battery Technologies and Based on the Requirement for Applications and Future Movement - S. Tsuda (Matsushita Electric Industrial Co., Ltd.) Tsuda (Matsushita Electric Industrial Co., Ltd.)
 12:00 **6** U.S. Army Portable Power Programs - R. Hamlen, G. Au, M. Brundage, M. Hendrickson, and E. Plichta (Army Power Division)
 12:30 **7** Lithium-Ion Batteries for Aerospace Applications - R. Marsh, S. Vukson (HQ Air Force Materials Command), S. Surampudi, R. Bugga, M. Smart (Jet Propulsion Laboratory), M. Manzo, and P. Dalton (NASA John H. Glenn Research Center)
 13:00 Lunch in Ala Lario

Anodes I

Chair: M. Broussely

- 14:30 **8** From Rome to Como: Twenty Years of Active Research on Carbon Based Electrodes for Lithium Batteries at INP-Grenoble - R. Yazami (CNRS) Batteries at INP-Grenoble - R. Yazami (CNRS)

Time Abs. #

- 15:00 9 The Complex Electrochemistry of Graphite Electrodes in Lithium-Ion Batteries - P. Novak, F. Joho, M. Lanz, B. Rykart, J.-C. Panitz, D. Alliata, and R. Koetz (Paul Scherrer Institute)
- 15:30 10 High-Capacity Carbons for Lithium-Ion Batteries Prepared from Rice Husk - G.T.-K. Fey and C.-L. Chen (National Central University)
- 16:00 Coffee Break in Ala Lario
- 16:30 Poster Session in Ala Cernobbio

TUESDAY, MAY 30, 2000

Anodes II

Chair: G. A. Nazri

- 8:30 11 Searching for Anode Materials for the Li-Ion Technology: Time to Deviate from the Usual Path - P. Poizot, S. Laruelle, E. Baudrin, S. Denis, M. Touboul, and J.-M. Tarascon (Université de Picardie Jules Verne)
- 9:00 12 Film-Forming Electrolyte Additives for Li-Carbon and Li-Alloy Anodes - J.O. Besenhard, G.H. Wrodnigg, K.-C. Moller, H. Buqa, M. Wachtler, and M. Winter (Graz University of Technology)
- 9:30 13 Novel Anodes for Lithium Ion Batteries - T. Brousse, O. Crosnier, P. Fragnaud, and D.M. Schleich (Ecole Polytechnique de l'Université de Nantes)
- 10:00 14 New Composite Anode Systems Combined with $\text{Li}_{2.6}\text{Co}_{0.4}\text{N}$ - Y. Takeda and J. Yang (Mie University)
- 10:30 Coffee Break in Ala Lario

Cathodes I

Chair: K. M. Abraham

- 11:00 15 Layered LiMnO_2 and Spinel-Based Compounds as Positive Electrodes in Rechargeable Batteries: Structure, Transformation and Properties - P.G. Bruce, A.R. Armstrong, A.D. Robertson, M.J. Duncan, A.J. Fowkes, and T.E. Quine (University of St. Andrews)
- 11:30 16 Charge-Discharge Properties of Spinel Oxides as the Cathode for Lithium Secondary Battery - M. Wakihara (Tokyo Institute of Technology)
- 12:00 17 Novel Layered Cathode Materials for Advanced Lithium Ion Batteries - B. Ammundsen, J. Desilvestro, R. Steiner, and P. Pickering (Pacific Lithium Limited)
- 12:30 18 STM Study on Lithium Manganese Oxide Cathodes - M. Inaba, T. Abe, and Z. Ogumi (Kyoto University)
- 13:00 Lunch in Ala Lario

Cathodes II

Chair: S. Panero

- 14:30 19 Effects of Cationic Disorder and Defects on the Structural Behaviour of the $\text{Li}_x(\text{M}, \text{L})\text{O}_2$ ($\text{M} = \text{Ni}, \text{Co}$) Phases - C. Delmas (Ecole Nationale Supérieure de Chimie et Physique de Bordeaux)
- 15:00 20 The Source of First-Cycle Capacity Loss in LiFePO_4 - A.S. Andersson and J.O. Thomas (Uppsala University)

Time Abs. #

- 15:30 21 A Survey of Polyanionic Structures Hosts For Reversible Lithium Insertion - C. Masquelier, C. Wurm (Université Paris-Sud Orsay), J. Rodriguez-Carvajal (CEA-CNRS Saclay), J. Gaubicher, and L. Nazar (University of Waterloo)
- 16:00 Coffee Break in Ala Lario
- 16:30 Poster Session in Ala Cernobbio

WEDNESDAY, MAY 31, 2000

Liquid Electrolytes

Chair: I. Exner

- 8:30 22 Lithium Fluoralkylphosphates, A New Class of Conducting Salts for Electrolytes for High Energy Lithium-Ion Batteries - M. Schmidt, U. Heider, A. Kuehner, R. Oesten, M. Jungnitz (Merck KGaA), N. Ignat'ev, and P. Sartori (Gerhardt-Mercator-University)
- 9:00 23 Low Temperature Behavior of Li-Ion Cells - H.-P. Lin, M. Salomon, H.C.A. Shiao (MaxPower, Inc.), M. Hendrickson, E. Plichta, and S. Slane (U.S. Army)
- 9:30 24 Composition, Depth Profiles and Lateral Distribution of Materials in the SEI Built on HOPG -TOF SIMS and XPS Studies - E. Peled, D. Bar Tow, A. Merson, A. Gladkich, and L. Burstein (Tel Aviv University)
- 10:00 25 In Situ Studies of SEI Formation - F. Kong, R. Kostecki (Lawrence Berkeley National Laboratory), G. Nadeau (Institut de Recherche d'Hydro-Quebec), X. Song (Lawrence Berkeley National Laboratory), K. Zaghib (Institut de Recherche d'Hydro-Quebec), K. Kinoshita, and F. McLarnon (Lawrence Berkeley National Laboratory)
- 10:30 Coffee Break in Ala Lario

Polymer Electrolytes

Chair: B. Scrosati

- 11:00 26 Volta Award Address-Batteries for Transportation: Are We Missing the Boat? - M. Armand (University of Montreal)
- 11:30 27 PEO-Based Nanocomposite Polymer Electrolytes - F. Croce, L. Persi, and B. Scrosati (Università "La Sapienza")
- 12:00 28 Electrochemical Characteristics of Polymer Electrolytes Based on P(VDF-co-HFP)/PMMA Ionomer Blend for PLIB - J.-K. Park and Y.-G. Lee (Korea Advanced Institute of Science and Technology)
- 12:30 29 Self-Doped Block Copolymer Electrolytes (SDBCEs) for Solid-State, Rechargeable Lithium Batteries - D. Sadoway, A. Mayes, B. Huang, P. Trapa, P. Soo, and P. Bannerjee (Massachusetts Institute of Technology)
- 13:00 Lunch in Ala Lario
- 14:30 Afternoon free for sightseeing activities

THURSDAY, JUNE 1, 2000

Battery Materials

Chair: J. R. Selman

- 8:30 30 Electrochemical and Synchrotron Radiation XAS Studies of Lithium Intercalation Into Vanadium Pentoxide Aerogels and Nanocomposites - W. Smyrl (UMN), S. Passerini (ENEA), M. Giorgetti (UMN), F. Coustier (Polystor Corporation), M. Fay, and B. Owens (UMN)

Time	Abs. #	
9:00	31	Light Scattering and Computational Studies on Ionic Interaction and Dynamics in Polymer Based Gel Electrolytes - P. Johansson, C. Svanberg, R. Bergman, and P. Jacobsson (Chalmers University of Technology)
9:30	32	Solid State NMR Studies of Lithium Ion Battery Materials - S. Greenbaum, Y. Wang, S. Chung, and X. Guo (Hunter College of the City University of New York)
10:00	33	<i>In-Situ</i> and <i>Ex-Situ</i> Strategies for the Study of Lithium Battery Electrodes - L. Rendek Jr., D. Totir, G. Chottiner, and D. Scherson (Case Western Reserve University)
10:30		Coffee Break in Ala Lario

Chair: K. Amine

11:00	34	Rechargeable Magnesium Battery Technology, a Comparison with Li Battery Systems - D. Aurbach, Y. Gofer (Bar-Ilan University), Z. Lu (Dalhousie University), A. Schechter (Case Western Reserve University), O. Chusid, H. Gizbar, Y. Cohen, V. Ashkenazi, M. Moshkovich, R. Turgeman, and E. Levi (Bar-Ilan University)
11:30	35	Nanomaterial-Based Li-Ion Battery Electrodes - C. Martin, N. Lee (University of Florida), and B. Scrosati (University of Rome "La Sapienza")
12:00	36	Microstructure Effects in Plasticized PVDF-HFP-Based Electrodes for Plastic Li-Ion Batteries - A. Du Pasquier, T. Zheng, G. Amatucci, and A. Gozdz (Telcordia Technologies)
12:30	37	Investigations of Non-Flammable Phosphazene Based Compounds for Lithium Ion Batteries - J. Prakash and C.-W. Lee (Illinois Institute of Technology)
13:00		Lunch in Ala Lario

Batteries I

Chair: R. J. Brodd

14:30	38	Development of Lithium Polymer Batteries with Gel Polymer Electrolyte - S. Narukawa and I. Nakane (Sanyo Electric Co., Ltd.)
15:00	39	Glassy Materials for Lithium Batteries - Theoretical Aspects and Devices Performances - M. Duclot and J.-L. Souquet (Laboratoire d'Electrochimie et de Physicochimie des Matériaux et des Interfaces (LEPMI))
15:30	40	Research on Highly Reliable Solid-State Lithium Batteries in NIRIM - K. Takada, T. Inada, A. Kajiyama, M. Kouguchi, S. Kondo, and M. Watanabe (NIRIM)
16:00		Coffee Break in Ala Lario
16:30		Poster Session in Ala Cernobbio
20:30		Banquet in Villa Antica

FRIDAY, JUNE 2, 2000

Batteries II

Chair: J. T. S. Irvine

9:00	41	Materials Development for High-Performance Lithium Batteries - R.A. Huggins, A. Netz, V. Thangadurai, J. Schwenzel, S. Stramare, and W. Weppner (Christian-Albrechts-University)
9:30	42	Modeling Lithium-Ion Battery Oven Exposure Tests - J.R. Dahn, T. Hatchard, D. MacNeil (Dalhousie University), and L. Christensen (3M Company)
10:10	43	Recent Investigations on Thin Films and Single Particles of Transition Metal Oxides for Lithium Batteries - I. Uchida, M. Mohamedi, M. Nishizawa, and T. Itoh (Tohoku University)
10:30		Coffee Break in Ala Lario

Time Abs. #

Batteries III

Chair: M. Conte

- 11:00 44 Recent Advances on Rechargeable Lithium Ion Polymer Batteries in Korea - K.-S. Yun, B.-W. Cho, W.-I. Cho, and H.-S. Kim (Korea Institute of Science and Technology)
- 11:30 45 Lithium Metal/Polymer Battery - T. Osaka (Waseda University)
- 12:00 46 Solid State Polymer Battery Based on Lithium Titanate Anode - P. Birke and F. Salam (Fraunhofer Institut Siliziumtechnologie (ISIT))
- 12:30 47 Shaped Charge: Adjustable Form-Factor Lithium-Ion Batteries - W. van Schalkwijk (SelfCharge Inc) and M. Juzkow (PolyStor Corporation)
- 13:00 Lunch in Ala Lario

Medical Batteries

Chair: B. B. Owens

- 14:30 48 The Role of Lithium Batteries in Modern Health Care - C.F. Holmes (Greatbatch-Hittman, Inc.)
- 15:00 49 The Future of Lithium and Lithium-Ion Batteries in Implantable Medical Devices - C. Schmidt and P. Skarstad (Medtronic Energy & Components Center)
- 15:20 50 Primary Batteries for Implantable Pacemakers and Defibrillators- J. Drews, G. Fehrmann, R. Staub, and R. Wolf (LITRONIK GmbH & Co.)
- 15:40 51 Medical Batteries for External Medical Devices - S. Passerini (ENEA) and B. Owens (University of Minnesota)
- 16:00 Coffee Break in Ala Lario

Supercapacitors

Chair: M. Morita

- 16:30 52 Advanced Capacitors and Their Application - S. Nomoto, H. Nakata, K. Yoshioka (Matsushita Electric Industrial Co., Ltd.), A. Yoshida (Matsushita Electric Industrial Co., Ltd.), and H. Yoneda (Matsushita Electronic Components Co., Ltd.)
- 17:00 53 Polymer-Based Supercapacitors - M. Mastragostino, C. Arbizzani, and F. Soavi (Universita' di Bologna)
- 17:30 54 New Conducting Polymers for Supercapacitors and Lithium Batteries - K. Naoi (Tokyo University of Agriculture and Technology)
- 18:00 Concluding Remarks by F.R. McLarnon

POSTER PRESENTATIONS

Ala Cernobbio, Villa Erba Conference Center

Authors presenting posters should prepare their materials with a total dimension of 100 cm wide by 150 cm high. Presenters may begin setting up their posters at 14:00 on Sunday, May 28, 2000 in Ala Cernobbio. Authors should look for the corresponding abstract number to see where to set up their posters. All posters will remain available for viewing throughout the entire week. Specific segments of posters will be highlighted in conjunction with the oral presentations each day. Authors are advised to be available at these times to answer questions and provide feedback. Afternoon poster sessions are planned from 16:30 to 19:00 on Monday, Tuesday, and Thursday to offer additional time for viewing the posters.

Abs. #

Anodes Posters

Co-Chairs: M. Brousely and G. A. Nazri

- 55 Tin/Tin Oxide Thin Film Electrodes for Lithium-Ion Batteries - J. Sarradin, N. Benjelloun, G. Taillades, and M. Ribes (Université Montpellier II)
- 56 Optimization of Physicochemical Characteristics of a Lithium Anode Interface for High-Efficiency Cycling - M. Ishikawa and M. Morita (Yamaguchi University)
- 57 Improved Carbon Anode Properties: Pretreatment of Particles in Polyelectrolyte Solution - M. Gaberscek, M. Bele, R. Dominko, J. Drofenik (National Institute of Chemistry), and S. Pejovnik (University of Ljubljana)
- 58 Graphite-Tin Composites as Anode Materials for Lithium-Ion Batteries - G.X. Wang (University of Wollongong), J.-H. Ann (Andong National University), L. Sun, M.J. Lindsay, D.H. Bradhurst, S.X. Dou, and H.K. Liu (University of Wollongong)
- 59 Study on Electrochemical Behavior of Carbon Materials for Lithium-Ion Battery - D. Wang, Y. Gao, D. Wang, Z. Li, X. Ping, and X. Wang (Tianjin Institute of Power Sources)
- 60 On The Possibility of forming Superdense Lithium Graphite Intercalation Compounds by Electrochemical Means - E. Peled, D. Bar Tow, V. Yufit, and Y. Rosenberg (Tel Aviv University)
- 61 Charge/Discharge Characteristics of the Coal-tar Pitch Carbon as Negative Electrodes in Li-Ion Batteries - J.-S. Kim and Y.-T. Park (University of Seoul)
- 62 Fast Electrochemical Formation of Nanostructure Alloys as Anodes in Lithium - Ion Batteries - E. Peled, A. Ulus, and Y. Rosenberg (Tel Aviv University)
- 63 Irreversibility Compensation of SnO Anodes by $\text{Li}_{2.6}\text{Co}_{0.4}\text{N}$ - J. Yang, Y. Takeda, N. Imanishi (Mie University), and O. Yamamoto (Genesis Research Institute, INC)
- 64 Impedance Measurements of Graphite Negative Electrode for Lithium-Ion Batteries - K. Sawai and T. Ohzuku (Osaka City University)
- 65 Direct Evidence on Anomalous Expansion of Graphite Negative Electrodes on 1st Charge by Dilatometry - T. Ohzuku, N. Matoba, and K. Sawai (Osaka City University)
- 66 Dispersed Silicon-Graphite Powder: A High Capacity Anode Material for Rechargeable Lithium-Ion Batteries - J. Niu and J. Lee (National University of Singapore)
- 67 Electrochemical Performance of $\text{Pb}_3(\text{PO}_4)_2$ Anodes in Secondary Lithium Batteries - Z. Liu (Institute of Materials Research and Engineering) and J.Y. Lee (National University of Singapore)
- 68 Electrochemical/Interfacial Studies of Carbon Films in Non-aqueous Electrolytes - D. Allia (Paul Scherrer Institut), R. Kostecki, X. Song, K. Kinoshita (Lawrence Berkeley National Laboratory), and R. Koetz (Paul Scherrer Institut)
- 69 Reversible Reaction of Li with Grain Boundary Atoms in SnMn_3C - L. Beaulieu (Dalhousie University), D. Larcher (Université de Picardie-Jules Verne), R. Dunlap, and J. Dahn (Dalhousie University)
- 70 The Influence of the Structure of Initial Material and the Ways of Its Modification on Electrochemical Properties of the Graphite Anodes in Lithium-Ion Systems. - E. Shembel, N. Globa, N. Zaderey, A. Baskevich, O. Ksenzhek, K. Kylyvnyk, T. Pastushkin (Ukrainian State Chemical Technology University), L. Vishnyakov, and V. Kokhany (Institute for Problems of Materials Science of NAS of Ukraine)
- 71 Nitride Electrode for Rechargeable Lithium Battery - Y. Nitta, J. Yamaura, M. Hasegawa, S. Tsutsumi (Matsushita Electric Industrial Co., Ltd.), H. Ohzono, and H. Miyake (Matsushita Battery Industrial Co., Ltd.)
- 72 Nano-Crystalline Multi-Phase Materials from the Ternary System Ag-Sb-Sn as New Anodes with Increased Lithium Storage Capacities - M. Wachtler, J.H. Albering, M. Winter, and J.O. Besenhard (Graz University of Technology)

Abs. #

- 73 Influence of the Binder on the Cycling Performance of Composite Electrodes with Nano-Structured Lithium Storage Metals and Alloys - M.R. Wagner, M. Wachtler, M. Schmied, P. Preishuber-Pflügl, F. Stelzer, J.O. Besenhard, and M. Winter (Graz University of Technology)
- 74 Anion Intercalation into Heat-Treated XP_3 Coke - J.A. Seel and J.R. Dahn (Dalhousie University)
- 75 Metallic Anode Materials for Li-ion Batteries - G. Ehrlich, C. Durand, M. Hetzel, J. McGuinn (Yardney Technical Products, Inc.), X. Chen, T. Hugener, F. Speiss, and S. Suib (University of Connecticut)
- 76 Relation Between Surface Properties and First-Cycle Irreversible Charge Loss of Graphite Electrodes for Lithium-Ion Batteries - F. Joho, B. Rykart, B. Andreas, P. Novak (Paul Scherrer Institut), and S. Michael E. (Timcal Group)
- 77 Origins of Reversible and Irreversible Capacity Losses of Graphite-Lithium Anode - A. Martinet and R. Yazami (CNRS)
- 78 Nanocrystalline Mg_2Sn As an Anode Materials for Li-ion Battery - H. Kim, Y.-J. Kim, D.-G. Kim, H.-J. Sohn, T. Kang, and B. Park (Seoul National University)
- 79 Al-Based Active/Inactive Composite Anodes for Lithium Rechargeable Batteries - G.-J. Jeong, Y.-U. Kim, H.-J. Sohn, T. Kang (Seoul National University), H.-R. Kang, and S.-W. Kim (NESS Coroperation Ltd.)
- 80 The Effect of Electrolyte Temperature on the Passivity of Solid Electrolyte Interphase formed on Graphite Electrode - S.-I. Pyun and S.-B. Lee (Korea Advanced Institute of Science and Technology)
- 81 Improvement of Charge/Discharge Characteristics of Al-X-Li Alloys by Means of Varying the Alloy Composition. - G. Vladimir, O. Victoria, and B. Aleksey (Rostov State University)
- 82 Carbon Electrode Morphology and Thermal Stability of the Passivation Layer - L. Fransson, A.M. Andersson, A. Hussenius, and K. Edstrom (Uppsala University)
- 83 Thermal Stability of a Hopg/Liquid Electrolyte Interface Using *In-Situ* Electrochemical Atomic Force Microscopy - K. Edstrom and M. Herranen (Uppsala University)
- 84 CaSi_2 : A New Anode Material for Lithium-Ion Batteries - S.R.S. Prabakaran, T.T. Yong (Multimedia University), and S. Michael (Advanced Materials Research Center)
- 85 The Correlation Among Surface Chemistry, 3D Structure, Morphology, Electrochemical and Impedance Behavior of Lithiated Carbon Electrodes - D. Aurbach, J. Gnanaraj (Bar-Ilan University), J. Fischer, and A. Claye (University of Pennsylvania)
- 86 A Comparison Between the Electrochemical Behavior of Reversible Magnesium and Lithium Electrodes - D. Aurbach, Y. Gofer (Bar-Ilan University), A. Schechter (Case Western Reserve University), O. Chusid, H. Gizbar, Y. Cohen, M. Moshkovich, and R. Turgeman (Bar-Ilan University)
- 87 Novel SnS_2 Anode for Rechargeable Lithium Battery - T. Momma, N. Shiraishi, T. Osaka (Waseda University), A. Gedanken, J. Zhu, and L. Sominski (Bar-Ilan University)
- 88 The Effects of Electrolyte Composition on the Electrochemical Behavior of Li-Alloy Electrode - G.-J. Jeong (Seoul National University), Y.-J. Kim (Kyushu University), H. Kim, H.-J. Sohn, and T. Kang (Seoul National University)
- 89 Amorphous Sn-Ca Alloy as Lithium Ion Battery Anode - L. Fang (Institute of Materials Research and Engineering) and B.V.R. Chowdari (National University of Singapore)
- 90 Influence of Edge and Basal Plane Sites on the Electrochemical Behavior of Flake-Like Natural Graphite for Li-Ion Batteries - K.V. Zaghib, G. Nadeau (Institut de Recherche d'Hydro-Quebec), and K. Kinoshita (Lawrence Berkeley National Laboratory)
- 91 Nanopartical Size Carbon Materials for Lithium Batteries - B. Banov (Bulgarian Academy of Sciences)

Abs. #

- **92** Study on $\text{Li}[\text{Li}_{1/3}\text{Ti}_{5/3}]\text{O}_4$ as Anode Material for Lithium Ion Batteries - M. Arrabito (Polytechnic of Turin), S. Panero, P. Reale, and B. Scrosati (University of Rome La Sapienza)
- **93** *In-Situ* TEM Study of the Interface Carbone/Electrolyte - M. Dolle, S. Grugeon, A. Cressent, B. Beaudoin, L. Dupont, and J.-M. Tarascon (Université de Picardie Jules Verne)
- **94** The Electrochemical Behaviour and Structural Changes of Tin-Lead Anodes During Li Reversible Insertion - A. Momtchilov (Bulgarian Academy of Sciences)
- **95** Aggregation and Li_2O Formation Reaction in the Sn-Based Oxide Anodes - Y.-J. Kim, H.-J. Sohn, and T. Kang (Seoul National University)
- **96** Capacity Losses and Cycle Behaviors in Sn-Based Anodes - Y.-J. Kim, H.-J. Sohn, and T. Kang (Seoul National University)
- **97** Hard Carbon Prepared from Anthracite Coal for Lithium Ion Batteries - I. Mochida, C.-H. Ku, Y.-J. Kim, and Y. Korai (Institute of Advanced Material Study)
- **98** Development and Manufacturing of the Lithium Sources and Novel Generation Electrode's Materials in Novosibirsk - V. Afanasjev, V. Rozhkov, A. Alexandrov, V.V. Moukhin (Joint Stock Novosibirsk Chemical Concentrates Plant), V.N. Mitkin (RAS), V. Purgin, V. Sergeev, A. Gorev, M. Medjutov, V. Telezhkin, A. Enin, V. Yakimov, B. Antipenko, and V. Ogarkov (Joint Stock Novosibirsk Chemical Concentrates Plant)
- **99** Aluminum Negative Electrode in Lithium Ion Batteries - Y. Hamon, T. Brousse (Ecole Polytechnique de l'Université de Nantes), F. Jousse, P. Topart, P. Buvat (CEA Le Ripault), and D.M. Schleich (Ecole Polytechnique de l'Université de Nantes)
- **100** Influence of Particle Size and Matrix in "Metal" Anodes for Li-ion Cells - O. Crosnier (Ecole Polytechnique de l'Université de Nantes), X. Devaux (Ecole des Mines de Nancy), T. Brousse, P. Fragnaud, and D.M. Schleich (Ecole Polytechnique de l'Université de Nantes)
- **101** Mechanically Alloyed Sn-V Powders as Anode Materials for Lithium-Ion Batteries - Y. Xia, T. Sakai, T. Fujieda, K. Tatsumi (Osaka National Research Institute), S. Sakurai, and A. Kawabata (Taiyokoko Co., Ltd.)
- **102** TPD/GC-MS Analysis of Solid Electrolyte Interface in Propylene Carbonate/Ethylene Sulfite Electrolyte on Graphite Anode for Lithium Batteries - H. Ota (Center for Analytical Chemistry and Science, Inc. (CACs)), T. Sato, H. Suzuki (Mitsubishi Chemical Corporation), and T. Usami (Center for Analytical Chemistry and Science, Inc. (CACs))
- **103** ^7Li -NMR Study on Li^+ Storage/De-Storage Mechanisms in Non-Graphitizable Carbons - C.W. Park, J.K. Hong, and S.M. Oh (Seoul National University)
- **104** Mg_2Sn : A New Anode Material for Rechargeable Lithium Batteries - H. Sakaguchi, M. Kubota, H. Honda, and T. Esaka (Tottori University)
- **105** Surface Condition and Conductivity Homogeneity: Are the Key Factors for Obtaining High Power and Long Life Carbon Anode of Li-ion Battery - J. Suzuki, M. Yoshida, K. Yamaguchi, M. Kikuchi, K. Sekine (Rikkyo University), and T. Takamura (Petoca, Ltd.)
- **106** Graphite-Metal Oxide Composites as Anode for Li-ion Batteries - H. Huang, E. Kelder, and J. Schoonman (Delft Interfaculty Research Center)
- **107** Key Factors for Material Designing of High Power Carbon Anode of Li-Ion Secondary Battery - T. Takamura (Petoca, Ltd.), J. Suzuki, K. Yamaguchi, T. Katsuta, and K. Sekine (Rikkyo University)
- **108** Doped Tin Oxides as Potential Lithium Ion Battery Negative Electrodes: Effects of Milling Process - F. Belliard and J.T.S. Irvine (University of St. Andrews)
- **109** Novel Tin Oxide Based Anodes for Li-Ion Batteries - P.A. Connor and J.T.S. Irvine (University of St. Andrews)

Abs. #

- **110** The Effect of Lithium Insertion on the Structure of Tin Oxide Based Glasses - C. Gejke, E. Zanghellini, L. Borjesson (Chalmers University of Technology), L. Fransson, and K. Edstrom (Uppsala University)
- **111** Electrochemical Properties of Tin-Containing Thin Films - H. Kobayashi (Osaka National Research Institute), Y. Uebou (Ritsumeikan University), T. Ishida, S. Tamura, S. Mochizuki, T. Mihara, M. Tabuchi, H. Kageyama (Osaka National Research Institute), Y. Yamamoto, M. Matsuoka, and J. Tamaki (Ritsumeikan University)
- **112** Antimony Doping Effect on the Electrochemical Behavior of SnO₂ Thin Film Electrodes - J. Santos-Pena, T. Brousse (University of Nantes), L. Sanchez, J. Morales (University of Cordoba), and D.M. Schleich (University of Nantes)
- **113** Investigation of Solvated and Unsolvated Lithium Intercalation Processes into Graphitic Carbons by Electrochemical Dilatometry - G.H. Wrodnigg (Graz University of Technology), P. Novak (Paul Scherrer Institute), J.O. Besenhard, and M. Winter (Graz University of Technology)
- **114** Stress Effect on Cycle Properties of the Silicon Thin film Anode - S.-J. Lee, J.-K. Lee, H.-K. Baik (Yonsei University), and S.-M. Lee (Kangwon National University)
- **115** Electrochemical Properties of MnV₂O₆ and Its Derivatives as New Anode Material for Lithium Secondary Battery - S.-S. Kim, Y. Suzuki, H. Ikuta, and M. Wakihara (Tokyo Institute of Technology)
- **116** Thermally Oxidised Graphites as Anodea for Lithium-Ion Cells - M. Natchi, R. Meenakshisundaram, T. Prem Kumar, A.S. Manual, V. Subramanian, S. Gopukumar, and N.G. Renganathan (Central Electrochemical Research Institute)
- **117** X-ray Absorption Study of Cobalt Vanadates During Cycling Usable as Negative Electrode in Lithium Battery - S. Laruelle, P. Poizot (Université de Picardie Jules Verne), E. Baudrin (UCLA), V. Briois (Centre Universitaire Paris Sud), M. Touboul, and J.-M. Tarascon (Université de Picardie Jules Verne)
- **118** Reversible Li Uptake in Fe₃BO₆, a New Anode Material - J. Gaubicher, L. Nazar, and J. Rowsell (University of Waterloo)
- **119** Structural and Mechanistic Studies of Intermetallic Electrodes - J.T. Vaughey, C.S. Johnson, B. Roy, M.M. Thackeray (Argonne National Laboratory), L. Fransson, K. Edstrom, and J. Thomas (Uppsala University)
- **120** Modified Carbons for Improved Anodes in Lithium Ion Cells - H. Buqa, P. Golob, M. Winter, and J.O. Besenhard (Graz University of Technology)
- **121** Surface Modification of Graphite Anodes by Combination of High Temperature Gas-Treatment and Silylation in Nonaqueous Solution - M. Santis, H. Buqa, C. Grogger, J.O. Besenhard, and M. Winter (Graz University of Technology)
- **122** Effects of Synthesis Condition of Graphitic Carbon Tube on Anodic Property of Li Ion Battery - T. Ishihara, A. Kawahara, H. Nishiguchi (Oita University), M. Yoshio (Saga University), and Y. Takita (Oita University)
- **123** Anodic Property of Graphitic Carbon Nanotube in Propylene Carbonate Based Organic Electrolyte - A. Kawahara, T. Ishihara, H. Nishiguchi (Oita University), M. Yoshio (Saga University), and Y. Takita (Oita University)
- **124** Improved Rate Performance of Active Materials Coated on Surface-Modified Carbon Black - H. Huang and L. Nazar (University of Waterloo)
- **125** Electrochemistry and Impedance Analysis of Intermetallic Electrodes for Lithium-Ion Batteries - C.S. Johnson, J.T. Vaughey, D.W. Dees, A.N. Jansen, M.M. Thackeray (Argonne National Laboratory), T. Sarakonsri, and S.A. Hackney (Michigan Technological University)
- **126** Benchmark Study on High Performing Carbon Anode Materials - C. Lampe-Onnerud, J. Shi, B. Barnett, and P. Onnerud (Arthur D. Little, Inc.)
- **127** Effects of SEI on the Kinetics of Lithium Intercalation - R. Bugge, M. Smart, and S. Surampudi (Jet Propulsion Laboratory)

Abs. #

- **128** In Situ AFM Observation of Lithium Deposition at Elevated Temperatures - R. Mogi, M. Inaba, T. Abe, and Z. Ogumi (Kyoto University)
- **129** Boronated Mesophase Pitch Coke for Lithium Insertion - E. Frackowiak (Poznan University of Technology), J. Machnikowski (Technical University), and F. Beguin (CNRS-Université)
- **130** A Composite Carbonaceous Anode Material for Lithium Ion Batteries - G. Zhang, J. Han, C. Du, Y. Chen, and Q. Liu (University of Science and Technology Beijing)
- **131** Electrochemical Lithium Intercalation in TiO_2 with Ramsdellite Structure - R. Amandi, A. Kuhn, and F. Garcia-Alvarado (Universidad San Pablo CEU)
- **132** Investigation of Lead Tin Fluorides as Possible Negative Electrodes for LI-Ion Batteries - L. Garza, P.A. Connor, F. Belliard (St. Andrews University), L. Torres (UANL), and J.T.S. Irvine (St. Andrews University)
- **133** A Microtextural Approach of Lithium Insertion in Hard Carbons : The "Corridor" Model - S. Gautier (CNRS-University), E. Frackowiak (Poznan University of Technology), F. Chevallier, J.N. Rouzaud, and F. Beguin (CNRS-University)
- **134** Neutron Diffraction Studies on Lithium Non-Graphitizable Carbon - R. Kanno, A. Hirano (Kobe University), T. Kaminya (University of Tsukuba), K. Tatsumi (Osaka National Research Institute), M.A. Mostafa, M. Furusaka, and T. Otomo (High Energy Accelerator Research Organization)
- **135** Investigation of the Solid Electrolyte Interface Film on the Graphitic Anodes Surface - D. Zane (CNR-Italy), A. Antonini, and M. Pasquali (University of Rome "La Sapienza")
- **136** Determination of the Ratio of Basal Plane Surfaces and Prismatic Surfaces of Graphites And its Impact on Graphite Anode Performance in Lithium Ion Batteries - J.P. Olivier (Micromeritics Instrument Corp, Inc.), P. Golob, and M. Winter (Graz University of Technology)
- **137** First Principles Calculations for Li Insertion into InSb - R. Benedek, M.M. Thackeray (Argonne National Laboratory), L. Yang (Lawrence Livermore National Laboratory), and R. Prasad (Indian Institute of Technology Kanpur)
- **138** Phase Separation and Amorphization in Lithium Inserted Cu-In-Sn Sulfospinel. Theoretical and Experimental Approach - R. Dedryvere (Université Montpellier II), S. Denis (CNRS), P.E. Lippens, J. Olivier-Fourcade, and J.-C. Jumas (Université Montpellier II)
- **139** Experimental and Theoretical Analysis of Li Insertion Mechanisms in Anode Materials - J. Chouvin, P.E. Lippens (Université Montpellier II), C. Perez Vicente (Universidad de Cordoba), J. Olivier-Fourcade, and J.-C. Jumas (Université Montpellier II)
- **140** The Effects of Chemical Composition of Adsorbed Organic Molecular Layers on Lithium Electrode/Polymer Electrolyte Interface Stabilization - M. Le Granvalet-Mancini (Université de Nantes), S. Gadad, and D. Teeters (The University of Tulsa)

Cathodes Posters

Co-Chairs: K. M. Abraham and S. Panero

- **141** Synthesis and Characterization of $\text{Li}_2\text{Mn}_4\text{O}_9$ Cathode Material - W.P. Kilroy, W.A. Ferrando, and S. Dallek (Naval Surface Warfare Center)
- **142** Preparation and Characterization of $\text{Li}_{1+x}\text{Co}_y\text{Mn}_{2-y}\text{O}_4$ Spinel for Lithium Battery Applications - B.W. Lee and S.H. Kim (Korea Maritime University)
- **143** Highly Rechargeable $\text{Li}_x\text{Mn}_{1-y}\text{Me}_y\text{O}_2$ Mixed Oxides Synthesized via LT Techniques - S. Franger, S. Bach, J.-P. Pereira-Ramos, and N. Baffier (CNRS)
- **144** Voltage Prediction from Coulomb Potential Created by Atoms of a Cathode Active Material for Li Ion Cells - J.-I. Yamaki, M. Egashira, and S. Okada (Kyushu University)

Abs. #

- **145** Influences of the Electrolyte Composition on the Charge and Discharge Characteristics of $\text{LiCr}_{0.1}\text{Mn}_{1.9}\text{O}_4$ Positive Electrode - M. Morita, T. Nakagawa, O. Yamada, N. Yoshimoto, and M. Ishikawa (Yamaguchi University)
- **146** Cathode Material For Primary Lithium Cells Based On Modified Manganese Dioxide - N.D. Ivanova, Y.Y. Boldyrev, and G.V. Sokolsky (Ukrainian Academy of Sciences)
- **147** Advantages of $\text{LiNi}_{0.8}\text{Co}_{0.2}\text{O}_2$ Blending into $\text{Li}_{1+x}\text{Mn}_{2-x}\text{O}_4$ Cathode - T. Numata, C. Kanbe, M. Shirakata, and M. Yonezawa (NEC Corporation)
- **148** Pyrolysis/GC/MS Analysis of the Surface Film Formed on Graphite Negative Electrode - Z. Ogumi, A. Sano, M. Inaba, and T. Abe (Kyoto University)
- **149** Corrosion of Cathodic Sulphide Materials in Melted Ionic Salt Electrolytes - V.A. Dushenko, V.V. Radshenko, and V.U. Buryak (Kiev State Trade and Economic University)
- **150** A Novel Method for Preparing Lithium Manganese Oxides and its Electrochemical Characteristics - Y. Azuma, K. Katayama (Tokai University), and M. Suhara (Seimi Chemical Co., Ltd.)
- **151** Structure and Electrochemical Properties of the New Layered $\text{Li}_3\text{Cu}_2\text{O}_4$ and $\text{Li}_2(\text{Na}_{0.68}\text{Li}_{0.313})\text{Cu}_2\text{O}_4$ - E. Raekelboom, A. Hector, M. Weller, and J. Owen (University of Southampton)
- **152** Physical and Electrochemical Characterisation of $\text{LiNi}_{0.8}\text{Co}_{0.2}\text{O}_2$ Thin Film Electrodes Deposited by Laser Ablation - G.X. Wang, M.J. Lindsay, M. Ionescu, D.H. Bradhurst, S.X. Dou, and H.K. Liu (University of Wollongong)
- **153** Effects of Conducting Carbon on the Electrochemical Performance of LiCoO_2 and LiMn_2O_4 Cathodes - Z. Liu (National University of Singapore), J.Y. Lee (National University of Singapore), and H.J. Lindner (National University of Singapore)
- **154** Structure and Electrochemical Properties of $\text{LiSi}_x\text{Co}_{1-y}\text{O}_2$ Cathode for Lithium Rechargeable Battery - T. Zhiyuan, X. Jianjun, L. Jiangang, and C. Gaoping (Tianjin University)
- **155** Spontaneous Modification of the Electrode Surface in Contact with Non-Aqueous Electrolyte - D. Ostrovskii, P. Jacobsson (Chalmers University of Technology), F. Ronci, and B. Scrosati (University "La Sapienza")
- **156** Improvement of Cycle Performance of Orthorhombic $\text{LiMn}_{0.95-x}\text{M}_x\text{Cr}_{0.05}\text{O}_2$; $\text{M}=\text{Al}, \text{Ga}, \text{Yb}, \text{Y}$ and In , Synthesized by Hydrothermal Technique - T. Sakurai, T. Kimura, and T. Sugihara (Mitsubishi Materials Corporation)
- **157** Electrochemical Synthesis, Characterization and Lithium Insertion Behavior of $\text{e-M}_{0.15}\text{V}\{2\}\text{O}\{5\}$ Compounds ($\text{M}=\text{Ni}^{2+}, \text{Cu}^{2+}, \text{Mn}^{4+}$) - E. Potiron, A. Le Gal La Salle, A. Verbaere, Y. Piffard, and D. Guyomard (University of Nantes)
- **158** Synthesis by Sol-Gel Process and Characterization of $\text{LiCr}_x\text{Mn}_{2-x}\text{O}_4$ Cathode Materials - T. Zhiyuan, L. Jiangang, X. Jianjun, and C. Gaoping (Tianjin University)
- **159** Lithiated Electrolytic Oxides of d-Metals in Cathodes of Lithium Accumulators - E. Shembel, R. Apostolova, V. Nagirny (Ukrainian State Chemical Technology University), D. Aurbach, and B. Markovsky (Bar-Ilan University)
- **160** Improved LiCoO_2 for Li-ion Battery Applications - Y. Gao, M. Yakovleva, and J. Engel (FMC Corporation)
- **161** Li-Insertion Behavior in Nanocrystalline $\text{TiO}_2\text{-(MoO}_3)_z$ Core-Shell Materials - G. Moore, A. Le Gal La Salle, D. Guyomard (CNRS - University of Nantes), and S. Elder (Pacific Northwest National Laboratory)
- **162** Relationship Between Cycling Performance and Structural Phase Transitions of $\text{Li}_{1+y}\text{Mn}_{2-y}\text{O}_4$ Cathode Materials Studied by Synchrotron X-ray Diffraction - X.-Q. Yang, X. Sun, M. Balasubramanian, J. McBreen (Brookhaven National Laboratory), Y. Xia, T. Sakai (Osaka National Research Institute), and M. Yoshio (Saga University)
- **163** Preparation and Electrochemical Properties of $\text{LiAl}_y\text{Mn}_{2-y}\text{O}_4$ - Q. Zhong (E-One Moli Energy (Canada) Limited), J. Faiers (Simon Fraser University), and U. von Sacken (E-One Moli Energy (Canada) Limited)

Abs. #

- **164** New Phases and Phase Transitions Observed in Over-Charged States of LiCoO_2 based Cathode Materials - X. Sun, X.-Q. Yang, J. McBreen (Brookhaven National Laboratory), Y. Gao, M. Yakovleva (FMC Corporation), X.-K. Xing, and M. Daroux (Gould Electronics Inc)
- **165** Structural Behavior of Some NASICON Compounds upon Lithium Electrochemical Intercalation/Deintercalation - J. Gaubicher (Université Pierre et Marie Curie), G. Vaughan (European Synchrotron Radiation Facility (ESRF)), C. Masquelier, C. Wurm (Laboratoire de Chimie des Solides), Y. Chabre (Université Joseph-Fourier, and CNRS), and L. Nazar (University of Waterloo)
- **166** Electroactivity of Natural and Synthetic Triphylite - N. Ravet, Y. Chouinard (Université de Montréal), J.-F. Magnan, S. Besner (Hydro Quebec), M. Gauthier, and M. Armand (Université de Montréal)
- **167** The Kinetics of Lithium Transport Through $\text{Li}_{1-x}\text{CoO}_2$ Thin Film Electrode by Theoretical Analysis of Current Transient and Cyclic Voltammogram - S.-I. Pyun and H.-C. Shin (Korea Advanced Institute of Science and Technology)
- **168** Lithium Transport Through $\text{Li}_{1-x}\text{Mn}_2\text{O}_4$ Electrode Involving the Ordering of Lithium Ions - S.-I. Pyun and S.-W. Kim (Korea Advanced Institute of Science and Technology)
- **169** Analysis of Lithium Transport Through Vanadium Pentoxide by Using Potentiostatic Current Transient Technique - S.-I. Pyun and M.-H. Lee (Korea Advanced Institute of Science and Technology)
- **170** Synthesis of $\text{LiAl}_y\text{Co}_{1-y}\text{O}_2$ Using Acrylic Acid and its Electrochemical Properties for Li Rechargeable Batteries - K.Y. Chung, W.-S. Yoon, and K.-B. Kim (Yonsei University)
- **171** A Study on the Effect of Lithium Deintercalation on the Local Structure of $\text{LiAl}_y\text{Co}_{1-y}\text{O}_2$ Cathodes Using X-ray Absorption Spectroscopy - W.-S. Yoon, K.-K. Lee, and K.-B. Kim (Yonsei University)
- **172** Electrochemical Characterization of Layered LiCoO_2 Films Prepared by Electrostatic Spray Deposition - S.-H. Ban, W.-S. Yoon, and K.-B. Kim (Yonsei University)
- **173** Electrical and Thermal Properties of $\text{LiNi}_{1-y}\text{Co}_y\text{O}_2$ ($0 < y < 0.2$) During Initial Cycle - K.-K. Lee, W.-S. Yoon, and K.-B. Kim (Yonsei University)
- **174** Characterization of $\text{LiNi}_{0.85}\text{Co}_{0.10}\text{M}_{0.05}\text{O}_2$ ($\text{M}=\text{Co, Al, Fe}$) for Lithium Secondary Batteries - K.-K. Lee, W.-S. Yoon, and K.-B. Kim (Yonsei University)
- **175** Correlation Between Structural and Electrochemical Properties of Some Lithium-Metal Vanadates - M. Arrabito, S. Bodoardo, N. Penazzi (Politecnico di Torino), S. Panero, B. Scrosati (Università "La Sapienza"), X. Guo, Y. Wang, and S. Greenbaum (Hunter College of CUNY)
- **176** Mechanisms of Manganese Spinel Dissolution and Capacity Fade at High Temperature - T. Aoshima, K. Okahara, C. Kiyohara, and K. Shizuka (Mitsubishi Chemical Corporation)
- **177** Defect Structure of Li-Mn-O Spinel Prepared at Different Annealing Temperatures - S. Ishida and K. Numata (Mitsui Mining & Smelting Co., Ltd.)
- **178** On the Correlation Between the Electroanalytical Behavior and Crystallographic Features of Li Intercalation Electrodes - D. Aurbach, M. Levi, E. Levi (Bar-Ilan University), U. Heider, R. Oesten, and M. Schmidt (Merck KGaA)
- **179** Li Insertion into Thin Vacuum-Deposited V_2O_5 Films Characterized by a Variety of In-Situ Techniques - D. Aurbach, M. Levi (Bar-Ilan University), L. Zhonghua (Dalhousie University), M. Moskovich, Y. Cohen, and E. Levi (Bar-Ilan University)
- **180** Study of Lithium Insertion into Electrochemically Synthesized Sodium Vanadate - D. Aurbach, B. Markovsky, G. Salitra, Y. Cohen (Bar-Ilan University), E. Shembel, R. Apostolova, and V. Nagirny (Ukrainian State Chemical Technology University)
- **181** Characterization of LiFePO_4 as the Cathode Material for Rechargeable Lithium Batteries - M. Takahashi, S. Tobishima, K. Takei, and Y. Sakurai (NTT)

Abs. #

- **182** Magnesium Insertion into $\text{Mg}_{0.5+y}(\text{Fe}_y\text{Ti}_{1-y})_2(\text{PO}_4)_3$ - K. Makino, Y. Katayama, T. Miura, and T. Kishi (Keio University)
- **183** Preparation of Todorokite MnO_2 for Rechargeable Battery Cathode - N. Kumagai, S. Kornaba, H. Sakai, and N. Kumagai (Iwate University)
- **184** A Study on the Preparation and Characterization of Au-Codeposited $\text{LiM}_{n-2}\text{O}_4$ Electrode - M.-R. Lim and K.-B. Kim (Yonsei University)
- **185** Lithium and Proton Insertion in Spinel Structured Manganese Oxides - M.S. Islam (University of Surrey), B. Ammundsen, and J. Roziere (Université Montpellier II)
- **186** Synthesis and Characterization of Nonstoichiometric LiCoO_2 - M. Fujii, N. Imanishi, and Y. Takeda (Mie University)
- **187** Yttrium-Doped $\text{Li}(\text{Ni},\text{Co})\text{O}_2$: An Improved Cathode for Li-Ion Battery - G.V.S. Rao (Institute of Materials Research and Engineering), B.R. Chowdari (National University of Singapore), and H.J. Lindner (Institute of Materials Research and Engineering)
- **188** Electrochemical Properties of Li-Mn-Spinel Using Hydrothermal Method - T. Kanasaku, K. Amezawa, and N. Yamamoto (Kyoto University)
- **189** Synthesis Process of Lithiated or Overlithiated Manganese Oxide Active Materials for Positive Electrode - H. Rouault, F. Le Cras, C. Bourbon, and D. Bloch (Commissariat Energie Atomique)
- **190** General Behaviour Upon Cycling of LiNiVO_4 as Battery Electrode - C. Rossignol and G. Ouvrard (Institut des Matériaux Jean Rouxel)
- **191** Microimpedance Spectroscopy of Cathode Materials Prepared from Polyelectrolyte-Pre-treated Particles - A. Sever Skapin, M. Bele, J. Drogenik, R. Dominko (National Institute of Chemistry), S. Pejovnik (University of Ljubljana), and M. Gaberscek (National Institute of Chemistry)
- **192** $\text{Li}_2\text{Mn}_4\text{O}_9$ Revisited: Crystallographic and Electrochemical Studies - P. Strobel, A. Ibarra Palos, and M. Anne (C.N.R.S.)
- **193** Structural and Electrochemical Studies of Layered $\text{Li}(\text{Mn}_{1-y}\text{M})\text{O}_2$ Based Compounds. I. $\text{M} = \text{Co}$ - A.D. Robertson, A.R. Armstrong, A.J. Fowkes, and P.G. Bruce (University of St. Andrews)
- **194** Cyclic Voltammetric Study on Stoichiometric Spinel LiMn_2O_4 Electrode at Elevated Temperature - S. Ma, H. Noguchi, and M. Yoshio (Saga University)
- **195** Electrical Conductivity and Structural Behaviour of $\text{Li}_{(1+x)}\text{MM}'(\text{PO}_4)_3$ ($\text{M}, \text{M}' = \text{Fe}, \text{Zr}, \text{Ti}$) Phases - C.M. Mari, R. Ruffo, and M. Catti (University of Milano-Bicocca)
- **196** $\gamma\text{-MnO}_2$ Compounds as Insertion Hosts for Li^+ and H^+ - S. Sylvere, J. Severine, L.G.L.S. Annie, P. Yves, and G. Dominique (University of Nantes)
- **197** Charge Ordering in $\text{Li}_{0.5}\text{CoO}_2$? A Single-Crystal XRD Study - J. Howing, T. Gustafsson, J. Thomas (Uppsala University), and H. Sakaebe (ONRI - Osaka)
- **198** Synthesis of $\text{Li}_2\text{M}_{1+x}\text{Mn}_{3-x}\text{O}_8$ ($\text{M} = \text{Co}, \text{Fe}$) as Positive Active Material for Lithium Cells - S. Panero, D. Satolli, and B. Scrosati (University of Rome La Sapienza)
- **199** Lithiated Cobaltates for Li-Ion Batteries. Structure, Morphology and Electrochemistry of Oxides Grown by Solid-State Reaction, Wet Chemistry and Film Deposition - J. Christian (LMDH Université Pierre et Marie Curie)
- **200** Evidence for Structural Defects in Non-Stoichiometric HT- LiCoO_2 : Electrochemical, Electronic Properties and Li MAS NMR Studies - S. Levasseur, M. Menetrier, and C. Delmas (Institut de Chimie de la Matière Condensée de Bordeaux CNRS and Ecole Nationale Supérieure de Chimie et de Physique de Bordeaux)
- **201** Synthesis of Nanocrystalline Layered Manganese Oxides by the Electrochemical Reduction of AMnO_4 ($\text{A} = \text{K}, \text{Li}$) - G. Moore, R. Portal, A. Le Gal La Salle, and D. Guyomard (CNRS - University of Nantes)
- **202** LiMBO_3 ($\text{M} = \text{Mn}, \text{Fe}, \text{Co}$) Orthoborates : Synthesis, Crystal Structure and Lithium Deinsertion/Insertion Properties - L. Vanessa, L.G.L.S. Annie, P. Yves, V. Alain, and G. Dominique (CNRS-University of Nantes-Chemin de la Houssinière)

- Abs. #**
- **203** Electrochemical Investigations of Pure and Poped Lithium Cobaltate - A. Momtchilov (Bulrarian Academy of Sciences)
 - **204** Electrochemical and In Situ Structural Investigation of $\text{Li}_x\text{Ni}_{0.8}\text{Co}_{0.2}\text{O}_2$ - A. D'Epifanio, F. Croce, L. Persi, F. Ronci, and B. Scrosati (University of Rome "La Sapienza")
 - **205** Synchrotron X-Ray Diffraction Study of the Spinel LiMn_2O_4 at Low Temperatures - G. Rousse, C. Masquelier (Université Paris-Sud), J. Rodriguez-Carvajal (CNRS), E. Elkaim, and J.-P. Lauriat (Université Paris-Sud)
 - **206** Electrochemical Performances of Different Li-VOPO_4 Systems - N. Dupre, J. Angenault, G. Wallez, and M. Quarton (Université Pierre et Marie Curie) Wallez, and M. Quarton (Université Pierre et Marie Curie)
 - **207** Structural Transformation Associated with the Extra 3.3 and 4.5V in Spinel LiMn_2O_4 - R. Gwenaëlle (Université Paris-Sud), D. Loic (Université de Picardie), H. Maryvonne (CRISMAT), M. Mathieu (Université de Picardie), P. Maria Rosa (ICMAB (CSIC)), M. Christian (Université Paris-Sud), and T. Jean-Marie (Université de Picardie)
 - **208** Influence of the Synthesis Conditions of LiMn_2O_4 on the Extent of the Spinel to Double Hexagonal Transformation Associated to the Anomalous 3.3/3.95 V and 4.5 V Redox Steps - R.M. Palacin (ICMAB (CSIC)), G. Rousse (Université de Paris-Sud), M. Morcrette, L. Dupont (Université de Picardie and CNRS), C. Masquelier (Université de Paris-Sud), Y. Chabre (Université Josep Fourier Grenoble and CNRS), and J.-M. Tarascon (Université de Picardie and CNRS)
 - **209** Performance and Mechanical Safety of 26650-size Mn-spinel Li-ion Cells for High Power Applications - A.M. Wilson, W. Chow, and U. von Sacken (E-One Moli Energy (Canada) Limited)
 - **210** Use of Aluminum Vanadates as Cathodes in Lithium Rechargeable Cells - E. Andrukaitis, I. Hill, and G. Torlone (Department of National Defence (Canada))
 - **211** Boron Additives to Lithiated Cobalt Dioxide and Lithiated Nickel-Cobalt Dioxide for Lithium Ion Cells - G. Blomgren (Blomgren Consulting Services Ltd.)
 - **212** Manganese Spinel Li-ion Cells With Improved High Temperature Characteristics - W. Chow, M. Zhang, Y. Wang, J. Reimers, and U. von Sacken (E-One Moli Energy (Canada) Limited)
 - **213** Mechanochemical Synthesis Of $\text{Li}_y\text{Mn}_2\text{O}_{4-d}$: Positive Electrode for Lithium Batteries - S. Soiron, A. Rougier, L. Aymard, and J.M. Tarascon (Laboratoire de Réactivité et Chimie des Solides)
 - **214** Two-Phase LiCoO_2 based Oxides for Rechargeable Lithium Batteries - F. Croce (Università "La Sapienza"), H.-P. Lin, H.C.A. Shiao, M. Salomon (Max Power Inc.), J. Wolfenstine (Army Research Lab.), W. Lada, A. Deptula (Institute of Nuclear Chemistry and Techn.), and D. Chua (Max Power Inc.)
 - **215** Defect Spinel $\text{Li}_{8n/n+4}\text{Mn}_{8/n+4}\text{O}_4$ Cathode Materials for Lithium Polymer Batteries - Y. Xia (Osaka National Research Institute), K. Takahashi (Japan Metals & Chemicals Co., Ltd.), T. Sakai, K. Tatsumi, T. Fejieda (Osaka National Research Institute), and M. Yoshio (Saga University)
 - **216** ^7Li MAS-NMR and Electrochemical Studies of LiMn_2O_4 -Based Spinel for Lithium Rechargeable Batteries - M.C. Tucker, J.A. Reimer, and E.J. Cairns (University of California, Berkeley)
 - **217** Mechanochemical Way for Preparation of Disordered Lithium-Manganese Spinel Compounds - N. Kosova, E. Devyatkina, N. Uvarov (Institute of Solid State Chemistry), and S. Kozlova (Institute of Inorganic Chemistry)
 - **218** In Situ XAFS Analysis of the Li Deintercalation Process of $\text{Li}(\text{Mn}, \text{M})_2\text{O}_4$ ($\text{M}=\text{Cr}, \text{Co}, \text{Ni}$), Cathode Materials for 5V Lithium Batteries - I. Nakai (Science University of Tokyo)
 - **219** ESR Analysis of Electrochemical Oxidation on Cathode in a Lithium Ion Battery - H. Kurokawa, T. Ota, S. Matsuta, Y. Kato, S. Yoshimura, S. Fujitani, and I. Yonezu (Sanyo Electric Co. Ltd.)

Abs. #

- 220 Preparation of Lithium Manganese Oxides Including Iron - M. Tabuchi, H. Shigemura, K. Ado, H. Kobayashi, H. Sakaebe, H. Kageyama (Osaka National Research Institute), and R. Kanno (Kobe University)
- 221 In Situ Neutron Powder Diffraction Analysis of the Li Deintercalation Process of $\text{Li}_{1.1}\text{Mn}_{1.9}\text{O}_4$ - Y. Terada (Science University of Tokyo)
- 222 In Situ Total Reflection X-ray Fluorescence Analysis of Mn Dissolution from LiMn_2O_4 During Charge-Discharge Process of the Li Secondary Battery - Y. Nishiwaki, Y. Terada, and I. Nakai (Science University of Tokyo)
- 223 Lithium Ion Transport Through LiCoO_2 Thin-Film Electrode Under Intercalation-Induced Stress - J.-K. Lee, S.-J. Lee, H.-K. Baik (Yonsei University), and S.-M. Lee (Kangwon National University)
- 224 Local Structure of Substituted Layered LiMnO_2 Cathode Materials Probed by X-ray Absorption Fine Structure and ^6Li Nuclear Magnetic Resonance - B. Amundsen, H. Desilvestro, R. Steiner, P. Pickering (Pacific Lithium Limited), D. Jones, J. Roziere (Laboratoire des Agregats Moleculaires et Materiaux Inorganiques), Y.J. Lee, C. Pan, and C. Grey (State University of New York at Stony Brook)
- 225 LiMoVO_6 - A Candidate Cathode Material for Solid-Polymer Batteries at Elevated Temperatures - H. Sakaebe, M. Shikano, Y. Xia, T. Sakai (Osaka National Research Institute, AIST), T. Eriksson, T. Gustafsson, and J. Thomas (Uppsala University)
- 226 Structure, Phase Relationship and Transitions in Lithium Manganese Oxide Spinel - R. Kanno, M. Yonemura, Y. Kawamoto (Kobe University), M. Tabuchi (Osaka National Research Institute), and T. Kamiyama (University of Tsukuba)
- 227 Storage and Cycling Performance of Stoichiometric Spinel at Elevated Temperatures - X. Wang, Y. Yagi (Saga University), Y. Xia, T. Sakai (Osaka National Research Institute of Japan), and M. Yoshio (Saga University)
- 228 Capacity Failure of Lithium Manganese Oxide Spinel Cathode at Elevated Temperature - M. Okada, K. Kamioka, T. Mouri (Tosoh Corporation), and M. Yoshio (Saga University)
- 229 Synthesis and Characterization of Lithium Manganese Oxides for Rechargeable 3 V Lithium Batteries - A. Perner, M. Wohlfahrt-Mehrens (Center for Solar Energy and Hydrogen Research), K. Holl (VARTA Batteries AG), J. Garche (Center for Solar Energy and Hydrogen Research), and D. Ilic (VARTA Batteries AG)
- 230 MALDI-MS Spectroscopic Analysis of Products on LiMn_2O_4 Electrode - T. Fukushima, Y. Matsuda, T. Abura, and R. Arakawa (Kansai University)
- 231 Effect of Aluminum Addition in Co Substituted Ni Oxide Cathodes - M. Kanda, Y. Tatebayashi, M. Sekino, Y. Isozaki, and I. Mitsuishi (Toshiba Corporation)
- 232 Cathode Properties of Phospho-Olivine LiMPO_4 for Lithium Secondary Batteries - S. Okada, S. Sawa, M. Egashira, J.-I. Yamaki (Kyushu University), M. Tabuchi, H. Kageyama (Osaka National Research Institute), T. Konishi, and A. Yoshino (Asahi Chemical Industry Co., Ltd.)
- 233 Soft-Combustion Synthesis of a New Cathode-Active Material, LiVWO_6 , for Li-Ion Batteries - S.R.S. Prabaharan (Multimedia University), C.C. Pei, A.F. Mohd Noor (Universiti Sains Malaysia), and M.S. Michael (SIRIM Bhd)
- 234 Electrochemical Characterization of a New High Capacity Cathode - C. Storey (National Research Council of Canada), I. Kargina, Y. Grincourt, I. Davidson, Y. Yoo (National Research Council of Canada), and D.-Y. Seung (Samsung Advanced Institute of Technology (SAIT))
- 235 Continuous Production of Cathode Materials for Lithium Batteries by Hydrothermal Synthesis Under Supercritical Condition - Y. Hakuta, T. Adschiri (Tohoku University), K. Kanamura (Tokyo Metropolitan University), and K. Arai (Tohoku University)

Abs. #

- **236** Synthesis, Structure, and Charge-Discharge Characteristics of the New Layered Oxides at $\text{Li}_{1.8}\text{Ir}_{0.6}\text{M}_{0.6}\text{O}_3$ (M=Fe,Co,Ni) - H. Kobayashi (Osaka National Research Institute), M. Waki (Osaka Electro-Communication University), Y. Uebou (Ritsumeikan University), M. Tabuchi, H. Kageyama (Osaka National Research Institute), Y. Takigawa (Osaka Electro-Communication University), Y. Yamamoto, M. Matsuoka, and J. Tamaki (Ritsumeikan University)
- **237** The $\text{Li}_{1-x}(\text{Ni}_{1-y}\text{Mg}_y)_{1+z}\text{O}_2$ System: Structural Modifications Observed Upon Cycling - C. Poullierie, L. Croguennec (Ecole Nationale Supérieure de Chimie et Physique de Bordeaux), P. Biensan (SAFT), P. Willmann (CNES), and C. Delmas (Ecole Nationale Supérieure de Chimie et Physique de Bordeaux)
- **238** Synthesis and Characterization of $\text{LiFe}_x\text{Co}_{1-x}\text{O}_2$ Cathode Materials for Lithium Batteries - S. Venkatachalam, R. Sriram, G. Sukumaran, N.G. Renganathan, A. Mani, M. Natchi, R. Meenakshisundaram, and R. Meenakshisundaram (Central Electrochemical Research Institute)
- **239** Electronic and Electrochemical Properties of $\text{Li}_x\text{Co}_y\text{Ni}_{1-y}\text{O}_2$ Cathodes Studied by Impedance Spectroscopy - F. Croce (Università "La Sapienza"), F. Nobili, R. Tossici (Università di Camerino), B. Scrosati, L. Persi (Università "La Sapienza"), and R. Marassi (Università di Camerino)
- **240** $\text{Li}_{1+d}\text{Mn}_{2-d}\text{O}_4$ Performance Measured by Leaching - E. Kelder, F.G.B. Ooms, R. Perego, and J. Schoonman (Delft University of Technology)
- **241** Tungsten Oxysulfide Thin Films as Positive Electrode in Lithium Microbatteries - I. Martin-Litas, P. Vinatier, A. Levasseur (ENSCP), J.C. Dupin, and D. Gonbeau (Université de Pau et des Pays de l'Adour)
- **242** Electronic Structure in LiMn_2O_4 Based Spinel Oxides from Transition Metal L-edge and O K-edge XANES - Y. Uchimoto and T. Yao (Kyoto University)
- **243** Effect of Cr^{6+} on the Jahn-Teller Distortion of Spinel LiMn_2O_4 - S. Venkatachalam, V. S. G. Sukumaran, P. T. R. N.G. M. Natchi, and R. Meenakshisundaram (Central Electrochemical Research Institute)
- **244** 3 V Manganese Oxide Electrode Materials for Lithium Batteries - C.S. Johnson and M.M. Thackeray (Argonne National Laboratory)
- **245** The Spinel Phases $\text{LiMg}_y\text{Mn}_{2-y}\text{O}_4$ as the Cathode for Rechargeable Lithium Batteries - I.-S. Jeong and H.-B. Gu (Chonnam National University)
- **246** Characterisation of Nanoparticles of LiMn_2O_4 Synthesized by Citric Acid Sol-Gel Method - B.-J. Hwang, R. Santhanam, and D.G. Liu (National Taiwan University of Science and Technology)
- **247** Theoretical Approach of the Lithium Intercalation in Host Materials - F. Lantelme, H. Groult (Université P&M Curie), and N. Kumagai (Iwate University)
- **248** The Influence of the Synthesis Conditions on the Structural and Electrochemical Properties of Cathodes Based on Manganese Oxides in Nonaqueous Electrolytes - E. Shembel, N. Globa, N. Zaderey, V. Pismany, and K. Kylyvnyk (Ukrainian State Chemical Technology University)
- **249** A New 3.8V Cathode for Lithium-Ion Batteries: ϵ - Li_xVOPO_4 - T. Kerr, J. Gaubicher, L. Nazar, and H. Huang (University of Waterloo)
- **250** Aluminium Substituted LiCoO_2 as an Intercalation Cathode for Lithium Polymer Battery - S. Venkatachalam, M.A. Stephan, S. Venkatraman, G. Sukumaran, T. Premkumar, N.G. Renganathan, M. Natchi, and R. Meenakshisundaram (Central Electrochemical Research Institute)
- **251** The Jahn-Teller Distortion in Li_xNiO_2 and Li_xMnO_2 - C. Marianetti, D. Morgan, and G. Ceder (Massachusetts Institute of Technology)
- **252** Theory of Lithium Diffusion in Li_xCoO_2 : A First Principles Investigation - A. Van der Ven and G. Ceder (Massachusetts Institute of Technology)

Abs. #

- 253 Lithium Insertion of $(V_{1-y}Mo_y)_2O_5$ - M. Eguchi, F. Maki, S. Iwabe, and Y. Momose (Ibaraki University)
- 254 Effect of Lanthanum Dopant on the Structural and Electrical Properties of $LiCoVO_4$ Cathode Materials Investigated by EXAFS - B.-J. Hwang (National Taiwan University of Science and Technology), Y.-W. Tsai (National Taiwan University of Science and Technology, Taipei, Taiwan, R.O.C.), G.T.-K. Fey (National Central University), and J.-F. Lee (Synchrotron Radiation Research Center)
- 255 Long-life Lithium Manganese Spinel Cathodes for High Power Secondary Batteries for Electric Vehicle Use - M. Kasai, Y. Kumashiro, K. Nishimura, H. Andou, Y. Muranaka, Y. Kozono (Hitachi Ltd.), and T. Horiba (Shin-Kobe Electric Machinery Co. Ltd.)
- 256 Synthesis of $Li_xCo_{0.085}Cr_{0.015}O_2$ by the PVA Precursor Method and Application as Cathode in Lithium Ion Batteries - R. Vasanthi, I. Ruth Mangani, R. Chandrasekaran (Anna University), and S. Selladurai (Anna University)
- 257 $LiCr_xMn_{2-x}O_4$ Solid Solutions for Lithium Batteries - R. Thirunakaran, P. Periasamy, B. Ramesh Babu, N. Kalaiselvi, N.G. Renganathan, M. Raghavan, and N. Muniyandi (Central Electrochemical Research Institute)
- 258 Solid-State Synthesis and Characterization of $LiCoO_2$ and $LiCo_{1-y}Ni_yO_2$ Solid Solutions - P. Periasamy, B. Ramesh Babu, R. Thirunakaran, N. Kalaiselvi, N.G. Renganathan, M. Raghavan, and N. Muniyandi (Central Electrochemical Research Institute)
- 259 Electrochemical Behaviour of $LiMn_{2-y}MyO_4$ ($M = Cu, Cr; 0 < y < 0.4$) - B. Ramesh Babu, P. Periasamy, R. Thirunakaran, N. Kalaiselvi, N.G. Renganathan, M. Raghavan, and N. Muniyandi (Central Electrochemical Research Institute)
- 260 Structural and Electrochemical Studies of Layered $Li(Mn_{1-y}M_yO_2)$ Based Compounds. II $M=Ni$ - T.E. Quine, M.J. Duncan, P.G. Bruce, A.D. Robertson, and A.R. Armstrong (University of St. Andrews)
- 261 Iron-Doped Lithium Cobalt Oxides as Lithium Intercalating Cathode Materials - N. Kalaiselvi, P. Periasamy, R. Thirunakaran, B. Ramesh Babu, T. Prem Kumar, N.G. Renganathan, M. Raghavan, and N. Muniyandi (Central Electrochemical Research Institute)
- 262 Redox Reactions of Substituted Lithium Manganese Spinel Compounds in Lithium Cells - Y. Shao-Horn and R. Muddaugh (Eveready Battery Company, Inc.)
- 263 Electronic Structure of Li_xNiO_y Thin Films - A. Urbano, S. deCastro, R. Landers, J. Morais, M. Fantini, and A. Gorenstein (Gleb Wataghin Physics Institute - UNICAMP)
- 264 Electrochemical Performance of Cathodes Based on $LiMn_2O_4$ Spinel Obtained by Combustion Synthesis - E. Santiago, S. Amancio, P. Bueno, and L. Bulhoes (Universidade Federal de Sao Carlos)
- 265 The Structure Property Relationship Of Lithium Nickel Cobalt Oxides - R. Gover, R. Kanno (Kobe University), B. Mitchell (Argonne National Laboratory), and Y. Kawamoto (Kobe University)
- 266 Electrochemical Characteristics of $LiMn_2O_4$ -Polypyrrole Composite Cathode for Lithium Polymer Batteries - J.-U. Kim, J.-A. Lee, S.-I. Moon, and H.-B. Gu (Chonnam National University)
- 267 Effects of Powder Characteristics of $LiMn_2O_4$ on the Electrochemical Properties - H.-T. Chung and S.-T. Myung (Dongshin University)
- 268 Electrocopolymerization of Carbazole Derivatives - A.S. Sarac (Istanbul Technical University)
- 269 Influence of the Particle Size on the Electrochemical Properties of Lithium Manganese Oxide - C.-H. Lu and S.-W. Lin (National Taiwan University)
- 270 Synthesis of Nanosized $LiMn_2O_4$ Powder by Reverse Emulsion Process for Li-Ion Batteries - C.-H. Lu, S.K. Saha, and S.-W. Lin (National Taiwan University)

Abs. #

Liquid Electrolytes Posters

Co-Chairs: I. Exner and E. Spila

- 271 High Purity Lithium Carbonate for Batteries Applications - S. Harrison (Limtech Inc.), K. Amouzegar (Limtech Inc.), and G. St-Amant (Limtech Inc.)
- 272 Viscosities, Conductivities and Activation Energies for Transport Processes in Liquid Electrolytes. The Quasi Lattice Approach - A. Chagnes, B. Carre (Université de Tours), P. Willmann (Centre National d'Etudes Spatiales), and D. Lemordant (Université de Tours)
- 273 Optimisation of the Polyelectrolyte used in Carbon Anode Pretreatment Procedures - R. Dominko, J. Drogenik, M. Bele, S. Pejovnik, and M. Gaberscek (National Institute of Chemistry)
- 274 New Fusible Lithium Salt with High Conductivity in Solutions - W. Xu, M. Videa, and C.A. Angell (Arizona State University)
- 275 Application to Lithium Battery Electrolyte of Lithium Chelate Compounds with Boron - Y. Sasaki, M. Handa, S. Sekiya, K. Kurashima (Tokyo Institute of Polytechnics), and K. Usami (Denso Corporation)
- 276 Microporous PVDF Membrane for Lithium-Ion Batteries - F. Bodin, C. Lenhof, G. Caillon, and I. Olsen (SAFT)
- 277 Synthesis of a New Family of Fluorinated Boronate Compounds as Anion Receptors and Studies of Their Use as Additives in Lithium Battery Electrolytes - H.-S. Lee, X.-Q. Yang, X. Sun, and J. McBreen (Brookhaven National Laboratory)
- 278 Lithium Bis(perfluoroalkyl)sulfonimides: Primary and Secondary Lithium Battery Electrolyte Salts - S. Boyd, B. Johnson, L. Krause, W. Lamanna, P. Pham, and H. Shimada (3M Company)
- 279 Thermal Stability of LiPF_6 EC:EMC Electrolyte for Lithium Ion Batteries - G. Botte, R. White (University of South Carolina), and Z. Zhang (Celgard, Inc)
- 280 Trans-Esterification of Ethylmethyl Carbonate in Lithium Ion Batteries - B. Dobler, I. Exnar, W. Haupt, and R. Imhof (RENATA Batteries SA)
- 281 Kinetic Aspects of HF Generation in a LiPF_6 Based Electrolyte Solution - I. Exnar, B. Dobler, W. Haupt, and R. Imhof (RENATA Batteries SA)
- 282 New Li-Ion Electrolytes for Low Temperature Applications - S. Herreyre, O. Huchet (SAFT), S. Barusseau (Alcatel-Alsthom Recherche), F. Pertion, J.-M. Bodet, and P. Biensan (SAFT)
- 283 Electronic Structures and Electrochemical Properties of $\text{LiPF}_{(6-n)}(\text{CF}_3)_n$ - F. Kita, H. Sakata, A. Kawakami (Hitachi Maxell Ltd.), H. Kamizori, T. Sonoda, H. Nagashima (Kyushu University), N. Pavlenko, and Y. Yagupolskii (Ukrainian Academy of Science)
- 284 Asymmetrical Alkyl Carbonate as Solvent for Li-ion Batteries Electrolytes - I. Geoffroy, B. Carre, D. Lemordant (Université de Tours), S. Herreyre, and P. Biensan (SAFT)
- 285 Database and Models of Electrolyte Solutions for Lithium Battery - S. Zhang, A. Tsuboi, H. Nakata, and T. Ishikawa (Mitsubishi Chemical Corporation)
- 286 An Exceptional Additive to the Electrolyte for Lithium-Ion Batteries : The Vinylen Carbonate - B. Philippe, B. Jean-Marie, P. Francoise, B. Michel, J. Christophe (SAFT), B. Sylvie (Alcatel), H. Sylvie, and S. Bernard (SAFT)
- 287 An Evidence of Preventing the Decomposition of PC at the Surface of Well Graphitized Carbon without Any Additions - K. Yamaguchi, J. Suzuki, M. Saito, T. Katsuta, K. Sekine (Rikkyo University), and T. Takamura (Petoca, Ltd.)
- 288 Effect of Organic Additives in Electrolyte Solutions on Behavior of Lithium Metal Anode - Y. Matsuda and T. Takemitsu (Kansai University)

Abs. #

- **289** Cyclic and Acyclic Sulfites - New Solvents and Electrolyte Additives for Lithium Ion-Batteries with Graphitic Anodes? - G.H. Wrodnigg, J.O. Besenhard, and M. Winter (Graz University of Technology)
- **290** Fluorinated Organic Solvents in Electrolytes for Lithium Ion Cells - K.-C. Moller, T. Hodal (Graz University of Technology), W.K. Appel (Deutschland GmbH & Co. KG), M. Winter, and J.O. Besenhard (Graz University of Technology)
- **291** Performance of Solupor Separator Materials - F.G.B. Ooms, E.M. Kelder, J. Schoonman (Delft University of Technology), N. Gerrits, and G. Calis (DSM Solutech)
- **292** Fast Charge in Non-Aqueous Li Cells: Investigation of a Novel Hybrid Solution - G. Amatucci, F. Badway, and A. Du Pasquier (Telcordia Technologies)
- **293** Temperature and Concentration Effects on the Ionic Transport Behavior of LiAlCl_4 SOCl_2 Electrolyte Solutions - G.T.-K. Fey, W.-K. Liu (National Central University), and Y.-C. Chang (Tamkang University)
- **294** Mass Transport and Kinetic Aspects of Thionyl Chloride Reduction at the Platinum Microelectrode - G.T.-K. Fey, M.-C. Hsieh (National Central University), and Y.-C. Chang (Tamkang University)
- **295** Novel Superacid-based Lithium Electrolytes for Lithium Ion and Lithium Polymer Rechargeable Batteries - H.V. Venkatesetty (H.V. Setty Enterprises, Inc.)

Polymer Electrolytes Posters

Co-Chairs: E. Spila and I. Exner

- **296** Interfacial Stability of Lithium Electrode in IPN Electrolytes Based on Crosslinked PEGMEM and PMMA - X. Hou and K.S. Siow (National University of Singapore)
- **297** Diffusion Mechanism in the Cross-Linked Poly(ether) Doped by $\text{LiN}(\text{CF}_3\text{SO}_2)_2$ - Y. Aihara, T. Bando, T. Iguchi, J. Kuratomi (Yuasa Corporation), K. Sugimoto, and K. Hayamizu (National Institute of Materials and Chemical Research)
- **298** Ion Conduction Mechanism in Solid $\text{Li}_x\text{-P}(\text{EO})_n$ -based Polymer Electrolytes - D. Golodnitsky, E. Lifshits, E. Peled (Tel Aviv University), S. Chung, and S. Greenbaum (Hunter College of CUNY)
- **299** Preparation of Microporous PVDF Based Polymer Electrolytes - H. Huang, H. Wang, and S. Wunder (Temple University)
- **300** Room Temperature Amorphous-Phase Stabilization of PEO-Based Nanocomposite Polymer Electrolytes: An Impedance Spectroscopy Study - F. Croce, L. Persi, and B. Scrosati (University "La Sapienza")
- **301** Gel Electrolytes Based on Amphiphilic Copolymers - R. Ljungback, P. Gavelin, P. Jannasch, and B. Wesslen (Lund University)
- **302** Ionic Conduction and Electrochemical Properties of New Poly(acrylonitrile-itaconate) Based Gel-electrolyte - Y.W. Kim, M.S. Gong, and B.K. Choi (Dankook University)
- **303** Studies of the Interface Between Lithium Deposits and Polymeric Electrolyte Systems Using in situ FTIR Spectroscopy - D. Aurbach, O. Chusid, Y. Gofer (Bar-Ilan University), M. Watanabe (Yokohama National University), T. Momma, and T. Osaka (Waseda University)
- **304** Polymeric Gel Electrolyte Reinforced with Glass Fiber Cloth for Lithium Secondary Battery - S.I. Jo, J.-S. Jung, H.-J. Sohn (Seoul National University), H.-C. Park, J.H. Chun, H. Kim, and J.-M. Ko (Taejon National University of Technology)
- **305** Polymer Electrolytes Based On Hyperbranched Polymers - T. Itoh, N. Hirata, Z. Wen, M. Kubo, and O. Yamamoto (Mie University)
- **306** Spectroscopic Estimation of Dielectric Constant and Donor Number in Polymer Electrolytes - C.S. Kim, J. Lee, and S.M. Oh (Seoul National University)
- **307** Electrochemical Properties of Gel Electrolytes - A. Reiche, A. Weinkauff, and B. Sandner (Martin-Luther-Universitat Halle-Wittenberg)

Abs. #

- **308** A Novel PEG-borate Based Solid Polymer Electrolytes; Conductivity and Application to Li-ion Battery - S. Yokoyama (NOF Corporation), T. Kobayashi, Y. Kato, H. Ikuta, and M. Wakihara (Tokyo Institute of Technology)
- **309** Determination of Diffusion Co-Efficient of Lithium Ion in Plasticized PVC Electrolytes - A.S. Manual, R. Sudalaimuthu, T. Premkumar, N.G. Renganathan, R. Meenakshisundaram, and M. Natchi (Central Electrochemical Research Institute)
- **310** Effects of Diethylaluminum Carboxylate and EC/PC on Dielectric Relaxation and Ionic Conductivity of PEO Based Polymer Electrolytes - J. Dygas, B. Misztal-Faraj, F. Krok, Z. Florjanczyk, E. Zygodlo-Monikowska, and E. Rogalska (Warsaw University of Technology)
- **311** Studies of Conductivity and Ionic Mobility in Polymer Gel Electrolytes - H. Hubbard, M. Williamson, and I. Ward (IRC in Polymer Science and Technology)
- **312** Conductivity and Structure of Li-Containing Pervoskite Solid Electrolytes - J.-S. Chen and K.-Z. Fung (National Cheng Kung University)
- **313** Self-Tracking, Solvent-Free Low-Dimensional Polymer Electrolyte Blends with Lithium Salts - Y. Zheng, F. Chia, G. Ungar, and P.V. Wright (University of Sheffield)
- **314** The Role of the Inorganic Oxide in Nanocomposite Polymer and Gel Electrolyte Structure And Ion Transport Mechanism: An NMR Study - S. Greenbaum, S. Chung, Y. Wang (City University of New York), L. Persi, F. Croce, and B. Scrosati (Università di Roma La Sapienza)
- **315** Plasticising Effect in Phase-Separated Polymer Electrolytes Based on Poly(Ethylene oxide) and Poly(perfluoroethers) - M. Furlani (Goteborg University and Chalmers University of Technology), K. Bandara (University of Peradeniya), and B.-E. Mellander (Goteborg University and Chalmers University of Technology)
- **316** Characteristics of PVDF/Pan Based Polymer Electrolyte for Lithium Ion Polymer Battery - J.-A. Lee, J.-U. Kim, G.-C. Park, and H.-B. Gu (Chonnam National University)
- **317** Structure, Porosity and Conductivity of PVdF Films for Polymer Electrolytes - A. Magistris, P. Mustarelli, E. Quartarone (University of Pavia), P. Piaggio, and A. Bottino (University of Genova)
- **318** Spectroscopic Conductivity Studies on the Ionic Motion in the Electrolytic Complexes (Polyethylene Glycol 400)/(LiCl)_x - V. Di Noto, M. Fauri, S. Biscazzo, and M. Vittadello (Università di Padova)
- **319** Fabrication of All Solid Polymer Electrolytes based on Block-Graft Copolymers - K. Hirahara, M. Ueno, O. Watanabe, and T. Nakanishi (Shin-Etsu Chemical Co., Ltd.)

Battery Posters

Co-Chairs: R. J. Brodd and J. T. S. Irvine

- **320** Power Management: The Path to the Future - J. Barbarello, M. Molz, and R. Hamlen (U.S. Army - CECOM)
- **321** High Energy Density, Thin Film, Rechargeable Lithium Batteries for Marine Field Operations - D. Sadoway, A. Mayes, B. Huang, S. Mui, P. Soo, D. Staclin, and C. Cook (Massachusetts Institute of Technology)
- **322** Cycling Performance of 10 Wh class Lithium Metal Rechargeable Battery with New-type Lithium Imide Electrolyte - H. Saito and K. Usami (Denso Corporation)
- **323** Fabrication of Composite Electrodes for Rechargeable Lithium Batteries by Using Electrophoretic Deposition Process - K. Kanamura, A. Goto, and T. Umegaki (Tokyo Metropolitan)
- **324** Developments in Multichannel Impedance Instrumentation for the Characterization of Energy Storage Devices - A. Hinton and B. Sayers (Solartron)

Abs. #

- 325 Hydrothermal Synthesis - T. Kanasaku, K. Amezawa, and N. Yamamoto (Kyoto University)
- 326 New High-Surface-Area 3-Dimensional "On-Chip" Lithium-Ion Microbattery - M. Nathan, D. Haronian, D. Golodnitsky, Y. Lavi, E. Sverdlov, and E. Peled (Tel Aviv University)
- 327 Opportunities for Lithium Batteries in Electric Vehicle and Hybrid Electric Vehicle Applications - M. Corbett (Kline & Company, Inc.)
- 328 New Thin Lithium-Ion Batteries Using an Organic Liquid Electrolyte with Thermal Stability - N. Takami, M. Sekino, T. Ohsaki, M. Kanda, and M. Yamamoto (Toshiba Corporation)
- 329 Development of 6Ah Prismatic Cells for High Rate, Low Temperature Applications - G. Ehrlich, M. Hetzel (Yardney Technical Products, Inc.), and S. Slane (U.S. Army CECOM)
- 330 A Study of the Overcharge Reaction of Li-ion Batteries - M.J. Palazzo, R.A. Leising, E.S. Takeuchi (Wilson Greatbatch Ltd.), and K.J. Takeuchi (SUNY at Buffalo)
- 331 Fast Charging of Lithium-Ion Batteries - J.R. van Beek (Philips Research Laboratories)
- 332 Factors Responsible for Impedance Rise in High Power Lithium Batteries - K. Amine, M. Hammond, J. Liu, C. Chen, D.W. Dees, A.N. Jansen, and G. Henriksen (Argonne National Laboratory)
- 333 Promising Modifying Additives for Lithium Power Sources - E. Shembel, O. Chervakov, I. Maksyuta, N. Globa, N. Zaderey, L. Romanovskaya, A. Ribalka (Ukrainian State Chemical Technology University), and D. Meshri (Advance Research Chemical, Inc.)
- 334 Overcharge Protection Additives for 4 Volt Lithium Ion Batteries - T. Richardson and P. Ross (Lawrence Berkeley National Laboratory)
- 335 Comparative Study of Thermal Behaviors of Various Lithium-Ion Batteries - Y. Saito, K. Takano, K. Kanari, A. Negishi, K. Nozaki, and K. Kato (Electrotechnical Laboratory)
- 336 Thermal Behaviors of Lithium-Ion Batteries During Overcharging - Y. Saito, K. Takano, and A. Negishi (Electrotechnical Laboratory)
- 337 Charge-Discharge Cycle Performance of Lithium Secondary Batteries using Hybrid Carbon as Negative Electrode Materials - K. Yanagida, A. Yanai, Y. Kida, A. Funahashi, T. Nohma, and I. Yonezu (Sanyo Electric Co., Ltd.)
- 338 Cycle Life Estimation of Lithium Secondary Battery by Extrapolation Method and Accelerated Aging Test - T. Katsuhito, K. Kazuma, K. Yo, M. Hajime, T. Nobuyuki, I. Toru, and T. Toshikatsu (Central Research Institute of Electric Power Industry (CRIEPI))
- 339 A New Method to Study Li-Ion Cell Safety: Laser Beam Initiated Reactions on Both Charged Positive and Negative Electrodes - J.-P. Peres, F. Perton, C. Audry, P. Biensan (SAFT - Direction de la Recherche), G. Blanc (Insavalor), and M. Broussely (SAFT)
- 340 Development of Large-scale Lithium Secondary Battery Cell - T. Akiyama, T. Hashimoto, H. Tajima (Mitsubishi Heavy Industries, Ltd.), K. Adachi, and S. Taniguchi (Kyushu Electric Power Co., Inc.)
- 341 Effect of Iron Disulfide Structure and Nonaqueous Electrolyte Composition on the Characteristics of High-Energy Li-FeS₂ System - E. Shembel, L. Neduzhko, O. Chervakov, I. Maksyuta, K. Kylyvnyk, Y. Polychuk (Ukrainian State Chemical Technology University), D. Reisner, and T. Xiao (US Nanocorp)
- 342 Safety and Performance of In-Service Lithium-Sulphur Dioxide Batteries - I. Hill, E. Andrukaitis, and G. Torlone (Canadian Department of National Defence)
- 343 Fabrication of Dye-Sensitized Solar Cells by the Spray Pyrolysis Deposition (SPD) Technique - M. Okuya, K. Nakade, and S. Kaneko (Shizuoka University)

Abs. #

- **344** High Temperature Characteristics of Lithium Ion Batteries Using Spinel Lithium Manganese Oxides as the Cathode - H. Watanabe, N. Imachi, K. Saishou, and S. Narukawa (Sanyo Electric Co., Ltd.)
- **345** Li-Ion Cells using a New High Capacity Cathode - Y. Grincourt, C. Storey (NRC), I. Davidson, P. Whitfield, I. Kargina, and H. Slegre (National Research Council)
- **346** Thermal Analysis of a 40-Ah Lithium-Ion Cell - H. Vaidyanathan (COMSAT Laboratories) and G. Rao (NASA)
- **347** Overview of ENEA's Projects on Lithium Batteries - F. Alessandrini, M. Conte, S. Passerini, and P.P. Prosini (ENEA)
- **348** Properties of Explosively Compacted Li-Ion Battery Components - M. Jak, N. Van Landschoot, E. Kelder, and J. Schoonman (Delft University of Technology)
- **349** New PVDF Binder for Li-Ion Batteries - B. Barriere (Elf Atochem)
- **350** Effect of Separator Properties on the Performance of Lithium-Ion Cells - D.-J. Ihm, H.-S. Sin, K.-S. Roh, J.-H. Lee, and Y.-J. Shim (SKC Co., Ltd.)
- **351** Advanced Li-Ion Technology for the MSP01 MARS Lander - C. Marsh, R. Gitzendanner, F. Puglia (Yardney Technical Products, Inc.), and J. Byers (Lockheed Martin Astronautics)
- **352** Characterization of Lithium Thionyl Chloride Cells by Impedance Techniques - F. Walsh, M. Pozin, A. Cherniy, and K. Tikhonov (Tracer Technologies Inc.)
- **353** High Rate Performance Of Moltech Prismatic Rechargeable Cells - Y. Geronov and T. Skotheim (Moltech Corporation)
- **354** Manganese Type Lithium Ion Battery for Pure and Hybrid Electric Vehicles - T. Horiba, K. Hironaka, T. Matsumura, T. Kai, M. Koseki (Shin-Kobe Electric Machinery Co., Ltd.), and Y. Muranaka (Hitachi, Ltd.)
- **355** Status of Lithium Battery for Electric-Based Transportation - G.A. Nazri (University of Michigan)
- **356** Performance Characteristics of LiMn_2O_4 /Polymer/Carbon Electrochemical Cells - N. Kamaruddin (MARA University Of Technology), Z. Osman, N.S. Mohamed, and A.K. Arof (University of Malaysia)
- **357** Cooperative Research on Safety Fundamentals of Lithium Batteries - J.R. Selman, S. Al Hallaj (I.I.T.), I. Uchida, and Y. Hirano (Tohoku University)
- **358** Development of High Energy Density Li-Ion Batteries Based on $\text{LiNi}_{1-x-y}\text{Co}_x\text{Al}_y\text{O}_2$ - J. Weaving, F. Coowar, D. Teagle, J. Cullen, V. Dass (AEA Technology Batteries), P. Bindin, R. Green (Engineering Images Ltd.), and B. Macklin (AEA Technology Batteries)
- **359** Recycling of Lithium Ion Cells and Batteries - M. Lain (AEA Technology Batteries)
- **360** Modulation of Discharge Process of a Lithium Battery by Changes of Battery Inner Medium Influence on Process of Discharge - A. Skekhtman (KVANT)
- **361** Application of Impedance Measurements in the Development of Lithium Ion Cells - F. Walsh, M. Pozin, and K. Tikhonov, Jr. (ECO Energy Conversion)

Polymer Batteries Posters

Co-Chairs: B. Macklin and M. Conte

- **362** Liquid-free Rechargeable Li Polymer Battery - S. Matsui, T. Muranaga, H. Higobashi, S. Inoue, and T. Sakai (Daiso Co., Ltd.)
- **363** High Temperature Stable Lithium Ion Polymer Battery - C.-K. Park, A. Kakirde, W. Ebner, V. Manivannan, C. Chai (SKC America, Inc.), and D.-J. Ihm (SKC Co., Ltd.)
- **364** Solid Polymer Electrolyte Cells Using $\text{SnSb}_x/\text{Li}_{2.6}\text{Co}_{0.4}\text{N}$ Composite Anodes - J. Yang, Y. Takeda, N. Imanishi, Q. Li, H.Y. Sun (Mie University), and O. Yamamoto (Genesis Research Institute, Inc.)

Abs. #

- **365** Elucidation of the Charge-Discharge Mechanism of Lithium/Polymer Electrolyte/Pyrite Batteries - E. Stauss, D. Golodnitsky, and E. Peled (Tel Aviv University)
- **366** Development of a Bipolar Li/Composite Polymer Electrolyte/Pyrite Battery for Electric Vehicles Application - V. Livshits, A. Blum, E. Strauss, G. Ardel, D. Golodnitsky, and E. Peled (Tel Aviv University)
- **367** Near-Room-Temperature Rechargeable Lithium/Pyrite Battery - G. Ardel, D. Golodnitsky, E. Peled (Tel Aviv University), G. Appetecchi, P. Romagnoli, and B. Scrosati (University "La Sapienza")
- **368** The Two-Phase Battery Concept: A New Strategy for High Performance Lithium Polymer Batteries - P.P. Prosini, M. Carewska, F. Alessandrini, and S. Passerini (ENEA)
- **369** Investigations on Lithium Polymer Electrolyte Batteries - G. Appetecchi, F. Alessandrini, M. Carewska, P.P. Prosini, S. Scaccia, and S. Passerini (ENEA)
- **370** Cycling Performance and Interface Properties of Li/PEO-Li(CF₃SO₂)₂N-Ceramic Fillers/LiNi_{0.8}Co_{0.2}O₂ - L. Qi, Y. Takeda, N. Imanishi, J. Yang, H.Y. Sun (Mie University), and O. Yamamoto (Genesis Research Institute, Inc.)
- **371** Fabrication and Electrochemical Characteristics of All-Solid-State Lithium-Ion Rechargeable Batteries Composed of LiMn₂O₄ Positive and V₂O₅ Negative Electrodes - M. Baba (Iwate University)
- **372** A Lithium-Ion Polymer Battery Using PVdF-HFP/Polyethylene Composite Gel Electrolyte - X. Liu, H. Kusawake, and S. Kuwashima (National Space Development Agency of Japan)
- **373** Development of Solid-Polymer Lithium Secondary Batteries - J. Kuratomi, T. Iguchi, T. Bando, Y. Aihara, T. Ono, and K. Kuwana (Yuasa Corporation)
- **374** Electrochemical Performance of Gel-Type Lithium Polymer Battery - Y.-M. Choi, J.-I. Han, S.-G. Doo, and D.-Y. Seung (Samsung Advanced Institute of Technology)
- **375** Onset of Dendritic Growth in Lithium/Polymer Cells - C. Brissot, M. Rosso, J.-N. Chazalviel (Ecole Polytechnique - CNRS), and S. Lascaud (EDF/DER)
- **376** Influence of Added Plasticizer on Dispersion of Electrode Active Materials and on the Discharge Performance of Plastic Lithium Ion Batteries - S. Ahn, H. Lee, T.H. Kim, and H.M. Lee (Battery Research Institute)
- **377** Use of Grafted PVdF-based Polymers in Lithium Rechargeable Lithium Batteries - C. Jarvis, B. Macklin, A. Macklin, N. Mattingley (AEA Technology Batteries), and E. Konfli (RMCS)
- **378** Production and Study of Physical and Chemical Properties of Thin-Film CC-ES - V.A. Dusheiko (Kiev State Trade and Economic University), L.P. Paskal, and V.U. Buryak (Kiev Taras Shevchenko University)

Battery Materials Posters

Co-Chairs: J. R. Selman and K. Amine

- **379** ⁷Li-Nuclear Magnetic Resonance Observation of Lithium Insertion into Coke Carbon Modified with Mesophase-Pitch - Y. Sato, K. Tanuma, T. Takayama, K. Kobayakawa (Kanagawa University), T. Kawai, and A. Yokoyama (Nippon Carbon Co., Ltd)
- **380** X-ray Photoemission Studies of Surface Pre-treated Graphite Electrodes - R.I.R. Blyth (Karl-Franzens Universität Graz), H. Buqa (Graz University of Technology), F.P. Netzer, M.G. Ramsey (Karl-Franzens Universität Graz), J.O. Besenhard, P. Golob, and M. Winter (Graz University of Technology)
- **381** Raman Microscopy as a Quality Control Tool for Electrodes of Lithium-Ion Batteries - P. Novak and J.-C. Panitz (Paul Scherrer Institute)

Abs. #

- **382** Structural and Concentrational Changes in Lithium Polymer Electrolytes Under Current Flow: In Situ Micro-Raman Investigation - D. Ostrovskii and P. Jacobsson (Chalmers University of Technology)
- **383** Studies of Lithium Battery Materials using Cold Neutron Depth Profiling - G. Lamaze, H. Chen-Mayer, D. Becker (National Institute of Standards and Technology), F. Vereda, A. Gerouki, N. Clay, P. Zerigian, T. Haas, and R. Goldner (Tufts University)
- **384** Application of EELS to Characterization of Cathode Materials for Lithium Secondary Batteries - Y. Shiraishi, I. Nakai (University of Tokyo), K. Kimoto, and Y. Matsui (National Institute for Research in Inorganic Materials)
- **385** Mechanisms and Dynamics of the Microcorrosion Phenomena in the Coin Cells of an Electrochemical System " CF_{1+x} - Lithium" - V.N. Mitkin, T.N. Denisova, V.E. Kerzhentseva, E.A. Shinelev (RAS), and V.V. Moukhin (JS Novosibirsk Chemical Concentrates Plant)
- **386** *In Situ* Raman Study of a Lithium-Polymer Battery - C. Naudin, J.L. Bruneel (Université Bordeaux I), M. Deschamps (Bollere Technologies), C. Edwards, J. Grondin (Université Bordeaux I), S. Lascaud (EDF-DER), J.C. Lassegues, and L. Servant (Université Bordeaux I)

Supercapacitors Posters

Co-Chairs: M. Morita and F. R. McLarnon

- **387** Quinone-Introduced Conducting Polymers for Supercapacitor Material - S. Suematsu, A. Manago, T. Ishikawa, and K. Naoi (Tokyo University of Agriculture and Technology)
- **388** New Gel Electrolytes for Batteries and Supercapacitor Applications - J. Chojnacka (Instituto de Ciencia y Tecnologia de Polimeros C.S.I.C.), J.L. Acosta (Instituto de Ciencia y Tecnologia de Polimeros C.S.I.C.), and E. Morales (Instituto de Ciencia y Tecnologia de Polimeros C.S.I.C.)
- **389** Electric Capacitance of Active Carbon Fiber Electrode in Aqueous Electrolyte Solutions - Y. Matsuda, S. Ohmura, and K. Ohno (Kansai University)
- **390** Nanotubular Materials for Supercapacitors - E. Frackowiak (Poznan University of Technology), K. Metenier, and F. Beguin (CNRS-University)
- **391** Charge/Discharge Characteristics of V_2O_5 -Carbon Composite for Supercapacitor - M.-S. Kim, J.-U. Kim, B.-K. Park, and H.-B. Gu (Chonnam National University)
- **392** Application of Conducting Polymer Composite Electrode for Supercapacitor - K.-W. Kang, J.-U. Kim, and H.-B. Gu (Chonnam National University)

INDEX OF AUTHORS

Abe, T.	18, 128, 148,	Bach, S.	143
Abura, T.	230	Badway, F.	292
Acosta, J.L.	388	Baffier, N.	143
Adachi, K.	340	Baik, H.-K.	114, 223
Ado, K.	220	Balasubramanian, M.	162
Adschiri, T.	235	Ban, S.-H.	172
Afanasjev, V.	98	Bandara, K.	315
Ahn, S.	376	Bando, T.	297, 373
Aihara, Y.	297, 373	Bannerjee, P.	29
Akiyama, T.	340	Banov, B.	91
Al Hallaj, S.	357	Bar Tow, D.	24, 60
Alain, V.	202	Barbarello, J.	320
Albering, J.H.	72	Barnett, B.	126
Aleksey, B.	81	Barriere, B.	349
Alessandrini, F.	347, 368, 369	Barusseau, S.	282
Alexandrov, A.	98	Baskevich, A.	70
Alliata, D.	68, 9	Baudrin, E.	11, 117
Amancio, S.	264	Beaudoin, B.	93
Amandi, R.	131	Beaulieu, L.	69
Amatucci, G.	292, 36	Becker, D.	383
Amezawa, K.	188, 325	Beguin, F.	129, 133
Amine, K.	332	Bele, M.	191, 273, 57
Ammundsen, B.	17, 185, 224	Belliard, F.	108, 132
Amouzegar, K.	271	Benedek, R.	137
Andersson, A.M.	82	Benjelloun, N.	55
Andersson, A.S.	20	Bergman, R.	31
Andou, H.	255	Bernard, S.	286
Andreas, B.	76	Besenhard, J.O.	113, 12, 120, 121, 289, 290, 380, 72, 73
Andrukaitis, E.	210, 342	Besner, S.	166
Angell, C.A.	274	Biensan, P.	237, 282, 284, 3, 339
Angenault, J.	206	Bindin, P.	358
Ann, J.-H.	58	Birke, P.	46
Anne, M.	192	Biscazzo, S.	318
Annie, L.G.L.S.	196, 202	Blanc, G.	339
Antipenko, B.	98	Bloch, D.	189
Antonini, A.	135	Blomgren, G.	211
Aoshima, T.	176	Blum, A.	366
Apostolova, R.	159, 180	Blyth, R.I.R.	380
Appel, W.K.	290	Bodet, J.-M.	282
Appetecchi, G.	367, 369	Bodin, F.	276
Arai, K.	235	Bodoardo, S.	175
Arai, N.	1	Boldyrev, Y.Y.	146
Arakawa, R.	230	Botte, G.	279
Arbizzani, C.	53	Bottino, A.	317
Ardel, G.	366, 367	Bourbon, C.	189
Armand, M.	166, 26	Boyd, S.	278
Armstrong, A.R.	15, 193, 260	Bradhurst, D.H.	152, 58
Arof, A.K.	356	Briois, V.	117
Arrabito, M.	175, 92	Brissot, C.	375
Ashkenazi, V.	34	Brousse, T.	100, 112, 13, 99
Au, G.	6	Broussely, M.	3, 339
Audry, C.	339	Bruce, P.G.	15, 193, 260
Aurbach, D.	159, 178, 179, 180, 303, 34, 85, 86	Brundage, M.	6
Aymard, L.	213	Bruneel, J.L.	386
Azuma, Y.	150	Bueno, P.	264
Börjesson, L.	110	Bugga, R.	127, 7
Béguin, F.	390	Bulhoes, L.	264
Baba, M.	371	Buqa, H.	12, 120, 121, 380

Burstein, L.	24	Dalton, P.	7
Buryak, V.U.	149, 378	Daroux, M.	164
Buvat, P.	99	Dass, V.	358
Byers, J.	351	Davidson, I.	234, 345
Caillon, G.	276	deCastro, S.	263
Cairns, E.J.	216	Dedryvére, R.	138
Calis, G.	291	Dees, D.W.	125, 332
Carewska, M.	368, 369	Delmas, C.	19, 200, 237
Carre, B.	272, 284	Denis, S.	11, 138
Catti, M.	195	Denisova, T.N.	385
Ceder, G.	251, 252	Deptula, A.	214
Chabre, Y.	165, 208	Deschamps, M.	386
Chagnes, A.	272	Desilvestro, H.	224
Chai, C.	363	Desilvestro, J.	17
Chandrasekaran, R.	256	Devaux, X.	100
Chang, Y.-C.	293, 294	Devyatkina, E.	217
Chazalviel, J.-N.	375	Di Noto, V.	318
Chen, C.	332	Dobler, B.	280, 281
Chen, C.-L.	10	Dolle, M.	93
Chen, J.-S.	312	Dominique, G.	196, 202
Chen, X.	75	Dominko, R.	191, 273, 57
Chen, Y.	130	Doo, S.-G.	374
Chen-Mayer, H.	383	Dou, S.X.	152, 58
Cherniy, A.	352	Drews, J.	50
Chervakov, O.	333, 341	Drofenik, J.	191, 273, 57
Chevallier, F.	133	Du Pasquier, A.	36, 292
Chia, F.	313	Du, C.	130
Cho, B.-W.	44	Duclot, M.	39
Cho, W.-I.	44	Duncan, M.J.	15, 260
Choi, B.K.	302	Dunlap, R.	69
Choi, Y.-M.	374	Dupin, J.C.	241
Chojnacka, J.	388	Dupont, L.	208, 93
Chottiner, G.	33	Dupré, N.	206
Chouinard, Y.	166	Durand, C.	75
Chouvin, J.	139	Dusheiko, V.A.	149, 378
Chow, W.	209, 212	Dygas, J.	310
Chowdari, B.V.R.	187, 89	Ebner, W.	363
Christensen, L.	42	Edstrom, K.	110, 83, 119, 82
Christian, J.	199	Edwards, C.	386
Christian, M.	207	Egashira, M.	144, 232
Christophe, J.	286	Eguchi, M.	253
Chua, D.	214	Ehrlich, G.	329, 75
Chun, J.H.	304	Elder, S.	161
Chung, H.-T.	267	Elkaim, E.	205
Chung, K.Y.	170	Engel, J.	160
Chung, S.	298, 314, 32	Enin, A.	98
Chusid, O.	303, 34, 86	Eriksson, T.	225
Clay, N.	383	Esaka, T.	104
Claye, A.	85	Exnar, I.	280, 281
Cohen, Y.	179, 179, 180, 34, 86	Faiers, J.	163
Connor, P.A.	109, 132	Fang, L.	89
Conte, M.	347	Fantini, M.	263
Cook, C.	321	Fauri, M.	318
Coowar, F.	358	Fay, M.	30
Corbett, M.	327	Fehrmann, G.	50
Coustier, F.	30	Fejieda, T.	215
Cressent, A.	93	Ferrando, W.A.	141
Croce, F.	204, 214, 239, 27, 300, 314	Fey, G.T.-K.	10, 254, 293, 294
Croguennec, L.	237	Fischer, J.	85
Crosnier, O.	100, 13	Florjanczyk, Z.	310
Cullen, J.	358	Fowkes, A.J.	15, 193
D'Epifanio, A.	204	Frackowiak, E.	129, 133, 390
Dahn, J.R.	42, 69, 74	Fragnaud, P.	100, 13
Dallek, S.	141	Francoise, P.	286

Franger, S.	143	Hammond, M.	332
Fransson, L.	110, 119, 82	Hamon, Y.	99
Fujieda, T.	101	Han, J.	130
Fujii, M.	186	Han, J.-I.	374
Fujitani, S.	219	Handa, M.	275
Fukushima, T.	230	Haronian, D.	326
Funahashi, A.	337	Harrison, S.	271
Fung, K.-Z.	312	Hasegawa, M.	71
Furlani, M.	315	Hashimoto, T.	340
Furusaka, M.	134	Hatazawa, T.	4
Gaberscek, M.	191, 273, 57	Hatchard, T.	42
Gadad, S.	140	Haupt, W.	280, 281
Gao, Y.	160, 164, 59	Hayamizu, K.	297
Gaoping, C.	154, 158	Hector, A.	151
Garche, J.	229	Heider, U.	178, 22
Garcia-Alvarado, F.	131	Hendrickson, M.	23, 6
Garza, L.	132	Henriksen, G.	332
Gaubicher, J.	118, 165, 21, 249	Herranen, M.	83
Gauthier, M.	166	Herreyre, S.	282, 284, 3
Gautier, S.	133	Hetzl, M.	329, 75
Gavelin, P.	301	Higobashi, H.	362
Gedanken, A.	87	Hill, I.	210, 342
Gejke, C.	110	Hinton, A.	324
Geoffroy, I.	284	Hirahara, K.	319
Geronov, Y.	353	Hirano, A.	134
Gerouki, A.	383	Hirano, Y.	357
Gerrits, N.	291	Hirata, N.	305
Giorgetti, M.	30	Hironaka, K.	354
Gitzendanner, R.	351	Hodal, T.	290
Gizbar, H.	34, 86	Holl, K.	229
Gladkikh, A.	24	Holmes, C.F.	48
Globa, N.	248, 333, 70	Honda, H.	104
Gnanaraj, J.	85	Hong, J.K.	103
Gofar, Y.	303, 34, 86	Horiba, T.	255, 354
Goldner, R.	383	Hou, X.	296
Golob, P.	120, 136, 380	Hsieh, M.-C.	294
Golodnitsky, D.	298, 326, 365, 366, 367	Huang, B.	29, 321
Gonbeau, D.	241	Huang, H.	106, 124, 249, 299
Gong, M.S.	302	Hubbard, H.	311
Gopukumar, S.	116	Huchet, O.	282
Gorenstein, A.	263	Hugener, T.	75
Gorev, A.	98	Huggins, R.A.	41
Goto, A.	323	Hussénius, A.	82
Gover, R.	265	Hwang, B.-J.	246, 254
Gozdz, A.	36	Ibarra Palos, A.	192
Green, R.	358	Ignat'ev, N.	22
Greenbaum, S.	175, 298, 314, 32	Iguchi, T.	297, 373
Grey, C.	224	Ihm, D.-J.	350, 363
Grincourt, Y.	234, 345	Ikuta, H.	115, 308
Grogger, C.	121	Ilic, D.	229
Grondin, J.	386	Imachi, N.	344
Groult, H.	247	Imanishi, N.	186, 364, 63, 370
Grugeon, S.	93	Imhof, R.	280, 281
Gu, H.-B.	245, 266, 316, 391, 392	Inaba, M.	128, 148, 18
Guo, X.	175, 32	Inada, T.	40
Gustafsson, T.	197, 225	Inoue, S.	362
Guyomard, D.	157, 161, 201	Ionescu, M.	152
Gwenaelle, R.	207	Irvine, J.T.S.	108, 109, 132
Höwing, J.	197	Ishida, S.	177
Haas, T.	383	Ishida, T.	111
Hackney, S.A.	125	Ishihara, T.	122, 123
Hajime, M.	338	Ishikawa, M.	145, 56
Hakuta, Y.	235	Ishikawa, T.	285, 387
Hamlen, R.	320, 6	Islam, M.S.	185

Isozaki, Y.	231	Kerzhentseva, V.E.	385
Itoh, T.	305, 43	Kezuka, K.	4
Ivanova, N.D.	146	Kida, Y.	337
Iwabe, S.	253	Kikuchi, M.	105
Jacobsson, P.	155, 31, 382	Kilroy, W.P.	141
Jak, M.	348	Kim, C.S.	306
Jannasch, P.	301	Kim, D.-G.	78
Jansen, A.N.	125, 332	Kim, H.	304, 78, 88
Jarvis, C.	377	Kim, H.-S.	44
Jean-Marie, B.	286	Kim, J.-S.	61
Jean-Marie, T.	207	Kim, J.-U.	266, 316, 391, 392
Jeong, G.-J.	79, 88	Kim, K.-B.	170, 171, 172, 173, 174, 184
Jeong, I.-S.	245	Kim, M.-S.	391
Jiangang, L.	154, 158	Kim, S.-S.	115
Jianjun, X.	154, 158	Kim, S.-W.	168, 79
Jo, S.I.	304	Kim, S.H.	142
Johansson, P.	31	Kim, T.H.	376
Johnson, B.	278	Kim, Y.-J.	78, 88, 95, 96, 97
Johnson, C.S.	119, 125, 244	Kim, Y.-U.	79
Joho, F.	76, 9	Kim, Y.W.	302
Jones, D.	224	Kimoto, K.	384
Jousse, F.	99	Kimura, T.	156
Jumas, J.-C.	138, 139	Kinoshita, K.	25, 68, 90
Jung, J.-S.	304	Kishi, T.	182
Jungnitz, M.	22	Kita, F.	283
Juzkow, M.	47	Kiyohara, C.	176
Kageyama, H.	111, 220, 232, 236	Ko, J.-M.	304
Kai, T.	354	Kobayakawa, K.	379
Kajiyama, A.	40	Kobayashi, H.	111, 220, 236
Kakirde, A.	363	Kobayashi, T.	308
Kalaiselvi, N.	257, 258, 259, 261	Koetz, R.	68, 9
Kamaruddin, N.	356	Kokhany, V.	70
Kaminya, T.	134	Komaba, S.	183
Kamioka, K.	228	Kondo, S.	40
Kamiyama, T.	226	Konfli, E.	377
Kamizori, H.	283	Kong, F.	25
Kanamura, K.	235, 323	Konishi, T.	232
Kanari, K.	335	Korai, Y.	97
Kanasaku, T.	188, 325	Koseki, M.	354
Kanbe, C.	147	Kosova, N.	217
Kanda, M.	231, 328	Kostecki, R.	25, 68
Kaneko, S.	343	Kouguchi, M.	40
Kang, H.-R.	79	Kozlova, S.	217
Kang, K.-W.	392	Kozono, Y.	255
Kang, T.	78, 79, 88, 95, 96	Krause, L.	278
Kanno, R.	134, 220, 226, 265	Krok, F.	310
Kargina, I.	234, 345	Ksenzhek, O.	70
Kasai, M.	255	Ku, C.-H.	97
Kaszejna, P.	3	Kubo, M.	305
Katayama, K.	150	Kubota, M.	104
Katayama, Y.	182	Kuehner, A.	22
Kato, K.	335	Kuhn, A.	131
Kato, Y.	219, 308	Kumagai, N.	183, 183, 247
Katsuhito, T.	338	Kumashiro, Y.	255
Katsuta, T.	107, 287	Kurashima, K.	275
Kawabata, A.	101	Kuratomi, J.	297, 373
Kawahara, A.	122, 123	Kurokawa, H.	219
Kawai, T.	379	Kusawake, H.	372
Kawakami, A.	283	Kuwana, K.	373
Kawamoto, Y.	226, 265	Kuwashima, S.	372
Kazuma, K.	338	Kylyvnyk, K.	248, 341, 70
Kelder, E.	106, 240, 348	Lada, W.	214
Kelder, E.M.	291	Lain, M.	359
Kerr, T.	249	Lamanna, W.	278

Lamaze, G.	383	Ma, S.	194
Lampe-Onnerud, C.	126	Machnikowski, J.	129
Landers, R.	263	Macklin, A.	377
Lantelme, F.	247	Macklin, B.	358, 377
Lanz, M.	9	MacNeil, D.	42
Larcher, D.	69	Magistris, A.	317
Laruelle, S.	11, 117	Magnan, J.-F.	166
Lascaud, S.	375, 386	Maki, F.	253
Lasségués, J.C.	386	Makino, K.	182
Lauriat, J.-P.	205	Maksyuta, I.	333, 341
Lavi, Y.	326	Manago, A.	387
Le Cras, F.	189	Manivannan, V.	363
Le Gal La Salle, A.	157, 161, 201	Manual, A. S.	116, 238, 250, 309
Le Granvalet-Mancini, M.	140	Manzo, M.	7
Lee, B.W.	142	Marassi, R.	239
Lee, C.-W.	37	Mari, C.M.	195
Lee, H.	376	Maria Rosa, P.	207
Lee, H.-S.	277	Marianetti, C.	251
Lee, H.M.	376	Markovsky, B.	159, 180
Lee, J.	306, 66	Marsh, C.	351
Lee, J.-A.	266, 316	Marsh, R.	7
Lee, J.-F.	254	Martin, C.	35
Lee, J.-H.	350	Martin-Litas, I.	241
Lee, J.-K.	114, 223	Martinent, A.	77
Lee, J.Y.	153	Maryvonne, H.	207
Lee, J.Y.	67	Masquelier, C.	165, 205, 208, 21
Lee, K.-K.	171, 173, 174	Mastragostino, M.	53
Lee, M.-H.	169	Mathieu, M.	207
Lee, N.	35	Matoba, N.	65
Lee, S.-B.	80	Matsuda, Y.	230, 288, 389
Lee, S.-J.	114, 223	Matsui, S.	362
Lee, S.-M.	114, 223	Matsui, Y.	384
Lee, Y.-G.	28	Matsumura, T.	354
Lee, Y.J.	224	Matsuoka, M.	111, 236
Leising, R.A.	330	Matsuta, S.	219
Lemordant, D.	272, 284	Mattinlgey, N.	377
Lenhof, C.	276	Mayes, A.	29, 321
Levasseur, A.	241	McBreen, J.	162, 164, 277
Levasseur, S.	200	McGuinn, J.	75
Levi, E.	178, 179, 34	McLarnon, F.	25
Levi, M.	178, 179	Medjutov, M.	98
Li, Q.	364	Meenakshisundaram, R.	116, 238, 238,
Li, Z.	59	243, 250, 309
Lifshits, E.	298	Mellander, B.-E.	315
Lim, M.-R.	184	Menetrier, M.	200
Lin, H.-P.	214, 23	Merson, A.	24
Lin, S.-W.	269, 270	Meshri, D.	333
Lindner, H.J.	153, 187	Michael E., S.	76
Lindsay, M.J.	152, 58	Michael, M.S.	233
Lippens, P.E.	138, 139	Michael, S.	84
Liu, D.G.	246	Michel, B.	286
Liu, H.K.	152, 58	Middaugh, R.	262
Liu, J.	332	Mihara, T.	111
Liu, Q.	130	Misztal-Faraj, B.	310
Liu, W.-K.	293	Mitchell, B.	265
Liu, X.	372	Mitkin, V.N.	98, 385
Liu, Z.	153	Mitsuishi, I.	231
Livshits, V.	366	Miura, T.	182
Ljungbäck, R.	301	Miyake, H.	71
Loic, D.	207	Mochida, I.	97
Lu, C.-H.	269, 270	Mochizuki, S.	111
Lu, Z.	34	Mogi, R.	128
Möller, K.-C.	12, 290	Mohamed, N.S.	356
Méténier, K.	390	Mohamedi, M.	43

Mohd Noor, A.F.	233	Ogarkov, V.	98
Molz, M.	320	Ogumi, Z.	128, 148, 18
Momma, T.	303, 87	Oh, S.M.	103, 306
Momose, Y.	253	Ohmura, S.	389
Momtchilov, A.	203, 94	Ohno, K.	389
Moon, S.-I.	266	Ohsaki, T.	328
Moore, G.	161, 201	Ohzono, H.	71
Morais, J.	263	Ohzuku, T.	64, 65
Morales, E.	388	Okada, M.	228
Morales, J.	112	Okada, S.	144, 232
Morcrette, M.	208	Okahara, K.	176
Morgan, D.	251	Okuya, M.	343
Morita, M.	145, 56	Olivier, J.P.	136
Moshkovich, M.	34, 86	Olivier-Fourcade, J.	138, 139
Moskovich, M.	179	Olsen, I.	276
Mostafa, M.A.	134	Onnerud, P.	126
Moukhin, V.V.	98, 385	Ono, T.	373
Mouri, T.	228	Ooms, F.G.B.	240, 291
Mui, S.	321	Osaka, T.	303, 45, 87
Muniyandi, N.	257, 258, 259, 261	Osman, Z.	356
Muranaga, T.	362	Ostrovskii, D.	155, 382
Muranaka, Y.	255, 354	Ota, H.	102
Mustarelli, P.	317	Ota, T.	219
Myung, S.-T.	267	Otomo, T.	134
N.G. Renganathan	238, 243, 309, 250	Ouvrard, G.	190
Nadeau, G.	25, 90	Owen, J.	151
Nagashima, H.	283	Owens, B.	30, 51
Nagirny, V.	159, 180	Pérez Vicente, C.	139
Nakade, K.	343	Palacin, R.M.	208
Nakagawa, T.	145	Palazzo, M.J.	330
Nakai, I.	218, 222, 384	Pan, C.	224
Nakajima, K.	4	Panero, S.	175, 198, 92
Nakane, I.	38	Panitz, J.-C.	381, 9
Nakanishi, T.	319	Park, B.	78
Nakata, H.	285, 52	Park, B.-K.	391
Naoi, K.	387, 54	Park, C.-K.	363
Narukawa, S.	344, 38	Park, C.W.	103
Natchi, M.	116, 238, 243, 250, 309	Park, G.-C.	316
Nathan, M.	326	Park, H.-C.	304
Naudin, C.	386	Park, J.-K.	28
Nazar, L.	118, 124, 165, 21, 249	Park, Y.-T.	61
Nazri, G.A.	355	Paskal, L.P.	378
Nechev, K.	3	Pasquali, M.	135
Neduzhko, L.	341	Passerini, S.	30, 347, 368, 369, 51
Negishi, A.	335, 336	Pastushkin, T.	70
Netz, A.	41	Pavlenko, N.	283
Netzer, F.P.	380	Pei, C.C.	233
Nishiguchi, H.	122, 123	Pejovnik, S.	191, 273, 57
Nishimura, K.	255	Peled, E.	24, 298, 326, 365, 366, 367, 60, 62
Nishiwaki, Y.	222	Penazzi, N.	175
Nishizawa, M.	43	Perego, R.	240
Nitta, Y.	71	Pereira-Ramos, J.-P.	143
Niu, J.	66	Peres, J.-P.	339
Nobili, F.	239	Periasamy, P.	257, 258, 259, 261
Nobuyuki, T.	338	Perner, A.	229
Noguchi, H.	194	Persi, L.	204, 239, 27, 300, 314
Nohma, T.	337	Perton, F.	282, 339
Nomoto, S.	52	Pham, P.	278
Novák, P.	113	Philippe, B.	286
Novak, P.	9, 76, 113, 381,	Piaggio, P.	317
Nozaki, K.	335	Pickering, P.	17, 224
Numata, K.	177	Piffard, Y.	157
Numata, T.	147	Ping, X.	59
Oesten, R.	178, 22	Pisniy, V.	248

Plichta, E.	23, 6	Saishou, K.	344
Poizot, P.	11, 117	Saito, H.	322
Polyschuk, Y.	341	Saito, M.	287
Portal, R.	201	Saito, Y.	335, 336
Potiron, E.	157	Sakaebe, H.	197, 220, 225
Pouillier, C.	237	Sakaguchi, H.	104
Pozin, M.	352, 361	Sakai, H.	183
Prabaharan, S.R.S.	233, 84	Sakai, T.	101, 162, 215, 225, 227, 362
Prakash, J.	37	Sakata, H.	283
Prasad, R.	137	Sakurai, S.	101
Preishuber-Pfogl, P.	73	Sakurai, T.	156
Prem Kumar, T.	116, 261	Sakurai, Y.	181
Proisini, P.P.	347, 368, 369	Salam, F.	46
Puglia, F.	351	Salitra, G.	180
Purgin, V.	98	Salomon, M.	214, 23
Pyun, S.-I.	167, 168, 169, 80	Sanchez, L.	112
Qi, L.	370	Sandner, B.	307
Quartarone, E.	317	Sano, A.	148
Quarton, M.	206	Santhanam, R.	246
Quine, T.E.	15, 260	Santiago, E.	264
R. Sriram	238	Santis, M.	121
Radshenko, V.V.	149	Santos-Pena, J.	112
Raekelboom, E.	151	Sarac, A.S.	268
Raghavan, M.	257, 258, 259, 261	Sarakonsri, T.	125
Ramesh Babu, B.	257, 258, 259, 261	Sarradin, J.	55
Ramsey, M.G.	380	Sartori, P.	22
Rao, G.	346	Sasaki, Y.	275
Rao, G.V.S.	187	Sato, T.	102
Ravet, N.	166	Sato, Y.	379
Reale, P.	92	Satolli, D.	198
Reiche, A.	307	Sawa, S.	232
Reimer, J.A.	216	Sawai, K.	64, 65
Reimers, J.	212	Sayers, B.	324
Reisner, D.	341	Scaccia, S.	369
Rendek Jr., L.	33	Schechter, A.	34, 86
Renganathan, N.G.	116, 257, 258, 259, 261	Scherson, D.	33
Ribalka, A.	333	Schleich, D.M.	13, 99, 100, 112
Ribes, M.	55	Schmidt, C.	49
Richardson, T.	334	Schmidt, M.	178, 22
Robertson, A.D.	15, 193, 260	Schmied, M.	73
Rodriguez-Carvajal, J.	205, 21	Schoonman, J.	106, 240, 291, 348
Rogalska, E.	310	Schwenzel, J.	41
Roh, K.-S.	350	Scrosati, B.	155, 175, 198, 204, 239, 27, 300, 314, 35, 367, 92
Romagnoli, P.	367	Seel, J.A.	74
Romanovskaya, L.	333	Sekine, K.	105, 107, 287
Ronci, F.	155, 204	Sekino, M.	231, 328
Rosenberg, Y.	60, 62	Sekiya, S.	275
Ross, P.	334	Selladurai, S.	256
Rossignol, C.	190	Selman, J.R.	357
Rosso, M.	375	Sergeev, V.	98
Rouault, H.	189	Servant, L.	386
Rougier, A.	213	Seung, D.-Y.	234, 374
Rousse, G.	205, 208	Sever Skapin, A.	191
Rouzaud, J.N.	133	Shao-Horn, Y.	262
Rowell, J.	118	Shembel, E.	159, 180, 248, 333, 341, 70
Roy, B.	119	Shi, J.	126
Rozhkov, V.	98	Shiao, A.	214
Roziere, J.	185, 224	Shiao, H.C.A.	23
Ruffo, R.	195	Shigemura, H.	220
Ruth Mangani, I.	256	Shikano, M.	225
Rykart, B.	76, 9	Shim, Y.-J.	350
S��verine, J.	196	Shimada, H.	278
Sadoway, D.	29, 321	Shin, H.-C.	167
Saha, S.K.	270		

Shinelev, E.A.	385	Takano, K.	335, 336
Shiraishi, N.	87	Takayama, T.	379
Shiraishi, Y.	384	Takeda, Y.	14, 186, 364, 370, 63
Shirakata, M.	147	Takei, K.	181
Shizuka, K.	176	Takemitsu, T.	288
Sin, H.-S.	350	Takeuchi, E.S.	330
Siow, K.S.	296	Takeuchi, K.J.	330
Skarstad, P.	49	Takigawa, Y.	236
Skekhtman, A.	360	Takita, Y.	122, 123
Skotheim, T.	353	Tamaki, J.	111, 236
Stane, S.	23, 329	Tamura, S.	111
Slegr, H.	345	Tanaka, T.	1
Smart, M.	127, 7	Taniguchi, S.	340
Smyrl, W.	30	Tanuma, K.	379
Soavi, F.	53	Tarascon, J.-M.	11, 117, 208, 93
Sohn, H.-J.	304, 78, 79, 88, 95, 96	Tarascon, J.M.	213
Soiron, S.	213	Tatebayashi, Y.	231
Sokolsky, G.V.	146	Tatsumi, K.	101, 134, 215
Sominski, L.	87	Teagle, D.	358
Song, X.	25, 68	Teeters, D.	140
Sonoda, T.	283	Telezkin, V.	98
Soo, P.	29, 321	Terada, Y.	221, 222
Souquet, J.-L.	39	Thackeray, M.M.	2, 119, 125, 137, 244
Speiss, F.	75	Thangadurai, V.	41
St-Amant, G.	271	Thirunakaran, R.	257, 258, 259, 261
Staelin, D.	321	Thomas, J.	119, 197, 225
Staniewicz, R.J.	3	Thomas, J.O.	20
Staub, R.	50	Tikhonov, Jr., K.	361
Stauss, E.	365	Tikhonov, K.	352
Steiner, R.	17, 224	Tobishima, S.	181
Stelzer, F.	73	Topart, P.	99
Storey, C.	234, 345	Torlone, G.	210, 342
Stramare, S.	41	Torres, L.	132
Strauss, E.	366	Toru, I.	338
Strobel, P.	192	Toshikatsu, T.	338
Subramanian, V.	116	Tossici, R.	239
Sudalaiimuthu, R.	309	Totir, D.	33
Suematsu, S.	387	Touboul, M.	11, 117
Sugihara, T.	156	Trapa, P.	29
Sugimoto, K.	297	Tsai, Y.-W.	254
Suhara, M.	150	Tsuboi, A.	285
Suib, S.	75	Tsuda, S.	5
Sukumaran, G.	238, 243, 250	Tsutsumi, S.	71
Sun, H.Y.	364, 370	Tucker, M.C.	216
Sun, L.	58	Turgeman, R.	34, 86
Sun, X.	162, 164, 277	Uchida, I.	357, 43
Surampudi, S.	127, 7	Uchimoto, Y.	242
Suzuki, H.	102	Uebou, Y.	111, 236
Suzuki, J.	105, 107, 287	Ueno, M.	319
Suzuki, Y.	115	Ulus, A.	62
Svanberg, C.	31	Umegaki, T.	323
Sverdlov, E.	326	Ungar, G.	313
Sylvère, S.	196	Urbano, A.	263
Sylvie, B.	286	Usami, K.	275, 322
Sylvie, H.	286	Usami, T.	102
T. Prem Kumar	243, 250, 309	Uvarov, N.	217
Tabuchi, M.	111, 220, 226, 232, 236	Vaidyanathan, H.	346
Taillades, G.	55	van Beck, J.R.	331
Tajima, H.	340	Van der Ven, A.	252
Takada, K.	40	Van Landschoot, N.	348
Takahashi, K.	215	van Schalkwijk, W.	47
Takahashi, M.	181	Vanessa, L.	202
Takami, N.	328	Vasanthi, R.	256
Takamura, T.	105, 107, 287	Vaughan, G.	165

Vaughey, J.T.	119, 125	Yakimov, V.	98
Venkatachalam, S.	238, 243, 250	Yakovleva, M.	160, 164
Venkatesetty, H.V.	295	Yamada, O.	145
Verbaere, A.	157	Yamaguchi, K.	105, 107, 287
Vereda, F.	383	Yamaki, J.-I.	144, 232
Victoria, O.	81	Yamamoto, M.	328
Videa, M.	274	Yamamoto, N.	188, 325
Vinatier, P.	241	Yamamoto, O.	305, 364, 370, 63
Vishnyakov, L.	70	Yamamoto, Y.	111, 236
Vittadello, M.	318	Yamaura, J.	71
Vladimir, G.	81	Yanagida, K.	337
von Sacken, U.	163, 209, 212	Yanai, A.	337
Vukson, S.	7	Yang, J.	14, 364, 370, 63
Wachtler, M.	12, 72, 73	Yang, L.	137
Wagner, M.R.	73	Yang, X.-Q.	162, 164, 277
Waki, M.	236	Yao, T.	242
Wakihara, M.	115, 16, 308	Yazami, R.	77, 8
Wallez, G.	206	Yo, K.	338
Walsh, F.	352, 361	Yokoyama, A.	379
Wang, D.	59, 59	Yokoyama, S.	308
Wang, G.X.	152, 58	Yoneda, H.	52
Wang, H.	299	Yonemura, M.	226
Wang, X.	59	Yonezawa, M.	147
Wang, X.	227	Yonezu, I.	219, 337
Wang, Y.	175, 212, 314, 32	Yong, T.T.	84
Ward, I.	311	Yoo, Y.	234
Watanabe, H.	344	Yoon, W.-S.	170, 171, 172, 173, 174
Watanabe, M.	303, 40	Yoshida, A.	52
Watanabe, O.	319	Yoshida, M.	105
Weaving, J.	358	Yoshimoto, N.	145
Weinkauf, A.	307	Yoshimura, S.	219
Weller, M.	151	Yoshino, A.	232
Wen, Z.	305	Yoshio, M.	122, 123, 162, 194, 215, 227, 228
Weppner, W.	41	Yoshioka, K.	52
Wessén, B.	301	Yufit, V.	60
White, R.	279	Yun, K.-S.	44
Whitfield, P.	345	Yves, P.	196, 202
Williamson, M.	311	Zaderey, N.	248, 333, 70
Willmann, P.	237, 272	Zaghib, K.	25
Wilson, A.M.	209	Zaghib, K.V.	90
Winter, M.	113, 12, 120, 121, 136, 289, 290, 380, 72, 73	Zane, D.	135
Wohlfahrt-Mehrens, M.	229	Zanghellini, E.	110
Wolf, R.	50	Zerigian, P.	383
Wolfenstine, J.	214	Zhang, G.	130
Wright, P.V.	313	Zhang, M.	212
Wrodnigg, G.H.	113, 12, 289	Zhang, S.	285
Wunder, S.	299	Zhang, Z.	279
Wurm, C.	165, 21	Zhaolin, L.	67
Xia, Y.	101, 162, 215, 225	Zheng, T.	36
Xia, Y.	227	Zheng, Y.	313
Xiao, T.	341	Zhiyuan, T.	154, 158
Xing, X.-K.	164	Zhong, Q.	163
Xu, W.	274	Zhonghua, L.	179
Yagi, Y.	227	Zhu, J.	87
Yagupolskii, Y.	283	Zygadlo-Monikowska, E.	310

Notes

Notes

Notes

IMLB 11

11th
International
Meeting on
Lithium Batteries

JUNE 23-28, 2002

**MONTEREY CONFERENCE CENTER
& DOUBLETREE HOTEL**

**MONTEREY,
CALIFORNIA**

www.electrochem.org/meetings/011/imlb11.html

**10th International Meeting
on Lithium Batteries
"Lithium 2000"**

**Villa Erba Conference Center
Como, Italy**

May 28-June 2, 2000

IMLB

DISTRIBUTION STATEMENT A
Approved for Public Release
Distribution Unlimited

Copyright 2000

by

The Electrochemical Society, Inc.

Presentation of a paper at a technical meeting sponsored by The Electrochemical Society (ECS) does not guarantee publication in full by ECS. Not all illustrations to be presented during a paper delivery are reproduced here. Production limitations to this volume caused illustration reduction to a point where a phenomenon described by the author may have, in some cases, been lost in reproduction. All magnifications are those existing before photographic reproduction. Statements and opinions given in this abstracts volume are those of the contributors and neither The Electrochemical Society, Inc. nor the other sponsors of this meeting assume any responsibility for them.

.....

The Abstracts contained herein may not be reprinted and may not be digested by publications other than those of The Electrochemical Society, Inc. in excess of 1/6 of the material presented. Rights and permissions requests should be addressed to: Director of Publications, The Electrochemical Society, Inc., 65 South Main Street, Pennington, New Jersey 08534-2839, USA.

.....

ISBN 1-56677-283-4

Printed in the United States of America

CHAIRMAN

Bruno Scrosati
Dipartimento di Chimica
Università "La Sapienza"
Piazzale A. Moro 5
00185 Rome, Italy
Phone: +39-6-49913530
Fax: +39-6-491769
Email: scrosati@axrma.uniroma1.it

CO-CHAIRMEN

Peter G. Bruce - University of St. Andrews, Scotland
Frank R. McLarnon - Lawrence Berkeley Laboratory, USA
Zempachi Ogumi - Kyoto University, Japan

INTERNATIONAL SCIENTIFIC COMMITTEE

K. M. Abraham - Covalent Associates, Inc, USA
M. Armand - Université de Montréal, Canada
R. Atanasoski - 3M Research Center, USA
D. Aurbach - Bar-Ilan University, Israel
J. O. Besenhard - Technische Universität Graz, Austria
M. Broussely - SAFT, Advanced Batteries, France
K. R. Bullock - C&D Technologies, Inc., USA
J. Dahn - Dalhousie University, Canada
G. C. Farrington - Lehigh University, USA
G. T-K. Fey - National Central University, Taiwan, ROC
R. Marassi - Università di Camerino, Italy
M. Mastragostino - Università di Bologna, Italy
R. Neat - AEA Technology, Harwell, UK
B. B. Owens - Research International, USA
T. Osaka - Waseda University, Tokyo, Japan
J. -K. Park - KAIST, Korea
E. Peled - Tel Aviv University, Israel
W. H. Smyrl - University of Minnesota, USA
E. Spila - Eldor Corporation, Italy
J. M. Tarascon - Université de Picardie Jules Verne, France
M. Thackeray - Argonne National Laboratory, USA
J. Thomas - Uppsala University, Sweden
R. Vellone - ENEA, Rome, Italy
C. A. Vincent - University of St. Andrews, Scotland
M. Wakihara - Tokyo Institute of Technology, Japan
K. West - Technical University of Denmark
O. Yamamoto, Mie University, Japan

LOCAL ORGANIZING COMMITTEE

Fausto Croce, Università di Roma, Italy
Roberto Marassi, Università di Camerino, Italy
Marina Mastragostino, Università di Bologna, Italy
Stefania Panero, Università di Roma, Italy
Francesca Schiatti, Villa Erba, S.p.A., Italy
Bruno Scrosati, Università di Roma, Italy
Eraldo Spila, Eldor Corp, S.p.A., Italy

MEETING ORGANIZATION

Administration
The Electrochemical Society, Inc
65 South Main Street
Penninton, NJ 08534-2839, USA
Phone: 609.737.1902
Fax: 609.737.2743
E-mail: ecs@electrochem.org
Responsible Persons: Brian E. Rounsavill & Elizabeth Brennfleck

LOCAL ARRANGEMENTS

Centro Volta
Villa Olmo, Via Cantoni 1
22100 Como, Italy
Phone: 39-031-579-812
Fax: 39-031-573-395
E-mail: stefanetti@icil64.cilea.it
Responsible persons: Chiara Stefanetti & Nadia Tasini

SPONSORS



Comitato Comasco per le Manifestazioni Voltiane nel Bicentenario
dell'Invenzione della Pila 1997-2000;



The Electrochemical Society, Inc, Battery Division;
The Electrochemical Society Inc; European Local Section;



Electrochemical Society of Japan, Committee of Battery Technology;
Electrochemical Society of Japan, Committee on Capacity Technology;

Università "La Sapienza" di Roma;

Elettrochimica ed Energia, Roma

Divisione Elettrochimica della Società Chimica Italiana;



ENEA, Ente per le Nuove Tecnologie, l'Energia e l'Ambiente, Roma



Lithium Battery Energy Storage Technology Research Association



US Army European Research Office, London



ARCOTRONICS ITALIA SpA



AUSIMONT SpA



ELDOR Corporation

**Abstract
Number**

IMLB 10 - TENTH INTERNATIONAL MEETING ON LITHIUM BATTERIES
The Electrochemical Society, Inc. / Centro Volta - Como

- 1 Year 2000 R&D Status of Large-Scale Lithium Secondary Batteries in the National Project of Japan
T. Tanaka and N. Arai
- 2 From Gems to Lithium Battery Electrodes
M.M. Thackeray
- 3 Aging Mechanism in Li Ion Cells and Calendar Life Predictions
M. Broussely, S. Herreyre, P. Biensan, P. Kaszlejna, K. Nechev, and R.J. Staniewicz
- 4 The Status of Sony Li-Ion Polymer Battery
K. Nakajima, K. Kezuka, and T. Hatazawa
- 5 Battery Technologies and Based on the Requirement for Applications and Future Movement
S. Tsuda
- 6 U.S. Army Portable Power Programs
R. Hamlen, G. Au, M. Brundage, M. Hendrickson, and E. Plichta
- 7 Lithium-Ion Batteries for Aerospace Applications
R. Marsh, S. Vukson, S. Surampudi, R. Bugga, M. Smart, M. Manzo, and P. Dalton
- 8 From Rome to Como: Twenty Years of Active Research on Carbon Based Electrodes for Lithium Batteries at INP-Grenoble
R. Yazami
- 9 The Complex Electrochemistry of Graphite Electrodes in Lithium-Ion Batteries
P. Novak, F. Joho, M. Lanz, B. Rykart, J.-C. Panitz, D. Alliaata, and R. Koetz
- 10 High-Capacity Carbons for Lithium-Ion Batteries Prepared from Rice Husk
G.T.-K. Fey and C.-L. Chen
- 11 Searching for Anode Materials for the Li-Ion Technology: Time to Deviate from the Usual Path...
P. Poizot, S. Laruelle, E. Baudrin, S. Denis, M. Touboul, and J.-M. Tarascon
- 12 Film-Forming Electrolyte Additives for Li-Carbon and Li-Alloy Anodes
J.O. Besenhard, G.H. Wrodnigg, K.-C. Möller, H. Buqa, M. Wachtler, and M. Winter
- 13 Novel Anodes for Lithium Ion Batteries
T. Brousse, O. Crosnier, P. Fragnaud, and D. Schleich
- 14 New Composite Anode Systems Combined with $\text{Li}_{2.6}\text{Co}_{0.4}\text{N}$
Y. Takeda and J. Yang
- 15 Layered LiMnO_2 and Spinel-Based Compounds as Positive Electrodes in Rechargeable Batteries: Structure, Transformation and Properties
P.G. Bruce, A.R. Armstrong, A.D. Robertson, M.J. Duncan, A.J. Fowkes, and T.E. Quine
- 16 Charge-Discharge Properties of Spinel Oxides as the Cathode for Lithium Secondary Battery
M. Wakihara
- 17 Novel Layered Cathode Materials for Advanced Lithium Ion Batteries
B. Ammundsen, J. Desilvestro, R. Steiner, and P. Pickering
- 18 STM Study on Lithium Manganese Oxide Cathodes
M. Inaba, T. Abe, and Z. Ogumi
- 19 Effects of Cationic Disorder and Defects on the Structural Behaviour of the $\text{Li}_x(\text{M,L})\text{O}_2$ (M = Ni, Co) Phases
C. Delmas
- 20 The Source of First-Cycle Capacity Loss in LiFePO_4
A.S. Andersson and J.O. Thomas
- 21 A Survey of Polyanionic Structures Hosts For Reversible Lithium Insertion
C. Masquelier, C. Wurm, J. Rodriguez-Carvajal, J. Gaubicher, and L. Nazar
- 22 Lithium Fluoralkylphosphates, A New Class of Conducting Salts for Electrolytes for High Energy Lithium-Ion Batteries
M. Schmidt, U. Heider, A. Kuehner, R. Oesten, M. Jungnitz, N. Ignat'ev, and P. Sartori
- 23 Low Temperature Behavior of Li-Ion Cells
H.-P. Lin, M. Salomon, H.C.(A. Shiao, M. Hendrickson, E. Plichta, and S. Slane
- 24 Composition, Depth Profiles and Lateral Distribution of Materials in the SEI Built on HOPG -TOF SIMS and XPS Studies
E. Peled, D. Bar Tow, A. Merson, A. Gladkikh, and L. Burstein
- 25 *In Situ* Studies of SEI Formation
F. Kong, R. Kostecki, G. Nadeau, X. Song, K. Zaghib, K. Kinoshita, and F. McLarnon
- 26 Batteries for Transportation: Are We Missing the Boat?
M. Armand
- 27 PEO-Based Nanocomposite Polymer Electrolytes
F. Croce, L. Persi, and B. Scrosati
- 28 Electrochemical Characteristics of Polymer Electrolytes Based on P(VDF-co-HFP)/PMMA Ionomer Blend for PLIB
J.-K. Park and Y.-G. Lee

Abstract
Number

- 29 Self-Doped Block Copolymer Electrolytes (SDBCEs) for Solid-State, Rechargeable Lithium Batteries
D. Sadoway, A. Mayes, B. Huang, P. Trapa, P. Soo, and P. Bannerjee
- 30 Electrochemical and Synchrotron Radiation XAS Studies of Lithium Intercalation Into Vanadium Pentoxide Aerogels and Nanocomposites
W. Smyrl, S. Passerini, M. Giorgetti, F. Coustier, M. Fay, and B. Owens
- 31 Light Scattering and Computational Studies on Ionic Interaction and Dynamics in Polymer Based Gel Electrolytes
P. Johansson, C. Svanberg, R. Bergman, and P. Jacobsson
- 32 Solid State NMR Studies of Lithium Ion Battery Materials
S. Greenbaum, Y. Wang, S. Chung, and X. Guo
- 33 *In Situ* and *Ex Situ* Strategies for the Study of Lithium Battery Electrodes
L. Rendek Jr., D. Totir, G. Chottiner, and D. Scherson
- 34 Rechargeable Magnesium Battery Technology, a Comparison with Li Battery Systems
D. Aurbach, Y. Gofer, Z. Lu, A. Schechter, O. Chusid, H. Gizbar, Y. Cohen, V. Ashkenazi, M. Moshkovich, R. Turgeman, and E. Levi
- 35 Nanomaterial-Based Li-Ion Battery Electrodes
C. Martin, N. Lee, and B. Scrosati
- 36 Microstructure Effects in Plasticized PVDF-HFP-Based Electrodes for Plastic Li-Ion Batteries
A. Du Pasquier, T. Zheng, G. Amatucci, and A. Gozdz
- 37 Investigations of Non-Flammable Phosphazene Based Compounds for Lithium Ion Batteries
J. Prakash and C.-W. Lee
- 38 Development of Lithium Polymer Batteries with Gel Polymer Electrolyte
S. Narukawa and I. Nakane
- 39 Glassy Materials for Lithium Batteries - Theoretical Aspects and Devices Performances
M. Duclot and J.-L. Souquet
- 40 Research on Highly Reliable Solid-State Lithium Batteries in NIRIM
K. Takada, T. Inada, A. Kajiyama, M. Kouguchi, S. Kondo, and M. Watanabe
- 41 Materials Development for High-Performance Lithium Batteries
R.A. Huggins, A. Netz, V. Thangadurai, J. Schwenzel, S. Stramare, and W. Weppner
- 42 Modeling Lithium-Ion Battery Oven Exposure Tests
J. Dahn, T. Hatchard, D. MacNeil, and L. Christensen
- 43 Recent Investigations on Thin Films and Single Particles of Transition Metal Oxides for Lithium Batteries
I. Uchida, M. Mohamedi, M. Nishizawa, and T. Itoh
- 44 Recent Advances on Rechargeable Lithium Ion Polymer Batteries in Korea
K.-S. Yun, B.-W. Cho, W.-I. Cho, and H.-S. Kim
- 45 Lithium Metal/Polymer Battery
T. Osaka
- 46 Solid State Polymer Battery Based on Lithium Titanate Anode
P. Birke and F. Salam
- 47 Shaped Charge: Adjustable Form-Factor Lithium-Ion Batteries
W. van Schalkwijk and M. Jozkow
- 48 The Role of Lithium Batteries in Modern Health Care
C.F. Holmes
- 49 The Future of Lithium and Lithium-Ion Batteries in Implantable Medical Devices
C. Schmidt and P. Skarstad
- 50 Primary Batteries for Implantable Pacemakers and Defibrillators
J. Drews, G. Fehrmann, R. Staub, and R. Wolf
- 51 Medical Batteries for External Medical Devices
S. Passerini and B. Owens
- 52 Advanced Capacitors and Their Application
S. Nomoto, H. Nakata, K. Yoshioka, A. Yoshida, and H. Yoneda
- 53 Polymer-Based Supercapacitors
M. Mastragostino, C. Arbizzani, and F. Soavi
- 54 New Conducting Polymers for Supercapacitors and Lithium Batteries
K. Naoi
- 55 Tin/Tin Oxide Thin Film Electrodes for Lithium-Ion Batteries
J. Sarradin, N. Benjelloun, G. Taillades, and M. Ribes
- 56 Optimization of Physicochemical Characteristics of a Lithium Anode Interface for High-Efficiency Cycling
M. Ishikawa and M. Morita

**Abstract
Number**

- 57 Improved Carbon Anode Properties: Pretreatment of Particles in Polyelectrolyte Solution
M. Gaberscek, M. Bele, R. Dominko, J. Drofenik, and S. Pejovnik
- 58 Graphite-Tin Composites as Anode Materials for Lithium-ion Batteries
G.X. Wang, J.-H. Ann, L. Sun, M.J. Lindsay, D.H. Bradhurst, S.X. Dou, and H.K. Liu
- 59 Study on Electrochemical Behavior of Carbon Materials for Lithium-Ion Battery
D. Wang, Y. Gao, D. Wang, Z. Li, X. Ping, and X. Wang
- 60 On The Possibility of forming Superdense Lithium Graphite Intercalation Compounds by Electrochemical Means
E. Peled, D. Bar Tow, V. Yufit, and Y. Rosenberg
- 61 Charge/Discharge Characteristics of the Coal-tar Pitch Carbon as Negative Electrodes in Li-Ion Batteries
J.-S. Kim and Y.-T. Park
- 62 Fast Electrochemical Formation of Nanostructure Alloys as Anodes in Lithium - Ion Batteries
E. Peled, A. Ulus, and Y. Rosenberg
- 63 Irreversibility Compensation of SnO Anodes by $\text{Li}_{2.6}\text{Co}_0.4\text{N}$
J. Yang, Y. Takeda, N. Imanishi, and O. Yamamoto
- 64 Impedance Measurements of Graphite Negative Electrode for Lithium-Ion Batteries
K. Sawai and T. Ohzuku
- 65 Direct Evidence on Anomalous Expansion of Graphite Negative Electrodes on 1st Charge by Dilatometry
T. Ohzuku, N. Matoba, and K. Sawai
- 66 Dispersed Silicon-Graphite Powder: A High Capacity Anode Material for Rechargeable Lithium-Ion Batteries
J. Niu and J. Lee
- 67 Electrochemical Performance of $\text{Pb}_3(\text{PO}_4)_2$ Anodes in Secondary Lithium Batteries
L. Zhaolin and L. J.Y.
- 68 Electrochemical/Interfacial Studies of Carbon Films in Non-aqueous Electrolytes
D. Alliata, R. Kostecki, X. Song, K. Kinoshita, and R. Koetz
- 69 Reversible Reaction of Li with Grain Boundary Atoms in SnMn_3C
L. Beaulieu, D. Larcher, R. Dunlap, and J. Dahn
- 70 The Influence of the Structure of Initial Material and the Ways of Its Modification on Electrochemical Properties of the Graphite Anodes in Lithium-Ion Systems.
E. Shembel, N. Globa, N. Zaderey, A. Baskevich, O. Ksenzhek, K. Kylyvnyk, T. Pastushkin, L. Vishnyakov, and V. Kokhany
- 71 Nitride Electrode for Rechargeable Lithium Battery
Y. Nitta, J. Yamaura, M. Hasegawa, S. Tsutsumi, H. Ohzono, and H. Miyake
- 72 Nano-Crystalline Multi-Phase Materials from the Ternary System Ag-Sb-Sn as New Anodes with Increased Lithium Storage Capacities
M. Wachtler, J.H. Albering, M. Winter, and J.O. Besenhard
- 73 Influence of the Binder on the Cycling Performance of Composite Electrodes with Nano-Structured Lithium Storage Metals and Alloys
M.R. Wagner, M. Wachtler, M. Schmied, P. Preishuber-Pfogl, F. Stelzer, J.O. Besenhard, and M. Winter
- 74 Anion Intercalation into Heat-Treated XP3 Coke
J.A. Seel and J.R. Dahn
- 75 Metallic Anode Materials for Li-ion Batteries
G. Ehrlich, C. Durand, M. Hetzel, J. McGuinn, X. Chen, T. Hugener, F. Speiss, and S. Suib
- 76 Relation Between Surface Properties and First-Cycle Irreversible Charge Loss of Graphite Electrodes for Lithium-Ion Batteries
F. Joho, B. Rykart, B. Andreas, P. Novak, and S. Michael E.
- 77 Origins of Reversible and Irreversible Capacity Losses of Graphite-Lithium Anode
A. Martinent and R. Yazami
- 78 Nanocrystalline Mg_2Sn As an Anode Materials for Li-ion Battery
H. Kim, Y.-J. Kim, D.-G. Kim, H.-J. Sohn, T. Kang, and B. Park
- 79 Al-Based Active/Inactive Composite Anodes for Lithium Rechargeable Batteries
G.-J. Jeong, Y.-U. Kim, H.-J. Sohn, T. Kang, H.-R. Kang, and S.-W. Kim
- 80 The Effect of Electrolyte Temperature on the Passivity of Solid Electrolyte Interphase formed on Graphite Electrode
S.-I. Pyun and S.-B. Lee
- 81 Improvement of Charge/Discharge Characteristics of Al-X-Li Alloys by Means of Varying the Alloy Composition.
G. Vladimir, O. Victoria, and B. Aleksey
- 82 Carbon Electrode Morphology and Thermal Stability of the Passivation Layer
L. Fransson, A.M. Andersson, A. Hussénius, and K. Edstrom

**Abstract
Number**

- 83 Thermal Stability of a Hopp/Liquid Electrolyte Interface Using *In Situ* Electrochemical Atomic Force Microscopy
K. Edström and M. Herranen
- 84 CaSi_2 : A New Anode Material for Lithium-Ion Batteries
S.R.S. Prabakaran, T.T. Yong, and S. Michael
- 85 The Correlation Among Surface Chemistry, 3D Structure, Morphology, Electrochemical and Impedance Behavior of Lithiated Carbon Electrodes
D. Aurbach, J. Gnanaraj, J. Fischer, and A. Claye
- 86 A Comparison Between the Electrochemical Behavior of Reversible Magnesium and Lithium Electrodes
D. Aurbach, Y. Gofer, A. Schechter, O. Chusid, H. Gizbar, Y. Cohen, M. Moshkovich, and R. Turgeman
- 87 Novel SnS_2 Anode for Rechargeable Lithium Battery
T. Momma, N. Shiraishi, T. Osaka, A. Gedanken, J. Zhu, and L. Sominski
- 88 The Effects of Electrolyte Composition on the Electrochemical Behavior of Li-Alloy Electrode
G.-J. Jeong, Y.-J. Kim, H. Kim, H.-J. Sohn, and T. Kang
- 89 Amorphous Sn-Ca Alloy as Lithium Ion Battery Anode
L. Fang and B.V.R. Chowdari
- 90 Influence of Edge and Basal Plane Sites on the Electrochemical Behavior of Flake-Like Natural Graphite for Li-Ion Batteries
K.V. Zaghib, G. Nadeau, and K. Kinoshita
- 91 Nanoparticle Size Carbon Materials for Lithium Batteries
B. Banov
- 92 Study on $\text{Li}[\text{Li}_{1/3}\text{Ti}_{5/3}]\text{O}_4$ as Anode Material for Lithium Ion Batteries
M. Arrabito, S. Panero, P. Reale, and B. Scrosati
- 93 *In Situ* TEM Study of the Interface Carbon/Electrolyte
M. Dolle, S. Grugeon, A. Cressent, B. Beaudoin, L. Dupont, and J.-M. Tarascon
- 94 The Electrochemical Behaviour and Structural Changes of Tin-Lead Anodes During Li Reversible Insertion
A. Momtchilov
- 95 Aggregation and Li_2O Formation Reaction in the Sn-Based Oxide Anodes
Y.-J. Kim, H.-J. Sohn, and T. Kang
- 96 Capacity Losses and Cycle Behaviors in Sn-Based Anodes
Y.-J. Kim, H.-J. Sohn, and T. Kang
- 97 Hard Carbon Prepared from Anthracite Coal for Lithium Ion Batteries
I. Mochida, C.-H. Ku, Y.-J. Kim, and Y. Korai
- 98 Development and Manufacturing of the Lithium Sources and Novel Generation Electrode's Materials in Novosibirsk
V. Afanasjev, V. Rozhkov, A. Alexandrov, V. Moukhin, V. Mitkin, V. Purgin, V. Sergeev, A. Gorev,
M. Medjutov, V. Telezhkin, A. Enin, V. Yakimov, B. Antipenko, and V. Ogarkov
- 99 Aluminum Negative Electrode in Lithium Ion Batteries
Y. Hamon, T. Brousse, F. Jousse, P. Topart, P. Buvat, and D.M. Schleich
- 100 Influence of Particle Size and Matrix in "Metal" Anodes for Li-ion Cells
O. Crosnier, X. Devaux, T. Brousse, P. Fragnaud, and D.M. Schleich
- 101 Mechanically Alloyed Sn-V Powders as Anode Materials for Lithium-ion Batteries
Y. Xia, T. Sakai, T. Fujieda, K. Tatsumi, S. Sakurai, and A. Kawabata
- 102 TPD/GC-MS Analysis of Solid Electrolyte Interface in Propylene Carbonate/Ethylene Sulfite Electrolyte on Graphite Anode for Lithium Batteries
H. Ota, T. Sato, H. Suzuki, and T. Usami
- 103 ^7Li -NMR Study on Li^+ Storage/De-Storage Mechanisms in Non-Graphitizable Carbons
C.W. Park, J.K. Hong, and S.M. Oh
- 104 Mg_2Sn : A New Anode Material for Rechargeable Lithium Batteries
H. Sakaguchi, M. Kubota, H. Honda, and T. Esaka
- 105 Surface Condition and Conductivity Homogeneity Are the Key Factors for Obtaining High Power and Long Life Carbon Anode of Li-ion Battery
J. Suzuki, M. Yoshida, K. Yamaguchi, M. Kikuchi, K. Sekine, and T. Takamura
- 106 Graphite-Metal Oxide Composites as Anode for Li-ion Batteries
H. Huang, E. Kelder, and J. Schoonman
- 107 Key Factors for Material Designing of High Power Carbon Anode of Li-Ion Secondary Battery
T. Takamura, J. Suzuki, K. Yamaguchi, T. Katsuta, and K. Sekine
- 108 Doped Tin Oxides as Potential Lithium Ion Battery Negative Electrodes: Effects of Milling Process
F. Belliard and J.T.S. Irvine
- 109 Novel Tin Oxide Based Anodes for Li-Ion Batteries
P.A. Connor and J.T.S. Irvine

**Abstract
Number**

- 110 The Effect of Lithium Insertion on the Structure of Tin Oxide Based Glasses
C. Gejke, E. Zanghellini, L. Börjesson, L. Fransson, and K. Edström
- 111 Electrochemical Properties of Tin-Containing Thin Films
H. Kobayashi, Y. Uebou, T. Ishida, S. Tamura, S. Mochizuki, T. Mihara, M. Tabuchi, H. Kageyama, Y. Yamamoto, M. Matsuoka, and J. Tamaki
- 112 Antimony Doping Effect on the Electrochemical Behavior of SnO₂ Thin Film Electrodes
J. Santos-Pena, T. Brousse, L. Sanchez, J. Morales, and D. Schleich
- 113 Investigation of Solvated and Unsolvated Lithium Intercalation Processes into Graphitic Carbons by Electrochemical Dilatometry
G.H. Wrodnigg, P. Novák, J.O. Besenhard, and M. Winter
- 114 Stress Effect on Cycle Properties of the Silicon Thinfilm Anode
S.-J. Lee, J.-K. Lee, H.-K. Baik, and S.-M. Lee
- 115 Electrochemical Properties of MnV₂O₆ and Its Derivatives as New Anode Material for Lithium Secondary Battery
S.-S. Kim, Y. Suzuki, H. Ikuta, and M. Wakihara
- 116 Thermally Oxidised Graphites as Anodea for Lithium-Ion Cells
M. Natchi, R. Meenakshisundaram, T. Prem Kumar, A. Manuel Stephan, V. Subramanian, S. Gopukumar, and N.G. Renganathan
- 117 X-ray Absorption Study of Cobalt Vanadates During Cycling Usable as Negative Electrode in Lithium Battery
S. Laruelle, P. Poizot, E. Baudrin, V. Briois, M. Touboul, and J.-M. Tarascon
- 118 Reversible Li Uptake in Fe₃BO₆, a New Anode Material
J. Gaubicher, L. Nazar, and J. Rowsell
- 119 Structural and Mechanistic Studies of Intermetallic Electrodes
J. Vaughey, C. Johnson, B. Roy, M. Thackeray, L. Fransson, K. Edstrom, and J. Thomas
- 120 Modified Carbons for Improved Anodes in Lithium Ion Cells
H. Buqa, P. Golob, M. Winter, and J.O. Besenhard
- 121 Surface Modification of Graphite Anodes by Combination of High Temperature Gas-Treatment and Silylation in Nonaqueous Solution
M. Santis, H. Buqa, C. Grogger, J. Besenhard, and M. Winter
- 122 Effects of Synthesis Condition of Graphitic Carbon Tube on Anodic Property of Li Ion Battery
T. Ishihara, A. Kawahara, H. Nishiguchi, M. Yoshio, and Y. Takita
- 123 Anodic Property of Graphitic Carbon Nanotube in Propylene Carbonate Based Organic Electrolyte
A. Kawahara, T. Ishihara, H. Nishiguchi, M. Yoshio, and Y. Takita
- 124 Improved Rate Performance of Active Materials Coated on Surface-Modified Carbon Black
H. Huang and L. Nazar
- 125 Electrochemistry and Impedance Analysis of Intermetallic Electrodes for Lithium-Ion Batteries
C.S. Johnson, J.T. Vaughey, D.W. Dees, A.N. Jansen, M.M. Thackeray, T. Sarakonsri, and S.A. Hackney
- 126 Benchmark Study on High Performing Carbon Anode Materials
C. Lampe-Onnerud, J. Shi, B. Barnett, and P. Onnerud
- 127 Effects of SEI on the Kinetics of Lithium Intercalation
R. Bugga, M. Smart, and S. Surampudi
- 128 *In Situ* AFM Observation of Lithium Deposition at Elevated Temperatures
R. Mogi, M. Inaba, T. Abe, and Z. Ogumi
- 129 Boronated Mesophase Pitch Coke for Lithium Insertion
E. Frackowiak, J. Machnikowski, and F. Beguin
- 130 A Composite Carbonaceous Anode Material for Lithium Ion Batteries
G. Zhang, J. Han, C. Du, Y. Chen, and Q. Liu
- 131 Electrochemical Lithium Intercalation in TiO₂ with Ramsdellite Structure
R. Amandi, A. Kuhn, and F. Garcia-Alvarado
- 132 Investigation of Lead Tin Fluorides as Possible Negative Electrodes for LI-Ion Batteries
L. Garza, P. Connor, F. Belliard, L. Torres, and J. Irvine
- 133 A Microtextural Approach of Lithium Insertion in Hard Carbons : The "Corridor" Model
S. Gautier, E. Frackowiak, F. Chevallier, J.N. Rouzaud, and F. Beguin
- 134 Neutron Diffraction Studies on Lithium Non-Graphitizable Carbon
R. Kanno, A. Hirano, T. Kaminya, K. Tatsumi, M.A. Mostafa, M. Furusaka, and T. Otomo
- 135 Investigation of the Solid Electrolyte Interface Film on the Graphitic Anodes Surface
D. Zane, A. Antonini, and M. Pasquali

**Abstract
Number**

- 136 Determination of the Ratio of Basal Plane Surfaces and Prismatic Surfaces of Graphites And its Impact on Graphite Anode Performance in Lithium Ion Batteries
J.P. Olivier, P. Golob, and M. Winter
- 137 First Principles Calculations for Li Insertion into InSb
R. Benedek, M. Thackeray, L. Yang, and R. Prasad
- 138 Phase Separation and Amorphization in Lithium Inserted Cu-In-Sn Sulfospinels. Theoretical and Experimental Approach
R. Dedryvére, S. Denis, P.E. Lippens, J. Olivier-Fourcade, and J.-C. Jumas
- 139 Experimental and Theoretical Analysis of Li Insertion Mechanisms in Anode Materials
J. Chouvin, P.E. Lippens, C. Pérez Vicente, J. Olivier-Fourcade, and J.-C. Jumas
- 140 The Effects of Chemical Composition of Adsorbed Organic Molecular Layers on Lithium Electrode/Polymer Electrolyte Interface Stabilization
M. Le Granvalet-Mancini, S. Gadad, and D. Teeters
- 141 Synthesis and Characterization of $\text{Li}_2\text{Mn}_4\text{O}_9$ Cathode Material
W.P. Kilroy, W.A. Ferrando, and S. Dallek
- 142 Preparation and Characterization of $\text{Li}_{1+x}\text{Co}_y\text{Mn}_{2-y}\text{O}_4$ Spinel for Lithium Battery Applications
B.W. Lee and S.H. Kim
- 143 Highly Rechargeable $\text{Li}_x\text{Mn}_{1-y}\text{Me}_y\text{O}_2$ Mixed Oxides Synthesized via LT Techniques
S. Franger, S. Bach, J.-P. Pereira-Ramos, and N. Baffier
- 144 Voltage Prediction from Coulomb Potential Created by Atoms of a Cathode Active Material for Li Ion Cells
J.-I. Yamaki, M. Egashira, and S. Okada
- 145 Influences of the Electrolyte Composition on the Charge and Discharge Characteristics of $\text{LiCr}_{0.1}\text{Mn}_{1.9}\text{O}_4$ Positive Electrode
M. Morita, T. Nakagawa, O. Yamada, N. Yoshimoto, and M. Ishikawa
- 146 Cathode Material For Primary Lithium Cells Based On Modified Manganese Dioxide
N.D. Ivanova, Y.Y. Boldyrev, and G.V. Sokolsky
- 147 Advantages of $\text{LiNi}_{0.8}\text{Co}_{0.2}\text{O}_2$ Blending into $\text{Li}_{1+x}\text{Mn}_{2-x}\text{O}_4$ Cathode
T. Numata, C. Kanbe, M. Shirakata, and M. Yonezawa
- 148 Pyrolysis/GC/MS Analysis of the Surface Film Formed on Graphite Negative Electrode
Z. Ogumi, A. Sano, M. Inaba, and T. Abe
- 149 Corrosion of Cathodic Sulphide Materials in Melted Ionic Salt Electrolytes
V.A. Dusheiko, V.V. Radshenko, and V.U. Buryak
- 150 A Novel Method for Preparing Lithium Manganese Oxides and its Electrochemical Characteristics
Y. Azuma, K. Katayama, and M. Suhara
- 151 Structure and Electrochemical Properties of the New Layered $\text{Li}_3\text{Cu}_2\text{O}_4$ and $\text{Li}_2\text{Na}_{0.687}\text{Li}_{0.313}\text{Cu}_2\text{O}_4$
E. Raekelboom, A. Hector, M. Weller, and J. Owen
- 152 Physical and Electrochemical Characterisation of $\text{LiNi}_{0.8}\text{Co}_{0.2}\text{O}_2$ Thin Film Electrodes Deposited by Laser Ablation
G.X. Wang, M.J. Lindsay, M. Ionescu, D.H. Bradhurst, S.X. Dou, and H.K. Liu
- 153 Effects of Conducting Carbon on the Electrochemical Performance of LiCoO_2 and LiMn_2O_4 Cathodes
Z. LIU, J.Y. LEE, and H.J. LINDNER
- 154 Structure and Electrochemical Properties of $\text{LiSi}_y\text{Co}_{1-y}\text{O}_2$ Cathode for Lithium Rechargeable Battery
T. Zhiyuan, X. Jianjun, L. Jiangang, and C. Gaoping
- 155 Spontaneous Modification of the Electrode Surface in Contact with Non-Aqueous Electrolyte
D. Ostrovskii, P. Jacobsson, F. Ronci, and B. Scrosati
- 156 Improvement of Cycle Performance of Orthorhombic $\text{LiMn}_{0.95-x}\text{M}_x\text{Cr}_{0.05}\text{O}_2$; $\text{M}=\text{Al, Ga, Yb, Y and In}$, Synthesized by Hydrothermal Technique
T. Sakurai, T. Kimura, and T. Sugihara
- 157 Electrochemical Synthesis, Characterization and Lithium Insertion Behavior of $\text{e-M}_{0.15}\text{V}_2\text{O}_5$ Compounds ($\text{M}=\text{Ni}^{2+}, \text{Cu}^{2+}, \text{Mn}^{4+}$)
E. Potiron, A. Le Gal La Salle, A. Verbaere, Y. Piffard, and D. Guyomard
- 158 Synthesis by Sol-Gel Process and Characterization of $\text{LiC}_{r-x}\text{Mn}_{2-x}\text{O}_4$ Cathode Materials
T. Zhiyuan, L. Jiangang, X. Jianjun, and C. Gaoping
- 159 Lithiated Electrolytic Oxides of d-Metals in Cathodes of Lithium Accumulators
E. Shembel, R. Apostolova, V. Nagirny, D. Aurbach, and B. Markovsky
- 160 Improved LiCoO_2 for Li-ion Battery Applications
Y. Gao, M. Yakovleva, and J. Engel
- 161 Li-Insertion Behavior in Nanocrystalline $\text{TiO}_2\text{-(MoO}_3)_2$ Core-Shell Materials
G. Moore, A. Le Gal La Salle, D. Guyomard, and S. Elder

**Abstract
Number**

- 162 Relationship Between Cycling Performance and Structural Phase Transitions of $\text{Li}_{1+y}\text{Mn}_{2-y}\text{O}_4$ Cathode Materials Studied by Synchrotron X-ray Diffraction
X.-Q. Yang, X. Sun, M. Balasubramanian, J. McBreen, Y. Xia, T. Sakai, and M. Yoshio
- 163 Preparation and Electrochemical Properties of $\text{LiAl}_y\text{Mn}_{2-y}\text{O}_4$
Q. Zhong, J. Faiers, and U. von Sacken
- 164 New Phases and Phase Transitions Observed in Over-Charged States of LiCoO_2 based Cathode Materials
X. Sun, X.-Q. Yang, J. McBreen, Y. Gao, M. Yakovleva, X.-K. Xing, and M. Daroux
- 165 Structural Behavior of Some NASICON Compounds upon Lithium Electrochemical Intercalation/Deintercalation
J. Gaubicher, G. Vaughan, C. Masquelier, C. Wurm, Y. Chabre, and L. Nazar
- 166 Electroactivity of Natural and Synthetic Triphylite
N. Ravet, Y. Chouinard, J.-F. Magnan, S. Besner, M. Gauthier, and M. Armand
- 167 The Kinetics of Lithium Transport Through $\text{Li}_{1-d}\text{CoO}_2$ Thin Film Electrode by Theoretical Analysis of Current Transient and Cyclic Voltammogram
S.-I. Pyun and H.-C. Shin
- 168 Lithium Transport Through $\text{Li}_{1-d}\text{Mn}_2\text{O}_4$ Electrode Involving the Ordering of Lithium Ions
S.-I. Pyun and S.-W. Kim
- 169 Analysis of Lithium Transport Through Vanadium Pentoxide by Using Potentiostatic Current Transient Technique
S.-I. Pyun and M.-H. Lee
- 170 Synthesis of $\text{LiAl}_y\text{Co}_{1-y}\text{O}_2$ Using Acrylic Acid and its Electrochemical Properties for Li Rechargeable Batteries
K.Y. Chung, W.-S. Yoon, and K.-B. Kim
- 171 A Study on the Effect of Lithium Deintercalation on the Local Structure of $\text{LiAl}_y\text{Co}_{1-y}\text{O}_2$ Cathodes Using X-ray Absorption Spectroscopy
W.-S. Yoon, K.-K. Lee, and K.-B. Kim
- 172 Electrochemical Characterization of Layered LiCoO_2 Films Prepared by Electrostatic Spray Deposition
S.-H. Ban, W.-S. Yoon, and K.-B. Kim
- 173 Electrical and Thermal Properties of $\text{LiNi}_{1-y}\text{Co}_y\text{O}_2$ ($0 \leq y \leq 0.2$) During Initial Cycle
K.-K. Lee, W.-S. Yoon, and K.-B. Kim
- 174 Characterization of $\text{LiNi}_{0.85}\text{Co}_{0.10}\text{M}_{0.05}\text{O}_2$ ($\text{M}=\text{Co}, \text{Al}, \text{Fe}$) for Lithium Secondary Batteries
K.-K. Lee, W.-S. Yoon, and K.-B. Kim
- 175 Correlation Between Structural and Electrochemical Properties of Some Lithium-Metal Vanadates
M. Arrabito, S. Bodoardo, N. Penazzi, S. Panero, B. Scrosati, X. Guo, Y. Wang, and S. Greenbaum
- 176 Mechanisms of Manganese Spinel Dissolution and Capacity Fade at High Temperature
T. Aoshima, K. Okahara, C. Kiyohara, and K. Shizuka
- 177 Defect Structure of Li-Mn-O Spinel Prepared at Different Annealing Temperatures
S. Ishida and K. Numata
- 178 On the Correlation Between the Electroanalytical Behavior and Crystallographic Features of Li Intercalation Electrodes
D. Aurbach, M. Levi, E. Levi, U. Heider, R. Oesten, and M. Schmidt
- 179 Li Insertion into Thin Vacuum-Deposited V_2O_5 Films Characterized by a Variety of *In Situ* Techniques
D. Aurbach, M. Levi, L. Zhonghua, M. Moskovich, Y. Cohen, Y. Cohen, and E. Levi
- 180 Study of Lithium Insertion into Electrochemically Synthesized Sodium Vanadate
D. Aurbach, B. Markovsky, G. Salitra, Y. Cohen, E. Shembel, R. Apostolova, and V. Nagirny
- 181 Characterization of LiFePO_4 as the Cathode Material for Rechargeable Lithium Batteries
M. Takahashi, S. Tobishima, K. Takei, and Y. Sakurai
- 182 Magnesium Insertion into $\text{Mg}_{0.5+y}(\text{Fe}_y\text{Ti}_{1-y})_2(\text{PO}_4)_3$
K. Makino, Y. Katayama, T. Miura, and T. Kishi
- 183 Preparation of Todorokite MnO_2 for Rechargeable Battery Cathode
N. Kumagai, S. Komaba, H. Sakai, and N. Kumagai
- 184 A Study on the Preparation and Characterization of Au-Codeposited LiMn_2O_4 Electrode
M.-R. Lim and K.-B. Kim
- 185 Lithium and Proton Insertion in Spinel Structured Manganese Oxides
M.S. Islam, B. Ammundsen, and J. Roziere
- 186 Synthesis and Characterization of Nonstoichiometric LiCoO_2
M. Fujii, N. Imanishi, and Y. Takeda
- 187 Yttrium-Doped $\text{Li}(\text{Ni},\text{Co})\text{O}_2$: An Improved Cathode for Li-Ion Battery
G.V.S. Rao, B.V.R. Chowdari, and H.J. Lindner
- 188 Electrochemical Properties of Li-Mn-Spinel Using Hydrothermal Method
T. Kanasaku, K. Amezawa, and N. Yamamoto

**Abstract
Number**

- 189 Synthesis Process of Lithiated or Overlithiated Manganese Oxide Active Materials for Positive Electrode
H. Rouault, F. Le Cras, C. Bourbon, and D. Bloch
- 190 General Behaviour Upon Cycling of LiNiVO_4 as Battery Electrode
C. Rossignol and G. Ouvrard
- 191 Microimpedance Spectroscopy of Cathode Materials Prepared from Polyelectrolyte-Pretreated Particles
A. Sever Skapin, M. Bele, J. Drofenik, R. Dominko, S. Pejovnik, and M. Gaberscek
- 192 $\text{Li}_2\text{Mn}_4\text{O}_9$ Revisited: Crystallographic and Electrochemical Studies
P. Strobel, A. Ibarra Palos, and M. Anne
- 193 Structural and Electrochemical Studies of Layered $\text{Li}(\text{Mn}_{1-y}\text{M})\text{O}_2$ Based Compounds. I. $\text{M} = \text{Co}$
A.D. Robertson, A.R. Armstrong, A.J. Fowkes, and P.G. Bruce
- 194 Cyclic Voltammetric Study on Stoichiometric Spinel LiMn_2O_4 Electrode at Elevated Temperature
S. Ma, H. Noguchi, and M. Yoshio
- 195 Electrical Conductivity and Structural Behaviour of $\text{Li}_{1+x}\text{MM}'(\text{PO}_4)_3$ ($\text{M}, \text{M}' = \text{Fe}, \text{Zr}, \text{Ti}$) Phases
C.M. Mari, R. Ruffo, and M. Catti
- 196 $\gamma\text{-MnO}_2$ Compounds as Insertion Hosts for Li^+ and H^+
S. Sylvère, J. Séverine, L.G.L.S. Annie, P. Yves, and G. Dominique
- 197 Charge Ordering in $\text{Li}_{0.5}\text{CoO}_2$? A Single-Crystal XRD Study
J. Höwing, T. Gustafsson, J. Thomas, and H. Sakaebe
- 198 Synthesis of $\text{Li}_2\text{M}_{1+x}\text{Mn}_{3-x}\text{O}_8$ ($\text{M} = \text{Co}, \text{Fe}$) as Positive Active Material for Lithium Cells
S. Panero, D. Satolli, and B. Scrosati
- 199 Lithiated Cobaltates for Li-Ion Batteries. Structure, Morphology and Electrochemistry of Oxides Grown by Solid-State Reaction, Wet Chemistry and Film Deposition
J. Christian
- 200 Evidence for Structural Defects in Non-Stoichiometric HT- LiCoO_2 : Electrochemical, Electronic Properties and Li MAS NMR Studies
S. Levasseur, M. Menetrier, and C. Delmas
- 201 Synthesis of Nanocrystalline Layered Manganese Oxides by the Electrochemical Reduction of AMnO_4 ($\text{A} = \text{K}, \text{Li}$)
G. Moore, R. Portal, A. Le Gal La Salle, and D. Guyomard
- 202 LiMBO_3 ($\text{M} = \text{Mn}, \text{Fe}, \text{Co}$) Orthoborates : Synthesis, Crystal Structure and Lithium Desinsertion/Insertion Properties
L. Vanessa, L.G.L.S. Annie, P. Yves, V. Alain, and G. Dominique
- 203 Electrochemical Investigations of Pure and Poped Lithium Cobaltate
A. Momtchilov
- 204 Electrochemical and *In Situ* Structural Investigation of $\text{Li}_x\text{Ni}_{0.08}\text{Co}_{0.02}\text{O}_2$
A. D'Epifanio, F. Croce, L. Persi, F. Ronci, and B. Scrosati
- 205 Synchrotron X-Ray Diffraction Study of the Spinel LiMn_2O_4 at Low Temperatures
G. Rousse, C. Masquelier, J. Rodriguez-Carvajal, E. Elkaim, and J.-P. Lauriat
- 206 Electrochemical Performances of Different Li- VOPO_4 Systems
N. Dupré, J. Angenault, G. Wallez, and M. Quarton
- 207 Structural Transformation Associated with the Extra 3.3 and 4.5V in Spinel LiMn_2O_2
R. Gwenaëlle, D. Loic, H. Maryvonne, M. Mathieu, P. Maria Rosa, M. Christian, and T. Jean-Marie
- 208 Influence of the Synthesis Conditions of LiMn_2O_4 on the Extent of the Spinel to Double Hexagonal Transformation Associated to the Anomalous 3.3/3.95 V and 4.5 V Redox Steps
R.M. Palacin, G. Rousse, M. Morcrette, L. Dupont, C. Masquelier, Y. Chabre, and J.-M. Tarascon
- 209 Performance and Mechanical Safety of 26650-size Mn-spinel Li-ion Cells for High Power Applications
A.M. Wilson, W. Chow, and U. von Sacken
- 210 Use of Aluminum Vanadates as Cathodes in Lithium Rechargeable Cells
E. Andrukaitis, I. Hill, and G. Torlone
- 211 Boron Additives to Lithiated Cobalt Dioxide and Lithiated Nickel-Cobalt Dioxide for Lithium Ion Cells
G. Blomgren
- 212 Manganese Spinel Li-ion Cells With Improved High Temperature Characteristics
W. Chow, M. Zhang, Y. Wang, J. Reimers, and U. von Sacken
- 213 Mechanochemical Synthesis Of $\text{Li}_y\text{Mn}_2\text{O}_{4-d}$: Positive Electrode for Lithium Batteries
S. Soiron, A. Rougier, L. Aymard, and J.M. Tarascon
- 214 Two-Phase LiCoO_2 based Oxides for Rechargeable Lithium Batteries
F. Croce, H.-P. Lin, A. Shiao, M. Salomon, J. Wolfenstine, W. Lada, A. Deptula, and D. Chua
- 215 Defect Spinel $\text{Li}_{8/n+4}\text{Mn}_{8/n+4}\text{O}_4$ Cathode Materials for Lithium Polymer Batteries
Y. Xia, K. Takahashi, T. Sakai, K. Tatsumi, T. Fejieda, and M. Yoshio

**Abstract
Number**

- 216 ⁷Li MAS-NMR and Electrochemical Studies of LiMn₂O₄-Based Spinel for Lithium Rechargeable Batteries
M.C. Tucker, J.A. Reimer, and E.J. Cairns
- 217 Mechanochemical Way for Preparation of Disordered Lithium-Manganese Spinel Compounds
N. Kosova, E. Devyatkina, N. Uvarov, and S. Kozlova
- 218 *In Situ* XAFS Analysis of the Li Deintercalation Process of Li(Mn, M)₂O₄ (M=Cr, Co, Ni), Cathode Materials for 5V Lithium Batteries
I. Nakai
- 219 ESR Analysis of Electrochemical Oxidation on Cathode in a Lithium Ion Battery
H. Kurokawa, T. Ota, S. Matsuta, Y. Kato, S. Yoshimura, S. Fujitani, and I. Yonezu
- 220 Preparation of Lithium Manganese Oxides Including Iron
M. Tabuchi, H. Shigemura, K. Ado, H. Kobayashi, H. Sakaebe, H. Kageyama, and R. Kanno
- 221 *In Situ* Neutron Powder Diffraction Analysis of the Li Deintercalation Process of Li_{1.1}Mn_{1.9}O₄
Y. Terada
- 222 *In Situ* Total Reflection X-ray Fluorescence Analysis of Mn Dissolution from LiMn₂O₄ During Charge-Discharge Process of the Li Secondary Battery
Y. Nishiwaki, Y. Terada, and I. Nakai
- 223 Lithium Ion Transport Through LiCoO₂ Thin-Film Electrode Under Intercalation-Induced Stress
J.-K. Lee, S.-J. Lee, H.-K. Baik, and S.-M. Lee
- 224 Local Structure of Substituted Layered LiMnO₂ Cathode Materials Probed by X-ray Absorption Fine Structure and ⁶Li Nuclear Magnetic Resonance
B. Ammundsen, H. Desilvestro, R. Steiner, P. Pickering, D. Jones, J. Roziere, Y.J. Lee, C. Pan, and C. Grey
- 225 LiMoVO₆ - A Candidate Cathode Material for Solid-Polymer Batteries at Elevated Temperatures
H. Sakaebe, M. Shikano, Y. Xia, T. Sakai, T. Eriksson, T. Gustafsson, and J. Thomas
- 226 Structure, Phase Relationship and Transitions in Lithium Manganese Oxide Spinel
R. Kanno, M. Yonemura, Y. Kawamoto, M. Tabuchi, and T. Kamiyama
- 227 Storage and Cycling Performance of Stoichiometric Spinel at Elevated Temperatures
X. Wang, Y. Yagi, Y. Xia, T. Sakai and M. Yoshio
- 228 Capacity Failure of Lithium Manganese Oxide Spinel Cathode at Elevated Temperature
M. Okada, K. Kamioka, T. Mouri, and M. Yoshio
- 229 Synthesis and Characterization of Lithium Manganese Oxides for Rechargeable 3 V Lithium Batteries
A. Perner, M. Wohlfahrt-Mehrens, K. Holl, J. Garche, and D. Ilic
- 230 MALDI-MS Spectroscopic Analysis of Products on LiMn₂O₄ Electrode
T. Fukushima, Y. Matsuda, T. Abura, and R. Arakawa
- 231 Effect of Aluminum Addition in Co Substituted Ni Oxide Cathodes
M. Kanda, Y. Tatebayashi, M. Sekino, Y. Isozaki, and I. Mitsuishi
- 232 Cathode Properties of Phospho-Olivine LiMPO₄ for Lithium Secondary Batteries
S. Okada, S. Sawa, M. Egashira, J.-I. Yamaki, M. Tabuchi, H. Kageyama, T. Konishi, and A. Yoshino
- 233 Soft-Combustion Synthesis of a New Cathode-Active Material, LiVWO₆, for Li-Ion Batteries
S.R.S. Prabakaran, C.C. Pei, A.F. Mohd Noor, and M.S. Michael
- 234 Electrochemical Characterization of a New High Capacity Cathode
C. Storey, I. Kargina, Y. Grincourt, I. Davidson, Y. Yoo, and D.-Y. Seung
- 235 Continuous Production of Cathode Materials for Lithium Batteries by Hydrothermal Synthesis Under Supercritical Condition
Y. Hakuta, T. Adschiri, K. Kanamura, and K. Arai
- 236 Synthesis, Structure, and Charge-Discharge Characteristics of the New Layered Oxides at Li_{1.8}Ir_{0.6}M_{0.6}O₃ (M=Fe, Co, Ni)
H. Kobayashi, M. Waki, Y. Uebou, M. Tabuchi, H. Kageyama, Y. Takigawa, Y. Yamamoto, M. Matsuoka, and J. Tamaki
- 237 The Li_{1-x}(Ni_{1-y}Mg_y)_{1+z}O₂ System: Structural Modifications Observed Upon Cycling
C. Pouillier, L. Croguennec, P. Biensan, P. Willmann, and C. Delmas
- 238 Synthesis and Characterization of LiFe_xCo_{1-y}O₂ Cathode Materials for Lithium Batteries
S. Venkatachalam, S. R. G. Sukumaran, R. N.G. M. A. M. Natchi, R. Meenakshisundaram, and R. Meenakshisundaram
- 239 Electronic and Electrochemical Properties of Li_xCo_yNi_{1-y}O₂ Cathodes Studied by Impedance Spectroscopy
F. Croce, F. Nobili, R. Tossici, B. Scrosati, L. Persi, and R. Marassi
- 240 Li_{1+d}Mn_{2-d}O₄ Performance Measured by Leaching
E. Kelder, F. Ooms, R. Perego, and J. Schoonman
- 241 Tungsten Oxsulfide Thin Films as Positive Electrode in Lithium Microbatteries
I. Martin-Litas, P. Vinatier, A. Levasseur, J.C. Dupin, and D. Gonbeau

**Abstract
Number**

- 242 Electronic Structure in LiMn_2O_4 Based Spinel Oxides from Transition Metal L-edge and O K-edge XANES
Y. Uchimoto and T. Yao
- 243 Effect of Cr^{6+} on the Jahn-Teller Distortion of Spinel LiMn_2O_4
S. Venkatachalam, V. S. G. Sukumaran, P. T. R. N.G. M. Natchi, and R. Meenakshisundaram
- 244 3 V Manganese Oxide Electrode Materials for Lithium Batteries
C.S. Johnson and M.M. Thackeray
- 245 The Spinel Phases $\text{LiMg}_y\text{Mn}_{2-y}\text{O}_4$ as the Cathode for Rechargeable Lithium Batteries
I.-S. Jeong and H.-B. Gu
- 246 Characterisation of Nanoparticles of LiMn_2O_4 Synthesized by Citric Acid Sol-Gel Method
B.J. Hwang, R. Santhanam, and D.G. Liu
- 247 Theoretical Approach of the Lithium Intercalation in Host Materials
F. Lantelme, H. Groult, and N. Kumagai
- 248 The Influence of the Synthesis Conditions on the Structural and Electrochemical Properties of Cathodes Based on Manganese Oxides in Nonaqueous Electrolytes
E. Shembel, N. Globa, N. Zaderey, V. Pisiy, and K. Kylyvnyk
- 249 A New 3.8V Cathode for Lithium-Ion Batteries: Epsilon- Li_xVOPO_4
T. Kerr, J. Gaubicher, L. Nazar, and H. Huang
- 250 Aluminium Substituted LiCoO_2 as an Intercalation Cathode for Lithium Polymer Battery
S. Venkatachalam, S. Manual. A, V. S. G. Sukumaran, P. T. R. N G, M. Natchi, and R. Meenakshisundaram
- 251 The Jahn-Teller Distortion in Li_xNiO_2 and Li_xMnO_2
C. Marianetti, D. Morgan, and G. Ceder
- 252 Theory of Lithium Diffusion in Li_xCoO_2 : A First Principles Investigation
A. Van der Ven and G. Ceder
- 253 Lithium Insertion of $(\text{V}_{1-y}\text{Moy})_2\text{O}_5$
M. Eguchi, F. Maki, S. Iwabe, and Y. Momose
- 254 Effect of Lanthanum Dopant on the Structural and Electrical Properties of LiCoVO_4 Cathode Materials Investigated by EXAFS
B.-J. Hwang, Y.-W. Tsai, G.T.-K. Fey, and J.-F. Lee
- 255 Long-life Lithium Manganese Spinel Cathodes for High Power Secondary Batteries for Electric Vehicle Use
M. Kasai, Y. Kumashiro, K. Nishimura, H. Andou, Y. Muranaka, Y. Kozono, and T. Horiba
- 256 Synthesis of $\text{Li}_x\text{Co}_{0.085}\text{Cr}_{0.015}\text{O}_2$ by the PVA Precursor Method and Application as Cathode in Lithium Ion Batteries
R. Vasanthi, I. Ruth Mangani, R. Chandrasekaran, and S. Selladurai
- 257 $\text{LiCr}_x\text{Mn}_{2-x}\text{O}_4$ Solid Solutions for Lithium Batteries
R. Thirunakaran, P. Periasamy, B. Ramesh Babu, N. Kalaiselvi, N.G. Renganathan, M. Raghavan, and N. Muniyandi
- 258 Solid-State Synthesis and Characterization of LiCoO_2 and $\text{LiCo}_{1-y}\text{Ni}_y\text{O}_2$ Solid Solutions
P. Periasamy, B. Ramesh Babu, R. Thirunakaran, N. Kalaiselvi, N.G. Renganathan, M. Raghavan, and N. Muniyandi
- 259 Electrochemical Behaviour of $\text{LiMn}_{2-y}\text{MyO}_4$ ($\text{M} = \text{Cu, Cr}$; $0 < y < 0.4$)
B. Ramesh Babu, P. Periasamy, R. Thirunakaran, N. Kalaiselvi, N.G. Renganathan, M. Raghavan, and N. Muniyandi
- 260 Structural and Electrochemical Studies of Layered $\text{Li}(\text{Mn}_{1-y}\text{M}_y\text{O}_2)$ Based Compounds. II $\text{M}=\text{Ni}$
T.E. Quine, M.J. Duncan, P.G. Bruce, A. Robertson, and R. Armstrong
- 261 Iron-Doped Lithium Cobalt Oxides as Lithium Intercalating Cathode Materials
N. Kalaiselvi, P. Periasamy, R. Thirunakaran, B. Ramesh Babu, T. Prem Kumar, N.G. Renganathan, M. Raghavan, and N. Muniyandi
- 262 Redox Reactions of Substituted Lithium Manganese Spinel Compounds in Lithium Cells
Y. Shao-Horn and R. Midaugh
- 263 Electronic Structure of Li_xNiO_y Thin Films
A. Urbano, S. deCastro, R. Landers, J. Morais, M. Fantini, and A. Gorenstein
- 264 Electrochemical Performance of Cathodes Based on LiMn_2O_4 Spinel Obtained by Combustion Synthesis
E. Santiago, S. Amancio, P. Bueno, and L. Bulhøes
- 265 The Structure Property Relationship Of Lithium Nickel Cobalt Oxides
R. Gover, R. Kanno, B. Mitchell, and Y. Kawamoto
- 266 Electrochemical Characteristics of LiMn_2O_4 -Polypyrrole Composite Cathode for Lithium Polymer Batteries
J.-U. Kim, J.-A. Lee, S.-I. Moon, and H.-B. Gu
- 267 Effects of Powder Characteristics of LiMn_2O_4 on the Electrochemical Properties
H.-T. Chung and S.-T. Myung
- 268 Electrocopolymerization of Carbazole Derivatives
A.S. Sarac
- 269 Influence of the Particle Size on the Electrochemical Properties of Lithium Manganese Oxide
C.-H. Lu and S.-W. Lin

**Abstract
Number**

- 270 Synthesis of Nanosized LiMn_2O_4 Powder by Reverse Emulsion Process for Li-Ion Batteries
C.-H. Lu, S.K. Saha, and S.-W. Lin
- 271 High Purity Lithium Carbonate for Batteries Applications
S. Harrison, K. Amouzegar, and G. St-Amant
- 272 Viscosities, Conductivities and Activation Energies for Transport Processes in Liquid Electrolytes. The Quasi Lattice Approach
A. Chagnes, B. Carré, P. Willmann, and D. Lemordant
- 273 Optimisation of the Polyelectrolyte used in Carbon Anode Pretreatment Procedures
R. Dominko, J. Drogenik, M. Bele, S. Pejovnik, and M. Gaberscek
- 274 New Fusible Lithium Salt with High Conductivity in Solutions
W. Xu, M. Videa, and C.A. Angell
- 275 Application to Lithium Battery Electrolyte of Lithium Chelate Compounds with Boron
Y. Sasaki, M. Handa, S. Sekiya, K. Kurashima, and K. Usami
- 276 Microporous PVDF Membrane for Lithium-Ion Batteries
F. Bodin, C. Lenhof, G. Caillon, and I. Olsen
- 277 Synthesis of a New Family of Fluorinated Boronate Compounds as Anion Receptors and Studies of Their Use as Additives in Lithium Battery Electrolytes
H.-S. Lee, X.-Q. Yang, X. Sun, and J. McBreen
- 278 Lithium Bisperfluoroalkylsulfonimides: Primary and Secondary Lithium Battery Electrolyte Salts
S. Boyd, B. Johnson, L. Krause, W. Lamanna, P. Pham, and H. Shimada
- 279 Thermal Stability of LiPF_6 EC:EMC Electrolyte for Lithium Ion Batteries
G. Botte, R. White, and Z. Zhang
- 280 Trans-Esterification of Ethylmethyl carbonate in Lithium Ion Batteries
B. Dobler, I. Exnar, W. Haupt, and R. Imhof
- 281 Kinetic Aspects of HF Generation in a LiPF_6 Based Electrolyte Solution
I. Exnar, B. Dobler, W. Haupt, and R. Imhof
- 282 New Li-Ion Electrolytes for Low Temperature Applications
S. Herreyre, O. Huchet, S. Barusseau, F. Pertion, J.-M. Bodet, and P. Biensan
- 283 Electronic Structures and Electrochemical Properties of $\text{LiPF}_{(6-n)}(\text{CF}_3)_n$
F. Kita, H. Sakata, A. Kawakami, H. Kamizori, T. Sonoda, H. Nagashima, N. Pavlenko, and Y. Yagupolskii
- 284 Asymmetrical Alkyl Carbonate as Solvent for Li-ion Batteries Electrolytes
I. Geoffroy, B. Carre, D. Lemordant, S. Herreyre, and P. Biensan
- 285 Database and Models of Electrolyte Solutions for Lithium Battery
S. Zhang, A. Tsuboi, H. Nakata, and T. Ishikawa
- 286 An Exceptional Additive to the Electrolyte for Lithium-Ion Batteries : The Vinylen Carbonate
B. Philippe, B. Jean-Marie, P. Francoise, B. Michel, J. Christophe, B. Sylvie, H. Sylvie, and S. Bernard
- 287 An Evidence of Preventing the Decomposition of PC at the Surface of Well Graphitized Carbon without Any Additions
K. Yamaguchi, J. Suzuki, M. Saito, T. Katsuta, K. Sekine, and T. Takamura
- 288 Effect of Organic Additives in Electrolyte Solutions on Behavior of Lithium Metal Anode
Y. Matsuda and T. Takemitsu
- 289 Cyclic and Acyclic Sulfites - New Solvents and Electrolyte Additives for Lithium Ion-Batteries with Graphitic Anodes?
G.H. Wrodnigg, J.O. Besenhard, and M. Winter
- 290 Fluorinated Organic Solvents in Electrolytes for Lithium Ion Cells
K.-C. Möller, T. Hodal, W.K. Appel, M. Winter, and J.O. Besenhard
- 291 Performance of Solupor Separator Materials
F.G.B. Ooms, E.M. Kelder, J. Schoonman, N. Gerrits, and G. Calis
- 292 Fast Charge in Non-Aqueous Li Cells: Investigation of a Novel Hybrid Solution
G. Amatucci, F. Badway, and A. DuPasquier
- 293 Temperature and Concentration Effects on the Ionic Transport Behavior of LiAlCl_4 SOCl_2 Electrolyte Solutions
G.T.-K. Fey, W.-K. Liu, and Y.-C. Chang
- 294 Mass Transport and Kinetic Aspects of Thionyl Chloride Reduction at the Platinum Microelectrode
G.T.-K. Fey, M.-C. Hsieh, and Y.-C. Chang
- 295 Novel Superacid-based Lithium Electrolytes for Lithium Ion and Lithium Polymer Rechargeable Batteries
H.V. Venkatesetty
- 296 Interfacial Stability of Lithium Electrode in IPN Electrolytes Based on Crosslinked PEGMEM and PMMA
X. Hou and K.S. Siow
- 297 Diffusion Mechanism in the Cross-Linked Poly(ether) Doped by $\text{LiN}(\text{CF}_3\text{SO}_2)_2$
Y. Aihara, T. Bando, T. Iguchi, J. Kuratomi, K. Sugimoto, and K. Hayamizu

Abstract
Number

- 298 Ion Conduction Mechanism in Solid $\text{Li}_x\text{-P(EO)}_n$ -based Polymer Electrolytes
D. Golodnitsky, E. Lifshits, E. Peled, S. Chung, and S. Greenbaum
- 299 Preparation of Microporous PVDF Based Polymer Electrolytes
H. Huang, H. Wang, and S. Wunder
- 300 Room Temperature Amorphous-Phase Stabilization of PEO-Based Nanocomposite Polymer Electrolytes: An Impedance Spectroscopy Study
F. Croce, L. Persi, and B. Scrosati
- 301 Gel Electrolytes Based on Amphiphilic Copolymers
R. Ljungbäck, P. Gavelin, P. Jannasch, and B. Wesslén
- 302 Ionic Conduction and Electrochemical Properties of New Poly(acrylonitrile-itaconate) Based Gel-electrolyte
Y.W. Kim, M.S. Gong, and B.K. Choi
- 303 Studies of the Interface Between Lithium Deposits and Polymeric Electrolyte Systems Using in situ FTIR Spectroscopy
D. Aurbach, O. Chusid, Y. Gofer, M. Watanabe, T. Momma, and T. Osaka
- 304 Polymeric Gel Electrolyte Reinforced with Glass Fiber Cloth for Lithium Secondary Battery
S.I. Jo, J.-S. Jung, H.-J. Sohn, H.-C. Park, J.H. Chun, H. Kim, and J.-M. Ko
- 305 Polymer Electrolytes Based On Hyperbranched Polymers
T. Itoh, N. Hirata, Z. Wen, M. Kubo, and O. Yamamoto
- 306 Spectroscopic Estimation of Dielectric Constant and Donor Number in Polymer Electrolytes
C.S. Kim, J. Lee, and S.M. Oh
- 307 Electrochemical Properties of Gel Electrolytes
A. Reiche, A. Weinkauff, and B. Sandner
- 308 A Novel PEG-borate Based Solid Polymer Electrolytes; Conductivity and Application to Li-ion Battery
S. Yokoyama, T. Kobayashi, Y. Kato, H. Ikuta, and M. Wakihara
- 309 Determination of Diffusion Co-Efficient of Lithium Ion in Plasticized PVC Electrolytes
S. Manual.A, R. Sudalaimuthu, P. T, R. N.G, R. Meenakshisundaram, and M. Natchi
- 310 Effects of Diethylaluminum Carboxylate and EC/PC on Dielectric Relaxation and Ionic Conductivity of PEO Based Polymer Electrolytes
J. Dygas, B. Misztal-Faraj, F. Krok, Z. Florjanczyk, E. Zygadlo-Monikowska, and E. Rogalska
- 311 Studies of Conductivity and Ionic Mobility in Polymer Gel Electrolytes
H. Hubbard, M. Williamson, and I. Ward
- 312 Conductivity and Structure of Li-Containing Pervoskite Solid Electrolytes
J.-S. Chen and K.-Z. Fung
- 313 Self-Tracking, Solvent-Free Low-Dimensional Polymer Electrolyte Blends with Lithium Salts
Y. Zheng, F. Chia, G. Ungar, and P.V. Wright
- 314 The Role of the Inorganic Oxide in Nanocomposite Polymer and Gel Electrolyte Structure And Ion Transport Mechanism: An NMR Study
S. Greenbaum, S. Chung, Y. Wang, L. Persi, F. Croce, and B. Scrosati
- 315 Plasticising Effect in Phase-Separated Polymer Electrolytes Based on Poly(Ethylene oxide) and Poly(perfluoroethers)
M. Furlani, K. Bandara, and B.-E. Mellander
- 316 Characteristics of PVDF/Pan Based Polymer Electrolyte for Lithium Ion Polymer Battery
J.-A. Lee, J.-U. Kim, G.-C. Park, and H.-B. Gu
- 317 Structure, Porosity and Conductivity of PVdF Films for Polymer Electrolytes
A. Magistris, P. Mustarelli, E. Quartarone, P. Piaggio, and A. Bottino
- 318 Spectroscopic Conductivity Studies on the Ionic Motion in the Electrolytic Complexes (Polyethylene Glycol 400) (LiCl)_x
V. Di Noto, M. Fauri, S. Biscazzo, and M. Vittadello
- 319 Fabrication of All Solid Polymer Electrolytes based on Block-Graft Copolymers
K. Hirahara, M. Ueno, O. Watanabe, and T. Nakanishi
- 320 Power Management: The Path to the Future
J. Barbarello, M. Molz, and R. Hamlen
- 321 High Energy Density, Thin Film, Rechargeable Lithium Batteries for Marine Field Operations
D. Sadoway, A. Mayes, B. Huang, S. Mui, P. Soo, D. Staelin, and C. Cook
- 322 Cycling Performance of 10Wh class Lithium Metal Rechargeable Battery with New-type Lithium Imide Electrolyte
H. Saito and K. Usami
- 323 Fabrication of Composite Electrodes for Rechargeable Lithium Batteries by Using Electrophoretic Deposition Process
K. Kanamura, A. Goto, and T. Umegaki
- 324 Developments in Multichannel Impedance Instrumentation for the Characterization of Energy Storage Devices
A. Hinton and B. Sayers

**Abstract
Number**

- 325 Hydrothermal Synthesis
T. Kanasaku, K. Amezawa, and N. Yamamoto
- 326 New High-Surface-Area 3-Dimensional "On-Chip" Lithium-Ion Microbattery
M. Nathan, D. Haronian, D. Golodnitsky, Y. Lavi, E. Sverdlov, and E. Peled
- 327 Opportunities for Lithium Batteries in Electric Vehicle and Hybrid Electric Vehicle Applications
M. Corbett
- 328 New Thin Lithium-Ion Batteries Using an Organic Liquid Electrolyte with Thermal Stability
N. Takami, M. Sekino, T. Ohsaki, M. Kanda, and M. Yamamoto
- 329 Development of 6Ah Prismatic Cells for High Rate, Low Temperature Applications
G. Ehrlich, M. Hetzel, and S. Slane
- 330 A Study of the Overcharge Reaction of Li-ion Batteries
M.J. Palazzo, R.A. Leising, E.S. Takeuchi, and K.J. Takeuchi
- 331 Fast Charging of Lithium-ion Batteries
J.R. van Beek
- 332 Factors Responsible for Impedance Rise in High Power Lithium Batteries
K. Amine, M. Hammond, J. Liu, C. Chen, D. Dees, A. Jansen, and G. Henriksen
- 333 Promising Modifying Additives for Lithium Power Sources
E. Shembel, O. Chervakov, I. Maksyuta, N. Globa, N. Zaderey, L. Romanovskaya, A. Ribalka, and D. Meshri
- 334 Overcharge Protection Additives for 4 Volt Lithium Ion Batteries
T. Richardson and P. Ross
- 335 Comparative Study of Thermal Behaviors of Various Lithium-ion Batteries
Y. Saito, K. Takano, K. Kanari, A. Negishi, K. Nozaki, and K. Kato
- 336 Thermal Behaviors of Lithium-ion Batteries During Overcharging
Y. Saito, K. Takano, and A. Negishi
- 337 Charge-Discharge Cycle Performance of Lithium Secondary Batteries using Hybrid Carbon as Negative Electrode Materials
K. Yanagida, A. Yanai, Y. Kida, A. Funahashi, T. Nohma, and I. Yonezu
- 338 Cycle Life Estimation of Lithium Secondary Battery by Extrapolation Method and Accelerated Aging Test
T. Katsuhito, K. Kazuma, K. Yo, M. Hajime, T. Nobuyuki, I. Toru, and T. Toshikatsu
- 339 A New Method to Study Li-Ion Cell Safety: Laser Beam Initiated Reactions on Both Charged Positive and Negative Electrodes
J.-P. Peres, F. Pertion, C. Audry, P. Biensan, G. Blanc, and M. Broussely
- 340 Development of Large-scale Lithium Secondary Battery Cell
T. Akiyama, T. Hashimoto, H. Tajima, K. Adachi, and S. Taniguchi
- 341 Effect of Iron Disulfide Structure and Nonaqueous Electrolyte Composition on the Characteristics of High-Energy Li-FeS₂ System
E. Shembel, L. Neduzhko, O. Chervakov, I. Maksyuta, K. Kylyvnyk, Y. Polyschuk, D. Reisner, and T. Xiao
- 342 Safety and Performance of In-Service Lithium-Sulphur Dioxide Batteries
I. Hill, E. Andrukaitis, and G. Torlone
- 343 Fabrication of Dye-Sensitized Solar Cells by the Spray Pyrolysis Deposition (SPD) Technique
M. Okuya, K. Nakade, S. Kaneko, N. none, N. none, and N. none
- 344 High Temperature Characteristics of Lithium Ion Batteries Using Spinel Lithium Manganese Oxides as the Cathode
H. Watanabe, N. Imachi, K. Saishou, and S. Narukawa
- 345 Li-Ion Cells using a New High Capacity Cathode
Y. Grincourt, C. Storey, I. Davidson, P. Whitfield, I. Kargina, and H. Slegre
- 346 Thermal Analysis of a 40-Ah Lithium-ion Cell
H. Vaidyanathan and G. Rao
- 347 Overview of ENEC's Projects on Lithium batteries
F. Alessandrini, M. Conte, S. Passerini, and P.P. Prosini
- 348 Properties of Explosively Compacted Li-Ion Battery Components
M. Jak, N. Van Landschoot, E. Kelder, and J. Schoonman
- 349 New PVDF Binder for Li-Ion Batteries
B. Barriere
- 350 Effect of Separator Properties on the Performance of Lithium-Ion Cells
D.-J. Ihm, H.-S. Sin, K.-S. Roh, J.-H. Lee, and Y.-J. Shim
- 351 Advanced Li-Ion Technology for the MSP01 MARS Lander
C. Marsh, R. Gitzendanner, F. Puglia, and J. Byers
- 352 Characterization of Lithium Thionyl Chloride Cells by Impedance Techniques
F. Walsh, M. Pozin, A. Cherniy, and K. Tikhonov

**Abstract
Number**

- 353 High Rate Performance Of Moltech Prismatic Rechargeable Cells
Y. Geronov and T. Skotheim
- 354 Manganese Type Lithium Ion Battery for Pure and Hybrid Electric Vehicles
T. Horiba, K. Hironaka, T. Matsumura, T. Kai, M. Koseki, and Y. Muranaka
- 355 Status of Lithium Battery for Electric-Based Transportation
G.A. Nazri
- 356 Performance Characteristics of LiMn_2O_4 /polymer/Carbon Electrochemical Cells
N. Kamaruddin, Z. Osman, N.S. Mohamed, and A.K. Arof
- 357 Cooperative Research on Safety Fundamentals of Lithium Batteries
J.R. Selman, S. Al Hallaj, I. Uchida, and Y. Hirano
- 358 Development of High Energy Density Li-Ion Batteries Based on $\text{LiNi}_{1-x-y}\text{Co}_x\text{Al}_y\text{O}_2$
J. Weaving, F. Coowar, D. Teagle, J. Cullen, V. Dass, P. Bindin, R. Green, and B. Macklin
- 359 Recycling of Lithium Ion Cells and Batteries
M. Lain
- 360 Modulation of Discharge Process of a Lithium Battery by Changes of Battery Inner Medium Influence on Process of Discharge
A. Skekhtman
- 361 Application of Impedance Measurements in the Development of Lithium Ion Cells
F. Walsh, M. Pozin, and K. Tikhonov, Jr.
- 362 Liquid-free Rechargeable Li Polymer Battery
S. Matsui, T. Muranaga, H. Higobashi, S. Inoue, and T. Sakai
- 363 High Temperature Stable Lithium Ion Polymer Battery
C.-K. Park, A. Kakirde, W. Ebner, V. Manivannan, C. Chai, and D.-J. Ihm
- 364 Solid Polymer Electrolyte Cells Using $\text{SnSb}_x/\text{Li}_{2.6}\text{Co}_{0.4}\text{N}$ Composite Anodes
J. Yang, Y. Takeda, N. Imanishi, Q. Li, H.Y. Sun, and O. Yamamoto
- 365 Elucidation of the Charge-Discharge Mechanism of Lithium/Polymer Electrolyte/Pyrite Batteries
E. Stauss, D. Golodnitsky, and E. Peled
- 366 Development of a Bipolar Li/Composite Polymer Electrolyte/Pyrite Battery for Electric Vehicles Application
V. Livshits, A. Blum, E. Strauss, G. Ardel, D. Golodnitsky, and E. Peled
- 367 Near-Room-Temperature Rechargeable Lithium/Pyrite Battery
G. Ardel, D. Golodnitsky, E. Peled, G. Appetecchi, P. Romagnoli, and B. Scrosati
- 368 The Two-Phase Battery Concept: A New Strategy for High Performance Lithium Polymer Batteries
P.P. Prosini, M. Carewska, F. Alessandrini, and S. Passerini
- 369 Investigations on Lithium Polymer Electrolyte Batteries
G. Appetecchi, F. Alessandrini, M. Carewska, P. Prosini, S. Scaccia, and S. Passerini
- 370 Cycling Performance and Interface Properties of $\text{Li}/\text{PEO-Li}(\text{CF}_3\text{SO}_2)_2\text{N-Ceramic Fillers}/\text{LiNi}_{0.8}\text{Co}_{0.2}\text{O}_2$
L. Qi, Y. Takeda, N. Imanishi, J. Yang, H.Y. Sun, and O. Yamamoto
- 371 Fabrication and Electrochemical Characteristics of All-Solid-State Lithium-Ion Rechargeable Batteries Composed of LiMn_2O_4 Positive and V_2O_5 Negative Electrodes
M. Baba
- 372 A Lithium-Ion Polymer Battery Using PVdF-HFP/Polyethylene Composite Gel Electrolyte
X. Liu, H. Kusawake, and S. Kuwashima
- 373 Development of Solid-Polymer Lithium Secondary Batteries
J. Kuratomi, T. Iguchi, T. Bando, Y. Aihara, T. Ono, and K. Kuwana
- 374 Electrochemical Performance of Gel-Type Lithium Polymer Battery
Y.-M. Choi, J.-I. Han, S.-G. Doo, and D.-Y. Seung
- 375 Onset of Dendritic Growth in Lithium/Polymer Cells
C. Brissot, M. Rosso, J.-N. Chazalviel, and S. Lascaud
- 376 Influence of Added Plasticizer on Dispersion of Electrode Active Materials and on the Discharge Performance of Plastic Lithium Ion Batteries
S. Ahn, H. Lee, T.H. Kim, and H.M. Lee
- 377 Use of Grafted PVdF-based Polymers in Lithium Rechargeable Lithium Batteries
C. Jarvis, B. Macklin, A. Macklin, N. Mattinlgey, and E. Konfli
- 378 Production and Study of Physical and Chemical Properties of Thin-Film CC-ES
V.A. Dushenko, L.P. Paskal, and V.U. Buryak
- 379 ^7Li -Nuclear Magnetic Resonance Observation of Lithium Insertion into Coke Carbon Modified with Mesophase-Pitch
Y. Sato, K. Tanuma, T. Takayama, K. Kobayakawa, T. Kawai, and A. Yokoyama

Abstract
Number

- 380 X-ray Photoemission Studies of Surface Pre-treated Graphite Electrodes
R.I.R. Blyth, H. Buqa, F.P. Netzer, M.G. Ramsey, J.O. Besenhard, P. Golob, and M. Winter
- 381 Raman Microscopy as a Quality Control Tool for Electrodes of Lithium-Ion Batteries
P. Novak and J.-C. Panitz
- 382 Structural and Concentrational Changes in Lithium Polymer Electrolytes Under Current Flow: *In Situ* Micro-Raman Investigation
D. Ostrovskii and P. Jacobsson
- 383 Studies of Lithium Battery Materials using Cold Neutron Depth Profiling
G. Lamaze, H. Chen-Mayer, D. Becker, F. Vereda, A. Gerouki, N. Clay, P. Zerigian, T. Haas, and R. Goldner
- 384 Application of EELS to Characterization of Cathode Materials for Lithium Secondary Batteries
Y. Shiraishi, I. Nakai, K. Kimoto, and Y. Matsui
- 385 Mechanisms and Dynamics of the Microcorrosion Phenomena in the Coin Cells of an Electrochemical System " CF_{1+x} - Lithium"
V.N. Mitkin, T.N. Denisova, V.E. Kerzhentseva, E.A. Shinelev, and V.V. Moukhin
- 386 In Situ Raman Study of a Lithium-Polymer Battery
C. Naudin, J.L. Bruneel, M. Deschamps, C. Edwards, J. Grondin, S. Lascaud, J.C. Lasségues, and L. Servant
- 387 Quinone-Introduced Conducting Polymers for Supercapacitor Material
S. Suematsu, A. Manago, T. Ishikawa, and K. Naoi
- 388 New Gel Electrolytes for Batteries and Supercapacitor Applications
J. Chojnacka, J.L. Acosta, and E. Morales
- 389 Electric Capacitance of Active Carbon Fiber Electrode in Aqueous Electrolyte Solutions
Y. Matsuda, S. Ohmura, and K. Ohno
- 390 Nanotubular Materials for Supercapacitors
E. Frackowiak, K. Méténier, and F. Béguin
- 391 Charge/Discharge Characteristics of V_2O_5 -Carbon Composite for Supercapacitor
M.-S. Kim, J.-U. Kim, B.-K. Park, and H.-B. Gu
- 392 Application of Conducting Polymer Composite Electrode for Supercapacitor
K.-W. Kang, J.-U. Kim, and H.-B. Gu

Abstract No. 1

Year 2000 R&D Status of Large-Scale Lithium Secondary Batteries in the National Project of Japan

T. Tanaka, Central Research Institute of Electric Power Industry (CRIEPI), and N. Arai, the Lithium Battery Energy Storage Technology Research Association (LIBES), Tokyo, Japan

As part of the New Sunshine Program promoted by the Agency of Industrial Science and Technology (AIST), MITI, a 10-year project to develop dispersed-type energy storage technology commenced in FY1992 and will be completed in FY2001. The Lithium Battery Energy Storage Technology Research Association (LIBES) was entrusted with this challenge by a project-managing agency, the New Energy and Industrial Technology Development Organization (NEDO), and has been conducting research and development.

Based on the results of 10-Wh-class cell developments in Phase I, the subsequent five years, which began in FY1997, were designated Phase II. As originally planned, the program of Phase II aims at further improvement of the performance of large-scale cells, including safety issues, and battery modules using these high-performance large-scale cells, and the formulation of roadmaps toward worldwide dissemination of large-scale lithium secondary batteries. In addition to the above R&D programs, a new target has been presented particularly for sooner practical application of several-kWh class battery modules¹⁾.

Two types of battery modules have been developed, i.e., for stationary device and electric vehicle applications. Cathode materials for these cells are either nickel-cobalt oxides or manganese oxides. It is projected that they should have the following performance targets. Battery modules for stationary devices such as customer-use small-scale energy storage, sometimes called load conditioners, should be characterized by battery capacity, 2 kWh; specific energy, 120 Wh/kg; energy density, 240 Wh/L; cycle life, 3500 cycles; energy efficiency, 90%. Those for the electric vehicle application should be characterized by battery capacity, 3 kWh; specific energy, 150 Wh/kg; energy density, 300 Wh/L; specific power, 400 W/kg; cycle life, 1000 cycles; energy efficiency, 85%.

Exterior views of the four battery modules developed in this project are shown with their respective material composition and shape in Fig.1. Parameters such as battery capacity and energy efficiency have already achieved their original targets for both the types. Specific power has also reached its target in the battery module level for EV purpose.

Currently, further improvements in energy density and the cycle life of the cells themselves are being pursued. For that purpose, the materials for cathodes and anodes, the shapes and structures for batteries and the methods for cell connections are being re-investigated. This should lead to the improvement of the performance of the battery modules. Some examples are described below.

Cathode Materials: In the Ni-Co active material system selected, the crystal structure has been stabilized by the substitution of some Ni by Co, which has contributed to the improvement of the cycle life of the battery. The Co substitution has also led to the improvement of the thermal

stability of the cathode due to the rise of the onset temperature of thermal decomposition of the active material and the reduction of the decomposition reaction heats. In the Mn active material system selected, the crystal volume changes during charging and discharging have been decreased as a result of the reduction in the lattice constant caused by increasing the amount of Mn^{4+} in the crystal, which leads to an extension of the cycle life.

Anode Materials: In the graphite/coke hybrid anode chosen, the side reaction between the electrode surface and the electrolyte is suppressed by the characteristics of the coke, and the high capacity density is simultaneously maintained. Therefore, for the battery composed of this material, the cycle life is improved and a high energy density is achieved. In the Ag-dispersed graphite anode material system chosen, the improvement of the electronic conductivity and the forming of the LiAg alloy resulting from Ag addition will lead to the cycle life extension and high energy density in the batteries, respectively.

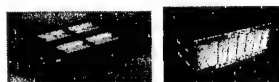
Newly developed cells and battery modules based on the preceding R&D procedures are compared in terms of their short-term and long-term performances.

Since FY1998, the development of medium-capacity battery systems for small- and medium-size electric vehicles, as well as for demand-side stationary device applications has been under way. This new development is not only based on the results for large-scale cells and battery modules obtained thus far, but also aims at further performance improvements of the battery systems. This project in Phase II is expected to realize sooner practical application of lithium secondary batteries.



EV-application type

EV-application type



Stationary type

Stationary type

Fig. 1 Battery Modules Developed in the Project

References

- [1] T. Iwahori, Y. Ozaki, A. Funahashi, H. Murase, I. Mitsuishi, S. Shiraga, S. Yoshitake and H. Awata. J. Power Sources 8-82 (1999) 872-876.

Abstract No. 2

**FROM GEMS TO LITHIUM BATTERY
ELECTRODES**

by
Michael M. Thackeray
Electrochemical Technology Program
Chemical Technology Division
Argonne National Laboratory
Argonne, Illinois 60439

The materials that are used for the negative and positive electrodes of rechargeable "lithium-ion" batteries have host structures that can accommodate and release lithium over a wide compositional range. Carbon and intermetallic compounds have been widely exploited as the negative electrodes and transition metal oxides as the positive electrodes in these batteries. In order for a lithium-ion battery to perform adequately, it is essential that the structural integrity of the electrode host structures be maintained throughout the discharge and charge processes for many hundreds of cycles. Nature provides us with many examples of stable compounds that can be produced from solution or melt, or by solid-state or ion-exchange reactions under variable conditions of temperature and pressure. As such, the mineral world can be used as a guide in the selection of materials for technological applications. In this presentation, the relationships that exist between the structure-types of precious and semi-precious gems and insertion electrodes for lithium batteries will be highlighted.

Abstract No. 3

Aging mechanism in Li Ion cells and calendar life predictions

M. Broussely¹, S. Herreyre², P. Biensan²

P. Kasztejna³, K. Nechev³, R.J. Staniewicz³

¹SAFT BP 1039, 86060 Poitiers, France;

²SAFT, 111 Bvd A. Daney, 33074 Bordeaux, France;

³SAFT America, 107 Beaver court, Cokeysville, MD, USA

Due to its excellent energy density and specific energy Li ion system appears to be the best solution for many applications such as for example standby power sources or satellites. If outstanding cycle life at small DOD has now been demonstrated, a pending question is the ability of these cells to operate over very long life, currently more than 10 years, in various environmental conditions. Calendar life prediction of such cells, which must take in account possible aging reactions, independently of cycling, has been very few reported so far. In order to evaluate such calendar life, different cell designs were tested for long period of time, and the results will be described.

Cell aging, resulting in energy losses, can be the result of degradation of the active materials structure, or secondary reactions at the interface of active material with the electrolyte.

On the positive side, slow oxidation of electrolyte can form passive films on the surface, and active material loss due to particles insulation. That results in capacity loss, associated with a polarization resistance increase. This phenomenon is enhanced by temperature and electrode potential, i.e. material oxidizing activity.

On the negative electrode, the most common side reaction is the electrolyte slow reduction through the passivation layer, consuming lithium, or degradation of carbon structure, reducing its ability to insert lithium.

Temperature being the usual accelerating factor, complete cells have been stored at different temperatures, up to 60°C. A constant "floating" voltage has been applied to the cells, to be in controlled conditions regarding the electrodes reactivity towards the electrolyte, and to simulate the actual conditions of utilization. "Diagnostic tests" are applied periodically, to follow the cells characteristics as a function of time.

The example of $\text{LiNi}_x\text{M}_{(1-x)}\text{O}_2$ / Graphite "40Ah" High Energy cells aging will be described, showing a negligible permanent capacity loss after 8 months storage at 40°C under a constant voltage of 3.9V, while under the more severe condition of 60°C, the capacity loss is limited to less than 5% during the same period.

This capacity loss at high temperature can be attributed to the lithium corrosion from the negative electrode by the electrolyte, through the passivation layer. A corrosion kinetic model has been established, assuming that the rate-limiting factor is the electronic semi-conductivity of the SEI layer by having the general simple equation:

$$t = A/(2.B) \cdot x^2 + e_0/B \cdot x$$

With

$$A = [d \cdot n / (1 + r)]$$

$$B = k \cdot \chi \cdot s$$

t = time elapsed from initial, after formation

x = amount of Li corroded,

The constant parameters are:

χ = Specific electronic semi-conductivity

s = interface area considered

e_0 = initial layer thickness after cell formation

r = ratio of insoluble / soluble reaction products

k, n and d are coefficients of proportionality

Thanks to additional results obtained from previous designs, tested for more than 1 year, a very good fitting with experimental data has been obtained, and will be discussed. Assuming an Arrhenius law applied to the semi-conductivity of the layer, $\chi = \chi_0 \cdot e^{-E/RT}$, an activation energy could be deduced from several temperature testing, and capacity loss predictions can be made as a function of temperature, confirmed by other experimental data.

Cell post mortem analysis, which will be described, have demonstrated that the negative capacity loss is not related to a carbon aging, which properties remained quite similar to initial state.

Assuming that the negative electrode corrosion is the main aging factor, excellent calendar life predictions can be extrapolated, especially with the nickel-based oxides design. Additional capacity loss can result from the positive electrode degradation, which is associated with cell polarization increase. Stable resistance of the last cell generation during on-going aging test gives credit to this assumption.

Abstract No. 4

"The status of Sony Li-ion polymer battery"

Koichiro Kezuka, Tsuyonobu Hatazawa, Kaoru Nakajima

Sony Corporation, Energy Co, Nishi Battery Laboratories(Sendai Technology Center)
3-4-1 Sakuragi, Tagajo, Miyagi 985-0842 Japan

The appearance of lithium-ion rechargeable battery ten years ago comes now supporting to an epoch of mobile telecommunication, mainly because of the high energy density. In the viewpoint of reliability, the leakage of organic solvents used in the electrolyte may cause undesirable matters, such as peculiar odor of organic solvents, catching a fire to the worse and so on. Authors have been developing for several years polymer electrolytes to apply to a lithium-ion battery for the purpose to enhance the reliability. Solidifying electrolyte spread into an entire cell with ingenious polymer gel technology(Fig.1), authors succeeded in developing an ultra thin and light battery suitable for mobile phones. The features are:

- (1) Thin and light
- (2) No solvent leakage
- (3) Enhanced safety
- (4) The same performance as a conventional Li-ion battery, such as high drain and low temperature capability in addition to durability in high temperature storage(Table 1, from latest R & D).

As known in general, the ion mobility in gel was supposed to be insufficient to perform practical battery functions. The major breakthrough leading to (4) is no doubt due to the improvement in ion conductivity of gel electrolyte, as shown in Fig.3. It is speculated that trapped ions stabilized with solvents in the matrix of polymer molecules work elaborately in the high drain condition and even at low temperature.

As the result of polymer gel method, authors could eliminate liquid or fluid, thus there is no fear of electrolyte leakage even if cell cases are broken. In addition there is no increase in internal vapor pressure, therefore it is possible to utilize thin film of Al and plastic layers for cell cases, as commonly used in retort food packs. Since there is no significant solvent vapor, there is no chance to cause a fire, resulting in enhancing reliability and safety.

In this paper the authors report the R & D status of Sony's lithium-ion polymer battery, its gel technology and results.

Table 1. Updated results in R & D

Size (DxWxH)	3.8 x 35 x 62(54) mm
Weight	15.5 g
Nominal Capacity	690 mAh
Nominal Voltage	3.7 V
Charge Voltage	4.2 V
Charge Time	90 min.
Energy Density (Volume)	375 Wh/L
Energy Density (Weight)	165 Wh/kg
Cycle performance	83 % @ 1,000 Cycle
Temperature Range	-20 ° ~ 60 °
Cathode	LiCoO ₂
Anode	Graphite

Fig.1 Sony's gel electrolyte



Fig.2

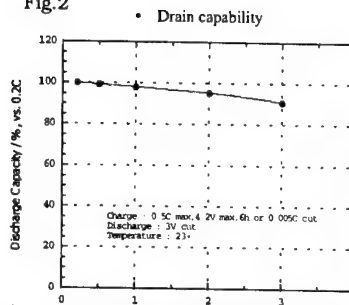
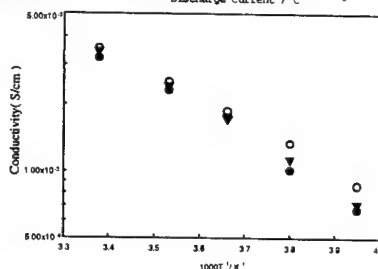


Fig.3 Ionic conductivity of Sony gel electrolyte



Abstract No. 5

"Battery Technologies Based on the Requirements for Applications and Future Movement"

Presentation by Mr. Shingo Tsuda, Director of
Battery Product Development Center
Matsushita Battery Industrial Co., Ltd.
1-1 Matsushita-Cho, Moriguchi city, Osaka,
572-8511 JAPAN

Abstract:

Historically, battery development has changed its course in accordance with the characteristics of battery applications.

Various battery systems have been developed to satisfy the demands of the age.

Especially, during these 15 years, the competition in the development of small consumer batteries has rapidly strained, in response to the remarkable diversification and spread of portable appliances.

In the 21st century, the development of "solution-type" products will be necessary, to meet the characteristics of each portable product which is in a rapid growth in the consumer market.

From the viewpoint of the device design according to the market needs as above, the development of the following items will be continued:

- materials as the source of various battery systems;
- core technologies in order to improve the efficiency and output characteristics of batteries;
- quality with high reliability and safety of battery products;
- environmentally-friendly battery elements/materials.

Figure 1 shows the trend of battery development in Matsushita Electric Industrial Co., Ltd. (MEI).

As shown in the Figure, we started to introduce our advanced NiCd batteries with high energy density to the VCR market around 1985, based on our success to improve the battery's structure.

Next, technology with new active material was introduced to alkaline rechargeable battery systems. After this innovative change of the systems, NiMH rechargeable battery was developed; this promoted the expansion of the application of portable rechargeable batteries, such as cellular phones and personal computers.

The rise of such small batteries with high energy density as above caused a revolution of market structure, and the demand for downsized batteries with higher capacity has increased.

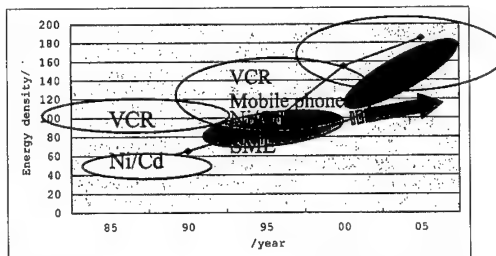
In 1992, Lithium-ion rechargeable battery was put on the market. With its remarkably improved volumetric/gravimetric energy density, the market demand for small rechargeable batteries in the area of telecommunication and personal computers was dramatically promoted.

During the battery development as above, various materials have been developed to improve the volumetric efficiency and core technologies have been accumulated, and as a result, a variety of new appliances with high capacity and high reliability has been introduced.

With these efforts, MEI has first succeeded in the world to commercialize lithium-polymer battery, which features light weight and thinner shape, and to meet the demands which have not been satisfied by other conventional ion batteries.

In order to timely respond to the continuous demands for higher energy density and the rapid diversification of small consumer applications as mentioned, it is urgently needed for us to discover new active materials for different operating voltages and shapes and develop core technologies for high reliability and safety.

In this paper, the trend of battery development in MEI is overviewed, along with the changing needs for appliances, and the future movements of our development is also discussed.



Abstract No. 6

U.S. Army Portable Power Programs
R. Hamlen, G. Au, M. Brundage,
M. Hendrickson, E. Plichta
U.S. Army-CECOM-C2D
AMSEL-RD-C2-AP
Fort Monmouth, NJ 07703 USA

The U.S. Army Communications-Electronics Command has had a significant program over the past several years aimed at providing for lighter primary and rechargeable batteries, as well as providing for more convenient charging in the field. This work is being conducted in conjunction with both battery developers and charger manufacturers. Improved primary batteries are being developed for special man-portable uses such as the Land Warrior, where the amount of electronic equipment is increasing and longer missions are required. There are no commercial primary batteries available that exhibit the required high capacities at the high energy and power densities desired. The emphasis on rechargeable batteries started about 5 years ago in response to the increasing cost of the primary lithium sulfur-dioxide batteries, especially during training. This has led to the fielding of relatively large lithium and nickel-metal hydride batteries, and to the need for versatile charging equipment which can be employed both in the front lines and rear support areas.

The main user concerns are energy content, power, weight, safety and ease of recharging, while those of the logistics and support personnel are cost, disposal requirements, unused capacity and proliferation of battery types. These impose additional limitations on the types of systems that can be considered.

PRIMARY BATTERIES: In the area of primary, or non-rechargeable, batteries, there has been a major effort over the past few years to provide an improved battery to replace the very good lithium-sulfur dioxide battery which has been the workhorse for Army high-performance portable equipment for the past 15-20 years. We are now providing new prototype batteries to the Land Warrior program that have 50-80% more capacity, and in addition are safer. They are based on lithium and manganese dioxide, and are packaged in foil pouches rather than metal cans. If the initial successes continue these types will replace the current batteries. However, the lithium-sulfur dioxide batteries have two outstanding characteristics that will be difficult to match. They operate very well at low temperatures (-40 C) and have long storage lives. Studies show that they can be expected to lose only about 10% of their capacity after 10 years of random storage. Prototype lithium-manganese dioxide pouch batteries have been tested in various sizes and applications with positive results. For example, the experimental BA-3847 primary pouch battery has a capacity of 14 Ah at 6-8 volts, as compared to 7 Ah for the older BA-5847 sulfur dioxide primary and 3.8 Ah for the rechargeable lithium-ion version of this battery.

In addition, we are developing very high energy density zinc-air batteries which, though limited in low temperature and high rate performance, can serve as silent portable battery chargers and as power sources for remote sensors and similar devices.

RECHARGEABLE BATTERIES AND CHARGERS: CECOM has introduced the lithium-ion and nickel-metal hydride batteries to replace the older nickel-cadmium

batteries over the past few years. These have 1.5 to 3 times the capacities of the nickel-cadmium batteries that they replaced. Wherever possible, these are based on commercial cells. Since cells used in commercial batteries are generally smaller than those used by the military, this has required the use of larger numbers of cells in a single package, and therefore more complex safety and charge control circuitry.

Programs are under way with contractors, as well as with the Air Force and NASA, to provide enhanced military capabilities for lithium-ion batteries, particularly in the area of low-temperature performance and of maximizing energy content. A portion of this work is being carried out in CECOM's laboratories, and we have developed one of the promising low temperature electrolytes. Figure 1 shows the performance over a range of temperatures of a cell with this electrolyte, as compared in Figure 2 with a cell using a standard commercial electrolyte. The data shows that the performance of a cell with the new electrolyte is about the same at -30 C as a conventional cell at -20 C.

We are also working with the Dismounted Battlespace Battle Lab at Ft. Benning, as well as others, to develop and field a range of new battery chargers, from on-the-move vehicle chargers to smart cables that can be carried by an individual warfighter. The first of these is a charger that can be bolted into the back of a vehicle. It will accept the military standard batteries, and fits into the charger in a manner that provides contact with circuitry that provides the appropriate charging regimen. 150 initial chargers have been fabricated and are now seeing service in a number of locations, including Kosovo.

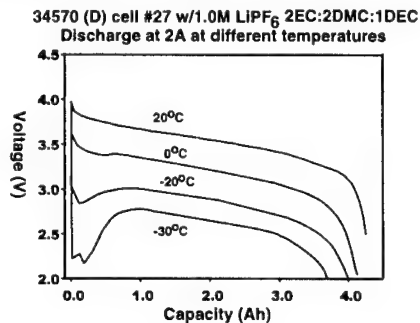


Figure 1 - Low Temperature Electrolyte

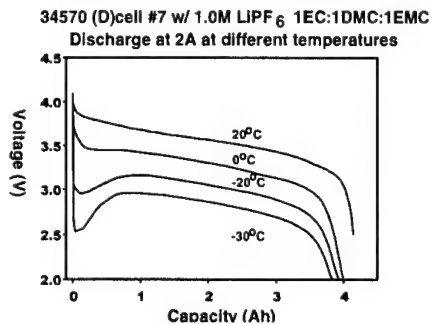


Figure 2 - Conventional Electrolyte

Abstract No. 7

Lithium-Ion Batteries for Aerospace Applications

R. A. Marsh & S. Vukson
U.S. Air Force Research Laboratory, HQ Air Force
Materials Command
Wright Patterson AFB, OH
S. Surampudi, B. V. Ratnakumar and M. C. Smart
Jet Propulsion Laboratory, Pasadena, CA
M. A. Manzo & P. J. Dalton
NASA Glenn Research Center, Cleveland, OH

Rechargeable lithium-ion batteries offer significant performance and cost benefits for many future space missions. The projected benefits include reduced weight and volume of the energy storage system, improved reliability and low power system life cycle costs. In view of these advantages, NASA is considering the use of lithium ion-batteries in many aerospace applications such as planetary landers, planetary rovers, planetary orbiters, earth orbiting spacecraft (GEO and LEO) and astronaut equipment. Air Force is considering using these batteries in various applications, such as unmanned aerial vehicles, military aircraft and earth orbiting spacecraft (GEO & LEO). Some of NASA's missions that are scheduled to use these batteries in the near term include the Mars 2001 Lander, the Mars 2003 Rover, Europe, Pluto fly-by, and Solar Probe. Plans are also being made to replace the existing hydraulic Auxiliary Propulsion Unit (APU) of the Shuttle with an electrically controlled system using 100 - 150 kWh Li-Ion batteries. These batteries are also being considered for use in cameras, astronaut equipment, satellite tools etc.

Planetary missions such as landers and rovers require lithium-ion batteries (28 V, 6-35 Ah) that are capable of operating at temperatures as low as -20°C . Low earth orbiting spacecraft and planetary orbiters require lithium-ion batteries that can provide 30,000-50,000 cycles at 30-40% depth of discharge. GEO spacecraft require lithium-ion batteries that have an operating life greater than ten to fifteen years. Some aircraft applications require high voltage (28-300V), and high capacity (30-100 AH) batteries that can operate from -40°C to $+60^{\circ}\text{C}$. Further, these batteries need to meet stringent environmental requirements such as vibration, shock, and high impact. Commercially available lithium-ion cells do not meet many of the space mission requirements. Small capacity lithium-ion cells (1-4 Ah) that only provide 500-1000 cycles are presently available commercially. Further, battery packs limited to 2-4 cells are being supplied for consumer applications. State-of-art lithium-ion cells need improvements in several areas, such as cell size/capacity, cycle life, and operating temperature. In addition, the safety of large capacity cells and batteries is also a serious concern for space applications.

A joint DOD/NASA program has been established to develop lithium-ion batteries with the capabilities required by future NASA and DOD missions. The specific objectives of this program are to 1) develop high specific energy and long cycle life lithium-ion cells and batteries, 2) establish production sources, and 3) demonstrate technology readiness for rovers and landers by 2000, GEO missions by 2001, aviation/UAV's by 2001, military terrestrial applications by 2001 and LEO missions by 2003. The technical approach involves a) development of advanced electrode materials and electrolytes to achieve improved low temperature performance and cycle life, b) optimization of cell design to achieve high specific energy, c) development of cells (6-100 Ah) and batteries (16-300 V) of various sizes required for various future missions, and d) the development of control electronics for smart battery

management. These batteries will be initially used in missions where weight and volume are critical and cycle life requirements are low to moderate (200-1000).

The development of lithium-ion cells for lander and rover applications is nearing completion. Prototype cells developed for these applications were evaluated for their performance characteristics, including room temperature cycle life, low temperature cycle life (-20°C), rate capability as a function of temperature, pulse capability, self-discharge and storage characteristics, as well as, mission profile capability. The results obtained so far indicate that they can meet mission performance needs such as low temperature operational capability, eight to ten month cruise stand storage requirement, cycle life and pulse capabilities. Testing of the cells for GEO and LEO missions and aircraft applications is in progress. This paper gives an outline of the DOD-NASA Li-ion program and progress made so far by US Air Force and NASA in developing lithium ion cells for future aerospace missions.

Acknowledgments

Some of the work described in this paper was performed by the Jet Propulsion Laboratory, California Institute of Technology, under a contract with the National Aeronautics and Space Administration (NASA).

Abstract No. 8

From Rome to Como: Twenty Years of Active Research on Carbon Based Electrodes for Lithium Batteries at INP-Grenble

Rachid Yazami¹

¹CNRS

BP 75

INPG/LEPMI

St Martin d'Hres 38402

France

This paper will review twenty years (1980-2000) of uninterrupted research activity of our group in the field of carbonaceous materials for application as negative and positive electrode materials in lithium batteries. This work was initiated after the first paper showing the potential use of graphite intercalation compounds (GICs) as positive electrodes in organic electrolyte lithium primary and secondary batteries [1].

Two major problems were then identified regarding the application of GICs in secondary batteries: the solvent co-intercalation and the solubility in the electrolyte.

One of the option was the use of dry polymer electrolytes to cope with co-intercalation/exfoliation phenomenon. This allowed the reversible lithium intercalation into graphite to be achieved for the first time [2] and opened the way for its use in practical lithium-ion batteries ten years later. A great deal of work was then devoted to characterize the carbon-lithium-polymer electrolyte system at mild temperature (50-100°C). The mechanism of lithium storage in poorly ordered carbons which yield a huge capacity (up to 1600 mAh/g [3]) was clarified together with that of passivation [4]. After the finding that EC does not co-intercalate into graphite and forms a stable passivation film which we studied in details recently [5], much of our work was devoted to better characterize such SEI film by SEM [6, 7], FTIR [7] and coupled XPS and AFM [8].

The use of strongly covalent or iono-covalent GICs such as graphite oxide [9] and graphite fluoride [10] as positives prevents them from dissolution into the electrolyte and makes them very attractive materials for primary and secondary batteries. In addition, their practical specific capacity exceeds by far that achieved with most metal oxide based materials.

We are currently pursuing research on different areas such as: 1) new carbon phases for improved performances and 2) the mechanisms behind lithium storage and capacity losses in relation with the passivation phenomenon.

[1] Ph. Touzain and M. Armand, *Mat. Sci. Eng.* 31(1977)319 [2] R. Yazami and Ph. Touzain, *J. Power Sources* (1983) [3] M. Deschamps and R. Yazami, *J. Power Sources* 68(1997)236 [4] R. Yazami and M. Deschamps *Mat. Res. Soc. Symp. Proc.* Vol. 369 (1995)165 [5] R. Yazami and S. Geniès, *Denki Kagaku* 66(1998)1293 [6] K. Zaghib, R. Yazami and M. Brousely, *J. Power Sources* 68(1997)239 [7] S. Geniès, R. Yazami, J. Garden and J. C. Frison *Synthetic Metals* 93(1998)77 [8] S. Genis, R. Yazami, H. Estrade-Schwarckopf, B. Rousseau, *ITE Battery Letters* 1 (1999)15 [9] Ph. Touzain, R. Yazami and J. Maire, *J. Power Sources* (1985)99 [10] A. Hamwi, M. Daoud, J. C. Cousseins and R. Yazami, *J.*

Abstract No. 9

The Complex Electrochemistry of Graphite Electrodes in Lithium-Ion Batteries

Petr Novák, Felix Joho, Martin Lanz, Beat Rykart, Jan-Christoph Panitz, Dario Allia, and Rüdiger Kötz

Paul Scherrer Institute, Laboratory for Electrochemistry, CH-5232 Villigen PSI, Switzerland

Nowadays, carbons, and particularly graphites, seem to be established as the negative electrode materials most commonly used in rechargeable lithium-ion batteries. Much knowledge has been gained about them in recent years, but some important scientific challenges still remain. It is the aim of this talk to discuss the interrelated phenomena of solid electrolyte interphase (SEI) formation and the irreversible "charge loss" which occurs during the first cycle of a graphite electrode, as well as their relevance to the cycling stability of lithium-ion batteries. Thus, results from several advanced interface characterization methods, namely *in-situ* mass spectrometry, *in-situ* infrared spectroscopy, *in-situ* Raman mapping, and *in-situ* scanning probe microscopy were combined for a more thorough understanding of observations made in cycling experiments.

From electrochemical cycling tests we have learned that a high specific charge (~360 Ah/kg of carbon), satisfactory cycle life of the graphite electrodes (Fig. 1), and a charge loss of less than 7 % during SEI formation can only be obtained when water contamination of the cell is avoided (<10 ppm H₂O in the electrolyte). The irreversible charge loss is proportional to the BET surface area of the graphite and rapidly increases with increasing water content in the cell. In dry EC/DMC-based electrolytes, a significant reduction current due to SEI formation is observed at potentials ≤0.8 V vs. Li/Li⁺. At ~0.8 V ethylene gas (the prominent volatile product of SEI formation reactions) starts to evolve. Hydrogen gas can be detected by *in-situ* mass spectrometry (DEMS) when water is present in the electrolyte solution, while the amount of evolved ethylene appears to be lower.

From *in-situ* measurements we know that the infrared spectra and, thus, the SEI layers are similar on different carbons. For convenience, therefore, we chose the basal surface of HOPG for our SEI morphology studies. In EC/DMC the SEI starts to form at ca. 0.7 V (Fig. 2), which is after the start of ethylene evolution. The *in-situ* AFM technique revealed that the SEI is very rough at first, and does not cover the whole surface of the electrode, but later on the SEI film is about 200 Å thick and covers the entire surface. Thus, combining our results with literature data we can conclude that at first the carbonate solvent(s) are reduced, forming ethylene gas, organic radicals, oligomers, and polymers. Then a SEI film precipitates on the surface via a nucleation and growth mechanism. DEMS experiments show that ethylene gas evolution is completed within very short periods of time on thin (<10 μm) model electrodes, but on ~100 μm thick electrodes, as in the example of Fig. 3, much more time is required for formation of an effective SEI film, and ethylene gas continues to be generated even at open circuit when the potential of the (lithiated) graphite electrode is more negative than ~0.8 V.

This work was supported in part by the Swiss Federal Office of Energy, Swiss National Science Foundation, and Timcal AG. We are grateful to Dr. M.E. Spahr, Timcal Group, and Dr. O. Haas, Paul Scherrer Institute, for graphite samples and numerous stimulating discussions.

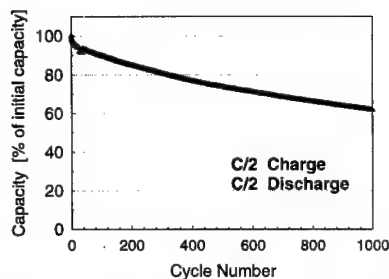


Fig. 1: Cycle performance of a coin cell containing graphite (Timrex® SLM 44) and lithium manganese oxide (BASF) as electrode materials, and 1M LiPF₆ + EC/DMC as the electrolyte. For each cycle, the cell was cycled to 100% of the capacity exhibited in the last prior cycle (initially 3.8 mAh/cm²).

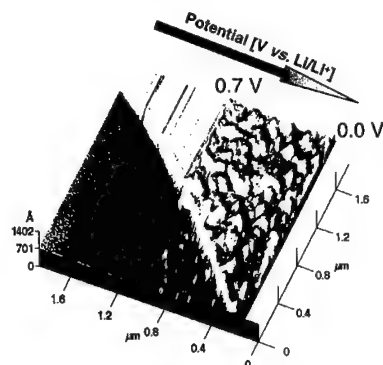


Fig. 2: *In-situ* AFM image (one line per second) of the basal surface of a HOPG electrode in 1M LiClO₄ + EC/DMC (1:1) recorded during a 5 mV/s potential scan from 1.3 V to 0 V vs. Li/Li⁺.

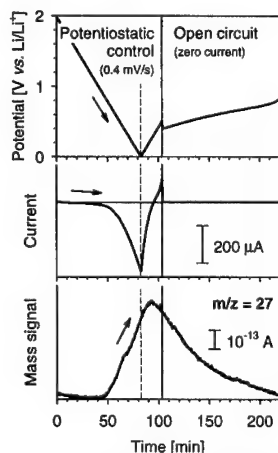


Fig. 3: DEMS experiment with a ~100-μm graphite sheet electrode in 1M LiPF₆ + EC/DMC (1:1) (second cycle at 0.4 mV/s followed by an open-circuit step). The mass signal *m/z* = 27 represents ethylene.

High-Capacity Carbons for Lithium-Ion Batteries Prepared from Rice Husk

George Ting-kuo Fey and Chung-lai Chen

Department of Chemical Engineering
National Central University
Chungli, Taiwan 32054, Republic of China

The search for low-cost and high-capacity carbon anode materials is now arousing interest world-wide, stimulated by increasing demand for lithium-ion batteries used to power portable electronic devices such as notebook computers and phones [1] and for vehicle propulsion in zero-emission vehicles (ZEVs) [2]. Rice husk is a form of agricultural biomass and a major by-product in the rice milling industry. The estimated world-wide rice husk production was about 100 million tons according to a 1996 report by the Food and Agricultural Organization [3]. Disposal of such vast amounts of rice husk has been one of the main problems facing the rice milling industry. The major constituents of rice husk are silica (20%-25%) and cellulose, which yields carbon when pyrolysed under inert atmosphere [4]. We consider rice husk to be an excellent low-cost source for high-capacity amorphous carbon containing micro amounts of silicon.

Except for some studies on the thermal degradation of rice husk [5,6] and the preparation of silica from rice husks [4,7], no report on preparing carbon anode materials for lithium-ion batteries has been published.

In this work, we developed a procedure for obtaining high-capacity hard carbon with a very high specific surface area from rice husk. The raw material, rice husk obtained from a local rice mill, was thoroughly washed with water, to remove adhering soil and clay, and dried at 110°C in an oven overnight. The dried husk (ca. 30 g) was refluxed with 400 ml of 3N HCl solution for 1 hour. After leaching, the husk was thoroughly washed with distilled water until the filtrate was free from acid. The leached husk was then dried at 110°C for 2 hours. After drying, the husk was first transferred into a quartz tube, which was then purged with argon for 30 minutes. The tube was initially heated at 150°C for 1 hour to remove water from the husk and then heated at a

5°C/min rate to reach pyrolysis temperature (from 500 to 900°C) for another hour. The black residues (about 8 g) was ground as carbon product.

The effect of pyrolysis temperatures from 500 to 900°C on the capacity of Li/Carbon coin cells was studied. The optimum pyrolysis temperature was 700°C in terms of the discharge and charge capacity of the first cycle, 691 and 319 mAh/g, respectively. The reversible capacity was about 280 mAh/g at the 10th cycle.

When pretreated using a proprietary additive (X) of a higher concentration prior to pyrolysis, the resulting hard carbon product showed a tremendous increase in cell capacity. The first discharge and charge capacity values were 2374 and 1055 mAh/g, respectively. At the fifth cycle, the reversible capacity remained 1051 mAh/g. To our best knowledge, both irreversible and reversible capacity values are the highest ever reported for any carbon anode materials of lithium-ion batteries. The surface chemistry and relationship between the capacity and specific surface area of these new hard-carbon materials will be studied. The impact of this new super hard-carbon material will be discussed.

References

- [1] R. Krause, *Pop. Sci.*, Feb., 64 (1993).
- [2] K. M. Abraham, *Electrochimica Acta*, 18, 1233 (1993).
- [3] *Production Yearbook. Basic Data Unit Statistics Division*, Food and Agricultural Organization, Rome.
- [4] C. Real, M. D. Alcala, and J. M. Criado, *J. Am. Ceram. Soc.*, 79, 2012 (1996).
- [5] M. A. Hamad, *J. Chem. Tech. Biotechnol.*, 31, 624 (1981).
- [6] A. Chakraverty, P. Mishra, and H. D. Banerjee, *Thermochim. Acta*, 94, 267 (1985).
- [7] A. Chakraverty, P. Mishra, and H. D. Banerjee, *J. Mat. Sci.*, 23, 21 (1988).

Searching for anode materials for the Li-ion technology:
Time to deviate from the usual path...

**P. Poizot, S. Laruelle, E. Baudrin, S. Denis,
M. Touboul, and J.M. Tarascon***

*Laboratoire de Réactivité et Chimie des Solides, UPRES-A
6007*

*Université de Picardie Jules Verne, 33 rue Saint-Leu,
80039 Amiens, France*

Today's research on negative electrodes for the Li-ion technology is mainly split between 1) enhancing the electrochemical characteristics of the carbonaceous negative electrode by chemical (pyrolytic processing of organic materials) or physical (mechanical milling of carbons) means, and 2) finding alternative materials to substitute for the presently used carbonaceous negative electrode composites. The second approach has sequentially led to the discovery of new oxides (ternary vanadates (R-V-O) [1], amorphous tin composite oxides (ATCO) [2-3] or composite negative alloy electrodes (SnFe₃C) [4] that can display large electrochemical capacities vs. Li at low voltages. Therefore, the poor capacity retention of these new materials upon cycling is limiting their use in practical cells.

Fundamental studies, directed towards a better understanding of the Li reactivity mechanism, were undertaken to solve these materials electrochemical limitations. For the ATCO's or alloys electrodes, once the first discharge is achieved, it is believed that the Li uptake/removal proceeds in accordance with a classical Li-Sn alloying mechanism that is reversible over limited amounts of cycles because of cycling-driven aggregation issues. Interestingly, while the unusual low voltage Li uptake/removal with the vanadates was discovered first, the Li reactivity mechanism with these materials still remains an open question.

To answer this question a must is to monitor, by means of in-situ techniques, structural evolution as well as oxidation states changes of the cations during subsequent cell discharge/charge cycles. Herein, we took advantage of the shape and design flexibility offered by the plastic Li-ion technology to design unusual electrochemical cell configurations for specific in-situ X-rays, XANES, Mössbauer and microscopy studies. Plastic batteries laminates, consisting of a 3d-metal(M)-based Vanadate positive electrode of general Formula $MVO_4 \cdot nH_2O$ and of a Li negative plastic laminate separated by a PVdF-HFP copolymer plastic matrix swollen in liquid electrolyte, were assembled by lamination under heat and pressure, and packed in a hermetically sealed thin and soft metal laminate bag.

For all the vanadates studied, the first electrochemical reduction vs. Li (e.g. first discharge) was found to produce an amorphous composite matrix consisting mainly of Li₂O, M-O, and Li-V-O nanoparticles. If one considered $FeVO_4 \cdot nH_2O$, we

noted for instance that during the first discharge Fe^{+3} was fully reduced to "metallic Fe", and then reoxidized to Fe^{+n} upon the following charge, while the oxidation state of V (+5 to start with) was simultaneously decreasing to +2, and converting back to about +4. The same observation applies to most of the studied vanadates. Interestingly, none of the involved metals (neither Fe or V) alloys with lithium implying a mechanism different from the one reported for the ATCO's or alloys composites. A different mechanism, in which the Li reactivity in the vanadates is governed by the nanoparticle surfaces/grain boundaries will be presented. In light of this mechanism several materials, precluded to react with Li on the basis of the classical Li insertion/deinsertion process or Li-alloying process were investigated, and their electrochemical performance as anodes in Li-ion batteries will be reported.

*** Invited speaker**

1. I. Yoshio, Eur. Patent 0567749 AI.
2. Y. Idota et al., U.S. Patent 5,478,671 (1995).
3. Y. Idota, T. Kubota, A. Matsufuji, Y. Maekawa, T. Miyasaka, Science, Vol. 276, 1395 (1997).
4. J. Dahn et al. J. of the Electrochemical Society, 146 (2) 423-427 (1999).

Film-Forming Electrolyte Additives for Li-Carbon and Li-Alloy Anodes

J. O. Besenhard, G. H. Wrodnigg, K.-C. Möller,
H. Buqa, M. Wachtler, M. Winter

Institute for Chemical Technology of Inorganic
Materials, Graz University of Technology,
Stremayrgasse 16, A-8010 Graz, Austria

The protection of metallic Li anodes in organic and inorganic electrolytes by formation of a solid electrolyte interphase (SEI) consisting of decomposition products of the electrolyte has been demonstrated as early as in the 1970ies by Dey [1] and Peled [2]. Later on, the effective operation of Li-alloy and Li-carbon anodes far beyond the reductive stability limit of various organic electrolytes could be explained by the same filming mechanism. The use of graphitic carbons in lithium ion cells is only possible because the SEI prevents the solvent molecules from co-intercalation [3].

Composition, properties and rate of formation of the SEI depend very much on the kind of electrolyte and in particular, on the kind of solvent. Carbonate solvents such as ethylene carbonate (EC) have been identified as excellent filming agents. On the other hand, it has been demonstrated that even small amounts of reactive electrolyte additives may improve very much the behavior of the SEI [4] e.g. with respect to thickness, conductivity, rate of formation and last but not least "irreversible capacity" required to form it. Self-discharge, safety at elevated temperatures and low temperature rate capabilities of lithium ion cells may also depend strongly on SEI properties.

So far in commercial batteries bulk solvents with reasonable filming properties - mostly cyclic and linear carbonates - are used, although their physical properties such as freezing point (e.g. of EC) or flash points (e.g. of methyl- and ethyl-carbonates) are not really satisfactory. By effective film-forming additives the filming process may "de-coupled" from the bulk components of the electrolyte, i.e., the bulk components could be selected in view of low temperature behavior, safety, cost, etc. [5].

SEI formation on carbons is related to "electropainting" as an electronically insulating film has to be deposited by an electrochemical process such as a "solution-precipitation" process. Uniformity, thickness and time, and charge required to achieve a pin-hole free film depend not only on the electrolyte composition but also on the surface characteristics and the pre-treatment of the substrate electrode to be filmed. This is in fact a process controlled by nucleation and growth of nuclei as illustrated by Fig. 1.

Whereas the irreversible reduction of standard bulk solvent components of the electrolytes is usually kinetically strongly hindered and hence does not occur until the carbon or alloying metal electrode approaches the potential of Li-insertion, additives may be chosen in a way that filming occurs at much more positive potentials,

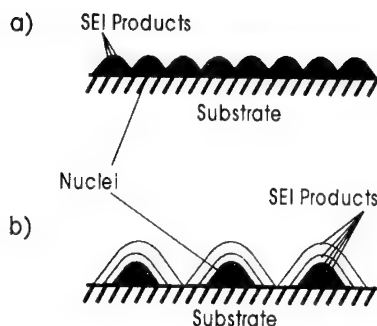


Fig. 1. Schematic representation of the filming process on substrates offering a) good and b) poor conditions for nucleation.

i.e. before any solvent co-intercalation will occur. This is true e.g. for some sulfur containing [5-7] and fluorine containing [8] additives. Even "chemical" pre-filming by reducing agents included in the anode composition may be considered.

Filming of Li-alloy anodes is slightly different from filming of Li-carbon anodes as the volume changes of Li-alloys during cycling are much more drastic. Therefore, there is still some irreversible capacity even after prolonged cycling. Filming of nano-structured multiphase lithium storage alloy [9] does preferably occur by filming of the whole particle rather than by filming of the individual phases within the particle.

- [1] A. N. Dey, Abstract No. 62, The Electrochemical Society Meeting, Atlantic City NJ (1970), p. 154
- [2] E. Peled, *J. Electrochem. Soc.* **126**, 2047 (1979)
- [3] M. Winter and J. O. Besenhard, in: *Handbook of Battery Materials*, J.O. Besenhard (Ed.), Wiley-VCH, Weinheim (1999) p. 383
- [4] J. O. Besenhard and P. Castella, in: *Intercalation Compounds*, D. Tchoubar, I. Conard (Eds.), Trans Tech Publications, Zürich (1992) p. 647
- [5] G. H. Wrodnigg, J. O. Besenhard, and M. Winter, *J. Electrochem. Soc.* **146**, 470 (1999)
- [6] G. H. Wrodnigg, T. M. Wrodnigg, J. O. Besenhard, and M. Winter, *Electrochem. Comm.* **1**, 148 (1999)
- [7] G. H. Wrodnigg, C. Reisinger, J.O. Besenhard, and M. Winter, *ITE Batt Lett.* **1**(1), 111 (1999)
- [8] L. H. Lie, T. Hodal, K. Ch. Möller, G. H. Wrodnigg, W. K. Appel, J. O. Besenhard, and M. Winter, *ITE Batt. Lett.*, **1**(1) 106 (1999)
- [9] M. Winter and J. O. Besenhard, *Electrochim. Acta* **45**, 31 (1999)

Support by the Austrian science fund in the special research program "Electroactive Materials" is gratefully acknowledged.

Novel Anodes for Lithium Ion Batteries

T. Brousse, O. Crosnier, P. Fragnaud and D.M. Schleich

Laboratoire de Genie des Matériaux
Ecole polytechnique de la université de Nantes
Nantes, France

Carbon electrodes have been the anode material of choice for lithium ion batteries. There has been a gradual progression of the carbon material used from coke type carbons to graphitic type carbons in order to increase the reversible capacity of the electrode. There appears to be a theoretical limit to capacity if one remains within the simple graphite system allowing for the formation of the lithiated compound LiC_6 (372mAh/g). One of the substantial benefits of using graphite is that even upon the full insertion of lithium there is a very small volume change, thus readily allowing for a large number of charge/discharge cycles of the electrode. Alternative anode systems have been recently explored in order to bypass the capacity of LiC_6 . Initial efforts were put forth by Fuji in the use of various tin oxide compounds which showed reversible capacities far greater than those obtained for carbon. However, these oxide materials all exhibited substantial first cycle irreversibility.

A variety of alternatives to carbon anode have been explored and at this point various problems still remain that prevent the replacement of carbon. A series of materials, including binary alloys and simple metals is explored with various concentrations as well different binders and additives. The goals are to control the substantial expansion coefficients upon the uptake of lithium as well as to prevent a large first cycle irreversible capacity. The irreversible capacity can be substantially limited by not using oxide materials as the cathode; however mechanical problems associated with expansion and contraction are still present even if very small particle sizes or used for the active component. We will describe a variety of materials and methods used to optimize both capacity and cycle life in alternative anode materials.

New Composite Anode Systems Combined with $\text{Li}_{2.6}\text{Co}_{0.4}\text{N}$

Y. Takeda and J. Yang

Department of Chemistry, Faculty of Engineering, Mie
University
Kamihama-cho, Tsu, Mie 514-8507, Japan

In the efforts of making the higher capacities of lithium secondary batteries, various new anode materials have been proposed. Among them, the revival of Li-alloys systems such as Sn, Sb, Si is especially noticeable. The

Fig.1. The first cycle profiles of different electrodes. Electrode composition: (a) 10% Ni, 10% PE and 80% $\text{SnSb}_{0.14}$; (b) 10% Ni, 10% PE, 20% $\text{Li}_{2.6}\text{Co}_{0.4}\text{N}$ and 60% $\text{SnSb}_{0.14}$; (c) 12% Ni, 10% PE and 78% $\text{Li}_{2.6}\text{Co}_{0.4}\text{N}$.

mechanical and cycling stability can be significantly improved by decreasing the particle size to sub-micron or nano scale. For example, the sub-micron size and multi-phase SnSb_x largely increased their cycling behavior [1]. Although these materials show a good cycle life performance, the serious disadvantage for the practical use is the relatively high irreversible capacity in the first cycle attributed to the formation of irreversible Li compounds.

As the another class of a high capacity new anode material, lithium cobalt nitride, $\text{Li}_{3-x}\text{Co}_x\text{N}$ ($x=0.4-0.5$) has been studied [2,3]. $\text{Li}_{2.6}\text{Co}_{0.4}\text{N}$ shows a high capacity of more than 700mAh/g with good cycle performance (0.7V to Li on average). Matsushita and NTT groups reported the high performance $\text{Li}_3\text{CoO}_2/\text{Li}_{2.6}\text{Co}_{0.4}\text{N}$ battery system [4]. One difficulty for the practical use is that the high potential cathodes such as LiCoO_2 cannot be combined because this nitride has already contained the full amount of Li in the structure. However, if $\text{Li}_{2.6}\text{Co}_{0.4}\text{N}$ is mixed with the Li-alloy systems, it is expected that reactive lithium in $\text{Li}_{2.6}\text{Co}_{0.4}\text{N}$ can compensate the first irreversible capacity.

Figure 1 shows the first discharge and charge curves of three types of composite electrodes. The cells were constructed with Li counter electrode and organic electrolyte of 1M $\text{LiClO}_4/\text{EC}+\text{DEC}(1:1)$. $\text{SnSb}_{0.14}$ ($\text{SnSb} + \text{Sn}$ two phase alloy, $< 0.2\mu\text{m}$)-based electrode has a low coulombic efficiency (ca.62%). Its high irreversible capacity can be entirely compensated by adding $\text{Li}_{2.6}\text{Co}_{0.4}\text{N}$ into the electrode. This is because Li-rich $\text{Li}_{2.6}\text{Co}_{0.4}\text{N}$ has very low discharge capacity (ca.100mAh/g), but very high charge capacity (ca.900mAh/g) in the first cycle. The first efficiency of the $\text{SnSb}_{0.14}$ and $\text{Li}_{2.6}\text{Co}_{0.4}\text{N}$ based electrode is adjustable by controlling the ratio of $\text{SnSb}_{0.14}$ to $\text{Li}_{2.6}\text{Co}_{0.4}\text{N}$.

Figure 2 gives a comparison of the cycling behavior between the $\text{SnSb}_{0.14}$ and the mixed-host electrode. The addition of $\text{Li}_{2.6}\text{Co}_{0.4}\text{N}$ can not only compensate the irreversible capacity in the first cycle, but also improve the electrode cyclability. The better cycling stability can, at least in part, be attributed to a small volume change of $\text{Li}_{2.6}\text{Co}_{0.4}\text{N}$ structure during cycling, which alleviates the volume effect of the whole electrode. Figure 3 shows charge-discharge profiles of a cell using $\text{SnSb}/\text{Li}_{2.6}\text{Co}_{0.4}\text{N}$ composite anode and $\text{LiCoO}_2\text{Ni}_{0.8}\text{O}_2$ cathode. The cell shows good performance.

A combination of the Li-alloys with $\text{Li}_{2.6}\text{Co}_{0.4}\text{N}$ can effectively compensate the first irreversible capacity. This offers a solution for the similar problems for Sn- or Si-based composite oxides and high capacity hard carbons.

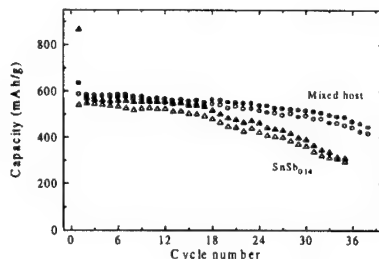


Figure 1 shows the first discharge and charge curves of three types of composite electrodes.

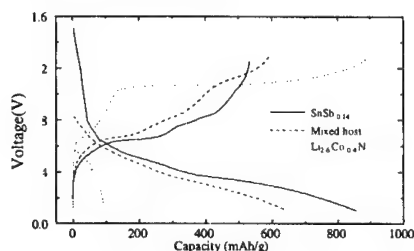


Fig.2. The cycling behaviors of different electrodes. Electrode composition: (a) 10% Ni, 10% PE, 80% $\text{SnSb}_{0.14}$; (b) 10% Ni, 10% PE, 20% $\text{Li}_{2.6}\text{Co}_{0.4}\text{N}$ and 60% $\text{SnSb}_{0.14}$. Filled symbols: Li-insertion, open symbols: Li-extraction.

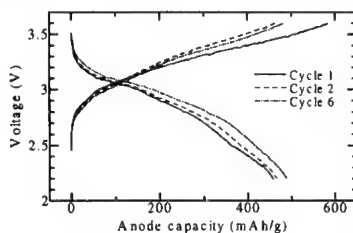


Fig.3. Charge-discharge profiles for a cell using $\text{SnSb}_{0.14}/\text{Li}_{2.6}\text{Co}_{0.4}\text{N}$ composite anode and $\text{LiCoO}_2\text{Ni}_{0.8}\text{O}_2$ cathode. Current density: $0.4\text{mA}/\text{cm}^2$.

Reference

- [1] J. Yang, Y. Takeda, N. Imanishi, T. Ichikawa, and O. Yamamoto, *J. Power Sources*, **79**, 220 (1999).
- [2] M. Nishijima, T. Kagohashi, M. Imanishi, Y. Takeda, O. Yamamoto, and S. Kondo, *Solid State Ionics*, **83**, 107 (1996).
- [3] T. Shodai, S. Okada, S. Tobishima and Y. Yamaki, *Solid State Ionics*, **86**, 785 (1996).
- [4] M. Hasegawa, J. Yamaura, S. Tsutsumi, Y. Nitta, T. Shodai, and Y. Sakurai, The 1999 Joint Int. Meeting, Hawaii, Oct. 17-22, 1999. Abstract No.174

Abstract No. 15

Layered LiMnO_2 and spinel-based compounds as positive electrodes in rechargeable batteries: structure, transformation and properties

P.G. Bruce, A.R. Armstrong, A.D. Robertson, M.J. Duncan, A.J. Fowkes and T.E. Quine

School of Chemistry, University of St. Andrews, St. Andrews, Fife, KY16 9ST, U.K.

During the last decade of the twentieth century we have witnessed a phenomenal growth in the use of rechargeable lithium-ion batteries. Technologically, however, lithium-ion cells are only in the adolescent stages of development thus during the initial years of the twenty-first century major advances will surely be made. Amongst these will be the exploration and exploitation of new positive electrode materials. In recent years there has been a considerable refocusing of interest on low cost, low toxicity and safe compounds such as the lithium manganese oxides. Major advances have been achieved in the performance of lithium manganese oxide spinels as practical battery materials. However there remains a need to develop lithium manganese oxides with higher capacities than spinel, while retaining low cost, low toxicity and high degrees of safety.

In the search for new lithium manganese oxide based positive electrode materials, compounds based on layered LiMnO_2 are of interest (1-8). Extensive doping is possible by replacing, in part, manganese by a variety of other ions, and research on these materials is expanding rapidly.

We have prepared a range of LiMnO_2 materials based on the layered O3 structure (LiCoO_2 structure type). These materials are formed by first preparing the sodium phase then ion exchanging sodium by lithium. Rich variations in the synthesis conditions for these materials are possible and we have exploited this to introduce subtle but important differences in the composition and structure of the materials which result in considerable variations in their electrochemical properties.

We have prepared a family of Co doped materials $\text{Li}(\text{Mn}_{1-y}\text{Co}_y)\text{O}_2$ and by varying the ion exchange conditions, layered phases with different c/a ratios and different electrochemical performances can be prepared. The materials convert to a spinel-like phase on cycling, however, the transformation becomes less facile with increasing cobalt content and with lower ion exchange temperatures. Such trends will be discussed in the paper. The doped materials can achieve stable discharge capacities of more than 190 mAhg^{-1} on cycling, Fig. 1. The performance is particularly promising at very low dopant levels e.g. with only a few per cent Co. Such capacities can be obtained at rates of 25 mAhg^{-1} . The capacity drops by only around 10 mAhg^{-1} on cycling at rates of 50 mAhg^{-1} . More details concerning the synthesis, structure and electrochemical performance of these phases will be presented.

$\text{Li}(\text{Mn}_{1-y}\text{Ni}_y)\text{O}_2$ may also be prepared and yields slightly higher initial discharge capacities than the Co doped systems, achieving values of around 200 mAhg^{-1} for low levels of Ni doping, Fig. 1. Fade is slightly greater for the nickel doped materials than those doped with Co. The Ni doped compounds also convert to spinel on cycling, Fig. 2, and, depending on the synthesis conditions, can exhibit some spinel-like character in the as-prepared form. The rate of conversion to spinel also depends on the synthesis conditions.

Further results on layered LiMnO_2 and materials doped with various ions will be described along with the influence of synthesis on structural transformations and electrochemical performance

REFERENCES

1. A.R. Armstrong and P.G. Bruce, *Nature*, **381**, 499 (1996).
2. F. Capitaine, P. Gravereau and C. Delmas, *Solid State Ionics*, **87** 197 (1996).
3. M. Tabuchi, K. Ado, H. Kobayashi, H. Kageyama, C. Masquelier, A. Kondo and R. Kanno, *J. Electrochem. Soc.* **145**, L49 (1998).
4. A.R. Armstrong, R. Gitzendanner, A.D. Robertson and P.G. Bruce, *J.C.S. Chem. Comm.* **1998** 1833-1834 (1998).
5. Y.-I. Jang, B. Huang, Y.-M. Chiang and D.R. Sadoway, *Electrochem. Solid State Lett.* **1** 13 (1998).
6. S.K. Mishra and G. Ceder, *Phys. Rev. B*, **59** 6120 (1999).
7. A.R. Armstrong, A.D. Robertson, R. Gitzendanner and P.G. Bruce, *J. Solid State Chem.*, **145** 549 (1999).
8. A.R. Armstrong, A.D. Robertson and P.G. Bruce, *Electrochimica Acta*, **45** 285 (1999).

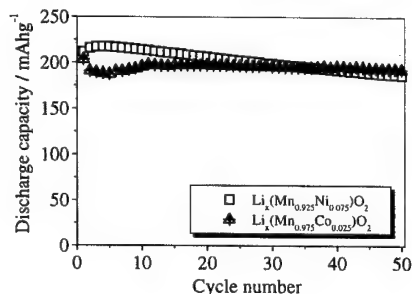


Figure 1. Cycling data for $\text{Li}_x\text{Mn}_{1-y}\text{M}_y\text{O}_2$, $\text{M} = \text{Co}, \text{Ni}$. Rate = 25 mAhg^{-1} , $V_{\text{limits}} = 2.4-4.6 \text{ V}$.

CHARGE-DISCHARGE PROPERTIES OF SPINEL OXIDES AS THE CATHODE FOR LITHIUM SECONDARY BATTERY

Masataka WAKIHARA

School of Applied Chemistry, Tokyo Institute of Technology,
2-12-1 Ookayama, Meguro-ku, Tokyo 152-8552, Japan

Spinel compound LiMn_2O_4 has been paid much attention as the most promising cathode material for 4V lithium ion batteries, because of its moderate cost and low toxicity. There are, however, certain problems to be solved before it can be fully exploited in commercial cells. Capacity fade upon repeated charge/discharge cycling has been observed, especially at an elevated temperature which is higher above 50°C . The capacity fading is usually linked to the dissolution of Mn^{3+} from the spinel to organic electrolyte^{1,2)}.

Bittihn et al.³⁾ have mentioned that the partial replacement of Mn by Co stabilizes the spinel structure. In my research group, we have showed that among the quaternary spinel phases $\text{Li}_x\text{M}_y\text{Mn}_{2-y}\text{O}_4$ in which a part of Mn is replaced by Cr, Co, Ni, Al or Mg prepared by solid-state reaction^{4,7)}, the bonding energy of octahedral M-O in $\text{Li}_x\text{M}_y\text{Mn}_{2-y}\text{O}_4$ (M=Cr etc.) is stronger than that in the parent LiMn_2O_4 ⁵⁾. The stability of MO_6 octahedral framework of the spinel leads to the suppression of Mn^{3+} dissolution from the MO_6 and results in the improvement of the cyclabilities at elevated temperature. Here, it can be considered that there is a correlation between Mn dissolution and capacity fading, however, it does not mean the Mn dissolution is the only factor of capacity fading.

In Fig.1, the Mn amount of dissolution from the $\text{LiM}_{1/6}\text{Mn}_{11/6}\text{O}_4$ is shown depending on the cycles. Co substituted spinel shows no marked dissolution of Mn compared with other spinels.

In Table 1, volume change in various $\text{Li}_x\text{M}_{1/6}\text{Mn}_{11/6}\text{O}_4$ are summarized before and after lithiation at 50°C . $\text{Li}_x\text{Co}_{1/6}\text{Mn}_{11/6}\text{O}_4$ shows the smallest volume change which actually exhibited better cycle performance compared to other active materials studied even at 50°C and is shown in Fig.2.

From the in situ XANES spectra during charge, it became clear that only Mn^{3+} in $\text{Li}_x\text{M}_y\text{Mn}_{2-y}\text{O}_4$ contributes the energy capacity. Diffusion coefficient of lithium in $\text{Li}_x\text{M}_y\text{Mn}_{2-y}\text{O}_4$ increased with the increase of the amount y of the substituted metal M. It seems that the more stable MO_6 in the octahedron makes stronger π -d bonding which causes easier diffusion of lithium in 8a-16c-8a diffusion path.

In order to increase the capacity of $\text{Li}_x\text{M}_y\text{Mn}_{2-y}\text{O}_4$, we prepared the nonstoichiometric spinel oxides with defects by controlling the partial pressure of oxygen at 750°C . The slight increase of Mn^{3+} enhances the capacity of the spinel. However, the capacity of the nonstoichiometric spinel oxides increased only slightly and there is no remarkable cycling improvement. There are two possible models for the nonstoichiometric spinel oxides, one is simple oxygen defect $(\text{Li})_{8a}[\text{Mn}_2]_{16d}\text{O}_{1.8}$ and the other metal excess model $(\text{Li})_{8a}[\text{Li}_y\text{M}_{1-y}\text{Mn}_{2-y}]_{16d}\text{O}_4$. From the data of density measurement, the above metal excess model rather than the simple oxygen defect model was proposed as the defect structure.

Through these studies, $\text{Li}_x\text{M}_y\text{Mn}_{2-y}\text{O}_4$ especially $\text{LiCo}_{1/6}\text{Mn}_{11/6}\text{O}_4$ is found to be a promising candidate cathode even at elevated temperature i.e. above 50°C .

Table 1 Volume change of various substituted spinel $\text{Li}_x\text{M}_{1/6}\text{Mn}_{11/6}\text{O}_4$ upon charging process at 50°

Sample	$V(x=0)$ (\AA^3)	$V(x=0.3)$ (\AA^3)	Volume Change(%)
$\text{Li}_x\text{Co}_{1/6}\text{Mn}_{11/6}\text{O}_4$	541.3	525.6	2.9
$\text{Li}_x\text{Ni}_{1/6}\text{Mn}_{11/6}\text{O}_4$	555.4	531.4	4.3
$\text{Li}_x\text{Al}_{1/6}\text{Mn}_{11/6}\text{O}_4$	557.4	529.5	5.0
$\text{Li}_x\text{Mn}_2\text{O}_4$	559.7	523.3	6.5

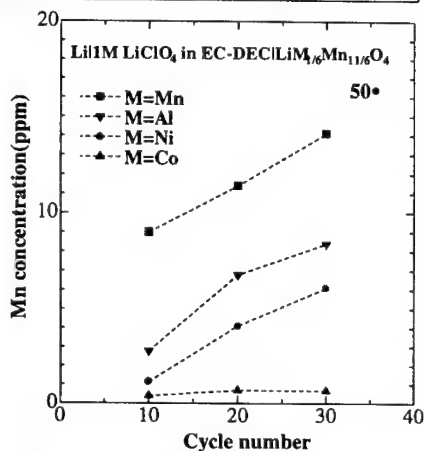


Fig.1 The concentration of dissolved Mn from the $\text{LiM}_{1/6}\text{Mn}_{11/6}\text{O}_4$ depending on the cycles

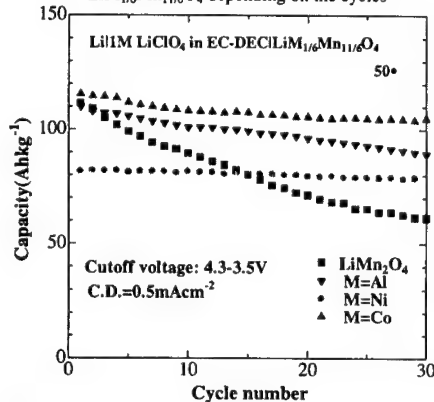


Fig.2 Cycle performance of $\text{LiM}_{1/6}\text{Mn}_{11/6}\text{O}_4$ at 50°C .

References

- 1) Dong H. Jang, Young J. Shin and Seung M. Oh, *J. Electrochem. Soc.*, **144**, 2204 (1997).
- 2) Y. Xia, Y. Zhou and M. Yoshio, *ibid.*, **144**, 2593 (1997).
- 3) R. Bittihn, R. Herr and D. Hoge, *J. Power Sources*, **43/44**, 223 (1993).
- 4) G. Li, H. Ikuta, T. Uchida and M. Wakihara, *J. Electrochem. Soc.*, **143**, 178 (1996).
- 5) M. Wakihara, G. Li and H. Ikuta, *Lithium Ion Batteries*, M. Wakihara and O. Yamamoto (Eds.), p26, Kodansha-Wiley-VCH, Tokyo (1998).
- 6) D. Song, H. Ikuta, T. Uchida and M. Wakihara, *Solid State Ionics*, **117**, 151 (1999).
- 7) N. Hayashi, H. Ikuta and M. Wakihara, *J. Electrochem. Soc.*, **146**, 1351 (1999).

Novel layered cathode materials for advanced lithium ion batteries

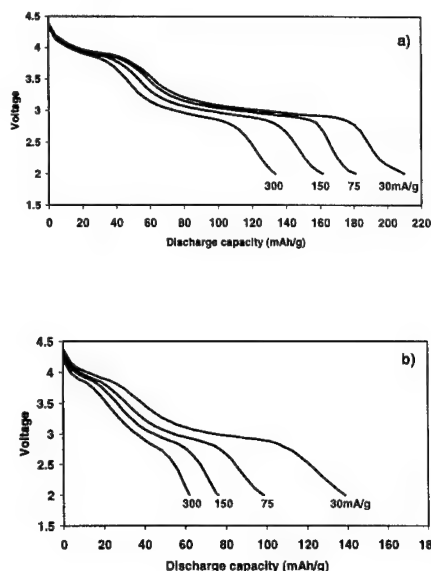
B. Ammundsen, J. Desilvestro, R. Steiner & P. Pickering
Pacific Lithium Limited, P.O. Box 90725, Auckland,
New Zealand

Current work on cathode active materials for secondary lithium batteries is focussed on replacing LiCoO_2 with less expensive manganese oxides. Since spinel-type lithium manganese oxides have relatively low practical capacities, lithium manganese oxides with other structures, such as layer-type LiMnO_2 , have been increasingly investigated in recent years [1]. However these materials, although having relatively high reversible capacities, generally have insufficient rate capability for practical applications. Apart from spinel LiMn_2O_4 which has tetrahedral sites for Li, manganese oxides also intercalate lithium at a lower operating voltage than LiCoO_2 (ca. 3 V or less vs. a Li metal anode). Most lithiated manganese oxides furthermore tend to phase-transform to spinel-type structures with cycling, and in many cases require complex preparation routes to obtain the lithiated oxide.

We have investigated the effect of incorporating Al and Cr into layered LiMnO_2 on the capacity, rate capability, and stability of the layered structure with cycling [2,3]. In the case of Cr, even small amounts of substitution allow LiMnO_2 with a well-crystallised layer structure to be obtained by solid state reaction. Cr-stabilised LiMnO_2 compounds may also be cycled without transformation to spinel. When cycled at moderately elevated temperatures (e.g. 55 °C) the substituted materials show stable reversible capacities of up to 200 mAh/g at medium to high current rates (see Fig. 1a). However the capacities at ambient temperature and below are considerably lower, highlighting the rate limitation (Fig. 1b).

Further work has shown that the rate capability of layered Mn oxides, and therefore the accessible capacity at practical rates, can be significantly increased by modifying the materials chemistry. The modified materials also show increased energy density due to a higher average operating voltage. Materials have been prepared which can deliver in excess of 150 mAh/g at the C/2 rate and ambient temperature to a voltage cutoff of 2.5 V vs. Li/Li^+ , representing a 50% improvement on earlier work (as shown in Fig. 1b). Furthermore the discharge is delivered in a smooth curve with an average voltage of 3.5 V, which makes these compounds highly attractive for application in second generation lithium batteries. In this paper we will address the key relationships between composition and structure which underlie these improvements in electrochemical properties.

1. A.R. Armstrong & P.G. Bruce, *Nature*, **381**, 499 (1996).
2. B. Ammundsen, J. Desilvestro, T. Groutso, D. Hassell, J.B. Metson, E. Regan, R. Steiner & P.J. Pickering, in *New Materials for Batteries and Fuel Cells* (1999), MRS Proceedings Series, in press.
3. B. Ammundsen, J. Desilvestro, T. Groutso, D. Hassell, J.B. Metson, E. Regan, R. Steiner & P.J. Pickering, Abstract 138, 196th Meeting of the Electrochemical Society (1999).



Figures: Discharge curves of 2032 Li button cells at 30, 75, 150 and 300 mA/g current rates for a Cr-stabilised LiMnO_2 at (a) 55°C and (b) 22°C.

STM Study on Lithium Manganese Oxide Cathodes

Minoru Inaba, Takeshi Abe, and Zempachi Ogumi
 Department of Energy and Hydrocarbon Chemistry,
 Graduate School of Engineering, Kyoto University,
 Sakyo-ku, Kyoto 606-8501, Japan

Spinel LiMn_2O_4 is a promising 4-V cathode material for lithium-ion batteries in the near future. Although the charge/discharge process is largely reversible, repeated cycling of LiMn_2O_4 cathodes results in a significant capacity fade. Proposed explanations for this capacity fade include (1) instability of electrolyte, (2) dissolution of Mn ions, and (3) cooperative Jahn-Teller effect. In this work, we prepared LiMn_2O_4 thin films by pulsed laser deposition (PLD) as test samples and observed the morphological change of the films by electrochemical STM to clarify the origin of the capacity fade of LiMn_2O_4 cathodes.

$\text{Li}_{1+x}\text{Mn}_2\text{O}_4$ thin films were prepared by PLD on Au substrates at 873 K. A KrF excimer laser was used as a light source. Their electrochemical properties were examined by cyclic voltammetry and galvanostatic charge/discharge cycling. In situ STM observation of the films was carried out in 1 M LiClO_4/PC using an SPI-3600 system (SEIKO Instruments) equipped with an apiezone wax-coated Pt/Ir tip. All measurements were carried out at room temperature in an argon-filled glove box (dew point less than -60°C).

Spinel thin films with a nearly stoichiometric composition ($\text{Li}/\text{Mn} \approx 0.51$)¹⁾ had an initial discharge capacity of 116 mAh/g, but it decreased to 109 mAh/g after 100 cycles. Cyclic voltammetry (Fig. 1) showed two couples of redox peaks at ca. 3.9 and 4.1 V, which are characteristic of LiMn_2O_4 cathodes. The peaks, in particular the couple at ca. 4.1 V, were broadened after repeated cycling. Figure 2 shows STM images of the film obtained at 3.5 V in 1 M LiClO_4/PC before and after repeated cycling between 3.5 and 4.25 V. Before cycling, the surface consisted of grains of ca. 400-nm in diameter. After 20 cycles, fine particles (120-250 nm) were formed on the original grains. The size of the particles decreased, while the number increased with repeating cycling. The observed round-shaped particles suggest that they were formed from the solution during cycling, which may be correlated with the dissolution of Mn ions. It is most likely that the particles were formed through a kind of dissolution/precipitation reactions. To know the effect of potential on the fine-particle formation, cyclic voltammetry was carried out separately between 3.50 and 4.09 V, and between 4.04 and 4.25 V, and the resulting STM images were compared. Fine-particle formation was more marked after cycled in the high potential region than in the lower potential region.

Lithium-excess spinel thin films ($\text{Li}/\text{Mn} = 0.52$) were prepared by increasing the energy fluence of the laser. Cyclic voltammograms of the Li-excess spinel thin film was quite stable, and broadening of the peaks was hardly observed even in the 75th cycle. Figure 3 shows STM images before and after 75 potential cycles between 3.50 and 4.36 V. Before cycling, the surface consisted of grains of ca. 400-nm in diameter. After 75 cycles, the shape of the grains was slightly deformed, but no fine particles appeared on the surface. The absence of fine-particle formation would lead to the stability of Li-excess spinel.

As mentioned earlier, the dissolution of Mn-ions

has been proposed as the origin of the capacity fading; however, the dissolution mechanism does not solely explain the capacity fade because the capacity fade of LiMn_2O_4 cathode is usually much larger than that calculated from the amount of dissolved Mn-ions. Because the fine particles observed in the present study were mainly formed at potential higher than 4 V, it is reasonable to think that the dissolved Mn-ions are oxidized at high potentials and precipitated on the electrode surface. The reversible capacity of such precipitates is probably less than that of the original spinel, which explains the discrepancy mentioned above.

Reference

- 1) M. Inaba, T. Doi, Y. Iriyama, T. Abe, and Z. Ogumi, *J. Power Sources*, **81-82**, 554-557 (1999).

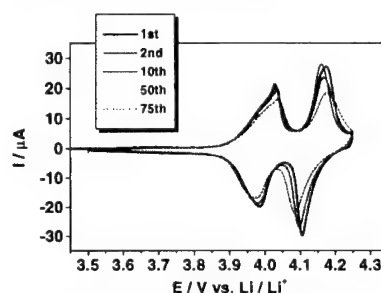


Fig. 1. Cyclic voltammograms of LiMn_2O_4 thin film/Au electrode (0.19 cm^2) in 1 M LiClO_4/PC . Scan rate was 1 mV/s.

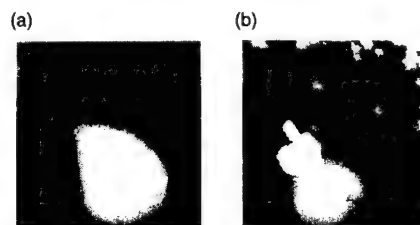


Fig. 2. STM images ($2 \times 2 \mu\text{m}$) of LiMn_2O_4 thin film (a) before and (b) after 20 potential cycles in the range 3.50 to 4.25 V in 1 M LiClO_4/PC .

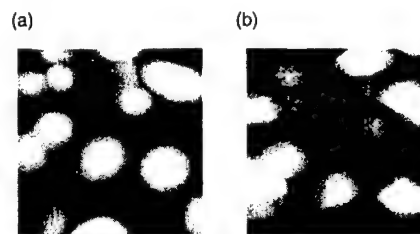


Fig. 3. STM images ($2 \times 2 \mu\text{m}$) of $\text{Li}_{1.04}\text{Mn}_2\text{O}_4$ thin film (a) before and (b) after 75 potential cycles in the range 3.50 to 4.36 V in 1 M LiClO_4/PC .

This work was supported by CREST of JST (Japan Science and Technology).

Effects of cationic disorder and defects on the structural behaviour of the $\text{Li}_x(\text{M,L})\text{O}_2$ ($\text{M} = \text{Ni, Co}$) phases

C. DELMAS

Institut de Chimie de la Matière Condensée de Bordeaux
ICMCB-CNRS and Ecole Nationale Supérieure de
Chimie et Physique de Bordeaux,
Av. Dr Schweitzer, 33608 Pessac Cedex (France).

The electrochemical behaviour of layered oxides in lithium batteries is very sensitive to the existence of reversible or irreversible phase transitions. The behaviour of $\text{Li}_x(\text{M,L})\text{O}_2$ ($\text{M} = \text{Ni, Co}$) derivatives is considered in this paper from a general point of view. The $\text{Li}_{x-2}\text{Ni}_{1+x}\text{O}_2$ system has been intensively investigated as a result of the difficulty to obtain a material close to the ideal stoichiometry and exhibiting good electrochemical properties. Moreover, the strong fading upon cycling and the thermal instability on the lithium deintercalated phases have induced a considerable number of studies on substituted materials. On the contrary, due to the facility to obtain electrochemically active LiCoO_2 , the number of studies devoted to the derivatives of this material is comparatively limited.

In the $\text{Li}_{x-2}\text{Ni}_{1+x}\text{O}_2$ system the phase transitions appear only for small departure from the ideal stoichiometry, they are due to the formation of lithium/vacancy ordering. The presence of a significant amount of extra-nickel ions (5 to 7 %) prevents from the ordering and in this case there is no structural transition. Cationic substitution in the nickel plane tends also to prevent the formation of superstructure in the lithium plane. In the case of 2D structure like $\text{Li}(\text{Ni}_{1-y}\text{Co}_y)\text{O}_2$ a significant substitution rate is required to inhibit the monoclinic distortion. When the cationic substitutions (or the condition syntheses) lead to the presence of a non negligible amount of extra-cations in the lithium plane the ordering can be killed even for low substitution rate.

A more complicated behaviour can occur if irreversible cationic redistributions occur during the lithium deintercalation/reintercalation process. In the case of the $\text{Li}_{x-2}(\text{Ni}_{1-y}\text{Mg}_y)_{1+x}\text{O}_2$ system almost ideal 2D structure are observed for $y < 0.1$. During lithium deintercalation an irreversible magnesium migration from the nickel layer to the lithium one occurs. In this case there is no structural transition upon lithium deintercalation even for $y = 0.05$.

When almost all lithium ions are removed from LiCoO_2 , Amatucci and Tarascon have observed an reversible transition to the CdI_2 type structure. The behaviour of NiO_2 or its derivatives is much more complicated. For the ideal material without nickel in the lithium site, the ABAB packing is expected. In fact there are always AB CA type stacking faults due to the presence of remaining extra-nickel ions in the Van der Waals gap. For the $\text{Ni}_{1.07}\text{O}_2$ composition the amount of extra-nickel ions is enough high to destabilise the ABAB packing, therefore the ABCABC one is preserved.

In the last step of the lithium deintercalation in the $\text{Li}_x\text{Ni}_{1.02}\text{O}_2$ system a large two phase domain is observed between $x = 0.30$ and $x = \epsilon'$. Both phases exhibit the ABCABC oxygen packing, the most deintercalated one has a very reduced c parameter, as previously mentioned by Dahn, Ohzuku, Arai and Amatucci. When most of the lithium ions have been deintercalated the interslab space collapse; when the last lithium ions are deintercalated a

structural gliding occurs to screen the orbital interaction throw the empty Van der Waals gap leading to the ABAB oxygen packing. One can assume that the existence of the large two phase domain results from the destabilisation of large Ni^{3+} ions in the NiO_2 slabs (where Ni^{4+} are prevalent) for the $\text{Li}_x\text{Ni}_{1.02}\text{O}_2$ ($x < 0.30$) composition. One can assume from the electronic configuration that in these materials the electrons are localised. On the contrary in the homologous cobalt system which exhibits metallic properties such a destabilisation is not expected. Recently, Van der Ven and Ceder have shown from first principle calculations the theoretical presence of an intermediate phase for the $\text{Li}_{0.15}\text{CoO}_2$ composition with an ordered succession of hc and fcc packings. A material very close to this ideal one but with stacking faults has been recently obtained in our laboratory.

In the Li_xCoO_2 system, XRD characterisation, electronic property and NMR studies show that the two-phase domain observed in the 0.75-0.94 range results from the existence of an insulator-metal transition in good agreement with theoretical calculation performed by Ceder's group. The very slight monoclinic distortion observed for the $\text{Li}_{1/2}\text{CoO}_2$ composition has been related by Dahn and Reimers to a lithium/vacancy ordering. If the Li/Co ratio is larger than 1 in the starting lithium cobalt oxide, localised structural defects are formed. The NMR study shows unambiguously the presence of low spin divalent cobalt in the structure. The compilation of X-ray diffraction, neutron diffraction, ^7Li MAS NMR data and chemical analyses leads to conclude to the simultaneous presence of cobalt and oxygen vacancies in the layered structure. During lithium deintercalation from this material the potential plateau and the monoclinic distortion ($\text{Li}_{0.50}\text{CoO}_2$ composition) have disappeared. The X-ray diffraction study of deintercalated materials shows the existence of a solid solution in the whole domain while the ^7Li MAS NMR shows the continuous formation of metallic domains. All these data shows that the presence of localised structural defects prevent from the demixion reaction which in ideal Li_xCoO_2 requires only electrons and lithium ions displacement. A very similar behaviour occurs in the $\text{Li}_x(\text{Co}_{0.97}\text{Ni}_{0.03})\text{O}_2$ system. If the pristine phase exhibits a Li/(Co + Ni) ratio equal to one, the two phase domain has disappeared while the monoclinic distortion remains upon lithium deintercalation. On the contrary, for material with lithium in excess both features have disappeared. The very small amount of nickel in the cobalt site is sufficient to inhibit the demixion reaction but not the lithium vacancy ordering.

Acknowledgements

The author wish to thank M. Ménétrier, L. Croguennec, C. Poullerie, S. Levasseur, G. Prado and D. Carlier for their collaboration and SAFT, CNES, REGION AQUITAINE and UNION MINIERE for financial support.

The Source of First-Cycle Capacity Loss in LiFePO_4

A.S. Andersson and J.O. Thomas

*Inorganic Chemistry, Angstrom Laboratory,
Uppsala University, Box 538, SE-751 21 Uppsala, Sweden.*

Through its flat voltage curve at 3.5V vs. Li/Li^+ , theoretical capacity of ca. 170mAh/g, good cyclability and, above all, its potential cheapness, LiFePO_4 has quickly emerged as a highly viable candidate cathode material for EV-battery applications [1]. Under charging, it passes from the structure of the mineral triphylite (LiFePO_4) to that of the mineral heterosite (FePO_4); both materials have the olivine-type structure: orthorhombic - $Pnma$. It has been found that 0.6-0.7 Li^+ ions can readily be removed and reinserted and, indeed, even larger amounts of lithium are suggested to be cyclable using smaller particle-sizes [2]. More recently, it has been shown that higher capacities can also be achieved at somewhat elevated temperatures [3]; moreover, as high as 95-100% utilisation has been claimed through the use of "a new synthetic technique" [4].

This would all suggest that efficient commercial exploitation of LiFePO_4 as a battery cathode material requires a solid understanding of the factors controlling (especially first-cycle) capacity loss. To this end, we have here followed the first-cycle delithiation-re lithiation process in a series of "coffee-bag" cells of type $\langle \text{LiFePO}_4 | \text{liq. el.} | \text{Li-metal} \rangle$ (where the liquid electrolyte used is 1 M LiBF_4 in EC:DMC 2:1), by a combination of electrochemical cycling, *in situ* powder XRD and ND, and Mossbauer spectroscopy [5]. Excellent internal consistency has been obtained in observing a ca. 20% first-cycle capacity loss from each of these techniques. A careful analysis of these data is currently underway to distinguish intrinsic material properties from particle-size effects and from other battery-engineering features.

References

- [1] A.K. Padhi, K.S. Nanjundaswamy and J.B. Goodenough, *J. Electrochem. Soc.*, **144** (1997) 1188.
- [2] J.B. Goodenough and V. Manivannan, *Denki Kagaku*, **66** (1998) 1173.
- [3] A.S. Andersson, J.O. Thomas, B. Kalska and L. Haggstrom, *Electrochem. and Solid State Letts.*, **3**(2) (2000) 66.
- [4] N. Ravet, J.B. Goodenough, S. Besner, M. Simoneau, P. Hovington and M. Armand, Abstracts of the Fall Meeting of the Electrochemical Soc., Hawaii, 1999.
- [5] A.S. Andersson, B. Kalska, L. Haggstrom and J.O. Thomas. *Solid State Ionics*. *In press*.

A Survey of Polyanionic Structures Hosts For Reversible Lithium Insertion

C. Masquelier¹, C. Wurm¹, J. Rodriguez-Carvajal²,
J. Gaubicher³ and L. Nazar³

1. Laboratoire de Physico-Chimie des Solides, UMR-CNRS #8648, Université Paris-Sud, 91405 Orsay cédex, France.

2. Laboratoire Léon Brillouin (CEA-CNRS), CEA/Saclay, 91191 Gif sur Yvette, France

3. Dept. of Chemistry, University of Waterloo, ESC 131, Waterloo, Ontario N2L 3G1, Canada

Along with the identification of alternative cathode materials operating on the Ti^{4+}/Ti^{3+} , Fe^{3+}/Fe^{2+} , V^{4+}/V^{3+} or V^{5+}/V^{4+} redox couples, investigation of polyanionic structures recently allowed a systematic tuning of transition-metal redox energies through the inductive effect. The effect of the nature of the polyanion (XO_4^{n-} ; X = Mo, W, S, P, As) and of the crystal structure on the energy level of the $M^{n+}/M^{(n-1)+}$ redox couples was shown to be particularly important [1-10].

Compounds such as $LiFePO_4$, $Li_3M_2(PO_4)_3$ (M = Fe, V), $VOPO_4$, $LiMPO_4$ (M = Fe, V), $Fe_4(P_2O_7)_3$, Fe_3PO_7 , $FePO_4$, $LiFeAs_2O_7$ and $FeAsO_4$ show very distinct electrochemical behavior at redox potentials between 2.0 and 3.8 V vs. Li^+/Li . A review on how the MO_x polyhedra are linked to each other via PO_4 tetrahedra in these framework structures will be presented.

Special attention will be given to the description of $Li_3M_2(PO_4)_3$ (M = Fe, V) compositions that may adopt two distinct crystallographic forms, denoted "A-LMP" (monoclinic, $P2_1/n$) and "B-LMP" (rhombohedral $R\bar{3}$) which differ in the way the $M_2(PO_4)_3$ "lantern-units" are connected. They illustrate in particular the great adaptability of the NASICON framework $[M_2(PO_4)_3]$ towards various alkali cation contents: Li insertion into $Li_3Fe_2(PO_4)_3$ to give $Li_3Fe_2(PO_4)_3$ occurs at an average potential of 2.8 V vs. Li^+/Li while Li extraction from $Li_3V_2(PO_4)_3$ to give $LiV_2(PO_4)_3$ occurs at an average potential of 3.7 V vs. Li^+/Li . A precise investigation of these materials by means of temperature-controlled synchrotron X-ray and neutron diffraction was undertaken. We will concentrate here on the order-disorder transitions observed on heating NASICON B- $Na_3M_2(PO_4)_3$ (M = Fe, V) and on the crystal structure of the lithium analog B- $Li_3Fe_2(PO_4)_3$.

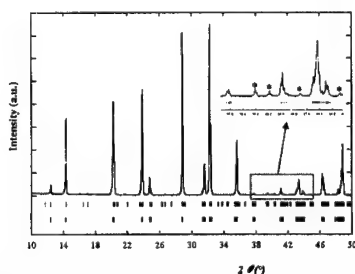


Fig. 1 : XRD Pattern ($CuK\alpha$) of α - $Na_3Fe_2(PO_4)_3$. Stars refer to the most intense superstructure reflections.

The NASICON framework of $Na_3M_2(PO_4)_3$ (M = Fe, V) exhibits long-range sodium ordering at room temperature

that induces slight monoclinic distortions and characteristic superstructure reflections in the XRD pattern (Fig. 1). The supercell of the vanadium phase, which is not identical to the iron analogue, disappears on heating above 220°C, where the global symmetry becomes rhombohedral. An alkali transfer from the Na(1) to the Na(2) crystallographic site upon heating $Na_3Fe_2(PO_4)_3$ between room temperature and 200°C occurs [11]. It has a peculiar effect on framework relaxations due to an increase of electrostatic repulsions between adjacent FeO_6 faces along [001].

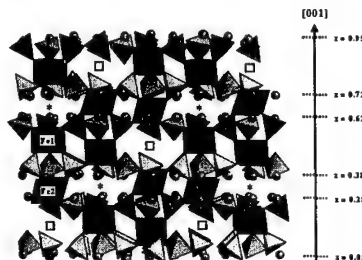


Fig. 2 : Crystal structure of $Li_3Fe_2(PO_4)_3$. Projection along [110].

The crystal structure of rhombohedral $Li_3Fe_2(PO_4)_3$ obtained through ion exchange from the sodium analog $Na_3Fe_2(PO_4)_3$ was recently determined [11] from neutron diffraction. It displays an unusual lithium-ion distribution as the replacement of Na^+ by Li^+ removes the alkali cation ordering on the M(1) and M(2) sites of the NASICON interstitial space. These two crystallographic sites are empty in $Li_3Fe_2(PO_4)_3$, and Li occupies a new, single intermediate position between M(1) and M(2). The coordination of Li in $Li_3Fe_2(PO_4)_3$ is then found to be 4. This new distribution gives rise to an important increase of the c lattice parameter that can be explained by the absence of alkali cations in the M(1) site. Evacuation of this site which is located halfway between two FeO_6 octahedra along [001], results in stronger O-O repulsions between adjacent octahedral faces.

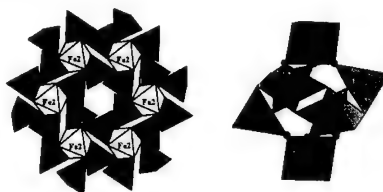


Fig. 3 : LiO_6 rings surrounding the Fe(2) (left) and Fe(1) (right) sites of the rhombohedral $Li_3Fe_2(PO_4)_3$.

References

1. A. Manthiram et al., *J. Power Sources* **26**, 403 (1989).
2. S. Okada et al., *36th Power Sources Conf.*, June (1994).
3. A. K. Padhi et al., *J. Elec. Soc.*, **144**(4), 1188-1194 (1997).
4. A. K. Padhi et al., *J. Elec. Soc.*, **144**(8), 2581 (1997).
5. A. K. Padhi et al., *J. Elec. Soc.*, **144**(5), 1609 (1997).
6. K. S. Nanjundaswamy et al., *S. S. Ionics*, **92**, (1996).
7. J. Gaubicher et al., *Mol. Cryst. Liq. Cryst.*, **311**, 45 (1998).
8. C. Masquelier et al., *J. Solid State Chem.*, **135**, 228 (1998).
9. J. Gaubicher, *Ph.D. doctoral thesis*, Paris (1998).
10. N. Ravet et al., *196th Meeting of the Electrochemical Society*, Hawaii, Oct. 1999.
11. C. Masquelier et al., *Chem. Mater*, Feb. 2000.

Lithium Fluoroalkylphosphates, A New Class of Conducting Salts for Electrolytes for High Energy Lithium-Ion Batteries

M. Schmidt, U. Heider, A. Kühner,
R. Oesten, M. Jungnitz
Merck KGaA
Frankfurter Straße 250
64293 Darmstadt
Germany

N. Ignat'ev, P. Sartori
Gerhard-Mercator-University
Lotharstraße 1
47048 Duisburg
Germany

Lithium secondary batteries, commercially available since the early nineties in Japan, are going to be more and more important for portable electronic devices and even EV applications. The electrolytes under discussion are mixtures of aprotic organic solvents and conducting salts.

Among the conducting salts Lithiumhexafluorophosphate is the most commonly used one in high-energy lithium-ion batteries. Nevertheless, its low thermal and chemical stability and its sensitivity towards hydrolysis restrict its use, especially if one keeps in mind larger lithium ion batteries.

It is commonly accepted that the problems with the use of LiPF_6 in lithium batteries result from the ease of breaking the P-F bond and the high heat of linkage of LiF. On one hand this leads to a formation of PF_5 and F⁻ at higher temperatures and on the other hand this is the reason for the sensitivity of LiPF_6 towards hydrolysis.

With this in mind, our recent work suggests that the substitution of one or more fluorine atoms of LiPF_6 with electron withdrawing perfluorinated alkyl chains should lead to stabilised P-F bonds and therefore to

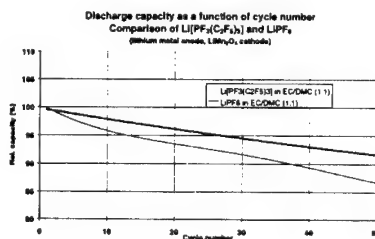
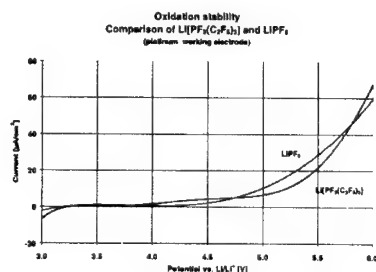
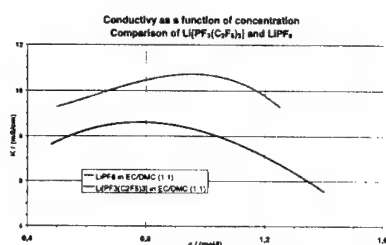
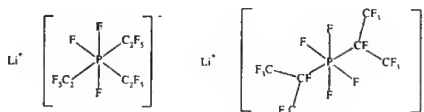
- a very low (ideal case: none) sensitivity towards hydrolysis, due to the steric shielding of the phosphorus through the hydrophobic perfluorinated alkyl chains,
- a conductivity comparable to LiPF_6 , due to the strong electron withdrawing effect of the perfluorinated alkyl chains that leads to a weak association of the anion and the lithium cation and,
- as a result of both mentioned effects to an improved thermal stability of the corresponding lithium salt.

The presentation will focus on the synthesis, chemical and electrochemical properties of some of these derivatives and discuss the application in high-energy lithium batteries.

References:

Lithium Fluorophosphates and their Use as Conducting Salts; DE 196 41 138, WO 98/155562
Electrochemical Synthesis of Perfluoroalkylphosphoranes; DE 198 466 36

Typical structure of the synthesised Lithium Fluoroalkylphosphates



Abstract No. 23

Low Temperature Behavior of Li-Ion Cells

H.-p. Lin, M. Salomon and H.-C. Shiao
MaxPower, Inc., 220 Stahl Road,
Harleysville, PA 19438, USA
M. Hendrickson, E. Plichta and S. Slane
US Army CECOM RDEC
Ft. Monmouth, NJ 07703-5601, USA

Introduction

The major focus of the research discussed in this paper concerns the low temperature behavior of a carbon anode typically found in Li-ion rechargeable cells. Our objectives are to provide insight into the limiting factors which effect cell performance over the temperature range from ambient to -40°C . As is well known, both the nature of the electrolyte solution and the properties of the SEI (the Solid Electrolyte Interface) are key problem areas for operation below 20°C . Recent results addressing these key areas are the bases for the present research.

The first part of our presentation deals with new advances in the area of electrolyte solutions. Details on the conductivities as a function of temperature for new ternary solvent mixtures containing methylpropyl carbonate (MPC) with LiPF_6 and $\text{LiC}(\text{SO}_2\text{CF}_3)_3$ electrolytes will be reported in our full presentation. Our studies include conductivity measurements down to -50°C and improved SEI formation on graphite anodes.

The second part of our presentation deals with capacity retention and rate as a function of temperature as these relate to the properties of the SEI. We present data confirming that a major problem is related to metallic Li deposition at temperature $\leq 30^{\circ}\text{C}$ which is strongly dependent upon the charging rate of carbon materials. Our results show that when deposition of metallic Li occurs, the newly formed mossy deposit of Li quickly reacts with the electrolyte solution. Besides depleting available Li^+ for subsequent cycling, the increase in resistivity of the SEI results in a large IR drop which limits the available capacity when the cell discharge and charge voltage limits are reached (normally between 0.01 V and 4.15 V). A brief review of our studies is presented below.

Experimental

To determine the temperature effect on MCMB 2825 anode material, two electrochemical cells were employed. The first is a Li-ion cell represented by



A Li reference electrolyte was used in these cells. The second is a "half-cell" designed to study the intercalation and deintercalation properties of MCMB represented by



The electrolyte used in these experiments was 1 mol dm^{-3} LiPF_6 in an EC:EMC mixture (1:3 v/o) incorporated in a PVDF membrane. Type [1] cells were charged at constant current (0.25 mA/cm^2) to 4.15 V and then at constant potential to a cutoff current of 0.025 mA/cm^2 . It was discharged at 0.25 mA/cm^2 to a cutoff of 3.0 V at 25°C , and 2.5 V at low temperatures. Type [2] cells were discharged (i.e. Li intercalation) at constant current (0.25 mA/cm^2) to 0.01 V followed by constant potential to a current cutoff of 0.025 mA/cm^2 . All cells were preconditioned by cycling three times at 25°C at which point we obtained essentially 100 % efficiency based on 270 mAh/g for MCMB. Figure 1 shows the 3rd cycle

potentials for cell [1] charged and discharged at 25°C . Figure 2 shows the 14th cycle for this cell charged and discharged at -30°C . The major feature revealed from these results is the deposition of metallic Li at -30°C . The charging potential of the cell cycled at 25°C does reach 0 V vs. Li/Li^+ , and some deposition of metallic Li probably occurs even for room temperature charging. The problem of Li deposition at low temperatures is very severe. Fig. 3 shows the charging (deintercalation) of the half cell [2] at -20°C , -30°C and -40°C . Charging was initiated at 0.01 V, and the cutoff voltage was 1.5 V. A major feature revealed in Fig. 3 is the large IR drop at -40°C due to a combination of solution resistivity and SEI resistivity. Note that we obtained an efficiency of close to 120 % for the -20°C and -30°C charging which is due to the excess plating of Li during discharge (e.g. see Fig. 2).

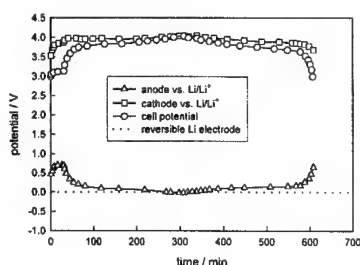


Fig. 1
(25°C)

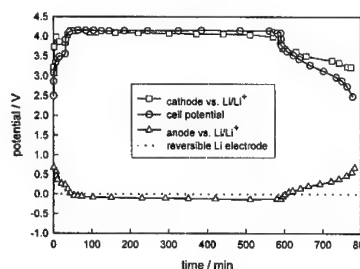


Fig. 2
(-30°C)

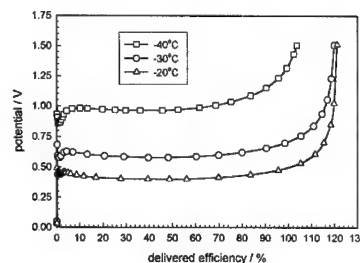


Fig. 3

Conclusions

Recently developed electrolyte solutions which possess high conductivities of the order of 10^{-3} S/cm at -40°C based on ternary mixtures containing MPC as one component show improved SEI stability at room temperatures. However, capacity retention after cycling at temperatures $\leq -30^{\circ}\text{C}$ remains a problem due to deposition of metallic Li and its subsequent effect on the SEI. Additional data and discussion will be presented in our full paper.

Composition, Depth Profiles and Lateral Distribution of Materials in the SEI Built on HOPG -TOF SIMS and XPS Studies.

E. Peled^{a,*}, D. Bar Tow^a, A. Merson^a, A. Gladkikh^b and L. Burstein^b

a- School of Chemistry, Tel Aviv University Tel Aviv, Israel 69978

b- The Wolfson Applied Materials Research Center, Tel Aviv University, Tel Aviv 69978, Israel

The SEI on both lithium and carbonaceous electrodes consists of many different materials including LiF, Li₂CO₃, LiCO₂-R, Li₂O, lithium alkoxides and according to some researchers, nonconductive polymers as well. We previously suggested that these materials form simultaneously and precipitate on the electrode as a mosaic of microphases. Many reports based on FTIR measurements failed to detect polymers in the SEI. Graphite is a major anode material in the lithium-ion battery industry. The SEI functions differently on the different planes of graphite particles: on the basal plane, it is enough to have an electronic non-conducting film, while on the cross section (zigzag and armchair planes) it must also be a good lithium ion conductor. These different tasks entail differences in composition. Therefore it is important to study separately the composition and properties of the SEI on these two planes (basal and cross section). The goal of this work was to provide, with the use of TOF SIMS and XPS techniques, details of the microphase morphology of the SEI and evidence for the existence of polymers in the SEI formed on HOPG in LiPF₆ - EC, DEC solutions. The lateral distribution of SEI materials was determined for the first time (at submicron lateral resolution) with the use of TOF SIMS. The SEI on the HOPG can be described as nonhomogeneous. The SEI on the cross-section is dominated by Li⁺ and F⁻ regions ranging in size from 0.5 (or less) to several dozen microns. The distributions of C₂H (and other C_xH_y-based fragments), O, C₂H₃O₂ (59), and C₂H₃O (43), show full coverage and are fairly homogeneous. There is an overlap of Li⁺ and F⁻ images with those of the organic species indicating an intimate mixture of these species at the submicron level. The SEI on the basal plane is dominated by organic materials (some contain oxygen, C₂H₃O has the highest contribution) and shows that Li⁺ and F⁻ are concentrated in large regions (100 microns), with some smaller micron (or submicron) sized particles. There is little or no correlation with graphite topography. Here also, C₂H (and other C_xH_y based fragments)

, O, C₂H₃O₂ (59), and C₂H₃O (43) show full coverage and are fairly homogeneous. No carbonates were found by XPS measurements on the cross section and the Li/F ratio is close to one (13). Thus most oxygen species are bonded to polymers. These measurements provide also direct evidence for the existence of polymers (or insoluble long oligomers) in the SEI, a (CH₂)_n sequence was proved. The polymer content of the SEI is an important issue. On the one hand, they can add flexibility to the SEI, but on the other they block lithium migration and cause uneven current distribution. At elevated temperatures, polymers and other organics (such as alkylcarbonates) may dissolve, leaving voids in the SEI and this can trigger thermal runaway.

In Situ Studies of SEI Formation

F. Kong^a, R. Kostecki^a, G. Nadeau^b, X. Song^a, K. Zaghbi^b, K. Kinoshita^a and F. McLarnon^a

^aLawrence Berkeley National Laboratory, 1 Cyclotron Road, Berkeley, CA, 94720, USA

^bInstitut de Recherche d'Hydro-Québec, 1800 boul. Lionel-Boulet, Varennes, Québec, J3X 1S1, Canada

Introduction

Both hard (non-graphitizable) and soft (graphitizable) carbonaceous materials are used in Li-ion cells. Electrolyte decomposition and the formation of a solid electrolyte interface (SEI) layer occur on the carbon surface during the first few charge/discharge cycles. Ideally, this so-called SEI layer should form a passivating layer which is sufficiently compact to prevent the penetration of electrolyte and solvated Li compounds that contribute to irreversible capacity loss and possible exfoliation of the graphite structure. At the same time, the SEI layer should be sufficiently ionically conductive to permit reversible intercalation/deintercalation of Li⁺ ions at suitable rates. Even though various electrochemical, spectroscopic and surface analytical techniques have been used to study the formation and growth of SEI layers, our understanding of the relationships between the SEI layers, electrodes, electrolytes and experimental conditions are quite limited. This paper describes our approach to characterize the formation of SEI layers on various carbonaceous materials by *in situ* ellipsometry and other techniques. This investigation extends a preliminary study of SEI layer formation on pyrolyzed photoresist (1).

Experimental

Five types of carbon samples were used: (i) electron-beam evaporated carbon film on glass (Tufts University), (ii) carbon film on glass (International Crystal Manufacturing Co.), (iii) highly oriented pyrolytic graphite (HOPG, Advanced Ceramics Corp.), (iv) natural graphite powder (HydroQuebec) and (v) pyrolyzed carbon films on silicon wafer produced in the Microfabrication Facility in the Electronics Research Laboratory on the campus of the University of California at Berkeley (2). The carbon sample surfaces were specular, except for the natural graphite powders. In this case, the powder was compressed in a die at high pressures (~50,000 psi) to form a thin disk with a smooth surface. The physicochemical properties of the carbon materials were characterized by Raman spectroscopy, atomic force microscopy (AFM) and spectroscopic ellipsometry.

A special test cell for *in situ* ellipsometry/electrochemical studies of carbon anodes in non-aqueous electrolytes was constructed. The polypropylene-body cell was designed with a prismatic shape and openings for two optical windows, a working electrode, a counter electrode, and a reference electrode. The ellipsometric parameters Ψ and Δ were measured as the carbon electrode was scanned from its open-circuit potential (~3.0 V) to 0 V and then back to 3.5 V at 1-5 mV/s. The electrolyte was typically 1 M LiPF₆/ethylene carbonate (EC)-dimethyl carbonate (DMC) (1:1) obtained from EM Industries Inc. (Selectipur Battery Electrolyte LP30) with a nominal water content <30 ppm. In some experiments with HOPG and the carbon films, 1 M LiClO₄/EC-DMC (1:1) was also used.

Results and Discussion

Raman spectroscopy showed that the carbon films deposited on glass contain broad overlapping peaks from 900 cm⁻¹ to 1700 cm⁻¹, which is indicative of the highly disordered nature of the carbon films. The other carbon samples showed two distinct Raman peaks in the vicinity of 1600 cm⁻¹ and 1350 cm⁻¹, corresponding to the G band and D band, respectively. In addition, the carbon obtained from pyrolyzed photoresist showed evidence for a peak at 1620 cm⁻¹ attributed to the D' band. Further analyses of the Raman spectra are underway to observe changes to the microstructure following charge/discharge cycling.

Ellipsometric parameters were measured with all of the carbon samples in air prior to the electrochemical experiments. The *in situ* experiments with the natural graphite disk were not successful because it swelled or mechanically disintegrated when the potential was scanned from open circuit to 0 V. Changes in the ellipsometric parameters were observed during the *in situ* experiments with the other carbon samples. The parameters Ψ and Δ changed when the SEI layer was formed during the initial charge (intercalation). The potential at which the parameters changed, and the magnitude of the change, varied with the carbon sample. For example, Ψ and Δ increased by ~3° and ~10°, respectively, when the potential of the pyrolyzed carbon film (produced at 1100°C) reached about 1.5 V. On HOPG with predominantly of basal plane surface, Ψ and Δ also exhibited sharp change but at a more cathodic potential of about 0.4 V. Optical modeling of observed data indicated that changes in Ψ and Δ reflect the changes of the surface layer compactness and its apparent absorption. In conclusion, *in situ* ellipsometry provides a sensitive technique to observe SEI layer formation and growth during charge/discharge cycling. When these studies are complemented by other analytical measurements, important information on the properties of the SEI layer can be obtained.

Acknowledgment

This work was supported by HydroQuebec and the Assistant Secretary for Energy Efficiency and Renewable Energy, Office of Transportation Technologies, Office of Advanced Automotive Technologies of the U.S. Department of Energy under Contract No. DE-AC03-76SF00098 at Lawrence Berkeley National Laboratory. The authors would like to thank R. Goldner and N. Clay of Tufts University (Medford, MA) for kindly supplying several carbon films used in this study.

References

1. F. Kong, J. Kim, X. Song, M. Inaba, K. Kinoshita and F. McLarnon, *Electrochem. and Solid-State Lett.*, **1**, 39 (1998).
2. J. Kim, X. Song, K. Kinoshita, M. Madou and R. White, *J. Electrochem. Soc.*, **145**, 2314 (1998).

**BATTERIES FOR TRANSPORTATION:
ARE WE MISSING THE BOAT?**

Michel Armand
University of Montréal
C.P. 6128, succursale Centre Ville
Montréal, Québec H3C 3J7 Canada;
e-mail armandm@chimie.umontreal.ca

Volta's invention of the "pile" has ushered, at an unprecedented rate, an era of discoveries both in chemistry and physics throughout the two following centuries. Yet, at a time when all indicators point at a complete fraying of the planet ecosystem, the world seems unable to cope, both in terms of technology and policy, with one of the principal culprit, the wasteful ICE transportation system. History will decide whether the refusal by the most conspicuous plunderer of earth resources to ratify the Kyoto agreement is sheer greed through lobbying or mere short-sightedness. The well orchestrated enthusiasm -and bullish stock values - for fuel cells and without minimising the rapid progresses made in this field, still leaves this system remote from a practical and economical application. It is tempting to see this as a semi-scientific strategy to buy time.

One cannot contend that EVs will be the ultimate solution to tailpipe poisons or oil slicks, but it could certainly contribute to a change in attitude towards power and speed, which are addictive. An all-electric vehicle or a hybrid has never been technically so close to a feasible product and the principles set forth two decades ago still hold.

Advanced electrochemical systems differ from the original devices in two respects – i) technological: systems are thinner, particles smaller which is favourable to all the parameters imposed by kinetics (conductivity, diffusion) – ii) chemical: extreme operating voltages are sought, well beyond the thermodynamic compatibility of components, placing the emphasis on metastability and surface science.

Besides the special case of hydrogen, the electropositive light elements that can be plated in non-aqueous systems are lithium, sodium to some extent and aluminium. For the latter, the justified temptation to use this element in batteries has not progressed, without any practical positive electrode material applicable in the chemically aggressive electrolytes. Sodium falls in the same category as lithium: a neutral electrochemistry where intercalation is the main path through any solid-state redox reaction. However, the much wider choice and stoichiometry range of intercalation or intercalation/displacement reactions for the smaller Li^+ ion has practically shifted all activity towards this element.

The almost provocative choice of a moderately conducting polymer electrolyte (polyethylene oxide)

was initially seen as a response to electrode volume change and ease of thin film processing. An added benefit, whose importance is becoming a key issue, is safety. Despite myriads of testing and mixing, liquid electrolytes have not been able to provide the faultless metastability needed, neither with lithium metal nor carbon-based negative electrodes. While hybrid vehicles (and future fuel cells) will require batteries operating under ambient condition, the temperature of operation (50-80°C) needed for pure EVs is a non-issue, or even an advantage. It also translates in facilitated lithium plating mechanism as the softer metal is less prone to develop a dendritic morphology.

The most apparent progress in polymer electrolytes has been indirect, with the development of new salts, the imide $\text{Li}(\text{CF}_3\text{SO}_2)_2\text{N}$ followed by several new families optimised for cost or performance. A less publicised improvement has been made, keeping the basic PEO structure with minimum modifications but allowing for easy processing and crosslinking into mechanically robust films.

The intercalation electrode, as said, has given lithium system in an unassailable advantage. The need for greener materials has resulted in an enormous effort to tame the manganese oxide systems, with limited success. Vanadium oxides of various stoichiometries have up to now represented the best compromise. Organic materials have impressive energy density, an advantage becoming marginal when considering their low specific gravity. The future seems to lie with a new generation of iron or manganese oxyanions, as proposed by Goodenough and co-workers. While compounds like LiFePO_4 obviously lack the electronic conductivity for complete access to the redox site, they are amenable to surface conductivity enhancement resulting in impressive kinetics and cycle life. This compound probably foreshadows nanostructured materials where the ionic and electronic conductivity can be addressed separately, widening the choice considerably.

Solid-state batteries for EV applications can be considered as advanced enough to merit commercialisation, and no major hurdle has still to be overcome, before performance, safety and cost are acceptable. Though, *laissez faire* prevails. It is quite clear that neither governments Inc. nor shareholders-first economics will provide the necessary time and money for an inevitably long term return on research and commercialisation investment. It is probably time for motivated scientists to unite world-wide, share information and express their concern at any possible decision level.

Abstract No. 27

PEO-Based Nanocomposite Polymer Electrolytes

F. Croce

Dipartimento di Chimica, Università "La Sapienza"

P.Le A. Moro, 5 - 00185 Roma, Italy

Great attention has been devoted the last years by the scientific community to modify the conventional polymer/salt polymer electrolyte systems. Recently it has emerged that the addition of suitable inert oxide nanoparticles can improve both the ionic conductivity and the stability vs lithium electrodes of these electrolytes. However the mechanism by which these dispersoids influence the properties of the native materials are still not satisfactory understood: contradictory results have been reported and no clear pictures at microscopic level have been proposed.

From practical point of view the ideal achievement in electrolyte of PEO-LiX type would be the enhancement of low temperature ionic transport by modifications which avoid any liquid contamination.

Recently we have proposed¹ a novel approach to this problem consisting on the addition of 'solid plasticizers' in the form of oxide (e.g. TiO₂, SiO₂ or Al₂O₃) powders having nano-particles size to the PEO-LiX bulk. The idea was to develop solid-state PEO-LiX composite polymer electrolytes having in the 30-80°C range good mechanical stability (promoted by the cross-linking ability of the ceramic fillers toward the polymer chains) and high ionic conductivity. We based our hypothesis on the assumption that the surface groups of the ceramic particle could play an active role in both influencing the recrystallization kinetics of the PEO polymer chains and in promoting salt dissociation.

Some results obtained²⁻⁴ on various samples of different nanocomposite polymer electrolytes confirm the validity of this model and provide important indications that this nanocomposite polymer electrolytes combine important properties such as good mechanical stability, enhanced ionic transport and great interfacial stability with lithium metal electrode.

References

- 1) F. Croce, G.B. Appetecchi, F. Ronci, Y. Wang, Y. Dai, S. Greenbaum and M. Salomon, *Electrochemical Society Proceedings Volume* 96-17, p.162-167;
- 2) B. Scrosati, *Nature*, 373, 557(1995);
- 3) F. Croce, G.B. Appetecchi, L. Persi and B. Scrosati, *Nature*, 394, (1998) 456;
- 4) F. Croce, R. Curini, L. Persi, F. Ronci, B. Scrosati, R. Caminiti, *J. Phys. Chem.*, in press

Electrochemical Characteristics of Polymer Electrolytes Based on P(VdF-co-HFP)/PMMA Ionomer Blend for PLIB

Jung-Ki Park and Young-Gi Lee

Department of Chemical Engineering,
Korea Advanced Institute of Science and Technology,
373-1, Kusung-dong, Yuseong-gu, Daejeon, 305-701, Korea

The polymer electrolytes composed of the blend of poly(vinylidene fluoride-co-hexafluoropropylene), [P(VdF-co-HFP)] and poly(methyl methacrylate-co-lithium methacrylate), [P(MMA-co-LiMA)] ionomer, and the mixed solvent of ethylene carbonate (EC) and dimethyl carbonate (DMC), and LiPF_6 salts have been prepared for plastic lithium ion batteries (PLIB).

The introduction of the ionomer into P(VdF-co-HFP) matrix was found to enhance the compatibility of porous polymer matrix with the liquid electrolyte through their ion-dipole interactions^{1,2} between the ion groups in the ionomer and the polar groups in the liquid electrolyte. This increase of compatibility could lead to the increase in uptake amount of the liquid electrolyte into the porous matrix (Figure 1) and the ionic conductivities at ambient and subambient temperature were also enhanced.

The interfacial behavior of the polymer electrolytes with the electrode was investigated. The polymer electrolytes based on the P(VdF-co-HFP)/P(MMA-co-LiMA) blend showed better interfacial stability with the increase in the ion content of the ionomer in the blend (Figure 2).

The charge/discharge behavior of the carbon/polymer electrolytes/ LiCoO_2 cell was also investigated. Suppression of leakage of organic solvent from the porous polymer matrix is expected to be the principle reason for the long-term stability in the charge/discharge behavior with cycles.

Acknowledgement

This work was performed with the cooperation of Samsung SDI Co. in Korea.

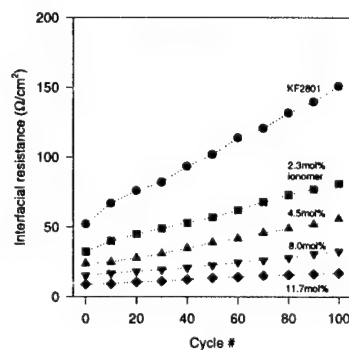
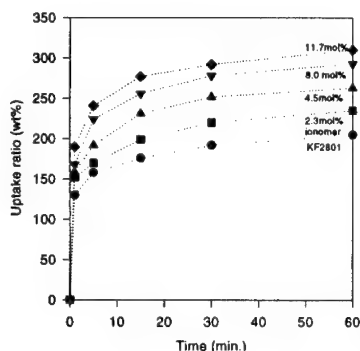
References

1. J.K. Park et al., *Electrochimica Acta*, **43** (1998) 1421.
2. J.K. Park et al., *Journal of Polymer Science, Part B: Polymer Physics*, **37** (1999) 247.

Figure 1. Uptake ratio ((wt. liquid electrolyte/wt. matrix polymer)×100%) of liquid electrolyte into the porous polymer matrix based on the P(VdF-co-HFP)/PMMA Ionomer blend (8/2, w/w).

(liquid electrolyte : 1M LiPF_6 in EC/DMC)

Figure 2. Interfacial resistances between the polymer electrolytes based on the P(VdF-co-HFP)/PMMA Ionomer blend (8/2, w/w) and electrode with CV cycles. (scan rate : 10 mV/sec, Li/polymer electrolytes/Li symmetric cell, $2 \times 2 \text{ cm}^2$)



Self-doped Block Copolymer Electrolytes (SDBCEs) for Solid-State, Rechargeable Lithium Batteries

Donald R. Sadoway, Anne M. Mayes, Biying Huang, Patrick E. Trapa, Philip P. Soo, and Pallab Bannerjee

Department of Materials Science and Engineering
Massachusetts Institute of Technology
Cambridge, Massachusetts
U.S.A. 02139-4307

The ideal electrolyte material for a solid-state battery would have the ionic conductivity of a liquid, the mechanical properties of a solid, and the formability of a commodity thermoplastic. In this laboratory it has been shown that this challenge can be met with a class of polymers known as block copolymers [1]. Block copolymers consist of two chemically dissimilar polymers covalently bonded end-to-end. Under appropriate conditions, a net repulsion between the polymer blocks induces their local segregation, or "microphase separation", into periodically-spaced nanoscale domains. By choosing a lithium salt-solvating polymer as one block component, continuous ion-conducting pathways can be formed. The nanoscale morphology confers solid-like mechanical properties to the material at macroscopic scales even if both polymer blocks reside well above their respective glass transition temperatures [2,3]. By choosing two low T_g , noncrystallizing blocks, films with mechanical properties similar to a crosslinked rubber can be obtained, without sacrificing the high local chain mobility required for Li^+ conductivity. Because microphase separation is thermodynamically reversible with the addition of a common solvent, block copolymers can be readily processed by conventional polymer coating methods.

Proof of this concept has been demonstrated here in our laboratory by the synthesis of POEM-PLMA block copolymers that are mechanically stable but exhibit nearly the same ionic conductivity as the molten POEM homopolymer [1]. Using this copolymer as both the electrolyte and cathode binder thin film, solid-state rechargeable lithium batteries of the type Li/BCE/LiMnO_2 have been constructed. These cells have been multiply cycled at room temperature. Additionally, to demonstrate the utility of the BCE at subambient temperatures, Li/BCE/Al cells have been repeatedly cycled at temperatures as low as -20°C [1]. Although our first-generation BCEs possess properties not previously exhibited by solids, a number of materials issues still need to be addressed to meet the demanding requirements of a commercially viable rechargeable battery. The focus of the present work is the effort to raise the transference number of Li^+ to nearly unity.

The approach is to synthesize a self-doped BCE (SDBCE) in which organic counterions are tethered to the secondary block of the copolymer. Preliminary work has identified a class of very low charge density organic anions that might be suitable for this purpose. Upon copolymer ordering, these attached anions become sequestered within the secondary block nanodomains, while Li^+ ions are localized to the ion-conducting block nanodomains. By localizing the counterions, their mobility should be reduced substantially, resulting in a dramatic rise in the Li^+ transport number to values approaching 1. With the SDBCE the anions are prohibited from accumulating at the polymer/oxide interface, and the

potential barrier for cation removal from the intercalation compound during charging is thereby reduced. This should enable the passage of larger currents through the cell, and reduce or eliminate polarization.

The SDBCE offers other advantages. For example, higher t_{Li^+} translates into a lower thermal load as a greater fraction of the total cell current is borne by Li^+ ions which participate in faradaic processes at the two electrodes. An increase in t_{Li^+} results in a decrease in the amount of unwanted joule heating of the cell per unit of current, which lessens the chances of thermal runaway. Hence the SDBCE would enable a safer, more efficient battery capable of operating at higher currents. Moreover, the salts presently used to dope conventional polymer electrolytes are subject to electrochemical breakdown at moderate to high voltages. This limit of electrochemical stability of the salt constrains the accessible voltage range, and consequently the capacity, of lithium polymer batteries. The SDBCE is expected to exhibit improved electrochemical stability and to confer higher energy storage capacity on the battery.

Block copolymer electrolytes with anions incorporated into the secondary block can be prepared via anionic synthesis methods, e.g., a living synthesis starting with the secondary block, e.g., poly t-butyl methacrylate, or a random acrylate copolymer containing t-butyl methacrylate. The monomer for the ionically conducting block of the copolymer, e.g., methoxy (polyethylene glycol) methacrylate, is then added to the reactor and allowed to polymerize. Upon completion of the growth of this block the synthesis is terminated with methanol or another appropriate reagent. The t-butyl methacrylate segments in the secondary block can be easily and quantitatively converted into a methacrylic acid by hydrolysis or trans-alcoholysis. Neutralization of this hydrolyzed block copolymer can be accomplished with appropriate metal bases such as lithium methoxide (LiOCH_3).

Following the general polymerization scheme described above, we have prepared a SDBCE structure of poly(lauryl methacrylate-*r*-lithium methacrylate)-*b*-poly(oligoxyethylene methacrylate). The molar ratio of the monomer components was 1:1:1 LMA:LiMA:OEM, giving an effective $\text{EO}:\text{Li}^+$ ratio of 9:1. Electrochemical impedance spectroscopy on this SDBCE (no added lithium salt) shows that this polymer exhibits significant ionic conductivity. By stepped-potential current decay a Li^+ transference number of 0.9 was measured. Cyclic voltammetry has shown the SDBCE to be immune to electrochemical breakdown at voltages exceeding 5 V.

This work was sponsored by the Office of Naval Research and the MIT Center of Materials Science and Engineering with funds from the National Science Foundation.

1. P.P. Soo, B. Huang, Y.-I. Jang, Y.-M. Chiang, D.R. Sadoway, and A.M. Mayes, *J. Electrochem. Soc.*, **146** (1), 32-37 (1999).
2. F. S. Bates, *Macromolecules* **17**, 2607 (1984); J.H. Rosedale, and F.S. Bates, *Macromolecules* **23**, 2329 (1990).
3. T.P. Russell, T.E. Karis, Y. Gallot, and A.M. Mayes, *Nature* **368**, 729 (1994).

**ELECTROCHEMICAL AND SYNCHROTRON
RADIATION XAS STUDIES OF LITHIUM
INTERCALATION INTO VANADIUM
PENTOXIDE AEROGELS AND
NANOCOMPOSITES**

William Smyrl¹, Stefano Passerini², Marco Giorgetti¹,
Fabrice Coustier³, Matthew Fay¹ and Boone Owens¹

¹Corrosion Research Center
Department of Chemical Engineering & Materials
Science
221 Church St. SE, 112 Amundson Hall
University of Minnesota
Minneapolis, MN 55455 USA

²ENEA
Electrochemical Energy Conversion Division
Via Anguillarese 301
Rome 00060 Italy

³Polystor Corporation
6918 Sierra Court
Dublin, CA 94568 USA

Vanadium pentoxide hosts have excellent intercalation capacity and reversibility, and are universal hosts for both univalent and polyvalent cations (Li^+ , Na^+ , Zn^{+2} , Mg^{+2} , and Al^{+3}). All the cations may be inserted to high concentrations of at least four equivalents of Li^+ , Mg^{+2} , and Al^{+3} , and more than three equivalents of Zn^{+2} per mole of V_2O_5 . Sol-gel synthesis of xerogels and aerogels yield materials that are amorphous and very versatile. Aerogel processing at supercritical conditions, or at near supercritical conditions yield highly porous solids as powders or thin films. Solvent exchange during the aerogel drying process also modifies the solid and causes "pillaring" of vanadium pentoxide. The pillaring is associated with the retention of a small amount of the organic solvent. Thus, the aerogel and aerogel-like materials are nanocomposites of vanadium pentoxide and the pillaring agent. Pillaring is limited and does not pack the entire intercalation gallery. It is associated with larger interlayer gaps and the larger gaps lead to facile and fast insertion of polyvalent cations. Other nanocomposites have also shown high rates of insertion. Lithium intercalation has been cycled one thousand times and was found to be completely reversible with respect to charge, mass and stress. In addition, *in situ* synchrotron X-Ray absorption spectroscopy (XAS) at the vanadium edge was used recently to demonstrate that the local atomic and electronic structure around the vanadium sites is completely reversible upon cycling as well. Further, the local structure around Zn and Cu sites in intercalated or doped materials was also reversible in other *in situ* XAS studies at the Zn and Cu edges respectively. For the Mg^{+2} , Al^{+3} , and Zn^{+2} ions, electrochemical intercalation studies have also demonstrated high reversibility.

To enhance the rate of insertion, the electronic conductivity of amorphous V_2O_5 , was increased by doping. Ag and Cu doping to the level of 0.1 mole/mole of V_2O_5 increased the conductivity by three

orders of magnitude. Doping with Ni, Mg, and Al was also studied. Subsequent intercalation of Li^+ into the doped materials was very facile and highly reversible. Nanocomposites of the doped host were shown to support exceptionally high rates of For the Cu doped samples, XAS studies showed that the Cu^{+2} was reduced to the metallic state during lithium insertion, but was re-oxidized and returned to the same sites in the lattice upon lithium release. Thus, not only is the intercalation reversible for guest species like Li^+ , but doping species are not lost into the solution upon electrochemical cycling. In the case of Cu, the metallic clusters that form in the reduced state are thin sheets that are presumably located near the intercalation sites from which they came, and to which they return on the reverse portion of the cycle.

The strategy of using sol-gel processing as a general route to prepare other porous, pillared intercalation hosts will be discussed.

Acknowledgment

This work was supported by DARPA/ONR N/N00014-92-J-1875; IIT/ARO DAA-H04-93-R-BAA10; and DOE DE-FG02-93ER14384.

Light scattering and computational studies of ionic interaction and dynamics in polymer based gel electrolytes

P. Johansson, C. Svanberg,
R. Bergman, P. Jacobsson*.

Department of Experimental Physics.
Chalmers University of Technology
SE-41296 Göteborg Sweden

Solid polymer electrolytes (SPE) have gained a strong scientific and technological interest due to their applicability in many electrochemical devices [1]. However, along with such advantages as electrochemical and mechanical stability the classical SPE based on poly(ethylene oxide) and a lithium salt have a rather low ionic conductivity at ambient temperature due to a low segmental mobility of the polymer matrix. In order to improve the conducting properties of the SPE several new approaches have been suggested. One of them is to utilise the mechanical properties of polymer membranes with the high conductivity of liquid electrolytes in polymer based gel electrolytes [2]. These gel electrolytes are not as well characterised as the SPE compounds and therefore offer fundamental scientific challenges in materials science as well as established technological promises.

Typical gel electrolytes consists of a non-aqueous solvent (like ethylene carbonate, EC, propylene carbonate, PC, dimethyl carbonate, DMC, etc., or mixtures thereof), lithium salt and an immobilising polymer matrix. Commonly used polymers are for example poly(acrylo-nitrile), poly(methylmethacrylate) and poly(vinylidene-fluoride) etc., but also functionalized polymers like PEO chains grafted on acrylate backbones [3-6].

Various intermolecular interactions between the components of the gel electrolytes affect both the transport properties and the important mechanical and electrochemical stability of the gels. In this work we compare vibrational spectroscopy investigations of the competition between polymer-ionic and solvent-ionic interaction in a functionalised gel-electrolyte with *ab-initio* calculations of the binding energy for different types of interaction.

Previous photon correlation spectroscopy, PCS, work [7] have shown that in PMMA-EC/PC/LiClO₄ based gels the ionic conductivity is largely decoupled from the polymer and instead related to the fast diffusive process of the low molecular solvents. Comparing with conductivity measurements it was found that the measured self diffusion coefficient was in qualitative agreement with the diffusion of the ions as determined from the Stoke-Einstein relation.

In the present study PCS is used to probe dynamic processes in the time range from 10⁻⁷ - 10³ s on two different polymer gel electrolytes. One based on an inert polymer matrix (PMMA) with low solvent interaction and one based on a polymer matrix (PAN) with pronounced solvent-polymer and cation-polymer interactions. A complex relaxation behaviour is observed with multiple relaxation processes with different temperature and wave-vector dependencies.

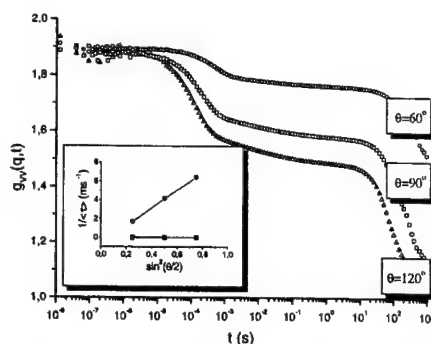


Figure 1: Angle dependence of the homodyne correlation function ($\approx 1 + (S(Q,t))^2$), as measured by photon correlation spectroscopy for a PMMA-EC/PC-LiClO₄ gel. Inset shows Q -dependence of the characteristic times of the fast diffusive motion (\bullet) and the segmental relaxation processes (\circ).

References

1. F. M. Gray, Solid Polymer Electrolytes, VCH Publishers: New York, 1991.
2. B. Scrosati, Nature 373 (1995) 557.
3. D. Ostrovskii, L.M. Torell, G.B. Appetecchi, B. Scrosati, Solid state Ionics 106 (1998) 19.
4. E. Cazzanelli, G. Mariotto, G.B. Appetecchi, F. Croce, Ionics 2 (1996) 81.
5. J.P. Southall, H. Hubbard, S.F. Johnston, V. Rogers, G.R. Davies, J.E. McIntyre, I.M. Ward, Solid State Ionics 85 (1996) 51.
6. J. Adebahr, P. Gavelin, P. Jannasch, D. Ostrovskii, B. Wesslén, P. Jacobsson, Solid State Ionics. (in press).
7. C. Svanberg, G.B. Appetecchi, J. Adebahr, H. Ericsson, L.M. Torell, L. Börjesson, and B. Scrosati, J. Chem. Phys.

**Solid State NMR Studies of Lithium Ion
Battery Materials**

S.G. Greenbaum, Y. Wang, S.H. Chung, and X. Guo
Physics Dept., Hunter College of CUNY
695 Park Avenue, New York, NY 10021 USA

Structural studies of materials utilized in lithium battery technology are often hampered by the lack of long-range order found only in well-defined crystalline phases. Powder x-ray diffraction, while being an indispensable technique in the characterization of cathode materials for example, yields only structural parameters that are averaged over hundreds of lattice sites. Our laboratory utilizes solid state nuclear magnetic resonance (NMR) methods to investigate structural and chemical aspects of lithium ion anodes, cathodes, and polymer electrolytes.

NMR is one of very few powerful methods to probe the immediate environment of ions such as Li^+ in solids, especially in disordered materials. Thus NMR methods have contributed much toward our current fundamental understanding of lithium intercalation or other insertion reactions in lithium battery electrodes, and ion transport in solid electrolytes. These methods are particularly useful when the results are correlated with data from other analytical means, such as x-ray diffraction, x-ray absorption spectroscopy, AC impedance, or even cell performance tests. This paper will review some background aspects of NMR that illustrate its strength in studying battery materials, including elemental (nuclear) specificity and sensitivity to short-range ($< \text{nm}$) interactions and dynamics. Results of several recent NMR investigations on various battery materials, in collaboration with other research groups, will be presented.

In partnership with E. Peled's group at Tel Aviv University, we have undertaken studies of the effect of mild oxidation of natural graphite on lithium capacity, and formation of the solid electrolyte interphase (SEI). Previous work by our groups has shown that mild oxidation of graphite can increase its reversible lithium capacity and facilitate the formation of a chemically bonded SEI. Both wide line and high resolution (magic angle spinning) ^7Li NMR measurements were conducted on electrochemically lithiated graphite, both untreated and partially oxidized (8 - 15% mass burn-off for the latter). Several sites are identifiable: the stage-1 intercalated LiC_6 phase, characterized by a central transition peak of 43 ppm (relative to aqueous LiCl) and nuclear quadrupole coupling constant (QCC) of 33 kHz, an edge site at 11-13 ppm with QCC of 39 kHz, and a high stage compound, presumably LiC_{18} , at 3 ppm with QCC of 36 kHz. The 3 ppm feature is present only at relatively low Li concentration ($< 30\%$ capacity), above which the major spectral feature is due to the LiC_6 phase. In addition, there is NMR intensity at zero ppm attributed to lithium salts and organolithium compounds which constitute the SEI. The edge site occupation is present at intermediate levels of lithiation, and is attributed to a stacking defect, and increases strongly with pre-oxidation of the graphite. Further lithiation reduces the edge site occupancy, which then converts to LiC_6 .

In collaboration with D. Fauteux (Powercell, Inc., formerly of Hirion), and K. Amine (Argonne National Lab), we have studied a series of substituted LiNiO_2 compounds, of the general form $\text{LiNi}_{1-x-y}\text{M}_x\text{M}'_y\text{O}_2$, where $\text{M} = \text{Co, Ti, Mg}$, and x is up to 0.20 for Co; $\text{M}' = \text{Al, and Ga}$, and $y = 0.05$ for Ga and values up to 0.10 for Al.

Although wide line ^7Li NMR linewidths are dominated by broadening from paramagnetic Ni^{3+} , all samples containing Co with at least $x = 0.15$ exhibit varying degrees of Co segregation, whereby some of the Li sites are characteristic of a diamagnetic LiCoO_2 - like environment (i.e. Co^{3+} neighbors in the first cation coordination shell, which yield a narrow line component centered at the zero ionic reference frequency) and others characterized by a broad and paramagnetically shifted line component arising from at least one nearby Ni^{3+} ion. We have also observed the ^{27}Al NMR signal, characteristic of Al^{3+} in a very distorted octahedral environment, in samples with as little as 5% Al substitution.

Finally, we present results on anisotropic ion transport in poly(ethylene oxide) (PEO) - lithium salt complexes under uniaxial stress, again in collaboration with E. Peled's group. ^7Li NMR spectra in stretched films reveal changes in short-range structure that are consistent with alignment of the PEO helices. There is also preliminary evidence of anisotropy in both cation and anion diffusion, as determined from pulsed field gradient NMR measurements. These results are correlated with the observed enhancement in ionic conductivity due to stretching.

Acknowledgments

This research was supported in part by grants from the U.S. Department of Energy and the U.S. Office of Naval Research.

IN SITU AND EX SITU STRATEGIES FOR THE STUDY OF LITHIUM BATTERY ELECTRODES

Louis J. Rendek Jr.[†], Dana Totir, Gary S. Chottiner[‡],
Daniel A. Scherson[†]

Departments of Chemistry[†] and Physics[‡]
Case Western Reserve University
Cleveland, Ohio 44106, USA

A better understanding of the reactivity of carbon and transition metal oxides and sulfides toward Li-containing non-aqueous solutions is expected to provide insights into the factors that control the performance of secondary Li and Li⁺ batteries. This presentation will focus on two strategies developed and implemented at CWRU for studies of the chemistry and electrochemistry of such electrodes.

A. Ex situ assembly and characterization of Li passive films in ultrahigh vacuum (UHV) by photon-, and electron-based techniques

This experimental approach, described in detail elsewhere,¹ relies on the vapor deposition of Li onto a nominally unreactive clean substrate metal, such as Ni, followed by exposure to the non-aqueous solvent of interest in gas phase in UHV. Fig. 1 shows infrared reflection absorption spectra (IRAS) of a Li/Ni(poly) film exposed to propylene carbonate (PC), diethyl carbonate (DEC), and dimethyl carbonate (DMC) vapors, in the form of $\Delta R/R = (R_{\text{amp}} - R_{\text{ref}}) / R_{\text{ref}}$ vs wavenumber, using the spectrum of bare Li/Ni(poly) as a reference. The C-O stretching modes between 1050 and 1150 cm⁻¹ in these spectra are characteristic of Li-O-C present in alkoxide-type species reported by Aurbach et al.^{2,3} The clear absence of features for the CO₂ symmetric and asymmetric modes at 1350 and 1650 cm⁻¹ respectively, rules out formation of an alkyl carbonate under these reaction conditions.

B. In situ X-ray absorption spectroscopy (XAS) and Raman scattering of particle electrodes embedded in inert metal supports

This strategy allows for the electrochemical and spectroscopic properties of battery grade particle electrodes to be characterized in the absence of binders and other additives.⁴ In particular, Fig. 2 displays a series of fluorescence Mn K-edge X-ray absorption near edge structure (XANES) for a Li₂MnO₂/Au electrode polarized at the potentials indicated in the cyclic voltammetry recorded in the same cell (see insert). Analysis of these results, as well as those of extended X-ray absorption fine structure (not shown here) were found to be in excellent agreement with those reported by other authors. Another illustration of the use of embedded particle electrode approach is provided by the *in situ* Raman spectra of graphite particles embedded in softened Ni foils as a function of the applied potential shown in Fig. 3.

Also to be discussed are possible extensions of these techniques to the study of a much wider variety of electrode materials, as well as of real operating devices.

ACKNOWLEDGEMENTS

This work was supported through a grant from the US Department of Energy. Additional funding was provided by a grant from NEDO Japan.

REFERENCES

1. See, for example, D. Scherson In *Nonaqueous Electrochemistry*, D. Aurbach Ed. Marcel Dekker, 1999, Chapter 5.
2. Aurbach, D., Daroux, M. L., Faguy, P. W., and Yeager, E., *J. Electrochem. Soc.*, **134**, 1611 (1987)
3. Aurbach, D., Daroux, M. L., Faguy, P. W., and Yeager, E., *J. Electrochem. Soc.*, **135**, 1863 (1988)
4. Totir, D. A., Cahan, B., D. and Scherson, D. A., *Electrochim. Acta.*, **45**, 161 (1999).

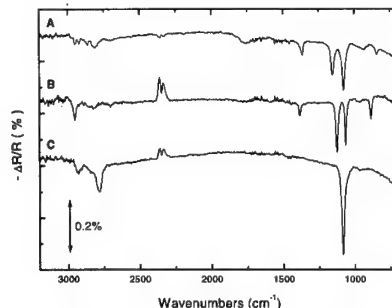


Figure 1. IRAS spectra of Li/Ni(poly) exposed to PC (curve A), DEC (curve B), and DMC (curve C) vapors at room temperature.

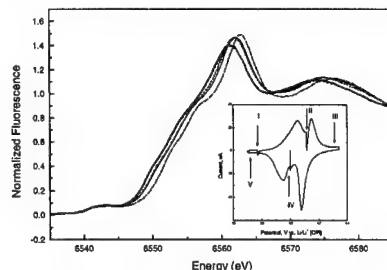


Figure 2. Series of fluorescence Mn K-edge XANES for a Li₂MnO₂/Au electrode polarized at the potentials indicated in the cyclic voltammetry recorded in the same cell (see insert).

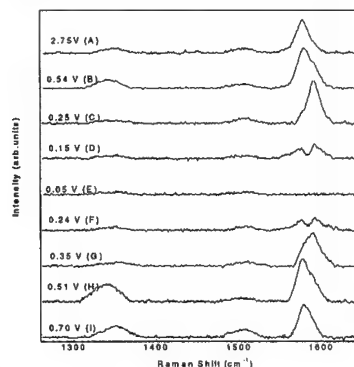


Figure 3. Series of Raman spectra as a function of potential for a KS-44 graphite powder electrode.

**Rechargeable Magnesium Battery Technology, a
Comparison with Li Battery Systems**

D. Aurbach, Y. Gofer, Z. Lu,^(a) A. Schechter,^(b) O. Chusid,
H. Gizbar, Y. Cohen, V. Ashkenazi, M. Moshkovich, R.
Turgeman and E. Levi

Department of Chemistry
Bar-Ilan University,
Ramat-Gan 52900, Israel

a. Department of Chemistry & Physics, Dalhousie
University, Halifax, Nova Scotia, Canada B3H 3J5,
b. Department of Chemical Engineering, Case Western
Reserve University, Cleveland, OH 44106, USA.

Introduction

An active metal that should be considered as an anode material in high energy density batteries is definitely magnesium. It is relatively cheap, much safer to use and handle than lithium, and its compounds are usually nontoxic.

Similar to lithium, magnesium is covered by surface films in any 'inert' atmosphere that contains atmospheric contaminants, and in most of the relevant electrolyte solutions for batteries. In contrast to lithium where the surface films covering the active metal are Li-ion conductors, surface films formed similarly on magnesium can not conduct the bivalent Mg^{++} ions.⁽¹⁾ Electrolyte systems in which magnesium electrodes behave reversibly are Grignard salt solutions in ethers ($RMgX$; R=alkyl, aryl and X=Cl, Br). It was found that in these solutions, Mg electrodes are not passivated.⁽²⁾ However, these solutions are not suitable for battery application, because they are strongly reducing agents that are not compatible with any possible relevant cathode for rechargeable magnesium batteries.

About 10 years ago there was a report in the literature on an attempt to develop rechargeable Mg batteries based on ethereal solutions of $Mg(BR_4)_2$ salts (R=alkyl, aryl groups) and Mg insertion cathodes: Mg_xCoO_y .⁽³⁾ The use of magnesium organo borate salts definitely produced electrolyte solutions of a wider electrochemical window than that of the $RMgX$ /ether solutions. However, the data presented in this report⁽³⁾ were not at all promising from the practical point of view. Over the past years there have been continuous efforts to develop host materials that can intercalate electrochemically with bivalent ions, including Mg^{++} , and thus can be used as cathodes for rechargeable Mg batteries.⁽⁴⁾ However, since the publication of the $Mg-Mg_xCoO_y$ battery system⁽³⁾ we have not seen any reports in the literature on integrated, practically important, prototypes of magnesium batteries. The aim of this presentation is to report on a novel Mg battery system that we developed recently. At this stage: the publication of this abstract, only limited information can be released. However, a comprehensive presentation of this battery system will be given at the IOILMB

Results and discussion

The R&D of the new Mg battery systems benefited from the use of the most novel tools in material and surface science, with the emphasis on the use of *in situ* techniques (FTIR, XRD, STM, EQCM and EIS). We developed new electrolyte solutions based on ethers of the 'glyme' family, and magnesium aluminates whose electrochemical window is 2.5 V wide. It was confirmed by *in situ* FTIR, STM, EQCM and EIS that magnesium electrodes do not develop passivating surface films in these solutions. The efficiency of Mg deposition-dissolution cycles in these solutions was higher than 99%, confirmed by EQCM and standard electrochemical measurements. We also developed a cathode material which is an Mg ion insertion compound of

the Mg_xMS_y type (M=transition metal) whose working potential is 1.3 – 1 V vs. magnesium (during discharge), and its practical charge capacity may reach >100 mAh/gr. This cathode is completely compatible with the above electrolyte solutions, and behaves highly reversibly at practical rates. Prototype batteries in coin cell configurations were constructed and tested. Preliminary tests showed that these battery systems may possess an energy density > 90 Wh/Kg of the active components, can be cycled at 100% DOD over a thousand charge-discharge cycles with negligible capacity fading, and can function at practical rates (0.1 – 1 mA/cm² of the electrodes). It should be noted that cathode modification can increase both the potential and the energy density of these batteries (work on this is presently in progress).

These batteries are totally environmentally friendly and are composed of cheap, abundantly available materials. They are expected to be superior in terms of energy density and environmental aspects than commonly used rechargeable batteries. They are inferior in energy density compared with Li-ion batteries, but should be safer and cheaper, and hence, may be suitable for applications which require large size batteries.

Acknowledgment

This work was partially supported by Advance Technology Upgrading (ATU Ltd.), Israel.

References

1. Z. Lu, A. Schechter, M. Moshkovich, and D. Aurbach, *J. Electroanal. Chem.* 466, 2203 (1999).
2. D. Aurbach, M. Moshkovich, A. Schechter, and R. Turgeman, *Electrochemical and Solid State Letters* 3, 31 (2000).
3. T. Gregory, R. Hoffman and R. Winterton. *J. Electrochem. Soc.* 137, 3 (1990).
4. P. Novak, R. Tuhof and O. Haas, *Electrochimica Acta* 45, 351 (1999).

Abstract No. 35

Nanomaterial-Based Li-Ion Battery Electrodes

Charles R. Martin, Nichao Li and Bruno Scrosati^a
Department of Chemistry, University of Florida,
Gainesville, FL 32611

^aDepartment of Chemistry, University "La Sapienza",
00185 Rome, Italy.

Template synthesis is a general method for preparing nanomaterials that entails synthesis of the desired material within the pores of a microporous membrane or other solid.^{1,2} The membranes employed contain cylindrical pores with monodisperse diameters that run the complete thickness of the membrane (typically 5 to ~50 μm). Corresponding cylindrical nanostructures of the desired material are obtained within the pores. Of particular interest to battery research and development, the template method can be used to prepare nanostructures of Li-ion battery electrode materials.³⁻⁷ High-density ensembles of these nanostructures, where the nanostructures protrude from a current collector surface like the bristles of a brush, can be prepared.

We have demonstrated that these nanostructured Li-ion battery electrodes show better rate capabilities than conventional electrodes composed of the same materials.^{3-6,7} Better rate capabilities are obtained because the distance over which Li^+ must diffuse in the solid state is dramatically decreased in the nanostructured electrode. Furthermore, the surface area of the nanostructured electrode is larger, making the effective current density during discharge smaller than for a conventional electrode discharged at the same current density.

This lecture will focus on rate capabilities and recyclability of nanostructured Sn-based anodes prepared via the template method. Such anodes (derived from oxides of tin, e.g., SnO_2) have been of considerable recent interest because they can, in principle, store over twice as much Li^+ as graphite.^{8,9} However, large volume changes occur when Li^+ is inserted and removed from the Sn-based materials, and this causes internal damage to the electrode resulting in loss of capacity and rechargeability.¹⁰⁻¹³ We describe here a new nanostructured SnO_2 -based electrode that can deliver very high capacity (600 mAhg^{-1}) at very high discharge currents, and still retain the ability to be discharged and recharged through many cycles.

Nanofibrous Sn-based anodes were prepared by doing sol-gel template synthesis of SnO_2 within the pores of a commercially-available microporous polycarbonate filtration membrane (Poretics). This procedure yields monodisperse 110 nm-diameter, 6.0 μm -long nanofibers that protrude from the current collector surface like the bristles of a brush. The charge storage capacity of the nanostructured electrode (and a thin-film-control electrode containing the same quantity of SnO_2) were investigated by doing constant current charge/discharge experiments between potential limits of 0.2 and 0.9 V vs. Li^+/Li .

At very low discharge rates both electrodes showed an experimental capacity that was essentially identical to the theoretical capacity associated with Li alloying of tin over this potential range. As is always observed, capacity fell off with increasing discharge rate; however, the extent of capacity loss was dramatically

reduced for the nanostructured electrode. This is because in order to achieve full capacity all of the Li^+ in the electrode must be removed during the discharge. This is more easily accomplished when the distance over which Li^+ must diffuse in the electrode material is decreased, as it is in the nanomaterial.³⁻⁷

In addition to this rate capability advantage, the nanostructured anode showed absolutely no loss of capacity with cycling. Furthermore, the charging and discharging were done at a very high rate, 32 C, which corresponds to a current density of 1.33 mA cm^{-2} . In spite of this high rate, the capacity was still large, ~600 mA h g^{-1} . The thin-film-control electrode delivered an order of magnitude less capacity at this rate.

This combination of high capacity, long cycle life, and extraordinary rate capability has never been observed for an electrode of this type. The extended cycle life is undoubtedly related to the small size of the nanofibers that make up the electrode, over an order of magnitude smaller than achieved for any previous electrode of this type. In addition, the nanofibers are composed of very small grains of electrode material, which has also been shown to be beneficial to the cycle life of these materials.^{10,12}

1. J. C. Hulthen and C. R. Martin, *J. Mater. Chem.*, **7**, 1075 (1997).
2. C. R. Martin, *Science*, **266**, 1961 (1994).
3. G. Che, K. B. Jirage, E. R. Fisher, C. R. Martin, and H. Yoneyama, *J. Electrochem. Soc.*, **144**, 4296 (1997).
4. C. J. Patrissi and C. R. Martin, *J. Electrochem. Soc.*, **146**, 3176 (1999).
5. M. Nishizawa, K. Maukai, S. Kuwabata, C. R. Martin, and H. Yoneyama, *J. Electrochem. Soc.*, **144**, 1923 (1997).
6. G. Che, B. B. Lakshmi, E. R. Fisher, and C. R. Martin, *Nature*, **393**, 346 (1998).
7. N. Li and C. R. Martin, *J. Electrochem. Soc.* In press.
8. Tahara, K., Ishikawa, H., Iwasaki, F., Yahagi, S. S., Sakkata, A. & Sakai, T. *Eur. Pat. Appl.* 93111938, 2 (1993).
9. Y. Idota, T. Kubota, A. Matsufuji, Y. Maekawa, T. Miyasaka, *Science* **276**, 1395-1397 (1997).
10. J.O. Basenhard, J. Yang, and M. Winter, *J. Power Sources* **68**, 87-90 (1997).
11. T. Brousse, P. Paillard, R. Retoux, and D. Schleich, *J. Electrochem. Soc.* **145**, 1-4 (1998).
12. I.A. Courtney, and J.R. Dahn, *J. Electrochem. Soc.* **144**, 2045-2052 (1997).
13. I.A. Courtney, and J.R. Dahn, *J. Electrochem. Soc.* **144**, 2943-2948 (1997).

Microstructure effects in plasticized PVDF-HFP-based electrodes for plastic Li-ion batteries

Aurelien Du Pasquier, Tao Zheng,
Glenn G. Amatucci and Antoni S. Gozdz

Telcordia Technologies (formerly Bellcore)
Red Bank, NJ 07701, USA

Plasticized composite electrodes for plastic lithium-ion batteries^{1,2} possess several readily adjustable characteristics, e.g., microporosity, the plasticizer and methods of its removal, that make them convenient systems to study structure-property relationships. For a given thickness and volume fraction of the binder, active material and conducting additive, and depending on its microstructure, the rate capability and energy density of an electrode may widely.

In the present study, we have investigated several parameters affecting microstructure of the electrode. These included the crystallinity of PVDF-based binders with variable HFP content, and the effect of the nature of the plasticizer (PC, DBP or no plasticizer) and its removal method (solvent extraction or evaporation). Changes in the crystallinity of the polymeric binder affected by processing conditions were investigated by DSC, XRD and mechanical tests.

The effect of microstructure on the physical properties of the electrode was studied by mechanical testing, pore size distribution by mercury porosimetry, specific surface area and SEM imaging. Further, rate capability (specific power), specific energy and electrochemical stability (capacity fade) of the electrodes was determined as a function of the electrode thickness [Fig.1]. Our results indicate that carefully designed plasticized-polymer Li-ion systems can achieve very high specific power and energy values even at low temperatures (-20°C). Their characteristics are fully competitive with those of liquid-electrolyte Li-ion cells based on non-plasticized electrodes [Fig.2].

References

- [1] A. Du Pasquier and A. S. Gozdz
Proceedings of the Joint 196th Meeting of The Electrochemical Society, Inc. and 1999 Fall Meeting of The Electrochemical Society of Japan; October 17-22, 1999; Honolulu, HI (in press)
- [2] A. Du Pasquier, G. G. Amatucci, I. Plitz, T. Zheng, A. S. Gozdz, and J.-M. Tarascon
Solid State Ionics (in press)

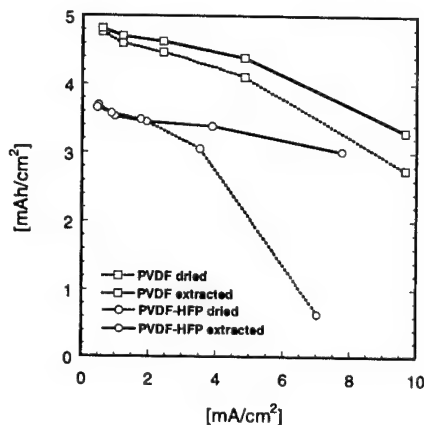


Fig.1. Effect of electrode binder and plasticizer removal method on discharge rate capability of PLiON™ cells with electrodes having the same composition.

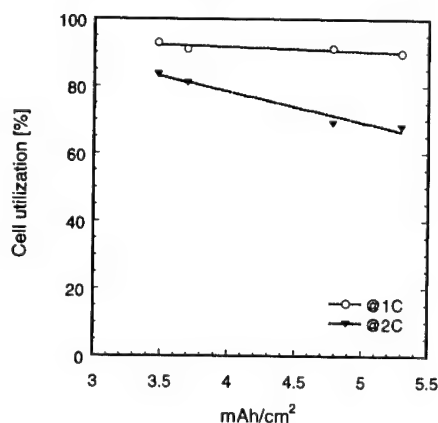


Fig. 2. Effect of electrode capacity on discharge rate capability.

Abstract No. 37

Investigations of Non-Flammable Phosphazene Based Compounds for Lithium Ion Batteries

Jai Prakash and Chang Woo Lee

Center for Electrochemical Science and Engineering,
Department of Chemical and Environmental Engineering,
Illinois Institute of Technology, Chicago, IL, USA

Introduction

Lithium batteries possess high energy density compared to other secondary batteries. Small Li-ion batteries with a capacity of 1300 to 1900 mAh are currently commercially available to power portable electronic devices such as camcorders, computers, cameras, etc. In addition, Li-ion and Li-polymer batteries are being developed as power sources for electric vehicles (EV)¹⁻³ to provide longer drive ranges, higher accelerations and longer lifetimes. However, safety concerns have limited the full utilization of Li batteries in EV applications. The primary challenge in designing the Li-ion and Li-polymer EV batteries is its safety under abusive as well as normal operating conditions. Under certain conditions, the flash point of the electrolyte can be exceeded and the Li-ion can be overheated, thereby resulting in major safety problems.⁴ Thus, nonflammability⁵ of the electrolyte is an essential property for the safe design and operation of EV batteries. This paper describes the preliminary results of the electrochemical and thermal investigations carried out on the electrolyte systems modified by incorporation of a non flame-retardant additive in the electrolyte.

Experimental

The effect of the flame-retardant additive hexa-methoxy-cyclo-tri-phosphazene (HMTP) on the electrochemical stability and the performance was investigated in Li/LiNi_{0.8}Co_{0.2}O₂ cells. The thermal stability of the electrolyte with and without the flame-retardant additive was investigated using a differential scanning calorimeter (DSC 7, Perkin-Elmer) and an accelerating rate calorimeter (ARC 2000TM, Arthur D Little Inc.).⁴⁻⁵

Results and Discussion

Cyclic voltammetry showed that the electrolyte containing the flame-retardant additive hexa-methoxy-cyclo-tri-phosphazene (HMTP) [NP(OCH₃)₂]₃ is stable up to 5.0 V vs. Li. Fig. 1 shows the electrochemical performance of Li/LiNi_{0.8}Co_{0.2}O₂ cells in the presence and absence of the flame-retardant additive in the electrolyte. The capacity of the cells was determined under the same current regimes. The charge and discharge capacities of the cell containing the 1.5 wt. % flame-retardant additives increased somewhat compared with the cell in the absence of the flame-retardant additive.

Fig. 2 shows the self-heat rate profile of the electrolyte with and without the flame-retardant additive in the ARC. It is evident that the maximum self-heat rate of the electrolyte without the flame-retardant additive is 0.68°C/min, which occurs at T=177.6°C. This can be attributed to the reaction of lithium metal with the electrolyte. As the reaction proceeds, the lithium metal is consumed, and thus the exothermic peaks decrease as the temperature increases beyond 177.6°C. On the other hand, the maximum self-heat rate of the electrolyte with the flame-retardant additive is only 0.1957°C/min at T=170.2°C. The peaks were suppressed in comparison with those for the electrolyte without the flame-retardant additive, which may be attributed to passivation layer that is formed on the surface of the lithium metal by the flame-retardant additive. Results of these thermal investigations strongly suggest that the addition of the flame-retardant additive in the electrolyte significantly reduces the self-heat rate. The reduced self-heat rate, in turn, helps in improving the nonflammability of the electrolyte.

Acknowledgment

This work was supported by the Lawrence Berkeley

National Laboratory under Contract No. 6487465. The authors would like to thank Dr. Kim Kinoshita (Lawrence Berkeley National Laboratory) for the encouragement and helpful discussions.

References

1. J. M. Tarascon and D. Guyomard, *Electrochim. Acta*, **38**, 1221 (1993)
2. J. A. R. Stiles, in *Rechargeable Lithium Batteries*, S. Subbarao, V. R. Koch, B. B. Owens, and W. H. Smyrl, Editors, PV 90-5, p. 127, The Electrochemical Society Proceedings Series, Pennington, NJ (1990)
3. S. Megahed and B. Scrosati, *Electrochem. Soc. Interface*, **3** (4), 34 (1994)
4. J. S. Hong, H. Maleki, S. Al Hallaj, L. Redey, and J. R. Selman, *J. Electrochem. Soc.*, **145**, 1489 (1998)
5. Subhash C. Narang, Susanna C. Ventura, Brian J. Dougherty, Ming Zhao, Stuart Smedley, Gary Koolpe, U. S. Patent No. 5,830,600 (1998).

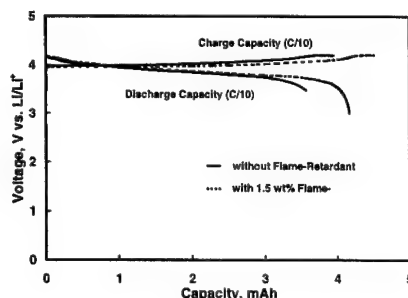


Figure 1. The cycling performance of Li/LiNi_{0.8}Co_{0.2}O₂ cell containing 1.5 wt. % flame-retardant additive.

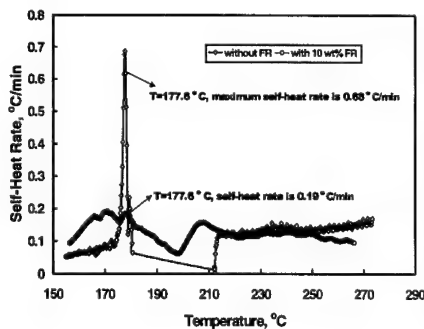


Figure 2. Thermal behavior of 1 M LiPF₆ with EC-DMC containing 0.0 and 10.0 wt. % of the flame-retardant additive using ARC.

Development of Lithium Polymer Batteries with Gel Polymer Electrolyte

Satoshi Narukawa and Ikuro Nakane¹

Soft Energy Technology Development Center

¹New Battery Division

Soft Energy Company, Sanyo Electric Co., Ltd.

222-1, Kaminaizen, Sumoto, Hyogo 656-8555, Japan

Introduction

Recently, Li-ion polymer battery with gel polymer electrolyte is applied increasingly for some commercial uses, for example, mobile phone etc. The some domestic battery makers started the mass-production of Li-Ion polymer battery last year. Many kinds of polymer, for example, polyethylene oxide (PEO), poly(vinylidene fluoride) (PVdF) and polyacrylonitrile (PAN), etc., have been studied for battery chemical [1-5]. We selected a new polymer material for electrolyte and have succeeded in developing an excellent leakage-proof battery in 3.6 mm thickness by filling up any room in the cell with the gel polymer electrolyte as well as penetrating into electrode. This battery has good charge-discharge performance and storage performance. The influence of the composition of the gel polymer electrolyte on its electrochemical characteristics and the performance of the battery applied with this gel polymer electrolyte will be discussed in this work.

Experimental

Polyether type polymer with bridge structure is used for the gel polymer electrolyte. The ionic conductivity of the electrolyte was measured by putting polymer electrolyte between blocking electrodes, which is made of stainless steel by AC impedance method. The gel polymer electrolyte was prepared by the following process. We mixed the pre-polymer with the Li-salt dissolved by electrolyte (1M LiPF₆ EC/DEC (3/7)) at several weight ratios and then coated it on a glass, and finally had it polymerized by heating. The electrochemical cell constructed in a globe box filled with argon gas and the measuring of the cell performance was done in an incubator controlled at several temperature. The test battery was constructed as following process;

- > Used a positive electrode of LiCoO₂ and a negative electrode of graphite. This is the same process as the current Li-Ion battery.
- > Wound the pair of the electrodes with micro porous polyethylene film, then inserted into a case which is made of resin laminated Al sheet.
- > Heat-sealed after infusing the gel polymer/electrolytes mixture into the case.

Results and Discussion

We have developed the gel polymer electrolytes, which can hold electrolyte solution about ten times as much as of its weight sufficiently. Figure 1 shows the temperature dependence of ionic conductivity of gel polymer electrolyte prepared at various weight ratios. We got tendency that ionic conductivity increase in all temperature range as ratio of electrolyte increases. This result is considered that a part of ionic conductivity is influenced by the electrolyte solution in the gel [6]. Under the ratio of polymer vs. electrolyte is 1:10, the ionic conductivity shows 5×10^{-3} S/cm at 25 °C and 2×10^{-3} S/cm at -10 °C. This high conductivity is almost the same to that of electrolyte solution. As concerns the

composition of electrolyte solution, we were able to reduce the swelling of the battery using LiN(SO₂C₂F₅)₂ much less than LiPF₆ under the storage at 60 °C. It was thought that this low swelling was attributed from better stability of LiN(SO₂C₂F₅)₂ than LiPF₆ at high temperature.

Li-polymer battery (model:UPF363562) by using the gel polymer electrolyte was constructed. The capacity is 570mAh, dimension is 3.6mm in thickness, 35mm in width, 62mm in height and the weight is about 13.5g. This battery has the energy density of 270Wh/l (294Wh/l in excepting sealed area), 150Wh/kg and shows good performance in the high rate discharge and low temperature discharge. In addition, the battery shows good leakage-proof, so that the electrolyte solution doesn't leak out when pressed, even though it has a small hole in its case. We therefore conclude that this polymer material is very suitable for polymer electrolyte because of its high ionic conductivity and high reliability.

References

- [1]P. V. Wright, Br. Polymer. J., 7, 319(1975)
- [2]J. F. Le Nest, S. Callens, A. Gandini and M. Armand, Electrochim. Acta., 37, 1585(1993)
- [3]K. M. Abraham and M. Alamgir, J. Electrochem. Soc., 137, 1657(1994)
- [4]G. B. Appetecchi petecchi, F. Croce and B. Scrosati, Electrochim. Acta., 40, 991(1994)
- [5]T. Fujii, I. Nakane, K. Teraji and S. Narukawa, Abstract of International Conference on Applications of Conducting Polymers: Batteries, Electrochromics, Supercapacitors and other devices, p.146(1997)
- [6]I. I. Olsen and R. Koksang, J. Electrochem. Soc., 143, 570(1996)

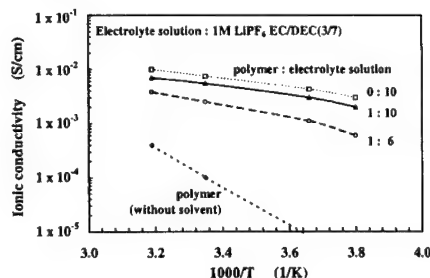


Fig.1 Temperature dependence of ionic conductivities of gel polymer electrolytes prepared at various ratio of polymer/electrolyte solution.

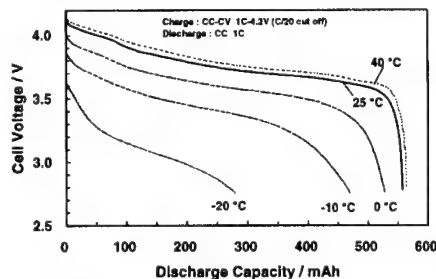


Fig.2 Discharge curves of lithium polymer battery (model:UPF363562) in various temperatures at 1C rate.

**GLASSY MATERIALS FOR LITHIUM
BATTERIES.
THEORETICAL ASPECTS AND
DEVICES PERFORMANCES.**

Michel DUCLOT*, Jean-Louis SOUQUET
Laboratoire d'Electrochimie et de
Physicochimie des Matériaux et des
Interfaces (LEPMI)
(UMR CNRS INPG N° 5631, associée à
l'Université Joseph Fourier Grenoble)
ENSEEG BP 75 - F - 38402 Saint Martin
d'Hères - France

Amorphous or glassy materials are used as active materials in Lithium batteries either as electrolyte or electrode materials (1, 2, 3).

By optimisation of their composition, Lithium conductive glasses have reached conductivities up to 10^{-4} S.cm⁻¹ at room temperature. The transport number of the alkali is unity and they present large Red/Ox windows. Some of them have been successfully used as solid electrolytes in electrochemical cells. The less conductive (oxide glasses) are deposited as thin films (≈ 1 μ m) for microgenerators (4, 5, 6) the most conductive, (sulphide glasses), are shaped in layers of about 1 mm by isostatic pressure to form button cells (7, 8). In commercially available button cells, the glassy electrolyte is an oxi-sulphide glass doped with Lithium iodide associated with a Lithium anode and a Titanium disulphide cathode. Such a cell can deliver current densities of 40 to 80 μ A.cm⁻² until 200°C and allows several hundred of cycles at temperature until 200°C (7). Nevertheless the high resistivity of the glassy electrolyte below room temperature is a limit to the potential application of these all solid state cells.

Oxide or oxi-sulphide glasses have been tested as mixed conductive electrodes for primary or secondary lithium batteries. The electronic conduction mechanism is a small polaron hopping between d-orbitals of a transition metal (Ti, V, Fe,...). Their

association with a glassy oxide allowed the recently industrial development of thin film microgenerators able to deliver a current density of 300 μ A.cm⁻² and a cyclability allowing about 1000 charge/discharge cycles (4).

1 K.J.Rao, M. Ganguli, in Handbook of Solid State Batteries and Capacitors, M.Z.A Munshi Ed., p 189, World Scientific, Singapore (1995).

2 N. Machida, R. Fuchida, T. Minami, J.of Electrochem. Soc **137** 1315 (1990)

3 Yuong-Ling Li, T. Kudo, Solid State Ionics **86-88** 1295 (1996)

4 A. Levasseur, P. Vinatier, in Solid State Ionics : Science and Technology, B.V.R Chowdari Ed., p 421, World Scientific, Singapore (1998).

5 S.D. Jones, J.R. Akridge, Solid State Ionics **86-88** 1291 (1996)

6 C.H. Chen, E.M. Kelder, J. Schoonman, J.of Power Sources **68** 377 (1997)

7 S.D. Jones, J.R. Akridge, in Handbook of Solid State Batteries and Capacitors, M.Z.A Munshi Ed., p 209, World Scientific, Singapore (1995).

8 K. Takada, S. Kondo, Ionics **4** 42 (1998).

* corresponding author : Tel : 33/(0)4 76 82 65 69 Fax 33/(0)4 76 82 66 70
E-mail : Michel.DucLOT@lepmi.inpg.fr

Research on highly reliable solid-state lithium batteries in
NIRIM

Kazunori Takada, Taro Inada, Akihisa Kajiyama, Masaru Kouguchi, Shigeo Kondo, and Mamoru Watanabe
National Institute for Research in Inorganic Materials
Namiki 1-1, Tsukuba, Ibaraki 305-0044 JAPAN

The usage of solid electrolytes is a fundamental solution to improve the reliability of conventional lithium batteries. National Institute for Research in Inorganic Materials (NIRIM) started developing highly reliable lithium batteries at July in 1999. Solid-state batteries can be safety, and suppress various side reactions because lithium ion is only a mobile species in solid electrolytes. We investigate some materials that have not been considered as candidates for electrode materials and found that they act as electrode materials in a solid electrolyte system.

FeS_2 has been studied as a cathode material in thermal cells. It shows two plateaus at 2.3 V and 1.6 V during its reduction in a Li^+ ion conductive electrolytes [1]. The former was reported to be reversible reaction, but the later to lead to formation of Fe metal, which seems to be irreversible. We have investigated the reduction process of Li_2FeS_2 in a Li^+ ion conductive oxysulfide glass and found that the reaction is reversible as shown in fig. 1. Our some analytical data suggested that the conversion rate from a meta-stable phase, which was formed by the reduction, to Fe metal was so slow in the solid-state system that the meta-stable phase acted as a reversible electrode. In other words, the formation of Fe metal was suppressed owing to the solid electrolyte, so that the electrode reactions remained reversible.

LiVS_2 was also studied as an electrode material in lithium batteries. Murphy et al. reported that the $\text{Li}_2\text{VS}_2 / \text{LiVS}_2$ couple was reversible, but further extraction of Li^+ ions rapidly led to deterioration [2]. But in a solid-state battery, we show, the reaction is successfully reversible as displayed in fig. 2.

One of the examples, which demonstrate the potentiality of solid electrolyte, is the electrochemical behavior of Li_2FeCl_4 in the solid-state system. The chloride has a high ionic conductivity [3] and contains Fe^{2+} ions available for a redox reaction. One can imagine that it will be an electrode material in lithium batteries. However its ionicity is so high that it is easily dissolved in a liquid electrolyte and therefore can not be used as an electrode material. Fig. 3 indicates a potential profile of Li_2FeCl_4 during the oxidation in the solid electrolyte. It shows a plateau at ca. 3.5 V vs. Li/Li^+ . In our further studies, the reaction was revealed to be extraction of Li^+ ions from Li_2FeCl_4 . The phenomenon suggests that ionic materials can also be candidates for electrode materials by using solid electrolytes.

Details of these examples as well as the concept of our research will be presented at the meeting.

References

- [1] R.Fong, J.R.Dahn, and C.H.W.Jones, J. Electrochem. Soc., **136**, 3206 (1989).
- [2] D.W.Murphy and J.N.Carides, J. Electrochem. Soc., **126**, 349 (1979).
- [3] R.Kanno, Y.Takeda, and O.Yamamoto, Solid State Ionics, **28-30**, 1276 (1988).

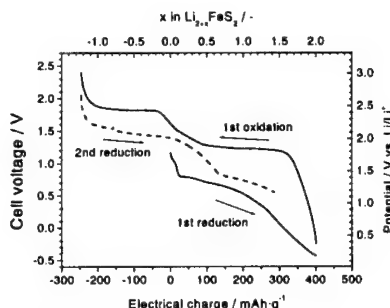


Fig. 1 Potential profile of Li_2FeS_2 .
In-Li alloy was used as a counter electrode.

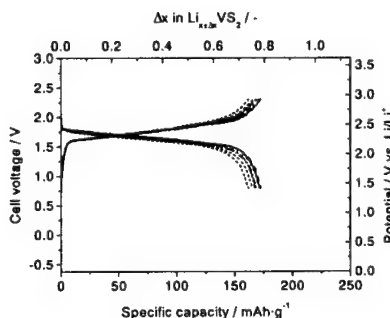


Fig. 2 Charge-discharge cycle of the cell, In-Li alloy / LiVS_2 .

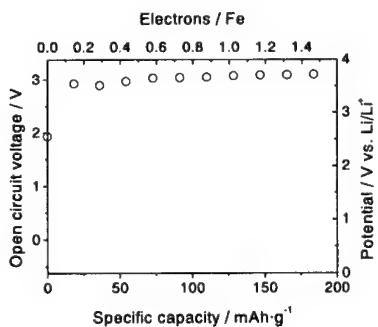


Fig. 3 Potential profile (open circuit voltage) of Li_2FeCl_4 during the oxidation in the Li^+ ion conductive glass. Counter electrode was In-Li alloy.

Abstract No. 41

Materials Development for High-Performance Lithium Batteries

R.A. Huggins, A. Netz, V. Thangadurai, J. Schwenzel, S. Stramare and W. Weppner

Chair for Sensors and Solid State Ionics
Faculty of Engineering
Christian-Albrechts-University, 24143 Kiel

A large variety of materials is presently being considered for improved lithium batteries. Many of those suffer from irreversible capacity losses and reduced kinetics of the electrodes in the course of an increasing number of cycles. These problems are related to interfacial solid state chemical reactions in view of the lack of thermodynamic stabilities of the electrolyte-electrode phases and because of poor reproduction of the geometry of the phases being formed in the electrodes.

Similar to semiconductor junctions, the electrostatic potential drop occurs only at interfaces. The driving forces by the chemical potential differences for both ions and electrons across the electrolyte-electrode interfaces are compensated by the formation of an electrical field to build up the same electrochemical potentials for the ions and electrons at both sides of the interfaces.

In contrast to semiconductors with space charge layer thicknesses of the order of $1\mu\text{m}$, the Debye length of fast ionic conductors and good electronically conducting electrodes is quite small, i.e. of the order of one atomic layer. Accordingly, high chemical stability is mandatory for the electrolyte-electrode contact. Common approaches of using immobile ions, as often considered in the case of semiconductor devices, are not applicable because of the functionally essential requirement of mobile ions moving across the interfaces.

Thermodynamic equilibria may be commonly not achieved because of the different electronic properties required for the electrolyte and electrode materials and the unlikeliness of such phases in thermodynamic equilibrium with each other. Furthermore, the electrode phases show large variations in the compositions and lithium activities upon discharge. This does not only cause problems of chemical instabilities between the electrolyte and electrodes, but causes also quite different local arrangements of the various phases depending on the kinetic paths of the chemical reaction.

The achievement of high performance batteries is based on the development of materials with improved interfacial stabilities. Kinetic aspects with regard to the ionic mobilities of all components of both the electrolyte and the electrodes are taken into account for the selection of appropriate materials compositions.

Furthermore, various additional compounds were dissolved in the electrolyte for varying the electronic properties in view of the equilibration of the electronic charge carriers across the interfaces besides that of the electrochemically active ionic species.

Successful previous applications of Li_xCoO_2 and $\text{Li}_x\text{Ni}_2\text{O}_7$ cathodes depend on the performance of these

materials just like quasi-binary compounds. The two phases which are being formed and decomposed upon discharge and charging of the battery are in line with the direction toward the lithium corner the Gibbs triangle. Structural variations are small in addition. That is not the case for other cations under investigation in place of Ni and Co.

Thermodynamic relationships between the various components of the electrodes result in kinetic paths within the phase diagram which are locally considerably different from thermodynamically expected overall equilibrium compositions.

Furthermore, electronic bulk properties are taken into consideration for enhanced chemical diffusion and accordingly improved power rates.

Various oxides, which are presently being considered for anodes, behave kinetically quite unfavorable because of blocking tarnishing layers. Other approaches seem to be more favorable in view of high energy and power densities.

Transport of lithium ions across interfaces appears to be a considerable problem in all-solid-state batteries. It appears favorable to avoid these impedances and to develop "monolithic lithium batteries" which are based on a single material without interfaces between structurally different compounds. The feasibility of this concept will be discussed. Such systems may play an important role for applications with energy densities in the range between those of supercaps and high energy density lithium batteries.

Abstract No. 42

Modeling lithium-ion battery oven exposure tests

J. R. Dahn, T. D. Hatchard, D.D. MacNeil and L. Christensen*

Departments of Physics and Chemistry, Dalhousie University, Halifax, Nova Scotia, Canada B3H 3J5

a - 3M Co. 3M Center, St. Paul, MN, 55144-1000, USA.

Calorimetric experiments using ARC and DSC are used to develop kinetic expressions for the reactions between electrode materials and electrolyte as a function of temperature and reaction history. These so-called "power functions" are then combined with Newton's law of cooling and the heat equation to produce a full thermal model capable of accurately predicting thermal runaway in Li-ion cells of any size or shape.

A Visual C++ program has been developed that is user friendly and allows the battery designer to simulate the effects of design changes (cell radius, surface heat transfer coefficient, cell shape) on oven exposure test results. (1) This program will be demonstrated during this presentation. Figure 1 shows a comparison between model and experiment for commercial 18650 cells.

During this work, we realized the importance of radiation heat transfer from the cell surface. Radiation provides approximately 50% of the heat flow from the cell to the environment during the oven test, while conduction and convection provide the rest. The radiated power is directly proportional to the emissivity of the surface, which is a characteristic of the material (usually the cell label) making up the outermost surface of the cell.

Figure 2 shows oven exposure tests for Li-ion 18650 cells that have been first charged to 4.2V. One result is for a cell as received from the manufacturer and the other result is for a cell from the same manufacturer with the label removed. The emissivity of metal surfaces generally ranges from 0.1 to 0.35 while that of plastic can be near 0.8. Therefore, labeled cells transfer heat more effectively to the environment and do not exhibit thermal runaway until the temperature has been increased by 15 to 20°C above the point where the unlabelled cells exhibit runaway.

This work suggests that cell labels and battery pack cases should be made from materials with emissivities as close to 1 as possible. (2)

Acknowledgement: Funding for this work was provided by 3M Co. and the Natural Sciences and Engineering Research Council of Canada

References

1. J.R. Dahn, T.D. Hatchard and D.D. MacNeil, U.S. Patent Application, Filed Dec 29, 1999.
2. J.R. Dahn, T.D. Hatchard and D.D. MacNeil, U.S. Patent Application filed Dec 28, 1999.

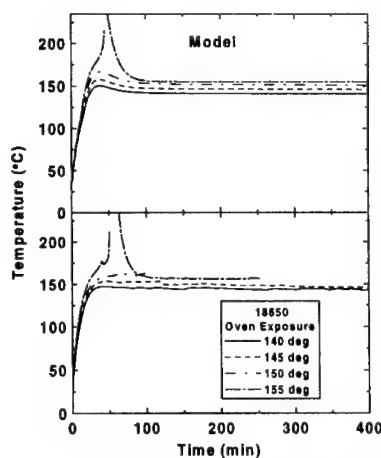


Figure 1. Comparison between oven exposure test results measured for 18650 cells at 4.2V (lower panel) and the model predictions.

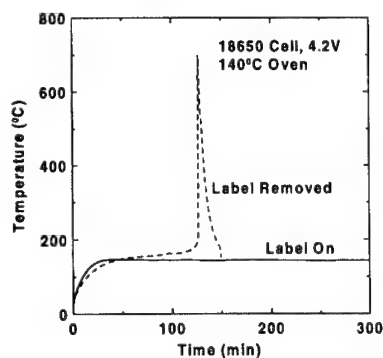


Figure 2. Oven exposure test results for 18650 cells charged to 4.2V. Solid line - cell as received dashed line - label removed.

Abstract No. 43

-Recent Investigations on Thin Films and Single Particles of Transition Metal Oxides for Lithium Batteries

Isamu Uchida, Mohamed Mohamedi, Matsuhiko Nishizawa, Takashi Itoh
Tohoku University

Department of Applied Chemistry, Graduate school of Engineering, 07 Aramaki Aoba, Aoba-Ku, Sendai 980-8579, Japan

An extensive research program dealing with several aspects related to battery systems is being carried out in our group.

Part of this program is to develop both new anode and cathode materials that would improve the performance of the actual batteries such as lithium-ion batteries and nickel-metal hydride batteries. Other argued phenomena for instance lithium insertion/extraction mechanism and manganese dissolution are also being investigated in our group. The present lecture will highlight some recent research and development on cathode materials that have been carried out in our laboratory.

Lithium insertion/extraction mechanism

Thin film electrodes permit evaluations of the active material itself without effect of conductive additives and organic binder. A uniform, dense film of spinel LiMn_2O_4 (0.1 μm thick) has been prepared by the electrostatic spray deposition (ESD) technique. The electroanalytical behavior of this electrode was elucidated by use of electrochemical impedance spectroscopy (EIS). The data have been modeled using an equivalent circuit approach following rigorous criteria. An excellent fit was found between measured data and the derived model, comprising Li^+ migration through surface layer, potential-dependent charge transfer resistance, semiinfinite Warburg-type element, reflecting solid state Li^+ ion diffusion and a finite space Warburg-type element, describing both diffusion and accumulation of lithium at the very low frequency. Specific parameters of interest were determined in this investigation: (i) diffusion coefficient, (ii) redox capacitance, (iii) surface film capacitance, resistance, and (iv) exchange-current density. The apparent chemical diffusion coefficient of lithium in the spinel phase was found within $10^{-12} < \bar{D}_{\text{Li}} < 10^{-9} \text{cm}^2 \text{s}^{-1}$ as function of electrode potential with minima at the potentials corresponding to the voltammetric peaks. The robustness of the model was checked by changing the experimental conditions (electrolyte, temperature, film thickness, etc).

The lithium insertion/extraction reaction has also been investigated by means of a microelectrode technique recently developed in our group (Fig.1).^{1,2} We were able to perform transient as well as stationary electrochemical methods by means of this microelectrode. Impedance was carried out on LiMn_2O_4 and LiCoO_2 single particles and the data have been analyzed according to an equivalent circuit approach.

Manganese dissolution

Manganese dissolution is believed to be responsible for the low capacity fading of LiMn_2O_4 in LiPF_6 containing solutions at elevated temperatures. The

microelectrode technique has been applied to a single particle of LiMn_2O_4 in 1M $\text{LiPF}_6/\text{PC}+\text{EC}$ (1:1) solution at 50°C. Multi-cyclic voltammetry showed a significant decrease in capacity (ca. 25% decrease upon 50 cycles). This was attributed to the dissolution of manganese oxide promoted by acidic species (HF) originated from the reaction of LiPF_6 with water. We have confirmed subsequently, the role of water in the dissolution process.

The manganese dissolution was further investigated by means electrochemical quartz crystal microbalance (EQCM) technique on thin LiMn_2O_4 films. This technique enables a direct measurement of the manganese dissolution process. The open circuit voltage and mass of LiMn_2O_4 were followed upon exposure in a 1M $\text{LiPF}_6/\text{PC}+\text{EC}$ (1:1) solution at 50°C. After 20 hrs of storage, the mass started to decrease while the OCV increased to about 4.3V vs. Li/Li^+ and sustained till the LiMn_2O_4 was completely dissolved.

All these results are very likely to support that the manganese dissolution (probably induced by the H^+ attack) proceeds with the formation of $\gamma\text{-MnO}_2$ phase at the surface.

Cathode materials

The microelectrode technique was successfully applied to various single particles of transition metal oxides such as LiCoO_2 , LiNiO_2 and $\text{Li}_{1.10}\text{Mn}_{1.852}\text{Cr}_{0.048}\text{O}_4$. An important result concerns the $\text{Li}_{1.10}\text{Mn}_{1.852}\text{Cr}_{0.048}\text{O}_4$ single particle. This material exhibited no significant capacity fading even in the 1M $\text{LiPF}_6/\text{PC}+\text{EC}$ (1:1) solution at 50°C upon 50 cycles. It is suggested that chromium doping because of Cr-O bond is stronger than Mn-O bond stabilized the spinel structure.

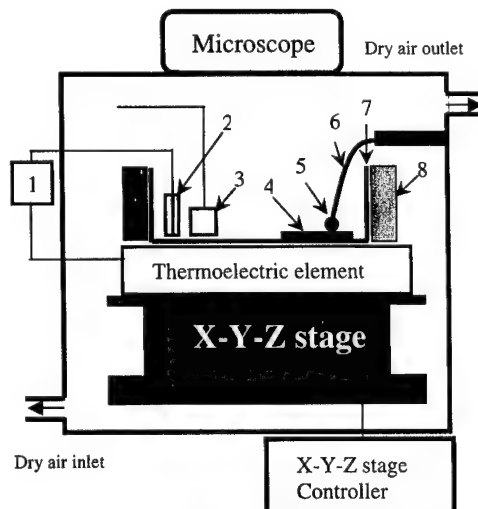


Fig.1 Sketch of the experimental set-up for single particle investigations. 1: thermal controller, 2: thermocouple, 3: Li foil, 4: Teflon mesh, 5: single particle, 6: Pt-Rh filament, 7: Teflon cell, and 8: alumina wool.

References

- [1] Uchida et al, *J. Power Sources*, **68**, 139 (1997).
- [2] M. Nishizawa and I. Uchida, *Electrochim. Acta*, **44**, 3629 (1999).

Recent Advances on Rechargeable Lithium Ion Polymer Batteries in Korea

K.S. Yun, B.W. Cho, W.I. Cho and H.S. Kim
Battery and Fuel Cell Research Center
Korea Institute of Science and Technology
39-1 Hawolgok-dong, Sungbuk-ku, Seoul 136-791, Korea

Many local battery makers recently announced one by one to begin mass production of the lithium ion polymer battery in Korea with the mobile phone boom. There are five or six potential suppliers of lithium ion polymer batteries, which are preparing for mass production by this year or early next year. This is because secondary batteries, in particular, the lithium ion polymer battery have been called one of the next generation commodities with bright prospects. According to the prospects of the related institutions, the rate of increase of secondary batteries in the domestic market is estimated 20.7% yearly growth until the year 2002 and 17% until the year 2005 respectively, which values are far exceed the global increase rates of 13.2% - 11.4% in the same period. In monetary amounts, the domestic market will have the size of 510 billion won(\$425 million) in this year and 1.12 trillion won(\$933 million) by the year 2005 and the world market share will increase from 7% to 9% in the same period. In spite of several technological and marketing problems for the mass production, the local battery makers are in believe that the lithium ion polymer battery will make inroads into the lithium ion battery market soon or later, because of several advantages such as leakage free, safety and design flexibility etc.

The research activities on polymer batteries in Korea are covered almost every fields from materials to manufacturing processes. Presently two national research projects are ongoing; one for development of small power sources and the other for electric vehicle. Although the research projects on the polymer batteries hold a minority in these national research programs, around 20 companies and research institutions including universities are involved in the development of polymer battery. The majority of research groups are supported by other governmental or private research funds.

Major researches are focused on the development of the polymer electrolytes, which might be classified into hybrid and gel type electrolytes. The R&D on the hybrid electrolyte originated from Bellcore are concentrated mainly on the process engineering and the others are to exploit a new polymer electrolyte blended with different polymers such as poly(acrylonitrile), poly(vinylidene)fluoride, poly(methylmetacrylate), etc.

Besides of a good ionic conductivity, the polymer electrolyte must be extrusive easily as a free-standing film for mass production and exhibit an excellent mechanical property with strong adhesive character as well as a good chemical and electrochemical stability. In figures 1-3 some of the recent advances of R&D in polymer batteries are demonstrated. The poly(acrylonitrile) based polymer electrolyte met so far the requirements mentioned above. Including these, the recent activities on advanced batteries in Korea will be outlined.

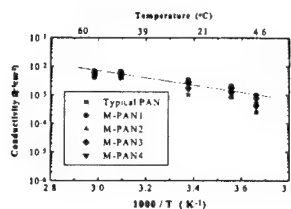


Figure 1. Ionic conductivity of PAN-based polymer electrolytes.

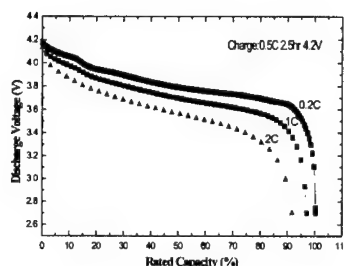


Figure 2. Rate characteristic of lithium ion polymer battery (charge rate : C/2 at room temperature).

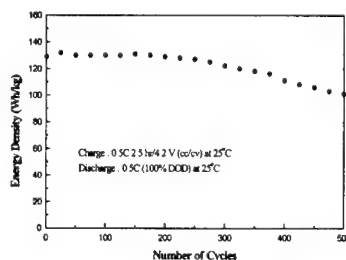


Figure 3. Cycle performance of lithium ion polymer battery (charge and discharge rate : C/2 at room temperature).

Lithium Metal / Polymer Battery

Tetsuya OSAKA

Department of Applied Chemistry, Waseda University
Shinjyuku, Tokyo 169-8555, Japan

For the next generation rechargeable battery, lithium secondary battery using lithium metal as the anode is the most attractive candidate for higher energy power sources for portable electric devices, electric vehicles, and load leveling systems. Lithium metal demonstrates remarkable low electrochemical equivalent and the most negative redox potential among all metallic elements. There are, however, some disadvantages of the lithium metal anode compared to the carbon anode of Li-ion battery [1,2].

In order to enhance the lithium anode properties, the effect of additives to the liquid electrolyte was studied, e.g., CO₂ [9-13], HF [3,4] and so on. In addition, the dendritic growth of lithium was suppressed in poly(ethylene oxide) (PEO)-based gel electrolyte [5].

The gel electrolyte, which consists of polymer matrix, organic solvent and supporting electrolyte, was introduced as a novel material in the field of rechargeable battery applications [6-8]. By applying the gel electrolyte to the batteries, the electrolyte solution does not leak out from the cell, and the electrolyte can be prepared as a thin film, which enables to construct a solid state and high energy density battery. In particular, the gel electrolytes demonstrates highly ionic conductivity about 10^{-3} S cm⁻¹ at room temperature and has a sufficient mechanical strength, e.g., poly(acrylonitrile) [9,10], poly(methyl methacrylate) [8,9], a new copolymer of vinylidene fluoride with hexafluoropropylene (PVdF-HFP) [4,12] based gel electrolytes. In 1997, on the basis of these background, the first reliable and practical rechargeable Li-ion plastic battery, which contained the carbon material as an anode, was developed by applying the PVdF-HFP copolymer type gel electrolyte [13]. In addition, we demonstrated the high charge-discharge performance of lithium metal anode in the PVdF-HFP gel electrolyte system. Furthermore, the higher performance was obtained by the combination of the CO₂ addition and gel electrolyte.

As described previously [5,14], the dendritic deposition was suppressed in the PEO gel electrolytes owing to the immobility of the electrolyte molecules. We thought that the efficiencies for the gel electrolytes depend on the kind of polymer matrix. There are some apparent differences between the PEO and PVdF-HFP gel electrolyte, i.e., the chemical behavior of polymer matrix and the immobility of the electrolyte molecules. It was most likely that the interface between the gel electrolyte and lithium played the most important role in the cycling characteristics. When the poly(tetrafluoroethylene) (PTFE), which has similar chemical structure to the copolymer of PVdF-HFP, became black in color like as carbon by contact with lithium metal, it seemed that the PTFE polymer was reduced by lithium metal and lithium surface was covered with lithium compounds. In consideration of this fact, it is probably that the enhancement property for the PVdF-HFP was due to the formation of some protective layers on the lithium by the reductive reaction of PVdF-HFP copolymer by lithium metal.

The effect CO₂ addition to the PVdF-HFP gel electrolyte and PEL gel electrolyte was also examined. The efficiency was increased by the CO₂ addition. These results confirm that the CO₂ addition is effective not only in the liquid electrolyte but also in the gel electrolyte.

Considering results as reported elsewhere [15], the combination of the PVdF-HFP gel electrolyte and CO₂ addition did enhance the efficiency of lithium anode effectively.

Additionally, the morphology of lithium deposited (charged) in the gel electrolytes was improved. In case of the PEO gel electrolyte, the morphology became rough gradually by proceeding the cycling. On the contrary, the lithium tested in the PVdF-HFP gel possesses more uniform surface than that in the PEO gel. It was due to the differences in chemical behavior and immobility of the electrolyte molecules. By the addition of carbon dioxide to the PVdF-HFP gel, the surface becomes smooth slightly. Simultaneously, an ac impedance measurement confirmed that the interface resistance was decreased [16,17].

These results suggest that there are possibilities of enhancing the lithium anode properties by selecting and designing host polymer, supporting electrolyte, solvent and additives. Further analyses and discussion should be required for understanding the characteristics of the lithium anode in the PVdF-HFP gel system. We believe that further studies will clarify the potential for the application of lithium metal to rechargeable Li batteries.

References

- [1] D. Aurbach, Y. Gofer, M. B.-Zion, and P. Aped, *J. Electroanal. Chem.*, 339, 451 (1992).
- [2] D. Aurbach and A. Zaban, *J. Electroanal. Chem.*, 348, 155 (1993).
- [3] S. Shiraishi, K. Kanamura, and Z. Takehara, *J. Appl. Electrochem.*, 25, 584 (1994).
- [4] K. Kanamura, S. Shiraishi, and Z. Takehara, *J. Electrochem. Soc.*, 143, 2187 (1996).
- [5] T. Osaka, T. Momma, T. Momma, and H. Yarimizu, *J. Electroanal. Chem.*, 421, 153 (1997).
- [6] G. Feuilleade and P. Perche, *J. Appl. Electrochem.*, 5, 63 (1975).
- [7] K. M. Abraham and M. Alamgir, *J. Electrochem. Soc.*, 137, 1657 (1990).
- [8] G. B. Apetecchi, F. Croce, and B. Scrosati, *Electrochim. Acta*, 40, 991 (1995).
- [9] S. Kakuda, T. Momma, T. Osaka, G. B. Apetecchi, and B. Scrosati, *J. Electrochem. Soc.*, 142, L1 (1995).
- [10] T. Osaka, T. Momma, H. Ito, and B. Scrosati, *J. Power Sources*, 68, 392 (1997).
- [11] J. Fuller, A. C. Breda, and R. T. Carlin, *J. Electrochem. Soc.*, 144, L67 (1997).
- [12] Z. Jiang, B. Carroll, and K. M. Abraham, *Electrochim. Acta*, 42, 2667 (1997).
- [13] J. -M. Tarascon, A. S. Gozdz, C. Schmutz, F. Shokoohi, and P. C. Warren, *Solid State Ionics*, 86-88, 49 (1996).
- [14] Y. Uchida, S. Komaba, T. Osaka, and N. Eda, in *Batteries for Portable Applications* and [17] T. Osaka, T. Momma, T. Tajima, and Y. Matsumoto, *J. Electrochem. Soc.*, 142, 1057 (1995).
- [15] M. Ishikawa, Y. Takai, M. Morita, and Y. Matsuda, *J. Electrochem. Soc.*, 144, L90 (1997).
- [16] T. Osaka, T. Momma, T. Tajima, and Y. Matsumoto, *J. Electrochem. Soc.*, 144, 1709 (1997).
- [17] T. Osaka, T. Momma, Y. Matsumoto, and Y. Uchida, *J. Electrochem. Soc.*, 144, 1709 (1997). *Electric Vehicles*, C. F. Holmes and A. R. Landgrebe (Eds.), *The Electrochemical Society Proceeding Series*, Pennington, NJ, PV 97-18, 70-76 (1997).

Abstract No. 46

Solid State Polymer Battery based on Lithium Titanate Anode

Peter Birke¹ and Fatima Salam¹

¹Fraunhofer Institut Siliziumtechnologie (ISIT)
Fraunhofer Str. 1
Itzehoe 25 524
Germany

Lithium-ion/polymer rechargeable batteries are attracting attention as being key to create thinner and lighter mobile communication and information technology devices.

The present contribution describes the development of a new all solid state-polymer battery technology which includes an innovative process that enables thin rechargeable batteries to be manufactured with lower costs.

The performance of a laboratory prototype cell composed of lithium aluminium silicate-polymer electrolyte, lithium cobalt oxide and lithium titanate electrodes will be reported.

Abstract No. 47

Shaped Charge: Adjustable Form-Factor Lithium-Ion Batteries

Walter A. van Schalkwijk
SelfCharge, Inc.
Redmond, Washington

Marc Juzkow
PolyStor Corporation
Livermore, California

For too long lithium polymer batteries have shown the promise of ease of manufacture and performance equal to that of liquid electrolyte systems. The perceived advantage has generally been for the manufacturer.

In a joint effort, we have been developing a lithium-ion polymer battery based on PolyStor's LiNiCoO₂ chemistry. Utilizing the thermoplastic properties of some of the battery materials, the cells can be shaped in two axes to fit an OEM required shape. Without the metal can the batteries are lighter and thinner thus yielding a higher energy density. The cell is flexible prior to thermoforming, but is rigid once the desired shape is made.

In principle, any degree of bend in any axis should be possible. In practice, we have made and tested cells curved to a radius of about 1.2 cm or as to make a cylinder to fit around the index finger.

Discharge capacity measurements for C-rate, C/10 and GSM performance compare favorably to the can-packaged product currently in production.

This technology is a new development and limited data exists at the abstract deadline. Test data, including projections of cycle life, electrical abuse, overcharge, forced discharge, short circuit, high-rate charge, seal integrity, and mechanical and environmental abuse will be reported at the meeting.

The batteries are not at an advanced stage of manufacture and as such have not been submitted for regulatory certifications.

The Role of Lithium Batteries in Modern Health Care

Curtis F. Holmes
Greatbatch-Hittman, Inc.
Columbia, MD 21045 USA

The first medical device using a lithium primary battery was implanted in Italy in 1972 (1). This device, a cardiac pacemaker, marked a new era in the treatment of disease by implantable devices. Before that time, pacemakers were generally powered by zinc/mercuric oxide batteries that provided only 24 – 36 months of longevity and ceased operation with little or no warning. Lithium batteries permitted the development of devices with many years of longevity. Moreover, the devices could be hermetically sealed and offered greater reliability than those previously available.

The use of lithium batteries to power implantable devices soon became standard, and by the late 1970's virtually all pacemakers were powered by primary lithium batteries. Indeed, it can be argued that the use of lithium batteries in implantable devices represented the first successful commercialization of such cells. Several cathode materials were used in the early days of lithium-powered pacemakers, including iodine-polyvinylpyridine (PVP), silver chromate, copper sulfide, and thionyl chloride. By the mid 1980's virtually all pacemakers used the lithium/iodine-PVP system.

Today's pacemakers are equipped with very advanced microprocessor circuitry and can adjust therapy to the needs of the patient by sensing physiological parameters and adjusting pacing parameters accordingly. The use of telemetry to communicate the state of the battery and medical information is common. Pacemakers of the future will likely need the higher current drains provided by systems such as manganese dioxide and carbon monofluoride.

By the mid 1970's the pacemaker was well-established as a standard treatment for bradycardia, and physicians and biomedical engineers soon became involved in the development of battery-powered devices to treat a variety of other illnesses. Today many diseases are routinely treated by devices powered by lithium batteries, and it is estimated that well over five million lithium batteries have been implanted in patients.

In 1980 the first implantable defibrillator/cardioverter (ICD) was implanted in a human (2). Dr. Michel Morowski and his colleagues developed the device, which could sense the onset of ventricular fibrillation and apply a shock of around 35 joules directly to the heart, restoring normal cardiac rhythm and saving the life of the patient. The first devices were quite large and required that an electrode be sutured directly to the heart, and could only supply the life-saving high energy shock. During the next twenty years, significant development has occurred, and devices today are smaller by around a factor of four. Transvenous leads have been developed that eliminate the need for a thoracotomy. In addition to providing the high energy shock necessary to arrest ventricular fibrillation, today's devices provide anti-tachycardia pacing as well as normal bradycardia pacing. They can store and transmit important clinical data to the physician. Most ICD's use lithium/silver vanadium oxide batteries today, although lithium/manganese dioxide batteries are also used.

Implantable neurostimulators are devices that provide therapy by stimulating various nerves in the human

body. The first use of such devices was for the treatment of some types of chronic intractable pain by stimulation of the spinal cord (3). The treatment of pain is still a common use of such devices, but newer applications such as the treatment of Parkinson's disease and epilepsy have been developed (4). The epilepsy application has been approved by the U. S. FDA, and has been shown to be effective in reducing the frequency and severity of epileptic seizure (5). These devices are typically powered by lithium/thionyl chloride or lithium/carbon monofluoride batteries.

Implantable drug delivery systems have been developed to administer controlled doses of drugs to patients in need of such drugs. The devices contain a reservoir, a pumping mechanism, electronic circuitry, and a battery. They are refilled transcutaneously through a septum on the device. These devices treat cancer, multiple sclerosis, cerebral palsy, and diabetes (6). These devices are also powered by lithium/thionyl chloride or lithium/carbon monofluoride batteries.

Several devices require rechargeable lithium ion batteries for power. Among them are left ventricular assist devices (LVAD's), the totally artificial heart, and modern implantable hearing assist devices (7). The LVAD is an implantable pumping device that provides long-term circulatory support to patients with serious heart disease. It is implanted in the thorax and is attached to the heart. The power requirements are so high that secondary batteries, worn externally, are used for power. The devices typically also contain an internal secondary battery, recharged transcutaneously, to provide backup power and allow patients an hour or so of freedom from the external pack. Implantable hearing devices have been developed to treat hearing loss in patients who are not adequately treated by conventional hearing aids. Their small size and high power requirements are well served by rechargeable implantable lithium ion cells.

Lithium batteries have served a variety of health care needs since the first implant in 1972. They have enabled the development of a wide variety of life-saving and health-giving devices. Both primary and secondary lithium/lithium ion cells serve well in this important medical role.

References:

1. G. Antonioli, F. Baggioni, F. Consiglio, G. Grassi, R. LeBrun, and F. Zanardi, Stimulatore cardiaco impiantabile con nuova batteria a stato solido al litio, *Minerva Med.* 64, 2298, (1973).
2. M. Miroski, M. M. Mower, and P. R. Reid, The automatic implantable defibrillator, *Am. Heart. J.*, 100, 1089, (1980).
3. A. J. Salkind, A. J. Spotnitz, B. V. Berkovits, B. B. Owens, K. B. Stokes, and M. Bilitch, Electrically driven implantable prostheses, in B. B. Owens, ed., *Batteries for Biomedical Implantable Devices*, Plenum Press, New York, 1986, p. 25.
4. C. F. Holmes, Electrochemical power sources – an important contributor to modern health care, *J. Power Sources*, 65, xv, (1997).
5. R. Terry, W. B. Tarver, and J. Zabara, An implantable neurocybernetic prosthesis system, *Epilepsia*, 31, Suppl. 2:S33, (1990).
6. Reference 4, p.xvii.
7. C. F. Holmes, R. A. Leising, D. M. Spillman, and E. Takeuchi, Batteries for biomedical implantable devices, *ITE Battery Letters*, 1, 132, (1999).

The Future of Lithium and Lithium-ion Batteries in Implantable Medical Devices

Craig L. Schmidt and Paul M. Skarstad
Medtronic, Inc.
Minneapolis, MN 55430, USA

Lithium primary batteries have played a vital role in the successful development of a wide range of battery-powered, implantable medical devices. The universal adoption of lithium battery technology in these applications can be ascribed to the high energy density and high voltage afforded by the lithium anode. High energy density is critically important to minimizing the size of the implanted device, and high voltage allows circuits to be powered by a single cell. The ability to develop systems that exhibit excellent long-term (> 10 years) material and performance stability has been of equal significance.

The major battery chemistries used in implantable applications are summarized in Table 1. With careful attention to battery design and manufacturing practices, each of these battery chemistries has proven to be extremely safe and reliable and well suited to its particular application. Thus, the development and/or implementation of other battery technologies will occur only if there are substantial driving forces.

In fact, there are many such driving forces that are likely to dramatically change the battery technology used in implantable medical devices over the next several years. Many developing technologies will affect either the peak power requirements or average power requirements for the battery. Some examples are summarized below.

Microprocessor-based devices – Modern pacemakers (and most of the other devices in Table 1) incorporate microprocessors and substantial amounts of memory. The development of complex processing algorithms drive the implementation of higher clock speeds, more memory, and longer processor duty cycles. All of these contribute to higher peak power requirements and tax the rate capability of the lithium/iodine batteries used in present-day pacemakers.

Improved telemetry systems – Transfer of data to or from an implanted device is accomplished via an antenna internal to the implanted device and an external antenna ("programming head") placed directly over the device. Future devices will be capable of communication over greater distances (several meters) to facilitate remote monitoring of the device via the Internet.

Smaller size – Batteries occupy approximately 30% to 60% of the volume of a typical implanted device. For power intensive applications such as ventricular defibrillation, smaller battery size can only be achieved by improving power density.

New applications – A prime example is the extension of conventional pacemaker technology to congestive heart failure applications. This involves pacing the left ventricle in addition to the right side of the heart, thus increasing the average power requirement.

Improved efficacy – The number of chronic-pain patients treatable by neurostimulators can be dramatically expanded by increasing the number of sites (along the spinal cord) that can be stimulated. This is accomplished by increasing the number of stimulation electrodes and, proportionately, the average power requirement.

Treatment of multiple disease states – Future devices will continue the trend towards treatment of multiple disease states. A recent example is the Medtronic Jewel AF[®] which provides therapies for ventricular tachycardia and fibrillation, atrial tachycardia and fibrillation, as well as conventional pacing.

Technical Approaches

There are several technical approaches for addressing these new challenges.

Modeling and power management – In many instances, increasing peak power demands can be addressed by careful power management. This requires accurate discharge and transient response models of the battery. We have developed such models for the lithium/iodine and lithium/silver vanadium oxide battery systems. These models are physically-based and can be used to accurately predict the performance of new battery designs (1-4).

New primary chemistries – These batteries must maintain the high energy density and reliability of the lithium/iodine battery while offering much higher power capabilities. Possible replacements include existing chemistries such as Li/CF_x or new technologies such as the Li/hybrid cathode systems (5,6).

Rechargeable batteries – For those systems that require high average power or extended longevity, rechargeable batteries are a viable option. The batteries can be recharged by inductive coupling as was successfully demonstrated in a commercial pacemaker in the late 1960s. It is likely that future implementations will involve lithium-ion technology due to its high voltage, high energy density, and low self-discharge. We have already verified acceptable performance of the technology using commercial cells. The tests consisted of simulated application conditions (37°C, 2 hr. charge, weekly or monthly discharge rate) over a period of five years. It is also likely that the use of rechargeable batteries will be limited to non-life support applications or involve the use of a primary battery backup. The latter concept has already been proposed by Terumo, a Japanese company that is developing rechargeable pacemaker technology (7).

References:

1. C. Schmidt and P. Skarstad, "Power Sources 13," (T. Keily and B. Baxter eds.), 1991, pp. 347-361.
2. C. Schmidt and P. Skarstad, "Power Sources 16," (T. Keily and A. Attewell eds.), 1997, pp. 121-128.
3. J. Norton and C. Schmidt, The Electrochem. Soc. Proceedings, Vol. 97-18, 197, pp. 389-393.
4. C. Schmidt, A. Crespi, and P. Skarstad, The Electrochem. Soc. Proceed., Fall 1999, (in press).
5. C. Holmes, E. Takeuchi, S. Ebel, PACE, Vol. 19, 1996, pp. 1836-1840.
6. D. Weiss et al., U.S. Patent 5,180,642
7. K. Kuwana et al., Japanese Patent H6-125994

Table 1
Typical Implantable Applications
and Battery Chemistries

Application	Device Type	Chemistry
Bradycardia	Cardiac Pacemaker	Li/I ₂
Tachycardia	Cardioverter/ Defibrillator	Li/SVO
Pain Management	Neurological Stimulator	Li/SOCl ₂
Spasticity	Drug Pump	Li/SOCl ₂

**Primary Batteries for
Implantable Pacemakers and Defibrillators**
J.Drews, G.Fehrmann, R.Staub, R.Wolf
LITRONIK GmbH & Co.
Birkwitzer Str. 79, D-01796 Pirna, Germany

Presently all primary batteries for implantable medical devices contain a lithium anode. This is based on the well known excellent energy and power density of lithium batteries. Defibrillators/ Cardioverters are either powered by lithium-silvervanadiumoxide (SVO) or lithium-manganesedioxide (MDX) cells respectively doublecells. Development, production and use of MDX batteries within implanted ICD's during the last years have confirmed the capabilities of MDX batteries which are able to comply with the extremely high pulse power requirements of that application.

Recent results of a 6-V-MDX battery development are presented. Figure 1 shows the results of a pulse discharge to illustrate the high power capability of the design. Power density of the battery is >660 W/l, low rate (600 k ζ) energy density is 410 Wh/l. The doublecell is part of a hybrid system used within ICD's. The hybrid concept makes use of two different battery chemistries within one application. In the case of ICD's the two basic requirements to the power source are high power plus longevity whereas pacemakers require longevity at low rate currents from their batteries. Therefore a hybrid system consisting of a MDX battery plus a lithium-iodine cell has been developed in order to increase pulse power capabilities and energy density of the system. The capacity requirement on the lithium iodine battery is 0.68 Ah which is considerably less than the capacity of a typical pacemaker battery. To be able to deliver sufficient power to pace and sense with the ICD, the internal design of this small cell lead to the use of a folded anode which increases the active lithium-surface resulting in a lower current density. A further power density increase of lithium iodine batteries is difficult to achieve because of the solid state system properties. Therefore the development of batteries suitable to comply with extended electrical requirements of future applications, e.g. pacemakers with increased functionalities, neurostimulators and implantable micromechanical devices has to evaluate the performance of MDX and other systems under the specific conditions and requirements of implantable batteries.

As a result of this work the electrical performance data of a medium rate MDX cell are presented. Figure 2 shows the results of a pulse discharge. The energy density of this battery is 680 Wh/l. The battery is able to supply up to 400 mA pulses for 10 s at 2.5 V BOL, this compares to a power density of 103 W/l. Low rate pulsing capacity of this battery is >2.5 Ah down to 2.0 V end voltage under the following conditions: 1 min 120 Hz pulsing current (0.5 ms pulse of 110 mA, 8.33 ms OC interval) followed by 9 min OC interval, plus constant background load of 8.6 μ A.

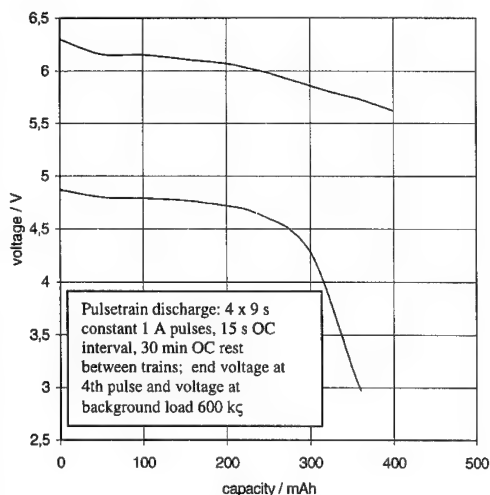


Fig.1 LiS 32125/K6+ Pulsetrain discharge

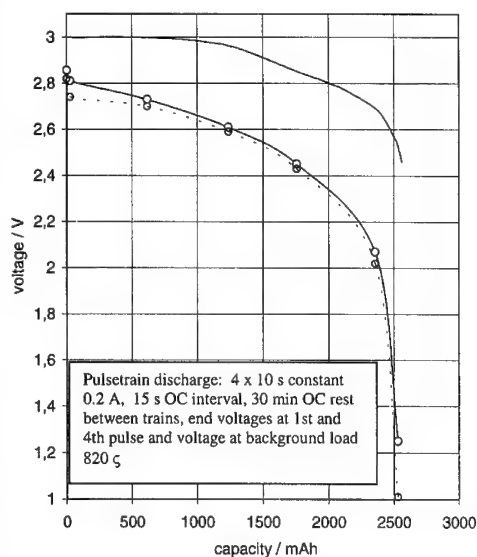


Fig.2 LiS 4087 Pulsetrain discharge

Abstract No. 51

Medical Batteries for External Medical Devices

Stefano Passerini^a and Boone B. Owens^b

a) ENEA, ERG-TEA-ECHI, C.R. Casaccia

Via Anguillarese 301, 00060 Rome, Italy

b) Corrosion Research Center, University of Minnesota,
221 Church St. SE, Minneapolis, MN 55455, USA

External medical devices are widely used, worldwide. Such devices have been used for treating scoliosis by periodic muscle stimulation, alleviating pain through transdermal electrical nerve stimulation (TENS), and for sound amplification in hearing aid devices (HAD). Primary batteries are used in most of the devices to afford free mobility to the user. Use of secondary cells would provide a number of benefits to the user.

It has been estimated that over 25 million persons in the United States suffer hearing loss and approximately 7 million use a hearing aid device (HAD). The majority of these miniature sound amplifiers are powered by Zn/air cells. A typical HAD user will replace this battery every 5 to 15 days so approximately 150-250 million of these small button cells are consumed annually in the United States. Such a high replacement rate is the source of several problems that include the following:

1. Cost. Several replacement batteries each year.
2. Environment. 150-250 million used batteries must be disposed of each year, in the United States alone.
3. Health Hazard. The proliferation of millions of small batteries annually leads to cases of the accidental ingestion of cells or the insertion of cells into the ear or nose, especially by children and the elderly.

Each of these problems can be mitigated by a user friendly medical device containing a reliable rechargeable battery. One of the major reasons that rechargeable external medical devices are not widely used is the limited performance found in present, commercially available rechargeable batteries or coin cells of appropriate size. Although large sizes of Li-ion cells are under development for medical devices (1) no small button cells are currently available.

The high level of interest in lithium batteries today is a direct result of the needs for lightweight portable power sources and the unique properties of lithium. Lithium is the lightest of the alkali metals, and as a result, can offer a higher density of energy storage than any other metallic anode material. For this reason, lithium batteries represent the ultimate in advanced, high performance batteries for the growing markets in portable consumer electronic products, communications and other cordless devices, at least in the context of present battery technology.

We⁽²⁾ developed a small, 3.6V Li-ion button cell to overcome the problems cited above for the primary battery powered HAD, and also to offer a high energy density, low impedance cell as an alternative to small NiCd and NiMH button cells.

The external medical batteries developed have a typical lithium-ion chemistry schematically depicted as:



where copper (foil) and aluminum (foil) are the current collectors and the electrolyte is one molar lithium hexafluoroarsenate in ethylene carbonate-dimethyl carbonate (50:50 by volume). The graphite and the lithium cobalt oxide are the two intercalation compounds.

Beyond the formation cycle, the batteries were tested to characterize the design and the electrochemical

performance as required for the hearing aid application. Engineering prototype batteries were used for the tests. For comparison purposes, commercially available cells based on the lithium-alloy anode/ vanadium oxide and zinc/air (Zn-air) chemistries, and also a small developmental nickel/metal hydride (Ni-MH) cell were tested. In this presentation we report the results of the investigations on the capacity, the rate performance, the cycle life, pulsed discharge performance and preliminary safety characterization of the new lithium-ion batteries we have developed for external medical applications.

Acknowledgements

This publication was made possible by Grant No. 5 R44 AG12711-03 from the National Institute on Aging, to Research International, Inc., Woodinville WA, USA. The contents are solely the responsibility of the authors and do not necessarily represent the official views of the National Institute on Aging or NIH.

References:

1. C. F. Holmes, R. A. Leising, D. M. Spillmar and E. S. Takeuchi, "Batteries for Biomedical Implantable Devices", 12th IBA Grenoble-Anneecy Battery Materials Symposium", Sept. 20, 1998.
2. US Patent pending to Research International, Inc. 1998.

Figure 1. Delivered capacity versus cell voltage behavior of a battery discharged at two different rates: C/12 (dashed line) and C (solid line). A typical charge cycle at C/12 rate is also shown (dotted line). Voltage cut-off limits: 2.75V-4.1V.

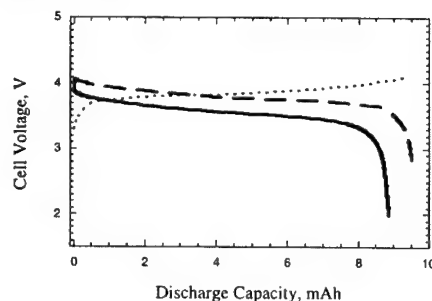
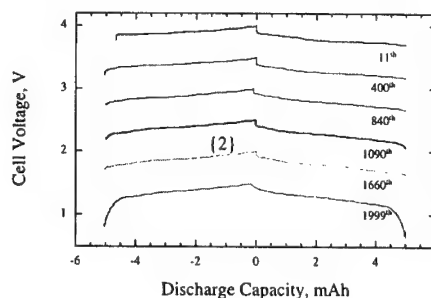


Figure 2. Cell voltage versus capacity plots of a battery in several different cycles (see legend). The cells were discharged to a fixed capacity of 5 mAh. Discharge/charge currents: 1.0/3.0 mA (C/9 - C/3 rate). Voltage cut-off limit: 4.0V. Cathodic safety limit: 2.75 V.



Advanced Capacitors and Their Application
S.Nomoto, H.Nakata, K.Yoshioka, A.Yoshida, and
H.Yoneda*

Matsushita Electric Industrial Co., Ltd.
Moriguchi Osaka JAPAN

*Matsushita Electronic Components Co., Ltd.
Uji Kyoto JAPAN

1.Introduction

An electric double-layer capacitor (EDLC) is an energy storage device, in which an electric charge is stored in the electric double layer¹⁾ formed at the interface between carbon materials and electrolytic solutions when dc voltage is applied. The EDLC has a pair of polarizable electrodes with collector electrodes, a separator, and an electrolytic solution. The capacitor is charged and the electrical energy stored in the capacitor is discharged at loads. Although an energy density of EDLCs is considerably low compared with rechargeable batteries, the capacitor shows many features, i.e. a higher power density, a stable charge-discharge performance in a wide temperature range, an environmental advantage, etc. Many studies on EDLCs have been carried out in correlation with physical and chemical properties of carbon electrode materials.²⁾

2.History and Present Status of the Capacitors

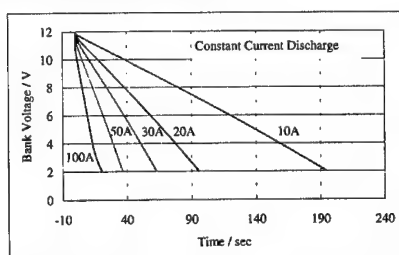
In later 1970s, with increasing application of ICs and LSI's, micro-power sources are required to back-up for microprocessors with lower voltages and currents. Matsushita started to produce EDLCs in 1978, which have been widely used as memory back-up devices in many electrical appliances, e.g. VCRs, cameras, etc. In 1980s, the EDLCs were used for the energy source to drive wristwatches with solar cells. In early 1990s, EDLCs are used as actuator back-up sources for toys, electric appliances, home equipment, etc. Recently, EDLCs with higher capacitances and lower resistances are under development for higher electric power sources in EV systems, electric power storage systems, etc.

3.Effective Factors to Capacitor Characteristics

The EDLC is supposed to be assembled micro-capacitors connected in series and parallel. Physical, chemical, and electrical properties of activated carbon materials, electrolytic solutions, collector electrode materials, separator materials, etc. are very important to determine the capacitor characteristics. The construction of carbon electrodes and collector electrodes is also an effective factor to capacitor characteristics.

4.New Capacitor for Power Uses.

Recently Matsushita Electronic Components Co., Ltd. released a new-type capacitor for power uses "UP-Cap" which shows 1.7 times higher capacitance density and almost half times lower resistance compared with conventional EDLCs. A newly developed activated carbon materials, polarizable electrode layers with a high filling density of activated carbons, and new construction of collector electrodes, realized novel characteristics of the new EDLC. Figure 1 and 2 show a representative discharge characteristics and an appearance of the capacitor developed, respectively.



• Figure 1 Discharge characteristics of EDLC bank.



Figure 2 Appearance of the new capacitor.

5.Application of the Capacitors. •

EDLCs have been applied to many kinds of electrical equipment and systems as energy back-up devices. Small coin-type EDLCs are used as memory back-up devices for microcomputers at less than mA-rate-load in VCRs, handy telephones, pagers, etc. Tubular-type EDLCs have such a low inner resistance that they are used as back-up devices for actuators at less than A-rate-load in toys, measuring equipments, traffic signals, electric thermo pots, etc. to drive motors or LEDs.^{3,4)} Many applications of the power-type EDLCs have been studied in the system of electric heated catalysts, EVs, elevator systems, AC-cordless devices, etc. In these capacitor-systems, EDLCs work as energy-storage devices for a temporary period in which EDLCs are charged by solar cells, batteries, AC sources, inner combustion engines, fuel cells, etc.

6. Future Prospect of the Capacitors

To attain high energy density and power density, high reliability, low cost of EDLCs, and electric circuits for efficient charges-discharges of EDLCs, development of new material for electrodes and electrolytic solutions, and power electronics study with inverter-converter components are significant. In the next century, the EDLC-system will play an important role in the field of energy storage or energy management.

References

1. H. L. F. von Helmholtz, *Ann. Phys.*, 3, 337 (1879).
2. A. Yoshida, *Denki Kagaku*, 66, 884 (1998).
3. A. Yoshida, I.Aoki, S. Nonaka, and A. Nishino, *J. Power Sources*, 60, 213 (1996).
4. A. Yoshida, S. Nonaka, and A. Nishino, *ECS Proc.*, 95-29, 210 (1995).

Polymer-based supercapacitors

Marina Mastragostino¹, Catia Arbizzani², Francesca Soavi²

¹Università di Bologna, Ist. di Scienze Chimiche,
via San Donato 15, I-40127 Bologna, Italy

²Università di Bologna, Dip. di Chimica 'G. Ciamician',
via Selmi 2, I-40126 Bologna, Italy

The use of electronically conducting polymers (ECPs) as pseudocapacitive electrode materials in high-power supercapacitors is a challenge to overcome the performance of carbon-based double-layer supercapacitors for applications requiring high power levels (1-5).

ECPs provide different supercapacitor configurations but devices with the polymer n-doped form as the negative electrode and the p-doped form as the positive one are the most promising in term of energy and power. This type of supercapacitor has indeed a high operating voltage, it is able to deliver all the doping charge and it has in the charged state both electrodes in the conducting (p- and n-doped) states.

The distinction between a polymer-based supercapacitor and a polymer-based battery is not very sharp. In the early 1980's Kaneto et al. (6) proposed a poly(thiophene)-based battery in which the electrodes become p- and n-doped upon charge, and undoped upon discharge. A criterion that can be used to distinguish batteries and supercapacitors might be the function they are expected to explicate in terms of specific energy and power. A supercapacitor is required to deliver a high specific power for a short period (10-30 s), whereas the energy is significantly lower than that of conventional and advanced batteries.

The difficulty to find conventional polymers that feature a truly efficient n-doping-undoping process has driven research efforts towards polymers yielded by new, non conventional molecules. This study reports some data on supercapacitors based on both conventional and non conventional polymers which can be p- and n-doped. Some criteria in the selection of polymer electrodes and cell design for high performance supercapacitors are reported as well as experimental results of devices based on selected polymer materials. The replacement of n-doped polymers with more suitable negative electrodes (without loosing the energy and power performance of supercapacitors based on p- and n-doped polymers) is also envisioned.

ACKNOWLEDGEMENTS

The authors would like to acknowledge the European Commission for the financial support within JOULE III contract n° JOE3-CT97-00437 and the project partners CNAM (France), ENEA's Department of Energy (Italy), Arcotronics Italia S.p.A. (Italy) and CEAC-Exide (France).

REFERENCES

1. B. E. Conway, in *New Sealed Rechargeable Batteries and Supercapacitors*, Edited by B. M. Barnett, E. D'Agostino, G. Halpert, Y. Matsuda and Z-i. Takeara, Editors, **PV 93-23**, p.15, The Electrochemical Society Proceedings Series, Pennington, NJ (1993)
2. C. Arbizzani, M. Mastragostino, B. Scrosati in *Handbook of Organic Conductive Molecules and Polymers*, H.S. Nalwa, Editor, Vol. 4, p. 595, John Wiley & Sons, Chichester, (1997).
3. (a) A. Rudge, J. Davey, I. Raistrick, S. Gottesfeld and J. P. Ferraris, *J. Power Sources* **47**, 89 (1994); (b) J. P. Ferraris, M. M. Eissa, I. D. Brotherston and D. C. Loveday, *Chem. Mater.* **10**, 3528 (1998)
4. (a) C. Arbizzani, M. Mastragostino, L. Meneghello, R. Paraventi, *Adv. Mater.* **8**, 331 (1996); (b) M. Mastragostino, C. Arbizzani, M. G. Cerroni and R. Paraventi in *Electrochemical Capacitors II*, F. M. Delnick, D. Ingersoll, X. Andrieu and K. Naoi, Editors, **PV 96-25**, p. 109, The Electrochemical Society Proceedings Series, Pennington, NJ (1997); (c) M. Mastragostino, C. Arbizzani, R. Paraventi and A. Zanelli, *J. Electrochem. Soc.* **147** (2), 2000; M. Mastragostino, R. Paraventi and A. Zanelli, *J. Electrochem. Soc.* in press.
5. (a) X. Andrieu, L. Josset and J. F. Fauvarque, *J. de Chim. Phys.* **92**, 879 (1995); (b) A. du Pasquier, J. Gonzales, C. Sarrazin and J. F. Fauvarque, in *Electrochemical Capacitors II*, F. M. Delnick, D. Ingersoll, X. Andrieu and K. Naoi, Editors, **PV 96-25**, p. 127, The Electrochemical Society Proceedings Series, Pennington, NJ (1997)
6. K. Kaneto, K. Yoshino, Y. Inuishi, *Jap. J. Appl. Phys.* **22**, L567-L568 (1983)

New Conducting Polymers for Supercapacitors and Lithium Batteries

Katsuhiko Naoi

Department of Applied Chemistry,
Tokyo University of Agriculture and Technology
2-24-16 Naka-Cho, Koganei, Tokyo 184-8588, Japan
E-mail: naoi_lab@cc.tuat.ac.jp

The author's research group has been studying new class of conducting polymer materials which has high potential applicability as high energy/power electrochemical capacitor and lithium battery materials. The author will present various types of new conducting polymer materials (see Fig. 1) which involves the moieties of an aniline and other redox systems (such as quinone and disulfide) in a molecule. These polymers exhibit stabilized cycling characteristics for more than 10^3 cycles with high specific capacities as compared with the conventional conducting polymers like polypyrrole, polyaniline, and polythiophene derivatives.

Poly(2, 2'-Dithiodianiline) [poly(DTDA)][1], a conducting polymer having disulfide(S-S) bond in it, is proposed here as a new class of high energy storage material. DTDA has one S-S bond interconnected between two moieties of anilines. DTDA was electrochemically polymerized to form an electroactive thin film. The structure of the poly(DTDA) was similar to that of polyaniline in addition that the S-S bond is preserved after electropolymerization of DTDA. The electropolymerized poly(DTDA) had enhanced redox processes due to an intramolecular electrocatalytic effect

of aniline/anilinium and thiol/thiolate redox couples. The poly(DTDA) has some advantages because of its high theoretical energy density, fast kinetics and high electrical conductivity. The discharge test of a Li/Gel electrolyte/poly(DTDA) cell showed good discharge behavior with an energy density in excess of 675 Wh kg^{-1} -cathode.

A poly(1,5-diaminoanthraquinone) [poly(DAAQ)][2] film, a new class of conducting polymer which is a hybrid of an aniline and a benzoquinone. A poly(DAAQ) film showed high electrical conductivity ($0.3\text{--}2.0 \text{ S cm}^{-1}$) and reproducible redox cycling behavior in a wide range of electrochemically active potential window (2.3 V span). By utilizing poly(DAAQ) films as both anode (π -conjugated system of the polymer) and cathode (quinone redox reaction) one can construct a novel type of electrochemical capacitor device. The charge-discharge mechanism for poly(DAAQ) / poly(DAAQ) capacitor is similar to that with Type III (p- and n-doping) polythiophene derivatives which are regarded as the most promising conducting polymers in terms of energy and power densities. A poly(DAAQ) / poly(DAAQ) electrochemical capacitor exhibited higher specific energy (46 Wh kg^{-1}) and power (30 kW kg^{-1}) than those for conventional conducting polymer materials.

References

- [1] K. Naoi *et al.*, *J. Electrochem. Soc.*, **144** (6), L173 (1997).
- [2] K. Naoi, S. Suematsu and A. Manago, *J. Electrochem. Soc.*, in press.

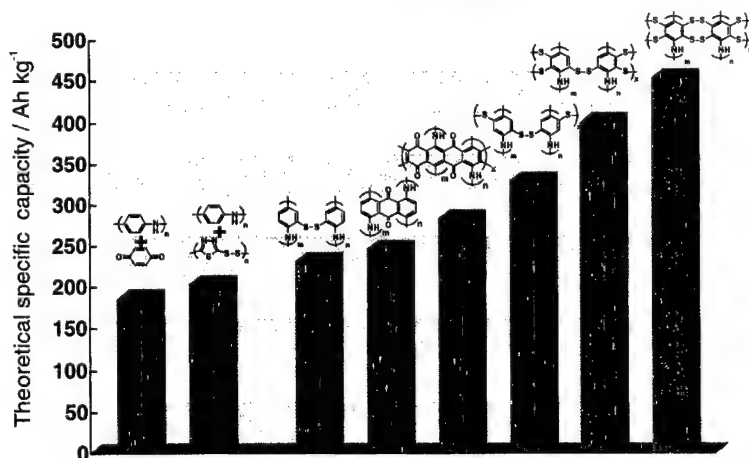


Figure 1 Theoretical specific capacities for various proposed conducting polymers

Tin / Tin oxide thin film electrodes for lithium-ion batteries.

J. Sarradin, N. Benjelloun, G. Taillades and M. Ribes.

Laboratoire de Physicochimie de la Matière Condensée – UMR 5617 Université Montpellier II 34095 Montpellier cedex 5, France.

Thin film-based lithium-ion batteries have high energy density and are capable to power microelectronics devices such as computer memory chips, implantable medical sensors, smart cards, etc...

Vitreous matrixes are well suited to the production of thin film-based host electrode allowing insertion/de-insertion of lithium ions without major change in volume. As a consequence, a better cycleability may be expected, the capacity losses often being the result of a partial destruction of the core structure of the electrode.

Carbon based electrodes are widely used as the anode in lithium-ion batteries, but promising results were recently obtained with tin-based composite oxides (TCOs) including bulk [1] as well as thin film electrodes [2, 3].

Since the electrochemical reversible part of the TCOs materials can be attributed to the alloying/de-alloying process [3,4,5], our objective was to increase the tin amount while keeping up the coexistence with the wrapping glassy matrix. In this way, sputter deposited thin films were elaborated from a Sn / $\text{SnP}_{0.4}\text{B}_{0.4}\text{O}_{2.9}$ composite target with an high Sn/matrix ratio.

Physical and chemical characteristics of the thin films were investigated. Depending on the sputtering conditions, diffraction peaks corresponding to metallic tin were observed by XRD (figure 1). SEM was used to measure the thickness of the layers and figure 2 shows a cross sectional view of a sputtered thin film elaborated under argon plasma. XPS and EDX measurements were carried out on the thin layers. Electrical conductivity of the thin films is close to 2 S cm^{-1} , a mid value between the conductivity of the bulk vitreous matrix (10^{-7} Scm^{-1}) and metallic tin (10^5 Scm^{-1}).

Regarding the electrochemical behavior, the average value of potentials corresponding to the uptake and release of Li ions occurred at 0.5 V/Li and 0.7 V/Li respectively (1st cycle excepted).

Running tests on thin film electrodes are currently in progress to obtain the best compromise between high specific capacity and cycleability.

Figure 1 : XRD patterns of sputter deposited thin films elaborated under argon plasma $P = 10^{-2}$ Torr. (a) 30 W, (b) 50 W, (c) 70 W.

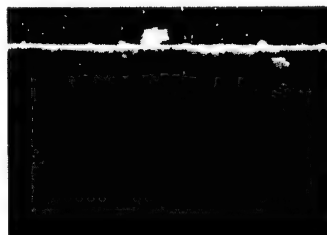
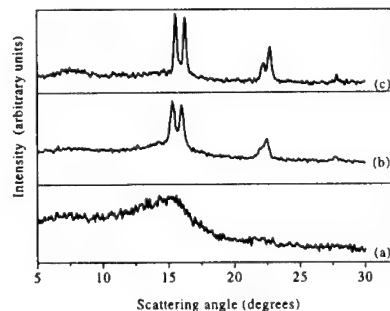


Figure 2 : Cross sectional view of a sputtered thin film elaborated under argon plasma.

References.

- [1] Y.Idota, T.Kubota, A.Matsufuji, Y.Mackawa T.Miyasaka, Science, 276, 1395-97 (1997).
- [2] C.Branci, N.Benjelloun, J.Sarradin and M.Ribes. 12th Int'l Conf. on Solid State Ionics-Greece 1999 (accepted)
- [3] F.Ding, Z.Fu, M.Zhou and Q.Qin, J.Electrochem. Soc., 146 (10) 3554-59 (1999).
- [4] I.A.Courney, W.R.McKinnon and J.R.Dahn, J.Electrochem.Soc., 146 (1) 59-68 (1999).
- [5] W.Liu, X.Huang, Z.Wang, H.Li and L.Chen J.Electrochem.Soc., 145 (1) 59-62 (1998).

Abstract No. 56

Optimization of Physicochemical Characteristics of a Lithium Anode Interface for High-Efficiency Cycling

Masashi Ishikawa and Masayuki Morita

Department of Applied Chemistry & Chemical Engineering, Faculty of Engineering,

Yamaguchi University

2-16-1 Tokiwadai, Ube 755-8611, Japan

To overcome poor charge-discharge cycleability of lithium (Li) metal anodes, we have modified physicochemical characteristics of a Li interface by our techniques proposed recently: (i) optimization of a Li metal interface by utilizing electrolyte-temperature effects, (ii) modification of a Li interface with electrochemically active additives in electrolytes. In this regard we recently found that low-temperature "precycling" improves Li cycleability in PC/DMC with LiPF_6 (1) and that some additives such as AlI_3 and MgI_2 enhance Li cycling efficiency in appropriate electrolytes (2,3). We reports herein extended investigation based on such approaches under various conditions.

1. Electrolyte-temperature effects on Li metal interface properties

Low-temperature (253 K) precycling considerably reduced impedance at a Li interface in PC/DMC with LiPF_6 , and high efficiency cycling of a Li anode was observed at the low temperature and even after elevating temperature to 298 K (1). In PC/DMC with a Li imide, $\text{Li}(\text{C}_2\text{F}_5\text{SO}_2)_2\text{N}$ (LiBETI), an uniform Li interface was observed with an in situ CCD microscope during cycling especially at such a low temperature. This favorable interface brought about extended cycling, more than 350 cycles corresponding to an efficiency of 98 % with depth of discharge of 10 %. In this electrolyte system, furthermore, the cycling efficiency at a high temperature (323 K) was found to be comparable to that at a room temperature (298 K). In contrast to the results obtained in the LiPF_6 system, however, change of electrolyte temperature during cycling reduced the efficiency in the LiBETI electrolyte. Thus, the LiBETI electrolyte should be favorable for Li cycling under constant-temperature conditions.

Based on ac impedance analysis, it was found that the low-temperature cycling in the LiBETI system provides a thin and uniform LiF film at the Li interface; this film would contribute to the high efficiency at the low temperature. The impedance analysis suggests, however, this film would be broken with a drastic change of electrolyte temperature. It is concluded that one can realize modification of a Li interface favorable to Li cycling by appropriate electrolyte temperature control suitable for respective electrolyte systems.

2. Control of a Li metal interface by metal iodide additives

Addition of MgI_2 to LiPF_6 -PC/DMC improved Li cycleability while AlI_3 addition reduced the cycleability because of solvent fluorination via LiPF_6 decomposition with AlI_3 at a Li interface (2). By contrast, in LiBETI-PC/DMC the addition of both the additives resulted in an excellent efficiency, ca. 95 %. Based on the observation of the interface in the LiBETI system containing AlI_3 with the in situ CCD microscope, a surface layer had hilly Li-Al (or Mg) alloy without mossy/dendritic Li. Such macroscopic structure would be suitable for the cycling than fine dendritic (or mossy) structure.

It is notable that in the LiBETI-PC/DMC system a Li electrode cycled in the presence of MgI_2 at the initial cycle showed high cycleability in the subsequent cycles even without MgI_2 . This result suggests that the additives would be regarded as promising "pretreatment reagents" for the cycleability enhancement of a Li electrode; undesirable reactions such as self-discharge caused by the additives can be avoided if the "additives" are not used as additives in electrolytes but utilized as pretreatment reagents.

ACKNOWLEDGMENTS

This work was supported by Grant-in-Aids (Nos. 10131250 and 11118253) for Scientific Research on Priority Area of "Electrochemistry of Ordered Interfaces" from Ministry of Education, Science, Sports and Culture, Japan. This study was partially supported as a partial study of "Dispersed type Battery Energy Storage Technology Research and Development" under the contact with New Energy and Industrial Technology Development Organization (NEDO) for the "New Sunshine Program" by Agency of Industrial Science and Technology, Ministry of International Trade and Industry, Japan.

REFERENCES

1. M. Ishikawa, M. Kanemoto and M. Morita, *J. Power Sources*, **81-82**, 217-220 (1999).
2. M. Ishikawa, S. Machino and M. Morita, *J. Electroanal. Chem.*, **473**, 279-284 (1999).
3. M. Ishikawa, S. Machino and M. Morita, *Electrochemistry*, **67**, 1200-1202 (1999).

Abstract No. 57

Improved Carbon Anode Properties: Pretreatment of Particles in Polyelectrolyte Solution

Miran Gaberšček¹, Marjan Bele¹, Jernej Drofenik¹, Robert Dominko¹, and Stane Pejovnik^{1,2}

¹National Institute of Chemistry, Hajdrihova 19, SI-1000 Ljubljana, Slovenia

²Faculty of Chemistry and Chemical Technology, University of Ljubljana, Slovenia

In lithium ion rechargeable batteries, the problem of passive film formation on the surface of carbon anode during the first cycle(s) has still not been solved to a satisfactory degree. On one hand, the passive film formation consumes irreversibly a considerable amount (15-35%) of the lithium present in the cathode upon cell assembly while, on the other hand, the passive film itself represents an additional barrier for lithium ion transfer during cycling. Since the formation of a passive film cannot be avoided due to thermodynamical reasons¹, the reduction of the problem is limited to optimisation of the film properties.

The film properties can be influenced through selection of the type of carbon used², selection of electrolyte composition^{2,4}, electrolyte modification using additives^{2,5}, and through pretreatment of carbon particles leading to appropriate surface modification⁶⁻⁸.

In this paper, we present an approach in which carbon (graphite) particles, before being used in the conventional procedure of anode preparation, are pretreated in an aqueous solution of a polyelectrolyte⁹. The polyelectrolyte solution may be modified by appropriate addition of salt(s), surfactant(s) etc. in such a way that a maximum adsorption of polyelectrolyte molecules on carbon particle surface occurs. The adsorbed polyelectrolyte molecules contain a large number of active groups (cationic, anionic and nonionic) which may serve as nucleation sites for passive film formation.

Various polyelectrolyte types have been tested on various carbon particle types. Typically, the Li loss on pretreated particles in the first cycle is as low as 10-15%, while the reversible capacity remains higher than 300 mAh/g (current rates between to C/7 and C/3 have been checked).

As regards the influence of polyelectrolyte molecules on passivation, the results are explained in terms of a generalised passivation model verified using impedance spectroscopy measurements. In a recent paper¹⁰, we showed that the high surface density of nucleation sites should in principle lead to uniform film growth over entire particle surface rather than to a coarse and porous film as occurring in conventional systems. Moreover, the polyelectrolyte molecules selected for the present investigation have a sticky character and some of them extend far away from the particle surface (up to 0.5 μm). These special properties help carbon particles to bind together strongly enough that no conventional binder has to be added to the anode material to prepare mechanically stable anodes. The binding properties of the

polyelectrolyte molecules are explained on the basis of separate Atomic Force Microscopy experiments.

Acknowledgements

This research is sponsored by NATO's Scientific Affairs Division in the framework of the Science for Peace Programme. The financial support from the Ministry of Science and Technology of Slovenia is also fully acknowledged.

References

1. M. Winter and J.O. Besenhard, in *Lithium Ion Batteries, Fundamentals and Performance*, Eds. M. Wakihara and O. Yamamoto, Kodansha, Tokyo and Wiley-VCH, 1998, pp 135-140.
2. J. R. Dahn, A. K. Sleight, H. Shi, B. M. Way, W. J. Weydanz, J. N. Reimers, Q. Zhong, and U. V. Sacken, *Lithium Batteries - New Materials, Developments and Perspectives*, Ed. G. Pistoia, Chapter 1, Elsevier, 1994.
3. S. Megahed and B. Scrosati, *J. Power Sources*, **51**, 79 (1994).
4. A. N. Dey and B. P. Sullivan, *J. Electrochem. Soc.*, **117**, 222 (1970).
5. Z. X. Shu, R. S. Mc Millan, and J.J. Murray, *J. Electrochem. Soc.*, **140**, L101 (1993).
6. E. Peled, C. Menachem, D. Bar-Tow, and A. Melman, *J. Electrochem. Soc.*, **143**, L4 (1996).
7. N. Imanishi, Y. Takeda, and O. Yamamoto, in *Lithium Ion Batteries, Fundamentals and Performance*, Ed. M. Wakihara, O. Yamamoto, Kodansha, Wiley VCH, Chapter 5, 1998.
8. M. Winter, et al., *ITE Battery Letters*, **1**, 129 (1999).
9. M. Gaberšček, M. Bele, S. Pejovnik, J. Drofenik, and R. Dominko, Patent application No. P-9900238, Bureau for Intellectual Property of the Republic of Slovenia, Ljubljana, Slovenia, October, 1999.
10. M. Gaberšček, M. Bele, S. Pejovnik, J. Drofenik, and R. Dominko, *Electrochemical and Solid-State Letters*, in print.

Graphite-Tin Composites as Anode Materials for Lithium-ion Batteries

G. X. Wang^{*1}, Jung-Ho Ahn², M. J. Lindsay¹, L. Sun¹,
D.H. Bradhurst¹, S.X. Dou¹ and H.K. Liu¹

¹Energy Storage Materials Research Program, Institute for Superconducting & Electronic Materials, University of Wollongong, NSW 2522, Australia

²Department of Materials Engineering, Andong National University, Andong, Gyeongbuk 760-749, Korea

Lithium-ion batteries are state-of-the-art power sources for portable electronics and also show promise for use in electric vehicles (EVs). The development of a new generation of lithium-ion batteries demands new cathode and anode materials with high energy density. The capacity of carbon anode materials has been improved greatly in the past few years from early types of soft carbons (200-240 mAh/g) to more recent MCMB graphites (300-340 mAh/g). Some carbonaceous compounds (hard carbon) have demonstrated even higher capacity of about 700 mAh/g. In addition to carbon materials, some binary or ternary lithium alloys and intermetallic alloys have recently attracted worldwide attention. In particular, tin was used as the active element because it can combine with Li to form Li_2Sn_5 alloys with a theoretical capacity of 990 mAh/g. The main shortcoming for Sn and MSn alloys is the volume expansion during the process of alloying with Li, which causes crumbling and cracking of the electrode, inducing a very short cycle life.

The objective of this research was to utilize the high lithium storage capacity of Sn and the stable cyclability of graphite. Graphite-tin composites with different content of tin were prepared by high energy ball milling. The element Sn was nano-dispersed in a ductile carbon matrix. The physical properties and microstructure of the C-Sn composites were characterized by XRD, TEM and HREM. The electrochemical performance of the composites as anodes in lithium cells was tested using coin cells.

Typical XRD patterns of the ball-milled C-Sn composites are shown in Fig. 1. The diffraction peaks of graphite and Sn became very broad, indicating the decrease of the crystalline size. The crystalline size of C and Sn was calculated to be 2-10 nm. The diffraction line (002) of graphite shifted to a lower angle, corresponding to the increase of the interlayer distances (d_{002}). Through ball-milling, the elementary Sn was embedded in the C matrix on a nanometer scale.

The discharge/charge profiles of the ball milled graphite and one of the C-Sn composite electrodes are shown in Fig. 2. The first discharge capacities for ballmilled C, $\text{C}_{0.9}\text{Sn}_{0.1}$ and $\text{C}_{0.8}\text{Sn}_{0.2}$ electrodes were 820 mAh/g, 1250 mAh/g and 1070 mAh/g respectively. With the addition of Sn in graphite, the specific capacity increased but not in proportion to the Sn content. The $\text{C}_{0.9}\text{Sn}_{0.1}$ composite electrode demonstrated the highest capacity and good reversibility.

A C-Sn composite anode with 2-3 times the capacity of MCMB and good cycle life might be achieved by optimizing the preparation of graphite-tin composites.

^{*}Corresponding author, email: gw14@uow.edu.au.

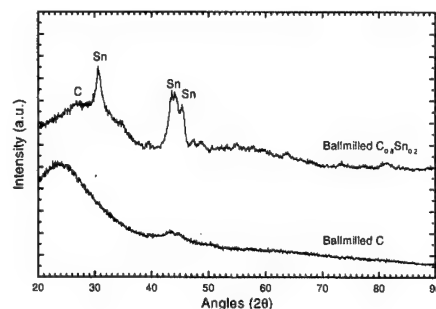


Fig. 1. Typical XRD patterns of ball milled graphite and graphite-tin composite.

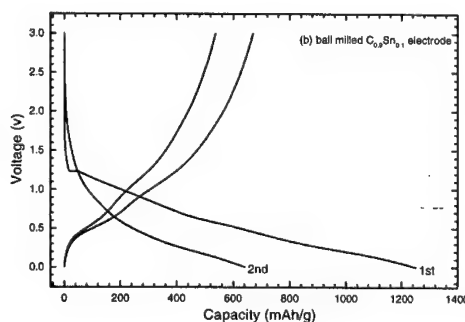
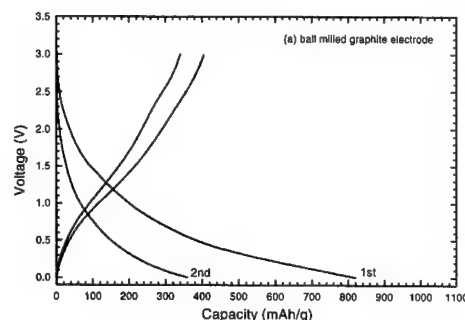


Fig. 2. The charge/discharge profiles of graphite-tin composite electrodes.

Study on Electrochemical Behavior of Carbon Materials for Lithium-ion Battery

Wang Dequan, Gao Ying, Wang Dongxi, Li
Zhongtao,
Ping Xiaoshan and Wang Xiaofeng

Tianjin Institute of Power Sources
P.O. Box 277 Tianjin 300381, P.R. China.

Abstract

Various Carbonaceous materials are used in lithium-ion battery as anode materials, such as petroleum coke, treated artificial graphite, nature graphite, mesophase carbon microbeads (MCMB), carbon fiber, graphite fiber and hard carbon, etc. Low irreversible capacity loss is one of the principle requirements for carbonaceous materials. The treatment of Carbonaceous materials and the selection of electrolyte are the key to reduce the irreversible capacity loss. The intercalation / deintercalation properties of MCMB, graphite, carbon and carbon fiber were studied in coin cells, in which the domestic MCMB showed good performance. The reversible capacity of the domestic MCMB is up to 310-320mAh/g. The cycling life, low temperature performance and rate-discharge performance of 18650 size lithium-ion cells with domestic MCMB as anode materials were also studied in this paper. The first discharge capacity of 18650 size cells is over 1.4Ah at 1C. The domestic MCMB showed excellent performance.

On The Possibility of forming Superdense Lithium Graphite Intercalation Compounds by Electrochemical Means

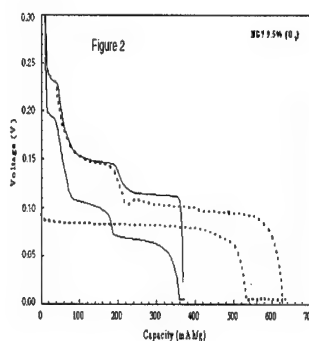
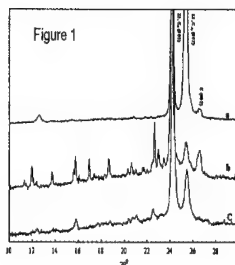
E. Peled, D. Bar Tow, V. Yufit and Yu. Rosenberg[#]

School of Chemistry and (#) Wolfson Applied Materials Research Center, Tel-Aviv University, Tel-Aviv, Israel 69978

Superdense lithium graphite intercalation compounds (GIC) with x , in Li_xC_6 , as high as 3 were obtained only at high temperatures and under high pressures (1-4). After release of the pressure the Li_3C_6 phase decomposes to yield a $\text{Li}_{2.67}\text{C}_6$ phase which is stable for several of months¹⁻³. This phase is yellow² while the color of Li_1C_6 is golden. The superdense phases have the same c value (3.7Å) and their other physical properties are similar to those of Li_1C_6 stage 1 phase⁴. The goal of this work was to synthesize superdense Li_xC_6 (x larger than 1) by electrochemical means at room temperature and under atmospheric pressure. Here we report preliminary results. We used pristine NG7 and 8 to 9.5 % burnt NG7. We use oxidized graphite as it has a higher capacity and better stability^{5,6}. In several attempts we obtained yellow GIC samples. Fig. 1 presents XRD patterns (obtained with $\lambda = 1.5406$ Å) for a, common Li_xC_6 where x is close to (but smaller than) 1; b, x about 1.55; c, x about 1.1. Under our experimental test conditions the Li GIC reacts slowly with the air that penetrates the sample. The positions of the 002 peaks of both the $x=1$ and $x=0.5$ phases of the three samples are similar. This is in agreement with recent finding⁴. We could not find any rationale for the peaks at the small angles. However these peaks do not exist in the Li_1C_6 phase. After 24 hours the XRD patterns of all the samples turn (due to air penetration) to the common pattern of pristine graphite. Fig. 2 depicts the intercalation - deintercalation curves for 9.5 % burnt superdense $\text{Li}_{1.7}\text{C}_6$ sample (dotted line) in comparison to curves for a common Li_1C_6 sample (smooth line). Intercalation was carried out at 0.1 mA/cm² to 5 mV vs. Li plus 4 hours at 5mV, deintercalation was at 0.1 mA/cm². After the superdense phase was obtained, capacity dropped and it took about four cycles to return to a normal ($x=1$) behavior. It can be seen (Fig. 2) that the intercalation potential for the superdense phase is higher than that of the common stage 1 phase. The deintercalation potential for the stage 1 and beyond is lower than that for the common stage 1. At stage 2 and at higher stages the intercalation curves of the superdense GIC and that of the common coincide. At this stage of the research we are far from controlling the conditions for the electrochemical formation of superdense lithium GIC. Much work is needed to understand this system.

Reference

1. V.A. Nalimova, D. Guerard, D.E. Sklovsky and D. Cox in *J.Phys.Chem.Solids*, pp. 771-774, 1996
2. V.Z. Mordkovich in *Synthetic Metals* 80 pp. 243-247 (1996).
3. C. Bindra, V. Nalimova, D.E. Sklovsky, Z. Benes and J.E. Fischer in *J.Electrochem.Soc.*, vol. 145, No.7, pp. 2377-2380 (1998).
4. C. Bindra, V.A. Nalimova, D.E. Sklovsky, W.A. Kamitakahara and J.E. Fischer in *Physical Review B*, volume 57, Number 9, pp. 5182-5190 (1998)
5. C. Menachem, E. Peled, L. Burshtein, Y. Rosenberg in *Journal of Power Sources*, vol. 68, No.2, pp. 277-282 (1997)
6. C. Menachem, D. Golodnitsky, E. Peled in *Proceedings of the Symposium on Batteries for Portable Applications and Electric Vehicles*. Electrochem. Soc., pp.95-102 (1997)



Charge /Discharge Characteristics of the Coal-tar Pitch Carbon as Negative Electrodes in Li-Ion Batteries

Jung-Sik Kim and Young-Tae Park

University of Seoul
Seoul, Korea

Recent works^(1,2) have demonstrated that carbons obtained by pyrolyzing organic precursors such as phenolic and epoxy resins at low temperature can reversibly intercalate Li atoms with capacities greater than that of graphite (≈ 372 mAh/g). Most of these carbons were found to be disordered and contain a large fraction of single graphene layers that have large amount of nanoporosity. In the present study, carbon was synthesized by pyrolyzing organic precursors of coal tar pitch under the condition preferentially to form anisotropic mesophase pitch, then its electrochemical performance as an anode for the Li-ion cell was investigated.

In pyrolyzing process the coal tar pitch was held in a quartz tube furnace flowing N_2 gas at 300° for 3hrs at the first stage to remove the low molecular weight compounds, then heated at 400° for 3hrs to enhance the formation of anisotropic mesophase at the second stage prior to being cooled down to room temperature. In order to extract anisotropic mesophases the pitch was dissolved in tetrahydrofuran (THF) solution for a day and washed by ethanol. The solidified pitch was then heat treated at various temperatures ranging from 700° to 1300° for 1hr in N_2 atmosphere. Carbon electrodes were prepared by coating slurries of carbon powders and polyvinylidene fluoride (PVDF) dissolved in N-methyl pyrrolidinone (NMP) on a copper foil. The electrochemical experiment was carried out in the three-electrode glass-cell using lithium foils as the counter and reference electrodes. The electrolyte was made by dissolving 1 M $LiPF_6$ in a mixture of ethylene and diethyl carbonates as 50:50 by volume. The electrochemical tests were performed using a potentiostat/galvanostat (EG&G inst. Co. 263A)

Fig.1 shows the extracted anisotropic mesophase pitches which are spherical particles below 30° diameter. Fig.2 shows the reversible capacity and irreversible capacity as a function of heat treatment temperature for the pyrolyzed carbons without extraction (solid lines) and with extraction of anisotropic mesophases from the coal tar pitch (dotted lines), respectively. As the heat treatment temperature increased, the reversible capacity for the coal tar pitch carbon (CTPC) increased progressively by about 1000° , while the irreversible capacity decreased continuously. Also, a carbon of anisotropic mesophase by the THF extraction shows higher reversible capacity (C_{rev}) and lower irreversible capacity (C_{irr}) than carbons without extraction. Fig.3 shows

the charge/discharge capacities with cyclic number for the CTPC which was pyrolyzed, extracted and heat-treated at 900° . Discharge capacity decreased significantly at the first cycle, and then gradually by about 220 mAh/g after the 2nd cycle. Also, the difference in capacity between discharge and charge occurred with large amount of about 300 mAh/g at the 1st cycle and a little amount of less than 30 mAh/g after 2nd cycle number.

In addition the BET surface area, crystallization, and cyclic voltammogram were analyzed for the CTPC.

REFERENCES

1. W. Xing, J. S. Xue, T. Zheng, A. Gibaud, and J. R. Dahn, J. Electrochem. Soc., vol. 143, No. 11, 3482 (1996).
2. K. Tokumitsu, A. Mabuchi, H. Fujimoto, and T. Kasuh, J. Electrochem. Soc., vol. 143, 2235 (1996).

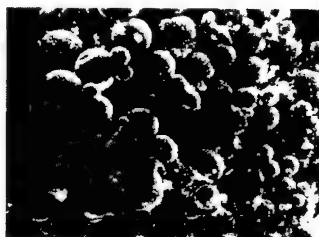


Fig.1 SEM micrograph of anisotropic mesophase carbons by extraction.

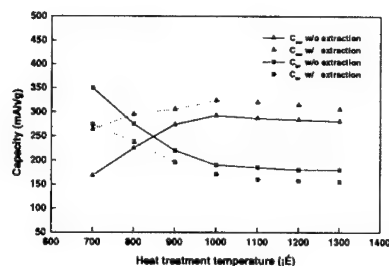
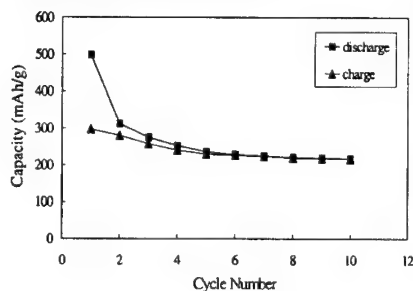


Fig.2 Reversible capacity and irreversible capacity vs. heat treatment temperature for carbons pyrolyzed from the coal-tar pitch without extraction (solid line), and with extraction of mesophase (dotted line).

Fig.3 Capacity as a function of cycle number for carbons extracted and heat treated at 900° .



**FAST ELECTROCHEMICAL
FORMATION OF NANOSTRUCTURE
ALLOYS AS ANODES IN LITHIUM - ION
BATTERIES**

A. Ulus, Yu. Rosenberg⁽¹⁾ and E. Peled

**School of Chemistry and (1) Wolfson Applied
Materials Research Center Tel-Aviv
University, Tel Aviv, Israel 69978**

Tin based sub-micron alloys and glasses are potential candidates for the anode of the lithium-ion battery. These materials are produced in several ways: glass formation and grinding, mechanical alloying by ball milling, and electrochemical deposition. The processes of glass formation and ball milling are costly and time consuming. We present here a fast electrochemical method for the preparation of tin- and zinc-based nanostructure alloys, directly on the current collector, with no need for a polymeric binder.

Two important properties make tin and zinc alloys promising candidates for use as anodes in lithium-ion batteries: high reversible capacity and high melting point of the Li_xM phases. It has been shown that reducing the size of the tin alloy particles results in a longer cycle life. It was also proven that the aggregation of tin nanoparticles to form larger agglomerates is delayed when spectator atoms are present within the tin matrix.

In this work we studied electrochemical methods of preparation of nanostructure tin and zinc alloys containing 50- 90% (v/v) tin or zinc and other elements including antimony and copper. The plating takes less than 5 minutes per electrode. Fractal-like or honeycomb morphologies were obtained. The thickness of the particles or the honeycomb wall is generally less than 100nm.

Anodes made from tin and zinc alloys were cycled versus lithium between 0 to 1.0V in 1M LiPF_6 EC/DEC solutions and at current densities of 0.02 and 0.2 mA/cm². Tin-copper-antimony alloys have capacities of 350-700mAh/g depending on the alloy composition.

The anode with the best performance was a tin-copper-antimony alloy that gave 400mAh/g (based on the total electrode mass excluding the current collector).

This electrode had over 30 stable 100% charge-discharge cycles with a capacity loss of 0.13% per cycle.

Zinc-tin alloys with Zn:Sn 6:1 atomic ratio have a capacity of 250mAh/g for 10 stable 100% charge-discharge cycles with a capacity loss of 0.9% per cycle. XRD patterns of tin-zinc alloys show only the typical peaks for each element, indicating the existence of micro-phases of pure tin and pure zinc. This finding is in disagreement with the tin-zinc phase diagram, which shows solid solution behavior.

The correlation among capacity, cycle life, alloy composition, and morphology will be addressed.

Irreversibility Compensation of SnO Anodes by $\text{Li}_{2.6}\text{Co}_{0.4}\text{N}$

J. Yang, Y. Takeda, N. Imanishi, and O. Yamamoto*

Department of Chemistry, Mie University
Kamihama-cho, Tsu, Mie 514-8507, Japan

* Genesis Research Institute, INC., Nagoya, Japan

Since Idota et al. found that amorphous Sn-based composite oxide possessed a high reversible capacity and satisfied cycle life [1], SnO and related materials have been intensively investigated for anodes in lithium ion batteries. It is believed that highly dispersed active Sn-domains in inert phases such as Li_2O greatly alleviates the volume effect of the electrode and suppresses the aggregation of the active phase, which significantly improves the cycle stability. However, a conversion of tin-bond oxygen into Li_2O produces a high irreversible capacity at the first cycle, which limits the potential application of electrodes of this kind. In this study, we try to compensate this irreversibility by $\text{Li}_{2.6}\text{Co}_{0.4}\text{N}$. The first Li-insertion and -extraction capacity of $\text{Li}_{2.6}\text{Co}_{0.4}\text{N}$ is, respectively, about 70 mAh/g and over 800 mAh/g. Such a Li-rich compound should be able to compensate the initial irreversible capacity of the SnO host, if these two host materials are combined together.

Three types of SnO powders with different particle sizes were used for the mixed-host electrodes. Fig. 1 shows the first charge-discharge profiles for SnO and mixed-host electrodes in 1M $\text{LiClO}_4/\text{EC}+\text{DEC}$. A high efficiency close to 100% is obtained, when 65% SnO (particle size: 10-30 μm) is mixed with 35% $\text{Li}_{2.6}\text{Co}_{0.4}\text{N}$ to form an electrode. There is a potential plateau near 0.95 V vs. Li/Li^+ for SnO electrode, which is related to the reduction of SnO into metallic Sn. After introducing $\text{Li}_{2.6}\text{Co}_{0.4}\text{N}$ powder into the electrode, this potential plateau almost disappears. It means that lithium can directly be transferred from $\text{Li}_{2.6}\text{Co}_{0.4}\text{N}$ into SnO to form Li_2O and Sn before cycling. The cycle stability of the mixed-host electrodes is strongly dependent on the SnO particle size and the kind of electron conductors within the electrodes. The best capacity retention was obtained with an ultrafine SnO powder ($< 0.2 \mu\text{m}$) prepared by chemical precipitation (Fig. 2). X-ray diffraction measurement indicates that the ultrafine SnO has been reduced to metallic Sn before the electrode is soaked into an electrolyte. With an increase in the SnO particle size, only part of the SnO can be transferred into metallic Sn before soaking. This can be attributed to a slow reaction kinetic due to poor connection and small contact area between the two active materials. The complete SnO reduction usually occurs after the electrode is soaked in the electrolyte for over 2 hrs. The larger the SnO particles, the greater the volume effect and the stronger the tendency to aggregation of active Sn phase. This results in a fast degradation of the electrode based on coarse SnO particles.

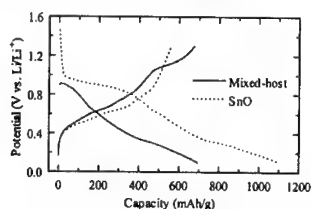


Fig. 1. A compensation of irreversible capacity of SnO host by $\text{Li}_{2.6}\text{Co}_{0.4}\text{N}$ in the first cycle. $i_c = i_d = 0.4 \text{ mA/cm}^2$.

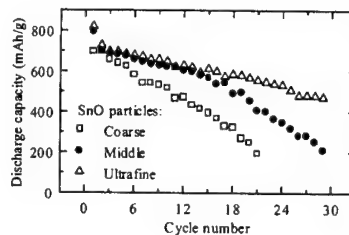


Fig. 2. Cycling behavior of $\text{SnO}/\text{Li}_{2.6}\text{Co}_{0.4}\text{N}$ composite electrodes with different SnO particle size.

Acknowledgements

This work was financially supported by Genesis Research Institute, INC., Nagoya, Japan.

References

- [1] Y. Idota, T. Kubota, A. Matsufuji, Y. Maekawa, and T. Miyasaka, Science, 276, 1395 (1997).

Impedance Measurements of Graphite Negative Electrode for Lithium-Ion Batteries

Keiichi SAWAI and Tsutomu OHZUKU

Electrochemistry and Inorganic Chemistry Laboratory,
Department of Applied Chemistry,
Faculty of Engineering,
Osaka City University
Sugimoto 3-3-138, Sumiyoshi, Osaka 558-8585, Japan

A graphite is one of the most attractive materials as a negative electrode for lithium-ion batteries because of the lowest operating voltage among the insertion materials reported so far, excellent rechargeability, highest volumetric capacity of ca. 600 mAh cm⁻³ based on the observed density and rechargeable capacity, and nontoxicity in addition to an economical reason. Solid-state electrochemical reaction of graphite was known to be two-phase reactions mainly consisting of the 1st / 2nd, 2nd / 3rd, 3rd / 4th stage compounds. Two-phase reactions associated with the staging phenomena are characteristic of graphite forming the lithium-graphite intercalation compounds in which diffusing away of lithium ions or atoms due to concentration gradient in the solid matrix are hardly imagined.

The negative electrodes for lithium-ion batteries are normally made of graphite powder with an organic binder. The negative electrode layers with thickness of 30-100 μm depending on the cell design for specific application are usually formed on a thin copper foil which is a current feeder or collector, also a media to transfer heat from inside a cell to outside in practical high-volume lithium-ion batteries. The densities of negative electrode layers based on the weight of electrode mix and thickness are usually low compared with the XRD density of graphite (2.27 g cm⁻³), indicating a porous matrix consisting of graphite particles glued together with binder.

Figure 1(a) shows the Cole - Cole plots of the impedance data of the lithiated graphite electrode in a coexistence region of the 1st / 2nd stages. The locus of the Cole - Cole plots consists of two distinct regions, i.e., a semi-arc in a high-frequency region and a sloping line in a low-frequency region. As frequency decreased below 0.1 Hz, the line with an angle of 45 degrees with respect to the real axis appeared in the locus of the impedance data, indicating a diffusion process. We tried to calculate a diffusion coefficient by a usual method from the impedance data. As can be seen in Fig.1(b), both Z' versus $f^{1/2}$ and -Z'' versus $f^{1/2}$ plots exhibit almost parallel lines, in which -Z'' versus $f^{1/2}$ line approaches the origin of the plot as frequency increases. From the slope of the lines in Fig.1(b) and geometrical surface area of the graphite particles, the diffusion coefficient was calculated to be the order of 10⁻¹⁶ cm² s⁻¹, which was not a realistic value. If the diffusion coefficient in a solid matrix was the order of 10⁻¹⁶ cm² s⁻¹, it would take at least a year depending on a graphite particle size to consume or accumulate half of lithium ions in the first stage compound of LiC₆. Conversely, the diffusion coefficient analyzed by assuming lithium salt diffusion in an organic solvent gave a reasonable value of about 10⁻⁸ cm² s⁻¹ which was consistent with the diffusion coefficient observed for a lithium metal electrode in the same electrolyte.

Figure 2 shows the chronoamperograms together with the capacity (quantity of electricity passed) curves for the oxidation of the first-stage compound at a constant

voltage, in which the current (mA g⁻¹) and the charge (mAh g⁻¹) are given based on the mass of graphite in the electrode. A rate-capability is highly influenced by a free volume inside a porous electrode matrix consisting of graphite particles and binder. A rate-determining step of the charge and discharge reaction and possible ways to improve the kinetic problems of a graphite electrode for lithium-ion batteries will be discussed therefrom.

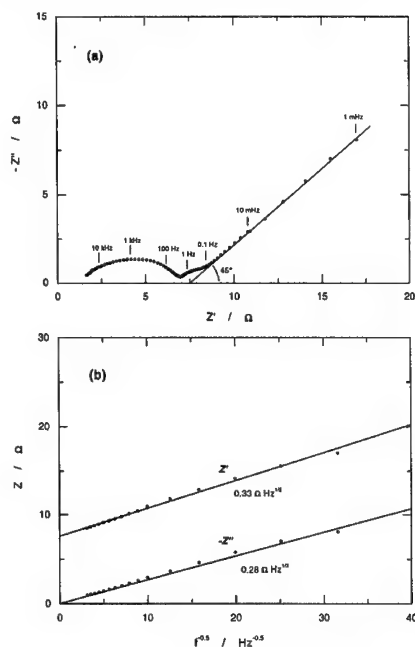


Fig.1 (a) Cole - Cole plots of the impedance data for the lithiated graphite electrode at $x = 0.73$ in Li_xC₆ in 1M LiClO₄ EC/DME (1/1 by volume) solution and (b) Z' or -Z'' versus $f^{1/2}$ plots, where f indicates frequency in Hz. The electrode consisted of 97 wt% graphite and 3 wt% Teflon. Graphite sample weight and geometrical electrode area were 54.5 mg and 3 cm².

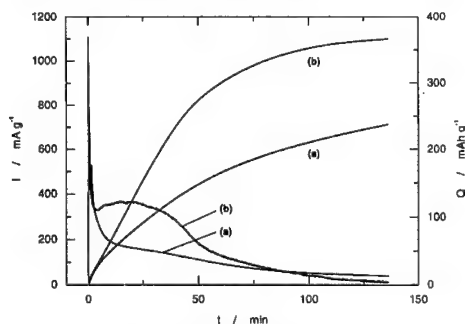


Fig.2 Chronoamperograms and capacity curves given based on the mass of graphite for the oxidation of the first-stage compound at 0.5 V vs. Li. The electrode mix consisted of (a) 97 wt% graphite (57.9 mg) and 3 wt% Teflon, and (b) 60 wt% graphite (28.9 mg), 20 wt% acetylene black, and 20 wt% Teflon.

Direct Evidence on Anomalous Expansion of Graphite Negative Electrodes on 1st Charge by Dilatometry

Tsutomu Ohzuku, Naoki Matoba, and Keiji Sawai

Electrochemistry and Inorganic Chemistry Laboratory,
Department of Applied Chemistry,
Faculty of Engineering,
Osaka City University
Sugimoto 3-3-138, Sumiyoshi, Osaka 558-8585, Japan

A graphite has been of great interest as a negative electrode material for lithium-ion batteries among battery researchers and electrochemists. A characteristic feature of lithium-graphite intercalation compounds is a staging phenomenon with a periodic sequence of lithium-intercalated layers between graphite sheets. When lithium is intercalated into graphite matrix, the interlayer distance between graphite layers increases about 10 %, which has been followed by XRD. However, a change in electrode thickness via visual inspection especially on the first reduction of graphite is often larger than that expected from XRD data. We could not so far express directly and efficiently such observation. In-situ measurement to monitor a change in electrode thickness will give important information which aids systematic investigation of materials for advanced lithium batteries. We report here a dilatometer technique to follow directly a change in electrode thickness and introduce it to graphite electrode in nonaqueous electrolytes, focusing on the first reduction.

A schematic illustration of dilatometer used in this study is shown in Fig.1. The electrochemical cell consisted of graphite electrode and lithium electrode, between which a microporous polypropylene separator was placed. The electrodes were under a constant load by a weight attached to a spindle. The change in total electrode thickness of both electrodes was measured using a displacement transducer mounted on a rigid frame.

Figure 2 shows change in graphite electrode thickness and voltage curve of graphite(NG-7) in 1M LiClO₄ PC/DME(1/1 by volume) during the first reduction. The graphite electrode used was a compressed pellet of natural graphite without any binder. The change in graphite electrode thickness was calculated by subtracting the thickness of lithium electrode (4.85 $\mu\text{m mAh}^{-1} \text{cm}^{-2}$) from the observed change in the overall thickness of both electrodes. When the current was switched on, the voltage dropped from ca. 3 V to ca. 1.1 V and then showed shoulders in the voltages 1.1 - 0.5 V, which were observed only for the first reduction. As can be seen in Fig.2, the graphite electrode expanded anomalously in such region on the first reduction with drawing a characteristic curve with changing a slope at transition points in the voltage curve. Upon further reduction to 0 V vs. Li, the thickness increased monotonously as the lithium intercalation reaction proceeded.

Figure 3 shows the result for the first reduction of graphite in 1 M LiClO₄ in EC/DME(1/1 by volume) solution. The graphite electrode expanded also in the initial part of the first reduction, although the expansion itself was less pronounced compared with that in PC/DME. As can be seen in Figs. 2 and 3, anomalous expansion of graphite was observed in the initial part of the first reduction in so-called irreversible capacity region. No change in lattice dimension of graphite was

observed by XRD in such a region. The observed change in electrode thickness was larger than that of 10 % expected from XRD, due mainly to anomalous expansion in the initial part of the first reduction. Factors affecting such anomalous expansion of graphite electrodes will be elucidated by dilatometry combined with in-situ optical microscopy and acoustic emission histometry.

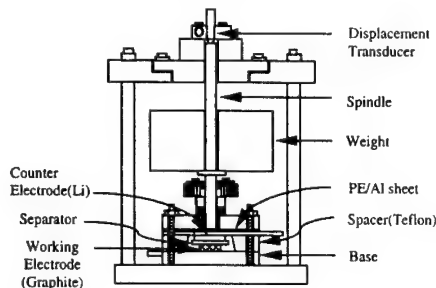


Fig.1 Schematic illustration of dilatometer used to monitor change in electrode thickness.

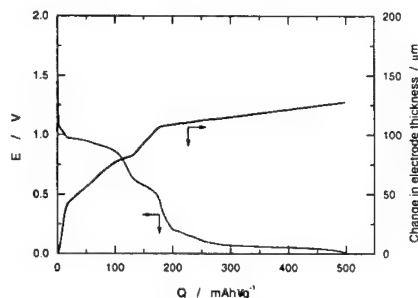


Fig.2 Change in graphite electrode thickness and operating voltage curve for the first reduction in 1 M LiClO₄ PC/DME(1/1 by volume) at a rate of 0.15 mA cm⁻². The graphite electrode was a compressed pellet (19.8 mg, 119 μm thick.) with no binder.

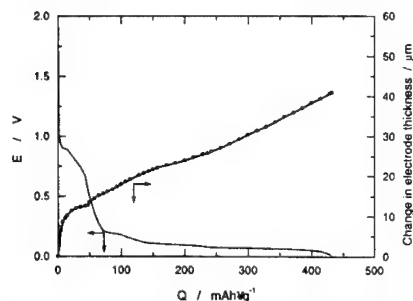


Fig.3 Change in graphite electrode thickness and operating voltage curve for the first reduction in 1 M LiClO₄ EC/DME(1/1 by volume) at a rate of 0.15 mA cm⁻². The graphite electrode was a compressed pellet (21.0 mg, 130 μm thick.) with no binder.

Dispersed Silicon-Graphite Powder: A High Capacity Anode Material for Rechargeable Lithium Ion Batteries

Jianjun Niu and Jim Yang Lee*

Department of Chemical & Environmental Engineering
National University of Singapore
10 Kent Ridge Crescent, Singapore 119260
Singapore

Lithium alloys are high energy density materials with potential applications in rechargeable lithium-ion batteries. Among them silicon has the highest theoretical capacity of 4000 mAh/g Si as a result of the favorable Li/Si stoichiometry (e.g. $\text{Li}_{22}\text{Si}_5$) and the low atomic weight of Si. However, silicon based anodes have severe cyclability problem because of their poor mechanical properties. This paper describes a new synthesis method based on sol-gel processing¹, which is used in conjunction with mechanical grinding to produce more usable Si based composite materials.

The preparation of this new anode material includes firstly the formation of porous organic silicon modified carbons by sol-gel techniques^{2,3}. Silicon particles are then dispersed in this sol-gel based carbon-ceramic medium by mechanical grinding. The sol-gel process takes place at room temperature, using various alkoxysilanes such as tetramethoxy silane (TMOS), methyltrimethoxy silane (MTMOS), phenyltriethoxy silane (PTEOS), and tetraethoxy silane (TEOS) as precursors.

The silicon embedded graphite powder prepared as such is a ceramic-like material with a porous structure deriving from the formation of 3-D gel network of percolating graphite particles. The scanning electron micrograph in Fig.1 (from a MTMOS precursor) confirms that silicon is uniformly distributed. This new anode material gives the lowest irreversible capacity and the highest reversible capacity reported to date (e.g. at 19.2 wt % of elemental silicon, the irreversible capacity and reversible capacity are 4586 mAh/g Si and 3705 mAh/g Si, respectively). Typical charging (Li intercalation) and discharging (Li deintercalation) curves for the first five cycles are shown in Fig.2. The material cycles well, with $R_{10/1}$ (the ratio of capacity in the 10th cycle to the 1st) = 0.98. The first cycle coulombic efficiency is also a high 79%, surpassing the performance of most of the current implementations of silicon based anodes. The first cycle discharge (intercalation) capacity of 4586 mAh/g Si is equivalent to an uptake of about 4.9 Li atoms per Si atom ($\text{Li}_{4.9}\text{Si}$), which exceeds the commonly accepted maximum of 4.4 Li per Si atom. Powder x-ray diffraction (Fig.3) shows no significant broadening of the graphite diffraction peaks. However, very small shifts and a new diffraction peak at $2\theta = \sim 11^\circ$ are found upon closer examination of the pattern. The formation of sol-gel-graphite composites therefore has not brought about structural changes to the carbon host, but instead induces beneficial synergistic interactions between the two Li hosts. Such interactions could be the principal contributor to the high Li/Si stoichiometry observed here. The diffraction peaks at $2\theta = 28-29^\circ$, $2\theta = 47-48^\circ$, $2\theta = 56-57^\circ$, and $2\theta = 69-70^\circ$ all pertain to Si as they only appear after Si addition and their intensities increase with the increase in the Si content of the composites (Fig.3). These experiments show that the capacities of the composites are dependent on the details of the sol-gel process and the inorganic silicon content. The cycle life is undoubtedly an improvement compared to other silicon-based anodes. The modification of the carbon microstructure by sol-gel chemistry seems to be the key factor for this improvement.

References

1. J. Niu and J.Y.-Lee, *Anal. Commun.*, **36** (1999) 81.
2. L.L.Hench, J.K.West, *Chem. Rev.*, **90** (1999) 33.
3. P.S.Gilman and J.S.Benjamin, *Ann. Rev. Mater. Sci.*, **13** (1983) 279.

Fig.1 Scanning electron micrograph of a dispersed Si composite (5.8% silicon particles).



Fig.2 The first five cycle charging and discharging curves of the silicon-graphite composite.

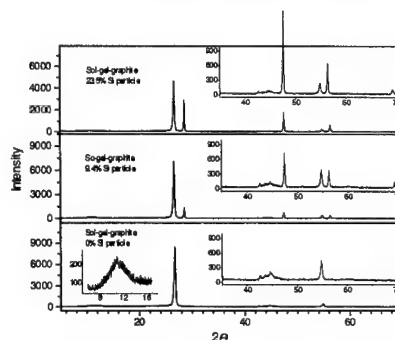
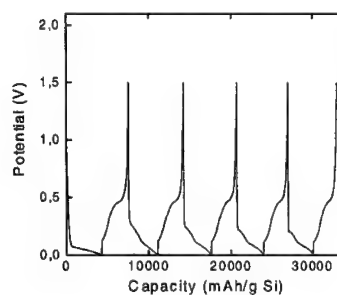


Fig.3 XRD patterns of silicon-graphite composites.



ELECTROCHEMICAL PERFORMANCE OF $\text{Pb}_3(\text{PO}_4)_2$ ANODES IN SECONDARY LITHIUM BATTERIES

LIU Zhaolin¹ and J. Y. LEE²

¹Institute of Materials Research and Engineering,
3 research link, Singapore 117602

²Department of Chemical and Environmental
Engineering, National University of Singapore,
Singapore 119260

Li-alloys such as Li-Al, Li-Sn and Li-Pb are attractive anode materials for lithium ion cells because of their high charge densities and fast room temperature lithium mobility in the alloys^[1]. However, many reports have indicated that it is difficult to realize the theoretical capacity with these Li-alloy electrodes because of the mechanical and conductivity instabilities caused by large volume changes of the lithium storage phase during cycling. There was no industrial interest in the possible use of these alloys in the negative electrodes of commercial cells. The situation was changed when Fuji Photo Film Co., Ltd., announced the development of lithium batteries based on amorphous tin composite oxide negative electrodes^[2]. Since then, much attention has been given to the possibility of substituting similar classes of compounds for carbon negative electrodes in Li-ion batteries. Both pristine and doped tin oxides have been extensively investigated as anode materials, but reports about Pb composite oxides as anode material in Li-ion batteries are relatively scarce. In this on-going work, we consider $\text{Pb}_3(\text{PO}_4)_2$ as intrinsic P-doped Pb oxide composites and investigated their performance as anode materials for Li-ion batteries.

Crystalline $\text{Pb}_3(\text{PO}_4)_2$ was supplied by Johnson Matthey and used as received. Its crystal structure was verified by powder X-ray diffraction. Amorphous $\text{Pb}_3(\text{PO}_4)_2$ was obtained by melting the crystalline polymorph at 1020°C for 2 hours followed by quenching. Inductively coupled plasma spectroscopic analysis of the quenched product showed no changes in elemental composition and XRD confirmed the total lack of crystallinity. Mixture of $\text{Pb}_3(\text{PO}_4)_2$ with poly(vinylidene fluoride) binder and acetylene black in the weight ratio of 80:7:13 were compressed at 2.0×10^6 Pa to form anode pellets 1.6cm in diameters. Lithium foil was used as the counter electrode together with a polypropylene separator. The electrolyte was 1M LiPF_6 in a 1:1 mixture of ethylene carbonate/diethyl carbonate. Cyclic voltammetry and galvanostatic measurements were used to evaluate the electrochemical characteristics of $\text{Pb}_3(\text{PO}_4)_2$.

The cyclic voltammograms of Fig. 1 show substantial differences between the first cycle and subsequent cycles. In Fig. 1a, a large cathodic peak around 1.25V appears only during the first cathodic scan. The underlying reaction is irreversible because there is no similar feature from the second scan onward. Upon scan reversal, there is one anodic peak around 0.6V. This peak is found to decrease in size with increasing cycle number. A prominent cathodic peak appears at 0.1V from the second cycle onward. For amorphous $\text{Pb}_3(\text{PO}_4)_2$ (Fig. 1b), a large cathodic peak around 0.1V and smaller cathodic peaks around 1.6V, 1V and 0.7V are found in the first cathodic scan. There are also two anodic peaks at 0.55V and 0.7V in the reverse scan, indicating that there are at least two energetically different sites for the lithium ions in this polymorph. A comparison of the voltammetric features between the second scan and the fifth scan shows that the lithium insertion/extraction reactions are more reversible in amorphous $\text{Pb}_3(\text{PO}_4)_2$. Figure 2 shows the first five charging and discharging cycles of crystalline and amorphous $\text{Pb}_3(\text{PO}_4)_2$ between 5mV and 1.4V (vs. Li^+/Li) at the constant current of 30 mA/g. In Fig. 2a for crystalline $\text{Pb}_3(\text{PO}_4)_2$, the charge capacity for the second cycle is 278 mAh/g, which is a great reduction from the initial charge capacity of 742 mAh/g. This lower value of charge capacity is however retained in the next three cycles. In Fig. 2b for amorphous $\text{Pb}_3(\text{PO}_4)_2$, the charge capacity for the second cycle is 298 mAh/g, which is lower than the initial

charge capacity of 568 mAh/g but higher than the 278 mAh/g from crystalline $\text{Pb}_3(\text{PO}_4)_2$. Cycling tests also confirm amorphous $\text{Pb}_3(\text{PO}_4)_2$ as a more reversible anode material with a higher specific capacity.

References

- [1] J. Wang, P. King, R. A. Huggins, *Solid State Ionics*, 20 (1986) 185.
- [2] Y. Idota, M. Nishima, Y. Miyaki, T. Kubota, and T. Miyasaka, *Canada Pat. Appl.* 2,134,053 (1994).

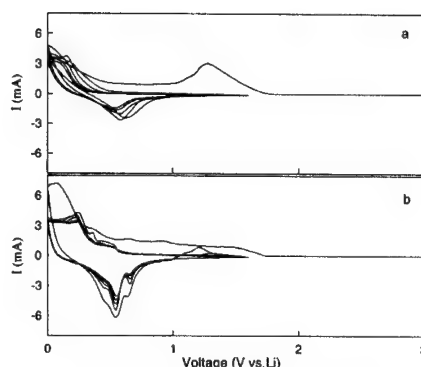


Figure 1. Cyclic voltammograms of (a) crystalline and (b) amorphous $\text{Pb}_3(\text{PO}_4)_2$ at 0.1 mV/s.

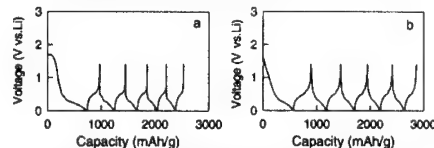


Figure 2. Charge and discharge curves for the first five cycles of Li/(a) crystalline and (b) amorphous $\text{Pb}_3(\text{PO}_4)_2$ cells.

Abstract No. 68

Electrochemical/Interfacial Studies of Carbon Films in Non-aqueous Electrolytes

D. Allia^a, R. Kostecki^b, X. Song^b,
K. Kinoshita^b and R. Kötz^a

^a Paul Scherrer Institut
Villigen PSI, CH-5232, Switzerland
^b Lawrence Berkeley National Laboratory
Berkeley, CA 94702, USA

Spin coating thin layers of photoresist on silicon wafers and subsequent photolithographic patterning are well-developed technologies in the semiconductor industry. The microscopic structures that are routinely produced provided an opportunity to fabricate useful microstructures for microbatteries [1]. As an extension of the development of interdigitated microelectrodes, the application of carbon films obtained from pyrolyzed photoresist was investigated as negative electrodes for microbatteries.

A thin layer of positive photoresist (OiR-897, Olin Corporation) was spin coated onto a 10-cm diameter silicon wafer. The photoresist was heated in nitrogen for 20 hr at 150°C, followed by heating for 1 hr at 600°, 700°, 800°, 900° or 1000°C in nitrogen to form the carbon film [2].

The electrical properties of the carbon films were investigated by current-sensitive atomic force microscopy (CSAFM) and four-point probe techniques. The carbon/non-aqueous electrolyte interface was also studied by *in-situ* electrochemical scanning probe microscopy. Cyclic voltammograms were recorded in 1 M LiClO₄ (EC:DMC) electrolyte during *in-situ* AFM measurements.

According to the CSAFM (see Figure 1) and four-point probe measurements, highly conductive carbon films were obtained when the photoresist is pyrolyzed at temperatures higher than 700°C. At 600°C, the carbon film shows a non-linear resistance behavior.

The electrochemical activity of the carbon in LiClO₄ also depends on the heat-treatment temperature. For example, carbon films obtained at 900°C show a cathodic current much higher than carbon films produced at 700°C (see Figure 2). As a consequence, the SEI film formed in the non-aqueous electrolyte is thicker on the carbon films obtained at 900°C, as indicated by the *in-situ* AFM measurements (see Figure 3).

Acknowledgements

Financial support by the Swiss National Science Foundation, Grant No. 4036-044040, and by the Office of Energy Research, Office of Basic Energy Sciences, Chemical Sciences Division of the U.S. Department of Energy, contract No. DE-AC03-76SF00098, are gratefully acknowledged.

References

- [1] K. Kinoshita, X. Song, J. Kim and M. Inaba, J. Power Sources, **81**, 170 (1999).
- [2] R. Kostecki, X. Song and K. Kinoshita, Electrochem.

Solid-State Lett., **2**, 465 (1999).

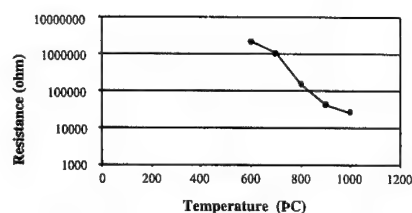


Fig 1: Resistance of carbon films vs. temperature of pyrolysis

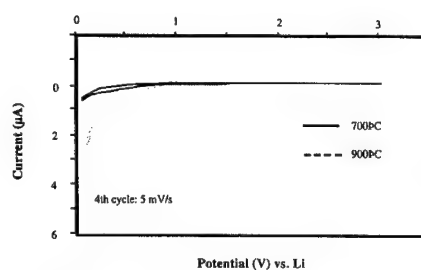


Fig. 2: Voltammograms of carbon films pyrolyzed at different temperatures

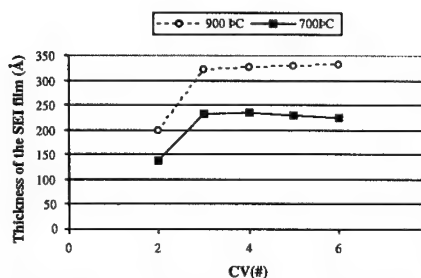


Fig. 3: Thickness of SEI films formed in 1 M LiClO₄ (EC:DMC)

Reversible Reaction of Li with Grain Boundary Atoms in SnMn_3C

L. Beaulieu, D. Larcher, R.A. Dunlap and J.R. Dahn.
Department of Physics, Dalhousie University
Halifax, NS. B3H 3J5 Canada.

Bulk SnMn_3C is a perovskite-structure material that does not react with lithium. However, when SnMn_3C is prepared by mechanical alloying, it reacts reversibly with about 1 lithium atom per formula unit. Mechanically-alloyed samples are comprised of approximately $10\ \mu\text{m}$ particles consisting of 10 nm grains. Here we show that the reversible reaction with lithium involves only tin atoms located at grain boundaries.

Figure 1 shows the voltage versus capacity and capacity versus cycle number of mechanically-alloyed SnMn_3C cycled against pure Li metal. The reversible capacity is about 25% of its expected value of 400mAh/g (based on reaction of all Sn in the compound to form Li_{14}Sn), and the cell shows excellent capacity retention.

Figure 2 shows the *in-situ* x-ray diffraction patterns of a mechanically-alloyed $\text{SnMn}_3\text{C}/\text{Li}$ cell cycled between 0-1.3 V. Unlike most materials which react with substantial lithium, the structure of SnMn_3C is not disturbed by the reaction with lithium. Neither the amount of the phase, nor its lattice constants are changed, even though about 1 Li atom per formula unit has reacted. How can this be?

Figure 3 shows the *in-situ* ^{119}Sn Mössbauer spectrum of the fresh cell and the fully discharged cell. The spectra have been fitted with two components: 1) a lorentzian centered at $1.7\ \text{mm/s}$ which is from the nanocrystals of SnMn_3C and 2) a component which is from tin at the grain boundaries. Component 1 does not change as lithium reacts, but component 2 moves smoothly from a center shift of $2.5\ \text{mm/s}$ to a center shift of about $2.0\ \text{mm/s}$ (consistent with the center shift seen in Li-rich Li-Sn alloys [1]) as the cell discharges.

Our model for the reaction is therefore that Sn atoms at the grain boundaries throughout the structure can react with lithium, and Sn atoms within SnMn_3C nanocrystals cannot. One does not expect grain boundary atoms, with positions uncorrelated to the atomic planes of the nanocrystals to contribute to the sharp peaks of the diffraction pattern. Thus the Bragg peaks in figure 2 do not change. On the other hand, a broad peak near 23° does appear in the discharged cell. This is thought to arise from small clusters of tin atoms at the corners of a tetrahedron with Li atoms nearby, as explained in reference 2. The tin atoms needed to form these clusters are in the grain boundaries.

This work clearly shows the importance of the grain boundary atoms in materials that are otherwise inactive with respect to lithium. Grain boundary materials may one day replace graphite as the anode of choice in lithium-ion batteries.

References:

- [1] R.A. Dunlap, D.E. Small, D.D. MacNeil, M.N. Obrovac and J.R. Dahn, *J. Alloys and Compounds*, **289**, 135-142 (1999).
- [2] Jeff Dahn, I. A. Courtney, and O. Mao, *Solid State Ionics* **111**, 289 (1998)

Figure 1: a) Voltage versus capacity and b) capacity versus cycle number of SnMn_3C . The solid line represents the discharge cycle while the dashed line represents the discharge cycle. Panel b shows the results for 2 SnMn_3C cells.

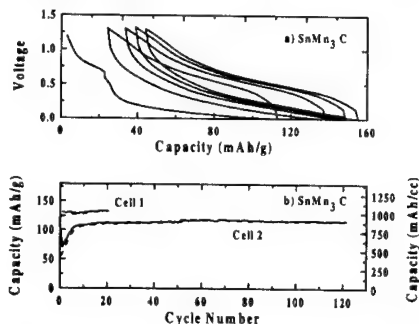


Figure 2: In-situ x-ray diffraction pattern of SnMn_3C showing the a) fully discharged cell and b) the fresh cell.

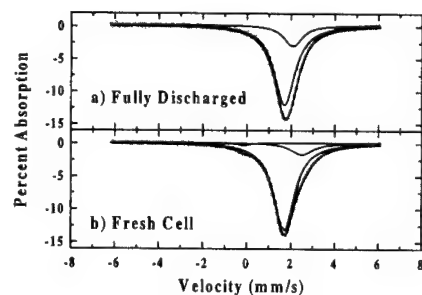
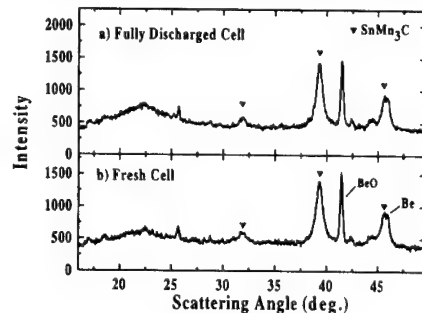


Figure 3: In-situ Mössbauer absorption spectra of SnMn_3C showing the a) the fully discharged cell and b) fresh cell.

THE INFLUENCE OF THE STRUCTURE OF INITIAL MATERIAL AND THE WAYS OF ITS MODIFICATION ON ELECTROCHEMICAL PROPERTIES OF THE GRAPHITE ANODES IN LITHIUM-ION SYSTEMS.

E.M.Shembel, N.I.Globa, N.D.Zaderey, A.S.Baskevich, O.S.Ksenzhek, K.Ye.Kylynyk and T.V.Pastushkin
Ukrainian State Chemical Technology University,
Dnipropetrovsk
E-mail: shembel@onil.dp.ua

L.R.Vishnyakov and V.A.Kokhany
The Institute of Materials Problems of the Academy of Sciences of Ukraine, Kiev

The following factors determining the efficiency of intercalation process of lithium ions in a carbon material have been studied: the catalytic properties of graphite materials relative to the cathodic reduction process of electrolyte components, the properties of the passivating film, formed in this case, the structure and microstructure of carbon material, determining the kinetics of intercalation process and the amount of intercalated lithium ions. Investigations were carried out with natural Ukrainian graphites, synthetic graphites and with the same materials after a special chemical modification.

By XRD analysis the parameters of crystalline lattice, crystallite sizes and the texture of graphite samples have been determined.

The mutual effect of graphite material nature and the composition of nonaqueous electrolyte on the electrochemical stability of the system have been established by the methods of potentiodynamic cycling.

Galvanostatic investigations were carried out in flat disk cells of 2325 size in Li-C and C-LiMn₂O₄ systems.

As the electrolytes EC, DMC, LiClO₄; EC, DMC, LiPF₆; EC, DMC, LiBF₄ were used.

The cathode material of LiMn₂O₄ has been synthesized at the authors' laboratory on the basis of Ukrainian manganese ores.

The salts were produced at ARC (USA) by the methods developed by Dr.Meshri, and the solvents were gifts of Dr.U.Heider, the Merck company, Germany.

The developed method of graphite modification allows us to increase significantly the discharge capacity of intercalation graphite anode. The discharge capacity of the modified graphites depends slightly on the nature of an initial material and reaches 320 mAh/g at 40mA/cm². At the same time the nature of the initial material determines the self-discharge of anodes intercalated by lithium.

The mutual influence of LiMn₂O₄, graphite and the composition of nonaqueous electrolyte on the nature of electrochemical processes in LiMn₂O₄ - graphite system during a storage and cycling has been studied.

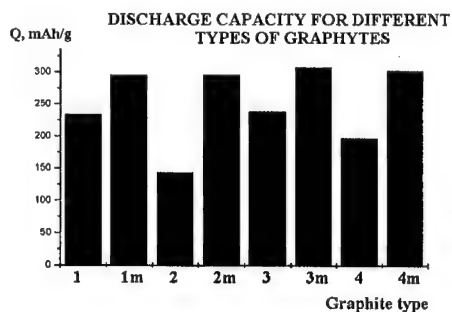
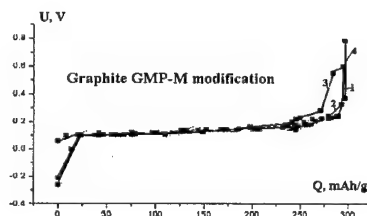
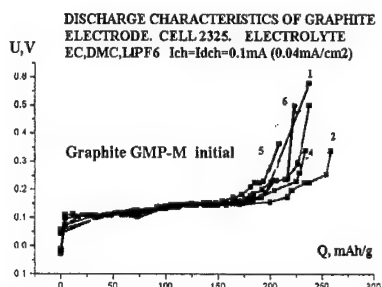
The ways of the characteristics stabilization of lithium-ion power source C-LiMn₂O₄ at a long storage have been determined.

Acknowledgement.

This work is supported by the STCU Project # 656 and the Ministry of Science of Ukraine, Grant 2c/1458-97.

Table 1. The electrochemical characteristics of investigated graphites

Type of graphite		Q, mh/g, I=40 μ A/cm ²	Q _{dis} , mAh/g, I=500 μ A/cm ²
GMP-M initial	1	260-280	250-260
GMP-M modified	1m	310-320	264
GMP-K initial	2	130-150	80
GMP-K modified	2m	260-280	230
GP initial	3	220-240	200
GP modified	3m	310-320	275
Natural (initial)	4	220	200
Natural modified.	4m	300-310	265



Nitride electrode for rechargeable Lithium BatteryYoshiaki Nitta, Junichi Yamaura, Masaki Hasegawa
and Shuji Tsutsumi

Battery research and development center

Matsushita Electric Industrial Co., Ltd.

Hiroshi Ohzono* and Hajime Miyake*

Materials Characterization Dept.*

Matsushita Battery Industrial Co., Ltd.

1-1 Matsushita-cho Moriguchi Osaka, 570-8511 Japan

Nitride compounds as negative electrode have been investigated because of a large capacity[1,2]. $\text{Li}_2\text{Co}_0.4\text{N}$ has a large reversible capacity (700mAh/g) and has a possibility to achieve higher energy density in comparison with conventional carbon system. It is known that the structural changes in this material during electrochemical reaction show extraordinary behavior, changing from crystalline phase at initial state to amorphous phase after an anodic reaction at once. We reported some of the characterization on this material[3]. In this paper, we will present the cell performances and the behavior of cobalt in conjunction with electrochemical behavior.

Fig.1 shows the typical discharge curves of test cell (A-size) employing $\text{Li}_2\text{Co}_0.4\text{N}$ as anode material and Li_xNiO_2 as cathode material. The test condition of charge/discharge was carrying out for the range of 1.5V-4.1V. The cell showed remarkable large capacity which was almost the twice of conventional system and also the discharge rate characteristics were excellent.

Fig.2 shows the result of ^7Li -NMR on the initial state and charged/discharged states after a cycle. A broad spectrum at around 5ppm with spinning side band was observed in the initial state, while almost the same spectra at around 1ppm were observed after charging to 0.1V and discharging to 1.4V vs.Li. Each of the spectra has good symmetry in common. It might be considered that the line broadening in NMR spectra is attributed to the paramagnetic effect of cobalt. The reason why a slight difference in those samples happens might be thought that the state of electronic structure of cobalt was changing or a fine structure in a solid was changing before and after charge/discharge reaction.

Fig.3 shows the result of XAFS (Co-K absorption) data measured at initial state, at discharged state up to 1.4V and at charged state to 0.1V respectively. As can be seen, these spectra showed the same absorption edge although the XANES spectrum on the sample discharged up to 1.4V show different configuration from others. The EXAFS spectra on the samples of discharged and charged state are different from that of initial state. This enable us to think that there is a long range ordering in the initial state, while it is difficult to see a long range ordering in the other two samples which has been experienced lithium extraction reaction at once.

From these evidences, we believe that in spite of the appearance of amorphous phase in XRD view caused by lithium extraction, which has been known, charge/discharge reaction for following cycles can carry out in a short range order. This is because supposing a loss of long range ordering, the presence of a short range ordering of which electronic configuration for cobalt preserve almost the same as in the initial state even after the first discharge, enables redox reaction to proceed.

References

- [1] M.Nishijima, Y.Takeda, N.Imanishi, O.Yamamoto and M.Takano, J. Solid State Chem., 113, 205(1994)
- [2] T.Shodai, S.Okada, S.Tobishima and J.Yamaki, J.Solid State Ionics, 785,86 (1996)
- [3] Y.Nitta, J.Yamaura, M.Hasegawa, S.Tsutsumi, T.Shodai and Y.Sakurai The 1999 Joint International Meeting Abstracts Vol.99-2 236(1999)

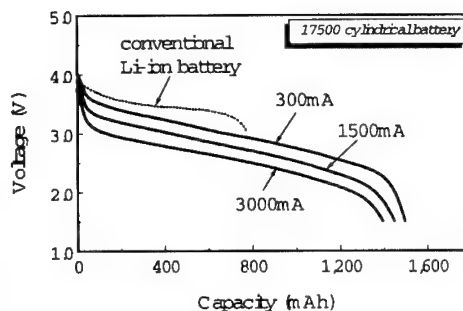


Fig.1 Discharge curves at various currents of $\text{Li}_x\text{NiO}_2/\text{Li}_2\text{Co}_0.4\text{N}$ (A-size) battery. Voltage range is 1.5-4.1V, charge current is 300mA.

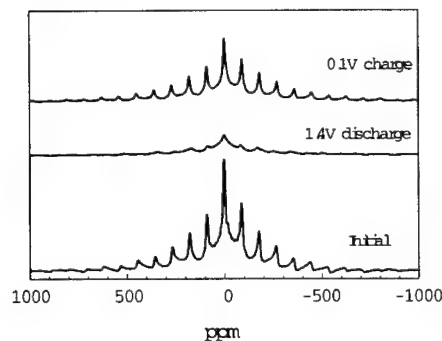


Fig.2 ^7Li -NMR spectra for the samples at initial state and after charge/discharge states.

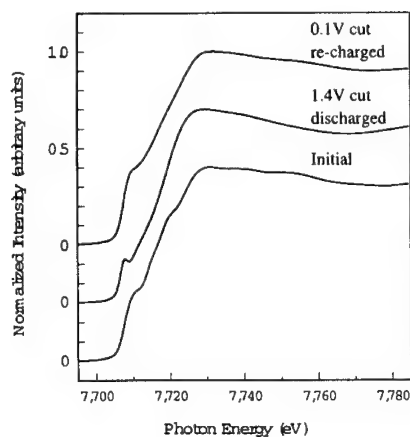


Fig.3 XANES spectra (Co-K) on each step during charge/discharge

Nano-crystalline multi-phase materials from the ternary system Ag-Sb-Sn as new anodes with increased lithium storage capacities

Mario Wachtler, Jörg H. Albering, Martin Winter, and Jürgen O. Besenhard

*Institute for Chemical Technology of Inorganic Materials
Graz University of Technology
Stremayrgasse 16, A-8010 Graz, Austria*

Due to their high lithium storage capacities metals like Al, Si or Sn have frequently been proposed as substitutes for metallic Li or carbon materials as anode materials in rechargeable lithium ion cells. However, their breakthrough has so far been prevented by the poor cycling stability of conventional coarse-grained materials, which is a result of the large absolute volume changes occurring during Li uptake and release.

The cycling stability can be improved by limiting the cut-off potentials (limited capacity cycling) [1-3] or by diluting the reacting component in a more or less inactive matrix. The latter point resembles the situation in Fuji's amorphous tin-based composite oxide [3,4]. Unfortunately, both approaches result in a decreased capacity of the overall electrode.

Other ways of improving the cycling stability of these metallic systems without losing capacity were shown up in previous works on Sn and Sn/"SnSb" [1,2]. These include a proper design of the morphology (small particle size, porosity), the use of multi-phase instead of single-phase materials, and the use of intermetallic compounds, such as "SnSb", which undergo phase separation and restoration during Li uptake and release.

These investigations are now extended to various other multi-phase materials from the ternary system Ag-Sb-Sn. According to Oberndorff et al. [5] these system

exhibits a number of binary intermetallic compounds, namely Sn_4Sb_3 , Sn_3Sb_4 , SnAg_3 , SnAg_4 , SbAg_3 , and SbAg_4 (at 220 °C). No ternary compounds have been found.

The nano-crystalline multi-phase powders were obtained by chemical precipitation with NaBH_4 in aqueous solution as described in Ref. [1]. The multi-phase compositions, such as Sn/"SnSb", Sb/"SnSb" Sn/SnAg₃, or Sb/SbAg₃, were confirmed by X-ray diffraction. The BET surface areas of the powders are typically in the range of 20 - 50 m² g⁻¹.

Composite electrodes were prepared with these powders and electrochemically characterized. Cyclic voltammogrammes as well as preliminary galvanostatic cycling studies are presented and discussed. For comparison, results obtained with single-phase Sn, Sb, and Ag, as well as with pure "SnSb" are given.

- [1] J. Yang, M. Wachtler, M. Winter, and J.O. Besenhard, *Electrochem. Solid-State Lett.* **2**, 161 (1999)
- [2] M. Winter and J.O. Besenhard, *Electrochim. Acta* **45**, 31 (1999)
- [3] Y. Idota, T. Kubota, A. Matsufuji, Y. Maekawa, and T. Miyasaka, *Science* **276**, 1395 (1997)
- [4] I.A. Courtney and J.R. Dahn, *J. Electrochem. Soc.* **144**, 2943 (1997)
- [5] P.J.T.L. Oberndorff, A.A. Kodentsov, V. Vuorinen, J.K. Kivilahti, and F.J.J. van Loo, *Ber. Bunsenges. Phys. Chem.* **102**, 1321 (1998)

Financial support from the Austrian Science Fund and the Oesterreichische Nationalbank in Project 12768 and in the Special Research Programme "Electroactive Materials" as well as support by Mitsubishi Chemical Corp. (Japan) are gratefully acknowledged.

Influence of the binder on the cycling performance of composite electrodes with nano-structured lithium storage metals and alloys

Markus R. Wagner¹, Mario Wachtler¹, Mario Schmied², Peter Preishuber-Pflügl³, Franz Stelzer³, Jürgen O. Besenhard¹, and Martin Winter¹

¹Institute for Chemical Technology of Inorganic Materials

²Research Institute for Electron Microscopy

³Institute for Chemical Technology of Organic Materials
Graz University of Technology
A-8010 Graz, Austria

It is state of the art in primary as well as in secondary lithium batteries to use the active materials as powders in composite electrodes (both for the anode and the cathode), where the particles are held together by a suitable polymer binder. Poly(vinylidene fluoride) (PVdF) and polytetrafluoroethylene (PTFE) are by far the most frequently used binders, though a literature research shows that a vast variety of other materials have been tested for their binding properties and patented, especially in Japan.

PVdF is quite a good solution for composite electrodes with carbon materials or transition metal oxides, where volume changes during Li uptake and release are rather small, and hence the electrodes are dimensionally stable. This must, however, not necessarily be the case for alloys, such as Sn/SnSb which was investigated in this contribution, or for metallic and intermetallic systems in general.

In the case of Sn, for example, the theoretical volume increase due to Li insertion is approximately 260 % (from Sn to Li₂₂Sn₃). This leads to serious problems with the cycling stability of the active material (i.e. to cracking and crumbling and to loss of contact between the single particles), which, however, can be relieved by applying appropriate strategies, as was shown in [1,2]. But this volume increase is also a challenge to the binder: on the one hand it should show a certain flexibility to allow for the "breathing" of the metal / intermetallic during cycling, on the other hand it has to guarantee the stability of the composite material and the support of sufficient electrical contact between the single particles of the active material all throughout cycling. Additionally, the interplay of the composite electrode with the electrolyte has to be considered, since filming

reactions will occur at the surface of active material and the conductive additive. Obviously, the rigidity and the swelling behaviour of the binder are most important parameters for long-term cycling.

Recent publications usually deal with binders for carbon materials, e.g., with ethylene-propylene-diene terpolymer (EPD) and PVdF-copolymers as binders for mesocarbon microbeads [3], or with silica-based gel binders for carbon films [4]. Only little has been done in the case of metals / intermetallics, e.g., a study on polyethylene (PE) and PTFE as binders for Sn and Sn/SnSb, where especially PE appears promising [5].

In this contribution some other binders are investigated in combination with Sn/SnSb and discussed. One approach is, for example, the use of cross-linked binders. The polymer may be incorporated as already cross-linked powder, or it may be incorporated as monomer and then cross-linked during the electrode preparation, either by ultraviolet light, though this requires ultra-thin films of composite material, or thermally, as was applied here.

But it is not only the nature of the binder, which determines the (long-term) cycling stability, but also its distribution within the composite electrode, which is a result of the electrode preparation. The effects of homogenous or inhomogeneous distribution of the binder in the composite material and of partial or complete encapsulation of the active material in the binder are discussed for the case of PVdF.

- [1] J. Yang, M. Wachtler, M. Winter, and J.O. Besenhard, *Electrochem. Solid-State Lett.* **2**, 161 (1999)
- [2] M. Winter and J.O. Besenhard, *Electrochim. Acta* **45**, 31 (1999)
- [3] M.N. Richard and J.R. Dahn, *J. Power Sources* **83**, 71 (1999)
- [4] G. Oskam, P.C. Searson, and T.R. Jow, *Electrochem. Solid-State Lett.* **2**, 610 (1999)
- [5] J. Yang, Y. Takeda, N. Imanishi, T. Ichikawa, and O. Yamamoto, *J. Power Sources* **79**, 220 (1999)

Financial support from the Austrian Science Fund and the Oesterreichische Nationalbank in Project 12768 and in the Special Research Programme "Electroactive Materials" as well as support by Mitsubishi Chemical Corp. (Japan) are gratefully acknowledged.

Anion intercalation into heat-treated XP3 Coke

J. A. Seel and J. R. Dahn
Departments of Physics and Chemistry, Dalhousie
University, Halifax, Nova Scotia, Canada B3H 3J5

In typical lithium-ion cells the carbon electrode acts as the anode. It is possible, however, to use carbon as both the anode and cathode creating a dual carbon cell. In other words, lithium ions can intercalate into one carbon electrode and the anion, such as PF_6^- or ClO_4^- , can intercalate into the other carbon electrode. There has been work done in the past on anion intercalation [see for example refs. 1-5] as well as recent work on dual carbon cells [6-9].

To fully understand the electrochemical processes in a dual carbon cell, anion intercalation must be fully investigated. It has been shown that the anion (PF_6^-) reacts with the carbon electrode (graphite) by an intercalation process [10]. This paper will show that anion intercalation is also possible into other carbon materials with different amounts of disorder, such as XP3 cokes heated to different temperatures.

The amount of turbostratic disorder can be determined by analyzing X-ray patterns for each material with the "Structure Refinement Program for Disordered Carbons" developed by Shi et al. Samples of Fluka graphite, and XP3 coke heated to 1500, 1800, 2300 and 2600°C were studied. The fractions of layers in turbostratic misalignment (p) are indicated in the x-ray patterns shown in Figure 1. The three samples shown in figure 1 all show anion insertion upon charging cells to voltages higher than 4.8 V, see Figure 2. Though the capacity is lower for the more disordered systems, preliminary results suggest that the capacity balance is improved.

The XP3 cokes, as with graphite, intercalate anions. The intercalation process is verified with in-situ X-ray experiments. The results for a cell with an XP3 2300°C electrode in 2M LiPF_6/EMS electrolyte are shown in Figure 3. It can be seen easily that the reaction process is anion intercalation as the structure of the carbon electrode displays a series of staged phases. The first 'pure' stage that can be seen easily is stage 3, at about scan 13, 5.1V. As the cell is charged to even higher voltages, stage 2 is present at scan 23, 5.2V. The results of in-situ x-ray diffraction studies on each of the heat treated samples will be presented here.

- [1] H. Zaleski, P. K. Ummat and W. R. Datars. Solid State Communications, **55**, #5 (1985) 401-403
- [2] W. Rüdorff and U. Hofmann, Zeitschrift für Anorganische und Allgemeine Chemie. **238** (1938) 1-99
- [3] F. Beck, H. Junge and H. Krohn. Electrochimica Acta, **26** (1981) 797-809
- [4] D. Billaud, A. Chenite and A. Metrot. Carbon, **20**, #6 (1982) 493-497
- [5] R. Santhanam and M. Noel. J. Power Sources, **66** (1997) 47-54
- [6] F. P. McCullough, A. Levine, R. V. Snelgrove; US. Patent #4,830,938, May 16, 1989
- [7] F. P. McCullough; US. Patent, #5,532,083, (1996).
- [8] R. T. Carlin, et al. Materials Research Bulletin Symposium Proceedings, **393** (1995) 201-206
- [9] R. Santhanam and M. Noel. Journal of Power Sources, **76** (1998) 147-152
- [10] J.A. Seel and J. R. Dahn, J. Electrochem. Soc., (in press)

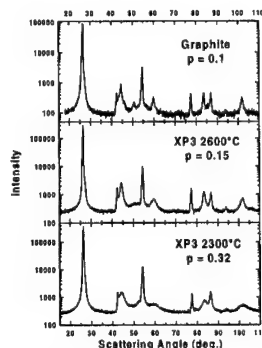


Figure 1: Comparison of the X-ray patterns for graphite, XP3 2600°C and XP3 2300°C

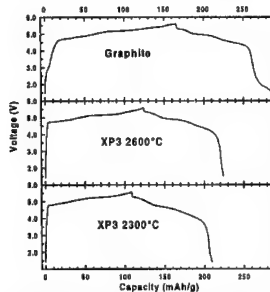
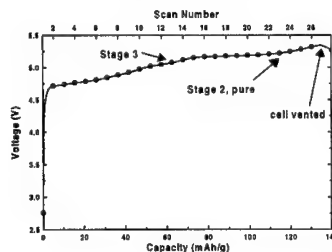


Figure 2: Comparison of voltage profiles for graphite, XP3 2300°C and XP3 2600°C

(a)



(b)

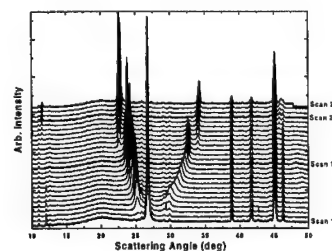


Figure 3: In-situ cell made of XP3 2300°C in 2M LiPF_6/EMS cycled up to 5.32V (a) voltage profile and (b) X-ray measurements.

Metallic Anode Materials for Li-ion Batteries

G. M. Ehrlich[†], C. Durand[†], M. Hetzel[†], J. McGuinn[†], X. Chen[†], T. A. Hugener[‡],
F. Spiess[‡], and S. L. Suib[‡]

[†]Yardney Technical Products, Inc., Pawcatuck, Connecticut, 06379, USA

[‡]The University of Connecticut, Storrs, Connecticut, 06269, USA

An attractive characteristic of Li-ion cells is their energy density and power density. Current 18650 cells offer over 410 Wh/l and as described in the open literature Li-ion cells can offer power density greater than that available from other common technologies, including NiCd or NiMH cells¹. To improve energy and power density, materials with improved energy density and conductivity are required. In particular, there is renewed interest in tin based materials that alloy with lithium at potentials less than 1V vs. Li².

We have prepared alloys based on elements known to alloy with lithium, including Sn, Si, Ag, and Ge. These alloys have been prepared by either mechanical mixing of fine powders of the elements in a mechanical mill or treatment of mixtures of the elements at elevated temperature (500°C to 1000°C) under dry Argon. Electrode materials have been fabricated from the resulting alloys and characterized in electrochemical cells with either Li or LiCoO₂ counter electrodes.

One promising material is a nickel-tin alloy. The reversibility of the reaction of Li with nickel-tin alloys is illustrated by the cyclic voltammogram shown in Figure 1. As shown, Li alloys with the material at 0.25V vs Li and the process offers good reversibility, not observed are significant irreversible processes as is typical for materials based on tin oxides. When alloyed with Li to 400mAh/g, the irreversible capacity observed on the first cycle was

22%, comparable to that observed with many graphitic carbon materials.

The synthesis and performance characteristics of candidate alloys will be discussed.

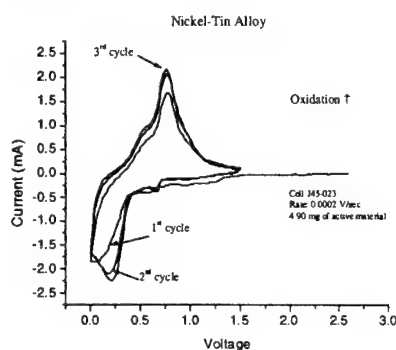


Figure 1. Cyclic voltammogram of a nickel-tin alloy.

Acknowledgement

The authors thank NASA/JSC for support under contract NAS9-99148.

References:

1. A. M. Wilson, J. N. Reimers. *J. Power Sources* 81-82 (1999) 642-646.
2. J. Yang, M. Winter, J. O. Besenhard. *Solid State Ionics* 90 (1996) 281-287. R. Retoux, T. Brousse, D. M. Schleich. *J. Electrochem. Soc.* 146 (1999) 2472-2476.

Relation between Surface Properties and First-cycle Irreversible Charge Loss of Graphite Electrodes for Lithium-Ion Batteries

Felix Joho, Beat Rykart, Andreas Blome, Petr Novák, and Michael E. Spahr¹

Paul Scherrer Institute, Laboratory for Electrochemistry, CH-5232 Villigen PSI, Switzerland

¹TIMCAL Group, CH-6743 Bodio, Switzerland

During recent years extensive work has been carried out toward increasing the energy density of lithium-ion batteries. Progress has mainly been made by improving the carbonaceous material of the negative electrode [1]. One of the major problems of these materials is their "charge loss" during the first cycle, which consumes lithium that must be brought into the cell in the form of a relatively heavy lithium metal oxide such as LiCoO_2 . More recently, several research groups began to improve the reversible capacity and to reduce the irreversible charge loss of graphitic materials. But care must be exercised when comparing their results, because both the irreversible charge loss and reversible capacity depend on the measuring conditions [2].

It is generally accepted in literature [3,4] that the irreversible charge loss occurring during the first reduction cycle depends on the BET surface area of the graphite. Figure 1 shows the quasi linear relation between the irreversible capacity and the BET surface area measured for different synthetic TIMREX[®] graphites. A linear regression fit of the measured values resulted in the relatively value of 95 % for the correlation factor R^2 . In these measurements the first electrochemical lithium insertion occurred at 10 mA/g graphite in an 1M LiPF_6 DMC/EC electrolyte. The current was reduced to 5 mA/g when a potential of 5 mV vs. Li/Li^+ was reached. The first cycle of an electrode containing TIMREX[®] E-SLX 50 as the active material is presented as an example in figure 2. The BET surface area of this sample was 3.9 m^2/g . The formation of the electrode consumed 385 Ah/kg, whereas the reversible capacity was 360 Ah/kg. The irreversible capacity of this sample is 6.5 % as calculated by the formula:

$$L_{\text{cap}} = \frac{C_{\text{dis}} - C_{\text{rev}}}{C_{\text{dis}}} \cdot 100\%$$

L_{cap} : irreversible charge loss
 C_{dis} : first discharge capacity
 C_{rev} : reversible capacity of the first cycle

All graphites investigated had reversible capacities of ca. 360 Ah/kg. The irreversible charge losses and the BET surface areas are listed in table 1 and plotted in figure 1.

A linear function is also obtained when the double layer capacities of the same graphites are measured and plotted against their BET surface area. However, preliminary results of these impedance spectroscopic investigations show that the electroactive graphite surface which is wetted by the liquid electrolyte, and thus gives rise to the irreversible charge loss, is smaller than the BET-graphite surface that is measured with gas absorption techniques. Differential porosity measurements show that the major contribution to the BET surface area is made by the graphite's porosity. This means that only a fraction of the graphite pores are filled with liquid electrolyte and thus can influence the irreversible capacity.

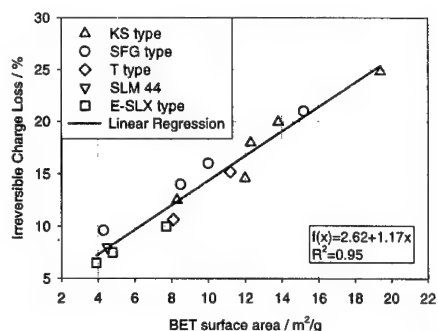


Fig. 1: Measured irreversible charge losses vs. BET surface area from table 1.

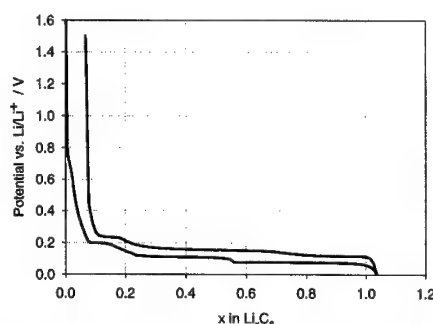


Fig. 2: First cycle of an TIMREX[®] E-SLX 50 electrode (electrolyte: 1M LiPF_6 DMC/EC)

Table 1: Properties of investigated TIMREX[®] graphites

Product	BET surface area m^2/g	charge loss %	d_{50} μm
KS 6	19.4	24.8	3.6
KS 10	13.8	20.0	5.6
KS 15	12.3	18.0	7.5
KS 25	12.0	14.6	8.2
KS 44	8.3	12.5	16.2
SFG 6	15.2	21.0	3.4
SFG 10	10.0	16.0	5.8
SFG 15	8.5	14.0	7.5
SFG 44	4.3	9.6	23.6
T 15	11.2	15.2	8.6
T 44	8.1	10.7	20.2
SLM 44	4.5	8.0	24.0
E-SLX 20	7.7	10.7	10.2
E-SLX 30	4.8	7.5	18.5
E-SLX 50	3.9	6.5	28.0

- [1] A. Yoshino, Abstract ISIC 10 (1999) 31A5, Okazaki, Japan.
- [2] F. Joho, B. Rykart, R. Imhof, P. Novák, M.E. Spahr, and A. Monnier J. Power Sources 81-82 (1999) 243.
- [3] R. Fong, U. von Sacken, and J.R. Dahn, J. Electrochem. Soc. 137 (1990) 2009.
- [4] B. Simon, S. Flandrois, A. Février-Bouvier, and P. Biensan, Mol. Cryst. Liq. Cryst. 310 (1998) 333.

Abstract No. 77

Origins of reversible and irreversible capacity losses of graphite-lithium anode

Audrey Martinent¹ and Rachid Yazami²

¹LEPMI/CNRS-INPG

BP 75

St Martin d'Hres 38402

France

²LEPMI/CNRS-INPG

BP 75

St Martin d'Hres 38402

France

In the present paper study the changes in the electrochemical performances induced by an elevated temperature storage of Li/ LiPF₆ + EC-DMC 1M/ graphite cells.

Thermal storage is carried out at 60°C between a series of C/5-rate galvanostatic cycles in the [-0.005 V ; 1.5 V vs Li/Li+] voltage range. This led to an irreversible capacity loss during the first cycle after the storage. Moreover, Electrochemical Impedance Spectrometry (EIS) measurements showed that the cell polarization resistance increased during storage.

The evolution of the EIS spectra is tentatively related to the concomitance of two phenomena:

1) dissolution of the organic/polymer part of passivation film (SEI) formed on lithiated graphite electrodes during storage at elevated temperature. This would account for the re-appearance of an irreversible capacity after storage. 2) increase of the inorganic part of the SEI resulting from the electrolyte reaction with residual lithium present in the carbon structure even after de-intercalation at 1.5 V vs. Li.

Being the most resistive part of the SEI, this inorganic internal layer should play a major role in the apparent irreversible capacity losses of the graphite

Nanocrystalline Mg_2Sn As an Anode Material for Li-ion BatteryH. Kim^a, Y.-J. Kim^a, D.-G. Kim^b, H.-J. Sohn^b,
T. Kang^b, B. Park^b^a Department of Mineral and Petroleum Engineering,^b School of Materials Science and Engineering,
Seoul National University
Seoul, 151-742, Korea

Mg_2X (X=Si, Ge, Sn, Pb) has been studied as alternatives to current commercial anode materials for Li-ion battery due to several advantages including high capacity, safety and favorable voltage plateau [1-3]. In our previous study [3], it was found that three sequential reactions occurred during Li insertion into Mg_2Si , i.e., Li intercalation into Mg_2Si lattice, Li-Si alloying reaction followed by Li-Mg alloying reaction. It was also found that poor cyclability of Mg_2Si was attributed to the volume change during the alloying/dealloying reaction between Li and Si as well as between Li and Mg. Saito et al reported that the Mg_2Sn and Mg_2Pb (the same structure as Mg_2Si) showed better cyclability than Mg_2Si [1]. The reaction mechanism of these materials would be almost the same with Mg_2Si . And the better cyclability of these materials is probably due to the ductility of element X in Mg_2X (X= Sn, Pb) since ductile materials showed better capacity retention characteristics [4]. Also nanocrystalline structure may insignificantly improve the ductility of brittle materials such as ceramics and intermetallics [5]. In this study, nanocrystalline magnesium stannide (Mg_2Sn) was examined as anode materials for Li-ion battery

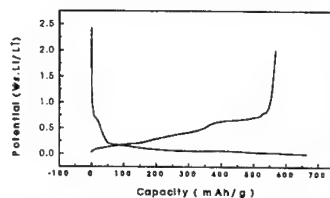
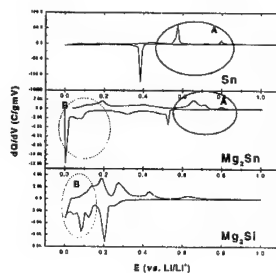
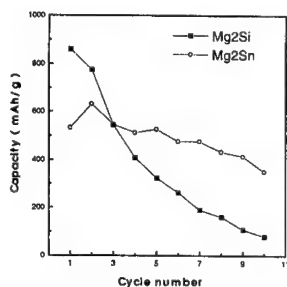
Nanocrystalline Mg_2Sn powders were prepared by conventional mechanical alloying process. Pure Mg (99.9 %, 325 mesh size) and Sn (99.8%, 325 mesh size) were blended and milled under Ar atmosphere using lab-made vibratory mill. Electrode preparation and electrochemical test were performed as described in Ref. 3.

Crystalline Mg_2Sn powders could be obtained after 24 h and the estimated grain size through Hall-Williamson plot was 31 nm which indicated powders obtained had nanocrystalline structure. Figure.1 shows the voltage profile of Mg_2Sn electrode for the first cycle. The first charge (Li alloying) and discharge (Li dealloying) capacities are 660 mAh/g ($\text{Li}_{4.12}\text{Mg}_2\text{Sn}$) and 570 mAh/g ($\text{Li}_{3.56}\text{Mg}_2\text{Sn}$), respectively and the initial cycling efficiency is 86.3 % which is higher than Mg_2Si and tin-based oxide materials. To investigate electrochemical behavior of Mg_2Sn during Li insertion/removal, differential capacity plots of Mg_2Sn , Sn and Mg_2Si are compared in Figure.2. Differential capacity plots of Mg_2Sn and Sn show similarities at region A, which indicates that Li-Sn alloying/dealloying reaction occurred and those of Mg_2Sn and Mg_2Si shows similarities at region B. The latter indicates that the reaction of Mg_2Sn with Li was similar to the reaction of Mg_2Si with Li. Figure.3 compare the cycle performances of Mg_2Sn and Mg_2Si . It was noteworthy that the Mg_2Sn electrode exhibited better capacity retention characteristics than the Mg_2Si electrode.

Dozono and M. Inagaki, U.S.Pat., 5,770,330, 1998

2. H. Sakaguchi, H. Honda, and T. Esaka,
J. Power Sources, 81-82, p.229, 19983. H. Kim, J. Choi, H.-J. Sohn and T. Kang,
J. Electrochem. Soc., 146, p.4401, 19994. D. Fauteux and R. Koksang, *J. Appl. Electrochem.*

23, p. 1, 1993.

5. K. Lu, *Mater. Sci. & Eng. R*, 16, p.161, 1996Figure.1 Voltage profile of Mg_2Sn electrodeFigure. 2 Differential capacity plots of Sn, Mg_2Sn and Mg_2Si Figure. 3 Cycle performances of Mg_2Si and Mg_2Sn

References

1. A. Saito, Y. Aono, T. Horiba, H. Kodama, T.

Al-based active/inactive composite anodes for lithium rechargeable batteries

G.J. Jeong^a, Y.U. Kim^b, H.-J. Sohn^b, T. Kang^b,
H.R. Kang^c, S.W. Kim^c

^aDepartment of Mineral and Petroleum Engineering,
Seoul National University, Seoul 151-742, Korea

^bSchool of Materials Science and Engineering,
Seoul National University, Seoul 151-742, Korea
^cNESS Corporation Ltd., Soowon 442-380, Korea

Introduction

Graphite has been used as an anode material in lithium-ion batteries. Since graphite has a limited capacity of 372 mAh/g, there has been a demand for anode materials with higher capacity. Recently, Fujifilm Celltec reported tin-based oxide as a high-capacity anode material which has higher energy density and specific capacity compared to graphite[1]. After this publications, the lithium alloy anodes attract attention for alternative anode materials again. In this alloy system, the large change in volume that was observed during the reaction resulted in a severe cracking of the particle and loss of electric contact that is responsible for poor cycle performance. To overcome this problem, intermetallic compounds[2,3] or active/inactive nanocomposite materials[4] have been considered instead of pure metals. Of the various metals that can alloy with lithium, aluminum has merits of a relatively high capacity (992mAh/g for β -LiAl formation), very flat charge/discharge voltage plateau, and relatively low volume change between the lithium-free and lithated state (ca. 97%). But, up to date, there have been a little reports about Al-based composite or intermetallic compound for anode materials. In this study, we synthesized Al/ Al_2O_3 or Al/SiC composite materials by ball milling technique and examined the possibility for anode materials. The internal structure of this ball-milled composite powder can be considered as a nanocomposite containing the inactive phase of Al_2O_3 or SiC, and active phase of Al. These nanocomposite materials have been studied in the aerospace and automotive industry for the enhanced mechanical strength[5].

Experimental

The composite powders of Al/ Al_2O_3 or Al/SiC were prepared by ball milling. The volume fraction of Al_2O_3 or SiC particulates in the composite powder was varied from 20 to 50%. The powders were put into a hardened steel vessel (80 cm^3) with steel balls (combination of 3/8 and 3/16 inch), and ball to powder ratio was 20. Ball milling was performed from 0 to 36 hrs using lab-made vibratory mill. The electrode were prepared by coating the slurries (composite powders (80wt%), carbon black (10wt%) and PVDF (10wt%) dissolved in NMP) on a Cu foil substrate. Coin-type test cells were assembled in an argon-filled glove box using a Celgard 2400 as a separator, 1 M $\text{LiPF}_6/\text{EC}/\text{DEC}$ (1:1) as an electrolyte, and Li foil as counter electrodes. The charge (Li insertion) / discharge (Li deinsertion) experiments were performed galvanostatically with a current density of 30 mA/g.

Results and Discussion

Figure 1 and 2 show the charge/discharge voltage profiles of Al-20vol% Al_2O_3 and Al-20vol%SiC composite electrode. In both cases, the typical voltage profiles of pure Al electrode were observed and the cycle performance of electrode that was ball-milled for 12 hours

was better than that of not-ball-milled one. Figure 3 and 4 show the capacity vs. cycle number for Al-50vol% Al_2O_3 and Al-50vol%SiC composite electrodes. In the same way, the cycle performance of electrode that was ball-milled for 12 hours was enhanced. And the capacity retention increases as the amount of Al_2O_3 or SiC phase in the composite increases. From these results, it seems that inactive Al_2O_3 or SiC phases in the composite powder plays an important role to enhance the cycle performance.

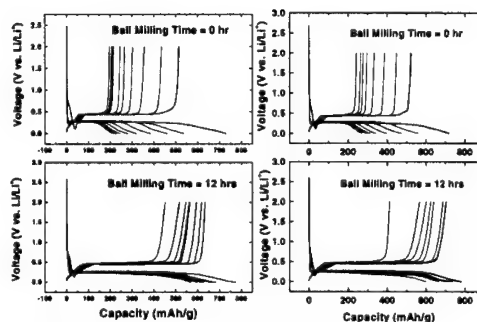


Figure 1. The charge/discharge curve of Al-20vol% Al_2O_3 composite electrodes. (Left)

Figure 2. The charge/discharge curve of Al-20vol%SiC composite electrodes. (Right)

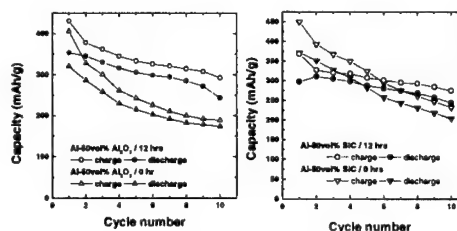


Figure 3 and 4. The capacity vs. cycle number of Al-50vol% Al_2O_3 and Al-50vol%SiC composite electrode

References

- [1] Y. Idota, T. Kubota, A. Matsufuji, Y. Maekawa, and T. Miyasaka, *Science*, **276**, 1395 (1997)
- [2] O. Mao and J.R. Dahn, *J. Electrochem. Soc.*, **146**, 414 (1999)
- [3] J.T. Vaughey, J.O'Hara, and M.M. Thackeray, *Electrochem. Solid-State. Lett.*, **3**(1), 13, (2000)
- [4] R.A. Huggins in: J.O. Besenhard(Ed.), *Handbook of Battery Materials*, Wiley-VCH, Weinheim, (1999), Part III, Ch.4.
- [5] M. S. El-Eskandarany, *J. Alloys Comp.* **279**, 263, (1998)

**THE EFFECT OF ELECTROLYTE
TEMPERATURE ON THE PASSIVITY OF SOLID
ELECTROLYTE INTERPHASE FORMED ON
GRAPHITE ELECTRODE**

Su-Il Pyun*, and Seung-Bok Lee

*Department of Materials Science and Engineering,
Korea Advanced Institute of Science and Technology,
373-1 Kusong-Dong, Yusong-Gu, Taejeon 305-701,
KOREA*

The effect of electrolyte temperature on the passivity of solid electrolyte interphase (SEI) [1] was investigated in a 1M LiPF₆-ethylene carbonate (EC) / diethyl carbonate (DEC) (50:50 vol.%) electrolyte, using galvanostatic charge-discharge experiment, and ac-impedance spectroscopy combined with in-situ Fourier transform infra-red (FT-IR) spectroscopy [2,3].

From the galvanostatic charge-discharge curves in Fig. 1, it was found that the irreversible capacity loss with cycling was markedly increased with rising SEI formation temperature from 0 ° to 35 °C. This implies that more structural damages such as exfoliation and amorphization of the graphite electrodes took place at higher SEI formation temperature. The in-situ FT-IR spectra of the SEI layer formed at various temperatures showed that the main chemical constituents of the SEI layer on the graphite electrodes were Li₂CO₃, ROCO₂Li, and Li_xPF_y. However, the relative amounts of the surface species formed on the graphite electrode were strongly dependent on the SEI formation temperature. This is due to the enhanced gas evolution reaction during SEI formation, which leads to the more defects in the SEI layer as easy co-intercalation paths for lithium ions and solvated electrolyte molecules with increasing SEI formation temperature. From the analysis of measured ac-impedance spectra, it was found that the resistance associated with the SEI layer decreased with SEI formation temperature, which is attributable to the formation of the defect-rich SEI layer.

The electrochemical lithium intercalation into the graphite electrodes was discussed in terms of the effect of the SEI formation temperature on both the structure and composition of SEI layer.

References

- [1] A. M. Andersson, K. Edström, and J. O. Thomas, *J. Power Sources* 81-82 (1999) 8.
- [2] S.-I. Pyun, and Y.-G. Ryu, *J. Electroanal. Chem.* 455 (1998) 11.
- [3] D. Aurbach, B. Markovsky, I. Weissman, E. Levi, and Y. Eim-Eli, *Electrochim. Acta* 45 (1999) 67.

*Corresponding author. Tel: (82) 42-869-3319; Fax: (82) 42-869-3310; E-mail: sipyun@sorak.kaist.ac.kr

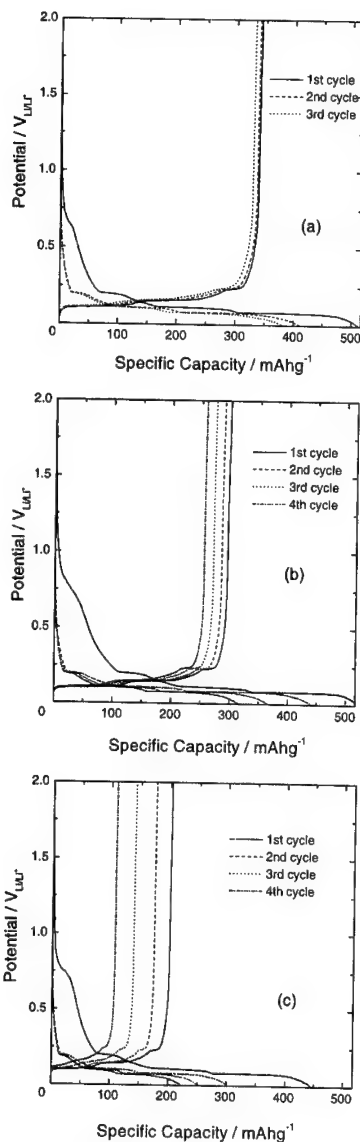


Fig.1. Galvanostatic charge-discharge curves of the Timrex SFG 6 graphite electrodes in a 1M LiPF₆-EC/DEC electrolyte at 20 °C. The electrodes were previously subject to a potential of 0.6 V_{Li+/Li-} for 2 h at various SEI formation temperatures of : (a), 0 °C; (b), 20 °C; (c), 35 °C. The lithium was charged and discharged at a 10 h rate.

Improvement of Charge/Discharge Characteristics of Al-X-Li Alloys by Means of Varying the Alloy Composition.

V. Guterman*, V. Ozeryanskaya and A.
Bratuhin.

Department of Electrochemistry, Rostov State University,
Zorge st., 7. 344090, Rostov-on-Don, Russia. E-
mail:vguter@chimfak.rsu.ru

New effective anodic materials for lithium batteries, based on metallic composites were produced the latest time [1]. Metal alloys, intermetallics, oxides or other inorganic compounds may be used as components of such materials. In accordance with the role of each phase component of such systems during charge-discharge process the components may be conditionally divided on three groups: 1st –phases-absorbers, which can reversibly interact with lithium (reactants); 2nd – components, which interact with lithium irreversibly; 3rd – morphological consolidating components, which does not interact with lithium. Knowledge about the electrochemical behavior of individual substances and their compounds or mixtures is necessary for the choice of best components for composite anodes.

Earlier we in detail described the electrochemical behaviour of solid solutions on the base of aluminium during lithium cycling [2]. The aim of the work is the study of the influence of the composition of two-component aluminum alloys (intermetallics and binary mixtures) on the phase formation peculiarities and lithium cycling efficiency in the aprotic solvent electrolytes.

It have been established for intermetallic substrates that either pure lithium phase layer is formed on the anode surface (AlNi) or the phase transformation of Al_3M_2 to $LiAl$ and M takes place (Al_2Cu and Al_3Mg_2 in part)[3].

Lithium intercalation-deintercalation processes in two-phase electrodes take place for the both alloy phases in a parallel way. At that the influence of the alloy composition on the cycling efficiency and the charge-discharge capacity aren't obey to the additive scheme, as it would be expected in accordance with an "independent realization of electrode reactions" principle. An electrochemical behavior of such anodes is well imitated by the "hydrodynamic" model of the system of tanks joined with one source of a liquid.

The filling and pouring out of the system is equivalent to charge-discharge process. The height of each tank disposition is identical to the value of equilibrium potential (Li^+/Li -compound). The capacity of each tank is determined by the lithium capacity of the compound (the composition of lithium-containing phase) and depends on the nature and concentration of the component in the alloy. The rate of the tank filling (pouring out) is determined by the kinetics of corresponding cathodic (anodic) reaction and may be imitated by the temporal change of traffic capacity for the leading (rejecting) pipe. A potentiostatic cycling conditions are reproduced by means of the support of constant liquid level in the

system. Galvanostatic charge-discharge corresponds to the constant rate of the liquid afflux (drain).

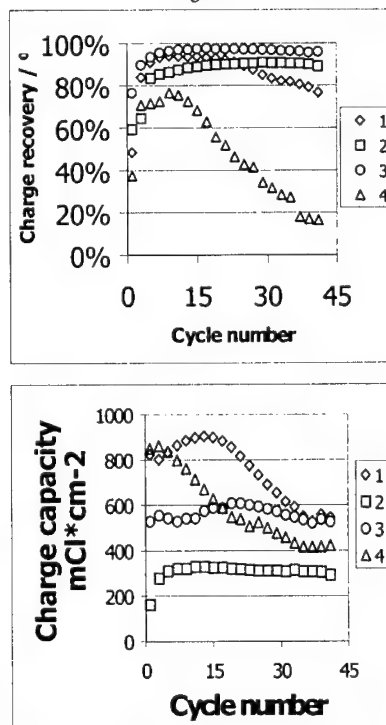
Consequent phase transformation of lithium-containing compounds (based on the one component) and solid phase diffusion of lithium from one phase to another admits the opportunity of the connection among some tanks.

In general it has been established how the alloy composition changing influences on the electrode charge-discharge capacity, lithium cycling efficiency and on the character of the parameters changing during the cycling.

References.

1. M. Winter, J.O.Besenhard, *Electrochimica Acta* 45 (1999) 31.
2. V.E.Guterman *et al*, *Russian Journal of Electrochemistry* 30 (1994) 663; 30 (1994) 768.
3. V.V.Ozeryanskaya, V.E.Guterman, V.P.Grigor'ev, *Russian Journal of Electrochemistry* 35 (1999) 275.

Figures



Cycle life performance of Sn-(Li) (1), Al-(Li) (2), Al60Sn40-(Li) (3) and Al20Sn80-(Li) (4) in 0.5M $LiClO_4/PC$. Potentiodynamic cycling in the potential range +2,2 -0,2 V with the rate 10 mV.s⁻¹.

CARBON ELECTRODE MORPHOLOGY AND THERMAL STABILITY OF THE PASSIVATION LAYER

Linda Fransson¹, Anna M. Andersson¹, Anita Hussénius² and Kristina Edström¹

1) Inorganic Chemistry, Ångström Laboratory, Uppsala University, Box 538, SE-751 21 Uppsala, Sweden.

2) Department of Organic Chemistry, Institute of Chemistry, Uppsala University, Box 521, SE-751 21 Uppsala, Sweden.

A solid electrolyte interface (SEI) is formed during the first discharge of a graphite electrode. This passivation layer is responsible for an irreversible capacity loss but also serves as a protection of the graphite surface from exfoliation. A complete understanding of the chemistry and morphology of this layer is therefore crucial, and there have been numerous investigations of these features in recent years [1-3].

The choice of lithium-salt anion in the electrolyte solvent EC/DMC has been shown to be of a vital importance for the thermal stability of this passivation layer [4,5]. The thermal stability of the SEI-layer formed using LiCF_3SO_3 and $\text{LiN}(\text{SO}_3\text{CF}_3)_2$ will here be discussed and compared with results from similar earlier studies based on the salts LiPF_6 and LiBF_4 [4,5].

A C/Li half-cell configuration was used in all experiments. Different types of carbon, synthetic graphite, MCMB and carbon black, were investigated in combination with EC/DMC-based electrolytes containing 1 M LiCF_3SO_3 or $\text{LiN}(\text{SO}_3\text{CF}_3)_2$ salt. Cells were precycled at room temperature to create a SEI-layer on the carbon surface. They were then stored in charged (deintercalated) or discharged (intercalated) state at different temperatures. After storage, a number of different techniques were used to analyse the electrodes and the resulting electrolyte solutions: continued electrochemical cycling to probe electrochemical response to temperature treatment; *in situ* XRD and SEM studies to characterize morphology; DSC to investigate the thermal response; NMR to determine changes in the electrolyte, and XPS measurements to analyse compositional and SEI layer thickness changes.

We find a clear correlation between the lithium salt in use and the degradation of the SEI layer at elevated temperature. In Table 1 the starting temperature for SEI-degradation, based on DSC measurements, is presented for each salt.

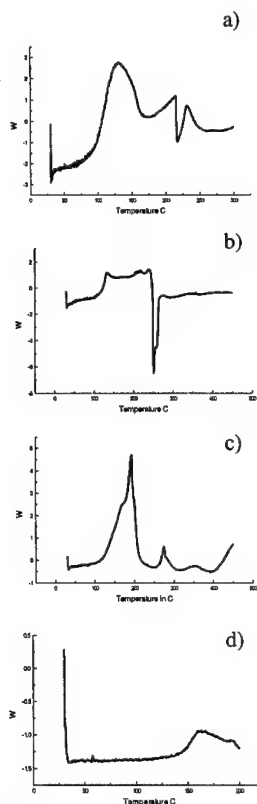
Table 1

1 M lithium salt in EC/DMC 2:1	Onset temp. for breakdown of passivation layer/ °C
LiBF_4	58
LiPF_6	89
LiSO_3CF_3	105
$\text{LiN}(\text{SO}_3\text{CF}_3)_2$	120

Not only does the onset temperature differ between the salts, but also the shape of the exothermic isotherm (Fig. 1 a-d), which suggests different thermal breakdown mechanisms.

Reaction mechanisms will be discussed in relation to the lithium salt used and the morphology of the carbon electrode.

Fig. 1 The DSC ΔH isotherms in J for: a) LiBF_4 , b) LiPF_6 , c) LiSO_3CF_3 and d) $\text{LiN}(\text{CF}_3\text{SO}_3)_2$



References

- [1] D. Aurbach, Y. Ein-Eli, B. Markovsky, A. Zaban, S. Luski, Y. Carmeli and H. Yamin. *J. Electrochem. Soc.*, **142** (1995) 2882.
- [2] S. Geniès, R. Yazami, J. Garden and J. C. Frison. *Syn. Metals*, **93** (1998) 77.
- [3] S. Mam J. Li, X. Jing and F. Wang. *Solid State Ionics*, **86-88** (1996) 911.
- [4] A. M. Andersson, K. Edström and J. O. Thomas. *J. Power Sources*, **81-82** (1999) 8.
- [5] A.M. Andersson, K. Edström, Å. Wendsjö and N. Rao. *J. Power Sources*, **81-82** (1999) 287.

**THERMAL STABILITY OF A HOPG/LIQUID
ELECTROLYTE INTERFACE USING *IN SITU*
ELECTROCHEMICAL ATOMIC FORCE
MICROSCOPY**

Kristina Edström and Merja Herranen

Inorganic Chemistry, Ångström Laboratory, Uppsala
University, Box 538, SE-751 21 Uppsala, SWEDEN

In situ atomic force microscopy (AFM) has been used to follow morphological changes of the thermal stability of a highly oriented pyrolytic graphite (HOPG)/electrolyte interface. The novelty of this study is that the morphological changes of the HOPG/electrolyte interface are studied *in situ* as a function of temperature. Hence the thermal stability of the electrolyte could be studied. An organic solvent of 1 M LiBF_4 in EC/ γ BL 2:1 was used as electrolyte with a water content of 1%. Cyclic voltammetry was performed and showed a water reduction as expected at 1.3 V vs. Li/Li^+ . A passivation layer, sometimes called a Solid Electrolyte Interface,

formed on the HOPG surface at 0.8 V as followed by *in situ* AFM (Fig. 1a and b). Lithium-ion intercalation into the graphite started at 0.2V. *In situ* AFM temperature measurements were carried out at 25, 40, 50, 60 and 70 °C. At 50 °C a destruction of the passivation layer, changing its morphology, could be detected. The SEI-layer was cracking forming islands with unprotected graphite surface in between (Fig. 2a). At higher temperatures the reaction products – islands – were even more concentrating to the HOPG edge planes (Fig. 2b). The effect of the lithium salt (here LiBF_4) and water are discussed in the light of the morphological changes in comparison with electrochemical cycling results, XPS and DSC studies.

Acknowledgements

Financial support from the Foundation for Environmental Strategic Research (MISTRA) and the Swedish Science Research Councils; NFR and TFR. Dr. Ute Schmidt at Molecular Imaging is hereby acknowledged.

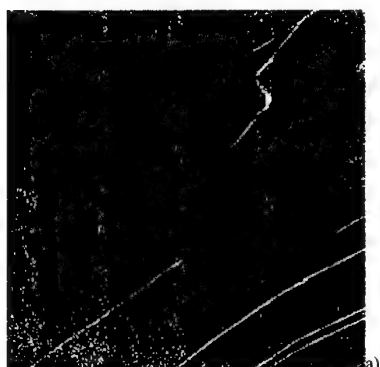


Figure 1 AFM images (scan size $1 \times 1 \mu\text{m}^2$) of a) an untreated HOPG surface in electrolyte and b) the SEI layer formed on the surface after CV.

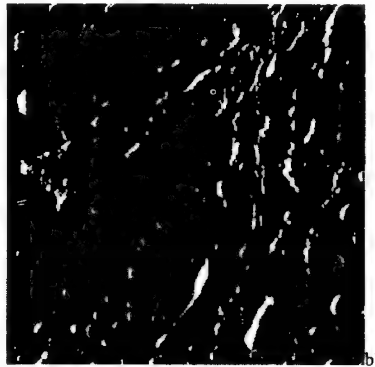
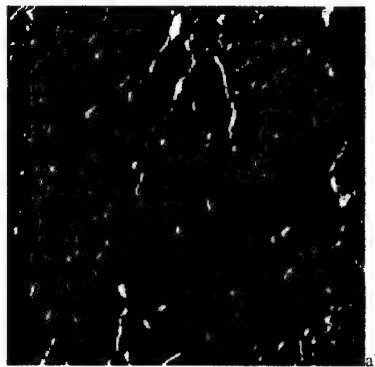


Figure 2 AFM images (scan size $3 \times 3 \mu\text{m}^2$) of the SEI layer at a) 50° C and b) 70° C.

CaSi₂ : A New Anode Material for Lithium-Ion BatteriesS.R. Sahaya Prabakaran¹, Tou Teck Yong¹, and M. Siluvai Michael²¹ Center for Smart Systems and Innovation, Faculty of Engineering, Multimedia University, 63100 Cyberjaya, Selangore, Malaysia.² Advanced Materials Research Center, SIRIM Bhd., 40911 Shah Alam, Selangore, Malaysia.

There have been a variety of carbon compounds studied as possible anodes for lithium-ion cells including graphite [1] coke, [2] and various poorly crystalline carbons [3]. Although these materials have shown reasonable behaviour in commercial cells, there are certain limitations associated with the carbon intercalation anode. In search for newer anode materials to replace carbon systems with respect to its limited capacity of < 370 mAh/g [4] in commercial systems, an alternative system has recently been announced by Fuji in a series of patents [5,6] and publications [7]. The system is based on an inorganic amorphous anode system containing metallic elements of groups III, IV, or V. The most impressive results were reported for oxides of tin, SnO, or SnO₂.

We propose here, for the very first time, another new inorganic anode material, CaSi₂, which can possibly insert Li⁺ ions into its host lattice and behave reversibly in a lithium containing cells. Our preliminary analysis on this new material shows promising reversible behaviour over extended cycles. In view of its novelty in lithium battery applications, we report here the preliminary electrochemical properties in actual test cells in a flooded electrolyte environment.

The structure of CaSi₂ has a trigonal-rhombohedral crystal lattice [8]. The stacking sequence of Ca trigonal layers repeats after six layers (tr6). The cell constant $a = 10.4 \text{ \AA}$ with the space group D_{3d}^5 ($R\bar{3}m$). Our electrochemical studies prove that the existence of the open structures facilitate the insertion of Li⁺ comfortably into its host lattice leading to the probable stoichiometry of Li_xCaSi₂. This prompted us to explore this compound for lithium-ion battery application.

Electrochemical studies were carried out in order to ascertain the lithium ion insertion into CaSi₂ matrix. The test cells were fabricated in the following configurations:

(1) Li metal/ CaSi₂ (Cell #1) [OCV = 2.98 V](2) LiMn₂O₄ / CaSi₂ (Cell #2) [OCV = 0.12 V]

The CaSi₂ powders were procured from Fluka (Germany) and used as received. The powders were mixed with a PTFE binder and an electroconductive carbon (black carbon) powder in a weight ratio 90:5:5, respectively and compressed into circular pellets (20 mm) on copper mesh (Exmet, U.S.A). The composite CaSi₂ electrode was mounted in a 2450 coin type cell hardware with a celgard 2400 polypropylene microporous separator sandwiched between lithium metal (Cell #1) and also with composite spinel LiMn₂O₄ (Cell #2) [9]. The electrolyte used was 1M LiBF₄ in EC + DMC (1:1). The cells were fabricated in a argon filled glove box.

The test cells were subjected to potentiostatic charge/discharge cycles using BAS (LG 50). The CV results obtained for Cell #2 is shown in figure 1.

The galvanostatic charge/discharge studies on cell #1 surprisingly proved that the CaSi₂ exhibits the similar charge/discharge trend of a carbon based Li/C₆ system. The curve of Li/CaSi₂ shows that the working potential range of 0.015 to 0.7 V versus Li/Li⁺ which is very much suitable for use as negative-electrode active material in Li-Ion batteries.

The complete details on the obtainable reversible Li-Ion storage capacity and number of possible cycles and the self-discharge details will be presented. Also, another a couple of new materials in this family, NiSi₂ and CoSi₂ will also be proposed.

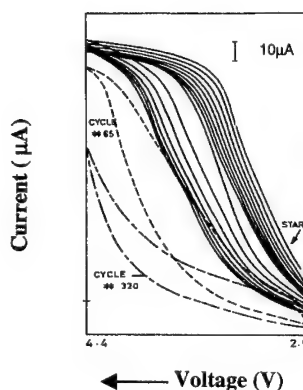


Fig.1: Typical cyclic voltammetric curves of LiMn₂O₄/CaSi₂ cells

References:

1. M.B. Armand, in *Materials for Advanced Batteries*, D.W. Murphy, J. Broadhead, and B.C. Steele, Editors, p.145, Plenum Press, New York (1980).
2. D. Guyomard and J.M. Tarascon, *J. Electrochem. Soc.*, 139, 937 (1992).
3. J.R. Dahn, R. Fong, and M.J. Spoon, *Phys. Rev.B*, 42, 6424 (1990).
4. T. Zheng, Q.Zhong, and J.R. Dahn, *J. Electrochem. Soc.*, 142, L211 (1995).
5. Y. Idota, M. Mishima, M. Miyaki, T. Kubota, and T. Miyasaka, *Eur. Pat. Appl.* 651450 A1 94116643.1 (1994).
6. K. Tahara, H. Ishikawa, F. Iwasaki, S. Yahagi, A. Sakata, and T. Sakai, *Eur. Pat. Appl.* 93 111 938.2 (1993).
7. Y. Idota, T. Kubota, A. Matsufuji, Y. Maekawa, T. Miyasaka, *Science*, 276 (1997).
8. J. Evans, *J. Solid State Chem.*, 28, 369 (1979).
9. S.R.S. Prabakaran, Nasiman B. Saparil, S.S. Michael, M. Massot, C. Julien., *Solid State Ionics* 112, 25 (1998).

The Correlation among Surface Chemistry, 3D Structure, Morphology, Electrochemical and Impedance Behavior of Lithiated Carbon Electrodes

D. Aurbach and J. S. Gnanaraj
Department of Chemistry
Bar-Ilan University
Ramat-Gan 52900, Israel

J. E. Fischer and A. Claye
Department of Material Science
University of Pennsylvania
Philadelphia, PA 19104-6272
USA

Introduction

The work related to this abstract involved a rigorous study of the correlation among surface chemistry (FTIR, XPS), 3D structure (X-ray and neutron scattering), morphology (SEM, AFM), and electrochemical and impedance behavior of lithiated carbon electrodes in commonly used liquid electrolyte solutions. Of special importance was the fact that four different types of carbons were explored in a single study. These included, for comparison, two types of hard, disordered carbons, carbon nanotubes⁽¹⁾ and synthetic graphite powder.

Experimental

Graphite powders from Timcal Inc., hard, disordered carbons from Mitsubishi Inc., carbon nanotubes from Rice University, and ready to use, Li battery grade electrolyte solutions from Merck KGaA, have been used. The preparation of composite carbon electrodes and the performance of their FTIR, XPS morphological, electrochemical and impedance measurements were already described.⁽²⁾ The nanotubes (NT) could be used as electrodes as received ('bucky paper'⁽³⁾). The performance of the 3D analysis by diffraction methods is described in ref. (4). In this study we used two types of disordered carbons, denoted as C_A and C_B. The former exhibits a higher degree of order (R factors calculated from XRD are 9.1 and 6, respectively). The H/C ratios for these carbons (0.04 and 0.13, respectively) were obtained from prompt gamma activation analysis. These carbons can insert lithium at capacities of >400 mAh/gr for C_A and >750 mAh/gr for C_B (irreversible capacity around 25%), as reported by their manufacturer.

Results and discussion

An important experimental result is the excellent coherence in the results obtained from FTIR and XPS surface measurements. All the pristine carbons are covered by surface groups containing carbonyl groups (e.g. ketones, aldehyde, carboxyl). Judging from the percentage of surface oxygen (XPS) and the intensity of the surface C=O peaks, the disordered carbons contain more surface groups than the graphite and the nanotubes (the latter seem to be the most surface-group free of the four carbons studied). Regarding the disordered carbons, C_A, which possesses the lower hydrogen content of the two, is the richest in surface groups (it may be connected with the low H content).

We used LiPF₆, LiAsF₆ and LiC(SO₂CF₃)₃ solutions in EC/DMC mixtures. Polarization of all carbons to low potentials (>0. V vs. Li/Li⁺) leads to their coverage by surface films, which are dominated by solvent reduction products (organic carbonates). All the salts mentioned above are also reduced on the lithiated carbons. Hence, the surface films also contain species of the Li_xAsF_y, Li_xS₂O_z, Li_xPF_y type (in the relevant salt solutions), and LiF. The surface chemistry developed on all of these carbons is similar, and the solution reduction is more dominant in the surface film formation than reduction of the surface groups covering the pristine materials.

Galvanostatic and voltammetric cycling shows that the disordered carbons indeed possess a very high reversible capacity (>> 372 mAh/gr), which deteriorates upon cycling. The behavior of the nanotubes and graphite upon cycling is definitely more stable than that of the disordered carbons.

Highly interesting is a comparison of the impedance behavior of these electrodes. Nyquist plots obtained with all four electrodes show a very similar, high frequency behavior: a semicircle which reflects Li-ion migration through the surface films, coupled with film and interfacial capacitances. It is very significant that the high frequency behavior of electrodes comprised of the disordered carbons depends slightly on the potential, and that of the Li-graphite electrodes depends pronouncedly on the electrode's potential. These differences definitely reflect different reversible structural changes as Li insertion-deinsertion proceeds.

The low frequency behavior of these electrodes, which basically constitutes straight lines of -Z'' vs. Z', whose slopes increase as the frequency decreases, reflects pronounced differences in the kinetics of Li insertion into the 4 carbons studied. The impedance spectra of the Li-graphite and Li-nanotube electrodes clearly reflect solid state diffusion of Li ions into the carbon bulk, ('Warburg'-type elements). The impedance behavior of the disordered carbon electrodes seems to indicate that Li is not intercalated into them, but rather inserted in chemisorption-type processes.

Acknowledgment

This work was supported by NEDO Japan.

References

1. A. Claye and J.E. Fischer, *Mol. Cryst. Liq. Cryst.* (2000). In press.
2. D. Aurbach, B. Markovsky, I. Weissman, E. Levi, and Y. Ein-Eli, *Electrochimica Acta* 45, 67 (1999) and references therein.
3. A.G. Rinzler, J. Liu, P. Nikolaev, C.B. Huffman, F.J. Rodriguez-Macias, P.J. Boul, A.H. Lu, D. Heymann, D.T. Colbert, R.S. Lee, J.E. Fischer, A.M. Rao, P.C. Eklund and R.E. Smalley, *Applied Physics A* (bif 67), 29 (1998).
4. A. Claye and J.E. Fischer, *Electrochimica Acta* 45, 107 (1999) and references therein.

A Comparison Between the Electrochemical Behavior of Reversible Magnesium and Lithium Electrodes

D. Aurbach, Y. Gofer, A. Schechter,^{*} O. Chusid, H. Gizbar, Y. Cohen, M. Moshkovich and R. Turgeman

Department of Chemistry, Bar-Ilan University
Ramat-Gan 52900, Israel

a. Dept. of Chemical Engineering, Case Western Reserve University, Cleveland OH 44106, USA

Introduction

In a similar manner to lithium, magnesium is usually covered by surface films.⁽¹⁾ However, in contrast to the case of lithium, the surface films which cover Mg electrodes in a large variety of non-aqueous systems (e.g. solutions based on alkyl carbonates, esters, acetonitrile, and other polar solvents) can not conduct the bivalent Mg^{++} ions. It is well known that Mg electrodes may behave reversibly in Grignard salt solutions in ethers ($RMgX$; R = alkyl, aryl, X = Cl, Br).⁽²⁾ In addition, there was a report on the reversible behavior of Mg electrodes in THF/ $Mg(BR_4)_2$ solutions (R = alkyl, aryl groups).⁽³⁾ The present work is aimed at a rigorous study of Mg electrodes in solutions in which reversible deposition-dissolution of magnesium can be obtained. The study benefited from the use of a variety of *in situ* spectroelectrochemical techniques, including FTIR, EIS, STM and EQCM, and *ex situ* surface sensitive tools such as SEM, EDAX and XPS in conjunction with electrochemical techniques.

Experimental

The use of EQCM, FTIR, EIS, electrode preparation, and the configuration of the electrochemical cells, as well as other details on the experimental set-up, has already been reported.^(1,4) The application of *in situ* STM to highly reactive electrochemical systems is described in ref. 5. Grignard salts were purchased from Aldrich and $Mg(BR_4)_2$ were prepared as described in ref. 3.

Results and discussion

In addition to Grignard salts ($RMgX$)⁽²⁾ and $Mg(BR_4)_2$ ⁽³⁾ we also studied solutions of new electrolytes that we developed with the general structure of $Mg(AX_{4-n}R^n)_2$ where $A=Al$ or B , $X=Cl$ or Br , R =various alkyl or aryl groups, and $0 \leq n \leq 4$; $n^+ + n^- = n$. Relevant solvents are cyclic ethers such as THF and polyethers from the 'glyme' family. Magnesium deposition and dissolution processes are reversible in the three classes of electrolyte solutions, namely, the Grignard salts, borates and aluminates. However, the electrochemical window of the $RMgX$ /ether solutions is around 1.2 V (i.e. the salt is oxidized at this potential). The electrochemical windows with the Mg borates and aluminates are 1.8 V and up to 2.5 V, respectively. Hence, the latter ones can be used as electrolytes in rechargeable Mg batteries. In all three types of electrolyte solutions, magnesium electrodes are not covered by passivating, stable surface films. This was evident from *in situ* FTIR, STM and EQCM measurements. Hence, reversible Mg deposition-dissolution is possible due to the development of film free conditions on the Mg surfaces. It should be mentioned that if passivating surface films covered the Mg surfaces, it would be impossible to obtain the high resolution STM images that could be seen. However, Mg deposition is not a simple process of the Mg/Mg^{++} red-ox couple.

In a separate study, we accumulated evidence that highly complicated structures are formed in these solutions, which involve the formation of cationic complexes comprised of Mg halide ions and solvent molecules, whose counter ions are halides, alkyl anions and/or organoborate and organo aluminate anions. The Mg deposition-dissolution processed are accompanied by adsorption processes that lead to a high impedance that Mg electrodes develop during storage at

OCV. However, as Mg deposition-dissolution proceeds, the electrode impedance drops due to the dynamics of these processes, which interfere with the stability of the adsorbed species on the Mg surfaces (which cause the high impedance developed with Mg electrodes at rest).

Hence, we see a pronounced difference in the behavior of reversible Li and Mg electrodes. In the former case, stable, passivating films protect the active metal from reactions with solution species and hence, the electrochemical processes occur by migration of Li-ions through the surface films.

In the case of Mg electrodes, a condition for reversibility is inertness with solution species, and hence, the absence of passivation phenomena. It should be mentioned that cycling efficiency close to 100% could be obtained with magnesium electrodes during hundreds of charge-discharge cycles in selected electrolyte solutions comprising ethers and Mg aluminate salts.

Acknowledgment

This work was partially supported by the BMBF, the German Ministry of Science within the framework of the DIP program, and by the Israeli Ministry of Science.

References

1. M. Moshkovich and D. Aurbach, *J. Electroanal. Chem.* 466, 2203 (1999).
2. C. Liebenow, *J. Appl. Chem.* 27, 221 (1997).
3. T. Gregory, R. Hoffman and R. Winterton, *J. Electrochem. Soc.* 137, 3 (1990).
4. D. Aurbach, M. Moshkovich, A. Schechter and R. Turgeman, *Electrochemical and Solid State Letters* 3, 31 (2000).
5. D. Aurbach and Y. Cohen, *Rev. Sci. Instrum.* 70, 4668 (1999).

Novel SnS_2 Anode for Rechargeable Lithium Battery

Toshiyuki Momma, Nobuhiro Shiraishi and Tetsuya Osaka

Kagami Memorial Lab. for Materials Science and Technology; School of Science and Engineering, Waseda University
Shinjyuku, Tokyo 169-8555, JapanAharon Gedanken, Junjie Zhu and Lena Sominski
Department of Chemistry, Bar-Ilan University
Ramat Gan 52900, Israel

In recent years, Li-Sn alloy compounds have attracted many researchers in the sense of application to the anode material of rechargeable lithium battery. SnO_2 was attempted to create the Li-Sn alloy by electrochemical reducing. In order to use the Li-Sn alloy for the anode of rechargeable Li battery, some other Sn compounds can be the starting material for Li-Sn alloy. In this study we have examined the possibility of using SnS_2 as a starting material for the lithium battery anode.

The amorphous SnS_2 powder was made as follows. The aqueous solution of $\text{SnCl}_4 \cdot 5\text{H}_2\text{O}$ and thioacetamide was sonicated for 30 minutes at room temperature under air. The amorphous SnS_2 was obtained as a precipitate. Part of resulting amorphous SnS_2 was sintered at 400°C to convert to the crystalline SnS_2 .

The SnS_2 powder was mixed with poly(vinylidene fluoride hexafluoropropylene) (PVdF-HFP) (10 wt. %) and carbon powder (10 wt. %) in THF solvent. The mixture was casted onto the Ni form and dried. The resulting electrode was pressed and used for the electrochemical tests.

Figure 1 shows the cyclic voltammograms for the SnS_2 electrodes. At the first potential sweeping towards the anodic direction of voltammetry, a large cathodic current was observed around 0.9 V vs. Li/Li^+ , while in the subsequent potential cycling no more large cathodic current was detected around 1 V vs. Li/Li^+ . There appear redox peak couple at 0.1 V vs. Li/Li^+ in the cathodic scan and at 0.3 V vs. Li/Li^+ in the anodic scan for all the cycling. From these results, the large cathodic irreversible current was supposed to exhibit the formation of Sn metal particle from the SnS_2 powder with the Li_2S formation. And the redox couple will be the charge discharge reaction of Li with Sn particle.

Figure 2 shows the potential curve of SnS_2 electrode. The first cycling of both electrodes exhibits enormous irreversible capacitance. That indicates the formation of Sn particle from the SnS_2 powder similar with the SnO_2 electrode. During the subsequent cycling, the electrode was charged in the potential range of $0.5 - 0\text{ V vs. Li/Li}^+$ and discharged in the potential range of $0.5 - 0.7\text{ V vs. Li/Li}^+$. The discharge capacity and coulombic efficiency for these electrodes are shown in Fig. 3. Comparing the capacity of SnS_2 electrodes, it is clear that the crystalline SnS_2 has larger capacity as the rechargeable lithium battery anode. The initial capacity of crystalline SnS_2 shows above 600 mAh g^{-1} , and decreases gradually to 400 mAh g^{-1} , while the capacity of amorphous SnS_2 decreases from 300 to 200 mAh g^{-1} . The value of coulombic efficiency shows same tendency. In the initial cycling, the efficiency was less than 50% and showed sudden jumping to 80% in the second cycling. After the third cycling, the efficiency was kept at the value of about $90 - 95\%$. These results indicate that the conversion of SnS_2 into Sn metal or Sn-Li alloy was taken place in the initial

cycle and completed after a few cycling. Almost the same amount of charge was stored in the resulting metal compound in subsequent charge-discharge cycling as the charge of conversion. These results exhibit a good agreement with the results obtained from the cyclic voltammetry.

In conclusion, amorphous SnS_2 and crystalline SnS_2 were studied in order to apply as the novel anode material to rechargeable lithium battery. The crystalline SnS_2 showed a high capacity as the anode with the value of 600 mAh g^{-1} at the initial stage. The amorphous SnS_2 had the capacity of about 300 mAh g^{-1} . The crystalline SnS_2 was revealed as a promising candidate for the rechargeable lithium battery anode.

This study was financially supported in part by NEDO International Joint Research Grant.

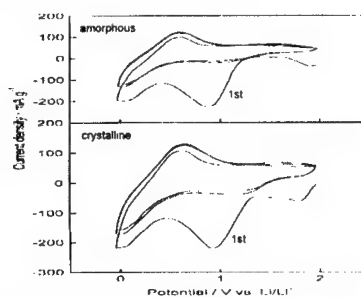


Fig. 1 Cyclic voltammograms for amorphous or crystalline SnS_2 electrodes obtained at 0.1 mV s^{-1} in $1.0\text{ M LiClO}_4/(\text{EC}:\text{PC}=1:1)$ electrolyte solution

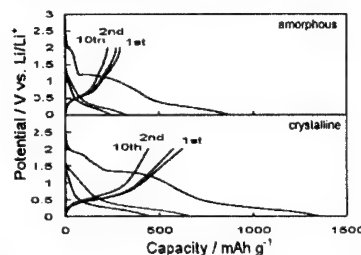


Fig. 2 Charge and discharge curves for SnS_2 electrode in $1.0\text{ M LiClO}_4/(\text{EC}:\text{PC}=1:1)$ under constant current density of 50 mA g^{-1} . The operated potential range was $0 - 2\text{ V vs. Li/Li}^+$.

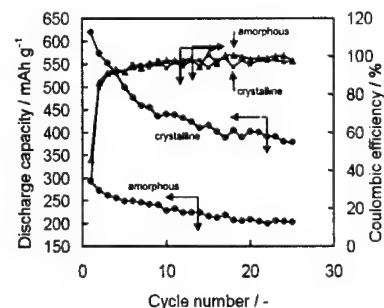


Fig. 3 Cycling performance of SnS_2 in $1.0\text{ M LiClO}_4/(\text{EC}:\text{PC}=1:1)$ under constant current density of 50 mA g^{-1} . The operated potential range was $0 - 2\text{ V vs. Li/Li}^+$.

The Effects of Electrolyte Composition on the Electrochemical Behavior of Li-Alloy Electrode.

G.J. Jeong^a, Y.-J. Kim^c, H. Kim^a, H.-J. Sohn^b, T.Kang^b^aDepartment of Mineral and Petroleum Engineering, Seoul National University, Seoul 151-742, Korea^bSchool of Materials Science and Engineering, Seoul National University, Seoul 151-742, Korea^cInstitute of Advanced Material Study, Kyushu University, Kasuga 816-8580, Japan

Introduction

Although the basic features of battery performance (operating voltage, energy density, etc.) are essentially determined by the active materials used as the cathode and anode, the chemistry of electrolyte often affects battery performance significantly. Up to now, much attention has been focused on the effects of electrolyte composition on the charge/discharge characteristics of various carbonaceous anode materials. PC(propylene carbonate)-based electrolyte tend to decompose electrochemically on the highly graphitized carbon anodes during the charging process, so the more stable EC(ethylene carbonate)-based electrolytes are used in lithium-ion batteries. In this study, we investigated the effects of the electrolyte composition on the charge/discharge characteristics of Sn electrodes during Li insertion/removal.

Experimental

The electrode materials used in this study were Sn(99.8%, -325mesh, Aldrich) and Al(99.9%, ca. 20 μ m, Kojundo). The electrodes were prepared by coating slurries (active material powders (80wt%), carbon black(10wt%) and PVDF(10wt%) dissolved in NMP) on a Cu foil substrate. Coin-type test cells were assembled in an argon-filled glove box using a Celgard 2400 as a separator and Li foil as counter electrodes. The tested electrolytes were 1 M LiPF₆, EC/DEC(1:1), 1 M LiClO₄, PC/DME(1:1) and 1 M LiPF₆, PC/DME(1:1). The charge-discharge experiments were performed galvanostatically within a fixed voltage window.

Results and Discussion

Figure 1 shows the the voltage profile of Sn electrode for the first cycle in 1 M LiPF₆, EC/DEC (1:1) with constant current density of 30 mA/g. As shown in Figure 1, the first voltage plateau was observed at about 1.5 V (vs. Li/Li⁺). Because first voltage plateau of Li-Sn alloying reaction was reported at 0.8 V (vs. Li/Li⁺), it is difficult that the plateau observed at 1.5 V was assigned as Li-Sn alloying reaction. This voltage plateau was probably due to the electrolyte decomposition. It is noteworthy that the charge and discharge capacity of the first cycle were smaller than the value normally reported. On the other hand, voltage plateau above mentioned could be not observed in the case of Al electrode under same condition. (Figure 2). It indicates that electrolyte decomposition reaction on the metal electrode does not always occur. Figure 3 illustrates the voltage profile of Sn electrode for the first cycle under same condition with higher reaction rate (100 mA/g). It was found that higher reaction rate prevented from side reaction and charge-discharge value reached the value generally reported. Figure 4 shows the voltage profile of the Sn electrode for the first cycle in 1 M LiPF₆, PC/DME (1:1) with constant current density of 30 mA/g. The voltage profile

above mentioned was not observed at all in PC-based electrolyte. As a result, it was found that the electrochemical characteristics of Sn metal electrode were depended upon kinds of solvent in the electrolyte. In particular, side reaction was occurred significantly in EC-based electrolyte.

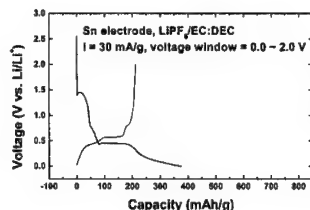


Figure 1. The Voltage profile for the first cycle of the Sn metal electrode.(LiPF₆, EC/DEC(1:1), 30 mA/g)

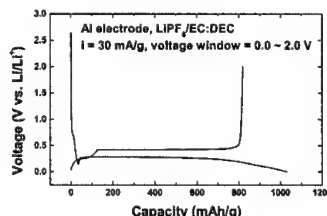


Figure 2. The Voltage profile for the first cycle of the Al metal electrode.(LiPF₆, EC/DEC(1:1), 30 mA/g)

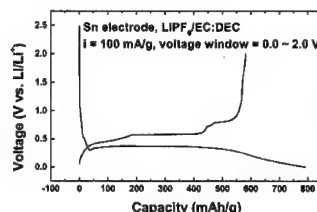


Figure 3. The Voltage profile for the first cycle of the Sn metal electrode.(LiPF₆, EC/DEC(1:1), 100 mA/g)

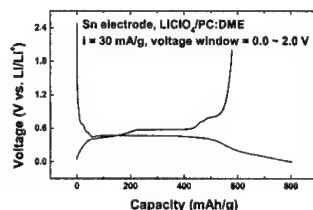


Figure 4. The Voltage profile for the first cycle of the Sn metal electrode.(LiClO₄, PC/DME(1:1), 30 mA/g)

Amorphous Sn-Ca Alloy as Lithium Ion Battery Anode

L.Fang¹ and B.V.R.Chowdari^{1,2}

¹ Institute of Materials Research and Engineering, Singapore 117602.

² Physics Department, National University of Singapore, Singapore 119260.

ABSTRACT

The announcement of new generation of lithium ion battery based upon the use of the amorphous tin based composite oxide (TCO) by Fujifilm Celltec Co.^[1] arose significant interest in amorphous alloys as anode materials. In TCO, tin oxide is converted to a lithium-tin alloy during cycling process and only the tin alloy^[2] serves as the active media. Making use of amorphous alloy directly may have some advantages over the tin oxide composite. In present work, Sn-Ca system was selected due to the fact that calcium has very high elastic modulus than other elements like Cu, Fe etc and it can absorb large mechanical strain and stress during the cycles of charge and discharge.

The amorphous Sn-Ca alloys were synthesized by reducing the SnCl_2 and CaCO_3 solution making use of NaBH_4 as the reducing agent. The amorphous state of the materials was confirmed by XRD and DSC techniques. Since the materials are synthesized by chemical route, the particles are homogeneous and their size is less than 100 nm. The amorphous state can be modified by using different synthesis conditions. DSC curves indicate that all amorphous materials exhibit endothermal transition in the range of 150 to 200 °C.

The capacity of the material is found to be 400 mAh/g and 62 % of it has been retained after 60 cycles (Fig.1). The ex-situ XRD technique was used to illustrate the progress of lithium intercalation. Cyclic voltammogram shows that two peaks located at 0.6 and 0.2 volt respectively correspond to the charge and discharge plateaus (Fig.2a). Fig.2b illustrates the first five cycle performance. The observation of voltage plateau at about 1.0 V confirms the formation of Solid Electrolyte Interphase (SEI) on the surface of the alloy anode.

REFERENCE

1. Y. Idota, T. Kubota, A. Matsufuji, Y. Maekawa and T. Miyasaka, Science, 276(1997)1395.
2. Binary alloy phase diagrams, Materials Park, Ohio : ASM International, 1996.

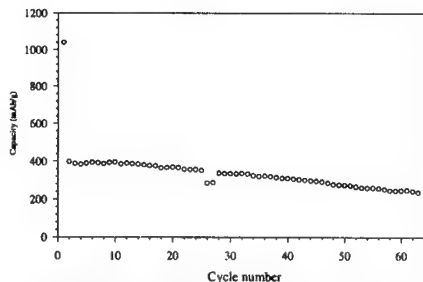
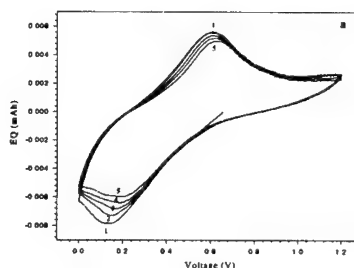


Fig.1 The capacity vs. cycle number of Li/Ca-Sn cells (1 mA/cm² and 0.0-1.1 V). (active material:super carbon:PVDF=80:5:15)



Influence of Edge and Basal Plane Sites on the Electrochemical Behavior of Flake-Like Natural Graphite for Li-Ion Batteries

K. Zaghib, G. Nadeau and K. Kinoshita*

Institut de Recherche d'Hydro-Québec, 1800 boul. Lionel-Boulet, Varennes, Québec, Canada, J3X 1S1

*Environmental Energy Technologies Division, Lawrence Berkeley National Laboratory, Berkeley, CA 94720 USA

Introduction

We have recently initiated studies to analyze the role of the edge and basal plane sites on the magnitude of the irreversible capacity loss (ICL) on natural graphite electrodes for Li-ion batteries. The aim of this effort is to develop a better understanding of the contribution of these two distinct surface sites to the ICL. To conduct this investigation, graphite particles that consist solely of edge and basal plane surface sites are desired. Unfortunately, this ideal structure is not available. As an alternative, flake-like graphite powders of varying average sizes were used to simulate the ideal graphite structure. In this paper we present the results of an analysis to illustrate the role of edge and basal plane sites on the electrochemical behavior of flake-like natural graphite. The electrochemical reactions involving the decomposition of nonaqueous electrolyte during the initial charge (intercalation) of carbon, which is associated with the ICL, was investigated

Experimental

Five samples of flake-like natural graphite powders were obtained from a commercial source. These samples have average dimensions of 2, 12, 20, 30 and 40 μm in the direction parallel to the basal plane, and it is these dimensions that are referred to as the average particle size. Scanning electron microscopy (SEM, Hitachi) was employed to determine the morphology and dimensions of the edge and basal plane. X-ray diffraction (XRD) analysis (Siemens D500 Diffractometer) was used to determine the d_{002} spacing and the crystallite size, L_c . The Brunauer-Emmett-Teller (BET) surface area was measured with a Quantachrome Autosorb automated gas sorption system using N_2 gas.

Electrochemical measurements of the charge/discharge of the natural graphite were conducted in an electrolyte containing 1 M LiClO_4 in 1:1 (volume ratio) ethylene carbonate (EC)-dimethyl carbonate (DMC) (Tomiyama Pure Chemical Industries Ltd). The working electrode was fabricated from a mixture of the natural graphite and poly(vinylidene fluoride) (PVDF) dissolved in 1-methyl-2-pyrrolidinone (NMP). The slurry was spread onto a copper grid and dried under vacuum at 95°C for 24 h. The working electrodes were evaluated in a three-electrode cell that contained metallic Li as both counter and reference electrodes. The cells were assembled in a glove box under an Ar atmosphere containing less than 5-ppm humidity. The natural graphite samples were cycled at a C/24 rate between 2.5 and 0 V vs Li/Li^+ with a MacPile II (Bio Logic, France).

Results

The surface area of the model structures was determined with the use of Eq :

$$S = 2(B + 2T) / \rho BT$$

where ρ is the density, B is the average particle size and T is the thickness of the edge plane. This value can be compared to the BET surface area, S_{BET} , which considers adsorption on essentially a smooth surface, and the BET surface area is used for the natural graphite samples. The ICL that was calculated for the model structures and the experimental data obtained for natural graphite is plotted in Fig. 1 as a function of surface area.

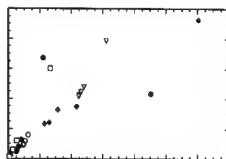
With the exception of the calculated ICL values for small particle size ($B < 5 \mu\text{m}$), the trend line shows a linear relationship between ICL and surface area. Closer inspection of the results indicates that differences exist in the slope of the data for the different flake and cube structures, indicating the contribution of the relative fraction of edge and basal

plane sites on the total ICL. The 2- μm flake has a proportionally higher fraction of edge sites than the other flake-like structures, and consequently its change in ICL with surface area is much greater. Based on the analysis of the two different prismatic structures, flake-like versus cube, the latter particle morphology appears to offer an advantage in electrochemical performance. That is, the cube structure has a lower ICL and higher CE than flake-like particles of comparable size.

Acknowledgment

The authors would like to acknowledge the support of HydroQuebec and the Assistant Secretary for Energy Efficiency and Renewable Energy, Office of Advanced Automotive Technologies of the U.S. Department of Energy under Contract No. DE-AC03-76SF00098 at Lawrence Berkeley National Laboratory.

Fig.1. Influence of surface area on ICL. Calculated values for flake-like and cube structures and experimental results obtained with natural graphite (NG). Line shows the trend of experimental data.



**Nanopartical size carbon
materials
for lithium-ion batteries**

**B. Banov, A. Momchilov, A.
Trifonova, B. Puresheva**

A. Kozawa

Central Laboratory of Electrochemical
Power Sources
Bulgarian Academy of Sciences, 1113
Sofia, BULGARIA

Recently a range of new carbons materials - Ultra Fin Carbon (UFC) and Graphite with nanopartical size appear on the battery marked as conductive additive for cathode application in both, aqueous and non aqueous medias. The use of UFC material as performing agent for aged Pb cells was demonstrated recently (Long Beach IBA Meeting 1997 and Marrakech IBA Meeting 1999). Having in mind that the UFC and nanopartical size Graphite are carbon materials we decide to test them also as hosting compounds for lithium ions in lithium - ion batteries.

The physicochemical parameters, as SSA, total pore volume, pore distribution, and the XRD analysis of this materials confirm our prediction that the characteristics of virgin material are very close to that of other carbon materials used as conductive binders or intercalating anodes in lithium ion cells. The UFC materials are available only as suspensions, aqueous or nonaqueous contrary to the nanopartical size graphite witch is powder. We have investigated and demonstrated that applying an appropriated technique it is possible to use aqueous and non aqueous suspensions or powder material as

conductive additives or active electrode materials in lithium cells. The electrochemical characteristics of thus investigated electrodes depend on the first lithiation, in the case of use of these materials as intercalating compounds (anodes), on the current density of intercalation deintercalation and the nature of the used electrolyte. A specific characteristics within 150-320 mAh/g at the 10th cycles are obtained in best conditions depending on UFC or Graphite samples at C/20, when the tested materials are used as anodes. An improvement of the cathode utilisation in the range of 7-15% is observed when the tested samples are used as conductive additives in the cathode mix.

Abstract No. 92

Study on $\text{Li}[\text{Li}_{1/3}\text{Ti}_{5/3}]\text{O}_4$ as Anode Material for Lithium Ion Batteries

M. Arrabito^a, S. Panero^b, P. Reale^b and B. Scrosati^b

^aPolytechnic of Turin, 10129 Turin, Italy

^bUniversity La Sapienza, 00185 Rome, Italy

Chemical and electrochemical studies have shown that various titanium oxides can incorporate lithium in different ratios. Other compounds with a spinel-type structure and corresponding to the spinel oxides LiTi_2O_4 and $\text{Li}_3\text{Ti}_5\text{O}_{12}$ have been evaluated in rechargeable lithium cells with promising features. One of the most attractive characteristics is the very constant potential of the materials during the electrochemical charge and discharge.

In this work the synthesis and the electrochemical characteristics of a mixed lithium spinel $\text{Li}[\text{Li}_{1/3}\text{Ti}_{5/3}]\text{O}_4$ obtained via a modified solid-state process are reported. According to the scanning electron microscopy of the $\text{Li}_3\text{Ti}_5\text{O}_{12}$ synthesized by this route, the particle sizes of the compound are less than $2\mu\text{m}$ (fig.1). The micron-sized material can reversibly insert 0.7-1 Li per mole and exhibits a capacity of $120\text{-}150\text{ mAhg}^{-1}$ after 100 cycles.

Lithium transport through $\text{Li}_3\text{Ti}_5\text{O}_{12}$ electrodes takes place in the coexistence of two phases, which are mutually interconvertible upon lithium exchange. The identification of the insertion mechanism is possible by the analysis of the impedance response of the electrodes during the electrochemical process.

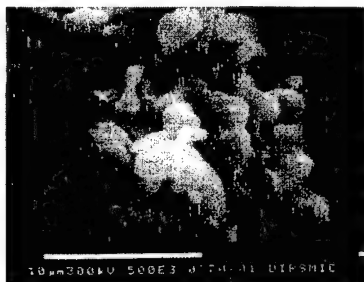


Fig.1. SEM micrographs for $\text{Li}_3\text{Ti}_5\text{O}_{12}$ powder

**In-situ TEM study of the interface
carbone/electrolyte**

M. Dollé, S. Grugeon, A. Cressent,

B. Beaudoin, L. Dupont, J.-M. Tarascon

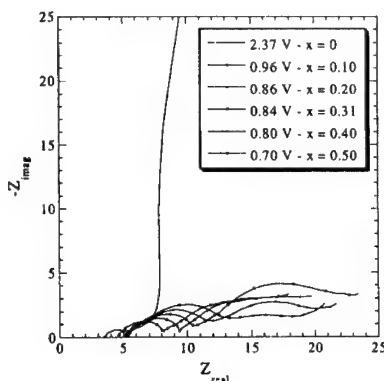
Laboratoire de Réactivité et de Chimie des Solides,

UPRES-A 6007, UPJV

33, rue Saint-Leu 80039 Amiens Cedex, France

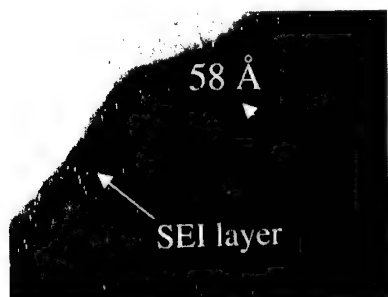
The recent development of the portable electronics market requires high energy density batteries. Li-ion batteries, which use carbon as negative electrode and lithium metal oxides as positive electrode, seem to be excellent candidates to make up for this need. It is known the carbons are covered during the first discharge by a passivating layer (SEI), which avoids the reduction of electrolyte. This film governs the electrochemical performances of this electrode (cycle life, reversible capacity, selfdischarge rate,...), hence the necessity to understand its growth mechanism. Since 20 years, numerous groups have been working on this topic using different electrolytes [1,2], but thickness, composition, density and nature are not yet unambiguously defined. The main reason being that most of studies were carried out under air, and it is well known that some compounds of the SEI are unstable in this atmosphere.

In order to study the carbone/electrolyte interface upon cycling, we performed electrochemical tests in Swagelok™ cells using different kinds of carbonaceous powders versus Li metal. The cells were stopped at different intercalation rates and the interface was observed by *in-situ* TEM (1), DSC and *in-situ* TF-IR. By *in-situ* TEM, we succeeded in visualizing the dual (organic and inorganic) nature of the passivating layer and the evolution of each of them upon high temperature cycling or storage performance. The evolution of this interface upon cycling was confirmed in 3-electrode cells by AC-impedance measurements (2). Finally, attempts to monitor the evolution of the organic part of the passivating layer upon various operating conditions by DSC and *in-situ* TF-IR will be shown. The results obtained by these four technics when performed in a water-free environment with samples never exposed to air provide very useful information regarding the SEI formation and more specifically its evolution with namely its ratio organic/inorganic parts. Findings turn out to be important with respect to the formation cycle in Li-ion cells.



(2) Impedance diagram of carbon SP according to intercalation rate

- [1] Young-Gyoon Ryu, Su-Il Pyun, J. of Electroanalytical Chemistry 433 (1997) 97
- [2] D. Aurbach, B. Markovsky, A. Shechter, Y. Ein-Eli, H. Cohen, J. Electrochem. Soc. 143 (1996) 3809



(1) Carbon SP at the end of first discharge at C/20

**THE ELECTROCHEMICAL
BEHAVIOUR AND
STRUCTURAL CHANGES OF
TIN-LEAD ANODES DURING Li
REVERSIBLE INSERTION**

A.Momchilov*, A.Trifonova*,
B.Banov*, B.Puresheva*,
I.Abrahams**

*Central Laboratory of
Electrochemical Power Sources,
"G. Bonchev" str., bl. 10, Sofia
1113, BULGARIA

*Queen Mary and Westfield
College, University of London, Mile
End Road, London E1 4NS, UK

The Sn based alloys and
intermetallic systems are attractive
materials as negative electrode in
lithium-ion batteries. The tin-lead
foil was investigated in the
electrochemical system

Li/1M LiPF₄ or 1M LiAsF₆
EC:DEC or DMC solution/Sn-Pb

as anode for Li-ion cell.

A destruction of the tin-lead foil
was established during the first
intercalation of the Li⁺ into the
structure. This process is illustrated
by the electron microscopic
pictures. The destruction is most
probably due to two facts. First one
is the changes in the host structure
during the first lithium insertion
which is established by X-ray
measurements. The changes
between the first and come after
semicycles in the curve shape of the

slow voltammetry measurements
also confirm these changes. The tin-
lead intermetallic compound was
electrochemically cycled in the
voltage range 10 mV - 900 mV at
different current densities. A large
irreversible capacity was
established between the first
intercalation and deintercalation.
This capacity is most probably due
to the forming of the passive film
on the forming particles during
destruction of the metal foil. A
reversible capacity of 600 mAh/g
was obtained from the investigated
materials during the cycling tests.

Aggregation and Li_2O Formation Reaction in Sn-Based Oxide Anodes

Young-Jun Kim^a, Hun-Joon Sohn^b, Tak Kang^b

^aDepartment of Mineral and Petroleum Engineering, Seoul National University, Seoul 151-742, Korea

^bSchool of Materials Science and Engineering, Seoul National University, Seoul 151-742, Korea

It is well known that Sn metal was formed via reconstruction reaction in tin-based oxide anodes [1]. During reconstruction reaction, they suggested that lithium ion reacted with oxygen, which resulted in Li_2O and Sn in the grains of pristine tin-based oxides. And sequentially, reversible reaction forming Li-Sn alloy compounds were proceeded to 0 V (vs. Li/Li^+).

Fuji Celltec[2] reported the good capacity retention material(ATCO) only under specific voltage range. Courtney and Dahn[3] has proposed that Sn metal aggregated to some dimension above 0.8 V during charge reaction in Sn-based oxide anodes based on the differential capacity plot. As can be seen in Fig. 1, we found the aggregates in SnO anode by SEM and analyzed the composition of aggregates (point A) and bottom (point B) by EDS simultaneously. In aggregates, the amount of Sn was larger than that of the matrix (bottom), but the oxygen content in point A was higher than expected because of surface contamination in spite of use of glove bag to transfer the sample into the chamber of instrument. Composition analysis was performed using Auger spectroscopy that provided the ion milling of surface. After ion milling, the ratio of Sn in aggregates increased from 47 % to about 70 %. And the main component in the bottom was oxygen that may be looks like "Lithia" proposed by Dahn[1]. The aggregates were found in 2nd discharge (lithium uptake) reaction, and the size of aggregates grew up upon cycling.

As shown in Fig. 2, the difference between 1st and 2nd cycle of the differential capacity plot of SnO_2 did not locate on specific potential but on all potential range during discharge. If Li_2O was formed initially near 0.9 V, the two curves are the same except the peak shown at 0.9 V. We calculated the difference of capacity between 1st and 2nd discharge reaction on the same potential, and converted it to the atomic ratio of Li/O . As a result, the atomic ratio was not 2 near 0.9 V, and when the reaction reached to 0 V, the atomic ratio was nearly 2 (Fig. 3). By Auger analysis, we compared the atomic ratio of Li/O in the sample using of Li_2O , which showed the similar trend with Fig. 3. From those results, we concluded that Li_2O formation was not completed in the initial stage of the reaction (0.9 V) and continued to 0 V during the first discharge reaction.

References

- [1] Ian A. Courtney and J. R. Dahn, *J. Electrochem. Soc.*, **144**(1997)2045
- [2] Y. Idota, T. Kubota, A. Matsufuji, Y. Mackawa, T. Miyasaka, *Science*, **276**(1997)1395
- [3] Ian A. Courtney and J. R. Dahn, *J. Electrochem. Soc.*, **144**(1997)2943

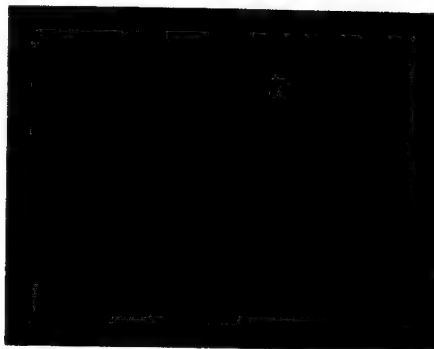


Fig. 1. SEM image of SnO electrode after 10 cycles between 0.5 and 1.5 V.

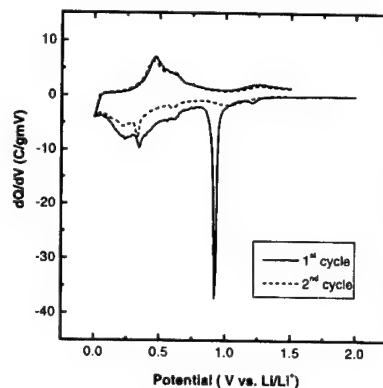


Fig. 2. Differential capacity plot of SnO_2 electrode.

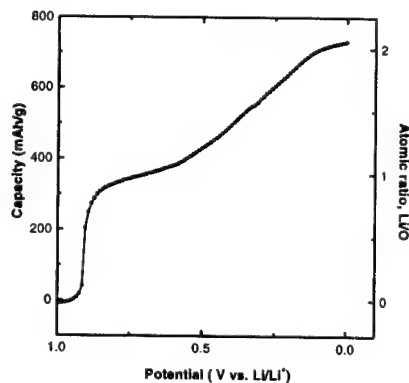


Fig. 3. Capacity difference between 1st and 2nd discharge reaction and the atomic ratio, Li/O in SnO_2 electrode.

Capacity Losses and Cycle Behaviors of Sn-Based Anodes

Young-Jun Kim^{a,*}, Hun-Joon Sohn^b, Tak Kang^b

^aDepartment of Mineral and Petroleum Engineering,
Seoul National University, Seoul 151-742, Korea

^bSchool of Materials Science and Engineering, Seoul
National University, Seoul 151-742, Korea

After the amorphous tin composite oxides (ATCO) had reported by Fuji Celltec[1], Sn-based anodes have attracted considerable attentions. Although the ability of the capacity retention was improved with ATCO, the development and commercialization are not realized yet using Sn-based oxide anodes, because of the irreversible capacity in the first cycle by reconstruction reaction. And Sn-based alloy compounds have the problems of low first cycle efficiency and poor cyclability. In this article, we investigated the reasons of the capacity losses and the problems of cycle behavior in Sn-based anodes.

In tin metal anodes, the first cycle efficiency is approximately 80 %. And the poor cyclability is due to the volume change, especially in low potential region. As shown in Fig. 1, even though the active materials were tin-based oxides, the capacity was decreased abruptly over the voltage range between 0 and 2 V vs. Li/Li^+ . This phenomenon was approximately in terms of the aggregation of Sn metal particles in pristine tin-based oxide materials[2]. When we tested the tin-based oxide anodes over the voltage range between 0.5 V and various upper voltages(1.0, 1.1, 1.2, ..., 2 V), the capacity was converged after a few cycles. The difference between the first cycle capacity and the converged one was close to the amount of the irreversible capacity of the first cycle in Sn metal. First of all, upon cycling, the aggregates grew up and the cycle characteristics of tin-based oxides resembled the tin metal anode. In addition, the crack was observed in aggregates by SEM in SnO electrode discharged to 0 V.

In SnO electrode, the capacity decreased gradually as the cycle went forward in spite of the selection of stable voltage window from 0.3 to 1.0 V in which aggregation reaction did not occur and volume change small. To find the factor that affecting the cyclability, we plotted the differential capacity loss curve by comparing the 2nd and 30th charge reaction (Fig. 2). The shape of the differential capacity loss curve was very similar with differential capacity plot, and this means the loss of active material from the test electrode. From the result of SEM observation, in active material, there were many cracks, so lithia did not act as a "pool" as mentioned in Ref[3]. Hence the small tin particles contained in lithia and some fractured active materials were released from the electrode during cycling. To confirm above result, we made the electrode with more binder(15 wt%), and that exhibited better cycle behaviors(Fig. 3).

References

- [1] Y. Idota, T. Kubota, A. Matsufuji, Y. Mackawa, T. Miyasaka, *Science*, **276**(1997)1395
- [2] Ian A. Courtney and J. R. Dahn, *J. Electrochem. Soc.*, **144**(1997)2943
- [3] Ian A. Courtney and J. R. Dahn, *J. Electrochem. Soc.*, **144**(1997)2045

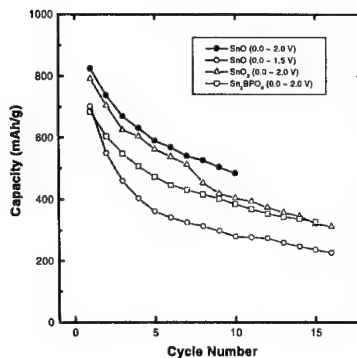


Fig. 1. Cycle characteristics of SnO, SnO₂ and Sn₂BPO₆.

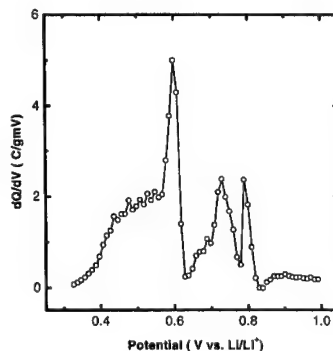


Fig. 2. Differential capacity loss curve between 2nd and 30th cycle charge reactions.

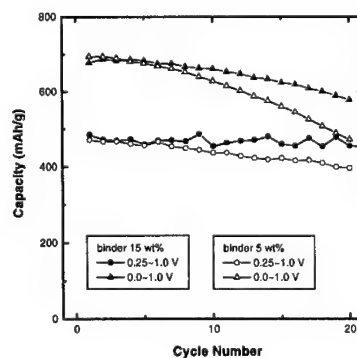


Fig. 3. Comparison of cycleability with the different content of binder.

Hard Carbon Prepared from Anthracite Coal for Lithium Ion Batteries

Isao Mochida, Cha-Hun Ku, Young-Jun Kim, Yozo Korai

Institute of Advanced Materials Study, Kyushu
University,
Kasuga, Fukuoka 816, Japan

Introduction

A number of carbon materials have been investigated to find the best performance as an anode for the lithium ion batteries. Non-graphitic carbons such as semi-coke and glass-like carbon are still targets to be studied to improve their anodic performance[1,2]. Coals of various ranks can provide a series of cokes, of which graphitic structure and properties vary continuously, reflecting their softening behavior[3]. Dahn et al.[4] have reported the anodic behavior of non-graphitic cokes derived from low rank coals. In this study, anthracite coal, which has the highest rank among the coals, was investigated for anodic performances of their cokes calcined at various temperatures. Non-graphitic nature and high density are expected with anthracite-derived carbon.

Experimental

Coal was carbonized in a Pyrex glass tube at 600°C for 1 hour under nitrogen flow at a heating rate of 1°C/min. The semi-coke thus prepared was further calcined at 1000-1800°C for 1 hour under Ar flow by a heating rate of 10°C/min. Test electrodes were fabricated by mixing active material with 5 wt% PTFE binder in mortar. The electrolyte used was 1M LiPF₆ dissolved in EC/DMC (1:1 in volume). The electrochemical performances were measured by constant current (25 mA/g) and constant voltage (0 V vs. Li/Li⁺) methods.

Results and discussions

Figure 1 illustrates XRD profiles of anthracite coke calcined at 1000 to 1800°C. The anthracite as-received showed a very broad peak at 22-28°. The heat treatment below 1200°C further broadened and shifted the peak to high. The heat treatment above 1600°C sharpened and intensified the peak very much, the progress of graphitization becoming very significant. Figure 2 shows the discharge voltage profiles of anthracite coal calcined at 1000, 1100, 1600, 1800°C. Coals calcined at 1000 and 1100°C exhibited a voltage plateau around 0.1 V during deinsertion of lithium, which is commonly observed with conventional hard carbons. The discharge capacities decreased as the progress of graphitization. The capacity of the cokes calcined at 1050 and 1150°C was found inferior to that at 1100°C. Hence, so far, the calcination at 1100°C provides the largest capacity, 270 mAh/g under 0.5 V and 340 mAh/g under 1.0 V (Figure 3).

Reference

- [1] K. Sato, M. Noguchi, A. Demachi, N. Oki and M. Endo, *Science*, 1994, **264**, 556
- [2] N. Sonobe, M. Ishikawa and T. Iwasaki, *The 35th Battery Symposium in Japan*, 1994, p.47
- [3] Y.C. Chang, H. J. Sohn, Y. Korai and I. Mochida, *Carbon*, 1998, **36**, 1653
- [4] Zheng, T., Xing, W. and Dahn, J. R., *Carbon*, 1996, **34**, 1501

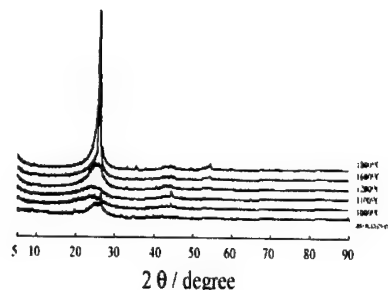


Figure 1. XRD patterns of carbon materials from anthracite.

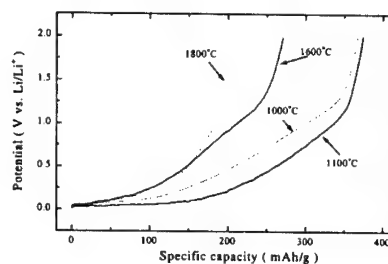


Figure 2. Discharge voltage profiles of carbon materials from anthracite. Heating rate : 10°C/min, holding time : 1h, constant current (25mA/g) +constant potential charge (0V, 40h) and constant current discharge (25mA/g).

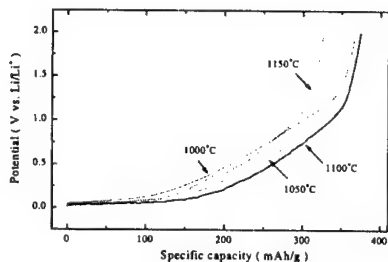


Figure 3. Discharge voltage profiles of hard carbons from anthracite calcined from 1050 to 1150°C. Heating rate : 10°C/min, holding time : 1h, constant current (25mA/g) +constant potential charge (0V, 40h) and constant current discharge (25mA/g).

Development and Manufacturing of the Lithium Sources and Novel Generation Electrode's Materials in Novosibirsk

V. Afanasjev, V. Rozhkov, A. Alexandrov, V. Moukhin, V. Mitkin *), V. Purgin, V. Sergeev, A. Gorev, M. Medjutov, V. Telezhkin, A. Enin, V. Yakimov, B. Antipenko, V. Ogarkov

Joint Stock Novosibirsk Chemical Concentrates Plant, 94, B. Khmel'nitsky str., Novosibirsk, 630110, RUSSIA

*) Institute of Inorganic Chemistry SB RAS, 3, Av. Lavrentjeva, Novosibirsk, 630090, RUSSIA

Base for competitive lithium chemical current source's (LCSC) issues by our Plant is the presence of own metal lithium and Li-Al alloys production and the development of effective electrode materials technology, mastering of complex assembly technologies and their patenting. The complex of these actions is carried out within the framework of the Interbranch Complex Scientific and Technical Program "Conversion". As a result of the spent developments the conventional technologies are mastered and created the perspective new classes of highly effective energyholders for LCSC based on various electrochemical systems. There is adjusted a necessary electrode materials for creation of modern production, and since 1992 the mass release of market production is begun. During the last decade the main attention was given to the coin LCSC release on the basis of the inexpensive electrochemical system "Li-MnO₂" in the field of production development and adaptation to internal Russian market.

The research and development activity (RD) in last ten year was devoted to the creation of novel generation of highly effective electrode materials and it's technologies. Taking into account the perspectives of porous carbon-containing material application in LSCS our efforts per 90 years the RD-complex was spent on the search and trials of effective electrode's composites for the primary and secondary cells with an achievable power density in a range of 1200-1500 Whr/kgs.

As a result of share actions the new families of carbon and fluorocarbon-containing Russian materials have been created including a novel superstoichiometric fluorocarbon material -FCM CF_{1.18-1.33} and a new carbon "chemical container" for reversible lithium intercalation. The latter material was developed by the way of graphite fluoroxide (FOG) study and creation, where FOG is a precursor for new carbon anodes design in the lithium ion rechargeable sources. Now this carbon material named as a thermal expanded graphite is patented and it has a specific surface ~200 m²/g.

At a results of research the processes proceeding in the electrochemical system "CF_{1+x} - Li" (δ=0.18-0.33), the interrelations between macro- (microstructure) and properties of FCM in lithium LCSC are established and the novel generation of the high-energy FCM cathodic composites with specific capacity up to 620 Ahr/kgs (1500 Whr/kgs) ensuring possibility of continuous cathodes load at current densities of bit up to 1.5 mA/cm² is developed. Their advantages are demonstrated by tables 1 and 2, in which the discharge data of new FCM cathodes in lithium

various typesize cells are adduced. The high electrical characteristics achieved in pilot series BR2325, CBR2325, BR6P and BR6C, are supplied with use FCM of a brand FS, and also new porous-forming additive - FOG. Thus in all cases a standard 1M LiClO₄ in the PC+DME was used.

There are developed a technical specifications for FCMs of brands FS and FT - TU 349735-0003-0353944-97, the hygienic certificates are authorized and the full complex of a control techniques for all required physical-chemical parameters is created. Thus the properties of FCMs of a type FS and FT on all parameters set appreciably exceed known for FCM, released by Japanese and American corporations (Daykin Industry - Japan, Allied Signal - USA). There are developed and authorized the technical specifications on the fluorocarbon cathodic composite (FUKM) TT 349735-0005-0353944-99 and consumer specification to market coin cell BR2325.

Table 1.
Results of discharge tests of 3 Volt cathodic materials in cylindrical lithium cells R6 and related types

Type size	O.C.V., Volts	Load current, mA	Average voltage, Volts	Typical electrical capacity, mAhour	Cathode efficiency, %
CR6C	3.25-3.38	10-50	2.58	1.4-1.8	98
CR6P	3.25-3.38	75-150	2.45	0.8-1.20	82-92
1/3CR6P	3.25-3.38	5-25	2.42	0.3-0.32	80-88
2/3CR6C	3.25-3.38	5-25	2.42	1.1-1.25	80-88
1/2CR6C	3.25-3.38	5-25	2.42	0.7-0.9	80-88
BR6C	3.03-3.25	1-5	2.54	1.8-2.45	92-98
BR6P	3.03-3.25	50-200	2.32	1.8-2.00	78-87

Table 2.
Results of the discharge tests of 3 Volt cathodic materials in coin lithium cells

Type size	Nominal current, iA	Maximal current, iA	Average voltage in discharge, Volts	Typical electrical capacity, mAhours	Year of R&D or industrial issue
CR2325	0.1	5-10	2.80	140-160	1988
BR2325	0.1	1.0	2.62	200-220	1993*)
CBR2325	0.1	5.0	2.80	200-220	1996
CR2032	0.1	5.0	2.80	160-170	1996
BR2032	0.1	1.0	2.62	190-200	1998*)
CR2025	0.1	5.0	2.80	120-130	1996
BR2025	0.1	1.0	2.62	150-160	1998*)
CR2016	0.1	0.5	2.77	65	1995*)
BR2016	0.1	0.5	2.5-2.7	95	1995*)
CR1616	0.1	0.5	2.75	40	1995*)
BR1616	0.1	0.5	2.5-2.7	46	1995*)

Note: *) - Experimental series

Aluminum Negative Electrode in Lithium Ion Batteries

Y. Hamon, T. Brousse, F. Jousse*, P. Topart*, P. Buvat* and
D.M. Schleich

Laboratoire de Génie des Matériaux
Ecole Polytechnique de l'Université de Nantes
La Chantrerie, rue Christian Pauc, BP50609
F44306 Nantes Cedex 3 – France

*CEA/DMAT/CMF
Centre du Ripault - BP16
F37260 Monts - France

Recently, tin has been proposed as a good candidate to replace graphite as a negative electrode for lithium ion cells [1]. The main advantage of tin compared to standard graphite is its high mass and volume capacities, respectively 994 mAh/g and 7254 mAh/cm³. Not only tin is able to form alloys with lithium. Bi, Si or Al for example can also react with lithium to form intermetallic compounds [2]. A first sight to the Al-Li binary diagram indicates that the aluminum-lithium richest alloy is Al₄Li₉. Therefore, the maximum theoretical lithium uptake for an aluminum electrode will be 2.25 Li for each Al atom. This value is below the 4.4 Li for each Sn atom observed in the Li₂₂Sn₅ alloy. However, due to its low atomic weight compared to tin, aluminum can present a mass capacity of 2234 mAh/g if the Al₄Li₉ alloy is reached, which is more than twice the theoretical capacity of metallic tin.

The use of an aluminum electrode in a lithium ion cell has been investigated in this study. In order to avoid the contribution of binder or conductive additive in the electrochemical tests, we have focused our interest on aluminum thin films. Layers ranging from 0.1 μm to 1 μm have been deposited by thermal evaporation of aluminum granules on copper substrates. All the samples are well crystallized according to the X-ray diffraction patterns. XPS analysis systematically indicate the presence of an oxidized layer on the surface of the films.

For the electrochemical tests, both potentiostatic and galvanostatic, the films have been used "as-deposited", i.e. without the use of any binder neither conductive additive. All the samples have been cycled versus a metallic lithium electrode in LiPF₆ in EC:DMC electrolyte between 1.2V and 10mV versus lithium. The cycling rate was 10mV/2min for the cyclic voltammetry experiments and C/4 rate for the galvanostatic experiments.

The electrochemical activity of aluminum is clearly evidenced on the cyclic voltamogram (figure 1) where sharp peaks are observed both during the charge and the discharge. On figure 2, it can be seen that the charge mainly consists in three regions : the initial lithium "insertion" between 2V and 0.26V, followed by a wide plateau 0.26V, and a final "insertion" occurring between 0.26 and 0.01V. The lithium uptake on the first voltage region is related to the presence of an oxidized layer of on the top of the aluminum thin films. The two last regions (between 0.26V and 0.01V) are probably due to the formation of Li-Al alloys.

The charge and discharge capacities are summarized in table 1. The capacities are high but never reach the value expected for the formation of the Al₄Li₉ alloy. The observations by scanning electron microscopy reveal microcracks in all the samples after one complete

cycle. However the surface of the thinnest sample seems less damaged than the 0.3 μm and 1 μm layers. Subsequently, it is not surprising that the highest capacity is measured for the 0.1 μm sample. Furthermore, this sample presents the best discharge to charge ratio (table 1) and exhibits the lowest capacity fade upon cycling.

It is difficult to exactly assume which alloy forms during the charge since the (111) aluminum peak on the XRD patterns of the as-deposited samples is no longer observed in the fully charged state. This suggests that the structure of aluminum is destroyed when lithium is inserted in the thin films electrodes, leading to an amorphous compound.

Even if the reaction mechanisms of lithium "insertion" in the aluminum thin film electrodes are still unclear, this study highlights the promising performances of this material as a negative electrode in lithium ion cells.

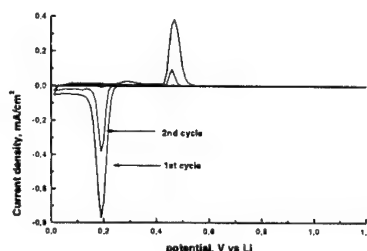


Figure 1 : typical cyclic voltamogram of an aluminum thin film (0.3 μm)

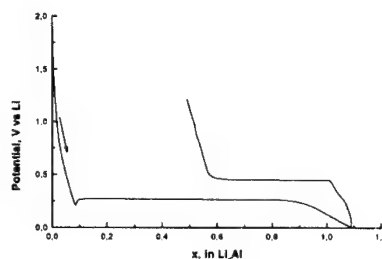


Figure 2 : typical galvanostatic plot of an aluminum thin film (0.3 μm, C/4 rate).

Thickness	Q _{charge} (mAh/g)	Q _{discharge} (mAh/g)	Q _{discharge} / Q _{charge}
0.1 μm	1390	800	58 %
0.3 μm	1090	610	56 %
1 μm	960	420	44 %

Table 1 : first charge and discharge capacities of aluminum thin films

[1] see for example J. Yang, M. Winter and J.O. Besenhard, Solid State Ionics **90**, 281 (1996).

[2] see for example S. Bourderau, T. Brousse and D.M. Schleich, Journal of Power **81-82**, 233 (1999).

Influence of Particle Size and Matrix in « Metal » Anodes for Li-ion Cells

O. Crosnier, X. Devaux*, T. Brousse, P. Fragnaud,
and D.M. Schleich

Laboratoire de Génie des Matériaux
Ecole Polytechnique de l'Université de Nantes
La Chantrerie, rue Christian Pauc, BP50609
F44306 Nantes Cedex 3 – France

* Laboratoire de Physique des Matériaux,
UMR CNRS 7556, Ecole des Mines,
Parc de Saurupt
F-54042 Nancy Cedex – France

Different metals and alloys have been recently investigated as possible anodes for lithium ion batteries [1]. The main advantage of these compounds is the huge mass and/or volume capacity compared to standard carbonaceous anodes. However, their main drawback is the impressive volume changes of the compounds upon cycling, which leads to the mechanical disintegration of the electrodes [2], and subsequently to a drastic capacity fade. In order to improve this cycling ability of metals and alloys, several studies have aimed at the improvement of both the microstructure of the materials and the matrix designed with a binder and a conductive additive. Bismuth has been chosen as a "model" metal to investigate the influence of particle size on the electrochemical performances of the bismuth electrodes. The second part of the study deals with the optimization of matrix composition, i.e. the influence of the respective percentages of active material, binder and conductive additive on the cycling properties of the electrode.

Electrodes films have been prepared by using a slurry technique involving a mixture of bismuth powder : carbon black : PVDF in a 85:10:5 weight ratio in n-methyl-2-pyrrolidinone. This slurry was coated on Cu foil. The bismuth powder was either commercially available material sieved down to 40µm and submicronic powder prepared by arc plasma processing. In this last technique, a bismuth ingot was set in a DC arc discharge under argon atmosphere at reduced pressure ($2.7 \cdot 10^{-7}$ Pa) [3]. The ingot was set down in a conical graphite crucible at the anode. The material was vaporized and carried out by a gas flow. Finally, it was trapped on a membrane filter. The bismuth powder was collected and stored in a glove box under high purity argon atmosphere.

Figure 1 shows the typical cyclic voltammogram of a bismuth electrode made with the ultrafine powder. The interesting point is the relatively "high" potential of Li-Bi alloys formation (0.8V to 0.6V) which prevents the carbon black from being electrochemically active versus lithium in this potential window.

The galvanostatic tests were performed between 1,2V and 0,5V (figure 2). Based upon the total amount of electrode material and the measured capacity, the calculation of lithium "inserted" during the charge process reveal that for the ultrafine powder, the alloy formed has the composition Li_3Bi . However, when the material with particle size in the range of 40µm is dispersed in the same matrix as for the ultrafine powder, the calculation indicates that only a small percentage of bismuth has reacted with lithium to form the alloys. Observations by scanning electron microscopy show in both cases

(ultrafine and 40µm powders) microcracks all over the electrodes.

The poor electrochemical performances of the large bismuth particles upon cycling led us to focus the study of the matrix influence with the ultrafine powder. In this case, the amount of bismuth in the electrode was varied from 85% to 6%. The cycling performances are greatly enhanced when the amount of active material is decreased.

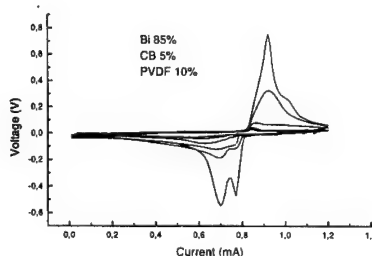


Figure 1 : typical slow scan voltammogram of a bismuth electrode

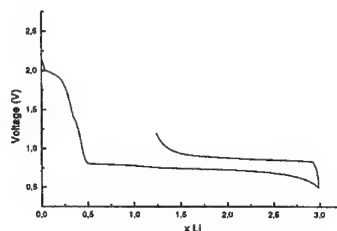


Figure 2 : galvanostatic cycle of the same bismuth electrode
(first discharge in 7 hours)

[1] see for example O. Mao, R.A. Dunlap and J.R. Dahn, J. Electrochem.Soc. 146, 405 (1999)

[2] see for example J. Yang, M. Winter and J.O. Besenhard, Solid State Ionics 90, 281 (1996).

[3] see for example F.Brochin, X.Devaux, J.Ghanbaja and H.Scherrer, Nanostruct. Mater., 11, 1 (1999)

Mechanically Alloyed Sn-V Powders as Anode Materials for Lithium-ion Batteries

Yongyao Xia^a, Tetsuo Sakai^a, Takuya Fujieda^a, Kuniaki Tatsumi^a, Seiji Sakura^b, and Akio Kawabata^b

^aBattery Section, Osaka National Research Institute, 1-8-31 Midorigaoka, Ikeda, Osaka 563-8577, Japan

^b•• Ako Laboratory, Taiyokoko Co., Ltd. 1603-1, Higashioki, Nakahiro, Hyogo 678-0232, Japan

•• Lithium-ion batteries based on a carbon/graphite anode and a transition metal oxide cathode have been commercially used in popular portable devices such as cellular phones and notebook PCs for about ten years. One of the next interesting and challenge steps is to develop increased capacity electrode materials for such type batteries in order to increase the energy density, including cathode and anode. The conventional anode material, graphite has a theoretical maximum capacity of 372 mAh/g, or a volumetric capacity of 840 Ah/L. Some low temperature heat-treated soft and hard carbons show capacity as large as 700 mAh/g, however, the volumetric capacity is still limited. Metals and alloys can be used as anode for lithium batteries, and have almost double volumetric capacity of these carbons, e.g., Sn yields a maximum theoretical capacity of 990 mAh/g or 7200 Ah/L. One major problem preventing them from practical use in Li-ion batteries is that alloy anodes undergo a significant volume change during cycling, which cause rapid cracking and crumbling of the metallic host and subsequent decline of battery performance. Approach for overcoming these problems is to introduce a matrix-glue to hold the particle together. One of the successful examples is the intermetallic compound Sn_xFe and Cu_6Sn_5 (SnM). These intermetallic alloys show improved reversible cycling behavior compared to pure Sn. However, for these intermetallic alloys, a displacement reaction occurs in which the intermetallic structure is broken down to form Li_xSn alloy and inactive metal Me when cycled with deep charge/discharge depth, and agglomeration of the inactive phase (M') into larger grains is responsible for the capacity decline upon cycling. These exciting works give an important information: Cycling behavior of the alloy is most likely dependent on the nature of introduced inactive metal (M').

With this in mind, we prepared Sn-V alloys by mechanically milling because metal vanadium has high

ductility and V-based hydrogen storage alloy has less decrepitation property. Our initial data provide exciting results that Sn-V alloys show excellent cycle behavior. Fig. 1 shows the first several cycles' charge/discharge curves of Li/Sn-V alloy compared to pure Sn. Fig. 2 gives rechargeable capacity vs. cycle number. Sn-V alloy delivers a rechargeable capacity of ca 450 mAh/g over 20 cycles when cycled between 0 and 0.8 V.

References:

1. O. Mao et al., *J. Electrochem. Soc.*, 145, 4195 (1998).
2. K. D. Kepler et al., *Electrochemical and Solid-State Letter*, 2, 307 (1999).

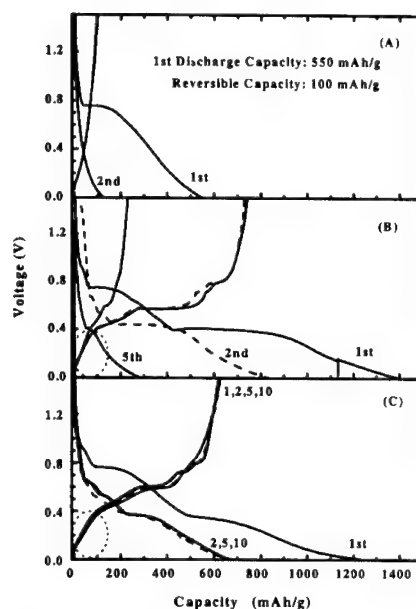
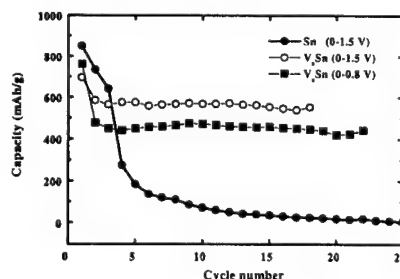


Fig. 1 Charge/discharge curves of Li/Sn alloy cell (A) TAB, (B) Sn, and (C) Sn-V



••• Fig. 2 Cycling behavior of Li/Sn-V alloy cell

TPD/GC-MS analysis of Solid Electrolyte Interface in Propylene Carbonate/Ethylene Sulfite Electrolyte on Graphite Anode for Lithium Batteries

Hitoshi Ota¹, Tomohiro Sato², Hitoshi Suzuki²
and Takao Usami¹

¹ Tsukuba Laboratory, Center for Analytical Chemistry and Science, Inc. (CACs), 8-3-1 Chu-o, Ami, Inashiki, Ibaraki 300-0332, Japan

² Tsukuba Research Center, Mitsubishi Chemical Corporation, 8-3-1 Chu-o, Ami, Inashiki, Ibaraki 300-0332, Japan

Introduction

It is well known that PC based electrolyte is easily decomposed electrochemically on the graphite and the intercalation efficiency of lithium is very low. However, the doping of lithium without decomposing the electrolyte becomes possible by adding additives to the PC solvent.¹ Recently, it was reported that the decomposition of electrolyte was suppressed by adding ethylene sulfite (ES).² It is very important to clarify the behavior of solid electrolyte interface (SEI) formation on the graphite and the role of additives. We examined the structure of the SEI formed on the graphite by TPD-GC/MS (Temperature Programmed Decomposition or Desorption - Gas Chromatography / Mass Spectrometry) in the case that ES was added to the PC solvent. In addition, XPS, FT-IR, SEM were used in order to analyze the SEI in detail, and the SEI was determined quantitatively by the chemical analysis.

Experimental

Synthetic graphite (KS44) provided by Timcal G&T was used as a carbon electrode and lithium metal foil was used as the counter electrode. The electrolyte of 10wt% ES in PC including 1M LiPF₆ was used. The experiment was carried out using two-electrode cell. The cell was discharged to 1.5V, 1.0V, 0.6V and 0V vs. Li/Li⁺ in the constant current. Currents were 8 A/cm² and 160 A/cm².

The organic components of SEI is generally decomposed below 200°. The analysis of the SEI structure was carried out by analyzing this thermal decomposition gas by GC/MS (TPD-GC/MS). The carbon electrode was heated under helium gas at rate of 10°/min, and the evolved gas up to 200° was collected in a trap cooled by liquid nitrogen. The collected decomposition gas was introduced into the GC/MS analysis unit by heating up the trap. Li⁺, CO₃²⁻, SO₄²⁻ and F⁻ ion in the SEI were determined quantitatively using ion chromatography by dissolving the SEI into water. XPS, FT-IR, SEM measurements were also carried out. All analysis except for the chemical analysis were done by transporting the samples to the analysis chamber using a inactive transfer vessel.

Results and Discussion

In the electrolyte of PC solvent, the continuing plateau in potential curve was observed around 0.9V due to the successive decomposition of PC. However the intercalation of lithium can be achieved by adding ES to the electrolyte. At the discharging rate of 160 A/cm², the first cycle intercalation efficiency of lithium was 88%. However, at the low discharging rate of 8 A/cm² the irreversible capacity increased, since the plateau appeared in high potential region. As for the thermal decom-

position of the SEI formed at low current density, propylene glycol (PG), CO₂ and SO₂ were detected as shown in Figure 1. These gases are formed by decomposing lithium alkyl carbonate (ROCOOLi) or lithium alkyl sulfite (ROSOOLi), where R = CH₃CH₂CH₂. However, at the high current density of 160 A/cm², these gases evolution from the SEI were not very much detected from 1.5 to 0.6 V region and PG, CO₂ were detected mainly in the potential region of 0.6V or lower. Concerning the chemical analysis, at the low current density, CO₃²⁻ and SO₄²⁻ ion were detected mainly in high potential region. On the other hand, at high current density, SO₄²⁻ ion was detected mainly in high potential region and CO₃²⁻ ion was seldom detected at 0.6V. It was proven that this SO₄²⁻ ion component came from Li₂SO₃ by XPS and FT-IR. The SEI including sulfur constituent was formed in high potential region prior to reductive decomposition of PC. The decomposition of the additives plays the main role in the effective SEI formation for intercalation.

In case of the high current density, the inorganic SEI component was formed first. Then the organic SEI was formed in the region where the intercalation of lithium occurs. In case of the low current density, the SEI was composed of not inorganic component but organic component from the initial stage. From these results, it was confirmed that the SEI structure greatly differed by the current density.

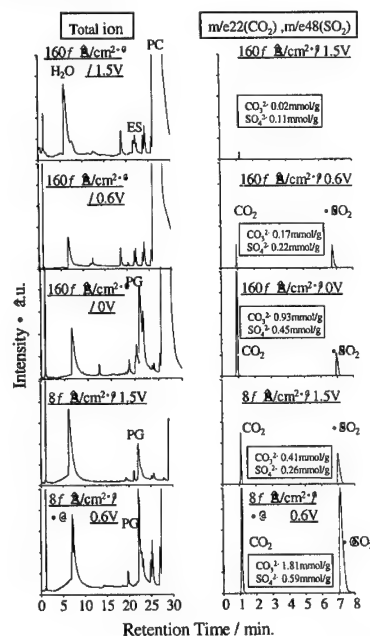


Fig.1 • TPD-GC/MS pattern at various potential and current density in 1M LiPF₆/PC+ES10% electrolyte. • @ The values in the square are the component ratio of CO₃²⁻ and SO₄²⁻ in the SEI estimated from the chemical analysis.

References

1. Y. Ein-Eli, S.R. Thomas, and V.R. Koch, J. Electrochem. Soc., **142**, 1159 (1997)
2. G. H. Wroldnigg, J.O. Besenhard, and M. Winter, J. Electrochem. Soc., **146**, 470 (1999)

Abstract No. 103

⁷Li-NMR study on Li⁺ storage/de-storage mechanisms in non-graphitizable carbons

Chul Wan Park, Jin Kyu Hong and Seung M. Oh

School of Chemical Engineering, College of Engineering,
Seoul National University

San 56-1, Shillim-dong, Kwanak-Gu, Seoul 151-742,
Korea

Non-graphitizable carbons that deliver a higher capacity than graphites have been studied for the application to Li secondary batteries. In this work, the Li⁺ storage/de-storage mechanisms involved in the non-graphitizable carbons were examined using ⁷Li-NMR spectroscopy.

The non-graphitizable carbons were prepared from the methylnaphthalene-derived isotropic pitches (MNIP) by a heat-treatment at 1000°C in Ar atmosphere. For the ⁷Li-NMR study, both the 1-D static and dynamic MAS spectra (spin rate = 4-9 kHz) were obtained using Bruker DSX400 (resonance frequency = 155.6 MHz).

The anodic performances of MNIP-derived carbons have been analyzed using electrochemical techniques.^{1,2} It was found that the carbons have at least three different Li⁺ storage sites, from which Li⁺ ions are de-stored at different potential regions: from site I at 0.0-0.12 V (vs. Li/Li⁺), from site II at 0.12-0.8 V, and from site III at > 0.8 V. During the charging reaction, Li⁺ ions are stored at site II first, then sites I and III in order. But Li⁺ de-storage takes place from site I first, then sites II and III.

Three different resonance absorptions are distinguished in the spectra shown in Fig. 1, supporting the presence of three different Li⁺ storage sites in these carbons. The resonance peaks appearing at 85, 14 and 8 ppm can be related to the Li species stored at sites I, II, and III, respectively. When the evolution of resonance peaks upon Li⁺ storage/de-storage is examined, the sequential order of Li⁺ storage/de-storage is well matched with that proposed by the electrochemical characterization.

The fully stored sample (the fifth spectrum in Fig. 1) gives rise to an abnormally high absorption at 85 ppm but low absorption at 14 ppm. When the sample is steadily cooled down to 140 K, the peak at 14 ppm grows at the expense of the peak at 85 ppm (Fig. 2). A certain interaction between the Li species stored at sites I and II is thus expected. It is, however, likely that the interaction prevails only in the fully stored state because the peak intensity variation is not significant in the partly stored sample.

REFERENCES

1. C. W. Park, S. I. Lee, S. -H. Yoon and S. M. Oh, The 193rd ECS symposium, No. 78, San Diego, USA, May 1, 1998.
2. C. W. Park, S. I. Lee, S. -H. Yoon and S. M. Oh, Carbon, in press.

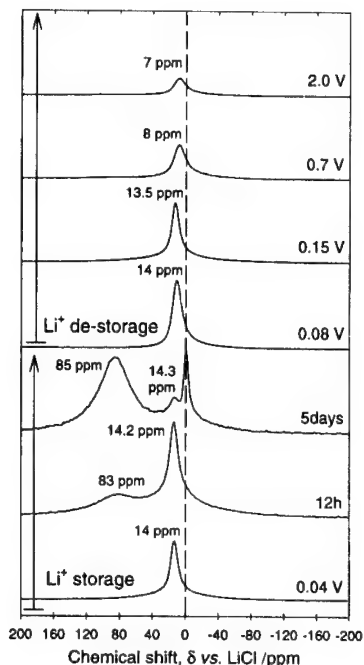


Figure 1. ⁷Li-NMR spectra according to the degree of Li⁺ storage/de-storage. Three resonance absorptions are distinguished in the spectra, indicative of three different Li⁺ storage sites in these carbons.

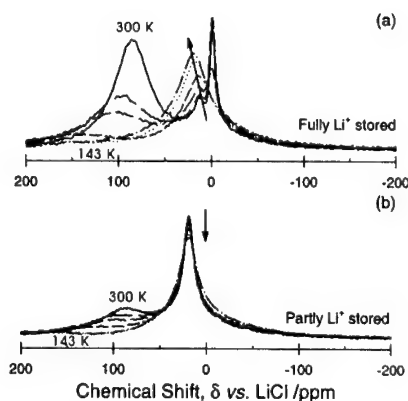


Figure 2. Variable-temperature ⁷Li-NMR spectra recorded with the fully (a) and partly stored sample (b).

Mg₂Sn : A New Anode Material for Rechargeable Lithium BatteriesHiroki Sakaguchi, Masaaki Kubota,
Hitohiko Honda, and Takao Esaka*Department of Materials Science, Faculty of Engineering,
Tottori University
Minami 4-101, Koyama-cho, Tottori 680-0945, Japan

Some intermetallic compounds, such as Mg₂Ge, appear to be promising anode materials for lithium secondary batteries, because the latent capacities of the electrodes consisting of the compounds are much larger than those of carbon materials, especially volumetric energy densities are excellent (1-3). In comparison with LiAl, this type of compounds has a characteristic that the damages during charge-discharge cycling would be avoided, because lithium atoms could accommodate at not lattice site but interstitial sites of the lattices. In the present study, we focused on Sn on behalf of Ge in Mg₂Ge, and synthesized a new anode material, Mg₂Sn, using mechanical alloying. The electrochemical performance of electrode consisting of the compound was investigated.

EXPERIMENTAL

Experimental conditions of mechanical alloying to prepare Mg₂Sn are as follows. A mixture of elemental Mg powder (particle size *ca.* 50 μ m) and Sn (chip size *ca.* 1 mm) chip put in a stainless steel vessel (80 ml) together with five balls (ϕ 15). The weight ratio of the balls to sample was about 15:1. The milling with the prescribed time interval was done using a high-energy planetary ball mill at 300 r.p.m. and at room temperature.

X-ray diffraction was done on the MA samples to identify phases and structures

Electrochemical performance of an electrode was estimated with a three-electrode cell. The electrode consisted of Mg₂Sn, acetylene black, and PVDF in 75:20:5 in wt % on a Cu mesh (1 \times 1 cm²). In the test cell, both counter and reference electrodes were 2 mm thick lithium metal sheets. 1 M LiClO₄ dissolved in propylene carbonate was used as an electrolyte. The cell performance was evaluated galvanostatically at current densities of 0.1 mA cm⁻² for both charge and discharge at

RESULTS AND DISCUSSION

Figure 1 shows XRD patterns of the mechanically alloyed products using elemental Mg and Sn as starting materials. The cubic Mg₂Sn phase was obtained by MA for only 3 hours which were much shorter than the case of Mg₂Ge previously reported (1-3). Interestingly, when the MA treatment proceeded for a longer time, the diffraction peaks of the orthorhombic Mg₂Sn phase appeared in the XRD pattern. Furthermore, the cubic phase disappeared, and single orthorhombic phase was obtained after 7.5 h MA treatment. It is noteworthy that such a phase transformation was never seen for Mg₂Ge and Mg₂Si (3).

Figure 2 gives the result of cycle life on the cubic, orthorhombic, and mixed phasic Mg₂Sn electrodes. The mixed phasic electrode showed the longest cycle life among the electrodes obtained. There is a big difference between the mixed phasic and cubic Mg₂Sn electrodes. At least, the cubic phase give obviously no contribution to the discharge capacity of the mixed phasic electrode. On the other hand, the orthorhombic Mg₂Sn electrode exhibited the similar result as the mixed phasic one, though the electrode showed a little bit lower performance than the mixed phasic Mg₂Sn one. Good performances of the mixed phasic electrode would be due to the

cooperative effect of cubic and orthorhombic phases. The orthorhombic phase may contribute to large capacity, while the cubic phase may assist the relaxation of internal stress generated at lithium insertion.

REFERENCES

1. H. Sakaguchi, H. Honda, and T. Esaka, *Denki Kagaku*, **66**, 1291 (1998).
2. H. Sakaguchi, H. Honda, and T. Esaka, *J. Power Sources*, **81-82**, 229 (1999).
3. H. Sakaguchi, H. Honda, H. Maeta, and T. Esaka, *The Japan Institute of Metals Proceedings (JIMIC-3)*, **12**, 1305 (1999).

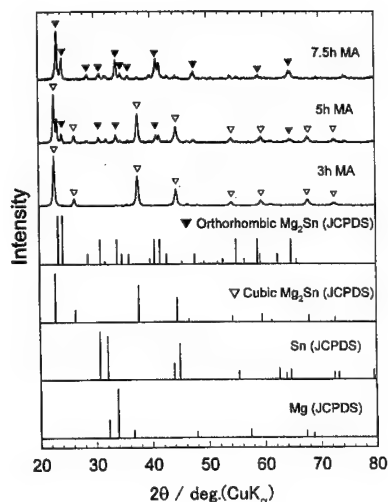


Figure 1 Changes in XRD patterns of Mg₂Sn with mechanical alloying (MA) time.

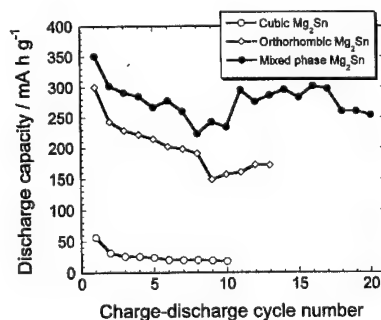


Figure 2 Dependence of discharge capacity on charge-discharge cycling for the Mg₂Sn electrodes with cubic, orthorhombic, and mixed phasic structures.

**Surface Condition and Conductivity Homogeneity
Are the Key Factors for Obtaining High Power and
Long Life Carbon Anode of Li-ion Battery**

*Junji Suzuki^a, Masaomi Yoshida^a, Keita Yamaguchi^a,
Masahiro Kikuchi^a, Kyoichi Sekine^a
and Tsutomu Takamura^b

^a Department of Chemistry, Rikkyo University,
Toshimaku, Tokyo 171-8501, Japan

^b Petoca, Ltd., Kioicho, Chiyodaku, Tokyo 102-0094,
Japan

Introduction

Graphitized carbon is one of the most promising anodic material for the anode of Li-ion secondary battery. But recent modernized electronic appliances require further improvement of the charge/discharge characteristics for heavy duty use. For the purpose of improving the charge/discharge characteristics we have focused our attention on the modification of carbon surface and found mild oxidation as well as metal film deposition on the carbon surface is important key factors^[1,2]. In this paper, we will make clear the importance of the decorated surface as well as the homogeneous distribution of conductivity on the surface.

Experimental

As the test material, mesophase carbon fiber felt (Melblon 3100, Petoca, Ltd. made, 7 μ m) prepared at 3100 °C was used. Ag (99.99%) was deposited on the fiber surface by vacuum evaporation. After the deposition, the felt sample was heated at Tammann temperature ($TT=0.33T_m$ where T_m is the melting point of metal) if necessary. Test electrode was prepared by cutting the felt sample into a piece of 1 mm thick and 1 X 1 cm square and sandwiched between expanded Ni sheets, whose rims were then spot-welded at several points. A cylindrical Pyrex glass cell with a three-electrode system was used for the measurement of linear sweep cyclic voltammogram (CV). Pure metallic lithium foils were used as reference and counter electrodes, respectively. Mixed solvent of EC and DMC (1:1 by volume) containing 1M LiClO₄ was used as an electrolyte. All the procedures were performed in a dry box in an argon atmosphere at room temperature.

Results and Discussion

The rate of Li deintercalation reaction from the carbon fiber is considered to be influenced not only by the surface condition but the process in the internal structure. If the carbon surface is contaminated by some foreign entities, the reaction site is considered to be passivated to provide only a slow reaction even though the mass transfer of Li is fast enough in the interior. In contrast, if the surface is kept active by cleaning or some modification, the overall rate is

expected to be controlled by the carbon interior condition, where phase change due to the stage change and diffusion of Li are the two major factors, and the shape of the deintercalation peak on CV is expected to be modified depending on both the rates of those mechanisms and the potential scan rate. When the scan rate is slow enough, several well separated current peaks could be observed, which correspond well to each stage change, while these peaks tend to merge when the scan rate is moderately fast.

If the conductivity is not uniform throughout the electrode, the SEI formed during the first charge is supposed to be not uniform (in chemistry and structure), causing a deterioration during the charge/discharge cycle, resulting in a poor cycle life.

When a few hundreds angstrom thick silver film was deposited, the peak height was enhanced remarkably as compared with that of pristine sample, indicating that the deintercalation reaction site on the silver surface which is in contact with the electrolyte is sufficiently active as compared with that on the pristine carbon. The cycleability was also improved remarkably. Deposition of silver is expected to improve the conductivity uniformity which gives rise to a long cycle life.

The sample treated with mild oxidation revealed also an enhanced deintercalation peak whose top was well splitted into two sharp subpeaks and that at negative potential side was much enhanced. This may be indicative of the reaction site to be cleaned. The cycleability, however, was rather poor, indicating that the conductivity uniformity was degenerated by the oxidation process.

When the silver covered sample was heated over the Tammann temperature, the resulting SEM picture revealed tiny silver drops spread all over the carbon surface, which is supposed to be formed by the melting of silver on the carbon surface and coagulated into drops. In the process of forming the silver drop deposits the carbon surface is expected to be cleaned. The CV of the drop deposit sample gave rise to a dramatically large peak. The cycleability, however, was rather poor, which is considered to be caused by the nonuniformity potential distribution during the discharge because too much current flew, resulting in a formation of heterogeneous SEI.

In conclusion, surface cleanness and the uniformity of high conductivity are the most important key factors for attaining high power and long cycle life.

References

- [1] M. Kikuchi, Y. Ikezawa and T. Takamura, J. Electroanal. Chem., 396 (1995) 451-455.
- [2] T. Takamura, K. Sumiya, J. Suzuki, C. Yamada and K. Sekine, J. Power Sources., 81-82 (1999) 368-372.

Graphite-Metal Oxide Composites as Anode for Li-ion Batteries

H.Huang, E.M.Kelder, and J.Schoonman
Delft Interfaculty Research Center:
Renewable Energy
Laboratory for Inorganic Chemistry
Delft University of Technology,
Julianalaan 136, 2628BL Delft, The Netherlands

Graphite as anode material for Li-ion batteries has many advantages over other types of carbon in a low-rate application. However, when a fast-rate charge capability is required such as in Electric Vehicles (EV), lithium-ion batteries with primary graphite as anode cannot meet the targets because of the limited insertion rate of lithium ions. Furthermore, graphite cannot match with the commonly used cathode in terms of rate, the capacity, the energy density, and the cycleability decrease and consequently once the battery is charged at a fast rate, a safety problem is encountered. Hence, in order to improve the insertion rate graphite needs to be modified for these types of applications.

Using graphite with dispersed ultrafine silver particles, a higher volumetric capacity and longer cycle life than conventional graphite was reported [1]. An improvement of the charge/discharge rate was shown by cyclic voltammograms of the graphitized mesophase carbon fibers on the surface of which Pd was deposited [2]. Recently, in our laboratory graphite-metal oxide composites were prepared by dispersing various metal oxides in a Graphite Oxide coarse suspension and the electrochemical performances were studied in detail [3,4]. The results on G-MO (G= graphite, MO = CuO, NiO, Fe₃O₄, and Pb₃O₄) composites will be presented and discussed in this paper.

XRD results show that the prepared G-MO samples are mainly a mixture of graphite and the corresponding metal oxide, while FTIR analyses confirm the existence of a certain bonding between the metal oxide and carboxylic groups on the surface of graphite.

During the first discharge a large irreversible plateau appears in all four samples. Combining the calculations and XRD analyses, these plateaus are a result of a reduction reaction of the metal oxide to the corresponding metal during discharging. Subsequently, only a small part of the formed metallic particles are oxidized upon charging. In the subsequent discharge/charge cycles such reduction/oxidation reactions are reversible.

The prepared graphite-metal oxide composites show a good cycleability (see Fig.1). This characteristic is attributed to the improvement of the electronic contact between the graphite particles as a result of the presence of the metallic particles formed after the first discharge process.

The reversible capacities at various discharge current densities are compared with pure graphite and the results are shown in Table. 1. A substantial improvement has been obtained with G-CuO composites as can be seen in Table 1 and Fig.2. The inset presents the same curves into the low voltage regions for better resolution. For G-CuO when discharged at a high current rate, i.e. $I=1.0\text{mA}/\text{cm}^2$, the completion of the initial-stage intercalation can be observed while for pure graphite not. In combination with electrochemical impedance spectroscopy results, the improvement of the rate capability of G-MO composites is attributed to the enhancement of both the electronic conductance and reaction kinetics especially considering

the lithium transport process along and across the interfaces where charge transfer occurs.

References

1. H.Morose, H.Honbo, S.Takeuchi, K.Nishimura, T.Horiba, Y.Muranaka, Y.Kozono, and K.Miyadera, *J. Power Sources*, 68(1997)208.
2. K.Skine, T.Shimoyamada, R.Takagi, K.Sumiyu, and T.Takamura, Abstract 126, Electrochemical Society Proceedings 97-18, Paris, France, 1997.
3. H.Huang, E.M.Kelder, L.Chen, and J.Schoonman, Abstract, Joint Meeting of The Electrochemical Society, Honolulu, USA, 1999.
4. H.Huang, Anode Materials for Lithium-ion Batteries, Ph.D.Thesis, Delft University of Technology, Universal Press, ISBN 90-9013379-8, 1999.

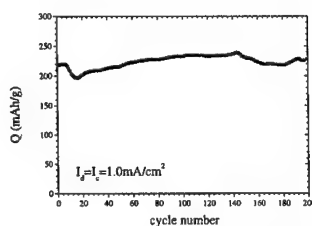


Fig.1 Capacity vs. cycling of G-CuO composite

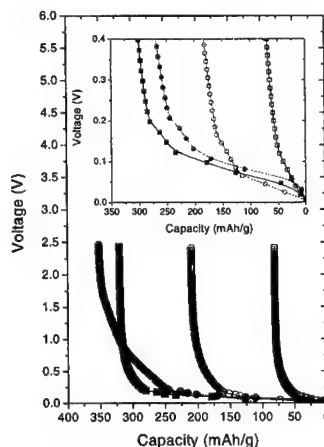


Fig.2 Discharge profiles of G (squares) and G-CuO (circles) composite at low ($I=0.1\text{mA}/\text{cm}^2$, solid) and high ($I=1.0\text{mA}/\text{cm}^2$, hollow) current densities, respectively.

Table.1 Capacity at low and high discharge current rate of G and G-MO composites

Samples	Q_l (mAh/g G) $I=0.1\text{mA}/\text{cm}^2$	Q_h (mAh/g G) $I=1.0\text{mA}/\text{cm}^2$	Q_h/Q_l (%)
G	320	80	25
G-NiO	325	125	38
G-Pb ₃ O ₄	675	260	38
G-Fe ₃ O ₄	325	135	41
G-CuO	350	210	60

Key Factors for Material Designing of High Power Carbon Anode of Li-Ion Secondary Battery

Tsutomu Takamura^a, Junji Suzuki^b, Keita Yamaguchi^b, Takumasa Katsuta^b and Kyoichi Sekine^b
^a*Petoca, Ltd, Kioicho, Chiyodaku, Tokyo 102-0094,*
^b*Department of Chemistry, Rikkyo University Nishiikebukuro, Tokyo 117-8501, Japan*

Introduction

Recent strong demand of portable electronic appliance, especially an advanced portable phones, is to enhance the operational power of the power source. The most promising power source is considered to be Li-ion secondary batteries. Attaining the increase in operational power of the battery causes to improve the cycleability as well.

The cell performance is strongly dependent on what type of material is used and also what type of the electrode designing is adopted. The influencing factor in the material designing is the structure not only based on the molecular level but also SEM microscope level. In addition, even though the same material is used, the cell performance differs to a great extent if the different electrode designing is adopted.

In the present study we focus our attention on the anode material of Li-ion battery, especially on the carbon material and would like to provide key factors for realizing a high power charge/discharge performance in view of what type of the carbon material and what type of the electrode designing are the most preferable.

Experimental

As the test active materials two types of mesophase carbon fibers of very well graphitized and low temperature-treated ones (Melblon 3100 and 800, Petoca made) were used. A single straight fiber with a diameter of 10 μ m, an integrated fiber felt and short cut fiber particles were tested.

A single fiber was immersed in the electrolyte vertically with a depth of 5 mm and the electrochemical test was done. For the fiber felt, it was sliced into 1 mm thick piece and sandwiched between two Ni expanded metal sheets, whose rims being spot-welded at several points for tight fixing and used as a test electrode. For preparing active material slurry the short cut fibers were mixed well with an electroconducting additive of carbon powder, PVDF binder, and n-methyl pyrrolidone, thus formed slurry being coated on a copper foil, dried at 120 $^{\circ}$ C, pressed, and used as a test electrode. Several kinds of electroconducting carbon powder including graphite powder were tested, where the mixing ratio was varied.

A 1:1(v/v) mixture of ethylene carbonate and dimethyl carbonate, or propylene carbonate, containing 1 M LiClO₄, was used as an electrolyte. The former was used for the graphitized carbon and the latter, for the non-graphitized one.

Several electrochemical tests were performed, where cyclic voltammogram (CV), constant current charge/discharge performance, and potential step

current-time curve were measured. SEM pictures and XRD patterns were taken if necessary.

Results and Discussion

Regarding the initial irreversible charging capacity of graphitized carbon, it appeared clearly the CV both for the felt type and the coated electrodes, while a single carbon fiber revealed no detectable irreversible capacity even the same source of the material was used. In the case of the single fiber, the electric conductivity is considered to be uniform throughout the specimen but that of the other is supposed to be inhomogeneous. This means that the irreversible capacity appearing on the CV of the graphitized carbon is not due to an intrinsic nature, and accordingly, taking a homogeneous good electric contact of each active material particle can minimize it. The homogeneous distribution of the conductivity was also effective to attain a good cycleability.

In contrast, a single fiber of 800 $^{\circ}$ C sample gave always a sharp cathodic peak on the first scan CV curve. The irreversible peak could not be removed unless the sample was heated over 1000 $^{\circ}$ C *in vacuo*, implying that it is an intrinsic one.

The Li charge/discharge capacity of over 600 mAh/g could be confirmed for the 800 $^{\circ}$ C felt sample only when the charge/discharge rate was extremely slow, implying that the Li insertion and removal rates of the material is intrinsically slow. Therefore, the low temperature sample is not suitable for the high power purpose though it has a very high latent charge capacity.

For the coated electrode comprised of short fiber, not only the cycleability but the depression of the initial irreversible capacity could be much improved when an appropriate amount of the conducting additives was loaded homogeneously. This means that the homogeneous distribution of the conductivity throughout the electrode surface is an important key factor for realizing high performance.

The surface of the fiber sample is covered with a thin hard skin formed by oxidation treatment. When the skin was thinned by mild oxidation treatment, the CV peak for Li discharge was enhanced showing the reaction rate to be increased.

Application of a thin metal film by vacuum deposition on the carbon surface was found also very effective to enhance the Li charge/discharge rate. Silver was found to be one the best candidate. The rates of the Li charge/discharge reactions were evaluated by a potential stepping chronoamperometry. The obtained value expressed based on diffusion coefficient was near 10⁻⁸ cm²/sec² for pristine graphitized carbon but it could be increased up to as high as 10⁻⁶ cm²/sec² when a silver film was deposited. Thus surface modification is also an important key factor to attain the high power charge/discharge performance.

References

- [1] K. Sumiya, J. Suzuki, R. Takasu, K. Sekine and T. Takamura, *J. Electroanal. Chem.*, **462**, 150(1999).
- [2] T. Takamura, K. Sumiya, J. Suzuki, C. Yamada and K. Sekine, *J. Power Sources*, **81-82**, 368(1999).

DOPED TIN OXIDES AS POTENTIAL LITHIUM ION BATTERY NEGATIVE ELECTRODES: EFFECTS OF MILLING PROCESS

Frédérique Belliard and John T.S. Irvine

School of Chemistry, University of St. Andrews, Kingdom
of Fife, Scotland, KY16 9ST.

Idota et al. (1) announced in 1997 that tin oxide compounds can replace the carbon as a negative electrode in the future. Courtney and Dahn (2) have proposed a model to explain the mechanism. Initially the tin oxide is reduced to form tin metal and Li_2O , then the lithium-tin alloy is formed and the reversible capacity comes from the alloying/dealloying of the tin metal. Some reports (3,4) have shown that ZnO follows the model suggested by Courtney and Dahn (2) for tin oxides. Since then, there have been an increasing number of studies on tin alloys and other tin oxide composites. Both strategies register some disadvantages: mechanical stress due to volume expansion for the alloys and large irreversible loss during the initial discharge for the oxides. The purpose of this work is to combine both metal oxides to improve the capacity. The inverse spinel Zn_2SnO_4 was prepared by hand-grinding and ball-milling followed by sintering. Also the same ratio of SnO_2 and ZnO with several periods of ball-milling were investigated as active material.

Milling is well known for decreasing particle size down to nanoscale, creating more disorder in the structure and new crystalline phase, and amorphous phases (5). In our case ball-milling does not alter the oxide structure and does not initiate new phases (see Figure 1). The oxides, after a long milling time, stopped decreasing and increased in particle size and become partially amorphous. During this process the existing plateaux of SnO_2 at 0.9V and ZnO at 0.6V are still visible.

The spinels exhibit an initial reversible capacity between 300 and 400 mAh/g, whereas the mixtures have a capacity between 400 and 550 mAh/g. As has been reported previously (6), the initial capacity increases as particle size decreases. The capacity is larger for the oxides milled separately than the co-milled oxides (see Figure 2). The milled spinel gives lower capacity compared to the ground spinel. Milled powders react better because of the smaller particle size of the reactants, therefore ball-milling before reaction might reduce the performance of the negative electrode.

After several cycles the capacity profile is modified. The spinel has better capacity compared to the mixture. The alloying and dealloying efficiency of lithium-tin and lithium-zinc is lower for the mixture. The spinel structure seems to lose less capacity during cycling.

In order to estimate the particle size before and after cycling some SEM were performed. Understanding the mechanisms that occur during cycling is challenging, because the processes proposed are not well understood. To clarify the phenomena *in-situ* and *ex-situ* measurements as EXAFS, XRD and SEM were performed.

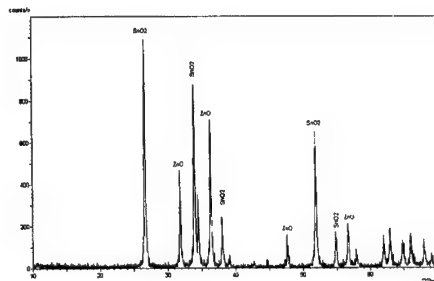


Figure 1 XRD of $\text{ZnO}:\text{SnO}_2$ (2:1) milled together for 22 hours

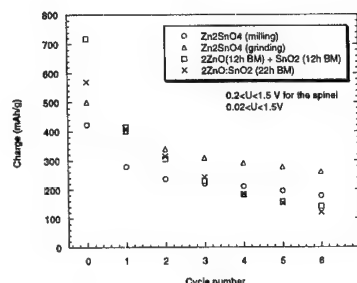


Figure 2 Reversible capacity Vs cycle number for ball-milled (O) and hand-ground (Δ) Zn_2SnO_4 spinels and ball-milled separately (□) and together (X) ZnO and SnO_2 powders

1. Y. Idota, T. Kubota, A. Matsufuji, Y. Maekawa, T. Miyasaka, *Science* **276**, 1395 (1997)
2. I. A. Courtney, J. R. Dahn, *J Electrochem. Soc* **144**, 2045 (1997)
3. T. Brousse, D. Defives, L. Pasquereau, S.M. Lee, U. Herterich, D.M. Scheich, *Ionics* **3**, 332 (1997)
4. J. Wang, P. King, R. A. Huggins, *Solid State Ionics* **20**, 185 (1986)
5. M. N. Obrovac, O. Mao, J.R. Dahn, *Solid State Ionics* **112**, 9 (1998)
6. J. Yang, M. Winter and J.O. Besenhard, *Solid State Ionics* **90**, 281 (1996)

NOVEL TIN OXIDE BASED ANODES FOR LI-ION BATTERIES

Paul A. Connor, and John T. S. Irvine

School of Chemistry, University of St Andrews, St Andrews, Fife KY16 9ST, Scotland

Tin oxides are a group of materials that show promise as Li-ion battery anodes (1,2,3) due to their large reversible lithium capacity. The mechanism of insertion of Li^+ into these oxides is thought to proceed by an initial reduction of the Sn(II or IV) to metallic tin particles [1] dispersed in the remaining oxide. This is followed by the reversible alloying of lithium into the dispersed metal particles [2] (1,2). This alloying of lithium into tin causes a large volumetric expansion, which makes bulk tin electrodes unusable. It is thought that the small particle size and the surrounding oxide matrix helps to stabilise these volume changes in the oxide based electrodes.

The form of the initial tin oxide used is important as it will effect both the size of the metallic particles as well as the type and structure of the surrounding oxide matrix.

To investigate the influence of the oxide matrix on electrode performance, a series of isostructural inverse spinels (M_2SnO_4 , $\text{M} = \text{Mg, Co, Mn, etc}$) were produced and investigated. Assuming the additional metals are inert to lithium insertion they should still follow the same model as insertion into SnO_2 but with the reduction step [1] forming a more complicated Li-metal oxide composite.

These materials were characterised, and studied as possible anode materials. Conventional voltammetric studies have been used to investigate the electrochemical behaviour of the materials. A selection is shown in Fig 1. There are significant differences between the various oxides, most readily apparent in the level of the voltage plateaux at low lithium insertion. The correlation between these potentials and the enthalpies of formation of the oxides will be discussed. There are also changes in the reversible cycling of the cell, with the amount of lithium inserted at different potentials varying between samples. This shows that the oxide framework has an influence on the insertion of the lithium into the electrode.

These results, coupled with other *in situ* and *ex situ* techniques, such as AC impedance, X-ray diffraction EXAFS, will be shown and discussed.

References

1. Y. Idota, T. Kubota, A. Matsufuji, Y. Maekawa and T. Miyasaka, Science **276**, 1395 (1997).
2. I. A. Courtney and J. R. Dahn, J. Electrochem. Soc. **144**, 2045 (1997).
3. W. F. Liu, X. J. Huang, Z. X. Wang, H. Li, and L. Q. Chen, J. Electrochem. Soc. **145**, 59 (1998).

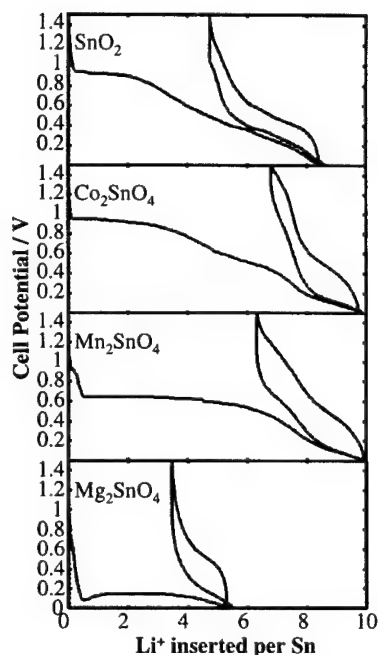
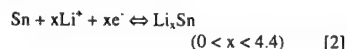
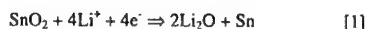


Fig 1 Galvanostatic cycling of various tin spinels, and SnO_2 for comparison

The effect of lithium insertion on the structure of tin oxide based glasses

C. Gejke, E. Zanghellini, and L. Börjesson
 Department of Applied Physics, Chalmers University of
 Technology, S-412 96 Göteborg, Sweden
 L. Fransson and K. Edström
 Inorganic chemistry, Ångström Laboratory, Uppsala
 University, Box 538, S-751 21 Uppsala, Sweden

Tin-based amorphous composite oxides have recently received much attention as the active component in anode materials for rechargeable lithium ion batteries [1]. These materials show an outstanding performance regarding the Li-storage capacity, more than 600 mAh/g (reversible). However, during the first cycle there is a large permanent capacity loss. The reaction causing the large irreversible capacity is believed to be the formation of metallic tin when the lithium ions, when inserted into the material, react with oxygen in the tin oxide [2]. New results indicate the importance of the constituents of the glass network and also the significance of oxygen participation for good cycleability [3]. The dependence of the glass network for the cycleability is not yet clear but by substituting the different components of the network it should be possible to lower the irreversible capacity.

We have earlier examined the behavior of boron and phosphorous in the glass network. This has been done by investigating electrodes from different stages of the first cycle with FT-IR. From FT-IR measurements it can be seen that the glass network is affected by the lithium insertion and that the changes are not fully recovered by lithium extraction.

We have performed micro-Raman spectroscopy measurements which indicate that the lithium, when entering the material, is first attracted by the oxygen's bonded to the phosphorous and thereby causes an irreversibly change in the local structure around it. Since the structure for phosphate and/or boron oxide glasses is well known it is possible to detect and understand how their part of the structure is affected by lithium. It appears like bonds between neighboring phosphate units are broken, while boroxol bridging units are less affected, see Figure (1). Results will be presented on glasses investigated both before and after the electrochemical cycling experiments. Due to the interaction between phosphate and lithium, measurements have been done on tin oxide glasses containing boron and aluminium but without phosphorous.

The irreversible capacity is not only being due to the aggregation of metallic tin and the formation of lithium oxide but also to the disruption of the original glass network.

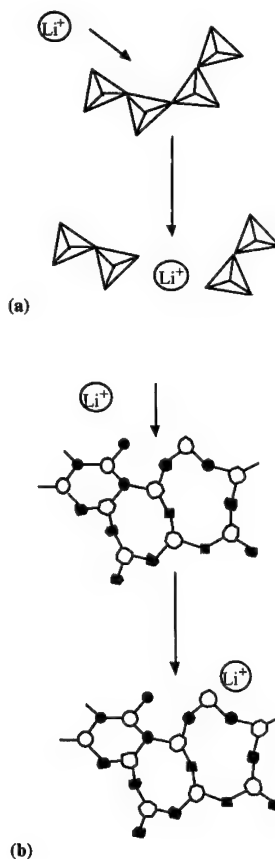


Figure 1. The effect of lithium insertion on the glass network; (a) the phosphate units, (b) the boroxol units.

- [1] Y. Idota, T. Kubota, A. Matsufuji, Y. Maekawa, T. Miyasaka, *Science* **276** (1997) 1395
- [2] I. A. Courtney and J. R. Dahn, *J. Electrochem. Soc.* **144** (1997) 2045
- [3] G. R. Goward, F. Leroux, W. P. Power, G. Ouvrard, W. Dmowski, T. Egami, L. F. Nazar, *Electrochem. Letters*, **2** (1999) 367

Electrochemical Properties of Tin-containing Thin Films

H. Kobayashi, Y. Uebou*, T. Ishida, S. Tamura, S. Mochizuki, T. Mihara, M. Tabuchi, H. Kageyama, Y. Yamamoto*, M. Matsuoka*, J. Tamaki*

Osaka National Research Institute, AIST, MITI, Ikeda, Osaka, 563-8577 Japan

*Department of Chemistry, Faculty of Science and Engineering, Ritsumeikan Univ., Kusatsu, Shiga, 525-8577 Japan

Introduction

Tin-containing materials have been studied for anode materials for lithium secondary batteries because of high capacity against carbon (1). From the viewpoint of high volumetric energy density, tin-containing thin films are also promising materials for anode materials of micro-battery (2,3). Tin metal has large capacity but shows poor cycle reversibility because of large volumetric change with lithium intercalation. In addition, the intrinsic electrochemical property of tin-containing materials was not completely clarified. Electrochemical tests using thin films might throw light on electrochemical properties without binder. Tin oxide thin films showed good cycle reversibility but need relative high temperature above 573 K for deposition on substrate. In this study, tin-containing thin films were synthesized and characterized by XRD and electrochemical measurements. Further, their electrochemical properties were tried to improve by the change of form and electrical test conditions.

Experimental

Tin metal (Sn) and tin-copper alloy (Sn_3Cu_6) films were prepared from tin ingot by a vapor deposition process. The tin oxide (SnO_2) films were prepared by a photochemical vapor deposition process. TMT and O_2 (containing 4 mol% O_3) were used as the source materials and a low pressure mercury lamp was used as the light sources. Electrochemical tests were carried out with a beaker-type configuration. The electrolyte used was 1M LiClO_4 in EC:DMC(1:1).

Results and discussion

Tin metal films were deposited on stainless substrate at R.T.–493 K. All XRD patterns showed the peaks of tin metal (JCPDS 4-673) except for ones of substrate. SEM image showed average grain size of about 2 μm at 393 K. Electrochemical tests showed typical curves of tin metal. From the volumetric change, the thin films were peeled off substrate during charge-discharge cycles between 0 and 1.1 V. The Li/Sn cell showed the capacity of 400 mAh/g at 10 cycles in the range of cut-off voltage of 0.2 and 0.8 V.

Tin-copper films were deposited on copper substrate. XRD patterns showed a single-phase tin metal at R.T. and tin-copper alloy appeared with increasing temperature. At 473 K, tin-copper alloy was mainly observed except for copper substrate. SEM image showed drastic changes with substrate temperature. A small spherical grain of 0.1–0.5 μm was observed at 463 K, while large grain of 2 μm was observed at 473 K. The plateaus around 0.4 V, which was characteristics for tin metal, was observed in initial charge process for samples synthesized under 433 K. The characteristic curves, corresponding to Sn_3Cu_6 alloy (4), were observed above

473 K. The Li/ Sn_3Cu_6 cell showed the capacity of 200 mAh/g after 100 cycles.

Tin oxide films were deposited on stainless substrate at 473–573 K. XRD patterns showed amorphous-like patterns at 473 and 523 K, while XRD pattern prepared at 573 K showed polycrystalline pattern, in which 110 and 211 peaks were indexed from orthorhombic SnO_2 (JCPDS 41-1445). The Li/ SnO_2 cell showed the reversible capacity of 600 mAh/g in the voltage range of 0.02–0.8 V. No different electrochemical behavior was observed with substrate temperature.

These results indicated that tin-containing materials were promising candidate for anode materials by controlling the grain size and cut-off voltage and clarified that the SnO_2 thin film suitable for electrode was possible to synthesis at low temperature of 473 K by photo-CVD method.

References

1. Y. Idota, A. Matsufuji, Y. Maekawa, and T. Miyasaki, *Science*, **276**, 1395 (1997)
2. T. Brousse, R. Retoux, U. Herterich, and D.M. Schleich, *J. Electrochem. Soc.*, **145**, 1 (1998).
3. S.C. Nam, Y.H. Kim, W.I. Cho, H.S. Chun, and K.S. Yun, *Electrochem. and Solid-State Lett.*, **2**, 9 (1999).
4. K.D. Kepler, J.T. Vaughey, and M.M. Thackeray, *Electrochem. and Solid-State Lett.*, **2**, 307 (1999).

Antimony doping effect on the electrochemical behavior of SnO₂ thin film electrodes

J. Santos-Peña, T. Brousse, L. Sánchez*, J. Morales* and
D.M. Schleich

ISITEM, Laboratoire de Génie des Matériaux,
La Chantrerie, BP 90604
F-44300 Nantes Cedex 3 - France

* Laboratorio de Química Inorgánica,
Facultad de Ciencias, E-14004 Córdoba - Spain

Since the announcement by Fuji Film Co. of the use of tin oxides as anode for lithium ion batteries, there has been an impressive amount of work on tin based electrodes [1]. One of the problem related to the use of tin oxide is that very fine particles are needed to get the high capacity expected for this material. Furthermore, the poor electronic conductivity is also a hinder to the reaction of tin oxide with lithium during the first charge.

In order to investigate the effect of the grain size and the electronic conductivity of tin oxide, we have prepared thin films of this material by a sol-gel technique. The electronic conductivity was enhanced by antimony doping [2]. Furthermore, it seems that some dopant, like Mo, are efficient to enhance the cycling properties of SnO₂ material [3].

Thin films were prepared from propyleneglycol solutions with a total metal concentration [Sn+Sb] equal to 0.05M. These solutions were obtained from chlorides titrated with AgNO₃. About 7-10 ml of the solution was slowly sprayed on a Cu foil at 498°K. Then, the films were annealed at 673°K during one hour.

Scanning electronic microscopy was used to examine some properties of the electrode surface. No special changes in particles morphology occur with the antimony doping. In addition, no antimony oxide particles apart from tin-antimony oxide particles were detected.

X-ray diffraction (XRD) patterns reveal a poor crystallinity of the samples according to the marked broadness of the peaks. In contrast, they can be easily correlated to a cassiterite (SnO₂) structure. Antimony doping remarkably decreases the crystallinity of the samples (see Table I). However, it seems that antimony doping has a slight effect on the cell.

Electrochemical tests were performed at 25°C, in a simple two electrode cell using metallic lithium as both reference and counter electrode. The electrolyte was a 1M solution of LiPF₆ dissolved in a two to one mixture of EC and DEC (Merck). Cells were cycled in a range de 50 mV-1.2V under a current density of 0.25 mA/cm², corresponding to a C/7 rate. As seen in Figure I, antimony doping leads to an initial capacity loss higher than the undoped sample. Nevertheless, the capacity fade upon cycling is lower for the antimony doped films. The best performances are obtained for the « 5% » Sb composition.

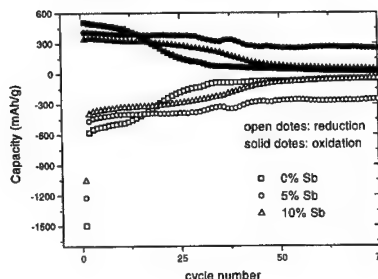
These preliminary results would indicate that Sb doping in SnO₂ thin films significantly enhances the performance of the electrode in a lithium ion cell. Several reasons can explain this feature. Firstly, a decrease in the grain size when tin oxide film is antimony modified. Secondly, the thin films must increase their electronic conductivity when doping. This last feature can also increase the reactivity of the material during the first cycle, when tin particles are formed in-situ. Further

investigation must be carried out in order to clarify the mechanism.

Table I. Structural data of the antimony doped tin oxide samples.

%Sb	Microsize (Å)	Spacing (Å)		
		(110)	(101)	(211)
0	68	3.333	2.626	1.754
5	40	3.402	2.641	1.766
10	32	3.536	2.617	1.738

Figure I. Capacity versus cycle number of cells with antimony-tin oxide thin films as anodes.



See for example :

- [1] T. Brousse, R. Retoux, U. Hertirich and D. M. Schleich, *J. Electrochem. Soc.* 145, 1 (1998).
- [2] B. Orel, U. Lavrencic-Stangar and K. Kalcher, *J. Electrochem. Soc.* 141, L127 (1994).
- [3] J. Morales, L. Sánchez, *J. Electrochem. Soc.* 146, 1640 (1999).

Investigation of solvated and unsolvated lithium intercalation processes into graphitic carbons by electrochemical dilatometry

Gerhard H. Wrodnigg¹, Petr Novák²,
Jürgen O. Besenhard¹, and Martin Winter¹

¹ Institute for Chemical Technology of Inorganic Materials, Graz University of Technology, Stremayrgasse 16, A-8010 Graz, Austria

² Paul Scherrer Institute, Laboratory for Electrochemistry, CH-5232 Villigen PSI, Switzerland

In many electrolyte solutions graphite electrodes tend to co-intercalate solvent molecules. This effect causes increased irreversible charge consumption due to solvent decomposition inside the graphite (i.e., between the graphene layers). The solvated lithium intercalates, $\text{Li}(\text{solvent})^+$, are much larger than the unsolvated lithium cations Li^+ . Therefore, solvated intercalation may cause irreversible structural damages of the graphite. To avoid solvated intercalation, only electrolyte compositions can be used, which form a protective "solid electrolyte interphase" (SEI). The SEI is in an ideal case a membrane permeable for unsolvated Li^+ cations only [1-3].

Here, we investigate and compare solvated and unsolvated intercalation reactions into graphites by electrochemical dilatometry. The method is able to *in-situ* monitor the macroscopic expansions (and contractions) of a graphite sample due to the electrochemical intercalation (and de-intercalation) of Li^+ and/or $\text{Li}(\text{solvent})^+$.

Graphite anodes charged in electrolytes based on propylene carbonate (PC) suffer from enormous PC co-intercalation between the graphene layers and, thus, the graphite exfoliates rapidly (Figure 1). This is indicated by the large irreversible volume expansion of the sample and the extensive irreversible solvent reduction negative to about 1 V vs. Li/Li^+ . The solvated intercalation reaction and the corresponding large volume changes can be diminished or even suppressed by using strong film-forming electrolyte additives, e.g., ethylene sulfite (ES, Figure 2). The ES is electrochemically reduced and forms a SEI at potentials more positive than the potential of solvent co-intercalation [3,4].

Results on the influence of other additives and electrolyte components, such as propylene sulfite [5] and chloroethylene carbonate [6] in combination with PC will be presented. The role of ethylene carbonate (EC) in electrolytes based on EC/PC solvent mixtures will receive particular attention.

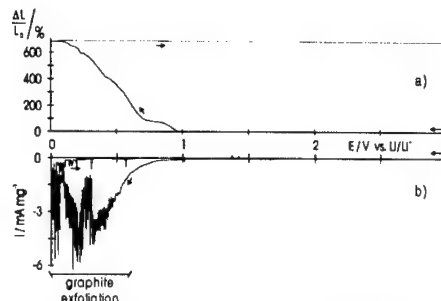


Fig. 1: Dilatation record (a) and cyclic voltammogram (b) of TIMREX® T 200 - 2000 synthetic graphite in 1 M $\text{LiN}(\text{SO}_2\text{CF}_3)_2/\text{PC}$; scan rate 0.1 mV s^{-1} .

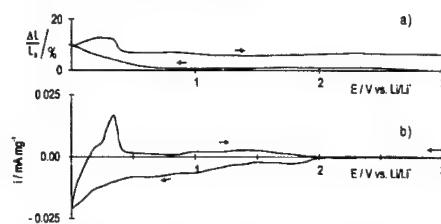


Fig. 2: Dilatation record (a) and cyclic voltammogram (b) of TIMREX® T 200 - 2000 synthetic graphite in 1 M $\text{LiN}(\text{SO}_2\text{CF}_3)_2/\text{PC}/\text{ES}$ (95/5 by volume); scan rate 0.1 mV s^{-1} . (Signal to background ratio and resolution of the CV is poor due to geometrical limitations of the dilatometry cell).

- [1] E. Peled, D. Golodnitzky, and J. Pencier, in: Handbook of Battery Materials, J. O. Besenhard (Ed.), Wiley-VCH, Weinheim, Part III, Ch. 6 (1999)
- [2] M. Winter, J. O. Besenhard, M. E. Spahr, and P. Novák, *Adv. Mater.*, **10**, 725 (1998)
- [3] G. H. Wrodnigg, J. O. Besenhard, and M. Winter, *J. Electrochem. Soc.*, **146**, 470 (1999)
- [4] M. Winter, G. H. Wrodnigg, J. O. Besenhard, W. Biberacher, and P. Novák, *J. Electrochem. Soc.*, submitted
- [5] G. H. Wrodnigg, T. M. Wrodnigg, J. O. Besenhard, and M. Winter, *Electrochem. Comm.*, **1**, 148 (1999)
- [6] Z. X. Shu, R. S. McMillan, J. J. Murray, and I. J. Davidson, *J. Electrochem. Soc.*, **14**, 2231 (1996)

This work was partially supported by the Austrian Science Fund within the special research program "Electroactive Materials" and by the Swiss Federal Office of Energy. We thank Dr. M. E. Spahr (Timcal Group, Bodio) and Merck (Darmstadt, Germany) for the donation of samples used in this study

Stress Effect on Cycle Properties of the Silicon
Thinfil Anode

Seung-Joo Lee, Jong-Ki Lee, and Hong-Koo Baik*
and Sung-Man Lee**

*Department of Metallurgical Engineering, Yonsei
University, Seoul 120-749, Korea

**Department of Advanced Material Science and
Engineering, Kangwon National University, Chuncheon
200-701, Korea

Rechargeable microbatteries for use in low power applications, such as micro electromechanical system (MEMS), and micro implantable medical devices, require high specific energy and cycle properties. To satisfy these requirements, anode materials, which have high specific capacity and no irreversible capacity at the first cycle, are necessary. In this viewpoint, carbonaceous materials and tin composite oxides are not adequate.

It is well known that silicon can alloy with lithium up to 4.4 Li per Si, at 400°C, but, silicon anode shows poor cycle properties. It is considered that volume change of Si-Li alloy with Li insertion and extraction leads to pulverization of silicon anode.

Silicon thinfil anodes were fabricated by rf magnetron sputtering method on copper and very thin glass substrate varying thickness. Microstructures, surface morphology were observed by X-ray diffraction (XRD), scanning electron microscopy (SEM), and X-ray photoelectron spectroscopy (XPS). Electro-chemical cells were assembled with EC/DEC based electrolyte containing 1M LiBF₄ salt. Charge and discharge test and in-situ stress measurement were carried out.

Effect of stress variation during lithium insertion and extraction processes on the cycle properties of silicon anode will be discussed.

REFERENCES

1. J. B. Bates, N. J. Dudney, D. C. Lubben, G. R. Gruzalski, B. S. Kwak, X. Yu, and W. R. A. Zuhr, J. Power Sources, 54 58 (1995)
2. B. A. Boukamp, G. C. Lesh, R.A. Huggins, J. Electrochem. Soc., 128, 725 (1981)
3. H. Ikuta, T. Morita, A. Modeki, and M. Wakihara, Extended Abstracts of the Ninth International Meeting on Lithium Batteries, Edinburgh, U.K., July (1998)

ELECTROCHEMICAL PROPERTIES OF MnV_2O_6
AND ITS DERIVATIVES AS NEW ANODE
MATERIAL FOR LITHIUM SECONDARY BATTERYSung-Soo KIM, Yasunori SUZUKI, Hiromasa IKUTA,
Masataka WAKIHARASchool of Applied Chemistry, Tokyo Institute of Technology,
2-12-1 Ookayama, Meguro-ku, Tokyo 152-8552, Japan

The carbonaceous anode material commonly used in lithium rechargeable batteries suffers from small capacity per unit weight (about 350mAh/g) and low capacity per unit volume due to its low density. To overcome these disadvantages, considerable amount of attempts have been made by several workers to find out alternative anode material in place of carbonaceous anodes.

As a part of this venture, we have recently explored the possibility of employing manganese vanadium oxide as anode material. The unique character of vanadium compound is that it can function either as anode or as cathode material in lithium ion batteries.^{1-*} Recently, Piffard *et al.*² have reported on the synthesis of amorphous and crystalline manganese vanadate MnV_2O_6 , by precipitation method and showed that the anode material with amorphous structure is capable of delivering high capacity compared to crystalline one.

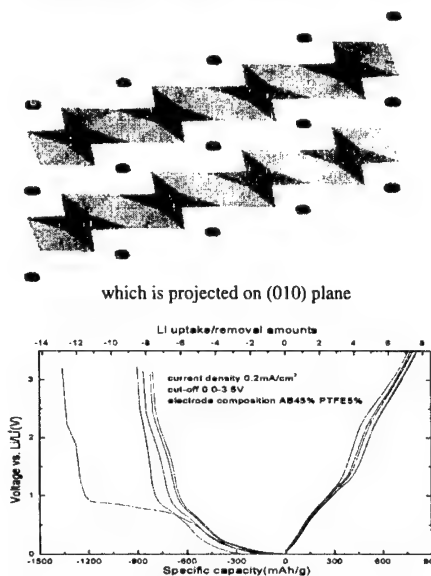
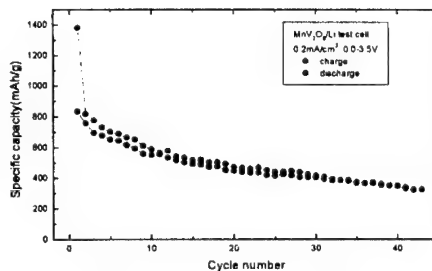
In this work, we report the synthesis of brannerite type crystalline MnV_2O_6 and its derivatives as anode material of lithium rechargeable battery via solution route using polymer resin as gelling agent which has advantage over solid state reaction³. The physical properties of above oxide are discussed and its electrochemical behavior as anode material has also been investigated.

In Fig. 1, the crystal structure of brannerite projected on (010) plane was presented. Kozłowski *et al.*⁴ had already prepared brannerite MnV_2O_6 to investigate its catalytic behavior. According to them, the brannerite structure composed of VO_6 octahedra which shares opposite corners forming chains running parallel to b-axis. The VO_6 octahedra in adjacent chains share the edges forming anion sheets parallel to (001) planes. Mn ions are situated between anionic sheets so that each Mn ion is coordinated by six O atoms arranged in a distorted octahedron. MnO_6 share edges forming chains paralleling the b-axis. These chains are not linked to each another. They provide a rather open structure between the VO_6 sheets.

The initial five charge-discharge pattern of MnV_2O_6 is depicted in Fig. 2. Note that the first charge profile is quite different from the rest of charge curves is indicative of the two different mechanism operating in the lithium insertion process. In order to understand the electrode process around this voltage region, XRD measurements were carried out for composite electrode. It is observed from the figure that the principal peaks appearing around $2\theta = 28^\circ$ ($\text{CuK}\alpha$) characteristics of brannerite crystalline MnV_2O_6 gradually decreases and at the end of the plateau at 0.7V, it disappeared completely. When the charged electrodes were discharged again, we could not observe recovery of crystalline peaks. From these, we assumed that irreversible transformation to amorphous lithiated material occurred only during the first lithium insertion stage into this structure. Fig.3 shows the cycling behavior of composite electrode under constant current density ($0.2\text{mA}/\text{cm}^2$) was tested between 0.0 and 3.5V over several tens of cycles. To improve the electrode

property including capacity retention and cycle property, Li and Mo were substituted with Mn and V, respectively. This substituted compounds ($\text{Li}_x\text{Mn}_{1-x}\text{V}_1-x\text{Mo}_x\text{O}_6$, $0 \leq x \leq 1$) were also identified as the same structure through XRD. The physical and electrochemical properties of these substituted materials will be presented.

Fig.1 Schematic diagram of Brannerite structure

Fig.2 Initial charge-discharge profile of $\text{MnV}_2\text{O}_6/\text{Li}$ cell.Fig.3 cycle behavior of $\text{MnV}_2\text{O}_6/\text{Li}$ cell.

References

1. S. Denis, E. Baudrin, M. Touboul and J.-M. Tarascon, *J. Electrochem. Soc.*, **144**, 4099 (1997)
2. E. Andrukaitis, *J. Power Sources*, **68**, 652 (1997)
3. Y. Piffard, F. Leroux, D. Guyomard, J.-L. Mansot and M. Tournoux, *ibid.*, **68**, 698 (1997)
4. E. Andrukaitis, J. P. Cooper and J. H. Smit, *ibid.*, **54**, 465 (1995)
5. F. Orsini, E. Baudrin, S. Denis, L. Dupont, M. Touboul, D. Guyomard, Y. Piffard and J.-M. Tarascon, *Solid State Ionics*, **107**, 123 (1998)
6. H.-J. Kwon, S. S. Kim, G. B. Kim and D. G. Park, *J. Mat. Sci. Lett.*, **17**, 1697 (1998)
7. R. Kozłowski, J. Ziokowski, K. Mocala and J. Haber, *J. Solid State Chem.*, **35**, 1 (1980)

**THERMALLY OXIDISED
GRAPHITES AS ANODES
FOR LITHIUM-ION CELLS**

T.Prem Kumar, A.Manuel Stephan,
V.Subramanian*, S.Gopukumar,
N.G.Renganathan, M.Raghavan and
N.Muniyandi #

Central Electrochemical Research
Institute, Karaikudi 630006, India.

increased number of sites for lithium
intercalation.

* Presenting author

Corresponding author

Abstract

Lithium intercalation and deintercalation processes occur through solid electrolyte interfaces on the zigzag and arm-chair faces of graphite. Such solid electrolyte interfaces are formed by reaction of surface groups on the graphite with lithium upon charging. The nature of this interface to a large extent determines the reversible and irreversible capacities of the graphite. We have investigated the influence of mild oxidation of samples of natural graphite exfoliated graphite and carbon nanotubes on the surface characteristics of the films formed on these materials upon lithium intercalation. These surface groups formed upon oxidation have been characterized using FTIR spectroscopy. The reversible and irreversible capacities of the thermally oxidised graphite samples are discussed in terms of the surface film composition as well as enhanced surface area that contributes to

X-RAY ABSORPTION STUDY OF COBALT VANADATES DURING CYCLING USABLE AS NEGATIVE ELECTRODE IN LITHIUM BATTERY.

S. Laruelle⁽¹⁾, P. Poizot⁽¹⁾, E. Baudrin⁽²⁾, V. Briois⁽³⁾, M. Touboul⁽¹⁾ and J.M. Tarascon⁽¹⁾

(1) LRCS, Université de Picardie and CNRS, 33 Rue St. Leu, F-80039, Amiens, France

(2) UCLA-SEAS, Department of Material Science and Engineering, 405 Hilgard Avenue, Los Angeles - CA - 90095, USA.

(3) LURE, Centre Universitaire Paris Sud - 91405 Orsay Cedex, France.

Vanadium-based oxides were reported to display attractive electrochemical properties vs. Li, such as uptake and removal of a large amount of lithium ions at low potential. Over the last few years, our group has devoted much effort towards the synthesis of a wide variety of either crystalline or amorphous divalent and trivalent element vanadates [1,2] containing occasionally structural water. Their electrochemical performances vs. Li were investigated, so as to screen the best material. Amongst them, numerous are those having an initial capacity as high as 1000 mAh/g. However, whatever their initial capacity, all of them exhibit a large capacity fading upon cycling, whose origin is not yet understood.

A possible clue to account for such a limited cycleability could arise from a better understanding of the relation between structure and electrochemical properties. Searching for such relation is complicated by the fact that these materials are becoming amorphous during the first discharge. So we are left with only a few techniques able to probe the structure of amorphous materials. One of them is the X-ray absorption spectroscopy (XAS). We then used this technique to characterize the structural and electronic modifications induced by cycling in a $\text{CoV}_2\text{O}_6/\text{Li}$ battery. The experiments have been performed at both vanadium and cobalt K edges using a plastic $\text{CoV}_2\text{O}_6/\text{Li}$ battery made according to Bellcore technology.

We monitored the evolution of the M-O ($\text{M}=\text{Co}$ and V) and M-M' ($\text{M}'=\text{Co}$ or V), distances and the electronic change within the CoV_2O_6 vanadate not only during the first discharge but through subsequent cycles. The first discharge voltage composition curve for CoV_2O_6 exhibits a first plateau at 2.4V and another one at 0.6 V having capacities of 2 and 2.5 lithiums, respectively, followed by a gradual voltage down to 0.02 V leading to a total Li uptake of 12.5 Li per formula units. XAS data were collected after each plateau and at the end of the discharge as well as on charge and discharge for the 10th cycle.

CoV_2O_6 consists of a 3-dimensional packing of CoO_6 chains and VO_5 bipyramids. The intense prepeak observed on the XANES spectrum (figure 1) is indicative of the vanadium fivefold coordination. As soon as the cell is discharged (e.g. upon Li uptake) we note a progressive vanishment of the prepeak implying an increase in the vanadium coordination symmetry that evolves from pyramidal to octahedral. Simultaneously, V-O distances are enhanced whereas V-M' ($\text{M}'=\text{V}$ or Co) are shortened once and then remain constant upon subsequent cycling. The Co-O and Co-M' distances exhibit the same behavior as the vanadium ones until the second plateau with therefore a drastic difference during the end of discharge (figure 2) with namely the decrease

in both distances and the appearance of an additional one around 2.45 Å. The XANES spectrum tends to prove that this distance corresponds to a metallic structural environment. During cycling the cobalt atom goes from this state, on discharge, to an oxide like environment on charge.

[1] S. Denis, E. Baudrin, M. Touboul, J.-M. Tarascon, J. Electrochem. Soc. 144 (1997) 4099.

[2] E. Baudrin, S. Laruelle, S. Denis, M. Touboul, J.-M. Tarascon, Solid state ionic 123 (1999) 139.

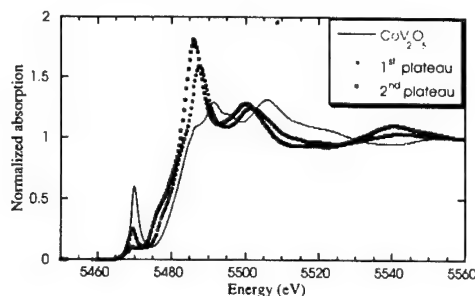


Figure 1: XANES spectra of vanadium K edge for various lithium content.

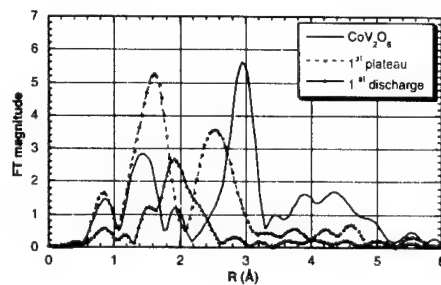


Figure 2: moduli of the cobalt K edge Fourier transform for various lithium content.

Reversible Li Uptake in Fe₃BO₆, a New Anode Material

J. Gaubicher, J. Rowsell and L.F. Nazar

Department of Chemistry, University of Waterloo,
Waterloo ON N2L 3G1, Canada

Recently, polyanion 3-D structures such as LiFePO₄ (olivine), some oxo-vanadates and NASICON-related frameworks built of (XO₄)ⁿ⁻ tetrahedra and MO₆ octahedra have engendered much interest (1-13). These structures have been shown to be promising hosts for the reversible insertion of lithium, as the Li insertion potential can be "tuned" by the adroit choice of X and M. Despite its low atomic weight, the investigation of boron as a polyanion (BO₃)ⁿ⁻ in these structures has not been reported to date. The present communication reports the investigation of a new class of materials for lithium batteries: the borates FeBO₃ and Fe₃BO₆. These two compounds are obtained by simple solid state reactions involving Fe₂O₃ and either B₂O₃ or H₃BO₃ at temperatures ranging from 670-800°C and 860-900°C for FeBO₃ and Fe₃BO₆ respectively. FeBO₃ crystallizes in the calcite structure, comprised of BO₃ and corner shared FeO₆ units (Fig.1). Above 800°C, FeBO₃ transforms to Fe₃BO₆, exhibiting the norbergite structure. The latter is similar to olivine, in that it has hcp packing of oxygen with both corner and edge shared FeO₆ octahedra and BO₄ tetrahedra (Fig.1), but it possesses a different ordering of the cations.

The first few cycles at 1Li/10h are shown on Figure 2 within a 3.1-0.8V potential window. Lithium uptake in both materials appears to correspond to reduction from Fe³⁺ to iron metal. In FeBO₃, the amorphous material that results on reduction exhibits cycling behavior characterized by a reversible phase transition at 1.6V. By contrast, Fe₃BO₆ shows a smooth decrease/increase of the potential corresponding to a single phase process that is centered at 1.25V. Accordingly, the average potential on oxidation is higher for FeBO₃ (2V) than for Fe₃BO₆ (1.6V). After the first cycle, this system shows a fairly good cyclability (Fig. 3) by comparison to that obtained for iron oxides such as α-Fe₂O₃. Since the reversible capacity for Fe₃BO₆ (480mAh/g) is much higher than that shown by FeBO₃ (260 mAh/g), our main interest resides in optimization of its electrochemical properties as an negative electrode material. As shown on Figure 3, the electrochemical performance of Fe₃BO₆ is better when H₃BO₃ is used rather than B₂O₃ as the iron precursor or when the depth of discharge is limited to 0.8V rather than 0.2V. In every case, the cyclability is much better, however, than that obtained for α-Fe₂O₃. In order to reduce the grain size, we have synthesized particles of Fe₃BO₆ (Ø<100 nm) from a freeze-dried precursor (α-Fe₂O₃) at temperatures as low as 600°C. These results will be discussed along with the electrochemical

behavior as a function of the potential window limits and the galvanostatic regime, as well as the influence of dopant ions (Al³⁺, V³⁺ and Mn³⁺) ions.

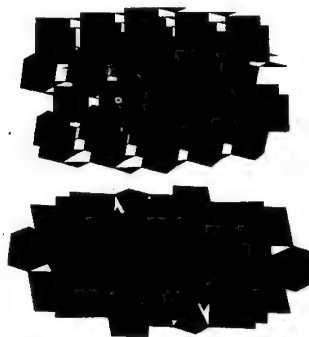


Fig. 1 : Crystal structures of calcite, FeBO₃ (top) and norbergite, Fe₃BO₆ (bottom).

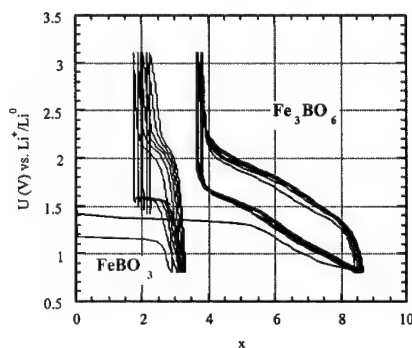


Fig. 2 Galvanostatic cycling of FeBO₃ and Fe₃BO₆ at 1Li/10h.

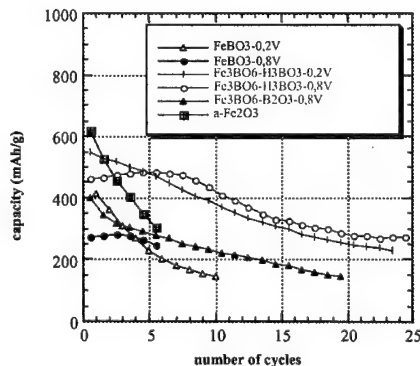


Fig. 3 Reversible capacity vs cycle number for iron borates and oxides at a 1Li/10h rate.

Structural and Mechanistic Features of Intermetallic Electrodes

J. T. Vaughey, C. S. Johnson, R. Benedek,
M. M. Thackeray
Electrochemical Technology Program
Chemical Technology Division
Argonne National Laboratory
Argonne, IL 60439, USA

and

L. Fransson, K. Edstrom, J. O. Thomas
Inorganic Chemistry, Angstrom Laboratory,
SE-751 21 Uppsala University, Sweden

State-of-the-art lithium-ion batteries commonly use graphite as the anode of choice. Although graphite works well, it delivers much of its capacity close to the potential of metallic lithium; therefore, safety concerns related to overcharging individual cells still persist and have warranted further research to find alternative anode materials. Recent research has included studies of tin oxide glass composite systems and intermetallic anodes that operate by a "matrix" effect in which a chemical breakdown of the initial anode structure occurs on lithiation, to create an "active" intermetallic phase within an "inactive" matrix. The inactive matrix absorbs some of the volume expansion usually associated with the lithiated intermetallic phase, thus aiding cycle life; however, many of these systems show unacceptably high irreversible capacity losses.

In our recent work, we have initiated investigations on a new class of mixed-metal intermetallic anode materials with NiAs- and zinc-blende-type structures [1,2]. We have found that lithium can react with the intermetallic anode to form ternary compounds without segregation of the metal components from their structures. In these structures, it is possible to substitute the metal atoms in the framework with others, thereby allowing the possibility of tailoring the electrochemical potential of the electrode.

We first studied the Li-Cu-Sn system because we noticed that there existed a crystallographic relationship between Cu_6Sn_5 and a lithiated copper-tin phase, Li_2CuSn ($\text{Li}_{10}\text{Cu}_5\text{Sn}_5$), in which the Cu:Sn ratio was close to that in Cu_6Sn_5 . The structures of Cu_6Sn_5 and Li_2CuSn are shown in Figures 1 and 2. The " $\text{Li}_2\text{Cu}_6\text{Sn}_5$ " system yields an electrochemical potential close to 400 mV vs. Li and delivers a capacity of approximately 200 mAh/g [1]. X-ray diffraction data and structural modeling provide evidence that lithium is initially inserted into the interstitial sites of the NiAs-type lattice; thereafter, a two-phase transformation takes place, during which the electrode transforms from the NiAs-type structure to a zinc blende (ZnS) type structure.

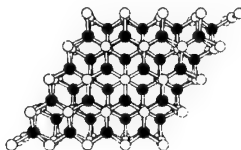


Figure 1. An (001) projection of the structure of Cu_6Sn_5

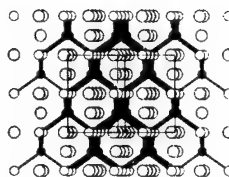


Figure 2. A (110) projection of the structure of Li_2CuSn .

Insights from structural observations on $\text{Li}_2\text{Cu}_6\text{Sn}_5$ prompted investigations of zinc-blende type structures, such as InSb, that show electrochemical properties superior to the NiAs-type structures [2]. In this presentation we will report on further structural features of these electrodes and on their reaction mechanisms, as gathered from X-ray diffraction, Mössbauer spectroscopy, and structural predictions from first principles calculations.

References

1. K. D. Kepler, J. T. Vaughey and M. M. Thackeray, *Electrochem. and Solid State Lett.*, **2** (7), 307 (1999).
2. J. T. Vaughey, J. O. O'Hara and M. M. Thackeray, *Electrochem. and Solid State Lett.*, **3** (1) 13 (2000).

Modified Carbons for Improved Anodes in Lithium Ion Cells

H. Buqa¹, P. Golob², M. Winter¹ and J. O. Besenhard¹

¹ Institute for Chemical Technology of Inorganic Materials, Graz University of Technology, Stremayrgasse 16, A-8010 Graz, Austria

² Institute for Electron Microscopy, Graz University of Technology, Steyrergasse 17, A-8010 Graz

Various research activities aim at the minimization of the irreversible losses of capacity associated with the formation of the SEI on carbon anodes. Basically the SEI can be described as film consisting of electrolyte decomposition products "plated" on the carbon surface. Apart from the well known effects of electrolyte variations on the SEI properties, recent works have been focussed also on the optimization of the anode performance by proper (surface) pre-treatment of the carbon material.

In this contribution we present results on graphitic carbons, which have been treated with different gases at elevated temperatures. We have used a special two-step pre-treatment procedure (Fig. 1), which allows a quite selective and systematic modification of the carbon surface. In the first step the surface groups of the pristine carbon prevalently containing oxygen-groups such as carboxyl- or hydroxyl-groups are removed at a certain temperature T_1 for a certain time t_1 ("outgassing"). Afterwards, the "cleaned" graphite surfaces, which can be anticipated to be highly reactive ("dangling bonds") are exposed to gases, such as O_2 , CO_2 , NH_3 , SO_2 , etc. ("gas treatment") at a temperature T_2 for a time t_2 . T_2 and t_2 may vary considerably from T_1 and t_1 . The separation of the outgassing step and the gas treatment step allows to change several treatment parameters independently from each other, and thus increases the chances for "tailoring" the carbon surface.

The carbon samples [for examination we were using graphite TIMREX® SFG 44 (TIMCAL AG)] were heated *in vacuo* or under Ar-atmosphere in an electric furnace (quartz tube) at various temperatures $T_1 = 1000^\circ\text{C}$ for $t_1 = 1\text{ h}$. Immediately afterwards the treated carbons were exposed to the gaseous reactants. Here we concentrate on O_2 - and CO_2 -treatment. (The gas treatment temperatures T_2 and treatment times t_2 are given in Table 1).

As a result from the treatment procedure, "new" carbon surfaces with different surface chemistry and morphology are formed, which also show different - in several cases improved - anode performance in the electrochemical experiments with comparison to the original (untreated) graphite (Table 1). Morphology changes have been determined with field resolution electron microscopy (F-REM). Even very mild treatments have caused some burn-off of carbon, in particular at the highly sensitive prismatic surfaces of the graphite. Graphites with roughened ("nanorough") prismatic surfaces show a significantly improved anode performance (cf. Table 1). Simple outgassing in Ar (without subsequent gas treatment) does not change the surface morphology very much and also does not improve the electrochemical performance.

XPS studies on the chemical composition of the surface of these graphite materials will be presented in a different paper at this meeting (see paper by R.I.R. Blyth et al.).

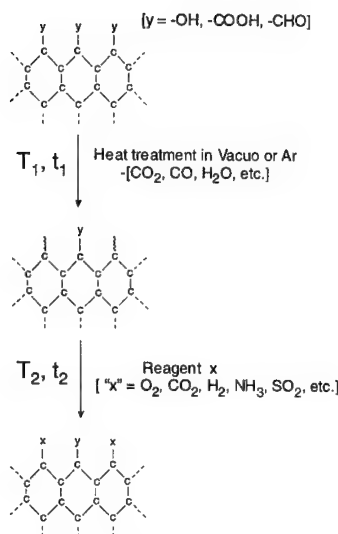


Fig. 1.: Two-step pre-treatment of carbon surfaces.

Table 1: Charge/discharge performance of TIMREX® SFG 44 (a) before and (b) after outgassing in Ar at 1000 °C, (c) after outgassing in Ar at 1000 °C and subsequent gas treatment with O₂ at T₂ = 420 °C for t₂ = 15 min, and (d) after outgassing in Ar at 1000 °C and subsequent treatment with CO₂ at T₂ = 1000 °C for t₂ = 15 min, i = ±20 mA g⁻¹, cut-off = 0.024/2.0 V vs. Li/Li⁺.

	cycle number	C _{discharge} / Ah kg ⁻¹	C _{charge} / Ah kg ⁻¹	efficiency/ %
(a)	1	339	406	83.1
	2	339	359	94.2
	3	340	356	95.4
	4	340	350	97.6
(b)	1	336	404	83.4
	2	336	357	94.5
	3	338	354	95.5
	4	340	351	97.4
(c)	1	344	401	88.3
	2	349	368	96.6
	3	352	362	97.3
	4	349	357	98.1
(d)	1	349	405	88.7
	2	351	362	97.1
	3	349	358	97.5
	4	349	354	98.9

- [1] H. Buqa, M. Winter, B. Evers, R. Blyth, M. Ramsey, F. Netzer, and J. O. Besenhard, *GDCb-Monographie*, 12, 619 (1998)
- [2] M. Winter, H. Buqa, B. Evers, T. Hodal, K.-C. Möller, C. Reisinger, M. V. Santis Alvarez, I. Schneider, G. H. Wrodnigg, F. P. Netzer, R. I. R. Blyth, M. G. Ramsey, P. Golob, F. Hofer, C. Grogger, W. Kern, R. Saf and J. O. Besenhard, *ITE Batt. Lett.* 1(2), 129 (1999)

Work has been supported by the Austrian Science Funds in the „Electroactive Materials“ special research program. We thank the Timal group (Bodio, Switzerland) and Merck (Darmstadt, Germany) for the donation of samples used in this study.

**Surface Modification of Graphite Anodes by
Combination of High Temperature Gas-Treatment
and Silylation in Nonaqueous Solution**

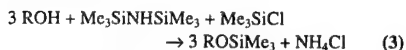
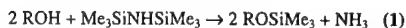
M. V. Santis Alvarez¹, H. Buqa¹, Ch. Grogger¹,
J. O. Besenhard¹, and M. Winter¹

¹ Institute for Chemical Technology of Inorganic
Materials, Graz University of Technology,
Stremayrgasse 16, A-8010 Graz, Austria,

² Institute for Inorganic Chemistry, Graz University of
Technology, A-8010 Graz, Austria

The surface of graphite is characterized by several parameters, such as surface area, chemical composition [surface groups (-COH, -COOH, etc.)], surface morphology, etc. Appropriate surface modification of graphitic carbons is a useful measure to improve the carbon anode performance in the lithium ion battery. We developed a two-step gas-treatment procedure, which allows to modify the above carbon surface parameters quite selectively. The process involves a "pre-cleaning" step in inert Ar atmosphere at elevated temperatures, in which the original surface groups are (partially) removed. Then, the cleaned carbon surfaces are exposed to (reactive) gaseous partners, e.g., O₂, CO₂, etc. at a certain temperature and for a certain time (see [1] and paper by H. Buqa et al. at this meeting).

We studied the effect of chemical surface modification of graphites with silanes in nonaqueous solution on the anode performance. By way of example, here we show results on TIMREX[®] SFG 44 graphites. For silylation we used the procedure reported in ref. [2], employing a 10/1 (by volume) mixture of hexamethyldisilazane (HMDS) and trimethyl chlorosilane (TMCS). The HMDS reacts with hydroxyl-containing surface-groups of the graphite material (hereafter abbreviated to ROH) whereby ammonia is eliminated (equation 1). The addition of the effective silyl donor TMCS increases the degree of silylation (equation 2). Hence, apart from the silylated surface group (ROSiMe₃) the complete reaction (equation 3) yields NH₄Cl as further product.



Whereas the silylation of the pristine (untreated) graphite (Table 1a and 1b) causes no significant change in the discharge capacities and the discharge/charge efficiencies, silylation after long-term pre-oxidation in oxygen considerably improves the efficiencies, not only in the first but also in the later cycles (Table 1d). This is evidently not due to the pre-oxidation step, which yields even worse performance compared to the untreated graphite, both with respect to discharge capacities and with respect to efficiencies (Table 1a and 1c). For an optimum anode performance the oxidative pre-treatment and the silylation procedure have to be carefully coordinated with respect to each other.

The improved or worsened anode performance might be due to the change (i) of the surface chemistry, (ii) of the surface area and morphology, and/or (iii) of the wettability of the samples with electrolyte (the silylated surfaces are highly lyophobic). One might also speculate that the silylated surfaces offer more favorable anchoring sites for the solid electrolyte interphase film.

In this contribution, the influence (i) of different gas pre-treatment according to the above concept, (ii) of different silylation procedures, e.g., by changing the silanes and (iii) of different carbon materials, e.g., changing from "standard" synthetic graphite powder to expanded graphites will be discussed. Finally, aqueous oxidative pre-treatments, e.g., in aqueous HNO₃, will be compared with the oxidative gas pre-treatments.

Table 1: Charge/discharge performance of TIMREX[®] SFG 44 synthetic graphite: (a) untreated, (b) untreated and silylated, (c) after outgassing in Ar and subsequent treatment with O₂ at 420 °C for 60 h, and (d) after outgassing in Ar, treatment with O₂ at 420 °C for 60 h and silylation. $i = \pm 20 \text{ mA g}^{-1}$, cut-off = 0.024/2.00 V vs. Li/Li⁺.

	cycle number	C _{discharge} / Ah kg ⁻¹	C _{charge} / Ah kg ⁻¹	efficiency/ %
(a)	1	339	406	83.1
	2	339	359	94.2
	3	340	356	95.4
	4	340	350	97.6
(b)	1	338	403	83.4
	2	338	357	94.0
	3	341	357	95.1
	4	341	352	97.2
(c)	1	323	397	80.1
	2	320	352	91.0
	3	320	346	94.0
	4	318	340	94.6
(d)	1	336	378	89.2
	2	340	350	97.1
	3	341	350	97.4
	4	338	346	97.6

[1] M. Winter, H. Buqa, B. Evers, T. Hodal, K.-C. Möller, C. Reisinger, M. V. Santis Alvarez, I. Schneider, G. H. Wroldnig, F. P. Netzer, R. I. R. Blyth, M. G. Ramsey, P. Golob, F. Hofer, C. Grogger, W. Kern, R. Saf and J. O. Besenhard, *ITE Batt. Lett.* 1(2), 129 (1999)

[2] A.E Pierce, *Silylation of Organic Compounds*, Pierce Chemical Co., Illinois (USA) 1968, p. 19

This work has been supported by the Austrian Science Funds in the "Electroactive Materials" special research program. We thank the Timcal group (Bodio, Switzerland) and Merck (Darmstadt, Germany) for the donation of samples used in this study.

EFFECTS OF SYNTHESIS CONDITION OF GRAPHITIC CARBON TUBE ON ANODIC PROPERTY OF Li ION BATTERY.

Tatsumi Ishihara, Akihiro Kawahara, Hiroyasu Nishiguchi, Masaki Yoshio¹⁾, and Yusaku Takita

Department of Applied Chemistry,
Faculty of Engineering, Oita University, Dannoharu 700,
Oita 870-1192, Japan

¹⁾Department of Chemical Engineering, Faculty of Science
and Engineering,
Saga University, Honjyou, Saga, Japan

Lithium-ion rechargeable battery incorporates a lithiated metal oxide (typically LiCoO_2) as the positive electrode, carbonous materials as the negative electrode, and an organic lithium-ion conducting electrolyte (1). Various type of carbon has been investigated extensively as the anode. Among them, carbon nanotube is attracting a much attention because of its high capacity. In the previous study, the authors investigated the Li intercalation capacity of carbon tubes obtained by CH_4 decomposition with Ni catalyst (2). It was found that carbon tube obtained by CH_4 decomposition exhibited a large capacity for Li intercalation, which is higher than 200 mAh/g. However, the relationship between Li intercalation capacity and synthesis condition is not thoroughly made clear.

Carbon tube was synthesized by using a conventional fixed bed reactor. Ni catalyst was always used as a catalyst for CH_4 decomposition. After reaction, Ni was separated from carbon tube by dissolving with HF acid solution. Li intercalation capacity was measured with applying a constant current of 0.4 mA/cm². Li metal was always used as a counter electrode. Organic electrolyte of EC:DMC=1:2 was always used for electrolyte.

XRD pattern of the obtained carbon tube was always the typical diffraction pattern from graphitic carbon. Therefore, the large part of the obtained carbon was graphitic carbon, although the decomposition temperature of CH_4 was as low as 673 K. Observation with TEM confirmed that the obtained graphite was tubular of which average diameter was 20 nm and thickness of wall was around 5 nm. It was found that the size and crystallization of tubular carbon was strongly dependent on the synthesis condition, in particular, reaction temperature and contact time of CH_4 . The capacity for Li intercalation increased with increasing the decomposition temperature and it attained the maximum at 973 K. Therefore, the optimum reaction temperature for CH_4 decomposition seems to exist at 973 K.

Figure 1 shows the initial and reversible capacity for Li intercalation as a function of contact time of CH_4 on Ni catalyst. It is clear that both initial and reversible capacity increased with increasing contact time and it attained to a constant value at W/F larger than 100 g-cat.h/mol. In Raman spectroscopy, two absorption peaks at around 1350 and 1570 cm⁻¹, which could be assigned to amorphous and graphitic carbon respectively, were observed. Since the intensity ratio of these two peaks, I_{1350}/I_{1570} , decreased with increasing contact time, the content of graphitic carbon seems to be improved by increasing contact time. Therefore, it seems likely that the formation rate of graphitic carbon was rather slow and it is expected that the formation of amorphous carbon can be suppressed at a slow feed rate of CH_4 . Consequently, the capacity for Li intercalation increased with increasing constant time of CH_4 . The initial and reversible capacity for Li intercalation

were attained to a value of 430 and 320 mAh/g, respectively at the contact time higher than 100 g-cat.h/mol.

The cycle stability of the carbon tube obtained at W/F=400 g-cat.h/mol was further measured. Figure 2 shows the capacity for Li intercalation as a function of cycle number. Although the large irreversible capacity was observed at first cycle, coulomb efficiency was always almost 100 % after second cycles. Both intercalation and de-intercalation capacity decreased gradually with increasing the cycle number. However, after 50 cycles, the intercalation capacity of 270 mAh/g was still sustained. Therefore, it can be said that the carbon tube obtained by CH_4 decomposition is attractive as the anode for Li rechargeable battery.

Refencies

- 1) J.R.Owen, Chemical Society Review, **26**, 259 (1997).
- 2) T. Ishihara, A.Fukunaga, R. Akiyoshi, M. Yoshio, and Y. Takita, Electrochemistry, **68**, 38 (2000).

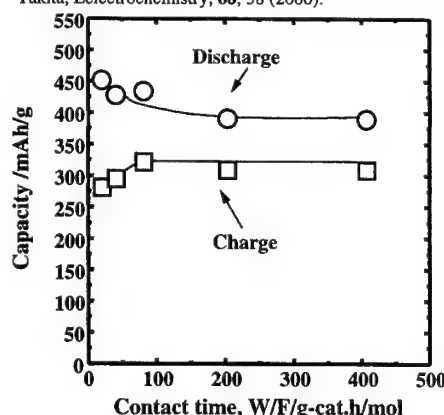
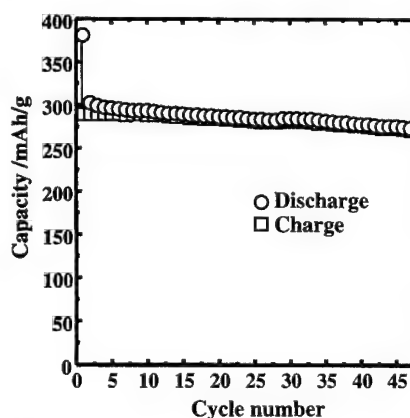


Fig.1 Charge and discharge capacity for Li intercalation as a function of contact time of CH_4 on Ni catalyst during



preparation.

Fig.2 Capacity for Li intercalation into graphitic carbon tubes as a function of cycle number.

ANODIC PROPERTY OF GRAPHITIC CARBON NANOTUBE IN α -PROPYLENE CARBONATE BASED ORGANIC ELECTROLYTE

Akihiro Kawahara, Tatsumi Ishihara, Hiroyasu Nishiguchi, Masaki Yoshio¹⁾, and Yusaku Takita

Department of Applied Chemistry,
Faculty of Engineering, Oita University, Dannoharu 700,
Oita 870-1192, Japan

¹⁾Department of Chemical Engineering, Faculty of Science
and Engineering,
Saga University, Honjyou, Saga, Japan

Li ion rechargeable battery is currently absorbing a much interest as an electric source for mobile electric equipment. At present, Li rechargeable battery uses an organic lithium-ion conducting electrolyte, mainly, ethylene carbonate-dimethyl carbonate (EC-DMC) dissolving LiPF_6 . This electrolyte exhibits a high electrical conductivity at high temperature. However, application of propylene carbonate based system for electrolyte has an advantage in improving the performance of the Li ion battery at low temperature. However, propylene carbonate is easily decomposed on carbon anode so that the irreversible capacity became large when propylene carbonate based system is used for electrolyte (1). In the present study, the authors investigated the anodic performance of graphitic carbon nanotube in propylene carbonate based electrolyte.

It is well-known that larger surface area of carbon anode easier decomposes electrolyte and accelerates the formation of so-called "SEI (Solid Electrolyte Interface)". Therefore, the irreversibility capacity for Li intercalation became larger with increasing surface area of carbon anode. On the other hand, in spite of a fairly large surface area like $30 \text{ m}^2/\text{g}$, graphitic carbon nanotube obtained by the decomposition of CH_4 on Ni catalysts exhibits a large capacity for Li intercalation of ca. 300 mAh/g (2). Consequently, it is anticipated that the graphitic carbon nanotube obtained by decomposition of CH_4 is usable for the anode of Li ion battery utilizing propylene carbonate based electrolyte.

Carbon tube was synthesized by using a conventional fixed bed reactor at 973 K . Ni catalyst was always used as a catalyst for CH_4 decomposition. After reaction, Ni was separated from carbon nanotube by dissolving with HNO_3 acid solution. Li intercalation capacity was measured with applying a constant current of $0.4 \text{ mA}/\text{cm}^2$. Li metal was always used as a counter electrode.

Figure 1 shows the charge-discharge curves of the carbon nanotube in propylene carbonate (PC)-dimethyl carbonate (DMC) electrolyte system. In similar manner with the bulk graphitic carbon, decomposition of electrolyte was observed and it became significant with increasing the content of propylene carbonate. At the propylene carbonate content higher than 30 vol%, large plateau in charge-discharge curve, which might correspond to the decomposition of electrolyte, was observed at 0.5 V . However, at the content of propylene carbonate of 25 vol%, there is no significant peak observed at 0.5 V . In addition, capacity for Li intercalation and de-intercalation were 402 and 284 mAh/g , respectively. Therefore, it can be said that PC-DMC system can be used as electrolyte if the content of PC was smaller than 25 vol%.

Figure 2 shows the cycle stability of Li intercalation capacity of graphitic carbon in PC-DMC(1:3) electrolyte. It is clear that the fairly large capacity for Li intercalation was stably exhibited after 40 charge and discharge cycles. Although a large irreversible capacity was observed at the first cycle, almost 100 % coulomb efficiency was always exhibited in the following cycles. Therefore, after SEI formation at the initial few cycles, intercalation of Li into graphitic carbon tube was highly reversible even in PC based electrolyte.

This study revealed that graphitic carbon tube obtained by decomposition of CH_4 exhibits a large capacity for reversible Li intercalation in PC based electrolyte if the content of PC is smaller than 25 %.

References

- 1) C. Wang, H. Nakamura, H. Komatsu, H. Noguchi, M. Yoshio, and H. Yoshitake, *Denki Kagaku* **66**, 286 (1998).
- 2) T. Ishihara, A. Fukunaga, R. Akiyoshi, M. Yoshio, and Y. Takita, *Electrochemistry*, **68**, 38 (2000).

Fig.1 Charge-discharge curves of the carbon nanotube in propylene carbonate (PC)-dimethyl carbonate (DMC) electrolyte system.

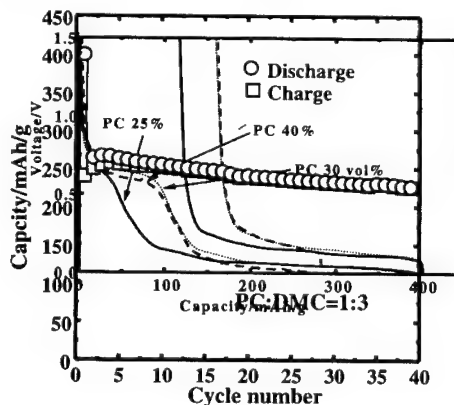


Fig.2 Cycle stability of Li intercalation capacity of graphitic carbon in PC-DMC(1:3) electrolyte.

Improved Rate Performance of Active Materials Coated on Surface-Modified Carbon Black

H. Huang, J. Gaubicher and L. F. Nazar*

Chemistry Department, University of Waterloo
Waterloo, Ontario, Canada, N2L 3G1

To achieve high charge/discharge currents without significant loss of capacity is a significant challenge for many lithium or lithium-ion battery electrodes [1]. This is particularly a problem for materials that are poor electronic or ionic conductors, such as V_2O_5 , and many materials that fall into the new class of "polyanionic" structures such as $LiFePO_4$ or $VOPO_4$.

In an attempt to address the above problem, we have developed a nanostructured composite which is based on the coating of the active materials on functionalized carbon black. In this composite, the incorporated carbon supports the thin layer of surface-coated active material. The functional coating acts to bind the active material to the surface and provide good contact. We have applied this approach to several active materials.

As proof-of-concept, we have first investigated V_2O_5 coated-functionalized carbon black as the cathode in a lithium battery. V_2O_5 is a well-known cathode material that has somewhat limited conductivity. The composite was prepared using a sol-gel method [2] to coat the V_2O_5 on the functionalized carbon black ($V_2O_5@C_F$), to give a composite 18 wt% in carbon. For comparison, we also coated V_2O_5 on unfunctionalized carbon black ($V_2O_5@C$).

Fig. 1 shows the first cycles of V_2O_5 xerogel, $V_2O_5@C$, and $V_2O_5@C_F$. V_2O_5 gel yielded an initial capacity of 185 mAh/g, and very significant irreversibility (~15%). $V_2O_5@C$ showed a significant improvement of capacity (240 mAh/g) and a decrease of the irreversible component (~9%). The best results were obtained for $V_2O_5@C_F$, with a capacity of 320 mAh/g and negligible irreversibility.

Capacities vs. current densities for the three samples are shown in Fig. 2. The capacity of V_2O_5 gel decreased rapidly upon increasing the current density; for example, a capacity of only ~30 mAh/g was available at a rate of 500 mA/g (~3.5C). The nanostructured composite, however, can sustain a 200-fold increase in the current density while maintaining almost the same capacity as the initial capacity of V_2O_5 xerogel. Thus, $V_2O_5@C_F$ at a current of 2000 mA/g (~14C) yields a capacity of 190 mAh/g. This new nanostructured composite is very suitable for high current (power) applications.

Cycling behavior of the materials are illustrated in Fig. 3. After 100 cycles, 68% of the initial capacity was maintained for V_2O_5 gel. $V_2O_5@C$ showed improved cycling stability (82% after 100 cycles). $V_2O_5@C_F$ possesses excellent stability with less than 10% capacity loss after 100 cycles.

In conclusion, the nanostructured composite can sustain much higher capacities, with better stability, at significantly higher rates than V_2O_5 xerogel. The applications of this method to potentially useful cathode materials which are limited by very low conductivity such as $VOPO_4$ will also be discussed.

References

- [1] Brodd R. J. *The Electrochem. Soc. Interface*, 8(3): 20-23 (1999)

[2] Livage J. *Solid State Ionics*, 50, 307 (1992)

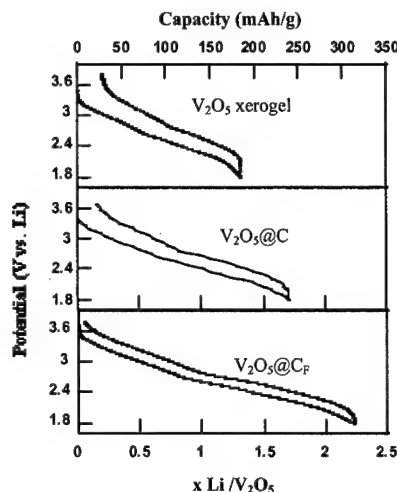


Fig. 1 First discharge/charge sweep for V_2O_5 xerogel, $V_2O_5@C$, and $V_2O_5@C_F$ (10 mA/g; 3.8-1.8 V)

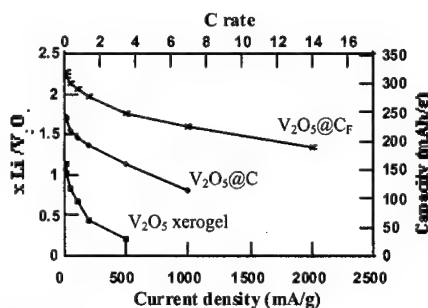


Fig. 2 Capacity vs. current density for V_2O_5 xerogel, $V_2O_5@C$, and $V_2O_5@C_F$

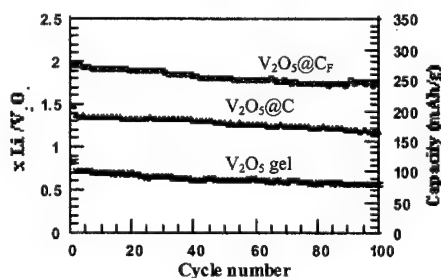


Fig. 3 Cycling stability of V_2O_5 xerogel (100 mA/g), $V_2O_5@C$ (200 mA/g), and $V_2O_5@C_F$ (200 mA/g)

Electrochemistry and Impedance Analysis of Intermetallic Electrodes for Lithium-Ion Batteries

C. S. Johnson, J. T. Vaughey, D. W. Dees,
A. N. Jansen and M. M. Thackeray,
Electrochemical Technology Program,
Chemical Technology Division,
Argonne National Laboratory
Argonne, IL 60439, USA

and
T. Sarakonsri and S. A. Hackney
Department of Metallurgical and Materials Engineering,
Michigan Technological University
Houghton, MI 49931, USA

Intermetallic compounds such as η' - Cu_3Sn and InSb that have NiAs and ZnS (zinc blende) structure types, respectively, exhibit promising electrochemical properties as anodes for lithium-ion batteries [1,2]. These materials provide, in practice, moderate gravimetric capacities (200-300 mAh/g) that translate into large volumetric capacities (>1000mAh/ml) because of their high densities. Our studies of η' - Cu_3Sn show that the NiAs-type structure acts initially as a host for lithium, but that during lithium insertion, one-half of the tin atoms are displaced in a topotactic (two-phase) reaction to yield a Li_2CuSn -type structure in which the copper and tin atoms adopt a zinc-blende configuration [1]. Further lithiation causes a breakdown of the Li_2CuSn structure into Cu and lithiated Sn, Li_xSn ($0 < x < 4.4$). By contrast, our preliminary work on InSb has indicated that the zinc-blende framework, which contains a three-dimensional space for lithium, remains essentially intact on lithiation to an approximate composition Li_xInSb [2]. Thereafter, In is extruded from the lattice to provide a $\text{Li}_{2x}\text{In}_{1-x}\text{Sb}$ phase that reaches the composition Li_2Sb at $x=1$. The cubic unit cell of InSb expands by only 5.6% on full lithiation to Li_2Sb .

We have compared the differences in electrochemical behavior of intermetallic electrodes based on NiAs and zinc-blende type structures. Our studies have included analyses of rate capability, impedance and elevated temperature operation. For example, Figure 1 shows the typical cyclic voltammograms (CV's) of η' - Cu_3Sn (----) and InSb (—) electrodes obtained from separate Li cells. It is immediately clear from the large peak separation in the CV data (----) that the reaction kinetics associated with Li extraction from the η' - Li_2CuSn electrode (Li_2CuSn -type structure) are substantially inferior to Li extraction from the Li_xInSb electrode. The cycling voltage hysteresis in the copper-tin system can be attributed to the displacement of the tin atoms during the phase transition from the lithiated zinc-blende-type structure to the NiAs-type structure. By contrast, the Li_xInSb maintains its zinc-blende framework upon Li insertion and extraction, at least over the range $0 \leq x < 2$.

The impedance of $\text{Li/Cu}_3\text{Sn}$ and Li/InSb cells is lowered markedly after the initial reaction with lithium and on further cycling. This improvement is believed to be attributed to two factors: 1) a break-up of the electrode structures, particularly at high lithium loadings and the generation of finely divided metal particles (e.g., Cu, In) in the cycled electrodes, and 2) an increase in the electronic conductivity of the intermetallic electrode as more lithium, and hence electrons, are added to the structures. The improvement in cell impedance is clearly evident in the Nyquist plots for a delithiated electrode (Li_xInSb ; $0 < x \leq 1$) obtained at 1.2 V, compared to a lithiated $\text{Li}_{2x}\text{In}_{1-x}\text{Sb}$ electrode obtained at 0.2 V. Results

show that in the lithiated electrode the interfacial charge transfer resistance is approximately six-times lower than in the delithiated electrode and that the Li diffusion is 4 to 5-times higher.

In particular, InSb electrodes show a remarkable rate capability due to their good electrical properties. These electrodes can easily deliver >250 mAh/g or >1400 mAh/cc at a current density of 2.4 mA/cm² with excellent coulombic efficiency.

Acknowledgment

This work was performed under the auspices of the U.S. Department of Energy, Office of Basic Energy Sciences; Division of Chemical Sciences, under Contract No. W-31-109-ENG-38.

References

1. K. D. Kepler, J. T. Vaughey and M. M. Thackeray, *Electrochem. and Solid State Lett.*, **2** (7), 307 (1999).
2. J. T. Vaughey, J. O. O'Hara and M. M. Thackeray, *Electrochem. and Solid State Lett.*, **3** (1) 13 (2000).

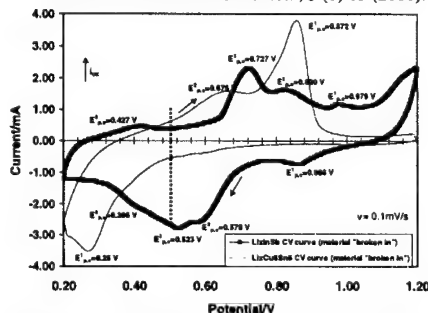


Figure 1. CV of η' - $\text{Li}_2\text{Cu}_3\text{Sn}$ and Li_xInSb type electrodes in lithium cells.

Benchmark Study on High Performing Carbon Anode Materials C. Lampe-Onnerud, J. Shi, B. Barnett, P. Onnerud Arthur D. Little, Inc. Acorn Park, Cambridge, MA 02140, USA As lithium-ion batteries are dominating the portable power industry for laptop computers and mobile telephones today, there is a renewed interest in refining the basic chemistry and process parameters in order to bring new and improved products to the market place. We believe that there are opportunities for major gains in capacity and high rate capability in the near future. Major improvements need to come from both a systems perspective, in which both active materials properties and advanced process knowledge are utilized, and from an in-depth knowledge on properties that define performance on a component level. This presentation will focus on the active carbon anode material and its dependence on formulation. In assessing the active carbon material, several properties need to be considered as they define many of the key performance attributes of the lithium-ion battery. The surface termination and morphology of the active material play crucial roles, both in selecting other battery components and in determining the extent of improvements that subsequent processing can allow. For example, identical slurries of active material, carbon additive, binder, and solvent system, may yield quite different results as the coating parameters are varied. The performance is greatly dependent on slurry formulations and coating processes. Each graphite material therefore has to be optimized with regards to slurry composition and processing settings in manufacturing and a wide range of parameters have to be considered in this optimization. The ratio between the active carbon and binder/conductive carbon compositions is not only critical to the battery performance but also to the utilization of the active material. We are reporting new results that show some of the complexity in making high-quality electrodes and will include results based on several types of graphite materials ranging from mesophase carbon fibers, carbon microbeads (MCMB), and graphite flakes.

Effects of SEI on the Kinetics of Lithium Intercalation

B. V. Ratnakumar, M. C. Smart and S. Surampudi
Electrochemical Technologies Group
Jet Propulsion Laboratory
4800 Oak Grove Dr., Pasadena, CA 91109

The successful operation of Li-ion cells is attributed mainly to the surface films on carbonaceous anode materials. These films provide the much-needed kinetic stability to the electrolyte species even at the thermodynamically reducing anode potential. Unlike the passive films on valve metals or in primary Li cells, the anode films in Li ion cells have moderate ionic conductivity and hence termed solid electrolyte interface.

Understandably, the performance of the anode is dictated largely by the characteristics of SEI, i.e., its resistance, ability to prevent further electrolyte reduction, amenability to charge transfer or Li intercalation process and to some extent the diffusivity of Li^+ ions, even though it is difficult to distinguish the slow diffusion across the SEI from the slow diffusional process within the bulk anode. The corresponding performance characteristics of Li-ion cells that would be affected by the SEI include cycle life, self-discharge, rate capability and low temperature. The characteristics of the SEI depend on several factors such as the nature of the carbonaceous material and electrolyte, temperature and mode of forming the SEI (rate and temperature).

Our recent research studies at JPL, have focussed on enhancing the low temperature performance of Li-ion cells, by a judicious selection of electrolyte, especially the solvent mixture. The characteristics of the SEI in the selected-solvent solutions have been determined in three-electrode cells by a variety of electrochemical techniques, such as ac impedance, DC micro polarization and Tafel polarization at various temperatures. These measurements have been supported by charge-discharge measurements at different temperatures and rates. For enhancing the low temperature performance, we have adopted the approach of initially optimizing the carbonate-based electrolytes, e.g., equi-proportion mixture of ethylene carbonate, dimethyl carbonate and diethyl carbonate¹ for achieving the desired SEI and later the use of quaternary additives, e.g., aliphatic esters such as methyl acetate, ethyl acetate, ethyl propionate and ethyl butyrate that have relatively poor filming properties, especially with low molecular weight esters and yet form highly conducting solutions at low temperatures (Fig. 1).² Also, we have used electrolyte additives, e.g., pyrocarbonates (Fig. 2),³ that would enable the formation of suitable SEI. In all these studies, we have found that the interfacial properties are more critical than bulk ion migration processes in the electrolyte at low temperatures.

Acknowledgments

This work was performed by JPL, California Institute of Technology, under a contract with the National Aeronautics and Space Administration and supported by NASA Code AE Battery and DARPA sponsored-SAFT TRP programs.

References

1. M. C. Smart, B. V. Ratnakumar, and S. Surampudi, *J. Electrochem. Soc.*, **146**, 486 (1999).
2. M. C. Smart, B. V. Ratnakumar, S. Greenbaum and S. Surampudi, *Proc. 194th Meeting of Electrochem. Soc.*, **98-2**, Boston, MA, Nov. 1-6, 1998.
3. M. C. Smart, B. V. Ratnakumar, and S. Surampudi, *196th ECS Meeting*, Honolulu, HI, Oct. 17-24, 1999.

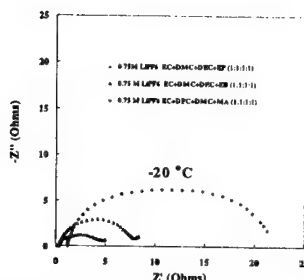


Fig. 1: EIS plots of graphite anode in solutions containing esters as quaternary solvent additive at -20°C .

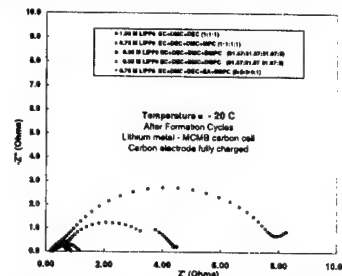


Fig. 2: EIS plots of graphite anode in solutions containing pyrocarbonate additives, dimethyl and dibutyl pyrocarbonates at -20°C .

In Situ AFM Observation of Lithium Deposition at Elevated TemperaturesRyo Mogi, Minoru Inaba, Takeshi Abe,
and Zempachi OgumiDepartment of Energy and Hydrocarbon Chemistry,
Graduate School of Engineering, Kyoto University
Sakyo-ku, Kyoto-606-8501, Japan**Introduction**

Lithium metal is the most attractive material for the negative electrode in rechargeable lithium batteries because of its high energy density; however, the low cycling efficiency and the safety problems owing to its dendrite formation prevents its use in commercially available cells. Many researchers have so far studied the surface morphology of deposited lithium and the protecting surface film in various electrolyte systems. Scanning electron microscopy (SEM) has been mainly used for this purpose; however, the deposited lithium is so reactive that the surface morphology may be changed during washing residual electrolyte solution and transferring the sample to the sample chamber of SEM. Atomic force microscopy (AFM) enables us to observe surface morphology *in situ* in liquid, and began to be used to observe lithium deposition in organic electrolyte solutions.¹⁻³⁾ In the present study, we observed the morphology of lithium deposited on nickel substrate in polyether electrolyte solution at elevated temperatures by *in situ* AFM. The morphology of the deposits at elevated temperatures was compared with that at room temperature, aiming at the use in dry polymer batteries at elevated temperatures.

Experimental

In situ AFM images were obtained with a PicoSPM system (Molecular Imaging). The working electrode was mirror-polished nickel plate, and lithium was deposited at constant currents. The electrolyte solution was a mixture of poly(ethylene glycol) dimethyl ether (PEGDM) and lithium bis(perfluoroethylsulfonyl)imide (LiBETI, $\text{LiN}(\text{C}_2\text{F}_5\text{SO}_2)_2$) with a ratio O/Li = 25. The counter and reference electrodes were lithium metal. The cell was set on a heating sample stage, and its temperature was controlled with a temperature controller. All experiments were carried out in an argon-filled glove box with a dew point lower than -60°C .

Results and Discussion

First we observed lithium deposition at 0.5 mA cm^{-2} at room temperature. Fine particles of lithium appeared after deposited by 0.09 C cm^{-2} , and the number of the particles increased with an elapse of time. At 0.12 C cm^{-2} , the whole surface was covered completely with the particles. Figure 1 shows AFM images obtained after deposited by 0.3 C cm^{-2} . The surface was covered with fine particles with relatively uniform particles 200-300 nm in diameter.

After lithium was deposited by 0.3 C cm^{-2} at room temperature, the temperature of the cell was elevated stepwise and the morphology changes were observed. At 70°C , the shape of the deposited particles began to change, and the shape of the particles partly became obscure at 80°C as shown in Fig. 2.

Figure 3 shows AFM images after deposited by 0.3 C cm^{-2} when lithium was deposited at 0.5 mA cm^{-2} at 80°C . The particle size was larger than that deposited at

room temperature, and the crevices between the large particles seemed to be filled with lithium metal. At elevated temperatures, surface diffusion of lithium is promoted, which may have resulted in the observed changes of the morphology of lithium deposit.

References

- 1) D. Aurbach and Y. Cohen, *J. Electrochem. Soc.*, **144**, 3355 (1997).
- 2) S. Shiraishi and K. Kanamura, *Langmuir*, **14**, 7082 (1998).
- 3) K. Morigaki and A. Ohta, *J. Power Sources*, **76**, 159 (1998).

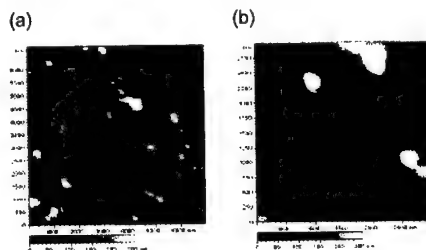


Fig. 1. AFM images of lithium deposited on Ni (0.3 C cm^{-2}) in LiBETI/PEGDM at room temperature. (a) $7 \mu\text{m} \times 7 \mu\text{m}$. (b) $3 \mu\text{m} \times 3 \mu\text{m}$.

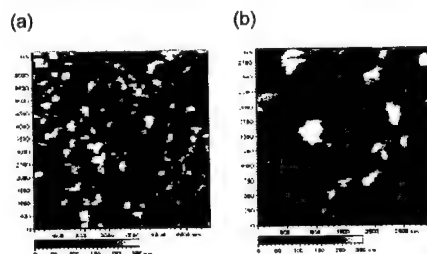


Fig. 2. AFM images of lithium deposited on Ni (0.3 C cm^{-2}) in LiBETI/PEGDM at room temperature, followed by heated at 80°C . (a) $7 \mu\text{m} \times 7 \mu\text{m}$. (b) $3 \mu\text{m} \times 3 \mu\text{m}$.

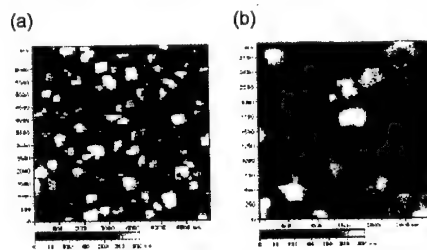


Fig. 3. AFM images of lithium deposited on Ni (0.3 C cm^{-2}) in LiBETI/PEGDM at 80°C . (a) $7 \mu\text{m} \times 7 \mu\text{m}$. (b) $3 \mu\text{m} \times 3 \mu\text{m}$.

BORONATED MESOPHASE PITCH COKE FOR LITHIUM INSERTION

*E. FRACKOWIAK, *J. MACHNIKOWSKI, F. BEGUIN

*Poznan University of Technology, ul. Piotrowo 3, 60-965 Poznan, Poland

*Technical University, ul. Gdanska 7/9, 50-344 Wroclaw, Poland

CRMD-CNRS-University, 1B rue de la Férollerie, 45071 Orléans, France

Introduction

The electrochemical insertion of lithium into non-boronated mesocarbon microbeads (MCMB) has been already studied [1]. The promising results encouraged us to the further modification of the mesophase carbon by boron as heteroatom.

Boron as a substitutional element in the carbon matrix facilitates graphitization, improves the oxidation resistance of carbon, the mechanical stability and the thermal conductivity [2-3].

Due to the fact that boronated carbon has electronic deficiency we can expect materials with better electron acceptor properties without any large distortion of structure.

Chemical and electrochemical intercalation of lithium into boronated carbons synthesized by chemical vapor deposition from acetylene and boron trichloride was investigated [4, 5]. However, even if the amount of inserted lithium was enhanced, an aggravation of electrochemical characteristics was observed. Our target was to study the electrochemical properties of differently boronated mesophase pitch coke during the lithium insertion/deinsertion process and to analyze the effect of boron.

Experimental

Co-pyrolysis of a filtered coal tar pitch with the pyridine-borane complex has been performed to obtain boron doped carbon following the method introduced earlier [3]. Above 120°C the pyridine-borane complex decomposes into highly reactive borane BH_3 which reacts as a Lewis acid catalyst for polymerization and condensation of polynuclear aromatic molecules. Simultaneously, a hydro-boronation of aromatics takes places forming a boron-substituted polyaromatic mesophase.

Our experiments pointed out that the efficiency of the carbonization of pitch at a temperature from 400°C to 450°C for 0.5 h, 4h or 6h varied from 73% to 82%, being higher of a few % in the case of boron additive.

During carbonization under the atmospheric pressure, about 50% of boron used for reaction is in-built in the structure of carbon. The final product was further pyrolysed at 700°C, 850°C and 1000°C to obtain cokes with a suitable conductivity for electrochemical insertion of lithium.

To study the influence of boron on the structure of carbon, the boronated semi-cokes and cokes were characterized by X-ray diffraction ($CuK\alpha$).

The amount of boron in the carbon was estimated by ICP emission spectrometry.

Optical microscopy was used to image the isotropy of the carbon material.

Boron doped carbons were used as materials for lithium insertion in aprotic medium: 1M $LiPF_6$ in (EC:DEC) or (EC:DMC). Investigation of lithium insertion has been performed in carbon/lithium cells (two electrode swagelok construction) using a multichannel generator Mac Pile II (Biologic-France).

Results-Discussion

Non-homogenous optical texture of boronated carbon with a less developed degree of anisotropy proved a strong local influence of boron during the polymerization and cross-linking process in which boron is in-built in aromatic layers. Even if the total amount of boron ranges only between 1.7% to 2.0% by weight, it drastically changes the texture of carbon. The dimensions of anisotropic units become smaller and the disorder is well remarkable from the optical microscopy and X-ray diffractograms. From the galvanostatic charge-discharge characteristics between 3V and $-0.02V$ vs Li at a current density of 20 mA/g, the reversible and irreversible capacity of lithium insertion was evaluated. A high value of 400 mAh/g was obtained for the boronated coke treated at 1000°C. Additionally, a lack of divergence between the lithium insertion and extraction was observed. In the case of cokes treated at lower temperatures (700°C and 850°C), even if the values of reversible capacity are higher, the presence of hysteresis, more remarkable for coke 700°C, discriminates the cokes obtained below 1000°C.

Potentiodynamic investigations (0.2mV/s to 5mV/s) and galvanostatic intermittent titration technique (GITT) were used for detailed studies of all the kind of polarization during insertion and removal of lithium.

References

- [1] S. Gautier, E. Frackowiak, J. Machnikowski, J.N. Rouzaud, F. Béguin *Mol. Cryst. & Liq. Cryst.* **310** (1998) 359.
- [2] A. Marchand, in: P.L. Walker ed. *Chemistry and Physics of Carbon*, vol. 7, Marcel Dekker, NY (1971) p. 155.
- [3] T. Eichner, M. Braun, K.J. Hütinger *Carbon* **34** (1996) 1367.
- [4] T. Shirasaki, A. Derré, K. Guérin, S. Flandrois *Carbon* **37** (1999) 1961.
- [5] B.M. Way, J.R. Dahn *J. Electrochem. Soc.* **141** (1994) 907.

A Composite Carbonaceous Anode Material for Lithium Ion Batteries

Gang Zhang, Jingli Han, Cuiwei Du, Yanbin Chen and Qingguo Liu

University of Science and Technology Beijing
Beijing 100083, China

Various types of carbon materials have been used for the anode material of Li-ion batteries. The anode of the first Sony's commercial Li-ion battery was composed of non-graphitizable (hard) carbon. The hard carbon shows a high lithium diffusion rate, and less exfoliation problem. The Li-ion battery assembled with the hard carbon anode shows good kinetics, long cycle life.

Artificial and natural graphite are now widely used as the anode materials of Li-ion batteries. The high density and high lithium intercalation capacity of graphite make Li-ion battery exhibiting a high energy density. The powder grains of graphite typically are plate-like shapes. This gives the rise to anisotropic flow properties under shear, so that rolled or pressed graphite anode film might exhibit a high degree of preferred orientation. The plate-like shape and the preferred orientation may cause lithium ions to diffuse longer distances, resulting in large polarization and reasonably less cycleability.

In this work, a process for preparing a composite carbonaceous material consisting of graphite core embedded in hard carbon shell was studied. Natural graphite particles were covered with ethylene-cracking residual. Then the covered graphite powder was pre-oxidized in air and oxygen atmosphere at 250-350°C, resulting in stereo cross-linked in the residual. The cross-linked residual/graphite precursor was pyrolyzed at different temperatures in argon atmosphere. Thus, the hard-carbon/graphite composite powders were obtained.

Figure 1 shows the effect of the pre-oxidized time on the electrochemical performance of the composite anode pyrolyzed at 1000°C. The button cells with lithium foil as the counter electrodes and composite carbonaceous as the working electrodes were galvanostatically charged and discharged with different current densities. In the first ten cycles, the current density was 0.30 mA/cm², then the current density increased to 0.60 mA/cm² in the second ten cycles, and in the third and fourth ten cycles to 0.90 and 1.20 mA/cm², respectively. It can be seen that the lithium intercalation capacities were almost same for all samples at lower current density of 0.30 mA/cm². However, when the current density increased to 0.60, 0.90 and 1.20 mA/cm², the samples pre-oxidized for 1 and 5 hours at 350°C in flowing air showed higher relative capacities. Without pre-oxidizing, and too short pre-oxidizing time, the residual did not have enough cross-link structure, the pyrolyzed coke shell mainly shows soft carbon properties. So, in comparison with soft carbon, the hard carbon shell can greatly improve the kinetics of graphite.

After pre-oxidized at 350°C in flowing air for 3 hours, the pre-oxidized residual/graphite composite was pyrolyzed (heat-treated) at different temperature from 500 to 1700°C. Fig. 2 shows the effect of heat treatment temperatures on the Coulomb efficiency of the first cycle. Although the composite carbonaceous materials pyrolyzed at lower temperature showed higher lithium inter-

calation capacities, but the Coulomb efficiency at the first cycle was much lower. The large irreversible capacity at the first cycle would seriously reduce the specific power density of lithium ion battery.

The diffusion coefficient of lithium ions in graphite, ethylene-cracking residual coke and core-shell composite carbonaceous anode films were measured by using potential step technique. The experimental results are listed in Table 1. It can be seen that the diffusion coefficient of lithium ions in anode films can be increased by means of the covering of hard carbon on graphite particle surface.

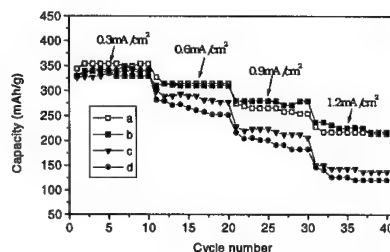


Figure 2. The effect of pre-oxidized time on the Property of composite carbonaceous material
a: 5 hours; b: 1 hour; c: 0.5 hours;
d: without pre-oxidizing

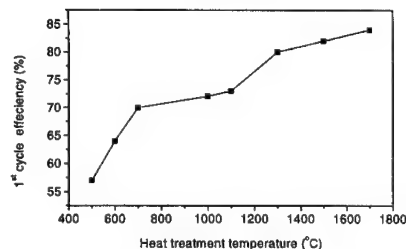


Figure 3. The effect of heat treatment temperature on the Coulomb efficiency of first cycle

Table 1 Diffusion coefficient of lithium ion in graphite, ethylene-cracking residual coke and core/shell composite (cm²/s)

Y in Li ₇ C ₆	graphite	residual coke	Core/shell Composite
0• 1	5.75• 10 ⁻¹⁰	5.25• 10 ⁻⁸	7.83• 10 ⁻⁹
0• 2	5.03• 10 ⁻¹⁰	5.84• 10 ⁻⁸	1.87• 10 ⁻⁹
0• 5	1.15• 10 ⁻¹⁰	4.10• 10 ⁻⁹	•

Electrochemical lithium intercalation in TiO_2 with ramsdellite structure

R. Amandi, A. Kuhn and F. García-Alvarado
Departamento de Química Inorgánica y Materiales de la
Universidad San Pablo-CEU
Urbanización Montepríncipe, 28668 Boadilla del Monte
Madrid, SPAIN

Lithium intercalation is well known for most of the TiO_2 polymorphs. Small amounts can be inserted at room temperature into rutile (0.13 Li/Ti), anatase (0.5 Li/Ti) and brookite (0.5 Li/Ti) [1] if compared with the expected quantity to reduce all Ti^{4+} ions to Ti^{3+} (1 Li/Ti). Hollandite is able to accept a higher quantity (0.75 Li/Ti) [2] and hence it can develop the highest specific capacity c.a. 250 Ah/Kg. Although the ramsdellite polymorph was synthesised as single crystal in 1994 [3], more recently a route to prepare pure powder has been reported [4]. Taking into account that reduction of Ti^{4+} in an octahedral coordination uses to take place at low potential, the electrochemical properties of this latter polymorph, when it is intercalated with lithium, may be of interest for anodic applications in lithium batteries.

In this work we present a study of the electrochemical intercalation of lithium into Li_xTiO_2 ($x \approx 0.3$ and 0). The results are compared with those reported for other titanium ramsdellites that have been proposed as possible anodic materials.

A Li_xTiO_2 compound having ramsdellite structure has been synthesised following the procedure previously reported [4]. Chemical analysis showed that the composition is $\text{Li}_{0.075}\text{TiO}_2$. Lithium can be extracted electrochemically under nearly equilibrium conditions to give a quasi lithium-free compound $\text{Li}_{0.075}\text{TiO}_2$. Afterwards lithium can be reversibly intercalated between 3 and 1 V versus lithium. Figure 1 shows the first discharge-charge cycle (obtained by the application of current pulses of 0.1 mA/cm^2 for 30 minutes and 60 minutes of relaxation) in a cell using $\text{Li}_{0.075}\text{TiO}_2$ as the positive electrode (10% w/o carbon black, 5% w/o binder). The maximal theoretical specific capacity (336 Ah/Kg) is almost reached. When the cell is discharged at higher current density the electrode keeps fairly well the capacity (70% at 1.0 mA/cm^2).

Figure 2 shows the cycling behaviour of the ramsdellite $\text{Li}_{0.075}\text{TiO}_2$ for 0.5 mA/cm^2 . The reversibility of the intercalation reaction is acceptable and the polarisation is not too high if one takes into account that the starting compound is white, i.e. it is expected to have a very low electronic conductivity.

When compared with other ramsdellites such as $\text{Li}_2\text{Ti}_3\text{O}_7$ [5], the capacity of Li_xTiO_2 is clearly advantageous, so that we could propose this latter compound as a new electrode material. However, the major advantage of titanium oxides is that, presenting low intercalation voltages, they may be useful as the anode for rocking chair batteries. This is fulfilled for the case of $\text{Li}_2\text{Ti}_3\text{O}_7$ but not for $\text{Li}_{0.075}\text{TiO}_2$. As it can be seen in Figure 1, intercalation proceeds between 2.3 and 1.2 V, while for $\text{Li}_2\text{Ti}_3\text{O}_7$ an unique plateau situated at 1.5 V is observed. Therefore, although the studied compound Li_xTiO_2 shows a higher capacity, its use as anode material would be more limited than for this other ramsdellite.

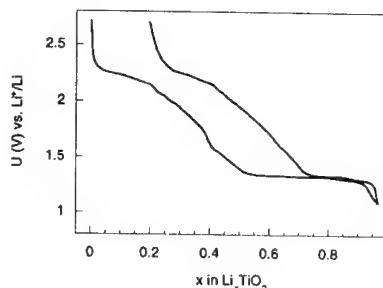


Figure 1. First discharge-charge cycle of a cell Li/LiPF_6 (1M)+EC+DMC (1:1)/ TiO_2 (current pulses of 0.1 mA/cm^2 for 30 minutes and 60 minutes of relaxation).

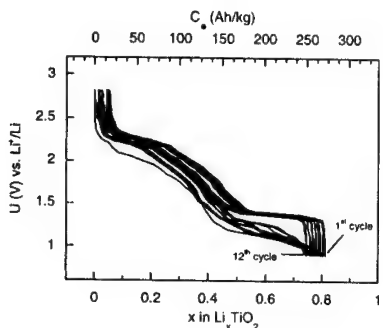


Figure 2. Cycling behaviour of a cell Li/LiPF_6 (1M)+EC+DMC (1:1)/ TiO_2 at a constant current density of 0.5 mA/cm^2 .

Acknowledgements

This work has been financially supported by the projects MAT98-1053-C04-04, CAM 07N/0012/1998 and USP 7/99

References

- [1] B. Zachau-Christiansen, K. West, T. Jacobsen and S. Atlung, *Solid State Ionics* 28-30 (1988) 1176.
- [2] F. García-Alvarado, M.E. Arroyo y de Dompablo, E. Morán, M.T. Gutiérrez, A. Kuhn and A. Várez, *J. Power Sources* 81-82 (1999) 85.
- [3] J. Akimoto, Y. Gotoh, M. Sohma, K. Kawaguchi and Y. Oosawa, *J. Solid State Chem.* 110 (1994) 150.
- [4] J. Akimoto, Y. Gotoh, Y. Oosawa, N. Nonose, T. Kumagai and K. Aogi, *J. Solid State Chem.* 113 (1994) 27.
- [5] M.E. Arroyo y de Dompablo, E. Morán, A. Várez and F. García-Alvarado, *Mater. Res. Bull.* 32 (1997) 993.

INVESTIGATION OF LEAD TIN FLUORIDES AS POSSIBLE NEGATIVE ELECTRODES FOR LI-ION BATTERIES

Lorena L. Garza-Tovar^{1,2}, Paul A. Connor¹, F. Belliard¹,
Leticia M. Torres-Martinez² and John T. S. Irvine¹

1. School of Chemistry, University of St Andrews, St Andrews, Fife KY16 9ST, Scotland
2. Facultad Ciencias Químicas, UANL, Monterrey, N.L. México, CP 64570

Tin oxides have been the subject of considerable investigation as possible new negative electrodes in lithium-ion batteries (1-3). The initial mechanism of lithium incorporation into these anodes is generally attributed to the formation of metal clusters capable of reversible lithium insertion surrounded by a protecting metal oxide matrix. In this study, we have investigated a series of tin fluorides associated with high anionic mobility, following on from earlier phase equilibria and solid state electrochemical studies of this system.

PbSnF_4 is a well-known fluoride ion conductor exhibiting one of the highest ionic conductivities at room temperature of any material. Ionic conductivities, $>10^{-2} \text{ Scm}^{-1}$ at 300K and activation energies $<0.2\text{eV}$ have been observed. PbSnF_4 exhibits three principal polymorphs, α , β , γ . The γ form has the cubic fluorite structure and is isomorphous with $\beta\text{-PbF}_2$. The α - and β - forms have distorted fluorite-related structures with different tetragonal modifications. The cubic fluorite polymorph ($\beta\text{-PbF}_2$ or $\gamma\text{-PbSnF}_4$) is observed to exist at high temperatures from 0 - 80% SnF_2 and is stabilised to room temperature between ~15 and ~30 mol% SnF_2 . The α and β forms of PbSnF_4 are found in the vicinity of 50 mol% SnF_2 . The α form is only found over a narrow range of composition and is not stable at temperatures above 543K. The β form is stable over a much wider range of temperatures and compositions.

In this study, we have investigated electrochemical incorporation of lithium into the high temperature cubic fluorite forms of PbF_2 , $\text{Pb}_{0.75}\text{Sn}_{0.25}\text{F}_2$, $\text{Pb}_{0.15}\text{Sn}_{0.85}\text{F}_2$ the tetragonally distorted fluorite $\text{Pb}_{0.48}\text{Sn}_{0.52}\text{F}_2$ and the rutile form of SnF_2 . Samples have been prepared by solid state reaction under inert and fluoridising atmospheres. The resulting phases have been studied by X-ray diffraction, DSC, quenching and ac impedance spectroscopy techniques.

These materials have been investigated as possible anode materials, using two electrode galvanostatic and potentiostatic cycling techniques. For PbF_2 initial lithium insertion occurs in two steps at 2 and 1.5 V_{Li} , corresponding to the formation of 2LiF per formula unit. Limited further lithium insertion occurs and reversibility is poor. For Sn containing fluorides, the initial insertion is poor. For Sn containing fluorides, the initial insertion of 2 Li per formula unit occurs over the potential range ~2.7-1.5 V. There is significantly more insertion for the Sn-containing compounds at potentials below 0.5V and some degree of reversibility is exhibited. The main differences from the oxide are the higher potential for the irreversible insertion stage ($>2\text{V}$ for the fluoride and $\sim 1\text{V}$ for the oxide) and the lower potential observed for the reversible stage ($<0.5\text{V}$ for the fluoride, $>0.5\text{V}$ for the oxide).

References

1. I. A. Courtney and J. R. Dahn, J. Electrochem. Soc. **144**, 2045 (1997).
2. W. F. Liu, X. J. Huang, Z. X. Wang, H. Li, and L. Q. Chen, J. Electrochem. Soc. **145**, 59 (1998).
3. Y. Idota, T. Kubota, A. Matsufuji, A. Mackawa and T. Miyasaki, Science, **276**, 1394-1397 (1997)

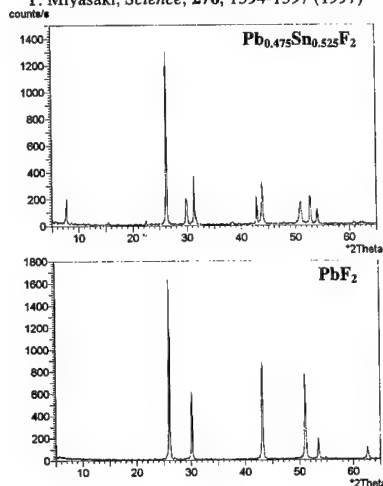


Figure 1 Powder X-ray diffraction patterns comparing the tetragonally distorted fluorite $\beta\text{Pb}_{0.475}\text{Sn}_{0.525}\text{F}_2$ and the cubic fluorite βPbF_2

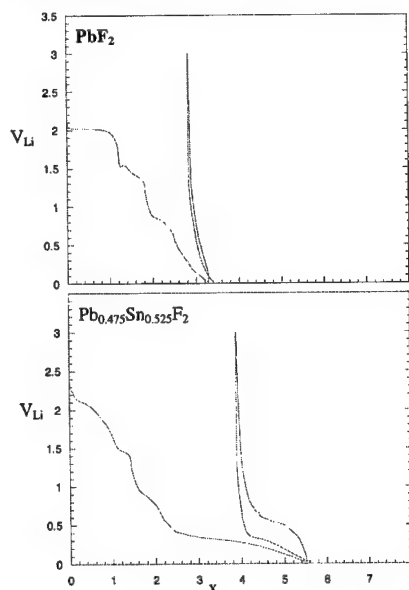


Fig 2 Comparison of galvanostatic cycling data for PbF_2 and $\text{Pb}_{0.475}\text{Sn}_{0.525}\text{F}_2$, x is Li per formula unit.

A MICROTTEXTURAL APPROACH OF LITHIUM INSERTION IN HARD CARBONS: THE « CORRIDOR » MODEL

S. GAUTIER, E. FRACKOWIAK, F. CHEVALLIER, J. N. ROUZAUD, F. BEGUIN
CRMD, CNRS-University, 1B, rue de la Férollerie, 45071 Orléans cedex 02, France.

Hard carbons are expected to be very promising anode materials for lithium-ion batteries, able to store more lithium than graphite. However, the irreversible capacity and the polarization between charge and discharge are usually more important than with graphite. In order to improve the performance, there is a need to interpret more clearly the reasons for the deviations to the ideal behavior of graphite. From electrochemical investigations of hard carbons, TEM observations and ^7Li NMR at various degrees of lithium insertion, we suggest a model which explains the mechanism of lithium insertion and de-insertion.

For this work, we have selected a cellulose precursor. Films have been precarbonized several weeks at ca. 400°C and then heat-treated one minute at 1000°C. The reversible capacity of the carbon product was 250 mAh/g and the irreversible capacity 120 mAh/g. In another experiment, the same precursor was precarbonized at 450°C during 7 minutes and heat-treated during 7 minutes at 1000°C, applying anisotropic mechanical strains during all the process. The reversible capacity was of the order of 500 mAh/g and its irreversible capacity of 160 mAh/g; a noticeable hysteresis was remarked in comparison with the other sample.

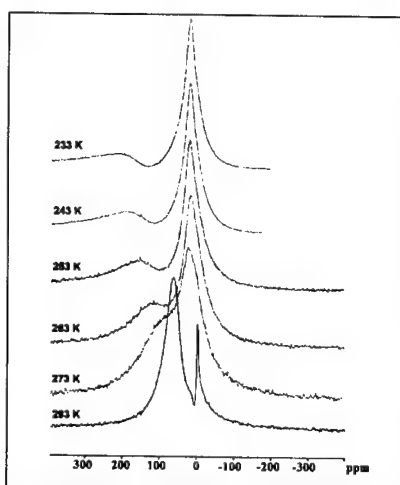
For the analysis of the nature of lithium sites and type of lithium-carbon bonding, ex-situ ^7Li NMR has been performed on fully lithiated samples in the range of temperatures from 293K to 233K. A peak centered at 66ppm observed at ambient temperature on the strained sample gives two different contributions at 233K, i.e. a paramagnetic with a value of 220ppm and peak at 18ppm independent of temperature. The results suggest the existence of two different lithium species in the hard carbon: a pseudometallic lithium forming clusters into micropores and a covalent lithium "truly" intercalated as in LiC_6 .

On the other hand, TEM observations on the strained carbon precursor showed a tendency to a preferential orientation of the aromatic layers. Image analysis brought out a distribution of the interlayer distances, with values ranging from ca. 3.5 to 6 Å.

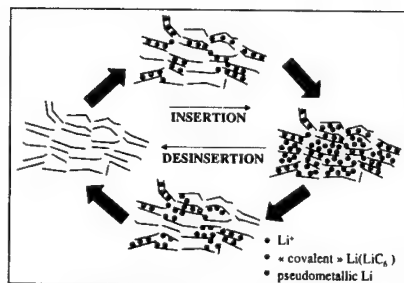
Our model of insertion/deinsertion elucidates that intercalation with charge transfer to the graphitic layers forming corridors is the first process; then electron back-donation takes place for the filling of the pores by pseudometallic lithium. During deinsertion, intercalated species are extracted firstly through the corridors; then, the removal from pores

proceeds with additional polarization for charge transfer from Li clusters to the carbon matrix.

The process of lithium insertion was also investigated on samples especially modified under hydrogen flow and by thermal treatment under secondary vacuum in order to elucidate the exact influence of heteroatoms (O, H) and open porosity on the electrochemical properties. Outgassing at high temperature turned out to be a very efficient way for the reduction of irreversible capacity.



Low temperature ^7Li NMR on fully lithiated carbon



The « corridor » model of lithium insertion/deinsertion in hard carbons

Neutron Diffraction Studies on Lithiated Non-Graphitizable Carbon

Ryoji KANNO, Atsushi HIRANO, Takashi KAMIYAMA*, Kuniaki TATSUMI**, Mamun Al MOSTAFA***, Michihiro FURUSAKA***, and Toshiya OTOMO

Department of Chemistry, Faculty of Science, Kobe University, Nada, Kobe, Hyogo, 657-8501 Japan

*Institute of Materials Science, University of Tsukuba, Tsukuba, Ibaraki, 305-8673 Japan

**Osaka National Research Institute, 1-8-1, Midorigaoka, Ikeda, Osaka, 653-8577 Japan

***High Energy Accelerator Research Organization, Tsukuba 305-0801, Japan,

Non-graphitizable carbons heat-treated at ca. 1000°C give the capacity higher than LiC_6 with a significant capacity in the potential range from 0 to 0.1 V (vs. Li/Li^+). The capacity below 0.1 V looks as a plateau in charge and discharge and is very attractive for anodes of high energy-density batteries. The charge-discharge mechanism studied by ^7Li -nuclear magnetic resonance (^7Li -NMR) suggested two types of lithium species during lithiation process; the lithium same as those in graphitizable carbons, and the species with quite different from those in graphitizable carbons(1). The former is thought to be in the interlayer space between graphite layers, and the latter is inferred to be lithium clusters with metallic character which causes a significant capacity below 0.1V (2). The structure information on the lithiation mechanism is, however, still ambiguous, because weakly periodic structures of the carbon make it difficult to understand the structural changes during lithium insertion and extraction by X-ray diffraction analysis. In the present study, the structures of the carbon and lithiated carbon were studied using neutron diffraction to clarify the structure changes during the lithiation process.

Carbon fiber prepared from an isotropic petroleum pitch (nominal diameter of 10 μm , FIP, Petoca), which was used as a precursor of non-graphitizable carbons, was heat-treated at 1200°C. Electrochemical lithium insertion were performed in a three-electrode cell with 1 mol $\cdot \text{dm}^{-3}$ solution of LiClO_4 in a 50:50 (by volume) mixture of ethylene carbonate and diethylcarbonate (DEC) (battery grade, Tomiyama Pure Chemical Industry) at 27°C. The reference and counter electrodes were lithium metal. The fully lithiated carbons were prepared by short circuiting the cells for 12 h after galvanostatic reduction (25 mA $\cdot \text{g}^{-1}$) to 0 V. Partially lithiated carbons were prepared by a charge to 0.1V. The neutron diffraction data were taken on a time-of-flight (TOF) diffractometer VEGA, and the small-angle neutron scattering (SANS) were taken on a TOF diffractometer, SWAN, at the KENS pulsed spallation neutron source at KEK.

Figure 1 shows the VEGA data on the carbon and fully lithiated carbon. The patterns fitted by the graphite-2H model with a hexagonal structure led to lattice parameters with $a=2.4064(7)$, $c=6.985(11)\text{\AA}$, and $2.4186(6)$, $c=7.074(9)\text{\AA}$ for the carbon and the lithiated carbon respectively. No significant differences were found in the peak positions between the fully lithiated and

the partially lithiated samples. This indicates the intercalation reaction in a graphite region from shallow lithiation process.

SANS data of the carbon and the fully lithiated carbon differ slightly at ca. $Q = 0.2 \text{\AA}^{-1}$ and 1\AA^{-1} (Fig. 2). However, it is reasonable to assume that the framework of the carbon does not change appreciably, because both data are commonly consist of three parts: the Porod term with Q^{-4} dependency, the Debye-Bueche term with a double Lorentzian form and a constant incoherent scattering: $I(Q) = A \times Q^{-4} + B / \{1 + (\xi \times Q)^2\}^2 + I_{\text{inc}}$. The second term is relevant to the micropores with diameter of about 7 to 8 \AA surrounded by layered crystallites in the carbon. The slight difference at ca. $Q = 0.2 \text{\AA}^{-1}$ and 1\AA^{-1} corresponds to the value of ξ , the correlation length, which is related to a radius of the micropore. Both data were excellently fitted with this formula in the Q range $0.02 - 0.8 \text{\AA}^{-1}$. The obtained ξ was 2.9 and 3.4 for FIP and Li-doped FIP, respectively. The diameter of the micropore is simply approximated by $2 \times \xi$ (3). It is concluded that the micropore becomes larger with lithiation.

Using VEGA and SWAN data on the lithiated carbon, the structure informations concerned directly to the intercalation and lithium cluster formation process were clarified.

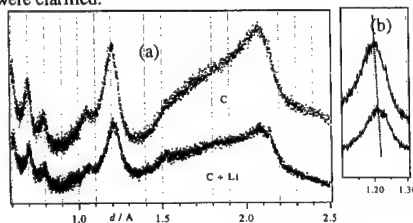


Fig. 1 The VEGA data for carbon and fully lithiated carbon.

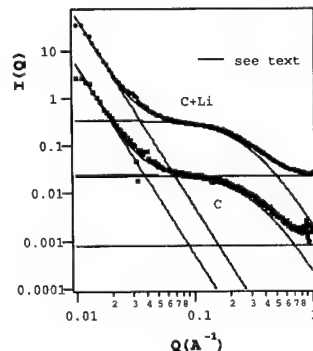


Fig. 2 The SANS data and fitting results.

REFERENCE

1. K. Tatsumi, *et al.*, *J. Power Sources*, **81-82**, 397 (1999).
2. K. Tatsumi, *et al.*, *Chem. Commun.*, 687 (1997).
3. K. Suzuya, *et al.*, *J. Mater. Res.*, **11**, 1169 (1996).

Abstract No. 135

Investigation of the solid electrolyte interface film on the graphitic anodes surface.

D. Zane^{*1}, A. Antonini^{°2}, M. Pasquali^{°2}

^{*}CNR-CECFI, Rome

[°]Dept. Chemical Engineering,

University of Rome "La sapienza"

^{1,2} v. Castro Laurenziano 7 Rome, Italy

Lithiated graphite is recognised as a good anode in lithium-ion cells for its high theoretical capacity (372mAh/g) and voltage respect to lithium leading at an high cell voltage and good power density¹. On the other hand, it is rather sensitive to electrolyte composition, in fact the electrolytes are reduced on the electrode surface especially during the first discharge forming an electron insulating but ionic conducting protective layer². The growth of this passivating layer causes an irreversible capacity loss which has a certain importance in constructing practice lithium-ion batteries. This film plays a fundamental rule in good performing of the electrode and its composition is dependent on the electrolytic solution in which the electrode have to work. It is well known that graphite is exfoliated by propylene-carbonate upon electrochemical intercalation of lithium^{3,4} while behaves well with ethylene-carbonate and in fact most of solutions which lead to a good cycleability are EC based in mixture with a variety of others solvents. In this work we report our results about a study of graphitic electrode surface morphology in several electrolytic mixtures and in hard temperatures conditions. Because of its employ in practice electronic devices (i.e. computer, cameras ...) the lithium-ion cells may work in such temperature conditions reaching at maximum 55°C this causing some problems with the evaporation of solvents and with stability of solutions, for this reason a little quantity of PC are added. We have studied the surface morphology of natural graphite (NG7) electrodes by SEM and tried to correlated the passivating film morphology with self-discharge properties following this phenomenon by impedance spectroscopy. The solution used are: LiPF₆ EC/DMC, LiBF₄ EC/PC 1/1, LiBF₄ EC/PC 3/1, LiClO₄ 2/1. In fig. 1 are reported first discharges obtained with previous solutions and the effect of the presence of propylene carbonate on the electrolyte decomposition is evident only in the 1/1 ratio with EC. The curves plotted for other solutions have more or less the same shape also for LiPF₆ reported as reference solution because of its wide presence in practical batteries. In every case the irreversible capacity loss consists in about the 20% of the total amount, except for the LiClO₄ EC/PC 1/1 with a 40%. In the fig.2 SEM picture as an exemple is reported the film obtained in LiClO₄ EC/PC 2/1 after the first discharge.

In fig.2, as an exemple, SEM pictures is reported for the film obtained in LiClO₄ EC/PC 2/1 after the first discharge. We have followed the electrode self-discharge by impedance spectroscopy and the data show a continous degradation of the film. The depression angle trend seems to be correlated with a progressive porosity of the passivating film as is clearly evident in others SEM pictures.



Fig. 1. Voltage vs time profiles for the first discharge of graphite in different electrolytes.

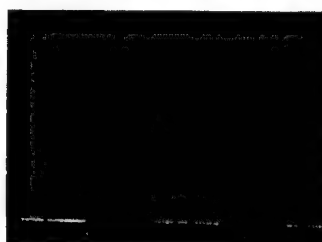


Fig. 2. SEM picture for a SEI film growth in LiClO₄ EC/PC 2/1

V/Volts OCV	Depression angle	R _{ct} (ohms)	C _{dl} (farads)
0,05	11,9	39,41	6,3 *10 ⁻⁶
0,096	18,7	45,1	6,2 *10 ⁻⁶
0,137	21,88	70,3	4,2 *10 ⁻⁶
0,155	26,22	80,9	3,8 *10 ⁻⁶

Table 1. Impedance data for a sample in OCV conditions after the first discharge in LiClO₄ EC/PC 2/1

ACKNOWLEDGEMENTS

This work was carried out with the financial support of the "PF MSTA II" of the National Research Council of Italy.

REFERENCES

- 1.D. Fauteaux, R. Koksang, J. Applied Electrochem. 23, 1 (1993)
2. D. Aurbach, B. Matkovsky, I. Weissman, E. Levi, Y. Ein-Eli, Electrochimica Acta 45, 67 (1999)
3. R. Fong, V. Von Sacken, J. R. Dahn, J. Electrochem. Soc. 137, 2009 (1990)
4. A. N. Dey, B. P. Sullivan, J. Electrochem. Soc. 117, 222 (1970)

Determination of the Ratio of Basal Plane Surfaces and Prismatic Surfaces of Graphites And its Impact on Graphite Anode Performance in Lithium Ion Batteries

James P. Olivier¹, Peter Golob², and Martin Winter³¹ Micromeritics Instrument Corp, Inc.
Norcross GA 30093 USA² Research Institute for Electron Microscopy, Graz
University of Technology, Steyrergasse 17, A-8010 Graz,
Austria³ Institute for Chemical Technology of Inorganic Materials,
Graz University of Technology,
Stremayrgasse 16, A-8010 Graz, Austria

Solid-electrolyte-interphase (SEI) formation on graphite anodes in lithium ion cells inevitably involves the irreversible consumption of both charge capacity and material (lithium and electrolyte). This "irreversible capacity" C_{ir} depends largely on the electrode surface accessible to electrolyte wetting. Basically, the electrode structure (type of binder, binder content, porosity, mechanical properties, etc.) and the type of graphite (characterized by properties, such as surface area, particle shape and size distribution, etc.) determine this surface.

The structure of layered graphite gives rise to basically two kinds of surfaces, prismatic (edge) surfaces and basal plane surfaces. Ideal (= defect free) basal plane surfaces are homogeneous and "smooth" and consist only of carbon atoms. In contrast the prismatic surfaces are heterogeneous and "rough" and apart from carbon contain various, mostly oxygen-containing surface groups. It is widely accepted that the chemistry and morphology of the prismatic surfaces of graphite play a major role in chemical and electrochemical reactivity, interaction with the SEI, etc., e.g., [1]. Besides, transport of either solvated or unsolvated lithium cations from/into the electrolyte take place via the prismatic surfaces. In accordance with the fact that surface group reduction and solvated intercalation take place at the prismatic surfaces, it was suggested, that prismatic surfaces contribute more to the overall C_{ir} than basal plane surfaces [2]. In conclusion, the information about the relative and absolute amounts of prismatic and basal plane surfaces in a graphite material are essential for understanding the irreversible (and reversible) reactions of the graphite anode.

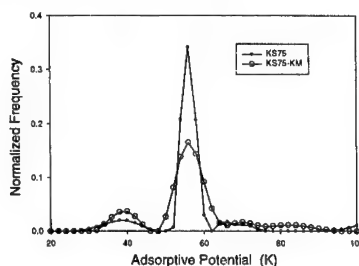
The adsorption of nitrogen at 77K is a commonly used measurement for the determination of the surface area of graphites and other materials through application of the well known BET equation. We show in this work how the same measurements can be used to estimate the extent of prismatic and basal plane surfaces present in a graphitic material.

The method is based on the premise that the two surfaces of interest will adsorb nitrogen with different affinities, or adsorptive potentials. In the case of physical adsorption, this potential is largely determined by the density of the adsorbent constituent atoms at the adsorbing interface. For graphite, this means that the basal plane, having a higher areal density of carbon atoms, will have a greater adsorptive potential, hence adsorb more strongly than the less dense prismatic surfaces. The task of extracting the adsorptive potential distribution from adsorption data has been described in detail elsewhere [3]. In simple terms, the adsorption isotherm on a heterogeneous surface is expressed as the convolution integral

$$Q(p) = \int q(p, \epsilon) f(\epsilon) d\epsilon \quad (1),$$

where $Q(p)$ is an experimental adsorption isotherm, $f(\epsilon)$ is the adsorptive potential distribution by area, and $q(p, \epsilon)$ is a function describing the theoretical adsorption isotherm on an energetically uniform surface having an adsorptive potential ϵ . In this work, the function $q(p, \epsilon)$ is evaluated by using non local density functional theory [4].

The materials investigated were several TIMREX[®] powder graphites (Timcal). By way of example, the normalized adsorptive potential distributions for two graphites with similar particle size distribution but quite different surface area, named KS75 and KS75KM, are shown below. The KS75KM has been prepared from the KS75 by a special milling procedure. The surface area of sample KS75 by the present method was $5.51 \text{ m}^2 \text{ g}^{-1}$ (BET 5.73) and sample KS75KM was 25.63 (BET 25.37).



From previous work with graphite [3], it is known that the peak centered at 57 K represents the basal plane surface. From physical considerations, the lower energy peak represents the prismatic surface. Dislocations, defects and surface steps (= "defect surface") can account for the higher energy portions of the distribution. By integrating under the peaks, we find that the ratio of basal plane surface / prismatic surface / "defect surface" for sample KS75 is $8.6 / 1.2 / 1.0$, while it is $5.5 / 1.2 / 1.0$ for KS75KM.

We will relate these ratios qualitatively with the first cycle charge curves of the samples. One has, however, to be careful, with a relation on a quantitative basis. The influence of surface groups, in particular for milled graphites like the KS 75 KM, as well as the amounts of the respective surface areas wetted by the electrolyte can not be determined. Furthermore, the electrode structure (see above) has to be considered, meaning that C_{ir} of a certain graphite material may vary in dependence of other electrode components and of the electrode preparation process. Finally, the SEI products at basal planes and prismatic surfaces and thus the C_{ir} for their formation may differ considerably, too [5].

- [1] M. Winter et al., *ITE Batt. Lett.* 1(2), 129 (1999)
- [2] M. Winter, P. Novák, and A. Monnier, *J. Electrochem. Soc.* 145, 428 (1998)
- [3] J. P. Olivier, in: *Surfaces of Nanoparticles and Porous Materials*, J. A. Schwartz and C. I. Contescu (eds.), Marcel Dekker, New York, 1999
- [4] P. Tarazona, *Phys. Rev.* 31, 2672 (1985)
- [5] D. Bar-Tow, E. Peled, and L. Burstein, *J. Electrochem. Soc.* 146, 824 (1999)

Support by the Austrian science fund in the special research program "Electroactive Materials" is acknowledged. We thank the Timcal group (Bodio, CH) and the Paul Scherrer Institute (Villigen, CH) for the donation of graphites used in this study.

First Principles Calculations for Li
Insertion into InSb

R. Benedek, M. M. Thackeray
Electrochemical Technology Program
Chemical Technology Division
Argonne National Laboratory
Argonne, IL 60439, USA

L. H. Yang
Lawrence Livermore National Laboratory
Livermore, CA 94551

R. Prasad
IIT Kanpur
Kanpur, India 208016

Intermetallic compounds have long been under consideration as possible anode materials in Li batteries, however, sluggish insertion/extraction behavior, large volume expansion, and relatively small capacity have discouraged their widespread use. Recent work has been motivated by the possibility that Li-intercalating intermetallics may exhibit better electrochemical behavior than the Li-compound-forming systems that have received most attention previously. Systems bearing the NiAs and ZnS structures have been investigated by our group [1-3]. To complement the experimental effort, we present here results of first principles calculations within the local-density-functional theory framework that shed further light on the intercalation properties of Li in InSb[2].

Calculations were performed primarily with the plane wave pseudopotential method, but some calculations were also done with the full-potential linear muffin tin orbital method. Pseudopotentials of the Troullier-Martins form were employed, with the In and Sb 4d electrons treated as valence. Calculated equilibrium lattice constants for zinc-blende InSb were within 1% of experiment. In order to analyze some possible decomposition reactions that occur upon lithiation, calculations were performed also for pure In in the tetragonal structure, and for the compound Li_3Sb .

Calculations for Li_xInSb have been performed at several compositions. In the dilute limit, a single Li atom ($x=0.25$) was treated in a conventional cubic unit cell. Tetrahedral interstitial sites coordinated to either In or Sb, as well as substitution for In were considered. The In-coordinated site is preferred to the Sb-coordination, and substitutional Li on In sites was found energetically unfavorable. Although direct experimental verification is lacking, the preference for In-coordinated tetrahedral can be rationalized on the basis of simple electrostatic considerations.

The composition $x=1$, with either the In- or Sb-coordinated tetrahedral interstitials filled, was considered. The equilibrium lattice constant at this composition is approximately 3% larger than in pristine InSb. In contrast to our predictions for $x=0.25$, the Sb-coordination was preferred at $x=1$. Calculations for $x=2$, which corresponds to the filling of all tetrahedral interstitial sites, suggest that the zinc blende structure is unstable at this composition.

Although isolated substitutional Li in InSb is found to be unfavorable, the In-extrusion reaction in which Li_3Sb is formed, is found to be

energetically competitive with Li insertion into tetrahedral interstitial sites at $x=0$.

The calculations described above, in conjunction with x-ray diffraction measurements [3], suggest the following scenario for the first cycle of Li intercalation of InSb. The first intercalated Li atoms occupy In-coordinated tetrahedral interstitial sites, but with subsequent filling a preference for Sb-coordinated interstitial sites develops. At a Li interstitial level between 0.5 and 1 Li per formula unit (if not lower), an In-extrusion reaction occurs. In this reaction, pure In is extruded, and domains of Li_3Sb are created in the InSb matrix.

Support by the Chemical Sciences Division of the Office of Basic Energy Sciences, U. S. Department of Energy, under Contract No. W-31-109-Eng-38 is gratefully acknowledged.

References

1. K. D. Kepler, J. T. Vaughey and M. M. Thackeray, *Electrochem. and Solid State Lett.*, **2** (7), 307 (1999).
2. J. T. Vaughey, K. D. Kepler, R. Benedek, and M. M. Thackeray, *Electrochem. Commun.*, **1**, 517 (1999).
3. J. T. Vaughey, J. O. O'Hara and M. M. Thackeray, *Electrochem. and Solid State Lett.*, **3** (1) 13 (2000).

Phase separation and amorphization in lithium inserted Cu-In-Sn sulfospinels. Theoretical and experimental approach.

R. Dedryvère¹, S. Denis², P.E. Lippens¹, J. Olivier-Fourcade¹ and J.C. Jumas¹

¹ Laboratoire des Agrégats Moléculaires et Matériaux Inorganiques, CNRS UMR5072

Sulfide compounds with spinel-related structure have been widely studied for their properties as host materials for lithium insertion and their potential use as electrode in lithium-ion batteries [1,2]. Post-transition metals of groups 13 and 14 provide many examples of such compounds. Particularly, indium and tin sulfospinels like MIn_2S_4 ($M = Mn, Fe, Co, Ni$) [3], $CuMo_{0.5}Sn_{1.5}S_4$ ($M = Mn, Fe, Co, Ni$) [4] and the cation deficient $In_2Sn_{0.5}S_4$ [5] have been previously studied as host lattices for lithium insertion. The oxidation/reduction potentials observed during electrochemical tests are lower than those observed for oxide spinels, and so these materials are currently investigated for their possible application as negative electrodes [6]. Unfortunately, their practical use has been limited up to now by a low specific capacity and a high capacity fading with cycling, in contrast to carbon electrodes.

A previous work has shown the interest of copper and indium containing sulfospinels to obtain low specific potentials [7]. We present here a study on copper, indium and tin containing compounds: $Cu_{0.5+4x}In_{2.5-3x}Sn_{2x}S_4$ ($0 \leq x \leq 0.5$), belonging to the spinel-related structure domain of the pseudo-ternary phase diagram $Cu_2S-In_2S_3-SnS_2$. This work includes lithium insertion on these materials by chemical (via n-butyllithium) and electrochemical (using Li / LiPF₆ 1M (EC:DMC) / sulfospinel cells) routes.

Characterization was performed by X-ray powder diffraction (XRD), ¹¹⁹Sn Mössbauer spectroscopy and X-ray absorption spectroscopy (XAS). Diffraction measurements show a spinel-rocksalt transformation at the beginning of the insertion, and then an important amorphization takes place with further lithium insertion. The Mössbauer results allow to analyze the evolution of the tin oxidation state throughout the insertion: initial Sn^{IV} is reduced to Sn^{II} in the rocksalt phase and to Sn⁰ in the amorphous phase (Fig. 1).

Changes in the partial electronic structure due to Li insertion have been studied by XAS. A qualitative analysis is proposed which explains some observed main trends in the variations of the XAS spectra as a function of the Li content. *Ab initio* calculations have been performed in order to give a more quantitative interpretation of these changes in terms of the modifications in the local environment of the different atoms. First results are given here for binary Sn-S and Cu-S compounds used as reference materials for the complex quaternary compounds. A good agreement is obtained between the experimental and the calculated XAS spectra (Fig.2) which allows to attribute the orbital contributions to the XAS peaks.

- [1] M. Eisenberg, *J. Electrochem. Soc.*, **127** (1980) 2382.
- [2] A.C.W.P. James, B. Ellis, J.B. Goodenough, *Solid State Ionics*, **27** (1988) 37, 45
- [3] C. Pérez Vicente, C. Bousquet, A. Krämer, J.L. Tirado, J. Olivier-Fourcade, J.C. Jumas, *J. Solid State Chem.*, **134** (1997) 238
- [4] C. Branci, J. Sarradin, J. Olivier-Fourcade, J.C. Jumas, *Chem. Mater.*, **11** (1999) 2846
- [5] M.L. Elidrissi Moubtassim, C. Bousquet, J. Olivier-Fourcade, J.C. Jumas, J.L. Tirado, *Chem. Mater.*, **10**(4) (1998) 968

Université Montpellier II, CC15, Place Eugène Bataillon, 34095 Montpellier Cedex 5, France

² Laboratoire de Réactivité et Chimie des Solides (UPRES-A 6007) 33, rue Saint-Leu, 80039 Amiens Cedex, France

- [6] P. Lavela, C. Pérez-Vicente, J.L. Tirado, C. Branci, J. Olivier-Fourcade, J.C. Jumas, *Chem. Mater.*, **11** (1999) 2687
- [7] J. Morales, J.L. Tirado, M.L. Elidrissi Moubtassim, J. Olivier-Fourcade, J.C. Jumas, *J. Alloys Comp.*, **217** (1995) 176

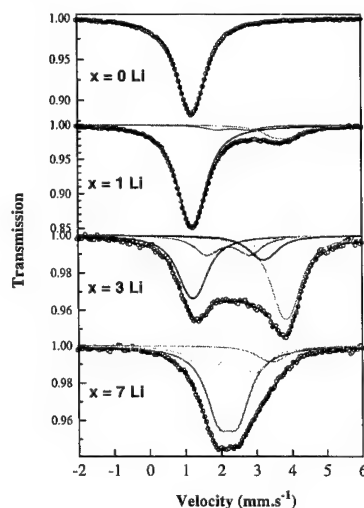


Fig.1 ¹¹⁹Sn Mössbauer spectra of $CuInSnS_4$ at different lithium contents per mole of compound.

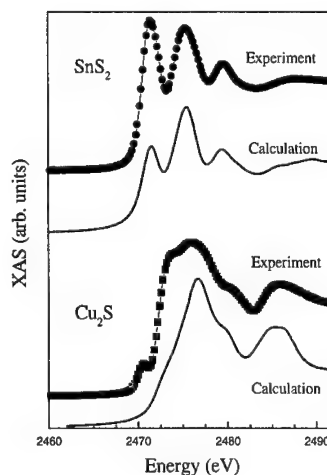


Fig.2 XAS spectra at the S K edge of the two reference materials SnS_2 and Cu_2S .

Experimental and theoretical analysis of Li insertion mechanisms in anode materials

J. Chouvin, P.E. Lippens, C. Perez-Vicente*, J.
Olivier-Fourcade and J.C. Jumas

Laboratoire des Agrégats Moléculaires et Matériaux
Inorganiques, CNRS UMR 5072
Université Montpellier II, Place Eugène Bataillon, F-
34095 Montpellier Cedex 05, France

*Laboratorio de Química Inorgánica, Facultad de
Ciencias,
Universidad de Córdoba, 14071 Córdoba, Spain

We present a method for the study of the effects of the Li insertion in new anode materials upon the structure, the electronic and the electrochemistry properties. This method which has been previously used for chalcogenide materials [1] is based on complementary experimental techniques including X-ray and neutron diffractions, Mössbauer spectroscopy, X ray photoelectron and absorption spectroscopies. The experimental results are analysed by different models including semi-empirical and *ab initio* calculations. This approach has been used by our group for different insertion materials and results obtained for tin based anode materials are shown here as an example. This study concerns Li insertion in the α -SnO crystalline phase considered as a reference material and in amorphous tin composite oxides (ATCO).

The electronic structure of α -SnO has been studied from both experiments and *ab initio* calculations. A new interpretation of the occupied and unoccupied electronic states based on the LAPW method [2] is proposed in terms of chemical bonding. Accurate results have been obtained in particular for the XAS spectra (Fig.1). This provides a reference for the interpretation of the experimental data obtained for Li insertion in both the crystalline and amorphous phases.

Results of X-ray absorption and ^{119}Sn Mössbauer spectroscopies let to conclude that the Li-Sn cluster are embedded in a Li_2O matrix with important Sn-O interactions (up to 4 Li/mol), which can be only neglected at very large depth of discharge (more than 4 Li/Sn) [3]. The different environments of tin atoms found during the discharge (Fig.2) agree well with Sn^{II} (up to 2 Li/mol), "metallic" tin (from 2 to 4 Li/mol) and Li-Sn (from 4 Li/mol). At the end of the discharge deformation of $\text{Li}_{22}\text{Sn}_5$ was confirmed [4].

The Li insertion in ATCO leads to structural changes and the new active phases have been studied by the different techniques [5]. The results have been compared to those obtained for reference materials in order to provide an interpretation of the insertion mechanisms and to improve the electrochemical properties.

References

- [1] P.E. Lippens, J.Olivier-Fourcade and J.C. Jumas, *Hyperfine Interact.* 113, 341 (1998).
- [2] P. Blaha, K. Schwarz and J. Luitz, WIEN97, Vienna University of Technology, Vienna 1997, Updated version of P. Blaha, K. Schwarz, P. Sorantin and S.B. Trickey, *Comp. Phys. Commun.* 59, (1990) 399.
- [3] J. Chouvin, J. Olivier-Fourcade, J.C. Jumas, B. Simon, Ph. Biensan, F.J. Fernández Madrigal, J.L. Tirado and C. Pérez Vicente, *J. Electroanal. Chem.* (submitted).
- [4] I.A. Courtney, R.A. Dunlap, J.R. Dahn, *Electrochim. Acta* 45, 51 (1999).
- [5] J. Chouvin, J. Olivier-Fourcade, J.C. Jumas, B. Simon and O. Godiveau, *Chem. Phys. Letters* 308, 413 (1999).

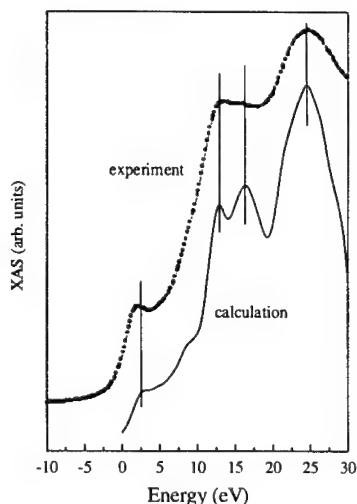


Fig.1 Experimental and calculated XAS spectra at the Sn L_3 edge of α -SnO

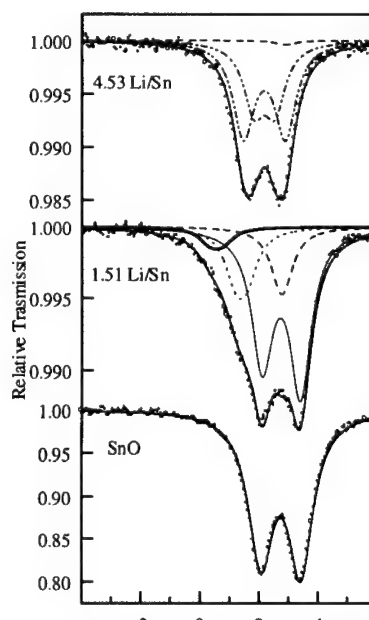


Fig.2 ^{119}Sn Mössbauer spectra of the Li-SnO materials. Velocity (mm/s)

Abstract No. 140

The Effects of Chemical Composition of
Adsorbed Organic Molecular Layers on
Lithium Electrode/Polymer Electrolyte
Interface Stabilization

Maryline Le Granvalet-Mancini
Universite de Nantes
Nantes, France

Shailesh Gadad and Dale Teeters
University of Tulsa
Tulsa, Oklahoma

Previous work in our laboratory has shown that the adsorption of self-assembled molecular layers on a polymer electrolyte surface can make the interface between the electrolyte and a lithium metal electrode more stable and hinder the formation of passivation layers that inhibit ion movement between the electrode and electrolyte. This work studies the effect that the molecular composition of the adsorbed layer has on interface stability and passivation inhibition. Several compounds have been studied particularly those having a portion of the molecule that will adsorb on the surface of the electrolyte and a portion that may self-assemble, forming the layer that comes in contact with the lithium electrode. Studies have been conducted on compounds of the form $\text{H}-(\text{CH}_2)_n-(\text{CH}_2-\text{CH}_2-\text{O})_m-\text{H}$, where the length of the hydrocarbon chains, n , have been varied. In addition molecules that have had the straight-chain $-(\text{CH}_2)-$ portion of the molecule replaced with branched hydrocarbon chains, aromatic groups, and organosilicon groups have been studied. Characterization of the molecular layers' ability to stabilize the electrode/electrolyte interface have been done using a.c. impedance spectroscopy. Impedance data will be correlated with chemical make-up of the molecular layer and the ability of some molecules to form more ordered self-assembled structures.

Synthesis and Characterization of $\text{Li}_2\text{Mn}_4\text{O}_9$ Cathode Material

W. P. Kilroy, W. A. Ferrando, and S. Dallek
Naval Surface Warfare Center, Carderock Division
West Bethesda, MD 20817, USA

ABSTRACT

Lithium manganospinel $\text{Li}_2\text{Mn}_4\text{O}_9$ has been investigated extensively in recent years as a lithium insertion cathode for lithium-ion batteries (1). The difficulty in preparing the fully oxidized $\text{Li}_2\text{Mn}_4\text{O}_9$ material in a reproducible manner, is well known (2). Strict control of experimental conditions such as temperature, time, particle size of the precursor materials, and oxygen partial pressure is essential for producing highly oxidized, single-phase material. Reported results to date show clearly that the fully oxidized $\text{Li}_2\text{Mn}_4\text{O}_9$ phase has not been prepared successfully.

We report here on the synthesis of $\text{Li}_2\text{Mn}_4\text{O}_9$ using a new precursor mixture, $\text{LiMnO}_4 \cdot 3\text{H}_2\text{O}$ and MnCO_3 . The rationale for choosing $\text{LiMnO}_4 \cdot 3\text{H}_2\text{O}$ as one of the precursors was that it forms a melt, which has recently been reported to improve contact between the reactants (3). The effectiveness of using LiMnO_4 as a reagent to prepare layered manganese oxides has also been reported (4).

Our objective was to prepare and characterize the fully oxidized spinel material, $\text{Li}_2\text{Mn}_4\text{O}_9$, and to determine its electrochemical behavior. Thermogravimetry (TG) was employed to determine the optimal experimental conditions for the synthesis of the cathode material and to determine the extent of oxidation of the product. The stoichiometry was determined from potentiometric titration and elemental analysis of Li and Mn. The electrochemical behavior of the material was investigated using single cell tests in hermetically sealed glass laboratory cells.

TG curves of our highly oxidized $\text{Li}_2\text{Mn}_4\text{O}_9$ material and a commercial LiMn_2O_4 sample are shown in Figure 1. The measured weight plateau ratio for the LiMn_2O_4 sample in curve (a) is in exact agreement with the theoretical value of 0.9410 for the thermal decomposition of LiMn_2O_4 to LiMnO_2 and Mn_2O_3 . The interpretation of the TG curve of our highly oxidized material (b) has been discussed previously (5). The value of z in $\text{Li}_2\text{Mn}_4\text{O}_{8+z}$ determined from the molecular weights of the solid phases and the TG weight plateaus was 0.83. The highest value of z obtained in this study was 0.88. We attribute the difficulty in preparing the fully oxidized phase, in part, to the simultaneous decomposition reaction of the product to LiMn_2O_4 .

The cycling behavior of the highly oxidized material and a commercial LiMn_2O_4 sample is shown in Figure 2. The tests were conducted in coin cells with a lithium anode and an EC:DMC:DEC electrolyte at 1.5 mA/cm². These results show the excellent capacity retention of the new cathode material relative to that of the commercial LiMn_2O_4 . We also observed that there was very low charge acceptance on the first cycle of the cell with the new cathode. This is considered strong evidence of the high oxidation state of the Mn in the material.

We will present details of the solid state synthesis parameters and properties of the new cathode material including lattice parameters, hygroscopicity, and thermal stability.

References:

1. M. M. Thackeray and M. H. Rossouw, *J. Solid State Chem.*, **113**, 441 (1994), and references therein.
2. C. Masquelier, M. Tabuchi, K. Ado, R. Kanno, Y. Kobayashi, Y. Maki, O. Nakamura, and J. B. Goodenough, *J. Solid State Chem.*, **123**, 255 (1996).
3. F. Leroux, D. Guyomard, and Y. Piffard, *Solid State Ionics*, **80**, 299 (1995).
4. J. Tarascon, W. McKinnon, F. Coowar, T. Bowmer, G. Amatucci, and D. Guyomard, *J. Electrochem. Soc.*, **141**, 1421 (1994).
5. S. Dallek, in Proc. 38th Power Sources Conf., p. 378 (1998).

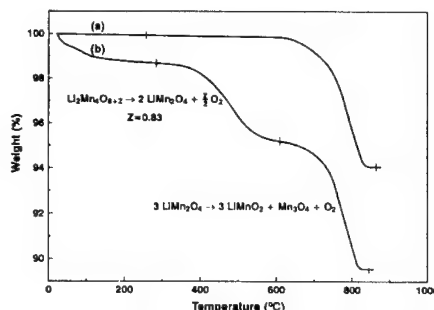


Figure 1. TG curves of manganospinel cathode materials a) LiMn_2O_4 b) $\text{Li}_2\text{Mn}_4\text{O}_{8.8}$

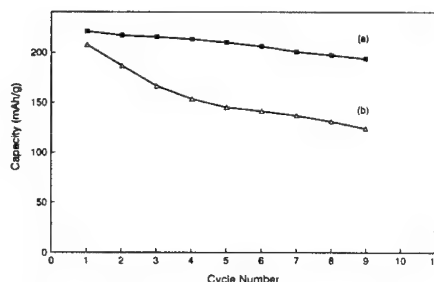


Figure 2. Cycling behavior of manganospinel cathode materials a) $\text{Li}_2\text{Mn}_4\text{O}_{8.8}$ b) LiMn_2O_4

Preparation and Characterization of $\text{Li}_{1+x}\text{Co}_y\text{Mn}_{2-y}\text{O}_4$ Spinel for Lithium Battery Applications

S. H. Kim and B. W. Lee

Department of Materials Engineering, Korea Maritime University, Pusan 606-791, Korea

Lithium transition metal oxides are of great interest as cathode materials of lithium rechargeable batteries. Among the potential cathode materials, LiMn_2O_4 spinel is most promising because of its economical and environmental advantages. An important problem prohibiting it from wider use as a cathode material is the unstable rechargeability as capacity fading during cycling. The capacity fading of the spinel has not been well clarified. A dissolution of the spinel cathode into the electrolyte and a tetragonal distortion caused by the Jahn-Teller effect are believed to contribute the capacity fading[1,2]. To overcome the problem, several research groups have studied the properties of transition metal doped spinels, $\text{LiM}_x\text{Mn}_{2-y}\text{O}_4$ ($M=\text{Ni, Fe, Co, Cr}$)[3,4], and nonstoichiometric lithium rich spinels, $\text{Li}_{1+x}\text{Mn}_{2-x}\text{O}_4$ [5,6]. Considerable improvement in rechargeability on cycling was obtained, but they delivered significant loss of initial capacity. As the lithium excess and the dopant concentration were increased, the initial capacity loss was also increased. In order to suppress the capacity loss and capacity fading, a low temperature preparation of the spinel powder having high degree of crystal quality without undesirable phases and a controlled addition of minimum amount of both excess lithium and dopants are required.

The quality of LiMn_2O_4 based materials for the applications on lithium ion batteries also depends on powder morphology and particle size. The electrode materials, which have smaller particle size and larger surface area, usually deliver a high capacity[7]. Wet chemical process makes it possible to prepare the high quality spinel at a low heating temperature in a shorter time with a high surface area product.

In the present study, $\text{Li}_{1+x}\text{Co}_y\text{Mn}_{2-y}\text{O}_4$ ($x=-2 \sim 2$, $y=0, 1/9, 1/6$) spinel powders, both the excess lithium and cobalt added, have been prepared by oxalate precipitation method as the wet chemical process. Their synthesis and high temperature properties were characterized by TG, DTA, x-ray diffractometry(XRD), FTIR spectroscopy, BET and electrochemical measurements. Moreover, the results for the prepared powders are compared to the results for powders prepared by solid state reaction of oxides and carbonates.

Oxalate derived spinel was synthesized by heating of precipitates at temperature lower than 650°C . FTIR results showed that the powders prepared even at 600°C had high degree of crystal quality comparing with the solid state reaction powders prepared at 750°C . The particle size of powders prepared by the oxalate precipitation at 600°C was smaller than $0.2\mu\text{m}$ and the specific surface area determined by BET was $11.01\text{m}^2/\text{g}$. The surface area is about ten times as large as that of the classical solid state reaction powders prepared at 750°C . As a result of the TG analysis, it was found that discontinuities of the curves started at temperatures T_1 as well as T_2 during heating and T_2 during cooling. The temperatures were related to reversible phase transitions. The transitions involved weight (oxygen) loss and gain during heating and cooling, which was in agreement with the results reported by Gao et al.[8]. Furthermore, DTA analysis showed that the transition over T_1 denoted a continuous decomposition

(endothermic) reaction, while the transition at T_2 and T_2 were related to additional endothermic and exothermic reaction, respectively. This suggests that the T_1 and T_2 were superheating and supercooling temperatures of transitions involving nucleation and growth of other phases. XRD measurements of samples quenched from temperatures above T_1 and T_2 showed that the other phases formed were oxygen deficient tetragonal, LiMnO_2 and Mn_2O_3 . For high temperature synthesis above 800°C followed by intermediate rate cooling, an irreversible second phase indexed to Li_2MnO_3 was also formed. It is considered that the transition at T_1 , was also responsible for the irreversible phase formation.

The addition of Co made the cubic spinel phase stable and led to a reduction in lattice constant, which might provide stable cell performance during cycling[4]. The increasing of Li excess (in the range of $x=-2 \sim 2$) for the fixed Co content also led to the continuous reduction in the lattice constant. The optimum amount of Li excess along with the Co content was studied.

The low temperature synthesis below 650°C avoided the undesirable second phase formation and the prepared powders showed improved compositional and physical properties for secondary lithium battery applications. The relationship between the spinel composition and the phase transition was analyzed. The effects of composition, powder synthesis condition and powder morphology on electrochemical properties will be elucidated.

ACKNOWLEDGMENTS

This work was supported by GRANT No. KOSEF 97-0300-05-01-3 from the Korea Science and Engineering Foundation.

REFERENCES

1. R. J. Gummow, A. de Kock and M. M. Thackeray, *Solid State Ionics*, **69**, 59 (1994).
2. W. Li, J. N. Reimers and J. R. Dahn, *Phys. Rev. B*, **49**, 826 (1994).
3. L. Guohua, H. Ikuta, T. Uchida and M. Wakihara, *J. Electrochem. Soc.*, **143**, 172 (1996).
4. W. Liu, K. Kowal and G. C. Farrington, *J. Electrochem. Soc.*, **143**, 3590 (1996).
5. D. Guyomard and J. M. Tarascon, *Solid State Ionics*, **69**, 222 (1994).
6. Y. Xia and M. Yoshio, *J. Electrochem. Soc.*, **143**, 825 (1996).
7. P. Barboux, J. M. Tarascon and F. K. Shokoohi, *J. Solid State Chem.*, **94**, 185 (1991).
8. Y. Gao and J. R. Dahn, *J. Electrochem. Soc.*, **143**, 1783 (1996).

Highly rechargeable $\text{Li}_x\text{Mn}_{1-x}\text{Me}_x\text{O}_2$ mixed oxides synthesized via low-temperatures techniques

S.Franger¹, S.Bach¹, J.P.Pereira-Ramos¹, N.Baffier²

1 : CNRS, UMR 7582, LECSO, 2 rue Henri Dunant, 94320 Thiais, France.

2 : CNRS, UMR 7574, LCAES, 11 rue Pierre et Marie Curie, 75231 Paris, France.

Lithiated transition metal oxides LiMO_2 ($\text{M} = \text{Co}, \text{Ni}, \text{Mn}$) have been extensively studied as cathode materials for commercial rechargeable lithium batteries [1-3]. Among these, lithium manganese oxides are promising candidates as cathodes in these systems due to their low cost, abundance and non toxicity.

Two kinds of synthesis ways are usually reported for preparing lithiated manganese oxides. One is a synthesis via solid state reaction. The other one is the use of low temperature techniques, consisting in ion - exchange reactions or sol-gel processes which give the advantage of homogeneity.

Sol-gel process chemistry provides homogeneous mixing of reactants on the molecular level and can also be used to control shape, morphology, and particle size in the resulting products. Previous results obtained in our group have shown the interest of using the sol-gel method to get new and/or high performance cathodic materials especially in the case of V_2O_5 -based compounds and MnO_2 oxides [4-6].

The major problem in developing sol-gel processes for the synthesis of manganese oxides with near MnO_2 stoichiometry is the lack of suitable Mn(IV) molecular precursors in aqueous solution. An alternative consists in the use of redox reactions between fumaric acid and aqueous permanganate solutions [5] in order to get Mn(IV) and then the building of Mn-O-Mn bonds to form an oxide network through polycondensation reactions.

In this paper, a new way of synthesis has been developed to prepare lithiated manganese oxides through an ionic-exchange procedure from the sol-gel lamellar $\alpha\text{-Na}_0.7\text{MnO}_2$. In a second step, these experiments have been performed with metallic ions in order to modify and to improve both the structure and the electrochemical properties of the lithiated manganese oxide.

These phases present attractive properties as rechargeable cathode materials for secondary lithium batteries (Figure 1). During cycling experiments performed at discharge-charge rates of $\text{C}/20$, a stabilization of the specific capacity around 200 mAh.g^{-1} (0.7 F.Mol^{-1}) occurs after the 40th cycle for the best compound obtained with an optimal composition of 15 % in cobalt ions, $\text{Li}_x\text{Mn}_{0.85}\text{Co}_{0.15}\text{O}_2$.

References :

- [1] : T.Ohzu, A.Ueda, M.Nagayama, Y.Iwakoshi and H.Komori, *Electrochimica Acta*, 38 (1993), 1159.
- [2] : M.Broussely, J.P.Planchat, G.Rigobert, D.Virey, G.Sarre, *J.Power Sources*, 68 (1997), 8.
- [3] : R.J.Gummow, A de Kock and M.M.Thackeray, *Solid State Ionics*, 69 (1994) 59.
- [4] : J.P.Pereira-Ramos, S.Bach, N.Baffier, R.Messina, *Solid State Ionics*, 40-41 (1990) 974.
- [5] : S.Bach, M.Henry, N.Baffier, J.Livage, *J.Solid State Chem.*, 88 (1990) 325.
- [6] : S.Bach, J.P.Pereira-Ramos, N.Baffier, *J.Power Sources*, 81-82 (1999) 273.

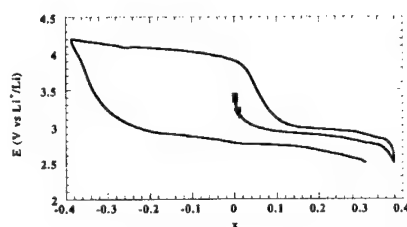


Figure 1 : Chronopotentiometric curves for the reduction/oxidation at low current density ($\text{C} / 20$ rate) of $\text{Li}_x\text{Mn}_{0.85}\text{Co}_{0.15}\text{O}_2$ heat-treated at 300°C in a $1 \text{ Mol.L}^{-1} \text{ LiClO}_4 / \text{Propylene Carbonate}$.

Voltage Prediction from Coulomb Potential Created by Atoms of a Cathode Active Material for Li Ion Cells

Jun-ichi Yamaki, Minato Egashira, and Shigeto Okada
Institute of Advanced Material Study, Kyushu University,
Kasuga Koen 6-1, Kasuga 816-8580, Japan

•The contribution of internal energy change for cathode voltage was studied assuming that the cathode material was completely ionic and only the Coulomb potential was effective. We assumed that an electron is inserted into the nearest metal of the inserted Li⁺. •From the internal energy change by one Li⁺ and one electron insertion (U_a), we have

$$E = -\frac{1}{F} \left[\left(\frac{\partial U}{\partial \xi} \right)_{P,T} + P \left(\frac{\partial V}{\partial \xi} \right)_{P,T} - T \left(\frac{\partial S}{\partial \xi} \right)_{P,T} \right] \approx -\frac{U_a}{F} - \frac{RT}{F} \ln \frac{y}{1-y}$$

$$= -\frac{1}{F} \left(\Phi_L - \Phi_M + I_M - I_L \pm \frac{e}{4\pi\epsilon_0 R_{L-M}} \right) - \frac{RT}{F} \ln \frac{y}{1-y} \quad [1]$$

$$\Phi_k = \frac{e}{4\pi\epsilon_0} \sum_{i,j} \frac{Z_i}{r_{i,j}} = 14.399 \sum_{i,j} \frac{Z_i}{r_{i,j}} \quad [2]$$

where E is potential vs. Li/Li⁺, U is internal energy, ξ is reaction coordinate, F is Faraday constant, P is pressure, V is volume, T is temperature, S is entropy, e is elementary charge, y is Li site occupancy, Φ_L is Coulomb potential of Li site, Φ_M is Coulomb potential of metal site, $(-\Phi_M + I_M)$ is energy level of the inserted electron, I_L is ionization energy of Li, R_{L-M} is the nearest distance between Li and M, ϵ_0 is permittivity of free space, Z_i is charge on species i in signed of electronic charge, $r_{i,j}$ (Å) is distance from an atom of species i to an atom k, Φ_k is Coulomb potential at the atom k, and the sign after I_L is + if Li exists already at the center of k for the calculation of Φ_k , and - if Li is vacant at the center. Φ_k was calculated using a personal computer (VIP Basic, Mainstay), for an ideal cathode Li_{1-x}MO₂ (R3m) (Li-O: 2Å, Ni-O: 2Å), which is a model compound of LiNiO₂. The summation was done for 8000 unit cells. The value of I_L is obtained to be -7.1076 eV from the enthalpy change of Li(cr)•Li⁺(g)+e. We assumed that the energy level of the metal atom is the sum of the electron energy level in vacuum and the Coulomb potential. Using DV-X α molecular orbital method (SCAT)¹, HOMO energy of [NiO₄]⁻¹ cluster was obtained to be -0.30858 eV, where nominal valence of Ni is 3 and that of O is -2/3. The contribution of the Coulomb potential of oxygen is -28.798 eV. Therefore $I_M = I_{Ni} = -0.30858 - 28.798 = -29.106$ (eV).

The voltage of Li_{1-x}MO₂ was calculated to be 0.593 V using $\Phi_L = -12.2485$ eV (empty Li site) and $\Phi_M = -38.7447$ eV (M⁴⁺ site). However the potential is too low. Let us consider an inter-layer Li⁺ ordering, namely Li⁺ occupancy along the c-axis. Li⁺ may occupy the nearest position to the Li⁺ inserted into the next layer just before, because the valence of M is reduced to 3, which decreases the repulsion force to Li⁺. In this case, we have to add -6.73329 eV to Φ_L and 6.73329 eV to Φ_M . Then, we have 3.879 V for the potential of Li_{1-x}MO₂. We assume in-plane Li ordering as shown in Fig. 1. Li_{1-x}MO₂ showed two phase co-existence for 0 < x < 0.25, and one phase for 0.25 < x < 1 by the comparison with the case of no ordering, as shown in Figs. 2 and 3.

From a similar calculation, spinel Li_{1-x}M₂O₄ showed a high potential of 6.839 V at x=0 using the same value of I_{Ni} , without assuming the inter-layer Li⁺ ordering. The potential at x=• was 7.057 V, assuming valence of M of 3.5. If Li-O length becomes shorter and the length of M-O changes to longer, the potential goes down.

Reference 1) H. Adachi editor, "Hajimete no densijoutai keisan / DV-X α bunsikidoukeisan eno nyumon (in Japanese)", ISBN 4-7827-0392-9, Sankyo, Tokyo (1998).

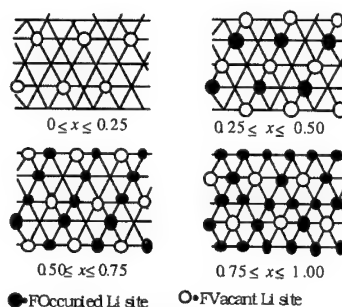


Fig.1 •Li ordering

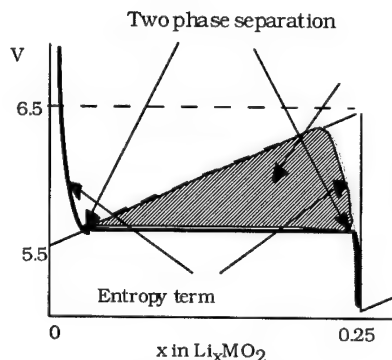


Fig. 2 Two phase separation

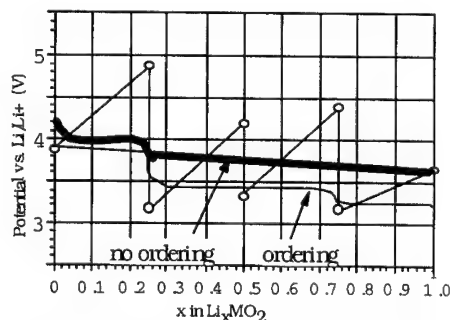


Fig. 3 Potential of ordered rock salt LiMO₂

Influences of the Electrolyte Composition on the Charge and Discharge Characteristics of $\text{LiCr}_{0.1}\text{Mn}_{1.9}\text{O}_4$ Positive Electrode

Masayuki Morita, Taiji Nakagawa, Otoo Yamada,
Nobuko Yoshimoto and Masashi Ishikawa

Department of Applied Chemistry & Chemical
Engineering, Faculty of Engineering,
Yamaguchi University,
2-16-1 Tokiwadai, Ube 755-8611, Japan

The charge and discharge performances of insertion-type electrodes for lithium (Li)-ion batteries are varied with the composition of the organic electrolyte solution (1,2). It is important to establish an optimum composition of the electrolyte system for a specific combination of the positive and negative electrodes. Up to the present, however, little has been known about the details in the effects of the electrolyte composition on the electrode characteristics in Li-ion battery systems. We have investigated the influences of the electrolyte composition on the charge and discharge performances of LiNiO_2 and LiMn_2O_4 cathodes (3-6). In this paper, the electrode characteristics of chromium-stabilized manganese spinel, $\text{LiCr}_{0.1}\text{Mn}_{1.9}\text{O}_4$, have been examined in organic electrolyte solutions with different compositions. We have tried to optimize the solvent composition for using LiBF_4 as the electrolytic salt. The cathode performances will be discussed in relation with the impedance behavior at the electrode/electrolyte interphase.

Ethylene carbonate (EC) or propylene carbonate (PC) was mixed with low viscosity solvent (LVS), dimethyl carbonate (DMC), with and without 1,2-dimethoxyethane (DME). The electrolytic salts were LiClO_4 , LiPF_6 and LiBF_4 . The test electrode was composed of 90 w% of active material, $\text{LiCr}_{0.1}\text{Mn}_{1.9}\text{O}_4$ (Tosoh), mixed with 5 w% of a conducting support and 5 w% of a binder resin. The charge and discharge characteristics were measured by cyclic voltammetry and constant-current polarization using a three-electrode beaker cell equipped with an Li/Li^+ reference electrode. The interfacial behavior was investigated by an ac impedance method (65 kHz - 5 mHz) using a three electrode system. All experiments were carried out under a dry-Ar atmosphere at room temperature (18-25 °C).

The charge and discharge capacities of $\text{LiCr}_{0.1}\text{Mn}_{1.9}\text{O}_4$ were varied with the electrolyte composition, especially with the electrolytic salt. The discharge capacity at the initial cycle decreased in the order of $\text{LiPF}_6 > \text{LiClO}_4 > \text{LiBF}_4$, which was generally consistent with the order of the ionic conductivity of the solution using mixed EC (or PC) and DMC solvents. The rate capability of the cathode for discharging also depended on the electrolyte solution. The discharge capacity in LiPF_6 was high at initial few cycles, but it gradually decreased with cycle repeating.

The ac impedance measurements showed that the charge and discharge characteristics of the $\text{LiCr}_{0.1}\text{Mn}_{1.9}\text{O}_4$ cathode are influenced by both bulk and interfacial impedance of the electrode/electrolyte system. That is, the bulk resistance of the electrolyte determines the initial discharge capacity of the cathode under relatively high rate conditions. The interphase resistance appeared at a moderate frequency region during the first discharge process relates with the capacity loss after the repeated cycles.

The discharge capacity in the LiBF_4 solution with EC+DMC (50+50 by volume) solvent was rather low even at low discharge rates. However, the capacity loss with the cycle repeating was quite low in the solutions containing LiBF_4 . As the LiBF_4 salt is superior to other salts from the viewpoints of safety and environmental compatibility, we have attempted to improve the discharge performances in the solutions using LiBF_4 as the salt. Partial substitution of DMC with equal volume of DME was efficient for the improvements in the ionic conductivity of the solution. The discharge capacity was also improved by the substitution of DMC with DME. That is, ternary solvent system, EC+DMC+DME, gave high discharge capacity even under high rate conditions. Almost ideal (theoretical) discharge capacity of ca. 115 Ah kg^{-1} was obtained for $\text{LiCr}_{0.1}\text{Mn}_{1.9}\text{O}_4$ in LiBF_4 (1 mol dm^{-3})/EC+DMC+DME system. The discharge capacity did not decreased with the repeated charge/discharge cycles in this electrolyte system, in which the ac impedance gave both low bulk resistance and low interfacial resistance.

This work was financially supported by a Grant-in Aid for Scientific Research from the Ministry of Education, Science, Sports and Culture (No. 11650846). This work was also conducted as a partial study of "Dispersed type Battery Energy Storage Technology Research and Development" under the contract with New Energy and Industrial technology Development Organization (NEDO) for the "New Sunshine Program" by AIST, MITT, Japan.

REFERENCES

1. J. M. Tarascon and D. Guyomard, *Solid State Ionics*, **68**, 293 (1994).
2. D. Guyomard and J. M. Tarascon, *J. Power Sources*, **54**, 92 (1994).
3. M. Morita, O. Yamada, M. Ishikawa and Y. Matsuda, *J. Applied Electrochem.*, **28**, 209 (1998).
4. M. Morita, O. Yamada, K. Adachi and M. Ishikawa, *Denki Kagaku*, **66**, 1304 (1998).
5. O. Yamada, M. Ishikawa and M. Morita, *Electrochim. Acta*, **44**, 1607 (1999).
6. M. Morita, O. Yamada and M. Ishikawa, *J. Power Sources*, **81-82**, 425 (1999).

Cathode Material For Primary Lithium Cells Based On Modified Manganese Dioxide

N.D.Ivanova, Y.I.Boldyrev, G.V.Sokolsky

Institute of General & Inorganic Chemistry of Ukrainian Academy of Sciences, 32-34 Prospect Palladina, 252680 Kiev 142, Ukraine

Manganese dioxide finds widespread use in batteries as cathode material. Among five crystalline forms of manganese dioxide electrochemical $\gamma\text{-MnO}_2$ (EMD) is known to be the most electrochemically active. It is nonstoichiometric oxide compound. It has been found that the rate of mass transfer during solid phase electrochemical process is higher in nonstoichiometric oxide compounds. The rate of electrochemical reaction increases with the degree of deviation from stoichiometry [1].

The aim of this work is the increasing of the discharge current density (the rate of electrochemical process) and of the battery capacity. The structure distortion is one of the ways of achievement of this aim.

It can be done electrochemically on the basis of bifunctional electrochemical system principles [2] or chemically by modifying manganese dioxide [3]. These methods allow to increase the degree of deviation from stoichiometry.

The structure distortion is a consequence of the presence of Mn^{3+} and Mn^{4+} ions. The presence of Mn^{3+} in the same crystallographic position as Mn^{4+} occupies is known to be stabilized by hydroxide ions. The amount of OH-group in the bulk of material depends on the nature of manganese dioxide - on the preparation procedure of it.

Modified samples of EMD (1 - Republic of Georgia, 2 - I. S. 10) and CMD (3 - Ukraine) were prepared by insertion of small amount of alkaline metals ions (1', 2') and (3'). The electrical parameters were determined at different loads resistance. The measurements were carried out in two real coin elements: diameter 23, height 2.5 and diameter 20 height 1.6. The discharge curves are presented in figure. It is shown that elements with modified manganese dioxide (1', 2', 3') differ from elements with usual cathodic material (1, 2 and 3). The higher rate of mass transfer in nonstoichiometric oxides makes it possible to operate at low external loads: 1.0-5.6 kOm. In this case a discharge current density of the order of $2.5\text{mA}/\text{cm}^2$ can be realized in the cathode material, which is several times greater than with usual oxide. In accordance with degree of deviation from stoichiometry ionic fraction of conductivity is increased (nearly 20-30%).

The ionic conductivity can be quantitative parameter of degree of deviation from stoichiometry. The comparison of our data with results of prominent firms shows advantages of modifying manganese dioxide, table.

Thus, essential increasing of the discharge characteristics could be achieved by the modifying process. It is necessary to admit that any type of manganese dioxide can be modified. This process is very simple. The general process of preparing cathodic material with operation(stage) modifying is simpler than usual.

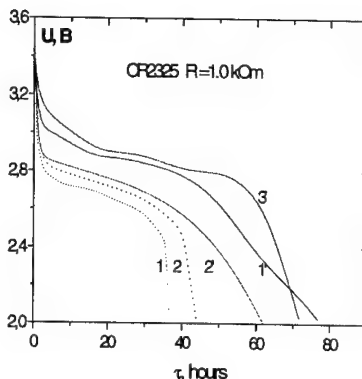


Figure. Discharge curve of Li elements with unmodified (1,2) and modified (1',2',3') cathodic material at external loads 1 kOm.

Table. Discharge characteristics of Li elements. CR2016, 30 kOm

	Our data $\text{MnO}_2 - 1'$	Panasonic	Sony
Nominal Voltage, V	3	3	3
Nominal Capacity, mAh	105	90	72

REFERENCES

1. J.D.Besenhard, J.Heydecke, Fitz H.P. Solid State Ionics.-1982.-6, N3.-p215-224.
2. N.D. Ivanova, S.V. Ivanov. Russian Chemical Reviews, 62, 907 (1993).
3. M.A.Dzieciuch, N.Gupta, and H.S.Wroblowa J.Electrochem. Soc. 135, N10 2415-2418.

Advantages of $\text{LiNi}_{0.8}\text{Co}_{0.2}\text{O}_2$ blending into $\text{Li}_{1+x}\text{Mn}_2-x\text{O}_4$ cathode

Tatsuji Numata, Chika Kanbe, Masato Shirakata,
Masatomo Yonezawa

NEC Corporation
4-1-1, Miyazaki, Miyamae-ku, Kawasaki, Kanagawa,
216-8555, Japan
E-mail: numata@fm1.cl.nec.co.jp

Introduction

Manganese spinel, $\text{Li}_{1+x}\text{Mn}_2-x\text{O}_4$, is one of the most prominent materials as cathode for lithium ion rechargeable batteries, because it has environmental and economic advantages as well as remarkable safety properties compared with LiCoO_2 . Consequently manganese spinel is expected not only for small-size cell with high energy density but also for large-size cell with high power density [1,2] in the near future. However, storage and cycle performance of the cell with manganese spinel cathode declines at elevated temperature (above 45°C). Mn dissolution from spinel structure is reported as one of the causes of this capacity loss [3]. HF in electrolyte, which is formed from supporting salt by contaminated water, causes Mn dissolution from spinel structure.

Therefore some additives that can consume water or prevent acid forming in electrolyte are solutions for avoiding Mn dissolution. LiNiO_2 was expected to be useful additive because it shows high pH (app.10~12) when soaked into water and no water seems to be generated by consuming acid with it. However LiNiO_2 is hard to use for this purpose, because of its poor cycle performance and difficulty of electrode preparation. $\text{LiNi}_{0.8}\text{Co}_{0.2}\text{O}_2$ is preferable material in practical use.

Prevention of Mn dissolution

Blending powder (Manganese spinel and $\text{LiNi}_{0.8}\text{Co}_{0.2}\text{O}_2$) was put into a can with electrolyte (1M LiPF_6 EC/DEC=30/70 by vol.) and sealed completely, then stored 10days at 80°C . After the storing, HF and Mn concentrations were estimated by ion-chromatography and ICP respectively. Fig.1 shows the result. Both HF and Mn concentrations were decreased with the increasing of $\text{LiNi}_{0.8}\text{Co}_{0.2}\text{O}_2$ blending ratio. Mn dissolution was almost prevented with above 10wt% $\text{LiNi}_{0.8}\text{Co}_{0.2}\text{O}_2$ content even at 80°C .

Storage performance of batteries

Blending of $\text{LiNi}_{0.8}\text{Co}_{0.2}\text{O}_2$ with manganese spinel has a big impact on Mn dissolution. Storage performance of cells with the blended cathode and graphite anode at elevated temperature was examined. $\text{LiNi}_{0.8}\text{Co}_{0.2}\text{O}_2$ recipe was tried as 20wt% and [Recover capacity after the storage / initial capacity] was estimated as an indicator for storage performance. The results at 60°C are shown in Fig.2. There is no doubt that $\text{LiNi}_{0.8}\text{Co}_{0.2}\text{O}_2$ serves as a useful additive for improving of high temperature storage performance.

Capacity increase

$\text{LiNi}_{0.8}\text{Co}_{0.2}\text{O}_2$ is also alternate material for LiCoO_2 and has higher capacity than manganese spinel. Charge-discharge property of blended cathode can be explained by composition of each curves arose from

manganese spinel and $\text{LiNi}_{0.8}\text{Co}_{0.2}\text{O}_2$. In other words, capacity of blended cathode is represented as summated capacity of each component. The fact that capacity of blended cathode increases when $\text{LiNi}_{0.8}\text{Co}_{0.2}\text{O}_2$ content is getting higher was confirmed with capacity data measured by coin cells and 18650 cells. Blended cathode with 40 ~ 50% $\text{LiNi}_{0.8}\text{Co}_{0.2}\text{O}_2$ shows equal capacity (mAh/g) to LiCoO_2 .

Conclusion

$\text{LiNi}_{0.8}\text{Co}_{0.2}\text{O}_2$ was investigated as an additive to consume HF in electrolyte. $\text{LiNi}_{0.8}\text{Co}_{0.2}\text{O}_2$ serves as avoiding agent against HF generation in electrolyte after storage at elevated temperature. For this reason, blending of $\text{LiNi}_{0.8}\text{Co}_{0.2}\text{O}_2$ with manganese spinel drastically affects on prevention of Mn dissolution and improving self-discharge. $\text{LiNi}_{0.8}\text{Co}_{0.2}\text{O}_2$ content rising can increase capacity of blended cathode in the range of 3.0 ~ 4.3V vs. Li.

References

- [1] A.M.Wilson et al., the 39th Battery Symposium in Japan, p23, (1998)
- [2] T.Ohta, et al., 196th ECS Fall Meeting abstracts, Vol.99-2, No.95, (1999)
- [3] A.Bylr, A.D.Pasquier, et al., Ionics, Vol.3, p321, (1997)

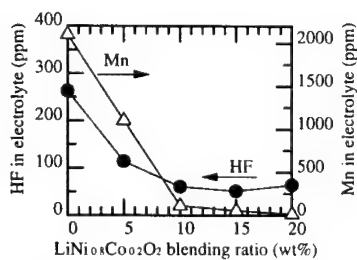


Fig.1 HF and Mn concentrations in electrolyte after 10days storage at 80°C

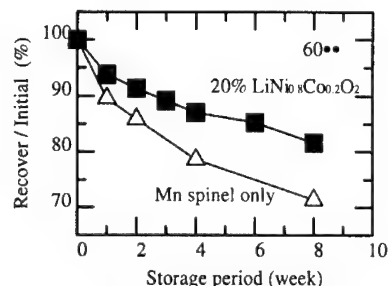


Fig.2 Storage performance at 60°C

Pyrolysis/GC/MS Analysis of the Surface Film Formed on Graphite Negative Electrode

Zempachi Ogumi, Atsushi Sano, Minoru Inaba, and Takeshi Abe

Department of Energy and Hydrocarbon Chemistry, Graduate School of Engineering, Kyoto University, Sakyo-ku, Kyoto 606-8501, Japan

Carbonaceous materials have been extensively studied for use as negative electrodes in rechargeable lithium batteries (lithium-ion batteries). Its charge (lithium intercalation) and discharge (deintercalation) reactions take place at extremely negative potentials close to Li/Li^+ (-3.045 V vs. NHE), and thereby nonaqueous solutions are used instead of aqueous solutions. Even nonaqueous solvents should not be thermodynamically stable at such negative potentials. It is generally believed that a kind of passive film, called solid electrolyte interface (SEI), is formed on carbon negative electrode in the initial stage of charging. The presence of SEI prevents further solvent decomposition and improves the safety and cycleability of lithium-ion cells. However, much of the SEI formation has not been clarified yet in spite of its importance in the battery reactions. In the present study, we used pyrolysis/GC/MS to identify the organic species in the SEI layer formed on graphite negative electrode.

Natural graphite flakes produced in China were used as the test samples. The graphite flakes (40 mg) were wrapped with nickel mesh and pressed moderately to obtain good electrical contacts between flakes. The test electrode did not contain any binder. A conventional three-electrode cell was used for electrochemical pretreatments. The test electrode was kept at a constant potential for 3 h, or charged to 0 V and discharged to 3 V at a C/24 rate in 1 M LiClO_4 dissolved in several kinds of solvent systems, such as ethylene carbonate (EC) and a 1:1 (by volume) mixture of EC and diethyl carbonate (DEC). The counter and reference electrodes were lithium metal. After removed from the cell, the test electrode was washed twice in 1,2-dimethoxyethane (DME), and then dried under vacuum for 10 min.

A schematic diagram of pyrolysis/GC/MS is shown in Fig. 1. The test electrode after an electrochemical pretreatment was introduced in the pyrolyzer kept at 300°C, without being exposed to air upon transfer. The decomposed products (gases) were analyzed by GC/MS to identify the organic species in SEI on the graphite electrode.

Figure 2 shows a gas chromatogram of thermally decomposed products of SEI on the graphite electrode after charge and discharged in 1 M LiClO_4/EC , in which organic species identified by MS are specified. In addition to the solvents (EC, DEC and DME), 1,3-butanediol, 3-methoxy-1,2-propanediol, and oligomers with repeated oxyethylene units, such as ethylene glycol and diethylene glycol, were detected. The presence of these compounds suggests that the SEI layer contained polymer-like substances with repeated oxyethylene units, which are similar to poly(ethylene oxide) (PEO). The similarity indicates that the SEI layer on graphite electrode has lithium-ion conductivity.

The gas chromatograms of graphite electrode after kept at constant potentials (not shown) revealed that the formation of diethylene glycol began to form at 1.0 V. When the potential was lowered, the amount of higher molecular-weight compounds increased, which suggests

that lower potentials accelerate the polymerization reaction.

When graphite electrode was charged and discharged in 1 M $\text{LiClO}_4/\text{EC}+\text{DEC}$, a quite similar result was obtained as shown in Fig. 3. This result shows that SEI is formed mainly by decomposition of EC, rather than DEC.

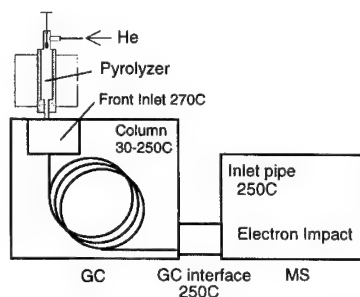


Fig. 1. Schematic diagram of the pyrolysis/GC/MS system.

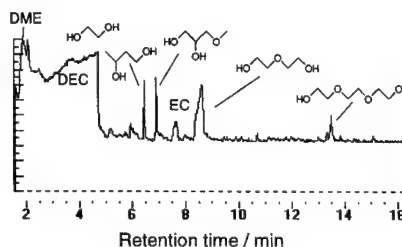


Fig. 2. Gas chromatogram of thermally decomposed product of SEI on natural graphite flakes after charged and discharged in 1 M LiClO_4/EC .

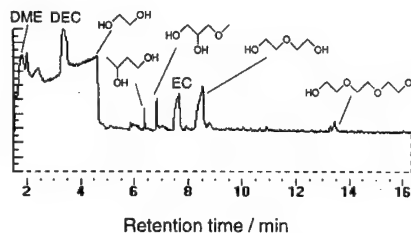


Fig. 3. Gas chromatogram of thermally decomposed product of SEI on natural graphite flakes after charged and discharged in 1 M $\text{LiClO}_4/\text{EC}+\text{DEC}$.

CORROSION OF CATHODIC SULPHIDE MATERIALS
IN MELTED IONIC SALT ELECTROLYTES

V.A. DUSHEIKO, V. V. RADSHENKO, V. U. BURYAK

Department of Chemistry, Kiev State Trade and Economic University, 19, Kioto St., Kiev, 253156, Ukraine
 Department of Chemistry, Ukrainian Transport University, 1 Suvorov St., Kiev, 252010, Ukraine

1. Introduction

Transition metal chalcogenides, in particular ferric sulphides, are of great interest for secondary lithium power sources with melted electrolytes. The merits of the electrochemical cells are stemming from high power capacities, the stability of basic electrochemical characteristics and from their relatively low cost.

However, the usage of melted salts dictates some problems in exploitation of high-temperature batteries, such as the corrosion of the cathode materials in hostile medium.

The objective of the study was to examine the interaction peculiarities of Fe, Ti, Cu, Al sulphides with melted electrolytes, namely mixed (LiCl-KCl) or monocationic ones (LiF-LiCl-LiBr) at 350-500°C range and to determine the solubility of these substances depending on the composition of the cathodic materials.

2. Experimental

The investigation was carried out by isothermal holding of metal sulphide powders in contact with melted electrolyte. The samples of the electrolyte were quenched and analyzed for sulphides and for Fe ions (if ferric sulphides were used). The analysis for sulphide ions was conducted by iodometry techniques and for Fe-ions by measuring electromotive force in concentration circuits.

3. Results and discussion

The data for solubility of Li_2S - FeS_2 -FeS samples in eutectic mixture of LiCl-KCl are given in Table 1.

Table 1

No	Composition of the samples	Solubility of Ferric sulphides, wt %	
		at 350°C, $\text{S} \times 10^4$	at 350°C, $\text{S} \times 10^4$
1	FeS_2	5,0	8,0
2	$\text{Li}_2\text{S} + 9\text{FeS}_2 + \text{FeS}$	6,0	5,0
3	$\text{Li}_2\text{S} + 7\text{FeS}_2 + \text{FeS}$	3,0	3,0
4	$\text{Li}_2\text{S} + 5\text{FeS}_2 + \text{FeS}$	6,0	2,0
5	$\text{Li}_2\text{S} + 3\text{FeS}_2 + \text{FeS}$	10,0	10,0
6	$\text{Li}_2\text{S} + \text{FeS}_2 + \text{FeS}$	20,0	25,0
7	$\text{Li}_2\text{S} + \text{FeS}$	60,0	70,0

The results for measurements of metal sulphides solubility in melted monocationic electrolyte are summarized in Table 2.

Table 2

No	Composition	Solubility of sulphides, wt %		
		at 460°C	at 500°C	at 550°C
1	Li_2S	1,15	1,35	1,77
2	TiS	0,028	0,026	0,023
3	TiS_2	0,051	0,047	0,037
4	$\text{Li}_2\text{S} \cdot \text{TiS}_2$	0,29	0,39	0,50
5	FeS	0,033	0,027	0,030
6	Al_2S_3	1,15	1,19	0,67
7	Cu_2S	0,155	0,195	0,21

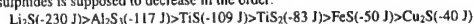
The values obtained make it clear that the samples with Li_2S , which contains the same cation as the electrolyte, possess the highest solubility. The relatively high solubility of different metal sulphides and their distinctive changes with temperature are likely to be caused by ionic double exchange reactions of cathodic material with electrolyte:



where $\text{Me} = \text{Ti, Al, Fe, Cu}$, $\text{Hal} = \text{F, Cl, Br}$.

In effect, the proceeding of the exchange reaction leads to dissolving of Li_2S and MeHal_y in the electrolyte. It seems reasonable that the similarity in properties of metal sulphide with those of lithium sulphide (e.g. ionicity of the bonds, the charge and ionic radius of the ions) favors the run of the reaction above, thus increasing the solubility of metal sulphides.

According to Pauling, the heat of formation per equivalent weight can be taken as a measure of bond ionicity. Using this criterion, the ionicity of sulphides is supposed to decrease in the order:



As a consequence, Al_2S_3 possess the greatest similarity in bond ionicity with Li_2S , and so do their cationic radii. The tendency to form a stable hexafluoroaluminate complex (Li_2AlF_6) also favors the proceeding of the ion exchange reaction between monocationic electrolyte and Al_2S_3 . As the exchange

reaction is supposed to be exothermal, a raise in temperature should adversely affect the equilibrium, thus lowering the sulphide solubility.

The match in ionic charges (+1), which ultimately can counterbalance the effect of bond ionicity, might explain a relatively high solubility of Cu_2S .

Furthermore, one should take into account the role of some other factors on the equilibrium of the exchange reactions, namely fugacity of metal halides and the formation of metal thiosalts Li_2MeS_y .

4. Conclusion

To summarize briefly, the phenomenon of cathodic materials' solubility in melted electrolytes is of major importance for the usage of high-temperature lithium batteries. The deterioration of cathodic materials may be a principal cause for power sources self-discharge and consequently the above mentioned lend impetus to a search for efficient separators used in lithium batteries.

A Novel Method for Preparing Lithium Manganese Oxides and its Electrochemical Characteristics

Yasuo Azuma*, Keiichi Katayama*
and Manabu Suhara**

*Department of Industrial Chemistry, Faculty of
Engineering, Tokai University, Hiratsuka 259-1292, Japan

**Seimi Chemical Co., Ltd., Chigasaki 253-8585, Japan

Introduction

Layered LiMnO_2 compounds are attractive cathode materials for lithium ion batteries in terms of high capacity, abundant resources and environmental concern. Many papers on the synthesis of layered LiMnO_2 have been published, and electrochemical performances have been reported. Lithium manganese oxides have orthorhombic[o-] and monoclinic[m-] crystal forms. Y-I Jang et.al. synthesized o- LiMnO_2 and m- LiMnO_2 by solid state reaction and observed gradual increase in discharge capacity with cycling at room temperature[1][2]. M.Tabuchi et.al. and K.Katayama et.al. synthesized m- LiMnO_2 and doped m- LiMnO_2 by hydro-thermal reaction[3][4]. In this study, we proposed new synthetic method of LiMnO_2 by use of fused salt and electrochemical characteristics were investigated.

Experimental

Mn_2O_3 ($x=0$ to 0.4) was prepared by firing mixtures of MnO_2 and $\text{Mn(NO}_3)_2 \cdot n\text{H}_2\text{O}$ at temperature of 650°C for 3hr in air. LiOH H_2O and KOH were heated at 500°C in a crucible to form an eutectic. Mn_2O_3 was added into the eutectic at temperature of 400 to 900°C in argon atmosphere. After a few minutes of reaction, the crucible was quenched to room temperature. The resultant products were washed with water and dried at 60°C . The products were characterized by XRD. The cathode was prepared by mixing the products with carbon black and PTFE powder into a sheet. The anode was Li foil. An electrolyte composition of ethylene carbonate and diethyl carbonate in the ratio of 1:1 and a salt of LiPF_6 were used. Coin cells of 2032 type were constructed in argon atmosphere. Electrochemical properties were measured at a current of 30mA/g with charge-discharge voltage limit of 2.0 to 4.3V .

Results and Discussion

The formation of LiMnO_2 with LiOH eutectic with Mn_2O_3 in the eutectic proceeded quite rapidly at temperature of 500 to 800°C . After addition of Mn_2O_3 into the eutectic, the precipitate was immediately formed and the formation of floating compounds on the eutectic surface was also observed. The reaction was continued for 5 minutes. The precipitate and floating compounds were separated and washed with water. The phases in these compounds were identified by XRD. XRD pattern of the precipitate is shown in Figure 1. The precipitate was multi-phase and the main phase was found to be o- LiMnO_2 . The floating substance was identified as Li_2MnO_3 by XRD. Prolonged reaction time and high reaction temperature resulted in an increase in the formation of Li_2MnO_3 .

The electrochemical properties of the precipitate were measured. Charge and discharge curves for first cycle is shown in Figure 2. The initial discharge capacity was 110mAh/g at 25°C , and 168mAh/g at 60°C . Thus, it

was found that lithium manganese oxide for lithium battery was quite rapidly and easily synthesized by one-step reaction.

Also it was found that an addition of KOH to LiOH eutectic enhanced the reactivity of the Mn_2O_3 and formation of m- LiMnO_2 . The effect of KOH on the formation of m- LiMnO_2 seems to be quite similar to that observed in hydro-thermal reaction.

Synthesis of a doped LiMnO_2 using this new method was attempted. $\text{Mn}_{1-x}\text{M}_x\text{O}_3$ ($\text{M}=\text{Fe}, \text{Co}, \text{Ni}, \text{Cr}, \text{Al}$ etc.) was treated in LiOH-KOH at 600°C . Reaction time was 5 minutes. Formation of Li_2MnO_3 was not observed. Battery performances of the resultant precipitate were measured. Discharge capacity and energy density for the first cycle at 25°C was 208mAh/g and 626mWh/g , respectively. These values are quite high compared to those reported previously. The first discharge capacity and energy density measured at 60°C were 228mAh/g and 702mWh/g .

Conclusion

A novel method for preparing layered lithium manganese oxide was developed by using LiOH eutectic. The cathode material obtained using this process was found to possess higher battery performance.

References

- [1] Y-I Jang, B Huang, H Wang, D.R.Sadoway and Y-M Chiang, J.Electrochem.Soc., 146, 3217 (1999).
- [2] Y-M Chiang, D.R.Sadoway, Y-I Jang, H Wang, B Huang and H Wang, Electrochemical and Solid-State Letters, 2, 107 (1999).
- [3] M.Tabuchi, K.Ado, H.Kobayashi, H.Kageyama, C.Masquelier, A.Kondo and R.Kano, J.Electrochem.Soc.Lett., 145, L49 (1998)
- [4] K.Katayama, S.Ishii, Y.Azuma, T.Ogihara and M.Suhara J. MRS Japan (in press).

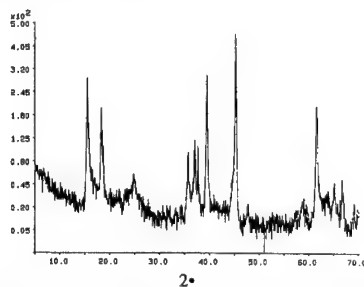


Fig 1 XRD pattern of the precipitate obtained from Mn_2O_3

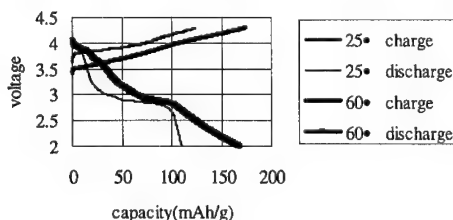


Fig 2 Initial charge and discharge curve of the precipitate obtained from Mn_2O_3

Structure and electrochemical properties of the new layered $\text{Li}_3\text{Cu}_2\text{O}_4$ and $\text{Li}_2(\text{Na}_{0.687}\text{Li}_{0.313})\text{Cu}_2\text{O}_4$.

E. Rackelboom, A. L. Hector, M. T. Weller and J. R. Owen

Department of Chemistry
University of Southampton
Highfield
SO17 1BJ Southampton**Abstract**

The mixed valence lithium sodium cuprate oxide $\text{Li}_3\text{Cu}_2\text{O}_4$ and $\text{Li}_2(\text{Na}_{0.687}\text{Li}_{0.313})\text{Cu}_2\text{O}_4$ have been synthesised and their structures refined from time-of-flight powder neutron diffraction data. The materials are isostructural and contain layers of edge-sharing CuO_4 planes perpendicular to the c direction separated by octahedrally and tetrahedrally coordinated lithium ions. In $\text{Li}_2\text{NaCu}_2\text{O}_4$, the sodium ions occupy octahedral sites. Electrochemical behaviour of both $\text{Li}_3\text{Cu}_2\text{O}_4$ and $\text{Li}_2\text{NaCu}_2\text{O}_4$ was investigated using the Cyclic Voltammetry and the Coulometric Titration Techniques.

Introduction

Various LiMO_2 compounds with layer structures have attracted great interest as cathode materials for secondary lithium batteries. Among them LiCoO_2 has been utilised in commercial battery systems [1]. LiNiO_2 and LiVO_2 have also been studied [2,3]. Lithium extraction from LiCuO_2 would also be of interest because $\text{Li}_{1-x}\text{CuO}_2$ cathode might produce a very high voltage. However previous work in this laboratory has shown that the synthesis of LiCuO_2 by the solid-state calcination method, even under high oxygen pressure results in the formation of: Li_2CuO_2 , $\text{Li}_3\text{Cu}_2\text{O}_4$ [4] and CuO rather than LiCuO_2 . We present here the synthesis, the structure and the electrochemical properties of the layered compounds $\text{Li}_3\text{Cu}_2\text{O}_4$ and $\text{Li}_2(\text{Na}_{0.687}\text{Li}_{0.313})\text{Cu}_2\text{O}_4$.

Description of the structure of $\text{Li}_3\text{Cu}_2\text{O}_4$

The structure contains square-planar CuO_4 units parallel to the b direction linked via their edges to form infinite chains of the stoichiometry CuO_2 . This gives rise to layers perpendicular to the c direction. The layers are separated by lithium atoms occupying tetrahedral sites derived from oxygen atoms in three separate cuprate chains. The remainder of the lithium ions occupy an elongated octahedral oxide ion cavity.

Experimental

$\text{Li}_3\text{Cu}_2\text{O}_4$ and $\text{Li}_2(\text{Na}_{0.687}\text{Li}_{0.313})\text{Cu}_2\text{O}_4$ were synthesised from Li_2O and CuO under high pressure oxygen at 700°C and 250 atm for 3 hours. The electrochemical tests were conducted in a three-electrode cell. The working electrode was a mixture of 60 wt.% active material, 20 wt.% carbon black and 20 wt.% polytetrafluoroethylene (PTFE) binder. Electrode pellets (diam: 14 mm, thickness: 0.3mm) were generated from this mixture and were compression moulded on a mesh. The reference and counter electrodes consist of Li metal foil and the electrolyte of 1 M LiPF_6 in a 1:1 (volume ratio) mixture of ethylene carbonate (EC) and dimethyl carbonate

(DMC). All the electrochemical tests were performed at room temperature with home-built galvanostatic and potentiostatic systems. Constant-current charge-discharge studies were carried out between 2V and 4.6 V at a current density of 1.6 mA/cm^2 . In the cyclic voltammetry, voltage was scanned at the scan rate 0.1 mV/s .

Results

The $\text{Li}_3\text{Cu}_2\text{O}_4$ and $\text{Li}_2(\text{Na}_{0.687}\text{Li}_{0.313})\text{Cu}_2\text{O}_4$ cells delivered discharge capacities of 90 and 50 mAh.g^{-1} respectively during which ~ 0.7 and ~ 0.4 lithium ions were inserted respectively.

The oxidation reaction $\text{Cu}^{2+} \rightarrow \text{Cu}^{3+}$ occurs at a higher potential in $\text{Li}_2(\text{Na}_{0.687}\text{Li}_{0.313})\text{Cu}_2\text{O}_4$ (3.8 V) than in $\text{Li}_3\text{Cu}_2\text{O}_4$ (3.4 V). However the capacity to a 4.5V limit is larger in $\text{Li}_3\text{Cu}_2\text{O}_4$ and the capacity fade on cycling is reduced.

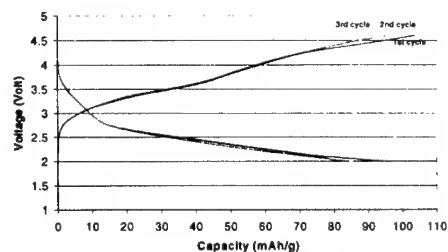


Fig.1: Early charge-discharge curves of $\text{Li}_3\text{Cu}_2\text{O}_4$ at 1.6 mA/cm^2 between 2V and 4.6V

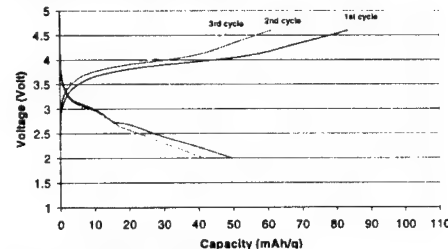


Fig.2: Early charge-discharge curves of $\text{Li}_2(\text{Na}_{0.687}\text{Li}_{0.313})\text{Cu}_2\text{O}_4$ at 1.6 mA/cm^2 between 2V and 4.6V

References

- [1] T. Naugara, *Prg. Batt. Mater.* **10** (1991) 209
- [2] M.G.R.S Thomas, W.I.F. David, J.B. Goodenough, *Mat. Res. Bull.* **20** (1985) 1137
- [3] L.A. de Picciotto, M.M Tackeray, W.I.F David, P.G. Bruce, J.B Goodenough, *Mat. Res. Bull* **19** (1984) 1497
- [4] D.B.Currie and M.T. Weller. *J. Mater. Chem.* **3** (1993) 229-232

Physical and Electrochemical Characterisation of $\text{LiNi}_{0.8}\text{Co}_{0.2}\text{O}_2$ Thin Film Electrodes Deposited by Laser Ablation

G. X. Wang*, M. J. Lindsay, M. Ionescu, D. H. Bradhurst, S. X. Dou and H. K. Liu

Energy Storage Materials Research Program, Institute for Superconducting & Electronic Materials, University of Wollongong, NSW 2522, Australia

Thin-film lithium microbatteries provide the best power sources for miniature microelectronic devices such as back-up power for computer memory chips, micromechanics and ultra-thin watches[1]. The preparation of thin-films plays a critical role in manufacture of thin-film microbatteries. Many techniques, including CVD, e-beam evaporation, pulse laser deposition (PLD) and sol-gel, can be used to produce thin films. Laser ablation has several advantages. It can deposit thin-films with complex stoichiometries, high deposition rate, uniform thickness and no requirement for post annealing treatment[2].

The thin-film electrodes of $\text{LiNi}_{0.8}\text{Co}_{0.2}\text{O}_2$ were deposited by pulse laser ablation. The x-ray diffraction showed that the thin films have the same phase as the target. The morphology was observed by AFM as shown in Fig. 1. The average thickness of the thin films was measured to be approximately 620 nm.

The thin-film electrodes have a structure and geometry without pores, conductive additives or binders. This provides a pure and clean interface for fundamental electrochemical study. A variety of electrochemical measurements were performed on the $\text{LiNi}_{0.8}\text{Co}_{0.2}\text{O}_2$ thin-film electrodes. Galvanostatic charge/discharge cycling was used to determine the capacity and cycle life of thin-film electrodes. The kinetic parameters of lithium insertion and extraction in $\text{LiNi}_{0.8}\text{Co}_{0.2}\text{O}_2$ thin-films were determined from AC impedance and cyclic voltammetry measurements. The CV curves of one of these electrodes are shown in Fig. 2. Three oxidation and reduction peaks were observed, which might correspond to the phase transformation of the $\text{LiNi}_{0.8}\text{Co}_{0.2}\text{O}_2$ phase during lithium intercalation and de-intercalation.

The pulse laser ablation technique can be used to produce thin-films with high quality. Therefore, thin-film lithium microbatteries could also be manufactured via this technique.

References

- [1] J. B. Bates, N. J. Dudney et. al., *J Power Sources*, **54**, 58 (1995).
- [2] K. A. Striebel, C. Z. Deng, S. J. Wen, and E. J. Cairns, *J. Electrochem. Soc.*, **143**, 1821(1996).

* Corresponding author, email: gw14@uow.edu.au



Fig.1. AFM surface morphology of a $\text{LiNi}_{0.8}\text{Co}_{0.2}\text{O}_2$ thin film.

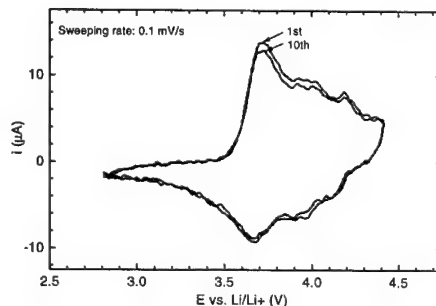


Fig. 2. The cyclic voltammetry curves of $\text{LiNi}_{0.8}\text{Co}_{0.2}\text{O}_2$ thin-film electrodes.

Effects of conducting carbon on the electrochemical performance of LiCoO₂ and LiMn₂O₄ cathodes

Zhaolin LIU¹, J. Y. LEE² and H. J. LINDNER¹¹Institute of Materials Research and Engineering, 3 research link, Singapore 117602²Department of Chemical and Environmental Engineering, National University of Singapore, Singapore 119260

Introduction

Layer LiCoO₂, layer LiNiO₂, and spinel LiMn₂O₄ are common cathode materials for today's high energy density and long life lithium-ion batteries. Since these oxides have low intrinsic electronic conductivities, they have to be mixed with a conductive additive such as carbon black to form a working cathode. Jang et al.^[1] reported recently that the cell capacity can fade rather severely if the carbon content in the LiMn₂O₄ cathode is low. Excess carbon may be advantageous for cyclability but the cell energy and power densities are necessarily lower after the addition. It is therefore important to optimize the amount of carbon in working cathodes.

In this paper, we report the effects of carbon loading on the electrochemical performance of LiCoO₂ and LiMn₂O₄ cathodes. Polarization losses and capacity losses upon cycling were examined for different carbon loadings, and electrochemical impedance spectroscopy was used to determine the major factors affecting long-term cyclability.

Experimental

LiCoO₂ was prepared by reacting stoichiometric amounts of CoCO₃ and Li₂CO₃ in air for 24h at 850°C. Spinel LiMn₂O₄ was prepared by heating stoichiometric amounts of Li₂CO₃ and MnCO₃ in air for 24h at 450°C, followed by another 24h at 750°C. The crystal structures of the oxides were determined by X-ray diffraction. LiCoO₂ and LiMn₂O₄ were mixed with 2-10% of carbon black (except stated otherwise) and 8% of PVDF in NMP, and coated onto Al disk electrodes 1.6cm in diameters. The electrolyte was 1M LiPF₆ in a 1:1 mixture of ethylene carbonate (EC) and dimethyl carbonate (DMC). Lithium foils were used as the counter and the reference electrodes in the electrochemical measurements. Cyclic voltammetry and battery life cycle tests were carried out on an EG&G model 273 potentiostat/galvanostat and a Bitrode battery tester, respectively.

Results and discussion

At the low charging rate of 0.2C, carbon content does not affect the charge and discharge capacities of LiCoO₂ and LiMn₂O₄. The LiCoO₂ electrode is however highly sensitive to carbon loading at higher rates of charging. At 1C rate, for instance, higher charge and discharge capacities are obtained with 10% of carbon loading relative to 2% and 5% of carbon. The charge and discharge capacities of LiMn₂O₄ electrodes at the 1C rate are not as dependent on the carbon content, showing only a general reduction in the capacity at the higher charging rate.

A typical cyclic voltammogram of the LiCoO₂ electrode is shown in Fig. 1a. Three clearly resolved redox pairs can be identified: the peaks at 3.93V, 4.08V, and 4.18V due to Li⁺ intercalation, and the corresponding peaks at 3.90V, 4.07V, and 4.17V due to Li⁺ de-intercalation are in good agreement with the results of Plichta^[2], Dahn^[3] and Uchida^[4]. LiCoO₂ electrodes with 10% of carbon show stronger and sharper peaks than that loaded with 2% of carbon, where only broad and indistinct features indicative of a disordered electrochemical response were obtained. The pasted-cathode is a resistive and porous system where clean electrochemical response can only be obtained using excess carbon (e.g. 10% carbon loading) and very slow scan rates. In the cyclic voltammogram of LiMn₂O₄ in Fig. 1b, the anodic and cathodic features around 4.2V and 3.9V respectively pertain to the reversible oxidation and reduction reactions in Li⁺ extraction and insertion. The peaks are split which, according to Tarascon and Guyomard^[5], are indications of insertion and extraction reactions occurring in stages. The integrated areas below the two oxidation (or reduction) peaks are approximately equal, suggesting that in each stage Li⁺ ions occupy half of the total available crystallographic sites. The splitting in the

voltammograms is most easily detected for 10% carbon loading of the LiMn₂O₄ electrode, but the effects of carbon loading on the voltammogram is not as sensitive as in LiCoO₂ electrode. This is consistent with results from galvanostatic charging.

The cyclability of LiCoO₂ and LiMn₂O₄ electrodes with 2% and 10% of carbon loadings were examined. At 1C charging rate, capacity fade is higher in electrodes loaded with 2% of carbon. Cyclability improves generally at lower rates of charging. LiCoO₂ with 10% of carbon cycles well but electrodes with only 2% of carbon still fare poorly. The effects on carbon loading on the cyclability of LiMn₂O₄ electrodes are similar. Carbon abundance is therefore beneficial to cyclability. This advantage is however realized at the expense of lower energy and power contents of the resulting cells, as electrically conductive but electrochemically inactive carbon necessarily adds weight and volume to the cells. Good capacity retention (at 1C charging rate) may be obtained in practice with 5% or more of carbon in the LiCoO₂ and LiMn₂O₄ cathodes. The reduced discharge capacity after charging at the 1C rate is due to incomplete charging from deteriorating electrical contact between oxide and carbon particles, which increases the cathode polarization.

References

- [1] D. H. Jang, Y. J. Shin, and S. M. Oh, *J. Electrochem. Soc.*, 143 (1996) 2204.
- [2] E. Plichta, S. Slane, M. Uchiyama, M. Salomon, D. Chua, W. B. Ebner and H. W. Lin, *J. Electrochem. Soc.*, 136 (1989) 1865.
- [3] J. N. Reimers and J. R. Dahn, *J. Electrochem. Soc.*, 139 (1992) 2091.
- [4] I. Uchida and H. Sato, *J. Electrochem. Soc.*, 142 (1995) L139.
- [5] D. Guyomard and J. M. Tarascon, *J. Electrochem. Soc.*, 139 (1992) 937.

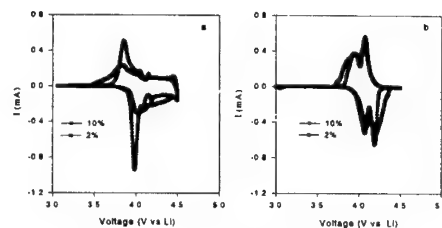


Fig. 1 Cyclic voltammograms (at 0.03mV/s) for (a) LiCoO₂ and (b) LiMn₂O₄ cathodes of different carbon loadings.

Structure and electrochemical properties of $\text{LiSi}_y\text{Co}_{1-y}\text{O}_2$ cathode for lithium rechargeable battery

Tang Zhiyuan Xue Jianjun Li Jiangang Cao
Gaoping
School of chemical engineering, Tianjin university
Tianjin300072, China
e-mail: jj-xue@263.net

Introduction

Various transition metal oxides have been studied as cathode materials of rechargeable lithium battery. Because of easy preparation and high theoretical specific capacity, LiCoO_2 is mostly used as the cathode material of commercial secondary lithium battery. But its high cost limits the further expansion of the application for lithium battery. Introduction of Al ion into the structure of LiCoO_2 may reduce the cost and stabilize the layered solid [1,2], but the discharge capacity is low. The focus of this study is to investigate silicon-doped LiCoO_2 as cathode materials for lithium secondary battery. LiCoO_2 and silicon-doped LiCoO_2 cathode materials were prepared by solid state reaction. Structure characterization of the oxides $\text{LiSi}_y\text{Co}_{1-y}\text{O}_2$ has been performed by X-ray diffraction. Electrochemical characterization of the prepared materials as cathode for lithium battery has been investigated by using galvanostatic charge and discharge, electrochemical voltage spectroscopy and cyclic voltammetry.

Result and Discussion

LiCoO_2 and silicon-doped $\text{LiSi}_y\text{Co}_{1-y}\text{O}_2$ cathode material were prepared by mixing stoichiometric amount of Li, Si, Co salt and then calcining in air for 24h. The crystal structure of $\text{LiSi}_y\text{Co}_{1-y}\text{O}_2$ ($y=0, 0.05, 0.10, 0.15, 0.20, 0.30$) was characterized by X-ray diffraction(XRD) and powder XRD pattern was recorded using $\text{Cu K}\alpha$ radiation. Figure 1 shows the XRD pattern for the silicon-doped $\text{LiSi}_y\text{Co}_{1-y}\text{O}_2$ cathode materials. Impurity of the prepared cathode materials is observed when the silicon content is above 0.1.

The $\text{LiSi}_y\text{Co}_{1-y}\text{O}_2$ ($y=0, 0.05, 0.10, 0.15, 0.20, 0.30$) electrodes was prepared by casting a mixed slurry of the prepared materials, acetylene black, PTFE binder (80:10:10) onto aluminum foil. The composite electrodes were dried under vacuum at 120°C for at least 12h before use. The charge and discharge cycle test was conducted in the voltage range of 3.30–4.25V at the current density 8mA/g. A three electrode electrochemical cell was employed for electrochemical measurement in which lithium foil was used for both reference and counter electrodes. Figure 2 shows the first discharge curves of $\text{LiSi}_y\text{Co}_{1-y}\text{O}_2$ at $y=0.10, y=0.20$ and 0.30. Although there is impurity in the prepared cathode material when the silicon content is 0.2, its first discharge capacity is 112 mAh/g. But decline of the first discharge capacity is observed with increase of silicon content of the cathode materials. It can be explained by the high coexisting impurity when silicon content is high.

Reference

[1]G. Ceder, Y. -M. Chiang, D.R. Sadoway, M. K.

Aydinol, Y.-I.Jang, and B. Huang, *Nature*, 392, 694(1998).

[2]R. Alcantara, P. Lavela, P. L. Relano, J. L. Tirado, E. Zhecheva, and R. Stoyanova, *Inorg. Chem.*, 37, 264(1998).

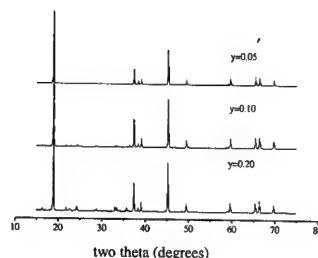


Figure 1 X-ray diffraction pattern of silicon-doped $\text{LiSi}_y\text{Co}_{1-y}\text{O}_2$ cathode material

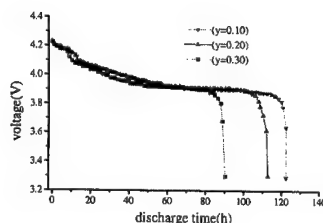


Figure 2 Discharge curves illustrating the capacity of the oxides $\text{LiSi}_y\text{Co}_{1-y}\text{O}_2$ at discharge current density 8 mA/g.

Spontaneous modification of the electrode surface in contact with non-aqueous electrolyte

D. Ostrovskii, P. Jacobsson
 Department of Experimental Physics, Chalmers
 University of Technology, SE-41296 Göteborg, Sweden

F. Ronci, B. Scrosati,
 Department of Chemistry, University "La Sapienza",
 Rome, Italy

Lithium polymer batteries (LPB) have a great potential for numerous practical applications varying from the microbatteries for portable electronics to the power sources for electric vehicles. To the present time, various electrolytes and electrode materials have been tested in order to optimize the batteries. It is clear that along with the properties of each battery's component themselves, the electrode-electrolyte interfacial behavior determines in a large extent the performance.

It has been found that a layer appears on the lithium electrode surface when it is stored or cycled in an electrolyte [1]. The mechanism of formation of this passivating layer (or solid electrolyte interface, SEI) and its physico-chemical properties have been intensively studied by various techniques [1-5]. Now it is generally accepted that only in the case of alkali-metal electrodes (due to their extremely high reactivity) a SEI may appear already at contact with an electrolyte, without applied potential [2,3]. For all other commonly used electrode materials, formation of the passivating layer is believed to start after the first charge/discharge cycle, and no signs of reduction of the electrolyte or electrode material solely due to the contact between them have been observed [5].

However, in recent study [6] we found that some new compounds or functional groups appear on the surface of $\text{LiNi}_{0.75}\text{Co}_{0.25}\text{O}_2$ -based electrode during the storage in non-aqueous organic electrolytes. Moreover the type of those compounds depends on the type of electrolyte used (see Fig. 1). It was therefore suggested that the appearance of new compounds on a $\text{LiNi}_{0.75}\text{Co}_{0.25}\text{O}_2$ surface is due to a decomposition of the electrolyte components.

In this work we report on results of an extended spectroscopic investigation of the behavior of several typical electrode materials in contact with organic non-aqueous electrolytes. The electrodes have been stored in various electrolytes over times varying from 1 to 4 weeks and then examined by IR diffuse reflectance and Raman spectroscopy. An analysis of the newly formed compounds is presented. The dependence of the layer composition on the type of electrolyte is discussed along with some possible mechanisms of layer formation.

In addition, we observed a significant alteration of the "real" SEI, which has been previously formed on the electrode surface by electrochemical cycling, during the storage of the samples in liquid electrolyte. This finding agrees well with the results of electrochemical investigation [7], where degradation of SEI layer on carbon-based electrodes at storage was reported. The reasons of this phenomenon are also discussed.

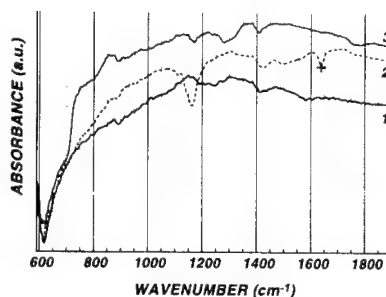


Fig. 1. IR diffuse reflectance spectra of $\text{LiNi}_{0.75}\text{Co}_{0.25}\text{O}_2$ -based cathode: 1 - initial; 2 - after 10 days storage in 1M LiClO_4 - PC; 3 - after 10 days storage in 1M LiPF_6 - EC/DMC.

Acknowledgments

DO and PJ wish to thanks MISTRA (Sweden) for financial support.

References

- [1] A.N. Dey, B.P. Sullivan, J. Electrochem. Soc. **117** (1970) 222.
- [2] E. Peled, J. Electrochem. Soc. **126** (1979) 2047.
- [3] E. Peled in *Lithium Batteries*, (Chapter 3) ed. J.-P. Gabano, Academic Press, 1983.
- [4] D. Aurbach et al., J. Electrochem. Soc. **142** (1995) 2873.
- [5] M. Jean, A. Chausse, R. Messina, Electrochim. Acta **43** (1998) 1795.
- [6] D. Ostrovskii, P. Jacobsson, F. Ronci, B. Scrosati, A FTIR and Raman Study of the $\text{LiNi}_{0.75}\text{Co}_{0.25}\text{O}_2$ electrode/Non-aqueous Electrolyte Interface, International Conference on Interfacial Phenomena in Batteries, Dec. 12-15, 1999, Rome, Italy.
- [7] A. Andersson, K. Edström, 196th Meeting of The Electrochemical Society, 1999 Fall Meeting of The Electrochemical Society of Japan with technical cosponsorship of The Japan Society of Applied Physics Honolulu, Hawaii October 17-22, 1999. Abstract No. 244.

Abstract No. 156

Improved cycle performance of orthorhombic $\text{LiMn}_{0.95-x}\text{M}_x\text{Cr}_{0.05}\text{O}_2$; $\text{M}=\text{Al}, \text{Ga}, \text{Yb}, \text{Y}$ and In , synthesized by hydrothermal technique

Takeshi Sakurai, Takashi Kimura and Tadashi Sugihara
Microelectronics laboratories, Central Research Institute,
Mitsubishi Materials Corporation
1-297 Kitabukuro, omiya, saitama 330-8508, JAPAN

The effect of Mn substitution by other trivalent elements on the cycle performance was examined for the orthorhombic manganese oxide (o- LiMnO_2). Though Ozuku, et.al. [1] reported high capacity up to 190mAh/g, irreversible phase transformation occurred from orthorhombic to spinel related structure during first charge [2]. So, this suggested poor cycle performance causing to the phase transformation. If the phase stability was achieved, the cycle performance seemed to be improved.

Samples were synthesized by hydrothermal technique [3]. Concerning to the reproducibility of fine powders, this process is superior to the conventional solid state reaction method [4]. In this work, powders having average grain size of 800nm were synthesized. Resulted powders were characterized by X.R.D., T.E.M. observations and charge-discharge properties.

For the preparation of electrodes, the recipe is mainly based on Richard's conditions [5]. As grain size of cathode powders should be different, condition of preparing cathode electrode was carefully refined. Cathode films with 10mm x 10mm each were settled on both side of 500-meshed Al current collector, and hot pressed by applying 24kgf/cm² for 5min at 130C.

Cycle performances were evaluated by measuring charge and discharge properties using open cells assembled under the dry Ar atmosphere. Counter and reference electrodes were consisting of Li foil. The electrolyte composition was 1.0M of LiPF_6 in a mixture of ethylene carbonate and propylene carbonate in a volume ratio of 1:1. This electrolyte was selected by the reason for the stability of high voltage. Cells were charged by cvcc mode and discharged cc mode, respectively. Charging up to 4.3V, current density was 20mA/cm². After potential reached to 4.3V, current density was decreased continuously in order to keep the same potential until the scheduled period had passed. Discharging down to 2.5V, current density was 10mA/cm².

Fig.1. Shows cycle performances of $\text{LiMn}_{0.95-x}\text{M}_x\text{Cr}_{0.05}\text{O}_2$ samples. All of samples are confirmed to be single phase by x-ray diffraction. Discharge capacities are monotonically decreased for the samples consisting of the combinations of (Al, Cr, Mn), (Ga, Cr, Mn) and (Y, Cr, Mn). In other samples consisting of the combinations of (Yb, Cr, Mn) and (In, Cr, Mn), cycle performance are found to be improved. It can be said that controlling average ionic radius larger than 0.645Å is effective method for this propose.

Fig.2 shows the x-ray diffraction patterns of $\text{LiMn}_{0.95-x}\text{In}_x\text{Cr}_{0.05}\text{O}_2$ samples. Solid solution of o- LiMnO_2 is exhibited in the composition range between 0 and 0.03. Reduction of crystalline size or increasing strain of crystalline seem to be reasons why the diffraction peaks are broadened at $x=0.03$. In_2O_3 is obtained as an impurity phase at $x=0.05$, which exhibit rapid degradation of cycle performance.

As the result of our study, it is concluded that improved cycle performance is achieved around the solubility limit of o- LiMnO_2 , whose average ionic radius

at Mn site is controlled to be larger than 0.645Å of trivalent Mn.

A part of this work was performed by Mitsubishi Materials Corporation, under the management of the Micromachine Center, as the Industrial Science and Technology Frontier Program "Research and Development of Micromachine Technology" of MITI, supported by the New Energy and Industrial Technology Development Organization.

- [1] T.Ozuku, A.Ueda and T.Hirai, Chem. Express, 7(1992)193-196
- [2] I.M.Kotchou and J.R.Dahn, J.Electrochem, 145(1998)2672-2677
- [3] M.Tabuchi, et.al., Solid.state.ionics, 89(1996)53-63
- [4] R.J.Gummow and M.M.Thacheray, J.Electrochem.Soc., 141(1994)1178
- [5] M.N.Richard, I.Koetschau and J.R.Dahn, J.Electrochem.Soc., 144(1997)554-557

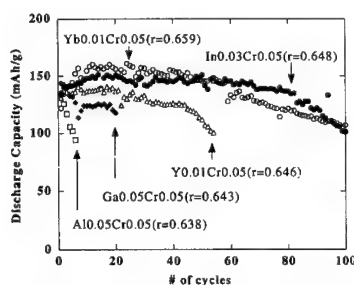


Fig.1 Cycle performance of $\text{LiMn}_{0.95-x}\text{M}_x\text{Cr}_{0.05}\text{O}_2$ samples obtained by hydrothermal technique. Average ionic radius at Mn site is varied from 0.638 to 0.659Å by controlling the combinations of additive elements; M and content; x.

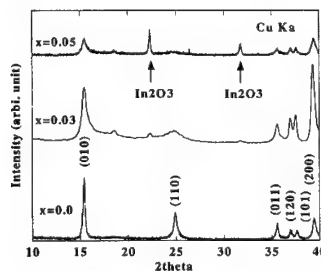


Fig.2 x-ray diffraction patterns of $\text{LiMn}_{0.95-x}\text{In}_x\text{Cr}_{0.05}\text{O}_2$ samples obtained by hydrothermal technique. Peaks belonging to LiMnO_2 are indexed by orthorhombic unit cell of $a=4.57\text{\AA}$, $b=5.75\text{\AA}$ and $c=2.81\text{\AA}$. It is found that solid solution of o- LiMnO_2 is formed where x is smaller than 0.03. Broadened diffraction peaks are observed at the increased content range. In_2O_3 as an impurity phase formed by excess In at $x=0.05$.

Abstract No. 157

Electrochemical synthesis, characterization and lithium insertion behavior of $e\text{-M}_0.15\text{V}_2\text{O}_5$ compounds ($\text{M}=\text{Ni}^{2+}$, Cu^{2+} , Mn^{4+}).

E. Potiron, A. Le Gal La Salle, A. Verbaere, Y. Piffard and D. Guyomard

Institut des Matériaux Jean Rouxel, CNRS - University of Nantes, BP 32229 - 44322 Nantes Cedex 3, France.

The preparation of oxide materials by oxidation of aqueous solutions is well known and the preparation of V_2O_5 by oxidation of VOSO_4 solutions has been reported recently [1,2]. Vanadium oxides are among the most studied cathode materials for rechargeable Li-metal batteries and vanadium oxide-based compounds present good performance in terms of specific capacity and cyclability [3] and can be considered as the short-term alternative for Li-metal batteries. This paper reports the preparation of new vanadium-based compounds by oxidation of mixtures of VOSO_4 and MSO_4 solutions (with $\text{M}=\text{Cu}$, Ni , Mn).

The synthesis was performed by applying a constant current density or voltage at a platinum electrode immersed in the aqueous solution. After being collected by scraping the Pt electrode, samples were first rinsed with distilled water and then dried at room temperature. An annealing procedure of 1 hr at 100°C under vacuum was used in order to dehydrate the samples in view of further Li insertion experiments. A combination of X-ray analyses, TGA, redox titrations, X-ray electron spectroscopy and X-ray absorption spectroscopy was used to characterize the samples. Composite electrodes were prepared by mixing the active material, a carbon black (Super-P from Chemetals Inc., Baltimore, MD, USA) and a binder (polyvinylidene difluoride: PVDF) with the mass ratio (85:10:5) and coating the mixture onto an Al disk serving as the current collector. Standard laboratory swagelok test cells were used with the composite electrode as the positive and Li metal as the negative, separated with glass paper soaked in the electrolyte. The electrolyte was made of 1M LiPF_6 dissolved in a 2:1 mixture of ethylene carbonate (EC) and dimethyl carbonate (DMC). The cells were tested using the Mac-Pile system (Biologic, Claix, France) operating in galvanostatic or potentiodynamic mode between 4 and 2 V/Li.

By oxidizing pure VOSO_4 solutions, hydrated vanadic acids, containing both VIV and VV are obtained [2]. Their formulation can be written $\text{V}_2\text{O}_5 \cdot 2\text{-} \frac{1}{2} \text{H}_2\text{O}$, where $0.08 < \frac{1}{2} < 0.4$ and $0.2 < n < 2$. When the mixture of

$\text{VOSO}_4 + \text{CuSO}_4$ (or NiSO_4) is oxidized, the Cu^{2+} (or Ni^{2+}) cations are incorporated into the electrodeposited products. Taking into account the VIV/Vtotal ratio (15%) of the products, their formulation can be formally written $\text{Cu}(\text{or Ni})_0.15\text{V}_2\text{O}_5 \cdot n\text{H}_2\text{O}$ ($1.1 < n < 1.3$). When the oxidation is performed in the presence of MnSO_4 , Mn^{2+} and VO_2^+ are oxidized simultaneously, and the products, that contain mainly VV and MnIV have the formulation $\text{Mn}_0.2\text{V}_2\text{O}_4 \cdot 9.1.7\text{H}_2\text{O}$ [4].

Upon the annealing procedure of 1 hr at 100°C under vacuum the water content of all compounds is comprised between 0.2 and 0.4 H_2O per formula unit, but the VIV, VV, MnIV, CuII (or NiII) contents are not modified.

The electrochemical behavior of the different compounds was compared to results obtained previously on pure vanadium oxides with the same VIV content [2]. The various compounds can be differentiated from their slightly different lithium insertion behavior. As a matter of fact, the presence of nickel or copper induces an increase of the average voltage and a decrease of the intercalation capacity (Figure), while the presence of manganese improves the cycling behavior.

[1] - Y. Sato, T. Nomura, H. Tanaka and K. Kobayakawa, J. Electrochem. Soc., 138(9) (1991) L37

[2] - E. Potiron, A. Le Gal La Salle, A. Verbaere, Y. Piffard and D. Guyomard, Electrochim. Acta, 45 (1999) 197

[3] - D. Guyomard, in "New Trends in Electrochemical Technology : Energy Storage Systems for Electronics", Editors : T. Osaka & M. Datta, Chapter C1-9, 1999, 253.

[4] - A. Le Gal La Salle, E. Potiron, S. Sarciaux, D. Guyomard and Y. Piffard, J. New Mat. Electrochem. Syst., 1(1) (1998) 89

Synthesis by Sol-gel Process and Characterization of $\text{LiCr}_x\text{Mn}_{2-x}\text{O}_4$ Cathode Materials

Tang Zhiyuan Li Jiangang Xue Jianjun Cao Gaoping
School of Chemical Engineering and Technology,
Tianjin University, Tianjin, 300072, China

Doping spinel lithium manganese oxide with chromium have been reported to be an effective way for improvement of its rechargeability^[1-3]. In these studies, the spinels have been synthesized using traditional solid-state reaction, which may result in non-homogeneity, abnormal grain growth, and poor control of stoichiometry. In the present study, we adapted a sol-gel method to the synthesis of $\text{LiCr}_x\text{Mn}_{2-x}\text{O}_4$ ($x=0.05, 0.20$). This process can provide for homogeneity on an atomic scale. Using the sol-gel method, it is possible to obtain the phase-pure, ultrafine $\text{LiCr}_x\text{Mn}_{2-x}\text{O}_4$ by employing temperatures as low as 600°C for several hours. The results of a series of electrochemical tests have revealed that the $\text{LiCr}_x\text{Mn}_{2-x}\text{O}_4$ materials obtained by the sol-gel method can offer high capacity and good rechargeability.

$\text{LiCr}_x\text{Mn}_{2-x}\text{O}_4$ were prepared by dissolving metal nitrates into citric acid solution, evaporating the solvent to form polymeric precursor, then calcining the precursors in air at various temperatures for 6h. For phase identification, a X-ray diffraction with $\text{Cu-K}\alpha$ radiation was used. The formation process for spinel was investigated by thermal analysis at a heating rate of $10^\circ/\text{min}$ from room temperature to 800°C in air. The cathode materials surface areas were determined by the BET method using a CHEMBET-3000 instrument. The electrochemical cell was used a two electrode Swagelok cell consisted of a lithium metal anode and a $\text{LiCr}_x\text{Mn}_{2-x}\text{O}_4$ cathode that were separated by a separator (Celgard 2500 membrane). The cathodes were prepared by pressing a blend of active material (15mg), acetylene black (5mg) and PTFE (5mg) onto a Al mesh. The electrolyte solution was 1M $\text{LiPF}_6/\text{EC}+\text{DEC}$ (1:1) solution. Cell fabrication was carried out in an Ar-filled dry box (MB150-BG, M.BRAUN). Constant-current charge-discharge studies were controlled with a battery cycler. Charge-discharge studies tests were performed at constant current density ($0.2\text{ mA}/\text{cm}^2$) with cutoff potentials of 3.35 to 4.3 V vs. Li/Li^+ .

The TGA and DTA result shows that the formation of the spinel phase product is completed at about 400°C , but the XRD patterns (Fig. 1) of the gel-derived materials calcinated at various temperatures demonstrates that the thermal treatment at 400°C only for 6h cannot lead to a pure mono-phase product. A single phase of chromium-doped LiMn_2O_4 is formed when the material is calcinated at 600°C . This result strongly suggests that the sol-gel preparation method requires lower calcination temperature and shorter calcination time than the solid-state reaction where the calcination temperature is almost 750°C and the calcination time is more than 24h. Crystallinity and growth of grain size increase with increasing firing temperature. This is consistent with the BET results, which shows that the surface area of the $\text{LiCr}_{0.2}\text{Mn}_{1.8}\text{O}_4$ material decreases from 13.1 to $5.2\text{ m}^2/\text{g}$ as the firing temperature is raised from 600°C to 800°C .

The effect of calcining temperature on the specific capacity is displayed in Fig. 2. Lower capacity of the samples fired at 400 and 500°C corresponds to the lower crystallinity and impurity phase. The first discharge capacity decreases slightly from a temperature higher than 700°C , which may be attributed to a disturbed structure that results from weight loss by the sample at high temperatures^[4]. The suitable calcinating temperatures for higher capacity is $600\sim 700^\circ\text{C}$. Fig. 3 shows the cyclability of $\text{LiCr}_x\text{Mn}_{2-x}\text{O}_4$ materials fired at 600°C . $\text{LiCr}_{0.05}\text{Mn}_{1.95}\text{O}_4$ and $\text{LiCr}_{0.20}\text{Mn}_{1.80}\text{O}_4$ initially delivered 138 and 108 mAh/g , remained at 128 and 106 mAh/g respectively at the tenth cycle, which is about 10 percent higher than the samples obtained from the solid-state reactions.

1. Li Guohua, H. Ikuta, T. Uchida et al., J. Electrochem. Soc., 143, 178 (1996)
2. A.D. Robertson, S.H. Lu, W.f. Averill et al., J. Electrochem. Soc., 144, 3500 (1997)
3. D. Zhang, B.N. Popov, R.E. White, J. Power Sources, 76, 81 (1998)
4. J.M. Tarascon, W.R. Mckinnon, F. Coowar, J. Electrochem. Soc., 141, 1421 (1994)

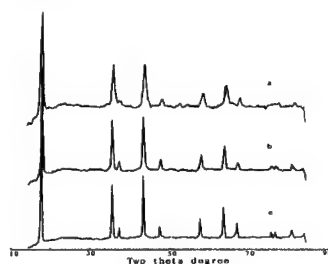


Fig. 1 XRD patterns of $\text{LiCr}_{0.20}\text{Mn}_{1.80}\text{O}_4$ (a) 400°C (b) 600°C (c) 800°C

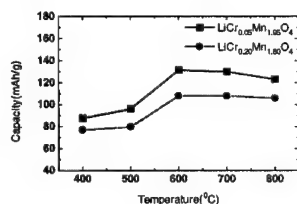


Fig. 2 Dependence of specific capacity on calcining temperature

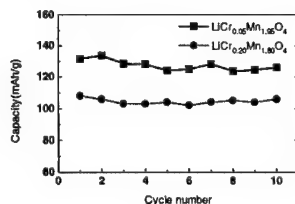


Fig. 3 Capacity vs. Cycle number for $\text{Li}/\text{LiCr}_x\text{Mn}_{2-x}\text{O}_4$

Lithiated Electrolytic Oxides Of D-Metals In Cathodes Of Lithium Accumulators

E.M.Shembel, R.D.Apostolova V.M.Nagirny
Ukrainian State Chemical Technology University,
49005, Dnipropetrovsk, Ukraine,
E-mail: shembel@onil.dp.ua

D.Aurbach, B.Markovsky
Department of Chemistry, Bar-Ilan University,
52900 Ramat-Gan, Israel.

One of the methods increasing a cycling efficiency of layered (LiMeO_2 , $\text{Me}=\text{Ni, Co, Mn}$) and spinel (LiMn_2O_4) compounds in the cathodes of lithium accumulators is a partial substitution of transient metals (Me) by other component (Me^1), stabilising the structure of cathode material with the final stoichiometry

$\text{LiMe}_{1-x}\text{Me}^1_x\text{O}_2$ and $\text{LiMn}_{2-x}\text{Me}^1_x\text{O}_4$ ($\text{Me}^1=\text{Al, Cr, Mg, Ni, Co, etc.}$). It is known that cycling efficiency of $\text{Li-Ni}_{1-x}\text{Co}_x\text{O}_2$ from the chemically co-deposited Ni-Co - precursors increases as compared with the same precursors obtained separately. The mentioned effect enables to suppose that electrolytically co-deposited transient metals oxides may be highly promising for the synthesis of lithiated oxide cathode materials with increased cycling efficiency.

The electrolysis opens the new possibilities for the correction of the co-deposited metal oxides characteristics. Changing the parameters of electrolysis and the subsequent heat treatment of deposits one can change the degree of dispersity and crystallinity of the deposits, stoichiometry of oxides and the structure of crystalline lattice of the synthesis products [1]. In this connection the electrolytic deposition of Co-oxide, Mn-oxide, the oxide mixtures of Mn-Co, Mn-Ni, Mn-Co-Ni was carried out. After a high-temperature effect the electrolysis products were lithiated by traditional ceramic technology with the use of the lithium compounds LiOH or Li_2CO_3 . Non-lithiated and lithiated oxide materials produced have been investigated. The electrochemical characteristics have been determined in the electrolyte: $\text{PC} + \text{DME} + 1\text{M LiClO}_4$.

Optimization of the technological parameters of electrolysis and the investigation of its products began in terms of cobalt oxides. Co-deposits were produced from the acid sulfate electrolytes on titanium anode.

Non-lithiated air-dried cobalt oxides (drying temperature 18 or 120°C) are X-ray - amorphous. After Co-oxide annealing (250, 600 or 800°C , 5h) its reflexes in X-ray diffractogram (d , nm: 0,466; 0,286; 0,244; 0,234; 0,202; 0,165; 0,155; 0,143) agree with those of Co_3O_4 oxide. Absorption IR-spectra and the data of thermal analysis have shown the composition change of electrolytic Co-oxide at annealing above 250°C .

IR-spectrum of Co-oxide (18 or 120°C) has one absorption band, showing oxygen-cobalt interaction with a maximum of 594cm^{-1} and the absorption bands, resulted from a moisture content of 3430cm^{-1} and 1639cm^{-1} . After Co-oxide annealing (250, 600 or 800°C) in its IR-spectrum two absorption bands, cm^{-1} appear: 560, 864, instead of one band at 594. Temperature variation from 250 to 800°C does not affect the position of these maxima and changes only their intensity and a band width, indicating oxide structure ordering. Loss in sample weight, occurring at two stages within the low-temperature range and also within the high-temperature range followed by a heat absorption with the corresponding Endo effects (130, 275 and 860, 975°C) is a feature of the TGA data of electrolytic Co-oxide. They are concerned with water and oxygen loss.

Galvanostatic discharge/charge curves of non-lithiated Co-oxide (800°C) have shown its uselessness as a cathode material for lithium accumulator. At $100\text{ }\mu\text{A}/\text{cm}^2$ current discharge voltage is low (1.0V). The discharge is followed by electrolyte decomposition with a gas evolution. Discharge reaction is irreversible. Co-oxides (18 and 800°C) were lithiated in the air (750°C , 10h). On the basis of X-ray diffraction analysis data the lithiated compounds contain 97-98% LiCoO_2 and 2-3% Co_3O_4 . The discharge capacity of lithiated Co-oxide was 116-120 Ah/kg ($I_{\text{disc}}=100\text{ }\mu\text{A}/\text{cm}^2$, $E=4,2-3,5\text{V}$). At lithiation the relation $\text{Li: Co}=1,05:1$, taking into account that electrolytic Co-oxide corresponds to the composition of Co_3O_4 . For improving cycling characteristics of cathode material it is necessary to determine the degree of non-stoichiometry of electrolytic Co-oxide depending on the conditions of electrolysis.

Influence of doping Co on the cycling efficiency of a spinel structure was determined with the compounds based on electrolytically co-deposited Co-Mn oxides, and also thermal treated LiMn_2O_4 mixture with lithiated electrochemical Co-oxide. The results of the investigations will be presented separately.

Acknowledgement

This work was supported by the Ukrainian and Israeli Ministries of Science within the framework of the joint Ukrainian-Israeli Binational Project for Exchange of Scientists (Project # 2m/1420-97)

Reference

1. E.Shembel, R.Apostolova, V.Nagirny, D.Aurbach and B.Markovsky. // J.Power Sources, 81-82, 480, (1999).

Abstract No. 160

Improved LiCoO_2 for Li-ion battery applications

Yuan Gao*, Marina V. Yakovleva**, and John F. Engel**

FMC Corporation, Lithium Division

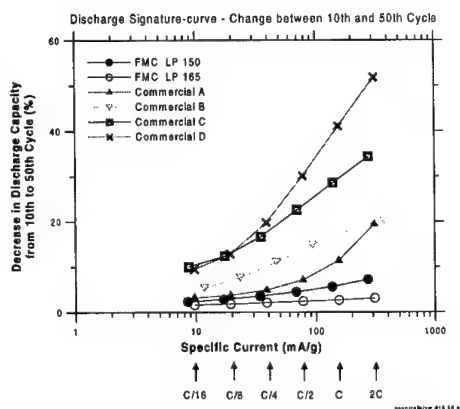
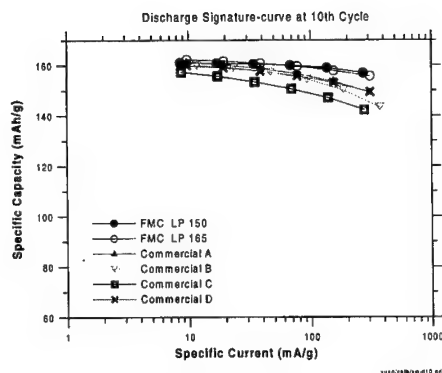
* Princeton, NJ 08543

** Bessemer City, NC 28016

Despite that LiCoO_2 has been mass produced and used as the cathode material in most of commercial Li-ion batteries since the early 1990s, there is still a lot of research activities in the area. This is in part because in-depth understanding of phase transformations during lithiation/delithiation processes is important for ensuring good electrochemical performance, and LiCoO_2 serves as a starting point for modeling other lithium metal oxides with the same layered structure of the $R\bar{3}m$ symmetry, as these materials offer relatively large capacity.¹⁻⁴ On the application side, the charge limit has been pushed higher and higher, and the amount of Li taken out has been increased from about 140mAh/g to 160mAh/g equivalent of lithium or from 0.5 Li to 0.6 Li per formula unit of LiCoO_2 . Seemingly good materials that performed well with the lower delithiation limit can perform quite differently with the larger delithiation limit, especially when large discharge current is applied. Obviously, materials that can consistently perform well with the larger delithiation limit are more desirable. We were able to identify key factors affecting the performance with the in-depth understanding of the reaction mechanism and the phase diagram. Especially, We found that the impedance growth on the LiCoO_2 electrode upon cycling is the main contributor to the performance inconsistency and is related to the fundamental properties of the LiCoO_2 itself. With carefully engineered LiCoO_2 , We were able to control the impedance growth and thereby greatly enhance its performance, especially for the high load applications. The latest results will be presented at the conference.

References:

1. J.N. Reimers & J.R. Dahn, J. Electrochem. Soc. **139**, 2091 (1992).
2. A. Van der Ven, M. K. Aydinol, G. Ceder, G. Kresse, & J. Hafner, Phys. Rev. B **58**, 2975 (1998).
3. C. Wolverton & A. Zunger, J. Electrochem. Soc. **145**, 2424 (1998).
4. Haifeng Wang, Young-Il Jang, Biying Huang, Donald R. Sadoway, & Yet-Ming Chiang, J. Electrochem. Soc. **146**, 473 (1999).



Li-insertion Behavior in Nanocrystalline TiO₂-(MoO₃)_z Core-Shell Materials

G. J. Moore^a, A. Le Gal La Salle^a,
D. Guyomard^a and S.H. Elder^b

^aInstitut des Matériaux Jean Rouxel
CNRS - University of Nantes
BP 32229 - 44322 Nantes Cedex 3 - France

^bPacific Northwest National Laboratory
Richland, Washington 99352 - U.S.A.

Nanocrystalline TiO₂ is a promising negative electrode material for rocking chair battery assemblies [1]. It has been cycled against LiCoO₂ demonstrating its ability to insert up to over 0.5 Li/Ti. TiO₂, as a mesoscopic insertion compound, has been further investigated using zirconium as a stabilization component [2]. TiO₂ has a tendency to undergo thermal induced crystalline growth, accompanied by partial phase transformation to rutile. The nanoarchitected TiO₂/zirconium materials proved to be resilient against these transformations, and could potentially make them amenable for battery applications. It is therefore of interest to exploit the potential of TiO₂ as a Li-insertion compound, as well as exploring nanocomposite architectures as a means to stabilize and enhance its electrochemical properties. To this end, we have studied the Li-intercalation cycling properties of TiO₂-(MoO₃)_z core-shell nanocomposite materials [3]. These materials are composed of a nanocrystalline TiO₂ (anatase) core with MoO₃ as a shell. These materials were synthesized by a novel surfactant induced nucleation reaction, the details of which will be reported in the near future [3,4]. Some of the properties of these materials are shown in table I.

At low concentrations ($z = 0.18$ & 0.54) of MoO₃, the shell only partially covers the TiO₂ core and can be viewed as existing as discrete MoO₃ islands. At 38 wt% ($z = 1.1$) MoO₃, the shell is a monolayer of corner sharing MoO₆ octahedra, and at 44 wt% ($z = 1.8$) it is a double layer of edge sharing MoO₆ octahedra. It was our goal to understand how the MoO₃ shell influences the electrochemical performance and properties of these materials.

Composite electrodes were prepared by mixing the active material (85% by mass) with carbon black (Super P, from Chemetals) (10%) and an organic binder (PVDF) (5%). The Li insertion behavior was studied in two-electrode cells using EC/DMC/LiPF₆ as an electrolyte. A Mac-Pile galvanostat/potentiostat was used for all of the electrochemical experiments.

Table I. Properties of the synthesized TiO₂-(MoO₃)_z

z in TiO ₂ -(MoO ₃) _z	Particle Size (in Å)	Wt. % MoO ₃	V _i =1/2(V _{red} +V _{ox}) (in Volts vs. Li)
0	100	0	-
0.18	80	4	1.833
0.36	70	10	-
0.54	60	17	1.850
1.10	50	38	1.886
1.80	40	44	1.893

Slow rate potentiodynamic experiments have been performed for all samples. Figure 1 compares the voltage vs. Li composition curves recorded for several compounds during the first discharge-charge cycle. It shows that the

materials insert from 0.4 to 1 Li per transition metal. Current-voltage curves are compared in Figure 2. The current peaks observed at V_{red}=1.7-1.8V during Li insertion and at V_{ox}=1.9-2.0V during Li deinsertion which corresponds to bulk Li insertion within the TiO₂ core [1]. No current peak due to Li insertion into MoO₃ was observed in these experiments. The bulk redox processes of the TiO₂ core appear to be strongly influenced by the extent of core-shell interactions (i.e. V_i is a function of the Ti-O-Mo bonding at the core-shell interface). The Li insertion voltage, measured by V_i = 1/2(V_{red}+V_{ox}), is reported in Table I as a function of the MoO₃ shell coverage. It increases with increasing coverage. The interpretation of such a significant variation is currently under study.

Further experiments are under way in order to verify if the observed increase in Li insertion capacity is due to the increase in MoO₃ shell coverage, or from the decrease in the particle size (see Table I). In addition, we aim to get a better general understanding of the Li insertion properties of these novel nanocrystalline TiO₂-(MoO₃)_z core-shell materials.

References

- [1] S. Y. Huang et al., J. Electrochem. Soc. **142**, L142 (1995).
- [2] L. Kavan et al., J. Electrochem. Soc., submitted.
- [3] S. H. Elder et al., J. Amer. Chem. Soc., in press.
- [4] S.H. Elder et al., to be published.

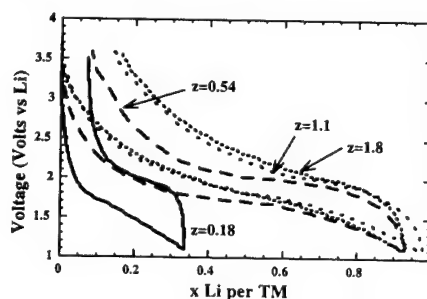


Figure 1. Comparison of the voltage - Li composition behavior of some TiO₂-(MoO₃)_z core-shell materials measured under potentiodynamic conditions (20mV/h).

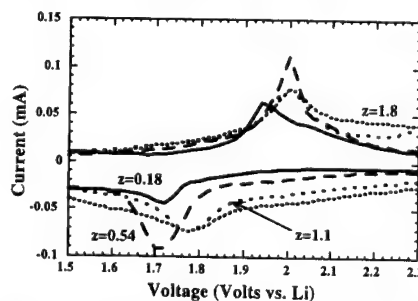


Figure 2. Comparison of the current - voltage behavior of some TiO₂-(MoO₃)_z core-shell materials measured under potentiodynamic conditions (20mV/h).

Relationship Between Cycling Performance and Structural Phase Transitions of $\text{Li}_{1+y}\text{Mn}_{2-y}\text{O}_4$ Cathode Materials Studied by Synchrotron X-ray Diffraction

X. Q. Yang, X. Sun, M. Balasubramanian and J. McBreen
Brookhaven National Laboratory, Upton, NY 11973, USA

Yongyao Xia and T. Sakai
Osaka National Research Institute, 1-8-31
Midorigaoka, Ikeda, Osaka, Japan

M. Yoshio
Department of Applied Chemistry, Saga University,
Saga, 840-8502, Japan

Introduction

$\text{Li}_{1+y}\text{Mn}_{2-y}\text{O}_4$ ($y=0$ to 0.3) compounds with spinel structure have been widely studied as promising cathode materials for lithium batteries because of their low cost, low toxicity, and high energy density. Recent studies have focused on the problem of capacity fading of this material during cycling. Early ex situ x-ray diffraction studies of $\text{Li}_x\text{Mn}_2\text{O}_4$ were performed by Ozhuku et al.¹ They found that two cubic phases coexist for $0.60 > x > 0.27$, and a single cubic phase is present for $1.0 > x > 0.6$. Xia and Yoshio² reported that this cubic to cubic phase transition was suppressed in cathode materials which were prepared "lithium rich" ($y=0.04$) or "oxygen rich". They also claimed that this phase transition is one of the key factors for the capacity fading during cycling. Yang et al.³ proposed a three-cubic-phase model with two two-phase coexistence regions for these materials resulted from in situ XRD studies. In this paper, we report our studies on the relationship between the cycling performance and the structural phase transitions of these spinel materials during cycling in both 3V and 4V regions.

Experimental

$\text{Li}_{1+y}\text{Mn}_{2-y}\text{O}_4$ ($y=0, 0.04$, and 0.10) samples were synthesized by solid state reactions. Cathodes were prepared by slurring $\text{Li}_{1+y}\text{Mn}_{2-y}\text{O}_4$ powder with 10% PVDF (KynarFlex 2801, Atochem), and 10% acetylene black (w/w) in a fugitive solvent, then coating the mix onto Al foil. After vacuum drying at 100 °C, the electrode disks (2.8 cm^2) were punched and weighed. The average weight of active material was 20mg. The electrodes were incorporated into the cells with a Li foil negative electrode, a Celgard separator and a 1 M LiPF_6 electrolyte in a EC:DMC (1:1 volume ratio) solvent (LP 30 from EM Industries Inc.). Mylar windows instead of beryllium windows were used in these in situ cells. In situ XRD spectra were collected on beam line X18A at National Synchrotron Light Source (NSLS) operated at an energy of 10375 eV ($\lambda=1.195 \text{ \AA}$)

Results and Discussion

In the in situ XRD spectra of stoichiometric lithium manganese oxide $\text{Li}_{1+y}\text{Mn}_{2-y}\text{O}_4$ ($y=0$), during the first charge from 3.5V to 4.5V at C/6 rate, three

cubic structures, phase I, II and III can be identified. Nevertheless, due to the relatively wide range of the lattice constant change of both phase I and II, the two-phase co-existence region between phase I and II is not as clear as that between phase II and III. This is also true for the XRD spectra during the subsequent discharge. However, the two-phase co-existence region between phase I and phase II become more prominent than during the first charge. After discharging the same cell to 1.8 V through the whole 3V plateau, the phase transition from phase I with cubic structure to a tetragonal phase was observed. Then the cell was charged back from 1.8 V to 4.5 V again. After the transition from the tetragonal phase to phase I, three cubic phases with different lattice constants can be clearly identified. Very interestingly, the changes in lattice constants of all three cubic phases are almost negligible during the second charge from 3.5 V to 4.5 V. The phase transition from phase I to Phase II and then to phase III can be clearly identified by the changes of the relative intensities of the Bragg peaks representing these three phases. This is quite different from that seen in the first charge and in a normal second charge from 3 V to 4.5 V, after a discharge limited to the 4 V plateau only. Therefore we conclude that the structural changes of this cathode material through the 4 V plateau depend on the cycling history of the cell. In the in situ XRD spectra of lithium rich $\text{Li}_{1+y}\text{Mn}_{2-y}\text{O}_4$ samples ($y=0.04$ and $y=0.10$), during the first charge from 3.5V to 4.5V at C/6 rate, the phase transition from phase I to phase II is very difficult to identify and the transition from phase II to phase III is indicated by peak broadening only. During the first discharge, the transition from phase III to phase II and the co-existence region between them are more prominent than during the first charge. The transition from phase II to Phase III during charge and from phase III to phase II during discharge are easier to identify from the spectra of moderately lithium rich sample ($y=0.04$) than those from the $y=0.10$ sample. The cycleability studies show that the capacity fading is closely related to the phase separation in the XRD spectra. The less the phase separation, the better the cycleability

Acknowledgment

This work was supported by the U. S. Department of Energy, on the Exploratory Technology Research Program under the Office of Advanced Automotive Technologies, Under Contract No. DE-AC02-98CH10886.

References

1. T. Ozhuku, M. Kitagawa, and T. Hirai, *J. of Electrochem. Society*, **137**, 769 (1990)
2. Y. Xia and M. Yoshio, *J. of Electrochem. Society*, **143**, 825 (1996)
3. X. Q. Yang, X. Sun, S. J. Lee, S. Mukerjee, J. McBreen, M. L. Daroux, and X. K. Xing, *Electrochemical and Solid State Letters*, **2**, 157(1999)

Abstract No. 163

Preparation and Electrochemical Properties of $\text{LiAl}_y\text{Mn}_{2-y}\text{O}_4$

Qiming Zhong, Jesse Faiers*, Ulrich von Sacken
E-One Moli Energy (Canada) Limited,
20000 Stewart Crescent, Maple Ridge, BC,
Canada, V2X 9E7

Recently $\text{LiAl}_y\text{Mn}_{2-y}\text{O}_4$ has been reported to improve the performance of Li/spinel coin cells at 55°C [1,2]. Aluminum doping was reported to stabilize the structure and F substituting for O in spinel was reported to increase the specific capacity. We tested Al_2O_3 , $\text{Al}(\text{OH})_3$, $\text{Al}(\text{NO}_3)_3$, AlF_3 , MnF_2 , and LiF as potential sources of Al and F. The products were characterized by XRD, TGA, Mn titration and evaluated in coin cells with Li metal anodes. The high temperature performance of the most promising $\text{LiAl}_y\text{Mn}_{2-y}\text{O}_4$ materials was also tested in 18650 Li-ion cells.

The synthesis of $\text{LiAl}_y\text{Mn}_{2-y}\text{O}_4$ was first attempted using Al_2O_3 according to Amatucci et al [1]. A series of samples (Series a) were prepared from EMD, Li_2CO_3 and Al_2O_3 with molar ratios chosen to give the theoretical formula $\text{LiAl}_y\text{Mn}_{2-y}\text{O}_4$ ($y = 0.05, 0.1, 0.2$). All the samples were fired at 750°C in air for a total of 14 hours with one intermediate regrind. A control series (Series b) was made using the same amounts of EMD and Li_2CO_3 but without added Al_2O_3 . Fig. 1 shows that both series have identical lattice constants. Furthermore, while series (b) dissolved completely in concentrated HCl, series (a) left a white powder residue identified by XRD as Al_2O_3 . We believe that most of the Al_2O_3 remains unreacted under these synthesis conditions.

The reactivity of Al_2O_3 , $\text{Al}(\text{NO}_3)_3$ and $\text{Al}(\text{OH})_3$ was compared by mixing and heating them with pre-made spinel in air at up to 800°C. $\text{Al}(\text{NO}_3)_3$ and $\text{Al}(\text{OH})_3$ caused changes in the lattice constant and T_{C} , indicating that some Al enters the lattice, but Al_2O_3 has no effect.

Finally, various combinations of Al_2O_3 , $\text{Al}(\text{OH})_3$, $\text{Al}(\text{NO}_3)_3$, AlF_3 , MnF_2 , LiF , Li_2CO_3 and EMD were tried to synthesize $\text{LiAl}_y\text{Mn}_{2-y}\text{O}_4$. The most interesting result is that the presence of LiF can dramatically improve Al doping into the spinel. Comparing Fig. 2 with Fig. 3 shows that when $\text{Al}(\text{NO}_3)_3$ and LiF are used together the XRD peaks become sharper, indicating a more homogeneous sample (i.e. better Al distribution). However we see no evidence of fluorine substitution into the spinel lattice. When AlF_3 or MnF_2 were used as F precursors, they extract Li from spinel to form LiF .

Conclusions

Al doping of spinel requires the use of active aluminum compounds like $\text{Al}(\text{NO}_3)_3$. Attempts to dope from Al_2O_3 produce Li rich spinel and unreacted Al_2O_3 . The presence of LiF can improve Al doping from active sources like $\text{Al}(\text{NO}_3)_3$, but we have no evidence for F in the spinel lattice. LiF is the only F containing compound that we observe in the product.

*Co-op student from University of British Columbia, BC, Canada

References

1. Glenn G. Amatucci, US patent (1998), US5,759,720
2. G.G Amatucci et al, J. Power Source, **81-82** (1999)

pg39.

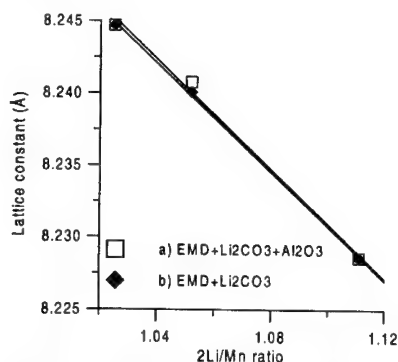


Fig.1 Cubic lattice constant of spinel vs Li/Mn ratio. Addition of Al_2O_3 has no measurable effect.

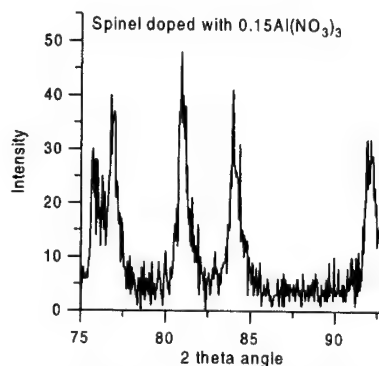


Fig. 2 XRD pattern (CuKα) of Al doped spinel ($y = 0.15$) using $\text{Al}(\text{NO}_3)_3$. Broad peaks indicate inhomogeneous product.

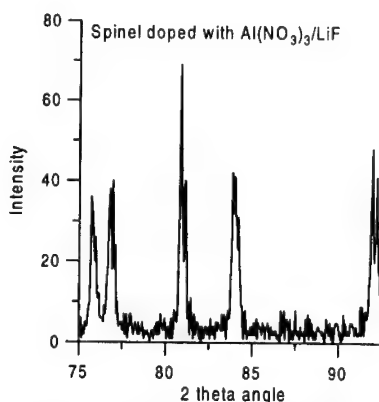


Fig.3 XRD pattern (CuKα) of Al doped spinel ($y = 0.15$) using $\text{Al}(\text{NO}_3)_3$ with LiF . Addition of LiF produces a more homogeneous product.

New Phases and Phase Transitions Observed in Over-Charged States of LiCoO₂ based Cathode Materials

X. Sun, X. Q. Yang and J. McBreen
Brookhaven National Laboratory
Upton, NY 11973

Y. Gao and M. V. Yakovleva
FMC Corporation, Princeton, NJ 08543

X. K. Xing and M. L. Daroux
Gould Electronics Inc., Eastlake, OH 44095

Introduction

LiCoO₂ is the most widely used cathode material in commercial lithium battery cells. LiNiO₂ has same theoretical capacity as LiCoO₂, but is less expensive. However its application in lithium batteries has not been realized due to serious safety concerns. Substituting a portion of Ni in LiNiO₂ with other cations has been pursued as a way to improve its safety characteristics. It was reported that Co doped LiNi_{0.8}Co_{0.2}O₂ showed better thermal stability than pure LiNiO₂. New materials, such as LiNi_{0.75}Mg_{0.125}Ti_{0.125}O₂, and LiNi_{0.65}Co_{0.25}Mg_{0.05}Ti_{0.05}O₂, have been developed. These materials exhibit even superior thermal stability to LiNi_{0.8}Co_{0.2}O₂. Using an *ex situ* XRD technique, Ohzuku¹ has performed interesting studies on some of the Li_{1-x}CoO₂ based materials. However, the charging voltage limit was set below 4.8 V in these studies. Dahn and co-workers have also published their results² on the structural changes of Li_{1-x}CoO₂ during charge using *in situ* XRD. The charging voltage used in that study was below 4.3 V. Amatucci and coworkers³ claimed a new phase transition, from a monoclinic phase M2 to a CdI₂ type single-layered hexagonal phase O1 for 0.9 < x < 1 in Li_{1-x}CoO₂. Using the state of art synchrotron based *in situ* x-ray diffraction, we have reported new findings on phase transitions for both Li_{1-x}CoO₂ and Li_{1-x}NiO₂ systems.^{4,5} In this paper, we report systematic studies on the structural changes of LiCoO₂, LiCo_{0.8}Ni_{0.2}O₂, LiCo_{0.5}Ni_{0.5}O₂, LiCo_{0.2}Ni_{0.8}O₂, and LiNi_{0.65}Co_{0.25}Mg_{0.05}Ti_{0.05}O₂ cathode materials during charge in the voltage range from 3.5 V to 5.2 V.

Experimental

LiCoO₂, LiCo_{0.2}Ni_{0.8}O₂ and LiNi_{0.75}Mg_{0.125}Ti_{0.125}O₂ were provided by FMC. LiCo_{0.8}Ni_{0.2}O₂ and LiCo_{0.5}Ni_{0.5}O₂ were synthesized by solid state reaction in our Lab. Cathodes were prepared by slurring the active material powder with 10% PVDF (KynarFlex 2801, Atochem), and 10% acetylene black (w/w) in a fugitive solvent, then coating the mixture onto Al foil. The cathodes were incorporated into cells with a Li foil negative electrode, a Celgard separator and a 1 M LiPF₆ electrolyte in a 1:1 EC: DMC solvent (LP 30 from EM Industries Inc.). Mylar windows were used in these *in situ* cells. *In situ* XRD spectra were

collected on beam line X18A at National Synchrotron Light Source (NSLS) at Brookhaven National Laboratory operated at an energy of 10375 eV ($\lambda=1.195$ Å).

Results and Discussion

It was reported that a monoclinic phase M2 is located in the region of 0.75 < x < 0.85 for Li_{1-x}CoO₂ in the over-charged state. However, in our *in situ* XRD data, no signature for the presence of a monoclinic phase M2 was observed. In the same composition region, we did observed more diffraction peaks. However, these new peaks can be indexed as two sets of O1 type structures. In other words, the formation of O1 structure takes two steps. An intermediate structure O1a is formed before the cathode totally converts to the final O1 structure. In the *in situ* XRD spectra of a LiNi_{0.65}Co_{0.25}Mg_{0.05}Ti_{0.05}O₂ cathode, the formation of the O1 type structure was also observed when the cell was over-charged to 5.2 V. However, at the end of charge at 5.2 V, the system is a mixture of two phases. Only a small portion is in the O1 type structure, while the majority of the material has a CdCl₂ type structure. Similar phenomena were also observed in LiCo_{0.8}Ni_{0.2}O₂, LiCo_{0.5}Ni_{0.5}O₂, and LiCo_{0.2}Ni_{0.8}O₂ samples. In these samples, at the end of charge at 5.2 V, the percentage of the O1 type structure increases with increasing Co content.

Acknowledgment

This work was supported by the U. S. Department of Energy Division of Materials Science of the Office of Basic Energy Sciences, and the Office of Energy Research, Laboratory Technology Research Program, Under Contract No. DE-AC02-98CH10886.

References

1. T. Ohzuku and A. Ueda, *J. Electrochem. Soc.*, **141**, 2972 (1994).
2. J. N. Reimers, and J. R. Dahn, *J. Electrochem. Soc.*, **139**, 2091 (1992).
3. G. G. Amatucci, J. M. Tarascon, and L. C. Klein, *J. Electrochem. Soc.*, **143**, 1114 (1996).
4. X. Q. Yang, X. Sun, and J. McBreen, *Electrochem. Communi.*, **1**, 227 (1999).
5. X. Q. Yang, X. Sun, and J. McBreen, *Electrochem. Communi.*, **2**, 100 (2000).

Structural behavior of some Nasicon compounds upon lithium electrochemical intercalation/deintercalation

J. Gaubicher^{1,5}, G. Vaughan²,
C. Masquelier³, C. Wurm³, J. Angenault¹,
Y. Chabre⁴, L. Nazar⁵ and M. Quarton¹

¹Laboratoire de Cristallographie du Solide, Université Pierre et Marie Curie, 4 place Jussieu 75252 Paris Cedex 05, France

²ESRF, Grenoble, France

³Laboratoire de Chimie des Solides, Bat. 414, Université Paris-XI Orsay, 91405 Orsay, France

⁴Laboratoire de Spectrométrie Physique, Université Joseph-Fourier, and CNRS BP 87, 38402 St Martin d'Hères, France

⁵Department of Chemistry, University of Waterloo, Waterloo ON N2L 3G1, Canada

Recently, polyanion 3-D structures built of corner sharing $(XO_4)^n$ tetrahedra and MO_6 octahedra, such as $FePO_4$, $VOXO_4$ and $Li_xM_2(XO_4)_3$ (M =transition metal; X =S, P) (1-13) have engendered much interest. These structures have been shown to be promising hosts for the reversible insertion of lithium, as the Li insertion potential is higher than in the corresponding oxide and can be "tuned" by the adroit choice of X and M . The present communication is devoted to examination of the structural behavior of Nasicon compounds $Li_xM_2(XO_4)_3$ (M =V, Fe; X =S, P) upon Li (de)intercalation. We have found that uptake/removal of two Li within the Nasicon framework can be characterized by either reconstructive phase transitions, exemplified by the sulfate $V_2(SO_4)_3$, or displacive transitions, exemplified by the phosphates where only slight distortions of the framework occur.

The $Li/V_2(SO_4)_3$ system exhibits a complex electrochemical behavior where two new deintercalation steps emerge on cycling at the expense of an initial oxidation process that progressively disappears. *In situ* synchrotron studies (with time resolution on the order of minutes) show a strong correlation between the electrochemical and structural behavior: the completion of the first reduction process corresponds to the formation of a new monoclinic phase $Li_2V_2(SO_4)_3$. This phase is different from that observed at the end of the second reduction. This structural evolution involving a reorganization of the polyhedra connectivity such as creation of pairs of edge-sharing VO_6 (which are absent in the initial phase) accounts for the electrochemical behavior.

In contrast, in the isostructural phosphate compounds $Li_3Fe_2(PO_4)_3$ and $Li_3V_2(PO_4)_3$, Li can either be inserted ($Fe^{3+} \rightarrow Fe^{2+}$) or de-inserted ($V^{3+} \rightarrow V^{4+}$), to result in displacive phase transformations. These are characterized by lithium reorganization within their Nasicon frameworks but little change in the structure. For $Li_3Fe_2(PO_4)_3$ reversible intercalation of two Li occurs during 2 single phase processes and 3 two-phase processes which occur at an average potential of 2.8V. XRD experiments show that the integrity of the framework is maintained throughout. This suggests that the phase transitions represent lithium reordering within the interstitial space. This is the first time, to our

knowledge, that a Nasicon framework with five interstitial alkali cations has been characterized. For the corresponding vanadium phase $Li_3V_2(PO_4)_3$, deintercalation of two Li occurs at about 3.75V. $LiV_2(PO_4)_3$ is isostructural with the starting compound but with an 8% decrease of the c parameter that we believe is the result of the depopulation of the M2 cavity with concomitant population of the M1 site.

References

1. A. K. Padhi et al., *J. Elec. Soc.*, **144**(5), 1609 (1997).
2. A.S. Andersson et al., *J. Elec. Soc.*, **3**(2), 66 (2000).
3. J. Gaubicher et al. *J. Alloys & Compounds*, **262-263**, 34-38 (1997).
4. J. Gaubicher et al. *J. Elec. Soc.*, **146**(12), 4375 (1999).
5. J. Gaubicher, et al. *J. Solid State Chem.*, accepted, in press.
6. K. S. Nanjundaswamy et al., *S. S. Ionics*, **92**, (1996).
7. A. K. Padhi et al., *J. Elec. Soc.* **144**(4), 1188-1194 (1997).
8. A. K. Padhi et al., *J. Elec. Soc.*, **144**(8), 2581 (1997).
9. A. Manthiram et al. *J. Power Sources* **26**, 403 (1989).
10. S. Okada et al., *36th Power Sources Conf.*, June (1994).
11. J. Gaubicher et al. *Mol. Cryst. Liq. Cryst.*, **311**, 45 (1998).
12. C. Masquelier et al. *J. Solid State Chem.*, **135**, 228 (1998).
13. C. Masquelier et al., *Chem. Mater.*, Feb. 2000

Electroactivity of natural and synthetic triphylite

N. Ravet^a, Y. Chouinard^a, J. F. Magnan^b, S. Besner^b,
M. Gauthier^a and M. Armand^{a*}

^a Département de Chimie, Université de Montréal, QC, Canada, H3C 3J7

^b Laboratoire L.T.E.E d'Hydro-Québec, 600 de la Montagne, Shawinigan, QC, Canada G9N 7N5

Recent studies on synthetic triphylite[1-3] LiFePO_4 have shown that this material is an attractive cathode for 3V+ lithium batteries. The best results in terms of capacity, cyclability and power were obtained with electronically conductive samples [3]. For non-conductive samples, charge / discharge depths and redox kinetics seem to be related to grain size. Therefore we have investigated a new synthetic route allowing a better control of particles size and shape. Moreover, this process can make use of a wide variety of iron salts. In addition, we have studied the behavior of the similar double phosphate occurring as a mineral found in different mining locations.

Natural triphylite Li(Fe,Mn)PO_4 generally does not form well defined crystals. It occurs as compact cleavable masses in complex granitic pegmatite dykes. It is within the solid solution series ranging from lithiophilite $\text{LiMn}_{1-x}\text{Fe}_x\text{PO}_4$ which differs from triphylite by being on the manganese-rich side versus iron. To the best of our knowledge, no electrochemical studies have been reported on natural triphillite.

We report here on the electrochemical properties of synthetic triphylite obtained by different synthetic routes and natural samples with several Fe/Mn ratio from Lord's Hill, Maine; Palermo Mine, North Groton, New Hampshire and Custer, South Dakota.

Electrochemical tests were performed at 80 °C, in coin type cells using PEO-based polymer electrolyte. The natural samples were ground and directly used as cathode material. First voltammetric scans (Mac Pile[®], Claix, France) performed at 20mV/h obtained for different samples are presented figure 1.

The capacity obtained at 3V during the first discharge process is 53 % (93 mAh of the theoretical capacity) for the sample from the conventional ceramic route and 57 % (100 mAh) for the new synthesis. This moderate improvement in capacity comes with an increase of the redox reaction kinetics. For the natural sample the discharge depth represents 37 %. Interestingly, the redox process appears to be more reversible and the cathodic peak is shifted anodically. This later observation is probably due to the presence of a slight amount of Mn in the compound.

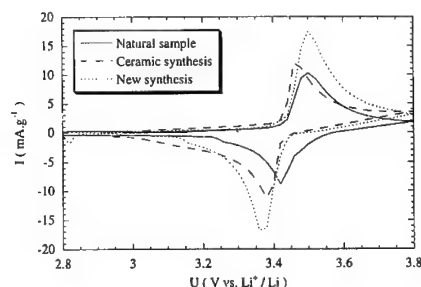


Figure 1: Potentiodynamic profiles for natural and synthetic triphylite samples. Scan rate 20 mV.h^{-1} ; temperature 80 °C; electrolyte PEO-Li salt O/Li = 20/1

The results for different natural samples as well as those from the two synthetic routes will be presented, in addition to the effect of the conductive additive whose effects on the redox kinetics, thus capacity, have been shown to be spectacular [3].

The well defined redox activity of double phosphates from various sources corroborates their interest as a new family of "plateau type" electrodes whose advantages over "sloping type" materials are worth consideration. Besides, attention should be drawn to the existence of an appreciable redox activity, yet unoptimized, from a natural compound found in relative abundance in nature; the triphylite family represents the second most abundant solid lithium ore. Again, these findings point towards the chemical sustainability of this environmentally benign compound.

References:

1. A. K. Padhi, K. S. Nanjundaswamy and J. B. Goodenough, Proc. 189th ECS Meeting, L.A., May. (1996)
2. A. K. Padhi, K. S. Nanjundaswamy and J. B. Goodenough, J. Electrochem. Soc., **144**, 1188 (1997)
3. N. Ravet, J.B. Goodenough, S. Besner, M. Simoneau, P. Hovington and M. Armand, Proc. 196th ECS Meeting, Honolulu., october. (1999)

* corresponding author

**THE KINETICS OF LITHIUM TRANSPORT
THROUGH $\text{Li}_{1.5}\text{CoO}_2$ THIN FILM ELECTRODE
BY THEORETICAL ANALYSIS OF CURRENT
TRANSIENT AND CYCLIC VOLTAMMOGRAM**

Su-Il Pyun*, and Heon-Cheol Shin

Department of Materials Science and Engineering, Korea
Advanced Institute of Science and Technology, 373-1,
Kusong-Dong, Yusong-Gu, Taejeon 305-701, KOREA

Lithium transport through lithium cobalt dioxide thin film electrode prepared by RF-magnetron sputtering was investigated in a 1M solution of LiClO_4 in propylene carbonate (PC) using galvanostatic intermittent titration technique (GITT), potentiostatic current transient technique [1,2] and cyclic voltammetry.

Electrode potential curve, determined from the GITT, showed clearly a potential plateau near $3.9 \text{ V}_{\text{Li/Li}^+}$, which indicates the coexistence of a Li-poor phase and a Li-rich phase. The current transients exhibited the non-Cottrell behaviour throughout the intercalation/deintercalation time, irrespective of the potential steps as can be seen in Fig. 1. Moreover, the initial current level was linearly proportional to the applied potential drop and jump, which means that the current-potential relation follows Ohm's law. From the comparison of the experimentally obtained current transients with those theoretically calculated, it is suggested that the occurrence of this abnormal behaviour is due to a 'cell-impedance-controlled' lithium transport, not a 'diffusion-controlled' lithium transport.

Cyclic voltammogram (CV) showed three sets of well-defined current peaks [3]. From the CV at various scan rates, anodic peak current I_{ap} vs. potential scan rate ν plot was obtained. 'Diffusion-controlled' CV and 'cell-impedance-controlled' CV were theoretically determined at various scan rates. Lithium transport during the potential scanning was discussed in terms of the shape of the CV and $I_{ap} - \nu$ relation.

References

- [1] H.-C. Shin, and S.-I. Pyun, *Electrochim. Acta* 44 (1999) 2235.
- [2] H.-C. Shin, and S.-I. Pyun, *Electrochim. Acta* 45 (1999) 489.
- [3] S.-I. Pyun, and H.-C. Shin, press in *Mol. Cryst. & Liq. Cryst.* (1999).

*Corresponding author. Tel: (82) 42-869-3319; Fax: (82) 42-869-3310; E-mail: sipyun@sorak.kaist.ac.kr

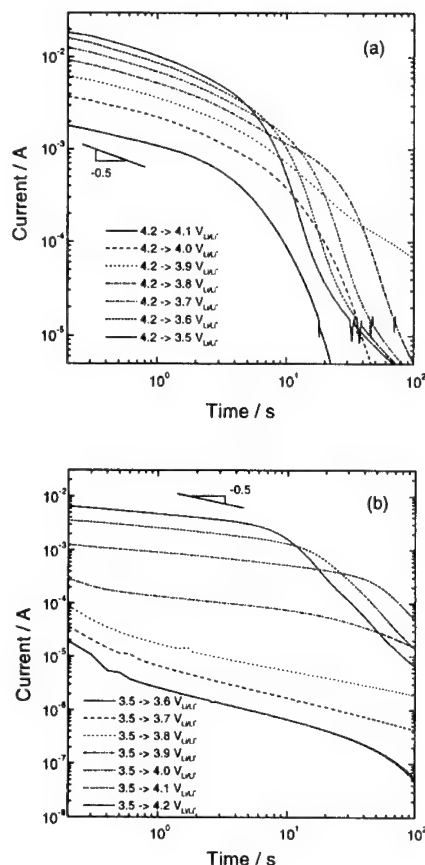


Fig. 1. (a) The cathodic and (b) anodic current transients obtained with the $\text{Li}_{1.5}\text{CoO}_2$ thin film electrode in a 1M LiClO_4 -PC solution at various potential steps as indicated in figures.

LITHIUM TRANSPORT THROUGH $\text{Li}_{1-\delta}\text{Mn}_2\text{O}_4$ ELECTRODE INVOLVING THE ORDERING OF LITHIUM IONS

Su-Il Pyun*, and Sung-Woo Kim

Department of Materials Science and Engineering,
Korea Advanced Institute of Science and Technology,
373-1 Kusong-Dong, Yusong-Gu, Taejeon 305-701,
KOREA

Lithium transport through $\text{Li}_{1-\delta}\text{Mn}_2\text{O}_4$ composite electrode, involving the ordering of lithium ions, was investigated by using potentiostatic current transient technique. For this purpose, the cathodic and anodic current transients were obtained from the electrode as functions of applied potential step and temperature.

The typical electrode potential vs. lithium content curve obtained from the $\text{Li}_{1-\delta}\text{Mn}_2\text{O}_4$ electrode shows a steep potential drop at about $(1-\delta) = 0.5$, due to the ordering of the intercalated lithium ions [1]. Using the Monte Carlo simulation for the repulsive ionic species in the cubic lattice based upon a lattice gas model, the ordering phenomenon during lithium intercalation was analysed from the thermodynamic viewpoint. In the electrode potential curves theoretically calculated and experimentally measured, the potential drop becomes steeper as temperature decreases, indicating the increase in the degree of order.

Non-Cottrell behaviour was observed in both cathodic and anodic current transients measured at various potential steps as shown in Fig. 1 (a) and (b). From the abnormal behaviour and temperature dependence of the current transient, it was suggested that lithium transport through the electrode in the disordered phase region is mainly controlled by cell-impedance [2].

As the applied potential step encountered the region where the lithium is intercalated in the ordered state, the current transient had a characteristic point, t_c , which was determined as the time of the local minimum in the derivative of the logarithmic current transient. At the same point, the characteristic peak was observed in the cell-impedance transient obtained from the current transient and the electrode potential curve. From the relative charge transferred during lithium intercalation, it was found that the characteristic point in those transients is corresponding to the point where the degree of order has the maximum value. Considering the degree of order which strongly depends on lithium content and temperature, lithium transport through the electrode in the ordered phase region was discussed from the kinetic viewpoint.

References

- [1] S.-I. Pyun, and S.-W. Kim, press in Mol. Cryst. & Liq. Cryst. (1999).
- [2] H.-C. Shin, and S.-I. Pyun, Electrochim. Acta 45 (1999) 489.

*Corresponding author. Tel: (82) 42-869-3319; Fax: (82) 42-869-3310; E-mail: sipyun@sorak.kaist.ac.kr

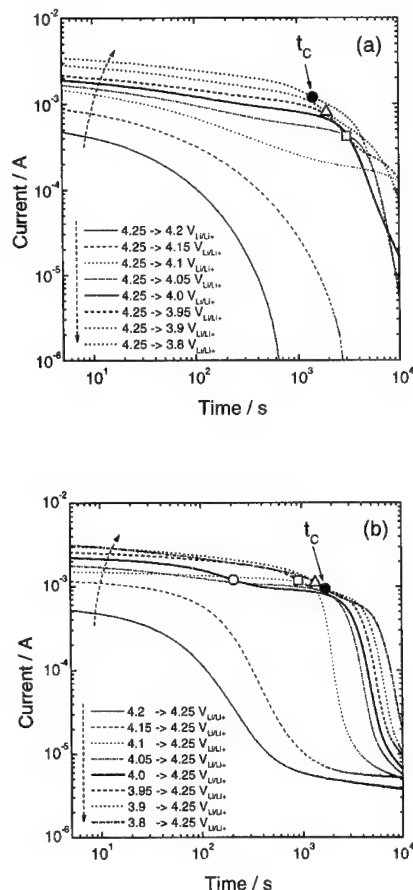


Fig. 1. (a) The cathodic and (b) anodic current transients in a logarithmic scale experimentally obtained from the $\text{Li}_{1-\delta}\text{Mn}_2\text{O}_4$ composite electrode in a 1M LiClO_4 -PC solution at 25 °C at various potential steps as indicated in figures.

ANALYSIS OF LITHIUM TRANSPORT THROUGH VANADIUM PENTOXIDE BY USING POTENTIOSTATIC CURRENT TRANSIENT TECHNIQUE

Su-Il Pyun*, and Min-Hyung Lee

Department of Materials Science and Engineering,
Korea Advanced Institute of Science and Technology,
373-1 Kusong-Dong, Yusong-Gu, Taejeon 305-701,
KOREA

Lithium transport through $\text{Li}_6\text{V}_2\text{O}_5$ composite electrode [1] was investigated in a 1M solution of LiClO_4 in propylene carbonate using galvanostatic intermittent titration technique (GITT) and potentiostatic current transient technique. The cathodic and anodic current transients obtained from the $\text{Li}_6\text{V}_2\text{O}_5$ composite electrode in Fig. 1 (a) and (b), showed the non-Cottrell behaviour. Moreover, the initial current level in the cathodic current transients was linearly proportional to applied potential drop as shown in Fig. 2. From these results, it seems reasonable to assume that lithium transport through the $\text{Li}_6\text{V}_2\text{O}_5$ composite electrode is governed by cell-impedance.

Under the assumption of cell-impedance-controlled lithium transport, the flux of lithium ions at the electrode/electrolyte interface is determined by cell-impedance and difference between applied potential and electrode potential, i.e., the current under the cell-impedance constraint is expressed by

$$I = -zF\tilde{D}_{\text{Li}} \frac{\partial c}{\partial x} = \frac{E - E_{\text{app}}}{R_{\text{cell}}} \quad \text{for } x = 0 \text{ at } t > 0,$$

where z is the valence of lithium ion; F , the Faraday constant; \tilde{D}_{Li} , the chemical diffusivity of lithium ion; E , the electrode potential; E_{app} , the applied potential and R_{cell} represents the cell-impedance [2]. Cell-impedance at various electrode potentials obtained from the current transient under the assumption of 'cell-impedance-controlled' lithium transport is nearly the same in value as that obtained from the electrochemical impedance spectroscopy.

In this work, lithium transport through the $\text{Li}_6\text{V}_2\text{O}_5$ composite electrode is theoretically analysed by numerical simulation of the current transient under the 'cell-impedance-controlled' constraint.

References

- [1] J.-S. Bae, and S.-I. Pyun, Solid State Ionics 90 (1996) 251.
- [2] H.-C. Shin, and S.-I. Pyun, Electrochim. Acta 45 (1999) 489.

*Corresponding author. Tel: (82) 42-869-3319; Fax: (82) 42-869-3310; E-mail: sipyun@sorak.kaist.ac.kr

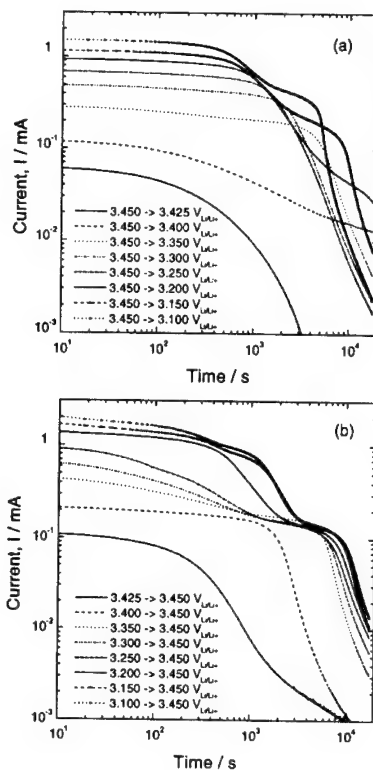


Fig. 1. (a) The cathodic and (b) anodic current transients in a logarithmic scale experimentally obtained from the $\text{Li}_6\text{V}_2\text{O}_5$ composite electrode in a 1M LiClO_4 -PC solution at various potential steps as indicated in figures.

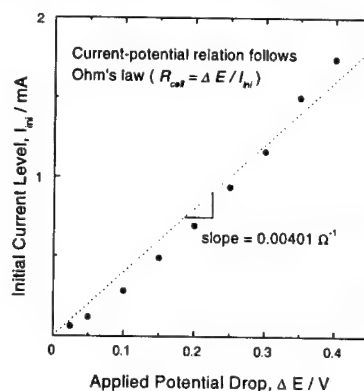


Fig. 2. Dependence of initial current level at 10 s on the applied potential drop from 3.45 $\text{V}_{\text{Li/Li}^+}$ to various lithium intercalation potentials.

Synthesis of $\text{LiAl}_x\text{Co}_{1-y}\text{O}_2$ Using Acrylic Acid and its Electrochemical Properties for Li Rechargeable Batteries

Kyung Yoon Chung, Won-Sub Yoon,
and Kwang-Bum Kim

Dept. of Metallurgical Eng., Yonsei University,
134 Shinchon-dong, Seodaemun-gu, Seoul, 120-749
Korea

Introduction

LiCoO_2 is most widely used as cathode material of commercial secondary lithium batteries due to its advantages including easy preparation and high theoretical specific capacity. Among the modifications to improve its electrode performance, one is the substitution of Co with metal ions which may stabilize the layered structure with or without participating in the redox processes. [1] Recently, Ceder et al. have shown that Al doping is potentially attractive to electrochemical application since Al-doped LiCoO_2 has advantages such as higher intercalation voltage, higher energy density, and a lower cost although it shows large capacity fading during cycling. [2] The focus of this study is to adopt Al-doped LiCoO_2 as a cathode material for lithium secondary battery. LiCoO_2 and Al-doped LiCoO_2 powders were prepared by a sol-gel method using acrylic acid and their structural and electrochemical properties have been investigated.

Experimental

A stoichiometric amount of lithium acetate, cobalt acetate, and aluminum nitrate with the cationic ratio of $\text{Li}:(\text{Co}+\text{Al}) = 1:1$ was dissolved in distilled water and mixed with an aqueous solution of acrylic acid. Nitric acid was slowly added to the solution with constant stirring until a pH of 2 was achieved. The resulting solution was mixed with a magnetic stirrer at 70 to 80°C for 6 to 8 h to obtain a clear viscous gel. The gel was dried in a vacuum oven at 100°C for 12 h. All the $\text{LiAl}_x\text{Co}_{1-y}\text{O}_2$ compounds were ground and calcined at 800°C for 24 h after precalcining the obtained gel precursor at 400°C for 1 h in air. The crystal structure of $\text{LiAl}_x\text{Co}_{1-y}\text{O}_2$ calcined at various temperatures was characterized by X-ray diffraction (XRD). Powder XRD pattern was recorded using an automated Rigaku powder diffractometer using $\text{Cu K}\alpha$ radiation. Cathode specimens were prepared by mixing the $\text{LiAl}_x\text{Co}_{1-y}\text{O}_2$ powders with 10wt% acetylene black and 6wt% PVDF (poly-vinylidene fluoride) in NMP (N-methyl pyrrolidone) solution. The mixture was spread on Al foil and pressed. The composite electrodes were dried under vacuum at 150°C for at least 12 h before use. A three-electrode electrochemical cell was employed for electrochemical measurements in which lithium foil was used for both reference and counter electrodes.

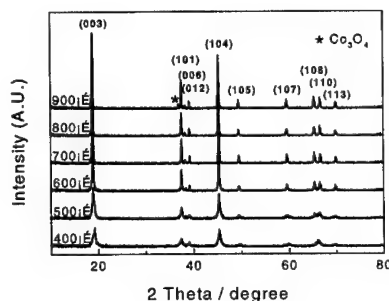
Results and Discussion

Fig. 1 shows XRD patterns for the gel-derived $\text{LiAl}_{0.25}\text{Co}_{0.75}\text{O}_2$ samples calcined at various temperatures for 24 h in air after precalcining the obtained gel precursor at 400°C for 1 h. For XRD patterns of the powders calcined in the temperature range of 600 and 800°C, (006) and (012) peaks and (108) and (110) peaks are well separated, which indicates that single-phase layered $\text{LiAl}_{0.25}\text{Co}_{0.75}\text{O}_2$ powders were obtained in the

temperature range of 600 and 800°C. More detailed discussion will be made about the relationship between electrochemical and structural properties in the meeting. Fig. 1 XRD patterns for the gel-derived $\text{LiAl}_{0.25}\text{Co}_{0.75}\text{O}_2$ powders calcined at various temperatures.

References

- [1] R. Alcantara, P. Lavela, P.L. Relano, J.L. Tirado, E. Zhecheva, and R. Stoyanova, *Inorg. Chem.*, 37, 264(1998).
- [2] G. Ceder, Y.-M. Chiang, D.R. Sadoway, M.K. Aydinol, Y.-I. Jang, and B. Huang, *Nature*, 392, 694(1998).



A Study on the Effect of Lithium deintercalation on the Local Structure of $\text{LiAl}_x\text{Co}_{1-x}\text{O}_2$ Cathodes Using X-ray Absorption Spectroscopy

Won-Sub Yoon, Kyung-Keun Lee,
and Kwang-Bum Kim

Dept. of Metallurgical Eng., Yonsei University,
134 Shinchon-dong, Seodaemun-gu, Seoul, 120-749
Korea

Introduction

Recently, Ceder et al. have shown that Al doping is potentially attractive to electrochemical application since Al-doped LiCoO_2 has advantages such as higher intercalation voltage, higher energy density, and a lower cost although it shows large capacity fading during cycling.[1] From the viewpoint of bulk structure, Jang et al. found with their XRD analysis that the layered structure of Al-doped LiCoO_2 is stable in its structure during cycling, which contrasts with its large capacity fading during cycling.[2] Thus, a more detailed analysis is needed in order to explain the cause of the capacity fading during cycling. Recently, a new structural analysis of X-ray absorption spectroscopy (XAS) is an excellent technique for characterizing the valency and local structure of an interesting atom in cathode materials with no long-range order. In the present study, $\text{LiAl}_x\text{Co}_{1-x}\text{O}_2$ powders were synthesized using acrylic acid as a chelating agent. The variations in the local structures with Li deintercalation and cycling process of LiCoO_2 and $\text{LiAl}_{0.25}\text{Co}_{0.75}\text{O}_2$ were systematically investigated on the basis of XAS study. The XAS analysis will give a better understanding of the mechanism for the capacity fading of cathode materials during the cycling process.

Experimental

XAS measurements were performed in transmission mode at beamline 3C1 of Pohang Light Source (PLS) using a Si(111) double-crystal monochromator detuned to 85% of its original intensity to eliminate the high order harmonics. The storage ring was operated with an electron energy of 2 GeV and a current between 120 and 150 mA. Calibration was carried out using the first inflection point of the spectrum of Co foil, i.e., Co K-edge = 7709 eV, as a reference. To remove an energy shift problem, the X-ray absorption spectrum for Co metal foil was measured simultaneously in every measurement as the metal foil was positioned in front of the window of the third ion chamber.

Results and Discussion

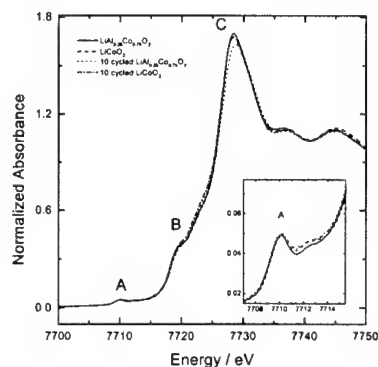
Figure 1 shows the normalized Co K-edge XANES spectra for LiCoO_2 and $\text{LiAl}_{0.25}\text{Co}_{0.75}\text{O}_2$ after 10 cycles. There is no substantial difference between XANES spectra for pristine LiCoO_2 and cycled LiCoO_2 . However, XANES spectrum for cycled $\text{LiAl}_{0.25}\text{Co}_{0.75}\text{O}_2$ is different from that of pristine $\text{LiAl}_{0.25}\text{Co}_{0.75}\text{O}_2$. There is a significant difference in the peak features between pristine $\text{LiAl}_{0.25}\text{Co}_{0.75}\text{O}_2$ and cycled $\text{LiAl}_{0.25}\text{Co}_{0.75}\text{O}_2$ after 10 cycles. Peak positions of A and C move towards the higher energy side, and this indicates an increase of remaining Co^{4+} ions in $\text{LiAl}_{0.25}\text{Co}_{0.75}\text{O}_2$ after 10 cycles. The results of XANES and EXAFS analysis for cycled

$\text{LiAl}_{0.25}\text{Co}_{0.75}\text{O}_2$ indicates that its large capacity fading is related to the more highly distorted environment of local structure around Co^{4+} ions remaining in the lattice.

Figure 1. Normalized Co K-edge XANES for LiCoO_2 and $\text{LiAl}_{0.25}\text{Co}_{0.75}\text{O}_2$ after 10 cycles.

References

- [1] G. Ceder, Y.-M. Chiang, D.R. Sadoway, M.K. Aydinol, Y.-I. Jang, and B. Huang, *Nature*, **392**, 694 (1998).
- [2] Y.-I. Jang, B. Huang, H. Wang, D.R. Sadoway, G. Ceder, Y.-M. Chiang, H. Liu, and H. Tamura, *J. Electrochem. Soc.*, **146**, 862 (1999).



Electrochemical Characterization of Layered LiCoO_2 Films Prepared by Electrostatic Spray Deposition

Sung-Ho Ban, Won-Sub Yoon,
and Kwang-Bum Kim

Dept. of Metallurgical Eng., Yonsei University,
134 Shinchon-dong, Seodaemun-gu, Seoul, 120-749
Korea

Introduction

Advances in the microelectronics industry have reduced the current and power requirements of electronic devices. This has made possible the use of thin-film rechargeable microbatteries as power sources for these devices. Thin films of various Li battery components have been synthesized by several methods, such as r.f. magnetron sputtering, pulse laser deposition, and chemical vapor deposition. Recently, Schoonman et al. have developed the electrostatic spray deposition (ESD) technique and applied it to preparing thin films of various Li-ion battery cathode active materials.[1] The ESD technique offers many advantages over some conventional deposition techniques, such as a simple and low cost set-up, high deposition efficiency, low temperature synthesis, and easy control of the composition and surface morphology of the deposited films. However, a systematic study of electrochemical properties of LiCoO_2 films prepared by ESD at various temperatures has not been reported so far. In this work, thin films of LiCoO_2 were prepared by ESD technique and their electrochemical properties were investigated.

Experimental

The ESD set-up used here and its working principles have been described in the literature.[1] A high DC voltage is applied between an electrically conductive substrate and a metal capillary nozzle, which is connected to a precursor solution. Under a suitable flow rate, the precursor solution is atomized at the orifice of the nozzle, generating a fine spray. The spray moves toward the heated substrate under the electrostatic force and, due to pyrolysis of the precursors, a thin layer is deposited on the substrate surface. An ethanol solution of $\text{LiNO}_3 + \text{Co}(\text{NO}_3)_2$ with a molar ratio $\text{Li}:\text{Co} = 1:1$ was used as the precursor solution (0.04 M). The precursor solution was pumped at a rate of 2 ml/h to a stainless steel nozzle, which placed 4 cm above the substrate. The deposition temperature was chosen generally between 200° and 400°. Electrochemical measurements were carried out using a three-electrode cell with 1M LiClO_4 / propylene carbonate (PC) solution in a glove box. Li foils were used as the counter and reference electrodes.

Results and Discussion

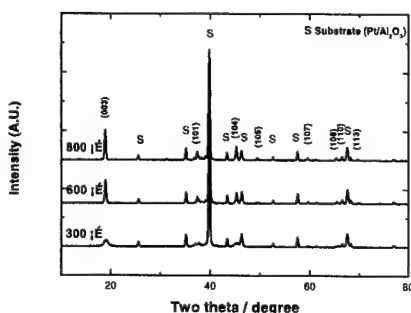
Fig. 1 shows XRD patterns for the LiCoO_2 films prepared at various temperatures for 30 min in air. For XRD patterns of the films prepared at 600° or above, (108) and (110) peaks are well separated, which indicates that single-phase layered LiCoO_2 films were obtained at 600° or above. Figure 2 presents cyclic voltammograms of a

LiCoO_2 film prepared at 600°. Typical cyclic voltammograms of HT- LiCoO_2 were observed, which were characterized by three sets of well-defined current peaks. More detailed discussion will be mentioned in the meeting.

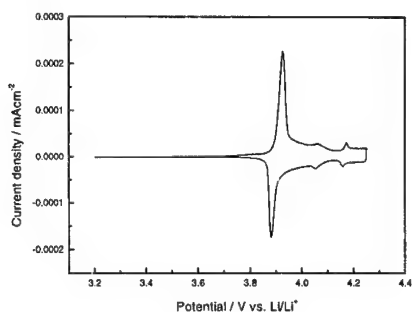
Figure 1. XRD patterns for the LiCoO_2 films prepared at various temperatures

Figure 2. Cyclic voltammograms of a LiCoO_2 film prepared at 600°.

References



[1] C. Chen, E. M. Kelder, P. J. J. M. van der Put, and J. Schoonman, *J. Mater. Chem.*, 6, 765-771 (1996)



Electrical and thermal properties of $\text{LiNi}_{1-y}\text{Co}_y\text{O}_2$ ($0 \leq y \leq 0.2$) during initial cycle

Kyung K. Lee, Won S. Yoon, and Kwang B. Kim

Dept. of Metallurgical Eng. Yonsei Univ. 134
Shinchon-dong, Seodaemun-gu, Seoul, Korea

Previous studies have shown that $\text{LiNi}_{1-y}\text{Co}_y\text{O}_2$ exhibits very interesting electrochemical properties leading to commercial batteries using this oxide.^{1,2} The structure of $\text{LiNi}_{1-y}\text{Co}_y\text{O}_2$ has two-dimensionally connected $\text{Ni}_{1-y}\text{Co}_y\text{O}_2$ layers which allow for easy intercalation/deintercalation of lithium ions into/from the inter-layer spaces. However, $\text{LiNi}_{1-y}\text{Co}_y\text{O}_2$ with little or no cobalt content ($y \leq 0.2$) exhibits a departure from stoichiometry because of the presence of excess nickel ions in its lithium sites. The oxidation of divalent excess nickel ions to trivalent ions reportedly leads to a local collapse of the inter-slab spaces during the first charge, and therefore limits lithium reintercalation during the next discharge.³ This capacity loss during the first discharge is about 20-30% of its initial value. Therefore, the behavior of $\text{LiNi}_{1-y}\text{Co}_y\text{O}_2$ during the initial charge/discharge cycling must be examined closely in order to develop this oxide into a potential electrode material.

As part of a larger study to develop $\text{LiNi}_{1-y}\text{Co}_y\text{O}_2$ with a high reversible capacity for a cathode material in lithium secondary batteries, we focused on the behavior of the $\text{LiNi}_{1-y}\text{Co}_y\text{O}_2$ observed in the initial charge/discharge cycles, and reported electrochemical and structural behavior of $\text{LiNi}_{1-y}\text{Co}_y\text{O}_2$ ($0 \leq y \leq 0.2$) during initial cycles.⁴

In this study, we investigate the electrical conductivity change of the $\text{LiNi}_{1-y}\text{Co}_y\text{O}_2$ induced by lithium ion intercalation/deintercalation. The electrical conductivity of the electrode material is one of the most important properties in design of high performance batteries. For this purpose, we adopt *in-situ* conductivity measurement technique using IDA electrodes.⁵ The *in-situ* method gives the conductivity of the electrodes in a whole potential region without taking out from the cells, showing the reliable relationships between conductivity and x in $\text{Li}_{1-x}\text{Ni}_{1-y}\text{Co}_y\text{O}_2$.

In addition, the thermal property of $\text{Li}_{1-x}\text{Ni}_{1-y}\text{Co}_y\text{O}_2$ must be considered in order to apply this oxide to the realistic battery, because the exothermic decomposition of the oxide releasing oxygen at elevated temperatures poses safety hazards. Therefore, the thermal behavior of $\text{Li}_{1-x}\text{Ni}_{1-y}\text{Co}_y\text{O}_2$ is closely observed using x-ray diffraction and differential scanning calorimetry.

Detailed discussion about the electrical and thermal properties of $\text{LiNi}_{1-y}\text{Co}_y\text{O}_2$ ($0 \leq y \leq 0.2$) will be made in the meeting.

370 (1992).

2. T. Ohzuku, A. Ueda, M. Nagayama, Y. Iwaoshi, and H. Komory, *Electrochim. Acta*, 38, 1159 (1993).
3. J. P. Peres, C. Delmas, A. Rougier, M. Broussely, F. Pertion, P. Biensan and P. Willmann, *J. Phys. Chem. Solids*, 57, 1057 (1996).
4. Kyung K. Lee and Kwang B. Kim, *J. Electrochem. Soc.*, accepted for publication.
5. M. Shibuya, T. Nishina, T. Matsue, and I. Uchida, *J. Electrochem. Soc.*, 143 (1996) 3157.

References

1. C. Delmas and I. Saadoune, *Solid State Ionics*, 53-56,

Characterization of $\text{LiNi}_{0.85}\text{Co}_{0.1}\text{M}_{0.05}\text{O}_2$ (M=Co, Al, Fe) for lithium secondary batteries

Kyung K. Lee, Won S. Yoon, and Kwang B. Kim

Dept. of Metallurgical Eng. Yonsei Univ. 134
Shincheon-dong, Seodaemun-gu, Seoul, Korea

Due to the increased production and use of portable devices, lithium secondary batteries with extended lives and higher power output are in demand. Since the performance of the lithium secondary batteries is limited by the properties of the positive electrodes, a significant amount of research has been focused on the synthesis, processing and/or electrochemical identification of positive cathode materials for use in these batteries.^{1,2} Several oxides are being considered for use as 4 V cathode materials for lithium batteries: the spinel LiMn_2O_4 and the layered oxide LiMO_2 (M=Co and/or Ni). Each of these cathode materials has advantageous and detrimental characteristics that have an impact on their further development for lithium-ion batteries.

Recently a unique combination of two or more cations substituting for M in LiMO_2 was reported to have some promising features, including a high capacity, a long cycle life, and an enhanced thermal stability, for use as a new cathode material.^{3,4}

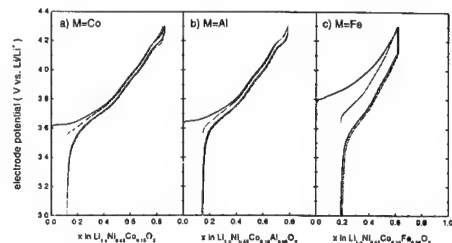
In this work, we report on the characterization of the four-cation oxide, $\text{LiNi}_{0.85}\text{Co}_{0.1}\text{M}_{0.05}\text{O}_2$ (M=Co, Al, Fe etc.). The electrochemical, structural and thermal behavior of these materials and the validity for application of these oxides to the realistic batteries are investigated.

Figure 1. shows the first two cycles during a constant current charge and discharge cycling at a 20 h rate. In contrast with $\text{LiNi}_{0.85}\text{Co}_{0.1}\text{O}_2$ or $\text{LiNi}_{0.85}\text{Co}_{0.1}\text{Al}_{0.05}\text{O}_2$, $\text{LiNi}_{0.85}\text{Co}_{0.1}\text{Fe}_{0.05}\text{O}_2$ has a large polarization and a small capacity. From x-ray diffraction results shown in Fig. 2, it is indicated that the $\text{LiNi}_{0.85}\text{Co}_{0.1}\text{Fe}_{0.05}\text{O}_2$ undergoes phase transition during the lithium deintercalation. The poor electrode property of the $\text{LiNi}_{0.85}\text{Co}_{0.1}\text{Fe}_{0.05}\text{O}_2$ maybe explained by the phase transition during the lithium deintercalation.

More detailed discussion about the electrochemical, structural and thermal properties of $\text{LiNi}_{0.85}\text{Co}_{0.1}\text{M}_{0.05}\text{O}_2$ (M=Co, Al, Fe etc.) will be made in the meeting.

References

1. R. Koksang, J. Baker, H. Shi, and M. Y. Saidi, *Solid State Ionics*, 69 (1994) 201.
2. T. Ohzuku, and A. Ueda, *Solid State Ionics*, 69 (1994) 201.
3. Z. Liu, A. Yu, and J. Y. Lee, *J. Power Sources*, 81-82 (1999) 416.



4. T. J. Boyle, D. Ingersoll, M. A. Rodriguez, C. J. Tafoya, and D. H. Doughty, *J. Electrochem. Soc.*, 146 (1999) 1683

Fig. 1. Charge and discharge curves of $\text{LiNi}_{0.85}\text{Co}_{0.1}\text{M}_{0.05}\text{O}_2$ in 1M LiClO_4 in PC at a 20h rate.

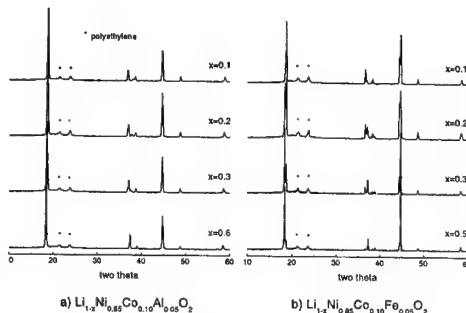


Fig. 2. X-ray diffraction patterns of $\text{Li}_{1-x}\text{Ni}_{0.85}\text{Co}_{0.1}\text{M}_{0.05}\text{O}_2$.

Correlation between structural and electrochemical properties of some lithium-metal vanadates

M. Arrabito*, S. Bodoardo*, N. Penazzi*
S. Panero**, B. Scrosati**,
X. Guo***, Y. Wang***, S. Greenbaum***

* Politecnico di Torino, Dip. Scienza dei Materiali ed Ingegneria Chimica, Torino, Italia

** Univ. La Sapienza Dip. di Chimica, Sez. Elettrochimica, Roma, Italia

*** Hunter College of the City of New York, Dep. of Physics, New York City, U.S.A.

Since the early 1960s, research on LiMVO_4 materials has focused on its preparation and characterization, where $M = \text{Cu, Ni, Zn, Cd, Mg, and Be}$ [1].

In this communication some lithium-metal vanadates containing metal ions as Cu, Ni, or Co have been synthesized using the solid state chemistry route.

Lithium carbonate (Li_2CO_3), metal oxide and vanadium oxide have been mixed, ballmilled and annealed in the narrow temperature range of 500°-520°C.

Structure characterization of each sample has been carried out by means of X Ray Powder Diffraction and solid state NMR techniques.

In the figure the RX powder diffraction patterns obtained in the case of the sample containing Ni is reported as an example.

Cyclic voltammetry and charge-discharge cycles have been performed in non-aqueous media in order to study the electrochemical activity.

The results of the morphological and structure characterization will be correlated with the electrochemical findings.

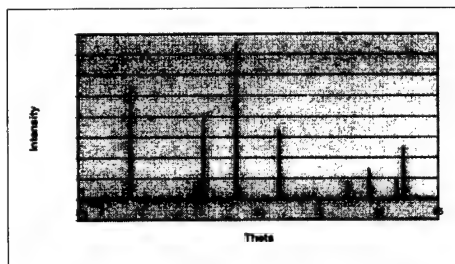


Figure: RX of LiNiVO_4 after some annealing at 500°C

References

- [1] T. L. Kulowa, L. S. Kanevskii, A.M. Skundin, E. I. Kachibaya, R. A. Imnadze, and T. V. Paikidze *Russian Journal of Electrochemistry*, Vol.35, N° 8, 1999, pp. 888-892.

Mechanisms of Manganese Spinel Dissolution and Capacity Fade at High Temperature

Takayuki Aoshima, Kenji Okahara, Chikara Kiyohara,
and Kenji Shizuka
Mitsubishi Chemical Corporation
1000, Kamoshida-cho, Aoba-ku, Yokohama 227-8502,
Japan

Introduction

The spinel LiMn_2O_4 is one of the most promising cathode materials for lithium secondary batteries. The disadvantage of the LiMn_2O_4 system is a capacity fade during charge-discharge cycling or storage at high temperature. It is well known that this deterioration is mainly caused by Mn dissolution from spinel.¹ Many mechanisms of spinel dissolution have been actively proposed,^{1,2} however, its detailed mechanism is still ambiguous. In this study, Mn dissolution from spinels was investigated to determine the detailed mechanism of capacity fade in lithium secondary batteries.

Reactivities of Spinel and Mn Dissolution

In order to clarify the origin of Mn dissolution at various discharge depths, the storage of the spinels, LiMn_2O_4 and $\lambda\text{-MnO}_2$,³ was performed in ethylene carbonate / diethyl carbonate electrolyte containing 1M LiPF_6 at 70 °C for a few weeks. As shown in Fig. 1, the amount of dissolved Mn from $\lambda\text{-MnO}_2$ increased continuously with storage times, while that from LiMn_2O_4 was constant after initially the slight Mn dissolution took place. In the case of LiMn_2O_4 , even if an electrolyte containing excess dissolved Mn and HF was used, the amount of the dissolved Mn after storage was same. These results indicate that the Mn at the surface of the LiMn_2O_4 is in equilibrium with a soluble species.

Analysis of the cathode capacity was also performed after storage of the cathode at 70 °C for 2 weeks in both discharged and charged states. It was found that capacity loss was larger if the cathode was stored in the discharged state.

In this study, the dissolved Mn was found to be deposited mainly on a graphite anode when in the charged state. Taking into account this reactivity, the capacity fade is induced by the increase in the anode resistance and the decrease in the amount of cyclable Li. In contrast, when the battery is in the discharged state, dissolved Mn forms a passivating layer on the cathode, leading to an increase in the cathode resistance. Figure 2 shows the proposed mechanism for the capacity fade.

Mechanism of Mn Dissolution from $\lambda\text{-MnO}_2$

As for the mechanism of Mn dissolution from $\lambda\text{-MnO}_2$, LiPF_6 plays a very important role in the course of Mn dissolution. The amount of the dissolved Mn increased with LiPF_6 concentration and no Mn dissolution was observed in the absence of LiPF_6 . Furthermore, during the course of Mn dissolution, CO_2 , C_2H_4 , EtOH, Et_2O , and AcOEt were detected as decomposition products of carbonates. From these results, we proposed the mechanism of Mn dissolution composed of 3 steps, (i) the decarboxylation of electrolyte catalyzed by $\lambda\text{-MnO}_2$ to give EtOH, (ii) reduction of $\lambda\text{-MnO}_2$ by EtOH to give acetate and MnO, (iii) Mn dissolution via Mn-O bond activation assisted by LiPF_6 (Fig. 3). Currently other aspects of this mechanism are under investigations.

References and Footnote

1. P. Arara, R. E. White, and M. Doyle, *J. Electrochem. Soc.*, **145**, 3647 (1998) and references therein.
2. A. D. Pasquier, A. Blyr, P. Courjal, D. Larcher, G. Amatucci, B. Gerand, and J.-M. Tarascon, *J. Electrochem. Soc.*, **146**, 428 (1999) and references therein.
3. $\lambda\text{-MnO}_2$ was chemically prepared by the reaction of LiMn_2O_4 with acid.

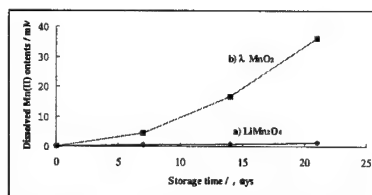


Figure 1. Dissolved Mn(II) content in electrolyte as a function of storage times. For this measurement, 150mg of spinel powder was dispersed in 8ml of electrolyte at 70 °C.

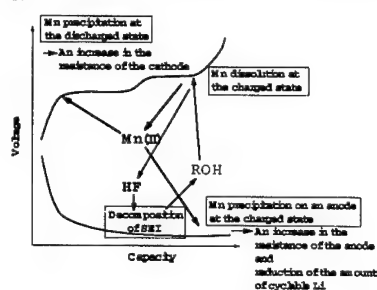


Figure 2. Proposed mechanism for capacity fade

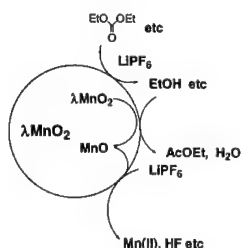


Figure 3. Proposed mechanism of Mn dissolution from $\lambda\text{-MnO}_2$

Abstract No. 177

Defect structure of Li-Mn-O spinels prepared at different annealing temperatures.

Shintaro Ishida and Koichi Numata
Battery Materials Research Laboratory
Mitsui Mining and Smelting Co., Ltd.
1-5-1 Shio-machi, Takehara
Hiroshima 725-0025 Japan

INTRODUCTION

Lithium manganese oxides with spinel structure ($[(Li_{1-x})_8(Mn_{2-x})_{16}(O_4)_{32}]$) prepared at different calcination conditions show different electrochemical properties.

There are some reports concerning the defect structure of Li-Mn-O spinel. Thermogravimetric analysis showed that the Li-Mn-O spinel lost oxygen at high temperature in an ambient atmosphere, and oxygen defect model was proposed (1). On the other hand, cation excess model was reported when the material was annealed in an inert atmosphere (2).

In this report, occupancy of both anion and cation in a unit cell of the samples that were annealed at different temperature was measured to investigate the relation between the defect structure and the electrochemical properties.

EXPERIMENTAL

Manganese oxide prepared from the wet process was mixed with lithium carbonate in a molar ratio of Li : Mn = 1.1 : 1.9. The mixture was calcined at 900°C in air and cooled rapidly in a ratio of 5°C/min and pulverized. Then the samples were annealed in different conditions listed in Table 1.

Chemical analysis was performed to determine lithium and manganese content, and manganese valence. Lattice constant was calculated from the X-ray diffraction data. True density of the powder samples was measured by He gas substitution technique.

Battery performance was measured using lithium foil as anode, 1 M LiBF₄/PC+DME (1 : 1) as electrolyte and polypropylene separator. Cut-off voltage of charge and discharge was 4.3 and 3.0 V, respectively.

RESULTS AND DISCUSSION

The lattice constant decreased when the annealing temperature was lowered. This can be explained by the increase of manganese valence caused by the absorption of oxygen. In this case, one can expect the increase of true density when the annealing temperature was lowered. However, the true density decreased by lowering the annealing temperature.

Figure 1 shows the occupancy of cations (8a and 16d sites) and anion calculated from the chemical analysis data, lattice constant and true density. The defect structure model of the sample annealed at 900°C that had less oxygen content could be the cation excess model, and occupancy of cation sites and anion site decreased while absorbing oxygen by lowering the annealing temperature.

Figure 2 shows the cycle durability of the samples annealed at different temperature. Samples that were annealed at lower temperature showed good cycle durability. The deficiency in anion and cation sites might be effective to tolerate the strain in the crystal structure during the charge and discharge process.

REFERENCES

1. Y. Gao and J. R. Dahn, J. Electrochem. Soc., **143**, 100 (1996).

2. M. Hosoya, H. Ikuta, T. Uchida and M. Wakiyama, J. Electrochem. Soc., **144**, L52 (1997).

Table 1. Sample description

No.	Annealing Temp. (°C)	Atmosphere	Cooling Rate (°C/min)
1	600	Air	5
2	700	Air	5
3	800	Air	5
4	900	Air	5
5	900	Oxygen	5

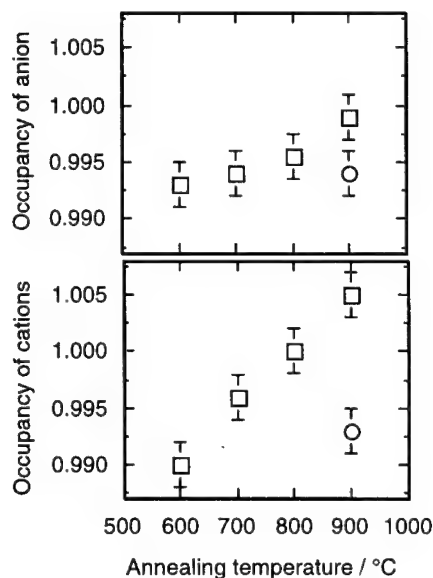


Figure 1. Dependence of occupancy of cations (Li + Mn) and anion (O) on the annealing temperature. Square and circle symbols denote the annealing atmosphere of air and oxygen, respectively.

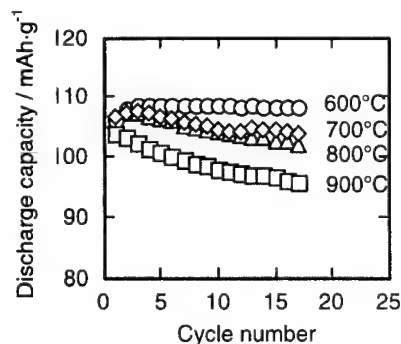


Figure 2. Cycle durability of spinels annealed at different temperature.

Abstract No. 178

On the Correlation between the Electroanalytical Behavior and Crystallographic Features of Li Intercalation Electrodes

M.D. Levi, E. Levi and D. Aurbach

Department of Chemistry, Bar-Ilan University
Ramat-Gan 52900, Israel

U. Heider, R. Oesten and M. Schmidt

Merck KGaA, 250 Frankfurter Str., Darmstadt, Germany

Introduction.

Recently we have reported on the electroanalytical behavior of thin composite Li_xMO_y electrodes studied by simultaneous application of slow-scan rate cyclic voltammetry (SSCV), potentiostatic intermittent titration (PITT) and electrochemical impedance spectroscopy (EIS) [1,2]. Several compounds such as LiNiO_2 and $\text{LiCo}_{0.2}\text{Ni}_{0.8}\text{O}_2$ can serve as almost ideal model systems for revealing and elucidation of the correlation between their structural features and electrochemical behavior.

Experimental.

LiMO_y ($M = \text{Co}, \text{Ni}, \text{Mn}$) powders were obtained from Merck ($0.5 - 1 \mu\text{m}$ particle size, in average). The electrode's active mass was 85 wt% of the corresponding oxide, 10 wt% conductive carbon black, and 5 wt% PVdF binder. The three-electrode cell contained a polyethylene frame with symmetrical slits on both sides. The frame held the working and counter electrodes in a parallel plate configuration with Li counter and reference electrodes. The electrolyte solutions were based on ethylene carbonate (EC) - dimethylcarbonate (DMC) mixtures (Merck's solvents) with different Li salts. The performance of the various electroanalytical and structural measurements has been already described [1-3].

Results.

Fig. 1a and b show as an example two highly resolved plots of differential intercalation capacity, C_{int} , and the chemical diffusion coefficient of Li-ions, D , vs. potential for Li_xNiO_2 and $\text{Li}_x\text{Co}_{0.2}\text{Ni}_{0.8}\text{O}_2$ electrodes, respectively. Phase diagrams indicating single and two-phase co-existence regions (hexagonal, H, and monoclinic, M, phases) obtained by in-situ XRD [3] are shown at the bottom of the figures. It is seen that a pronounced minimum in D is observed in the vicinity of $E = 3.57 \text{ V}$ (vs. $\text{Li}|\text{Li}^+$), corresponding to the maximum in C_{int} . The observed features were not practically dependent on the amplitude of the potential step, and thus were ascribed to high attractive electron-ion interactions with an interaction parameter $|\lg| < |\lg_{\text{crit}}|$ where the critical value \lg_{crit} defines the condition of first-order phase transition. This conclusion based on the application of lattice-gas models to Li-intercalation into transition metal oxides seems to be in excellent agreement with essentially single-phase mode of the reaction in this potential range (H_1 phase) for the two compounds.

In contrast, at higher de-intercalation levels (i.e. at $E > 3.6 \text{ V}$) the two electrodes exhibit quite different electroanalytical behavior: Rather sharp peaks on the C_{int} vs E plot for Li_xNiO_2 electrode correlate well with the distinct minima on $\log D$ vs. E curves, which become deeper as the amplitude of the potential increment decreases. In the case of $\text{Li}_x\text{Co}_{0.2}\text{Ni}_{0.8}\text{O}_2$, for the potential region between 3.60 and 4.15 V only two flat peaks at around 3.70 and 4.00 V appear on the C_{int} vs E plot. The corresponding $\log D$ vs. E relationship contains only minor, practically indistinguishable minima, such that this relationship is independent of the amplitude of the potential increment.

Conclusion.

Both types of the electroanalytical behavior have been found to strongly correlate with the character of structural changes occurring in the bulk of Li_xNiO_2 and $\text{Li}_x\text{Co}_{0.2}\text{Ni}_{0.8}\text{O}_2$ electrodes during Li-intercalation (as is seen in Fig. 1). This makes the application of lattice-gas models for the description of Li-intercalation into transition metal oxides both reliable and self-consistent.

References.

1. M. D. Levi, K. Gamolsky, U. Heider, R. Oesten and D. Aurbach, *J. Electroanal. Chem.* **477**, (1999)32.

2. D. Aurbach, M. D. Levi, E. Levi, H. Teller, B. Markovsky, G. Salitra, U. Heider, R. Oesten and D. Aurbach, *J. Electrochem. Soc.* **145** (1999) 3024.
3. E. Levi, M.D. Levi, G. Salitra D. Aurbach, R. Oesten, U. Heider and L. Heider, *J. Solid State Ionics* **126** (1999) 97.

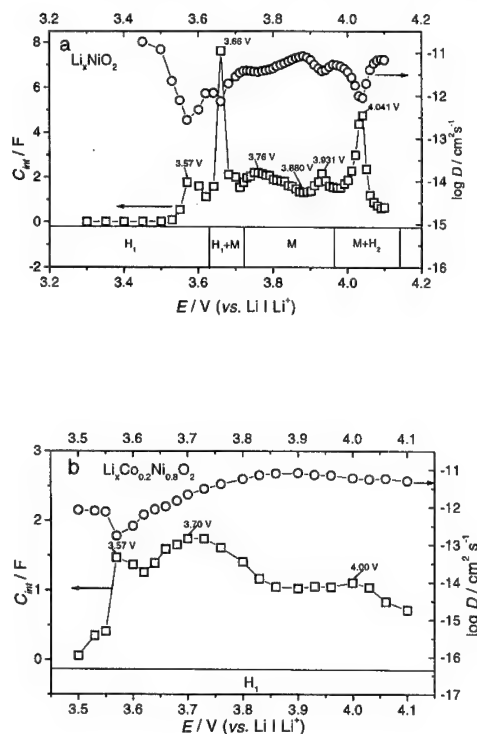


Fig. 1 Plots of differential intercalation capacity, C_{int} , and the chemical diffusion coefficient of Li-ions, D , vs. potential for Li_xNiO_2 and $\text{Li}_x\text{Co}_{0.2}\text{Ni}_{0.8}\text{O}_2$ electrodes (a and b, respectively). Phase diagrams shown in the bottom of the figures were obtained by in-situ XRD.

Abstract No. 179

Li Insertion into Thin Vacuum-Deposited V₂O₅ Films Characterized by a Variety of in-situ Techniques.

M.D. Levi, Z. Lu, M. Moskovich, Yaron Cohen, Yair Cohen, E. Levi, D. Aurbach

Department of Chemistry, Bar-Ilan University
Ramat-Gan 52900, Israel

Introduction.

Commercialization of rechargeable Li-ion batteries during recent years has stimulated interest in the elucidation of the mechanisms of Li intercalation into transition metal oxides which function usually as composite cathodes. Although electroanalytical characterization of these materials can be semi-quantitatively carried out, much more direct and precise information is expected to be obtained with pure oxide materials in the form of thin films. Vacuum-deposited V₂O₅ films, well-crystallized after annealing at about 400° C, present almost an ideal model system for the elucidation of Li-intercalation mechanisms using a variety of in-situ techniques: simultaneous application of SSCV, PITT, EIS [1] as well as conductometry [2], EQCM and AFM.

Experimental.

V₂O₅ films of ca. 1600 Å thick were thermally evaporated onto a Pt foil. The target used was V₂O₅ powder (Aldrich, 99.99%). The thermal deposition rate was 0.1 Å/s. After deposition, the microelectrode array covered with V₂O₅ film was annealed at 400° C in an oven over 1h, and then slowly cooled to a room temperature. The films morphology was characterized by AFM. The electrolyte solutions were comprised of Li salts in alkyl carbonates mixtures. The performance of the various measurements was already described [1,2].

Results.

Fig. 1 demonstrates a close correlation between a slow-scan rate cyclic voltammogram (in the form of the differential intercalation capacity, $C_{int} = I/v$, $v = 0.2 \text{ mV s}^{-1}$) and the plot of the chemical diffusion coefficient D vs potential for as-prepared V₂O₅ film. The potentiostatic titration was performed during electrode's discharge, thus the two minima in the D vs E dependence correspond almost precisely to the cathodic peaks of C_{int} . One can also see a similarity in the half-peak widths of the related C_{int} and D vs. E curves. These highly resolved data, which can hardly be obtained with the composite electrodes, are appropriate for theoretical modeling using lattice-gas approach. The above correlation is due to highly attractive electron-ion interactions during Li-intercalation. Above a critical value of the attraction constant (which appears as a parameter in the intercalation isotherm chosen for describing the intercalation reaction) the process proceeds in the form of first-order phase transition. Since SSCV and PITT reflect mainly the processes occurring in the long and medium-time domains, we have also applied EIS in order to receive a general view at the relaxation steps of the entire intercalation process, see Fig. 2. This figure shows as an example the complex-plane impedance spectra of thin Li_xV₂O₅ electrodes measured during Li-intercalation in the vicinity of the SSCV peak at 3.4 V (vs. Li⁺/Li⁰). The low frequency (long-time) domain of the spectra is represented by a sloping capacitive line. Horizontal lines in Fig. 2 mark the points related to different potentials (as indicated) but to the same lowest applied frequency of 2 mHz. It is seen that the Z' values which are reciprocals of C_{int} ($Z' = 1/\omega C_{int}$) reflect a deep minimum centered at ca. 3.4 V. The good correlation between the results obtained by SSCV and EIS demonstrates their reliability. The high frequency domain of the spectra (which cannot be reflected by SSCV) presents a slightly depressed semicircle shown as the insert in Fig. 2. We are accumulating evidence for the identification of this semicircle with surface layers, which cover the V₂O₅ electrodes, and can be attributed to acid-base reactions between the oxide and acidic solution species.

Conclusion.

SSCV, PITT and EIS applied in a single study in order to explore Li-ion intercalation into a thin V₂O₅ electrode were presented. The plots of C_{int} and D vs. potential correlate, and were practically independent of the technique used. Their

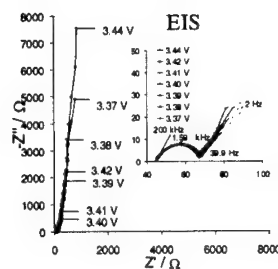
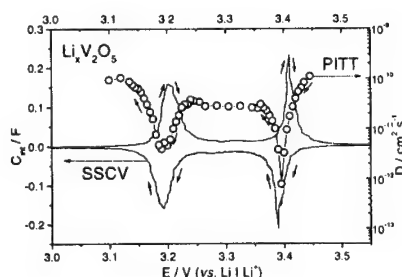
shape is consistent with a lattice-gas approach assuming highly attractive electron-ion interactions during Li-intercalation into this material. In-situ EQCM and AFM measurements of thin V₂O₅ electrodes during Li intercalation are in progress.

References.

1. Z. Lu, M. D. Levi, G. Salitra, Y. Gofer, E. Levi and D. Aurbach, *J. Electroanal. Chem.* (submitted).
2. M. D. Levi, Z. Lu, Y. Gofer, Yaron Cohen, Yair Cohen, D. Aurbach, E. Vieil, J. Serose, *J. Electroanal. Chem.* 479 (1999) 12 and references therein.

Fig. 1 Plots of differential intercalation capacity, C_{int} ($v = 0.2 \text{ mV s}^{-1}$) and the chemical diffusion coefficient of Li-ions, D , vs. potential for thin Li_xV₂O₅ film electrode.

Fig. 2 Nyquist plots for thin Li_xV₂O₅ film electrode measured in the vicinity of the CV peak centered at 3.4 V. The high frequency domain of the spectra is presented in the insert.



Study of Lithium Insertion into Electrochemically Synthesized Sodium Vanadium Oxide

D. Aurbach, B. Markovsky, G. Salitra and Y. Cohen
Department of Chemistry, Bar-Ilan University,
Ramat-Gan 52900, Israel

E. Shembel, R. Apostolova and V. Nagirny
Ukrainian State Chemical Technology University,
Dnipropetrovsk 320005, Ukraine

Introduction

In this work, we concentrated on the characterization of $\text{Na}_x\text{V}_2\text{O}_5$ ($0.2 < x < 0.4$) bronze as a cathode material for rechargeable Li batteries. We studied the correlation among the 3D structure, morphology, electroanalytical response (diffusion coefficient of Li-ions in the bulk, impedance behavior), and the surface chemistry and performance of these electrodes. The high capacity (>200 mAh/g) and the moderate red-ox potentials (around 3 V vs. Li/Li^+) make $\text{Na}_x\text{V}_2\text{O}_5$ bronze a suitable cathode for rechargeable batteries with Li metal anodes. The moderate red-ox potential is an advantage here, because the suitable electrolyte systems for Li metal-based rechargeable batteries (in which Li cycling efficiency is sufficiently high) are based on either cyclic ethers (liquid systems) or derivatives of PEO (polymeric systems). The anodic stability of these systems is limited to 4 V (vs. Li/Li^+). Another important advantage of these electrodes is their being monolithic, and hence can be used as-prepared, without the need for a composite structure and the use of a binder.

Experimental

Sodium-vanadium oxide $\text{Na}_x\text{V}_2\text{O}_5$ (bronze, $0.2 < x < 0.4$) was electrochemically synthesized from an aqueous electrolyte solution comprising vanadyl sulphate (0.2 M/l) and sodium sulphate (5 g/l of Na^+) as described recently.⁽¹⁾ The electrodes were thermally treated at 300°C , 2.5 h. The thickness of the sodium-vanadate films deposited on stainless steel plates was usually 2–4 μm (estimated by SEM and STM⁽²⁾ techniques). Electrolyte solutions comprised of EC, DMC (1:3 by volume, solvents from Merck) and 1M LiAsF_6 (FMC) were used for the electrochemical experiments. The various types of measurements used, including SSCV, PITT, EIS, FTIR spectroscopy, XPS, SEM-EDAX, and XRD were already described.⁽³⁾

Results and Discussion

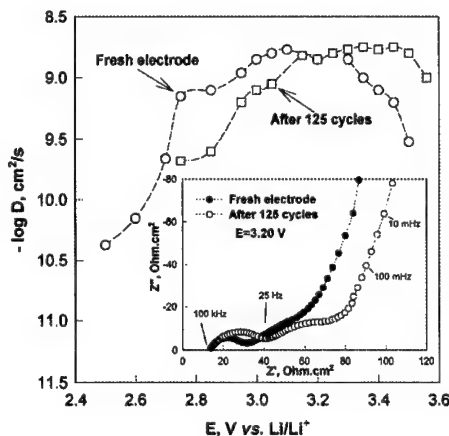
The potentiodynamic response of the $\text{Na}_x\text{V}_2\text{O}_5$ bronze electrode is characterized by a pronounced cathodic peak at 2.51 V and two shoulders positioned at 3.51 V and 2.84 V, respectively. The CV features of the electrochemically-synthesized material are very similar to those of the $\beta\text{-Na}_{0.33}\text{V}_2\text{O}_5$ bronze prepared by a sol-gel method.⁽⁴⁾

The capacity fading of our electrodes in the carbonate based solutions was less than 1 promil per cycle (100% DOD) and the effect of the charge-discharge rates (in the C/20h – C/2h range) was negligible. It thus appears that the kinetics of these electrodes is fast. FTIR spectral

studies revealed that the electrodes developed surface films (probably due to reactions of the vanadium oxide with trace Lewis acids in solutions). Highly resolved impedance spectra (Nyquist plots) could be obtained with the $\text{Li}_x\text{Na}_x\text{V}_2\text{O}_5$ electrodes after prolonged cycling. The impedance spectra nicely reflect all the stages of Li insertion into these electrodes: Li migration through surface films (high frequency semicircle), charge-transfer (medium frequency arc), Li-ion diffusion (a "Warburg"-type element), and Li accumulation in the bulk (capacitive behavior at the very low frequencies). The figure below compares Li-ion chemical diffusion coefficients as a function of potential, calculated from EIS data⁽⁵⁾ of fresh and cycled electrodes. The difference between these curves may reflect some structural changes occurring upon cycling. However, the possibility of calculating D vs. E of cycled electrodes at high precision from EIS proves the stability and integrity of these electrodes during prolonged cycling.

References

1. E. Shembel, R. Apostolova, V. Nagirny, D. Aurbach, and B. Markovsky, *J. Power Sources*, 80, 90 (1999).
2. Y. Cohen and D. Aurbach, *Rev. of Sci. Instr.*, 70, 4668 (1999).
3. D. Aurbach, B. Markovsky, M. D. Levi, E. Levi, A. Schechter, M. Moshkovich and Y. Cohen, *J. Power Sources*, 81-82, 95 (1999) and references therein.
4. S. Bach, J.P. Pereira-Ramos, N. Baffier and R. Messina, *J. Electrochem. Soc.*, 137, 1042 (1990).



The diffusion coefficient of Li-ion into $\text{Na}_x\text{V}_2\text{O}_5$ as a function of potential for pristine and cycled electrodes (as indicated), calculated from EIS (the "Warburg" region). Typical impedance spectra of these electrodes (at 3.2 V vs. Li/Li^+) are also presented.

Characterization of LiFePO_4 as the Cathode Material for Rechargeable Lithium Batteries

Masaya Takahashi, Shinichi Tobishima, Koji Takei and Yoji Sakurai

NTT Telecommunications Energy Laboratories
Tokai-mura, Naka-gun, Ibaraki-ken, 319-1193 Japan

LiFePO_4 , which has an olivine structure, is an attractive cathode material for lithium ion batteries in terms of environmental benignity and easy to availability. However, it was reported that high rate charging and discharging were difficult to achieve in an ordinary liquid electrolyte cell at room temperature [1]. LiFePO_4 was studied as a way to overcome this problem and recently this material has been reported to perform well in a lithium battery system [2]. We have studied the synthesis process and electrochemical characteristics of LiFePO_4 .

We prepared LiFePO_4 by firing a stoichiometric mixture of $\text{Fe}(\text{COO})_2 \cdot 2\text{H}_2\text{O}$, $(\text{NH}_4)_2\text{HPO}_4$ and $\text{LiOH} \cdot \text{H}_2\text{O}$ at various temperatures from 675 to 800 °C in an argon atmosphere. We evaluated its electrochemical characteristics by using a coin type cell with lithium metal anode and 1 M LiPF_6 in ethylene carbonate / dimethyl carbonate (1 : 1 in volume) electrolyte. The cells were cycled galvanostatically between 3.0 and 4.0 V.

Figure 1 shows charge and discharge curves of the $\text{Li}/\text{LiFePO}_4$ cells at the 10th cycle for different preparation temperatures of 675, 725 and 800 °C. The charge and discharge behavior was evaluated at 20 °C and at 0.5 $\text{mA} \cdot \text{cm}^{-2}$. The capacity of the cell increased as the preparation temperature decreased and reached 115 $\text{mAh} \cdot \text{g}^{-1}$ for the cell whose compound was prepared at 675 °C. This is about double the capacity for a cell whose compound was prepared at 800 °C. The voltages of the plateaus seen in the charge and discharge curves were almost the same regardless of the preparation temperature. This means the preparation temperature did not affect the overvoltage of the LiFePO_4 electrochemical reaction at the surface of the particles, where the early charge-discharge reaction proceeds. Our SEM observations showed that high temperature preparation causes particle growth and a reduction in the surface area. It has been reported that the capacity of the LiFePO_4 electrode is limited by the lithium diffusion rate in LiFePO_4 particles [1]. With large particles, the lithium ions must diffuse over a greater distance between the surface and center of the particles on insertion or extraction, and the LiFePO_4 near the particle center cannot contribute easily to the charge-discharge reaction. Hence the particle growth that occurs during high temperature LiFePO_4 preparation reduces the capacity.

Figure 2 shows the cycle performance of $\text{Li}/\text{LiFePO}_4$ cells operated at 20, 40, 60 and 80 °C. The LiFePO_4 compound used here was synthesized at 675 °C and the charge-discharge cycling test was undertaken at 0.5 $\text{mA} \cdot \text{cm}^{-2}$. The discharge capacity of the cell increased as the operating temperature was increased. At 80 °C, the initial discharge capacity reached 155 $\text{mAh} \cdot \text{g}^{-1}$, or about 1.35 times higher than that observed at 20 °C. This capacity increase indicates that the lithium diffusion in LiFePO_4 is enhanced by elevated temperature and that LiFePO_4 compounds nearer the center of the particle are utilized.

References:

1. A. K. Padhi, K. S. Nanjundaswamy and J. B. Goodenough, *J. Electrochem. Soc.*, 144, 1188 (1997).
2. N. Ravet, J. B. Goodenough, S. Besner, M. Simoneau, P. Hovington and M. Armand, Abstract No. 127, The 1999 Joint International Meeting, Hawaii, Oct. 17-22 (1999).

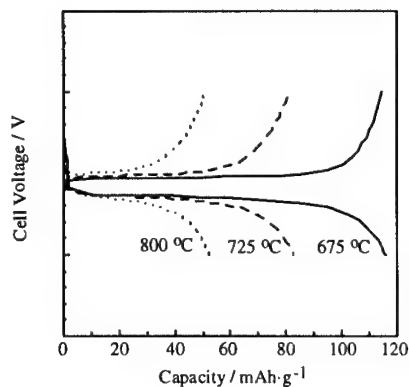


Fig. 1 Charge-discharge curves of $\text{Li}/\text{LiFePO}_4$ cells at 10th cycle with LiFePO_4 prepared at different temperatures, 675, 725 and 800 °C. Measurement temperature is 20 °C and current is 0.5 $\text{mA} \cdot \text{cm}^{-2}$.

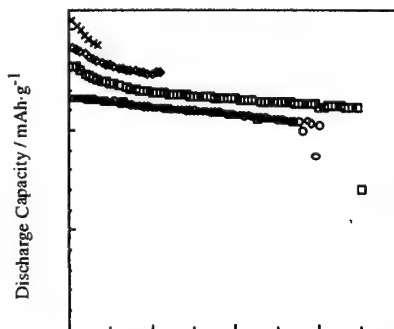
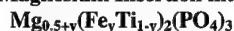


Fig. 2 Cycle performance of $\text{Li}/\text{LiFePO}_4$ cells at 20, 40, 60 and 80 °C. LiFePO_4 was prepared at 675 °C and charge-discharge current is 0.5 $\text{mA} \cdot \text{cm}^{-2}$.

Magnesium Insertion into



Koji MAKINO, Yasushi KATAYAMA,
Takashi MIURA, and Tomiya KISHI

Department of Applied Chemistry,
Faculty of Science and Technology, Keio University
Hiyoshi 3-14-1, Kouhoku-ku, Yokohama 223-8522, Japan

INTRODUCTION

Lithium ion cells are now widely accepted as high energy density secondary batteries. Rechargeable magnesium cells may be another candidates of a high energy density cell, because the raw material costs may lower those in lithium ion cells and because magnesium is less dangerous than lithium. However, Mg^{2+} insertion into ion-transfer host proceeds slowly owing to the strong solvation of small and divalent Mg^{2+} ion compared to Li^+ or Na^+ [1]. In this study, a series of transition metal phosphates, $\text{Mg}_{0.5+y}(\text{Fe}_y\text{Ti}_{1-y})_2(\text{PO}_4)_3$ (MFTP), modified from $\text{Mg}_{0.5}\text{Ti}_2(\text{PO}_4)_3$ (MTP) are investigated as a magnesium host. Since MTP and the well-known fast ion conductor of NASICON are isostructural, fast Mg^{2+} transport may be expected in the MTP lattice [2].

EXPERIMENTAL

$\text{Mg}_{0.5+y}(\text{Fe}_y\text{Ti}_{1-y})_2(\text{PO}_4)_3$ samples were prepared as follows; 0.1 mol/dm³ $\text{Mg}(\text{CH}_3\text{COO})_2 \cdot 4\text{H}_2\text{O}$ and 0.1 mol/dm³ $\text{NH}_4\text{H}_2\text{PO}_4$ aqueous solutions were prepared separately, in addition to 0.1 mol/dm³ FeCl_3 and 0.1 mol/dm³ $\text{C}_4\text{H}_9\text{O}[\text{Ti}(\text{OC}_4\text{H}_9)_2\text{O}]_4\text{C}_4\text{H}_9$ ethanol solutions. These solutions were mixed at the calculated ratio to give the composition y . The obtained sol solution was further stirred at 70°C for 6 h to form a gel, which was dried at 90 °C for 12 h to give a powder. It was heated at 300 and then 500 °C to remove ammonium and acetate groups, followed by final firing at 700°C for 24 h.

Electrochemical magnesium insertion from 1 mol/dm³ $\text{Mg}(\text{ClO}_4)_2/\text{PC}$ solution was performed in a cylindrical glass cell. Sample electrode was prepared from the mixture of MFTP (or MTP), acetylene black and PTFE (mass ratio; 70:25:5). Magnesium ribbon was used as a counter electrode. Reference electrode consisted of silver wire immersed in 0.1 mol/dm³ AgClO_4/PC , which was separated from the cell electrolyte by a glass filter.

RESULTS AND DISCUSSION

MFTP having the same lattice as MTP could be obtained as a single phase only at $0 < y < 0.5$, and FePO_4 appeared at $0.5 < y$ as the second phase. The effects of Ti^{4+} substitution with Fe^{3+} on lattice parameters are shown in Fig. 1, where the shrinkage in c -axis occurs due to the relaxed O-O repulsion in $(\text{Ti}, \text{Fe})\text{O}_6$ octahedra and to the bond formation between introduced excess Mg^{2+} and O in $(\text{Ti}, \text{Fe})\text{O}_6$ octahedra. On the other hand, a -axis expands to compensate the c -shrinkage in the flexible NASICON framework [3, 4], though a slight decrease in the unit volume is observed.

Discharge curves of MFTP ($y = 0.5$) and MTP are compared in Fig. 2. The plateau at about -1.6 V (vs. Ag^+/Ag) appears only for MTP. At $1.5 \times x$, MFTP and MTP show substantially identical discharge potential below -2.4 V, where x denotes the calculated amount of inserted Mg^{2+} per formulae. From these results, it may be suspected that the cation sites for foreign Mg^{2+} ions are available only in MTP and these sites are already occupied by preexisting Mg^{2+} in excess in MFTP. A

preliminary XRD study after discharge shows that magnesium insertion can proceed topotactically as a single phase reaction into both MFTP and MTP, where the unit cell parameters remain almost constant at various stages of magnesium insertion. It is possible to suppose that Mg^{2+} can be accommodated in the host without any phase transition, because there are large cation sites in NASICON-type compounds.

REFERENCES

- [1] P. Novák *et al.*, *J. Power Sources*, **54** (1995) 479.
- [2] J.B. Goodenough *et al.*, *Mat. Res. Bull.*, **11** (1976) 173.
- [3] C. Delmas *et al.*, *Solid State Ionics*, **28-30** (1988) 419.
- [4] O. Mentre *et al.*, *Solid State Ionics*, **72** (1994) 293.

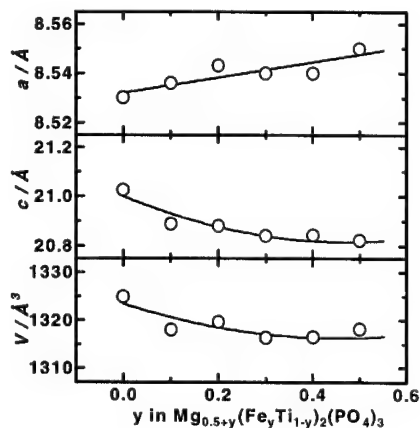


Fig.1. Unit cell parameters of $\text{Mg}_{0.5+y}(\text{Fe}_y\text{Ti}_{1-y})_2(\text{PO}_4)_3$.

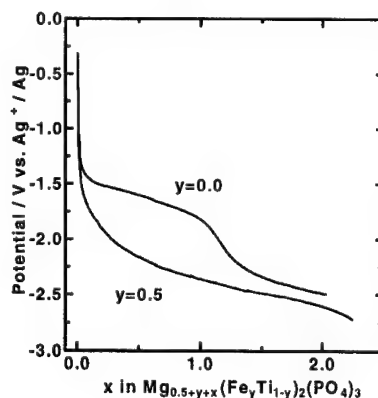


Fig.2. Discharge curves of $\text{Mg}_{0.5+y}(\text{Fe}_y\text{Ti}_{1-y})_2(\text{PO}_4)_3$ at $-50 \mu\text{A}\cdot\text{cm}^{-2}$.

Preparation of Todorokite MnO_2 for Rechargeable Battery Cathode

Naoaki Kumagai, Shinichi Komaba,
Hiroki Sakai, and Nobuko Kumagai
Department of Applied Chemistry & Molecular
Science, Faculty of Engineering,
Iwate University, Morioka 020-8551, Japan

Cathodic materials for rechargeable Li batteries have been the focus of intense research for a number of years. Among the candidates for cathodic materials, manganese oxides are particularly attractive. Much research is focusing currently on the application of the spinel LiMn_2O_4 phase to lithium-ion batteries. For the electrochemically reversible intercalation of lithium, vacant spacing in the host plays an important role to improve the intercalation dynamics. Among various manganese-based oxide frameworks which are roughly classified into tunnel structures (1D), layer phases (2D), and spinels (3D), "todorokite" would possess largest tunnel structure, which consists of triple chain of edge-sharing MnO_6 octahedra that form 3×3 channels as shown in Fig. 1 [1]. Recently, the synthesis of a thermally stable todorokite by combination of an aqueous solution and hydrothermal techniques was developed by Suib *et al.* [2,3], further a few reports appeared in a viewpoint of the lithium battery application of the synthesized todorokite [4-6]. We report here the fundamental properties and relationship between the synthetic condition and cathode performance of the todorokite.

The todorokite manganese oxide were prepared according to the previous literature [2] as follows:

1. $\text{Mn}(\text{OH})_2$ was precipitated by an addition of NaOH or KOH solution into MnCl_2 solution.
2. This $\text{Mn}(\text{OH})_2$ was oxidized by adding NaMnO_4 or KMnO_4 to obtain layered birnessite Na-MnO_2 powder at room temperature, and it was aged for one week.
3. Ion-exchange of the Na^+ for Mg^{2+} was achieved by dispersing the birnessite in MgCl_2 solution for one day to obtain busierite Mg-MnO_2 .
4. Todorokite was prepared by hydrothermal treatment ($120 \sim 200^\circ \text{C}$) of the Mg -busierite for four days in water.

Electrochemical investigation was undertaken in $1 \text{ mol dm}^{-3} \text{ LiClO}_4$ -propylene carbonate using a glass beaker-type cell at $25 \pm 2^\circ \text{C}$.

The todorokite electrode obtained here showed high electroactivity in Li cell due to

lithium de/intercalation. Figure 2 shows the cycle behavior of todorokite electrodes, which contained some magnesium ions and water. The todorokite obtained at 200°C through the hydrothermal process performed higher capacity of *ca.* 220 mAh g^{-1} at the initial and $> 100 \text{ mAh g}^{-1}$ during the initial 20 cycles. By further heat treatment of todorokites in air, the battery performance was improved. In case of magnesium insertion, todorokite exhibited higher capacity compared to the $\alpha\text{-MnO}_2$ which is a smaller tunnel material (2×2). We concluded that todorokite has a potential for the application as a new electrochemical intercalation host.

References

- [1] J. E. Post *et al.*, *Amer. Miner.*, **73**, 861 (1988).
- [2] S. L. Suib *et al.*, *Science*, **260**, 511 (1993).
- [3] S. L. Suib *et al.*, *J. Am. Chem. Soc.*, **116**, 11020 (1994).
- [4] Y. Yang *et al.*, *J. Power Sources*, **65**, 227 (1997).
- [5] L. F. Nazar *et al.*, *J. Electrochem. Soc.*, **145**, 3467 (1998).
- [6] Y. Yang *et al.*, *J. Power Sources*, **81-82**, 637 (1999).

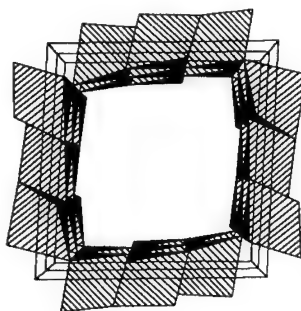


Fig. 1 Schematic illustration of todorokite structure refined by the Rietveld method [1].

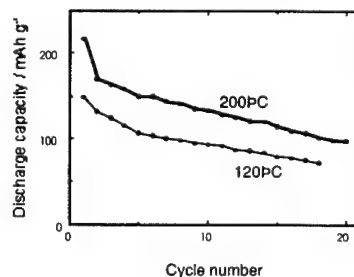


Fig. 2 Cycle number vs. discharge capacity plots of todorokite measured galvanostatically at 0.1 mA cm^{-2} in the potential range from 4.2 to 2.0 V vs. Li/Li^+ .

A Study on the Preparation and Characterization of Au-codeposited LiMn_2O_4 Electrode

Mi-Ra Lim and Kwang-Bum Kim*

Dept. of Chemistry, Chonnam National University, YoungBong-Dong, Buk-gu, Kwangju, 500-757, Korea

*Dept. of Metallurgical Eng., Yonsei University, 134 Shinchon-dong, Seodaemun-gu, Seoul, 120-749, Korea

Introduction

Numerous works have been done to study the electrochemical behavior of LiMn_2O_4 , however, almost all the studies were carried out with composite electrodes consisting of powdered electroactive materials, an organic binder and a conductive additive. Consequently, it is difficult to evaluate the intrinsic kinetic and electrochemical properties of the active materials. To avoid these complications, the preparation and characterization of an additive-free electrode such as a thin film of electrode materials should be an attractive approach. Electrochemical quartz crystal microbalance (EQCM) technique has been established as a powerful tool for in-situ monitoring of mass variation during electrochemical reactions. For a quartz crystal to oscillate, a very small quantity of active materials has to be loaded to the quartz crystal because the ratio of the resonant frequency shift to the original resonant frequency should be less than 0.02. Thin film cathode materials should be heat-treated at temperatures below the temperature of phase transition of quartz (573°) followed by deposition on the quartz crystal for the EQCM-based evaluation. However, the preparation of the thin film cathode materials usually requires heat treatments at temperatures higher than 573° , and it limits the use of EQCM technique. Therefore low temperature synthesis of thin film cathode materials has to be developed for studies using EQCM technique. Uchida et al. used the EQCM to investigate the lithium insertion/extraction reaction in LiMn_2O_4 film electrode prepared at 400° by electrostatic spray deposition (ESD)[1]. As an alternative to the low temperature synthesis of thin film cathode materials for EQCM study, we prepared additive-free, Au-codeposited LiMn_2O_4 electrodes with a very small amount of the powdered cathode materials and studied their physical and electrochemical properties.

Experimental

Au-codeposited LiMn_2O_4 electrode was prepared on a platinum substrate by embedding the particles of $\text{Li}_{1-x}\text{Mn}_2\text{O}_4$ (Kerr McGee Chemical LLC products, 210 grade, $x=0.06-0.08$) into an electrodeposited coating of metallic gold. Identification of the molecular structure of codeposited LiMn_2O_4 was done to observe any chemical changes of the particles during the preparation of electrode by microRaman spectroscopy. The electrode crystallographic structure was analyzed using X-ray diffraction and morphology change of the Au-codeposited electrode according to the deposition time was studied using scanning electron microscope. And electrochemical behavior of codeposited electrode was studied by cyclic voltammetry. Test cells were assembled using codeposited electrode as a working electrode, lithium foils as counter and reference electrode, and

a 1.0M lithium perchlorate (LiClO_4), propylene carbonate (PC) solution as the electrolyte.

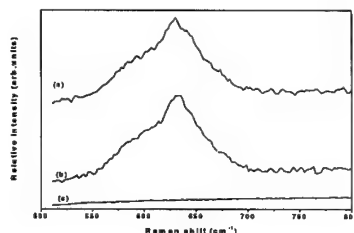
Results and Discussion

Fig. 1 shows the microRaman spectra of pure LiMn_2O_4 powders and Au-codeposited LiMn_2O_4 electrode. The lithium-excess pure LiMn_2O_4 powder showed band at 632 cm^{-1} and it could be clearly identified in Au-codeposited LiMn_2O_4 electrode. And Raman response of electrodeposited gold was negligible as shown in Fig. 1(c). No Raman shift observed in Fig.1 indicates that the molecular structure of Au-codeposited LiMn_2O_4 electrode has not been changed during electrode. Other physical and electrochemical properties of Au-codeposited electrode will be presented in the meeting.

Fig.1. MicroRaman spectra (a) pure LiMn_2O_4 powders, (b) Au-codeposited LiMn_2O_4 powders, (c) electrodeposited Au

References

- [1] M.Nishizawa, T. Uchiyama, T. Itoh, T. Abe, and I. Uchida, Langmuir, 15(1999), 49-51



**LITHIUM AND PROTON INSERTION
IN SPINEL-STRUCTURED
MANGANESE OXIDES**

**M. Saiful Islam^{*a}, Brett Ammundsen^b
and Jacques Roziere^b**

^a *Department of Chemistry, University of
Surrey, Guildford GU2 5XH, UK*

^b *Lab. des Agregats Moleculaires et
Materiaux Inorganiques, Universite
Montpellier 2, Montpellier Cedex 5,
France*

Atomistic computer simulation and x-ray absorption techniques are used to investigate lithium and proton insertion, and cation dopant sites in the LiMn_2O_4 - λ - MnO_2 system. We examine the mechanisms and pathways for lithium ion migration through the interstitial space of the spinel lattice. Evaluation of the data predicts that Li-ion diffusion in spinel manganates is rather slow compared with layered-structured materials. In aqueous acid the lithium ions in Mn(IV)-rich spinels are readily exchanged for protons without modification of the Mn oxidation state. The local structures around Mn vacancy defects are modelled to determine their effect on lithium and O-H configurations. This work includes simulations of the lattice (and O-H) vibrational modes allowing their Raman and infrared spectra to be assigned. Such phonon calculations support the assignment of two observed IR bands to vibrations of the hydroxyl group coordinated to a Mn vacancy. We have also examined the effects on local structure from substitution of Mn in LiMn_2O_4 by various cation dopants (e.g., Cr, Co, Ga); the simulations are compared with data from EXAFS studies. Results of recent modelling work on the effects of oxygen non-stoichiometry and fluoride substitution will be presented.

Ammundsen B., Islam MS et al., *J. Phys. Chem. B* **101**, 8156 (1997); *J. Phys. Chem. B* **103**, 5175 (1999); *J. Power Sources* **81**, 500 (1999)

Synthesis and Characterization of Nonstoichiometric LiCoO_2 Masaaki Fujii, Nobuyuki Imanishi, and Yasuo Takeda
Department of Chemistry, Mie University
1515 Kamihamacho, Tsu, Mie 514-8507, Japan

Introduction

LiCoO_2 is commercially used as positive electrode of lithium ion battery. The structure of high temperature LiCoO_2 is a space group of R-3m which has alternately ordered lithium and cobalt layers. This ion arrangement is not easily perturbed under usual synthetic conditions. Thus, LiCoO_2 has been believed to always occur in the stoichiometric form. This makes a sharp contrast to the identical structural material, LiNiO_2 , which inevitably contains cubic domains to some extent. The electrode behaviors based on lithium intercalation show strong and complicated dependence on degree of disorder of Li and Ni layers. On the other hand, there are few studies of LiCoO_2 from detailed structural aspects due to much less tendency to show such disordered structure.

Recent studies, however, show preparation of Li_xCoO_2 with $x > 1$, when initial nominal composition is set at $\text{Li/Co} > 1$. Delmas et al., reported that oxygen defects are generated in a lithium-rich Li_xCoO_2 together with the occurrence of divalent Co^{2+} . They found that Co^{2+} in cobalt layer decreases electronic conductivity and restrains phase transition. As shown in these literatures, slight structural defects play a crucial role even in LiCoO_2 .

In this study the relation between synthetic condition, non-stoichiometry and electrode characteristics of LiCoO_2 is discussed. We at first synthesize Li_xCoO_2 ($x > 1$) with wider range of compositions in order to survey the structural change. Secondary, the products are characterized in detail by X-ray diffraction, $^1\text{LiNMR}$, iodometry, Induced coupled plasma spectroscopy (ICP) etc. Our TG measurements indicate that the sample loses oxygen around 800°C with increasing Li/Co ratio. In order to evaluate effect of oxygen vacancies on structure and electrochemical properties, products are treated under high oxygen pressure to reduce the number of defects.

Experimental

LiOH and Co_2O_3 were mixed well in an agate mortar at nominal compositions, $\text{Li/Co} = 1.02, 1.05, 1.10, 1.15, 1.20, 1.25, 1.30$. Cobalt content in Co_2O_3 was determined from thermogravimetric analysis. Six-hour calcination of the mixture was done at 750°C, followed by 24 hour annealing at 850°C in air atmosphere.

The stoichiometry of products was determined from combining two types of data. ICP measurement was used to determine Li/Co molar ratio. The sample was dissolved in hydrochloric acid 10ml, then diluted to adjust the concentration being within $1 \times 10\text{ppm}$ range. Fixed amount of yttrium was added to the tested solution as an internal standard. Cobalt valence was decided from iodometry. In this analysis, the reduction of Co^{3+} to Co^{2+} was achieved by adding I^- into the hydrochloric solutions of LiCoO_2 . Back titration of resulting I_2 was carried out by sodium thiosulfate. Oxygen content "y" in Li_xCoO_y was calculated based on the data "x" from ICP result. The average valence of cobalt was then obtained. ICP and iodometry results can only provide relative ratio between Li, Co and O. In order to obtain the absolute chemical formula, another information about stoichiometry such as specific density is necessary. Here, we use the relative compositions to refer each

sample.

The powder X-ray diffraction measurement was carried out at the tube voltage 40kV and current 150mA. Samples are scanned within 2θ range of 10° – 90° at a speed of $0.5^\circ/\text{min}$.

Results and Discussion

The determined stoichiometries of products and cobalt valence are summarized in Table 1. According to increase of Li/Co ratio, cobalt valence decreases monotonously. The valence of cobalt is classified into three groups. In $1.02 < \text{Li/Co} < 1.14$, the valence takes the value around 3.0. It means that Co^{2+} amount in these samples is quite small. The cobalt valence decreases to around 2.9 in the next region $1.20 < \text{Li/Co} < 1.26$. In the third group, the cobalt valence is abnormally low at $\text{Li/Co} = 1.60$, and it is the effect of impurity phase which appears in X-ray diffraction pattern. The sum of lithium and cobalt molar numbers in the formula takes a value beyond 2.0. This leads to that cobalt valence goes below 3.0. The actual crystal structure can be interpreted in two ways. One is considering the existence of oxygen defects, that is, oxygen stoichiometry is not 2.0. As the second possibility, it is assumed that more cations than total octahedral holes exist. Latter situation is unlikely to occur because it requires simultaneous occupation of tetrahedral and octahedral holes.

The lattice parameter of each sample refined by the Rietveld method is plotted against Li/Co ratio in Fig. 1. The lattice constant is continuously decreasing with Li/Co ratio. After high pressure oxygen treatment, the lattice parameter significantly increases. This confirms that oxygen is doped into the vacancies that were prepared under normal condition. The expansion of interlayer distance by the treatment is attributed to increasing electrostatic repulsion between oxygen layers.

Table 1 LiCoO_2 composition determined by ICP and iodometry. Oxygen stoichiometry is fixed as 2.0.

Nominal Li/Co	ICP value Li/Co	Cobalt valence	Composition
1.02	1.02	3.06	$\text{Li}_{1.02}\text{Co}_{0.98}\text{O}_{2.00}$
1.05	1.09	2.97	$\text{Li}_{1.07}\text{Co}_{0.99}\text{O}_{2.00}$
1.10	1.11	2.97	$\text{Li}_{1.09}\text{Co}_{0.99}\text{O}_{2.00}$
1.15	1.14	2.96	$\text{Li}_{1.11}\text{Co}_{0.98}\text{O}_{2.00}$
1.20	1.20	2.88	$\text{Li}_{1.17}\text{Co}_{0.98}\text{O}_{2.00}$
1.25	1.22	2.88	$\text{Li}_{1.19}\text{Co}_{0.98}\text{O}_{2.00}$
1.30	1.26	2.86	$\text{Li}_{1.22}\text{Co}_{0.97}\text{O}_{2.00}$
2.00	1.60	2.44	Two-phase

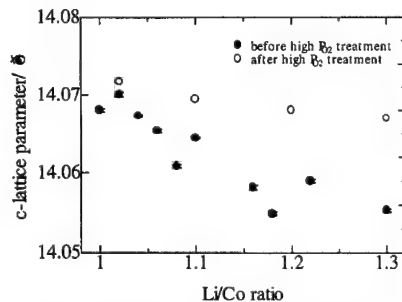


Fig. 1 c-axis lattice parameter change against Li/Co ratio.

Yttrium-doped $\text{Li}(\text{Ni},\text{Co})\text{O}_2$: an improved cathode for Li-ion BatteriesG.V. Subba Rao, B.V.R. Chowdari¹ and H.J. LindnerInstitute of Materials Research and Engineering,
3, Research Link, Singapore 117602.¹Also at Dept. of Physics, Natl. Univ. of Singapore,
Singapore 119260.**Introduction**

Recently mixed oxides of the formula $\text{Li}(\text{Ni}_{1-x}\text{Co}_x)\text{O}_2$, $x = 0.1-0.3$, have been examined as possible substitute for LiCoO_2 as the cathode material in lithium ion batteries[1,2]. Cobalt doping has a large beneficial effect in suppressing the crystallographic phase transitions in LiNiO_2 and thereby reduces the capacity-fading. It has been proved that only Ni-ions participate in the charge-discharge process in $\text{Li}(\text{Ni}_{1-x}\text{Co}_x)\text{O}_2$ for the voltage window of 2.5-4.3 V. Optimization of the parameters like particle size and morphology can yield higher initial capacities and lower capacity-loss during the first charge-discharge[2]. However, capacity-fading ranging from 25-35 % occurs after 50-100 cycles in cells with the above mixed oxide cathodes, with Li or graphite anode and liquid electrolyte. Presently we employed yttrium as an additional dopant and studied the cathodic behavior of phases, $\text{Li}(\text{Ni}_{1-x}\text{Co}_x\text{Y}_y)\text{O}_2$, $x = 0.3$ and $y = 0.02-0.05$.

Experimental

The compounds were synthesized by the high temperature solid state reaction using high-purity raw materials in an oxygen atmosphere and characterized by XRD, SEM, surface area and particle size analysis. Electrochemical tests were done on coin cells with the mixed oxide as cathode, Li metal foil as anode and LiPF_6 in EC+DEC as electrolyte and Bitrode (USA) battery-tester. Cathode was fabricated with 15 mg of oxide, super P carbon as additive and PVDF as binder and NMP solvent. The cells were cycled between 3.0-4.2 V at a current of 0.5 mA and up to 100 cycles.

Results and Discussion

Compounds with $x=0.3$ and $y=0.02, 0.05$ have been prepared and studied. We found that synthesis conditions need to be optimized to give best cathodic behavior. Using thoroughly mixed LiNO_3 , NiO , Co_3O_4 and Y_2O_3 , the heating conditions are: 300°C; 5 hrs; 750°C; 13-20 hrs; slow cool (60 °C/h; flowing O_2 gas(0.2-0.6 l/min). Black free-flowing powders with surface area (BET) ranging from 0.5-1.4 m^2/g and particle size of 10-15 μ are obtained. XRD has shown that single phase compounds are formed with the $\alpha\text{-NaFeO}_2$ structure with negligible cation-mixing. The lattice parameters are in agreement with those reported in Ref.[1,2]. The first-charge capacity for $\text{Li}(\text{Ni}_{0.7}\text{Co}_{0.3})\text{O}_2$ is 196 mAh/g (at 0.5 mA). The expected theoretical value, assuming that Ni-ions only will participate in the charging process(3.0-4.3V window) is 192 mAh/g. The second-charge capacity falls to 171 mAh/g indicating 87 % charge-efficiency. The first-discharge capacity also falls to 167 mAh/g and after a slight increase up to 5 cycles, slowly decreases to 111 mAh/g after 100 cycles. This works out to 58 % of the theoretical value. The discharge capacity, expressed as a % of theoretical value, is plotted against the cycle number in Fig.1.

For the Y-doped compound ($y=0.02$), the measured first-charge capacity is 180mAh/g and falls to 154mAh/g for the second-charge. The first-discharge capacity is 151 mAh/g, and after a slight increase to 155 mAh/g up to 5 cycles, gradually decreases to 124 mAh/g after 100 cycles (Fig.1). Thus a capacity-loss of only 16 % occurs for Y-doped phase compared to 29 % loss for undoped phase at

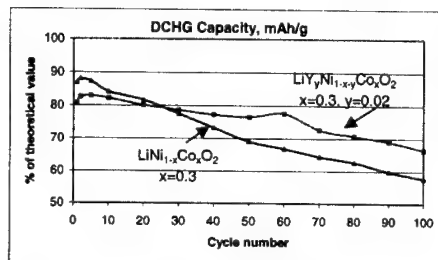
the end of 100 charge-discharge cycles.

Acknowledgement: Thanks are due to Ms. Doreen Lai for technical assistance.

References

- [1] I.Saadoun and C.Delmas, *J.Solid State Chem.*, **136**,8(1998).
- [2] J.Cho et al, *J.Electrochem. Soc.*, **146**, 3571(1999); **147**, 15 (2000).

Fig.1. Discharge capacity vs cycle number.



Electrochemical Properties of Li-Mn-spinel Using Hydrothermal Method.

T. Kanasaku, K. Amezawa and N. Yamamoto

Graduate School of Human and Environmental Studies,
Kyoto University
Yoshida-nihonmatsu-cho, Sakyo-ku, Kyoto 606-8501,
Japan**Introduction**

As well known, the lithium-manganese-spinel is one of the most attractive cathode material of Li-ion secondary batteries. The conventional synthetic method of the lithium-manganese-spinel is the calcination method [1]. However, high temperature firing is required in this synthetic process, because of making long-range diffusion of the reactants possible. Furthermore, such long-range diffusion of the reactants may cause non-homogeneity, abnormal grain growth and poor control of composition. It is known that the electrochemical properties of the lithium-manganese-spinel significantly depend on its homogeneity, grain size and composition [2].

From this background, our group adapted the hydrothermal method to synthesize the lithium-manganese-spinel. The hydrothermal method enables to synthesize a homogeneous material at far lower temperature than that of the conventional calcination method. We have already succeeded and reported to synthesize the lithium-manganese-spinel hydrothermally through γ -MnOOH in the LiOH aqueous solution at 150°C [3]. However the characteristics of the obtained spinel are rather complicated. The chemical composition and grain size, thus electrochemical properties, strongly depend on its synthetic conditions, e.g., the starting material, the concentration of aqueous solution, the reaction time, and the reaction temperature.

In this work, we aimed to determine the conditions for the lithium-manganese-spinel in the hydrothermal synthesis through γ -MnOOH. Afterward, the characteristics of the obtained spinel, especially the electrochemical properties, were investigated in detail.

Experimental

γ -MnOOH was chosen as a starting material of Mn compound. LiOH and/or LiCl were used as the Li ion supplier. When LiCl was chosen, MeOH (Me=Na, K, Li) aqueous solution was added for controlling OH⁻. The concentration of MeOH solution was between 0.050 and 1.000mol/l. After a certain amount of γ -MnOOH powder and Li ion supplier were dispersed in the MeOH solution, the reaction vessel was heated at the desired temperature at 130–170°C for 48–144h.

XRD and SEM were used for the characterization of the obtained precipitates. The molar ratio of Li to Mn was determined using ICP. The average valence of Mn ions was determined by the inverse oxidation-reduction titration using ferrous sulphate as a reducing agent [4]. The electrochemical properties of the lithium-manganese-spinel were investigated with coin type test cells. A positive electrode was made of a composite of the lithium-manganese-spinel, the acetylene black and PTFE. A negative electrode was an Li metal foil. An electrolyte was a solution of 1mol/l LiClO₄ in 1:1 mol% EC and DEC. The cells were charged / discharged at the

constant current density of 200 μ A/cm² and the cut-off voltages were 3.5 and 4.3V.

Results and Discussions

The single phase of the lithium-manganese-spinel was obtained using the hydrothermal reaction through γ -MnOOH both in the LiOH aqueous solution and in the LiCl + NaOH aqueous solution. The synthetic conditions for the single phase of the lithium-manganese-spinel were 0.050–0.150mol/l LiOH aqueous solution at 130–170°C and 0.100mol/l NaOH aqueous solution at 150–170°C. The spinels obtained in the LiOH aqueous solution had a rod-like shape with the particle size of 0.1 \times 0.1 \times 1 μ m, while the spinels obtained in the LiCl + NaOH aqueous solution had an octahedron shape with the particle size of 1 μ m.

The chemical composition and the theoretical capacity of the hydrothermally prepared lithium-manganese-spinel are summarized in Table 1. The lithium-manganese-spinel obtained using the hydrothermal method, in general, had a Li-rich composition. It was also found that the chemical composition of the lithium-manganese-spinel could be controlled by its synthetic conditions in the hydrothermal method.

The lithium-manganese-spinel obtained using the hydrothermal method showed similar charge/discharge properties as the lithium-manganese-spinel obtained using the conventional calcination method. These results indicated that the hydrothermal method is useful as the synthetic method of the lithium-manganese-spinel.

References

- [1] M. M. Thackeray, M. F. Mansuetto, D. W. Dees, and D. R. Vissers, *Mat. Res. Bull.*, 31 (1996) 133.
- [2] P. Barboux, J. M. Tarascon, and F. K. Shokoohi, *J. Solid State Chem.*, 94 (1991) 185.
- [3] T. Kanasaku, K. Amezawa and N. Yamamoto, *J. Japan Soc. of Powder and Powder Metallurgy* 45 (1998) 758.
- [4] A. Kozawa, *Memoirs of Faculty of Engineering, Nagoya University* 11 (1959) 243.

Table 1 Properties of the lithium-manganese-spinels

Concentration / mol/l	Li / Mn	Temperature / °C	Theoretical Li _{1+x} Mn _{2-2x} O _{4-y} capacity / mAhg
LiOH solution			
0.050	3.4	170	Li _{0.96} Mn _{2.04} O _{4.05} 149.00
0.100	6.7	150	Li _{1.08} Mn _{1.92} O _{3.97} 124.60
0.125	8.4	130	Li _{1.23} Mn _{1.77} O _{3.87} 91.16
LiCl + NaOH solution			
0.100	1.0	150	Li _{1.06} Mn _{1.94} O _{3.96} 136.16

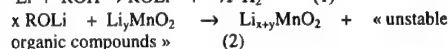
**SYNTHESIS PROCESS OF LITHIATED OR OVERLITHIATED
MANGANESE OXIDE ACTIVE MATERIALS
FOR POSITIVE ELECTRODE**

H. ROUAULT, F. LE CRAS, C. BOURBON, D. BLOCH
Commissariat à l'Energie Atomique (CEA), Grenoble
Research Center, CEA/DTA/DEM/SPCM,
17 rue des Martyrs, 38054 GRENOBLE cedex

Since 1996, the Commissariat à l'Energie Atomique (CEA) has pursued intensive research on active materials for positive electrode of lithium batteries, especially on lithiated manganese oxides. Indeed, these species suggest to be potentially outstanding active materials because of their insertion properties, due to their numerous possible structures (spinel or tunnelled or lamellar structures) and because of their high theoretic capacity (1 Li/Mn) and high electrochemical potential. Moreover, these materials are cheap and less toxic than the other metal oxide active materials for positive electrode.

Nevertheless, up to now, only lamellar or spinel lithium manganese oxide can be employed in carbon lithium-ion systems. For instance, these configuration is conceivable with spinel structures at 4V but the irreversible loss of 20% lithium in carbon negative electrode at the first charge does not permit to reach competitive performances (typically 115 mAh/g, 4V, [1]) against other oxides such as cobalt oxides (135 mAh/Co, 3.9V). For 3V manganese oxides, which can develop higher specific capacity like $\text{Li}_{0.33}\text{MnO}_2$ (150 mAh/g, 2.85V, 500 cycles, [2]), their integration in carbon lithium-ion battery are only envisageable in their fully inserted state. It is the why the CEA has engaged a research program to develop a synthesis process of overlithiated manganese oxides. The objective was proposing an innovative process, which would be rapid, efficient and cheap, compared to the n-butyl lithium based process, whose operating conditions are not easily scaled up to industrial applications, [3, 4].

The CEA process principle is based on the Li^+ ion transfer from metallic lithium to manganese oxide through an organic lithiated compound formed in situ. Operation is simple : it consists in mixing metallic lithium with manganese oxide to be treated in stoichiometric proportions in a common liquid alcohol. Lithium reacts with alcohol and forms lithium alkoxide and gaseous dihydrogen, according to chemical reaction (1). Lithium alkoxide therefore loses its lithium ion, that inserts into manganese oxide, (see chemical reaction (2)).



Synthesis process is performed under dried argon atmosphere between 80°C and 150°C depending on the alcohol medium. Powdered solid phase is then recovered, washed, dried and embedded in electrode matrix under dry conditions.

Tests were conducted in order to define different process parameters : operating conditions (temperature, concentrations, duration, ...), technics for separating, washing and recovering overlithiated manganese oxides, kind of alcohol $\text{C}_n\text{H}_{2n-1}\text{OH}$ (value of n, alcohol class, ...), principal process steps and additional specific treatments. These experiments were performed on two manganese oxides : spinel $\text{Li}_{1.03}\text{Mn}_{1.97}\text{O}_4$ and $\text{Li}_{0.33}\text{MnO}_2$. They showed that the lithium alkoxide/manganese oxide transfer factor was about 100% and that the reaction kinetics are therefore very fast ; in the best operating conditions, conversion factor reached 95% in less than 6 hours duration.

Moreover, overlithiated materials properties highlighted the CEA process efficiency. Their mean value of Mn valency is quite equal to 3.00. Their specific capacity reaches in average 90% of the specific capacity of initial compounds, (see figure 1). Morphology of overlithiated particles shows fractures, probably resulting from lithium insertion. Crystalline structure of manganese oxides overlithiated by CEA process closes to this one obtained electrochemically.

The lithiation treatment developed by the CEA shows that its application is simple, industrially feasible, fast and efficient with 90% of recovered initial capacity. Thus, integration of manganese oxide is today tested in lithium-ion batteries for electric vehicle application within the framework of the European Joule project SHEDELB. Moreover the CEA is now undertaking a research and development program to elaborate new outstanding lithiated manganese oxide variety owing to its process. Their use in portable applications (cellular phones, electronic devices, smart cards, ...) is today envisageable and the CEA is examining their electrochemical properties and rheological characteristics inside gelled polymer lithium ion systems.

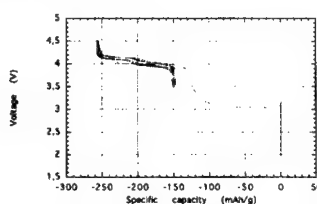


Figure 1 : cycling curve of overlithiated $\text{Li}_{1.03}\text{Mn}_{1.97}\text{O}_4$
(4V, C/10, EC/DMC/LiPF₆ 1M button cell)

References

- [1] H. Huang, C.A. Vincent, P.G. Bruce, J. Electrochem. Soc., **146**, 2, 481, (1999)
- [2] E. Levi, E. Zinigrad, H. Teller, J. Electrochem. Soc., **144**, 12, 4133, (1997)
- [3] M.B. Dines, Mat. Res. Bull., **10**, 287, (1975)
- [4] M.S. Whittingham, M.B. Dines, J. Electrochem. Soc., **124**, 9, 1387, (1977)

Abstract No. 190

General behaviour upon cycling of LiNiVO_4 as battery electrode

C. Rossignol, G. Ouvrard
Institut des Matériaux Jean Rouxel, 2 rue de la
Houssinière, BP 32229, 44322 Nantes Cedex 3, France

LiNiVO_4 is among the transition metal oxides which are performing candidates as negative in lithium-ion batteries. The mechanism of the lithium reaction is not understood yet, in both the structural and electronic aspects. We have used X-ray Absorption Spectroscopy (XAS) at the vanadium and nickel K edges to obtain information on the local atomic environment (EXAFS) and redox processes (XANES) during the first discharge and the first recharge of the battery. XAS experiments have been performed at LURE in using elements built according to the plastic battery technique.

LiNiVO_4 has been synthesized by a "chimie douce" method. The amorphous powder was annealed at 500°C and 600°C . Figure 1 compares the voltage vs. lithium content for the two samples. Both can reversibly react with 6 lithium per formula unit corresponding to a gravimetric capacity of about 850 Ah/kg but with a significant shift. XAS data have been collected on the first discharge and recharge curves referenced from 1 to 7 for $\text{LiNiVO}_4-600^\circ\text{C}$ and from A to G for $\text{LiNiVO}_4-500^\circ\text{C}$ as noted in figure 1.

Figure 2 represents various XANES spectra at the vanadium edge. In figures 3 and 4 are gathered some radial distribution functions (RDF's) extracted from EXAFS data collected at the nickel and vanadium edges respectively.

The starting compound LiNiVO_4 has a spinel structure in which vanadium atoms occupy tetrahedra and lithium and nickel are found in octahedra. The first fraction of added lithium atoms, corresponding to an important voltage drop, induces dramatic modifications in the XANES and EXAFS data. They indicate clearly that vanadium atoms move from tetrahedra to slightly distorted octahedra, with a large decrease of the prepeak in vanadium edge and an increase of the V-O distance from 1.74 Å to 1.98 Å and 2.08 Å. Another important feature is the occurrence of a shorter nickel-vanadium distance at about 3.00 Å. This transformation is complete for the sample 2. At the sample 2, a new distance of about 2.43 Å appears on the nickel K edge. Such a distance, attributed to metal neighbours, is not seen on the vanadium edge and corresponds to a pairing or clusterization of nickel atoms. Between samples 3 and 5, there are little change around the vanadium and the nickel. During the recharge, the vanadium comes back to a tetrahedral environment. At the same time, the XANES spectra at nickel K edge move slightly to the higher energy indicating a weak oxidation of the nickel, but it does not recover its initial site. A short distance Ni-Ni is always observed.

The shift in discharge curve of the 500°C compound is attributed to a slower initial transformation of the phase. As an example, the vanadium displacement from tetrahedra to octahedra occurs for the sample B instead of sample 2 in the 600°C compound. Furthermore, the short distance (2.43 Å) appears weakly at the sample C. Up to the end of the discharge and during the recharge, we observe the same behaviour as in the 600°C material study.

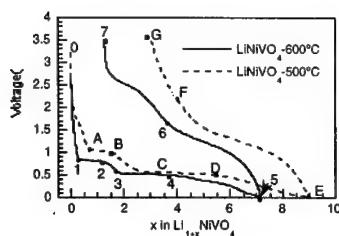


Figure 1 : First cycle of $\text{LiNiVO}_4-600^\circ\text{C}$ and $\text{LiNiVO}_4-500^\circ\text{C}$ /Li batteries

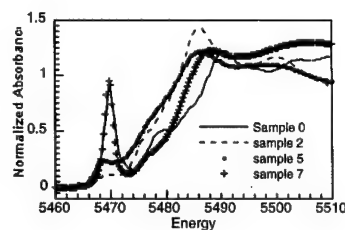


Figure 2 : Vanadium K edge for various lithium content

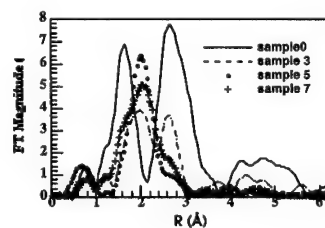


Figure 3 : Moduli of the Nickel K edge EXAFS Fourier transforms

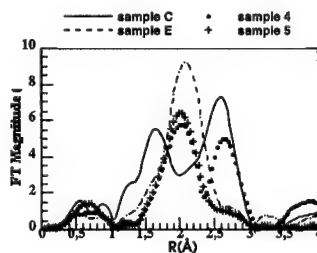


Figure 4 : Moduli of the Nickel K edge EXAFS Fourier transforms of LiNiVO_4-500 and LiNiVO_4-600

Abstract No. 191

Microimpedance Spectroscopy of Cathode Materials Prepared from Polyelectrolyte-Pretreated Particles

Andrijana Sever Škapin¹, Marian Bele¹, Jernej Drofenik¹, Robert Dominko, Stane Pejovnik^{1,2}, and Miran Gaberšek¹

¹National Institute of Chemistry, Hajdrihova 19, SI-1000 Ljubljana, Slovenia

²Faculty of Chemistry and Chemical Technology, University of Ljubljana, Slovenia

Electronic conductivity of cathode material (based on cobaltates, nictates etc.) is usually attained through addition of a known amount of carbon black¹ to selected cathodic particles. In the optimal case, the carbon black particles should surround each cathodic particle in a form of as thin as possible, but still continuous film. In such a case, electrons can reach the entire surface of each electroactive particle with a minimum amount of carbon black added.

In the present paper we pursue two goals:

1. To find an experimental procedure which leads to formation of a thin and homogeneous carbon black film on the surface cathodic particles
2. To check if the microimpedance technique can be used for detection of continuity of the carbon black film deposited on the surface of cathodic particles.

The cathodic particles (LiMn_2O_4 and LiCoO_2 both obtained from Merck) were immersed into a polyelectrolyte solution of known composition which allowed for a maximum adsorption of polyelectrolyte molecules on the surface of cathodic particles. Known amounts of the polyelectrolyte-pretreated particles were exposed to a series of dispersions of carbon black particles with different but known amounts of carbon black. By appropriate control of experimental conditions (variation of pH, temperature, mixing rate, salt content) we were able to deposit all carbon black particles on the surface or between cathodic particles, regardless of the concentration of the former. In this way, we could always determine the content of carbon black in the final cathode material. After deposition of carbon black had been finished, we separated the solid particles from the rest of dispersion and pressed them into cylinders (8 mm in diameter and 2 mm thick).

Cross sections for microimpedance measurements were prepared by polishing, but without the presence of water. Microimpedance spectra were recorded using a custom-designed microimpedance device: Karl Suss PM5 probe station with built-in thermochuck Lincam TMS 93. The Ag-coated tungsten tip (5 μm in diameter) of microelectrode was positioned on various surface regions of interest, such as the bulk grain of cathodic particle, the intergrain region etc., and the corresponding microimpedance spectra were recorded. It was found that in the case of continuous carbon black films, the intergrain conductivity was up to 10^7 times larger than the bulk grain conductivity. If the carbon black amount was below a critical level, i.e. the carbon black film became discontinuous, the intergrain conductivity decreased to a value comparable to the bulk grain conductivity of cathodic particle (about 10^{-9} Scm^{-1}). Applying the described technique to samples

with different content of carbon black, we have been able to determine the critical concentration at which the transition from the continuous carbon black film into discontinuous coating occurs. It is important to stress that in the case of polyelectrolyte-pretreated, this transition occurs at much lower carbon black content in cathode material ($<1 \text{ wt. } \%$) than in the case of classically prepared cathode materials (5-10 wt%).

Acknowledgements

This research is sponsored by NATO's Scientific Affairs Division in the framework of the Science for Peace Programme. The financial support from the Ministry of Science and Technology of Slovenia is also fully acknowledged.

References

1. J.M. Tarascon, D. Guyomard, *Electrochimica Acta*, 38, 1221-1231 (1993).

Li₂Mn₄O₉ revisited : crystallographic and electrochemical studies

P. Strobel, A. Ibarra Palos and M. Anne
Laboratoire de Cristallographie, C.N.R.S.
BP 166, 38042 Grenoble Cedex 9, France

The compound Li₂Mn₄O₉, initially reported by de Kock et al. (*Mat. Res. Bull.* **25** (1990) 657) is an interesting material for both fundamental crystallochemical studies and lithium intercalation, because (i) it contains tetravalent manganese only, (ii) its structure contains cation vacancies on both tetrahedral and octahedral sites, according to de Kock's study, which yielded the structural formula (Li_{8/9}vac_{1/9})[Mn_{16/9}vac_{2/9}]O₄, where () and [] indicate the contents of tetrahedral and octahedral sites, respectively. Such a high cation-deficiency could lead to high lithium intercalation capacity.

The synthesis of Li₂Mn₄O₉, however, is difficult, and subsequent attempts by several groups to reproduce de Kock's result yielded products with a manganese oxidation state never exceeding ca. +3.8. In this communication, we reconsider the Li₂Mn₄O₉ case, using three different preparation routes: (1) de Kock's low-temperature solid state reaction procedure, (2) chemical and (3) electro-chemical lithium deintercalation. In the latter two cases, the starting material was the non-lacunar Li-Mn-O spinel with appropriate Li/Mn ratio to yield the desired overall stoichiometry on lithium removal, i.e. Li[Li_{2/9}Mn_{16/9}]O₄.

Samples obtained by routes (1) and (2) were analyzed using chemical redox analysis and high-resolution powder neutron diffraction collected on the D2B powder diffractometer at Institut Laue-Langevin, Grenoble. Their electrochemical behaviour was investigated using coin-type or Swagelok cells containing Li metal/1M LiPF₆-EC:DMC/oxide-carbon black-PTFE positive.

Main results are following:

a) chemistry: samples 1, 2 and 3 are quite different from one another, with cubic cell parameters ranging from 0.809 nm for chemically-delithiated sample 2 to 0.817 nm for solid state reaction sample 1. The latter is not single-phase (it still contains unreacted lithium carbonate), and its average manganese oxidation state is only 3.69, compared to > 3.97 in lithium-deintercalated samples 2 and 3.

b) crystallography: For sample 1, Rietveld refinement of powder neutron diffraction data confirms the double-vacancy model (on both tetrahedral and octahedral sites). The vacancy concentration, however,

differs significantly from the ideal 1/9-2/9 scheme: our sample actually contains less vacancies on octahedral sites than on tetrahedral ones. Sample 2 contains no vacancies on octahedral sites, as expected from the preparation route.

b) electrochemistry: samples 1 and 2 were investigated both galvanostatically and by step-potential electrochemical spectroscopy (SPES). Both samples cycle on the "3V plateau" with clear characteristics of a 2-phase system. On first discharge, sample 1 exhibits an additional shoulder attributable to the filling of octahedral vacancies; this feature is not reversible.

In contrast, SPES and differential capacity curves show for sample 2 the occurrence of a prominent second current peak occurring at a potential ca. 150 mV above the main redox peak. This feature is reversible and does not become smeared out on cycling. It is not observed on non-lacunar manganese spinels LiMn₂O₄ or Li[Li_xMn_{2-x}]O₄. Using X-ray diffraction analysis of discharged batteries, the possible causes of this additional, reversible peak in cation-deficient sample 2 will be discussed.

Structural and Electrochemical studies of Layered $\text{Li}(\text{Mn}_{1-y}\text{M}_y)\text{O}_2$ based compounds. I. $\text{M} = \text{Co}$.

A.D. Robertson, A.R. Armstrong, A.J. Fowkes and P.G. Bruce

School of Chemistry, University of St. Andrews, St. Andrews, Fife, KY16 9ST, U.K.

Lithium-ion batteries are one of the major technological successes of the 1990's. Layered LiCoO_2 is commonly used as the positive electrode material, however, cost and safety concerns have intensified research into lithium manganese oxide-based compounds. The spinel, LiMn_2O_4 , represents a possible option but alternative materials with higher capacities are sought.

In the search for new lithium manganese oxide-based cathode materials, compounds based on layered LiMnO_2 are of particular interest (1-8). Extensive doping is possible by replacing, in part, manganese by a variety of other ions, and research on these materials is expanding rapidly.

Following our initial studies on stoichiometric layered LiMnO_2 (1) we have prepared a range of transition metal substituted layered lithium manganese oxides with the O3 structure ($\alpha\text{-NaFeO}_2$ type). These materials are formed by first preparing the sodium phase then ion exchanging sodium by lithium. Initial studies on the Co-doped system (4,7,8) showed a relatively facile conversion to spinel within the first few cycles. Conversion to spinel was hindered, however, with increasing Co content.

More recently we have varied the synthesis conditions to produce Co-doped materials with subtle, yet important, compositional and structural differences. These newly developed compounds demonstrate improved capacity retention and conversion to spinel-like structures occurs less readily, Figures 1 and 2. The transformation to spinel is inhibited to a greater extent with increasing Co content.

Rate capability data is encouraging with stable capacities in excess of 190mAhg^{-1} being obtained on cycling at $25\text{mA}\text{g}^{-1}$, dropping by only about 20mAhg^{-1} on increasing the rate to $100\text{mA}\text{g}^{-1}$, which corresponds to a practical C rate of C/1.5.

The effects of synthesis on stoichiometry, structure and electrochemical properties of these Co-doped intercalation compounds will be discussed in more detail.

REFERENCES

1. A.R. Armstrong and P.G. Bruce, *Nature*, **381**, 499 (1996).
2. F. Capitaine, P. Gravereau and C. Delmas, *Solid State Ionics*, **87** 197 (1996).
3. M. Tabuchi, K. Ado, H. Kobayashi, H. Kageyama, C. Masquelier, A. Kondo and R. Kanno, *J. Electrochem. Soc.* **145**, L49 (1998).
4. A.R. Armstrong, R. Gitzendanner, A.D. Robertson and P.G. Bruce, *J.C.S. Chem. Comm.* **1998** 1833-1834 (1998).
5. Y.-I. Jang, B. Huang, Y.-M. Chiang and D.R. Sadoway, *Electrochem. Solid State Lett.* **1** 13 (1998).
6. S.K. Mishra and G. Ceder, *Phys. Rev. B*, **59** 6120 (1999).

7. A.R. Armstrong, A.D. Robertson, R. Gitzendanner and P.G. Bruce, *J. Solid State Chem.*, **145** 549 (1999).
8. A.R. Armstrong, A.D. Robertson and P.G. Bruce, *Electrochimica Acta*, **45** 285 (1999).

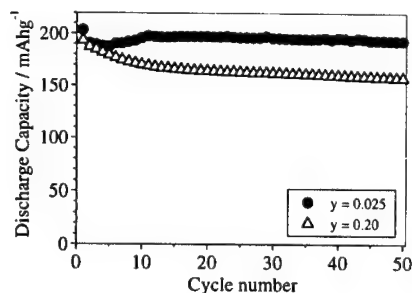
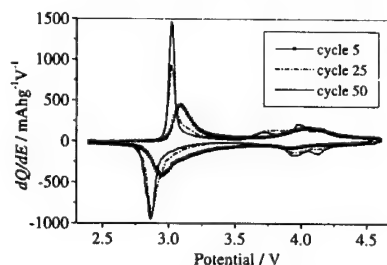


Figure 1. Cycling data for $\text{Li}_x\text{Mn}_{1-y}\text{Co}_y\text{O}_2$, prepared by low temperature ion exchange. Rate = $25\text{mA}\text{g}^{-1}$. $V_{\text{limits}} = 2.4\text{--}4.6\text{V}$.

Figure 2. Load curves for $\text{Li}_x\text{Mn}_{1-y}\text{Co}_y\text{O}_2$ ($y = 0.025$),



prepared by low temperature ion exchange. Rate = $25\text{mA}\text{g}^{-1}$.

Cyclic Voltammetric Study on
Stoichiometric Spinel LiMn_2O_4 Electrode at
Elevated Temperature

S. Ma, H. Noguchi, and M. Yoshio
Saga University
Saga, Japan

Spinel structure Li-Mn-O compounds are the most promising lithium ion insertion electrode materials for rechargeable lithium batteries. In order to overcome the capacity fading at elevated temperature, the comprehensive investigations on the high temperature electrochemical performance of the spinel cathode are very necessary. In this paper, we report on a new phenomenon found in the cyclic voltammometric study of stoichiometric spinel electrode at high temperature of more than 70°C .

As shown in Fig. 1, the second reduction peak at latter half intercalation stage, $x > 5.0$, has split, whereas for nonstoichiometric spinel the phenomenon is not observed. Fig. 2 displays the effect of scan rate on the split. At lower scan rate, 0.01 mV/s , a well-defined split, with a higher low-voltage peak, was found. With the increase of scan rate, the peak at low voltage increased, but became lower than the peak at high voltage, and finally the split disappeared at more than 0.1 mV/s of scan rate. Above result suggested that the insertion of Li^+ at $x > 0.5$ at high temperature, as normal insertion/extraction of Li^+ in spinel network, is also a process controlled by solid state diffusion of Li^+ ions. The process, analogous to staging insertion of Li^+ in graphitic carbon, can be tentatively considered relating to the domain separation of intercalatable vacancy energetically caused by more intense Li-Li interaction at high temperature.

References:

- 1.D. Guyomard, J.M. Tarascon, *J. Electrochem. Soc.*, 139, 937 (1991).
- 2.A. Momchilov, V. Manev and A. Nassalevska,

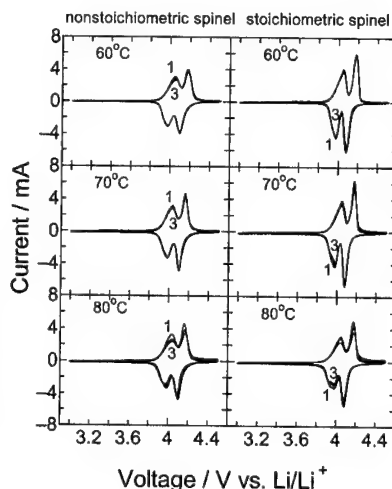


Fig.1. First three cyclic voltammograms of nonstoichiometric and stoichiometric spinel electrodes in the electrolyte of 1M LiPF_6 EC DMC 1:2 at different temperatures.

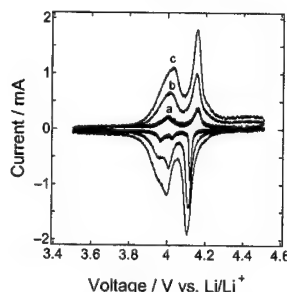


Fig.2. Cyclic voltammograms of stoichiometric spinel electrode in the electrolyte of 1M LiPF_6 EC DMC 1:2 at 80°C with different scan rates: (a) 0.01 mV/s , (b) 0.05 mV/s , (c) 0.1 mV/s .

Electrical conductivity and structural behaviour of
 $\text{Li}_{1+x}\text{MM}'(\text{PO}_4)_3$ ($\text{M}, \text{M}' = \text{Fe}, \text{Zr}, \text{Ti}$) phases

C.M. Mari, R. Ruffo, M. Catti

University of Milano-Bicocca, Department of Materials
 Science

Via R. Cozzi 53, 20125 Milano, Italy

The development of all-solid-state rocking chair batteries is of great interest. This goal is possible if the polymeric electrolytes are replaced with solid ion conductors. For this reason many lithium compounds have been and are investigated; among these NASICON type structure materials that generally show relatively high ionic conduction¹. However electrolytes having electrical conductivity, around 10^{-6} - $10^{-5} \Omega^{-1}\text{cm}^{-1}$, at room temperature, might be suitable for this application if their thickness is about 100-200 nm. To day low cost deposition techniques (dip and spin coating) are available and electrolyte layers could be obtained without great difficulties.

In the present paper $\text{Li}_2\text{FeZr}(\text{PO}_4)_3$ and $\text{Li}_2\text{FeTi}(\text{PO}_4)_3$ as well as the α and β $\text{LiZr}_2(\text{PO}_4)_3$ have been prepared and characterized by electrical conductivity measurements and by X-ray powder diffraction. The result are compared and analyzed in terms of the NASICON structural features.

All four phases were prepared by ceramic route starting from mixtures of Li_2CO_3 , $\text{NH}_4\text{H}_2\text{PO}_4$ and metal oxides, in proper ratios. The thermal treatments of pelletized samples were optimized according to each phase, with temperatures ranging from 900 to 1200 °C.

X-ray powder diffractometry (CuK α radiation) with high-temperature attachment gave the following values of the unit-cell constants: $\text{Li}_2\text{FeZr}(\text{PO}_4)_3$, orthorhombic: $a=8.708(3)$, $b=8.789(3)$, $c=12.230(4)$ Å at $T=25$ °C; $\text{Li}_2\text{FeTi}(\text{PO}_4)_3$, orthorhombic: $a=8.556(4)$, $b=8.628(4)$, $c=23.920(7)$ Å at $T=25$ °C. For the α' (triclinic, $T=25$ °C), α (rhombohedral, $T=110$ °C), β' (monoclinic, $T=25$ °C) and β (orthorhombic, $T=300$ °C) phases of $\text{LiZr}_2(\text{PO}_4)_3$; the values obtained confirmed previous results already published².

To obtain the specimens for electrical measurements, the powder of the phosphates were pressed and sintered at 900 °C for 8 hours, in air. The pellets (diameter = 13 mm) were then painted on both sites with platinum paste (Engelhard, Hanovia 6082) and successively heated for 2 hours, at 850 °C.

The electrical measurements were performed by complex impedance apparatus, using frequencies in the range $1\text{-}2 \cdot 10^4$ Hz.

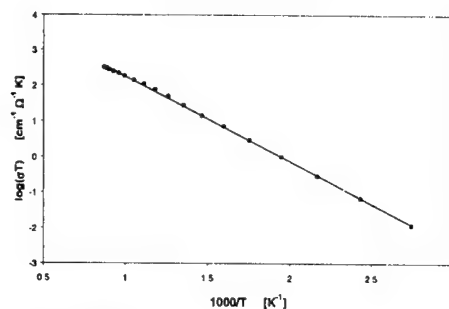
The conductance of the specimen was carried out in the temperature range 100-900 °C, in synthetic air. The impedance diagrams obtained at different temperatures show a semicircle terminated by a portion of straightline. Using a best fitting program the conductivity of the materials were obtained; the Arrhenius plots are reported in figures 1, 2, and 3. The activation energies were calculated to be 0.48 eV, 0.62 eV and 0.65 eV for the α - $\text{LiZr}_2(\text{PO}_4)_3$, $\text{LiFeZr}(\text{PO}_4)_3$ and $\text{LiFeTi}(\text{PO}_4)_3$ phases, respectively. The activation energy of the α - $\text{LiZr}_2(\text{PO}_4)_3$ is in good agreement with that earlier reported³.

On the base of the activated energies, the two ion containing compounds appear to be more promising

electrolytes for high temperature batteries than $\text{LiZr}_2(\text{PO}_4)_3$ phases.

References

1. A.D. Robertson, A.R. West, A.G. Ritchie, Solid State Ionics, 104 (1997) 1.
2. M. Catti, S. Stramare, R. Ibberson, Solid State Ionics, 123 (1999) 173.
3. F. Sudreau, D. Petit, J.P. Boilot, J. Solid State Chem.,



83 (1989) 78.

Figure 1. Conductivity versus temperature of the α - $\text{LiZr}_2(\text{PO}_4)_3$ phase.

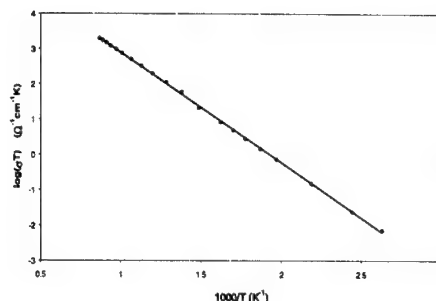


Figure 2. Conductivity versus temperature for the $\text{LiFeZr}(\text{PO}_4)_3$ phase.

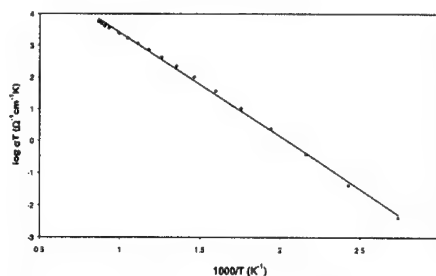


Figure 3. Conductivity versus temperature for the $\text{LiFeTi}(\text{PO}_4)_3$ phase.

γ -MnO₂ compounds as insertion hosts
for Li⁺ and H⁺.

S. Sarciaux, S. Jouanneau, A. Le Gal La Salle, Y. Piffard and
D. Guyomard.

Institut des Matériaux Jean Rouxel,
CNRS - University of Nantes
BP 32229 - 44322 Nantes Cedex 3 - France

γ -MnO₂ compounds (EMD: Electrolytic Manganese Dioxides, CMD: Chemical Manganese Dioxides and HTMD: Heat Treated Manganese Dioxides) are positive electrode materials of both rechargeable alkaline and lithium batteries. Their structure consists of a random intergrowth of blocks of the pyrolusite structure (De Wolff defects with a P, rate) within the ramsdellite structure, and contains microtwinning defects (with a Mt rate). Consequently, their structural characterization by diffraction techniques is complex and requires simulation of the powder patterns [1].

With the use of unusual preparation conditions [2,3], a large variety of γ -MnO₂ compounds was prepared to perform the present study. The compounds were characterized in terms of physico-chemical characteristics (average oxidation state of Mn: AOS(Mn), and content of crystallization water: n_c) and structural parameters (P, and Mt, determined by using an extension of the Pannetier's method [1]). Some of these compounds have been selected for a comparative study of H⁺ insertion in aqueous alkaline medium and Li⁺ insertion in a non-aqueous organic electrolyte, in order to study which structural parameter controls each cation insertion behavior.

Composite electrodes were prepared by mixing the active material (85% by mass) with carbon black (Super P, from Chemetals) (10%) and an organic binder (PVDF) (5%). Such electrodes were studied in two-electrodes cells, such as Li/EC + DMC + LiPF₆/electrode, and in three-electrodes cells, such as Pt/H₂O + 1M KOH (Ref=Hg/HgO)/electrode. Both potentiostatic and galvanostatic modes of a mac-pile battery tester were used.

The first electrochemical insertion of Li into γ -MnO₂ compounds induces an irreversible transformation leading to γ -Li_{0.5}MnO₂ compounds similar to those prepared by solid state reaction in the range 250-400°C, starting from a Li salt and γ -MnO₂. This transformation corresponds to important structural modifications, especially when the P, rate of De Wolff defects is high. Correlations have been established between the material characteristics and the performances in lithium batteries (reversible capacity and cycling behavior). The reversible Li intercalation capacity of γ -Li_{0.5}MnO₂ compounds is maximum for largest AOS(Mn) values (2.0) and for low Mt rates, with either low P, rates (ramsdellite-like compounds) or large P, rates (pyrolusites with structural defects) of the starting γ -MnO₂ compounds (figure 1).

Concerning the electrochemical H⁺ insertion behavior, 3 different types of voltamperograms were obtained at first discharge and 2 different types of behavior at first charge, as a function of the value of the structural parameters P, and Mt. These behaviors are discussed in comparison to the simplified H⁺ insertion mechanism published in the literature. The reversible insertion capacity depends strongly on the initial structure. Intermediate values of P, and Mt, in a range close to P_r=50-80% and Mt= 30-70%, give the largest reversible capacities.

As a summary, to get a maximum Li insertion reversible capacity, the optimal structure needs to contain a low amount of disorder. On the contrary, structures with maximum disorder lead to the largest proton insertion reversible capacities. It could be explained by the very small size of the proton compared to Li⁺ ion, leading to different diffusion paths for the two cations in the γ -MnO₂ structure.

References

- [1] - Y. Chabre and J. Pannetier, *Prog. Solid State Chem.*, 23 (1995) 1.
- [2] - A. Le Gal La Salle, S. Sarciaux, A. Verbaere, Y. Piffard and D. Guyomard, *J. Electrochem. Soc.*, accepted.
- [3] - S. Sarciaux, A. Le Gal La Salle, Y. Piffard and D. Guyomard, *J. Power Sources*, 81-82 (1999) 656.

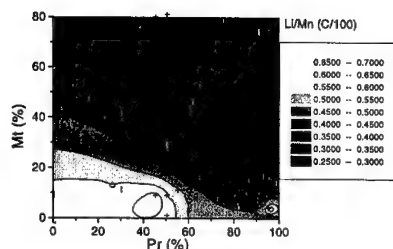


Figure 1: Influence of the structural parameters P, and Mt on the maximum reversible Li⁺ insertion capacity of γ -Li_{0.5}MnO₂ compounds.

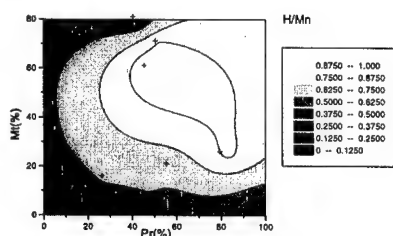


Figure 2: Influence of the structural parameters P, and Mt on the maximum reversible H⁺ insertion capacity of H- γ -MnO₂ compounds.

Abstract No. 197

**Charge Ordering in $\text{Li}_{0.5}\text{CoO}_2$?
A Single-Crystal XRD Study**

J. Höwing, T. Gustafsson, and J.O. Thomas

*Inorganic Chemistry, Ångström Laboratory
Uppsala University, Box 538, SE-751 21 Uppsala, Sweden.*

Hikari Sakaebe

*Battery Section, Department for Energy Conversion, Osaka
National Research Institute, AIST
1-8-31 Midorigaoka, Ikeda, Osaka 563-8577, Japan*

LiCoO_2 is today still the most commercially important cathode material in secondary Li-ion batteries. Despite its high cost, it is attractive because of its high capacity and excellent cyclability. The critical factor governing cyclability is structural stability during lithium insertion and extraction. The structure of LiCoO_2 can be described using a rhombohedral unit cell. An increase in unit-cell volume during lithium extraction has been observed from x-ray powder diffraction data. A distortion of the XRD pattern indicating a phase transformation to a monoclinic system[1] has been reported for the composition $\text{Li}_{0.5}\text{CoO}_2$. This transformation is probably caused by an ordering of the lithium ions, creating a superstructure with composition LiCo_2O_4 . Single-crystals have been synthesised in the Li-Co-O system with monoclinic symmetry and cell parameters corresponding to those obtained from powder XRD. A flux technique was used, with a lithium chloride melt in an aluminium oxide crucible. LiCoO_2 powder was used as starting material. Crystals suitable for single-crystal XRD could be separated from the flux. The structure and composition of this phase will be discussed.

[1] T. Ohzuku and A. Ueda,
J. Electrochem. Soc. **141**, 2972 (1994).

Abstract No. 198

**Synthesis of $\text{Li}_2\text{M}_{1-x}\text{Mn}_{3-x}\text{O}_8$ (M = Co, Fe) as Positive
Active Material for Lithium Cells**

S. Panero, D. Satolli and B. Scrosati

Department of Chemistry
University of Rome "La Sapienza"
Piazzale Aldo Moro, 5
00185 Rome, Italy

Several attempts have been carried out in order to prepare double metal ion doped manganese spinels. These samples act as reversible cathodes by extraction/insertion of lithium. Materials centered on LiMn_2O_4 show the electrochemical process at ca 4.0V, while materials centered on LiCoMnO_4 reveal charge-discharge properties at about 5V.

The double metal ion doped spinels seem to have a synergetic effect to the improvement of the cycling life of the electrodes. This effect may be the key point for the production of 5V cathode materials with excellent cycling life.

In this work high voltage, double metal ion spinels $\text{Li}_2\text{M}_{1-x}\text{Mn}_{3-x}\text{O}_8$ (M=Co and/or Fe) have been prepared by dissolving in aqueous acetic acid proper quantities of lithium hydroxide, cobalt nitrate and/or iron nitrate and Mn(II)acetate. The precursors have been annealed at 800°C for 24 hours under a flowing O_2 atmosphere. The chemical and electrochemical characterization has demonstrated that these materials behave as efficient, high voltage cathode materials.

**Lithiated cobaltates for Li-ion
batteries
Structure, morphology and
electrochemistry of oxides grown
by solid-state reaction, wet
chemistry and film deposition**

Christian JULIEN
Laboratoire des Milieux Désordonnés et
Hétérogènes, UMR 7603
Université Pierre et Marie Curie, 4 place
Jussieu, case 86
75252 Paris cedex 05, France

Lithium transition-metal oxides are functional intercalation compounds for their applications in rechargeable lithium-ion batteries. They are widely studied in search of structural stability and improved electrochemical performance. Compounds of α - NaFeO_2 -type structure are layered frameworks, which belong to the 4-volt class cathodes. LiCoO_2 with a theoretical gravimetric capacity of 273 mAh/g can deliver high electric energy and has adequately high reversibility in the range 3.5-4.5 volts. In this work, we wish to show the relationship between local cationic environment and electrochemical characteristics of 4-volt cathodes. We present the structural and electrochemical properties of various oxides of the cobaltate family grown by solid-state reaction, wet chemistry and film deposition techniques. It is shown that synthesis greatly affects the electrochemistry and cycle life characteristics of these layer structured cathode materials.

$\text{LiCo}_{1-y}\text{M}_y\text{O}_2$ materials doped with various M^{3+} cations, i.e., nickel, aluminum or boron, are also investigated. $\text{LiCo}_{1-y}\text{Ni}_y\text{O}_2$ oxides display a solid solution in the whole range $0 \leq y \leq 1$, while the solubility limit of $\text{LiCo}_{1-y}\text{Al}_y\text{O}_2$ and $\text{LiCo}_{1-y}\text{B}_y\text{O}_2$ is about $y=0.35$. Electrochemical features of $\text{LiCo}_{1-y}\text{Ni}_y\text{O}_2$ cathode materials show remarkable stability in their charge-discharge profiles. The overall capacity of

the $\text{LiCo}_{1-y}\text{B}_y\text{O}_2$ oxides has been reduced due to the sp metal substitution, however, a more stable charge-discharge cycling performances have been observed when electrodes are charged up to 4.4 volts as compared to the performances of the native oxides. Extensive damage including local strain variation, nano-domain formation, and change in cation ordering has been observed by local probes such as Raman scattering and FTIR spectroscopies, which are complementary tools for x-ray diffraction. Also, it is convenient to analyze these vibrational spectra in terms of localized vibrations, considering the layered structures built of CoO_6 and LiO_6 octahedra.

Evidence for structural defects in non-stoichiometric HT-LiCoO₂: Electrochemical, electronic properties and ⁷Li MAS NMR studies.

S. Levasseur, M. Ménétrier and C. Delmas

Institut de Chimie de la Matière Condensée de Bordeaux CNRS et Ecole Nationale Supérieure de Chimie et de Physique de Bordeaux, Château de Brivazac, 33608 PESSAC Cedex (France)

Considering previous studies lead on the Li_xCoO₂ system, it appears that ⁷Li NMR and galvanostatic results are strongly dependent on the synthesis conditions and particularly on the nominal Li/Co ratio (1, 2). However, the interpretation of the experiments remains rather confusing. In order to further investigate the question of non-stoichiometry in LiCoO₂, we synthesized Li_xCoO₂ materials with various nominal x₀ values and characterized them by X-ray and neutron diffraction, galvanostatic intercalation/deintercalation measurements and ⁷Li MAS NMR spectroscopy. In a second step, with reference to our previous work (3), we studied electrochemically deintercalated Li_xCoO₂ (x₀ = 1.10) materials by X-ray diffraction, electrical measurements and ⁷Li MAS NMR spectroscopy.

Starting Li_xCoO₂ materials were synthesized via direct reaction between Co₃O₄ and Li₂CO₃ at 900° C, with nominal Li/Co ratios x₀ = 0.90, 1.0, 1.05 and 1.10. While the galvanostatic charge curve of the stoichiometric material shows a voltage plateau at ca. 3.93V for 0.75 ≤ x ≤ 0.94 due to a semi-conductor to metal transition (3) and a particular feature for Li_{0.5}CoO₂ (x₀ = 1.0) due to a monoclinic distortion (4), the charge curves of materials with x₀ = 1.05 and 1.10 do not present the voltage plateau nor the monoclinic distortion (Fig. 1). XRD studies show the occurrence of a solid solution in the 0.60 ≤ x ≤ 1.10 domain. ⁷Li MAS NMR spectra of Li_xCoO₂ materials with x₀ > 1 exhibit three new signals at 190, -18 and -40 ppm in addition to the signal at 0 ppm resulting from the presence of diamagnetic Co^{III} (Fig. 2).

On the basis of our general knowledge of Li NMR in comparable materials with electron spins (3, 5), we suggest the presence of paramagnetic low spin Co^{II} and of a simultaneous cobalt and oxygen deficiency in samples with x₀ higher than 1.0. Furthermore, ⁷Li MAS NMR characterization of the materials obtained by electrochemical deintercalation and reintercalation of lithium from Li_{1.10}CoO₂ suggests that these defects prevent the long-range electronic delocalisation which is responsible for the two phase domain observed for stoichiometric Li_xCoO₂ (0.75 ≤ x ≤ 0.94) (3).

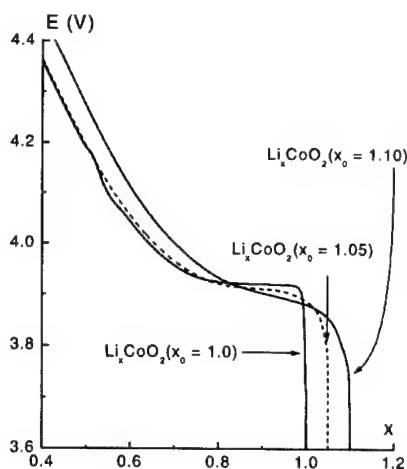


Fig. 1: First galvanostatic charge of Li/Li_xCoO₂ (x₀ = 1.0, 1.05 and 1.10) electrochemical cells. x₀ are nominal values and do not reflect exactly the actual composition.

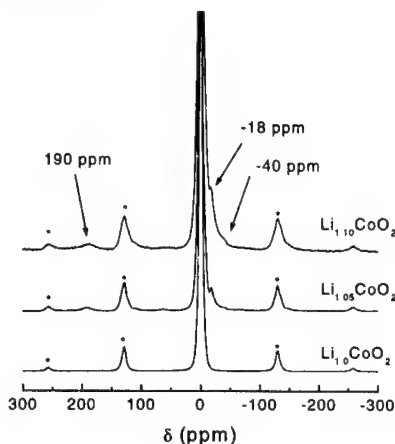


Fig. 2: ⁷Li MAS NMR spectra for the various Li_xCoO₂ phases (x₀ = 1.0, 1.05 and 1.10), (* = spinning sidebands).

- (1) M. P. J. Peeters, M. J. Van Bommel, P. M. C. Neilen-ten Wolde, H. A. M. Van Hal, W. C. Keur and A. P. M. Kentgens, *Solid State Ionics* 112 (1998) 41.
- (2) M. Carewska, S. Scaccia, S. Arumugam, Y. Wang and S. Greenbaum, *Solid State Ionics* 93 (1997) 227.
- (3) M. Ménétrier, I. Saadoun, S. Levasseur and C. Delmas, *J. Mater. Chem.* 9 (1999) 1135.
- (4) J. N. Reimers and J. R. Dahn, *J. Electrochem. Soc.* 139 (1992) 2091.
- (5) C. Marichal, J. Hirschinger, P. Granger, M. Ménétrier, A. Rougier and C. Delmas, *Inorg. Chem.* 34(1995) 1773.

Synthesis of Nanocrystalline Layered Manganese Oxides by the Electrochemical Reduction of AMnO_4 ($\text{A} = \text{K}, \text{Li}$)

G. J. Moore, R. Portal, A. Le Gal La Salle,
and D. Guyomard

Institut des Matériaux Jean Rouxel
CNRS - University of Nantes
BP 32229 - 44322 Nantes Cedex 3 - France

Manganese oxides are amongst the best positive electrode materials for lithium batteries due to their high insertion voltage, large specific capacity and good cyclability. Recent studies have shown that it is possible to prepare new compounds having interesting lithium insertion properties by the chemical reduction of permanganate solutions [1,2,3]. The Li-form of layered manganese oxides having the Rancieite-type structure were prepared previously by our group [4] by a 3-step procedure that consisted of an acid catalyzed reduction of an aqueous solution of KMnO_4 , followed by full proton exchange for the K, and finally Li was exchanged for the protons.

The aim of this project was to electrochemically reduce aqueous Mn (VII) solutions with the intent to form Li-manganese oxides directly. The procedure used here to make the pure Li form is of special interest since the electrochemical reduction is carried out only in the presence of Li rather than other cations such as K or protons. It was also of interest to study layered manganese oxide bulk deposits with varying ratios of interlayer cations, which in this project were K and Li.

The electrochemical reaction was carried out by using a 3 electrode system which consisted of an 80 cm^2 platinum working electrode mounted between 2 Pt counter electrodes, and a Ag/AgCl reference electrode. The method used to reduce the permanganate was chronopotentiometry set at 0.1 mA/cm^2 for 500 ml of a 0.075 M permanganate solution that was also mixed with 0.15 M A_2SO_4 salt. The K-permanganate solutions were made directly with KMnO_4 and the LiMnO_4 solutions were made by ion exchanging Li for the K using ion exchange resin. Figure 1 is a cyclic voltammetry curve that shows the reduction peak for the permanganate at -0.17 V . The electrodeposition reaction when run at 0.1 mA/cm^2 occurs at the reducing voltage of approximately -0.19 V at room temperature. It is noted here that the reactants are used in excess to maintain a relatively constant concentration throughout the reaction.

The results of x-ray diffraction show that the materials prepared by the electrochemical method are of the layered Rancieite-type structure; this can be seen in figure 2. Thermal analyses show that these materials can be dehydrated at 130°C . Elemental analyses via ICP-AAS are currently being carried out.

Composite electrodes were prepared by mixing the active material (85% by mass) with carbon black (Super P, from Chemetals) (10%) and an organic binder (PVDF) (5%). The Li insertion behavior was studied in two-electrode cells using EC/DMC/ LiPF_6 as an electrolyte. A Mac-Pile galvanostat/potentiostat was used for all of the electrochemical experiments. Prior to passing the cathodes into the argon filled dry-box, the samples were dried at 130°C under vacuum.

Preliminary studies of Li-insertion show capacities in the range of 100 mAh/g obtained at an average voltage of

3 V in the $4 - 2 \text{ V}$ range for some of the dehydrated samples. On-going studies are intended to understand the role of interlayer H_2O and the Li/K ratio on the Li-insertion behavior of the title compounds. Cycling of the cells are being analyzed to determine if there is a trend within the concentrations of K and Li that may permit the optimization of their Li-insertion performance within a window of relative amounts.

References

- [1] F. Leroux, D. Guyomard, and Y. Piffard, *Solid State Ionics*, **80**, 299 (1996)
- [2] F. Leroux and L. Nazar, *Solid State Ionics*, **100**, 103 (1997)
- [3] R. Chen and M. S. Whittingham, *J. Electrochem. Soc.*, **144**, L24 (1997)
- [4] F. Leroux, D. Guyomard, and Y. Piffard, *Mat. Res. Soc. Symp. Proc.*, **369**, 47 (1995)

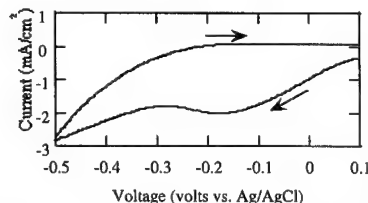


Figure 1. Cyclic voltammetry of 0.15 M Li_2SO_4 and 0.075 M KMnO_4 run at 50 mV/s at a Pt electrode at room temperature.

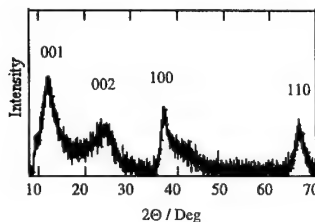


Figure 2. Powder x-ray diffraction pattern of one electrochemically synthesized $\text{Li}_x\text{K}_y\text{MnO}_z \cdot n\text{H}_2\text{O}$ compound with the peaks labeled for rancieite.

LiMBO₃ (M=Mn, Fe, Co) orthoborates : Synthesis, crystal structure and lithium deinsertion/insertion properties

V. Legagneur, A. Le Gal La Salle, Y. Piffard, A. Verbaere and D. Guyomard
 Institut des Matériaux Jean Rouxel
 2, rue de la houssinière, BP32229
 44322 Nantes Cedex3, France

As part of a search for new materials that could be used as electrode materials for lithium batteries, we have investigated the systems $\text{Li}_x\text{O-MO-B}_2\text{O}_3$ (M= Mn, Fe, Co). Such investigations were suggested by the growing interest of framework structures containing both first row transition metal cations, and polyanions. As a matter of fact, it has been shown that polyanions enable to reach low transition metal redox energies through the inductive effect, thereby allowing some sort of tuning of such energies [1-8]. However, polyanions also bring some inactive mass into the oxides that impedes both the specific capacity and the specific energy, and there is a need to minimize this drawback. Considering that up to now, most of the studies on the effect of the nature of the polyanion utilize tetrahedral groups $(\text{XO}_4)^3$ or $(\text{XO}_6)^3$ with X = Mo, W, S, P or V, this presentation intends to give a preliminary evaluation of the inductive effect of the much lighter BO_3 group through the study of the lithium deinsertion/insertion properties of three new compounds: h-LiMnBO₃, LiFeBO₃ and LiCoBO₃. It is also devoted to the synthesis and crystal structure characterization of these phases.

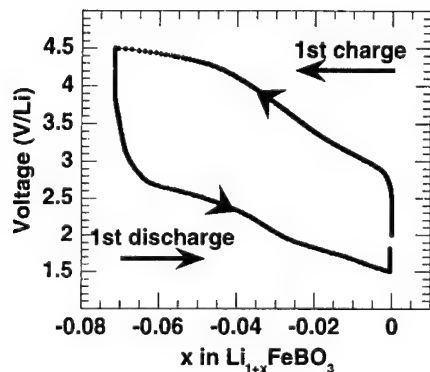
The LiMBO₃ (M= Mn, Fe, Co) compounds were synthesized by solid state reaction, and their crystal structures were determined from single crystal data. LiFeBO₃ and LiCoBO₃ [9] exhibit the same structure which is isotypic with that of other LiMBO₃ compounds (M= Mg[10], Mn[11], Zn[11]). The structure of h-LiMnBO₃ is isotypic with the hexagonal form of LiCdBO₃ [12,13].

The electrochemical behavior towards lithium deinsertion/insertion was investigated for the three compounds. The figure shows the voltage versus capacity curve obtained with LiFeBO₃. The capacities associated to the phenomena are small. However, it appears that the reduction of Fe^{3+} in $\text{Li}_{1-x}\text{FeBO}_3$ (discharge curve) is associated to a plateau at ~2.5V, whereas a similar reduction occurs at ~1.5V/Li in $\text{Li}_x\text{Fe}_2\text{O}_3$ [14]. Previous work has already shown that the $\text{Fe}^{3+}/\text{Fe}^{2+}$ redox couple lies between 2.5 V and 3.7 V in iron phosphates, reflecting the influence of P on the Fe-O bonding via the inductive effect. The relatively high voltage observed for the Fe^{3+} reduction in $\text{Li}_{1-x}\text{FeBO}_3$ is therefore a clear indication of a strong polarization of O^{2-} toward the B^{3+} cation. Similarly, for $\text{Li}_{1-x}\text{MnBO}_3$ and $\text{Li}_{1-x}\text{CoBO}_3$, the $\text{M}^{3+}/\text{M}^{2+}$ redox couple is unusually high, thus confirming an inductive effect of the $(\text{BO}_3)^3$ group.

Figure: First charge-discharge cycle obtained for LiFeBO₃ in galvanostatic mode at C/10.

References :

- [1] A. Manthiram and J.-B. Goodenough, J. Solid State Chem. 71 (1987) 349.
- [2] A. Manthiram and J.-B. Goodenough, J. Power Sources 26 (1989) 403
- [3] K. S. Nanjundaswamy, A. K. Padhi and J.-B. Goodenough, Solid State Ionics 92 (1996) 1.
- [4] A. K. Padhi, K. S. Nanjundaswamy and J.-B. Goodenough, J. Electrochem. Soc. 144(4) (1997) 1188.
- [5] A. K. Padhi, K. S. Nanjundaswamy, C. Masquelier, S. Okada and J.-B. Goodenough, J. Electrochem. Soc. 144(5) (1997) 1609.
- [6] A. K. Padhi, K. S. Nanjundaswamy, C. Masquelier and J.-B. Goodenough, J. Electrochem. Soc. 144(8) (1997) 2581.
- [7] A. K. Padhi, W. B. Archibald, K. S. Nanjundaswamy and J.-B. Goodenough, J. Solid State Chem. 128 (1997) 267.
- [8] C. Masquelier, A. K. Padhi, K. S. Nanjundaswamy and J.-B. Goodenough, J. Solid State chem. 135 (1997) 228.
- [9] Y. Piffard, K. K. Rangan, Y. An, D. Guyomard and M. Tournoux, Acta Cryst. C54 (1998) 1561.
- [10] R. Norrestam, Z. Kristallogr. 187 (1989) 103.
- [11] O. S. Bondareva, M. A. Simonov, Yu. K. Egorov-Tismenko et N. V. Belov, Sov. Phys. Crystallogr. 23 (1978) 269.
- [12] E. V. Kasanskaja, P. A. Sandomirskii, M. A. Simonov et N. V. Belov, Dokl. Akad. Nauk SSSR 238 (1978) 1340.
- [13] E. V. Sokolova, M. A. Simonov et N. V. Belov, Kristallografiya 25 (1980) 1285.
- [14] M. M. Thackeray, W. I. F. David and J. B. Goodenough, Mater. Res. Bull. 17 (1982) 785.



ELECTROCHEMICAL
INVESTIGATIONS OF PURE AND
DOPED LITHIUM COBALTATE

**A. Momchilov, A. Trifonova, B.
Banov, B. Puresheva**

Bulgarian Academy of Sciences
Central Laboratory of
Electrochemical Power Sources,
"G. Bonchev" str., bl. 10, Sofia
1113, BULGARIA

The last decade is marked with the spectacular development of the lithium-ion batteries with LiMn_2O_4 , LiCoO_2 and LiNiO_2 cathode materials. Of these only the cobalt compound has found wide commercial production by several Japanese companies. Both the Mn and Ni compounds have only a limited application mainly for the difficulties in their synthesis as well as for their irreversible capacity loss after long storage. The theoretical capacity of the cobaltate is rather high, 274 mAh/g, but practically it cannot yield more than 50-60% of this value. This is due to the fact that when charged to voltages above 4.25V the crystal structure of LiCoO_2 undergoes irreversible changes, leading to deterioration in its electrochemical characteristics: a steep reduction of the initial discharge capacity during cycling. Therefore the admissible voltage range during cycling of the LiCoO_2

cathode is limited between 3 and 4.25V.

The aim of this paper is to improve the specific capacity and cycling stability by using alternative precursors and doping transition metals, as well as by exchange of some of the lithium amount by potassium.

The LiCoO_2 cathode material and changing was synthesized by the nitrate precursors. The use of nitrate precursors leads to a considerable reduction in the synthesis temperature and improving of the electrochemical characteristics. The electrochemical behaviour of lithium cobaltate doped with potassium was investigated.

Abstract No. 204

Electrochemical and *in situ* Structural Investigation of $\text{Li}_x\text{Ni}_{0.8}\text{Co}_{0.2}\text{O}_2$

A. D'Epifanio, F. Croce, L. Persi, F. Ronci and B. Scrosati

Dipartimento di Chimica, Università "La Sapienza"

P.le Aldo Moro 5, 00185 Roma, Italy

Abstract

Layered compounds like LiNiO_2 and LiCoO_2 have been extensively studied as active cathodic materials in lithium or lithium-ion batteries.

A good compromise between the limited cyclability of LiNiO_2 and the high cost of LiCoO_2 is represented by the mixed Ni-Co-Li oxides having the general formula $\text{LiNi}_y\text{Co}_{1-y}\text{O}_2$ [1-4]. These compounds maintain the same structure of LiNiO_2 and LiCoO_2 (space group $\text{R}\bar{3}\text{m}$) and, especially when y is close to 0.8, they show an electrochemical behavior comparable to LiCoO_2 , but with substantial advantages in terms of cost.

In this work we report the electrochemical and structural properties of $\text{LiNi}_{0.8}\text{Co}_{0.2}\text{O}_2$.

The electrochemical characterization was based on galvanostatic cycling, performed at different C rates, and on cyclic voltammetry.

The structural changes during the intercalation process were investigated by means of the Energy Dispersive X-ray Diffraction (ADXRD) technique [5]. The results give clear information on the evolution of the crystal structure and of the lattice parameters of $\text{LiNi}_{0.8}\text{Co}_{0.2}\text{O}_2$ as the lithium content varies with the intercalation level.

In addition, electronic and ionic transport properties, as a function of the intercalation degree, were evaluated by using Electrochemical Impedance Spectroscopy (EIS) [6].

References

- [1] C. Delmas and I. Saadoune, *Solid State Ionics.*, **53-56**, 370 (1992).
- [2] R. J. Gummow and M. M. Tackeray, *Solid State Ionics.*, **53-56**, 681 (1992).
- [3] E. Zhecheva and R. Stoyanova, *Solid State Ionics.*, **66**, 143 (1993).
- [4] T. Ohzuku, A. Ueda, M. Nagayama, Y. Iwakoshi and H. Komori, *Electrochimica Acta*, **38-9**, 1159 (1993).
- [5] F. Ronci, B. Scrosati, V. Rossi Albertini and P. Perfetti, *Electrochemical and Solid State Letters*, Vol.3 N. 4 (2000).
- [6] F. Croce, F. Nobili, A. Deptula, W. Lada, R. Tossici, A. D'Epifanio, B. Scrosati and R. Marassi, *Electrochemistry Communications*, **1**, 605 (1999).

Abstract No. 205

Synchrotron X-Ray diffraction study of the spinel LiMn_2O_4 at low temperatures

G. Rousse¹, C. Masquelier¹, J. Rodríguez-Carvajal², E. Elkaim³, J.-P. Lauriat³

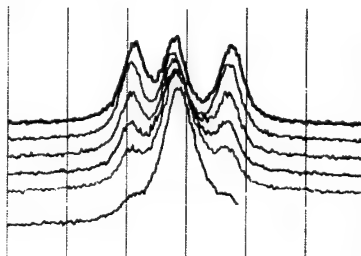
1. LPCS, UMR-CNRS 8648, Université Paris-Sud, 91405 Orsay, France

2. Laboratoire Léon Brillouin (CEA-CNRS), CEA/Saclay, 91191 Gif sur Yvette, France

3. LURE, Université Paris-Sud, 91405 Orsay, France

The phase transition observed for stoichiometric LiMn_2O_4 around room temperature, from cubic to orthorhombic symmetry^{1,2}, might be partly responsible for its poor cyclability in Li rechargeable battery systems. This transition induces a large modification of the conduction properties of the spinel : the conductivity decreases by one order of magnitude when the temperature is decreased below 290 K. It is also associated with a change in enthalpy and in entropy, as revealed by the great changes in the specific heat around room temperature.

Neutron diffraction allowed us to solve the crystal structure at 230 K (space group $Fddd$, $a = 24.743(1)$, $b = 24.840(1)$, $c = 8.199(1)$ Å). It corresponds to an orthorhombic $\sim 3a \times 3a \times a$ superstructure of the cubic spinel, induced by a charge ordering on the manganese sites^{2,3}. At $T < 300\text{K}$, the electrons become localized on three of the five manganese sites present in the structure.



Electrochemical performances of different Li-VOPO₄ systems

N. Dupré, J. Angenault, G. Wallez, M. Quarton
Laboratoire de Cristalchimie du Solide,
Université Pierre et Marie Curie, 4 place Jussieu
75252 Paris Cedex 05, France

Owing to the low density and the high reductive properties of lithium, a great amount of attention has been focused on the development of lithium batteries as power sources for use in portable devices or electric vehicles. So far, investigations have been mainly devoted to oxides as electrode intercalation compounds.

VOXO₄ compounds (X = S, P, As) present as well open 2D or 3D frameworks which facilitate lithium intercalation process. In addition, these compounds present good theoretical specific capacity (from 135 to 166 mA.h/g depending on the nature of the X element).

The present study deals with electrochemical performances and lithium intercalation mechanisms involving different lamellar phases of VOPO₄. The structural skeletons are built up from vertices-sharing distorted VO₆ octahedra to form chains connected by PO₄ tetrahedra. From one compound to the other one, the vanadyl bond V=O shows various orientations.

The different forms of VOPO₄ were prepared by simple and cheap methods [1]; we also obtained α_{II} -VOPO₄ (labelled p) from a new route involving a precursor. The X-ray diffraction patterns match those published by Bordes [2] and Calvo [3]. Chemical lithiations have been performed at room temperature using lithium iodide.

Electrochemical measurements were performed both in galvanostatic and potentiodynamic modes using SwagelokTM type cells [4] with Li metal as negative and reference electrode.

For all of these phases, the reduction-oxidation process occurs close to 3.7 V (Fig. 1), along with a structural transformation associated with an increase of the interplanar distance. This result is supported by XRD studies and is attributed to the size of inserted Li⁺ ions. Galvanostatic tests were performed at nominal regimes of C/5, C/10 and C/50. α_{II} , γ and δ -VOPO₄ show diverse capacities that can also vary according to the cycling regime: respectively 15, 25, 40 mA.h/g at C/5 (Fig. 2), 20, 30, 105 mA.h/g at C/10 and a lifetime going up to 400 cycles. Furthermore, α_{II} -VOPO₄-p presents a specific capacity of 80 mA.h/g at C/5 and 115 mA.h/g at C/10.

α_{II} -VOPO₄ and γ -VOPO₄ present a specific behavior on first reduction which has been attributed to a forming process continuing upon cycling. Then, chemical and electrochemical lithiation have been performed in order to

achieve this process before cycling experiments and to get stable performances from the beginning on.

From these results, it appears that the different forms of VOPO₄ are interesting as intercalation compounds. Further improvements are expected, concerning both the cyclability and the specific capacity, in order to lead to applications.

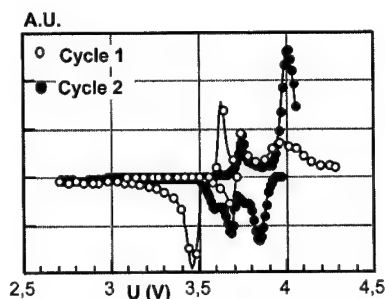


Figure 1 : Cyclic voltamogram for the two first cycles of α_{II} -VOPO₄.

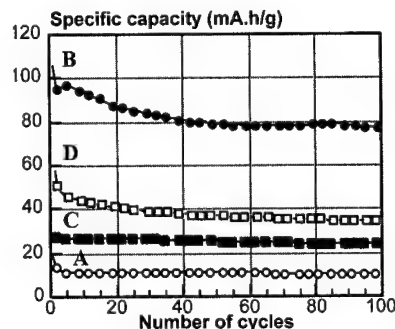


Figure 2 : Capacity vs cycle number (C/5) for : α_{II} -VOPO₄ (A), α_{II} -VOPO₄-p (B), γ -VOPO₄ (C) and δ -VOPO₄ (D).

- [1]: F. Ben Abdelouhab, M. Ziyad, C. Leclercq, J.M. Miller, R. Olier and J.C. Volta, *J. Chim. Phys.*, **92**, 1320 (1995).
- [2]: E. Bordes, *Catal. Today*, **1**, 499 (1987).
- [3]: C. Calvo and B. Jordan, *Can. J. Chem.* **51**, 2621 (1973).
- [4]: D. Guyomard, J.M. Tarascon, *J. Electrochem. Soc.*, **139**, 937 (1992).

STRUCTURAL TRANSFORMATION ASSOCIATED WITH THE EXTRA 3.3 AND 4.5V PLATEAUS IN SPINEL LiMn_2O_4

G. Rousse¹, L. Dupont², M. Hervieu³,
M. Morcrette², R. Palacin⁴, C. Masquelier¹,
and J.M. Tarascon²

(1) LPCS, UMR-CNRS 8648, Université Paris-Sud, 91405
Orsay, France.

(2) LRCS, Université de Picardie, 33 Rue St. Leu, 80039
Amiens, France

(3) CRISMAT, Caen, France.

(4) ICMAB (CSIC), Campus UAB, 08193 Bellaterra,
Catalonia, Spain

Peculiar electrochemical behavior during the extraction of lithium from LiMn_2O_4 was intensively investigated during the past few years [1], [2]. Electron diffraction showed recently that the two additional 3.3V (on discharge) and 4.5V plateaus are related to a phase transition from a cubic to a double hexagonal (DH) phase [3], [4], [5]. X-Ray diffraction on electrochemically deintercalated samples as well as on chemically delithiated spinels show additional peaks indexed in a unit cell similar to that of LiFeSnO_4 [6].

The spinel and DH structures were first described in stannoferrites systems in the early 80's [6]. They are both based on a compact closed packing of the oxygen atoms. Both structures consist of Kagomé [Oc_3] and [Td_2Oc] layers, as indicated in figure 1. The layers are ordered as "ABCABC.." sequences in the spinel and "ABAC.." sequences in the double hexagonal structure. In the spinel form, a tetrahedron is "blocking" a Kagomé window, inducing a $J_{K/T}$ (Kagomé/tetrahedron) junction, whereas in the DH structure, a junction $J_{K/T}$ is alternating with a $J_{K/O}$ (Kagomé/octahedron) junction (figure 2 and 3).

We focused on the spinel / DH transition. This helped us to predict whether or not a spinel will undergo a transition to a DH phase, that would induce the 3.3V and 4.5V plateaus. This prediction is of high interest, as it has a great influence on the cyclability and on the fading of the battery.

We studied stoichiometric spinels prepared from various $\gamma\text{-MnO}_2$ precursors. The de Wolff defects and the microtwinning faults of the manganese dioxide are of special importance for the growth of the spinel-DH transition. A special attention was paid on LiMn_2O_4 prepared from pyrolusite $\beta\text{-MnO}_2$, which up to now exhibits the most important capacity on these 3.3V and 4.5V extra-plateaus. We focused also on the effect of structural faults induced by ball milling of the pyrolusite precursor or of the LiMn_2O_4 itself. It appears that the structural defects induced by the ball milling prevent the transformation from spinel to DH phase. A lower crystalline coherence length in the spinel could explain this phenomenon.

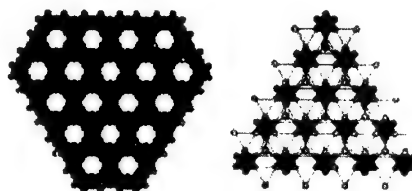


Figure 1 : A Kagomé [Oc_3] and a [Td_2Oc] layers.

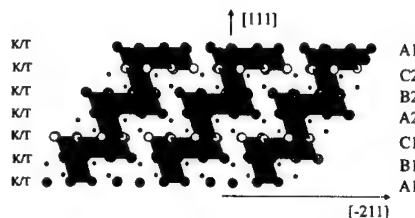


Figure 2 : The Spinel structure, built on [Oc_3] and [Td_2Oc] layers with $J_{K/T}$ junctions.

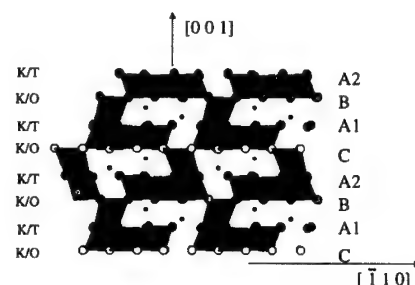


Figure 3 : The Double hexagonal structure, built on [Oc_3] and [Td_2Oc] layers with $J_{K/T}$ and $J_{K/O}$ junctions.

References

- [1] J.-M. Tarascon et al., J. Electrochem. Soc., **141**, 1421 (1994)
- [2] Y. Gao and J.R. Dahn, J. Electrochem. Soc., **143**, 100 (1996)
- [3] L. Dupont et al, submitted to J. Solid State Chem.
- [4] M. R. Palacin et al, IMLB-9, Edinburgh, Scotland, July 1998, J. Power Sources, **81-82**, 627 (1999)
- [5] M. R. Palacin et al, ECS Fall Meeting, Boston Nov.1998, J. Electrochem. Soc., in press
- [6] J. Choisnet et al., J. Solid State Chem., **40**, 344 (1981)

INFLUENCE OF THE SYNTHESIS CONDITIONS OF LiMn_2O_4 ON THE EXTENT OF THE SPINEL TO DOUBLE HEXAGONAL TRANSFORMATION ASSOCIATED TO THE ANOMALOUS 3.3/3.95 V AND 4.5 V REDOX STEPS

R. Palacin⁽¹⁾, G. Rousse⁽²⁾, M. Morcrette⁽³⁾, L. Dupont⁽³⁾, C. Masquelier⁽²⁾, Y. Chabre⁽⁴⁾ and J.M. Tarascon⁽³⁾

(1) ICMAB (CSIC), Campus UAB, 08193 Bellaterra, Catalonia, Spain

(2) LPCS, Université Paris-Sud, 91405 Orsay, France

(3) LRCS, Université de Picardie and CNRS, 33 Rue St. Leu, F-80039, Amiens, France

(4) LSP, UJF-Grenoble and CNRS, BP 87, F-38402, St. Martin d'Hères, France

Some LiMn_2O_4 spinel phases are known for long to present a peculiar reversible redox step at 4.5 V [1] as well as a reduction step at 3.3 V [2], which develop to the expense of the usual 4.0 and 4.1 levels. The origin of these additional states was very controversial at that time.

We have shown recently [3] that : a) oxidation of the 3.3 V reduction step occurs at the early stage of the deintercalation, namely before the usual plateau at 4V, in a specific oxidation occurring close to 3.95 V (Fig 1) ; b) it was two-phase behavior with appearance of a new set of diffraction lines, as shown from in situ X-rays diffraction experiments; and c) it is completely reversible upon further reduction. Moreover it was shown that these two additional redox 3.3/3.95 and 4.5 V levels are completely associated in the way that, if observed, they are both present, and they have the same charge capacity.

The additional lines observed upon oxidation at 3.95 V in the in situ XRD, were not numerous and well defined enough to be able to determine the new structure that appears at that time. By performing electron diffraction and High Resolution Electron Microscopy (HREM) studies on partially delithiated samples we observed that it corresponds to the formation of double hexagonal layers, consistent with the additional peaks observed in the "in-situ" experiments [4,5].

In previous studies undertaken for understanding the origin of the 3.3/3.95 and 4.5 V states, we looked at the influence of several parameters, mainly the stoichiometry of the compound that was varied by different synthesis conditions and further heat treatments. We were able to obtain samples in which each one of the two additional redox states contained up to 15% of the total available capacity [3,4]. And thus the spinel to double hexagonal transformation appeared limited to 30% of the material. This is attributed to the presence of structural defects that block the transformation.

Finding the conditions that would favor or block this spinel to double hexagonal transformation appears very interesting. We focused on the influence of the nature and amounts of structural defects initially present in the manganese dioxides used in the high temperature synthesis. Experiments were performed with pure pyrolusite and with several $\gamma\text{-MnO}_2$ with known amounts of de Wolff defects and microtwinning [6]. We also

looked at the influence of defects introduced mechanically by ball milling of the MD before the synthesis (fig. 2) or on the LiMn_2O_4 .

We will discuss the fact that the transformation can proceed only with concomitant removal of half of the Li of the initial LiMn_2O_4 spinel structure, as deduced from the fact that the 3.3/3.95 V and 4.5 V redox steps have identical capacities.

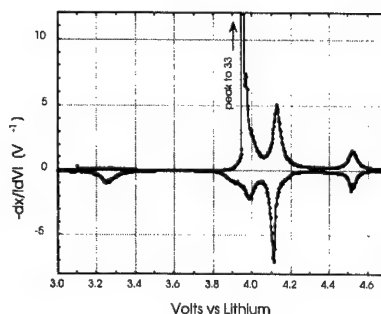


Figure 1: Incremental capacity voltammogram of a LiMn_2O_4 spinel, from very slow step potential electrochemical spectroscopy. Limited potential oxidation show that the peak at 3.95 V contains the reversible oxidation of the 3.3V reduction step [3].

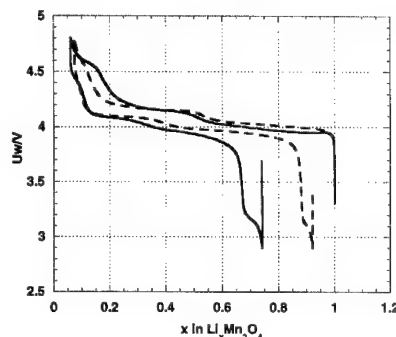


Figure 2: $V(x)$ curves for LiMn_2O_4 prepared from non-ground pyrolusite (plain curve) or from pyrolusite ground for 12h (dashed curve).

- [1] J.M. Tarascon et al., J. Electrochem. Soc., **141**, 1421 (1994)
- [2] Y. Gao and J.R. Dahn, J. Electrochem. Soc., **143**, 100 (1996)
- [3] M.R. Palacin et al, IMLB-9, Edinburgh, Scotland, 1998 J. Power Sources, **81-82**, 627 (1999)
- [4] M.R. Palacin et al, ECS Fall Meeting, Boston Nov.1998, vol.98-2 Ext. Abstr. 128 and J. Electrochem. Soc., in press
- [5] L. Dupont et al., submitted to J. Solid State Chem.
- [6] Y. Chabre and J. Pannetier, Prog. Solid St. Chem., **23**, 1-130 (1995)

Performance and Mechanical Safety of 26650-size Mn-spinel Li-ion Cells for High Power Applications

A.M. Wilson, Wendy Chow, and Ulrich von Sacken

E-One Moli Energy (Canada) Ltd.
20,000 Stewart Crescent, Maple Ridge, BC, V2X 9E7

For medium to high power applications, such as electric assist bicycles (EAB), electric vehicles and hybrid-electric vehicles, batteries must have excellent rate capability, high energy density and good mechanical safety. Mn-spinel shows good rate capability, excellent fundamental safety, and low cost. These factors make it an attractive candidate for large-size, high power Li-ion cell cathode material.

We are developing a Li-ion cell for medium to high power applications, such as EAB and power tools. Here we investigate the relationship between high specific power capability and mechanical safety (specifically nail penetration) as it is affected by electrolyte composition.

The rate capability of a cell is strongly influenced by the choice of electrolyte. Here we show how the rate capability of the cell improves by changing the principal electrolyte solvent from DEC to DMC.

Figure 1 shows a 5A discharge for Mn-spinel cathode 26650-size cells which contain DEC and DMC as principal electrolyte solvents. The effective impedance decreases significantly when DMC is substituted for DEC.

Figure 2 compares the specific power profiles (SPPs), using 2.5V as a lower voltage limit, for 26650 cells with either DEC or DMC as the principal electrolyte solvent. An SPP is acquired by performing various constant current discharges, and then plotting the data as specific power density versus time. The SPP is the highest power for a given time for constant current discharges. The details of this method have been published elsewhere.¹ Although the DMC cell performs better, even the DEC cell exceeds the long term criteria proposed by the USABC.²

Energy retention over multiple cycles is another important criteria for most applications. Figure 3 shows the discharge energy over multiple cycles for a cell with DEC as the principal electrolyte solvent. The cell is insulated (to simulate cycling in a pack) and discharged at 5A, constant current (it is recharged at 1.5A).

However, as the rate capability of the cell improves, the mechanical safety of the cell begins to deteriorate. This is especially important for larger cell sizes, as we will illustrate by comparing 26650- and 18650-size cells with similar electrolyte formulations.

References:

1. A.M. Wilson, J.N. Reimers, Journal of Power Sources 81-82 (1999) 642-646.
2. United States Advanced Battery Consortium (USABC) Electric Vehicle Battery Test Procedures Manual, Revision 2, DOE/ID-10479, Rev. 2, January 1996.

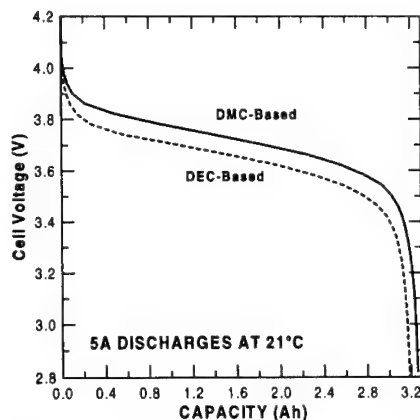


Figure 1. 5A constant current discharges (21°C ambient temperature) of 26650 cells with DEC and DMC as the principal electrolyte solvent.

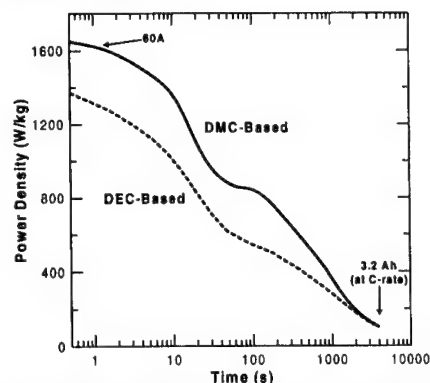


Figure 2. Specific power profiles (SPPs) for 26650 cells with DEC or DMC as the principal electrolyte solvent.

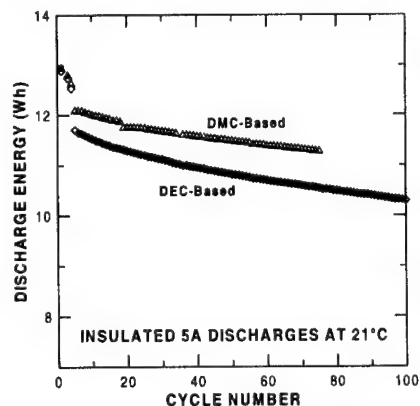


Figure 3. Energy fade plot for cells with DEC or DMC as the principal electrolyte solvent (cycled insulated at 21°C ambient, 5A discharge, 1.5A charge; first 3 discharges were done at lower currents).

USE OF ALUMINUM VANADATES AS CATHODES IN LITHIUM RECHARGEABLE CELLS

E. Andrukaitis*, G. L. Torlone and I.R. Hill
Defence Research and Development Branch,
National Defence Headquarters,
305 Rideau Street, Ottawa, Ontario, CANADA
K1A 0K2

Introduction

The metal vanadates, $Me_x(VO_3)_2$, reversibly intercalate lithium ions making them candidates for rechargeable lithium battery cathodes. Recent work on these vanadates has shown favourable specific capacities for use in lithium batteries (1-2). The potential use of non-transition metal vanadates, such as Al, was examined in this paper.

Experimental

The preparation for aluminum vanadates was similar to the preparation of transition metal vanadates described elsewhere (3). In this case, the aluminum salt replaces the transition metal salt used in the preparation. The vanadates can be prepared by two methods, a precipitation method or an electrodeposition method. Because the yields produced by the electrodeposition method were insufficient to make a complete range of aluminum vanadates, with different aluminum to vanadium ratios, for all the analysis required, the precipitation method was primarily used in this study. Coin cells were prepared by casting the vanadates on aluminum or copper foil (C 10 wt%, PVDF 5 wt%) with 1M $LiPF_6$ in 1:1 EC:DMC electrolyte and a counter electrode of lithium metal. The cells were then cycled continuously at a rate of about 20 mA/g discharge and 10mA/g charge.

Results and Conclusions

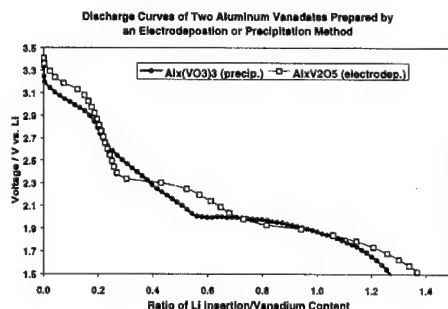
The aluminum vanadates with the general stoichiometry, $Al_x(VO_3)_2$, were made with different degrees of crystallinity and aluminum content. On average, specific capacities in the range of 300 to 350 Ah/Kg were obtained for the first discharge (see figure). By cycling, these aluminum vanadates were found to operate in a voltage range of 3.5 to 1.5 V. Structural changes occur on the second and subsequent cycles so that the discharge curve becomes smooth and free of phase changes with an average voltage of about 2.4V. Although specific capacities were not initially as high as that of some transition metal vanadates studied earlier (3), the aluminum vanadates did have superior cycling performance compared to these other vanadates. The specific capacity recovers to almost the full amount of the first discharge of the vanadate after about the 3rd cycle. This behaviour was unlike previous transition metal vanadates examined, where up to one half of the capacity could be lost after the first cycle. In this case the aluminum vanadate cathode capacity rebounds to almost 10% of the initial specific capacity and remained stable at that level for many cycles. This was believed to be due in large part to phase changes that occurs in the vanadate structure and also in part to the fact that the aluminum contained in the cathode material does not appear to actively participate in the lithium insertion process. This, perhaps, offers a more stable structure that was less likely to dissolve the cathode into the electrolyte, which is

a common problem for many vanadate species. Further study into use of non-transition metal vanadates for other suitable cathode candidates needs to be examined as well.

References

- (1) E. Andrukaitis, *Journal of Power Sources*, 68 (1997) 652-655.
- (2) S. Denis, E. Baudrin, M. Touboul, and J-M. Tarascon, *J. Electrochem. Soc.*, 144 (1997) 4099-4109.
- (3) E. Andrukaitis, J. Cooper and J. Smit, *Journal of Power Sources*, 54 (1995) 465-469.

* to whom which all correspondence should be addressed.



Boron Additives to Lithiated Cobalt Dioxide and
Lithiated Nickel-Cobalt Dioxide for Lithium Ion
Cells

George E. Blomgren
Blomgren Consulting Services Ltd.
1554 Clarence Ave.
Lakewood, OH 44107

Lithiated nickel dioxide is well known to have high initial capacity in lithium ion cells, but has shown many problems with cycle life and with preparation conditions. Several workers have pursued improvements in these properties through addition of other transition and main group elements to try to stabilize the layered structure material. The goal is to take advantage of the relatively low cost of nickel compounds and the high capacity compared to cobalt oxide based compounds. Lithiated cobalt dioxide has been shown to be a reliable, cathode material in lithium ion cells and many million cells have been manufactured with this material. In addition to the cost factor, the material has a problem with stability to high voltage charging and thermal excursions. These have been solved through the use of expensive control circuitry for each cell and expensive positive temperature coefficient materials placed in the cell.

The author has reviewed the use of aluminum and boron in the literature (1) and reported on experiments with aluminum additives as tested in lithium ion coin cells (2). This work presents results in demountable cells and coin cells for boron additives in LiCoO_2 and $\text{LiNi}_{1-x}\text{Co}_x\text{O}_2$.

Two electrolytes were employed in the experiments, 1M LiPF_6 in 1:1 EC:DEC and in 2:1 EC:DMC. Also, three doping levels of boron were employed (3, 5 and 10% of total transition metal cations). Cathode mixes (slurries) were coated on aluminum foil to mimic production positive electrodes as nearly as possible. All samples except LiCoO_2 were made by a spray decomposition method where solutions of precursor starting materials in the desired ratio of finished compounds were sprayed into a hot zone of air. Subsequent heat treatment of 750 to 800 °C for 2 hours in air was applied.

Table 1 gives the results in demountable cells for boron in LiCoO_2 . The capacity of the control electrode (LiCoO_2) was slightly higher than that of the boron doped because boron does not participate in the electrochemical reaction. The fading characteristic at the high charging voltage (4.4V) was much better for the boron containing material, particularly for the EC:DMC electrolyte.

Table 2 gives coin cell results for the boron in $\text{LiNi}_{1-x}\text{Co}_x\text{O}_2$. In this case, the EC:DMC electrolyte cells were charged to 4.4V, while the EC:DEC electrolyte cells were charged to 4.25V because, in view of the demountable cell results shown in Table 1, it was thought that the electrolyte would not perform well at the higher voltage. In this case, however, the results were very poor for EC:DMC, particularly in fade with cycle life. It is believed that the coin cell

hardware could not stand up to the high voltage, even though precautions had been taken by coating the can with a carbon conductive coating which we knew could stand up to at least the 4.25V condition. In the case of EC:DEC solutions, the boron containing samples showed better fading characteristics than the samples without boron, although the capacity at 20 cycles was not as good (as expected). The results for EC:DMC were mixed due to the high voltage effect, but one sample (B3) performed very well, while the control did very badly under this condition.

We concluded that boron substitution was as effective as aluminum in terms of cyclability, voltage stability and capacity. Further experimentation is desirable.

References

1. G. E. Blomgren, ITE Battery Letters, **1**, 60 (1999)
2. G. E. Blomgren, ITE Battery Letters, to be published

Table 1

Specific capacity of LiCoO_2 samples with and without boron in EC:DEC (A) and EC:DMC (B) electrolytes in demountable cells at different currents.

Elec	5% B		10% B		LiCoO_2	
	C/5	1C	C/5	1C	C/5	1C
A	167	150	163	134	172	140
B	169	155	164	149	164	117

Table 2

Specific Capacity at 20 cycles (Q_{20} - mAh/g) and fade characteristics (F) of $\text{LiNi}_{0.75}\text{Co}_{0.25}\text{O}_2$ samples with and without boron in A and B electrolytes in coin cells at C/5.

Elec	3% B		5% B		0% B	
	Q_{20}	F	Q_{20}	F	Q_{20}	F
A	140	Flat	139	Flat	156	Fade
B	132	Fade	145	Flat	-	Fade

Manganese Spinel Li-ion cells with Improved High Temperature Characteristics

By: Wendy Chow, Meijie Zhang, Yu Wang, Jan Reimers and Ulrich von Sacken

E-One Moli Energy (Canada) Ltd.
Maple Ridge, BC, Canada V2X 9E7

Spinel materials $\text{Li}_{1-x}\text{Mn}_2\text{O}_4$ have been studied intensively for the last decade. The main motivations have been the lower materials cost and the inherently better safety of spinel, making it an attractive alternative to $\text{Li}(\text{Co},\text{Ni})\text{O}_2$ cathode materials for large scale applications like EV batteries. Their major shortcoming has been relatively poor performance at elevated temperatures which is an important requirement for large scale applications.

Consequently the high temperature performance characteristics of spinel has been the subject of numerous studies. Our analysis of spinel Li-ion cells shows that the capacity loss at elevated temperatures is primarily due to increased irreversible loss of lithium at the Li_2C_6 electrode due to interaction with the spinel cathode. This type of capacity loss is completely masked in Li metal anode test cells (1).

We have previously proposed (2) a mechanism involving the conversion of trace amounts of H_2O to simple alcohols by reaction with the anode SEI, followed by diffusion of the alcohols to the $\lambda\text{-MnO}_2$ cathode where they are oxidized to produce even more H_2O . The ongoing generation of more and more H_2O then causes the irreversible loss of lithium at the anode. This mechanism is supported by the observation that unlike charged LiCoO_2 cathodes, charged spinel cathodes react with MeOH to generate H_2O as shown in Fig 1.

New developments make it possible to suppress these reactions. With a suitably modified spinel cathode material the rate of H_2O generation can be reduced to levels comparable to those observed on charged LiCoO_2 cathodes. As expected, Li-ion cells containing these modified spinel cathodes have high temperature storage characteristics similar to those of commercially available LiCoO_2 Li-ion cells (see Table I).

The results in Table I were obtained by storing fully charged 18650 cells at 60°C for 28 days, measuring their capacity at 1C rate discharge to obtain the retained capacity, then charging and discharging again to obtain the recovered capacity. These capacities are expressed as percentages of the cell capacity immediately prior to the storage period. All cells were charged to 4.2 volts for 2.5 hr with current limited to 1C rate.

In addition to good storage characteristics, spinel typically exhibits less impedance growth than cobalt after storage or cycling at elevated temperatures. As shown in Figure 2, long term 45°C cycling of our improved spinel cell does not show a downturn due to increasing impedance as is typical of LiCoO_2 Li-ion cells.

Conclusion

In view of their robust safety, lower materials cost and improved storage characteristics, spinel Li-ion cells are an attractive alternative to cobalt Li-ion cells, especially for large scale demanding applications.

References

- 1) Jan Reimers et al, Abstract #140, 196th Meeting of the Electrochem. Soc, Oct 17-22, 1999
- 2) Yu Wang and Jan Reimers, Extended Abstracts of 9IMLB, July 12-17, 1998

Table I - Capacity of 18650 Li-ion cells after 28 day 60°C Storage

Li-ion Cell Type	Retained Capacity (%)	Recovered Capacity (%)
Spinel 18650	82.0	90.6
Cobalt Competitor S	80.4	90.3
Cobalt Competitor Y	81.7	91.9

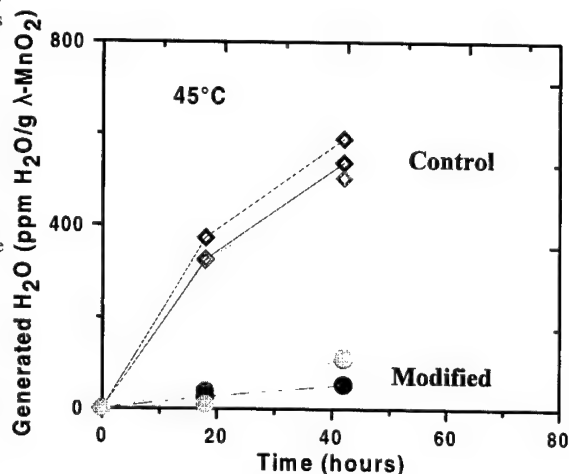


Figure 1- H_2O generation by charged ($\lambda\text{-MnO}_2$) cathode immersed in MeOH at 45°C . Modified spinel suppresses this reaction.

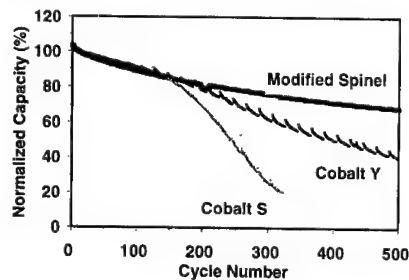


Figure 2 - Constant current cycling comparison of spinel with commercially available cobalt 18650 cells at 45°C . Discharge at 1C to 2.5v, 2.5hr constant voltage charge at 4.2v with current limited to 1C.

Mechanochemical Synthesis Of
 $\text{Li}_{1-y}\text{Mn}_2\text{O}_{4-d}$:
 Positive Electrode for Lithium Batteries

Sophie Soiron, Aline Rougier, Luc Aymard, and
 Jean Marie Tarascon

Laboratoire de Reactivite et Chimie des Solides
 Aimens, France

The spinel LiMn_2O_4 is of great interest for use in rechargeable lithium ion batteries because of its high voltage, low cost, low stability and low toxicity [1]. For commercial applications, it is important, on one hand, to reach low temperatures at which a phase can be synthesized without affecting the electrochemical properties and, on the other hand, to decrease the particle size to improve cell reversibility and capacity [2]. So, recently, mechanochemistry, a low temperature method, which allows nanometers scale materials, has been applied to electrode materials [3-5].

The aim of the present work is to study mechanochemical activation (MA) and mechanochemical synthesis of Li-Mn-O spinel and their electrochemical properties.

As a result of mechanochemical milling, lithium-manganese oxide $\text{Li}_y\text{Mn}_2\text{O}_{4.5}$ was successfully synthesized, for the first time, from a mixture of Li_2O and MnO_2 , ground for at least 5 hours in argon. The X-ray powder diffraction pattern (Fig. 1), indexed assuming the spinel structure (space group Fm3m), exhibits broad peaks in relation with small crystallites (80-150 Å) as confirmed by a TEM study. High surface areas of 16 m²/g were measured. SEM measurements showed the presence of agglomerates of few micrometers.

The electrochemical tests were performed in Swagelok™ cells $\text{Li}/\text{EC}+\text{DMC}+\text{LiPF}_6/\text{Li}_{1-y}\text{Mn}_2\text{O}_{4.5}$ at C/10 rate. The voltage/composition curves of cells using $\text{Li}_y\text{Mn}_2\text{O}_{4.5}$, prepared by mechanochemical synthesis reveal typical plateaus (3V-4V) of Li-Mn-O spinel (Fig. 2).

In this paper, we will emphasize that mechanical synthesis can be a powerful route of preparation for electrochemically active materials for lithium batteries.

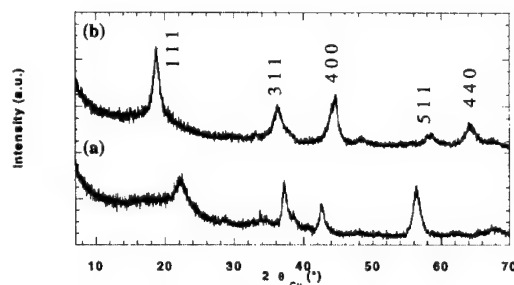


Fig. 1: Powder X-ray diffraction patterns of (a) starting mixture $\text{Li}_2\text{O}+\text{MnO}_2$ and of (b) $\text{Li}_y\text{Mn}_2\text{O}_{4.5}$ prepared by ball milling of $\text{Li}_2\text{O} + \text{MnO}_2$ for 5 hours in argon. The XRD pattern is indexed assuming the spinel structure (S.G.: Fm3m)

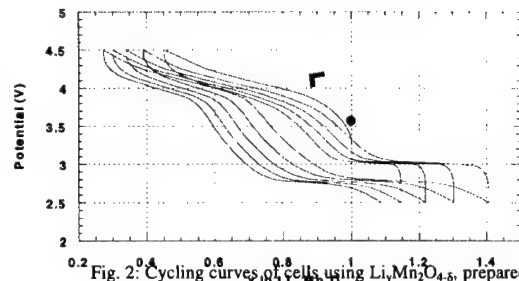


Fig. 2: Cycling curves of cells using $\text{Li}_y\text{Mn}_2\text{O}_{4.5}$, prepared by ball milling $\text{Li}_2\text{O} + \text{MnO}_2$ for 5 hours (C/10).

- [1]. J.M. Tarascon, and D. Guyomard, J. of Electrochem. Soc., 138, 2864 (1991)
- [2]. J.M. Tarascon, E. Wang, F.K. Shokoohi, W.R. McKinnon, and S. Colson, J. of Electrochem. Soc., 138, 2859 (1991)
- [3]. L. Aymard, C. Lenain, L. Courvoisier, F. Salver-Disma, and J.M. Tarascon, J. of Electrochem. Soc., 146 6 (1999)
- [4]. F. Salver-Disma, C. Lenain, B. Beaudoin, L. Aymard, and J.M. Tarascon, Solid State Ionics 98 145, (1997)
- [5]. N.V. Kosova, I.P. Asanov, E.T. Devyatkina, E.G. Avvakumov, J. Solid State Chem., 146, 184, (1999)

Two-Phase LiCoO₂ Oxides for Rechargeable Lithium BatteriesF. Croce¹, Hsiu-Ping. Lin², A. Shiao², M. Salomon², J. Wolfenstine³, A. Deptula⁴, W. Lada⁴ and D. Chua²

1. Dipartimento di Chimica, Università 'La Sapienza', P.le A. Moro 5, 00185, Roma, Italy

2. Max Power Inc., 220 Stahl Road, Harleysville, PA 19438, USA

3. U.S. Army Research Laboratory, 2800 Powder Mill Road, Adelphi, MD 20783-1197, USA

4. Institute of Nuclear Chemistry and Technology, 03-195 Warsaw, Poland

The exponentially growing demand for portable electronics, such as laptop computers and cellular phones, has rapidly increased interest for the development of more efficient Li-ion batteries, particularly for high rate applications. Presently, commercially available cells use LiCoO₂ as cathodic material, and in an effort to improve energy density, mixed LiNi_{1-x}Co_xO₂ layered compounds are presently receiving considerable attention (1,2). An alternate approach for increasing both rate and capacity capabilities, namely the use of 'two-phase' cathode materials, is the subject of this presentation. By increasing rate capability and at the same time decreasing polarization at the cathode, increases in energy and specific capacities are obtained.

Intercalation and deintercalation reactions of Li_xCoO₂ is accompanied by expansion (upon deintercalation) and contraction (upon intercalation) of the *c* axis (the *a* axis behaves in the opposite manner (2)) giving rise to significant mechanical stress in the oxide. The stress gradients produced will in turn result in Li-concentrated phases accompanied by phase boundary shifts which retard diffusion of Li⁺ across these phases or grain boundaries. One solution to this problem is the introduction of inert oxide materials to create stable grain boundaries which allow for greater stability upon contraction and expansion. In the present work, we report several materials used to create these stable grain boundaries which are the inert oxides TiO₂, SiO₂ and Al₂O₃.

By virtue of their Lewis-Base character, addition of these inert materials also facilitate rapid Li⁺ transport, and minimize the mechanical stresses produced during high rate charging and discharging. The key to successful syntheses of homogeneous two-phase oxides which can form these new grain boundaries is an even distribution of ceramic material on the molecular level: hence the need for innovative synthetic methods such as the sol-gel method. In the present work, we utilized a modified sol-gel method (3) to produce two-phase or 'composite' materials consisting of LiCoO₂ and a second inert phase intimately mixed on the nanometer scale. In a previous study (4), it was demonstrated that the modified sol-gel method used in the present study was able to produce two-phase oxide powders where the inert second phase is contained in the active oxide as nm-scale grains within the structure of the active oxide material. Here we report preliminary results obtained for composites based on LiCoO₂ as the main active phase, and SiO₂, TiO₂ and Al₂O₃ as second inert phases. In spite of the relatively low concentrations of these inert materials (between 0.5 and 1.0 mass %), these new two-phase cathodic materials are capable of being charged to 4.3 V vs Li/Li⁺ and capable of

sustaining very high discharge rates (5 mA/cm²). Tables 1, 2 and 3 confirm the improved rate and capacity retention for Li-ion /2-phase cathode cells at a discharge rate of 1 mA/cm². The electrolyte solution used in these studies was 1 mol dm⁻³ LiPF₆ in a 1:1:1 (by mass) mixture of EC:EMC:DMC. All cells reviewed in Tables 1 -3 were charged to 4.3 V and discharged to a 3.0 V cutoff. The data for the two-phase cathodes all show significant improvement in cathodic rate, energy and capacity capabilities compared to the pure, single-phase, LiCoO₂ parent compound. Additional data showing major improvements in energy and capacity for the new two-phase oxides at rates up to 5 mA/cm² will be presented in our full presentation.

Table 1
Discharge properties for cycle N° 2 at 1 mA/cm² at 25°C

Property	LiCoO ₂	0.5% SiO ₂	0.5% TiO ₂	0.5% Al ₂ O ₃	1% Al ₂ O ₃
mAh/g	138.9	136.7	132.8	132.6	132.5
mid volts	3.74	3.85	3.89	3.86	3.88
Wh/kg	518.8	526.3	515.9	511.8	512.7

Table 2
Discharge properties for cycle N° 50 at 1 mA/cm² at 25°C

Property	LiCoO ₂	0.5% SiO ₂	0.5% TiO ₂	0.5% Al ₂ O ₃	1% Al ₂ O ₃
mAh/g	130.9	132.2	---	130.7	132.0
mid volts	3.69	3.82	---	3.87	3.88
Wh/kg	483.0	505.5	---	505.8	512.7

Table 3
Discharge properties for cycle N° 70 at 1 mA/cm² at 25°C

Property	LiCoO ₂	0.5% SiO ₂	0.5% TiO ₂	0.5% Al ₂ O ₃	1% Al ₂ O ₃
mAh/g	125.4	132.4	131.7	128.2	131.4
mid volts	3.66	3.82	3.89	3.86	3.88
Wh/kg	459.0	506.2	511.9	494.7	509.8

References

1. J.R. Dahn, E.W. Fuller, M. Obravac and U. von Sacken, *Solid State Ionics*, 109, 265, (1994).
2. F. Croce, F. Nobili, A. Deptula, W. Lada, R. Tossici, A. D'Epifanio, B. Scrosati and R. Marassi, *Electrochemistry Communications* 1 (1999) 605-608.
3. F. Croce, A. D'Epifanio, A. Deptula, W. Lada, A. Ciancia, A. Di Bartolomeo, A. Brignocchi, *S. Francisco 1999 Spring MRS Meeting Proceedings MRS Book*, in press.
4. K.C. Goretta, Y. Xu, R.E. Cook, L.R. Feng, A. Deptula, W. Lada, T. Olczak, M. Xu and U. Balachandran, *Supercond. Sci. Technol.* 10 (1997) 853-856.

Acknowledgment

This research was sponsored by the U.S. Army Research Laboratory (ARL) under contract DAAD17-99-C-0004.

Defect Spinel $\text{Li}_{8n/n+4}\text{Mn}_{8n/n+4}\text{O}_4$ Cathode Materials for Lithium Polymer Batteries

Yongyao Xia^a, Koh Takahashi^b, Tetsuo Sakai^a,
Kuniaki Tatsumi^a, Takuya Fujieda^a, and M. Yoshio^c

^aBattery Section, Osaka National Research Institute,
1-8-31 Midorigaoka, Ikeda, Osaka 563-8577, Japan

^bJapan Metals & Chemicals Co., Ltd., Tsukuba,
Ibaraki 300-2635, Japan

^cDepartment of Applied Chemistry, Saga University,
Saga 840-8502, Japan

Solid state lithium polymer batteries is one of the most promising second batteries system for electric vehicle applications because of its advantages of no risk of leakage of liquid electrolyte, higher energy density, and shape flexibility compared with other systems. The cathode material currently used for such type battery was limited only to vanadium compounds. However, vanadium compounds are expensive, toxic, and unstable in atmosphere. One of the next challenge steps is to find a cheap, no toxic cathode materials instead of vanadium compounds. Manganese oxides are cheap, low toxic, and exist in many forms. Primary batteries in various sizes and rechargeable batteries in coin type with MnO_2 positive electrodes are commercially available. Spinel LiMn_2O_4 is capable of reversibly accommodating Li over a wide range (i.e., $\lambda\text{-MnO}_2$ to $\text{Li}_2\text{Mn}_2\text{O}_4$), corresponding to intercalation of lithium ion at two plateaus of 4 and 3 V vs. Li/Li^+ . Lithium intercalation at high voltage has been considered for lithium ion battery applications. The intercalation of lithium ion into LiMn_2O_4 at ca. 3 V leads to tetragonal $\text{Li}_2\text{Mn}_2\text{O}_4$, due to the Jahn-Teller effect. This gives rise to a decline in electrode capacity and consequently, poor rechargeability of battery. The Jahn-Teller distortion, however, can be suppressed by increasing average oxidation of manganese, e.g. the cubic symmetry can be preserved at least to $x = 2.5$ in $\text{Li}_{4+x}\text{Mn}_3\text{O}_{12}$, and $x = 1.7$ in $\text{Li}_{2+x}\text{Mn}_4\text{O}_9$ ¹. These compounds show better cyclability in the 3 V region.

In the present work, we used self-reaction method (JMC-method) to prepare stoichiometric defect spinel $\text{Li}_{8n/n+4}\text{Mn}_{8n/n+4}\text{O}_4$, $\text{Li}_4\text{Mn}_5\text{O}_{12}$ ($n=0.8$), $\text{Li}_2\text{Mn}_3\text{O}_7$ ($n=0.65$), and $\text{Li}_2\text{Mn}_4\text{O}_9$ ($n=0.5$) with an oxidation state of Mn close to 4+ by controlling the Li/Mn ratio, annealing temperature and time, as well as atmosphere. When assembled as positive electrode in both liquid and solid state polymer batteries, it behaves excellent battery

performance. Fig. 1 gives first 5 cycles charge/discharge curves of $\text{Li/Li}_4\text{Mn}_5\text{O}_{12}$ cell containing 1M $\text{LiPF}_6\text{-EC/DMC}$ and solid state polymer electrolyte $\text{Li}(\text{CF}_3\text{SO}_2)_2\text{P}(\text{EO/EM})$. It shows an initial capacity of 160 mAh/g close to the theoretical value, and a rechargeable capacity of 140 mAh/g. Rechargeable capacity of $\text{Li/SPE/Li}_4\text{Mn}_5\text{O}_{12}$ cell at C/3 rate at 65°C is plotted in Fig. 2 as a function of cycles. Cell shows excellent cyclability. The capacity decline is about 1.45% per cycle over 100 cycles at 65°C.

Synthesis, optimal cell configuration design, and mechanism of capacity decline upon cycling will present in the conference.

References:

1. M.M. Thackeray et al., J. Electrochem. Soc., 139, 363 (1992).

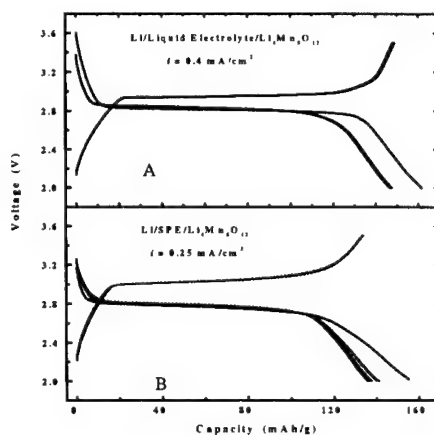


Fig. 1 charge/discharge curves of $\text{Li/Li}_4\text{Mn}_5\text{O}_{12}$ containing (A) 1M $\text{LiPF}_6\text{-EC/DMC}$ and (B) solid state polymer electrolyte $\text{Li}(\text{CF}_3\text{SO}_2)_2\text{P}(\text{EO/EM})$ at 65°C

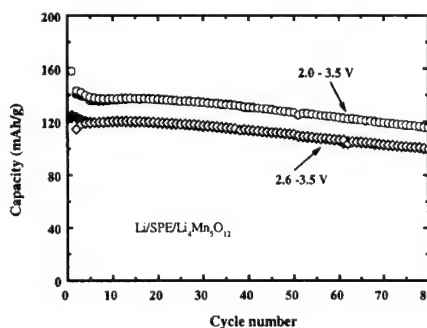


Fig. 2 Rechargeable capacity vs. cycle number of $\text{Li/SPE/Li}_4\text{Mn}_5\text{O}_{12}$ at C/3 rate at 65°C.

Abstract No. 216

⁷Li MAS-NMR and Electrochemical Studies of LiMn₂O₄-Based Spinel for Lithium Rechargeable Batteries

Michael C. Tucker, Jeffrey A. Reimer and Elton J. Cairns

Ernest Orlando Lawrence Berkeley National Laboratory
and
Department of Chemical Engineering
University of California, Berkeley
Berkeley, CA 94720
USA

Lithium manganese oxide spinels with substitution of certain metals for the manganese have been the subject of much interest as cathode materials for lithium rechargeable batteries.¹⁻³ This work attempts to elucidate the performance-improving effects that metal substitution has on the spinel structure by coupling MAS-NMR and electrochemical studies.

Substituted spinels, LiM_yMn_{2-y}O₄ (0 < y < 0.25, M=Li, Ni, Zn, Co, Al, Cr), have been prepared at 850°C (600°C for M=Li) in flowing oxygen. Selected compositions have been cycled vs. lithium foil on the 4-volt plateau. ⁷Li MAS-NMR spectra of LiMn₂O₄ as-prepared, after one cycle, and after 100 cycles are shown in Figure 1. Similar spectra for Li_{1.05}Mn_{1.95}O₄ are shown in Figure 2. The small shift in the normal tetrahedral lithium peak after cycling is due to a change in manganese oxidation state because of slightly different states-of-charge before and after cycling. The sharp peak at 0ppm is due to residual electrolyte salt.

role of the substituting metals in suppression of cycling-induced degradation.

ACKNOWLEDGMENTS

This work was supported by the National Science Foundation through a fellowship for M.C.T., and by the Director, Office of Basic Energy Sciences, Chemical Sciences Division of the U.S. Department of Energy, under Contract DE-AC03-76SF00098

REFERENCES

1. Gummow, R.J., A. de Kock, and M.M. Thackeray, *Solid State Ionics*, **69** 59 (1994).
2. Robertson, A.D., S.H. Lu, and W.F. Howard, *J. Electrochem. Soc.*, **144** 3505 (1997).
3. Hayashi, N., H. Ikuta, and M. Wakihara, *J. Electrochem. Soc.*, **146** 1351-1354 (1999).
4. Gee, B., C.R. Horne, E.J. Cairns and J.A. Reimer, *J. Phys. Chem. B*, **102** 10142-10149 (1998).
5. Lee, Y.J., F.Wang, and C.P. Grey, *J. Am. Chem. Soc.*, **120** 12601-12613 (1998).

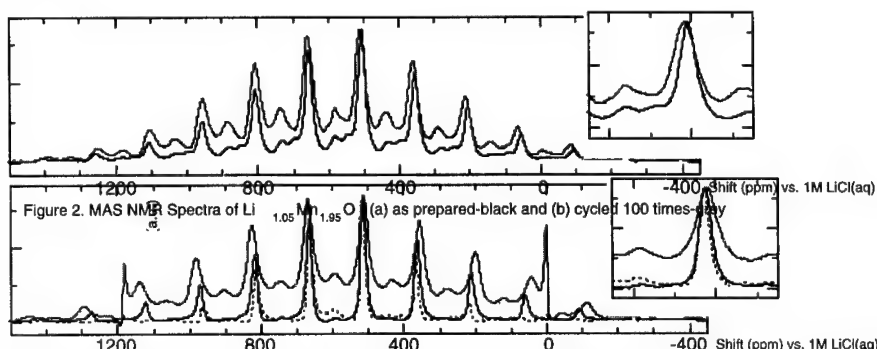


Figure 1. MAS NMR Spectra of LiMn₂O₄ (a) as prepared-black, (b) cycled once-dashed, and (c) cycled 100 times-grey

All spectra show a large peak around 500ppm, which is assigned to lithium in the normal spinel tetrahedral (8a) site.^{4,5} As-prepared Li_{1.05}Mn_{1.95}O₄ shows an additional peak at 580ppm. This peak is assigned to lithium in the tetrahedral (8a) environment near a manganese (16d) defect, specifically, a substitution for manganese by a lithium ion. Upon cycling, the peak at 580-590ppm becomes

apparent in the case of LiMn₂O₄ and grows in relative intensity in the case of Li_{1.05}Mn_{1.95}O₄. This suggests a replacement of manganese by lithium, and that this replacement is promoted by cycling.

The linewidth for the normal tetrahedral lithium peak is unchanged after one cycle, but substantially broadened after 100 cycles. This suggests the introduction of structural disorder to the 8a site upon cycling. The effect is greater for LiMn₂O₄, which showed a greater capacity fade, suggesting that the spinel structure is stabilized upon manganese substitution by structural consequences which are spatially removed from the substituting ion.

Currently, spinel electrodes are being subjected to different types of abuse in order to assess the changes in the NMR spectra each model process produces. It is expected that this will elucidate the changes introduced into the spinel structure upon repeated cycling, and the

Mechanochemical Way for Preparation of Disordered Lithium-Manganese Spinel Compounds

Nina Kosova,¹ Evgeniya Devyatkina,²
Nikolai Uvarov³ and Svetlana Kozlova⁴

¹Institute of Solid State Chemistry
Kutateladze 18, Novosibirsk 630128, Russia
Novosibirsk 630128
Russia

²Institute of Solid State Chemistry
Kutateladze 18, Novosibirsk 630128, Russia
Novosibirsk 630128
Russia

³Institute of Solid State Chemistry
Kutateladze 18, Novosibirsk 630128, Russia
Novosibirsk 630128
Russia

⁴Institute of Inorganic Chemistry
Lavrent'eva 3, Novosibirsk 630090, Russia
Novosibirsk 630090
Russia

Lithium-manganese oxide compounds with spinel structure attract a great deal of interest in both theoretical and applicative aspects. A great ability of Mn ions to change easily their valence state in Li-Mn spinels and possibility for cation mixing are the origin of interesting physical properties of these compounds. On the other hand, Li-Mn spinels were found to be prospective cathode materials in lithium batteries. Structural characteristics, particle size and crystallinity play very important role. Besides, disordered spinels are assumed to improve reversibility and to increase capacity of cathodes [1,2].

Mechanochemistry is one of the most promising low temperature method of synthesis. In these method nanoscale mixing of reagents occurs and nucleation process initiates at room temperature, exhibiting more homogeneous distribution, larger specific area and smaller particle size of final products as compared with the solid state reaction method. Besides, it is possible to obtain disordered spinel compounds. Disorder is achieved either through cation mixing (inverse spinel) or through cationic or anionic nonstoichiometry (deficient spinels).

Recently [3], we showed the possibility of direct mechanochemical synthesis of LiMn₂O₄ with poor crystallinity and specific surface area of about 50-100 m²/g. A significant influence of starting materials on the mechanism of synthesis was found.

In the present work we investigated the structural aspect of materials prepared using mechanochemical method.

Mechanochemical activation (MA) was carried out in AGO-2 activator with water cooling and stainless containers and balls (8 mm diameter, 660 rpm). The mass ratio of materials to balls was 1/40. MnO₂, LiOH and Li₂CO₃ were used as starting reagents. Two groups of activated mixtures (before and after chemical interaction) were then heated at 450, 600 and 800°C.

Phase analysis, changes of lattice parameters, oxygen stoichiometry, as well as local structure and cationic

environment have been performed using X-ray powder diffraction, thermogravimetry, ⁷Li NMR, EPR and IR spectroscopy. Specific surface area was measured by BET method.

It was found that in spite of different type of precursor, obtained by MA, thermal treatment brings to crystalline Li-Mn spinel starting from 450°C. All diffraction peaks were indexed by a cubic spinel structure and refined with a space group Fd3m. The crystallinity and the lattice parameter *a* of products increase with temperature and time of activation, the latter being lower for hydroxide samples, and doesn't achieve the value of 8.24 Å for stoichiometric LiMn₂O₄, prepared by solid state method. It indicates that they are disordered and enriched by Mn⁴⁺, and can be described by the formula (Li_{1-x}x)[(Mn³⁺+Mn⁴⁺)_{2-y}y]O₄, where y is vacancy, or LiMn₂O_{4+z}. The excess oxygen is released under heating. Oxygen nonstoichiometry was elucidated on the basis of thermogravimetry data. It decreased with the temperature of treatment.

IR studies showed the other kind of disordering in obtained spinels. IR spectra of all investigated samples are represented by two bands at 300-800 cm⁻¹. For samples heated at T_{450°C} they are degenerated, while for mechanochemically prepared samples and after heat treatment at lower temperatures the removal of degeneration is observed. The splitting of bands is explained as a consequence of Li and Mn ions distribution between tetrahedral and octahedral sites.

The quantitative data of Li ion distribution over nonequivalent crystallographic positions were obtained by ⁷Li NMR spectroscopy. If all Li ions occupy high symmetric tetrahedral 8a sites, NMR spectrum is represented by a narrow symmetric line. If all Li ions occupy octahedral sites, the broadening of line must appear owing to electric field gradient. In mechanochemically prepared Li-Mn spinels the asymmetry was observed due to the shift arising with the increasing number of neighboring oxygen atoms and indicating that Li ions occupy both tetrahedral and octahedral sites. Using the method of the least squares, the decomposition of the observed spectra was fulfilled.

The state of Mn⁴⁺ ions in prepared samples was elucidated by EPR spectroscopy. The analysis of signal width, g-factor value and their changes versus temperature allows to elucidate the degree of nonequilibrium of spinels.

Spinel, prepared mechanochemically, are characterized by high specific surface area. It sharply decreases with the increasing of temperature above 600°C and the time of MA. It is higher for hydroxide samples, that was explained by specific process of mixing [4] and the significant role of residual surface OH groups on the process of sintering of particles, determining moving apart effect.

The influence of disordering in Li-Mn spinels, prepared using MA, on their electrochemical properties was investigated in LiMn₂O₄/C, LiPF₆/EC/Li cell.

It is concluded that a control of the cationic distribution and oxygen nonstoichiometry in Li-Mn spinels is of a great importance for the improvement of their electrochemical properties.

REFERENCES. 1. J.M. Tarascon, W.R. McKinnon, F. Coowar, e.a. // J. Electrochem. Soc. 1994. V.141. P. 1421-1431. 2. M.M. Thackeray, A. de Kock, M.H. Rossouw, e.a. // J. Electrochem. Soc. 1992. V.139. P. 363-366. 3. N.V. Kosova, N.F. Uvarov, E.T. Devyatkina, E.G. Avvakumov // XII Int. Conf. on Solid State Ionics. Extended Abstracts. Greece, June 6-12, 1999. 4. N.V. Kosova, I.P. Asanov, E.T. Devyatkina, E.G. Avvakumov // J. Solid State Chem. 1999. V.146. P.184-188.

In situ XAFS analysis of the Li deintercalation process of $\text{Li}(\text{Mn}, \text{M})_2\text{O}_4$ ($\text{M}=\text{Cr}, \text{Co}, \text{Ni}$), cathode materials for 5V lithium batteries

Izumi Nakai, Yasuko Terada, Kenji Yasaka, Tokuzo Konishi¹, and Masaki Yoshio²

Dept. of Applied Chemistry, Faculty of Science, Science University of Tokyo,

Kagurazaka, Shinjuku, Tokyo 162-8601, Japan

¹⁾ Analytical Research Laboratory, Asahi Chemical Industry, Co., Ltd., Samejima, Shizuoka 416-8501, Japan

²⁾ Dept. of Applied Chemistry, Faculty of Science and Engineering, Saga University, Honjo, Saga 840-8502, Japan

Introduction

Recently, it was reported that $\text{Li}(\text{Mn}, \text{M})_2\text{O}_4$ ($\text{M}=\text{Cr}, \text{Fe}, \text{Ni}, \text{Co}, \text{Cu}$) exhibited a nearly 5V operating voltages after reaching the 4V plateau of voltage curves when they are used as cathode materials of the Li batteries(1-3). However, the structural variations of the dopant metals at the 5 V region remained to be elucidated. The X-ray absorption fine structure (XAFS) technique is most suitable for obtaining these information under an in situ condition. We have already developed a transmission in situ XAFS cell and revealed structural changes of LiCoO_2 , LiNiO_2 , $\text{Li}(\text{Co}, \text{Ni})\text{O}_2$, and LiMn_2O_4 with the electrochemical Li deintercalation (4-6). The present study was conducted to reveal variations in the chemical states and local structures of the Mn and M ($\text{M}=\text{Cr}, \text{Co}, \text{Ni}$) atoms in $\text{Li}_{1-x}(\text{Mn}, \text{M})_2\text{O}_4$ as a function of the Li content by in situ XAFS analysis. In particular, detailed structural behavior of the Ni-O₆ octahedra in $\text{Li}_{1-x}(\text{Mn}, \text{Ni})_2\text{O}_4$ during the charge process was clarified by analyzing EXAFS (extended X-ray absorption fine structure) oscillations.

EXPERIMENTAL

The partially substituted Mn spinels $\text{Li}(\text{Mn}_{2-y}\text{Cr}_y)\text{O}_4$ ($y=0.75$), $\text{Li}(\text{Mn}_{2-y}\text{Co}_y)\text{O}_4$ ($y=0.29$), and $\text{Li}(\text{Mn}_{2-y}\text{Ni}_y)\text{O}_4$ ($y=0.31, 0.4$) were prepared by a solid-state reaction. The in situ XAFS cell is composed of a thin film cathode, a liquid electrolyte 1M (LiPF_6 in EC+DMC: 1:2 in volume), and a lithium foil anode(6). The cell was charged to a desired voltage at a constant current, and then kept in a resting condition for ca. 40 minutes. Cr, Mn, Ni, and Co K-XAFS spectra were measured in a transmission mode at various stages of the charge process. The measurements were carried out at BL-7C and 12C, Photon Factory (PF), KEK, Tsukuba, Japan. A Si(111) double-crystal monochromator was used, and the intensities of the incident and transmitted X-rays were measured by the ion chamber detectors at room temperature. The EXAFS data were analyzed by conventional methods using REX2 data analysis software (7). Theoretical parameters of the backscattering amplitude and phase shifts used in the curve fitting analysis were calculated by FEFF 8 (8).

Results and Discussion

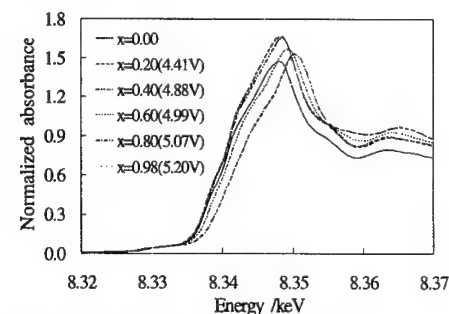
The XANES spectra of the transition metals show various changes with the Li deintercalation. As an example, the Ni K-XANES spectra of $\text{Li}_{1-x}\text{Mn}_{1.69}\text{Ni}_{0.31}\text{O}_4$ as a function of x are shown in Fig. 1. The spectrum shows an abrupt chemical shift at $x=0.4$, and the total shift is as large as 3.52 eV (Fig. 1). Because the Ni K-edge energy at $x=0$ (8340.7 eV) coincides with that of reference $\text{Ni}^{2+}(\text{CH}_3\text{COO})_2$ (8341.1 eV), the existence of Ni^{2+} in

$\text{LiMn}_{1.69}\text{Ni}_{0.31}\text{O}_4$ spinel is confirmed. It is reported that the chemical shift accompanied by the oxidation from Ni^{2+} to Ni^{4+} is 3.7 eV(9), which is in good agreement with the present result supporting the oxidation of Ni^{2+} to Ni^{4+} . The present XANES analysis has disclosed that, in summary, the oxidation of Mn^{3+} to Mn^{4+} is associated with the charge process at low voltage (3.9-4.3 V), and the high voltage (near 5 V) is due to the oxidations of Cr^{3+} and Ni^{2+} . The oxidation of Co^{3+} to Co^{4+} occurs at both the low and high voltage regions of the voltage curve.

The Fourier transforms (FT) of the EXAFS oscillation for each phase was calculated. The intensities of the first peak corresponding the Ni-O interaction in FT for the Ni phase show a peculiar variation. The height of the Ni-O peak begins to decrease when x exceeds 0.4, and then reaches a minimum at $x=0.6$. Then, the peak height increases significantly with the deintercalation of Li. An extraordinarily small Ni-O peak has also observed in LiNiO_2 (4). This was interpreted as due to the Jahn-Teller distorted $\text{Ni}^{3+}\text{-O}_6$ octahedron from the true octahedral coordination. Our results also suggest that the small Ni-O peaks at $x=0.6$ can be ascribed to the presence of a distorted $\text{Ni}^{3+}\text{-O}$ octahedron due to the Jahn-Teller effect. Consequently, it is found that Ni^{2+} is first oxidized to the low-spin Ni^{3+} , which is the d^7 Jahn-Teller ion; then, when x exceeds 0.6, Ni^{3+} starts to oxidize to Ni^{4+} . The average $\text{Ni}^{2+}\text{-O}$, $\text{Ni}^{3+}\text{-O}$, and $\text{Ni}^{4+}\text{-O}$ octahedral distances were calculated to be 1.99, 1.92, and 1.86 Å, respectively. The theoretical Ni-O distances calculated from the ionic radii 2.07 for $\text{Ni}^{2+}\text{-O}$, 1.94 for $\text{Ni}^{3+}\text{-O}$ (low-spin state), and 1.86 Å for $\text{Ni}^{4+}\text{-O}$, which is in fair agreement with the present results. It is concluded that the electrochemical Li deintercalation first causes the oxidation of Ni^{2+} to Ni^{3+} ; Ni^{3+} is then oxidized to Ni^{4+} . Thus, a dynamical change in the Ni oxidation state with the Li deintercalation can be elucidated experimentally for the first time.

Fig.1 Ni K-XANES spectra of $\text{Li}_{1-x}\text{Mn}_{1.69}\text{Ni}_{0.31}\text{O}_4$

References



- (1) H. Kawai et al., Chem. Mater. 10(1998)3266.
- (2) C. Sigalaet al., J. Solid State Chem. 132(1997)372.
- (3) K. Amine, et al., J. Electrochem. Soc. 143(1996)1607.
- (4) I. Nakai et al., J. Solid State Chem. 140(1998)145.
- (5) Y. Shiraishi et al., J. Solid State Chem. 133, (1997)587.
- (6) I. Nakai et al., Spectrochim. Acta B54(1999)143.
- (7) Cat. No. 2612S211, RIGAKU Co. (1996)
- (8) A.L. Ankudinov et al., Phys. Rev. B58 (1998)7565.
- (9) A.N.Mansour et al., J. Phys. Chem. A. 102(1998)65.

ESR Analysis of Electrochemical Oxidation on Cathode in a Lithium Ion Battery

Hiroshi Kurokawa, Taeko Ota, Shigeki Matsuta,
Yoshio Kato, Seiji Yoshimura,
Shin Fujitani and Ikuo Yonezu
New Materials Research Center,
SANYO Electric Co. Ltd.,
1-18-13, Hashiridani, Hirakata, Osaka 573-8534, Japan

1. Introduction

The decomposition of electrolyte in the lithium ion batteries is regarded as a major reason for the capacity decrease. Therefore, many studies have been carried out on decomposition mechanisms of electrolyte.¹

Many decomposition mechanisms of the electrolyte solutions on the negative electrode surface were suggested from the observation of the final decomposition products. For example, radical species of an intermediate state in this reaction mechanism were observed by electron spin resonance spectroscopy (ESR).^{1,3}

In this work, we used ESR to observe the reactive intermediate radical species in the reaction between the positive electrode and the electrolyte solution. Furthermore, we also discuss the intermediate radical structure and the capacity fade of the positive electrode during in a storage test at 80°C.

2. Experimental

Non-aqueous solvents (ethylene carbonate (EC), propylene carbonate (PC), dimethyl carbonate (DMC), ethyl methyl carbonate (EMC), diethyl carbonate (DEC) (Mitsubishi Chemical), lithium hexafluorophosphate (LiPF₆) and LiCoO₂ were used. The LiCoO₂ was oxidized by charging to the potential of 4.3 V vs. Li/Li⁺.

X-band ESR observations were carried out with an ESP350E electron spin resonance system (Bruker) at 80°C with microwave frequency of 9.49GHz, microwave power of 1mW, and measurement width between 313.6 and 363.6mT.

3. Results and Discussion

Cation Radical species were generated as an intermediate product in an electrochemical oxidation reaction of the charged positive electrode with the solution.

Direct ESR measurement was carried out for each sample after it was stored in the ESR equipment at 80°C for 1 hour. The result is shown in figure 1. These spectra were for the reactions of EC, PC, DMC, EMC, and DEC including 1 mol/l LiPF₆ on the charged positive electrode. All of g factor from those spectra were 2.0023. The radical quantity after the storage at 80°C was $3 \cdot 6 \times 10^{17}$ spins g⁻¹, which was approximately twice as large as that before the storage at 25°C.

Since hyperfine splitting was not observed, we used 0.32mT of the modulation width. The line width of the peak was also similarly different by the solvents in the range between 2.7 and 5.0mT. The line widths of the peak by the electrochemical oxidation in PC and DMC were over 10 times wider than those of the electrochemical reduction. The peak shape of each solution was symmetrical.

Possible explanations for these results are: transverse relaxation by spin-spin dipolar interaction, modulation of anisotropic tensors or intermolecular electron exchange broadening. Spin-spin dipole interaction depends on the spin concentration. In this case, the concentration of the

radical species was about 100ppm in the electrolyte solution. This radical concentration can be broaden the ESR peaks illustrated in figure 1. The open-shell cation radical species shown in figure 2 have an asymmetric line shape. However, the peak shape was symmetrical. Therefore, no asymmetric absorption was related to the effect of the modulation of anisotropic tensors by suppressed rotational diffusion of the open-shell species. This modulation is a transverse relaxation of electron exchange interaction like a intermediate anion radical species from a reduced reaction of an electrolyte solution in a negative electrode.

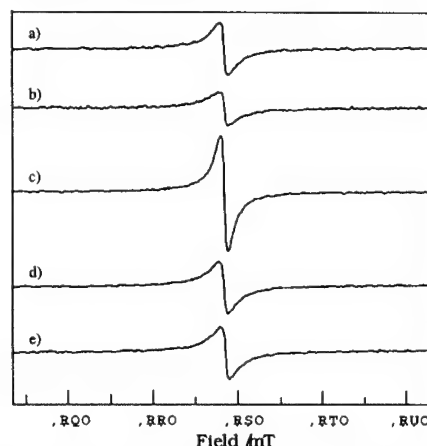


Figure 1 First-derivative ESR spectra obtained from oxidation reaction of a) 1.0 mol/l LiPF₆/EC; b) 1.0 mol/l LiPF₆/PC; c) 1.0 mol/l LiPF₆/DMC; d) 1.0 mol/l LiPF₆/EMC; e) 1.0 mol/l LiPF₆/DEC in contact with charged positive electrode (Li_{1-x}CoO₂) at 80°C after 1 hour.

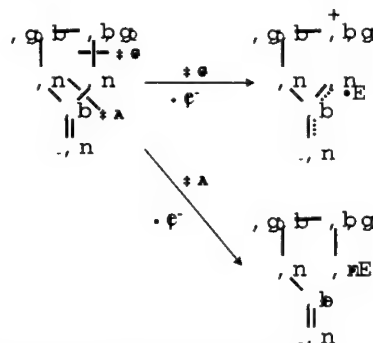


Figure 2 The open-shell cation radical species

4. Reference

1. E. Endo, M. Ata, K. Tanaka and K. Sekai, *J. Electrochem. Soc.*, 145, 3757 (1998).
2. N. Takami, A. Satoh, M. Oguchi, H. Sasaki and T. Ohsaki, *J. Power Source*, 68, 283 (1997)
3. L. Zhuang, J. Lu, X. Ai and H. Yang, *J. Electroanalytical Chem.*, 397, 315 (1995).

Preparation of Lithium Manganese Oxides Including Iron

Mitsuharu Tabuchi, Hikari Shigemura, Kazuaki Ado, Hironori Kobayashi, Hikari Sakaabe, Hiroyuki Kageyama and Ryoji Kanno*

Osaka National Research Institute, 1-8-31 Midorigaoka Ikeda Osaka 563-8577, Japan

*Kobe University, 1-1, Rokko-dai, Nada, Kobe, Hyogo, 657 Japan

1. Introduction

Lithium iron oxides, LiFeO_2 including metastable polymorphs are one of most attractive cathode materials for large-scale lithium-ion batteries due to abundance of natural resources. Although many researchers have succeeded to prepare electrochemically-active LiFeO_2 by soft-chemical method (ion-exchange reaction), only a few report has been presented concerning the formation of $\text{Fe}^{3+}/\text{Fe}^{4+}$ redox¹. However, the $\text{Fe}^{3+}/\text{Fe}^{4+}$ redox couple was observed in the cathodes of Fe doped LiNiO_2 and LiCoO_2 ². These reports raise a question whether Fe^{3+} can be oxidized independently from the oxidation of other cations or not. Therefore, we tried to prepare Fe doped Li_2MnO_3 to see the $\text{Fe}^{3+}/\text{Fe}^{4+}$ redox behavior in electrochemical inactive phase with one of layered rock salt structure similar to LiCoO_2 .

2. Experimental

Fe doped Li_2MnO_3 samples were obtained by hydrothermal reaction of Fe-Mn coprecipitate with lithium hydroxide under the presence of oxidant, KClO_3 at 220-240°C for 10-240h. The Fe-Mn coprecipitate was obtained by bubbling air through the precipitate (3-7days) which was made by adding dropwise NaOH solution to mixed $\text{Fe}(\text{NO}_3)_3$ - $\text{Mn}(\text{NO}_3)_2$ one. The hydrothermally-obtained samples were washed repeatedly with distilled water and filtered for eliminating the residual salt from the products and then they were dried at 100°C.

The samples were characterized by X-ray diffraction (XRD), transmission electron microscope (TEM), chemical analysis, Mn-K X-ray absorption and ^{57}Fe Mössbauer spectroscopy.

3. Results and Discussion

Although XRD patterns of 5% Fe doped samples (Fig. 1) was close to that of Li_2MnO_3 , the patterns of the doped one above 10% were similar to that of LiCoO_2 rather than that of Li_2MnO_3 . No other lithium manganese oxides, lithium iron oxides, manganese oxides and iron oxides were detected on these patterns. The $\text{Li}/(\text{Fe}+\text{Mn})$ values were 1.69(3) for 10% doped sample and 1.47(2) for 20% doped one. The $\text{Fe}/(\text{Fe}+\text{Mn})$ values were 0.10(1) for 10% doped sample and 0.21(1) for 20% doped one. These results indicate the samples are belong to Li_2MnO_3 - LiFeO_2 solid solution rather than LiMnO_2 - LiFeO_2 one. The pattern of 5% Fe doped Li_2MnO_3 could be fitted by monoclinic Li_2MnO_3 unit cell ($C2/m$, $a=4.9407(9)\text{\AA}$, $b=8.5465(10)\text{\AA}$, $c=5.0211(5)\text{\AA}$, $\beta=109.274(13)^\circ$). The α - NaFeO_2 type unit cell ($R\bar{3}m$, $a=2.85577(14)\text{\AA}$, $c=14.2181(10)\text{\AA}$) was used for fitting the XRD pattern of 10% Fe doped sample. The occupation of transition metal in lithium layer was estimated to be 3.2(2)%. The average grain size decrease with increasing Fe content (from ca. $0.3\mu\text{m}$ for 5% doped sample to $<0.1\mu\text{m}$ for 20% doped one). Therefore, the change in structure from monoclinic to pseudo-rhombohedral one could be attributed to suppression of cation ordering due to low preparation temperature. The hypothesis was supported by the experimental results; monoclinic form ($C2/m$, $a=4.9264(5)\text{\AA}$, $b=8.5246(6)\text{\AA}$, $c=5.0161(3)\text{\AA}$,

$\beta=109.266(7)^\circ$) of 10% Fe doped Li_2MnO_3 could be obtained by annealing at 400°C in air for 12h. The change in lattice parameters could be detected comparing to undoped sample ($a=4.9307(3)\text{\AA}$, $b=8.5313(4)\text{\AA}$, $c=5.0230(2)\text{\AA}$, $\beta=109.343(4)^\circ$) indicating that Fe ions were incorporated in Li_2MnO_3 structure. The occupation of transition metal in lithium layer was estimated to be 0.9(2)% which is smaller than that of as-prepared sample. The XRD pattern fitting of two 20% Fe doped samples (hydrothermally-obtained and annealed one at 400°C) were failed at present. Only peak position could be refined for obtaining lattice parameters ($R\bar{3}m$, $a=2.8648(2)\text{\AA}$, $c=14.2240(18)\text{\AA}$) for hydrothermally-obtained sample. Attempts for obtaining higher crystallinity sample by selecting higher annealing temperature were unsuccessful due to the formation of inverse spinel, i.e. LiFe_2O_4 at 450 °C.

No significant change in Mn-K XANES spectra for Fe doped samples (hydrothermally-obtained one) could be detected compared to that of Li_2MnO_3 , indicating that valence state of Mn was kept at 4+ after Fe doping. ^{57}Fe Mössbauer spectra at 300K could be fitted by a doublet with +0.32mm/s of isomer shift value for 10% Fe doped sample, which is typical one of high-spin Fe^{3+} compounds such as α - LiFeO_2 (+0.36 mm/s) and α - NaFeO_2 (+0.37 mm/s). These spectroscopy data supports the formation of Li_2MnO_3 - LiFeO_2 solid solution.

In conclusion, Fe could be incorporated into Li_2MnO_3 by hydrothermal reaction and post-annealing in air. Electrochemical data for these samples, and results for the sample obtained by solid state reaction will be presents at the meeting.

References

1. L.B. Guenne et al., *J. Mat. Chem.* 9, 1127, (1999).
2. G. Prado et al., Extended Abstracts of 194th Meeting of The Electrochemical Society, Boston, Massachusetts, 1998.
3. H. Kobayashi et al., *J. Electrochem. Soc.* in press (2000).

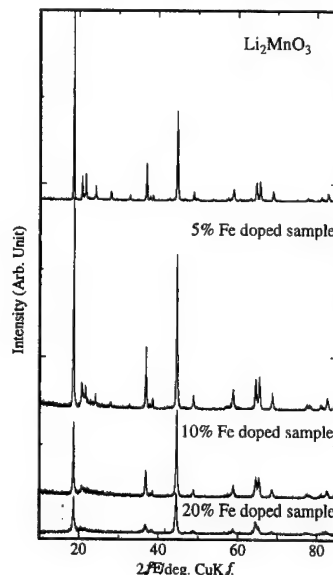


Fig. 1 XRD patterns of Fe doped and undoped samples obtained hydrothermally.

In situ neutron powder diffraction analysis of the Li deintercalation process of $\text{Li}_{1.1}\text{Mn}_{1.9}\text{O}_4$

Y. Terada, Y. Shiraishi, I. Nakai, T. Kamiyama^a,
S. Gotoh^a, K. Oikawa^b, F. Nishikawa^c and F. Izumi^d

Dept. of Appl. Chem., Fac. of Sci., Science University of
Tokyo, Kagurazaka, Tokyo 162-0825, Japan

^aInstitute of Material Science, University of Tsukuba,
Tsukuba, Ibaraki 305-8573, Japan

^bAdvanced Science Research Center, JAERI, Tokai,
Ibaraki 319-1195, Japan

^cBattery Development Lab., Asahi Chemical Industry,
Co., Ltd., Yako, Kawasaki, Kanagawa 210-0863, Japan

^dNational Institute for Research in Inorganic Materials,
Tsukuba, Ibaraki 305-0044, Japan

Strong attention has been focused on LiMn_2O_4 spinel because of its economic and environmental advantages over LiCoO_2 , which is currently used as a cathode material for lithium ion secondary batteries in a commercial base. However, there are several problems that remain to be solved such as capacity fading under high temperature before this new material can be used in practical applications. Study of crystal structure of lithium ion battery materials is necessary to understand the electrochemical behavior of the cathode materials, because it is directly related to the performance of the batteries. A large number of in-situ X-ray diffraction studies are carried out. Their structural information is limited to semi-quantitative such as a variation of lattice parameters. This is partly due to the small X-ray scattering factor of Li and O, and, it is difficult to obtain reliable structure parameters of these atoms. More precise structure determination can be realized by utilizing neutron diffraction. The present study was conducted to reveal the structure change of $\text{Li}_{1.1}\text{Mn}_{1.9}\text{O}_4$ as a cathode material during Li-deintercalation process by in situ neutron diffraction technique.

Figure 1 shows an arrangement of the in situ neutron diffraction cell developed in the present study. This cell can reduce Bragg reflections from components other than a cathode material. A Cu anode and a separator (PTFE) were placed out of the neutron beam path. A reservoir is used to store the electrolyte during neutron diffraction measurements. A composite cathode was prepared by mixing $\text{Li}_{1.1}\text{Mn}_{1.9}\text{O}_4$ with graphite, acetylene black and PVDF which was coated on an Al mesh. The electrolyte composition was 1M LiPF_6 in ethylene carbonate (EC): dimethyl carbonate (DMC) (1:2 in volume). The cells were charged to a desired capacity at a charge rate of 0.1 C. The measurements were made by the time-of-flight neutron diffractometer Vega at the pulsed spallation neutron facility KENS, KEK, Tsukuba.

The obtained neutron diffraction data were satisfactory in quality, and they were analyzed by the Rietveld method using RIETAN on the basis of the Fd-3m space group with three atomic sites, Li at 8a, Mn at 16d, and O at 32e. Occupancy of oxygen, g, was fixed at the value obtained from a separate refinement on the same cathode material: $g(\text{O})=0.946$. A small amount of foreign phases, i.e., Cu anode, Al collector and graphite binder were detected and were also included in the refinement. Using this model, diffraction data of the cathode after 50% charging were successfully analyzed. Its Rietveld refinement pattern is given in Fig. 2. The tick marks from

top to the bottom indicate the Bragg peak positions of $\text{Li}_{1.1}\text{Mn}_{1.9}\text{O}_4$, graphite, Cu and Al, respectively.

On the other hand, diffraction data of the cathode material after full charging could not be analyzed based on the above simple model. Figure 3 shows a shoulder peak of the 622 reflection, which indicates the coexistence of two phases. This result is consistent with that reported by the in situ X-ray diffraction study [1]. In order to extract structural information of each phase, we analyzed the data on the basis of the two-phase model, where slightly different structure parameters were assumed for each phase. The lattice parameter and the occupancy of the Li site, $g(\text{Li})$ of the first phase (original spinel) decreased with the Li deintercalation: 50% charged; $a=8.15153(5)$ Å and $g(\text{Li})=0.68(5)$, 100% charged; $a=8.11184(13)$ Å and $g(\text{Li})=0.53(8)$. It was estimated that a part of the Li ions exists at the 16c site in the second phase, which is believed to be an expected diffusion path of Li during the charge-discharge process. The lattice parameter and the occupancy of the second phase are calculated to be $a=8.08984(24)$ Å and $g(\text{Li})=0.47(21)$, respectively.

[1] M. N. Richard, I. Koetschau and J. R. Dahn, J. Electrochem. Soc., 144 (1997) 554.

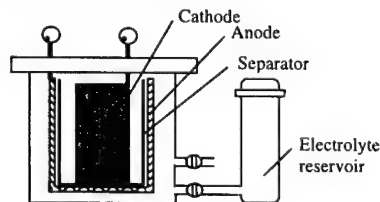


Fig. 1 Schematic drawing of the in situ cell.

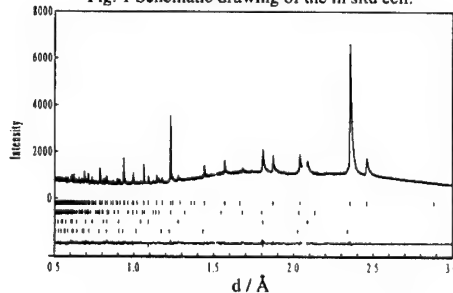


Fig. 2 Rietveld pattern for 50%-charged material.

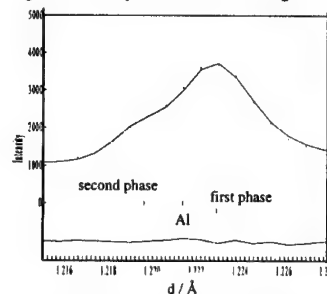


Fig. 3 The 622 reflection of the full-charged material.

In-situ total reflection X-ray fluorescence analysis of Mn dissolution from LiMn_2O_4 during charge-discharge process of the Li secondary battery

Y. Nishiwaki, Y. Terada, I. Nakai and F. Nishikawa^a

Dept. of Appl. Chem., Fac. of Sci., Science Univ. of Tokyo, Kagurazaka, Shinjuku, Tokyo 162-8601, Japan

^a Battery Development Lab., Asahi Chemical Industry, Co., Ltd., Kawasaki, Kanagawa 210-0863, Japan

Lithium manganese oxide spinel has been expected to be a candidate as a cathode material for lithium secondary batteries, however, it has a serious problem of the capacity fading. It is reported that the capacity fading is caused by Mn dissolution from LiMn_2O_4 cathode during cycling [1,2]. Determination of the Mn concentration in the electrolyte solution is essential to revealed the dissolution mechanism of the cathode. However, so far the sampling of the electrolyte solution has been made by disassembling the cell because a large amount of sample is necessary for chemical analysis such as inductively coupled plasma (ICP) atomic emission spectroscopy [3]. Total reflection X-ray fluorescence (TXRF) analysis is the most sensitive X-ray fluorescence technique, which requires a sample solution of as small as a few μl . We have applied this technique to monitor the concentration of Mn during the electrochemical cycling, because it enables us to collect electrolyte solution without disturbing the electrochemical reaction nor disassembling the cell.

In this study, an in-situ TXRF cell was developed and measurement conditions for TXRF analysis were optimized. Moreover, by applying this method, Mn dissolution behavior with charge-discharge cycle was clarified and variation of the Mn concentration in the cell were measured at 50 °C, 80 °C and room temperature.

We designed a glass beaker type electrochemical cell as shown in Fig. 1. A composite cathode was prepared by mixing $\text{Li}_{1-x}\text{Mn}_2\text{O}_4$ with graphite, acetylene black and PVDF which was coated on an Al foil. Li metal or graphite which was coated on a Cu foil was used as an anode. The electrolyte was 1M LiPF_6 dissolved in a mixture of ethylene carbonate (EC) and dimethyl carbonate (DMC). The ratio of EC to DMC was 2:1 by volume. The charge-discharge cycles were performed between 3.5-4.3 V at a current rate of 0.5 mA/cm^2 . Ten micro liters electrolyte solution was sampled by inserting a capillary with the outer diameter 0.35mm into the cell. The sample solution was incinerated at 1000 °C and dissolved by nitric acid. Then, 10 ppm Co solution was added to it as an internal standard. Finally, the sample solution was transferred to a sample holder of optically flat pyrex glass and was vacuum-dried for measurement.

The Mn concentrations in electrolyte were determined by TXRF analysis. Cu K_α X-ray from an X-ray tube was used as an excitation source, and, incident X-rays were monochromated by a $\text{LiF}(200)$ monochromator.

Figure 2 presents the variation of the capacity of the cell as a function of cycle number at room temperature. The arrows indicate sampling points for TXRF analysis. It was found that the sampling of 10 μl electrolyte solution did not affect on the cyclic

performance of the cell. Figure 3 shows a dependence of the Mn concentration on the cycle number at 50 °C and at room temperature. Mn concentration in the electrolyte solution increased with increasing the cycle number. Distribution of Mn concentration in the cell is measured and shown in Fig. 4. The concentration of the Mn was the highest at the center of the electrode. At the back of cathode and anode electrodes, almost the same values were obtained. This observation suggests that the dissolution of Mn occurs during the charge process followed by a diffusion in the cell. In this way, in situ determination of Mn concentration in the electrolyte has been successfully analyzed by using TXRF technique and the capillary technique.

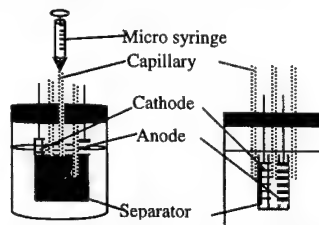
[1] G. Pistoia et al., *Electrochem. Acta*, 41 (1996) 2683.[2] Y. Xia et al., *J. Power Sources*, 66 (1997) 129.[3] D.H. Jang et al., *ibid.*, 143 (1996) 2201.

Fig. 1 Schematic illustration of the in situ cell for TXRF measurement.

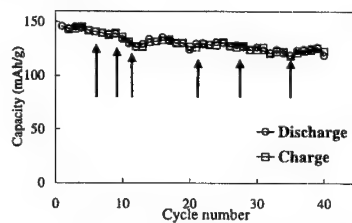


Fig. 2 Cycling behavior of the in situ cell.

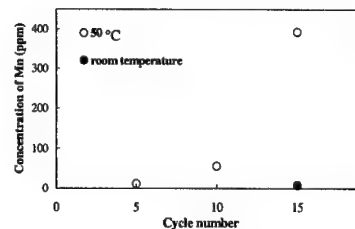


Fig. 3 The amount of Mn dissolution as a function of cycle number.

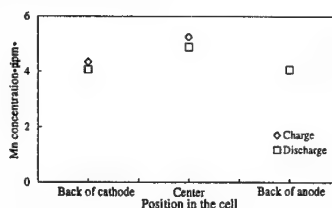


Fig. 4 Variation of the Mn concentration in the cell.

Lithium Ion Transport Through LiCoO₂ Thin-Film Electrode Under Intercalation-Induced Stress

Jong-Ki Lee, Seung-Joo Lee, Hong-Koo Baik* and Sung-Man Lee**

*Department of Metallurgical Engineering, Yonsei University, Seoul 120-749, Korea

**Department of Advanced Material Science and Engineering, Kangwon National University, Chuncheon 200-701, Korea

INTRODUCTION

Thin-film LiCoO₂ electrode as a cathode of Li secondary microbattery has been studied extensively due to its reversible storage capability for Li ion. Thin films without additives such as polymer binder and carbonaceous material have also received much attention from the viewpoint of investigating the intrinsic electrochemical properties of lithiated transition metal oxide [1-3].

The structure of LiCoO₂ consists of layers of lithium and cobalt atoms alternating each other that occupy the octahedral sites of a trigonal lattice (R-3m). Lithium ions can be intercalated and de-intercalated reversibly into and from these layers with a corresponding change of lattice parameters, in which the intercalation-induced stress is generated by the dimensional mismatch between regions having different Li concentrations.

There are two main driving forces which affecting the transport properties of Li ion through the oxide electrode *i.e.*, the concentration gradient and the stress gradient. Of these two factors, the stress gradient effect has been ignored as a trivial phenomenon.

In this study, we investigated the intercalation-induced stress gradient effect on the Li ion transport properties as a function of film thickness using the optical cantilever method.

EXPERIMENTAL

Thermally grown SiO₂ (about 2000 Å) on the (100) Si (total 100 µm thickness) was used as a substrate and its area for film deposition was 0.2 × 2 mm². The LiCoO₂ thin films were fabricated by r.f. magnetron sputtering with a stoichiometric LiCoO₂ target (2 inches in diameter). A 3000 Å Pt current collector was deposited prior to LiCoO₂ film deposition and a 300 Å Ti layer was incorporated between the substrate and Pt current collector in order to enhance the adhesion of Pt onto the SiO₂ surface. In order to obtain the desired structure, films were annealed at 800 °C in an oxygen atmosphere for 30 min with ±10 °C/min of heating and cooling rates.

The mechanical properties of LiCoO₂ thin-film cathode as a function of its thickness were investigated on an optical bench equipped with He-Ne laser beam source, splitter and linear position detector. Glass beaker-type cells were used to evaluate the electrochemical and mechanical properties of the LiCoO₂ cathodes. The cell consisted of lithium metal sheets as counter and reference electrodes and a LiCoO₂ film as a working electrode, and 1 M LiClO₄-PC electrolyte. The half-cell test was conducted at a constant voltage scan rate for cyclic voltammetry (CV) and constant current for charge-discharge experiments with a multichannel potentiogalvanostat. In order to measure the lithium ion diffusion coefficient in the thin-film LiCoO₂ cathode, the electrochemical impedance analysis (EIS) was

used

RESULTS AND DISCUSSION

The lattice parameter, *c*, and unit cell volume of LiCoO₂ increases linearly with decrease of Li concentration [4]. The changes in lattice parameter and volume generate intercalation-induced stress field between the regions having different Li concentration. The Li ion transport properties affected by the stress field gradient as well as the concentration gradient. Fig. 1 shows the deflection voltage variation associated with CV (scan rate = 1 mV/sec) of a LiCoO₂ thin-film electrode of 6000 Å thickness in the LiClO₄-PC electrolyte at room temperature.

The diffusion coefficient of Li ion through the thin-film LiCoO₂ cathode was a function of its thickness. The diffusion coefficient measured by EIS increases with the increase of film thickness at the same degree of Li concentration – at the same equilibrium potential. This phenomenon can be explained as a stress-field effect. The amount of stress generated by the intercalation process is not responsible for the variation of diffusion coefficient.

The stress variation for the samples with different thickness was measured by optical-cantilever method equipped with a He-Ne laser and linear position detector. The detailed experiments and results are proceeding. The results of this experiment would propose a very important criterion about the fabrication of thin-film electrode for the Li secondary microbattery.

REFERENCES

- [1] J. B. Bates, G. R. Gruzalski, N. J. Dudney, C. F. Luck and Xiaohua Yu, *Solid State Ionics*, **70/71**, 619 (1994)
- [2] Seung-Joo Lee, Jong-Ki Lee, Dae-Woo Kim, Hong-Koo Baik and Sung-Man Lee, *J. Electrochem. Soc.*, **143**, L268 (1996)
- [3] Jong-Ki Lee, Seung-Joo Lee, Hong-Koo Baik, Heon-Young Lee, Serk-Won Jang and Sung-Man Lee, *Electrochem. Solid-State Lett.*, **2** (10), 512-515 (1999)
- [4] Jan N. Reimers and J. R. Dahn, *J. Electrochem. Soc.*, **139**, 2091 (1992)

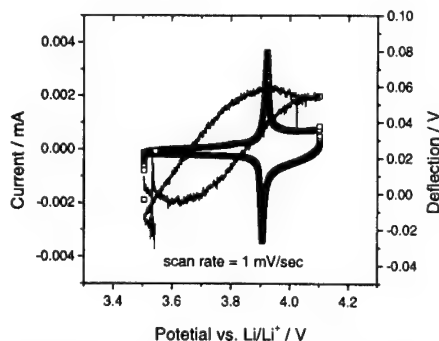


Fig. 1. Change in deflection voltage variation associated with CV of a LiCoO₂ thin-film cathode of 6000 Å thickness in the LiClO₄-PC electrolyte at room temperature.

Local Structure of Substituted Layered LiMnO_2 Cathode Materials Probed by X-ray Absorption Fine Structure and ^6Li Nuclear Magnetic Resonance

B. Ammundsen, J. Desilvestro, R. Steiner & P. Pickering
Pacific Lithium Ltd., P.O. Box 90725, Auckland, New Zealand

D. J. Jones & J. Rozière
Laboratoire des Agrégats Moléculaires et Matériaux
Inorganiques, CNRS ESA 5072, Université Montpellier 2, Place
Eugène Bataillon, Montpellier 34095 Cédex 5, France

Y. J. Lee, C. Pan & C. P. Grey
Department of Chemistry, State University of New York at Stony
Brook, Stony Brook, New York 11794-3400, U.S.A.

The formation and structural properties of layered LiMnO_2 cathode materials have recently been described for materials prepared by solid state processing, using Al or Cr to stabilise the $\alpha\text{-NaFeO}_2$ type structure [1]. For $0.05 < x \leq 0.1$, powder X-ray diffraction shows that the $\text{LiMn}_{1-x}\text{O}_2$ compounds have a well-ordered monoclinic crystal structure, with Al or Cr sharing the Mn sites and no detectable cation mixing between Mn and Li layers. Substitution therefore allows layered Li-Mn-O compounds to be obtained without the need for solution ion-exchange or hydrothermal methods of preparation.

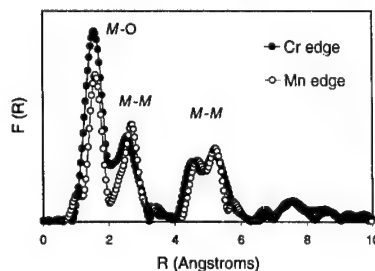
In order to better understand the effects of substitution in these materials, we have probed the local structures of Al- and Cr-substituted LiMnO_2 compounds by X-ray absorption fine structure (XAFS) spectroscopy at the Al, Cr and Mn *K*-edges. XAFS allows the local geometric and electronic structures with respect to the substituting element and Mn to be individually probed. In the case of Cr and Mn, detailed structural information can be obtained about the oxidation state of the ion and the distribution of nearest oxygen and transition metal neighbours. The data confirm that Cr and Mn occupy the same type of site in the compounds, but have different local coordination geometries in the first oxygen coordination shell and in the distribution of nearest-neighbour transition metal ions (see Fig. 1 for example of $\text{LiCr}_{0.1}\text{Mn}_{0.9}\text{O}_2$). The differences in local structure between Cr and Mn relate to a highly regular octahedral coordination around Cr ions, in contrast to a distorted octahedral environment around Mn ions due to the Jahn-Teller effect. Anomalous broadening of the $[2\ 0\ -1]$ diffraction lines in XRD of the monoclinic $\text{LiMn}_{1-x}\text{O}_2$ materials may arise from such local structural differences around atoms occupying the same crystallographic site.

XAFS data for cycled cathodes show significant modification of the local structure on the first charge, correlating with a phase change from monoclinic to hexagonal observed by powder X-ray diffraction. Al-substituted LiMnO_2 materials are known to undergo a structural transformation with cycling, and recent electron microscopy studies have shown the formation of small "ferroelastic" domains of spinel phase [2]. However, this process appears to be inhibited for materials modified by Cr. The changes which occur with removal and reinsertion of Li will be compared with data recorded recently for Cr-substituted spinel $\text{LiCr}_2\text{Mn}_2\text{O}_4$ [3].

Complementary structural and electronic information for the Cr-substituted materials has been obtained by probing

the Li local environment using solid state ^6Li magic angle spinning nuclear magnetic resonance spectroscopy. The ^6Li NMR spectra show a strong resonance characteristic of layered LiMnO_2 , and an additional resonance related to the Cr substitution (Fig. 2). Both resonances shift to higher frequency as the amount of Cr increases, indicating that the substitution perturbs the electronic structure and/or magnetic interactions of the Mn ions.

1. B. Ammundsen, J. Desilvestro, T. Grousto, D. Hassell, J.B. Metson, E. Regan, R. Steiner & P.J. Pickering, Abstract 138, 196th Meeting of the Electrochemical Society (1999).
2. H. Wang, Y.-I. Jang & Y.-M. Chiang, *Electrochem. Solid State Lett.* **2** (1999) 490.
3. B. Ammundsen, D. J. Jones, J. Rozière & F. Villain, *J. Phys. Chem. B* **102** (1998) 7939.



Mn-O	1.94 ± (% 4)	2.29 ± (% 2)
Cr-O	1.99 ± (% 6)	
Mn-M	2.82 ± (% 2)	3.05 ± (% 4)
Cr-M	2.81 ± (% 2)	2.97 ± (% 4)

Fig. 1: Fourier-transformed XAFS data at the Cr and Mn *K*-edges for layered $\text{LiCr}_{0.1}\text{Mn}_{0.9}\text{O}_2$, and interatomic distances (number of atoms at this distance in parentheses) determined from analysis of the XAFS data.

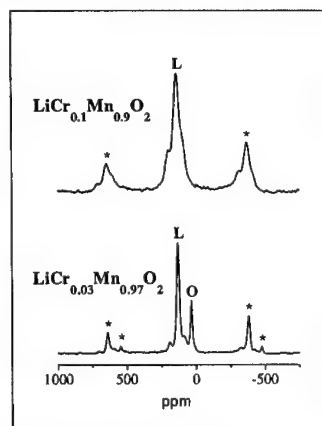


Fig. 2: ^6Li MAS NMR spectra of $\text{LiCr}_{0.1}\text{Mn}_{0.9}\text{O}_2$ and $\text{LiCr}_{0.03}\text{Mn}_{0.97}\text{O}_2$ acquired with a rotor-synchronized chemical-shift echo sequence ($\tau = 1$ rotor period) with spinning speeds of 15 kHz. The isotropic resonances of layered phase (L) and orthorhombic phase (O) are marked. * denotes spinning sidebands.

LiMoVO₆ – a Candidate Cathode Material for Solid-Polymer Batteries at Elevated Temperatures

Hikari Sakaebe, Masahiro Shikano, Yongyao Xia, and Tetsuo Sakai

Battery Section, Department for Energy Conversion,
Osaka National Research Institute, AIST
1-8-31 Midorigaoka, Ikeda, Osaka 563-8577, Japan

Tom Eriksson, Torbjörn Gustafsson, and Josh Thomas

Inorganic Chemistry, Ångström Laboratory, Uppsala
University, Box 538, SE-751 21 Uppsala, Sweden**Introduction**

A large number of vanadium compounds have been studied in a search for new, practicable cathode materials of lithium batteries, especially in conjunction with solid-polymer electrolytes. Brannerite-type LiMoVO₆ was first synthesized by Gary *et al.* [1]; it can be depicted as a "quasi-layered" structure with a capacity in excess of 250 mAh g⁻¹ between 1.5 and 3.8 V in a conventional lithium battery system [2,3]. In this study, rate properties of the LiMoVO₆ cell was investigated using a liquid electrolyte cell.

Experimental

LiMoVO₆ was prepared by solid state reaction of a stoichiometric mixture of Li₂CO₃, MoO₃ and V₂O₅ at 750-800 K. Its structure was determined by X-ray diffraction and Rietveld refinement using RIETAN97β software [4]. A liquid electrolyte cell was constructed from Li foil, a glass fiber separator soaked in electrolyte solution (1M LiBF₄; EC:DEC 2:1) and a cathode. These components were sealed into a plasticized Al "coffee-bag". The cathode mix (80 wt% LiMoVO₆, 15 wt% carbon black, and 5 wt% EPDM rubber dissolved in cyclohexane) was coated onto an Al current-collector. The solid-polymer battery was assembled by stacking cathode, polymer electrolyte (PEO-PEG), and Li foil. The cathode mixture (60 wt% LiMoVO₆, 8 wt% Ketjen Black, 8 wt% LiN(CF₃SO₂)₂, and 24 wt% PEG) was coated onto an Al current collector. Electrochemical properties were characterized mainly by galvanostatic discharge-charge testing between 1.5 and 3.8 V. Cycling was performed at room temperature, 40, and 80 deg.C for the liquid-electrolyte cell. The solid-polymer cell was cycled at 65 deg.C.

Results and Discussion

The rate dependence of the discharge-charge curves for the liquid-electrolyte cell, as shown in Fig.1, would suggest poor kinetics for Li insertion in LiMoVO₆ at room temperature. Fig. 2 illustrates the correlation between cell temperature and discharge-charge capacity for a current density fixed at 47.7 μA cm⁻² (41.7 mA g⁻¹-LiMoVO₆). These results clearly indicate that discharge capacity strongly depends on temperature, and that even a small increase in temperature (*ca.* 15 deg.C) above room temperature improves the discharge capacity greatly. At 80 deg.C, the discharge capacity increases to 310 mAh g⁻¹ and 256 mAh g⁻¹, respectively, for the first and the second cycles, corresponding to the insertion of 2.9 and 2.4Li per LiMoVO₆ unit.

At present, solid-polymer batteries generally require heating to enhance the Li-ion conductivity in the electrolyte. LiMoVO₆ would seem to have a clear advantage in this respect. LiMoVO₆ has also been evaluated as cathode material in a solid-polymer battery. Preliminary runs show a capacity of *ca.* 265 mAh g⁻¹ for the first discharge (at 20 mA g⁻¹) at 65 deg.C. Present cycling properties are inadequate for practical battery applications. This can be a result of degradation of the cathode composite at the end of the charge due to the presence of carbon black. Further optimization of the cell components and electrode composition are underway.

References

- [1] J. Gary *et al.*, *C. R. Acad. Sci., Fr.* **264**, 1477 (1967).
- [2] J.B. Goodenough *et al.*, *Denki Kagaku*, **66**, 1173 (1998).
- [3] M. Shikano *et al.*, *Abstracts of the 39th Battery Symposium in Japan*, 289 (1998). M. Shikano *et al.*, to be submitted to *Solid State Ionics*.
- [4] F. Izumi, *The Rietveld Method*, R. A. Young, Editor, Ch.13, Oxford University Press, Oxford (1993).

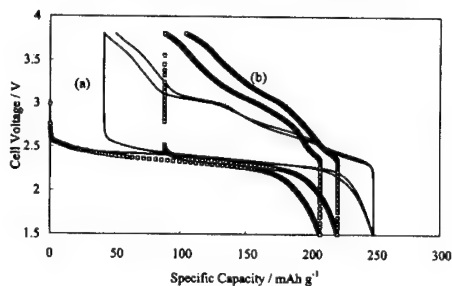


Fig. 1 Discharge-charge curves for LiMoVO₆ (1-2 cycle) at room temperature at current densities (a) 9.5 μA cm⁻² (8.3 mA g⁻¹) and (b) 47.7 μA cm⁻² (41.7 mA g⁻¹).

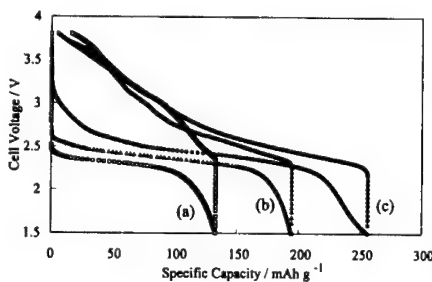


Fig. 2 Discharge-charge curves for LiMoVO₆ during the second cycle for current density 47.7 μA cm⁻² (41.7 mA g⁻¹) at: (a) room temperature; (b) 40 deg.C; and (c) 80 deg.C.

TE, TG and JOT acknowledge herewith support from NFR, NUTEK and The Swedish Environmental Strategic Foundation (MISTRA).

Structure, Phase Relationships and Transitions in Lithium Manganese Oxide Spinel

Ryoji KANNO, Masao YONEMURA, Yoji KAWAMOTO, Mitsuharu TABUCHI*, and Takashi KAMIYAMA**

Department of Chemistry, Faculty of Science, Kobe University, Nada, Kobe, Hyogo, 657-8501 Japan

*Osaka National Research Institute, 1-8-1, Midorigaoka, Ikeda, Osaka, 653-8577 Japan

**Institute of Materials Science, University of Tsukuba, Tsukuba, Ibaraki, 305-8673 Japan

Lithium manganese spinels are usually discussed in the triangle composition region of LiMn_2O_4 - $\text{Li}_4\text{Mn}_5\text{O}_{12}$ - $\text{Li}_2\text{Mn}_4\text{O}_9$. Changes in the Li/Mn ratio in $\text{Li}_{1+x}\text{Mn}_{2-x}\text{O}_4$ leads to the compositions along the tie line from LiMn_2O_4 to $\text{Li}_4\text{Mn}_5\text{O}_{12}$, and decreasing the heating temperature from 900°C varies the composition from LiMn_2O_4 towards $\text{Li}_2\text{Mn}_4\text{O}_9$. Oxygen vacancies have also been reported (1), however, the structures and the relation to the LiMn_2O_4 - $\text{Li}_4\text{Mn}_5\text{O}_{12}$ - $\text{Li}_2\text{Mn}_4\text{O}_9$ phase diagram are still ambiguous. In the present study, structures of the lithium manganese spinels synthesized at various synthesis conditions and Li/Mn ratio were determined by neutron powder diffraction at room temperature and low temperatures.

The neutron diffraction data were taken on a TOF diffractometer, VEGA and SIRIUS, at the KENS pulsed spallation neutron sources at KEK. The manganese spinels synthesized in this study were divided into four categories, oxygen deficient spinels, lithium-substituted spinels, cation deficient spinels, and the spinel close to the stoichiometric composition, LiMn_2O_4 .

Oxygen deficient spinels were synthesized at 750 - 900°C using Mn_2O_3 and Li_2CO_3 as starting materials. The ionic distribution of the spinels with a Li/Mn ratio of 0.5 were determined at 325K to be $(\text{Li}_{1-\delta}\text{Mn}_{2+\delta})_{\text{tet}}\text{O}_{4-\delta}$ ($0 < \delta < 0.18$) with a small amount of oxygen vacancy at 32e site. The oxygen vacancy decreased as the synthesis temperature was varied from 900 to 750°C. The oxygen vacancy increased from 0.132(12) to 0.276(16) after the spinel was treated under an evacuated tube using Ti metal.

The spinels close to the stoichiometric composition, LiMn_2O_4 , were obtained from the starting materials, MnO_2 obtained by the thermal decomposition of $\text{Mn}(\text{CH}_3\text{COO})_2$ and $\text{LiOH} \cdot \text{H}_2\text{O}$. The samples were heated at 470°C several times before being reacted at 750°C. The compositions determined by neutron diffraction measurements were close to the stoichiometric compositions.

Figure 1 shows the DSC curves of the oxygen deficient spinel A, ($\delta=0.132$) and the stoichiometric spinel B ($\delta=0$). The transitions were observed around 300 and 250K for the sample A and B, respectively, and the results are consistent with those reported by Sugiyama et. al (1)

Low-temperature structures of the oxygen deficient spinel with $\delta=0.132$ and a Li/Mn ratio of 0.5 were determined by a $3a \times 3a \times a$ orthorhombic superlattice structure(2) with oxygen vacancy model. There are five Mn sites, and the elongated Jahn-Teller axis of the trivalent manganese ions Mn1(8f), Mn4(16f),

and Mn5(16f) ordered along the z, x, and y direction, respectively, and the elongated axis of Mn5 increased with decreasing temperature (Fig. 2). The increase in the Jahn-Teller elongated axis of Mn5 site corresponds to the charge ordering process accompanying electron transfer from the Mn3 to Mn4 sites. The oxygen vacancy was ordered at one of nine oxygen sites.

The low temperature phase of the stoichiometric spinel has also an orthorhombic symmetry while the orthorhombic distortion is smaller than the oxygen vacancy spinel. The relationship between the compositions, structures, phase transitions, and electrochemical properties will be discussed.

REFERENCE

1. J. Sugiyama, T. Atsumi, A. Koiwai, T. Sasaki, T. Hioki, S. Noda, and N. Kamegashira, J. Phys.:Condens. Matter, 9, 1729 (1979).
2. G. Rousse, C. Masquelier, J. Rodriguez-Carvajal, and M. Hervieu, Electrochem. Solid-State Lett., 2, 6 (1999).

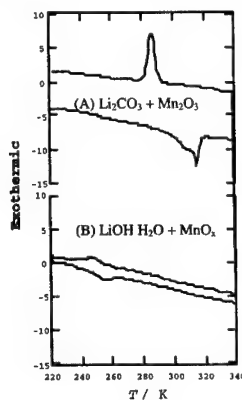


Fig. 1 The DSC curves of $\text{LiMn}_2\text{O}_{4-\delta}$.

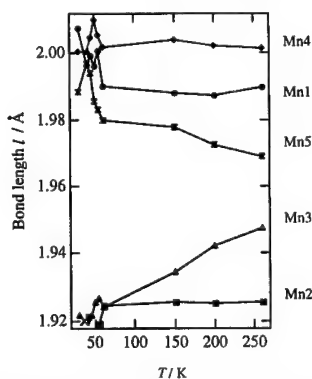


Fig. 2 Temperature dependence of the average Mn-O bond distances of five Mn sites in the low-temperature orthorhombic phase.

Storage and Cycling Performance of Stoichiometric Spinel at Elevated Temperatures

Xiaoqing WANG, Yoshin YAGI, Yongyao XIA[#],
Tetsuo SAKAI[#] and Masaki YOSHIO
Department of Applied Chemistry, Saga University,
Saga 840-8502, Japan
[#] Osaka National Research Institute, 1-8-31
Midorigaoka, Ikeda 563-8577, Japan

In the view of the economic and environmental advantages, there is no question that spinel $\text{Li}_x\text{Mn}_2\text{O}_4$ will be used as a cathode material for lithium-ion batteries instead of LiCoO_2 currently commercialized if the problem associated with the capacity fading on cycling and storage at the elevated temperature would be solved. We have demonstrated that both the change in the crystal structure and the dissolution of Mn into the electrolyte is major factors responsible for the capacity loss at the elevated temperature [1]. Recently, we found that the effects of both factors (structural change and Mn dissolution) on capacity fading are critically dependent on the operating temperature. We reported previously that capacity fading during cycling of the spinel electrode at room temperature occurred only in the high-voltage region and it was caused mainly by the unstable two-phase structure co-existing in this region for lithium ion insertion/extraction [2].

When cell was operated at the elevated temperature, capacity loss occurs in both regions.

Fig.1 (a) and (b) show the 4th and 50th charge/discharge profile of stoichiometric spinel at 50°C and 70°C, respectively. The capacity loss rate in the high and low voltage region depends on its operating temperature. The discharge capacity loss were found to be from 62 to 42 mAh/g in the high voltage region and from 66 to 52 mAh/g in low one at 50°C. The capacity retention in the high voltage region (65%) is much lower than that of low voltage region (79%). When cycled at 70°C, cell lost capacity from 53 to 32 mAh/g in the high voltage region and from 62 to 37 mAh/g in a low voltage region. The capacity retentions in both voltage regions are almost the same. We thereby speculate that the unstable two-phase structure co-existing for lithium ion insertion/extraction dominate the capacity fading during cycling at lower temperature, while Mn dissolution became major factor responsible for capacity fading at 70°C. It was confirmed that the capacity loss of stoichiometric spinel occurs mainly in high-voltage region even at the 60°C.

The capacity fading due to cycling or due to high temperature storage in the electrolyte would be commonly linked to Mn dissolution.

The solubility of stoichiometric spinel soaked in our highly purified electrolyte for 7 days were found to be 32.0, 60.7 and 592 ppM-Mn at 50°C, 60°C and 70°C, respectively.

Fig.1 (c) shows the typical charge/discharge curve of stoichiometric spinel, which was soaked in EC/DMC(LiPF_6) electrolyte for 2 weeks. This profile is strongly resembled to that of the 50th charge/discharge curve at 70°C.

Our tentative conclusion is as follows; At lower temperature (less Mn dissolution), the capacity loss mainly occurs in the unstable two phase structure coexisting (high voltage region). At high temperature, the capacity loss occurs in high and low voltage region both because of the spinel structure destruction due to the strong Mn dissolution. If the electrolyte were not so purified and thus Mn dissolution is high, then the capacity loss due to Mn dissolution would be dominant even at 50°C.

Detailed capacity fading mechanism will be discussed in the conference.

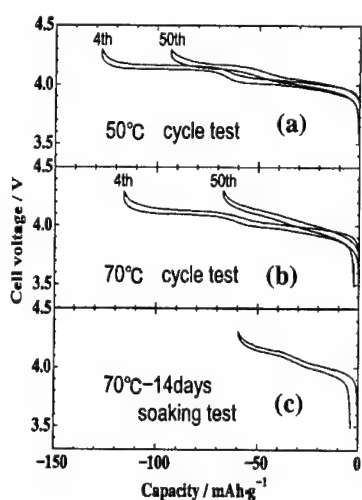


Fig.1. Typical charge/discharge profiles of stoichiometric spinel. (a) Cycling at 50°C and (b) at 70°C. (c) First room temperature charge/discharge profile of $\text{LiMn}_2\text{O}_4/\text{Li}$ cell after LiMn_2O_4 was soaked in a EC/DMC(1:2) electrolyte (LiPF_6) for 2 weeks.

Reference:

- 1) Y. Xia, Y. Zhou and M. Yoshio, J. Electrochem. Soc., 144, 2593 (1997)
- 2) Y. Xia and M. Yoshio, J. Electrochem. Soc., 127, 856 (1996).

Capacity Failure of Lithium Manganese Oxide Spinel Cathode at Elevated Temperature

Masaki Okada, Kunikazu Kamioka, Takashi Mouri
and Masaki Yoshio*

Nanyo Research Laboratories, TOSOH Corporation
4560, kaisei-cho, shin-nanyo, 746-8501, Japan

*Department of Applied Chemistry, Saga University
1, honjyoh, Saga, 840-8502, Japan

Introduction

Presently, much interest has been focused on applying lithium ion batteries for the electricity of power storage systems and hybrid electric vehicles (HEV) because of their high gravimetric and volumetric energy density. In these applications, lithium manganese oxide spinel compound ($\text{Li}_{1-x}\text{Mn}_2\text{O}_4$, $\text{Li}_{1-x}\text{M}_y\text{Mn}_{2-x-y}\text{O}_4$ M = transition metal, etc.) is the most promising alternatives as the cathode for lithium ion batteries, because of its low cost, less toxicity and material safety in the charge-state. One of the important problems for commercial use of it is the capacity failure at elevated temperature (1,2,3). In this work, we prepared the stored and cycled $\text{Li}_{1-x}\text{Mn}_2\text{O}_4$ at elevated temperature and examined their character change by XRD and chemical analysis to clarify the origin of the capacity failure.

Experimental

$\text{Li}_{1-x}\text{Mn}_2\text{O}_4$ samples were prepared by calcining a mixture of electrolytic manganese dioxide (EMD) and Li_2CO_3 . The prepared samples were characterized by XRD and chemical analysis. The XRD data were analyzed using RETAN94 of the Rietvelt program (4). The stored samples were prepared by soaking $\text{Li}_{1-x}\text{Mn}_2\text{O}_4$ in electrolyte solution and keeping for 4 days at 50°C or 85°C. The charge-discharge tests were carried out at constant current ($0.4\text{mA}\cdot\text{cm}^{-2}$) between 3.5V and 4.5V at room temperature (RT) or 50°C. The cathodes were consisted of 25mg of $\text{Li}_{1-x}\text{Mn}_2\text{O}_4$ and 12.5mg of teflonized acetylene black. The CR2032 type coin cells were constructed using the cathode, lithium metal as anode and 1M LiPF_6 EC-DMC(1:2 by volume) as electrolyte solution.

Results and Discussion

Figure 1 shows SEM images of the original and the stored $\text{Li}_{1.06}\text{Mn}_{1.94}\text{O}_4$. The surface morphology changed by the storage treatment at 85°C. From the result of chemical analysis of the filtered solution, Mn was detected. Figure 2 shows the cycle performance of the original $\text{Li}_{1.06}\text{Mn}_{1.94}\text{O}_4$ at RT and 50°C. Additionally, the cycling test results at 50°C of the stored samples was plotted. These samples exhibited the different performance for the capacity and the capacity failure on cycling. In order to understand the difference of the cycle performance, the analysis of crystal structure has been done. The results of XRD data analysis were summarized in Table I. It was found that the capacity failure increased with increase 8a site Mn occupancy in the original samples. It was suggested that Mn atom gradually migrated from 16d site to 8a site during the charge-discharge cycling at elevated temperature. From above results, we think that the capacity failure consists of two processes. One is the chemical change of surface condition with Mn dissolution bringing to large capacity failure. And another is the site occupancy change during charge-discharge cycling with Mn atom migration in the

crystal structure bringing to gradually capacity reduction. In the viewpoint of the crystal structure and chemical composition, the effect of the characters on the capacity failure will be discussed.

References

1. Yongyao Xia, Yunhong Zhou, Masaki Yoshio, J. Electrochem. Soc., 144, (1997), 2593.
2. G.G. Amatucci, A. Blye, C. Schmutz, J.M. Tarascon, Progress in Batteries and Battery Materials, 16, (1997), 1.
3. A. Du Pasquier, A. Blye, P. Courjal, G. Amatucci, B. Gerand and J-M Tarascon, J. Electrochem. Soc., 146, (1999), 428.
4. F. Izumi, "The Rietvelt Method", ed. by R.A. Young, Oxford Univ. Press, Oxford (1993), Chap.13.

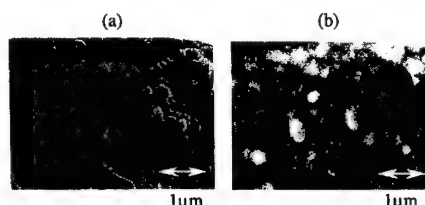


Fig.1. SEM images of (a) the original $\text{Li}_{1.06}\text{Mn}_{1.94}\text{O}_4$ and (b) after the stored $\text{Li}_{1.06}\text{Mn}_{1.94}\text{O}_4$ at 85°C.

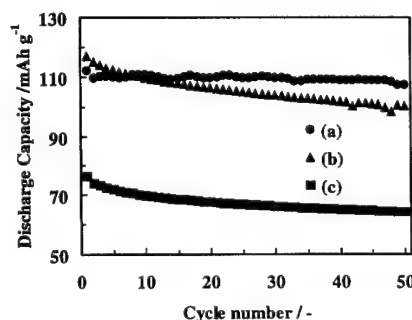


Fig.2. Cycle performance of (a) the original $\text{Li}_{1.06}\text{Mn}_{1.94}\text{O}_4$ at RT, (b) at 50°C and (c) at 50°C after stored sample at 85°C. The cells were cycled 4.5 and 3.5V at $0.4\text{mA}\cdot\text{cm}^{-2}$ using lithium metal as anode and 1M LiPF_6 EC-DMC(1:2 by volume) as electrolyte solution.

Table I. XRD data analysis of $\text{Li}_{1.06}\text{Mn}_{1.94}\text{O}_4$, after cycling test at RT and 50°C, and after stored at 85°C.

Sample	8a site occupancy, g		R_{wp} (%)
	(-)		
	8aLi	8aMn	
original ($\text{Li}_{1.06}\text{Mn}_{1.94}\text{O}_4$)	1.00	-	8.70
after cycling at RT	0.99	0.01	
after cycling at 50°C	0.93	0.07	7.93
after stored at 85°C	1.00	-	11.54

Calculation was made by assuming a space group $\text{Fd}3m$, 8a site; $\text{Li}+\text{Mn}=1.0$, 16d site; $\text{Li}+\text{Mn}=1.0$ and 32e site; $\text{O}=1.0$.

Abstract No. 229

SYNTHESIS AND CHARACTERIZATION OF LITHIUM
MANGANESE OXIDES FOR RECHARGEABLE 3 V
LITHIUM BATTERIES

A. Perner, M. Wohlfahrt-Mehrens, K. Holl*,
J. Garche, D. Ilie*

ZSW

Center for solar energy and hydrogen research,
Baden-Wuerttemberg
Helmholtzstrasse 8, D-89081 Ulm

*VARTA

Gerätebatterie GmbH
Daimlerstrasse 1
D-73479 Ellwangen

The structural and electrochemical properties of different lithiated α - MnO_2 have been studied for use as positive materials in 3 V rechargeable lithium cells. It is observed, that stabilizing foreign phases and the water content of the samples influences the obtained discharge capacities as well as the cycling performance.

X-ray diffraction studies show, that either a $\text{Li}_2\text{O} \cdot \text{MnO}_2$ phase or a Ramsdellite- MnO_2 phase stabilize the α - MnO_2 structure of these materials and provide better rechargeability.

Furthermore the presentation will discuss the relationship between the cycling behavior and the water content, measured by thermogravimetric analysis, within the large [2*2] channels of the α - MnO_2 structure. With the $\text{Li}_2\text{O} \cdot \text{MnO}_2$ stabilized α - Li_2MnO_2 , the water can be replaced by Li_2O and stabilize the framework structure. It was found, that lower water content leads to excellent cycling behavior over several hundreds of cycles.

Abstract No. 230

MALDI-MS Spectroscopic Analysis of Products on
 LiMn_2O_4 Electrode

Tsuyoshi Fukushima, Yoshiharu Matsuda, Tsutomu
Abura and Ryuichi Arakawa

Department of Applied chemistry, Faculty of
Engineering and High Technology Research Center,
Kansai University, Yamate-cho 3-3-35, Suita, Osaka 564-
8680, Japan

The possibility of chemical and electrochemical reactions between a positive electrode and an electrolyte solution in rechargeable lithium batteries has been reported in a few reports^(1,2). However the film formation on the positive electrodes has not been presented. At the present work, MALDI-MS spectroscopic analysis (Matrix Assisted Laser Desorption Ionization - Mass Spectrometry) was introduced to clarify the change of materials on LiMn_2O_4 electrode during the charge-discharge cycling.

Electrolyte solutions were 1mol/L LiPF_6 /EC (ethylene carbonate)-DMC (dimethyl carbonate) (1:1 vol) and 1mol/L LiPF_6 /EC (ethylene carbonate)-DEC (diethyl carbonate) (1:1 vol). A test cell was two electrodes cell and a working electrode was a tablet (diameter 12mm) of mixture of LiMn_2O_4 (25mg) and carbon powder - PVDF composite (25mg). A counter electrode was a lithium electrode with large surface area. The current density of the cycling was 0.4 mA/cm² and the potential range was between 3.5 and 4.3V. MALDI-MS measurement was applied to the positives or the thin layer chromatographically separated materials from the positive electrode.

The MALDI-MS measurement showed some peaks between 100 and 620 Mass (m/z) on the spectrogram of the charge-discharge cycled positives in EC-DMC containing 1mol/L LiPF_6 . These results would suggest that the reactions which included polymerization among the lithium salts, solvents and electrode proceeded on the positive electrode surface and the reaction products existed on the electrode. However the peaks on the spectrogram of the cycled positives in EC-DEC containing 1mol/L LiPF_6 were scarcely observed.

References

- [1] D.Aurbach, 9th Internat. Meeting on Lithium Batteries, Abst. Oral. 1, 14th July (1998)
- [2] M.Kato, S.Kanamura, and Z.Ogumi, 39th Battery Symposium in Japan, Abst. 3C05, 27th November (1998)

Abstract No. 231

Effect of Aluminum Addition in Co Substituted Ni Oxide Cathodes

Motoya Kanda, Yoshinao Tatebayashi, Masahiro Sekino, Yoshiyuki Isozaki and Iwao Mitsuishi

Power Supply Materials & Devices Laboratory,
R&D Center, Toshiba Corporation
72 Horikawa-cho, Saiwai-ku, Kawasaki 212-8572
JAPAN

E-mai/motoya.kanda@toshiba.co.jp

1. INTRODUCTION

Lithium nickel oxide (LiNiO_2) is one of the most promising positive materials for lithium ion batteries because of its high capacity and low cost. However, the material shows rather poorer cycle performance, lower first cycle charge-discharge efficiency and thermally less stable behavior than that of LiCoO_2 .¹⁾

We have improved the cycle performance and first cycle charge-discharge efficiency of LiNiO_2 by substituting for Ni with Co and have found that the suitable content of Co in LiNiO_2 was around 30-15%. For example, the material $\text{LiNi}_{0.81}\text{Co}_{0.19}\text{O}_2$ (19% of Ni was substituted with Co) showed 185mAh/g as the initial capacity and 90% as the first cycle efficiency (140mAh/g, 95% for LiCoO_2 and 200mAh, 85% for LiNiO_2). We have fabricated cylindrical cells with this material as positive electrodes and showed that they had about 20% higher capacity and the same degree of safety in overcharge tests as compared to the cells with LiCoO_2 as positive electrodes²⁾.

However, at the same time we found that the safety concerning nail-penetrating tests was not ensured with those cells, because in this case the cell temperature should reach very quickly to the decomposition temperature of the positive materials used in those cells.

Therefore, we have tried to improve the thermal decomposition behavior of Co substituted Ni oxide cathode materials by additional substitution for Ni with Aluminum (Al).

2. EXPERIMENTAL

The positive materials prepared were $\text{LiNi}_{1-0.2-x}\text{Co}_{0.2}\text{Al}_x\text{O}_2$, which were typically synthesized with a heat-treatment at 700°C under oxygen atmosphere with hydroxides containing Ni, Co and Al in the designed molar contents. These hydroxides were fabricated with co-precipitation method by adding NaOH solution into Ni, Co and Al sulfuric salt containing solutions.

The materials were mixed with acetylene black (AB) and binders (PTFE or PVdF) and kneaded with an NMP as pasting solutions to make compounds. Each compound was coated on an aluminum foil and dried and pressed to compose a sheet for positive electrode.

A part of electrode thus fabricated was put in a half-cell containing electrolyte of EC/MEC (1:2) with 1M-LiPF₆ and charged in CCCV to 4.4V vs. Li reference electrode. Then, the electrode was disassembled and washed with MEC and dried. The sample thus obtained was analyzed with a DSC.

The coated sheets were assembled as positive electrodes of 18650 type cylindrical cells. The carbon material of negative electrodes used was graphite MCF (mesophase pitch-based carbon fiber). Separators used were polyethylene with 25-micron thickness. The electrolytes were the same as used in the half-cells.

3. RESULTS and DISCUSSION

Figure 1 shows the thermal behaviors of the Al added Co-substituted Ni oxide materials, which were charged until 4.4V vs. Li reference electrode. We can see that the peak temperature of thermal decomposition was increased from 220°C at $x=0$ to 250°C at $x=0.107$.

Figure 2 shows the temperature changes at nail-penetrating test of the 18650 cells with $\text{LiNi}_{0.80}\text{Co}_{0.20}\text{O}_2$ and $\text{LiNi}_{0.717}\text{Co}_{0.20}\text{Al}_{0.083}\text{O}_2$ positive electrodes. The capacities of the cells were 1700 and 1600 mAh, respectively. Before conducting the tests, the cells were charged in condition of CCCV until 4.2V at 0.3C rate. The cell with $\text{LiNi}_{0.717}\text{Co}_{0.20}\text{Al}_{0.083}\text{O}_2$ positive electrode showed only electrolyte leakage and temperature rise was suppressed under 100°C by this test, while cell with $\text{LiNi}_{0.81}\text{Co}_{0.19}\text{O}_2$ positive electrode reached over 300°C and caught fire.

Therefore, it is clear that Al addition to Co-substituted Ni oxide materials is effective in raising the thermal decomposition temperature of the material and it contributes to the improvement of cell safety in the nail-penetrating tests.

ACKNOWLEDGEMENTS

A part of this work was performed under the financial support of the New Energy and Industrial Technology Development Organization (NEDO) of Japan.

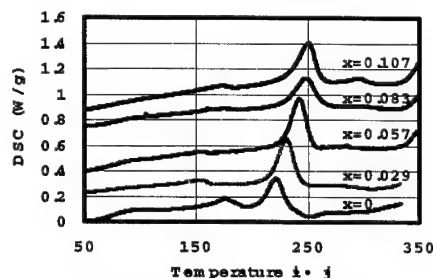
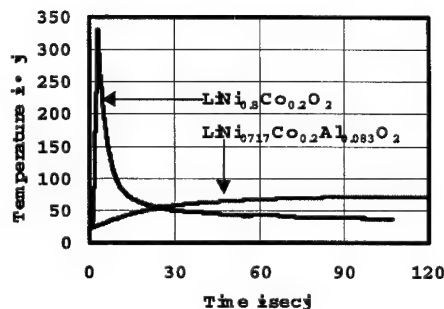


Fig.1 DSC curves of $\text{LiNi}_{1-0.2-x}\text{Co}_{0.2}\text{Al}_x\text{O}_2$

Fig.2 Nail-penetrating test results of the cells with $\text{LiNi}_{1-0.2-x}\text{Co}_{0.2}\text{Al}_x\text{O}_2$ positive electrodes

REFERENCES

- 1) H.Arai, S.Okada, H.Ohtsuka, M.Ichimura and J.Yamaki, *Solid State Ionics*, **80**, 261(1995).
- 2) M.Kanda, M.Sekino, A.Satoh, N.Matsuda and S.Arai, *Extended Abstract of IMLB9*, Poster III, Fri37(1998).



Cathode Properties of Phospho-olivine LiMPO_4 for Lithium Secondary Batteries

Shigeto OKADA, Syoichiro SAWA,
Minato EGASHIRA, Jun-ichi YAMAKI

IAMS, Kyushu University
6-1 Kasuga Kohen, Kasuga, 816-8580 Japan

Mitsuharu TABUCHI, Hiroyuki KAGEYAMA
Osaka National Research Institute, AIST,
1-8-31, Midorigaoka, Ikeda, Osaka, 563-8577 Japan

Tokuo KONISHI, Akira YOSHINO
Asahi Chemical Industry Co., Ltd.,
2-1, Samejima, Fuji, Shizuoka, 416-8501 Japan

Fey's paper on LiNiVO_4 [1] prompted the discovery of several high-voltage cathodes. However, they consist only of normal spinel and inverse spinel structure oxides and their reported capacities over 4.5 V vs. Li/Li^+ are less than 100 mAh/g.

We anticipated that ordered olivine LiMPO_4 would be a new high-voltage cathode candidate with superior capacity. The analogies and differences among their structures are summarized in Table 1. They can all be represented by the same formula $\text{LiMM}'\text{O}_4$ in which half the octahedral sites and one-eighth of the tetrahedral sites are occupied by cations. Unlike the normal spinel and inverse spinel structures with a cubic closed packed (ccp) oxygen framework, ordered olivine has a hexagonal closed-packed (hcp) oxygen array. In contrast, inverse spinel and olivine structure both have octahedral Li sites in their matrix.

In inverse spinel LiMVO_4 , Li and M randomly occupy the 16d octahedral site. M ions at the 16d site disturb Li conduction through the 16d - 8b - 16d path in an inverse spinel, while there is no obstacle cation except Li itself on the 16c - 8a - 16c diffusion path in a normal spinel.

However, in olivine, two types of octahedral site are crystallographically distinct and differ in size. The ordered olivine has orthorhombic symmetry with alternate *a-c* planes of Li and M occupying the octahedral sites, which makes the two dimensional Li diffusion paths possible between the hcp oxygen layers.

All four types of phospho-olivine LiMPO_4 (M: Co, Ni, Mn and Fe) that we obtained using the solid state reaction technique were indexed as orthorhombic in the space group Pmnb.

Of these investigated olivine cathodes, LiCoPO_4 exhibited the highest 4.8 V discharge plateau of 100 mAh/g vs. Li/Li^+ after initial charging to 5.1 V and its energy density was comparable to that of LiCoO_2 (120 mAh/g \times 4 V = 480 mWh/g) as shown in Fig.1.

During charging to 5.1 V, there were no other phases except Pmnb and the lattice constants *a* and *b* decreased, while *c* increased (Fig.2). This behavior is in good agreement with that of LiFePO_4 during chemical delithiation [5]. The cell volume change ratio ($\Delta V/V$) of LiCoPO_4 during the charging process was less than -5%.

In contrast, LiNiPO_4 and LiMnPO_4 did not show any voltage plateaus in their discharge profile even after initial charging to 5.2 V. In addition, we could not detect any reduction peaks in cyclic voltammogram of LiNiPO_4 between 3 and 5.5 V.

As shown in Fig.3, the rate capability of LiCoPO_4 seems to be better than that of LiFePO_4 . However, there is considerable room for improvement up to the theoretical upper limit of about 167 mAh/g for 1 Li per LiCoPO_4 .

References

1. G.Fey, W.Li and J.R.Dahn, *J.Electrochem.Soc.*, **141**, (1994) 2279.
2. H.Kawai, M.Nagata, H.Tsukamoto and A.R.West, *Electrochem. and Solid-State Letters*, **1**, (1998) 212.
3. S.Okada, H.Arai and J.Yamaki, *DENKI KAGAKU*, **65**, (1997) 802.
4. K.Amine, H.Yasuda and M.Yamachi, *ECS Meeting Abstracts*, 99-2, (1999) #277.
5. A.K.Padhi, K.S.Nanjundaswamy and J.B.Goodenough, *J.Electrochem.Soc.*, **144**, (1997) 1188.

Table 1. Typical High-voltage Cathodes over 4.5 V.

Structure	Spinel	Inverse spinel	Olivine
Symmetry	Cubic	Cubic	Orthorhombic
Space Group	Fd3m	Fd3m	Pmnb
Li site	Tetrahedral(8a)	Octahedral(16d)	Octahedral(4a)
Framework	ccp	ccp	hcp
Example	LiCoMnO_4	LiNiVO_4	LiCoPO_4
References	[2]	[1]	[3, 4]

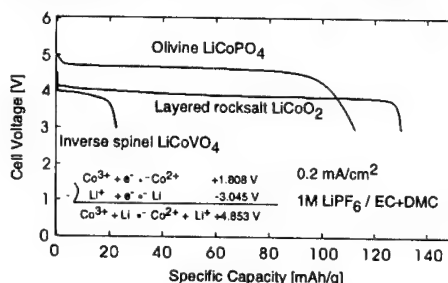


Fig. 1 First discharge profiles of Co-based high-voltage cathodes.

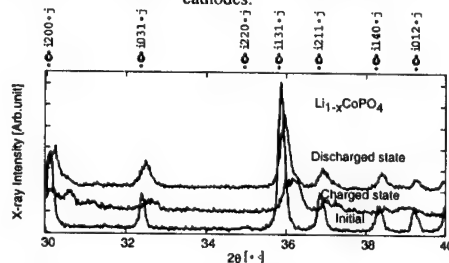
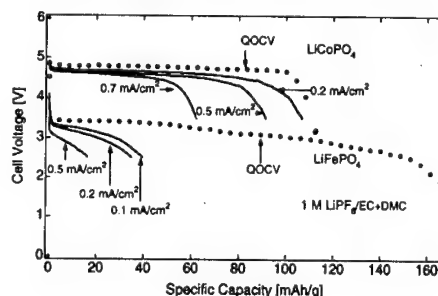


Fig. 2 Lattice behavior of LiCoPO_4 on the 1st charge-discharge cycle between 3.5 V and 5.1 V.

Fig. 3 Rate capability of LiCoPO_4 and LiFePO_4 .



Soft-Combustion Synthesis of a New Cathode-active Material, LiVWO_6 , for High Voltage Lithium-Ion Batteries

S.R. Sahaya Prabakaran¹, Chang Cheng Pei², Ahmad Fauzi² and M. Siluvai Michael³

¹ Center for Smart Systems and Innovation, Faculty of Engineering, Multimedia University, 63100 Cyberjaya, Selangore, Malaysia.

² School of Materials Engineering, Universiti Sains Malaysia, 31750 Tronoh, Perak D.R., Malaysia

³ Advanced Materials Research Center, SIRIM Bhd., 40911 Shah Alam, Selangore, Malaysia.

Transition metal oxides have been evaluated extensively in the past as cathode materials for lithium-ion cells. Lithium-Ion technology makes use of insertion compounds at both the anode and cathode of electrochemical cells. Candidate materials extensively investigated for positive electrodes include LiCoO_2 , LiNiO_2 , $\text{LiNi}_x\text{Co}_x\text{O}_2$, spinel LiMn_2O_4 , etc. In view of several environmental factors and also in the perspective of high yield in terms of capacity/high voltage, newer materials are being introduced recently [1,2]. We report here yet another new material, brannerite- LiVWO_6 , as cathode-active materials for 4-volt class category. We have synthesized this material using our proprietary technique recently announced [1]. We also report here the preliminary structural and electrochemical properties of the above material, LiVWO_6 in a lithium-containing cells under flooded electrolyte environment. This material behaves similar to its analogous materials, LiVMoO_6 reported by us recently [2].

LiVWO_6 crystallizes in brannerite structure of AB_2O_6 type [3,4], having a general formula $\text{LiM}'_2\text{O}_6$ (M' = transition metals) with lattice parameters $a = 9.347 \text{ \AA}$, $b = 3.670 \text{ \AA}$, $c = 6.593 \text{ \AA}$, $\beta = 111^\circ 50'$ [4]. Owing to its structural characteristics (Fig.1), it is predicted that this material could possibly be used as a high voltage intercalation material for Li-Ion battery applications. This paper presents our success in synthesizing this new material through a low temperature soft-combustion technique and its redox behaviour was investigated in lithium-containing electrochemical test cells.

LiVWO_6 was synthesized following the procedure described for LiVMoO_6 [2]. For tungstate counterpart, ammonium tungstate was used. Figure 2 illustrates the submicronic nature of grains synthesized/annealed ($560^\circ\text{C}/1 \text{ hr}$) product of LiVWO_6 . Figure 3 presents the galvanostatic first charge/discharge curve of the product against lithium counter electrode. The details will be presented.

References:

1. S.R.S. Prabakaran, M.S. Michael, S. Radhakrishna, C.Julien, J. Mater. Chem., 7(9), 1791 (1997)
2. M.S. Michael, Ahmad Fauzi, S.R.S. Prabakaran, Int. J. Inorg. Mater., 1, (1999)
3. R.Ruh, A.D. Wadsley, Acta Crystallagr., 21, 974 (1996)
4. J. Glay et al., J. Inorg. Nucl. Chem., 33, 2403 (1971)

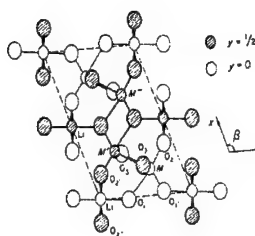


Fig.1: Structure of LiVWO_6 projected in the (010) plane



Fig.2: Typical SEM micrograph of LiVWO_6 synthesised powder showing the submicrometer grains.

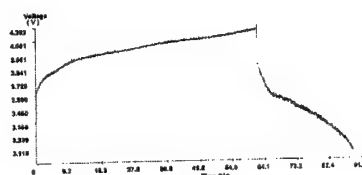


Fig.3: Typical first charge/discharge galvanostatic curve of Li/LiVWO_6

Electrochemical Characterization of a New High Capacity Cathode

C. Storey, I. Kargina, Y. Grincourt & I. J. Davidson
*Institute for Chemical Process and Environmental
 Technology, National Research Council,
 Ottawa, Ontario, K1A 0R6, Canada*

Y. Yoo and D. Y. Seung
*Samsung Advanced Institute of Technology,
 P.O. Box 111, Suwon, Korea, 440-600*

ABSTRACT

Although LiCoO_2 is extremely well suited for use in cathodes of lithium ion batteries, the high cost of batteries based on LiCoO_2 precludes their use in large scale or modestly priced applications. Cathodes based on LiMn_2O_4 provide a lower cost alternative, but suffer from lesser capacity and difficulties with capacity retention at elevated temperatures. Cathodes made from LiNiO_2 alone, or as a solid solution with LiCoO_2 , have attractive capacities but concerns about their safety persist. Consequently, there is still a need for improved cathode materials.

The ideal cathode material will combine low cost with the desirable performance characteristics of high capacity, good rate capabilities and long cycle life. Recently, we have developed a series of improved cathode materials that show considerable promise at meeting at least the first of these requirements. Details of the electrochemical performance of these materials will be presented in this paper.

For the initial characterization the materials were evaluated in 2325 size coin cells with metallic lithium anodes and LiPF_6 electrolyte. The cells were cycled between voltage limits of 2.5 and 4.5 volts at current densities ranging from 3.6 to 28.8 mA/g. The discharge voltage profiles for the first discharge of cells tested at the various rates are shown in figure 1. The average output voltage falls between 3.4 to 3.5 volts. In the preliminary evaluation, the specific capacities were quite rate dependent varying with the rate from 160 to 220 mAh/g. The capacity retention over the first 50 cycles, shown in figure 2, was quite good over the range of current densities. The stability of the discharge voltage profiles over the first 45 cycles is illustrated in figure 3 for the cell cycled at 30 mA/g.

The newly developed cathode materials show quite encouraging reversibility and specific capacities, but further improvement in their higher rate performance is required.

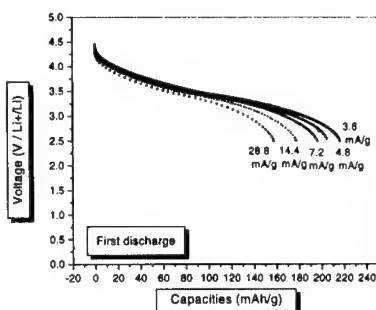


Fig.1 Voltage discharge profiles of new cathode material for the first cycle at 3.6, 4.8, 7.2, 14.4 and 28.8 mA/g

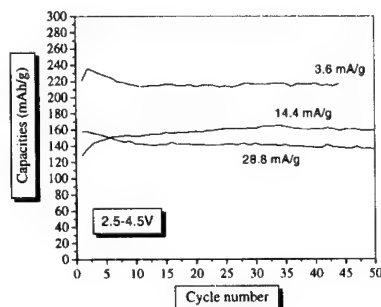


Fig. 2 Capacity retention plots of lithium half-cells with improved cathodes at indicated current densities.

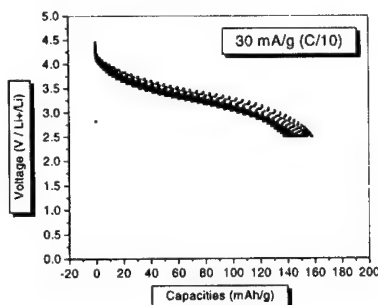


Fig.3 Evolution of the discharge voltage profile over 45 cycles for a lithium half-cell cycled between 2.5-4.5V at 30 mA/g.

Continuous Production of Cathode Materials for Lithium Batteries by Hydrothermal Synthesis under Supercritical Condition

Yukiya Hakuta*, Tadafumi Adschiri*, Kiyoshi Kanamura**, Kunio Arai*,

*Department of Chemical Engineering, Tohoku University, Aoba 07 Aramaki, 980-8579 Sendai, Japan

**Department of Applied Chemistry, Tokyo Metropolitan University, 1-1 Minami-Ohsawa, Hachioji, 192-0397 Tokyo, Japan

Hydrothermal crystallization (metal oxide formation from metal salt solution) is typically used at temperatures ranging from 373 to 474 K. We are developing a new process of hydrothermal crystallization method that uses supercritical conditions[1-7]. The supercritical state allows one to vary reaction rate and reaction equilibrium by shifting the dielectric constant and solvent density with pressure and temperature. In a series of fundamental studies, the specific features of this method were found to be as follows: ultrafine particles could be produced, morphology of the produced particles could be controlled by a little change of pressure and/or temperature, and reducing or oxidizing atmosphere could be controlled by introducing gases (O₂, H₂ etc.)[1].

Recently, we applied this method for the continuous production of highly functional materials including barium hexaferrite magnetic particles and YAG/Tb phosphor fine particles, LiCoO₂. In this paper, some typical results were demonstrated to show the key features of our proposed method. Especially, for the production of LiCoO₂ fine particles for a cathode material of rechargeable lithium ion batteries, details of the experimental results were explained. For a high electrochemical performance, smaller particle size is required for LiCoO₂. However, it is difficult to reduce the particle size down to a sub-micron order by conventional solid state reactions followed by comminution steps. For liquid phase synthesis methods, where Co²⁺ ion is a starting species, the oxidation conditions for Co²⁺ does not always match that required for the crystallization atmosphere. By using the supercritical hydrothermal synthesis method, we thought, ultrafine particles could be produced and the effective oxidation of Co²⁺ with O₂ could take place since a homogeneous reaction atmosphere is formed between O₂ and aqueous solutions under supercritical conditions. Thus the latter part of this paper is to provide a few examples regarding new applications for producing double oxides.

LiOH and Co(NO₃)₂ were used as starting materials. Feed aqueous solutions were prepared by dissolving each metal salt into distilled water. Aqueous KOH solution was used for adjusting a pH of solutions.

The schematic diagram for the experimental apparatus is shown in Figure 1. For oxidizing Co²⁺ in the reaction atmosphere, O₂ was introduced into the reactor after decomposing aqueous H₂O₂ solution. Aqueous Co(NO₃)₂ solution (0.02M) was first mixed with aqueous LiOH solution (0.4M) at a mixing point, MP1. The mixed solution of LiOH and Co(NO₃)₂ was contacted with a supercritical water-oxygen mixture fed from another line at a mixing point, MP2. At this mixing point, solutions were rapidly heated up to the reaction temperature (573, 623, or 673 K) and hydrothermal reaction occurred. The solution with formed particles was decompressed by a back-pressure regulator after the cooling. Particles recovered were washed several times with distilled water and then dried in an oven at 333K for 24 hours. Crystal structure of products was identified by a powder X-ray diffraction method (XRD).

Table I summarizes experimental conditions and results. It was found that LiCoO₂ were synthesized under a higher pH and a higher Li/Co molar ratios. Figure 2 shows XRD patterns for the particles of run 3. This figure indicates that LiCoO₂ particles were produced in a single phase at 673K, 30MPa. However, at 573K(run1) or at 623K(run2), Co₃O₄ was produced. Thus, at supercritical conditions, more effective oxidation of Co²⁺ took place than at 573K or 623K. One reason why the oxidation atmosphere at 673K is effective is probably due to the formation of the homogeneous reaction atmosphere of the solution and oxygen gas.

The electrochemical characterization was performed by a constant current discharge and charge test. The small decrease

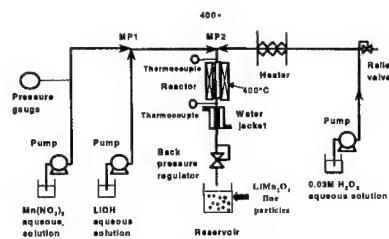


Figure 1. Experimental Apparatus

Table I. Experimental conditions and products.
([Co(NO₃)₂] = 0.02M, Pressure = 30MPa)

Run No.	LiOH M	KOH M	Temp. K	Products*
1	0.40	0	573	Co ₃ O ₄
2	0.40	0	623	Co ₃ O ₄
3	0.40	0	673	LiCoO ₂
4	0.10	0	673	Co ₃ O ₄
5	0.15	0	673	Co ₃ O ₄ (LiCoO ₂)
6	0.20	0	673	Co ₃ O ₄ (LiCoO ₂)
7	0.40	0	673	LiCoO ₂
8	1.0	0	673	LiCoO ₂
9	0.20	0.8	673	LiCoO ₂ (Co ₃ O ₄)
10	0.40	0.6	673	LiCoO ₂ , Co ₃ O ₄

*: Bracketed species indicate minor product

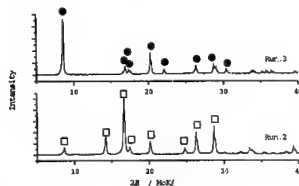


Figure 2. XRD profiles of particles obtained. (●: LiCoO₂; ○: Co₃O₄) in the discharge capacity suggests high stability of LiCoO₂ prepared by this method.

- 1). Adschiri, T., Kanazawa, K., and Arai, K., J. Am. Ceram. Soc., 75, 1019(1992).
- 2). Adschiri, T., Kanazawa, K., and Arai, K., J. Am. Ceram. Soc., 75, 2615(1992).
- 3). Hakuta, Y., Terayama, H., Onai, S., Adschiri, T. and Arai, K., J. Mater. Sci. Lett., 17, 1211(1998).
- 4). Hakuta, Y., Onai, S., Adschiri, T. and Arai, K., Proc. Int. Sympo. Supercrit. Fluids, B, 255(1997).
- 5). Hakuta, Y., Adschiri, T., Hirakoso, H., and Arai, K., Fluid Phase Equilibria, 158-160, 733 (1999).
- 6). Hakuta, Y., Adschiri, T., Suzuki, T., Seino, K., Arai, K., J. Am. Ceram. Soc., 81(9), 2461(1998).
- 7). Hakuta, Y., Seino, K., Ura, H., Adschiri, T., Takizawa, H., Arai, K., J. Mater. Chem., 9(10), 2671(1999).

Synthesis, Structure, and Charge-Discharge Characteristics of the New Layered Oxides $\text{Li}_{1.8}\text{Ir}_x\text{M}_{0.8-x}\text{O}_3$ ($M=\text{Fe}, \text{Co}, \text{Ni}$)

H. Kobayashi, M. Waki*, Y. Uebou**, M. Tabuchi, H. Kageyama, Y. Takigawa*, Y. Yamamoto**, M. Matsuoka**, J. Tamaki**

Osaka National Research Institute, AIST, MITI, Ikeda, Osaka, 563-8577 Japan

*Department of Electronics, Faculty of Engineering, Osaka Electro-Communication Univ., Neyagawa, Osaka, 572-8530 Japan

**Department of Chemistry, Faculty of Science and Engineering, Ritsumeikan Univ., Kusatsu, Shiga, 525-8577 Japan

Introduction

Li_2MO_3 ($M=\text{Ru}, \text{Ir}, \text{Pt}, \text{Mo}$) have a cubic close-packed oxide-ion lattice with basal planes of octahedral interstices filled alternately by Li^+ only and by $1/3\text{Li}^+$, $2/3\text{M}^{3+}$. The layered Li sites which are nearly identical to the $\alpha\text{-NaFeO}_2$ structure might allow reversible electrochemical extraction with fast electrode kinetics (1,2). Of these compounds, the $\text{Li/Li}_2\text{RuO}_3$ cell showed good reversibility with the cycle capacity of 160 mAh/g (3). We reported the structural studies of systematic substitution of Fe for Ru in Li_2RuO_3 and clarified that this substitution caused structural change from monoclinic to rhombohedral symmetry (4). However, the mechanism of delithiation from Fe-doped Li_2RuO_3 was not clarified. In this study, Fe-doped Li_2IrO_3 that was substituted by Fe for Ir in Li_2IrO_3 was synthesized and characterized by X-ray Rietveld analysis. Their electrochemical properties were investigated and delithiation mechanism was discussed. Further, Co- and Ni-doped Li_2IrO_3 was synthesized and their crystal structure, electrochemical properties, and delithiation mechanism were also investigated.

Experimental

$\text{Li}_2\text{Ir}_x\text{M}_{0.8-x}\text{O}_3$ ($M=\text{Fe}, \text{Co}, \text{Ni}$) (Nominal composition) was synthesized from appropriate molar ratios of Li_2CO_3 , Fe_2O_3 , Co_2O_3 , NiO , and IrO_2 at 1223-1373 K for 24-96 h in air. Samples obtained were characterized by XRD, magnetic, and ^{57}Fe Mössbauer measurements. Crystal structure was determined by X-ray Rietveld analysis. Electrochemical tests were carried out with a coin-type configuration. The electrolyte used was 1M LiClO_4 and 1M LiPF_6 in EC:DMC(1:1).

Results and discussion

Single phase $\text{Li}_2\text{Ir}_{0.8}\text{Fe}_{0.2}\text{O}_3$ (Nominal composition) was synthesized at 1348 K for 48 h in air. The valence state of Fe and Ir was confirmed to be 3+ and 4+, respectively, by ^{57}Fe Mössbauer spectra and magnetic susceptibility measurement and the ratio of Li:Fe:Ir was determined to be 3:1:1 by ICP emission spectrometry. X-ray Rietveld analysis clarified that $\text{Li}_{1.8}\text{Ir}_{0.8}\text{Fe}_{0.2}\text{O}_3$ had layered structure with the $\alpha\text{-NaFeO}_2$ -type and could be represented as $[\text{Li}]_{1.8}[\text{Li}_{0.2}\text{Ir}_{0.8}\text{Fe}_{0.2}]_{0.8}\text{O}_3$ (Fig.1). The lattice parameters refined were $a = 2.96749(5)$ and $c = 14.4970(3)$ Å. $\text{Li}_{1.8}\text{Ir}_{0.8}\text{Fe}_{0.2}\text{O}_3$ was electrochemically synthesized using coin-type cell. Lithium deintercalation from $\text{Li}_{1.8}\text{Ir}_{0.8}\text{Fe}_{0.2}\text{O}_3$ proceeded from $x=0$ to 1.36 with a single-phasic reaction from 1st charge quasi-OCV curves, while XRD patterns of delithiated samples basically remained layered structure but showed weak shoulder around 101 peak. The $\text{Li/Li}_{1.8}\text{Ir}_{0.8}\text{Fe}_{0.2}\text{O}_3$ cell showed reversible charge-discharge characteristics in the voltage

range, 2.0-4.4 V and the discharge capacity of about 90 mAh/g (Fig. 2).

Single phase $\text{Li}_2\text{Ir}_{0.8}\text{Co}_{0.2}\text{O}_3$ (Nominal composition) was synthesized at 1273 K for 72 h in air. The ratio of Li:Co:Ir was determined to be 3:1:1 by ICP emission spectrometry. X-ray Rietveld analysis clarified that $\text{Li}_{1.8}\text{Ir}_{0.8}\text{Co}_{0.2}\text{O}_3$ had layered structure with the $\alpha\text{-NaFeO}_2$ -type and the lattice parameters refined were $a = 2.91160(7)$ and $c = 14.2807(4)$ Å. The $\text{Li/Li}_{1.8}\text{Ir}_{0.8}\text{Co}_{0.2}\text{O}_3$ cell showed reversible charge-discharge characteristics in the voltage range of 2.5-4.3 V and the capacity of about 120 mAh/g at 10 cycles.

According to Ni-doped samples, it will be reported. In addition, the delithiation mechanism of these materials will be discussed in detail.

References

1. A. C. W. P. James and J. B. Goodenough, *J. Solid State Chem.*, **74**, 287 (1988)
2. A. C. W. P. James and J. B. Goodenough, *J. Solid State Chem.*, **76**, 87 (1988).
3. H. Kobayashi, R. Kanno, Y. Kawamota, M. Tabuchi, O. Nakamura, and M. Takano, *Solid State Ionics*, **82**, 25 (1995).
4. H. Kobayashi, R. Kanno, M. Tabuchi, H. Kageyama, O. Nakamura, and M. Takano, *J. Power Sources*, **68**, 686 (1997).

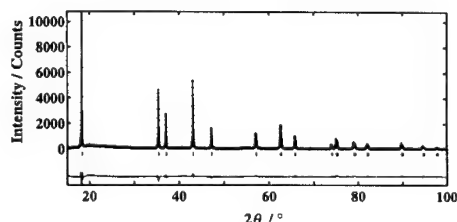


Fig.1 X-ray Rietveld refinement result of $\text{Li}_{1.8}\text{Ir}_{0.8}\text{Fe}_{0.2}\text{O}_3$

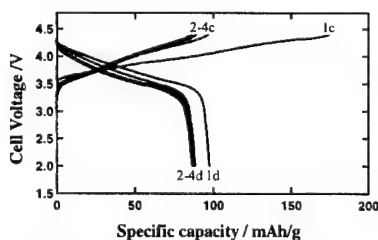


Fig.2 Charge and discharge curves of $\text{Li/Li}_{1.8}\text{Ir}_{0.8}\text{Fe}_{0.2}\text{O}_3$ cell. "1c" and "1d" mean the charge and discharge curves at 1st run, respectively.

The $\text{Li}_{1-x}(\text{Ni}_{1-y}\text{Mg}_y)_{1+z}\text{O}_2$ system: structural modifications observed upon cycling.

C. Pouillier^{*o}, L. Croguennec^{*}, Ph. Biensan^o,
P. Willmann[§] and C. Delmas^{*}.

^{*} Institut de Chimie de la Matière Condensée de Bordeaux and Ecole Nationale Supérieure de Chimie et Physique de Bordeaux, Château de Brivazac, Av. Dr. A. Schweitzer, 33608 Pessac cedex (FRANCE)

^o SAFT, Direction de la Recherche, 111 Bd Alfred Daney, 33074 Bordeaux cedex (FRANCE)

[§] CNES, 18 Av. Edouard Belin, 31055 Toulouse cedex (FRANCE)

New $\text{Li}_{1-x}(\text{Ni}_{1-y}\text{Mg}_y)_{1+z}\text{O}_2$ ($0 \leq y \leq 0.20$) layered oxides were synthesized by a co-precipitation method in aqueous solution followed by a high temperature thermal treatment. Rietveld refinements of the X-ray diffraction patterns showed that for small amounts of substitution ($y \leq 0.10$), these compounds exhibit a quasi-2D structure, isostructural to LiNiO_2 : only 2 % extra-ions (Mg^{2+} and/or Ni^{2+}) are present in the lithium sites (Figure 1). For the largest amounts of substitution, a significant lithium deficiency is observed. The charge compensation required due to lithium deficiency is preferentially associated with the presence of Mg^{2+} ions in the lithium sites.

The electrochemical study of the $\text{Li}/\text{Li}_x(\text{Ni}_{1-y}\text{Mg}_y)_{1+z}\text{O}_2$ systems showed a very good reversible behavior upon cycling (Figure 2). In fact, since the Mg^{2+} ions cannot be oxidized and have a size very similar to the Li^+ one, their presence in the interslab space prevents the local collapse of the structure which occurs for the $\text{Li}_{1-x}\text{Ni}_{1+z}\text{O}_2$ system and, therefore, improves the cycling stability. Nevertheless, even for the quasi-2D materials, a significant irreversible capacity is surprisingly observed at the end of the first discharge. A large capacity ($\geq 150 \text{ A.h.kg}^{-1}$) was found for the $\text{Li}_{1-x}(\text{Ni}_{1-y}\text{Mg}_y)_{1+z}\text{O}_2$ ($y \leq 0.02$), it obviously decreases when y increases.

The structural characterization of deintercalated $\text{Li}_x(\text{Ni}_{1-y}\text{Mg}_y)_{1+z}\text{O}_2$ ($y = 0.05$ and 0.10) phases showed that substitution of 5 % of magnesium for nickel is high enough to suppress the phase transitions observed for Li_xNiO_2 during the cycling process. In fact, the statistical distribution of Mg^{2+} ions in the structure prevents the lithium/vacancy ordering in the interslab space and the $\text{Ni}^{3+}/\text{Ni}^{4+}$ ordering in the slab, which are at the origin of these phase transitions.

Experiments performed at various depths for the charge showed that the mechanism responsible for the irreversible capacity at the end of the first discharge occurs at a potential higher than 4 V. Rietveld refinement of the X-ray diffraction patterns of the materials recovered after one cycle with an intermediate floating at high potential (4.35 V) or after 50 cycles (between 2.7 and 4.15 V), gave evidence for the migration of all the Mg^{2+} ions from the slab to the interslab space during the electrochemical process.

It is assumed that the presence of these Mg^{2+} ions in the lithium sites reduce the volume variations upon cycling and, therefore, is at the origin of the improvement

of the cycling properties observed for the magnesium substituted positive electrode materials.

Acknowledgements: The authors wish to thank SAFT, CNES, Région Aquitaine, ANRT and CEE (Contract CT960064) for financial support.

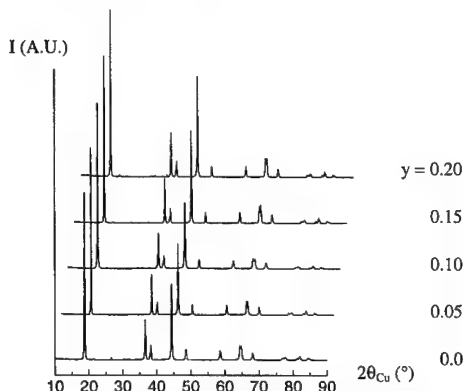


Figure 1: X-ray diffraction patterns of the magnesium substituted phases $\text{Li}_{1-x}(\text{Ni}_{1-y}\text{Mg}_y)_{1+z}\text{O}_2$ ($0 \leq y \leq 0.20$).

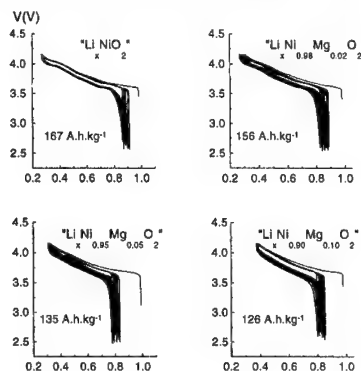


Figure 2: Cycling curve obtained for $\text{Li}/\text{Li}_x(\text{Ni}_{1-y}\text{Mg}_y)_{1+z}\text{O}_2$ batteries (C/10). The average reversible capacity calculated over the ten first cycles is also given.

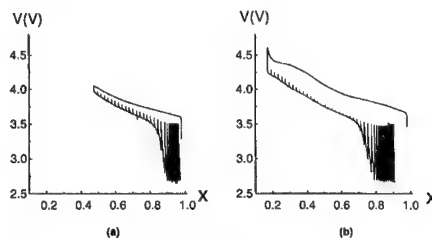


Figure 3: Electrochemical charges of $\text{Li}/\text{Li}_{0.92}\text{Mg}_{0.10}\text{O}_2$ batteries (C/100) up to 4.05 V ($x = 0.47$) (a) or up to 4.6 V ($x = 0.18$) (b), followed by an OCV discharge down to 2.7 V (relaxation criteria: $dV/dt \leq 1 \text{ mV.h}^{-1}$).

**Synthesis and Characterization
of $\text{LiFe}_x\text{Co}_{1-x}\text{O}_2$
cathode materials for Lithium
Batteries**

V. Subramanian*, R. Sriram, S.
Gopukumar[#], N. G. Renganathan, A.
Mani, N. Muniyandi and M.
Raghavan
Central Electrochemical Research
Institute, Karaikudi, India.

[#] Corresponding author, Fax: 91-4565-
38205,37779, e-mail:
gkumar41@hotmail.com

ABSTRACT

$\text{LiFe}_x\text{Co}_{1-x}\text{O}_2$ ($0.05 < x < 0.75$) solid solutions of $\alpha\text{-NaFeO}_2$ structure type with a well ordered layered structure have been synthesised by a sol-gel method using glycine as a chelating agent. Structure and particle morphology was examined by X-ray powder diffraction, FTIR & Scanning Electron Micrograph (SEM). The X-ray patterns of samples heated in air at 800°C show that single-phase solid solutions are formed up to a maximum of $x=0.5$ in $\text{LiFe}_x\text{Co}_{1-x}\text{O}_2$ studies reveal particles of sub-micron size and a high degree of homogeneity. Charge-discharge studies on non-aqueous liquid electrolyte cells using synthesised cathode materials show good electrochemical activity with an operating voltage of 4V.

*Presenting author

**Electronic and Electrochemical Properties of
 $\text{Li}_x\text{Co}_y\text{Ni}_{1-y}\text{O}_2$
 Cathodes Studied by Impedance Spectroscopy**

F. Croce^a, F. Nobili^b, R. Tossici^b, B. Scrosati^a, L. Persi^a
 and R. Marassi^b

^aDipartimento di Chimica, Università di Roma "La Sapienza", 00185 Roma, Italy

^bDipartimento di Scienze Chimiche, Università di Camerino, 62032 Camerino, Italy

It is well known that layered compounds such as Li_xCoO_2 , Li_xNiO_2 and mixed $\text{Li}_x\text{Co}_y\text{Ni}_{1-y}\text{O}_2$ change their electronic structure while intercalating or deintercalating lithium ions undergoing a semiconductor to metal transition^{1,2}. The transition occurs at the beginning of the deintercalation process in the very narrow range $x=1$ to $x \approx 0.9$. The electronic transition causes a contraction of the M-M distance: i.e. a lattice parameter. In a recent paper³, dealing with an AC impedance study of $\text{Li}_x\text{Co}_{0.25}\text{Ni}_{0.75}\text{O}_2$, we have interpreted the impedance spectra variation as a function of the intercalation degree in terms of change of the electronic structure by assigning the resistance associated to the lowest frequency semicircle to the electronic conductivity of the material. In this paper we present the results obtained by using Li_xCoO_2 .

The impedance spectra were obtained using the above compound as cathode in a Li_xCoO_2 / EC-DMC- LiClO_4 / Li cell at different potentials values (i.e. different x). The results have shown that the low frequency region of the spectra is dominated by a semicircle that, especially at high x value, tends to close on the real axis. As the electrode is non-blocking only for electrons, the high resistance associated with this semicircle has been interpreted in terms of the electronic conductivity of the material. The variation of this resistance, R_{el} , with x drops by several order of magnitudes over a potential range of about 100 mV corresponding to an x variation from 1 to about 0.9. After that the resistance appears to be potential independent. The plot is very similar to the one published by Ohzuku et al.⁴ who measured the conductivity of the same compound using a more complicated experimental apparatus. The spectra at lower x values show all the characteristic features of an intercalation electrode covered by a passivating layer, in agreement with published results⁵.

All the spectra have been analyzed using the non-linear least-square fitting program developed by Boukamp⁶. Here we like to stress the results obtained for the charge transfer resistance. The plot of this parameter Vs potential shows that, R_{ct} is rather constant over the entire potential range. This is consistent with a model in which the charge transfer in intercalation type electrodes, contrary to what happens in classical oxidation-reduction processes, is related to electrons that interact with the ions in the crystal lattice and not with the incoming ions. In this case no potential dependence of R_{ct} is expected⁷. Similar behavior have been found with parent compounds. Finally, to confirm our working hypothesis, we have repeated the entire set of measurements as function of the temperature in the temperature range $+5^\circ\text{C}$ - $+30^\circ\text{C}$. By plotting the $\log(1/\text{Rel})$ vs $1/T$ we have been able to obtain the activation energy, E_a , of the electronic conduction process as function of the intercalation degree x . A monotone decreasing of the value of this parameter from $E_a \approx 0.35$ eV to $E_a \approx 0.01$ eV has been observed for x

decreasing from $x=1$ to $x \approx 0.5$: i.e. for the material undergoing the semiconductor-metallic transition. Moreover, the numerical value for E_a we have found in the case of the fully intercalated compound, $x=1$, is in agreement with previously published results¹.

References

- 1) J. Molenda, A. Stopklosa, and T. Back, *Solid State Ionics*, 36 (1989) 53.
- 2) J. Molenda, *Phys. Stat. Sol. (b)*, 165 (1991) 419.
- 3) F. Croce, F. Nobili, A. Deptula, W. Lada, R. Tossici, A. D'Epifanio, B. Scrosati, R. Marassi, *Electrochemistry Communications*, 1 (1999) 605-608.
- 4) T. Ohzuku, A. Veda, *J. Electrochem. Soc.*, 144 (1997) 2780.
- 5) M.D. Levi, G. Salitra, B. Marcowsky, H. Teller, D. Aurbach, U. Heider, L. Heider, *J. Electrochem. Soc.*, 146 (1999) 419.
- 6) B.A. Boukamp, *Solid State Ionics*, 20 (1986) 31.
- 7) P.G. Bruce, M.Y. Saidi, *J. Electroanal. Chem.*, 322 (1992) 93.

Li_{1+δ}Mn_{2-δ}O₄ Performance Measured by Leaching

E.M. Kelder, F.J.B. Ooms, R. Perego, and J. Schoonman

Delft Interfaculty Research Center: Renewable Energy
 Laboratory for Inorganic Chemistry
 Delft University of Technology
 Julianalaan 136, 2628 BL Delft

In principle, LiMn₂O₄ (space group Fd3m) has manganese on octahedral sites and lithium on tetrahedral sites, but it was reported recently that part of the lithium resides on 16c octahedral sites (1). Furthermore, the Mn₂O₄ frame-work provides room for lithium ion transport, maintaining its structure over the compositional range Li_xMn₂O₄, with usually 0 < x < 1. Consequently, a gradual increase in the average Mn valency occurs, i.e. from 3.5 to 4.0, respectively. Upon Li-extraction Mn³⁺ is oxidised to Mn⁴⁺, and only Mn³⁺ ions contribute to the capacity at four Volt. However, it was found that lithium ions cannot be extracted at four Volt anymore, if the lithium content x is less than about 0.27 (2), reflected by a strong increase in the open-circuit-voltage (OCV). Hence, this leads to a capacity reduction of the spinel material compared to the theoretical capacity, i.e. 148 mAh/g, giving a practical capacity of about 120 mAh/g. In addition, the exact composition LiMn₂O₄ seems to be unstable in the current Li-ion battery systems (3). In order to stabilise the spinel for improved electrochemical performance extra lithium was added during synthesis, usually resulting in Li[Li_δMn_{2-δ}]O₄ (0 < δ < 0.33), with the ions between square brackets occupying 16d sites. Here the average Mn valency varies from 3.5 at δ=0 to 4 at δ=0.33, and thus the maximal amount of lithium ions that can be extracted theoretically is 1-3δ. It is believed that the regime reflecting the reduced capacity in LiMn₂O₄, i.e. between x=0.0 and x=0.27, can substantially be reduced by adding small amounts of extra lithium; small δ-values keep the number of Mn³⁺ acceptable. Here we report on the performance of Li[Li_δMn_{2-δ}] derived via redox titration (4) and a redox disproportionation reaction according to Hunter's method (5). The de-lithiated samples Li_x[Li_δMn_{2-δ}]O₄ agree with a composition indicating δ remain unaffected upon leaching. Based on this outcome, it can be seen that the Li/Mn-ratio is in favour for high δ, and from measurements it was found that higher δ leads to a pH that is significant closer to 7, indicating stabilisation of the material (Fig.1). During chemical de-lithiation a similar behaviour is observed as in electrochemical cells (Fig.2). Fig.3 shows curves recorded at different sulphuric acid dosing rates. These dosing rates can be performed in such a way that they match relevant C-rates, and thus reflecting the Li-ion transport in the insertion compound. Hence, diffusion coefficient can be established without interference of an interface; the interface dissolves during the leaching process.

In summary, by analysing the pH (1g in 250ml of water), the Mn valency (Jaeger-Vetter titration), and the chemical de-lithiation (a modified Hunter's method) the performance of the spinel material can be characterised.

Acknowledgements DSM SoluTech, Shell IEP, NWO-CW and STW are acknowledged for their financial support.

- (1) H. Berg, E.M. Kelder, and J.O. Thomas, J. Mater. Chem. 9 (1999) 427.
- (2) T. Ohzuku, M. Kitagawa, and T. Hirai, J. Electrochem. Soc., 137 (1990) 769.
- (3) P. Arora, R.E. White, and M. Doyle, J. Electrochem. Soc., 145 (1998) 3647.
- (4) E.M. Kelder, M.J.G. Jak, J. Schoonman, M.T. Hardgrave, and S. Yde-Andersen, J. Power Sources, 68 (1997) 590.
- (5) J. C. Hunter, J. Solid State Chem., 39 (1981) 142.

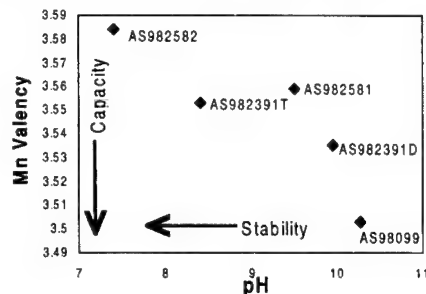


Fig. 1. Stability-capacity diagram versus pH and Mn valency

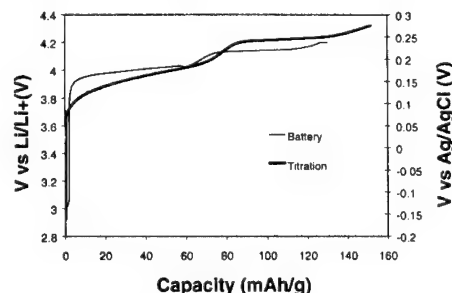


Fig. 2. Li-extraction capacity for chemical and electrochemical de-lithiation (sample AS982391D).

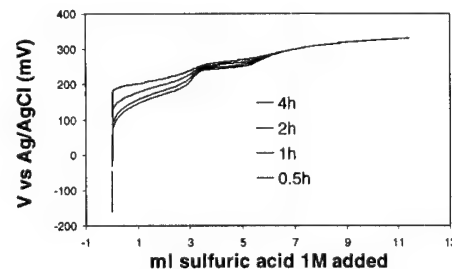


Fig. 3. Chemical de-lithiation at various sulphuric acid dosing rates.

Tungsten oxysulfide thin films as positive electrode in lithium microbatteries

I. Martin-Litas^a, P. Vinatier^a, A. Levasseur^a,
J.C. Dupin^b, D. Gonbeau^b

^a ICMCB-ENSCP Avenue Pey-Berland, BP 108, 33402
TALENCE-FRANCE

^b Laboratoire de Physico-Chimie Moléculaire (UMR5624)
Université de Pau et des Pays de l'Adour
2, Avenue du président Angot, 64000 PAU- FRANCE

Tungsten oxysulfide thin films (WO_xS_y) were prepared by r.f magnetron sputtering using a WS_2 target and a mixture of argon and oxygen discharge gas. The composition, the texture and the structure depend on two parameters : the oxygen partial pressure and the total pressure ($\text{Ar} + \text{O}_2$). For example, for a total pressure of 1 Pa, the range of chemical composition is large, from WS_2 when no oxygen gas is introduced in the chamber, to $\text{WO}_3\text{S}_{0.02}$ when the oxygen partial pressure is equal to 10^{-2} Pa. The different thin films were used as positive electrode in the cell : $\text{Li} / \text{LiAsF}_6, 1\text{M EMC} / \text{WO}_x\text{S}_y$ at different currents density and at different ranges of potential to study the reversible oxydo-reduction processes when the lithium is intercalated and de-intercalated.

Results for the cell : $\text{Li} / \text{LiAsF}_6, 1\text{M EMC} / \text{WO}_{0.9}\text{S}_{2.0}$

The electrochemical cell was cycled between 1.2 V and 3.0 V, at a current density of $3 \mu\text{A}/\text{cm}^2$. The three first cycles are shown in figure 1. During the first discharge, 2.44 lithium are intercalated and 1.65 are de-intercalated. To understand the different oxydo-reduction processes which exist in the first cycle, XPS (X-Ray Photoelectron Spectroscopy) studies were done.

Our previous studies by XPS have shown that in the tungsten oxysulfide thin films, the tungsten ions have three different environments with three different oxidation states : W^{4+} in a sulfide environment (S^{2-}), W^{5+} in a mixed oxygen-sulphur environment (O^{2-} , S^{2-} and S_2^{2-} ions) and W^{6+} in an oxide environment.

The XPS studies were done after intercalation of lithium to 1.85 V and to 1.20 V and after de-intercalation to 2.57 V. The evolution of the different tungsten (fig 2) and sulphur ions showed that during the intercalation, the main species involved are the W^{4+} ions reduced in W^0 species, and the S_2^{2-} ions reduced in S^{2-} . The process is reversible for the tungsten but not completely for the sulphur.

For a higher current density ($75 \mu\text{A}/\text{cm}^2$), between 1.6 V and 3.0 V (fig 3), 1.93 lithium are intercalated. During the charge 0.84 lithium is de-intercalated. The value of the initial capacity is $43 \mu\text{Ah}/\text{cm}^2$. The capacity decreases during the seven first cycles. Then the value is stable (140 cycles were done) and equal to nearly $14 \mu\text{Ah}/\text{cm}^2$; which correspond to 0.63 lithium intercalated.

Conclusion

The $\text{WO}_{0.9}\text{S}_{2.0}$ thin film has evidenced good properties as positive electrode in the ranges [1.6V-3.0V] and [1.2V-

3.0V] at different current densities. The XPS studies point out the presence at low potential of W^0 species in connection with the intercalation of so much lithium in our materials.

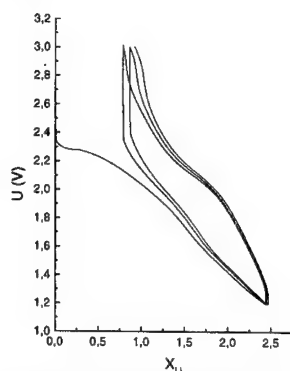


fig 1 : The three first cycles, at $3 \mu\text{A}/\text{cm}^2$, [1.2V-3.0V]

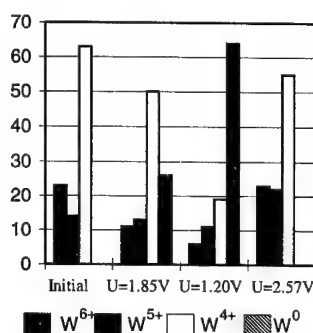


fig 2 : Evolution content of different tungsten at different stage of the cell.

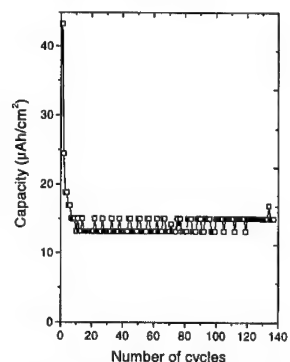


fig 3 : Evolution of the capacity with a current density of $75 \mu\text{A}/\text{cm}^2$,

Electronic Structure in LiMn_2O_4 Based Spinel Oxides from Transition Metal L-edge and O K-edge XANES

Yoshiharu UCHIMOTO and Takeshi YAO,
Department of Fundamental Energy Science,
Graduate School of Energy Science, Kyoto University,
Yoshida, Sakyo-ku, Kyoto 606-8501, JAPAN

LiMn_2O_4 based spinel type oxides are one of the most promising cathode materials used in lithium ion batteries because their low cost, high theoretical energy density. (1, 2) It is important to clarify the change of electronic structure during charge and discharge process in order to understand their electrochemical properties. In this study, the electronic structure of undoped and transition metal (Ni or Cr) doped LiMn_2O_4 spinel oxides were determined by using a measurement of Mn L₂₃-edge, Ni L₂₃-edge, Cr L₂₃-edge and Oxygen K-edge X-ray Absorption Near Edge Structure (XANES). XANES spectra were measured on BL-7A and BL-8B1 at UVSOR (Okazaki, Japan) with ring energy of 750 MeV in a mode of total electron yield.

LiMn_2O_4 , $\text{LiNi}_{0.4}\text{Mn}_{1.6}\text{O}_4$, $\text{LiCr}_{0.5}\text{Mn}_{1.5}\text{O}_4$ were prepared. The crystal structure of these oxides was determined by XRD using MoK α radiation. These XRD patterns were indexed to a cubic lattice. The lattice parameters and other structural parameters were refined by the Rietveld method. The Rietveld calculation was performed on the vector processor (Cray Y-MP2E/264) at the Institute for Chemical Research, Kyoto University, by using 'Rietvec' computer program (3, 4). It was confirmed that these oxides were belonging to cubic $Fd3m$ space group.

Fig. 1 shows the Mn L-edge XANES of $\text{Li}_x\text{Mn}_2\text{O}_4$ at various x values together with reference materials of MnO_2 (Mn^{4+}), Mn_2O_3 (Mn^{3+}), and MnCO_3 (Mn^{2+}). The spectra correspond to Mn2p⁶3dⁿ to Mn2p⁵3dⁿ⁺¹ transitions. This figure shows that the Mn L₃ absorption edge of Mn_2O_3 was about 642.0 eV and that of MnO_2 was 643.4 eV. These results indicate that increasing the oxidation state of manganese, the Mn L₃ absorption edge shifted to higher energy. As shown in Fig. 1, the peak of LiMn_2O_4 was a combination of peak of Mn_2O_3 and MnO_2 . At low x value of the $\text{Li}_x\text{Mn}_2\text{O}_4$, contribution of Mn^{4+} increased, whereas contribution of Mn^{3+} increased at large x values.

Fig. 2 shows the oxygen K-edge XANES of $\text{Li}_x\text{Mn}_2\text{O}_4$ at various x. A peak at about 529 eV is attributed to the band derived from the mixing of the Mn 3d majority (spin-up) e_g and minority (spin-down) t_{2g} states with oxygen 2p states. A peak at about 531.5 eV is attributed to the band derived from the mixing of the Mn 3d minority (spin-down) e_g states with oxygen 2p states. The broad structure about 540-545 eV is attributed to band of Mn 4sp character. The peak at about 529 eV increased with decreasing lithium content. This results shows that oxidation also take place on oxygen 2p orbital and the ground state of $\text{Li}_x\text{Mn}_2\text{O}_4$ ($x < 1.0$) is mixed state of $3d^3$ and $3d^4\bar{L}$, where \bar{L} represents a ligand hole state. These results are in good agreement with the result of First-Principles calculation for LiMn_2O_4 spinel oxides. (5, 6) At x values above 1.2, the peak at about 534 eV appeared. The peak at about 534 eV is attributed to minority (spin-down) $d_{x^2-y^2}$ state, which appeared by

cubic-to-tetragonal phase transition.

REFERENCES

- 1) T. Ohzuku, M. Kitagawa, and T. Hirai, *J. Electrochem. Soc.*, **137**, 769 (1990).
- 2) K. Kanamura, H. Naito, T. Yao, and Z. Takehara, *J. Material Chem.*, **6**, 33 (1997).
- 3) T. Yao, Y. Oka, and N. Yamamoto, *J. Mater. Chem.*, **32**, 331 (1992).
- 4) T. Yao, T. Ito, and T. Kokubo, *J. Materials Research*, **10**, 1079 (1995).
- 5) S.K. Mishra and G. Cedar, *Physical Review B*, **45**, 1612 (1999).
- 6) M.K. Aydinol and G. Cedar, *J. Electrochem. Soc.*, **144**, 3832 (1997).

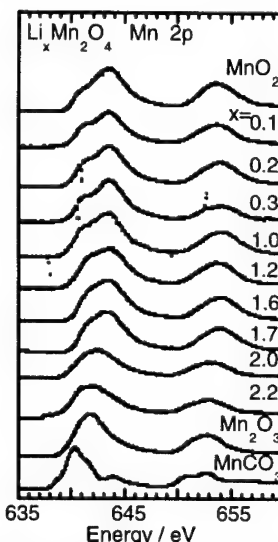


Fig.1 Mn 2p absorption spectra of $\text{Li}_x\text{Mn}_2\text{O}_4$, the value of x is indicated in the figure.

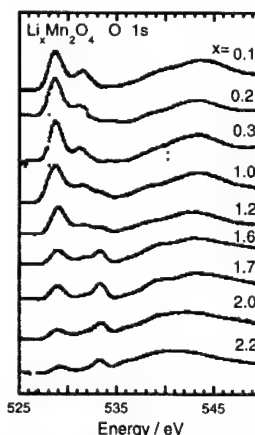


Fig.2 O 1s absorption spectra of $\text{Li}_x\text{Mn}_2\text{O}_4$, the value of x is indicated in the figure.

Effect of Cr^{6+} on the Jahn-Teller distortion of spinel LiMn_2O_4

V.Subramanian^{*}, S.Venkatraman,
S.Gopu Kumar[#], T.Prem Kumar,
N.G.Renganathan, N.Muniyandi and
M.Raghavan
Central Electrochemical Research
Institute, Karaikudi, India.

ABSTRACT

Hexavalent chromium $[\text{Cr(VI)}]$ doped LiMn_2O_4 spinels were synthesized for the first time by a sol-gel method using glycine as the chelant. The synthesized samples were analyzed using XRD for its phase purity. The change in the local structure was elucidated using FTIR. SEM studies reveals homogeneous particles of sub-micron size. The hexavalent chromium ion doping has led to very high capacity in the order of 400 mAh/g, confirming the recent theoretical investigation ^[1]. The effect of hexavalent ion doping on the Jahn-Teller distortion of the spinel LiMn_2O_4 is discussed in detail.

Reference:

- [1] Yanko M. Todrov, Yasufumi Hideshima, Hideyunki Noguchi, Masaki Yoshio
J. Power Sources 77 (1999) 198

^{*}Presenting author

[#] Corresponding author: Fax: 91-4565-38205,37779; e-mail: gkumar41@hotmail.com

3 V Manganese Oxide Electrode Materials for Lithium Batteries

Christopher S. Johnson
and Michael M. Thackeray,
Electrochemical Technology Program,
Chemical Technology Division,
Argonne National Laboratory
Argonne, IL 60439, USA

Lithium cells with manganese oxide cathodes that operate at 3 V compare favorably with 4 V $\text{Li/Li}_x\text{Mn}_2\text{O}_4$ (spinel) cells based on calculations of achievable energy densities. Table 1 compares these calculations. In short, if a Li_xMnO_2 electrode can deliver a practical capacity of 180 mAh/g at an average 3 V, then the system will provide an energy density of 504 Wh/kg (based on the masses of the active electrode materials only). From a stored energy standpoint, this makes it reasonably competitive with conventional 4 V Li-ion (spinel) cells (480 Wh/kg). We have been examining several 3 V manganese oxides that have delivered capacities in excess of 200 mAh/g and good cycling behavior.

Various MnO_2 structure types can be stabilized to lithium insertion/extraction by reacting the MnO_2 frameworks with lithia (Li_2O) [1]. Examples of lithia-stabilized compositions and structures include the α - MnO_2 (hollandite) structure ($0.15\text{Li}_2\text{O} \cdot \text{MnO}_2$) [2], ramsdellite- MnO_2 ($0.15\text{Li}_2\text{O} \cdot \text{MnO}_2$), the 3 V spinel structure $\text{Li}_x\text{Mn}_2\text{O}_4$ ($0.40\text{Li}_2\text{O} \cdot \text{MnO}_2$), and a layered structure derived from the rocksalt phase Li_xMnO_2 ($\text{Li}_2\text{O} \cdot \text{MnO}_2$) [3]. We have focused our efforts on stabilizing the α - MnO_2 and layered structures. In the α - MnO_2 system, stabilized structures with mixed-alkali dopants can also be prepared, such as ($0.11\text{Li}_2\text{O}/0.04\text{Na}_2\text{O} \cdot \text{MnO}_2$).

The capacity and cycling capability of α - MnO_2 electrodes can be increased by treating the structure with ammonia (NH_3) gas. When the beneficial effects of lithia doping and ammonia treatment are both implemented in this system, then excellent cycling properties result. Figure 1 shows that > 200 mAh/g can be obtained when lithia-doped α - MnO_2 , treated with ammonia is cycled between 3.8 and 2.0 V. This improvement in performance can be attributed to the stabilization of the hollandite framework by the partial occupancy of sites at the center of the (2x2) channels by both oxygen (from the lithia molecules) and nitrogen (from the ammonia).

Layered $\text{Li}_{1-x}\text{MnO}_{3/2}$ electrodes that are derived from the rock salt phase Li_2MnO_4 by acid treatment are of interest because, unlike layered LiMnO_2 electrodes obtained by Li-ion exchange from NaMnO_2 , they show a lesser tendency to convert to spinel. Good cycling behavior has been obtained when cells are cycled between 3.8 to 2.0V, but lower capacities (approximately 160 mAh/g) are achieved compared to stabilized α - MnO_2 electrodes. The electrochemical properties of $\text{Li}_{1-x}\text{MnO}_{3/2}$ electrodes, their thermal and structural stability, and the role that water plays in the structure will be discussed.

Acknowledgment

This work was performed under the auspices of the U.S. Department of Energy, Office of Basic Energy Sciences; Division of Chemical Sciences, under contract number W-31-109-ENG-38.

References

1. M. M. Thackeray, *Prog. Solid State Chem.*, **25**, 1 (1997).
2. C. S. Johnson, D. W. Dees, M. F. Mansueti, M. M. Thackeray, D. R. Vissers, D. Argyriou, C.-K. Loong and L. Christensen, *J. Power Sources*, **68/2**, 570 (1997).

3. C. S. Johnson, S. D. Korte, J. T. Vaughey, M. M. Thackeray, T. E. Bofinger, Y. Shao-Horn and S. A. Hackney, *J. Power Sources*, **81/82**, 491 (1999).

Structure Type	Average Discharge Voltage (V)	x range	Theory Capacity (mAh/g)	Practical Capacity (mAh/g)	% Electrode Utilization	Li per Mn	Energy Density (Wh/kg)
$\text{Li}_x\text{Mn}_2\text{O}_4$ spinel	4	$0 \leq x \leq 1$	148	110-120	81%	0.4	480
Li_xMnO_2 hollandite	2.8 (3)	$0 \leq x \leq 1$	308	160-180	58%	0.6	504

Table 1. Energy Densities of Li/MnO_2 Cells

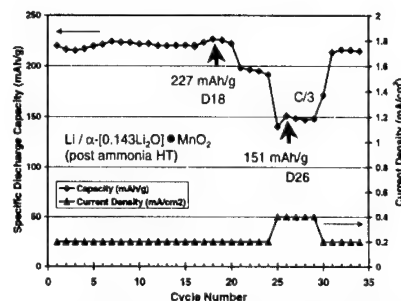


Figure 1. Cycling Performance of Advanced α - MnO_2 Electrode Materials

The Spinel Phases $\text{LiMg}_y\text{Mn}_{2-y}\text{O}_4$ as the Cathode for Rechargeable Lithium Batteries

In-Seong Jeong and Hal-Bon Gu

Introduction

Cathode material plays important part in the operation of a Lithium-ion cells. Among the intercalation compounds used as cathodes materials in lithium-ion batteries, spinel LiMn_2O_4 offers considerable advantages in price and reduced toxicity.¹ However, the published results for cell cycling performance of spinel compound show significant capacity fade. Despite considerable effort, preparation of high quality battery grade spinel with long cycle life capabilities has proven to be extremely difficult. Many researchers have also reported a marked improvement of the spinel cyclability but, unfortunately, this improvement was accompanied by a decrease in specific capacity of up to 30 percent of the theoretical value. Several investigations have been made for the performance of manganese-substituted spinel.²

In this work, the spinel phase $\text{LiMg}_y\text{Mn}_{2-y}\text{O}_4$ in which a part of Mn replaced by Mg^{2+} are prepared to improve the cycle performance of LiMn_2O_4 spinel.

Experimental

$\text{LiMg}_y\text{Mn}_{2-y}\text{O}_4$ samples were prepared by reacting stoichiometric quantities of $\text{LiOH}\cdot\text{H}_2\text{O}$, Mn_2O_3 and MgO in air at 800 °C for 36h. Powder X-ray diffraction using $\text{CuK}\alpha_1$ radiation was used to identify the crystalline phases of the material. Cathode specimens were prepared by mixing the $\text{LiMg}_y\text{Mn}_{2-y}\text{O}_4$ powder with 15wt.% sp-270 carbon black and 5wt.% PVDF (poly-vinylidene fluoride). A three electrode electrochemical cell was employed for electrochemical cell. The reference and counter electrodes were constructed from lithium metal as well and a 1M LiClO_4 -PC solution was used as the electrolyte. The charge and discharge test was carried out in the potential range of 3.0 ~ 4.3V with current of 0.1/.

Result and discussion

The powder XRD patterns of the $\text{LiMg}_y\text{Mn}_{2-y}\text{O}_4$ for $0 \leq y \leq 0.15$ are shown in Fig. 1. All samples were identified as a single-phase spinel with a space group $\text{Fd}3\text{m}$ in which the lithium ions occupy the tetrahedral (8a) sites and the transition metal ions reside at the octahedral (16d) sites. New peak can be slight seen at 42.94° (marked) when $y=0.05$ and is more apparent with increasing Mg^{2+} content. We presume that this peak is not other phase peak but co-spinel phase. The identity of the proposed co-spinel phase is not yet known. Therefore, it needs more work. The lattice parameter slightly decreased with increasing Mg^{2+} content.

The relationships between the discharge capacity and the cycle number of the $\text{Li}/\text{LiMg}_y\text{Mn}_{2-y}\text{O}_4$ cell are shown in Fig. 2. As can be seen, the capacity fading of the $\text{Li}/\text{LiMn}_2\text{O}_4$ cell was more severe than that of the substituted phases. In addition, $\text{Li}/\text{LiMg}_y\text{Mn}_{2-y}\text{O}_4$ cell substituted Mg^{2+} revealed more the high and stable discharge capacity than that of LiMn_2O_4 . Among these materials, $\text{LiMg}_{0.1}\text{Mn}_{1.9}\text{O}_4$ showed the best cycle performance in terms of the capacity and cycle life. The discharge capacity of the cathode for the $\text{Li}/\text{LiMg}_{0.1}\text{Mn}_{1.9}\text{O}_4$ cell at 1st cycle and at the 70th cycle was about 120 and 105mAh/g, respectively. While, $\text{Li}/\text{LiMn}_2\text{O}_4$ cell was about 117 and 73mAh/g. The cycle performance improved by the substitution could be explained by

Dept. of Electrical Eng., Chonnam National University
300 Yongbong-dong, Bukgu, Kwangju 500-757, Korea

considering that the doped metal cations enhance the stability of the octahedral sites in the spinel skeleton structure.

Fig. 1. X-ray diffraction pattern of $\text{LiMg}_y\text{Mn}_{2-y}\text{O}_4$.

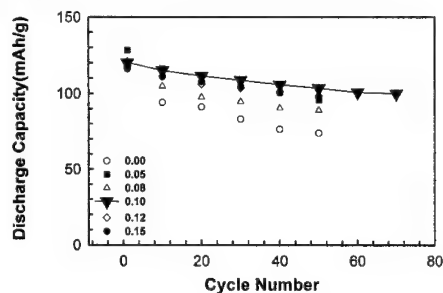
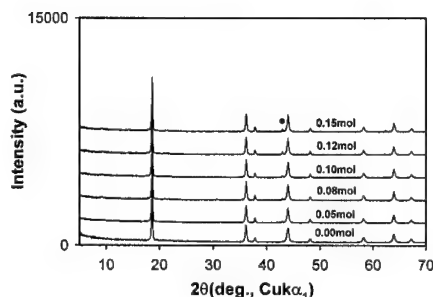


Fig. 2. Discharge capacity of $\text{LiMg}_y\text{Mn}_{2-y}\text{O}_4$.

Reference

1. J. M. Tarascon and D. Guyomard, *J. Electrochem. Soc.*, **138**, 2864 (1991)
2. R. J. Gummow, A. de Kock and M. M. Thackeray, *Solid State Ionics*, **69**, 59 (1994)



Characterisation of nanoparticles of LiMn_2O_4
synthesized
by citric acid sol-gel method
Department of Chemical Engineering
National Taiwan University of Science and
Technology
43 Keelung road, sec.4, 106 Taipei, Taiwan,
Republic of China
Fax : 00886-2-27376644
e-mail : bjh@ch.ntust.edu.tw

The spinel LiMn_2O_4 compound is of potential interest for lithium and lithium-ion batteries. This material has been synthesized by a sol-gel method using an aqueous solution of metal acetates containing citric acid as a chelating agent. The effects of various calcination temperatures on the physicochemical properties of the spinel LiMn_2O_4 powders have been investigated by means of X-ray diffraction (XRD), scanning electron microscopy (SEM) and transmission electron microscopy (TEM). XRD measurements show that crystallinity improves with increasing calcination temperature. SEM images reveal that LiMn_2O_4 particles calcined at 800°C exhibit uniform crystal shape and good crystallinity with an average size of ~ 80 nm (Fig.1), while LiMn_2O_4 particles calcined at low temperatures have an irregular shape and also smaller size than those of sample prepared at high temperature. TEM images of sample calcined at high temperatures show that the uniformity in particle size and particle size distribution.(Fig.2) Electrochemical measurements have been performed on a cell of $\text{Li}/1\text{M LiPF}_6$ in EC:DEC (50:50 v/v)/ LiMn_2O_4 which was assembled in a glove box with an argon inert atmosphere.



Fig.1. SEM image of LiMn_2O_4 powder calcined at 800°C

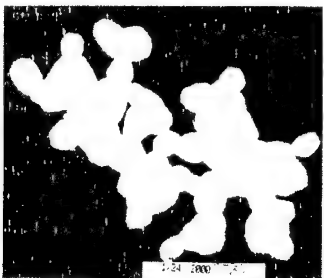


Fig.2 TEM image of LiMn_2O_4 powder calcined at 800°C

THEORETICAL APPROACH OF THE LITHIUM INTERCALATION IN HOST MATERIALS

F. Lantelme⁽¹⁾, H. Groult⁽¹⁾, N. Kumagai⁽²⁾⁽¹⁾Université P. & M. Curie - CNRS UMR 7612 - Laboratoire LI2C - Electrochimie ; Bât F74 4, Place Jussieu, 75252 Paris Cedex 05 - France⁽²⁾Dpt of Applied Chem., Faculty of Engineering, Iwate University, Ueda, Morioka, 020 Japan

In lithium batteries field, considerable attention has been paid for many years to the study of the electrochemical intercalation/deintercalation process of lithium in host materials. The latter is governed by the diffusion of Li^+ into the host material.¹

One of the most important kinetic characteristics of this electrochemical process is the lithium diffusion coefficient, \tilde{D}_{Li} . Several kinds of electrochemical studies were done for the determination of the \tilde{D}_{Li} such as galvanostatic intermittent titration technique (GITT), current pulse relaxation technique (CPR), impedance, etc. The experiments were interpreted in the frame of the solid state diffusion theory;² the classical mathematic approach provides algebraic equations which can be easily used for the exploitation of experimental transient curves in considering constant diffusion coefficients. But, a variation of \tilde{D}_{Li} with the lithium concentration into the host structure is usually observed.

Therefore, we propose a new approach based on the numerical integration of the diffusion equations taking into account a dependence of \tilde{D}_{Li} on the lithium concentration.³ This dependence can strongly modify the shape of the calculated chronopotentiograms as illustrated in Fig. 1 and then, must be introduced in the calculation to obtain a correct description of experimental results.

The new theoretical model was applied to the study of the Li^+ intercalation/deintercalation into Nb_2O_5 used as cathode material.⁴ As shown in Fig. 2, the experimental curve is perfectly fitted in considering a polynomial variation of \tilde{D}_{Li} vs lithium intercalation ratio, y :

$$\tilde{D}_{\text{Li}} = 2.63 \times 10^{-10} \times (1 - 1.37 y + 0.544 y^2) \text{ cm}^2 \text{ s}^{-1}$$

By contrast, the best fit of the experimental curve using the classical theory with a fixed diffusion coefficient is obtained for $\tilde{D}_{\text{Li}} = 6.78 \times 10^{-11} \text{ cm}^2 \text{ s}^{-1}$; nevertheless, the calculated curve does not well describe the experimental curve.

Therefore, it clearly shows that our new theoretical approach provides a significant improvement for the exploitation of experimental results and for the determination of \tilde{D}_{Li} .

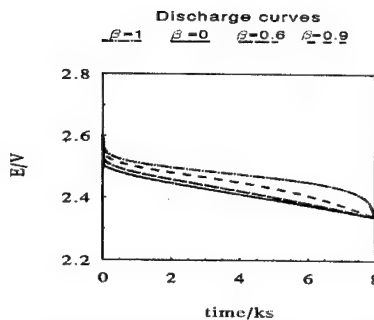


Fig. 1. Calculated chronopotentiograms for a variable component diffusion coefficient: $D = D_0 (1 - \beta y)$. Current density: -10 mA cm^{-2} . Variation of the potential according to [5]: $E = 2.5 - RT/F [\log (y / (1 - y))]$. The following $D \times 10^{14} \text{ cm}^2 \text{ s}^{-1}$ values are found: 4.5 ($\beta=0$), 9.45 ($\beta=0.6$), 20.7 ($\beta=0.9$) and 33.3 ($\beta=0$).

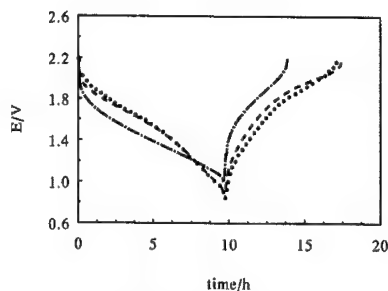


Fig. 2. Discharge-recharge curves for $\text{Li}_x\text{Nb}_2\text{O}_5$ in 1 M $\text{LiClO}_4\text{-PC}$ solution at 25°C . Current density: $\pm 100 \text{ mA cm}^{-2}$. •: experimental curves; dashed line: calculated curves with a concentration dependent diffusion coefficient; dotted line: calculated curves with a fixed diffusion coefficient.

References

1. M. Broussely, F. Pertion, P. Biensan, J. M. Bodet, J. Labat, A. Lecerf, C. Delmas, A. Rougier and J. P. Perès, *J. Power Sources*, **43**, 595 (1982).
2. C. Wagner, *Progress in Solid State Chemistry*, Vol. 10, Part 1, J. McCaldin and G. Somorjai, Editors, p. 3, Pergamon Press, Oxford (1975).
3. F. Lantelme, in *Modelling and Simulation in Metallurgical Engineering and Material Science*, Y. Zongsen, X. Zeqiang and X. Xishan, Editors, p. 133, Metallurgical Industry Press, Beijing (1996).
4. N. Kumagai, Y. Koishikawa, S. Komaba, N. Koshiba, *J. Electrochem. Soc.*, **146**, 3203 (1999).
5. C. Déportes, M. Duclot, P. Fabry, J. Fouletier, A. Hammou, M. Kleitz, E. Siebert and J.-L. Souquet, *Electrochimie des Solides*, Presses Universitaires de Grenoble, p. 311, Grenoble (1994).

The Influence Of The Synthesis Conditions On The Structural And Electrochemical Properties Of Cathodes Based On Manganese Oxides In Nonaqueous Electrolytes

E.M. Shembel, N.I.Globa, N.D.Zaderey, V.M.Pisniy, Kylyvnyk K.E.

Ukrainian State Chemical Technology University, Dnipropetrovsk, Ukraine, E-mail: shembel@onil.dp.ua

Ukrainian manganese ores are used as a starting raw material.

The main directions of investigation are the following:

1. The discharge/charge characteristics of the samples of secondary batteries with a cathode based on MnO_2 synthesized by different methods:

- 1.1. The treatment of electrolytic MnO_2 with a nitric acid (sample N1);
- 1.2. Oxidation of Mn_2O_3 with a nitric acid (different concentration);
 HNO_3 (delute)-sampleN2;
 HNO_3 (concentr.) - sample N3
- 1.3. The chemical method of the synthesis from $Mn(NO_3)_2 + NaClO_3$ mixture, samples N 4.

2. Studying discharge/charge characteristics of $LiMn_2O_4$ spinel, synthesized by different methods.

- 2.1. The synthesis is the high-temperature treatment of $MnO_2 + LiNO_3$, $MnO_2 + Li_2CO_3$, $MnO_2 + LiOH$.
- 2.2. Synthesis from the mixture of $MnCO_3$ and Li_2CO_3 .

3. The impedance testing of $Li-LiMn_2O_4$ accumulator at the different discharging stages .

The synthesis conditions of the efficient cathode materials for lithium secondary batteries have been developed on the basis on Ukrainian manganese ores.

Acknowledgement.

This work is supported by the STCU Project # 656 and the Ministry of Science of Ukraine, Grant 2c/1458-97.

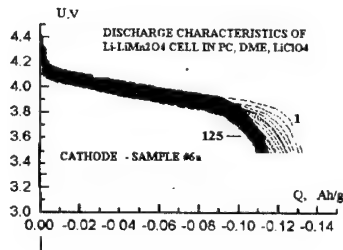
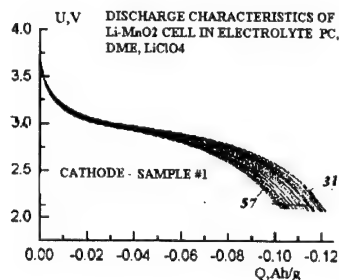
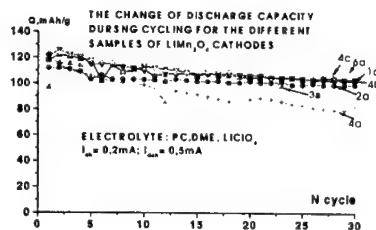
Table 1. The bulk density of $LiMn_2O_4$ at high-temperature synthesis from the different types of MnO_2

Parent components for the synthesis of $LiMn_2O_4$		Sample $LiMn_2O_4$ spinels	Bulk density initial $g \cdot m^{-3}$	Bulk density for $LiMn_2O_4$ $g \cdot m^{-3}$
MnO_2 / Type of structural modification	Li salt for synthesis			
Sample 1 / *	$LiNO_3$	1a	2.5	1.8
Sample 2 / *	$LiNO_3$	2a	1.1	1.2
Sample 3 / *	$LiNO_3$	3a	1.61	1.2
Sample 4 / *	$LiNO_3$	4a	2.5	2.4
Sample 4 / *	$LiOH$	4b	2.5	2.42
Sample 4 / *	Li_2CO_3	4c	2.5	2.55
-	$MnCO_3$, Li_2CO_3	6a	-	1.48

Table 2. The X-ray diffraction characteristics of parent MnO_2 and synthesized $LiMn_2O_4$

Type of a sample	Lattice parameters		Crystal lites size L_1 *	Crystal lites size L_2 *
Parent MnO_2	*	*		
1tetragonal structure	4.26	2.84	306	299
2tetragonal structure	4.39	2.87	572	545
3tetragonal structure	-	-	137	132
4tetragonal structure	-	-	278	-
5 pseudo-tetragon.	9.71	2.86	553	491

LiMn ₂ O ₄ spinels, cubic structure	1a	8.24		304	280
	2a	8.24		414	335
	3a	8.22		395	392
	4a	8.23		502	499
	4b	8.23		581	532
	4c	8.22		476	459
	6a	8.23		743	722



A New 3.8V Cathode for Lithium-Ion Batteries: ϵ -Li_xVOPO₄

T.A. Kerr, J. Gaubicher, and L.F. Nazar

Department of Chemistry, University of Waterloo
Waterloo, Ontario, N2L 3G1 Canada

Recently the search for new cathode materials for lithium ion batteries has lead to the study of metal oxide-polyanion structures such as the vanadium (V) phosphate, VOPO₄. Interest in vanadyl phosphates originates from the high potential of the V³⁺/V⁴⁺ redox couple (~3.85V) and their theoretical capacity of 165mAh/g.¹ Various forms of these structures are known that consist of distorted VO₆ octahedra that are bridged by PO₄ tetrahedra. The VO₆-PO₄ connectivity, however, is slightly different for each structural modification. The tetragonal α form² and the orthorhombic β form are the best known.³ The former is a lamellar compound characterized by a strong anisotropy of its chemical bonds, whereas the β form exhibits three-dimensional structure with interconnecting channels. This structural difference has a marked influence on the electrochemical behavior of the materials. Electrochemical cycling studies on the α_1 and β forms has shown that β -VOPO₄ has better performance yielding good stability with a capacity of ~95mAh/g after 100 cycles.¹

A third related polymorph, designated ' ϵ -VOPO₄', has recently been reported by Lim *et al.*⁴ We have synthesized this material by a hydrothermal reaction in the presence of an amine template at low pH, resulting in the formation of VPO₄·H₂O. The latter was then converted to ϵ -VOPO₄ by heating under oxygen to 550°C. The exact structure of ϵ -VOPO₄ has yet to be determined, although it is thought to be 3D and intermediate between VPO₄·H₂O and β -VOPO₄.⁴

In this communication, we will report our electrochemical study of the reversible Li insertion into ϵ -VOPO₄ and relate this to its structure. Initial electrochemical experiments (20% acetylene black) show that ϵ -VOPO₄ displays distinct reduction processes that occur in the voltage range of 4 V to 200 mV (3.85 V, 2.4V, and below 1 V; Fig. 1). The first two processes are typical first-order phase transitions and correspond to the V⁵⁺/V⁴⁺ and the V⁴⁺/V³⁺ redox couples respectively. Cycling between 4.5 and 3V at 1Li/10h yields good reversibility over the first 20 cycles but with a capacity that remains below 40 % of the theoretical value (Fig. 2). Chemical lithiation of ϵ -VOPO₄ using LiI leads to a lithiated, air stable form, ϵ -Li_xVOPO₄. X-ray diffraction shows that crystallinity is maintained after lithiation, albeit with changes to the framework structure. Structural studies of this phase are in progress. In initial experiments, at least 0.6Li could be extracted from composite electrodes prepared by ball-milling ϵ -Li_xVOPO₄ with 20% acetylene black and further optimization appears possible (Fig. 2). On-going cycling experiments at 1Li/10h yield a reversible capacity of over 100 mAh/g for the first 10 cycles (Fig. 2). Comparison of the galvanostatic curve of ϵ -Li_xVOPO₄ and ϵ -Li_xVOPO₄-(bm) (Fig. 3) indicates that the ball milling process gives rise to an

additional reversible single phase step centered on 3.7V. The influence of the synthetic conditions on the electrochemical behavior, further optimization of this system, along with structural studies will be presented.

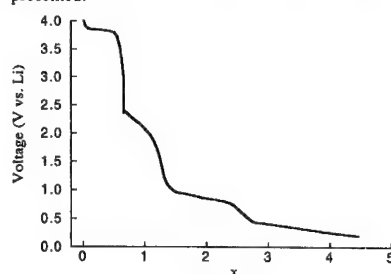


Fig.1: Voltage profile of Li/ ϵ -VOPO₄ at 1Li/10h

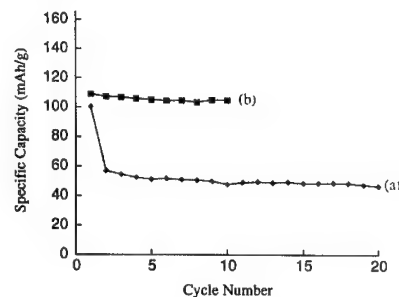


Fig.2: Reversible capacity vs cycle number for (a) ϵ -VOPO₄ (b) ϵ -Li_xVOPO₄-(bm).

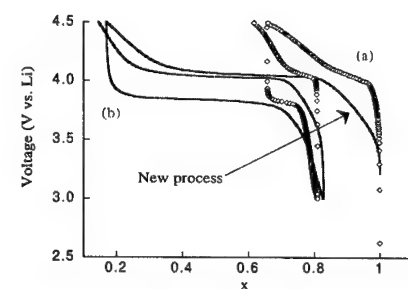


Fig.3: Voltage profile of (a) ϵ -Li_xVOPO₄, and (b) ϵ -Li_xVOPO₄-(bm).

¹ J. Gaubicher, T. Le Mercier, Y. Chabre, J. Angenault, and M. Quarton, *J. Electrochem. Soc.*, **146**, 4375, (1999)

² R. Tietz, *Aust. J. Chem.*, **34**, 2035, (1981)

³ R. Gopal and C. Calvo, *J. Solid State Chem.*, **5**, 432, (1972)

⁴ S.C. Lim, J.T. Vaghey, W.T.A. Harrison, L.L. Dussack, A.J. Jacobson, and J.W. Johnson, *Solid State Ionics*, **84**, 219, (1996)

**Aluminium substituted LiCoO_2
as an intercalation
cathode for lithium polymer
battery**

V.Subramanian*, A. M. Stephan,
S.Venkatraman, S.Gopu Kumar#,
T.Prem Kumar, N.G.Renganathan,
N.Muniyandi and M.Raghavan
Central Electrochemical Research
Institute, Karaikudi, India.

ABSTRACT

Aluminium doped lithium cobalt oxides $\text{LiAl}_{0.05}\text{Co}_{0.95}\text{O}_2$, was synthesized via a sol-gel method¹. Polymer gel electrolyte comprising, poly(methylmethacrylate) (PMMA), LiAsF_6 with a combination of EC and PC as plasticizer was prepared using doctor blade method. The thickness of the film was found to be 100 microns with the conductivity of $10^{-3} \text{ S cm}^{-1}$ at 25°C ². $\text{LiAl}_{0.05}\text{Co}_{0.95}\text{O}_2$ has a good electrochemical activity with a discharge capacity of 130 mAh/g^1 . The diffusion coefficient of the lithium ion has been extracted from the impedance data. A coin cell with $\text{LiAl}_{0.05}\text{Co}_{0.95}\text{O}_2$ as cathode and PMMA/EC/PC/ LiAsF_6 as electrolyte and lithium metal as anode was constructed and studied for its electrochemical activity, and its details will be presented in this paper.

References:

1. V. Subramanian, S. Venkatraman, S. Gopukumar, T. Prem Kumar, V. Sundaram, N.G. Renganathan, N.Muniyandi, M. Raghavan, A. Shivashanmugam and M.Wolfgang Mehrens, J. Materials Chemistry (Communicated).
2. A. Manual Stephan, T. Prem Kumar, V. Sundaram, N.G. Renganathan, S. Pitchumani and N.Muniyandi, Solid State Ionics (in press)

*Presenting author

Corresponding author, Fax: 91-4565-38205,37779, e-mail: gkumar41@hotmail.com

The Jahn-Teller distortion in Li_xNiO_2 and Li_xMnO_2 . C. Marianetti, D. Morgan and G. Ceder, Massachusetts Institute of Technology, USA

It is believed that the Jahn-Teller distortion significantly affects electrochemical performance of materials such as LiNiO_2 and LiMnO_2 . While a cooperative distortion occurs in LiMnO_2 , only local distortions are present in LiNiO_2 and LiMn_2O_4 . When Jahn-Teller ions become diluted with non-Jahn-Teller ions (either through delithiation or by chemical substitution) the cooperative distortion is expected to turn non-cooperative. Using detailed computational modeling, we study how local Jahn-Teller distortions can persist in the presence of non-Jahn-Teller ions. The effect on materials degradation and capacity fade will also be discussed, in particular in the context of the manganese system.

THEORY OF LITHIUM DIFFUSION IN Li_xCoO_2 : A FIRST PRINCIPLES INVESTIGATION

Anton Van der Ven¹ and Gerbrand Ceder¹
¹MIT
 Department of Materials Science Rm 13-4069
 Cambridge, MA 02139
 USA

Transport properties within the different components of a lithium battery are important in determining the rate at which the battery can be charged and discharged. For the cathode, the relevant transport property is the lithium diffusivity since it determines how fast lithium can be removed and reinserted into the cathode.

To better understand the lithium transport properties in layered transition metal oxides such as Li_xCoO_2 and Li_xNiO_2 , we have performed a first principles investigation of the lithium diffusion coefficient in Li_xCoO_2 as a function of the lithium concentration. We find that two different hopping mechanisms are available for lithium migration between neighboring octahedral sites. The first hopping mechanism involves the exchange of a lithium ion with an isolated vacancy, while the second hopping mechanism is mediated by a divacancy. We find that the activation barriers for the two mechanisms are very different and that they vary considerably with the local lithium-vacancy environment. This results in a diffusion coefficient that changes by several orders of magnitude with lithium concentration. The qualitative evolution of the diffusion coefficient is in good agreement with experiment.

We have implemented the calculated diffusion coefficients in continuum diffusion models in combination with continuum elasticity theory to investigate the effect of charging and discharging rates on the lithium concentration profiles within cathode particles. We find that large concentration gradients can be induced under typical charge and discharge rates and that the resultant lithium concentration profiles are accompanied by important stress build-ups that can be detrimental for the integrity of the cathode particle.

Lithium Insertion of $(V_{1-y}Mo_y)_2O_5$

Mika EGUCHI, Fumihiko MAKI, Satomi IWABE and Yoshihiro MOMOSE

Department of Materials Science, Faculty of Engineering, Ibaraki University.

Nakanarusawa 4-12-1, Hitachi, Ibaraki, 316-8511, Japan

INTRODUCTION

V_2O_5 having layered structure is of interest as an insertion cathode material for lithium secondary batteries. The crystal structure of lithium inserted $Li_xV_2O_5$ changes from α - to ϵ - to δ - form reversibly upon lithium insertion up to $x=1$, where the structural change to γ -form occurs irreversibly. Further γ -form changes finally to ω -form at $x=3$ [1].

Substitution of Mo for a part of V in V_2O_5 causes changes in the structure, and at $0.2 < y < 0.3$ in $(V_{1-y}Mo_y)_2O_5$, the oxide belongs to a monoclinic system [2]. Structural changes of these oxides upon lithium insertion, however, have not been reported.

In this study, effects of substitution of Mo for a part of V in V_2O_5 on stability range of each phase and rates and mechanisms of those structural changes were investigated. For this purpose, as the first step of a series of the studies, $(V_{0.75}Mo_{0.25})_2O_5$ was synthesized in powder form by the solid state reaction, and lithium insertion was carried out both by chemical and electrochemical methods. Electron spin resonance (ESR) and X-ray diffraction (XRD) measurements were used to analyse structural changes.

EXPERIMENTAL

Powder samples of $(V_{0.75}Mo_{0.25})_2O_5$ was prepared by a solid state reaction of reagent grade V_2O_5 , V_2O_4 and MoO_3 powders in evacuated quartz ampoules at 660°C for 72 hours [2] and then cooled down to room temperature at a rate of $2^\circ\text{C}/\text{min}$. XRD lines of the sample of $(V_{0.75}Mo_{0.25})_2O_5$ were well described as monoclinic system by Rietveld analysis using the data reported by K. West et al. for $y=0.3$ [2], excepting peaks at $2\theta > 40^\circ$, which could presumably be ascribed to any one of V_9MoO_{40} , $V_{0.87}Mo_{0.13}O_{2.17}$ or V_2MoO_8 .

For chemical lithiation of $(V_{0.75}Mo_{0.25})_2O_5$, n -BuLi/ n -hexane was added to $(V_{0.75}Mo_{0.25})_2O_5$ powder dispersed in n -hexane at $25\sim 85^\circ\text{C}$ under an argon atmosphere. The extent of lithiation was designated by $x = \text{Li} / (0.75V + 0.25Mo)$.

To prepare the electrode mixture of $(V_{0.75}Mo_{0.25})_2O_5$, acetylene black and poly(tetrafluoroethylene) powders in a weight ratio of 60 : 30 : 10 was pressed into a pellet on a porous nickel sheet. A $1 \text{ mol}\cdot\text{dm}^{-3}$ LiClO_4 solution of propylene carbonate (PC) was used as the electrolyte. The reference and counter electrodes were metallic lithium wires.

RESULTS AND DISCUSSION

The structural changes of $(V_{0.75}Mo_{0.25})_2O_5$ upon lithiation were investigated by XRD measurements. At about $x < 1$, peaks except for the starting material were not

observed, and no phase transformation characteristics of V_2O_5 occurred.

ESR spectra also provide a sensitive information on the phase transformations. A broad singlet signal of V(IV) was found, but those of Mo(V) was not detected. Line width of the signal V(IV) (see Fig. 1) increased steeply at about $x=1$.

The open circuit potentials of lithiated $(V_{0.75}Mo_{0.25})_2O_5$ were plotted against x in Fig. 2. In the composition region about $x < 1$, the electrode potential became less noble with increasing x , as is typical of a solid state electrode. At about $x=1$, the electrode potential drops steeply. These dependencies are almost coincided with that obtained from results of ESR and XRD analysis.

REFERENCES

- [1] C. Delmas, H. Cognac-Auradou, J. M. Cocciantelli, M. Ménétrier and J. P. Doumerc, *Solid State Ionics*, **69**, 257 (1994).
- [2] K. West, B. Zachau-Christiansen, S. Skaarup and T. Jacobsen, *Solid State Ionics*, **53-56**, 356 (1992).

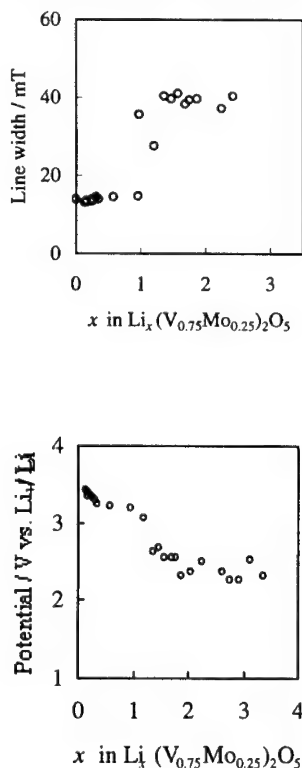


Fig. 1 Changes in the line width of V(IV) with x in $Li_x(V_{0.75}Mo_{0.25})_2O_5$.

Fig. 2 Open circuit potential for $Li_x(V_{0.75}Mo_{0.25})_2O_5$.

Abstract No. 254

Effect of Lanthanum Dopant on the structural and electrical properties of LiCoVO_4 cathode materials investigated by EXAFS

B. J. Hwang^{a)}, Y. W. Tsai^{a)}, G. T. K. Fey^{b)}, and J. F. Lee^{c)}

a) Department of Chemical Engineering, National Taiwan University of Science and Technology, Taipei, Taiwan, R.O.C.

b) Department of Chemical Engineering, National Central University, Chung-Li, Taiwan, R.O.C.

c) Synchrotron Radiation Research Center, Hsinchu, Taiwan, R.O.C.

Since the discovery of LiNiVO_4 and LiCoVO_4 as new cathode materials for secondary lithium batteries, interest in inverse spinel materials has arisen, due to their high voltage behavior [1]. Since both of them are poor electrical conductivity, it is necessary to mix it with significant amounts of good electrical conductor such as carbon black to ensure that the electrode has sufficient electrical conductivity. However, the addition of carbon black lowers the energy density.

Generally the use of a dopant or additive to materials of interest is widely employed to increase its electrical conductivity. In this studies we investigated the effects of lanthanum as dopant to LiCoVO_4 cathode material by using Co and V K-edges X-ray absorption fine structure (EXAFS) spectra. The structural and electrical properties has been discussed. It was observed that LiCoVO_4 has a inverse spinel structure and the coordination number of core Co is 6 in the first shell O. It was found that the Co-O distance is $2.08 \pm 0.01 \text{ \AA}$ and debye-waller factor is $0.012 \pm 0.001 \text{ \AA}$. The electrical conductivity of LiCoVO_4 material depends on the amount of lanthanum dopant.

Reference

1. G.T.K. Fey, W. Li and J.R. Dahn, J. Electrochem.Soc., 141, 227 (1994)

Long-life Manganese Spinel Cathodes for High-power Secondary Batteries for Electric Vehicle Use

Masahiro Kasai, Yoshiaki Kumashiro, Katsunori Nishimura, Hisashi Ando, Yasushi Muranaka
and Yuuzou Kozono

Hitachi Res. Lab., Hitachi Ltd.

7-1-1 Omika-cho, Hitachi-shi, Ibaraki, 319-1292, Japan

Tatsuo Horiba

Saitama Res. Lab., Shin-Kobe Electric Machinery Co., Ltd.

2200 Okabe-cho Oka, Saitama, 369-0297, Japan

High-power-density secondary batteries for electric vehicle (EV) use attract much interest from environmental aspects. Manganese spinel oxide LiMn_2O_4 is considered to be one of the best candidate as a cathode material for the EV use, because it has advantages in safety, cost and natural abundance. However the cycle life of the material was not enough to use as EV batteries. In this paper, we have studied cycle performance and structural change of the spinel manganese cathodes. Long-cycle life cathode materials were achieved for high-power lithium ion batteries like an electric vehicle use.

The cathode materials were synthesized by a solid reaction method varying the $[\text{Li}]/[\text{Mn}]$ molar ratio. X-ray diffraction measurement was performed using RIGAKU diffractometer and the lattice parameter was obtained by least-square fitting. Electrodes for measurement of the electrochemical characteristics were prepared by coating the mixed slurry consisting of the cathode material, conductive graphite powder, and a PVDF binder on an aluminum foil. The thickness of the electrodes was about 100 μm . A test cell with a lithium metal counter electrode and a reference electrode was used for the measurement. A mixed electrolyte of EC and DMC (1M LiPF_6) was used. Cycle tests were performed at room temperature at the voltage ranging from 4.3 to 3.0 volts vs lithium.

Synthesized cathode materials indicate single-phase spinel diffraction patterns. The lattice parameter of the $[\text{Li}]/[\text{Mn}]=0.50$ sample is $a=8.244 \text{ \AA}$, which is consistent with the value reported in JCPDS. As increasing the lithium composition, the lattice parameters decrease compared with the value of the $[\text{Li}]/[\text{Mn}]=0.50$ sample, indicating the increasing of the tetravalent Mn^{4+} ions. The change of the lattice parameters shows saturating behavior above $[\text{Li}]/[\text{Mn}]=0.56$. It is considered that the generation of a small amount of Li_2MnO_3 phase suppresses the increase of the manganese valence, although its diffraction peak cannot be clearly detected. Cycle performance improves dramatically for the Li-rich composition cathode. The capacity fade of the Li-rich cathode materials is less than 2% at 100 cycle. As shown in Fig. 1, cycle life of the cells, using carbon as anodes, shows a 23% capacity fade at 2300 cycles. Such improvement of the cycle performance makes it possible to apply the cathode material to EV use secondary batteries.

Open circuit voltage (OCV) measurement was also examined for $[\text{Li}]/[\text{Mn}]=0.50$ and the Li-rich cathode materials. The results reveals that the plateau, which shows the existence of two kinds of cubic phases with different lattice parameters, diminishes for the Li-rich cathode materials. It is considered that the Li-rich cathode

material shows good cycle performance, because the lattice volume change and the distortion accompanied by charge-discharge cycles decreases.

Especially, a hybrid Electric Vehicle (HEV) needs high-power batteries compared with a pure-EV. High-rate performance is also an important point for applying the Li-rich cathode to HEV batteries. High-rate discharge tests were examined to clarify this point. The Li-rich cathode material shows excellent performance at high discharge rate as shown in Fig. 2. The high-rate performance is also improved drastically. The discharge capacity at 2C is 90 % of the initial capacity. The results indicate that the Li-rich spinel cathode has a good potential for high-power batteries.

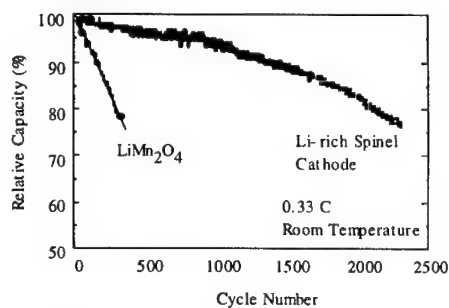


Fig.1 Cycle performance of manganese spinel cathodes.

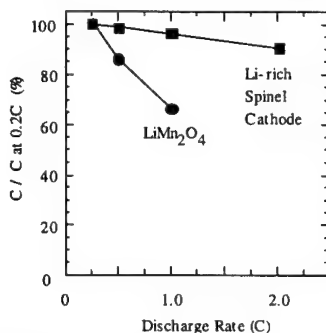


Fig.2 High-rate discharge characteristics of manganese spinel cathodes.

Acknowledgment

This work was supported by the New Energy and Industrial Technology Development Organization (NEDO).

References

- 1) Yuan Gao, J. R. Dahn, J. Elecchem. Soc. **143**, 100, (1996)
- 2) R. J. Gummow, A. de Kock, M. M. Thackeray, Solid state Ionics **69**, 59 (1994)
- 3) K. Nishimura, T. Douzono, M. Kasai, H. Andou, Y. Muranaka, Y. Kozono, J. Power Sources. **81**, 420 (1999)

Abstract No. 256

SYNTHESIS OF $\text{Li}_x\text{Co}_{0.085}\text{Cr}_{0.015}\text{O}_2$ BY THE PVA PRECURSOR METHOD AND APPLICATION AS CATHODE IN LITHIUM ION BATTERIES

Rajaraman Vasanthi,¹ Inachi Ruth Mangani,²
Ramu Chandrasekaran³ and subramanian selladurai⁴

¹Anna University
MIT, Anna University, Chennai-44, India
same
Chennai, Tamil Nadu 600 044
India

²Anna University
MIT, Anna University, Chennai-44
-do-
Chennai, Tamil Nadu 600 044
India

³Anna University
MIT, Anna University
-do-
Chennai, Tamil Nadu 600 044
India

⁴Anna University
MIT, Anna University, Chennai-44
-do-
Chennai, Tamil Nadu 600 044
India

Synthesis of polycrystalline powder of $\text{Li}_x\text{Co}_{0.085}\text{Cr}_{0.015}\text{O}_2$ from poly(vinyl alcohol) gel (a PVA-precursor) is reported. Charge-discharge property is studied by using a coin type cell containing $\text{Li}_x\text{Co}_{0.085}\text{Cr}_{0.015}\text{O}_2$ as cathode material, and Li metal as the anode, in a potential range of 2.5-4.5V. The cathode $\text{Li}_x\text{Co}_{0.085}\text{Cr}_{0.015}\text{O}_2$ exhibits reversible capacity of 160 mAhg⁻¹ initially. The cycling reversibility for the cell with $\text{Li}_x\text{Co}_{0.085}\text{Cr}_{0.015}\text{O}_2$ prepared from the PVA precursor was observed to be much better than that with the one prepared by the high cost of cobalt, LiMn_2O_4 [1] LiNiO_2 and $\text{LiCoXNi}_1\text{-XO}_2$ [2] are considered to be attractive because of the fact that they are inexpensive and they provide higher capacity. In addition, substituted LiCoO_2 may possess high reversible capacity and this is of great significance.

References:

- [1] T. Takada, H. Hayakawa, H. Enoki, J. Power sources 81-82, (1999) sept 505
[2] Y. Jang, B. Huang, H. Wang, J. Power sources 81-81, (1999) sept 589

Abstract No. 257

$\text{LiCr}_x\text{Mn}_{2-x}\text{O}_4$ SOLID SOLUTIONS FOR LITHIUM BATTERIES

R. Thirunakaran,¹ P. Periasamy,¹ B. Ramesh Babu,¹
N. Kalaiselvi,¹ N. G. Renganathan,¹ M. Raghavan¹
and N. Muniyandi¹

¹Central Electrochemical Research Institute
Central Electrochemical Research Institute
Karaikudi 630 006
India

Manganese dioxide has been widely employed as a cathode material in lithium non-aqueous cells. Because of good rechargeability spinel LiMn_2O_4 has gained importance as cathode material in lithium rechargeable cells. Several approaches have been made to combat the problem of Jahn-Teller distortion in the LiMn_2O_4 phase. Substitution of manganese in LiMn_2O_4 by trivalent transition metals is one such. In this paper, results of a study of the influence of Cr^{3+} as a substituent in LiMn_2O_4 are presented. The compositional range of $\text{LiCr}_x\text{Mn}_{2-x}\text{O}_4$ was $0 \leq x \leq 0.4$. Solid-state route has been employed for the preparation of this compound. Kinetics of formation of these compounds has been studied by TG-DTA and phase characterization has been done using XRD.

**SOLID-STATE SYNTHESIS AND
CHARACTERIZATION OF LiCoO₂ AND
LiCo_{1-y}Ni_yO₂ SOLID SOLUTIONS**

P. Periasamy,¹ B. Ramesh Babu,¹ R. Thirunakaran,¹
N. Kalaiselvi,¹ N. G. Renganathan,¹ M. Raghavan¹
and N. Muniyandi¹

¹Central Electrochemical Research Institute
Central Electrochemical Research Institute
Karaikudi 630 006
India

Since the commercialization of the carbon/LiCoO₂ cell by Sony Energytec in 1990, solid solutions of LiCo_{1-y}Ni_yO₂ (a NaFeO₂ type) and their end-members LiCoO₂ and LiNiO₂ have received much attention. The two homologous end-members possess high theoretical discharge capacities of 274 mAh/g which, however, cannot be tapped fully owing to structural instabilities in the former and cation disorder in the latter.

LiCo_{1-y}Ni_yO₂ solid solutions show lower insertion potentials compared to the pure LiCoO₂ phase. Nickel substituted LiCoO₂ phases are, therefore, expected to be oxidatively less taxing on the electrolyte and to retain good lamellar structure upon repeated cycling. In this paper we compare the physico-chemical characteristics of LiCoO₂ and LiCo_{1-y}Ni_yO₂ (0 ≤ y ≤ 0.2) obtained by a solid-state route and analyzed using XRD, FTIR and TG-DTA techniques. The effect of substitution of nickel for cobalt in layered LiCoO₂ phase on the cell voltage, discharge capacity and cyclability has been discussed.

**ELECTROCHEMICAL BEHAVIOUR OF
LiMn_{2-y}MyO₄ (M = Cu, Cr; 0 ≤ y ≤ 0.4)**

B. Ramesh Babu,¹ P. Periasamy,¹ R. Thirunakaran,¹
N. Kalaiselvi,¹ N. G. Renganathan,¹ M. Raghavan¹
and N. Muniyandi¹

¹Central Electrochemical Research Institute
Central Electrochemical Research Institute
Karaikudi 630 006
India

Spinel lithium manganese oxide, LiMn₂O₄, is beset with problems of capacity fading upon repeated cycling. The loss in capacity upon cycling is attributable to Jahn-Teller distortion and manganese dissolution in the electrolyte in the charged state. One way to circumvent this capacity fade is to introduce other 3d transition metal ions in the LiMn₂O₄ lattice. In this paper, we report on the effect of partial substitution of manganese in the LiMn₂O₄ phase with copper (II) and chromium (III) ions. The substituted compounds were synthesized using a solid-state fusion method and characterized using XRD, FTIR and TG-DTA techniques. Chromium bestows greater beneficial effect on the electrochemical discharge behaviour of the cathode than does copper.

Structural and Electrochemical Studies of Layered $\text{Li}(\text{Mn}_{1-y}\text{Ni}_y)\text{O}_2$ Based Compounds. II. $\text{M} = \text{Ni}$.

T.E. Quine, M.J. Duncan, A.D. Robertson,
A.R. Armstrong and P.G. Bruce

School of Chemistry, University of St. Andrews, St.
Andrews, Fife, KY16 9ST, U.K.

Considerable effort of late has focused on the advancement of Li-ion technology driven primarily by consumer demand for affordable renewable power sources. The properties required of a new material for application as a positive electrode in these state of the art devices are wide ranging. The material must be inexpensive, non-toxic and safe while retaining a high specific capacity and low fade rate over many cycles. In this regard, lithium manganese oxide based materials have shown much promise.

Manganese oxides exhibit numerous different structure types of which the 3D framework spinel, LiMn_2O_4 has been investigated extensively as a possible cathode candidate¹⁻⁴. However, compounds based on layered LiMnO_2 are of interest because they can support a higher specific capacity⁵⁻⁸. In particular, we have shown that doping with small quantities of Co into the layered O3 structure improved the fade on cycling^{9,10}. These results show that the properties of such materials can be tailored by changing subtly the composition.

Recently, we have prepared a family of single phase, nickel doped layered LiMnO_2 O3 type materials, $\text{Li}_x(\text{Mn}_{0.9}\text{Ni}_{0.1})\text{O}_2$ ($0 < y < 0.1$), Figure 1. These materials were formed by first preparing the sodium phase then ion exchanging in various Li media.

The dopant level and ion exchange conditions have a profound effect on the electrochemical performance. Figure 2 shows that $\text{Li}_x(\text{Mn}_{0.9}\text{Ni}_{0.1})\text{O}_2$ exhibits an initial capacity in excess of 220 mAhg^{-1} . On extended cycling (>50 cycles) at a cycling rate of 25 mA g^{-1} , $\text{Li}_x(\text{Mn}_{0.925}\text{Ni}_{0.075})\text{O}_2$ retains a capacity of 185 mAhg^{-1} , which corresponds to a cycling efficiency of >99.8% per cycle.

Structural investigation using ex-situ powder XRD has been carried out to elucidate the origin of the different behaviours exhibited by these Ni doped lithium Mn oxide materials. Analogous to the Co doped materials it appears that there is a transformation to a spinel-like material during cycling. The extent of conversion is very dependent on synthesis conditions.

This paper will discuss the interplay between preparation, structure and electrochemical properties of these Ni doped LiMnO_2 materials.

REFERENCES

1. M.M. Thackeray, W.I.F. David, P.G. Bruce and J.B. Goodenough, *Mat. Res. Bull.*, **18**, 461 (1983).
2. J.M. Tarascon, E.W. Wang, F.K. Shokoohi, W.R. McKinnon and S. Colson, *J. Electrochem. Soc.*, **138**, 2859 (1991).
3. R.J. Gummow, A. de Kock and M.M. Thackeray, *Solid State Ionics*, **69**, 59 (1994).
4. Y. Gao and J.R. Dahn, *J. Electrochem. Soc.*, **142**, 100 (1996).
5. A.R. Armstrong and P.G. Bruce, *Nature*, **381**, 499 (1996).
6. F. Capitaine, P. Gravereau and C. Delmas, *Solid State Ionics*, **87**, 197 (1998).
7. G. Ceder, Y.-M. Chiang, D.R. Sadoway, M.K. Aydinol, Y.-I. Jang and B. Huang, *Nature*, **392**, 694 (1998).
8. J.M. Paulsen, C.L. Thomas and J.R. Dahn, *J. Electrochem. Soc.*, **146**, 3560 (1999).
9. A.R. Armstrong, A.D. Robertson, R. Gitzendanner and P.G. Bruce, *J. Solid State Chem.*, **145**, 549 (1999).
10. A.R. Armstrong, A.D. Robertson and P.G. Bruce, *Electrochimica Acta*, **45**, 285 (1999).

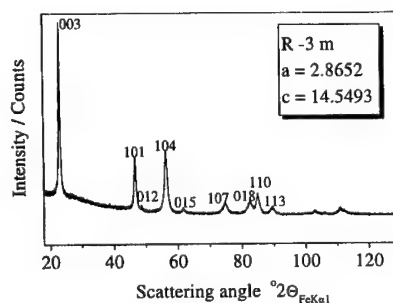


Figure 1. Powder XRD pattern of $\text{Li}_x\text{Mn}_{0.925}\text{Ni}_{0.075}\text{O}_2$.

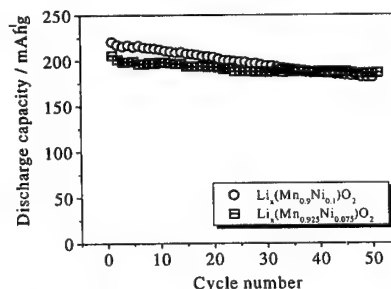


Figure 2. Cycling data for $\text{Li}_x\text{Mn}_{1-y}\text{Ni}_y\text{O}_2$, $y = 0.1, 0.075$
Rate = 25 mA g^{-1} , $V_{\text{limits}} = 2.4\text{--}4.8\text{ V}$.

Abstract No. 261

**IRON-DOPED LITHIUM COBALT OXIDES
AS LITHIUM INTERCALATING
CATHODE MATERIALS**

N. Kalaiselvi,¹ P. Periasamy,¹ R. Thirunakaran,¹
B. Ramesh Babu,¹ T. Prem Kumar,¹ N.
G. Renganathan,¹ M. Raghavan¹ and N. Muniyandi¹

¹Central Electrochemical Research Institute
Central Electrochemical Research Institute
Karaikudi 630 006
India

Layered transition metal oxides of the formula LiMO_2 have good lithium insertion properties for which reason LiCoO_2 and LiNiO_2 have been exploited in practical lithium rocking chair batteries. Another member of the LiMO_2 series, LiFeO_2 , should be an attractive cathode material considering the cheapness and environment-friendliness of iron compounds. Its rock-salt structure, however, does not allow significant amounts of lithium to be reversibly intercalated in its structure. Synthesis of layered LiFeO_2 and study of its lithium intercalating properties have been of limited success. Therefore, an attempt has been made here to study $\text{LiCo}_{1-y}\text{Fe}_y\text{O}_2$ solid solutions ($0 \leq y \leq 0.2$) as prospective cathode materials. Variation of cationic distribution in the $0 \leq y \leq 0.2$ compositional domain is discussed. The electrochemical discharge capacity of these materials is explained as a function of the iron content.

Redox Reactions of Substituted Lithium Manganese Spinel Compounds in Lithium Cells

Yang Shao-Horn and Richard Midaugh
Eveready Battery Company, Inc.
Westlake, OH 44145, USA

ABSTRACT:

Substitution of Mn with small amounts of other metal elements M (such as Li) on the 16d octahedral sites in the spinel structure has been found to improve the cycle life of $\text{Li/Li}_x[\text{M}_x\text{Mn}_{2-x}]\text{O}_4$ cells. These substituted metal elements on the octahedral sites are regarded as electrochemically inactive in the range of potentials studied (3.5 - 4.3 V). Recently, numerous publications reported a near 5 V redox reaction associated with substituted lithium manganese spinel $\text{Li}[\text{M}_x\text{Mn}_{2-x}]\text{O}_4$ compounds vs. lithium [1-14]. These materials are of interest for the positive electrode in the lithium rechargeable cells as they offer higher gravimetric or volumetric energy densities than standard LiMn_2O_4 . Structural characterization studies suggested that this lithium intercalation/deintercalation reaction near 5 V was attributed to the redox of substituted transition metal in the spinel structure. However, the similarity in the redox potentials of different transition metal elements in the spinel structure is abnormal as the redox reactions of 3d transition metal ions normally occur at distinct voltages. In addition, the first-principles calculations indicated that the raise in the lithium intercalation voltage was related to the increase in the tendency for the redox of oxygen [15-16]. Therefore, there is an apparent discrepancy between experimental and theoretical studies with regard to the origin of the ~5 V reaction. We believe that comparing the effects of non-transition and transition metal substitution on the lithium intercalation voltages might provide more insights into the root cause of this reaction. In addition, the change in the valence of manganese ions in the spinel structure upon substitution will be correlated with the presence of this ~5 V reaction.

Chemical, structural and electrochemical studies of cobalt, aluminum and titanium substituted lithium manganese spinel compounds were compared in this work. Single-phase $\text{Li}[\text{M}_x\text{Mn}_{2-x}]\text{O}_4$ ($x = 0.5$ and $\text{M} = \text{Co}, \text{Al}$ and Ti) spinel compounds were prepared. Structural refinements of X-ray powder diffraction patterns showed that the lattice parameter of the spinel structure was found to decrease upon substitution of Co^{3+} and Al^{3+} but to increase for Ti^{4+} substitution, as shown in Table I [17]. The change in the spinel lattice parameter was found consistent with the concentrations of Mn^{3+} and Mn^{4+} ions expected for Co^{3+} , Al^{3+} and Ti^{4+} substituted spinels.

Cyclic voltammetry data of $\text{Li/Li}[\text{Co}_{0.5}\text{Mn}_{1.5}]\text{O}_4$, $\text{Li/Li}[\text{Al}_{0.5}\text{Mn}_{1.5}]\text{O}_4$, and $\text{Li/Li}[\text{Ti}_{0.5}\text{Mn}_{1.5}]\text{O}_4$ cells, with a scanning rate of 0.1mV/s, are shown in Figure 1. A reversible reaction near 5 V was observed for the $\text{Li/Li}[\text{Co}_{0.5}\text{Mn}_{1.5}]\text{O}_4$ cell, which was associated with the redox of $\text{Co}^{3+}/\text{Co}^{4+}$ ions. This is consistent with that reported in the literature. However, an oxidation step at ~5 V was also observed in $\text{Li/Li}[\text{Al}_{0.5}\text{Mn}_{1.5}]\text{O}_4$ cells and it was not reversible upon reduction. The presence of this ~5 V reaction in $\text{Li/Li}[\text{Al}_{0.5}\text{Mn}_{1.5}]\text{O}_4$ could not result from the redox of Al^{3+} in the spinel structure. Therefore, this ~5 V reaction observed in $\text{Li}[\text{M}_x\text{Mn}_{2-x}]\text{O}_4$ spinels could not be attributed solely to the redox of substituted metal ions. Moreover, it was found that $\text{Li/Li}[\text{Ti}_{0.5}\text{Mn}_{1.5}]\text{O}_4$ cells, similar to $\text{Li/Li}[\text{Mn}_2]\text{O}_4$ cells, did not show any redox reactions at voltages above 4.6 V vs. lithium.

$\text{Li}[\text{Co}_{0.5}\text{Mn}_{1.5}]\text{O}_4$ and $\text{Li}[\text{Al}_{0.5}\text{Mn}_{1.5}]\text{O}_4$ that were found to possess a ~5 V reaction had Li/Mn^{3+} ratios larger than 1. They were different from standard $\text{Li}[\text{Mn}_2]\text{O}_4$ and $\text{Li}[\text{Ti}_{0.5}\text{Mn}_{1.5}]\text{O}_4$ in the Li/Mn^{3+} ratio, which had Li/Mn^{3+} ratios equal to 1. It is believed that having a Li/Mn^{3+} ratio larger than 1 is essential for the presence of ~5 V reaction in the $\text{Li}_x[\text{M}_y\text{Mn}_{2-y}]\text{O}_4$ spinels.

REFERENCES:

1. G. Fey, W. Li and J. R. Dahn, J. of Electrochem. Soc., **141**, 2279 (1994).
2. C. Sigala, D. Guyomard, A. Verbaere, Y. Piffard and M. Tournoux, Solid State Ionics, **81**, 167 (1995).
3. C. Sigala, D. Guyomard, A. Verbaere, Y. Piffard and M. Tournoux, J. Solid State Chem., **132**, 372 (1995).
4. Q. Zhong, A. Bonakdarpour, M. Zhang, Y. Gao and J. R. Dahn, J. Electrochem. Soc., **144**, 205 (1997).
5. Y. Ein-Eli and W. F. Howard, J. Electrochem. Soc., **144**, L205 (1997).
6. Y. Ein-Eli, W. F. Howard, S. H. Lu, S. Mukerjee, J. McBreen, J. T. Vaughey and M. M. Thackeray, J. Electrochem. Soc., **144**, L205 (1997).
7. J. McBreen, S. Mukerjee and X. Q. Yang and Y. Ein-Eli, Extended Abstracts of the 194th Electrochemical Society Meeting, Abstract No. 71 (1998).
8. H. Kawai, M. Nagata, H. Tukamoto and A. R. West, J. Power Sources, 3231 (1998).
9. H. Kawai, M. Nagata, H. Tukamoto and A. R. West, J. Mater. Chem., **8**(5), 1273 (1998).
10. H. Kawai, M. Nagata, H. Tukamoto and A. R. West, Electrochem. Solid State Letters, **1**(5), 212 (1998).
11. H. Kawai, M. Nagata, H. Tukamoto and A. R. West, J. Power Sources, in press (1999).
12. M. Y. Song, D. S. Ahn, S. G. Kang and S. H. Chang, Solid State Ionics, **111**, 237 (1998).
13. Y. Ein-Eli, Extended Abstracts of the 194th Electrochemical Society Meeting, Abs. # 70 (1998).
14. Y. Todorov and M. Yoshio, Extended Abstracts of the 194th Electrochemical Society Meeting, Abs. # 112 (1998).
15. G. Ceder, Y.-M. Chiang, D. R. Sadoway, M. K. Aydinol, Y.-I. Jang, B. Huang, Nature, **392**, 694 (1998).
16. T. Ohzuku, S. Takeda and M. Iwanaga, J. Power Sources, **81-82**, 90-94 (1999).
17. H. M. Rietveld, J. Appl. Cryst., **2**, 65-71 (1969).

ACKNOWLEDGMENTS:

Mr. Dennis Meyers and Mr. Steve Osmialowski were acknowledged for laboratory assistance. The authors would like to thank Professor Stephen A. Hackney at Michigan Technological University for fruitful discussions.

Table I Structural parameters of spinel compounds refined by the Rietveld method [17]

Nominal Compositions of Spinel Samples	Lattice Parameter (nm)	Oxygen Position "x"
$\text{Li}[\text{Mn}_2]\text{O}_4$	0.8242(1)	0.263(2)
$\text{Li}[\text{Co}_{0.5}\text{Mn}_{1.5}]\text{O}_4$	0.8134(1)	0.263(1)
$\text{Li}[\text{Al}_{0.5}\text{Mn}_{1.5}]\text{O}_4$	0.8166(2)	0.262(2)
$\text{Li}[\text{Ti}_{0.5}\text{Mn}_{1.5}]\text{O}_4$	0.8288(2)	0.262(2)

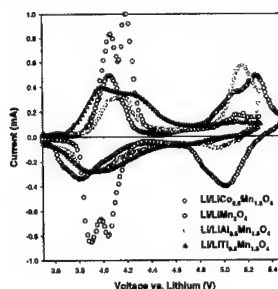


Figure 1 Cyclic voltammetry data of $\text{Li/Li}[\text{Co}_{0.5}\text{Mn}_{1.5}]\text{O}_4$, $\text{Li/Li}[\text{Al}_{0.5}\text{Mn}_{1.5}]\text{O}_4$, and $\text{Li/Li}[\text{Ti}_{0.5}\text{Mn}_{1.5}]\text{O}_4$ cells, under a scanning rate of 0.1mV/s.

Electronic structure of Li_2NiO_4 thin films

Urbano, A.¹, deCastro, Sandra C.¹, Landers, R.¹,
Morais, J.¹, Siervo¹, A. D., Gorenstein, A.¹, Tabacniks,
M.H.², Fantini, M.C.A.²

¹Universidade Estadual de Campinas, Instituto de Física
"Gleb Wataghin" - annette@ifi.unicamp.br

²Universidade de São Paulo, Instituto de Física-

In this work, thin films of Li_2NiO_4 were deposited by r.f. reactive magnetron sputtering in an O_2+Ar atmosphere. The target material was produced by heat treatment of $\text{LiOH}\cdot\text{H}_2\text{O}$ and $\text{Ni}(\text{NO}_3)_2\cdot 6\text{H}_2\text{O}$ mixture. The final powder was cold pressed, in the dimensions of the target. The total pressure during deposition was 7.0×10^{-3} mbar the power was 50_W, and the O_2 flow was varied. The target material and the films were analyzed by Rutherford Backscattering Spectroscopy (RBS) and X-Ray Diffraction. The electronic structure was analyzed by photoelectron spectroscopy, using either X-Ray ($\text{Al K}\alpha$) or Synchrotron Light (120 eV). The last experiments were done at the TGM beamline, National Lab. Synchrotron Radiation, LNLS, Campinas, Brazil, using the Surface Physics Station.

Table I presents the position and relative contribution of the carbon line (1s) obtained by Photoelectron Spectroscopy (XPS data). These lines present three main contributions. The most important contribution is centered at ~289 eV, and is characteristic of a carbonate contribution. The values for Li_2CO_3 reference powder are also shown. Table II presents the atomic ratios.

For the sample deposited in Ar atmosphere ($\phi=0$) the $\text{O1s}/\text{Ni2p}$ ratio is 31(XPS value), but the value obtained by RBS is $\text{O}/\text{Ni}=1.5$. For all samples, the $\text{O1s}/\text{Ni2p}$ ratio is very great, in comparison to the values obtained by RBS. These values can be accepted only if an important contamination of the film surface by Li_2CO_3 is assumed. The valence band spectra also presents the characteristic pattern of Li_2CO_3 contamination (Fig.1). The Li 1s line, e.g. is shifted to higher energies (55eV).

The target material were analyzed by XRD. The fresh powder did not present any carbonate contamination, but after some depositions, diffraction lines from carbonate were present in the diffratograms.

Table I

C1s Lines

Sample	C1s		
	A	B	C
$\phi=9$ sccm	289.2 [21]	287.4 [9]	284.6 [70]
$\phi=4.5$ sccm	289.9 [37]		284.6 [63]
$\phi=0$ sccm	289.9 [71]		284.6 [29]
Li_2CO_3	289.7 [37]		284.6 [63]

Table II

Atomic ratios

	O1s/ C1s	O1s/ C _{CO3}	O1s/ Ni2p	O2s/ O1s	Li1s/ O2s
$\phi=9$ sccm	0.7	3.2	10	1.6	0.70
$\phi=4.5$	0.8	2.2	37	1.5	1.02
$\phi=0$	1.6	2.3	31	1.4	1.05
Li_2CO_3	0.94	2.5		0.80	1.2

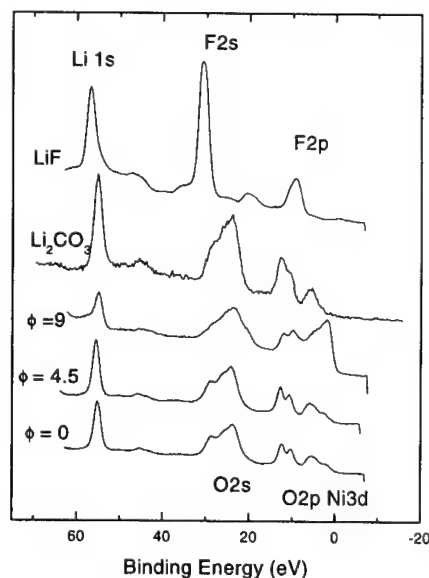


Figure 1

Photoemission spectra obtained at low photon energies (120 eV) for samples deposited at different O_2 flows. The spectra for LiF and Li_2CO_3 reference compounds are also presented.

ELECTROCHEMICAL PERFORMANCE OF CATHODES BASED ON LiMn_2O_4 SPINEL OBTAINED BY COMBUSTION SYNTHESIS

E. I. Santiago, S. T. Amâncio-Filho, P.R. Bueno and L.O.S. Bulhões

Universidade Federal de São Carlos, Departamento de Química, Laboratório Interdisciplinar de Eletroquímica e Cerâmica

Via Washington Luis km 235, Zip Code 13565-905, P.O. Box 676, São Carlos, SP, Brazil.

INTRODUCTION

Lithium secondary batteries have been intensively studied due to the technological importance provided by their high specific energy (1). Several materials have been investigated in order to improve the electrochemical performance of lithium secondary batteries. Layered and spinel oxides are promising materials to be used as cathode electrodes due to high potential *versus* lithium and high volume capacity which favors lithium ions intercalation/deintercalation. However, the synthesis complexity and expensive processes of the layered oxides have become the LiMn_2O_4 spinel more interesting as cathode electrode (2). The disadvantages of the LiMn_2O_4 are the lower specific capacity than cathodes based on layered oxides and capacity loss upon cycling (3). Therefore, several methods of synthesis have been evaluated to improve the electrochemical performance of these cathode electrodes.

The aim of the present work is to analyze the physical and electrochemical properties of the LiMn_2O_4 spinel powders obtained by combustion synthesis.

EXPERIMENTAL

The preparation of the LiMn_2O_4 powders by combustion synthesis was carried out by mixing manganese nitrate tetrahydrate and urea (fuel) with purified water in a glassy silica crucible. The manganese nitrate/urea ratio used was 1:1.75 mol%. The mixture was heated up to 200°C until the ignition and the combustion reaction carries out. The resulting material was heated at 800°C for 4 h using a heat rate of 5°C/min.

The resulting materials before and after heat treatment were analyzed by X-ray diffraction (XRD) (SIEMENS, model D5000, $\text{CuK}\alpha$) and scanning electronic microscopy (SEM) (ZEISS, model DSM 960). The specific surface area values were obtained by B.E.T. isotherms with N_2 adsorption (MICROMETRICS, model ASAP 2000).

Cathodes based on LiMn_2O_4 powders were prepared mixing poly(vinylidene fluoride) (PVDF), carbon black and LiMn_2O_4 powders in the ratio of 5:10:85 w/w% respectively.

Electrochemical cells were prepared using lithium metallic plates as counter and reference electrodes. The electrolyte used was a mixture of ethylene carbonate and dimethyl carbonate (1:1 v/v). The support electrolyte was lithium perchlorate anhydrous. All of electrochemical measurements were performed in a dry box with argon atmosphere.

Cyclic voltammograms were performed at 0.1 mVs^{-1} in the range from 3.5 to 4.5V. Charge-discharge curves were obtained at C/30 rate (70 μA) in the range from 4.2V to 2.5V. EIS data were obtained at 3.0V, 4.05V and 4.2V *dc* potentials that correspond to equilibrium potential, first anodic peak potential and second anodic peak potential

observed on cyclic voltammograms, respectively. The *ac* potential applied was 5 mV rms and the frequency range was 100 kHz up to 1 mHz. The equipment utilized were potentiostat/galvanostat (EG&G, model 283) and frequency response analyzer (SOLARTRON, model SI 1260).

RESULTS AND DISCUSSION

Physical Characterization

The formation of the LiMn_2O_4 was observed by X-ray diffraction. However, it was also observed the formation of the Mn_2O_3 spinel when the resulting materials were not calcinated. The LiMn_2O_4 single phase was observed after heat treatment at 800°C for 4 h. The specific surface area value observed was 1.9 m^2g^{-1} . SEM photomicrographs show that the particles are agglomerated and compacted with particle sizes in the range from 500nm up to 1.5 μm .

Electrochemical Characterization

Cyclic voltammograms of cathodes based on LiMn_2O_4 obtained by combustion synthesis presented two reversible process, usually observed in LiMn_2O_4 systems. The anodic scan is related to the oxidation of Mn^{3+} to Mn^{4+} with lithium ion deintercalation. The reverse processes are observed in the cathodic scan.

Charge-discharge curves showed the limite value of the energy capacity at the first discharge of 107 mAhg^{-1} . This value is in agreement to the values reported of LiMn_2O_4 cathodes obtained by different methods (1).

The impedance spectrum at 3.0V *dc* potential consists of a Randles circuit at high frequencies from 100 kHz up to ~0.1 kHz and a CPE behavior at intermediate and low frequencies range from ~0.1 kHz up to 1 mHz related to electrode interface (low frequency dispersion). In the 4.05V and 4.2V *dc* potential two arcs are observed at high and intermediate frequencies. At low frequency a linear diffusion impedance behavior is observed and can be represented as Warburg impedance. The first arc at higher frequencies is related to Randles circuit elements. The nature of the second arc could be related to the charge capacity or to the grain boundaries in the composite cathode.

CONCLUSIONS

LiMn_2O_4 spinel powders can be obtained by combustion synthesis as single phase presenting good performance to be used as cathode component. It was verified that LiMn_2O_4 -based cathodes have good electrochemical performance and are quite promising for lithium secondary batteries.

ACKNOWLEDGMENTS

We thank CNPq and FAPESP by financial support.

REFERENCES

1. R. Koksang, J. Barker, H. Shi and M.Y. Saïdi, *Solid State Ionics*, **84**, 1 (1996).
2. M.R. Palacin, *J. Electrochem. Soc.*, **144**, **12**, 4226 (1997).
3. Z. Liu, A. Yu and J.Y. Lee, *J. Power Sources*, **74**, 228 (1998).

The Structure Property Relationship Of Lithium Nickel Cobalt Oxides.

R. K.B. Gover, R. Kanno, B. J. Mitchell* and Y. Kawamoto.

Department of Chemistry, Kobe University, Japan.

*IPNS, Argonne National Laboratory, USA.

Introduction.

We present the findings of new studies on the structure of $\text{Li}_x(\text{Ni}_{1-y}\text{Co}_y)\text{O}_2$. The aims of these studies were to examine the effects of sintering temperature, sintering time, Li and Ni content on the structure of these phases and the effects on the electrochemical properties. The structures of the samples have been examined using powder x-ray and neutron diffraction. Structure determination was performed using Rietveld analysis. Studies 1 to 3 were performed on $\text{Li}_x(\text{Ni}_{0.8}\text{Co}_{0.2})\text{O}_2$ samples.

Results. 1. Effects of sintering temperature.

It was found that the sintering temperature primarily affects the degree of Li 3a site disorder. From our studies, we have found that a sintering temperature of 725°C produced the samples with the lowest disordering. This is shown in figure 1. When interpreted in conjunction with charge/discharge experiments it was clearly seen that the Li occupancy has a direct effect on electrochemical properties. However, it was noted that the Ni+Co occupancy varied as a function of sintering temperature, which has been interpreted as being due to the presence of Li on the 3b site.

2. Effects of sintering time.

In the second study, we examined the effects of sintering times on the structure. We prepared samples with sintering times of 3, 24, 48 and 96 hours. It was found that the Li occupancy on the 3a site increased as the sintering time increased, with a maximum obtained for the sample sintered for 48 hours (see figure 2). The sample sintered for 96 hours, however, was found to have the highest initial electrochemical capacities. This could be an indication of the effects of short-range order on the electrochemical properties [1, 2]

3. Effects of Li content.

For this study, we examined the effects of increased Li content in the initial starting mixture. Samples were identical to those presented in study 1, but with higher Li contents. It was found that these samples exhibited superior Li 3a site order, but the deviation in Ni+Co occupancy was greater than that seen in study 1. This is further evidence to support 3b Li. (shown in figure 3.)

4. Effects of Nickel content.

In this final study, we examined the role of Ni content on the structure of our materials. We prepared samples of $\text{Li}(\text{Ni}_{1-y}\text{Co}_y)\text{O}_2$ ($y=0$ to 0.3). Samples prepared with 0.25 and 0.3 were found to have small amounts of Li disorder (neutrons), which is contrary to previous reports in the literature. This is shown in figure 4. Electrochemical measurements on the 0.1 and 0.15 samples also suggested the probability of

phase transitions on charge, which are believed to be similar to that seen for LiNiO_2 .

Conclusions.

Our structural studies suggest that the structure-property relationships of lithium nickel cobalt oxides are more complex than originally envisaged. Our results have consistently suggested the possibility of a new structure model, with Li also present on the 3b site. We will present the findings of our new structure studies and show the effects that these subtle differences have on the electrochemical properties.

[1] J. Thomas, Private communication.

[2] R. Gover, *J. Power sources*, In press.

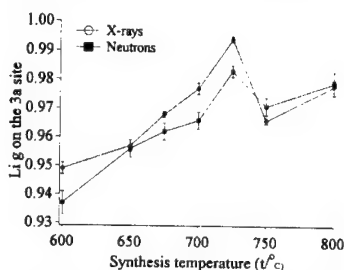


Figure 1. Li 3a g versus sintering temperature.

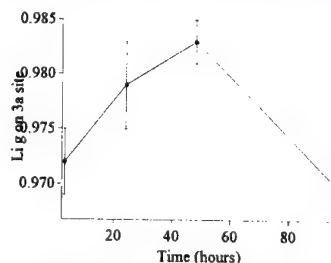


Figure 2. Li 3a g versus sintering time.

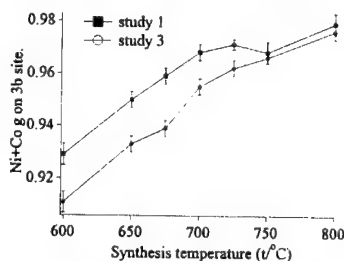


Figure 3. Ni+Co occupancy on 3b site.

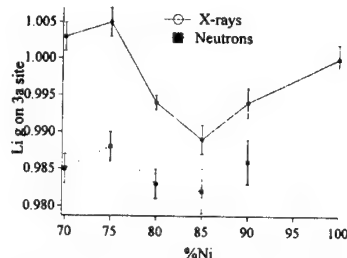


Figure 4. site occupancy of Li on 3a site from neutrons and x-rays diffraction.

**ELECTROCHEMICAL
CHARACTERISTICS OF LiMn_2O_4 -
POLYPYRROLE COMPOSITE CATHODE
FOR LITHIUM POLYMER BATTERIES**

Jong-Uk Kim, Jae-An Lee, Seong-In
Moon* and Hal-Bon Gu

Department of Electrical Engineering,
Chonnam National University
300 Yongbong-dong, Kwangju 500-757, Korea
*Battery Technology Team, Korea
Electrotechnology Research Institute,
28-1 Sungju-dong, Changwon, Kyungnam,
641-600, Korea

Polymer electrolytes were discovered by B. E. Fenton et al.[1] in 1973. P. V. Wright et al.[2] then showed that complexes formed with PEO and alkali metal salts exhibit high ionic conductivity. Subsequently these complexes were proposed by M. B. Armand et al.[3] as polymer electrolyte for solid state battery and electrochemical device applications. Polymer electrolyte have provided the interesting possibility of developing new types of lithium battery, so-called lithium polymer battery(LPB)[4], having thin layers. The LPB is an all-solid state system which consists of a lithium ion conducting polymer electrolyte and two lithium ion reversible electrodes. The LPB can be viewed as a suitable system for wide applications, from thin film batteries for microelectronics to electric vehicle batteries and load leveling batteries. Adding poly(vinylidene fluoride)[PVDF] to PC-EC- LiClO_4 electrolyte, its conductivity becomes higher than that of PEO-PC-EC- LiClO_4 . LiMn_2O_4 is an interesting active material for lithium rechargeable batteries. In this work we report the charge/discharge properties of LiMn_2O_4 -polypyrrole(PPy)/ SPE/Li- cells with cycling.

The polymer electrolyte films were prepared by solution casting and heating. SPE film was 150 μm . The complex impedance of the polymer electrolyte was measured by the AC two electrode method using IM6 Impedance Measurement System(Zahner Elektrik Co.). The AC signal was applied across the cells and its frequency range was from 100mHz to 2MHz. Composite cathode slurry was prepared by mixing LiMn_2O_4 powder with PPy and SPE solution. The mixture slurry was stirred for 6h. The composite cathode films were prepared by coating this slurry on Al foil current collector. The area of LiMn_2O_4 /SPE/Li cells were 2 X 2 cm^2 . The current density of charge/discharge cycling was 0.05 and 0.1mA/ cm^2 . Preparation and tests of cells were carried out in argon-filled glove box.

The conductivity of $\text{PVDFLiClO}_4\text{PC}_{10}\text{EC}_{10}$ with 25wt.% PVDF electrolytes was $2.3 \times 10^{-3}\text{S/cm}$ at room temperature $\text{PVDFLiClO}_4\text{PC}_{10}\text{EC}_{10}$ remains stable up to 4.7V vs Li/Li^+ . The discharge capacity of LiMn_2O_4 -PPy with 7wt.% PPy was 135 and

125mAh/g at 1st and 10th cycle, respectively. Also, the discharge capacity of LiMn_2O_4 -PPy with 10wt.% PPy was 132 and 122mAh/g, respectively. The capacity of LiMn_2O_4 composite with 7wt.% PPy was higher than that of LiMn_2O_4 composite with 10wt.% PPy. We suggest that capacity increasing is due to doping/undoping of anions in PPy.

References

- [1] B. E. Fenton et al., Polymer, Vol. 14, p. 589, 1973.
- [2] P. V. Wright, Brit. Polymer J., Vol. 7, p. 319, 1975.
- [3] M. B. Armand et al., 2nd Int. Meeting on Solid Electrolytes, St. Andrew, Scotland, p. 20, 1978.
- [4] K. M. Abraham and M. Alamgir, J. Power Source, Vol. 43-44, p. 195, 1993.

Abstract No. 267

**Effects of Powder Characteristics of LiMn_2O_4
on the Electrochemical Properties**

Hoon-Taek Chung¹ and Seung-Taek Myung²

¹Dongshin University
Department of Ceramic Engineering
Naju 520-714
South Korea

²Dongshin University
Department of Ceramics Engineering
Naju 520-714
South Korea

Powders of lithium manganese oxide are prepared by the emulsion drying method. The powder characteristics, particle size and shape, stoichiometry etc., could be controlled by changing the synthesis conditions. We investigated the relationship between powder characteristics and electrochemical properties.

ELECTROCOPOLYMERIZATION OF CARBAZOLE DERIVATIVES

A.Sezai SARAC

Istanbul Technical University, Department of Chemistry, 80626, Maslak,
Istanbul, TURKEY

In recent years, special attention has been paid to study, poly(N-vinylcarbazole) due to its high temperature dielectric, high softening points, photoconductive and fluorescence properties [1-4]. Many questions about increasing of stability and processability were not answered completely.

On the other hand, from the point of view of copolymerization of NVCz also holds a particular place, due to its capacity of forming macromolecular compounds leading to the formation of copolymers with properties close to those specificity of PVCz.

The copolymer is expected to gain both conductivity and good mechanical properties from its two components through sacrificing some of these qualities [5].

Recently it has been reported that the preparation of novel comonomers having low oxidation potential, extending conjugation and undergoing facile electrochemical polymerization to form stable electroactive polymers [6-9]. Our studies on the preparation of comonomers based on thiophene-ethylcarbazole and derivatives of pyrrole-ethylcarbazole (dimer and trimer)

suggest that the formation of alternating conjugated copolymers exhibiting the properties of both monomers. CV of such comonomers was compatible with the homopolymer of each constituent (Fig.1 a and b).

The thermal analysis (TGA, DSC) of carbazole/acrylamide(AAm) copolymers were indicated that inclusion of acrylamide into the structure thermally stabilised the polymer. The elipsometry was employed in-situ, monitor the growth of copolymer films, from the optical properties of the film layer thickness were determined. The rate of polymer film growth has a strong effect on the structure of the film. In-situ spectroelectrochemical results of copolymer formation indicated that stable oligomeric carbazole radical cations were copolymerized with other monomer (i.e. Th, AAm) grafting on the electrode surface. Electropolymerization mechanism was proposed. Several polymerization procedures were applied, i.e. electroinduced polymerization, electrochemical polymerization techniques. Conductivities of copolymer and composites were also on line with proposed mechanism.

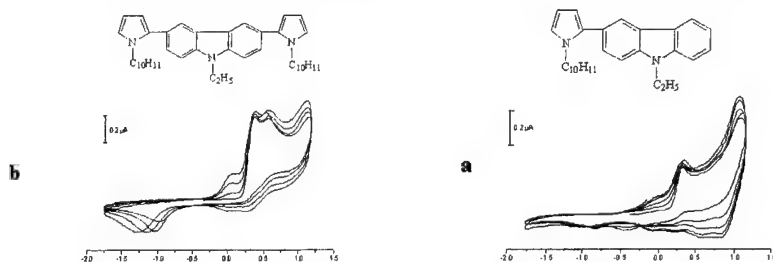


Fig.1 CV of DPETCz (a), and BDPEtCz (b) (10^{-2} M) in 0.1 M Bu₄NPF₆/Pt(0.5 mm) $t = -20^{\circ}\text{C}$

Influence of the particle size on the electrochemical properties of lithium manganese oxide

Chung-Hsin Lu and Shang-Wei Lin

Department of Chemical Engineering, National Taiwan University, Taiwan, R.O.C.

For the utilization of cathode materials in lithium ion batteries, lithium manganese oxide has been intensively developed on account of its inexpensive material cost, acceptable environmental characteristics, and good safety. However, LiMn_2O_4 has the disadvantage of low discharge capacity and significant capacity fading during cycling. Consequently, many researchers have presently focused on improving the electrochemical performance of LiMn_2O_4 . It is regarded that controlling the microstructure of powder can enhance the capacity of cyclability of LiMn_2O_4 . From the viewpoint of morphology, particle size of cathode materials is an important factor to influence the performance of batteries.

In this report, the effects of particle size on the electrochemical performance of LiMn_2O_4 have been studied. A supersonic sieving machine was used to sieve the powders with different size. Scanning electron microscopy (SEM) was used to ensure the sieving effect and examine the microstructure of obtained powder. Size distribution and the average particle size of the sieved powders were analyzed. Powders with different size were prepared as cathodes for cell test. Cells were charged and discharged at 0.2 mA/cm² within the potential ranging from 3 V to 4.3 V.

The relationship between the specific capacity and the cycle number is illustrated in Fig. 1. It is seen that the capacity increases with the decrease in the particle size. In the first cycle, the smallest power of 19.9 μm has the highest capacity of 122.3 mAh/g, while the largest powder of 53.83 μm has the lowest capacity of 110 mAh/g. In addition to the difference in capacity, the cyclability also varies with particle size. After cycling for 10 times, the smallest powder has the best cyclability. On the other hand, increasing the particle size causes more serious fading phenomenon. The above results imply that small powder exhibits better electrochemical performance than the large one. The large surface area and high packing density of the small particle is believed to improve the capacity and cyclability of LiMn_2O_4 [1, 2].

To further investigate the difference of various

particle size in electrochemical behavior, cyclic voltammetry test was carried out. All of the specimens show two distinct peaks, which represent the mixed phases and different stage intercalation of lithium ion. However, when particle size decreases, the oxidation potential is increased for the insertion of lithium ions. Moreover, the peaks become broader with decreasing particle size. The particle size is found to significantly affect the kinetics of intercalation/deintercalation processes.

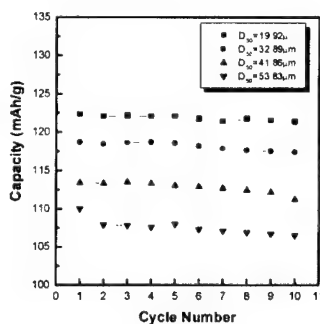


Figure 1. The effects of particle size on the capacity of LiMn_2O_4

Reference:

1. F. K. Shokoohi, J. M. Tarascon, B. J. Wilkens, D. Guyomard, and C. C. Chang, *J. Electrochem. Soc.* 139, 1845 (1992).
2. R. Vacassy, H. Hofmann, N. Papageorgiou, M. Gratzel, *J. Power Sources*, 81, 621 (1999)

Synthesis of nanosized LiMn_2O_4 powder by reverse emulsion process for Li-ion batteries

Chung-Hsin Lu, Susanta Kumar Saha, and Shang-Wei Lin

Department of Chemical Engineering, National Taiwan University, Taipei, Taiwan, R.O.C.

Nowadays, the demand for rechargeable batteries with high energy density and high voltage has increased rapidly due to the advancement and popularity of portable electronic devices. The spinel LiMn_2O_4 is an attractive cathode material for lithium ion batteries, because of its low cost and lower toxicity compared with the layered oxides LiCoO_2 and LiNiO_2 . For the consideration of practical application, it is important to produce LiMn_2O_4 powders with excellent capacity and cyclability.

Here we developed a new chemical method i.e., reverse emulsion process for synthesizing ultrafine LiMn_2O_4 powder. In the reverse emulsion process, kerosene was used as the oil phase, and the aqueous solution as the dispersed phase. The aqueous phase was prepared by dissolving appropriate amounts of lithium and manganese salts in de-ionized water. The ratio between the concentration of lithium ion and that of the manganese ion was 1:2. Surfactant was added to the oil phase for increasing the stability of emulsion. Then the prepared aqueous phase and oil phase were mixed together, and agitated by a homogenizer to obtain homogeneous water-in-oil emulsion. After drying the emulsion, the precipitates were obtained. The precipitates were heated in a furnace to obtain the precursor powder.

The precursor powder was heated at elevated temperature to synthesize the monophasic LiMn_2O_4 powder. X-ray diffraction (XRD) analysis was performed to identify the compounds formed in the quenched powder. It is found that pure phase LiMn_2O_4 was successfully prepared by quenching the precursor at as low as 400°C. No prolonged calcination is required. This emulsion process significantly shortens the reaction time for preparing LiMn_2O_4 .

To examine the reaction process and weight loss of the precursors, the dry precursors were subjected to thermal analysis at a heating rate of 10°C/min. In the DTA curve, one endothermic peak and one exothermic peak are observed around 120°C and 390°C, respectively. The endothermic peak is considered to be due to the removal of the moisture and volatile organic from the precursor. The exothermic peak at 390°C is attributed to the exothermic decomposition of residual organic present in the precursor.

Infrared spectrometry (IR) was used to examine the presence of organic species in the quenched samples. The bands at 865 and 1400-1600 cm^{-1} in the

sample quenched at 400°C indicate the presence of carbonyl groups from organic species. The samples quenched at 500°C or higher temperatures, the carbonyl group completely disappears, revealing the complete removal of the organic species from the sample. As for the bands appearing at around 500 and 620 cm^{-1} , it is attributed to the characteristic metal-oxygen absorption bands of LiMn_2O_4 .

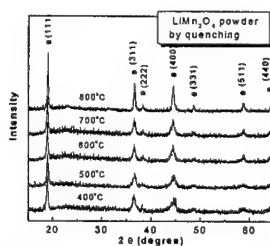


Figure 1. XRD pattern of quenched LiMn_2O_4 samples.

Scanning electron microscopy (SEM) and transmission electron microscopy (TEM) were carried out to observe the microstructures and particle size of the obtained powder. The powders exhibit a homogeneous morphology in a dispersed state. The particle size of the obtained powder is within narrow size distribution in the range of 30-50 nm. The electrochemical properties of obtained powder were investigated in an electrochemical cell, which comprised a cathode, an anode and an electrolyte of 1 M LiPF_6 in EC/DEC solution. As a result, this developed reverse emulsion process successfully prepared monophasic and nanosized LiMn_2O_4 with good electrochemical properties.

References:

1. M.M. Thackery, W.I.F. David, P.G. Bruce, J.B. Goodenough, *Mater. Res. Bull.* 18 (1983), 4611.
2. J.M. Tarascon, E. Wang, F. Shokoohi, W.R. Makinon, S. Colson, *J. Electrochem. Soc.* 138 (1991) 2859.
3. R.J. Gummow, M.M. Thackery, *J. Electrochem. Soc.* 141 (1994) 1178.
4. Y.H. Ikuhara, Y. Yamoto, K. Kikuta, S. Hirano, *J. Mater. Res.* 14 (1999) 31.

Abstract No. 271

High Purity Lithium Carbonate for Battery Applications
Stephen Harrison, Kamyab Amouzgar*
and Guy St-Amant*

LIMTECH Inc.
Tour de la Cité,
2600 boul. Laurier, Bureau 840,
Sainte-Foy, Québec
Canada G1V 4W2

*LTEE d'Hydro-Québec
600 avenue de la Montagne
Shawinigan, Québec
Canada G9N 7N5

Lithium carbonate is an important starting material in lithium ion and lithium metal battery applications. It is used in the manufacture of the electrolyte salts such as LiPF_6 and LiBF_4 as well as in the manufacture of both cobalt- and manganese-based cathode structures. This paper describes a unique patent process for the production of high purity lithium carbonate, as well as a new route to the production of battery grade lithium metal.

The overall process developed by LIMTECH for the production of lithium metal involves the purification of technical grade lithium carbonate obtained from brine salt flat purification in Argentina or Chile. The purification process can be used to produce lithium carbonate of different purities, ranging from 99.9 to 99.999 %. Once the lithium carbonate has been purified to the required purity it is then converted into lithium chloride by reaction with gaseous chlorine in a lithium chloride melt at temperatures between 450 and 650°C. This method of lithium chloride production produces lithium chloride that is extremely dry when compared with alternative routes. The lithium carbonate produced is then ready for direct use in molten salt electrolysis to give battery grade lithium metal. The high purity of the feedstock means that the lithium metal produced by electrolysis is, after filtration to remove salts and other insoluble materials, of a high enough purity to be used in the production of lithium metal batteries.

The process that has been developed for the purification of lithium carbonate is based on the formation of aqueous lithium bicarbonate by reacting lithium carbonate with carbon dioxide at ambient temperatures and pressures between 1 and 10 atmospheres of carbon dioxide. Insoluble impurities such as iron and silica are then removed by filtration from the solution. The solution, still under pressure, is then passed through a divalent selective cation exchange resin such as those containing aminophosphonic acid groups designed to absorb divalent ions such as calcium and magnesium from the solution. The next step in the new process is to increase the temperature to around 100°C and to release the applied pressure. Under these conditions the carbon dioxide is driven out of the solution and purified lithium carbonate is precipitated. The purified lithium carbonate is then filtered, washed and dried to complete the process. The solutions and the washings are partially recycled. The degree of recycle of these solutions determines the purity of the product, as key impurities such as sodium and sulfate remain in solution during the precipitation step of the process. A typical process flow sheet is shown in figure 1.

The effect of carbon dioxide pressure on the solubility of lithium carbonate is shown in figure 2; the effect of increasing the temperature on lithium carbonate solubility is shown in figure 3.

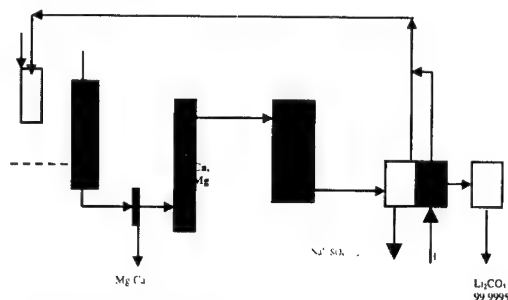


Figure 1: Process Flowsheet

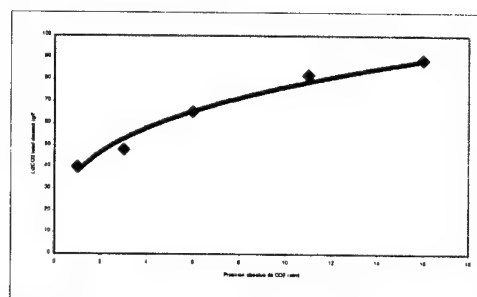


Figure 2: Effect of pressure on lithium carbonate solubility

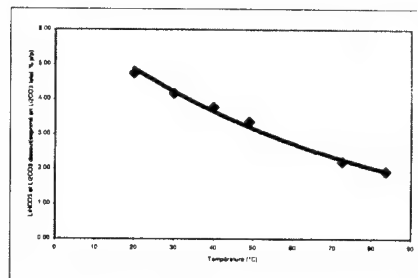


Figure 3: Decreasing solubility of lithium carbonate with temperature

Viscosities, Conductivities and Activation Energies for Transport Processes in Liquid Electrolytes. The Quasi Lattice Approach.

A. Chagnes¹, B. Carré¹, P. Willmann² and D. Lemordant¹

¹Laboratoire Physicochimie des Interfaces et des Milieux réactionnels, Université de Tours, Faculté des Sciences, parc de Grandmont, F 37200 TOURS.

²CNES, 18 Avenue E. Belin, F 31055 TOULOUSE Cedex

Knowledge of the viscosity and conductivity of electrolyte solutions is needed for Li-batteries use. At the same time, these physical properties provide useful insights into solution structure and interactions. Butyrolactone (BL) is a very common dipolar solvent having a dissociating power toward Li salts like LiClO₄. For this reason, it has been chosen for this study.

Concentration dependence of viscosity: the Jones-Dole equation¹

The viscosity-concentration relationship is illustrated in figure 1 for LiClO₄ in butyrolactone. The solid line is given by the Jones-Dole equation with a quadratic term added:

$$\eta/\eta^0 = 1 + A\sqrt{C} + BC + D C^2$$

At concentrations ranging from 0.2 to 2.0 M, the \sqrt{C} term is negligible and A is equal to zero. Curve fitting gives B and D values at 298K: B = 0.42 Lmol⁻¹, D = 0.98 L²mol⁻². The B term originates in the ion-solvent interaction and is dependent on the size of the ions. The D term is mostly controlled (as seen later) by coulombic interactions between ions.

Concentration dependence of conductivity: the lattice model²

The equivalent conductivity-concentration relationship is illustrated in figure 2 for LiClO₄ in BL. The Debye-Hückel-Onsager treatment of electrolytic conductivity has been adapted to the lattice model through the replacement of the Debye reciprocal length κ_D by $\kappa_L = M(2000 N_A C)^{1/3}$, where M is the analogous of the Magdelung constant for the pseudo-lattice, N_A the Avogadro's number and C the molarity of the salt. The solid line drawn on the graph reported in Fig. 2 fits equation (2):

$$\Lambda = \Lambda^0 - (H\Lambda^0 + J) \kappa_L / 3 = \Lambda^0 - K C^{1/3}$$

It is found that Λ^0 extrapolated from the cube root law does not differ significantly from Λ^0 obtained from the square root law

Temperature dependence of the viscosity and conductivity

Linear plots are obtained when the logarithms of the viscosity ($\ln \eta$) or the conductivity ($\ln \kappa$) are plotted against the reciprocal temperature $1/T$. The energies of activation for the two processes E_{η} and E_{κ} are deduced from the slope. If E_{η} varies linearly with the salt's concentration, E_{κ} exhibits a $C^{4/3}$ dependence as shown in Fig 3. The quasi lattice model adapted for the activation energy leads to:

$$\Delta E = E_{\kappa} - E_{\kappa}^{\infty} = k C^{4/3}$$

$$\text{with } k = 2 N_A^{4/3} e^2 M V_{\text{BL}} (10^3)^{4/3} / 4 \Pi \epsilon^0 \epsilon_r Z^{1/3}$$

Experimental value is $k = 1855 \text{ J}(\text{mol/L})^{-4/3}$

Theoretical value using $M=6$ is $k = 1680 \text{ J}(\text{mol/L})^{-4/3}$

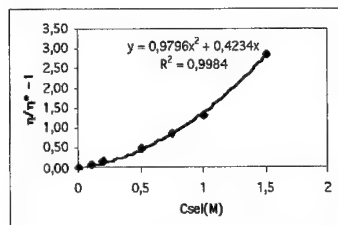


Figure 1

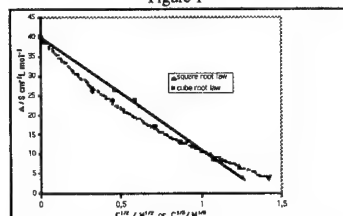


Figure 2

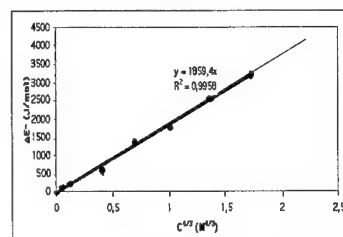


Figure 3

Conclusion

Here we present experimental evidence that the lattice model can be applied successfully to electrolytes solutions used in Li-batteries. The conductivity and viscosity dependencies on concentration and temperature have been highlighted. Nevertheless this model does not take into account the nature of the ions involved in the transport process. Further research is needed to better understand ion-ion and ion-solvent interactions in these media.

¹ G. Jones and M. Dole, J. Am. Chem. Soc., 51 (1929), 2950

² G. Murphy, J. Chem. Soc. Faraday Trans. 2, 79 (1983), 1607.

Abstract No. 273

Optimisation of the Polyelectrolyte used in Carbon Particle Pretreatment

Robert Dominko¹, Jernej Drofenik¹, Marjan Bele¹,
Stane Pejovnik^{1,2}, and Miran Gaberšek¹

¹National Institute of Chemistry, Hajdrihova 19,
SI-1000 Ljubljana, Slovenia

²Faculty of Chemistry and Chemical Technology,
University of Ljubljana, Slovenia

As reported earlier^{1,2} and, also, in this Symposium³ passivation of carbon particles used as anode material can be influenced by particle pretreatment in an aqueous solution of a polyelectrolyte. The Li loss on pretreated particles in the first cycle can be as low as 10-15%, while the reversible capacity remains higher than 300 mAh/g (current rates between to C/7 and C/3 have been checked). The reduction of passivation is due to formation of a thin uniform film the growth of which is governed by the uniformly distributed polyelectrolyte molecules on the surface of carbon particles. Furthermore, certain polyelectrolyte types have a sticky character which glue carbon particles together strongly enough that no conventional binder has to be added to the anode material to prepare mechanically stable anodes.

In this paper we present an optimisation of the polyelectrolyte properties with respect to 1) polyelectrolyte composition, 2) specific groups present on given polyelectrolyte molecule, 3) shape of polyelectrolyte molecule, 4) pH, temperature and concentration of the polyelectrolyte solution and 5) additives (salts and/or surfactants) in polyelectrolyte solution. It is shown that these parameters have a significant impact on both passivation and adhesion between carbon particles.

The results concerning passivation are explained in terms of a generalised passivation model verified using impedance spectroscopy measurements accompanied with typical charge-discharge curves for the selected case.

The binding properties of the polyelectrolyte molecules are explained on the basis of separate Atomic Force Microscopy experiments.

Acknowledgements

This research is sponsored by NATO's Scientific Affairs Division in the framework of the Science for Peace Programme. The financial support from the Ministry of Science and Technology of Slovenia is also fully acknowledged.

References

1. M. Gaberšek, M. Bele, S. Pejovnik, J. Drofenik, and R. Dominko, Patent application No. P-9900238, Bureau for Intellectual Property of the Republic of Slovenia, Ljubljana, Slovenia, October, 1999.
2. M. Gaberšek, M. Bele, S. Pejovnik, J. Drofenik, and R. Dominko, *Electrochemical and Solid-State Letters*, in print.
3. Miran Gaberšek, Marjan Bele, Jernej Drofenik, Robert Dominko, and Stane Pejovnik, this Symposium, see Contribution entitled "Improved Carbon Anode Properties: Pretreatment of Particles in Polyelectrolyte Solution".

NEW FUSIBLE LITHIUM SALT WITH HIGH CONDUCTIVITY IN SOLUTIONS

Wu Xu, Marcelo Videia and C. Austen Angell*

Department of Chemistry
Arizona State University
Tempe, AZ 85287-1604, USA

The application of ionic conductors as electrolytes in electrochemical devices requires the development of ionic conductors containing alkali metal cations which are the most mobile species and therefore the principal carriers of electrical current in the presence of a d.c. field. The ionic rubber systems are potentially superior electrolytes for ionic devices [1], but their application has been held back by the absence of suitable electrochemically stable low melting salts and salt combinations. To achieve this requirement a synthetic strategy that focuses on the size of the counter ion has been adopted. Synthesis of new salts which are chemically stable and have sufficiently low melting points to be incorporated in room temperature stable liquid phases has proven extremely difficult. Most new salts prove to have high melting points so high that decomposition occurs before fusion. In this work we describe the synthesis of a stable low melting lithium salt which has the additional advantage, from the electrolytic cell point of view, that it is heavily fluorinated. This confers certain advantages in cell performance.

The salt we have prepared is the lithium salt of an orthoborate in which the four oxygens are pairwise bridged by a perfluorinated derivative of pinacol, to give a giant anion containing 24 fluorine atoms. For easy visualization, the formula of the salt can be written $\text{LiB}[\text{OC}(\text{CF}_3)_2]_4$. The purified salt melts at 120°C, and can be sublimed at about 130°C under vacuum. The DTA-TGA thermogram shows that the melt remains stable up to about 160°C, the limit of heating in our experiments. The glass transition temperature cannot be measured directly because of the rapid crystallization on cooling below the melting point. However, by the $T_g/T_m = 2/3$ rule for glassformers, the T_g must be well below $(120+273) \times 2/3 = 262\text{K}$ (-11°C). The salt is soluble in all normal electrolyte solvents, though solubility in dimethoxy ethane, DME, is less than 1M at ambient temperature.

The conductivity of the salt in the molten state is shown in Arrhenius form in Figure 1. It is seen that the conductivity is only $7.1 \times 10^{-6} \text{ Scm}^{-1}$ at the melting point 120°C and has a very large temperature dependence. The behavior is that of a heavily ion-paired salt, presumably because the lithium ions find it difficult to relocate amongst the possible sites on and between the giant anion, special orientation of neighboring anions being a requirement for the jump to be possible.

When the salt is dissolved in solvents however the picture is quite different. The conductivity of a 0.6M solution in DME is $11.1 \times 10^{-3} \text{ Scm}^{-1}$ at 25°C, the same as that of the 1M DME solution of the salt reported by Barthel et al. [2], lithium bis(tetrafluoro-1,2-benzenediolate (2-)-O,O') borate $\text{LiB}(\text{OC}_6\text{F}_5)_2$, which was the highest of any 1M DME lithium organic salt solution reported. This makes the salt a candidate for application in any cells in which DME and other ether solvents are desirable. The conductivity of the 0.6M solution of $\text{LiB}[\text{OC}(\text{CF}_3)_2]_4$ in DME is shown as a function of temperature in Arrhenius form in Figure 1. The behavior of a 1M solution of $\text{LiB}[\text{OC}(\text{CF}_3)_2]_4$ in the solvent with higher dielectric constant, propylene carbonate (PC), is also shown in Figure 1. The conductivity, $2.1 \times 10^{-3} \text{ Scm}^{-1}$ at 25°C, is essentially the same as that of the common salt lithium triflate in PC.

The lithium ion transference number of this salt in DME was obtained as 0.57 using diffusivities measured by NMR pulse field gradient (PFG) Spin Echo technique ($D_{\text{anion}} = 5.5 \times 10^{-10} \text{ m}^2\text{s}^{-1}$ and $D_{\text{Li}^+} = 6.1 \times 10^{-10} \text{ m}^2\text{s}^{-1}$) and correcting for ion pairing [3]. In PC, the lithium ion transference number of this salt was measured as 0.53. The high lithium ion transference number for this salt is due to its giant perfluorinated anion. The electrochemical stability for each of the DME and PC solutions was determined from cyclic voltammograms which show the

electrochemical window is at least 4.5 V, probably limited by the solvent in each case.

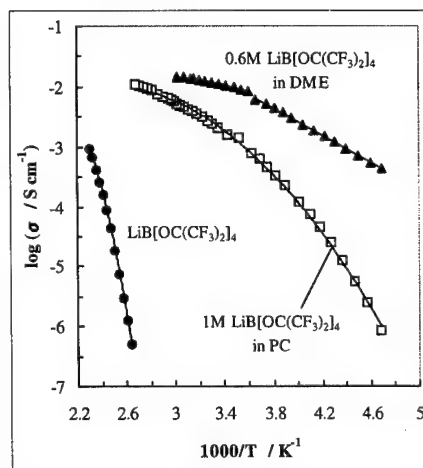
References

1. C. A. Angell, Changle Liu and E. Sanchez, *Nature*, **362**, 137 (1993).
2. J. Barthel, R. Buestrich, E. Carl and H. J. Gores, *J. Electrochem. Soc.*, **143**(11), 3572 (1996).
3. M. McLin and C. A. Angell, *J. Phys. Chem.*, **100**, 1181 (1996).

Acknowledgement

This work was supported by the DOE under contract no. DEFG0393ER14378-003.

Figure 1. Arrhenius plots of the ionic conductivity of the pure molten $\text{LiB}[\text{OC}(\text{CF}_3)_2]_4$ salt, a 0.6M solution in DME and a 1M solution in PC.



Application to Lithium Battery Electrolyte of
Lithium Chelate Compound with BoronY. Sasaki,¹ M. Handa, S. Sekiya, K. Kurashima, and
K. Usami²

- 1) Department of Applied Chemistry, Faculty of
Engineering, Tokyo Institute of Polytechnics
1583 Iiyama, Atsugi, Kanagawa 243-0297 JAPAN
2) Research & Development, DENSO CORPORATION
1-1 Showa-cho, Kariya, Aichi 448-8661 JAPAN

Many workers have attempted to develop improved electrolytes for lithium batteries with high energy density and good rechargeability as power sources for many portable instruments and electric vehicles because of protection against natural environment and resources. Recently, Barthel et al. reported new lithium organoborates as lithium salts for lithium battery electrolytes, such as lithium bis[1,2-benzenediolato(2-)-O,O']borate (LBBB), lithium bis[2,3-naphthalenediolato(2-)-O,O']borate (LBNB), lithium bis[2,2'-biphenyldiolato(2-)-O,O']borate (LBBPB) and lithium bis[salicylato(2-)-O,O']borate (LBSB), as shown in Fig. 1. In previous papers, we reported the thermal characteristics and the electrolytic behavior in propylene carbonate(PC)-1,2-dimethoxyethane(DME), ethylene carbonate(EC)-DME, PC-tetrahydrofuran(THF) and EC-THF binary solvent electrolytes containing these lithium salts.

The purpose of the present study is to elucidate the electrolytic behavior and charge-discharge characteristics of lithium electrode in PC- and EC-tetrahydrofurans such as 2-methyltetrahydrofuran(2-MeTHF) and 2,5-dimethyltetrahydrofuran(2,5-DMeTHF) binary solvent electrolytes containing these lithium organoborates in comparison with those in PC- and EC-based DME and THF binary solvent electrolytes.

The specific conductivities in PC- and EC-based equimolar binary solutions containing 0.3 mol dm⁻³ lithium organoborates at 25 °C are shown in Table I. The order of specific conductivities in Table I is LBBB>LBNB>LBSB>LBBPB, which is different from that of viscosities (LBBPB>LBNB>LBSB>LBBB) in these solutions. In LBNB and LBSB electrolytes, specific conductivity of LBNB electrolyte with higher viscosity than that of LBSB becomes high. This means that the conductivity of LBNB electrolyte depends on the increase in dissociation degree of LBNB rather than that of viscosity of LBNB electrolyte. The lithium cycling efficiencies in PC-based equimolar binary tetrahydrofurans electrolytes are shown in Fig. 2. The PC-2-MeTHF and PC-2,5-DMeTHF electrolytes containing LBSB show the highest cycling efficiencies, more than 90 % at a higher range of cycle number. Figure 3 shows the lithium cycling efficiencies in PC-DME, PC-2-MeTHF, PC-2,5-DMeTHF and EC-2-MeTHF equimolar binary solutions containing mixed electrolyte of 0.15 mol dm⁻³ LBBPB and 0.15 mol dm⁻³ LiPF₆ at 25 °C. The mixed electrolyte / PC-2,5-DMeTHF solution shows higher cycling efficiency than those in PC-2-MeTHF and PC-2,5-DMeTHF electrolytes containing LBSB with the highest efficiency in Fig. 2. It is found that the addition of LiPF₆ to LBBPB electrolyte contributes to the increase in cycling efficiency of the electrolyte containing LBBPB. In conclusion, the LBSB/PC-2-MeTHF and LBSB/PC-2,5-DMeTHF, especially the mixed electrolyte of LBBPB+LiPF₆/PC-2,5-DMeTHF solutions are good electrolytes for rechargeable lithium batteries.

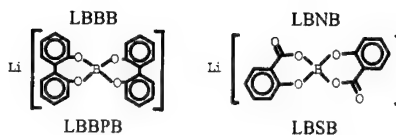
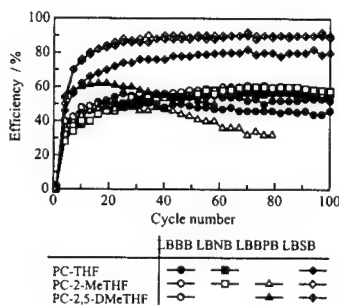
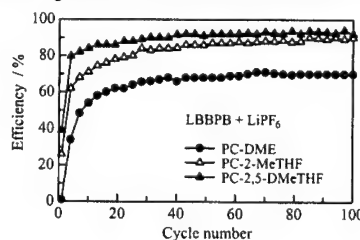


Fig. 1. Lithium compounds with boron.

Table I. Specific conductivities in PC- and EC-based equimolar binary solutions containing 0.3 mol dm⁻³ lithium organoborates at 25 °C.

Mixed solvent (mol ratio 1:1)	Specific conductivity / mS cm ⁻¹			
	LBBB	LBNB	LBBPB	LBSB
PC-DME	4.21	4.25	1.09	2.45
EC-DME	4.69	4.76	—	3.03
PC-THF	3.77	3.75	—	1.57
EC-THF	4.39	4.30	—	2.12
PC-2-MeTHF	3.07	2.97	0.92	1.28
EC-2-MeTHF	3.53	3.30	1.24	1.54
PC-2,5-DMeTHF	2.27	—	0.60	0.87

Fig. 2. Variation of lithium cycling efficiencies in 0.3 mol dm⁻³ PC-based tetrahydrofurans electrolytes containing lithium organoborates at 25 °C. $i = 0.1 \text{ mA cm}^{-2}$ Fig. 3. Variation of lithium cycling efficiencies in PC-based equimolar binary solutions containing 0.15 mol dm⁻³ LBBPB and 0.15 mol dm⁻³ LiPF₆ at 25 °C. $i = 0.1 \text{ mA cm}^{-2}$

ACKNOWLEDGMENTS

This study was conducted as a partial study of "Dispersed Type Battery Energy Storage Technology Research and Development" under a contract with the New Energy and Industrial Technology Development Organization (NEDO) for the "New Sunshine Program" by the Agency of Industrial Science and Technology (AIST), Ministry of International Trade and Industry (MITI).

MICROPOROUS PVDF MEMBRANE FOR LITHIUM-ION BATTERIES

F. Bodin, C. Lenhof, G. Caillon
Tel 33 5 57 10 68 89, Fax 33 5 57 10 68 77
e-mail francois.bodin@saft.alcatel.fr
Saft Direction de la Recherche, 111 bd Alfred Daney,
33074 Bordeaux, France

I.I. Olsen
SAFT America Inc. Lithium Battery Division, 313
Crescent Street, Valdeese NC 28690, USA

In lithium-ion technology, lithium ions are exchanged between negative and positive intercalation materials. Insulation between negative and positive electrode is provided by a microporous polyolefine separator that offers liquid electrolyte channels between the two electrodes. Its major characteristics are the following: polyolefin nature, thickness of 20 to 30 μm and 40% porosity. Its cost is expensive due to a complex manufacturing process. A microporous PVDF (polyvinylidene fluoride) matrix has been developed at the SAFT R&D center. This PVDF membrane is directly coated on the negative electrode by phase inversion process using two different techniques: either immersion in a non-solvent, or selective evaporation. The objective was to tailor its characteristics (microstructure, porosity and thickness) to manufacture flat lithium-polymer cells with electrochemical performances identical to lithium-ion batteries.

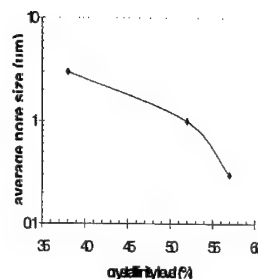
PVDF crystallinity has a direct influence on the microstructure type of the membrane obtained by phase inversion. Different commercial PVDF grades are available with very different crystallinity levels. For example Kynar Flex 2850 (PVDF copolymer with 5% HFP from Elf-Atochem) has 38% crystallinity and Kynar 741 (PVDF homopolymer from Elf-Atochem) 54% crystallinity. The higher the crystallinity level, the smaller the poresizes in the membrane is. At the same time, the swelling of PVDF in liquid carbonate based electrolytes is also linked to the crystallinity. Consequently the choice of PVDF grade is the first parameter to adjust membrane characteristics but it's not the only one. Membranes were prepared by immersion of an acetone + PVDF solution in an alcohol with different PVDF crystallinity levels. Membrane porosity was high (70 to 75 %) and independent of PVDF crystallinity for the range studied. The average pore size of the membrane (measured by Coulter porosimetry), however correlated well with PVDF crystallinity (figure 1).

At present, it has proved to be a challenge to manufacture uniform PVDF membranes on negative electrode with thicknesses less than 40 μm using phase inversion and retain the insulation properties. Therefore, additional post-treatments were tested. The objective was to reduce the PVDF membrane thickness preserving insulation properties and without affecting liquid electrolyte transport between the two electrodes. Another objective was to bond the positive electrode with the PVDF membrane coated negative electrode to form flat cells in one piece. Different combinations of pressure and temperature were tested to achieve the objectives.

PVDF membrane and the electrodes were made and assembled in a non-controlled environment to form flat cells in one piece. Standard active materials and electrolytes of lithium-ion were used. After careful drying, the cell stack was activated with liquid electrolyte and packed in a pouch,

manufactured from multi-layer plastic/metal foils. Impedance measurements and cycling tests at C and 2C rates were performed for different membrane characteristics and various stack manufacturing conditions.

Figure 1: Influence of PVDF crystallinity on average pore size of membrane manufactured by immersion of an acetone + PVDF solution in alcohol



Synthesis of a New Family of Fluorinated Boronate Compounds as Anion Receptors and Studies of Their Use as Additives in Lithium Battery Electrolytes

H. S. Lee, X. Q. Yang, X. Sun and J. McBreen
Brookhaven National Laboratory, Upton, NY
11973

Numerous studies have been done on developing new electrolyte for lithium battery with high ionic conductivity, and good chemical and electrochemical stability. In addition to the research on new salts and solvents, the use of cation receptors to reduce ion pairing in non-aqueous electrolytes has been considered as an approach to improve the properties of electrolytes.¹ Although both cation and anion receptors enhance the dissociation of ion pairs and increase the conductivity of electrolytes, the use of anion receptors is more attractive for a lithium battery electrolyte because anion receptors increase the lithium transference number in the electrolyte. However, most available neutral anion receptors complex with anions through hydrogen binding and cannot be used in lithium batteries.² Recently, we have reported on synthesis of a series of new neutral boron compounds as anion receptors based on the idea that electron-deficient boron would seek negative ligand from the ion pair. The anion complexation effect of these boron compounds was further enhanced by attaching electron-withdrawing groups.^{3,4} Here we report synthesis of another new family of boronate compounds. The effect of these new compounds on conductivity of lithium salts in non-aqueous solution was studied. The molecular weights of these new boronate compounds are lower than our previously reported boron compounds. Therefore, their effects on conductivity enhancement are superior. They also display high electrochemical stability up to 5 V.

Experimental

Ten fluorinated 1,3,2-benzodioxaborole and 1,3,2-Dioxaborolane compounds were synthesized in our laboratory. The chemical structure of these compounds was shown in Figure 1. Electrolyte conductivity measurements were made on a Hewlett-Packard 4129A Impedance Analyzer using a cell with Pt electrodes. Electrochemical stability measurements were performed using a Solatron SI 1287 Electrochemical Interface in the potential dynamic mode.

Results and Discussion

The ionic conductivity of electrolytes based on lithium salts $\text{CF}_3\text{CO}_2\text{Li}$ and $\text{C}_2\text{F}_5\text{CO}_2\text{Li}$ dissolved in DME are very low, with respective conductivities of only 3.3×10^{-5} and 2.1×10^{-5} S/cm at concentrations of 0.2 M. LiF is insoluble in this solvent. With addition of compound 1-9 as additive, the conductivities of 0.2 M solutions of $\text{CF}_3\text{CO}_2\text{Li}$ and $\text{C}_2\text{F}_5\text{CO}_2\text{Li}$ salts in DME were greatly increased to the range of 1.1×10^{-3} to 4.52×10^{-3} S/cm. The conductivity enhancement effect of these compounds increases with increasing number of the electron-withdrawing groups. Using compound 4 to 9 as an additive, even LiF was dissolved in DME at concentration as high as 1.2 M. For example, when fully fluorinated compound 5 was used as additive, the conductivity of LiF solutions in DME reached as high as 9.54×10^{-3} S/cm at 0.8M.

Acknowledgement

This work was supported by the U. S. Department of Energy Division of Materials Science of the Office Basic Energy Sciences, and the Office of Energy Research, Laboratory Technology Research Program, under Contract No. DE-AC02-98CH10886.

References

1. M. C. Lonergan, M. A. Ratner, D. Shriver, *J. Am. Chem. Soc.*, **117**, 2344 (1995).
2. F.P. Schmidtchen and M. Berger, *Chemical Reviews*, **97**, 1609 (1997).
3. H. S. Lee, X. Q. Yang, C. L. Xiang, J. McBreen, L. S. Choi, *J. Electrochem. Soc.*, **145**, 2813 (1998).
4. X. Sun, H. S. Lee, S. Lee, X. Q. Yang and J. McBreen, *Electrochem. Solid-state. Lett.*, **1**, 239 (1998).

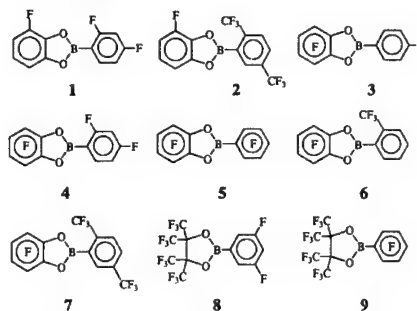


Figure 1 The chemical structures of fluorinated boronate compounds.

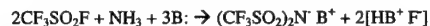
Abstract No. 278

Lithium Bisperfluoroalkylsulfonimides:
Primary and Secondary Lithium Battery Electrolyte Salts
SD Boyd*, BJ Johnson, LJ Krause, WM Lamanna,
PT Pham, H. Shimada
3M Company
236-2A-01
Maplewood, MN
55144-1000, USA

3M pioneered the use of lithium triflate ($\text{CF}_3\text{SO}_3^- \text{Li}^+$) FC-122, for high performance primary lithium batteries. This presentation highlights the utility of lithium imide salts, $(\text{RfSO}_2)_2\text{N}^- \text{Li}^+$ (Rf is a perfluoroalkyl moiety) for primary (1°) and secondary (2°) batteries.

In 1992, 3M commercialized the imide salt HQ-115, $(\text{CF}_3\text{SO}_2)_2\text{N}^- \text{Li}^+$, lithium bistrifluoromethylsulfonimide. HQ-115 shows excellent performance in 1° batteries and lower voltage 2° batteries. A limitation of HQ-115 is its aluminum pitting potential of 3.55V¹ which limits application in higher voltage lithium battery chemistries. This was resolved with introduction of the experimental product lithium bisperfluoroethylsulfonimide (BETI), $(\text{CF}_3\text{CF}_2\text{SO}_2)_2\text{N}^- \text{Li}^+$, shown to have an aluminum corrosion potential of 4.5V¹.

These products are based on the RfSO_2^- moiety, which is basic to 3M's electrochemical fluorination production capability. The imide salts are made by the reaction of RfSO_2F with ammonia, as, in the case of HQ-115:



Conducting the reaction in a stepwise manner allows flexibility for the production of a variety of imides, including unsymmetrical imides such as the methyl butyl imide (MBI), $\text{CF}_3\text{SO}_2(\text{C}_4\text{F}_9\text{SO}_2)_2\text{N}^- \text{Li}^+$.

Imide salts exhibit several features that are important for lithium ion batteries; i.e. thermal stability, hydrolytic stability, redox stability, solubility, corrosion resistance and conductivity. For example, Figure 1 shows the thermal stability of BETI relative to LiPF_6 by TGA analysis. BETI shows no evidence of decomposition beyond 300°C.

Hydrolytic stability of imide salts is excellent, being virtually unreactive with water. This lack of reactivity could require a less dry manufacturing environment (less capitol cost) and less concern with water that enters the battery during storage.

The aluminum corrosion potential with HQ-115 in secondary batteries is improved with BETI and MBI, 4.5V and 4.62V respectively¹. Figure 2 shows that BETI's corrosion current is comparable to LiPF_6 at 4.2V, approximately 2 $\mu\text{A}/\text{cm}^2$, at 1 h. HQ-115 and lithium triflate are, respectively 10 and 20 mA/cm^2 ; a 4 orders of magnitude improvement in the corrosion current.

1225 Coin cell battery tests have shown that high current rates can be achieved in 1 Molal imide solutions. Figure 3 shows the sustained discharge capacity versus discharge current density for BETI and LiPF_6 . These data support the use of BETI as a competitive 2° battery salt.

Imide salt issues with high temperature storage, high temp cycling and, thermal runaway, have been addressed and

will be presented. It has been found that additives such as organic and inorganic lithium salts can improve BETI performance under high temperature, 60°C, storage and cycling.

Figure 1. Thermal Gravimetric Analysis

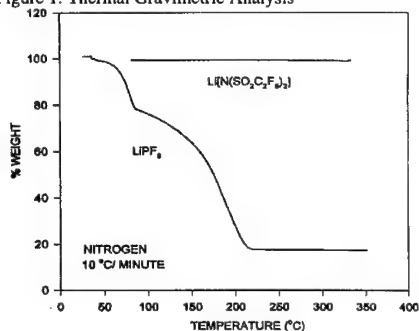


Figure 2. Chronoamperometry of 1M Electrolytes in PC at Aluminum Electrode at 4.2V (vs Li+/Li)

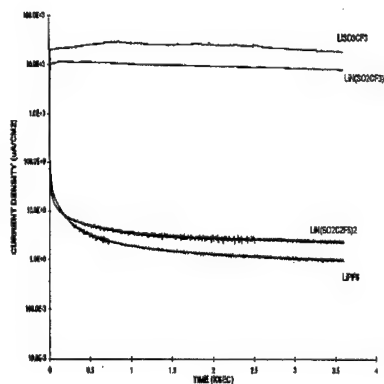
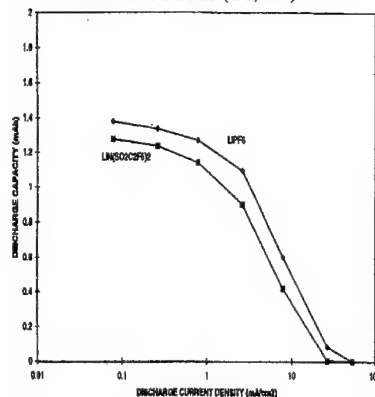


Figure 3 Sustained Discharge Rate, 1Molal LiPF_6 and BETI in EC:DMC (1/1;V/V)



¹Krause, L. J.; Lamanna, W.; Sumerfield, J.; Engle, M.; Korba, G.; Loch, R.; Atanasoski, R.; *J. Power Sources*, **68**, 320-325, (1997).

Thermal Stability of LiPF_6 EC:EMC Electrolyte for Lithium Ion Batteries

Gerardine G. Botte and Ralph E. White
Center for Electrochemical Engineering
Department of Chemical Engineering
University of South Carolina
Columbia, SC 29208

Zhengming Zhang
Celgard, Inc
13800 South Lakes Drive
Charlotte, NC 28173

Despite the improvement and developments in safety (PTC, CID, shutdown separator,^{1,2} chemical shuttles,^{3,4} cathode additives,^{1,5} etc) for the lithium ion battery, there are still some safety concerns associated with scale up to large scale applications such as electric vehicles. For this reason some researchers have performed thermal stability studies in these batteries.⁶⁻¹⁵ Adiabatic calorimeters (ARC)^{7,10-12} and differential scanning calorimeters (DSC)^{6,9,14} have been the most popular analytical techniques for these studies. These techniques have been used successfully to study the anode and cathode materials in the presence and absence of electrolytes.^{6,7,9-12,14} However, not much work has been done to study the thermal stability of the electrolytes *per se*.

In this work a DSC is used to perform a thermal stability study of LiPF_6 EC:EMC electrolyte. This is one of the electrolytes currently used in lithium ion batteries along with mixtures of other carbonates such as PC, DMC, and DEC.¹⁶ This work is the beginning of a project that involves the analysis of other solvents mentioned above.

The effect of different variables on the thermal stability of LiPF_6 EC:EMC was evaluated: salt (LiPF_6) concentration effect, solvents, EC:EMC ratios, and heating rates. The electrolyte solvents and salt were purchased from EM industries Inc. All of them were 99.9 % pure with less than 30 ppm of water. Stainless Steel Hermetic sealed pans from Haake were used in the experiments. Samples between 4.0 and 8.0 mg of electrolyte, salt, or solvents were placed in the DSC pans. The pans were hermetically sealed by crimping. The samples were prepared in a dry room at a temperature between 22-24 °C and a dew point of -60 °C. The samples were run in a DSC 2910 from TA Instruments. The weight of the samples (pans + electrolyte) was taken before and after the experiment to verify that the system was hermetic. In all the cases, the weight was kept constant indicating that there were no leaks during the experiments.

Figure 1 shows the DSC curves for the 1 M LiPF_6 EC:EMC electrolyte system and its individual components at 10 °C/min scan rate. The decomposition reaction of the salt with EC is exothermic, while the reaction of the salt with the EMC is endothermic. The reaction of the LiPF_6 EC:EMC is a combination of the individual reactions between LiPF_6 -EC and LiPF_6 -EMC, that is, the endothermic pick is due to the reaction of LiPF_6 -EMC and the exothermic pick is due to the reaction of LiPF_6 -EC. The EC, EMC and EC:EMC also decompose due to the temperature effect and these reactions are exothermic. The LiPF_6 melts before

decomposing. The decomposition reaction of LiPF_6 is endothermic. Further analysis and additional results will be presented.

REFERENCES

1. K. Ozawa, *Solid State Ionics* **69**, 212 (1994).
2. F. C. Laman, M. A. Gee, and J. Denovan, *J. Electrochem. Soc.* **140**, L51 (1993).
3. M. N. Golovin, D. P. Wilkinson, J. T. Dudley, D. Holonko, and S. Woo, *J. Electrochem. Soc.* **139**, 5 (1992).
4. T. J. Richardson and P. N. Ross, *J. Electrochem. Soc.* **143**, 3992 (1996).
5. U. von Sacken, Paper presented at *POWER '97*, 5th International Conference on Power Requirements for Mobile Computing and Wireless Communications, Santa Clara, CA, Oct 12-15 (1997).
6. Z. Zhang, D. Fouchard, and J. R. Rea, *J. Power Sources* **70**, 16 (1998).
7. U. von Sacken, E. Nodwell, A. Sundher, and J. R. Dahn, *Solid State Ionics* **69**, 284 (1994).
8. J. R. Dahn, E. W. Fuller, M. Obravac, and U. von Sacken, *Solid State Ionics* **69**, 265 (1994).
9. A. Du Pasquier, F. Disma, T. Bowmer, A. S. Gozdz, G. Amatucci, and J. M. Tarascon, *J. Electrochem. Soc.* **145**, 472 (1998).
10. M. A. Gee and F. C. Laman, *J. Electrochem. Soc.* **140**, L53 (1993).
11. J.-S. Hong, H. Maleki, S. Al Hallaj, L. Redey, and J. R. Selman, *J. Electrochem. Soc.* **145**, 1489 (1998).
12. M. N. Richard and J. R. Dahn, *J. Electrochem. Soc.* **146**, 2068 (1999).
13. A. Ohta, H. Koshina, H. Okuno, and H. Murai, *J. Power Sources* **54**, 6 (1995).
14. E. P. Roth, Abstract 388, The Electrochemical Society Meeting Abstracts, Vol. 99-2, Honolulu, Hw, Oct 17-22 (1999).
15. K. Kumai, H. Miyashiro, Y. Kobayashi, K. Takei, and R. Ishikawa, *J. Power Sources* **81-82**, 715 (1999).
16. S. Hossain, *Handbook of Batteries*, D. Linden (Ed.), McGraw-Hill, Inc., New York (1995).

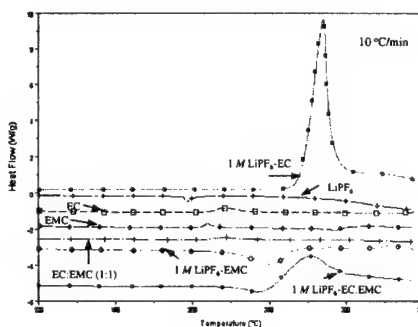


Figure 1. DSC curves for 1 M LiPF_6 EC:EMC (1:1) and its individual components.

Trans-Esterification of Ethylmethyl Carbonate in Lithium Ion Batteries

Beat Dobler, Ivan Exnar, Wolfgang Haupt, and Roman Imhof

RENATA Batteries SA
Kreuzenstrasse 30
CH-4452 Itingen, Switzerland
e-mail: roman.imhof@renata.com

Introduction

The choice of the electrolyte solution is one of the key issues in the development of lithium ion batteries. Electrolyte degradation reactions taking place during the formation process of the battery are of crucial importance for the electrochemical performance of the battery. Numerous studies have been performed during the past few years to clarify the degradation mechanism of different electrolyte solutions. However, the main object of most of these studies was focused on the analysis of the thin SEI film formed on the negative electrode, rather than on the composition and the influence of the electrolyte solution itself.

We present results about the trans-esterification reaction of ethylmethyl carbonate (EMC) to dimethyl carbonate (DMC) and diethyl carbonate (DEC) according to the following equation^{1,2}:



The ratio between the concentrations of [DMC + DEC] and [EMC] was monitored as a function of different constant current charging rates during the first charging cycle.

Experimental

Prismatic open type lithium ion batteries (950 mAh) with a 1:1 (w/w) mixture of ethylene carbonate (EC) and EMC (1 M LiPF₆) were used in this study. Neither traces of DMC nor DEC could be detected in the fresh electrolyte. In an argon filled glove box (H₂O, O₂ < 10 ppm) the freshly assembled open cells were charged to 4.10 V with different constant currents between 50 mA and 1900 mA (CCCV) and the concentrations of the resulting electrolyte solvents were determined by GC analysis. Additional batteries were closed after this first charging step and cycled 50 times between 2.75 and 4.10 V at a 1C/1C rate. Subsequently, the composition of the electrolyte solution was determined.

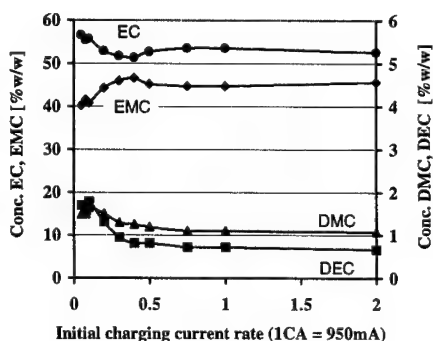
Results

The figure shows that DMC and DEC are formed during the initial charging step in the range of 1-2 weight %. However, the concentration of the four different electrolyte solvents EC, EMC, DMC, and DEC are functions of the applied charging current rate.

Small charging currents yield higher fractions of the trans-esterification products DMC and DEC.

Due to the different time frame of the formation process with the different charging currents and due to the open cell setup one has to scale the results according to the mass losses during the experiment. The scaled ratio between the concentrations of [DMC + DEC] and [EMC] increases by a factor of 2 going from a 2C to a C/20 charging current rate. Batteries where no charging current was applied do show no traces of DMC and DEC.

Further results about the cycling performance of the batteries and possible reaction mechanisms



will be discussed.

References

1. M. Terasaki, H. Yoshida, and H. Tukamoto, *Denki Kagaku*, **61**, 1417 (1993).
2. H. Yoshida, T. Fukunaga, T. Hazama, M. Terasaki, M. Mizutani, and M. Yamachi, *J. Power Sources*, **68**, 311 (1997).

Kinetic Aspects of HF Generation in a LiPF₆ Based Electrolyte Solution

Ivan Exnar, Beat Dobler, Wolfgang Haupt, and Roman Imhof

RENATA Batteries SA
Kreuzenstrasse 30
CH-4452 Itingen, Switzerland
e-mail: roman.imhof@renata.com

Introduction

Protic impurities in the ppm range are known to have major influence on the performance of lithium ion batteries. The high reactivity of LiPF₆ with trace amounts of water to produce HF is known¹ and the negative role of HF in lithium ion batteries is well documented². However, little is known about the kinetics of the LiPF₆ decomposition in electrolyte solutions which are used in consumer batteries.

We present results about the HF generation of a LiPF₆ based electrolyte solution in ethylene carbonate (EC) / ethylmethyl carbonate (EMC) upon addition of different amounts of water.

Experimental

Electrolyte solutions of the composition EC/EMC (1:1 w/w) with 1 M LiPF₆ of two suppliers (Merck, Germany and Tomiyama, Japan) were used (H₂O < 20 ppm, HF < 35 ppm). All experiments were carried out in an argon filled glove box under temperature control. A typical experiment was carried out as follows: 100 ml of the electrolyte solution was filled into a carefully cleaned aluminum bottle and a defined amount of water was added. The H₂O and HF content was checked periodically. The aluminum content of the electrolyte solution was determined at the end of the experiment by AAS. Experiments with additions of 100, 250, 500, 750, and 1000 ppm water have been performed.

Results

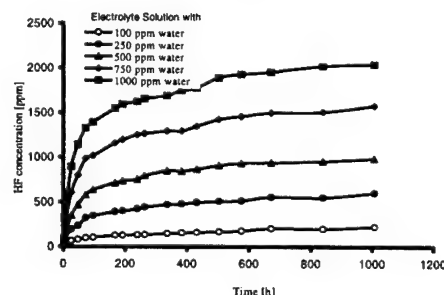
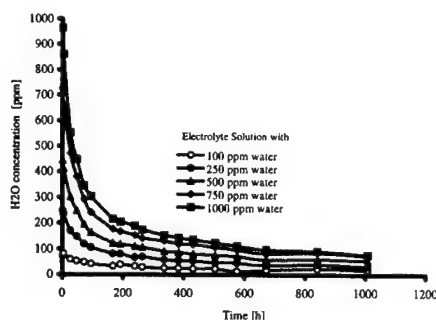
The figure shows the development of the concentrations of water (top) and HF (bottom) in the electrolyte solutions upon the addition of the specified amount of water. The initial reaction between water and LiPF₆ is described by the following overall reaction:



This first-order reaction was used to evaluate a rate constant of the initial reaction in the order of 10⁻³ s⁻¹ for both electrolyte solution systems. The value corresponds well with literature data about the direct decomposition of LiPF₆ salt with water¹. After prolonged reaction time the courses of the water and HF concentration show that the reaction kinetic slows down notably. An electrolyte solution without addition of water reveals no significant change in both, the water and HF con-

centration under the same experimental conditions.

The kinetic data, possible reaction mechanisms and a comparison of the two commercial samples will be discussed.



References

1. C.G. Barlow, *Electrochem. Solid State Lett.*, **2**, 362 (1999).
2. See for example: U. Heider, R. Oesten, and M. Jungnitz, *J. Power Sources*, **81-82**, 119 (1999).

NEW LI-ION ELECTROLYTES FOR LOW TEMPERATURE APPLICATIONS

S. Herreyre, O. Huchet, S. Barusseau, F. Perton,
J.M. Boder¹, Ph. Biensan

SAFT - DRE - 113 bld A. Daney, 33074 Bordeaux cedex FRANCE
¹ SAFT - rue G. Leclanché, BP 1039, 86060 Poitiers cedex FRANCE

INTRODUCTION

In order to allow new application fields for Li-ion batteries, one of the main goals is the increase of the performances at low temperature. The aim of this study is the development of new electrolyte compositions, able to lead to good discharge ability under -20°C , which is presently the limitation with carbonate solvent mixtures.

EXPERIMENTAL

Because of their very low freezing point [1], specific esters have been studied for low temperature applications: Methyl Acetate (MA) [2], but also Ethyl Acetate (EA) and Methyl Butyrate (MB).

Formulations were optimised in term of conductivity and compared to a EC/DEC/DMC mixture, recently studied at low temperatures [3].

Best compositions (with Vinylene Carbonate additive) have been tested in prismatic cells (ICP144350 - 2 Ah - graphite negative electrode), on an Arbin Battery Test system. Cells were charged at 4.1 V under a low rate (C/5), then put at low temperature during 15 h. A discharge was performed down to 2 V under different rates. Capacities were compared to the results obtained at room temperature (C/5 discharge rate).

RESULTS

Conductivity - Binary and ternary mixtures containing EA or MB displayed outstanding conductivity properties under -20°C : up to 7 mS/cm @ -20°C and 4 mS/cm @ -40°C have been reported, instead of 2 mS/cm (-20°C) for usual electrolytes.

Low temperature performances - Table 1 describes the discharge ability at low temperatures of cells filled with the optimised formulations. At -30°C , under a C/2 rate, about 85% initial capacity was recovered with EC/DMC/EA, EC/DMC/MB and PC/EC/MB formulations. On bigger cells (ICP176065), even at -40°C (C/5 rate), same mixtures enabled to recover more than 75% initial capacity. These experiments were also performed in cells with Nickel doped positive material, with similar exceptional results.

The discharge profile recorded at low temperature presents a voltage drop at the beginning of the discharge. This phenomenon, due to the high internal resistance of the cell at low temperatures, is the main limitation of the cell performance. Because of their high conductivities, EA and MB based electrolytes enabled to decrease the impact of this parameter.

Moreover, cells with these electrolyte compositions displayed fading rates at room temperature similar to those observed in carbonate mixtures (fig. 2). Even after 200 cycles, a fading rate between 0.03 and 0.05%/cycle was measured.

Self-discharge were also very similar, demonstrating the stability of the passivating layer formed on the graphite in EA and MB electrolytes. In terms of safety, these electrolytes displayed also a very good behaviour. All the results will be discussed in details in the full paper.

CONCLUSION

Contrary to previous results in MA mixture on Li/LiMn_{1.9}Co_{0.1}O₄ cell [2], EA and MB ternary mixtures enabled performances at room temperature similar to carbonate mixtures in Graphite/LiCoO₂ or Graphite/LiNi_{0.91}Co_{0.09}O₂ cells. This could be related to the chemical instability of metallic lithium in these esters, which would generate difficulties in the studies versus Li.

At low temperature, patent pending electrolyte compositions containing EA and MB enabled very good performances down to -30°C , even under a C rate.

Acknowledgements - Part of this work was done in collaboration with Merck KGaA and supported by the European Community in the frame of a Brite-Euram contract.

[1] *Industrial Solvents Handbook*, E.W. Flick, 4th edition, edited by Noyes Data Corp. (1991).

[2] K. Hayashi, Y. Nemoto, S. Tobishima, Y. Sakurai, *Key Eng. Mater.* **169-170**, 221 (1999).

[3] M.C. Smart, B.V. Ratnakumar, and S. Surampudi, *J. Electrochem. Soc.*, **146**, 486 (1999).

Table 1 - Discharge performances of ICP144350 cells at low temperatures with specific EA and MB electrolytes

Electrolyte composition	EC/DEC/DMC LiPF ₆ 1M	EC/DMC/EA LiPF ₆ 1M	EC/DMC/MB LiPF ₆ 1M	PC/EC/MB LiPF ₆ 1M
First rate efficiency	83%	92%	78%	84%
Rev. Capacity (C/5 rate)	1.98 Ah	1.98 Ah	2.0 Ah	1.96 Ah
-20°C				
Disch. capacity (C/2 rate)	96%	90%	91%	98%
Disch. capacity (C/5 rate)	92%	88%	91%	96%
-30°C				
Disch. capacity (C/2 rate)	0%	88%	84%	95%
Disch. capacity (C/5 rate)	0%	87%	90%	98%
-40°C				
Disch. capacity (C/2 rate)	0%	81%	87%	Not tested

** percentages were calculated from the discharges capacity at RT under a C/5 rate

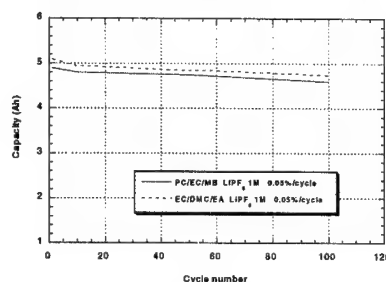


Figure 2 - Evolution of rev. capacity in ICP176065 cells with specific EA and MB electrolytes (RT - C rate)

Electronic Structures and Electrochemical Properties

of $\text{LiPF}_{6-n}(\text{CF}_3)_n$

Fusaji Kita, Hideo Sakata, Akira Kawakami, Haruki Kamizori*, Takaaki Sonoda*, Hideo Nagashima*, Natalya V. Pavlenko** and Yuri L. Yagupolskii
Hitachi Maxell Ltd. Battery R&D Laboratory, 1-1-88, Ushitora, Ibaraki, Osaka, 567-8567, Japan
* Institute of Advanced Material Study, Kyushu University, Kasuga, Fukuoka 816-8580, Japan
** Institute of Organic Chemistry Ukrainian Academy of Science, Dom5, Murmanskaya, Kiev-94, 253660, Ukraine

1. Introduction

We have developed some new organic lithium salts for lithium battery electrolyte such as $((\text{CF}_3)_2\text{CHOSO}_2)_2\text{NLi}^+$. A most advantageous feature of designing organic lithium salts is in a wide range of structural modification for improving their electrolyte properties. Although LiPF_6 salt is widely used as an effective electrolyte for lithium battery due to its high conductivity, it is thermally unstable and easily decomposed by hydrolysis. Our strategy to design new organic lithium salts $\text{LiPF}_{6-n}(\text{CF}_3)_n$ is to replace unstable P-F bond(s) of PF_6^- anion by P- CF_3 bond(s) keeping their high conductivity and electrochemical stability²⁾. We report here the structural effect of $\text{PF}_{6-n}(\text{CF}_3)_n$ anions on their properties for electrolyte such as HOMO energy level, dissociation constant, conductivity, and oxidation potential. We report also some performance of lithium battery with $\text{LiPF}_4(\text{CF}_3)_2$ which showed better cycle characteristics than that with LiPF_6 .

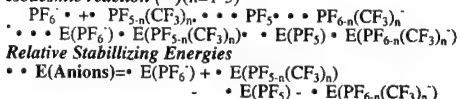
2. Results and Discussion

2.1 Syntheses of $\text{PF}_{6-n}(\text{CF}_3)_n$ Salts

$\text{LiPF}_{6-n}(\text{CF}_3)_n$ salts are prepared by electrochemical fluorination as in the case of $\text{KPF}_4(\text{C}_2\text{F}_5)_2$ salt³⁾. Recently Sartori et al. have reported the syntheses and conductivities of $\text{LiPF}_4(\text{i-C}_3\text{F}_7)_2$ and $\text{LiPF}_3(\text{C}_2\text{F}_5)_3$.

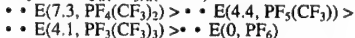
2.2 Thermal Stability of $\text{PF}_{6-n}(\text{CF}_3)_n$ Anions

As PF_6^- anion decomposes to give PF_5 and fluoride ion in pyrolysis, we evaluated the thermal stability of $\text{PF}_{6-n}(\text{CF}_3)_n$ anions by computational method considering a similar decomposition of $\text{PF}_{6-n}(\text{CF}_3)_n$ anions to give $\text{PF}_{5-n}(\text{CF}_3)_n$ and fluoride ion. The relative stabilizing energy of $\text{PF}_{6-n}(\text{CF}_3)_n$ anions ($\bullet \cdot \text{E}(\text{Anions})$) is obtained by the following isodesmic reaction(I) with total energy($\bullet \cdot \text{E}$) of optimized structures of PF_6 and $\text{PF}_{6-n}(\text{CF}_3)_n$ anions and PF_5 and $\text{PF}_{5-n}(\text{CF}_3)_n$ by B3LYP/6-31G* calculation.

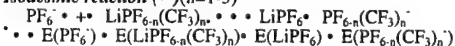
Isodesmic reaction ($\bullet \cdot$) (n=1-3)

where $\bullet \cdot \text{E}(\text{Anions})$ becomes positive when the $\text{PF}_{6-n}(\text{CF}_3)_n$ anion is more stable than PF_6^- anion.

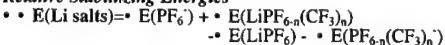
Table 1 shows that $\text{PF}_4(\text{CF}_3)_2$ anion is most stable among PF_6 and $\text{PF}_{6-n}(\text{CF}_3)_n$ (n=1-3) anions:

2.3 Conductivities of $\text{LiPF}_{6-n}(\text{CF}_3)_n$ Electrolytes

The conductivity of electrolyte solution is closely related with the dissociation level of lithium salt. The intrinsic and relative dissociation level of $\text{LiPF}_{6-n}(\text{CF}_3)_n$ salts is evaluated by the following isodesmic reaction(II):

Isodesmic reaction ($\bullet \cdot$) (n=1-3)

Relative Stabilizing Energies



The relative stabilizing energies of Li salts compared with LiPF_6 are shown in Table 1. As all $\bullet \cdot \text{E}(\text{Li salts})$ values of $\text{LiPF}_{6-n}(\text{CF}_3)_n$ salts are positive, these lithium salts are considered to be more dissociative than LiPF_6 .

Table 2 shows the conductivities of electrolyte solution with $\text{LiPF}_{6-n}(\text{CF}_3)_n$ (0.1 mol/l) in PC/DME(1/2 v/v). Although decreasing mobility of $\text{PF}_{6-n}(\text{CF}_3)_n$ anions with increasing number of CF_3 groups is predicted to reduce the conductivity of the electrolyte solution with $\text{LiPF}_{6-n}(\text{CF}_3)_n$ due to increased molecular weights of the anions, the conductivity of $\text{LiPF}_{6-n}(\text{CF}_3)_n$ electrolyte did not decrease so much because of their increased dissociation level.

2.4 Oxidation Potentials of $\text{LiPF}_{6-n}(\text{CF}_3)_n$ Salts

We investigated the oxidation stability of the $\text{PF}_{6-n}(\text{CF}_3)_n$ anions by calculating the HOMO energy levels of the anions as shown in Table 1. The HOMO level of $\text{PF}_4(\text{CF}_3)_2$ anion is slightly lower than that of PF_6^- anion and the electrolyte of $\text{LiPF}_4(\text{CF}_3)_2$ (0.1 mol/l) in PC solution showed slightly higher oxidation potential (6.2V) than that of LiPF_6 (6.0V).

2.5 Battery Performance

Finally, we checked the battery performance of the cell with $\text{LiPF}_4(\text{CF}_3)_2$. Since the conductivity of electrolyte solution with $\text{LiPF}_4(\text{CF}_3)_2$ (3.9 mS/cm) is slightly lower than that of LiPF_6 (4.4 mS/cm) as shown in Table 2, the discharge potential was also a little lower. But $\text{LiPF}_4(\text{CF}_3)_2$ -cell showed almost the same capacity as LiPF_6 -cell but better cycle characteristics than LiPF_6 -cell. Moreover, the impedance increase of $\text{LiPF}_4(\text{CF}_3)_2$ -cell for 60 - 20 days storage was smaller than that of LiPF_6 -cell.

References

- (1) F. Kita, H. Sakata, S. Shinomoto, A. Kawakami, H. Kamizori, T. Sonoda, H. Nagashima, J. Nie, N. Pavlenko, Y. L. Yagupolskii, J. Power Sources in press
- (2) H. Kamizori, T. Sonoda, H. Nagashima, F. Kita and Y. L. Yagupolskii, Abstracts of The 40th Battery Symposium in Japan, Kyoto, Nov.14-16, 477(1999).
- (3) L. M. Yagupolskii and Yu. L. Yagupolskii, J. Fluorine Chem., 72, 225(1995).
- (4) P. Sartori, N. Ignat'ev, R. Wenige, U. Heider and V. Hilarius, The Electrochem. Soc. Fall Meeting, Boston, Massachusetts, Nov.1-6, AB-160(1998).

Table 1. $\Delta\Delta\text{E}$ and HOMO Energies of $\text{PF}_{6-n}(\text{CF}_3)_n$ anion.

Li Salt	$\Delta\Delta\text{E}$ (kcal/mol)*		HOMO Energy of Anion (eV)
	Anion	Li Salt	
LiPF_6	0	0	-4.26
$\text{LiPF}_5(\text{CF}_3)$	4.4	0.5	-3.99
$\text{LiPF}_4(\text{CF}_3)_2$	7.3(trans)	2.1	-4.30
$\text{LiPF}_3(\text{CF}_3)_3$	4.1(mer)	8.6	-3.72

* B3LYP/6-31G*.

Table 2. Conductivities and Oxidation potentials of $\text{LiPF}_{6-n}(\text{CF}_3)_n$ Electrolytes at 25 °C.

Salt	Conductivity (mS/cm)	Oxidation Potential (V vs. Li/Li^+)
LiPF_6	4.4	6.0
$\text{LiPF}_6 + 3\text{DME}$	•	5.3
$\text{LiPF}_4(\text{CF}_3)_2$	4.2	6.2
$\text{LiPF}_4(\text{CF}_3)_2$	3.9	6.2
$\text{LiPF}_3(\text{CF}_3)_3 + 3\text{DME}$	3.9	5.1

*0.1 mol/l Salts in PC/DME(1/2 v/v).

**0.1 mol/l Salts in PC.

Asymmetrical Alkyl Carbonate as Solvent for Li-ion Batteries Electrolytes

I. Geoffroy¹, B. Carré¹, D. Lemordant¹,
S. Herreyre², Ph. Biensan²,

1: Laboratoire P.I.M.I.R. (EA 2098), Faculté des Sciences,
Parc de Grandmont, 37 200 Tours, France.

2: S.A.F.T., Direction de la recherche, 111, bd Daney,
33 074 Bordeaux, France.

Introduction

The aim of this work was to investigate new single or blended in order to optimize the performances of the electrolyte especially in terms of cyclability and conductivity at low temperature. For this purpose asymmetrical alkyl carbonate solvents (ACS) have been synthesized: methyl isopropyl carbonate (MiPC), ethyl isopropyl carbonate (EiPC) and ethyl propyl carbonate (EPC). Some of their mixtures with ethylene carbonate (EC) have also been studied.

Among the physico-chemical and electrochemical properties, those investigated were permittivity, viscosity, ionic conductivity, stability against lithium metal and cycling efficiency both carbon and LiCoO₂ electrodes.

Results

The influence of the temperature on the viscosity is well described by the Andrade law in the full range of temperature investigated. From the plots of $\ln(\eta)$ versus $1/T$, the activation energy for the viscous flow $E_{a\eta}$ has been calculated. E_a values are in the range of 10-11 kJ/mol for pure solvents and 12-13 kJ/mol for their mixtures with EC.

The temperature dependence of the conductivity of LiPF₆ (1M) solutions in the blended solvents has been examined in the range -40°C to 60°C (figure 1). If at ambient temperature (25°C), the conductivity of LiPF₆ in the single solvents are only 2 mS/cm, it raises sharply to 8-9 mS/cm at 25°C when EC is added.

The electrochemical properties of the ACS and the ACS:EC mixtures in presence of LiPF₆ (1M) have been determined by means of cyclic voltammetry. Upon reduction at a graphite anode, the formation of a passive layer occurred at 0.8V for all solvents. The reversible capacity at C/20 in EPC:EC is 275 mAh/g whereas the irreversible capacity is only 64 mAh/g (see figure 2).

The cycle life behavior is very promising as no fading is noted at the 10th cycle. The reversible capacity at a LiCoO₂ cathode is very high (146mAh/g) and the irreversible capacity very low (only 3 mAh/g)

Conclusion

ACS:EC mixtures are promising solvents for use in Li-ion batteries as they present at the same time:

- a low viscosity,
- high ionic conductivity even at low temperature,
- very good passivating properties at the graphite anode,
- large reversible capacity at both electrodes,
- non toxic, non volatile and stable.

Figure 1: conductivity of LiPF₆ (1M) in EC:ACS mixtures.

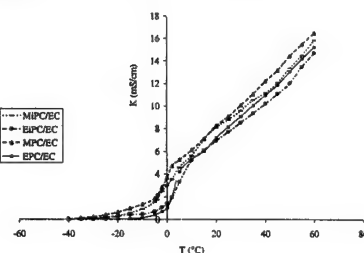
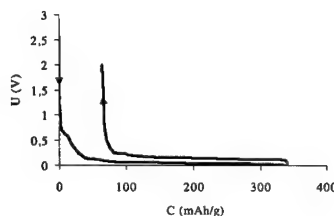


Figure 2: Cyclic voltammogram at a graphite electrode in the EPC:EC (LiPF₆, 1M) electrolyte.



Database and Models of Electrolyte Solutions for Lithium Battery

Suojiang Zhang, Akio Tsuboi, Hiroaki Nakata, Takeshi Ishikawa

Mitsubishi Chemical Corporation, DERC, Mizushima Plant,

Kurashiki, Okayama 712-8054, Japan

Fax: +81-86-457-2027 Email:

zhang@seigi2.mt.m-kagaku.co.jp

Electrolyte solutions are essential for lithium batteries, even in lithium polymer batteries a liquid electrolyte is also extensively employed by formation of gel with a polymer, known as a gel polymer electrolyte. It has been shown that the polymer is likely to have very little effect on the liquid electrolytes and hence the gelled electrolyte may be considered to be a liquid electrolyte entrapped in a polymer matrix as the polymer content is not high, e.g., below 30–35wt% [1,2,3]. So the optimal design of gel polymer electrolytes can also be reduced to optimizing liquid electrolyte compositions. The strategy of our researches is to develop an algorithm for quickly screening potential solvents and systemically optimizing the compositions of electrolyte solutions for lithium batteries like shown schematically in Figure 1. We believe that systematic approaches are important for the optimal design of lithium battery solutions, because many factors are highly interacted. For example, high salt solubility and high conductivity are related to dielectric constants (ϵ) and viscosity (η) of solvent mixtures. Also, they are contacted to ionic dissociation and hence mean ionic activity coefficients.

A reliable database is very useful. Collection of data is often a difficult procedure. Data are widely spread in the literature [4], many results that are not directly contacted to the researches of lithium batteries, e.g., electrolyte solution thermodynamics, could be very useful. The data covering a variety of properties such as thermodynamic, transport and thermal properties as well as electrochemical stability information have being compiled. The collected data are critically evaluated in terms of the accuracy and reliability before used for development of correlation and prediction models.

Property models, especially predictive type of models, are very important in realization of the systematically optimal design strategy. A number of correlation/prediction models for electrolyte solutions are evaluated, and some predictive models have been suggested/modified for lithium battery electrolytes based on the ionic group contribution idea [5] or other mixing rules. In Figure 2 it has been shown that molar conductance (Λ) can be fairly represented by the equation:

$$\Lambda = 1000\kappa / c = \Lambda_0 + B\sqrt{c} + Ec \ln c$$

where Λ_0 is the limiting molar conductance, B and E fitted parameters, κ conductivity with the unit s.cm^{-1} .

[1] A.M. Christie, L. Christie, C.A. Vincent, J. Power Sources, 74(1998), 77-86.

[2] O. Bohnke, G. Frand, M. Rezzazzi, C. Rousselot, C. Truche, Solid State Ionics, 66(1993), 105.

[3] O. Bohnke, G. Frand, M. Rezzazzi, C. Rousselot, C. Truche, Solid State Ionics, 66(1993), 97.

[4] J. Barthel, H.J. Gores, Pure & Appl. Chem., 57(1985), 1071.

[5] J. Li, H.M. Polka, J. Grmehling, Fluid Phase Equilib., 94(1994), 89.

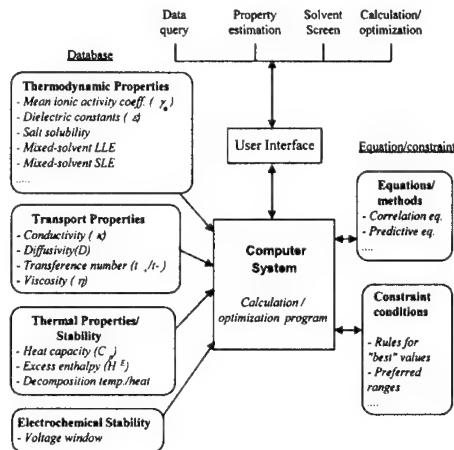


Figure 1. A Scheme of Strategic Researches on Optimal Design System of Electrolyte Solution for Lithium Battery

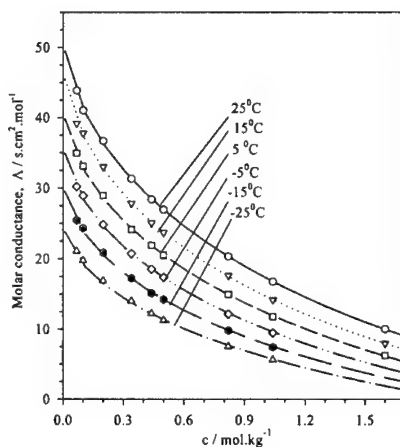


Figure 2. Comparison of Calculated Results with Literature [4] Molar Conductance Data for LiAsF_6 in $\text{PC}(32\text{wt}\%) + \text{DME}$

An exceptional additive to the electrolyte for Lithium-ion batteries : the vinylen carbonate

Ph. Biensan, J.M. Bodet¹, F. Pertion, M. Broussely,
C. Jehoulet, S. Barusseau, S. Herreyre and B. Simon
SAFT, 111 Boulevard A. Daney, 33074 Bordeaux, France
¹SAFT, BP 1039, 86060 Poitiers, France

Although good electric performances may be obtained with Li-ion, some aspects such as gas generation during formation, fading rate upon cycling and irreversible losses during storage are still to be improved. This paper aims to discuss how Vinylen Carbonate (VC) helps significantly in these domains.

VC for passivation :

The lowering of gas generation during formation, was discussed in a previous paper (1). This point is a striking figure of VC addition to the electrolyte (2). The gas production during formation, due to reduction of electrolyte solvents is far lower when VC is used (Fig1). This was explained by the stabilization of the radical intermediate with VC, leading to the displacement of the reaction towards solid, passivation compounds. VC has also the property to suppress exfoliation of graphites even with PC, but also with a very large number of more unusual solvents, due to its high reduction voltage (1.2 V vs. Li/Li^+). The main potential drawback associated to the use of VC is the slight increase of the passivation layer resistance with, if not taken into account, risks of lithium plating.

VC for fading :

The fading rate observed for LiCoO_2 /graphitized carbon cells appears very sensitive to the VC amount (Tab1). Capacity loss after cycling at rather high rate (C) decreases when VC amount in the electrolyte increases. In the same time, the impedance is more stable during cycling with VC than without, except for "too high" VC contents. Excellent results may be obtained with other positive active material like $\text{LiNi}_{1-x}\text{M}_x\text{O}_2$ family.

VC for irreversible losses :

Irreversible losses during storage are well known to be affected by the temperature or the cell voltage. The addition of small amounts of VC to the electrolyte leads to important reduction of the irreversible losses registered (Fig2) whatever the cell design. Moreover, cell impedance appears slightly more stable for cells containing 2% of VC additive than for the other one (Tab1). This point was related to the improvement of the passivation layer formed on the negative electrode. Exception can be made when VC amount is too high. Strong improvement of expected calendar life is thus observed.

Conclusion

The improvement of the electrochemical performances of Li-ion cells can be achieved through small addition of vinylen carbonate to the electrolyte. This excellent passivation additive helps to have performing Li-ion batteries for long range cycling and calendar life. Additional results, that demonstrate that this additive may be advantageously used in a very broad family of cell designs in term of active materials whether at the positive or negative electrodes but also in term of electrolyte compositions (carbonates, esters...), will be discussed.

Acknowledgements

The authors wish to thank MESR for financial support.

Reference

- (1) C. Jehoulet, P. Biensan, J.M. Bodet, M. Broussely, C. Moteau, C. Tessier-Lescouret, 197th ECS Meeting, Paris, p153-154, 1997
- (2) Patents Fr 94 04889, US 5,626,981

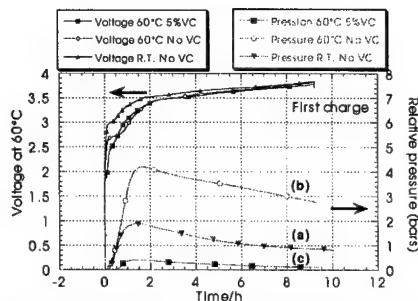


Fig1 : Gas generation during cell formation at R.T. without VC (a) at 60°C without VC (b) and at 60°C with VC (c). Electrolyte is PC/EC/DMC (1/1/3)+ LiPF_6 (1M). Positive is LiNiO_2 based material. Negative active material is a graphitized carbon.

VC Addition to the electrolyte	Fading after 150 cycles (%)	Cell Resistance before/after 60°C storage (mΩ)
No VC	18	101 / 162
1% VC	16.5	100 / 169
2% VC	13,5	100 / 137
5% VC	12	135 / 252

Tab1 : Performance evolution of LiCoO_2 / graphitized carbon cell during cycling at room temperature with or without VC content. Cycling rates are C rate (3 hours) in charge and C rate discharge. Electrolyte is EC/DMC/DEC+ LiPF_6 (1M).

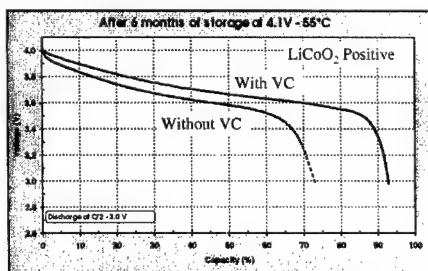


Fig2 : Capacity evolution after 6 months storage at 55°C with or without VC for LiCoO_2 / graphitized carbon cells. Electrolyte is EC/DMC/DEC+ LiPF_6 (1M).

An Evidence of Preventing the Decomposition of PC at the Surface of Well Graphitized Carbon without Any Additions

*Keita Yamaguchi ^a, Junji Suzuki ^a,
Morihiro Saito ^a, Takayuki Katsuta ^a,
Kyoichi Sekine ^a, and Tsutomu Takamura ^b

^a Department of Chemistry, College of Science,
Rikkyo University,
3-34-1, Nishiikebukuro, Toshimaku,
Tokyo 171-8501, Japan
^b Petoca, Ltd., 3-6, Kioicho, Chiyodaku,
Tokyo 102-0094, Japan

Introduction

The highly graphitized carbon is a mostly utilized anode material for Li-ion secondary batteries because of its high reliability. Propylene Carbonate (PC) is a very attractive electrolyte in view of ion conducting and cost as well. However, PC has never been utilized for graphite electrode, since PC decomposes without termination at the graphite surface during charging process^[1]. Such as PC decomposition has been reported to be accompanied with the co-intercalation of PC molecule which causes to destroy the graphite layer^[2]. We have pointed out that the conductivity of electrode strongly influences the anodic characteristics^[3]. We can expect, therefore, if the electrode is fabricated to maintain a homogeneous distribution of high conductivity, the PC decomposition might be prevented. In this paper, we have utilized a graphite single carbon fiber having a high and homogeneous conductivity, and examined whether the expectation can be realized in PC electrolyte.

Experimental

As the material, three types of mesophase pitch-based carbon fibers were used. (Melblon 3100, $\phi = 7 \mu\text{m}$, prepared at 3100 °C, Carbonic 3110, $\phi = 30 \mu\text{m}$, prepared at 3110 °C, NF415-3.4, $\phi = 10 \mu\text{m}$, prepared at 3110 °C, Petoca, Ltd. made.) A single fiber of Carbonic and NF415-3.4 was used as obtained monofilaments, and for Melblon, a single was picked out from the integrated fiber felt. A 15 mm long sample fiber was fixed on one end of 0.5 mm diameter Ni wire with conductive carbon-paste, which was used as a lead wire. A tip of the sample fiber was partially immersed vertically in the electrolyte with 5 mm depth. A cylindrical glass cell was used for the measurement of linear sweep cyclic voltammogram (CV). PC containing 1 M LiClO₄ was used as an electrolyte. All measurements were performed in a dry box in Ar atmosphere at room temperature.

Results and Discussion

The CVs obtained from pristine sample of Carbonic in PC electrolyte gave a stable CV with a satisfied cyclife, resulting in no reduction decomposition of PC. One may ascribe the stability to a thick surface skin layer of Carbonic. Then, we removed this skin by mild oxidation process^[4].

The resulting CVs gave larger charge / discharge current peaks with better cyclife as compared to the pristine sample, and no PC decomposition current was observed.

A single fiber of Melblon fiber felt and a monofilament of NF415-3.4 having much thinner skin layers gave satisfied CVs having a very good cyclife, accompanied with no reduction current

due to PC decomposition. These results imply that the existence of surface skin layer is not related to PC decomposition, and a homogeneous distribution of high conductivity of electrode is the key factor to prevent PC decomposition.

As an example of having lower and inhomogeneous distribution of high conductivity, we used the bundled carbon fibers. The CVs showed good cycle life and no decomposition current at sweep rate of 1 mV/sec, but the CVs became unstable and very large reduction current due to PC decomposition at higher sweep rate of 10 mV/sec.

We can conclude that the existence of surface skin layer to protect against exfoliation of grapheme layer is not related to PC decomposition, and that the homogeneous distribution of high conductivity in the electrode provided a stable cycleability even in PC electrolyte.

References

- [1] A. N. Dey and P. Sullivan, *J. Electrochem. Soc.*, **117**, 111 (1970).
- [2] D. Aurbuch, Yair. Ein-Eli, O. (Youngman) Chusid, Y. Cermeli, M. Babai and H. Yamin, *J. Electrochem. Soc.*, **141**, 603 (1994).
- [3] T. Takamura, K. Yamaguchi, M. Saito, and K. Sekine, Extended Abstract of the '99 Asian Conference on Electrochemistry, pp 184, Tokyo, Japan, 1999.
- [4] T. Takamura, H. Awano, T. Ura, K. Sumiya, *J. Power Sources.*, **68**, 114 (1997).

Effect of Organic Additives in Electrolyte Solutions on Behavior of Lithium Metal Anode
Yoshiharu Matsuda and Takatomo Takemitsu
 Department of Applied chemistry, Faculty of Engineering and High Technology
 Research Center, Kansai University, Yamatecho 3-3-35 Suita, Osaka 564-8680, Japan

Rechargeable lithium metal batteries have not been commercialized due to the decline of the lithium electrode performance on charge-discharge cycling. To prevent this problem, some additives, $\text{Al}_3^{1)}$, 2-methylfuran²⁾, $\text{CO}_2^3)$, sugar esters⁴⁾ were added in the electrolyte solutions. In the present work, organic additives, ex: poly(acrylonitrile)(PAN), poly(vinyl-pyrrolidone)(PVP), poly(ethylene oxide)(PEO), etc, were added in the electrolyte solution to improve the cycling behavior of lithium metal anode.

A three compartment cell with a lithium test, a lithium counter and a lithium reference electrodes was used and the electrolyte solutions were mainly 0.25 M LiBF_4 / 0.25 M LiPF_6 (Morita chemical), 0.25 M $(\text{CF}_3\text{SO}_2)_2\text{NLi}$, 0.25 M $(\text{CF}_3\text{SO}_2)(\text{C}_4\text{F}_9\text{SO}_2)\text{NLi}$ (Central glass) / ethylene carbonate(EC)-propylene carbonate(PC) (1:1 vol.) (Ube Industries). Usually 0.2g of the additive was dissolved in 50ml of the electrolyte solution. Interface resistance and capacitance were measured by a Solartron SI12280B and a charge-discharge equipment (Hokuto HJ-101 SM6) was used for the cycling of lithium electrode. The charge-discharge electricity was 1.0Ccm^{-2} (1.0mAcm^{-2} , 1000s). Measurement was proceeded in dry Ar atmosphere at ambient temperature. The addition of PVP in the electrolyte solution, 0.25 M $(\text{CF}_3\text{SO}_2)_2\text{NLi}/\text{EC-PC}$ Fig.1• and 0.25 M $\text{LiBF}_4/\text{EC-PC}$, suppressed the interface resistance and stable charge-discharge was achieved. Polarization resistance was measured during cycling in the electrolyte solutions with the additives. At the early stage of cycling, the polarization resistance was rather high, but after ca. one hundred cycles it was smaller and stable.

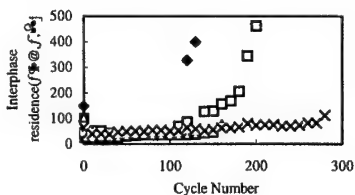


Fig.1• Interphase resistance on negative electrodes at low frequency range as a function of cycle number.

0.25 M $(\text{CF}_3\text{SO}_2)_2\text{NLi}/\text{EC-PC}$
 • Blank:• PAN:• PEO:×PVP

Refere

- 1) M. Ishi: *J. Electrochem. Soc.*, 141, L159 (1994)
- 2) M. Morita, S. Aoki, Y. Matsuda: *Electrochimica Acta*, 37, 119 (1992)
- 3) T. Osaka, T. Momma, T. Tajima, Y. Matsumoto: *J. Electrochem. Soc.*, 142, 1537 (1995)
- 4) M. Sekiya, Y. Matsuda: *Fall Meeting of Electrochem. Soc. Japan*, Abst. P14 (1998)

**Cyclic and Acyclic Sulfites –
New Solvents and Electrolyte Additives for Lithium
Ion-Batteries with Graphitic Anodes?**

Gerhard H. Wrodnigg, Jürgen O. Besenhard,
and Martin Winter

*Institute for Chemical Technology of Inorganic Materials
Graz University of Technology
Stremayrgasse 16, A-8010 Graz, Austria*

In lithium ion cells with propylene carbonate (PC) based electrolytes graphitic anodes usually co-intercalate PC molecules, resulting ultimately in large irreversible charge consumption and electrode destruction. This "solvated intercalation" has hindered the application of PC as electrolyte solvent in lithium ion cells with graphitic anodes so far [1].

We have studied the graphite anode performance with various sulfur-containing compounds, ethylene sulfite (ES) [2], propylene sulfite (PS) [3], dimethyl sulfite (DMS) [4], diethyl sulfite (DES) [4] for use as film forming electrolyte additives in PC based electrolytes. Basically, these sulfites (Figure 1) can be formally considered as structural analogues to the commonly used organic carbonates, ethylene carbonate, PC, dimethyl carbonate (DMC) and diethyl carbonate (DEC).

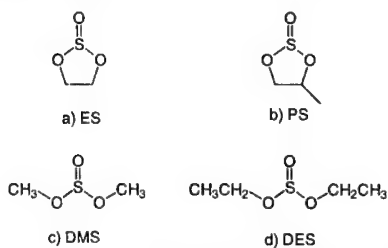


Fig. 1: Structural formulae and abbreviations of the sulfites investigated in this study.

The PC/sulfite mixtures have shown promising performance, with the filming capabilities (= capability for the formation of effective solid electrolyte interphase (SEI) films) decreasing in the order: ES > PS >> DMS > DES. The corresponding charge/discharge experiments will be presented at the meeting. Results obtained for different charging procedures in the first cycle will be particularly highlighted.

The low viscosities of DMS and DES also suggest their use as electrolyte co-solvents (50 vol.%) in combination with the highly viscous solvent EC (Table 1). The composed EC-based electrolytes exhibit better electrolyte conductivities at low temperatures than the corresponding electrolytes with the commonly used low-viscosity solvents DMC and DEC (Figure 2 and 3). Under "standard" constant current charge/discharge, however, the charge/discharge performance of the EC/DMS and EC/DES electrolytes can not compete with that of the EC/DMC and EC/DEC electrolytes. The influence of different charging procedures will be shown for these electrolytes, as well.

Tab. 1: Melting points (mp), boiling points (bp), flash points (fp), viscosities (η) and dielectric constants (ϵ) of cyclic carbonates, linear carbonates, and linear sulfites investigated in this study (at 25 °C).

Solvent	mp/ °C	bp/ °C	fp/ °C	η cP	ϵ
EC	36.5	238	160	1.9 *	90.36 *
PC	-54.5	242	132	2.512	64.95
DMC	4.6	90	18	0.5902	3.18
DEC	-43	126.8	31	0.748	2.82
DMS	-141	126	30	0.8732	22.5
DES	N/A	159	53	0.839 *	15.6 *

*at 40 °C, *at 20 °C

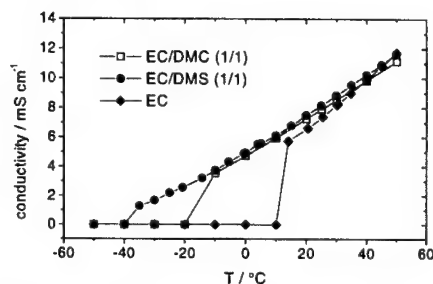


Fig. 2: Conductivity vs. temperature diagram of 1 M LiClO₄ in EC/DMC (1/1 by volume), EC/DMS (1/1 by volume) and EC, respectively.

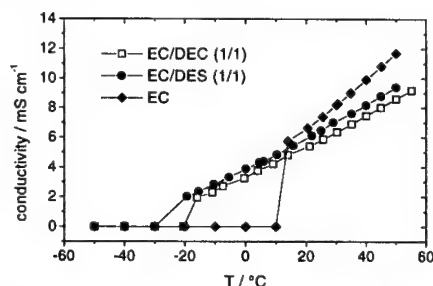


Fig. 3: Conductivity vs. temperature diagram of 1 M LiClO₄ in EC/DEC (1/1 by volume), EC/DES (1/1 by volume) and EC, respectively.

- [1] M. Winter and J. O. Besenhard, in: *Handbook of Battery Materials* (Ed. J. O. Besenhard), Part III, Ch. 5, Wiley-VCH, Weinheim (1999).
- [2] G. H. Wrodnigg, J. O. Besenhard, and M. Winter, *J. Electrochem. Soc.*, **146**, 470 (1999).
- [3] G. H. Wrodnigg, T. M. Wrodnigg, J. O. Besenhard, and M. Winter, *Electrochem. Comm.*, **1**, 148 (1999).
- [4] G. H. Wrodnigg, C. Reisinger, J. O. Besenhard, and M. Winter, *ITE Battery Letters*, **1**, 110 (1999).

This work was partially supported by the Austrian Science Fund within the special research program "Electroactive Materials". We thank the Timcal group (Bodio, Switzerland) and Merck (Darmstadt, Germany) for the donation of samples used in this study.

Fluorinated Organic Solvents in Electrolytes for Lithium Ion Cells

K.-C. Möller^a, T. Hodal^a, W. K. Appel^b, M. Winter^a,
and J. O. Besenhard^a

^aInstitute for Chemical Technology of Inorganic Materials, Graz University of Technology, Stremayrgasse 16/III, A-8010 Graz, Austria

^bAventis Research & Technologies, Deutschland GmbH & Co. KG, D-65926 Frankfurt, Germany

Currently, commercial graphite-based lithium ion batteries use mixed solvent electrolytes containing highly viscous ethylene carbonate (EC) and low viscosity diluents such as dimethyl or diethyl carbonate (DMC, DEC) as main solvents. EC is indispensable because of its excellent filming properties, DMC and/or DEC are required to get the low temperature performance of the electrolyte at least reasonable. Nevertheless, the low temperature performance of these EC based electrolytes needs still some improvement. In addition, DMC and DEC are highly volatile and their flash points are quite low (DMC 18 °C, DEC 31 °C), which may have a considerable impact on the battery safety.

Tab. 1: Physical properties of selected solvents (mp: melting point, bp: boiling point, fp: flashpoint, visc: viscosity ^aat 25 °C, ^bat 40 °C)

solvent	mp/ °C	bp/ °C	fp/ °C	visc/ mm ² /s ^a
EC	39	248	160	1.86 ^b
DMC	5	91	18	0.59
PC	-49	240	132	2.09
DTA	-42	135	72	1.09

Our aim was to employ low-viscosity partly fluorinated solvents as diluents for more viscous solvents such as propylene carbonate (PC), the latter being known for its better low temperature behaviour compared to EC. Exchange of some hydrogen for fluorine causes significant differences in the physical and chemical properties of polar solvents. In particular, viscosities but also melting and boiling points of fluorinated solvents are in most cases significantly lower, compared to their hydrogenated counterparts. Moreover, fluorinated solvents are in general much less flammable as less hydrogen is available. As a rule, oxidation stability of partly fluorinated solvents is quite good, due to the stability of the carbon-fluorine bond, and thus promising for lithium battery applications. On the other hand, costs and volumetric weight are obvious disadvantages of fluorinated solvents.

In this contribution, we present the partly fluorinated solvent *N,N*-dimethyl trifluoroacetamide (DTA, see fig. 1). The physical properties compared to the commercially used solvents EC and DMC are given in table 1. In mixtures with PC the DTA prevents the solvated intercalation of Li-PC, as can be

seen in fig. 2. The oxidation of a LiMn₂O₄ electrode in the same electrolyte is shown in fig. 3. In charge/discharge experiments the irreversible capacity losses are comparable to EC/DMC mixtures (fig. 4).

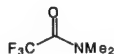


Fig 1: *N,N*-dimethyl trifluoroacetamide (DTA)

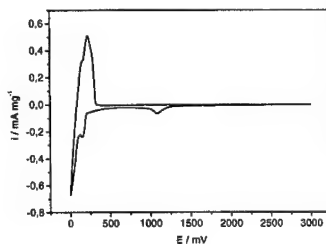


Fig. 2: Cyclic voltammogram of a KS 6 composite electrode in 1M LiN(SO₂CF₃)₂ + PC / DTA (50 : 50), scan rate 100 V/s; V vs. Li/Li⁺

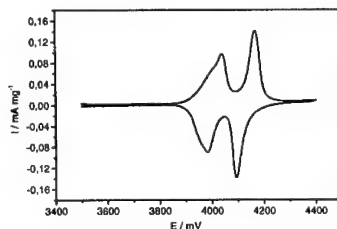


Fig. 3: Cyclic voltammogram of a LiMn₂O₄ composite electrode in 1M LiN(SO₂CF₃)₂ + PC / DTA (50 : 50), scan rate: 100 μV/s; V vs. Li/Li⁺

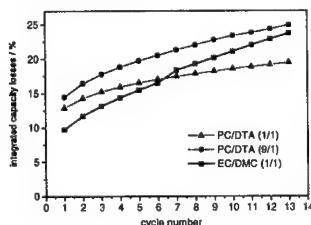


Fig. 4: Integrated capacity losses of EC/DMC and different PC/DTA mixtures

- [1] L. H. Lie, T. Hodal, K.-C. Möller, G. H. Wroldnig, W. K. Appel, J. O. Besenhard, M. Winter, *ITE Battery Letters* **1999**, 1(1), 105-109.

Acknowledgement: This work was supported by the Austrian Science Fund (FWF) in the "Electroactive Materials" special research programme. We thank Merck KGaA, Germany, and Timcal AG, Switzerland, for the donation of samples

Performance of Solupor® Separator Materials

F.G.B. Ooms*, E.M. Kelder*, J. Schoonman*,
N. Gerrits*, G. Calis*

*Delft University of Technology
Julianalaan 136, 2628 BL Delft, The Netherlands
Tel +31 15 278 2667 Fax +31 15 278 8047
Email F.G.B.Ooms@tnw.tudelft.nl

*DSM Solutech
Eisterweg 4, 6422 PN Heerlen, The Netherlands

Introduction

A separator in lithium ion batteries is a prerequisite, although inactive material. Despite the fact that theoretical battery capacity is determined by the amount of active materials, the real capacity is strongly dependent on the C-rate and the temperature during the charge/discharge procedure. However, the measured battery capacity varies noticeably for batteries containing different separator materials. The key properties of these materials are porosity, permeability (Gurley) and thickness.

In this study, a series of DSM Solupor® separator materials is compared with other commercially available separators.

Experimental

In order to see the effect of separator morphology on the rate capability, several series of test cells have been made using CR2320 coin cells (Hohsen Corp.). The cathode material is LiCoO_2 and the anode material Graphite or 0.3 mm Lithium foil (Chemetall Foote Corp.). The electrolyte is 1 M LiPF_6 in EC/EMC 1:2 vol (Mitsubishi Chem.). The cell-stack is always: can, gasket, LiCoO_2 (~2 mAh), separator, anode, $\varnothing 17 \times 0.5$ mm Cu press-plate, wave-spring and cap.

Cells are cycled on a Maccor S4000 with current densities between 0.3 and 2.4 mA/cm^2 (~C/7-1C rate). At 0.6 mA/cm^2 , the temperature is varied between +30 °C to -20 °C in a Vötsch VT4004 climate room.

Results

Figure 1 clearly shows that at +30 °C the materials do not show a significant difference in performance. At lower temperatures however, all tested Solupor separators perform better than its competitors.

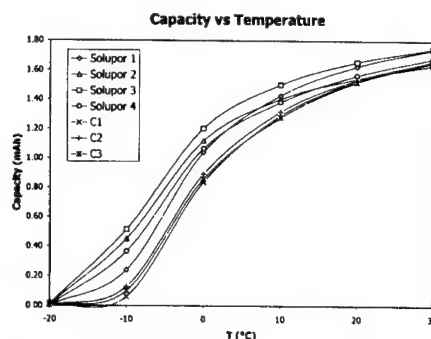


Figure 1: Effect of temperature on the discharge capacity for some Solupor and competitor (C1-C3) separators in LiCoO_2 /Graphite cells.

Conclusions

Optimizing the microstructure of separator materials results in better performance. Another way of looking at the data in Figure 1 is that at the same temperature a higher C-rate could be used applying Solupor. The experiments are extended to a wider range of Solupor and competitor materials with the goal to relate the results to the morphology of the materials.

Currently rate-capability tests, AC impedance measurements and thermal-shutdown experiments are in progress. A wider range of electrolytes will be included.

Fast Charge in Non-aqueous Li Cells: Investigation of a Novel Hybrid Solution

G. G. Amatucci, F. Badway, A. DuPasquier

Telcordia Technologies
331 Newman Springs Road, Red Bank, NJ 07701, USA

Li-ion battery technology is the present day state of the art battery technology for consumer electronics. Currently, a tremendous amount of research is focused on the development of new electrode materials and electrolytes which will result in improved energy density and lifetime for Li-ion batteries. A large, parallel effort is focused on entrapping this technology within polymer matrices. This has resulted in flat-plate bonded systems with lightweight packaging which allow further improvement in energy density and allow unprecedented form factor flexibility. The majority of these efforts are focused on the production of electrochemical cells with discharge rates ranging from C/2 to 3C. Most of the Li-ion batteries produced today perform acceptably well in these ranges.

Few electrochemical energy storage technologies allow fast charging of practical consumer cells. Li-ion technology is rarely charged faster than 1C. The negative electrode is typically graphite which has a Li^+ intercalation potential only 0.01V above Li plating. Fast charging can result in significant underpotential resulting in hazardous Li plating and subsequent deterioration of performance. In addition, fast charging of the positive electrode material may lead to significant diffusion induced concentration gradients within both the electrode bulk structure and liquid electrolyte resulting in deteriorated performance. NiCd is the fastest of the consumer viable technologies, capable of exceeding 10C discharge rates. Charging can also be performed at exceptional rates, but not in a sealed system. Pb-acid is the only commercial technology which can sustain such fast charge rates, especially with the use of high power density TMF^{TM} Pb-acid technology (Bolder Technologies). Charging in excess of 60C can be demonstrated by nonaqueous electrolytic double layer C-C supercapacitors, but energy density is typically well below that of battery technology and has poor self discharge characteristics.

To date, little effort has been focused on the design of electrochemical systems which enable fast charge capability of 10-30C. We have recently presented preliminary results of a research on a new type of electrochemical cell which combines the attributes of battery and supercapacitor technology that enables fast charging. In this non-aqueous electrochemical cell, the positive electrode stores charge as an electrolytic double layer capacitor through the adsorption and desorption of anion electrolyte species on the positive electrode. The negative electrode is an intercalation compound that reversibly intercalates lithium ions. A schematic comparison of the electrochemical reactions at the electrodes of a Li-ion battery, a non-aqueous supercapacitor based on Li, and the asymmetric hybrid cell is shown in Figs. 1-3, respectively. The use of an intercalation compound for the negative electrode of the hybrid results in much improved energy densities over C-C nonaqueous supercapacitors. The configuration also enables exceptionally fast charging of the cell with

respect to traditional consumer battery technology, with charge rates approaching 85% utilization at 20C.

This paper will explore a number of new aspects with respect to the fast charge Li hybrid technology. Particular attention will be on the optimization of energy densities, new configurations of this technology, and comparison with Li-ion cells with alternative electrode configurations. Parallel with this discussion we will focus on electrode material selection and the impact of their physio-electrochemical properties on electrochemical cell performance and diffusion limitations. Finally, performance in a flat plate bonded cell technology will be presented.

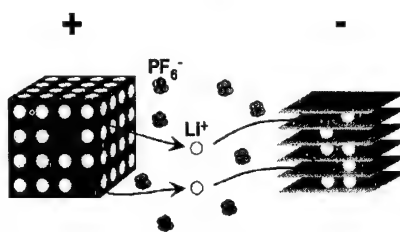
Li-ion Battery

Fig. 1. Simplified schematic showing electrode reactions with electrolyte salt in a Li-ion battery during charge.

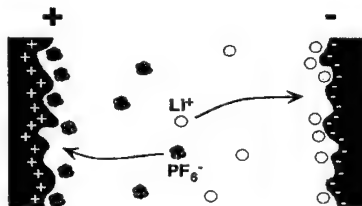
Supercapacitor

Fig. 2. Simplified schematic showing electrode reactions with electrolyte salt in supercapacitor during charge.

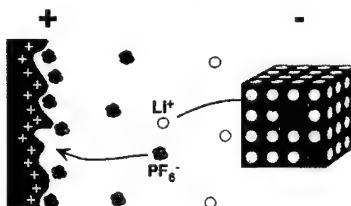
Asymmetric Hybrid

Fig. 3. Simplified schematic showing electrode reaction with electrolyte salt in an asymmetric hybrid cell during charge.

Temperature and Concentration Effects on the Ionic Transport Behavior of $\text{LiAlCl}_4/\text{SOCl}_2$ Electrolyte Solutions

George Ting-Kuo Fey and Wen-Kuei Liu
Department of Chemical Engineering,
National Central University
Chungli, Taiwan 320, R.O.C.

Yu-Chi Chang
Department of Chemical Engineering,
Tamkang University
Tamsui, Taiwan 251, R.O.C.

The lithium/thionyl chloride battery (Li/SOCl_2) using a $\text{LiAlCl}_4/\text{SOCl}_2$ inorganic electrolyte is capable of providing one of the highest energy densities among all practical primary battery systems known to date [1]. Though the kinetic, thermodynamic, and mechanistic aspects of thionyl chloride reduction have been extensively investigated [2-7], only a few studies have addressed the ionic conductivity of the electrolyte solutions [1, 8-10]. Lithium reacts with oxyhalide (SOCl_2) and forms a passivation film which protects it from any further reactions. The film grows with time and temperature of lithium storage in contact with the oxyhalide and is strongly influenced by the concentration of solute (LiAlCl_4) in the oxyhalide.

The objective of this work is to investigate, as much as possible, the temperature and concentration effects on the ionic transport behavior of $\text{LiAlCl}_4/\text{SOCl}_2$ electrolyte solutions by means of conductivity measurements and some spectroscopic techniques, such as ^7Li NMR and Raman spectroscopy. We hope that the results from this work will improve and advance our understanding of the molecular dynamics of ions in the $\text{LiAlCl}_4/\text{SOCl}_2$ inorganic electrolyte system.

The measured specific conductivity of the 1.8M LiAlCl_4 in SOCl_2 electrolyte solution as a function of temperature indicated that the solution's conductivity was greatest at 298K. We performed Raman experiments to examine the structural aspects of the ion-solvent adduct species in the solution. The results of Raman spectra suggest that the adduct compound is $\text{Li}(\text{SOCl}_2)_y \cdot x(\text{SO}_2)_x^+$, where y has a maximum value of 2. The conductivity was the outcome of the mobility and the degree of dissociation: $\text{Li}(\text{SOCl}_2)_y^+ + x\text{SO}_2 \rightleftharpoons \text{Li}(\text{SOCl}_2)_{y-x}(\text{SO}_2)_x^+ + x\text{SOCl}_2$. It is interesting to note that ion mobility

increased with rising temperature, but the degree of dissociation decreased with increasing temperature.

To further determine the structural environment of the lithium ions, ^7Li NMR measurements were conducted. The ^7Li spin-lattice relaxation rate indicated a change in the ionic structure of the electrolyte near 298K. We confirmed that a transition occurred at around 298K by the measurements of the chemical shifts and relaxation times under various temperatures and concentrations. The activation energies of spin-lattice relaxation for 1.8M LiAlCl_4 in SOCl_2 above and below 298K were 7.03 and 12.91 kJ/mol, respectively. The results of ^7Li NMR and Raman studies suggest that the structure of the adduct compound is $\text{Li}(\text{SOCl}_2)_y \cdot x(\text{SO}_2)_x^+$, and that the change in conductivity with temperature is related to the transformation between $\text{Li}(\text{SOCl}_2)_y^+$ and $\text{Li}(\text{SOCl}_2)_{y-x}(\text{SO}_2)_x^+$ ions.

References

1. G. T. K. Fey, W. G. Liu, T. J. Lee, H. J. Chuang, H. J. Cheng and S. Y. Chen, in "Proceedings of the Symposium on Lithium Batteries", S. Surampudi and V. R. Koch, eds., Proceeding Vol. 93-24, pp.146-155, The Electrochemical Society Inc., USA (1993).
2. W. K. Istone and R. J. Brodd, *J. Electrochem. Soc.*, Vol.131, 2467 (1984).
3. F. W. Dampier and T. A. Cole, *J. Electrochem. Soc.*, Vol. 133, 938 (1986).
4. W. M. Hedges, D. Pletcher, and C. Gosden, 32nd Int. Power Sources Symp., 542 (1986).
5. J. G. Chiu, Y. Y. Wang, and C. C. Wan, *J. Power Sources*, Vol. 21, 119 (1987).
6. L. D. Hansen and H. Frank, *J. Electrochem. Soc.*, Vol.134, 1 (1987).
7. Y. K. Choi, B. S. Kim, and S. M. Park, *J. Electrochem. Soc.*, Vol.140, 11 (1993).
8. G. T. K. Fey, *Progress in Batteries & Battery Materials*, Vol. 12, 145 (1993).
9. R. W. Berg, H. A. Hjuler, A. P. L. Sondergaard, and N. J. Bjerrum, *J. Electrochem. Soc.*, Vol.136, 323 (1989).
10. M. Jain, G. Nagasubramanian, R. G. Jungst, and J. W. Weidner, *J. Electrochem. Soc.*, Vol.146, 4023 (1999).

**Mass Transport and Kinetic Aspects of
Thionyl Chloride Reduction
at the Platinum Microelectrode**

George Ting-Kuo Fey and Ming-Chih Hsieh
Department of Chemical Engineering,
National Central University
Chungli, Taiwan 320, R.O.C.

Yu-Chi Chang
Department of Chemical Engineering,
Tamkang University
Tamsui, Taiwan 251, R.O.C.

The Li/SOCl₂ battery system holds an important place in the field of high power batteries because of their advantages in terms of high energy density, long storage life, low cost of materials, high open circuit voltage, and large operating temperature range (-55 to 70°C). Lithium/thionyl chloride batteries have been used for a number of applications in astronaut equipment [1,2] and biomedical devices [3,4]. Despite much progress in the design and optimization of these batteries, our fundamental knowledge of SOCl₂ reduction is limited. The reduction of thionyl chloride has been extensively investigated [5,9], but the detailed mechanism is still a subject of debate.

Film formation at the cathode during the reduction of thionyl chloride has been suggested [8,9]. Chiu et al. [8] estimated the values of diffusion coefficients ranging from 10⁻¹⁰ to 10⁻¹² cm²s⁻¹ for the 3.0M LiAlCl₄/SOCl₂ system, while Choi et al. reported that the diffusion coefficients were in the range of 10⁻⁹ to 10⁻¹¹ cm²s⁻¹ for the 1.5M LiAlCl₄/SOCl₂ system. The discrepancy between the reported values has been noted, but comprehensive studies have not been reported.

The object of the present paper is to systematically investigate the effects of reaction time, LiAlCl₄ concentration and temperature on the dynamics of film formation processes during the electroreduction of thionyl chloride using microelectrode techniques. The use of various transient electrochemical techniques to study the reaction provided an insight into the reduction of thionyl chloride. In addition, we also report the results of electrode kinetics at a nearly fresh electrode.

The mass transport and electron transfer characteristics of thionyl chloride reduction were studied using fast scan cyclic voltammetric, chronoamperometric, and pulse voltammetric

techniques. Diffusion coefficients are in the range of 10⁻¹¹ to 10⁻⁹ cm²s⁻¹, depending on the temperature, reaction time, and LiAlCl₄ concentration. The results obtained support the conjecture that a porous film formed on the Pt electrode surface during the electrochemical reduction of thionyl chloride. The standard rate constants range from 10⁻⁵ to 10⁻⁴ cm/s at a nearly fresh electrode surface, depending on the temperature and LiAlCl₄ concentration. We also conclude from this study that it is important to run the battery at a high LiAlCl₄ concentration because 0.5M LiAlCl₄ shows higher activation energy and a lower diffusion coefficient.

References

1. P. Chenebault, in "Lithium Batteries: New Materials, Developments and Perspectives", G. Pistoia, Ed., Elsevier Science B.V., The Netherlands, 347 (1994).
2. G. Halpert, H. Frank, and S. Surampudi, *Interface, The Electrochemical Society*, Vol.8, 25 (1999).
3. C. F. Holmes, in "Lithium Batteries: New Materials, Developments and Perspectives", G. Pistoia, Ed., Elsevier Science B.V., The Netherlands, 377 (1994).
4. C. F. Holmes, *Interface, The Electrochemical Society*, Vol.8, 32 (1999).
5. W. K. Istone and R. J. Brodd, *J. Electrochem. Soc.*, Vol.131, 2467 (1984).
6. F. W. Dampier and T. A. Cole, *J. Electrochem. Soc.*, Vol. 133, 938 (1986).
7. L. D. Hansen and H. Frank, *J. Electrochem. Soc.*, Vol.134, 1 (1987).
8. J. G. Chiu, Y. Y. Wang, and C. C. Wan, *J. Power Sources*, Vol. 21, 119 (1987).
9. Y. K. Choi, B. S. Kim, and S. M. Park, *J. Electrochem. Soc.*, Vol.140, 11 (1993).

Novel Superacid - based Lithium electrolytes for Lithium ion and Lithium polymer Rechargeable Batteries

H. V. Venkatesetty

H. V. Setty Enterprises, Inc.
12110 Red Oak Court So
Burnsville, MN 55337, U.S.A.

The objective of this work is to synthesize new and novel superacid-based lithium salts with improved ionic conductivity and good electrochemical stability for rechargeable lithium batteries which are useful in special medical devices and in Space applications. Several new lithium imide salts with large anions have been synthesized and characterized for electrochemical stability and conductivity in mixed solvent systems. Solid polymer electrolyte (SPE) films of the salts with polyethylene oxide with different compositions have been prepared and their conductivities have been measured as a function of temperature. Lithium transport properties and interfacial stability of the electrolyte in cells are influenced by the structure and properties of lithium polymer electrolyte material (1). Important factors that contribute to enhanced transport properties of lithium polymer electrolytes are the local segmental mobility of the solvating group in the polymer, the amorphous phase and the concentration of carrier ions (1-4). We have successfully synthesized eight new lithium superacid salts with large anions, purified them and characterized them for electrochemical stability and processability. Some of the promising salts are lithium 1,1,1-trifluoromethyl sulfonylperfluorobutylsulfonimide, $(CF_3SO_2NLiSO_2C_4F_9)$, lithium bis(nanofluorobutyl-sulfonyl) imide $(C_4F_9SO_2)_2NLi$, lithium 1,1,1-trifluoromethyl sulfonyl perfluorooctane sulfonimide $(CF_3SO_2NLiSO_2C_8F_{17})$ and N-(2-methoxyethyl) perfluorobutyl sulfonamide of lithium. The salts with low molecular weight have shown good solubility in mixed solvent system EC/DMC/DEC and all these salts are stable up to 5.0 V versus Li. The solution (1 M) of $CF_3SO_2NLiSO_2C_4F_9$ in solvent system shows conductivity at 6.6×10^{-3} S/cm at room temperature. We have prepared SPE films of these salts with polyethylene oxide with different Li/O ratios and measured their conductivity as a function of temperature. We have also studied the effect of filler materials such as amorphous silicon dioxide and aluminum oxide as well as polymer blends like polymethylmethacrylate (PMMA) in composite SPE films. We have fabricated lithium ion cells of nominal capacity of 100 m Ah to 2.3 Ah with carbon anode

mesocarbon microbeads (MCMB) and lithium cobalt oxide as well as lithium manganese dioxide cathodes. We have evaluated their performance for charge and discharge rates and cycle life. These cells show low impedance and excellent charge and discharge rate capability and very good cyclability. The experimental results are discussed in terms of lithium salt structures

Charge and discharge profiles of 100 m Ah cells at C/5 rate have been evaluated for cell voltage versus delivered efficiency and they show nearly 100 % efficiency. Irreversible capacity loss for cells with MCMB carbon in mixed solvent system EC/DMC/DEC is appreciably low. Cells with charge cut off at 4.15 V at C/10 rate and discharge at C/5 rate provide 80 cycles. 100 m Ah cells stored for two months, on discharging at C/5 rate with charge control at C/10 rate provide well over 450 cycle at 100 % efficiency. 100 m Ah cells on cycling at C/10 rate with charge control at C/10 provide more than 150 cycles with a loss of about 10 % capacity. Lithium metal polymer cells of about 100 m Ah capacity can be charged and discharged at low rates and efforts are being continued to prepare new electrolytes with high conductivity with a view to improve the rate capability.

Acknowledgment: Financial support from NIH, the Heart Lung and Blood Institute of the Department of Health and Human Services and NASA/JPL is gratefully acknowledged. Author thanks Prof. Thomas R. Hoyer of the University of Minnesota for help in the synthesis of lithium salts

References.

1. M. Armand, Solid State Ionics, 69, 309 (1994)
2. F. Capuano, F. Groce and B. Scrosati, J. Electrochem. Soc. 138, 1918 (1991)
3. H. V. Venkatesetty, Proc. Of 15th Annual Battery Conference on Applications and Advances, January 11-14 (2000) pp 109-114
4. G. Nagasubramania, D. H. Shen, S. Surampudi, Q. Wang, G. K. Suryaprakash, Electrochim. Acta, 40, (1996) pp 2280

**Interfacial Stability of Lithium Electrode in
IPN Electrolytes Based on Crosslinked
PEGMEM and PMMA**

Xinping Hou and Kok Siong Siow*

*Department of Chemistry, National University of
Singapore, 3 Science Drive 3, Singapore 117543*

It is now generally accepted that lithium batteries with solid polymer electrolytes offer attractive advantages such as elimination of electrolyte leakage, recharge ability, applicability of thin film technology in the production process [1]. However, few commercial products of this type are available to date due to severe problems with low conductivity and ambient temperature efficiency of cells.

Batteries with poly (ethylene oxide) (PEO)-based electrolytes have been widely examined [2,3]. The major problems lie with the following aspects: (i) PEO's crystallization affects its ionic conductivity and makes it poorly contact with electrodes. Crosslinking can eliminate the crystallization and improve its corresponding properties. (ii) Poor mechanical strength when plasticizers are used to improve ionic conductivity. Crosslinking or blending with another one or two polymers can solve such a problem to some extent. (iii) Poor stability in contact with lithium electrode because of its carbon / oxygen bonds and moisture sensitivity, which will result in a passivation layer in between lithium electrode and polymer electrolyte. The structure of this passivation layer is not well understood, but it is known that this uncontrolled passivation phenomena affect the cyclability of lithium electrodes and therefore the entire lithium battery.

Scrosati and co-workers [4,5] have demonstrated that the addition of inorganic fillers, such as LiAlO_2 or zeolites, improves electrode-electrolyte compatibility and reduces the passivation phenomena. It has been reported by Borkowska et al [6] that the growth of the resistance of passive layers is limited for blend-based poly (ethylene oxide) (PEO)- LiClO_4 electrolytes with various methacrylic and acrylic polymers used as additives. Scrosati et al [7] also reported an even stronger effect of poly (methyl methacrylate) (PMMA) on the stabilization of electrode-electrolyte interface for a variety of PMMA-based gel electrolytes. Recently, W. Wieczorek and J.R. Stevens [8] showed that the properties of lithium electrode-polymer electrolyte interface have been improved after the *in situ* polymerization of methyl methacrylate in a solution of LiCF_3SO_3 in an ethylene oxide-propylene oxide copolymer.

In the present paper, we will describe the synthesis of a new sequential interpenetrating polymer network (IPN) electrolyte based on methacrylate. The effect of polymerized MMA on the characteristic of lithium-polymer electrolyte interface is studied for this interpenetrating polymer network electrolytes obtained by polymerization of methyl methacrylate (PMMA) in crosslinked poly (ethylene glycol) methyl ether methacrylate (PEGMEM). The effect of the PMMA concentration on the conductivity and electrode-electrolyte interfacial resistance is discussed on the basis of impedance spectroscopy data obtained in a

symmetrical cell with two lithium electrodes. The thermal characteristics of these electrolytes have been studied by differential scanning calorimetry (DSC). Li^+ transference numbers were evaluated at room temperature on the basis of ac impedance and dc polarization measurements developed by Evans et al [9].

References

- [1]. M. Gauthier, A. Belanger, B. Kapfer, G. Vassort and M. Armand, Solid Polymer Electrolyte Lithium Batteries, in 'Polymer Electrolytes-Reviews II', (edited by C.A. Vincent and J.R. MacCallum) Elsevier Sequoia (1989), p. 289-295.
- [2]. F. Gray, Polymer Electrolyte-Based Devices, in 'Polymer Electrolytes: Recent Trends and Developments', VCH Publications, London, Berlin (1991).
- [3]. F. Gray, Polymer Electrolytes, The Royal Society of Chemistry, Cambridge, UK (1997).
- [4]. F. Capuano, F. Croce, B. Scrosati, J. Electrochem. Soc. 138 (1991) 1918.
- [5]. B. Scrosati, R. J. Neat, in 'Applications of Electroactive polymers', (edited by B. Scrosati) Chapman and Hall: London (1993), Chapter 6.
- [6]. R. Borkowska, J. Laskowski, J. Plochanski, J. Przyluski and W. Wieczorek, J. Appl. Electrochem. 23 (1993) 991.
- [7]. G. B. Appetecchi, F. Croce, B. Scrosati, Electrochim. Acta 40 (1995) 991.
- [8]. W. Wieczorek and J. R. Stevens, J. Phys. Chem. B 101 (1997) 1529.
- [9]. J. Evans, C. A. Vincent and P. G. Bruce, Polymer 28 (1987) 2324.

DIFFUSION MECHANISM IN THE CROSS-LINKED POLY(ETHER) DOPED BY $\text{LiN}(\text{CF}_3\text{SO}_2)_2$

Y. Aihara^a, T. Bando^a, T. Iguchi^a, J. Kuratomi^a,
K. Sugimoto^b and K. Hayamizu^b

^aYuasa Corporation,

4-5-1 Ohgi-cho, Odawara 250-0001, Japan, and

^bNational Institute of Materials and Chemical Research

INTRODUCTION

The cross-linked random copolymer of the ethylene oxide (EO) and the propylene oxide (PO), *poly*(EO-PO) is a candidate polymer for use in the lithium batteries. At present, the ion conductivity of these polymer electrolytes is not large enough for practical usage. We have reported the studies on the ionic conduction mechanisms in organic electrolytes and chemically cross-linked *poly*(ethylene oxide) gel electrolytes.¹⁻⁴⁾ In the present work, we measured the ionic conductivity and the self-diffusion coefficients by using pulsed gradient spin-echo (PGSE) NMR for clarification of the ionic conduction mechanism in the cross-linked polymer electrolytes. We found that the self-diffusion coefficients of the anion and lithium ions showed the dependence on the time (i.e., a measurement parameter Δ , the separation between the gradient pulses). Usually the a long Δ is adopted for the reliable value and the present phenomenon has not been reported.⁵⁻⁸⁾

EXPERIMENTAL PROCEDURE

The polymer electrolytes were prepared by cross-linking reaction of the tri-acryloyl terminated EO-PO macromer (Daiichi Kogyo Seiyaku) after dissolving $\text{LiN}(\text{CF}_3\text{SO}_2)_2$ (Central Glass Co., LTD). The various salt concentration electrolytes (O/Li=10/1, 20/1 and 30/1) were prepared. The ionic conductivity measurement was performed by ac impedance method. The self-diffusion coefficient of the cation (^7Li), anion (^{19}F) and polymer (^1H) were measured by PGSE-NMR method at various temperature, and also studied on the dependence of Δ . The spin-lattice relaxation time (T_1) and the spin-spin relaxation time (T_2) were also measured.

RESULTS AND DISCUSSION

The Arrhenius plots of the ionic conductivity for the polymer electrolytes are given a typical VTF behavior. The VTF equation was found to provide a good fit to the data and the results of the regression are shown in the figure. When the salt concentration was O/Li=20/1, the apparent temperature dependence of the ionic conductivity suggests higher performance compared to those with other salt concentrations, and at the same time higher ionic conductivity was obtained at higher temperature.

The anion diffusion behavior in the polymer can be explained by the single species diffusion, however, the measured diffusion coefficients depend on the time scale, Δ , the diffusion measurement parameter between the pulse gradients. (See Fig. 1.) These phenomena have not yet reported and are difficult to interpret by present theoretical treatment. However, the apparent activation energy (E_a) obtained by the Arrhenius plots of the anion diffusion coefficients at long Δ are closed to that from the ionic conductivity. On the other hand, the diffusion coefficients of the lithium are much smaller than those of the anions at every Δ . Also it is well known that low transport number of lithium ion, thus the ionic conduction strongly depends on the anion diffusion in these

electrolyte systems.

The T_1 relaxation curves were single exponential for the all components, but and spin-echo curves (T_2) curves were single exponential only for the anion. The temperature dependence of the T_1 value for the cation and the polymer were observed to have T_1 minima and calculated correlation times indicate that the reorientation motion of the cation is slower than the polymer motion.

CONCLUSION

In the present polymer electrolytes, clearly the ion transport phenomena are not the simple free diffusion. It seems to diffuse similar to a mode of diffusion in the fractal network, but can not be fully interpreted by the theory available. The motions of the lithium and the polymer are fast in the small region but the long-range diffusion is limited. The macroscopic ionic conduction is mainly carried out by the anion diffusion. As the polymer electrolytes without any solvent, the present electrolytes have relatively high ionic conductivity, but the transport number of the lithium is too small to be used practically. As well known, the slow cation diffusion is a serious problem in the polymer electrolytes. Since the lithium motions are closely correlated with those of the polymer, it is necessary to clarify the relationship between microscopic polymer structure and ion diffusion.

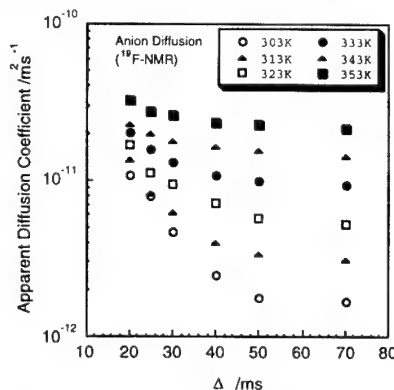


Figure 1. The apparent diffusion coefficients of the anion (^{19}F) are plotted versus large Δ at various temperature when the salt was LiTFSI (O/Li=20/1) used.

ACKNOWLEDGMENT

This study was supported by the Energy and Industrial Development Organization (NEDO).

REFERENCES

- 1) K. Hayamizu, Y. Aihara, S. Arai, and W. S. Price, *Solid State Ionics*, 107, 1 (1998)
- 2) K. Hayamizu, Y. Aihara, S. Arai, and C. Garcia-Martinez, *J. Phys. Chem.* 103, 519 (1999)
- 3) Y. Aihara, S. Arai, and K. Hayamizu, *Electrochimica Acta*, in press.
- 4) Y. Aihara, K. Sugimoto, W. S. Price, and K. Hayamizu, *J. Chem. Phys.*, in submitting.
- 5) S. Arumugam et al., *J. Phys. Condens. Matter* 5 (1993) 153-160
- 6) J. Shi et al., *Solid State Ionics* 60 (1993) 11-17
- 7) W. Gorecki et al., *J. Phys. Condens. Matter* 7 (1995) 6823-6832
- 8) C. Roux et al. *J. Phys. Condens. Matter* 8 (1996) 7005-7017

Ion Conduction Mechanism in Solid LiX-P(EO)_n-based Polymer Electrolytes

D. Golodnitsky¹, E. Livshits¹, E. Peled¹, S.H. Chung², and S. Greenbaum²

¹*School of Chemistry, Tel Aviv University, Tel Aviv 69978, Israel*

²*Physics Department, Hunter College of CUNY, New York, NY10021, USA*

Highly ionic-conductive polymer electrolytes (PE), formed by complexes of alkali metal salts and polyethers, currently attract considerable interest because of their potential applications as solid electrolytes in various electrochemical devices such as solid-state batteries, memory devices and "smart windows". Furthermore, PEs are of fundamental theoretical importance as model materials for investigations of conduction paths in anisotropic semicrystalline systems.

Most of the research on new PEs has been guided by the principle that ion transport is strongly dependent on local (segmental) motion of the polymer in the vicinity of the ion. Semi-crystalline solid poly(ethylene oxide) (PEO), having an extended helical structure with polar repeat units, is the most intensively studied polymer and serves as a prototype for the structural features in most advanced polymer-electrolyte hosts. The intrahelix location of the cations, found by Bruce [1], gives grounds to expect that cation transport may occur along the helical axis [2] and alignment of the polymer chains should be followed by an increase in ionic conductivity.

For the LiI-P(EO)₂₀ polymer electrolyte we were the first to find five-fold stretching-induced conductivity enhancement in the axial force direction [3]. With the use of solid state NMR it has been demonstrated that internuclear Li-H distances and local Li-O bond lengths and angles are altered upon the application of a uniaxial stress on a film of P(EO)₂₀-LiI [4]. Changes in the long-range structure, shown by the angular dependence of the lithium-7 NMR linewidths, clearly illustrates the alignment of the crystalline regions in the direction of the applied stress. On the basis of the negative correlation between segmental polymer motion and ionic conductivity enhancement, we raise the possibility of Li⁺ cation migration channels within the helical chain and possible anion movement on the helix envelope.

Of crucial importance, when discussing mechanisms of ion transport, is the number of charge carriers, since in concentrated polymer electrolytes, formation of ion aggregates strongly influences ion mobility. Because ion aggregation is strongly influenced by salt concentration and varies among anions, in this work we focus on the

effect of stretching on ionic conductivity and structural properties of LiX-P(EO)_n, (X=iodide and imide) with the ether oxygen-to-Li⁺ ratio (n) varying from 40:1 to 3:1.

AC impedance, XRD, XPS, SEM, DSC and solid-state NMR data will be presented.

References:

1. Solid State Electrochemistry, Ed: P.G. Bruce, Cambridge University Press, (1995)
2. M. B. Armand, Ann. Rev. Matter Sci., **16**, 245-261, (1986)
3. D. Golodnitsky and E. Peled, *Electrochimica Acta*, **45**, 1431-1436, (2000)
4. S. H. Chung, y. Wang, S. G. Greenbaum, D. Golodnitsky and E. Peled, *Electrochemical and Solid-State Letters*, **2**, 11, 553-555, (1999)

Preparation of Microporous PVDF Based Polymer Electrolytes

Haitao Huang, Hongpeng Wang, Stephanie L. Wunder*
Department of Chemistry, Temple University,
Philadelphia PA 19122, USA

Plasticized PVDF-HFP-SiO₂ polymer electrolytes have been widely prepared by a Bellcore's process, resulting in a nanoporous morphology [1]. It has been recently reported that increasing pore size (e.g. to microporous) in PVDF matrix can enhance its ionic conductivity and therefore improve the cell performance [2-4]. This paper presents a new method of preparing microporous PVDF-HFP film as follows:

PVDF/HFP copolymer (KYNAR 2801, ELF Atochem), PC and fumed silica, 30%:50%:20% by weight, were mixed in acetone/alcohol solvents. Acetone is a solvent and alcohol a non-solvent for PVDF-HFP. The resulting slurry was cast with a doctorblade onto a polyester sheet to form a thin blend film after solvent evaporation.

The PC component was removed under vacuum at room temperature. Fig 1 is the SEM micrograph of the film prepared from a casting solvent containing 75wt.% of acetone and 25wt.% of butanol, clearly showing a microporous morphology. Substitution of methanol and ethanol alcohol/acetone in the same ratios result in microporous structure, with the pore size being somewhat smaller in the case of methanol. After soaking in 1 M LiPF₆/EC+DMC electrolyte, conductivity measurements show a value of 1.8 mS cm⁻¹ for the films prepared from acetone/butanol and acetone/ethanol mixed solvents, and 0.9 mS cm⁻¹ for the methanol case. When no alcohol was present in the casting solvent, no microporous structure was observed and the film had lower conductivity, 0.7 mS cm⁻¹. The amount of butanol used in the mixed casting solvent were examined (14, 33, 40 and 50wt.%), and the mechanical properties became poor when more than 40wt.% of butanol was used.

The polymer blend film, prepared from acetone/butanol casting solvents, was placed between LiCoO₂ cathode and MCMB anode, and laminated by heating rolling. After removal of PC under vacuum and impregnation with the liquid electrolyte, the laminated cells were subjected to cycling test with cut-off voltages of 4.2 and 2.5 V. A discharge capacity of more than 100 mAhg⁻¹ at C/8 was obtained. This is a promising result considering that loading on the composite cathode used was around 27 mgcm⁻². Optimization of lamination process and rate capacity are under study.

These results indicate that using mixed casting solvents, with one of the components a

non-solvent for PVDF-HFP, microporous morphologies can be formed that result in increased conductivity and expect improved rate capability for the Li ion batteries.

REFERENCES

1. J. M. Tarascon, A. S. Gozdz, C. N. Schmutz, F. Shokoohi, P. C. Warren, *Solid State Ionics* **86-88** 49 (1996).
2. Hongpeng Wang, Haitao Huang and Stephanie L. Wunder, *J. Electrochem. Soc.* Submitted.
3. X. Andrieu, C. Jehoulet, F. Boudin, and I. I. Olsen, *Proceedings of 38th Power Sources Conference* 266 (1998).
4. A. Du Pasquier, P. C. Warren, D. Culver, A. S. Gozdz, G. G. Amatucci, J. M. Tarascon, 196th the electrochem. Soc. Meeting at Hawaii, B2 abs.116, Oct. 1999.

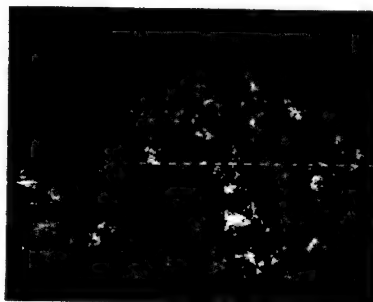


Fig 1. SEM of a cross section of the PVDF film (magnification:x2500)

* corresponding author, e-mail address:
slwunder@unix.temple.edu

ROOM TEMPERATURE AMORPHOUS-
PHASE STABILIZATION OF
PEO-BASED NANOCOMPOSITE POLYMER
ELECTROLYTES:
AN IMPEDANCE SPECTROSCOPY STUDY

F. Croce, L. Persi, B. Scrosati

Department of Chemistry, University "La
Sapienza"

P.le Aldo Moro, 5 - 00185, Roma, Italy

Lithium polymer electrolytes formed by dissolving a lithium salt in poly(ethylene oxide) PEO may find useful application as separators in lithium rechargeable polymer batteries. The main drawback of solvent-free PEO-based polymer electrolytes is their high crystallinity at room temperature, which reduces the conductivity to a level too low to satisfy the requirements of batteries or other devices. In this poster we show that the addition of nanometric filler (SiO_2 , TiO_2) in $\text{P(EO)}_n\text{LiClO}_4$ polymer electrolytes induces an increase of the transport properties respect to the corresponding unfilled ceramic-free polymer electrolyte. The increase in conductivity and cation transference number was attributed to the enlargement of the total amorphous phase in the polymer matrix and also to some possible ceramic-electrolyte interactions in according to an acid-base Lewis mechanism [1,2,3].

In order to study the effect that the addition of nanometric filler has on the crystallization kinetic of P(EO) -based polymer electrolytes we have undertaken an impedance spectroscopy study on samples with and without the ceramic filler. In particular in this poster we show that the nanometric filler can perform as a solid plasticizer for PEO by kinetically inhibiting crystallization. Furthermore, our results show that the filler addition deeply influences both the electrical conductivity and the fraction of the current transported by the cations of the samples.

- 1) G. B. Appetecchi, F. Croce, L. Persi, and B. Scrosati
Nature, 394 (1998) 4126.
- 2) R. Caminiti, F. Croce, A. Martinelli, L. Persi, F. Ronci and B. Scrosati
J. Phys. Chem., in press
- 3) F. Croce, G. B. Appetecchi, L. Persi, and B. Scrosati
Solid State Ionics, submitted

GEL ELECTROLYTES BASED ON AMPHIPHILIC COPOLYMERS

Ronnie Ljungbäck, Patrik Gavelin,
Patric Jannasch, and Bengt Wesslén

Department of Polymer Science & Engineering, Lund
University, P.O. Box 124, SE-221 00 Lund, Sweden,
www.polymer.lth.se

Amphiphilic copolymers synthesized by radical copolymerisation of methacrylates offer great flexibility in the design of polymer gel electrolytes and may be promising candidates for application in lithium polymer batteries. Amphiphilic copolymers consists of hydrophilic and hydrophobic parts. The polymers used in this study had a methacrylate backbone carrying hydrophilic diethylene glycol (DEG) chains, and hydrophobic fluoroalkyl chains. The cations of the lithium salt co-ordinate weakly to the hydrophilic units of the amphiphilic copolymer in competition with the solvent, when applied as a gel electrolyte.² The presence of DEG units ensures a high solubility of the copolymer, and that the gel electrolyte will not phase separate at a macroscopic level. The hydrophobic content was varied by the incorporation of different amounts of fluoroalkyl methacrylates in the copolymer (table 1).

Gel electrolytes based on PMMA have been thoroughly studied in several publications in recent years, and can basically be regarded as passive in the ion conductive process.³ The properties of gel electrolytes based on the amphiphilic copolymers were compared with the properties of a gel electrolyte based on PMMA. These copolymers function as 'active' polymer matrices, in contrast to the polymers commonly used in conventional gel electrolytes such as PMMA.

The copolymers were characterized with respect to structure by NMR and IR spectroscopy, and with respect to the thermal properties by differential scanning calorimetry. Gel electrolytes containing 30 wt % copolymer were prepared by using an electrolyte consisting of 1.0 M LiPF₆ dissolved in γ -butyrolactone. The thermal properties of the gel electrolytes were studied by differential scanning calorimetry, and the ion conductivity was measured in a broad temperature range (-20 to 60 °C) by electrochemical impedance spectroscopy (EIS).

The results showed that the introduction of DEG units on a polymethacrylate backbone did not increase the ion conductivity significantly, as compared to gel electrolytes based on PMMA. However, with the introduction of fluoroalkyl units in combination with DEG units, the ion conductivity increased substantially (Figure 1). The highest ion conductivity was observed for a gel electrolyte based on a copolymer containing 42 wt % fluoroalkyl methacrylate.

References.

1. P. Gavelin, P. Jannasch, B. Wesslén, *to be published*.
2. J. Adebahr, P. Gavelin, P. Jannasch, D. Ostrovskii, P. Jacobsson, B. Wesslén, *to be published*.
3. G.B. Appetecchi, F. Croce, B. Scrosati, *Electrochimica Acta*, **40**, 1995 (8), 991.

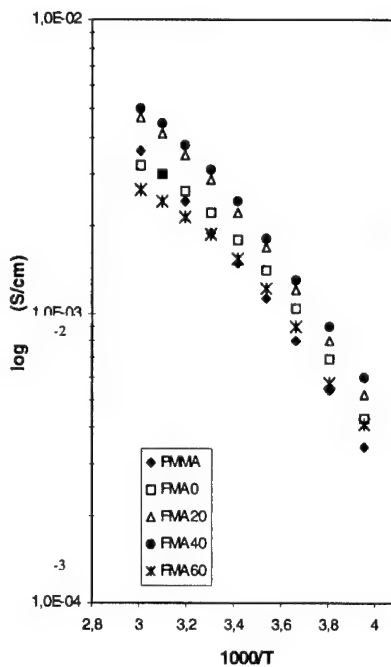
Acknowledgement.

The financial support from the Swedish Foundation for Strategic Environmental Research, MISTRA, is gratefully acknowledged. The work was done within the framework of the Jungner Centre.

Table 1. Polymer composition and glass transition temperature determined by ¹H NMR spectroscopy and DSC.

Polymer	Monomer content (wt %)		T _g (°C)
	FMA	DEGMA	
PMMA	-	-	100
FMA0	0	100	-34
FMA20	24	76	-27
FMA40	42	58	-8
FMA60	61	39	4

Figure 1. Conductivity plots for gel electrolytes based on amphiphilic copolymers and PMMA.



Abstract No. 302

IONIC CONDUCTION AND ELECTROCHEMICAL PROPERTIES OF NEW POLY(ACRYLONITRILE-ITACONATE) BASED GEL-ELECTROLYTE

Y.W. Kim, M.S. Gong* and B.K. Choi

Dankook University, Department of Science Education,
Seoul, 140-714, Korea

*Dankook University, Department of Chemistry,
Cheonan, 330-714, Korea

The poly(acrylonitrile)(PAN)-based polymer gel-electrolytes retain most of the high ionic conductivity characteristic of the liquid phase, but also are mechanically stable enough to fit the requirements of lithium polymer battery. Nonetheless, the PAN-based gel-electrolytes undergo solvent exudation upon long storage resulting in a progressive decrease in the ionic conductivity. The compatibility with the electrode materials is also poor when a lithium or a carbon anode is contacted by the PAN-gels.

To develop a new polymer gel-electrolyte based on the modified PAN, polyacrylonitrile-co-bis[2-(2-methoxyethoxy)ethyl]itaconate (abbreviated as PANI) copolymers were synthesized. Since the PANI as a host polymer did not form a freestanding film, PANI and PAN blend was complexed with organic solvents, ethylene carbonate (EC) and γ -butyrolactone (BL), and LiClO_4 salt. Polymer electrolytes of PAN-PANI-EC/BL- LiClO_4 were prepared for freestanding films by dissolving PAN and PANI in an appropriate amount of EC/BL- LiClO_4 solution at 120°C and evaporating off the excess solvents in Ar atmosphere. Various compositions were tested in order to obtain the best compromise between high conductivity, homogeneity, electrochemical and dimensional stability.

As the content of PANI was increased in PAN-PANI mixed gels, the crystallinity of the gels was greatly reduced as well as the organic solvents were thoroughly mixed, resulting in higher ionic conductivity. The highest room temperature conductivity of $1.9 \times 10^{-3} \text{ Scm}^{-1}$ was found for a film of 25PAN+10PANI+50EC/BL+15 LiClO_4 as shown in figure 1. The current-voltage response of a stainless steel electrode of a Li/electrolyte/SS cell was measured as shown in figure 2. The anodic limit of PAN-PANI blend film was about 5.1 V vs. Li and was slightly higher than that of PAN-based film. The time evolution of interfacial resistance of a Li/electrolyte/Li cell was monitored using frequency response analysis. The interfacial resistance of the electrolytes was steadily increased with time, but the increase is much lower in the case of PAN-PANI blend films. It reveals that the PAN-PANI film, as compared with pristine PAN-based film, is more stable toward lithium electrode, possibly because of its enhanced ability of trapping liquid solvent.

In conclusion, the addition of PANI as a host polymer in the PAN-based gels has beneficial effects such as higher ionic conductivity, better thermal stability, wider electrochemical stability, better ability of containing organic solvent and better interfacial stability with lithium electrode, though it exhibits slightly less mechanical rigidity. The PAN-PANI blend gel-electrolytes are considered to be a promising candidate for the solid electrolytes of lithium polymer batteries.

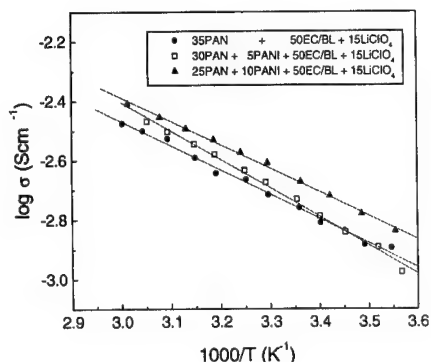


Fig. 1 Temperature dependence of the ionic conductivity of PAN + PANI + EC/BL + LiClO_4 electrolytes.

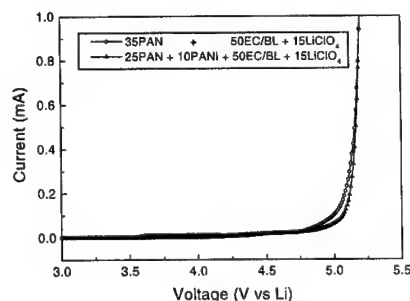


Fig. 2 Current-Voltage response of PAN + PANI + EC/BL + LiClO_4 electrolytes.

Studies of the Interface Between Lithium Deposits and Polymeric Electrolyte Systems Using *in situ* FTIR Spectroscopy

O. Chusid, Y. Gofer and D. Aurbach

Department of Chemistry, Bar-Ilan University, Ramat-Gan, 52900 Israel.

M. Watanabe

Department of Chemistry, Yokohama National University, Tokiwadai, Hodogaya-Ku, Yokohama 240, Japan

T. Momma and T. Osaka

School of Science and Engineering, Waseda University, Okudo 3-4-1, Shinjuku-Ku, Tokyo 169, Japan

Introduction

Special interest is currently being focused on the use of polymeric electrolytes in lithium battery systems. One of the solutions to the problem of their poor conductivity is the addition of plasticizers to form gel type membranes.⁽¹⁾ Another solution is R&D of new branched polymers with better conductivity at room temperature.⁽²⁾ The only way to explore the surface chemistry that is developed in the interface between lithium and polymeric electrolytes is to use *in situ* techniques, because the polymer electrolyte, can not be removed properly from the electrode for the performance of *ex situ* analysis. The best technique for studying the surface chemistry under these conditions is *in situ* FTIR spectroscopy. In this report we present the application of the single internal reflectance method,⁽³⁾ in order to investigate lithium-polymer electrolyte interfaces. In this method the IR beam hits the spectroelectrochemical window from the back and is reflected from the internal interface between the window and a thin metal layer W.E. The beam has some penetration depth beyond the reflective surface, and hence can be partially absorbed by the species at the metal-solution side. Windows inert to lithium and solution species such as KBr, NaCl, etc. can be used.

Experimental

The experimental setup included a spectroelectrochemical cell in which the working electrode is a thin layer of gold deposit on a KBr window (lithium disc counter electrodes). The polymer is positioned between the two electrodes, forming a thin layer type cell. The spectroscopic measurements used the single internal reflectance method⁽³⁾ (a Nicolet 860 FTIR spectrometer with a grazing angle reflectance accessory).

Each experiment included a measurement of an OCV spectrum before the electrochemical process, followed by galvanostatic steps (lithium deposition and dissolution) and measurements of spectra after each step. Two types of polymers were studied. One is a poly(vinylidene difluoride-hexafluoropropylene) (PVdF-HFP) gel type polymer for R.T.⁽¹⁾ with ethylene carbonate (EC) and propylene carbonate (PC) as plasticizers, and LiClO₄ as the salt. The concentration of EC/PC LiClO₄ 1M solution in the matrix was 20% by weight. The other one was poly[ethylene oxide-2-(2-methoxyethoxy)ethyl glycidyl ether] (P(EO/MEEGE)) with LiClO₄ as the salt.⁽²⁾ The [Li]/[O] ratio was 0.08. The second polymeric system was measured at elevated temperatures (>50 °C).

Results and discussion

We present herein a typical result of interfacial studies of these polymeric systems with lithium surfaces. The figure shows spectroscopic results that were measured with the PVdF-HFP gel type electrolyte at room temperature. Spectrum a was measured at OCV and contains mainly superimposed spectra of EC and PC (the plasticizers). Spectrum b was obtained by subtracting the OCV spectrum from the one that was measured after lithium deposition. In this spectrum the original features, belonging to the

electrolyte system, are absent due to successful subtraction, and new peaks are present around 1620-1550 cm⁻¹, 1300 cm⁻¹, 1200-1100 cm⁻¹ and 830 cm⁻¹.

Such a combination of peaks is an indication of the formation of lithium alkyl carbonates in the lithium-gel interface. These compounds are formed by the reduction of the EC/PC mixture⁽³⁾ in the gel, at potentials close to that of lithium deposition. From the spectroscopic results, there is no evidence that the PVdF itself undergoes a reduction process under these conditions. Studies of other polymeric systems are in progress.

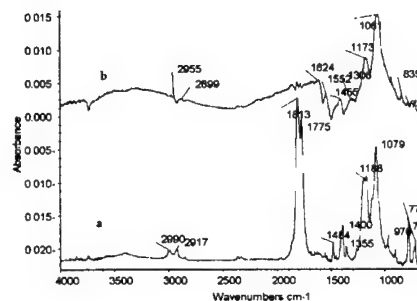
Acknowledgment

This work was supported by NEDO Japan.

References

1. T. Osaka, S. Komaba, X. Liu, *Nonaqueous Electrochemistry* Chap.7, D. Aurbach Editor, Marcel Dekker, Inc., New York, 1999.
2. A. Nishimoto, M. Watanabe, Y. Ikeda, S. Kohjiya, *Electrochimica Acta* 43, 1177 (1988).
3. E. Goren, O. Chusid, D. Aurbach, *J. Electrochem. Soc.*, 138, L6 (1991).

IR spectra of PVdF-HFP polymer with EC/PC 1M LiClO₄ plasticizer measured *in situ* in a Single Internal Reflectance Mode. a. OCV spectrum. b. A spectrum measured after lithium deposition (OCV spectrum subtracted).



Polymeric gel electrolytes reinforced with glass fiber cloth for lithium secondary battery

*Ho Cheol Park, Jong Han Chun, Sang Hern Kim, Jang Myoun Ko

**Soo Ik Jo, Jae Sik Jung, Hun-Joon Sohn

*Department of Industrial Chemistry, Taejon National University of Technology, 305-3, Samsung-2 dong, Dong-gu, Taejon 300-717, Korea.

**School of Materials Science & Engineering, College of Engineering, Seoul National University 56-1 Shinrim-dong, Kwanak-gu, Seoul 151-742, Korea.

The polymeric gel electrolytes(PGE), which consist of polymer matrix, plasticizer and Li salt, have been extensively studied for the application to lithium-based battery because of their high ionic conductivity over 10^{-3} S/cm at room temperature. However, there is no commercialization of Li based secondary battery using PGEs as an electrolyte, yet. One of crucial reasons seems to be its poor mechanical strength which do not allow easy construction of a unit battery cell configuration. The purpose of the present study is to investigate the possibility of improvement of the mechanical strength of PGE with the aid of glass fiber cloth(GFC) as a reinforcing material to be applicable to Li-ion battery. In particular, PAN-based composite polymer electrolytes with GFC as a reinforcing agent were prepared because PAN based polymer electrolyte have better performance and safety than conventional polyether-based gel electrolytes for battery applications. Polymeric gels were made by polyacrylonitrile(PAN) blended with poly(vinylidene fluoride-co-hexafluoropropylene) (P(VdF-co-HFP)), and reinforced by glass fiber cloth (GFC) to increase the mechanical strength. The PGE-GFC films with a thickness of 40-80 μ m were obtained by casting the gel solution onto a glass sheet substrate laying a GFC with thickness of 38 μ m in a dry argon box. Table 1 summarize the electrolyte compositions of the four different types of PGE-GFCs. To check the electrochemical stability of PGE-GFC, Fig. 1 illustrates the current-voltage responses of electrolytes obtained in different compositions. It can be seen that anodic decomposition voltage limits are close to 5.0 V for all PGE-GFCs, indicating that there is no decomposition of GFCs in the polymeric gel in this potential region. Table 2 shows ionic conductivities of the PGE-GFCs at room temperature. Ionic conductivities of the PGE-GFCs samples showed over approximately 10^{-3} S/cm at room temperature and it is almost the same with PAN based electrolytes without any reinforcing materials. This means that conductivities of polymeric gel electrolyte are not decreased with the introduction of the GFC to the gel, implying that GFC do not significantly inhibit the motion of Li ion in the polymeric gel matrix. Cycling performance of the test cell is given in Fig. 2. The cell continues to be cycled over 400 cycles without showing a significant drop in capacity and retains over 80% of the initial capacity. It has been well known that one of main causes of drop of cycle life is a creep phenomena observed in polymer gel electrolytes due to their viscoelasticity. However, our results suggest that GFC type of reinforcing material is very effective to prevent the creep of polymer gel electrolyte to keep the dimensional stability. Also, there is no interaction between glass fiber and Li^+ ion. In addition, it has been

known that when solid polymer electrolyte film based cross-linked polyethylene oxide was bent up to 180° , cracks were developed on the solid polymer electrolyte, depending on cross-linking density[1]. This indicates that a solid polymer electrolyte is fragile when the relative cross-linking density of polymer is too high to increase the mechanical strength. However, the GFC-GPE did not crack due to the flexibility of PGE and GFC

Table 1. Composition of PGE-GFC(wt%)

Sample #	Fiber GFC(mg)	Polymer		Plasticizer			Salt LiClO ₄
		PA N	PVdF	EC	PC	DE C	
1	4	8	0.8	37.2	37	13	4
2	4	8	1.6	36.7	36.7	13	4
3	4	8	2	37	37	12	4
4	4	7	0.4	35.8	35.8	15	4

Table 2. Ionic conductivities of PGE-GFC at room temperature

Sample #	Conductivities(S/cm)
1	2.88×10^{-3}
2	2.27×10^{-3}
3	1.69×10^{-3}
4	2.44×10^{-3}

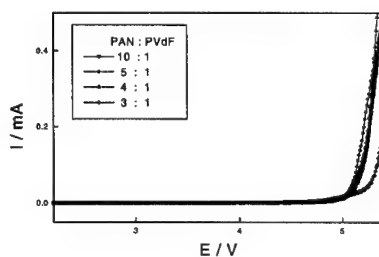


Fig.1.

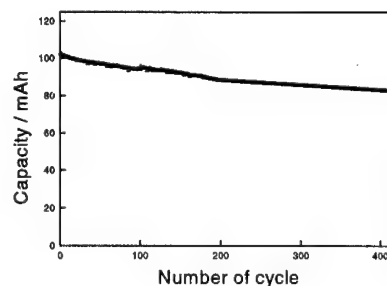


Fig.2

Reference

1. S. Izuchi, S. ochiai, K. takeuchi, *J. Power Source*, **68**, 37(1997)

Polymer Electrolytes Based On Hyperbranched Polymers
 Takahito Itoh, Nobuyuki Hirata, Zhaoyin Wen,
 Masataka Kubo, and Osamu Yamamoto
 Department of Chemistry for Materials,
 Faculty of Engineering, Mie University
 1515 Kamihama-cho, Tsu, Mie 514-8507, Japan

Previously, we prepared hyperbranched poly[bis-(diethylene glycol)benzoate] ($n=1$) (**poly-Ac1a**) and poly[bis(triethylene glycol)benzoate] ($n=2$) (**poly-Ac1b**) with terminal acetyl group and characterized their polymer electrolytes with lithium salts such as $\text{LiN}(\text{CF}_3\text{SO}_2)_2$ and LiCF_3SO_3 [1,2]. Higher ionic conductivity was observed for the hyperbranched polymer having triethylene glycol chain rather than diethylene glycol chain, and for $\text{LiN}(\text{CF}_3\text{SO}_2)_2$ rather than LiCF_3SO_3 . Moreover, addition of ceramic fillers to the **poly-Ac1b**/ $\text{LiN}(\text{CF}_3\text{SO}_2)_2$ electrolyte could increase the ionic conductivity and the mechanical strength of the electrolyte and even improve the interfacial stability with lithium metal [3]. In this work, hyperbranched polymer having hexaethylene glycol chain longer than triethylene glycol chain, poly[bis(hexaethylene glycol)benzoate] ($n=5$) (**poly-Ac1c**), was prepared and its polymer electrolyte with $\text{LiN}(\text{CF}_3\text{SO}_2)_2$ was characterized. And also, in order to investigate the effect of hyperbranched polymer as an additive, blend-based polymer electrolyte composed of **poly-Ac1b**, linear poly(ethylene oxide) (PEO), and $\text{LiN}(\text{CF}_3\text{SO}_2)_2$, was characterized.

Both monomers ($n=2$ and 5) were prepared according to the procedure reported [4], and then polymerized in the presence of a dibutyltin diacetate catalyst at 200°C for 120 min to give corresponding hyperbranched polymers with the molecular weight of 25000 for $n=2$ and of 30000 for $n=5$, respectively, in 60-70% yield, which were purified by reprecipitating each solution in THF into MeOH. Terminal hydroxy group of the resulting polymers was acetylated by the reaction with acetyl chloride according to the method reported previously [1], and both **poly-Ac1b** and **poly-Ac1c** were obtained as brown rubber-like solids in 70-80% yields.

Fig. 1 shows the isotherm curves of the ionic conductivity at the range of $30\text{--}80^\circ\text{C}$ against the lithium salt concentration from a [Li salt]/[repeat unit] ratio of 0.3 ($\text{Li}/\text{O}=0.02$) to 4.2 ($\text{Li}/\text{O}=0.28$) for the **poly-Ac1c**/ $\text{LiN}(\text{CF}_3\text{SO}_2)_2$ electrolyte. Conductivity maximum was observed at [Li salt]/[repeat unit] ratio of 0.6 ($\text{Li}/\text{O}=0.04$) similar to that of any other reported PEO-based polymer electrolytes, but this behavior is different from that of the **poly-Ac1b**/ $\text{LiN}(\text{CF}_3\text{SO}_2)_2$ electrolyte reported previously [1,2]. This indicates that the longer is ethylene oxide chain length in this hyperbranched polymer, the more the performance becomes similar to linear PEO. At a [Li salt]/[repeat unit] ratio of 0.6, the ionic conductivity reaches $9 \times 10^{-5} \text{ S/cm}$ at 80°C in the isotherm curve. After this maximum value, the conductivity decreases very slowly with increasing lithium concentration, different from linear PEO-based polymer electrolytes, probably due to hyperbranched structure.

The electrochemical stability of the **poly-Ac1c**/ $\text{LiN}(\text{CF}_3\text{SO}_2)_2$ electrolyte was determined by cyclic voltammetry using stainless steel (SS)/polymer electrolyte/SS cell at 70°C and the electrolyte was found to be stable until 5.2 V.

The effect of hyperbranched polymer (**poly-Ac1b**) as an additive on the ionic conductivity (σ) and lithium ion transference number (t_{Li}) of the $\text{PEO}/\text{LiN}(\text{CF}_3\text{SO}_2)_2$ ($\text{Li}/\text{O}=0.125$) electrolyte was examined at 80°C and the results

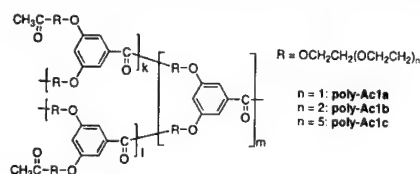
are summarized in Table 1. Addition of 10wt% **poly-Ac1b** enhanced the ionic conductivity and the ion transference number. And also, addition of the hyperbranched polymer was more effective to an improvement of the ionic conductivity in the region of relatively low temperature (Fig. 2).

ACKNOWLEDGEMENTS

We greatly acknowledge the financial support of Genesis Research Institute, Inc..

REFERENCES

- [1] T. Itoh et al., *J. Power Sources*, **81-82**, 874 (1999).
- [2] Z. Wang et al., *J. Electrochem. Soc.*, **146**, 2209 (1999).
- [3] Z. Wen et al., *J. Power Sources*, in press.
- [4] C. J. Hawker et al., *Macromolecules*, **29**, 3831 (1996).



Hyperbranched Polymers

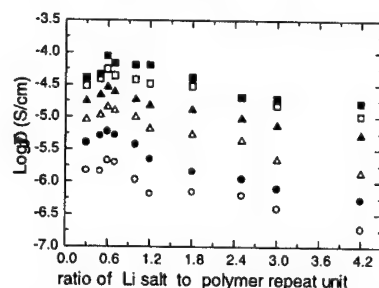


Fig. 1. $\text{LiN}(\text{CF}_3\text{SO}_2)_2$ concentration dependence of the conductivity of the electrolytes based on **poly-Ac1c**.

Table 1. σ and t_{Li} of the blend-based polymer electrolytes at 80°C with $\text{Li}/\text{O} = 1/8$ ratio

Poly-Ac1b /PEO in wt%	0/100	10/90	20/80	50/50
$\sigma \times 10^4 \text{ S/cm}$	7.0	8.1	6.8	2.9
t_{Li}	0.09	0.15	0.20	0.37

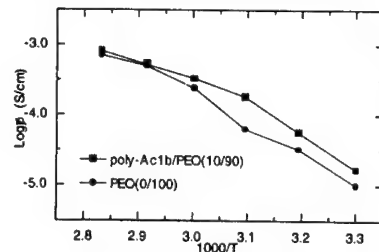


Fig. 2. Temperature dependence of the electrolytes for the **poly-Ac1b**/PEO and for the PEO with $\text{LiN}(\text{CF}_3\text{SO}_2)_2$.

Spectroscopic Estimation of Dielectric Constant and Donor Number in Polymer Electrolytes

Chi Su Kim, Jongwha Lee and Seung M. Oh

School of Chemical Engineering, College of Engineering,
Seoul National UniversitySan 56-1, Shillim-dong, Kwanak-Gu, Seoul 151-742,
Korea

The dielectric constant and donor number, which are the controlling factors for the charge carrier concentration in liquid or polymer electrolytes¹, were estimated utilizing the fluorescence and ultraviolet-visible (UV-VIS) spectroscopy. For the measurement of dielectric constant, pyrene was added into the electrolytes as the fluorescence probe and the resulting emission spectra were analyzed to obtain the Py values.² The donor number of electrolytes was estimated by monitoring the UV-VIS absorption maximum of a Cu complex that was used as the color indicator.³ When these methods were applied to organic solvents, there appeared a good correlation between the Py value and dielectric constant and also between the λ_{\max} and donor number (Fig. 1). The dielectric constant and donor number of gel-type polymer electrolytes were estimated using these methods. For example, when PEO was added into the liquid electrolytes composed of $\text{LiClO}_4(1)\text{EC}(8.3)\text{PC}(3.0)$ to have gel-type electrolytes, an increase of PEO addition led to an increase in the λ_{\max} and a decrease in the Py value, indicative of an increase in the donor number but a decrease in the dielectric constant (Fig. 2). The infrared study revealed that the free ion fraction in the gel electrolytes becomes enriched with PEO addition. It was thus concluded that the donor number is more effective than the dielectric constant in controlling the ion solvating ability of solvents or polymers.

REFERENCES

1. V. Gutmann, *Coordination Chemistry in Non-Aqueous Solutions*, Springer-Verlag, Wien (1968).
2. D.C. Dong and M.A. Winnik, *Photochem. Photobiol.*, **35**, 17 (1982).
3. Y. Fukuda and K. Sone, *Bull. Chem. Soc. Japan*, **45**, 465 (1972).

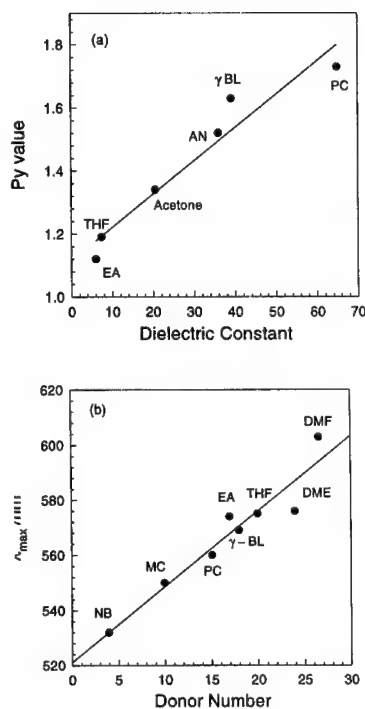


Figure 1. Calibration curve for the estimation of dielectric constant (a) and donor number (b) of organic solvents.

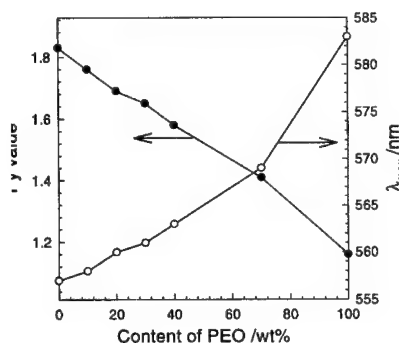


Figure 2. Variation of Py value and λ_{\max} with an addition of PEO into $\text{LiClO}_4(1)\text{EC}(8.3)\text{PC}(3.0)$ solution.

Abstract No. 307

Electrochemical Properties of Gel Electrolytes

A.Reiche, A.Weinkauf, B.Sandner

Martin-Luther-Universität Halle-Wittenberg, Institut für Technische und Makromolekulare Chemie, Geusaer Str. D-06217 Merseburg, Germany
e-mail: reiche@chemie.uni-halle.de

Gel electrolytes are potential candidates for application as electrolyte and separator in Li batteries because they combine a high mechanical stability with a high charge carrier mobility. However, it is expected in the literature that their electrochemical properties are comparable to that of the corresponding liquid electrolytes.

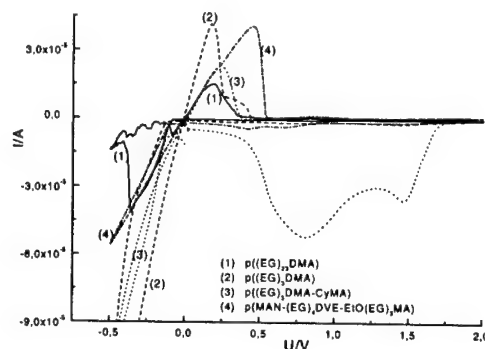
Meanwhile some studies^{1,2} indicate a reduced aggressivity of a liquid electrolyte in a gel towards the anode resulting in a stabilization of the interface between Li and electrolyte and an enhanced Li cyclability. For explication, it can be assumed that the polymer is involved in the formation of the solid electrolyte interface, due to the reactivity of functional groups at the polymer or the reduction of the reactivity of the plasticizer caused by interactions with the polymer, for example.

The present contribution focuses on the electrochemical properties of gel electrolytes on the basis of oligo(ethylene glycol)_ndimethacrylates ((EG)_nDMA)⁴ and on the basis of copolymers of maleic anhydride (MAN) with oligo(ethylene glycol)_n divinylether ((EG)_nDVE)³.

They have been prepared by photopolymerization of the monomers in the presence of a solution of LiCF₃SO₃ in a plasticizer, e.g. a mixture of oligo(ethylene glycol)_ndimethylethers ((EG)_nDME) with n = 4 and 11 ((EG)₁₁DME/((EG)₄DME = 1g/1g). Previous works indicate that the variation of monomer and plasticizer results in dramatic changes in the structure and thermal properties of the gels.⁴ Homogeneous and heterogeneous gel electrolytes were synthesized with significant differences in ionic conductivity and cationic transference number *t*⁺. Both are higher in the case of heterogeneous gel electrolytes, (ca. 5·10⁻⁵·10⁻⁴ S/cm at 25°C, *t*⁺ = 0,5 with ((EG)₁₁DME as a plasticizer) as a result of a higher attainable plasticizer content and a restricted ability of the polymer to interact with the cations^{3,4}.

Figure and Table show the results of cyclic voltammetry of various gel electrolytes, differing significantly in the electrochemical properties, despite of the use of the same liquid electrolyte. The highest Li-plating stripping efficiency is registered for gels on the basis of poly(MAN-(EG)₄DVE-EtO(EG)₃MA). EtO(EG)₃MA was used as a termonomer to decrease the network density. On the contrary, gels based on copolymers of ((EG)₃DMA with the polar monomer cyanomethyl methacrylate (CyMA) are not stable. The CV indicates a very low Li-plating stripping efficiency and the irreversible reduction of the electrolyte in the range between 1,7 and 0 V versus Li/Li⁺. Irreversible peaks in this potential range are also observed in the CV of the poly(MAN-(EG)₄DVE-EtO(EG)₃MA) based gels, however to a lower extent. It is assumed that these reactions lead to a stabilization of the Li electrolyte interface in the latter case as moreover indicated by a relatively constant impedance of the cell during the course of the experiment. Even gels on the basis of ((EG)_nDME with n = 3 and 23 differ concerning the Li plating-stripping efficiency and the anodic stability explicable by a stabilization of the salt in homogeneous gels due to simultaneous interactions of the charge carriers with the polymer and the plasticizer.

It can be expected that the activity of ethers versus Li is relatively low. Hence the Li surface chemistry is dominated by the reduction of the anion and contaminants providing Li surface layers with a low passivating ability⁵. There have been a number of additives for electrolytes for Li-batteries in the literature suitably to provide the formation of a smooth and stable interface between Li and electrolyte. The study indicates that this role can be played by the polymer in gel electrolytes.



Cyclic voltammograms of various gel electrolytes with a mixture of ((EG)₁₁DME and ((EG)₄DME as plasticizer, 0,6 mol/kg LiCF₃SO₃, 1 mV/s, Ni as WE, Li as CE and RE

Table of parameters calculated from the CV above

	% plast.	T [°C]	Eff. [%]	<i>I</i> _{ex} [mA/cm ²]	<i>U</i> _{decomp.} [V]
p((EG) ₁₁ DMA)	50	25	29	4,7	4,1
p((EG) ₄ DMA)	75	25	15	13	3,8
p((EG) ₃ DMA)-co-CyMA)	75	25	10	5,4	3,3
p(MAN-(EG) ₄ DVE-EtO(EG) ₃ MA)	75	40	48	8,3	4,1

¹ T.Osaka, et al., *J. Power Sources*, 81-82 (1999) 734

² M.Kono, et al., *J. Power Sources*, 81-82 (1999) 748

³ A.Reiche, B.Sandner et al., *Electrochimica Acta*, in press

⁴ A.Reiche, B.Sandner et al., *Polymer*, in press

⁵ D.Aurbach, E.Granot, *Electrochimica Acta* 42 (1997) 697

A Novel PEG-borate Based Solid Polymer Electrolytes; Conductivity and Application to Li-ion Battery

S.Yokoyama*, T.Kobayashi, Y.Kato, H.Ikuta, M.Wakihara

Dept. of Chemical Engineering, Tokyo Institute of Technology
2-12-1 Ookayama, Meguro-ku, Tokyo 152-8552, Japan
*Oleochemical Lab., NOF Corporation
3-3 Chidori-cho, Kawasaki, Kanagawa 210-0865, Japan

In recent years, ion conducting polymers has attracted interest because of their application to the solid polymer electrolytes (SPE). In the present study, we propose a new dry polymer electrolyte film (PEG-borate (M.W.1700) + polymerizable PEG(PEG-graft-crosslinked PMMA (PEG-PMMA) + lithium salt (LiClO_4 or $\text{Li}(\text{CF}_3\text{SO}_2)_2$ (LiTFSI)). PEG derivatives and boric acid anhydride were mixed in the reaction flask. The obtained slurry was heated to 100°C for one hour under vacuum condition. After increasing the temperature up to 130°C , the pressure in the flask was reduced gradually down to 20mmHg. A clear and yellowish PEG-borate fluid was obtained after cooling to room temperature. The polymer electrolyte film (500 μm thickness) was prepared from above mentioned PEG-borate, polymerizable PEG (methoxy PEG methacrylates or PEG dimethacrylates supplied by NOF Co.Ltd.) and anhydrous lithium salt. Stoichiometric amount of LiClO_4 or LiTFSI was dissolved in the mixture of the PEG-borate and the polymerizable PEG. Formed viscous solution was poured into small die made of Teflon and kept 110°C over 6h in vacuum to evaporate any liquid present in it.

Composition and structure of our polymer electrolyte is shown in Fig.1. PEG-borate and PEG-PMMA are well mixed in the polymer electrolyte film. Both PEG-borate and PEG-PMMA have a high solubility each other because of their common component PEG chain. Thus, our polymer electrolytes have good mechanical stability without any syneresis.

Temperature dependence of ionic conductivity for PEG-borate/PEG-PMMA is shown in Fig.2. The use of PEG-borate induces about half or one order higher conductivity than no use of it at room temperature. The electrical conductivity of the dry film which contents methoxy-PEG(550)-borate / PEG(600) dimethacrylate / methoxy-PEG(4000) methacrylate = 70/15/15 (wt) so formed was found to be $\sim 10^{-4} \text{S}\cdot\text{cm}^{-1}$ at room temperature.

The Li^+ transference number (t_{Li^+}) was obtained from combined method of four probe polarization and AC impedance measurement. The t_{Li^+} of described above electrolyte film was 0.38 at room temperature.

The lithium cell, $\text{Li} | \text{polymer electrolyte} | \text{LiMn}_2\text{O}_4$ was constructed, and the charge-discharge cycling property was carried out galvanostatically at a current density of $0.015 \text{mA}\cdot\text{cm}^{-2}$ (0.2C) and 50°C . The CV measurement shows the film was stable up to 4.50V at room temperature. The charge and discharge voltage limits were set at 4.45V and 3.5V, respectively. At the first discharge, energy capacity of $80 \text{Ah}\cdot\text{kg}^{-1}$ was obtained and at 40th cycle, it showed $60 \text{Ah}\cdot\text{kg}^{-1}$ accompanying slight retention at room temperature. And at 50°C , energy capacity of $107 \text{Ah}\cdot\text{kg}^{-1}$ and $87 \text{Ah}\cdot\text{kg}^{-1}$ at the first and the 40th cycle discharge respectively.

The EDX spectra were measured on the surface of lithium metal anode, on the surface of spinel cathode and regions of electrolytes near to the electrodes. These

results indicate that the dissolution of manganese from the cathode has completely been suppressed by the use of polymer electrolyte film. However, further emphasis can be made in the direction of film thickness reduction in order to minimize the internal resistance of the cell which will ultimately lead to high power and better cycle life.

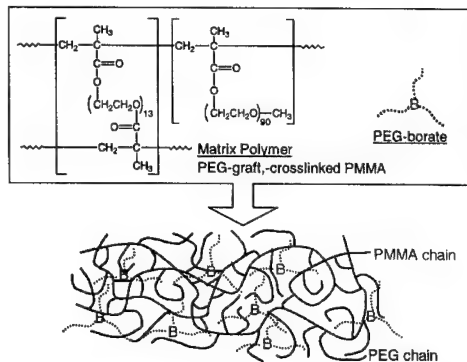


Fig.1 Composition and Structure of PEG-borate/PEG-PMMA Electrolyte.

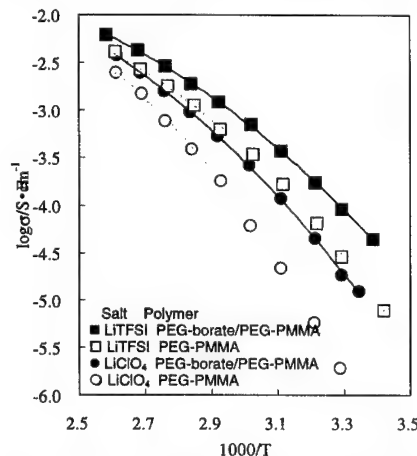
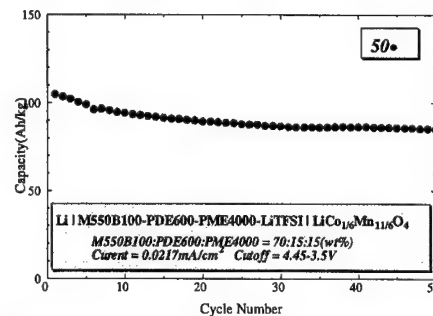


Fig.2 Temperature dependence of ionic conductivity for PEG-borate/PEG-PMMA and PEG-PMMA electrolyte film.

Fig.3 Cycle Performance of Polymer Test Cell at 50°C .

DETERMINATION OF
DIFFUSION CO-EFFICIENT OF
LITHIUM ION IN PLASTICIZED
PVC ELECTROLYTES

A. Manuel Stephan, S. Raman, T. Prem
Kumar, N.G.Renganathan, M.Raghavan
and N.Muniyandi[#].

Central Electrochemical Research
Institute, Karaikudi 630006, India.

Abstract

Polymer electrolyte films were cast from plasticized poly(vinyl chloride) (PVC) complexed with lithium perchlorate. The plasticizer employed was dibutyl phthalate (DBP) or diethyl phthalate (DEP). The films were subjected to impedance measurements at 25, 40, 50 and 60° C. The variation in ionic conductivity has been studied as a function of salt concentration at these temperatures. Using the impedance data, the diffusion co-efficient of lithium was calculated for different lithium salt concentrations. Diffusion co-efficient as calculated from pseudo capacitance due to non-faradaic contribution and those estimated by employing double layer capacitance have been compared.

References:

1. B. Scrosati, Applications of Electroactive Polymers, 1st ed., Chapman and Hall, London (1993).
2. A. Manuel Stephan, R. Thirunakaran, N.G. Renganathan, N.Muniyandi and S.Ramamoorthy, J.Power Sources, 81-81(1999) 752.
3. A. Manuel Stephan, N.G. Renganathan, T. Prem Kumar,

R. Thirunakaran, S.Pitchumani and N.Muniyandi, Solid State Ionics (In press).

4. A. Manuel Stephan, N.G. Renganathan, T. Prem Kumar, R. Thirunakaran, S.Pitchumani and N.Muniyandi, J.Power Sources (In press).

5. A. Manuel Stephan, M.Kamal Kumar, T. Prem Kumar, N.G. Renganathan, S.Pitchumani M.Raghavan and N.Muniyandi, Theor. Compu. Poly. Sci. (Communicated).

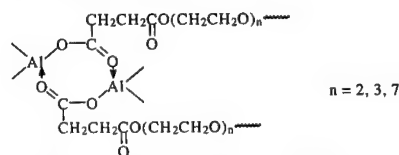
[#] Corresponding author

Effects of Diethylaluminum Carboxylate and EC/PC on Dielectric Relaxation and Ionic Conductivity of PEO Based Polymer Electrolytes

J.R. Dygas, B. Misztal-Faraj, F. Krok
Dept. of Physics, Warsaw University of Technology
Koszykowa 75, 00-662 Warszawa, Poland

Z. Florja* czyk, E. Zyga* o-Monikowska, E. Rogalska
Dept. of Chemistry, Warsaw University of Technology
Noakowskiego 3, 00-664 Warszawa, Poland

A new class of composite polymer electrolytes was obtained (1). The electrolytes consist of complexes of poly(ethylene oxide) with inorganic lithium salt and diethylaluminum carboxylates, which contain in their structure oxyethylene units:



Addition of diethylaluminum carboxylate causes increase of electrical conductivity and mechanical stability and decrease of crystallinity of PEO. The optimal electrical and mechanical properties were obtained for the composites containing 30-40 wt% of diethylaluminum carboxylate with $n=7$ oxyethylene monomeric units.

It seems that diethylaluminum carboxylate affects the local structure of polymer as well as dynamic properties of polymer chains. Coupling between movement of the polymer chains and ionic transport can be investigated by measurement of the ionic conductivity and dielectric relaxation. In this work such a coupling was studied for the system containing PEO and diethylaluminum carboxylate (33 wt%) with different lithium salts: LiClO_4 , LiCF_3SO_3 or $\text{LiN}(\text{CF}_3\text{SO}_2)_2$ (10% molar). For comparison, gel electrolytes based on PEO with plasticiser PC/EC were also investigated.

Complex impedance measurements of polymer electrolytes with stainless steel electrodes were performed using a computer controlled set-up based on Solartron 1260 Impedance Analyzer and Keithley 428 Current Amplifier. Impedance spectra were measured in the frequency range from 0.01 Hz to 10 MHz in heating-cooling cycles at temperatures between -30°C and 100°C . The impedance spectra were analyzed by non-linear least-squares fitting of the equivalent circuit shown in Fig. 1. The dielectric relaxation was clearly seen at low temperature. As an example data for the system containing diethylaluminum carboxylate and LiCF_3SO_3 are presented in Fig. 2.

The conductivity and the relaxation frequency data for the systems containing diethylaluminum carboxylate and different lithium salts are presented in Fig. 3. It was found that relaxation frequency obtained for composite electrolytes containing $\text{LiN}(\text{CF}_3\text{SO}_2)_2$ or LiCF_3SO_3 follow the Vogel-Tamman-Fulcher (VTF) function similarly as conductivity. This indicates that they are related to the same segmental movements of polymeric chain.

REFERENCES

- J.R. Dygas, F. Krok, B. Misztal-Faraj, Z. Florja* czyk, E. Zyga* o-Monikowska, E. Rogalska, Molecular Physics Reports, 27, 16 (2000).

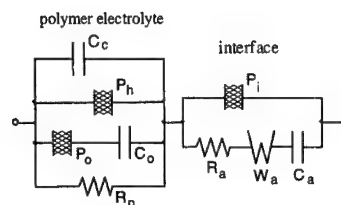


Fig.1. Equivalent circuit for polymer electrolyte with stainless steel electrodes.

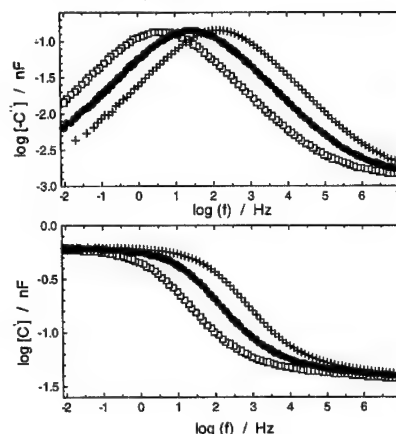


Fig.2. Logarithmic spectral plots of imaginary and real parts of complex capacitance of the polymer electrolyte with LiCF_3SO_3 at -32°C (\square), -25°C (\bullet), -18°C ($+$). Presented curves are the results of simulation for the part P_h , P_0 and C_0 of equivalent circuit with parameters obtained by fitting to the experimental spectrum.

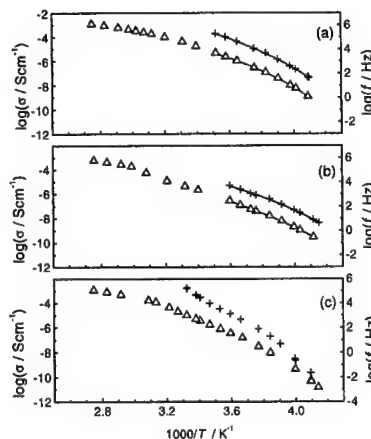


Fig.3. Temperature dependence of conductivity (\bullet) and frequency of dielectric relaxation ($+$) for composite polymer electrolytes with: (a) $\text{LiN}(\text{CF}_3\text{SO}_2)_2$, (b) LiCF_3SO_3 , (c) LiClO_4 . Continuous line – VTF function.

**STUDIES OF CONDUCTIVITY AND
IONIC MOBILITY IN POLYMER
GEL ELECTROLYTES**

H.V.St.A.Hubbard, M.J.Williamson and
I.M.Ward

IRC in Polymer Science and Technology,
University of Leeds, Leeds LS2 9JT, UK
I.M.Ward@leeds.ac.uk

Polymer gel electrolytes, combining high ionic conductivity with good mechanical properties are proving to be very useful materials as electrolytes in rechargeable lithium batteries.

Ionic conductivity and ionic mobility behaviour of polymer gel electrolytes based on polyvinylidene fluoride (PVDF) with N,N,-dimethylformamide (DMF) or tetraglyme with lithium triflate (LiCF_3SO_3) and their liquid electrolyte counterparts have been compared using pulsed field gradient NMR spin-echo technique to determine anion and cation diffusion coefficients. Measured ionic conductivities are compared with those calculated using the Nernst-Einstein equation with the NMR diffusivities for each of the systems over a range of salt concentrations and temperatures.

The results indicate that the polymer gel electrolytes are predominantly two phase systems comprising a liquid electrolyte providing the bulk of the ionic conduction and a polymer rich gel phase providing the mechanical matrix. There is also an important polymer-solvent-salt interaction involving both phases which also affects the ionic conductivity behaviour.

- [1] M.J.Williamson,
H.V.St.A.Hubbard and I.M.Ward,
Polymer 40, 7177-7185 (1999)
- [2] M.J.Williamson, J.P.Southall,
H.V.St.A.Hubbard, G.R.Davies
and I.M.Ward, Polymer 40, 3945-
3955 (1999)
- [3] I.M. Ward, M.J.Williamson,
H.V.St.A. Hubbard, J.P. Southall

and G.R. Davies, J.Power Sources
81-82, 700-704 (1999)

- [4] M.J.Williamson, J.P.Southall and
I.M.Ward, J.Chem.Phys. 109,
7893-7900 (1998)

CONDUCTIVITY AND STRUCTURE OF LI-CONTAINING PEROVSKITE SOLID ELECTROLYTES

Jian-Shiang Chen and Kuan-Zong Fung
Department of Materials Science and Engineering
National Cheng Kung University
Tainan 70101, TAIWAN, Republic of China

ABSTRACT

Since 1980s, lithium/lithium ion batteries have emerged as one of the most important power sources for portable electronics due to their high energy density. In order to reduce weight for portable electronics, the demand for lighter and thinner batteries is increasing. To reduce the battery size to micrometer range, using inorganic solid electrolyte is inevitable. In search for Li ion conducting solid electrolyte, cation-deficient perovskite with the addition of lithium ions has received considerable attention due to its high ionic conductivity. However, the stability, crystal structure and conductivity in Li-containing Pervoskite systems have not been thoroughly studied. Thus, the objective of this work was to study the effect of lithium ion addition on the crystal structure and conductivity of Li-containing perovskite.

In this work, two Li-containing perovskites $\text{La}_{2/3-x}\text{Li}_x\text{TaO}_3$ and $\text{La}_{1/3-x}\text{Li}_x\text{TaO}_3$ were prepared using La_2O_3 , Li_2CO_3 , TiO_2 and Ta_2O_5 as the starting materials. The concentration of lithium ions was varied from 0% to 50% of A-sites accordingly. The samples were sintered at 1300°C for 8h. Subsequently, the sintered samples were examined by XRD, SEM, and ICP.

The results show that both $\text{La}_{2/3}\text{TiO}_3$ and $\text{La}_{1/3}\text{TaO}_3$ tend to form a perovskite, ABO_3 structure with La ions located at A sites, respectively. However, La ion is trivalent and Ti ion is tetravalent. For lanthanum titanate to form a perovskite structure, the corresponding composition can be written as $\text{La}_{2/3}\text{TiO}_3$. In comparison with ABO_3 , there should be 33% of cation vacancies (in A sites) present in $\text{La}_{2/3}\text{TiO}_3$. On the other hand, La ion is trivalent and Ta ion is pentavalent. For lanthanum tantanate to form a perovskite structure, the formula can be written as $\text{La}_{1/3}\text{TaO}_3$. In comparison with ABO_3 , there should be 66% of cation vacancies (in A sites) present in $\text{La}_{1/3}\text{TaO}_3$. Such a high concentration of defects makes these structure unstable. Therefore, $\text{La}_{2/3}\text{TiO}_3$ cannot form a perovskite when sintered in air as shown in Fig. #1. Similar behavior was also found in $\text{La}_{1/3}\text{TaO}_3$.

The addition of Li ions into the A-site deficient perovskite can be rationalized using the following defect reaction:
 $\text{Li}_2\text{O} + \text{V}_\text{A}'' \rightarrow 2\text{Li}_\text{A}' + \text{O}_\text{O}^\times$
In this equation, V_A'' represents the available A-site cation vacancy. This reaction indicates that the addition of one Li_2O is able to eliminate one cation vacancy. Therefore, with the addition of lithium ions, the structure of perovskite is expected to be more stable. When 10% of Li was added, distorted perovskite structure was observed. As the concentration of Li increased to 0.5, the perovskite gradually shifted to cubic structure as shown in Fig. #2.

As described previously, the addition of Li ions tends to lower the concentration of cation vacancies. For ionic conductors, the conductivity, σ , can be expressed as the product of ion mobility, μ , carrier concentration, n , and ion charge, Ze , i.e. $\sigma = Zen\mu$.

However, the ion mobility is proportional to the concentration of defects (vacancies). In this work, the

lithium ion conductivity of perovskite should be proportional to the product of carrier concentration, i.e. $[\text{Li}]$ and the concentration of cation defects $[\text{V}_\text{A}']$. When $[\text{Li}]=0.5$, most of vacancies were filled with lithium ions so that $[\text{V}_\text{A}']$ became very small. The conductivity of $\text{La}_{0.5}\text{Li}_{0.5}\text{TiO}_3$ or $\text{La}_{0.5}\text{Li}_{0.5}\text{TaO}_3$ is expected to be small. When $[\text{Li}]=0.1$, on the other hand, the carrier concentration is so low that the conductivity of $\text{La}_{0.63}\text{Li}_{0.1}\text{TiO}_3$ or $\text{La}_{0.63}\text{Li}_{0.1}\text{TaO}_3$ would be low as well. In Figure #3, it was found that the maximum conductivity ($>10^{-5}$ S/cm) appeared at $[\text{Li}]=0.3$ in $\text{La}_{2/3-x}\text{Li}_x\text{TiO}_3$. Both $\text{La}_{0.5}\text{Li}_{0.5}\text{TiO}_3$ and $\text{La}_{0.63}\text{Li}_{0.1}\text{TiO}_3$ exhibited low conductivity ($\sim 10^{-7}$ S/cm). These results are in good agreement as what was described above. Based on the results obtained, the crystal structure and conductivity of cation-deficient perovskite were strongly affected by the addition of Li ions mainly due to elimination of cation defects.

Acknowledgment: This work is supported by NHRI, Taiwan under the contract # NHRI-GT-EX89E924L.

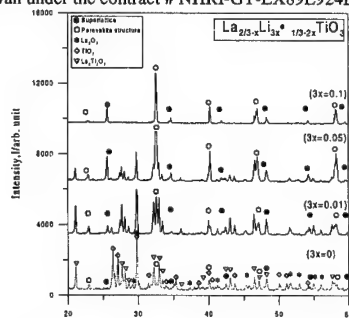


Figure #1. XRD trace of $\text{La}_{2/3-x}\text{Li}_x\text{TiO}_3$, ($3x=0, 0.01, 0.05$, and 0.1).

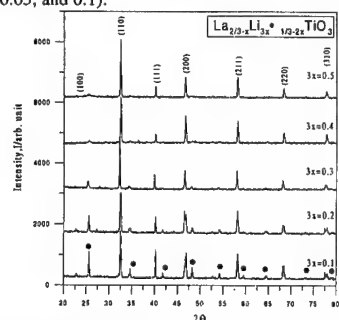


Figure #2. XRD trace of $\text{La}_{2/3-x}\text{Li}_x\text{TiO}_3$, ($3x=0.1, 0.2, 0.3, 0.4$, and 0.5).

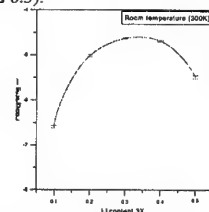
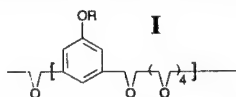


Figure #3. Electrical conductivity of $\text{La}_{2/3-x}\text{Li}_x\text{TiO}_3$, ($3x=0.1, 0.2, 0.3, 0.4$, and 0.5).

Self-Tracking, Solvent-free Low-Dimensional Polymer Electrolyte Blends with Lithium Salts

Y. Zheng, F. Chia, G. Ungar and P. V. Wright
Department of Engineering Materials, University of Sheffield, Sheffield S1 3JD, UK

Solvent-free polymer electrolyte blends comprising LiClO_4 complexes of poly[2,5,8,11,14-pentaoxapentadecamethylene(5-alkoxy-1,3-phenylene)]



(I) of molar mass 10^5 and random copolymers of poly(oxybutylene) (II) (3×10^4) have been prepared.
 $[-(\text{CH}_2)_4 - \text{O}]_x - \text{A} -$ $x \sim 30$ (II)

The n -alkyl side chains R in I are either $-\text{C}_{16}\text{H}_{33}$ or a random equimolar copolymer mixture with $-\text{C}_{12}\text{H}_{25}$. In (II) the units A are $-\text{CH}_2-$ or $-\text{CH}_2\text{C}(\text{=CH}_2)\text{CH}_2-$.

In cells with Li electrodes ($\text{Li} | \text{I} / \text{II} - \text{LiClO}_4 | \text{Li}$) DC polarised with 10 mV at $20^\circ - 30^\circ\text{C}$ (Fig.1) the current increases stepwise over ca. 24 hrs corresponding to Li^+ conductivity increases from ca $10^{-6} \text{ S cm}^{-1}$ to 3×10^{-4} and $4 \times 10^{-3} \text{ S cm}^{-1}$ at 20°C and 30°C respectively.

These changes are reflected in AC impedance measurements with indium-tin oxide glass electrodes showing transitions from ca $10^{-6} \text{ S cm}^{-1}$ to $6 \times 10^{-4} \text{ S cm}^{-1}$ at ambient after cooling from ca 100°C (Fig. 2).

Structural analysis indicates that in I side groups R condense together in crystal or liquid crystal phases to create an ionophobic layer causing the polyether segments to generate a helical substructure [1]. Alkali metal cations occupy the helical tubes whilst the anions occupy spaces between the helices with lamellar long spacing 40 - 45 Å. Strands of polymer II traverse the lamellae of I. (Fig.3). Shearing of II should promote rotation and development of the conducting planes of I in the direction *normal* to the electrode substrate.

'Tracking' occurs within the side-chain melting endotherm $20^\circ - 35^\circ\text{C}$ and perhaps involves both crystal melting-reorientation and ion tunnelling through II to maintain impedance matching with the channels of I.

1. P.V. Wright, Y. Zheng, D. Bhatt, T. Richardson and G. Ungar, *Polymer International*, 1998, **47**, 34.

Fig.1 DC polarisation with lithium electrodes. R= $-\text{C}_{16}\text{H}_{33}$, LiClO_4 , (a) 30°C , (b) 20°C .

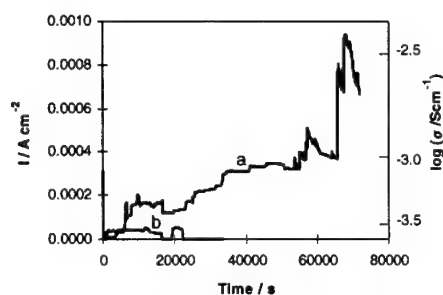
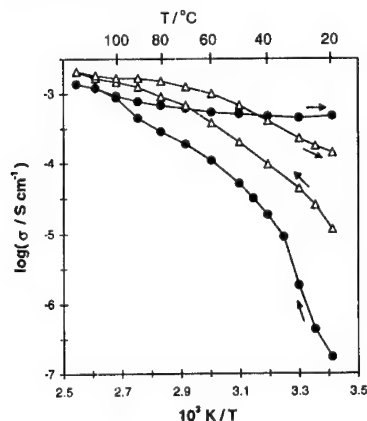


Fig.2 Conductivity by AC impedance (ITO electrodes) R= $-\text{C}_{16}\text{H}_{33}$, A= $-\text{CH}_2-$, LiClO_4 (—●) and R= $-\text{C}_{16}\text{H}_{33}/\text{C}_{12}\text{H}_{25}$, A= $-\text{CH}_2-$, LiClO_4 (—Δ). Arrows indicate the direction of heating.

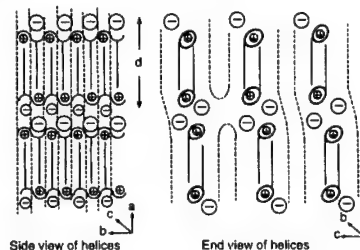


Fig.3 Schematic diagram of polymer electrolyte blend

**THE ROLE OF THE INORGANIC OXIDE
IN NANOCOMPOSITE POLYMER AND
GEL ELECTROLYTE STRUCTURE
AND ION TRANSPORT MECHANISM:
AN NMR STUDY**

S.G. Greenbaum*, S.H. Chung*,
Y. Wang*, X. Guo*,
L. Persi[#], F. Croce[#], and B. Scrosati[#]

*Physics Department
Hunter College of the City University of New
York
695 Park Avenue, New York, NY 10021 USA

[#]Dipartimento di Chimica
Universita di Roma, La Sapienza
P.le A. Moro, 5, 00185 Roma, ITALY

The addition of nanoscale inorganic powders (e.g. Al_2O_3 , SiO_2) to polymer and gel electrolytes for Li battery development has been shown to improve mechanical and electrochemical properties. In the case of gel electrolytes, the inorganic oxide component plays a vital role in providing a mechanical framework that allows maximum uptake and stabilization of the liquid electrolyte component. In the case of solvent-free, PEO-based polymer electrolytes, the finely divided inorganic component tends to inhibit the formation of crystalline phases, thus leading to a more highly conductive material. There is also recent evidence that interactions between the metal oxide surface and the polymer and/or salt may affect the ion transport mechanism.[1] This presentation summarizes recent activity on PEO: LiClO_4 composites containing nanoscale Al_2O_3 or TiO_2 . Lithium-7 was utilized to investigate the local environment about the mobile ions with particular emphasis on the effect of the added metal oxide component. The extent of surface interactions between metal oxide and polymer was studied by ^{27}Al NMR. Finally lithium self diffusion coefficients in the nanocomposite materials were determined by pulsed field gradient NMR and correlated with electrical conductivity data.

[1] F. Croce, G.B. Appetecchi, L. Persi, and B. Scrosati, *Nature*, **394** 456 (1998).

**Plasticising effect in Phase-separated
Polymer Electrolytes based on
Poly(ethylene oxide) and
Poly(perfluoroethers)**

M. Furlani, L. R. A. K. Bandara*,
and B.-E. Mellander,

Physics and Engineering Physics, Göteborg
University and Chalmers University of
Technology, SE-412 96 Göteborg, Sweden

*Department of Physics, University of
Peradeniya, Sri Lanka

Abstract

Polymer electrolytes for secondary lithium batteries are thoroughly studied in order to achieve better performance in terms of high ionic conductivity at room temperature and stability against lithium electrodes. Generally based on poly(ethylene oxide) (PEO) these electrolytes can be embedded in a gel or mixed with different additives, to avoid the polymer crystallisation and consequent decrease in conductivity. The addition of finely dispersed non-miscible particles in a polymer electrolyte generally enhances the ion conductivity. There are thus far no other examples of mixing these electrolytes with non-miscible liquids except the system presented here. The system poly(ethylene oxide) / lithium salts, with the addition of poly(perfluoroether) is a bi-phase stable emulsion. The micro-droplets present in the emulsion prevent or retard the crystallisation of the electrolyte when it is cooled from the melting temperature to ambient temperature. The ion conductivity below the melting point temperature maintains stable values as long as the re-crystallisation is prevented.

In this work we compared the properties of electrolytes containing lithium triflate (LiCF_3SO_3) and lithium bis-(trifluoromethanesulfonyl) imide ($\text{LiN}(\text{CF}_3\text{SO}_2)_2$) with a concentration range $8 < \text{O}:\text{Li} < 250$ (where O is the number of ether oxygen atoms) with more data around the eutectic point. Differential scanning calorimetry (DSC) and ionic conductivity measurements were performed on samples with different thermal history and the results show that the kinetics of re-crystallisation are strongly different. The use of a large anion like the imide besides drastically lowering the melting temperature of the complexes, serves to maintain a high mobility in the polymer segmental motion.

Notwithstanding the slowness of the process of re-crystallization, quenching samples that have previously been stored at room temperature for a long time to the initial temperature of the DSC experiment, we could obtain reproducible and accurate data and correlate them to the conductivity. Finally the changes in the phase diagram of these electrolytic systems due to the presence of the plasticiser suggest that the positive surface interaction of the electrolyte and the additive are modifying the material towards a less ordered system. In conclusion we suggest that the large area of contact between the additive and the electrolyte makes the superficial conductivity and superficial characteristics of the electrolyte prevail on the bulk ones.

References

- M. Furlani, L. R. A. K. Bandara and B.-E. Mellander, *Ionic Conductivity and Plasticizing Effect in the System Poly(ethylene oxide)/ LiCF_3SO_3 - Poly(perfluoro ethylene methylene oxide)*, *Electrochimica Acta*, 43 (10-11), 1517-23, (1998).
- “9th International Meeting on Lithium Batteries” in Edinburgh, Scotland, 12 -17 July 1998, poster: M. Furlani, G. B. Appetecchi, F. Ronci, B.-E. Mellander and B. Scrosati “Stability and ion conductivity of polyethylene oxide- LiCF_3SO_3 electrolytes plasticised with perfluoroethers in the presence of lithium electrodes”(poster).

**CHARACTERISTICS OF PVDF/PAN
BASED POLYMER ELECTROLYTE
FOR LITHIUM ION POLYMER
BATTERY**

Jae-An Lee, Jong-Uk Kim, Gye-Choon Park*,
Hal-Bon Gu

Department of Electrical Engineering, Chonnam
National University

300 Yongbon-dong, Kwangju, 500-757, Korea

*Department of Electrical Engineering,
Mokpo National University
61 Dorimri, Muan-kun, Chonnam 453-279,
Korea

Lithium ion polymer battery has excellent theoretical energy density and energy conversion efficiency. Lithium ion polymer battery (LIPB), included solid polymer electrolyte (SPE), can be viewed as a system suitable for wide applications from thin film batteries for microelectronics to electric vehicle batteries. Polymer electrolytes were discovered by B. E. Fenton et al. in 1973. P. V. Wright et al. [1,2] then showed that complexes formed with PEO and alkali metal salts exhibit high ionic conductivity. Subsequently these complexes were proposed by M.B. Armand et al. [3] as polymer electrolyte for solid state battery and electrochemical device applications. Generally, the SPE was only a low rate of self-discharge, good adhesion between the electrodes, and could be formed as a large-scale thin film. Especially, it is expected that application of the polymer problems concerned with safety. The importance of designing suitable polymer electrolyte for lithium polymer battery has been well demonstrated in the recent years.

The purpose of this study is to research and develop SPE for LIPB. This paper describes temperature dependence of conductivity, impedance spectroscopy, electrochemical properties of PVDF/PAN electrolytes as a function of a mixed ratio. PVDF/PAN based polymer electrolyte films were prepared by thermal gelification method of preweighted PVDF/PAN, plasticizer and Li salt. Steady state current method and ac impedance used for the determination of transference number in PVDF/PAN electrolyte film. The conductivity of PVDF/PAN electrolytes was 10^{-3} S/cm. 20PVDF5PANLiClO₄PC₁₀EC₁₀ electrolyte shows the better conductivity of the others. 20PVDF5PANLiClO₄PC₁₀EC₁₀ electrolyte remains stable up to 5V vs. Li/Li⁺. Steady state current method and ac impedance used for the determination of transference numbers in PVDF/PAN electrolyte film. The transference number of 20PVDF5PANLiClO₄PC₁₀EC₁₀ is 0.48.

References

- [1] B. E. Fenton, J. M. Parker and P. V. Wright, *Polymer*, Vol. 14, p. 589, 1973.
- [2] P. V. Wright, *Brit. Polymer J.*, Vol. 7, p. 319, 1975.
- [3] M. B. Armand et al., 2nd Int. Meeting on Solid Electrolytes, St. Andrew, Scotland, p.20, 1978.

Abstract No. 317

Structure, porosity and conductivity of PVdF films for polymer electrolytes

A. Magistris, P. Mustarelli, E. Quartarone
Department of Physical Chemistry and CSTE
CNR, Via Taramelli 16, 27100 Pavia, Italy

P. Piaggio, A. Bottino
Department of Chemistry, Via Dodecaneso,
16132 Genova, Italy

Poly(vinylidene fluoride) (PVdF) - hexafluoropropylene (HFP) copolymers have been widely studied for applications in rechargeable lithium batteries (1). Polymer electrolytes with room temperature conductivity of the order of 1 mS/cm have been obtained both by the standard casting procedure (2, 3), and by the absorption/extraction method (4). PVdF membranes with controlled porosity, in contrast, may be obtained by phase inversion methods (5). These last membranes seem to be good candidates as separators in polymer lithium batteries (6).

In order to obtain the best compromise among conductivity and thermal stability it is mandatory to characterize the pore structure and the interactions between the host polymer and the electrolyte solution, which are translated at a macroscopic level by thermodynamic observables like surface tension and solution viscosity.

In this paper we perform a structural, thermodynamic and electric characterization of PVdF porous membranes activated by a EC/DEC/LiPF₆ 1 M electrolyte solution. Starting from simple bulk measurements like apparent density and uptake rate, we are able to separate the contributions of pores and polymer swelling. These data are correlated with the pore structure and with the conductivity measurements.

We show that a proper tailoring of the porous structure of PVdF allows to easily obtain conductivity higher than 1 mS/cm at room temperature. The electrolyte solution goes chiefly to occupy the porous structure. However, a not negligible part gives origin to a swollen phase.

References

1. Z. Jiang, B. Carroll, K.M. Abraham, *Electrochim. Acta* 42 (1997) 2667.
2. J.-M. Tarascon, A.S. Gozdz, C. Schmutz, F. Shokkahi, P.C. Warren, *Solid State Ionics* 86-88 (1996) 49.
3. E. Quartarone, M. Brusa, P. Mustarelli, C. Tomasi, A. Magistris, *Electrochim. Acta*, 44 (1998) 677.
4. V. Arcella, A. Sanguineti, E. Quartarone, P. Mustarelli, *J. Power Sources*, 81-82 (1999) 790.
5. A. Bottino, G. Camera-Roda, G. Capannelli, S. Munari, *J. Membr. Sci.*, 57 (1991) 1.
6. T. Michot, A. Nishimoto, M. Watanabe, *Electrochim. Acta*, 45 (2000) 1347.

Spectroscopic conductivity studies on the ionic motion in the electrolytic complexes (polyethylene glycol 400)/(LiCl)_x

V. Di Noto¹, M. Fauri², S. Biscazzo², M. Vittadello¹

¹Dipartimento di Chimica Inorganica, Metallorganica ed Analitica, Università di Padova, Via Loredan 4, I-35131 Padova (Italy). Phone: +39 049 8275229. E-mail: dinoto@ux1.unipd.it.

²Dipartimento di Ingegneria Elettrica, Università di Padova

In the past decade various electrolyte polymers have been prepared and studied in many laboratories^{1,2}. Numerous studies have been carried out to understand the complicated nature of ionic conductivity and the complexation processes of cations and anions in the polymer host¹. Commonly these studies were carried out on systems obtained by doping an etheric oligomer or polymer with an inorganic salt. Several investigators suggested that segmental motions of polymer host appear to be largely responsible for the ionic transport mechanism in the polymer electrolytic complexes. Furthermore, it was also proposed that ionic conductivity occurs through a charge hopping mechanism between adjacent sites having equivalent coordination symmetries³.

This hopping process happens in two ways: the first type of hopping events involves hopping between sites of the same polymer chain, i.e. interchain hopping (*intra-CH*), and the second type occurs between different chains, i.e. interchain hopping (*inter-CH*).

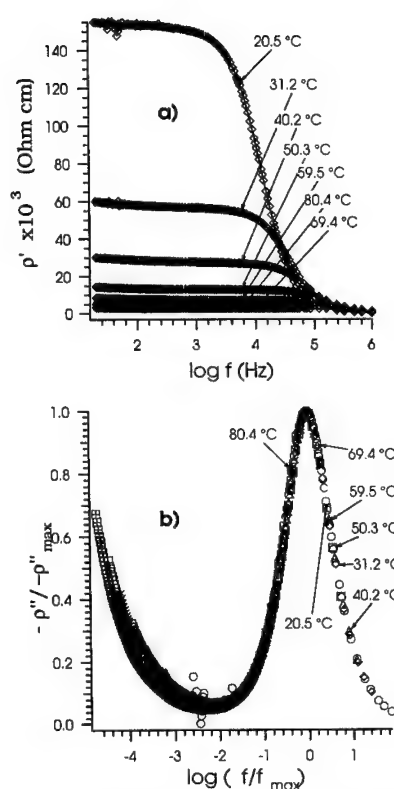
Recently, by reacting directly a new anhydrous LiCl salt with poly(ethylene glycol) with a molecular weight of 400 (PEG 400), we were able to prepare and to characterize structurally by FT-IR very pure solvent free polymer electrolytes.

Results revealed that in these systems³:

- the PEG chains assume a TGT type conformation;
- Li⁺ are coordinated by etheral oxygens of the PEG ligand;
- At a Li/O molar ratio less than 0.036, Cl⁻ ions form hydrogen bonding cages with the terminal OH groups of PEG chains;
- At a Li/O molar ratio greater than 0.036, Cl⁻ ions are present both in hydrogen bonds and as "free anions" along PEG chains.

The aim of this paper was to study the mechanism of the ionic motion in the electrolytic complexes PEG400/(LiCl)_x (0 ≤ x ≤ 1.40665).

This investigation was carried out obtaining accurate measurements of the complex impedance of the samples as a function of frequency and temperature (fig. 1). Detailed analysis of real and imaginary components of the complex conductivity, $\sigma^*(\omega) = \sigma'(\omega) + j\sigma''(\omega)$, indicated that a full characterization of the AC electrical response of the PEG400/(LiCl)_x complexes requires both equivalent circuit analysis and correlated ionic motion analysis⁴, which is based on the jump relaxation model. Both these investigations showed that the conductivity mechanism in PEG400/(LiCl)_x involves two distinct phenomena that are well described by the jump relaxation model. The first phenomenon is associated with ion hopping between the sites present in the material along the polyetheral chain (*intra-CH* hopping) and between different chains (*inter-CH* hopping) and the second is associated with the



imaginary components ($p''/p'max$) versus the logarithms of the ratio f/f_{max} . f_{max} is the frequency of the peak maximum.

structural relaxation of the host coordination site, which occurs after the ion hopping event. This last phenomenon is correlated with the segmental motion of polyetheral chains and contributes to the "successful" conductivity of each ion that hops between empty sites.

Finally, it is to be highlighted that PEG 400/(LiCl)_x polymer electrolytes present conductivities on the order of $1 \cdot 10^{-4} \text{ S cm}^{-1}$ at 25 °C, thus allowing us to classify these materials as good liquid polymer electrolytes.

References

- Gray, F.M. *Polymer Electrolytes*, RSC Materials Monographs; Royal Society of Chemistry: Cambridge, UK, 1997.
- Scrosati, B.; Neat, N.J. In *Applications of Electroactive Polymers*; Scrosati, B., Ed.; Chapman and Hall: London, 1993.
- Di Noto, V.; Longo, D.; Munchow, V. *J Chem. Phys. B* **1999**, *103*, 2636.
- Funke, K. *Zeit. Phys. Chem.* **1995**, *188*, 243.

Fig. 1. a) Real (p') component of complex resistivity versus natural logarithms of frequency, $f(\text{Hz})$, for PEG400/(LiCl)_{1.40665}. b) dependence of normalized

Fabrication of All Solid Polymer Electrolytes based on Block-Graft Copolymers

Kazuhiro Hirahara*, Masaya Ueno,

Osamu Watanabe, and Toru Nakanishi

Speciality Chemical Research Center,

Shin-Etsu Chemical Co., Ltd.

Nishifukushima 28-1, Kubiki, Nakakubiki,

Niigata 942-21 Japan

*E-mail: s02358@sec.shinetsu.co.jp

The batteries for EV or HEV have been researched for the long time and from the safety point of view all solid polymer electrolyte Li batteries seems to be one of the candidates. Though the main component of dry solid polymer must be ethylene oxide (EO), T_g of EO compound will be -60°C , much lower than the operation temperature of the battery ($60\sim 80^\circ\text{C}$), so mechanical strength of the EO film was greatly reduced. Thus it has been needed that the improvement of the mechanical strength is put into practice without reduction of ionic conductivity. The authors have tried to resolve above problem with the introduction of mechanically stable styrene component to form triblock-graft copolymer¹⁻³. The block-graft copolymers (Fig. 1) are synthesized through anionic procedures, thus EO and styrene components show the microphase-separated structure spontaneously and the mechanical stability and high ionic conductivity were realized simultaneously in the gelled block-graft copolymer system⁴. In this paper we report the application of the block-graft copolymer to the all solid polymer electrolyte systems.

All solid polymer electrolytes are derived from the block-graft polymer and lithium bistrifluoromethane sulfonyl imide in a proper manner³. The ionic

conductivities and dynamic moduli data are shown in Fig.2 and Fig.3, respectively. It is obvious that the block-graft copolymer obtains the dimensional stability under 100°C by the introduction of styrene component. Furthermore EO elastic component compensates the breakability of styrene component above 100°C . The ionic conductivity will be improved by addition of EO oligomers. The matter of safety will be ensured by EB radiation crosslinking of the oligomers.

The block-graft copolymer is thought to be suitable for the all solid polymer electrolyte materials.

References 1. K. Se, *et al.*, *Macromol. Chem., Macromol. Symp.* **25**, 249 (1989). 2. K. Se, *et al.*, *J. Poly. Sci., Poly. Chem.*, **36**, 302 (1998). 3. K. Hirahara, *et al.*, *Reactive & Functional Poly.*, **37**, 169 (1998). 4. K. Hirahara, *et al.*, *IMLB9 Abstracts* (1998).

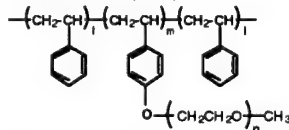


Fig. 1 The chemical structure of the block-graft polymer (ex. l 500, m 250, n 20)

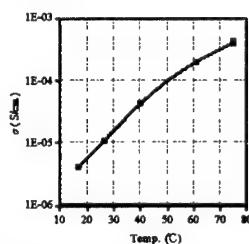


Fig.2 Ionic conductivity in the block-graft copolymer doped with LiTFSI(EO:Li=20:1)

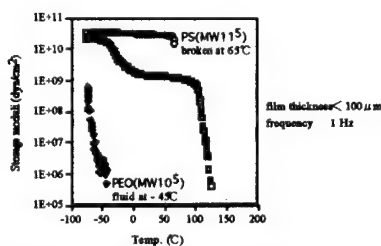


Fig.3 Storage moduli for the block-graft copolymer doped with LiTFSI(EO:Li=20:1)

Power Management, the Path to the Future

James J. Barbarello, Maureen Molz,
and Robert Hamlen

US Army CECOM, Ft Monmouth, NJ 07703

Commercial users and the Military will expect and demand extended operation time, reduced system weight and increased functionality from their portable computing systems. These will only be achieved through management of power usage. The United States Army is investing in a revolutionary approach for low-power system design that will have implications for the portable power industry.

As the United States Army moves to digitize the battlefield, power, especially man-portable power, has become a critical driver in the design of new systems. While advances in battery chemistries continue to provide extended life, they cannot be expected to keep pace with the demands of modern electronics and the increasing capabilities required by users.

For the last several years, the driver for improved portable power sources has been digital electronics, with the microprocessor at its core. So, much of the focus on power management has been seen initially in the microprocessor-based (computer) industry segment. In the past, the computer industry has only focused on increased performance in the areas of chip speed and size, while much of the power management effort has been the domain of the software used in the chips. The Army's desire is to expand the design criteria to include power as a major design driver for both the software and the hardware upon which it resides. This new focus is on direct and cumulative solutions to all levels of the system hierarchy.

While industry has and will continue to focus on the microprocessor as a system and the increased functionality of System on a Chip (SOC), the Army plans to focus on the "high level system" (which includes all elements along the system hierarchy model). The Army's current investment strategy addresses collective power optimization throughout this architecture to provide a complete and thorough power reduction approach for the future digitized battlefield.

In order to bring the power consumption of these future systems within reach of the battery source, power management (including low power technologies) has become a necessity. Two ways to achieve low power electronic systems are in the "static" design process and in the "dynamic" operation of these systems. The dynamic techniques used by designers at the system level allow a system or a device within a system to be placed

in which computer and device manufacturers can implement such power management techniques and maintain compatibility. ACPI is only an interface specification and will not specify how power consumption will be managed. Power management policies and procedures must be developed and tailored to specific system requirements. The United States Army's goal is to apply such dynamic power management to the future Land Warrior Systems, as well as other Army systems.

Additionally, the Army has invested in technology development that will enable electronic system designers to optimize the design for power efficiency at various levels of the systems design process. This holistic approach, referred to as the "static design process", looks at power reduction along all points of the digital design critical pathway in a cumulative manner. It necessitates a design tool that will automate the complete architectural design of a low-power application-specific system or System-On-a-Chip (SOC). Such a tool allows the designers to explore multiple system architectural options and choose the optimal design with the most appropriate tradeoffs (ex: power and cost). Until now, hardly any designer had the option to select the "best" (cost, performance and power) design because designing multiple system architectures for a given system requirement is a costly and time-consuming. This new automated approach will revolutionize the time required by designers to implement designs with power as an important tradeoff parameter. The Army is focused on reducing power by attacking the problem from both the hardware (mainly design) and software (which provides the robustness to manage that power).

It is highly likely that in the next five years, such design tools for high-level system design will mature, and general-purpose solutions will no longer be force-fit into an ever-expanding set of unique market segments. Researchers, designers, and manufacturers of portable power sources will most likely segment into two areas. The first area will be populated with those who continue to view the power source separate from the power-consuming device. The second area will include those who understand the synergy between power generation and consumption. They will join with their consumption-device design partners and be an innovating force. They will use their strategic knowledge gained from partnerships with the military and other unique-requirements market segments, and transition that knowledge into improved, general-purpose power sources. The key to being in the second area will not be technological expertise, but a willingness to embrace the change and participate.

High Energy Density, Thin Film, Rechargeable Lithium Batteries for Marine Field Operations

Donald R. Sadoway*, Anne M. Mayes*, Biying Huang*,
Simon Mui*, Philip P. Soo*, David H. Staelin[†],
Christopher C. Cook[†]

*Department of Materials Science and Engineering
[†]Lincoln Laboratory
Massachusetts Institute of Technology
Cambridge, Massachusetts
U.S.A. 02139-4307

Portable electrical power is an essential element for marines in field operations, being required for the operation of sensory enhancement equipment, automatic weapons, communications systems, etc. The lithium polymer battery (LPB) is an attractive option for the distributed power storage needs of soldiers, with projected practical energy densities of >300 Wh/kg, low safety risks and great flexibility in battery configuration. For underwater missions, the LPB has the added advantages of pressure tolerance and near neutral buoyancy. However, a number of materials and processing challenges must still be overcome to achieve these performance advantages.

All solid state, thin-film batteries have been designed, constructed, and cycle tested. The cathode consisted of a dense film of vanadium oxide, ~0.2 μm thick, deposited on aluminum foil. The cathode was prepared by laser assisted vapor deposition of vanadium metal in an oxygen atmosphere of controlled chemical potential. The cathode was additive-free – no carbon, no

binder. The electrolyte was a block copolymer of poly[oligo(oxyethylene) methacrylate] - *b* - poly(laurel methacrylate) containing LiCF_3SO_3 [1]. Preparation of the polymer is described in an accompanying presentation at this meeting [2]. The anode was metallic lithium.

Test cells were cycled at room temperature over the voltage range from 1.5 to 4.0 V. Cathode capacities of ~400 mAh/g were measured at a discharge rate of C/2 ($C = 400 \text{ mA/g}$). The cathode proved to be resistant to capacity fade as evidenced by a loss of 1% over 100 cycles. It was possible to draw substantial currents: routine testing was conducted at C/2; however, discharge rates as high as 1.6 C were achieved. Based upon these results, cells designed with these materials in optimal dimensions are projected to have energy densities exceeding ~400 Wh/kg and power densities exceeding 800 W/kg at C/2. Figure 1 shows cycle testing of the Li/BCE/ VO_x thin-film battery at room temperature with a C/2, C, and 1.6 C rate.

This work was sponsored by the Office of Naval Research, the MIT Center of Materials Science and Engineering with funds from the National Science Foundation, Intronic, and MIT Lincoln Laboratory Director's funds.

1. P.P. Soo, B. Huang, Y.-I. Jang, Y.-M. Chiang, D.R. Sadoway, and A.M. Mayes, *J. Electrochem. Soc.*, **146** (1), 32-37 (1999).
2. D.R. Sadoway, A.M. Mayes, B. Huang, P.E. Trapa, P.P. Soo, P. Bannerjee, "Self-doped Block Copolymer Electrolytes (SDBCEs) for Solid-State, Rechargeable Lithium Batteries," IMLB 10, Como, Italy.

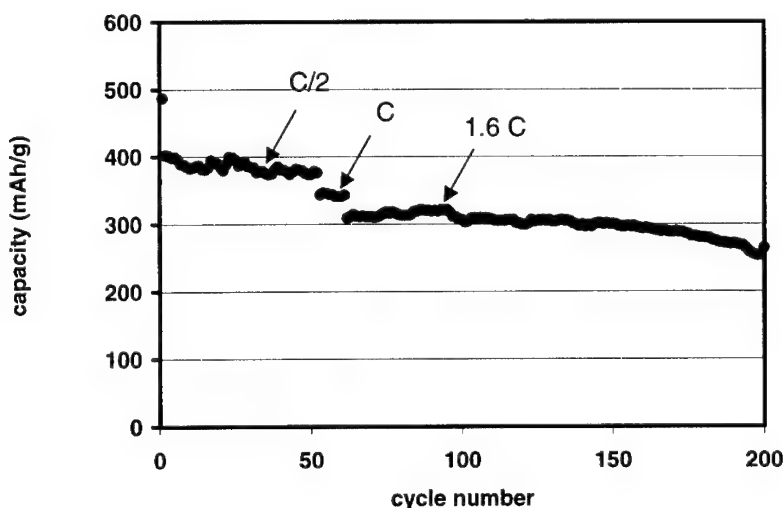


Figure 1. Cycle testing of the thin-film Li/BCE/ VO_x battery at room temperature at various C rates.

Cycling Performance of 10Wh class Lithium Metal Rechargeable Battery with New-type Lithium Imide Electrolyte

Hirohiko Saito and Kyohei Usami
Research & Development Department
DENSO CORPORATION

1-1 Showa-cho, Kariya, Aichi 448-8661, Japan

INTRODUCTION

A rechargeable lithium battery with a lithium metal anode has great advantages in high energy density. However, the insufficient coulombic efficiency of the lithium anode results in poor cycle characteristics. This is attributed to degradation of lithium metal caused by reactions between the lithium anode and the electrolyte as well as the formation of dendritic lithium. In this study, investigations were made on a new type electrolyte involving $\text{LiN}(\text{C}_2\text{F}_5\text{SO}_2)_2$ (LiBETI) and cyclic ether compounds as a salt and solvents, respectively [1]. And 10Wh-class $\text{Li/LiMn}_2\text{O}_4$ battery with this electrolyte was fabricated and examined.

EXPERIMENTAL

The lithium charge-discharge efficiencies [2] and the impedance spectrums were measured by using coin cells with 0.1mm and 0.4mm thickness of lithium foil as the working and the counter electrode, respectively. $\text{LiN}(\text{C}_2\text{F}_5\text{SO}_2)_2$ (LiBETI) supplied by 3M company was used as a salt, and ethylene carbonate (EC) and tetrahydropyran (THP), 1,3-dioxane (DOX) were used as the mixed solvents.

The 10Wh class lithium metal battery, 33.5mm in diameter and 63.7mm in height, was fabricated with LiMn_2O_4 and Li as a cathode and an anode, respectively. 0.9M LiBETI+0.1M $\text{LiPF}_6/\text{EC}+\text{THP}+\text{DOX}$ (40:30:30) was used as the electrolyte. The cycling performance was measured at DOD80%.

RESULTS AND DISCUSSION

Table 1 shows the results of measurements of the lithium charge-discharge efficiency. The lithium charge-discharge efficiencies were improved by using the electrolytes with LiBETI. Among the examined electrolytes, the lithium charge-discharge efficiency with the solvent composition of $\text{EC}+\text{THP}+\text{DOX}$ (40:30:30) achieved 99%. Fig.1 shows the cole-cole plots of Li / electrolyte / Li coin cells after 20 charge-discharge cycles. The semicircles of the LiBETI electrolyte system were smaller than that of the LiPF_6 electrolyte. This suggests that the lithium charge-discharge efficiency of the electrolyte with LiBETI is enhanced by the suppression of the reaction between the lithium and the electrolyte [3].

Based on the above results, 10Wh class $\text{Li/LiMn}_2\text{O}_4$ battery was fabricated with 0.9M LiBETI+0.1M $\text{LiPF}_6/\text{EC}+\text{THP}+\text{DOX}$ (40:30:30). Fig.2 shows the photograph of 10Wh class lithium metal battery. The shape of the battery is cylindrical, and the specific energy and capacity were 120Wh/kg and 242Wh/l, respectively. Fig.3 shows the cycling performance. The cycle life achieved over 350 cycles at DOD80%.

ACKNOWLEDGMENTS

This work was financially supported by New Energy and Industrial Technology Development Organization (NEDO) Japan. The authors thank Mitsubishi Chemical Corporation for supplying electrolytes.

REFERENCES

- [1] W. Xianming et.al., The 1999 Joint International Meeting, Hawaii, Abstract No 342 (1999)
- [2] K. Saito et.al., J. Power Sources, 68, 476 (1997)
- [3] K. Naoi et.al., J. Electrochem. Soc., 146, 469 (1999)

Table 1 Lithium charge-discharge efficiency at $0.2\text{mA}/\text{cm}^2$ in charge and at $0.6\text{mA}/\text{cm}^2$ in discharge.

salt	solvent	lithium charge-discharge efficiency
0.9MLiBETI+0.1MLiPF ₆	EC+THP(50:50)	98.4%
	EC+DOX(50:50)	98.9%
	EC+THP+DOX(40:30:30)	99.0%
1MLiPF ₆	EC+DOX(50:50)	93.9%

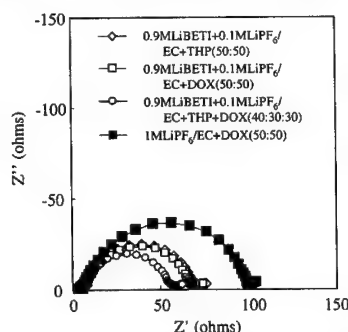


Fig.1 Cole-cole plots of Li/electrolyte/Li coin cells after 20 charge-discharge cycles at $0.6\text{mA}/\text{cm}^2$.



Fig.2 Photograph of 10Wh class Lithium Metal Battery.

Size : 33.5mm(D), 63.7mm(H)
Rated capacity : 3.4Ah
Specific energy : 120Wh/kg
Specific capacity : 242Wh/l

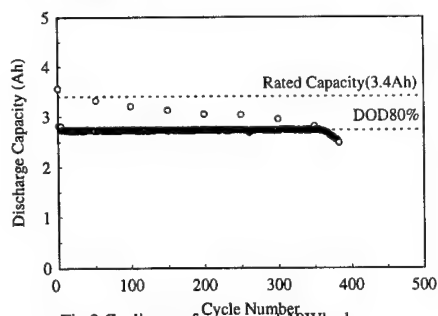


Fig.3 Cycling performance of 10Wh class Lithium Metal Battery with 0.9M LiBETI+0.1M $\text{LiPF}_6/\text{EC}+\text{THP}+\text{DOX}$ (40:30:30) at DOD80%.
Charge : $1/14.5\text{C}$; Discharge : $1/4\text{C}$

Fabrication of Composite Electrodes for Rechargeable Lithium Batteries by Using Electrophoretic Deposition Process

Kiyoshi Kanamura, Atsushi Goto, and Takao Umegaki
Department of Applied Chemistry, Graduate School of
Engineering, Tokyo Metropolitan University
1-1 Minami-Ohsawa, Hachioji, 192-0397 Tokyo, Japan

Composite electrodes for rechargeable lithium batteries have been fabricated by using a casting method. For example, three components, such as active material, conducting material (mostly carbon fine powder), and binding material (inactive polymer) were mixed in a proper solvent (*N*-methyl-2-pyrrolidone) to prepare a solution for a casting method. This solution was painted on a current collector (Cu or Al foil). After drying, composite electrodes are fabricated. In this study, we have used an electrophoretic deposition (EPD) process to fabricate such composite electrodes for rechargeable lithium batteries. The EPD process has been applied to a forming of ceramics powders. Thin films of BaTiO_3 , PbZrO_3 , and Apatite have been fabricated by the EPD.

In the EPD process, ceramic powders suspended in a proper solution moved toward negative or positive electrode according to its surface charge and then deposited on the electrode with a pressure generated by an electric field in the solution. Finally, a hard and thick film is fabricated on the electrode. In the case of the fabrication of positive or negative electrode in rechargeable lithium batteries, three components should be deposited on the current collector simultaneously with a proper weight ratio. We have already reported the fabrication of LiCoO_2 and LiMn_2O_4 electrodes. In this paper, $\text{Li}_4\text{Ti}_5\text{O}_{12}$ and graphite were used as anode materials of rechargeable lithium batteries. These electrodes were fabricated by the EPD process.

The EPD was conducted by using a standard electrochemical cell with two stainless steel electrode as anode and cathode. The solution for the EPD process was an acetone with a small amount of I_2 . The active material, conducting material, and binding material were suspended in the acetone solution with a optimized weight ratio. The conducting material for $\text{Li}_4\text{Ti}_5\text{O}_{12}$ electrode was graphite. The binding material for both graphite and $\text{Li}_4\text{Ti}_5\text{O}_{12}$ electrodes was PVdF.

Figure 1 shows a schematic illustration of the electrode production of rechargeable lithium batteries by using the EPD process. Both cathode and anode sheets can be produced through the EPD process. This is very simple and fast, compared with an ordinary one.

Figure 2 shows the scanning electron micrograph of the graphite and $\text{Li}_4\text{Ti}_5\text{O}_{12}$ composite electrodes. The particles of active material and conducting material were well mixed and uniformly distributed in the electrodes. The adhesion of composite electrodes to the Cu substrate was adequately high for production of rechargeable lithium batteries.

Figure 3 shows the discharge and charge curves of the graphite electrode fabricated by the EPD process. The initial discharge capacity of the electrode was 350 mA h g^{-1} and the charge one was 310 mA h g^{-1} . The graphite electrode prepared by a standard method was also tested using a standard nonaqueous electrolyte and exhibited similar discharge and charge capacities. Therefore, the EPD process is a good candidate of promising graphite electrode fabrication processes. $\text{Li}_4\text{Ti}_5\text{O}_{12}$ electrode prepared by the EPD process also exhibited a good performance.

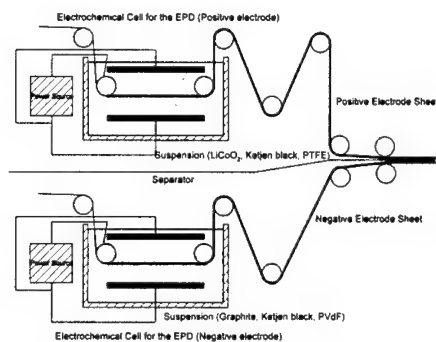


Figure 1 Schematic illustration of a fabrication process for rechargeable lithium batteries using the EPD process.

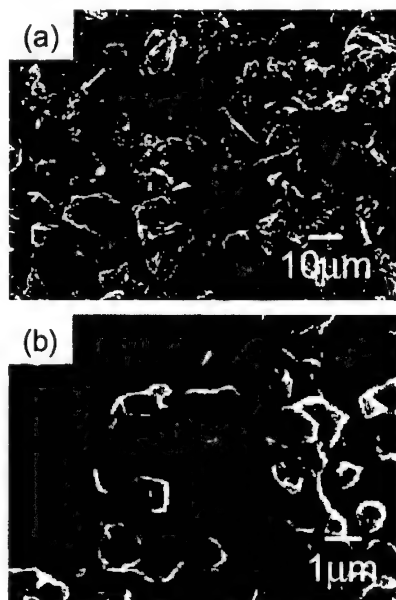


Figure 2 SEM photographs of (a) graphite and (b) $\text{Li}_4\text{Ti}_5\text{O}_{12}$ electrodes prepared by the EPD process.

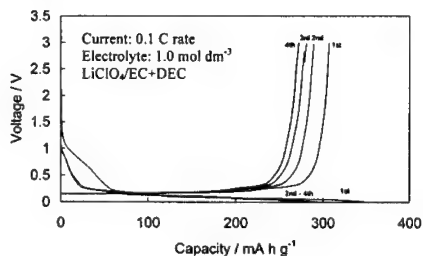


Figure 3 Discharge and charge curves of the graphite electrode fabricated by the EPD process.

Developments in Multichannel Impedance Instrumentation for the characterization of Energy Storage Devices

Andrew J. Hinton, Brian Sayers

Solartron – a Roxboro Group Company
Materials Test Division
Victoria Rd., Farnborough,
Hampshire
GU14 7PW
UK

For many years there has been a significant demand for instrumentation enabling manufacturers and suppliers of batteries to adequately quantify the performance of new battery materials and technologies. There has been a specific interest in running multi-channel high speed pulse and impedance tests on batteries, supercapacitors and fuel cells

The 1470 Multichannel Battery Test System is a novel battery test technology that is targeted at research, development and quality assurance applications. This instrumentation includes high-speed data acquisition components and the ability to connect to frequency response analyzers for impedance tests on any of the test channels, through a built-in multiplexer. Impedance (ac testing) is now widely recognized as giving valuable information regarding the prediction of the cycle life of secondary (rechargeable) batteries and is also useful for non-destructive tests on primary cells. The 1470 system not only allows the impedance of the whole cell to be tested; it can also test individual battery components including electrodes, separators and electrolytes by the use of auxiliary voltage inputs. The system is able to integrate impedance testing (upto 1MHz) over a wide frequency range with standard charge/discharge cycle testing. Typical applications include:- charge-discharge studies, lifetime performance, electrode/seperator reactions and GSM battery performance, the study of individual cell reactions, comparative analysis between new battery technologies and impedance tests determining mass/charge transfer effects.

The system is modular in design (8 channels per unit and up to 12 units per system giving a total channel count of 96). In practice however, any number of PCs can be added to the system giving a limitless number of test channels. The battery test units are designed both for bench top operation and also to fit into a standard 19" rack.

Constant voltage, current, power and load test strategies are available. The system makes use of analogue control loops for smooth control of applied signals (these are a similar design to that used in Solartron's research grade potentiostats e.g.1287). The maximum applied levels are up to +10V, -3V and at least 4A per channel.

The system is designed with multiple voltage and current ranges allowing resolution of very low level voltage and current signals; 3 microvolts / 1.5 nanoAmps (this is close to the performance of a single channel research grade potentiostat). The data acquisition sample rate is high, dual 16 bit / 10kHz analogue to digital converters per channel for simultaneous voltage and current sampling. The data is collected by a digital signal processor (one per battery channel), that allows compression of data and testing against safety or step termination limits.

The limiting factor of the system is designed to be in the communications linking back to the PC and in the speed of the PC itself, not in the battery tester. In this way as PCs, and communications standards such as Ethernet continue to develop, the system will automatically make use of the greater processing power, which is becoming available.

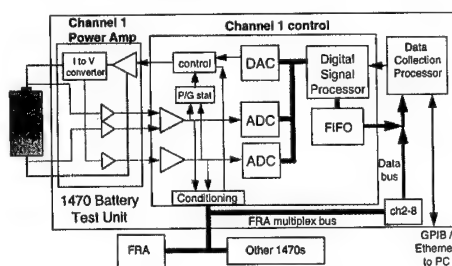


Fig. 1 Schematic of 1470 Battery Tester design

The schematic (Fig.1) shows a FRA added into the system linked to the battery tester. The FRA connects to the FRA multiplexer bus via a connector on the rear of the 1470. All channels within a 1470 are connected to this multiplexer bus. The PC software selects which channel actually forms a connection with the FRA via switches in the block named "conditioning" (see Fig. 1). Only one channel can be connected to a particular FRA at any time.

If only one FRA is available for the whole system (comprising of many 1470 battery test units), it is necessary to connect all of the 1470 FRA multiplexer connections together so that all channels in the system can be served by the single FRA. If more FRAs are available, then it is preferable to connect one FRA to each separate 1470 unit (in this case the multiplexer connections from each 1470 are not connected together). In this way each FRA only serves the eight channels inside its allocated battery test unit.

Electrochemical Properties of Li-Mn-spinel Using Hydrothermal Method.

T. Kanasaku, K. Amezawa and N. Yamamoto

Graduate School of Human and Environmental Studies,
Kyoto University
Yoshida-nihonmatsu-cho, Sakyo-ku, Kyoto 606-8501,
Japan

Introduction

As well known, the lithium-manganese-spinel is one of the most attractive cathode material of Li-ion secondary batteries. The conventional synthetic method of the lithium-manganese-spinel is the calcination method [1]. However, high temperature firing is required in this synthetic process, because of making long-range diffusion of the reactants possible. Furthermore, such long-range diffusion of the reactants may cause non-homogeneity, abnormal grain growth and poor control of composition. It is known that the electrochemical properties of the lithium-manganese-spinel significantly depend on its homogeneity, grain size and composition [2].

From this background, our group adapted the hydrothermal method to synthesize the lithium-manganese-spinel. The hydrothermal method enables to synthesize a homogeneous material at far lower temperature than that of the conventional calcination method. We have already succeeded and reported to synthesize the lithium-manganese-spinel hydrothermally through γ -MnOOH in the LiOH aqueous solution at 150°C [3]. However the characteristics of the obtained spinel are rather complicated. The chemical composition and grain size, thus electrochemical properties, strongly depend on its synthetic conditions, e.g., the starting material, the concentration of aqueous solution, the reaction time, and the reaction temperature.

In this work, we aimed to determine the conditions for the lithium-manganese-spinel in the hydrothermal synthesis through γ -MnOOH. Afterward, the characteristics of the obtained spinel, especially the electrochemical properties, were investigated in detail.

Experimental

γ -MnOOH was chosen as a starting material of Mn compound. LiOH and/or LiCl were used as the Li ion supplier. When LiCl was chosen, MeOH (Me=Na, K, Li) aqueous solution was added for controlling OH⁻. The concentration of MeOH solution was between 0.050 and 1.000 mol/l. After a certain amount of γ -MnOOH powder and Li ion supplier were dispersed in the MeOH solution, the reaction vessel was heated at the desired temperature at 130–170°C for 48–144h.

XRD and SEM were used for the characterization of the obtained precipitates. The molar ratio of Li to Mn was determined using ICP. The average valence of Mn ions was determined by the inverse oxidation-reduction titration using ferrous sulphate as a reducing agent [4]. The electrochemical properties of the lithium-manganese-spinel were investigated with coin type test cells. A positive electrode was made of a composite of the lithium-manganese-spinel, the acetylene black and PTFE. A negative electrode was an Li metal foil. An electrolyte was a solution of 1 mol/l LiClO₄ in 1:1 mol% EC and DEC. The cells were charged / discharged at the constant current

density of 200 μ A/cm² and the cut-off voltages were 3.5 and 4.3V.

Results and Discussions

The single phase of the lithium-manganese-spinel was obtained using the hydrothermal reaction through γ -MnOOH both in the LiOH aqueous solution and in the LiCl + NaOH aqueous solution. The synthetic conditions for the single phase of the lithium-manganese-spinel were 0.050–0.150 mol/l LiOH aqueous solution at 130–170°C and 0.100 mol/l NaOH aqueous solution at 150–170°C. The spinels obtained in the LiOH aqueous solution had a rod-like shape with the particle size of 0.1 \times 0.1 \times 1 μ m, while the spinels obtained in the LiCl + NaOH aqueous solution had an octahedron shape with the particle size of 1 μ m.

The chemical composition and the theoretical capacity of the hydrothermally prepared lithium-manganese-spinel are summarized in Table 1. The lithium-manganese-spinel obtained using the hydrothermal method, in general, had a Li-rich composition. It was also found that the chemical composition of the lithium-manganese-spinel could be controlled by its synthetic conditions in the hydrothermal method.

The lithium-manganese-spinel obtained using the hydrothermal method showed similar charge/discharge properties as the lithium-manganese-spinel obtained using the conventional calcination method. These results indicated that the hydrothermal method is useful as the synthetic method of the lithium-manganese-spinel.

References

- [1] M. M. Thackeray, M. F. Mansuetto, D. W. Dees, and D. R. Vissers, *Mat. Res. Bull.*, 31 (1996) 133.
- [2] P. Barboux, J. M. Tarascon, and F. K. Shokoohi, *J. Solid State Chem.*, 94 (1991) 185.
- [3] T. Kanasaku, K. Amezawa and N. Yamamoto, *J. Japan Soc. of Powder and Powder Metallurgy* 45 (1998) 738.
- [4] A. Kozawa, *Memoirs of Faculty of Engineering, Nagoya University* 11 (1959) 243.

Table 1 Properties of the lithium-manganese-spinels

Concentration / mol/l	Li / Mn	Temperature / °C	Theoretical Li _{1-x} Mn _{2-x} O _{4-y} capacity / mAh/g
LiOH solution			
0.050	3.4	170	Li _{0.94} Mn _{1.96} O _{4.02} 149.00
0.100	6.7	150	Li _{1.28} Mn _{1.92} O _{3.97} 124.60
0.125	8.4	130	Li _{1.23} Mn _{1.77} O _{3.87} 91.16
LiCl + NaOH solution			
0.100	1.0	150	Li _{1.40} Mn _{1.64} O _{3.84} 136.16

**New High-Surface-Area 3-Dimensional
"On-Chip" Lithium-Ion Microbattery**

**M. Nathan¹, D. Haronian¹,
D. Golodnitsky^{2,3}, Y. Lavi²,
E. Sverdlov¹, E. Peled²,**

**1. - Department of Electrical
Engineering, Physical Electronics 2.-
School of Chemistry,**

**3. - Wolfson Applied Materials Research
Center
Tel Aviv University, Tel Aviv, 69978,
Israel**

The miniaturization of electronic components with submicron- sized features and integration of millions of transistors on a "chip", has not been accompanied by a similar commercialization of batteries. The need for such sources is evident when taking into account the vast possibilities introduced by both microelectronics and the newer MEMS (micro-electro-mechanical systems) technologies to develop self-sustained mini- and micro-systems in a host of fields (smart cards with anti theft chips, sensors, miniature rf transmitters, microrobots, biochips, implantable medical and other MEMS devices). Battery capacity is directly proportional to the area and thickness of the thin-film (anode, electrolyte and cathode) layers, which form it. Thin-film planar lithium secondary battery research began about one decade ago, by Bates et al. [1]. An innovative way to increase the capacity is to utilize the volume of the substrate, upon which the layered thin-film structure is deposited and thus enable the film to follow the contour of a non-planar surface [2]. This can be achieved, for example, by etching the silicon to form an array of differently-shaped holes. The 3-dimensional high-surface-area and high-volume structure thus formed will result in increased battery capacity per unit volume. For example, for a hole with diameter d in a wafer of thickness h (aspect ratio = h/d), the ratio k of surface area after etching to the original, "planar" state is $2h/d$. For a square cavity with side a in the same wafer, $k=2h/a$. Thus, for a typical wafer with $h = 400\mu\text{m}$ and d or $a = 15\mu\text{m}$, the increase in area is $k=53$, while for $d=10\mu\text{m}$, $k=80$. This would result in a theoretical increase in capacity to over $1,000 \mu\text{Ah}/\text{cm}^2$ (geometric area).

The main goal of this work was to investigate electrode and solid electrolyte materials, as candidates for a high-capacity 3-dimensional lithium-ion thin-film

microbattery (3D-MB) on silicon. The following complementary tasks will be addressed: 1) identification and selection of the most suitable materials for electrode and solid electrolyte layers and 2) electrochemical characterization of the battery components.

Metal oxides and metal sulfides are considered as cathode-material candidates for 3D-MB. Several solid electrolytes are being considered. The ion-transport properties of ultra-thin polyethylene oxide-based solid polymer electrolytes (SPE) and charge-discharge characteristics of the cells will be presented. Microstructural and chemical data tests of the ultra-thin polymer electrolyte and cathode layers, performed with the use of XRD, SEM, AES/XPS, TOF SIMS will be shown.

References.

1. J.B. Bates, N. J. Dudney, G.R. Gruzalski et. A., J. Power Sources, **43**, 127 (1993)
2. Micro-Electrochemical Energy Storage Cell", M. Nathan, D. Haronian and E. Peled, U.S. pat. application 09/176,321, Oct. 1998

Abstract No. 327

**OPPORTUNITIES FOR LITHIUM BATTERIES
IN ELECTRIC VEHICLE AND HYBRID
ELECTRIC VEHICLE APPLICATIONS**

Michael Corbett
Business Manager, Advanced Materials
Kline & Company, Inc.
150 Clove Road
Little Falls, NJ 07424 USA

This paper will analyze and assess the future prospects for lithium batteries in electric vehicle (EV) and hybrid electric vehicle (HEV) applications.

The two major developing EV applications are pure EVs and HEVs. For the foreseeable future, HEVs appear to be more promising than pure EVs. Toyota already has over 10,000 of its PRIUS HEVs on the road. The PRIUS is doing well partly because Toyota is taking a loss on the initial production in the hope that volume sales will create economies of scale that can make this vehicle profitable. In addition, OEMs appear to be more comfortable with HEVs because they retain the internal combustion engine, can easily supply the acceleration power needed in passing situations, and can be used by consumers as a primary vehicle. The battery pack in the typical HEV is relatively small because the electric motor is used primarily for power boost during acceleration or in climbing hills.

The current battery technologies for HEVs include lead-acid, nickel cadmium (NiCd), and nickel metal hydride (NiMH). OEMs are investigating lithium ion (Li-ion) and lithium metal polymer (Li-P) batteries for HEVs, but the potential savings in weight is small compared with the alternatives to lead-acid batteries in a pure EV. The typical battery pack weights and potential weight savings by using Li-ion or Li-P are shown below:

Segment	Typical battery pack weight, lb	Potential weight savings from lithium packs, lb
HEV	100 - 200	25 - 50
Pure EV	500 or more	100 or more

In addition to current production efforts, it appears that many automobile companies are focusing their longer-term research on HEVs and other low-emission vehicles to a larger extent than on pure EVs. Key technology hurdles include increasing the operating range and increasing the power capabilities in order to deliver needed power in passing situations. With pure EVs, the battery life is an ongoing issue and for most people, the battery range is unacceptable. Although research has shown that 90% of travel is under 100 miles, there is a lack of comfort with most drivers knowing they only have 50 - 75 miles available to them. Another issue with pure EVs is the need for a second car, which increases the vehicle expense and the hesitancy of the general public to convert to pure EVs.

New Thin Lithium-Ion Batteries Using an Organic Liquid Electrolyte with Thermal Stability

Norio Takami*, Masahiro Sekino**, Takahisa Ohsaki*,
Motoya Kanda*, and Masao Yamamoto**

*Research & Development Center, Toshiba Corporation **Display
Devices & Components Company, Toshiba Corporation72,
Horikawa-cho, Saiwai-ku, Kawasaki 210-8572, Japan

Recently, thin film and prismatic polymer lithium-ion batteries (PLBs) using polymer gel electrolytes have been commercialized for some portable electronic devices. However, PLBs are subject to some problems in that their performance is inferior in some respects to that of LIBs. We have developed new thin LIBs using an organic liquid electrolyte with thermal stability. Here, we report the results of the performance and the safety of thin LIBs.

Experimental

Thin LIBs with thicknesses of 1.2 mm and 3.6 mm were constructed by using a graphitized mesophase-pitch-based carbon fiber (MCF) anode, a LiCoO_2 cathode, an organic liquid electrolyte, a separator, and an aluminum-plastic laminate bag. The anode and the cathode construction were the same as those described previously [2,3]. By molding the cathode, the anode, the cathode and the anode were in close contact with the separator. The charge-discharge characteristics were evaluated between 4.2 V and 3 V at 20°C.

Results

Liquid electrolyte-The electrolyte used for the thin LIBs was a solution of LiBF_4 in a mixture of high viscosity solvents. The electrolyte had the advantages of a high flash point of 129°C, a high boiling point of 216°C, a high viscosity of 6.6 cP at 20°C, a very low vapor pressure, and high conductivities of 6.04 mS/cm at 20°C and 2.1 mS/cm at -20°C.

Performance test data-Table 1 shows the performance parameters of thin LIBs with thicknesses of 1.2 mm and 3.6 mm. 363562-type LIB achieved an energy density of 156 Wh/kg, which is higher than that of prismatic LIB and thin film PLB [1,3]. Figure 1 shows the discharge curves of 363562-type LIB at various discharge rates. The capacity at 3 C (1710 mA) rate discharge was 95% of the capacity at 0.2 C rate discharge. The discharge performance of the thin LIB as a function of temperature at 1 C rate discharge between -20°C and 20°C was also measured (Fig.2). At -20°C, the capacity maintained 58% of that at 20°C. On the charge-discharge cycling tests at 1 C rate,

Table 1 Specifications of thin LIBs

Type	123562	363562
Dimensions (mm)	1.2 x 35 x 62	3.6 x 35 x 62
Thickness (mm)	1.2	3.6
Weight (g)	4.0	13.5
Capacity (mAh)	120	570
Voltage (V)	3.7	3.7
Energy density (Wh/kg)	120	156

the thin LIB maintained 80% of its initial capacity after 500 cycles. A high temperature storage test of 85°C for 24h after charging up to 4.2V showed a very small thickness change of less than 2 %. We consider that the excellent discharge performance, the long cycle life, and the small thickness change of thin LIBs are attributable to the high conductivity and the thermal stability of the LiBF_4 electrolyte and the rapid lithium intercalation into and deintercalation from the MCF anode [2,3].

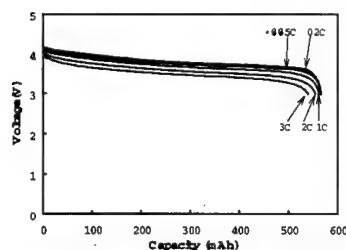


Fig.1 Discharge curves of 363562-type LIB at various rates.

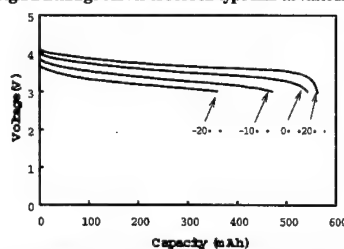


Fig.2 Discharge curves of the thin LIB at various temperatures.

Safety test data-The thin LIB had good safety performance. Specifically, the 363562-type LIB withstood overcharge tests up to 12 V, 5 C rate as well as oven tests up to 170°C for 1h at 4.4 V. Such safety performance is superior to that of any currently available LIB using 1M LiPF_6 -EC/methyl-ethyl carbonate (MEC) electrolyte. Figure 3 shows differential scanning calorimeter (DSC) profiles of unwashed LiCoO_2 after charging up to 4.2 V in the LiBF_4 electrolyte and the LiPF_6 electrolyte. The DSC peak of LiCoO_2 in the LiBF_4 electrolyte was smaller and shifted to a higher temperature than that of the LiPF_6 electrolyte. We consider that the safety results from the stability of the LiBF_4 electrolyte against the positive material in the high temperature ranges above 200°C. Finally, thin LIBs using the thermally stable liquid electrolyte and the MCF anode are the most promising thin batteries with high energy density, high power, and good safety.

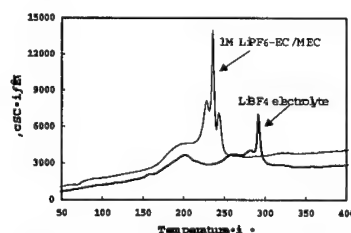


Fig.3 DSC profiles of unwashed LiCoO_2 after charging up to 4.2 V

References

1. C.Schmutz, J.M.Tarascon, A.S.Gozdz, P.C.Warren, and F.K.Shokoohi, The Electrochemical Society Proceedings Volume 94-28, p330 (1994)
2. N.Takami, A.Sato, M.Hara, and T.Ohsaki, J. Electrochem. Soc., **142**, 2564 (1995)
3. T.Ohsaki, M.Kanda, Y.Aoki, H.Shiroki, and Suzuki, J.Power Sources, **68**, 102 (1997)

Development of 6Ah Prismatic Cells for High Rate, Low Temperature Applications

G. M. Ehrlich[†], M. Hetzel[†], and S. Slane[‡]

[†]Yardney Technical Products, Inc,
Pawcatuck, Connecticut, 06379, USA

[‡]The U. S. Army CECOM, Ft. Monmouth,
N. J. USA

Li-ion cells are being applied to an increasing array of applications that value the high specific energy, high energy density, and long life delivered by the technology. One area is military batteries, where Li-ion cells are used for portable equipment, such as radios, detectors and imaging equipment. These devices are required to operate in all envisioned environments and many have high power requirements, in contrast to commercial equivalents. To enable their broadest application, Li-ion cells that offer high rate capability and low temperature capability are required.

To meet future military performance requirements prismatic "6Ah" Li-ion cells have been developed with high power and low temperature capability. The prismatic design permits efficient use of space within rectilinear military battery boxes. To optimize the cell rate capability, thus power density, a low resistance flat plate prismatic design was developed. The rate capability of the cell is illustrated in Figure 1 which shows constant current discharge curves at rates from 0.36A to 24A (4C). As shown, at 24A the cell delivered 6Ah, 88% of that delivered at the C/16 (0.36A) rate.

The cell also offers low temperature capability to -40°C as illustrated in Figure 2. As shown, at -40°C the cell delivered 4Ah, or 11.6Wh, 68% of the capacity and 54% of the energy delivered at 25°C.

The characteristics of these cells and batteries fabricated using these cells will be reported.

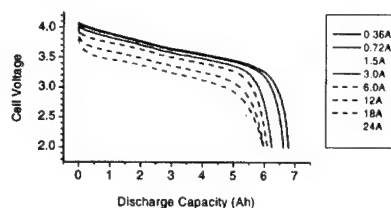


Figure 1. Voltage of a NCP-6 Cell when discharged at 25°C after charge to 4.1V at 1A.

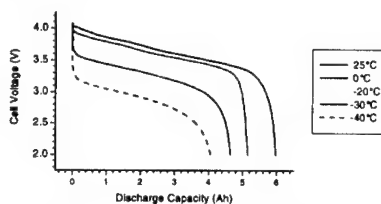


Figure 2. Voltage of a NCP-6 cell, charged to 4.1V at 25°C then discharged at 1A at various temperatures.

Acknowledgement

The authors thank the U.S. Army for support under contract DAAB07-97-C-D266.

A Study of the Overcharge Reaction of Li-ion Batteries

Marcus J. Palazzo, Randolph A. Leising
and Esther Sans Takeuchi*

Wilson Greatbatch Ltd.
10,000 Wehrle Drive
Clarence, NY 14031

Kenneth J. Takeuchi*

SUNY at Buffalo
Department of Chemistry
Buffalo, NY 14260

Introduction

The safety of lithium ion batteries, especially under abusive conditions, is a primary concern of battery manufacturers and their customers. In particular, the potentially violent reaction of lithium ion cells at very high temperatures or under extreme overcharge conditions has been documented.¹ There have been a number of studies published dealing with the thermal analysis of individual components of lithium ion battery systems,^{2,3} as well as considerable data generated on safety tests of commercially available lithium ion product.^{4,5} However, there has been little reported on the systematic variation of complete lithium ion batteries and the effect of these variations on the safety performance of the batteries. This report details the effect of cell balance (ratio of cathode to anode) on the overcharge characteristics of lithium ion cells.

Experimental

Prismatic, hermetically-sealed lithium ion cells enclosed in stainless steel cases were assembled using LiCoO_2 cathodes, graphite anodes, and polyethylene separator. The cells utilized a wound element design and liquid electrolyte. The anode weight was held constant, and the cathode weight was varied to yield cell balances of 2.3, 2.8 and 3.3 for three groups of cells. Cell balance is defined here as the weight of the active cathode material divided by the weight of the active anode material. The delivered cell capacity and anode capacity were experimentally determined for these cells as a function of cell balance and are plotted in Figure 1. The capacities plotted in Figure 1 were taken from cycle 3 discharge of the cells, where the cells were cycled between voltage limits of +4.1 and +2.75 V. Notably, the anode capacity at a cell balance of 3.3 was above the reversible capacity of the graphite anode material, and likely included lithium deposition at the anode in these cells.

Results and Discussion

The cells were fully charged to +4.1 V and then overcharged using a 1 amp constant current at room temperature. The voltage and current were monitored during the test, and the skin temperature of the cell was recorded using a thermocouple attached to the outside case surface. Typical voltage and temperature curves for a cell with a cell balance of 2.8 on overcharge test are plotted as a function of time in Figure 2. The temperature peaked at 115°C and the voltage at +5.3 V prior to the case rupturing as a result of the extreme overcharge. Interestingly, the onset time for the overcharge reaction was longer for cells with a higher cell balance, corresponding to the increased amount of cathode material in these cells.

Summary

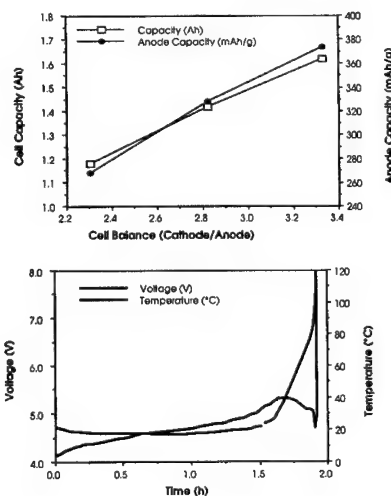
Experimental prismatic lithium ion cells were constructed with a systematic variation in cell balance. These cells were overcharged under a constant current, and displayed peak voltages of +5.3 to +5.5 V. The temperature remained stable throughout the test until very close to the end when it rapidly increased to 97 to 120°C. The onset time for the overcharge reaction was longer for cells with a higher cell balance.

References

- 1) Tobishima, S.; Yamaki, J. *J. Power Sources* **1999**, 81-82, 882.
- 2) Zhang, Z.; Fouchard, D.; Rea, J. R. *J. Power Sources* **1998**, 70, 16.
- 3) Richard, M. N.; Dahn, J. R. *J. Electrochem. Soc.* **1999**, 146, 2068.
- 4) Maleki, H.; Deng, G.; Anani, A.; Howard, J. J. *Electrochem. Soc.* **1999**, 146, 3224.
- 5) Lampe-Onnerud, C. *16th Int. Sem. on Prim. & Sec. Batt.*, FL, Mar 1 - 4, 1999.

Figure 1. Cell and anode capacity as a function of cell balance.

Figure 2. Voltage and temperature during overcharge at 1 amp constant current.



FAST CHARGING OF LITHIUM-ION BATTERIES

J. René van Beek
Philips Research Laboratories
Prof. Holstlaan 4
5656AA Eindhoven
The Netherlands

Faster charging of Li-ion batteries is not simply a matter of increasing the charging current, because capacity built-up is not linear during the usual CCCV charging method. The fast decreasing charging current in the CV-mode results in a very slow charge rate during the last part of the charging period. Increasing the maximum charge current I_{max} will advance the start of the CV-mode, but the total charging time is not much affected. An additional increase of the charge rate can be achieved by increasing the maximum charge voltage V_{max} . However, not only the charging time, but also the total charged capacity is affected by V_{max} . To a minor extent, end-of-charge criteria such as I_{min} or t_{max} determine the capacity or Depth-of-Charge (DOC) too. Hence, fast charging can only be defined as the total charging time for a certain amount of capacity (DOC). Increasing I_{max} and V_{max} results in faster charging, but also in faster degradation resulting in loss of cyclife. Faster degradation is possibly due to parasitic reactions like Li-metal deposition on the negative electrode and to decomposition of the electrolyte at the relative high voltage at the positive electrode. Investigations have revealed that charge rate, charged capacity and capacity decay (cyclife) depend on each other (see Fig. 1 and Fig. 2) and are determined by the charge parameters I_{max} , V_{max} and DOC.

In addition to the standard CCCV method (curves (a) and (c)), several charging algorithms have been investigated aiming for a decrease of the charging time without significant extra loss of cyclife, such as multi-CC charging, IR-compensated charging (curves (d) and (e)), 2-Step CCCV charging and COCV charging.

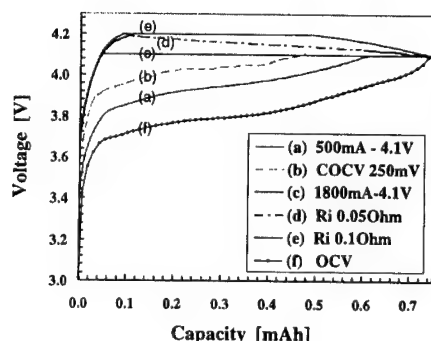


Figure 1: Voltage characteristics during various charging regimes (curves (a)-(e)) and OCV behavior (curve (f)).

A multi-CC charging algorithm is based on several charging steps with constant current. The charge current is gradually decreased from I_{max} till I_{min} in each consecutive step. A step is terminated when the maximum charge voltage V_{max} has been reached. The advantage of this charge regime is that the time the battery will be charged at V_{max} will be very limited.

For IR-compensated charging it is assumed that part of the internal resistance would be Ohmic, due to lead and contact resistances. The voltage drop on this resistance will not contribute to the overvoltage of the charging reactions. Consequently, the maximum charge voltage has been increased with an amount depending on the charging current. Figure 1, curves (d) and (e) shows the charge voltage profiles for a charge regime when a V_{max} of 4.1V is compensated for the charging current, assuming an Ohmic resistance of 0.05 Ω and 0.1 Ω , respectively.

The charge regime, called 2-Step CCCV, consists simply of 2 consecutive steps with a CCCV regime. During the first step, V_{max} is limited.

COCV charging has been developed as a new charging algorithm. COCV stands for a charging method with a Constant Overvoltage mode followed by a Constant Voltage mode. The CO-mode is based on the equilibrium voltage (OCV) of the battery and its corresponding DOC (see Figure 1). The charging voltage is continuously adapted to keep the difference with the OCV voltage at a constant value.

It has been shown that there is a clear relation between the overvoltage during charging and the degradation rate during cycling. Good results have been found with a COCV algorithm using an overvoltage of 250 - 300mV (curves (b)).

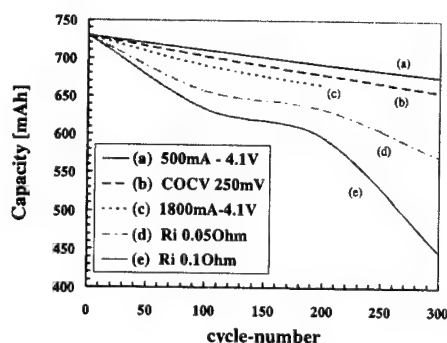


Figure 2: Capacity decay during cycling of Li-ion with the various regimes of Figure 1.

Factors Responsible for Impedance Rise in High Power Lithium Ion Batteries

K. Amine, M. Hammond, J. Liu, C. Chen, D. Dees, A. Jansen, and G. L. Henriksen
Argonne National Laboratory, 9700 South. Cass Ave.,
Argonne, IL 60439

Introduction

Lithium ion batteries have been proven to meet and even exceed the high power goals set by the Partnership for a New Generation Vehicle (PNGV). In this case, however, one of the major challenges that prevent this technology from being used as an energy storage system for hybrid vehicles, is its short calendar life. At the moment, the lithium ion technology has a 3-year calendar life, which is far shorter than the 10 years required by PNGV. In this case, the end-of-life of the high-power system is caused by power fade associated with the impedance rise of the cell, rather than the fading of the capacity, which is the typical cause of end-of-life for high-energy cells. To support the PNGV's industrial partners, the US Department of Energy (DOE) has created a multi-national laboratory program referred to as the "Advanced Technology Development Program", headed by Argonne National Laboratory, to identify the main causes responsible for calendar life limitation in the high power lithium ion technology, and propose potential solutions that can lead to meeting the life requirement.

Results and Discussion

The lithium-ion chemistry used in these high power batteries is based on $\text{LiNi}_{0.8}\text{Co}_{0.2}\text{O}_2$ as the positive active material and a blend of SFG-6 and MCMB-6 as the negative active material. This chemistry was investigated using $\text{LiPF}_6/\text{EC}+\text{DEC}$ electrolytes. Both the positive and negative electrodes were engineered with the aim of reducing initial cell resistance and enhancing power. A high power 18650-cell (36W) was then designed and fabricated using the above chemistry, and extensive accelerated calendar life testing was carried out. The cells were first characterized at 25°C in terms of AC impedance (at 0% and 100% SOC), C/1 capacity and a hybrid pulse power characterization (HPPC) test at 10 C rate. The cell was then discharged to 3.918 V and heated to 70°C. After equilibration, the cell was potentiostated at the rest voltage and allowed to age for two weeks at 70°C. After 2 weeks, the cell was disassembled and the electrodes were investigated via reference electrode and AC-impedance study. The hybrid pulse power characterization test (HPPC) was carried out on a large laboratory cell (32 cm²) containing a reference electrode. This test consists of a series of partial (but increasing) C/1 discharges at 10% depth of discharge (DOD) increments, each of which is followed by a pulse profile (18s at 10 C rate) and a recharge. The discharge and regenerative braking pulse power capability are calculated at each available DOD increment. The reference electrode used in this case was made of 25µm copper wire, insulated by a 3 micron layer of polyurethane enamel. The insulation layer was stripped from the tip of the wire and a 1 µm tin layer was electroplated onto the exposed copper. After cell assembly, the tin plated layer on the tip of the wire was charged with lithium from the positive electrode.

Figure 1 compares the area specific impedance (ASI), during the 18s pulse discharge of the cell, the positive and the negative electrodes of both a fresh, and an aged cell.

The initial ASI's of the cell, made with fresh electrode Fig.1c increased significantly from 40 ohm-cm² to 100 ohm-cm² after 2 weeks of accelerated calendar life testing at 70°C (Fig. 1a). The bulk of the impedance rise in this case, is due mainly to the positive electrode, as clearly indicated from the comparison of the ASI's of a fresh (Fig 1d) and aged (Fig 1b) positive electrodes. The increase in the ASI's of the aged negative electrode (Fig 1e) is not significant when compared to the ASI's of initial fresh negative electrode (Fig. 1f). To understand the cause of the impedance rise at the positive, we compared the AC impedance of two symmetrical cells made from two symmetric positive electrodes either fresh or aged cells. The positive symmetrical cells were built by taking two identical normal cells that were cycled, disassembling them, and then reassembling the positive electrodes of both regular cells as one symmetric positive cell. Fig. 2 compares the AC impedance of symmetrical positive cells made of fresh electrodes, after one cycle (Fig.2a), and aged electrodes (Fig.2b). The semi circle at medium frequency, which corresponds to lithium transport through the positive electrode interface, increases significantly after accelerated calendar life testing. Therefore, the impedance rise of the high power cell is mainly due to the charge transfer resistance at the positive electrode.

Acknowledgment

The authors acknowledge the financial support of DOE's Office of Advanced Automotive Technologies under contract No. W-31-109-ENG-38.

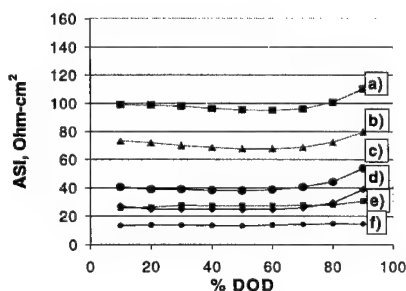


Fig. 1 Area specific impedance of a) aged cell, b) aged positive electrode, c) fresh cell, d) fresh positive electrode, e) aged negative electrode and f) fresh negative electrode

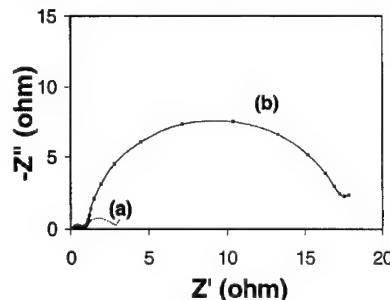


Fig.2 AC impedance spectra of symmetrical positive cells made of (a) fresh electrodes, and (b) aged electrodes subjected to calendar life testing at 70°C.

Promising Modifying Additives For Lithium Power Sources

*E.M.Shembel, O.V.Chervakov, I.M.Maksyuta,
N.I.Globa, N.D.Zaderey, L.G.Romanovskaya and
A.G.Ribalka*

Ukrainian State Chemical Technology University,
Dnipropetrovsk, Ukraine,
E-mail: shembel@onil.dp.ua

D.T.Meshri

Advance Research Chemical, Inc, Catoosa, OK, USA

Modification of electrolytes and electrode materials by organic additives is one of the promising methods for the improvement of operating characteristics of lithium power sources. The efficiency of using the modifying additives results in the following significant change in the properties of electrochemical system after introducing a minute quantity of the organic additive into the composition of electrode mass or directly into electrolyte:

- conductivity of liquid and polymer electrolytes increases;
- the range of the electrochemical resistance of electrolytes to oxidation/reduction processes becomes wider;
- during system storage and at cycling the interaction between electrode materials and electrolyte decreases.

As a result, stability of electrode system improves under the cycling conditions.

We have developed the method of synthesis and practical application of promising as the additives the following nitrogen-containing compounds:

- aromatic amines;
- diarylamines and their substituted amides of carboxylic acids;
- nitrogen-containing heterocycles;
- arilamide compounds;
- compounds with macrocyclic structure;
- ammonium siliconorganic compounds.

The following investigations were carried out:

- influence of the additives on the background potentiodynamic characteristics of nonaqueous electrolyte on a platinum electrode;
- electrochemical stability of electrolyte with the additives within the potential range of above 4.5 V;
- thermal stability of polymer electrolytes with the additives;
- potentiodynamic and galvanostatic cycling of electrode materials in the electrolytes with the additives;
- testing actual samples of chemical power sources within the size of disk lithium cells.

LiMn_2O_4 and graphite were investigated as electrode materials. Polymer electrolytes were prepared on the basis of chlorinated polyvinylchloride. Liquid electrolytes were fabricated on the basis of the following solvents: PC, DME, DMC, DEC and the salts: LiClO_4 , LiPF_6 , LiAsF_6 , LiSO_3CF_3 .

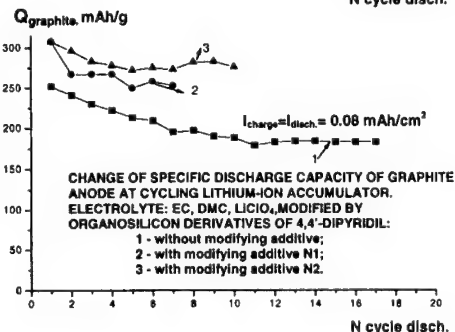
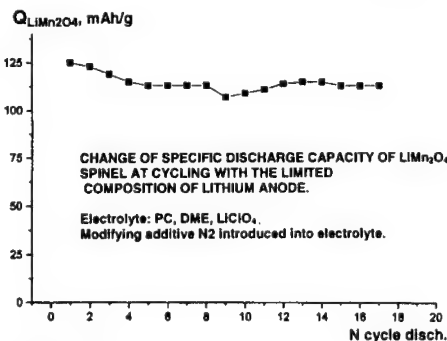
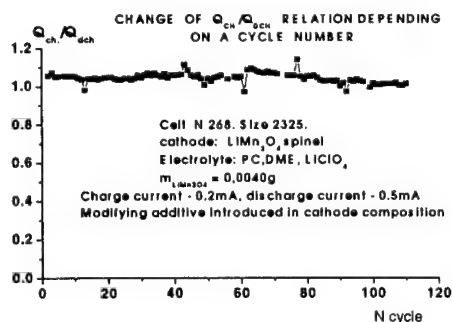
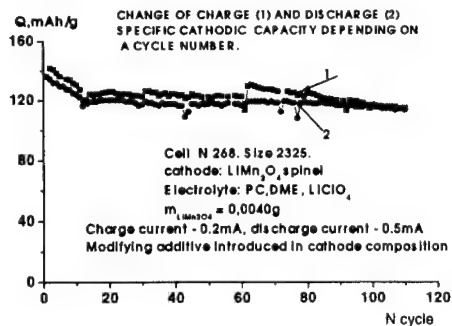
The investigations carried out have shown that the macrocyclic compounds, substituted heterylthiocarboxylic acids and the organosilicon derivatives of 4,4'-dipyridil are the most promising.

Introducing into LiMn_2O_4 -based cathode the modifying additives falling into the class of the compounds with a macrocyclic structure leads to the stabilization of cathode characteristics in the process of its cycling. After 120 cycles (Fig.1) the discharge capacity of cathode maintains higher than in the system without additive. It should be pointed out, that during all cycling the charge-discharge capacity relation is near 1 that indicates a good reversibility of the process (Fig.2).

Introduction of the developed pyridinium-containing organosilicon additives differing in ethylene oxide groups content affects positively both cathode (Fig.3) and anode (Fig.4) process.

Acknowledgement

This work was supported by the STCU Project #656 and the Ministry of Science of Ukraine, Grant 2c/1458-97.



Overcharge Protection Additives for
4 Volt Lithium Ion Batteries

T. J. Richardson and P. N. Ross, Jr.
Ernest Orlando Lawrence Berkeley National Laboratory
Berkeley, California 94720 USA

Overcharging of lithium and lithium ion batteries can not only reduce rechargeable capacity and shorten cell life, but can also create hazardous conditions. Redox shuttle additives may provide inexpensive overcharge protection for multi-cell battery stacks for electric vehicles and other high voltage applications.¹⁻³ The additive acts as an internal current shunt when the charging potential exceeds the oxidation potential of the additive (Fig. 1).⁴⁻⁶

A number of redox shuttle additives with shuttle current onset potentials ranging from 4.1 V to greater than 4.6 V have recently been discovered.^{1,2} Potential sweep results showing onset potentials and limiting currents at a 5 μ m diameter Pt microdisk electrode for some examples are shown in Figure 2.

In consumer battery applications, mechanical and thermal shutdown mechanisms are employed which prevent overheating, bursting or venting while terminating the life of the cell. This can also be accomplished through the use of electrolyte additives.

The electrochemical characteristics and performance evaluation of both types of additive will be discussed.

1. T. J. Richardson and P. N. Ross, Jr., *Proc. Electrochem. Soc.*, **99-25**, (2000).
2. M. Adachi, K. Tanaka, and K. Sekai, *J. Electrochem. Soc.*, **146**, 1256 (1999).
3. T. J. Richardson and P. N. Ross, Jr., *J. Electrochem. Soc.*, **143**, 3992 (1996).
4. S. R. Narayanan, S. Surampudi, A. I. Attia, and C. P. Bankston, *J. Electrochem. Soc.*, **138**, 2224 (1991).
5. M. N. Golovin, D. P. Wilkinson, J. T. Dudley, D. Holonko, and S. Woo, *J. Electrochem. Soc.*, **139**, 5 (1992).
6. Abraham, K. M., *Electrochim. Acta*, **38**, 1233 (1993).

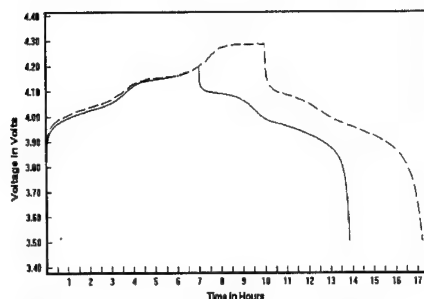


Figure 1. Galvanostatic cycling of $\text{LiMn}_2\text{O}_4/\text{LiPF}_6$ EC:2DMC/Li cell. Solid line: normal cycling with 4.2 V upper limit; dashed line: 50% overcharge.

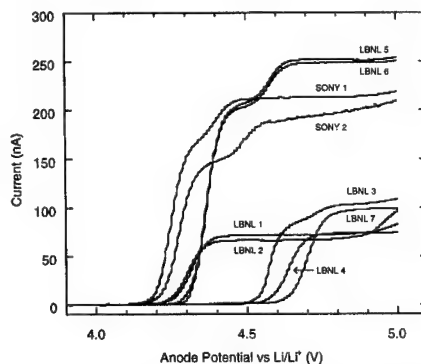


Figure 2. Pt microdisk electrode potential sweep data for redox shuttle additives in LiPF_6 EC:2DMC. Shuttle conc. 0.1 M, sweep rate 20 mV/s.

This work was supported by the Office of Energy Research, Basic Energy Sciences, Chemical Sciences Division of the United States Department of Energy under contract No. DE-AC03-76SF00098.

Comparative Study of Thermal Behaviors of Various Lithium-ion Batteries

Yoshiyasu Saito, Kiyonami Takano, Katsuhiko Kanari, Akira Negishi, Ken Nozaki, and Ken Kato
Electrotechnical Laboratory
1-1-4 Umezono, Tsukuba, Ibaraki 305-8568, Japan

INTRODUCTION

Since the first commercialization of the lithium-ion battery by SONY in 1991, we have studied the thermal behavior of the battery during charge and discharge from the viewpoint of safety [1]. In recent years, lithium-ion batteries have been produced by several companies. In this study, we will present the heat generation behaviors of the various lithium-ion batteries during charge and discharge.

EXPERIMENTAL

Four kinds of commercial batteries (Sample A, B, C, and D) produced by different companies were used as the test samples. The shape of the all batteries was cylindrical and the size was 18 mm in diameter and 65 mm in length. LiCoO_2 -based material was used in the cathode in all batteries. Graphite-based material had been selected for the anode except sample D in which hard carbon was used.

The heat generation of the batteries was measured by a twin-type heat conduction calorimeter (Setaram, C80-22) for constant current charging and discharging.

Depth of discharge, DOD, was defined from the battery capacity between charged state at 4.2V and discharged state at 2.7V for the all batteries.

RESULTS AND DISCUSSION

Figure 1 shows the results of calorimetric measurement for the batteries during 0.04C charging and discharging at 313K. The battery reaction is almost endothermic in charge while exothermic in discharge. This is related to the entropy change of the reaction.

The variation of the heat generation curves is extremely complicated. The peaks observed in region (a) are caused by the crystal phase transition of the cathode material. The cathode active material in sample A contains 2 wt% of Sn, and this might be effective to suppress the phase transition as shown in Fig. 1 (A). The thermal behaviors at region (a) in sample D are also somewhat different with those in sample B and C.

The heat generation curves of sample D appears unique while the others show similar variation at deeper discharged state than 30% of DOD. This is originated in the anode active material. Only in sample D, hard carbon is used. Hard carbon electrode shows voltage hysteresis between charging and discharging, which causes characteristic exothermic behaviors at region (e) and (f) during discharge and charge, respectively, and it results in asymmetric heat generation curves between charge and discharge [2].

It is well known that the graphite-based carbon that is used in sample A, B, and C shows stage structure when lithium ions are intercalated into the material. For sample A, it was suggested that the anode material at (b), (c), and (d) was attributed in single stage phase from the voltage profile, and XRD data showed that the stage was 2, 2L, and 4 in (b), (c), and (d), respectively. In addition, co-existence of stage 1 and 2 was observed in the fully charged state (DOD 0%), and dilute stage 1 in the fully discharged state (DOD 100%). Thus, it is concluded that the complex variation of heat generation at (b), (c), and (d) is caused by the change of the stage structure of the anode material. Fine distinctions of the variation among

sample A, B, and C is thought to be originated in the characteristics such as crystallinity and size of the crystallite of the anode material.

REFERENCES

- [1] Y. Saito, K. Kanari, K. Takano, *J. Power Sources*, 68 (1997) 451.
- [2] Y. Saito, K. Takano, K. Kanari, K. Nozaki, *Mat. Res. Soc. Symp. Proc.* 496 (1998) 551.

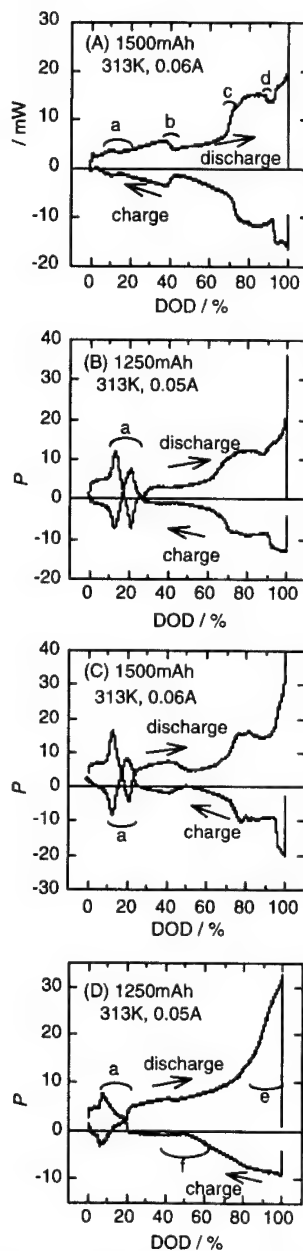


Figure 1. The heat generation curves during charge and discharge of 0.04C at 313K for (A) Sample A, (B) Sample B, (C) Sample C, and (D) Sample D.

Thermal Behaviors of Lithium-ion Batteries during Overcharging

Yoshiyasu Saito, Kiyonami Takano, Akira Negishi
Electrotechnical Laboratory
1-1-4 Umezono, Tsukuba, Ibaraki 305-8568, Japan

INTRODUCTION

For the prevention of the thermal-runaway, it is important to understand heat generation behaviors of the lithium-ion battery in the overcharge. The heat generation quantity in the overcharge of the various lithium-ion batteries was examined and discussed. It is also examined how the charging rate affects the heat generation behaviors.

EXPERIMENTAL

Commercial batteries were used mainly for the test. Samples A and D were an 18650 cylindrical type. LiCoO_2 -based active materials were used for the cathode of both samples. Anode active material was graphite in the sample A and hard carbon in the sample D. The solvents of electrolyte contained were EC/EMC in the sample A and PC/DMC/EMC in the sample D with LiPF_6 [1]. A trial manufacture battery was also tested, and LiMn_2O_4 was used for its cathode.

The heat generation in the batteries was measured by a twin-type heat conduction calorimeter (Setaram, C80-22) in constant current charging with a compliance voltage limit of 7.0V. The calorimeter was controlled at the constant temperature of 303K. Since the maximum range of C80-22 was about 3W, heat flow over the range was estimated from the inner temperature difference between the sample vessel and the reference vessel. Using specially designed sample vessels with a groove for a thermocouple, the temperature in the vessels was measured. The test was started from the fully discharged state.

RESULTS AND DISCUSSION

It has been proven that the cooling system must be able to remove an equivalent heat for electrical input in order to prevent the thermal-runaway that originates from the overcharge. In every battery, the heat generation flow gradually increased with the charged electricity at the beginning of overcharge, and then it rapidly increased from near 130% ~ 180% at the charged electricity to the battery capacity. The charged amount in which the heat flow begins to increase rapidly seems to be related to the composition ratio of the lithium contained in the cathode active material at the full charge. LiCoO_2 -based cathode materials contain much more lithium at the full charge than LiMn_2O_4 -based materials. The rapid increase in heat flow in the later battery began about 130% at the charged amount, while it in the former began at about 160% ~ 180%. Although the heat flow was almost proportional to the charging current at 0.2C and below, it was complicated at 0.5C and above. However, the heat flow almost agreed with electrical input, when the overcharge sufficiently advanced. Though the heat generation exceeding electrical input was also observed, the excess heat was about 20% of the electrical input at most as shown in Fig. 1 and Fig. 2. As shown in Fig. 3, the battery voltage monotonically increased with the charged amount until about 4.4V. In the range over 4.4V, there were plateaus and dents in the voltage curve. They were dependent on cathode material and charging current. In the sample A including Sn of about 2wt% in cathode active material, the increase in the voltage was limited under 5.3V.

REFERENCES

- [1] Y. Saito, K. Takano, A. Negishi, K. Nozaki, K. Kato, 1999 ESC-ECSJ Joint International Meeting, 3B-318 (1999).

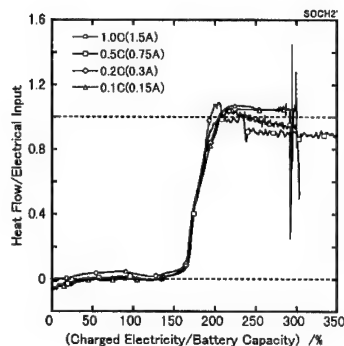


Fig. 1 Variations of (heat flow/electrical input) with (charged electricity/battery capacity) for various charging rates in the sample A with capacity of about 1630mAh.

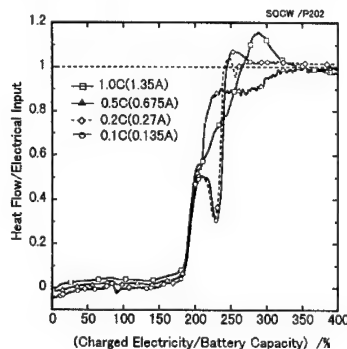


Fig. 2 Variations of (heat flow/electrical input) with (charged electricity/battery capacity) for various charging rates in the sample D with capacity of about 1300mAh.

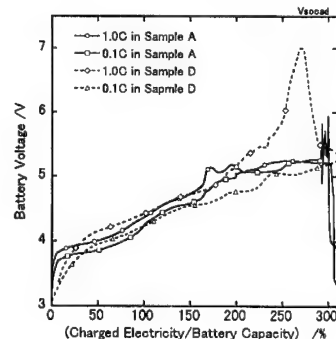


Fig. 3 Voltage variations in overcharging for different batteries and rates.

Charge-discharge cycle performance of lithium secondary batteries using hybrid carbon as negative electrode materials

K. Yanagida, A. Yanai, Y. Kida,
A. Funahashi, T. Nohma and I. Yonezu
New Materials Research Center, Sanyo Electric Co., Ltd.
1-1 Dainichi-higashimachi Moriguchi, Osaka, 570-8502,
Japan

Introduction

Recently, considerable attention has been given to the development of lithium secondary batteries for home-use load-leveling systems. These batteries require a much longer cycle life than those used for consumer electrical devices because they are designed for such long-term use as 10 years. Such a period implies a long cycle life of more than 3500 cycles. We have already reported the excellent charge-discharge cycle performance of lithium secondary batteries using $\text{LiNi}_{0.7}\text{Co}_{0.3}\text{O}_2$ as the positive electrode material and a mixture of graphite and coke (graphite-coke hybrid carbon) as the negative electrode material¹⁾.

In our previous work, it was found that a lithium secondary battery using a graphite-hard carbon hybrid carbon showed a higher discharge capacity and a better cycle performance than that using a graphite-coke hybrid carbon^{2), 3)}. In this work, the deterioration mechanism of graphite-hard carbon and that of graphite-coke hybrid carbon were investigated.

Experimental

The graphite-hard carbon or graphite-coke hybrid carbon was prepared by mixing natural graphite and hard carbon or coke. 2 Wh class cylindrical cells (14.2 mm in diameter and 50.0 mm in height) were fabricated by using the graphite-hard carbon or graphite-coke hybrid carbon as the negative electrode material and $\text{LiNi}_{0.7}\text{Co}_{0.3}\text{O}_2$ as the positive electrode material. The electrolyte was LiPF_6 of 1 mol/dm³ dissolved in a mixture of 50% ethylene carbonate (EC) and 50% diethyl carbonate (DEC) in volume ratio. In cycle tests, the cells were charged at a constant current of 220 mA to 385 mAh and discharged at a constant current of 220 mA to 2.7 V. In order to measure the entire discharge capacity, the cells were charged up to 4.2 V at a constant current of 80 mA and discharged to 2.7 V at a constant current of 70 mA at every 50 cycles.

Results and discussion

The graphite-hard carbon hybrid carbon (4/1 in weight ratio) exhibited a high discharge capacity of 371 Ah/kg. The 2 Wh class cells using the graphite-hard carbon hybrid carbon also exhibited a high specific energy of 120 Wh/kg, which was 5% higher than that of the cells using the graphite-coke hybrid carbon. As for the cycle performance, the 2 Wh class cells using the graphite-hard carbon hybrid carbon showed a discharge capacity of 76.6% at the 700th cycle compared with that at the initial state. These cells also had a slightly smaller deterioration rate in the discharge capacity than the cells using the graphite-coke hybrid carbon (Fig. 1).

In order to clarify the deterioration mechanism, hybrid carbon negative electrodes after charge-discharge cycle tests were analyzed by XPS. In the XPS spectra of O_{1s} and F_{1s} , there were peaks considered to be Li_2CO_3 and LiF (Fig. 2). The peak intensity of Li_2CO_3 grew stronger as the cycles increased. On the other hand, the change in peak intensity of LiF was smaller than that of Li_2CO_3 .

Therefore, it is assumed that LiF was produced by the decomposition of the solute mainly at the initial cycles and Li_2CO_3 was produced by the decomposition of the solvent during the cycles.

Furthermore, in order to measure the quantity of the decomposition products, hybrid carbon negative electrodes after charge-discharge cycle tests were analyzed by ^7Li NMR. In each negative electrode, there was a peak at 0 ppm that was attributed to inactive lithium in the decomposition products. We analyzed the rates of increase in the relative areas of the peak at 0 ppm to the peak indicating the lithium intercalated into the hybrid carbons during the cycles. Consequently, the rate of increase for the graphite-hard carbon hybrid carbon was found to be smaller than that for the graphite-coke hybrid carbon. It was therefore concluded that the graphite-hard carbon hybrid negative electrode suppressed the decomposition of the electrolyte and provided a better cycle performance than the graphite-coke hybrid carbon.

From these results, the graphite-hard carbon hybrid carbon is considered to be a promising negative electrode material for long-life lithium secondary batteries for load-leveling systems.

Acknowledgement

This work was supported by NEDO as a part of LIBES's R&D.

References

- 1) H. Kurokawa et al., Extended Abstracts of the 8th IMLB, p. 222 (1996).
- 2) A. Funahashi et al., Extended Abstracts of the 1999 ECS International Joint Meeting, Abstract No. 377 (1999).
- 3) K. Yanagida et al., Extended Abstracts of the 40th Battery Symposium in Japan, p. 1 (1999).

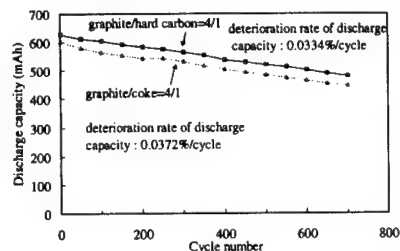


Fig. 1 Cycle performance of 2 Wh class cells using graphite-hard carbon and graphite-coke hybrid carbon.

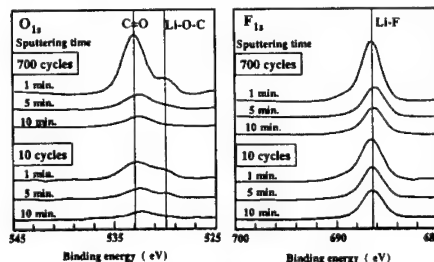


Fig. 2 XPS spectra of graphite-hard carbon hybrid carbon negative electrodes after charge-discharge cycle tests.

Cycle Life Estimation of Lithium Secondary Battery by Extrapolation Method and Accelerated Aging Test

K. Takei, K. Kumai, Y. Kobayashi, H. Miyashiro,
N. Terada, T. Iwahori and T. Tanaka
Central Research Institute of Electric Power Industry
(CRIEPI)

2-11-1 Iwado-kita, Komae-shi, Tokyo 201-8511, Japan
takei@criei.denken.or.jp

INTRODUCTION

Lithium secondary batteries for home-use load leveling systems are required to have long-cycle lives of 3500 cycles. This system is charged during the night for 5-8 hrs and discharged during the day for the same period. Therefore, time compression is an indispensable means to evaluate cycle lives of the batteries for a given period. In this study, two techniques were experimentally investigated in order to identify their applicability for the evaluation test. One was the extrapolation method that used limited data obtained from cycle operation under standard conditions. The other was the accelerated aging test involving five stress factors: charging rate, discharging rate, charging and discharging rate, depth-of-discharge (DOD) and static thermal stress.

EXPERIMENTAL

A commercialized cylindrical lithium ion cell of 1.25 Ah capacity (type US18650) from SONY was used as a typical sample. The standard operating condition is an 8-10 hr rate for both charging and discharging, and a DOD of 70 % from the fully charged state. The charging limit voltage was set at 4.2 V and charging methods of c.c.+c.v. and c.c. were compared. The discharging limit voltage was 2.5 V. The parameters of the rate accelerated test changed between 0.33 C and 1.0 C. The DOD was from 70 % to 100 % (fully discharged). All the operations, except for the static thermal test, were carried out at 25 °C. The temperature of thermal stress was set between 10 °C and 55 °C. A capacity test of full discharging at 8 hr rate was carried out every 50 cycles except in the static thermal stress test. Three cells were tested under the same conditions to elucidate the performance dispersion. Cycle tests were started in 1995 under 22 sets of conditions including 4 standard condition sets. The cycle life was judged from the cycle in which the discharge capacity dropped to 70 % of the initial capacity (0.875A) in the capacity test condition.

RESULTS AND DISCUSSION

1. Extrapolation method

The average cycle life under the standard conditions was approximately 2000 cycles. Discharge capacities under the capacity test condition almost linearly decreased. Cycle lives of 1700 cycles in c.c.+c.v. charging and 2200 cycles in c.c. charging were obtained. For understanding these phenomena, we carried out an additional cycle life tests of shallow DOD's with different voltage ranges. From these results, it was found that the operating voltage range played the important role in the cycle life of the cell. Above results can be explained to cause the difference in the period experienced the high voltage range over 4.0 V. Typical cycle performance under the standard condition is shown in Fig.1. The straight line extrapolated from the initial 500 cycles has been added. Based on this line, the cycle life was estimated to be 2200 cycles and this value has about 20% error against the experimental result.

2. Accelerated aging test

Accelerated coefficients against each of the accelerated factors are shown in Fig.2. These were calculated as the inverse ratio of the sustained periods against one of the standard conditions. Collectively, these tend to increase monotonously for all parameters. The thermal stress factor showed the most remarked acceleration of all factors and the charging rate factor was the second highest. On the other hand, DOD and the charging and discharging rate factors at 0.5 C were not effectively accelerated. In particular, in the latter case, the cycle life prolonged to twice that under the standard condition.

In evaluating the cycle life within limited periods, the accelerated condition fitted for the cell system should be selected, and both the extrapolation method and the accelerated aging test had better be conducted in parallel.

This work has been conducted as the partial R&D of LIBES under contract with NEDO for "New Sunshine Program" Japanese national project by AIST, MITI.

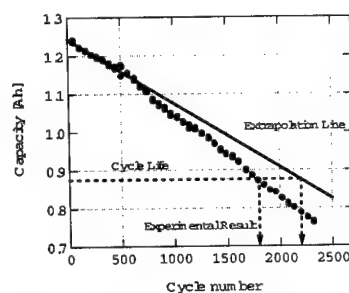


Fig.1 Typical cycle performance under standard conditions. Solid line represents the extrapolation from the initial 500cycles.

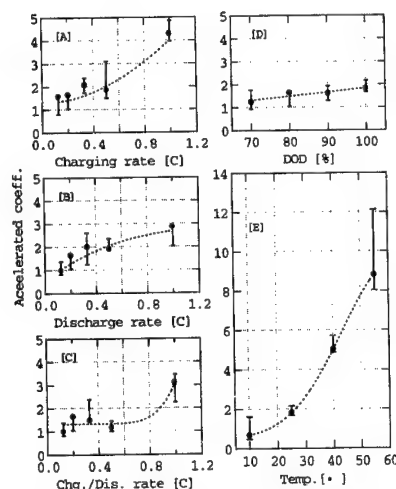


Fig.2 Accelerated coefficients of [A] charging rate, [B] discharging rate, [C] charging and discharging rate, [D] DOD and [E] the static thermal stress. Error bars represent the dispersion of the three cells.

**A new method to study Li-ion cell safety :
laser beam initiated reactions
on both charged negative and positive electrodes.**

J.P. Pères, F. Pertont*, C. Audry*, Ph. Biensan*,
G. Blanc** and M. Broussely***.*

*SAFT, 111 bvd Alfred Daney, 33074 Bordeaux,
FRANCE.

**CETHIL-INSA, 20, avenue Albert Einstein,
69621 Villeurbanne, FRANCE.

***SAFT, BP 1039, 86060 Poitiers, FRANCE.

A new tool to study Li-ion cell safety...

Safety of Li-ion cells is tightly linked to the unstability of charged positive and negative electrodes, in presence of liquid electrolyte. Many publications are relative to the evaluation of thermal stability of positive or negative materials by DSC experiments, or to the whole cell behavior during abusive tests at charged state. Not so much studies focusing on reactivity of whole single positive or negative electrodes have been reported so far.

The aim of this study is to evaluate the reactivity of a given positive or negative electrode, just recovered from dismantled Li-ion cells at charged state ($\geq 4.0V$ end charge voltage).

Different positive and negative electrodes definitions have been investigated. The nature of positive ($LiCoO_2$, doped $LiNiO_2$...) and negative (graphite, MCMB, carbons mixtures...) active materials is the main parameter which has been taken into account in the electrodes definitions.

The reactions between electrolyte and charged positive or negative electrodes have been initiated by a laser beam, having a monitored intensity and time pulse. From such a device, a strong and controlled heating can be generated, in a very short time scale, on a defined electrode surface area. This localized heating is supposed to be similar to that could occur from a cell internal short-circuit.

The behavior of electrodes under laser pulses has been followed by both video and IR camera. Very specific and different reaction propagation mechanisms have been observed in function of the laser power and of the positive or the negative electrode definitions.

On propagation phenomenon...

It has been possible to initiate self-propagation of reactions on both positive and negative electrodes from localized heating. Self-propagation is more easy to start on negative electrode. The differences between propagation mechanisms on negative and positive electrodes will be discussed in the paper.

On kinetics of reactions...

The kinetics of the involved propagation reactions speeds have been calculated from IR camera films. Results have been reported on Tables I and II for positive and negative electrodes respectively. Electrode ability to self-propagation has been linked to active material nature, electrode state of charge and laser power threshold (intensity, time, impact surface).

Correlation with other cell safety investigation techniques...

The obtained results have been compared to those of other safety investigation methods (DSC, ARC experiments). This new set of data has also allowed a better understanding of Li-ion cell abuse tolerance and an improvement of the ranking in thermal stability of charged negative and positive electrodes

Specific observations on positive electrode...

In addition to the known reactions between charged positive material and electrolyte, a highly energetic reaction has been identified and studied. It consists in an oxygen transfer between positive active material and aluminium collector. This very exothermic reaction occurs in the 700-900 °C temperature range and it must be taken into account to a better understanding of Li-ion cell behavior in abuse conditions.

Conclusion.

A new technique for a better understanding of Li-ion cell safety has been investigated. Useful and complementary results to those obtained from DSC and ARC experiments have been obtained and linked to Li-ion cell behaviour during abusive tests. Influence of the successive reactions kinetics on the overall process is particularly well evidenced.

Acknowledgements.

The authors wish to thank USABC for financial support.

Positive electrode (active material nature)	Pulse mode. Beam diameter [D=1 cm]		Total charged capacity mAh/g	Longitudinal kinetics
	I (mA)	t (ms)		
Type 1 $LiNi_{1-x}Co_xO_2$	10	300	180	0.68-0.74 cm/s Strong reaction.
Type 2 $LiCoO_2$	10	500	155	0.34 cm/s Localized reaction.
Type 3 $LiNi_{1-x-y}Co_xAl_yO_2$	10	300	180	0.58 cm/s Partial self-propagation.
Type 4 $LiNi_{1-x-y}Co_xAl_yO_2$	10	300	190	0.49-0.50 cm/s Partial self-propagation.
Type 5 New mixed oxide	10	1000	170	0.52-0.55 cm/s Auto- inhibition.

Table I

Positive electrodes reactivity ; propagation reaction kinetics.

Negative electrode (active material nature)	Pulse mode. Beam diameter [D=6 mm]		Total charged capacity mAh/g	Longitudinal kinetics
	I (mA)	t (ms)		
Type B (carbons mixture)	10	500	240	0.40 cm/s Partial self-propagation.
Type C (graphite)	10	300	270	1.20 cm/s Total self-propagation.

Table II

Negative electrodes reactivity ; propagation reaction kinetics.

Development of large-scale lithium secondary battery cell

*T. Akiyama, *T. Hashimoto, *H. Tajima,
K. Adachi and S. Taniguchi*Nagasaki R&D Center, Mitsubishi Heavy Industries,
Ltd.5-717-1, Fukahori-Machi, Nagasaki 851-0392, Japan
Kyusyu Electric Power Co., Inc.

2-1-47, Shiobaru, Minami-ku, Fukuoka 815-0032, Japan

Introduction

In recent years, expectation for the development of electric power storage devices such as power supply sources for electric vehicles or for load leveling has increasingly been intensified in recent issues including environmental issues such as air pollution or global warming and seasonal or daytime-to-nighttime differences in electricity demands.

Of them, the lithium secondary cell featuring its high operating voltage and its high energy density is regarded as the most promising candidate, and the research and development of large-scale lithium secondary cells are now actively in progress worldwide.

In commercialization for the above applications, such a secondary cell would require a high energy density and an extended cycle life exceeding 1000 cycles, an inexpensive cell cost and a high safety.

LiCoO_2 , LiNiO_2 and LiMn_2O_4 are known as cathode materials capable of discharging at 4V voltage and LiCoO_2 is most commonly used as the cathode material for the lithium secondary cell extensively available commercially. However, because cobalt is scarce in its resource and expensive, LiNiO_2 and LiMn_2O_4 can be promising as the cathode material for the large lithium secondary cell. Of them, LiMn_2O_4 in particular is rich in its resource and excellent in its thermal stability, and thus, it can be regarded as the best candidate for the cathode material for the large lithium secondary cell.

We have developed a 300Wh-class prismatic lithium secondary cell having an excellent energy density and cycle life by using LiMn_2O_4 for the cathode material and graphite for the anode material and its features are presented in this paper.

Experiment

The cathode was fabricated using lithium manganese as the cathode material, acetylene black as the conductive additive and PVdF as the binder. The anode was fabricated using graphite as the anode material and PVdF as the binder. Porous polypropylene films were used as the separator and 1mol/l LiPF_6 / ethylene carbonate (EC) + dimethyl carbonate (DMC) (1:2) was used as electrolyte. The cell size was 116mm in width, 175mm in height and 66.5mm in depth, and its weight was 2.64kg.

Charge / discharge cycle test was carried out at the C/8 rate, partial load operation of D.O.D.70%, and the capacity was confirmed every 50 cycles to calculate the deterioration rate.

Results

Fig.1 shows the discharge characteristics of 300Wh-class cell. Capacity of 77Ah and average discharge voltage of 3.9V were obtained. Specific energy and Energy density was 114Wh/kg and 222Wh/l respectively (Table 1).

Fig.2 shows the charge-discharge cycling efficiency of 300Wh-class cell. Cycling efficiency showed good stability throughout the cycling test.

Charge/discharge cycle test is still continuing, showing that over 70% of the initial capacity have been maintained after 500 cycles testing.

Table 1. Feature of 300Wh-class prismatic cell

Cathode	LiMn_2O_4	
Anode	Graphite	
Electrolyte	LiPF_6 / EC+DMC(1:2)	
Dimension	mm	116 ^W ×175 ^H ×66.5 ^D
Weight	kg	2.64
Volume		1.35
Average voltage	V	3.9
Capacity	Ah	77
Energy	Wh	300
Specific Energy	Wh/kg	114
Energy density	Wh/l	222

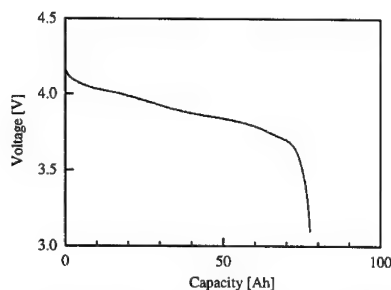


Fig. 1 Discharge characteristics of 300Wh-class prismatic cell

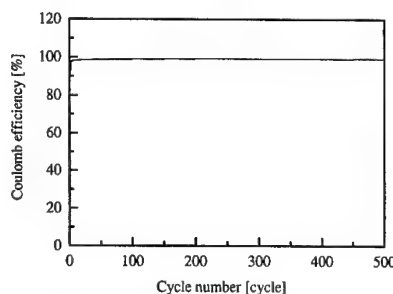


Fig. 2 Charge-discharge cycling efficiency of 300Wh-class prismatic cell

Effect of Iron Disulfide Structure and Nonaqueous Electrolyte Composition on the Characteristics of High-Energy Li-FeS₂ System

*E.M.Shembel, L.I.Neduzhko, O.V.Chervakov,
I.M.Maksyuta, K. Ye. Kylyvnyk and
Yu.V.Polyschuk*

*Ukrainian State Chemical Technology University,
Dnepropetrovsk*

E-mail: shembel@onil.dp.ua

*D.E.Reisner, T.D.Xiao
US Nanocorp, Inc. North Haven, CT, US.
E-mail: usnanocorp@aol.com*

This report is a continuation and development of the results presented previously concerning the development of a high-energy lithium battery based on Li-FeS₂ system operational at room temperature. Lithium system based on pyrite has well shown itself in primary cells. It has some significant advantages: high weight specific characteristics peculiar to sulfide systems, conditioned by a high density of pyrite, low self-discharge at a storage and during interruptions, environmentally friendly cathode materials. Application of polymer electrolyte based on chlorinated polyvinyl chloride and nanostructured FeS₂, prepared by a special method has permitted to produce a high efficient electrochemical system having reversible cycleability at room temperature.

In this work the investigation results of the synthesis conditions of iron disulfide influenced upon its structural and macrostructural characteristics are presented. As a consequence, the synthesis conditions of iron disulfide affect the efficiency of electrochemical redox processes in liquid and polymer electrolytes. Characteristics of natural pyrite, nanostructural FeS₂ and thermal sprayed films of FeS₂ were compared. The diffusion coefficients of lithium ions in a solid phase of different samples of iron disulfide have been measured. The characteristic properties of the kinetics of electrochemical processes on nanostructured materials have been studied.

The modification methods of polymer electrolyte aimed to increasing its conductivity at room and low temperatures have been developed. The influence of the amorphization degree of an initial polymer structure has been shown. The ways for controlling the amorphization degree of initial polymer and polymer electrolyte as a whole have been developed. Thermal stability of the system pyrite-polymer electrolyte has been studied. Additives to polymer electrolyte increasing the stability of Li-FeS₂ system have been substantiated and synthesized.

In the figures presented the cycling galvanostatic characteristics of the actual samples of

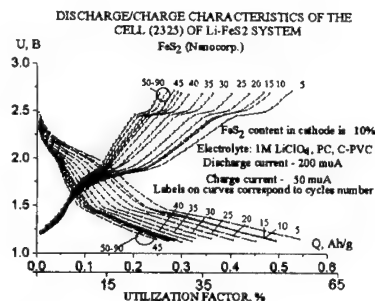
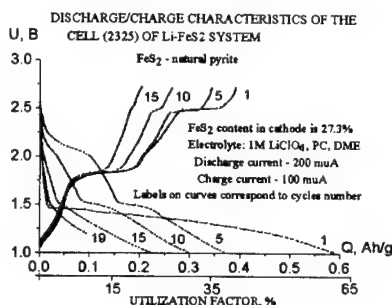
disk lithium cells (size 2325) Li-FeS₂ with liquid and polymer electrolytes have been compared. It is clear, that with the use of nanostructured pyrite synthesized by a special method and the polymer electrolyte based on modified chlorinated polyvinyl chloride the system Li-FeS₂ is cycling reversibly at room temperature with a high efficiency.

The performed developments, investigations and test show the prospects of the new type of high-energy lithium secondary battery, operational at room temperature.

The elaborations continue in the direction of increasing the utilization factor of pyrite at cycling. The results obtained are used for the optimization of the synthesis conditions of cathode material, cathode macrostructure, the composition of polymer electrolyte, stabilizing additives, production technology of lithium cells and cycling conditions.

Acknowledgements

This work was supported the CRDF Project #USB-384.



Reference

1. E.M.Shembel, L.I.Neduzhko, O.V.Chervakov, K.Ye.Kilyvnyk, I.M.Maksyuta, Yu.V.Polyschuk, H.Ye, T.D.Xiao, and D.E.Reisner. The 195th Meeting of the Electrochemical Society, Inc., May 2-6, 1999, Seattle, USA.
2. E.M.Shembel, O.V.Chervakov, N.I.Globa, D.T.Meshri, D.E.Reisner, T.Danny Xiao, L.R.Vishnyakov, V.A.Kokhany. 13th IBA Marrakesh Symposium, Nov. 7-11, 1999, Morocco.

**SAFETY AND PERFORMANCE OF IN-SERVICE
LITHIUM-SULPHUR DIOXIDE
BATTERIES**

Ian R. Hill, Ed E. Andrukaitis and Giulio L. Torlone,
Defence Research and Development Branch,
National Defence Headquarters,
305 Rideau Street, Ottawa, Ontario K1A 0K2,
Canada

Lithium-sulphur dioxide portable batteries (Li/SO₂, nominal cell OCV 3.0V) have been in extensive use with the Canadian Forces, and with the military of many other countries, for approximately 15 years. This medium-rate, non-rechargeable system is used in communications equipment and high-tech portable gadgets, such as a mass spectrograph for detecting poisonous gases in the battlefield. In recent years, there has been increased use of rechargeable batteries, for economic and environmental reasons. However, the available rechargeable batteries cannot match the low temperature performance of Li/SO₂, which has good performance at -40°C and acceptable performance at -50°C for lower rate applications. Because Canada has a cold climate, good performance at -40°C is an imperative. Alternative, safe, spirally wound primary couples, such as Li/MnO₂, do not support as high currents.

Li/SO₂ is perceived as dangerous by some people, because the steel can is pressurised and SO₂ is toxic. However, in service, very few incidents occur and many of these can be attributed to misuse (such as charging). Nevertheless, cells do infrequently vent violently (explode) during use and it is important to try and identify the mechanism, because the safety of personnel is involved. Usually, though, the evidence is destroyed during the explosion.

There has been an increased incidence of violent ventings since batteries, such as the BA5590 (15/30V, two 5-cell strings of D-size cells) and BA5800 (6V, two D-size cells), were fitted with a complete discharge device (CDD). The CDD is used to eliminate all of the metallic lithium from the cell by using a very low rate discharge. Although this device makes the batteries safe from the point of view of hazardous waste, a problematic cell may make the battery hazardous for the CDD user. This is likely during the early stages of the complete discharge, when there is sufficient energy in all

of the cells to melt lithium in the event of an internal short circuit.

Results will be presented from the autopsy of a BA5590 battery that had exploded whilst undergoing complete discharge. It was discovered that lithium metal had been deposited in the area of the glass-to-metal seal. Complete discharging of other batteries has been carried out in order to determine whether BA5590 batteries generally pose a hazard during the early stages of complete discharging.

Another problem with Li/SO₂ batteries is voltage delay at low temperatures. In fact, voltage delay is also a problem with other lithium couples, to a greater or lesser extent. In lithium metal-based couples, voltage delay is caused by the passivating layer on the Li, whilst for lithium-ion systems, it is the passive film on the carbon anode. Voltage delay can be particularly a problem when multi-cell strings are being discharged in parallel. In this case, the passivating layer on the lithium electrodes of the cells in one string may break down before those in another string, resulting in unevenly distributed currents. This could result in the electrical fuse for that string being blown, but certainly a big loss in discharge time, especially for higher rates.

Several communications radios use two BA5590 batteries in parallel, being operated at either 15V or 30V. Consequently, studies have been made on a variety of combinations of two BA5590 batteries of various dates -of-manufacture, using four parallel strings of 15V. The data showed that it is important to use matched batteries in parallel, from the point of view of efficient discharging, although no safety-related problems were encountered.

Fabrication of Dye-Sensitized Solar Cells
by the Spray Pyrolysis Deposition (SPD) Technique
Masayuki Okuya, Koji Nakade,
and Shoji Kaneko
Department of Materials Science and Technology,
Shizuoka University
3-5-1 Johoku, Hamamatsu 432-8561, JAPAN

INTRODUCTION

Recent global environmental problems require rapid progress of high performance solar cells as a clean energy source. A dye-sensitized solar cell is one of the most promising ones, since the photovoltaic system is quite simple. In order to produce the cell in a practical use, an industrial new electrode production technique should be developed. We adopt the spray pyrolysis deposition (SPD) technique that we have developed, since the technique is applicable to the electrode manufacture on a large scale.

EXPERIMENTAL

The schematic representation of the SPD apparatus is shown in Fig.1. TiO_2 films were synthesized from 0.1 M of $(\text{CH}_3\text{COCHCOCH}_3)_2\text{TiO}$ 2-butanol solution with 0.1% of $(\text{CH}_3\text{COCHCOCH}_3)_3\text{Al}$ or $\text{H}_2\text{PtCl}_6 \cdot 6\text{H}_2\text{O}$. The procedure in producing both transparent F-doped SnO_2 film and TiO_2 layer on glass substrates is described elsewhere[1-3]. The electrodes were then produced within a few hours by this technique. The crystal structure and the surface morphology of films were observed by XRD and SEM, respectively. The cell was fabricated utilizing dye-adsorbed TiO_2 layer on the transparent F-doped SnO_2 film as a working electrode, platinum coated glass as a counter electrode, and $(\text{C}_2\text{H}_5)_2\text{NI/I}_2$ in ethylene carbonate/propylene carbonate solution as an electrolyte.

RESULTS AND DISCUSSION

The XRD patterns of the obtained film showed anatase TiO_2 single phase at the substrate temperature above 450°C . The SEM images of the surface morphology of the films are shown in Fig.2. The film from the solution without any additives was consisted of a few hundreds of nanometer-sized particles due to the aggregation. On the other hand, the films from the solution with $(\text{CH}_3\text{COCHCOCH}_3)_3\text{Al}$ or $\text{H}_2\text{PtCl}_6 \cdot 6\text{H}_2\text{O}$ as additives were both consisted of needles of approximately 100 nm in length and 10 nm in width. The average transmittance of a typical film with the thickness of 10 μm was approximately 40% in the visible light region.

The current-voltage characteristic measurements of cells were done under AM-1.5 and 100 mW/cm^2 illumination. The light to current conversion efficiency was enhanced as high as 2.0% by adding a small amount of $(\text{CH}_3\text{COCHCOCH}_3)_3\text{Al}$ in the electrode due to the increase of the surface area of TiO_2 layer. Although the surface area was increased and then the short circuit current was enhanced by adding $\text{H}_2\text{PtCl}_6 \cdot 6\text{H}_2\text{O}$, the efficiency was as low as 0.5% due to the low fill factor and low open circuit voltage. Further improvement of the electrode is necessary to achieve the higher conversion efficiency for a practical use.

REFERENCES

- [1]K.Murakami *et al.*, *J.Am.Ceram.Soc.*, **79**, 2557 (1996).
- [2]M.Okuya *et al.*, *J.Euro.Ceram.Soc.*, **19**, 903 (1999).
- [3]M.Okuya *et al.*, *Ceram.Trans.*, in press.

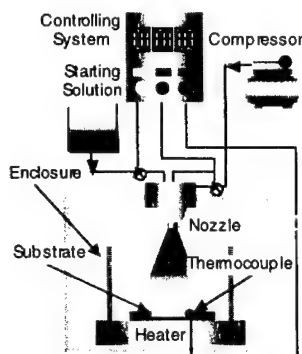


Fig.1 Schematic representation of the SPD apparatus. The film fabrication conditions are 1.25 $\text{ml/s} \times 0.5 \times 70$ at the substrate temperature of 510°C and 1.0 $\text{ml/s} \times 0.5 \times 500 \sim 1000$ at $450 \sim 500^\circ\text{C}$ for transparent F-doped SnO_2 and TiO_2 , respectively.

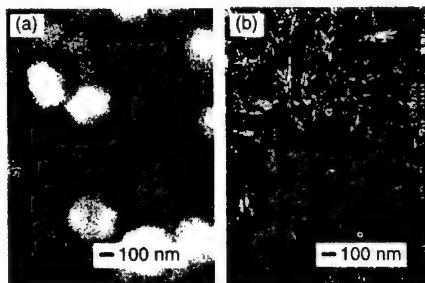


Fig.2 SEM images of the surface morphology of TiO_2 films deposited at the substrate temperature of 500°C with compressed air from 0.1 M of $(\text{CH}_3\text{COCHCOCH}_3)_2\text{TiO}$ 2-butanol solution with (a)no additives and with (b)0.1% of $(\text{CH}_3\text{COCHCOCH}_3)_3\text{Al}$.

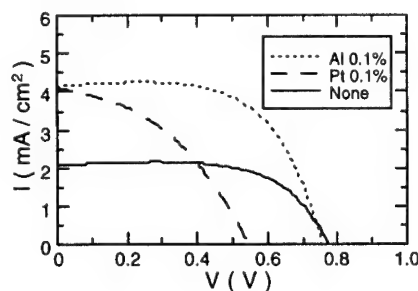


Fig.3 Typical current-voltage characteristics of the dye-sensitized solar cells with various electrodes fabricated by the SPD technique. The measurement was carried out under AM-1.5 and 100 mW/cm^2 illumination.

High Temperature Characteristics of Lithium Ion Batteries Using Spinel Lithium Manganese Oxides as the Cathode

Hiroshi Watanabe, Naoki Imachi, Keiji Saishou
and Satoshi Narukawa

Soft Energy Technology Development Center
Soft Energy Company, Sanyo Electric Co., Ltd.
222-1, Kaminaizen, Sumoto, Hyogo 656-8555, Japan

INTRODUCTION

Spinel lithium manganese oxide (LiMn_2O_4) is known as one of the promising cathode material for lithium secondary battery. But, this material has some problems concerning capacity and electrochemical stability at high temperature. Many works about this material have focused on the improvement of cycling performance of battery at high temperature. These results mentioned an effectiveness of Mn replacement with other element like Li, Cr, Co, and the like, on the cycling performances [1,2]. However, in storage test of battery using spinel lithium manganese oxide as the cathode and graphite as the anode at 60°C , we could not find the effect of replacement because large amount of gases were generated after storage. In order to improve a storage characteristics of lithium manganese oxide, mixed active materials of it with lithium cobalt oxide (LiCoO_2) and lithium nickel oxide (LiNiO_2) were investigated [3].

EXPERIMENTAL

As the cathode active materials, spinel manganese oxides, $\text{LiMn}_{2-x}\text{M}_x\text{O}_4$ ($\text{M}=\text{Li, Mg and Al}$), were used. LiCoO_2 and $\text{LiNi}_{0.8}\text{Co}_{0.2}\text{O}_2$ also used by mixing with $\text{LiMn}_{2-x}\text{M}_x\text{O}_4$. The slurry of these active materials mixed with carbon black and PVdF was coated on aluminum foil as the cathode sheet. Graphite coated on copper foil was used as the anode and 1M LiPF_6 EC/DEC (3/7) was used as electrolyte. Aluminum laminated film was used as battery case and test batteries with capacity of about 500mAh were constructed. The cell size was about $47 \times 40^w \times 80^h$ (mm). Charge-discharge test was carried out at the current of 500mA between 4.2V and 3.0V. Storage condition was 20 days at 60°C after charging or discharging.

RESULTS AND DISCUSSION

Table 1 shows the storage characteristics of the batteries using $\text{LiMn}_{2-x}\text{M}_x\text{O}_4$ ($\text{M}=\text{Li, Mg and Al}$) as the cathode active materials. Rather large increase of battery thickness was observed in storing both after charging and discharging. This trend was not so affected by the composition of manganese oxides. It was thought that increase of thickness was caused by generation of gaseous products due to a decomposition of electrolyte. Although a large swelling more than 30% was observed after storage at discharged state, capacity deterioration was smaller than that at charged state, so it seemed that deterioration of active material itself was not so hard in this case.

We thought that remarkable swelling of the battery in storing after discharge using lithium manganese oxide was induced by instability of crystal structure of lithium manganese oxide, especially at the end stage of discharge [4]. To stabilize the lithium manganese oxide near cutting-off voltage, we examined about mixed active materials of lithium manganese oxide with lithium cobalt oxide or lithium nickel oxide. It was expected that mixing

with lithium cobalt oxide or lithium nickel prevented lithium manganese oxide from radical decrease of the cathode potential because discharge potential of lithium cobalt oxide and lithium nickel oxide are lower than that of lithium manganese oxide. Particularly, lithium manganese oxide mixed with lithium cobalt oxide showed good storage characteristics and cycling performance (Fig.1) even if at 60°C . More detail results concerning an influence of lithium cobalt oxide on high temperature characteristics of battery will be reported.

REFERENCES

- [1] J. M. Tarascon, W. R. McKinnon, F. Coowar, T. N. Bowmer, G. Amatucci and D. Guyomard, *J. Electrochem. Soc.*, **141**, 1421(1994)
- [2] Li Guohua, H. Ikuta, T. Uchida and M. Wakihara, *J. Electrochem. Soc.*, **143**, 178(1996)
- [3] N. Imachi, K. Saishou, S. Nakamizo, H. Watanabe and S. Narukawa, The 40th Battery Symposium in Japan, Abstract No. 2C12, 297-298(1999)
- [4] T. Inoue and M. Sano, *J. Electrochem. Soc.*, **145**, 3674(1998)

Table 1 Storage characteristics of lithium ion batteries using $\text{LiMn}_{2-x}\text{M}_x\text{O}_4$ ($\text{M}=\text{Li, Mg and Al}$) as the cathode for 20 days at 60°C , which stored at (a) charged state and (b) discharged state ((Li+M)/Mn=0.59, 0.66 and 0.57, respectively).

(a) Charged state (4.2V cut off)				
	M	Li	Mg	Al
Rate of swelling (%)		17	17	17
Rate of capacity residual / retention (%)		63 / 72	65 / 73	66 / 76

(b) Discharged state (3.0V cut off)				
	M	Li	Mg	Al
Rate of swelling (%)		32	30	31
Rate of retention capacity (%)		92	93	93

*each rate means the relative value to the initial value

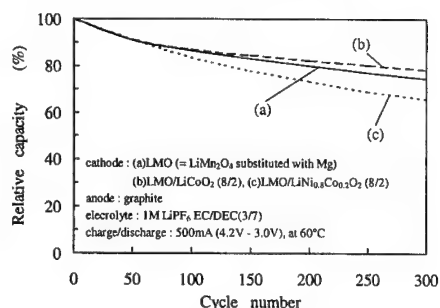


Fig.1 Cycle performance of lithium ion batteries using spinel lithium manganese oxide and its mixture with lithium cobalt oxide or lithium nickel oxide as the cathode at 60°C .

Li-Ion Cells using a New High Capacity Cathode

Y. Grincourt, C. Storey, I. J. Davidson, P.S. Whitfield, I. Kargina, & H. Sleg
*Institute for Chemical Process and Environmental
 Technology, National Research Council,
 Ottawa, Ontario, K1A 0R6, Canada*

ABSTRACT

There is a continuing demand for new alternative intercalation compounds suitable for use as positive electrodes in lithium ion batteries. Such compounds must combine large charge storage capacity, good reversibility at high to moderate current densities, low cost, a high degree of safety and absence of toxicity. Usually, an operating voltage near 3.5 V is desirable. The structure of the cathode material should remain stable while cycling. Recently, we have succeeded in preparing a series of new cathode materials displaying competitive capacities with reasonably good cycling stability at moderate current densities (1). These materials appear to be possible alternatives to LiCoO_2 , LiMn_2O_4 and $\text{LiNi}_{0.8}\text{Co}_{0.2}\text{O}_2$ for lithium ion cell cathodes. This paper will discuss the electrochemical characterization of these new compounds in lithium-ion and lithium half-cells under a range of operating conditions.

As a first step, the materials were evaluated in coin cells (2325 format) with lithium metal anodes. As shown in figures 1 and 2, capacities between 200 and 140 mAh/g were obtained at current densities of 10 and 30 mA/g, respectively. The materials were then evaluated in lithium ion cells with carbonaceous anodes based on materials such as mesocarbon microbeads (MCMB 25-28). The capacity retention of microbead anodes in half-cells with metallic lithium counter electrodes are shown in figures 1 and 2 for cells cycled between 0.005 and 2 volts at 10 and 30 mA/g.

Lithium ion cells combining the new cathode materials with mesocarbon microbead anodes were assembled in coin cells. Figure 3 shows the voltage profiles for the first five cycles of a lithium ion cell containing the new cathode material. The cycling of a lithium ion cell between 2.5 and 4.5 volts at current densities varying from 10 to 30 mA/g is shown in figure 4. The lithium ion cell demonstrated quite good reversibility and capacities as high as 160 mAh/g at low rates. Further improvement in the higher rate performance is required.

REFERENCES:

- (1) C. Storey, I. Kargina, Y. Grincourt, I.J. Davidson, Y. Yoo and D. Y. Seung, paper contributed to this conference.

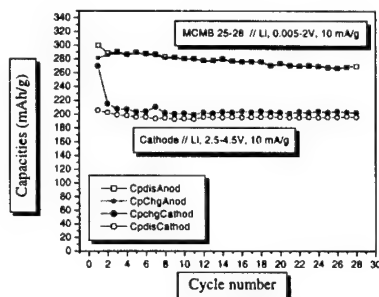


Fig. 1 Capacity retention plots of MCMB 25-28 and new cathode material versus Li at 10 mA/g.

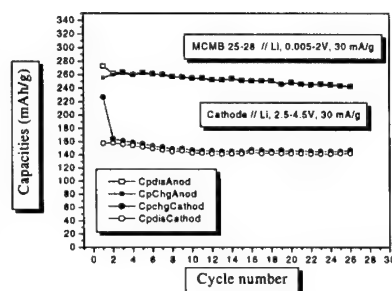


Fig. 2 Capacity retention plots of MCMB 25-28 and new cathode material versus Li at 30 mA/g.

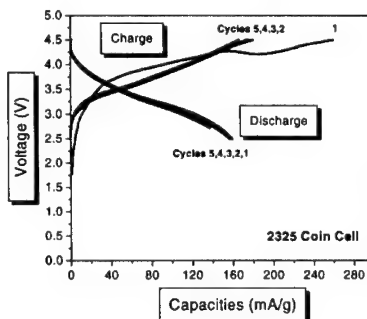


Fig. 3 Voltage profiles for the first five cycles of a Li-ion cell, MCMB 25-28 // cathode, at 10 mA/g.

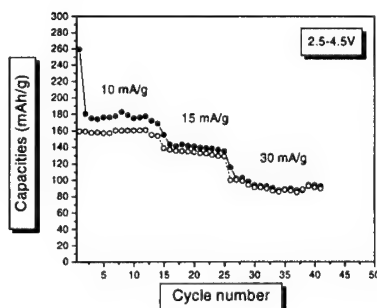


Fig. 4 Plot of capacity retention for a Li-ion cell MCMB 25-28 // cathode at : 10, 20, and 30 mA/g .

Thermal Analysis of a 40-Ah Lithium-ion Cell

H. Vaidyanathan
COMSAT Laboratories
Clarksburg, MD 20871 USA
and

G. M. Rao
NASA-Goddard Space Flight Center
Greenbelt, MD 20771 USA

NASA has successfully used 50-Ah nickel-cadmium (NiCd) and nickel-hydrogen (NiH₂) batteries for low-earth-orbit (LEO) applications. It is noteworthy that a lithium-ion (Li-ion) battery of similar ampere-hour size could reduce battery weight by about one-third compared with both NiCd and NiH₂ batteries. Also, in view of the interdependence of temperature and performance, the thermal behavior of batteries is of paramount importance in battery design, in-orbit battery management, and extending mission life. This study was conducted to determine the specific thermal capacity, heat generation rates during charge and discharge, and thermoneutral potential of an aerospace-type 40-Ah Li-ion cell. The test cell was a hermetically sealed cylindrical cell of 254 mm length and 54 mm diameter, consisting of a welded stainless steel container with a glass-to-metal seal for the positive terminal.

The cell was first characterized for capacity and self-discharge. It yielded a capacity of 33.4 Ah at 25°C, with a mid-discharge potential of 3.54 V when discharged at C rate. A radiative calorimeter was used to determine the specific thermal capacity and rate of heat dissipation during charge and discharge (1). The specific thermal capacity was 1,231 J/°C.

At C rate of discharge, the average heat dissipated was 8 W, and the maximum at the end of discharge at 2.75 V was 17.7 W. A plot relating the rate of heat dissipation to the state of charge during discharge at 40-, 20-, and 8-A rates exhibited waviness, as shown in Figure 1. The heat dissipation rate increased rapidly toward the end of discharge, and the increase was very large at the C rate of discharge. (The expected behavior was a gradual increase in the heat rate as discharge continued, followed by a rapid rise toward the end of discharge.) Waviness in the heat dissipation profile has also been reported by Hong *et al.* (2), and appears to be related to the changes in enthalpy of the cathode active material.

The average heat dissipated during constant-voltage charge at 4 V, with an initial current of 20 A and tapered current of 0.1 A, was lower than that obtained during constant-current charge at 20 A to 4 V, as presented in Table 1. Heat dissipation rates at various rates of charge and discharge are also recorded in the table. A notable feature of the heat rate profile obtained during charge was the absence of the initial spike that is generally attributable to the decomposition of the electrolyte (3).

The reactions at the cathode are believed to be more significant than those at the anode with regard to heat dissipation. The thermoneutral potential was found to vary with the state of charge, and an average value of 3.67 V was obtained.

REFERENCES

1. H. Vaidyanathan and G. M. Rao, *J. Power Sources*, **52**, 223 (1994).
2. J.-S. Hong, H. Maleki, S. Al Hallaj, L. Redey, and J. R. Selman, *J. Electrochem. Soc.*, **145**, 1489 (1998).
3. H. Vaidyanathan and G. M. Rao, paper presented at the Fall 1999 ECS Meeting, Extended Abstract No. 384, Honolulu, Hawaii, October 1999.

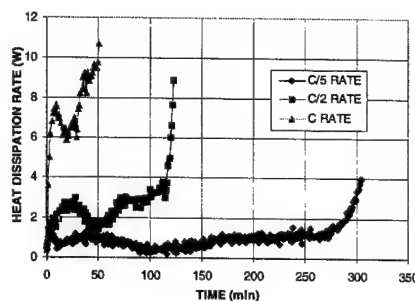


Figure 1. Heat Dissipation Rates at Various Rates of Discharge

Table 1. Heat Dissipation Data

Item	Max. Heat Rate (W)	Average Heat (W)
Charge		
C/5 (8 A) at 0°C	1.98	1.41
C/5 at 10°C	2.07	1.27
C/5 at 25°C	1.744	1.214
4 V Const. Max 20 A	4.82	2.42
15 A at 25°C	3.39	2.42
C/2 (20 A) at 25°C	4.981	3.51
Discharge		
C/5 (8 A) at 0°C	6.01	1.22
C/5 at 10°C	4.31	0.99
C/5 at 25°C	3.96	0.99
C/2 (20 A) at 25°C	10.07	2.67
C/2 (20 A) after 4 V Chg	8.81	2.64
C (40 A) at 25°C	17.70	7.99

Overview of ENEA's Projects on lithium batteries

F. Alessandrini, M. Conte, S. Passerini, P. P. Prosini
 ENEA, Advanced Energy Technology Division
 C. R. Casaccia, Via Anguillarese 301
 00060 Roma (Italy)

Since mid-80's ENEA, the Italian National Agency for New Technology, Energy and the Environment has been promoting research and development (R&D) programs on innovative and advanced batteries with improved performances (specific power and energy, cyclability, low maintenance and environmental impacts) and costs. According to its institutional role, ENEA has been working with research institutions and industries through cost-shared contracts, also on behalf of Ministries. At beginning of 1990's a research-oriented exploratory program was concluded, during which various batteries were analyzed and some proprietary results were obtained, particularly on innovative designs of lead-acid batteries and on novel polymer electrolyte with ceramic additives for lithium-metal batteries. Based on those interesting results and thanks to Program Agreements with some Ministries, new activities on lithium batteries were defined and started. This paper gives an overview of the major achievements of the recently concluded ALPE Project and two recently started MURST projects.

The ALPE Project. In the framework of a Program Agreement with the Ministry of Industry, ENEA started in 1994 the first national integrated project on lithium-metal batteries with polymeric components. The project, named ALPE (Accumulatori al Litio Per Elettrolizzazione), involved, along with ENEA, two scientifically advanced Universities (Bologna and Rome) and an industry (Arcotronics Italia), leader in equipment production. The goal of the first phase of ALPE Project, completed in 1999, has been the R&D of innovative materials and processes for lithium-metal batteries aimed at electric vehicle applications. The technical objectives of this phase of the project have been of precompetitive nature: good energy performance, acceptable cyclability, limited self-discharge, low-cost and environmentally benign materials and processes (1). The construction of planar cells and small-scale modules (of about 1 kWh) have been then used to verify the technologies and the concepts. Figure 1 shows the structure and the roles of the participants. The cell is basically composed by a lithium-metal anode on a copper current collector, a polymer electrolyte (including a lithium salt, PEO and ceramic fillers) and a composite cathode (mainly made of manganese-based insertion compounds) on an aluminum current collector. The cell works at a temperature of about 90 °C. Various classes of electrolytes and cathode materials have been investigated and developed with the main scope to have solvent-free processes and high performances. The final cell design is of double-anode type: a cathode is inserted between two anodes and separated by polymer electrolytes. The built pilot line starts from an extrusion phase for both cathodic and electrolytic films, a calendaring and then a lamination phase. Furthermore, a large dry room has been built at ENEA Casaccia Research Center. A stack of 10 unit cells is then assembled by parallel connection with ultrasonic welding. A final "softpack" is then produced inserting the stack in a soft envelope thermally welded (2). Chief achievements of the project are: a good selection of solvent-free electrolytes with ionic conductivity interesting also for lithium-ion batteries; an optimal behavior of the anode- polymer electrolyte interface with

an efficiency of lithium insertion and stripping exceeding sometimes 98% (3); an easy-to-built design with limited environmental impact during production and use; a flexible pilot line for small scale production of cells and "softpack. Some technical barriers still remain to be overcome: cathode capacity fading with limited cyclability, engineering of the module to control and manage thermal and safety aspects.

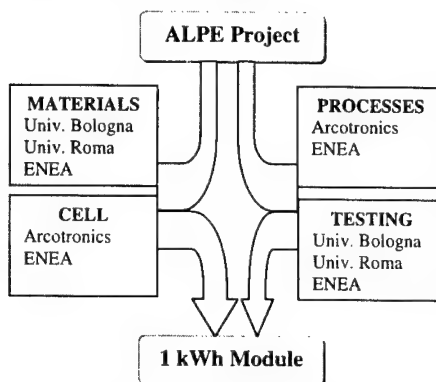


Figure 1. ALPE Project structure and main R&D tasks.

MURST Projects. Two new product-oriented projects on lithium batteries have been defined in 1998 and officially started in September 1999. Both projects are partially funded by the Ministry of Research and are regulated by a Program Agreement between such Ministry and ENEA. These projects are aimed to stimulate the collaboration between public research organizations and private institutions in order to favor the fast introduction of high-risk technologies. The first project is named "Rechargeable lithium batteries with polymeric components for consumer products" and is aimed at developing plastic-like polymer electrolyte lithium-ion (PLI) batteries in planar configurations. The technical objectives of the project are to research and develop pre-industrial prototypes with more than 110 Wh/kg (250 Wh/L) at about 4 V and a cycle life in excess of 500 cycles. Apart from ENEA, 12 public and private organizations are involved in the projects, combining large experience in lithium battery electrochemistry, materials development, thin film preparation with a variety of processes, and cell design and construction. The second project, called "Lithium Batteries with polymeric components for road electric vehicles", corresponds to the second phase of the ALPE project. In fact, the polymer lithium metal system will be further improved in terms of performances and usability. The goal is to improve specific performances of the systems of more than 20% with respect to the first phase and then to optimize the module technology introducing thermal and safety management systems in a fully monitored case.

REFERENCES

1. S. Saguatti et alii, in International Conference on Applications of Conducting Polymers/1997, B. Scrosati and O. Yamamoto, Editors, p. 160 (1997).
2. M.L. Borghini et alii, AEI, 85-3, 62, 1998.
3. P.P. Prosini, S. Passerini, R. Vellone and W. H. Smyrl, J. Power Sources, 75, 73 (1998).

Abstract No. 348

Properties of explosively compacted Li-ion battery components

M.J.G. Jak, N. Van Landschoot, E.M. Kelder, and J. Schoonman

Delft Interfaculty Research Center: Renewable Energy
Laboratory for Inorganic Chemistry
Delft University of Technology
The Netherlands

INTRODUCTION:

The use of thermally instable solid materials is a major problem for densification using elevated temperatures since reactions and undesired particle coarsening may occur. However, another way of increasing the density of these solids without a substantial temperature increase is by using high pressure pulses, also referred to as dynamic compaction. The high pressure pulses can be generated by using explosives or magnetic pulses. Here we focus on the use of explosive compaction resulting in high densities and improved material properties.

EXPERIMENTAL:

The ceramic electrolyte Li-doped BPO₄ [1,2] as well as the cathode material LiMn₂O₄ were compacted by using explosives. The Li-doped BPO₄ is a nano-structured powder material with a primary particle size of about 25 nm. The use of elevated temperatures (>300°C) result in massive grain growth causing a huge decrease of the total ionic conductivity. The materials were compacted by using an uniaxial setup. The explosives were placed on top of a dye filled with the to be compacted powder. The powders were pre-pressed in the dye. The generated pressure has been increased by increasing the explosive's density. Fig. 1 shows the pressure acting on the to be compacted powder. Pressures up to 50 GPa and a pulse duration of a few microseconds have been achieved.

RESULTS:

The relative densities of the Li-doped BPO₄ and LiMn₂O₄ powders were determined as a function of the applied pressure (Figs. 2 and 3). A maximum density of 86.6% has been found at a pressure 30 GPa for the Li-doped BPO₄, while a density of even 93.4% has been measured for the LiMn₂O₄. The compacted materials were not subjected to a heat-treatment after compaction.

From previous work [3] it is known that the ionic conductivity of the Li-doped BPO₄ material increases with up to three orders of magnitude when using explosive compaction instead of hot pressing due to the absence of grain growth. An increased electronic conductivity has been measured for explosively compacted LiMn₂O₄.

In this paper the specific capacity, electronic and ionic conductivity of LiMn₂O₄ will be reported as a function of the compaction pressure. The ionic conductivity of Li-doped BPO₄ as a function of the applied pressure will be reported as well.

REFERENCES:

- [1] M.J.G. Jak, "Dynamic compaction of Li-ion battery components and batteries" Ph.D.-Thesis, Delft University of Technology, The Netherlands, 1999.
- [2] E.M. Kelder, M.J.G. Jak, F. de Lange, and J. Schoonman, *Solid State Ionics* **85** (1996), 285.
- [3] M.J.G. Jak, E.M. Kelder, N.M. van der Pers, A. Weisenburger, and J. Schoonman, *J. of Electroceramics* **2** (1998), 127.

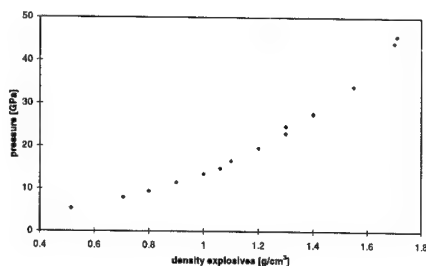


Figure 1: Pressure as a function of the explosive density.

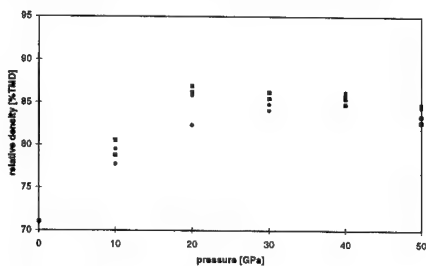


Figure 2: Final relative density of Li-doped BPO₄ as a function of pressure (squares=open setup, circles=closed setup).

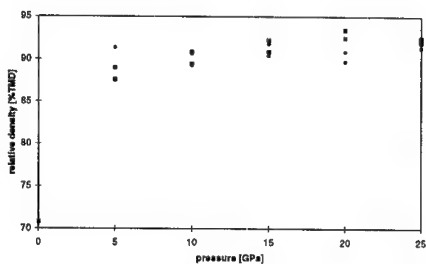


Figure 3: Final relative density of LiMn₂O₄ as a function of pressure (squares=open setup, circles=closed setup).

Abstract No. 349

A NEW PVDF BINDER FOR LI-ION BATTERIES

B. Barrière

Elf Atochem S.A. - CERDATO - F 27470

Serquigny – France

e-mail : benoit.barriere@cerd.elf-atochem.fr

In the manufacturing process of a Li-ion cell, the choice of the polymer used to bind the active materials at the anode and cathode is of critical importance for the final performance of the battery. Amid all kinds of polymers, polyvinylidene fluoride (PVDF) is now widely accepted as a material of choice for this purpose given its excellent chemical, thermal and electrochemical stability as well as its ease of processing.

Among the key properties of a binder, it must 1- have a good solubility in solvents that can be handled industrially (acetone, NMP etc...), 2- show enough adhesion to the metallic collector in order to prevent delamination phenomena during the charge and discharge cycles of the battery, 3- bring enough cohesion between active material particles (graphite or lithium metal salts) so that the electrode can be handled without occurrence of cracking 4- show a good initial efficiency at first cycle and be stable during the charge and discharge cycles of the battery.

In the first part of this presentation, we show how such key properties are controlled by the intrinsic parameters of the PVDF polymer like molecular weight, crystallinity or chemical functionality. As an example, the dissolution behavior is essentially governed by the amount of crystallinity of the polymer (in other terms, by its melting point) whereas adhesion or cohesion forces are mainly governed by the molecular weight and the chemical functionality. Such intrinsic parameters can be adjusted during the polymerization process, *e.g.* the chain length can be varied, comonomers like hexafluoropropene can be added in various ways and eventually some monomers can be functionalized with polar groups. As the world leader PVDF manufacturer, Elf Atochem has developed a wide range of PVDF resins that can answer the various needs of battery manufacturers.

In the second part of this presentation, we introduce a new binder which is specifically designed for Li-ion batteries, a high molecular

weight PVDF homopolymer functionalized in a small amount with polar groups. When used in an anode or a cathode, this binder leads to higher adhesion and cohesion forces compared to competitive binders. As a consequence, the binder content can be lowered in order to obtain a satisfactory electrode. Aging effects in carbonates will be discussed and eventually the cycling performance of this new polymer will be analyzed.

Effect of Separator Properties on the Performance of Lithium-ion Cells

D.-J. Ihm, H.-S. Sin, K.-S. Roh, J.-H. Lee, Y.-J. Shim,
SKC Co., Ltd.,
460 Chonhung-Ri, Songgo-Up, Chonan-City,
Chungchongnam-Do, 330-830 Korea

Introduction

The use of lithium secondary batteries has rapidly increased in recent years for portable telecommunication devices. To meet the requirements of these devices lithium-ion cells should have high capacity, good rate capability and good cyclability. Commercial lithium-ion cells consist of a carbon based anode, a lithium metal oxide based cathode, and a separator soaked with an organic electrolyte. There are numerous studies regarding the effect of cell components on the performance of lithium ion cells. They are mainly focused on cathode active materials, anode active materials, and electrolytes. The effect of separators on the performance of lithium ion cell was not studied extensively [1].

Separator is the one of key components of lithium ion cells. It provides not only the separation of cathode and anode so that no current can flow between them but also the path for the movement of lithium ion between cathode and anode. The inherent properties of separators including porosity, pore-size distribution, thickness and mechanical properties have a great effect on the properties of lithium ion cells especially on safety [1].

The properties of separator may be changed due to the deformation caused by any mechanical forces applied during the assembling process of the lithium ion cell and the pressure build-up inside the cell during formation of SEI layer and continuous cycling. Once the separator deformed, the performance of the cell will not be the same as we designed.

In this work, we will discuss the effect of separator properties on lithium-ion cell performances. The different degree of deformation of separator was manipulated and the performance of lithium ion cells including discharge rate and cycle life characteristics was characterized.

Experimental

Samples of separators were selected from commercial grades. To simulate the situation that separator may experience the deformation under the pressure during the assembly process of the cell and repeated cycling, the separators were pressed manually at different level of pressures. Test samples were prepared by cutting into 3x4 cm size and pressed with each pressure 0, 97, 194, 388kg/cm². The surface properties of separators as received and deformed were characterized by scanning electron micrograph. The degree of deformation of separator was determined by using air permeability method. Air permeability was measured using apparatus designed in house. Li-ion cell configurations containing a graphite anode, a LiCoO₂ cathode, and a separator were used for studying the electrochemical performance of the cell. Discharge rate dependence and cycle life performances of the test cells were characterized.

Results

Figure 1 shows the permeability result for separators having different applied pressures. It is clearly shown from the results that the permeability of the separator is reduced upon the increasing the pressure. The measurement of porosity and the pore size also shows the similar trend.

Figure 2 shows the cycle life results of the test cells consisted with various separators having different permeabilities. The cycle life performance of the test cell was deeply dependent on the permeability of the separator. The cycle characteristics of the test cell with less deformed separator (high permeability) was better than that of the test cell with more deformed separator (low permeability). The results also indicates that there is certain degree of allowable deformation of the given separator to have the same level of cyclability with undeformed state.

References

1. G. Venugopal, J. Moore, J. Howard, S. Pandalwar, J. Power Source, 77(1999), 34.

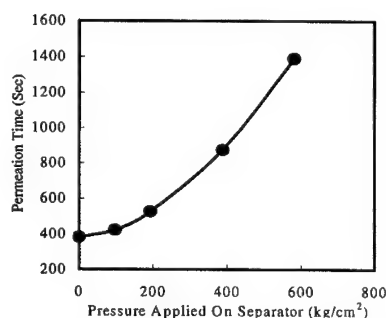


Figure 1. The influence of air permeability by applied press on separator SE2

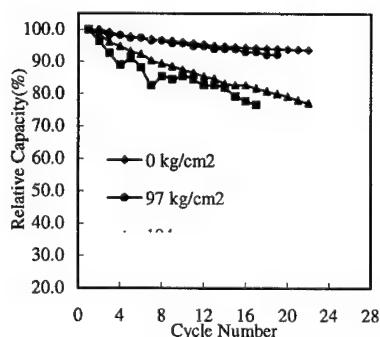


Figure 2. Cycle life performance of the test cells with various separators having different applied pressure.

Advanced Li-Ion Technology for the MSP01 MARS Lander

C. Marsh[†], R. Gitzendanner[†], F. Puglia[†], J. Byers[‡]

[†]Yardney Technical Products, Inc., 82 Mechanic
Street, Pawcatuck, CT 06379 USA

[‡]Lockheed Martin Astronautics, P.O. Box 179,
Denver CO 80201

Commercial Lithium-ion cells have demonstrated excellent performance, high energy density, high reliability, long cycle life and good safety characteristics for a wide range of applications. While commercially available cells demonstrate the viability, performance and economic potential of the Li-ion technology for consumer applications, they are not suitable for aerospace applications. Aerospace batteries require very high reliability, outstanding low temperature operation, exceptionally long cycle life, high specific energy and larger cell sizes. In addition, due to the high cost and inaccessibility of many of the aerospace applications, these battery systems must have designed-in lifetime reliability that far exceeds industry standards. Yardney Technical Products has designed and developed a lithium-ion cell that offers a unique weight, volume and reliability solution to these aerospace requirements.

The advanced Li-ion battery system for the MSP01 MARS Lander uses a space efficient and adaptable parallel-plate prismatic cell design. These cells deliver a specific energy of 145 Wh/kg, energy density of 325 Wh/l and demonstrate high sustained and pulse rate capability while providing superior low temperature performance that meets and exceeds the demanding MSP01 Lander requirements. These optimized cells have been configured into a battery, shown in Figure 1, that consists of two cell stacks, made of eight Li-ion cells connected in series, mounted to an aluminum deck plate with wiring harnesses, connectors and a connector bracket. The individual battery stacks are each 28 volt systems capable of supplying greater than 24 Ah capacity at a C/5 rate at -20°C and 33Ah capacity at a C/5 rate at +20°C. The batteries are designed to operate in temperatures ranging from -20°C to +40°C with non-operational excursions to -30°C and +50°C. As shown in Figure 2, the cells have been tested for performance to support mission requirements after a 10 month storage and cruise period. The batteries have also been designed to survive the vibration and acceleration levels required by the mission, and to maintain a delta temperature across the battery or from cell to cell in the battery stack no more than 3°C. The battery design is scheduled to complete full Qualification testing in early 2000 and will be flown in 2001. This paper will present the design considerations, battery development and the results of performance and life testing.

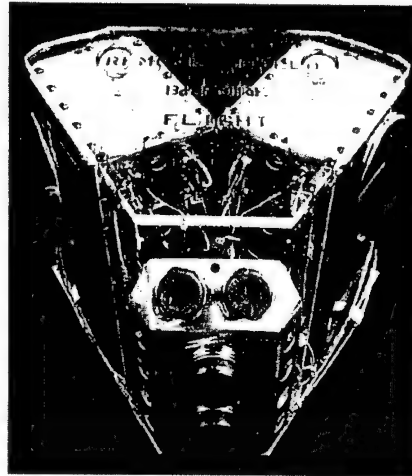


Figure 1. MSP01 Mars Lander Battery.

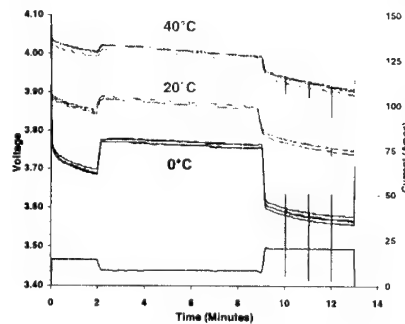


Figure 2. Voltage profile of Lander cells during Entry, Decent and Landing testing at 40°C, 20°C, and 0°C.

Acknowledgement: The authors thank Lockheed Martin, Inc., the U.S. Airforce and NASA for support under contracts RF9-356203 and F33615-98-C-2898.

CHARACTERIZATION OF LITHIUM THIONYL CHLORIDE CELLS BY IMPEDANCE TECHNIQUES

F. Walsh, M. Pozin, A. Cherniy, K. Tikhonov Jr.

Tracer Technologies, 20 Assembly Square Dr.,
Somerville, MA 02145, USA

INTRODUCTION

The voltage drop during initial polarization of lithium-thionyl chloride cells is caused by the high resistance passive film formed on the lithium metal surface during reaction of lithium with thionyl chloride (1). The Niquist plot of the lithium electrode in thionyl chloride solution includes a semicircle characterizing the passive film and the diameter of this semicircle correlates with the voltage drop during initial polarization of cells (2). During storage, the impedance of thionyl chloride cells as well as voltage drop increases due to the growth in thickness or density of the passive film (1,2). The ability to predict accurately the value of voltage drop for thionyl chloride cells after prolonged storage would be beneficial in practical applications. However, this analysis is complicated by the high dispersion of parameter values used to characterize the impedance of cells resulting from the extended storage time and temperature variation. In this paper we discuss the extent of dispersion observed as a function of storage time.

EXPERIMENTAL

Thirty ECO thionyl chloride cells of 8.7 Ah and geometric surface area of lithium 48 cm² were analyzed. Impedance measurements were performed using a Solartron 1280 in frequency range from 20 000 Hz to 0.05 Hz and 10 mV input signal amplitude. Polarization consisted of 10 sec discharge on 110 Ohm. Polarization was applied after a week and then again after three weeks following assembly. Cells tested were stored at room temperature.

RESULTS AND DISCUSSION

The Niquist plot of a thionyl chloride cell contains a depressed semicircle in the domain of high and medium frequencies and corresponds to the resistance of the passive layer on lithium metal. We found that the magnitude of the voltage drop during initial polarization of cells is proportional (Fig.1) to the value of R_{pl} (where R_{pl} is a segment cut by the semicircle on real axis). The expected value of a cell's voltage drop during polarization can be easily calculated based on the results of the impedance measurements. For this type of cell the dependence of the voltage drop under polarization on impedance can be described by the following equation $Y = -0.0004 \cdot X^2 + 0.392 \cdot X - 7.462$ with the R value of 0.96. This equation does not change with the storage time.

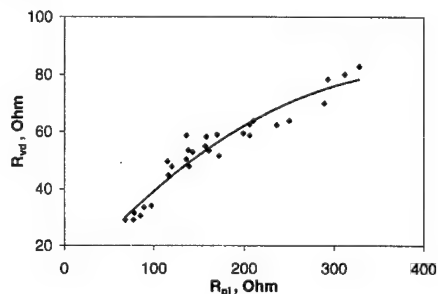


Fig.1. Resistance of cells calculated from the voltage drop (R_{vd}) vs. resistance of passive layer R_{pl} .

We also found that higher dispersion of the impedance of the cells corresponds to the higher average value of R_{pl} where during storage R_{pl} increases and dispersion of R_{pl} becomes higher. After polarization the value of R_{pl} drops with corresponding drop in dispersion and rises again with additional storage (Fig.2).

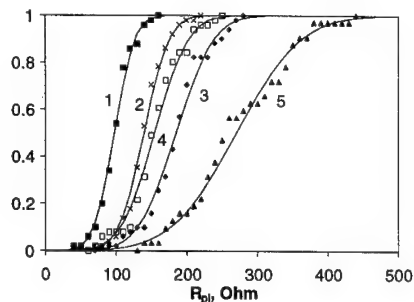


Fig.2. Cell resistance as a function of storage time.

1 - a week after assembly; 2 - one day after polarization; 3 - two weeks after polarization; 4 - nine days after second polarization; 5 - two months after second polarization.

REFERENCES

1. E. Peled, in *Lithium Batteries*, Jean-Paul Gabano, Editors, p.43, Academic Press Inc, New York (1983).
2. M. Gaberscek, S. Pejovnik, *J. of Electrochem. Soc.*, **146**, 933 (1999).

High Rate Performance Of Moltech Prismatic Rechargeable Cells

Y. Geronov and T. Skotheim
Moltech Corporation
9062 S. Rita Rd.
Tucson, Arizona 85747

Introduction

It was reported [1] that the Moltech rechargeable cells based on a sulfur containing cathode and Li anode have reached a specific energy close to 200 Wh/kg at moderate discharge rates. For portable tools, EV, and HEV applications, an energy density of 100 Wh/kg at a specific power of a minimum of 500 W/kg is required.

This paper presents the performance of Moltech rechargeable prismatic cells at high discharge rates where other Li systems deliver very limited specific energy.

Experiment

Two sizes of Moltech prismatic with a soft Al bag package were tested at 1 to 10 C discharge rates:

Size	Capacity	Spec. Energy @ 0.3C	Spec. Energy @ 0.3C
Prismatic	Ah	Wh/kg	Wh/l
33x44x6 (M08)	0.8	160	190
67x82x5.5 (M3)	3.0	200	210

For comparison Li ion cells from two manufacturers were discharged under the same conditions: Sanyo rectangular (Al can) 550 mAh, 18g and A.T. Battery Co. rectangular 750 mAh, 38g [2].

Results and Discussion

Ragone Plots

Fig. 1 compares the specific energy of Moltech M08 prismatic cell to the AT 0.75Ah and Sanyo 0.5 Ah Li ion cells. From the Ragone plots one can see that at a rate of 10C M08 cells deliver a specific power higher than 1kW/kg and energy of 120 Wh/kg. At 3C the specific energy of the tested Li ion cells was only 40 Wh/kg at a power of 250 W/kg. Fig. 2 depicts a typical voltage-time curve of M3 cells at 8C rate. A specific energy of 120 Wh/kg at 1070 W/kg was estimated. For comparison a Panasonic EV Energy -7 cell module of 6.5 Ah NiMH cells at peak pulse specific power of 625 W/kg for HEV application has only 7.5Wh/kg specific energy [3].

Cycle life at high rate charge

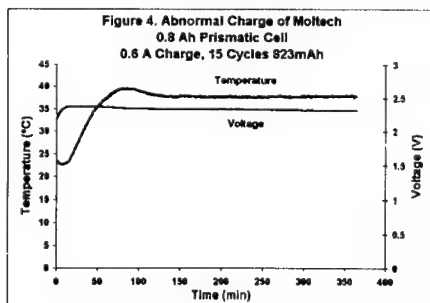
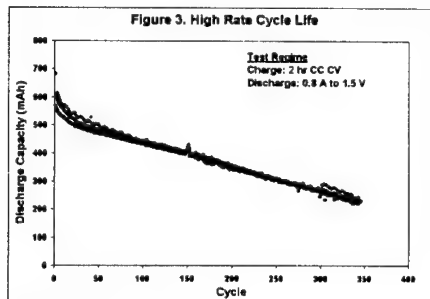
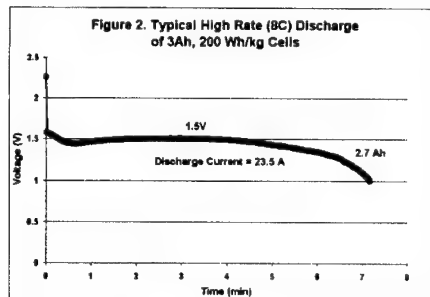
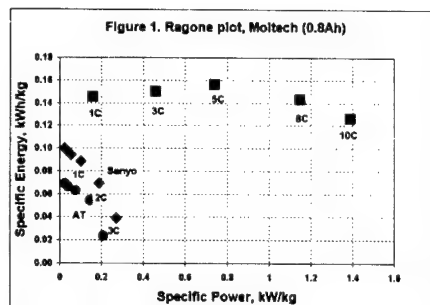
Because of Li dendrite formation the cycle life of the most advanced Li metal rechargeable cells is lower at high charge current density e.g. a 3 hour charge rate [4]. Moltech rechargeable cells can be charged at 1 to 2 hour charge rates without appreciable reduction of the cycle life. Fig 3 gives the cycle life of M08 at 2 hour taper charge and 0.8A discharge. 300 cycles to 50% of the capacity at the 5th cycle were achieved.

Safety

M08 and M3 prismatic Moltech cells tested according UL-1642 standard successfully passed all tests without any electronic protections. No safety failures were found for the cells containing a higher Li amount (M3 size). This suggests a very reliable self-protection of the Li deposit due to of a low concentration of Li polysulfides formed during the oxidation-reduction processes. The same soluble species are also responsible for the excellent overcharge protection shown in Fig 4 in an abnormal charge test. In the same test, the Li ion cells are unsafe and they require vent and cut-off protections.

References

1. J. Broadhead and Y. Geronov, Proceedings 16th International Seminar, March 1999 (USA)
2. ITE Battery Newsletter, #4, p. 48 (1998).
3. F. Kalhammer, 15th Ann. Bat Conf., Long Beach 2000
4. D. Aurbach et al, 199th Joint Int. Meeting, Abstr. #370



Manganese type lithium ion battery for pure and hybrid electric vehicles

T. Horiba, K. Hironaka, T. Matsumura, T. Kai, M. Koseki,

and *Y. Muranaka

Shin-Kobe Electric Machinery Co., Ltd.

Okabe-machi Ohsato-gun, Saitam 369-0297 Japan

*Hitachi Research Laboratory, Hitachi, Ltd.

Ohmika-cho Hitachi, Ibaraki 319-1292 Japan

Lithium ion batteries have now very important and promising position in battery market, though most of the batteries are Co type lithium ion batteries which use lithium cobaltate as positive electrode material. Co type Li ion batteries surely show good and well-balanced characteristics, but the small amount of the Co

resource suggests the difficulty in large-sized battery use such as electric vehicles. On the other hand Mn material has large natural abundance and steady background in battery industry, though the short cycle life and lower discharge capacity had been remaining in conventional technology. Thermal stability for lithium manganese spinel was another remarkable point for large-sized applications, for thermal management and safety occupy much serious position in the applications.

We concentrated on the improvement of cycle life at room temperatures and higher temperatures by means of crystallo-graphical approach and physicochemical approach to develop two types of Mn type Li ion batteries : one for pure-EV use of high energy density, another for HEV use of high power density.

The specification for Mn type Li ion single cell for pure-EV use is shown in Table 1. The energy density is almost same that for Co type. Cycle life at 40 % DOD and 25% showed more than 1000 cycles. 8 cells connected in series and a cell

controller were installed in a module case to form a module to mount on a car. Fig.1 is the photograph for the module.

Mn type Li ion cell for pure-EV use was modified to make it

high power density by reducing the internal resistance. Fig. 2

shows high rate discharge ability for our cell developed. Fig.3

is the photograph of battery module for HEV consisting of 48 cells connected in series and 6 cell controllers in the module case.

Acknowledgement

A part of this work is dependent on the results of the Development of Dispersed Type Battery Energy Storage Technology sponsored by MITI and NEDO.

References

- 1) K. Tamure, T. Horiba and T. Iwahori, J. Power Sources, 81-82, 156(1999).
- 2) S. Hossain and S. Megahed Symp. Proc. EVS-13, I-45 (1996).
- 3) A. M. Wilson and J. Reimer, Proc. IMLB-9, Poster II Thur 81 (1998).

Table1. Specification for developed single cell for pure-EV use

ratings	3.8 V-90 Ah
dimensions	•67×•410 mm
weight	3.2 kg
energy density	107 Wh/kg



Fig.1 Photograph of 8-cell module for pure-EV use

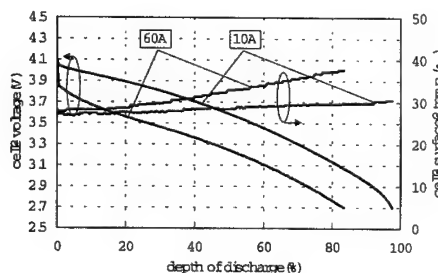


Fig.2 Discharge characteristics for HEV single cell



Fig.3 Photograph of 48-cell module for HEV use

Abstract No. 355

Status of Lithium Battery for Electric-based Transportation

G. Abbas Nazri

University of Michigan, Department of Chemistry, Ann Arbor, Michigan 48109, USA

There is a clear tendency of moving from combustion engines to a cleaner and more efficient electrochemical technology. It has been predicted that the combustionless technologies will dominate and replace the internal combustion engine in the next few decades. There will be a competing challenge between the lithium battery and the fuel cell driven vehicles.

The purpose of this work is to assess the status and viability of advanced lithium batteries for application in electric-based transportation. Technical challenges and opportunities for the development of advanced electric power sources have been explored, and the optimized lithium-ion battery is identified as the most advanced and promising energy storage system for future electric-based transportation. The abundance of lithium in the earth's crust and in the sea has been explored and it appears to satisfy the high lithium consumption of lithium battery for transportation applications. Recent innovations in materials engineering and new design concepts in battery packaging have provided a realistic optimism for the future of electric-based transportation. Breakthroughs in materials are key and eventually will determine the future technology for the electric-based transportation. The emerging battery technology will incorporate many recent breakthroughs in the field of solid state chemistry, physics, and materials science, and will benefit from numerous advances made in electronic control and power management systems. In addition, safety aspects of EV and HEV batteries have been improved considerably, and many intrinsic (chemical) and extrinsic (electronic) controls have been developed to provide extra safety margin. Furthermore, there is great possibility to further reduce the cost of advanced batteries through smart engineering of functional and low cost materials. The key improvements in performance, safety, and cost issues will be reported.

The electric propulsion systems are very advanced and energy efficient, however, improvement in batteries is crucial. There is tremendous potential for further improvement of lithium-ion battery performance and greater opportunity of lowering the cost of the battery.

There have been many proposals to combine two or more power sources in order to simultaneously satisfy the energy and power requirements of EVs and HEVs. Recent ICE-lithium battery hybrid will be discussed. Although the hybrid system benefits from the optimized performance of multiple-power units, the ideal scenario is to have only one power source, i.e. a battery capable of delivering both the required power and energy. Design and materials optimization of such a battery remains as a challenge for the next decade. Recent improvements in performance of high-power battery will be reported. The competing fuel cell technology, its potentials and limitations will be compared with the lithium battery technology.

Abstract No. 356

Performance Characteristics of LiMn_2O_4 polymer Carbon Electrochemical Cells

Norlida Kamaruddin,¹ Zurina Osman,² Nor Sabirin Mohamed³ and Abdul Kariem Arof²

¹MARA University Of Technology
Science Centre, MARA University of Technology,
Shah Alam, Malaysia 40450

²University of Malaya
Physics Department
Kuala Lumpur, Malaysia 50603

³University of Malaya
Centre for Foundation Studies in Science
Kuala Lumpur, Malaysia 50603

This paper discusses the performance characteristics of two types of cells of configuration $\text{LiMn}_2\text{O}_4/\text{chitosan}/\text{C}$. LiMn_2O_4 was prepared by the sol-gel method using lithium acetate and manganese acetate as starting reagents and tartaric acid as the gelling agent. The precursor obtained was heated at different temperatures. The performance of the LiMn_2O_4 prepared from heating the precursor at different temperature was determined. The performance characteristics of the different cells fabricated utilizing the lithium manganese oxide as the cathode active material, $\text{LiClO}_4\text{-EC-DMC}$ as the electrolyte and carbon as the anode was studied to ascertain the best condition for preparing the LiMn_2O_4 . The cell utilizing LiMn_2O_4 obtained by heating the precursor at 600 degrees celcius for 6 hours gave the best performance. The same LiMn_2O_4 material was then used in the fabrication of cells using the chitosan polymer based electrolytes. The electrolytes used were chitosan polymer doped with LiCF_3SO_3 to which EC was added as the plasticizer. In one of the cells, the chitosan polymer was doped with $40901.3 \times 10^{-3} \text{ S cm}^{-1}$ and that of the second the electrolyte $3.9 \times 10^{-3} \text{ S cm}^{-1}$. The cathode of all cells consist of 80 and 10 binder by weight. The characteristics of the cells was measured and analysed.

Cooperative Research on Safety Fundamentals of Lithium Batteries

J. Robert Selman and Said Al Hallaj
*Center for Electrochemical Science and Engineering (CESE),
 I.I.T., 10 West 33rd Street, Chicago, IL 60616.*
Isamu Uchida and Y. Hirano
*Tohoku University
 Department of Applied Chemistry
 Graduate School of Engineering
 07 Aramaki Aoba, Aoba-ku
 Sendai 980-8579, Japan*

A cooperative research program on the thermal characterization and safety of lithium batteries is being carried out at IIT/CESE (supported by U.S. Army Research Office) and Tohoku University (supported by NICHE). This research includes experimental work and performance prediction, for scaled-up secondary lithium batteries.

"Normal operation", and effects associated with "abnormal" operation.

The upper limit on the "normal" operating temperature of lithium-ion batteries is conservatively set (typically at 65°C for US Type 18650 lithium cobaltate cells). This is done to avoid rapid capacity fading and thermal runaway, which are both complicated and poorly predictable processes. The risk of thermal runaway is exacerbated under load conditions. Therefore, fundamental studies must take advantage of the more reproducible process at open circuit. As demonstrated at IIT, using an Accelerated Rate Calorimeter (ARC), thermal runaway at open-circuit is sensitive to the state-of-charge. It occurs at 104°C for cells charged to 4.06V open circuit, and only at 144°C for cells at 2.8V open circuit.[1]

Sources of heat generation and their effect on cell performance/ thermal runaway.

Three sources of heat generation must be considered in the analysis of capacity fading and thermal runaway.

- (1) The "reversible" heat released (or absorbed) by the chemical reaction of the cell;
- (2) The "irreversible" heat generated by ohmic resistance and polarization;
- (3) The heat generated by "side reactions", i.e., parasitic/corrosion reactions, and "chemical shorts".

In "normal operation", heat effects (1) and (2) are small. Therefore, no thermal runaway occurs even during prolonged operation, and capacity fading is not accelerated. Under "abnormal" conditions (high temperature or current, in prolonged operation) heat effects (1) and (2) trigger the self-accelerating effect (3).

Using the ARC to measure thermal runaway in small cells at open circuit, it is possible to extract information about heat effect (3), including kinetics.[2] When the "normal use" effects (1) and (2) are known, this can be combined to model heat generation in a scaled-up cell and predict thermal run-away or capacity fading. Since information on (3) is not consistent from one cell to the next, it must be "built up" from measurements on components. Also, the reversible heat (1), must be accurately known.

Heat generation under "normal" conditions

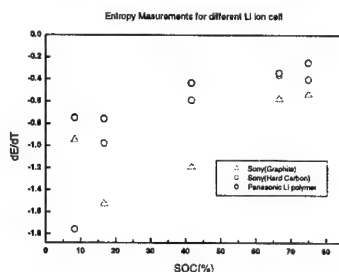
The reversible heat (1) can be measured by various techniques [3], or calculated from the thermodynamic equation:

$$Q_{rev} = nF \Delta S = T \left(\frac{\partial E_{eq}}{\partial T} \right) (I t)_{dc}$$

Therefore, in cooperative work [4], we have determined, for various lithium cells in normal operation, the "entropy coefficient" $(\partial E_{eq}/\partial T)$. The results are shown in Fig. 1

Fig.1. Coefficients $(\partial E_{eq}/\partial T)$ of various cells

References
 1. Al Hallaj, S., J. S. Hong, H. Maleki, and J. R. Selman, "Thermal Modeling and Design Considerations of Lithium Ion Batteries", *J.*



Power Sources, V. 83 (1-2), (1999)

2. S. Al Hallaj, "Scale-Up Design of Lithium-Ion Batteries: Electrochemical-Calorimetric, Thermal Modeling, and Safety Studies", Ph.D. thesis, I.I.T., Chicago, IL (May 2000)
3. J.S. Hong, H. Maleki, S. Al Hallaj, L. Redey, and J.R. Selman, *J. Electrochem. Soc.* **145** (1998) 1489-1501
4. EST Workshop NICHE, Tohoku University, Sendai, Aug.1999.

Development of High Energy Density Li-ion Batteries based on $\text{LiNi}_{1-x-y}\text{Co}_x\text{Al}_y\text{O}_2$

J S Weaving, F Coowar, D A Teagle, J Cullen, V Dass, *P Bindin, R Green* and W J Macklin
AEA Technology Batteries

Culham Science Centre, El Culham, Abingdon, Oxfordshire, OX14 3ED, U.K.

*Engineering Images Ltd., Malpas, Cheshire, SY14 8NE, U.K.

Introduction

$\text{LiNi}_{1-x}\text{Co}_x\text{O}_2$ ¹ is an attractive choice of cathode material in Li-ion cells due to its cost advantages and increased capacity compared with LiCoO_2 . In comparison with LiNiO_2 , $\text{LiNi}_{1-x}\text{Co}_x\text{O}_2$ offers improved safety benefits due to an increased structural stability at higher temperatures and voltages. Further, the introduction of small amounts of metal dopants, such as Al, into the $\text{LiNi}_{1-x}\text{Co}_x\text{O}_2$ lattice has also been reported² to stabilise the structure and improve cycle behaviour.

Experimental

Electrochemical characterisation of $\text{LiNi}_{1-x-y}\text{Co}_x\text{Al}_y\text{O}_2$ cathode material was conducted in lithium half-cell over the potential range 3.0 V to 4.2 V. Evaluation of $\text{LiNi}_{1-x-y}\text{Co}_x\text{Al}_y\text{O}_2$ performance with graphitic carbon anode has been undertaken in several alternative Li-ion cell types. These include a flat 'soft-packaged' 10 A h cell design and a high capacity 75 A h metal case cell design.

Results

The $\text{LiNi}_{1-x-y}\text{Co}_x\text{Al}_y\text{O}_2$ cathode material exhibited a high reversible capacity of 184 mA h / g and stable cycle performance, Figure 1. High energy densities in the range 150 – 160 W h / kg have been achieved for flat 10 A h Li-ion cells adopting a $\text{LiNi}_{1-x-y}\text{Co}_x\text{Al}_y\text{O}_2$ cathode. Such cells demonstrate encouraging cycle performance, as illustrated in Figure 2. In high capacity prismatic Li-ion cells increased energy densities in the range 130 – 140 W h / kg have been achieved with a $\text{LiNi}_{1-x-y}\text{Co}_x\text{Al}_y\text{O}_2$ cathode compared to that obtained with LiCoO_2 .

Conclusions

$\text{LiNi}_{1-x-y}\text{Co}_x\text{Al}_y\text{O}_2$ type cathode material demonstrates high reversible capacity and stable cycle performance for application in a range of Li-ion batteries of high energy density.

Figure 1 Cycle performance of $\text{LiNi}_{1-x-y}\text{Co}_x\text{Al}_y\text{O}_2$ cathode material versus lithium metal anode

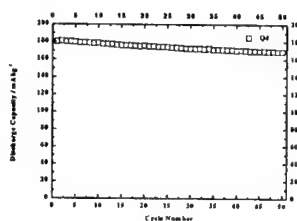
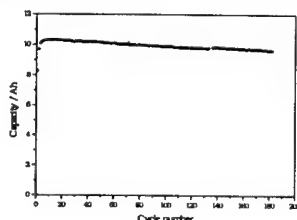


Figure 2 Cycle performance of $\text{LiNi}_{1-x-y}\text{Co}_x\text{Al}_y\text{O}_2$ cathode in flat 'soft-packaged' 10 A h Li-ion cell



References

1. C. Delmas, I. Saardoune & A. Rougier, J. Power Sources, **43-44** (1993) 595
2. K. Matsumoto, R Kuzuo, K. Takeya & A. Yamanaka, J. Power Sources, **81-82** (1999) 558

Recycling of Lithium Ion Cells and Batteries

M. J. Lain

AEA Technology Batteries
Culham Science Centre, E1 Culham, Abingdon,
Oxfordshire, OX14 3ED, U.K.

Lithium ion cells and batteries will form an increasing proportion of the battery waste stream, as products using them reach the end of their practical life. It is therefore important that an optimum recycling process is available for this battery chemistry. This process should be safe, economic, and recover as much of the battery material as possible. The absence of metallic lithium gives greater flexibility in cell disassembly, and subsequent processing.

The cobalt is the most valuable component of the lithium ion cell. However, the second most valuable component is the electrolyte. Therefore, any process seeking to extract the maximum value from the cell will need to recover the electrolyte. This imposes process limitations, because the lithium salt is hydrolysed by water, and thermally unstable above about 80 °C.

AEA Technology Batteries have been developing an alternative to the existing high and low temperature processes. It operates at around room temperature, and recovers more of the cell contents. The main process stages are as follows :-

1. Mechanical Shredding

The cells are posted into an inert, dry atmosphere for mechanical shredding. This avoids exposing the cell contents to water vapour, which would hydrolyse the electrolyte. It also reduces the impact of internal short circuits, which can be violent in contact with oxygen.

2. Electrolyte Extraction

The liquid electrolyte is dispersed in the pores of the electrodes and separator. However, by immersing in a suitable solvent for a few hours, the electrolyte can be extracted. After separation from the residual solids, the solvent can be recovered by evaporation at reduced pressure, leaving pure electrolyte.

3. Electrode Dissolution

The electrodes are cast using PVDF binder dispersed in a solvent. This process can be reversed to recover the electrode particles. The cell pieces are immersed in the solvent, which is stirred and heated to around 50 °C. The binder re-dissolves, separating the electrode particles from the residual copper, aluminium, steel and plastic. The latter can be further separated based on their physical properties e.g. density, magnetism. The electrode particles are filtered from the binder solution, which is then concentrated to recover the bulk of the solvent for re-use.

4. Cobalt Reduction

The residual electrode particles are lithium cobalt oxide, and one or more types of carbon. Before they can be reused, they need to be separated further. To avoid adding

any chemicals to the system, electrochemical reduction is used. As the cobalt(III) is reduced to cobalt(II), lithium is released from the solid structure. Oxygen is generated at the counter electrode.

The carbon particles increase the electronic conductivity during the electrochemical reaction. Any residual lithium is de-intercalated at the same time. Hydrogen evolution is an unwanted side reaction. Therefore, aqueous lithium hydroxide is used as electrolyte, and the current collector is graphite.

The individual steps of the process were initially investigated separately, on a small bench top scale. This allowed suitable solvents and operating conditions to be determined. The stages were then integrated into a demonstration unit. This had a number of advantages :-

- proper anhydrous operation where required.
- any cross-contamination between process steps revealed.
- consideration of preferred construction materials.
- control and safety issues resolved.
- identification of areas requiring further scale up effort.

Manufacturing waste is comparatively free of contamination, and generally localised. However, the predominant waste source is used batteries. All consumer lithium ion cells are sold as battery packs. Therefore, it is necessary to be able to disassemble the packs, and extract the cells. Unfortunately, there are already several hundred different pack sizes in existence, which makes fully automatic disassembly difficult. However, it is likely that a semi-automated process can be developed. The key safety requirement is to avoid rupturing the cell can during any cutting process. Contamination with other battery chemistries can be minimised by taking advantage of the non-standard cell sizes of lithium ion cells.

Given the projected numbers of cells available for recycling, and the value per cell of the contents, there is a significant market opportunity for recycling lithium ion cells and batteries. Unlike some recycling processes, the bulk of the income comes from the sale of the products, rather than from charges to the waste disposers. It seems unrealistic to charge the latter more than the costs of disposal through incineration or landfill.

A preliminary design has been produced for an operational plant with an annual throughput of around ten million cells. This has enabled the capital and operating costs to be estimated. With further assumptions on income, even a single plant shows a solid return on investment. The main complication is the variation in world prices of the recycled products. During the operating life of a plant, the prices can be expected to cycle up and down several times. This will obviously effect the degree of profitability, but only the degree, and not the fundamentally profitable nature of the process.

Modulation of discharge process of a lithium battery by changes of battery inner medium influence on process of discharge

A. Z. Shekhtman *

KVANT

Moscow, Russia

Influence of the lithium battery inner medium on process of battery discharge into an outer load can change its character during discharge. This change modulates discharge settling rate and can be researched by studying of the characteristic functions of discharge.

Here, we present the results on the inverse characteristic time of changes of value of some quantities characterizing discharge process of the lithium batteries during discharge. The polarization of the lithium battery, its inner resistance, and the quantity HI where I is the discharge current through the battery are among the researched quantities. The experimental data have been obtained by the intensive research method [1]. The VARTA CR 2032, CR 2016 GP, ENERGIZER CR 2025, BR 2020, and BR 2325 lithium batteries were used at the study.

Some of the results of the research are presented in Fig. 1-4. They give us the four-dimensional diagrams / 2, 3 / for the inverse characteristic time $1/\tau = (dr/dt)/r$ of changes of the inner resistance r of the investigated lithium batteries in process of discharge for the studied values of the outer load and the discharge time as one dependence on the battery's polarization H . Every value of $1/\tau$ in Fig. 1 - 4 is averaged on the nearest five values along the corresponding discharge. Fig. 3, 4 present the four-dimensional diagrams of $1/\tau$ obtained at different time for the same battery.

The results of the study show that $1/\tau$ has some not monotonous changes during discharge itself and from discharge to discharge. They are obviously connected with modulation of discharge process by changes of influence of the lithium battery inner medium on discharge process.

The fact itself of change of influence of the lithium battery inner medium on discharge process during discharge, is known. Two points present an interest here: the repeatable changes which occur at very small values of the discharge current [4] and possibility to research properties of the lithium battery inner medium by studying of the characteristic functions of discharge process.

Not monotonous changes of the behavior of $1/\tau$ in process of some discharges and from discharge to discharge in Fig. 1 - 4 point to appearance of alteration of medium influence on discharge process. Corresponding values of $1/\tau$ and H can give some estimates of the rate and the region of these alterations.

Acknowledgements

The author would like to thank his eldest son for the support of the study.

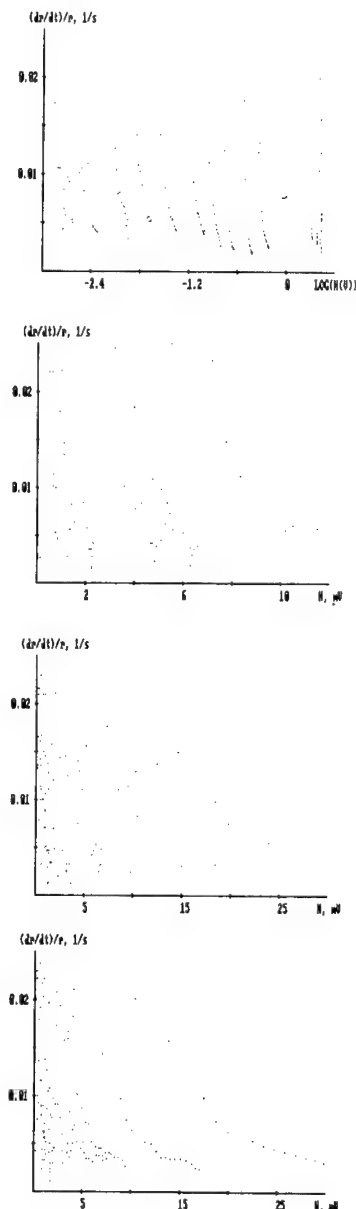
References

1. A.Z. Shekhtman, 1997 Joint International Meeting of the Electrochemical Societies, Paris 1997, Abstract # 925; The 194th Meeting of The Electrochemical Society, Inc., Boston 1998, Abstract #1073.
2. A.Z. Shekhtman, The 1999 Joint International Meeting of the Electrochemical Societies, Honolulu 1999, Abstract #2055.
3. A.Z. Shekhtman, The 197th Meeting of The Electrochemical Society, Inc., Toronto 2000.
4. A.Z. Shekhtman, *Elektrokimiya*, 30 (1994) 690 (in Russian).

* Current address: 71 Alicante Aisle, Irvine, CA 92614, USA.
Tel., fax: (949)7562682.

Fig. 1-2 The four-dimensional diagrams of $(dr/dt)/r$ for two VARTA CR 2032 batteries.

Fig. 3-4 The four-dimensional diagrams of $(dr/dt)/r$ obtained at different time for an ENERGIZER CR 2025 battery.



APPLICATION OF IMPEDANCE
MEASUREMENTS IN THE
DEVELOPMENT OF LITHIUM ION
CELLS

F. Walsh, M. Pozin, and K. Tikhonov Jr.
ECO Energy Conversion,
20 Assembly Square Dr., Somerville, MA
02145, USA

INTRODUCTION

It has been shown that it is possible to predict the performance of electrode materials for lithium ion cells based on impedance measurements. Impedance methods were used by several authors in order to determine the diffusion coefficients of lithium ions in transition metal oxides (1,2) and carbon materials (3,4). However, practically all experiments were performed in half-cell with "model" electrodes having thickness significantly lower compared to electrodes in real cells (1,2,3,4). As a result, interpretation of the correlation between impedance measurements and actual performance of cells becomes difficult. We will present data demonstrating that the investigation of the dynamic behavior of an electrodes' impedance, combined with the development of a theory of impedance of composite electrodes in lithium ion cells, can be applied as a effective tool for improvement of lithium ion cells.

EXPERIMENTAL

Cells tested were close to 18650 size. Anode of lithium ion cell was made from graphite SFG-44 with PVDF and was applied on copper foil. Cathode had the following composition: LiCoO_2 , SAB, PVDF; cathode material was applied on aluminum foil. Lithium metal reference electrode was a strip sealed in separator (Celgard 2300) and introduced into jelly roll in parallel with both electrodes.

Impedance measurements were performed using a Solartron 1280 in frequency range from 20000 Hz to 0.05 Hz (in some cases down to 0.002 Hz) and 10 mV input signal amplitude. Measurements were carried out both in charged and discharged state as a function of cycle number. Temperature of the cell was controlled to $\pm 1^\circ\text{C}$ accuracy.

RESULTS AND DISCUSSION

Based on results of the impedance measurement the contribution of the impedance of the anode into impedance of real lithium ion cell is negligible. Impedance of the cathode has a classical shape and consists of two arcs and the line of Warburg element at very low frequencies. The diameter of semicircle in low frequency domain noticeably depends on the state of the charge. The overall Niquist plot is well described by an equivalent circuit consisting of two resistors each in parallel with constant phase elements. Activation energies of the resistors in equivalent circuit were calculated to be close to 30 kJ/mol in the temperature range from -3°C to 40°C where the dependence of their values on temperature in Arrenius scale is linear.

The interpretation of the lithium ion cell impedance and the nature of equivalent circuit's elements as well as the correlation between capacity fade and changes in impedance of the lithium ion cell will be described.

REFERENCES

1. M.D.Levi, G.Salitra, B.Markovsky, H.Teller, D.Aurbach, U.Heider, L.Heider, J.Electrochem.Soc.,**146**,1279 (1999).
2. Y.-M.Choi,S.I.-Pyun, Solid State Ionics, **99**, 173 (1997).
3. N.Takami, A.Saton, M.Hara, and T.Ohsaki, J.Electrochem.Soc.,**142**,371 (1995).
4. M. D. Levi, D.Aurbach, J. Phys. Chem. B, **101**, 4641 (1999)

Liquid-free Rechargeable Li Polymer Battery

S. Matsui, T. Muranaga, H. Higobashi, S. Inoue
and T. Sakai

DAISO Co., Ltd.,
9, Otakasu-cho, Amagasaki-shi, Hyogo-ken 660-0842,
Japan

To improve safety and increase capacity of Li battery, development of liquid-free polymer battery system is one of the most important matters. High ionic conductive comb-shaped PEO based polymer, poly [ethylene oxide-co-2-(2-methoxyethoxy)ethyl glycidyl ether, (10^{-4} S/cm at 30°C) having high molecular weight ($M_w > 10^6$) has been developed by Daiso. The polymer is quite stable in contact with Li metal anode and it shows more than double figures higher conductivity than PEO on account of its low T_g (-70°C) owing to flexible branched ether units. [1], [2]

The polymer can form a self-standing film with so small quantity of crosslinking that the decline of the conductivity by crosslink can be minimized. The crosslinked film is elastic and has highly mechanical and electrochemical stability at room temperature and higher temperature.

In order to investigate into battery performance, testing cells were comprised of crosslinked polymer film as electrolyte, LiCoO_2 as cathodic active material and lithium metal anode. Cycleability has been highly improved by increasing electronic conductivity and heightening packaging density of cathode. The conductivity was an order of 10 ohm cm^2 and the density was close to theoretical value. Composite cathode was consisted of 82 wt % of LiCoO_2 , 5 wt % of acetylene black as an electronic conductor and 13 wt % of uncrosslinked copolymer as an ion-conducting binder.

All cells were charged at a constant current of 0.2 CmA ($=0.14 \text{ mA/cm}^2$) up to 4.2 V following at constant voltage and discharged at a constant current of 0.2 CmA to 3.0 V at 60°C . The typical initial charge and discharge capacity of the cell were 134 and 119 mAh/g. LiCoO_2 , respectively. As shown in Figure 1, the discharge capacity began to fall in after 10th cycle and reached down to 88 % and 60 % of its initial value at 50 and 125 cycles, respectively. The decline of the capacity was monotonous at the ratio of 0.32 % per cycle.

Cell impedance was measured before and after the cycle performance test in order to study the mechanism of the decrease in discharge capacity. No change in bulk impedance, R_b , was occurred throughout initial to 125 cycles cells. However, the significant increase in interfacial impedance, R_i , was observed. R_i after 125 cycles was approximately three times higher than that of initial state. From our experimental results regarding symmetrical cell, Li/SPE/Li , the interface between lithium and polymer electrolyte is extremely stable. So we presume that the reason of increasing impedance may be due to the deterioration of ionic and/or electronic path in the composite cathode or poor adhesion of current collector to cathode during cycles. Interfacial phenomena are still problems to be solved.

The details of the characteristics of the cell will be discussed.

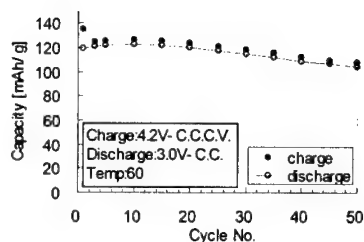


Fig.1: Cycle performance of liquid-free Li polymer battery.

Electrode size: 1.327 cm^2

Charge: C.C.-C.V.-4.2V ($0.2\text{C} = 0.14 \text{ mA/cm}^2$)

Discharge: C.C.-3.0V ($0.2\text{C} = 0.14 \text{ mA/cm}^2$)

Temp: 60°C

References

- [1] A. Nishimoto, M. Watanabe, Y. Ikeda, S. Kohjiya, *Electrochimica Acta* **43** (1998) 1177.
- [2] M. Watanabe, T. Endo, A. Nishimoto, K. Miura, M. Yanagida, *Journal of Power Source* **81-82** (1999) 786.

High Temperature Stable Lithium Ion Polymer Battery

C.-K. Park¹, A. Kakirde¹, W. Ebner¹,
V. Manivannan¹, C. Chai¹ and D.-J. Ihm²

¹SKC America, Inc., 850 Clark Drive, Mt. Olive, NJ 07828

²SKC Co., Ltd., #460 Chonhung-Ri, Songgo-Ub, Chonan-City, Chungchongnam-Do, 330-830 Korea

Introduction

Many investigations have been devoted to the study of lithium ion polymer batteries¹⁻³. Among the different technologies being evaluated, Bellcore's PLION technology is one of the most promising for commercialization. However, an important requirement for the battery is that it be able to cycle at elevated temperatures (at least up to 60 °C) to be accepted in varied portable electronics applications and Bellcore-type batteries typically do not cycle well under these conditions. The Bellcore type polymer battery employs 12 % hexafluoro propylene(HFP) unit substituted poly(vinylidene fluoride-co-hexafluoro propylene) as the separator and electrode binder because of its good solubility in organic solvents like acetone and high ionic conductivity with electrolyte. However, there has not been any detailed experimental report regarding the use of PVDF homopolymer or lower HFP content substituted PVDF copolymers as the separator or electrode binder. That was the objective of this investigation and our results showed a significantly enhanced high temperature cycle performance of lithium ion polymer batteries when having reduced HFP contents in the PVDF copolymer used as the electrode binder.

Experimental

Three different poly(vinylidene fluoride-co-hexafluoro propylene) compositions were selected for evaluation as the electrode binder: 0%, 5%, and 12% HFP. All electrodes were prepared by slurry coating directly onto aluminum or copper mesh. Separator membranes contained either a 1:1 blend of 5% HFP unit substituted copolymer and 12% HFP unit substituted copolymer (Separator A) or 12% HFP unit substituted copolymer alone (Separator B). Separators were prepared either by coating directly onto the electrodes or coating onto PET film followed by lamination to the electrodes. The experimental cells employed a bicell construction, graphite as the anode active material, LiCoO₂ as the cathode active material, and a 1 M LiPF₆/EC-DMC-DEC electrolyte solution.

Results and Discussion

Figure 1 shows the 60 °C cycle performance results for polymer batteries having different HFP compositions in the electrodes. Polymer batteries having 5% HFP unit substituted PVDF copolymer or PVDF homopolymer as their electrode binders showed good cycle performance at 60 °C, while capacity retention for the polymer battery with 12% HFP dropped to less than 80% after only 2 cycles. Thus, HFP content in the electrodes was found to have a significant impact on cycle life performance at 60 °C. Figure 2 shows the cycle performance data of the polymer batteries with the different separator membranes at room temperature and at 60 °C. The electrode binder used in these polymer batteries was 5% HFP substituted PVDF copolymer. The results showed the amount of HFP units in the PVDF copolymer used in the separator membrane does not affect cycle performance significantly at room temperature or at 60 °C. Additional experimental results will be discussed during the presentation.

References

1. C. Schmutz, J.M. Tarascon, A.S. Gozdz, P.C. Warren, and F.K. Shokoohi, Proceedings of the Symposium on Rechargeable Lithium and Lithium-Ion Batteries, 94-28, 330 (1994).
2. R. Koksang, I.I. Olsen, and D. Shackle, Solid State Ionics, 69, 320 (1994).
3. L. Sun, Y. Xu, M. Albu, S. Iqbal, and Y. Uetani, Proceedings of the 38th Power Sources Conference, 274 (1998).

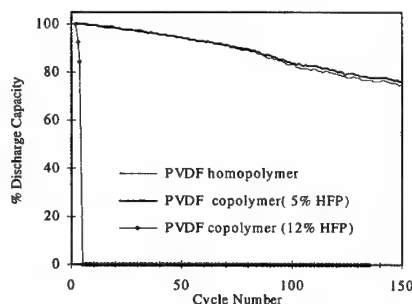


Figure 1. Cycle performance with different electrode binder at 60 °C.

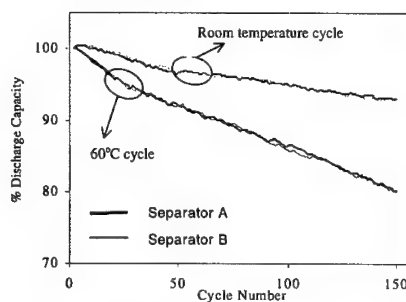


Figure 2. Cycle performance with different separator membranes at room temperature and at 60 °C.

Solid Polymer Electrolyte Cells Using $\text{SnSb}_x/\text{Li}_{2.6}\text{Co}_{0.4}\text{N}$ Composite Anodes

J. Yang, Y. Takeda, N. Imanishi, Q. Li, H. Y. Sun,
and O. Yamamoto*

Department of Chemistry, Mie University
Kamihamacho, Tsu, Mie 514-8507, Japan

* Genesis Research Institute, INC., Nagoya, Japan

Considerable effort has been devoted towards the development of lithium rechargeable batteries based on solid polymer electrolytes due to their potential increase in safety and energy density. Although the use of metallic lithium as anode can achieve the highest energy density, its high reactivity to polymer electrolytes can lead to uncontrolled passivation phenomena, even in the presence of a trace amount of water and impurity. Recently, we developed a new composite electrode based on SnSb_x alloy host and $\text{Li}_{2.6}\text{Co}_{0.4}\text{N}$ compound. This electrode demonstrated a high charge capacity ($> 500 \text{ mAh/g}$) and efficiency (close to 100% at the first cycle) in liquid electrolytes [1]. Taking account of its less-reactivity to electrolytes due to its operation potential above that of lithium, we examine, in this study, its electrochemical performance in solid polymer electrolytes.

PEO-based polymer electrolytes were prepared by the conventional casting technique. Using the electrolytes containing $\text{LiN}(\text{CF}_3\text{SO}_2)_2$ salt, the cells can be operated at a lower temperature ($\geq 70^\circ\text{C}$) than those containing LiCF_3SO_3 salt ($\geq 80^\circ\text{C}$). Moreover, the electrode/polymer electrolyte interface property appears to be also more stable with $\text{LiN}(\text{CF}_3\text{SO}_2)_2$ salt. For these reasons, a $\text{LiN}(\text{CF}_3\text{SO}_2)_2$ -PEO ($\text{MW} = 6 \times 10^5$) electrolyte system is adopted here.

Half-cell study with lithium as counter electrode shows that "shunting" effect related to lithium dendrite formation can not be avoided by the use of the PEO-based polymer electrolytes. This problem can be overcome by using insertion cathodes and adding ceramic fillers into the polymer electrolytes to enhance the mechanical strength. Fig. 1 shows charge/discharge profiles of a cell using $\text{SnSb}/\text{Li}_{2.6}\text{Co}_{0.4}\text{N}$ composite anode and $\text{LiNi}_{0.8}\text{Co}_{0.2}\text{O}_2$ cathode. The polymer electrolyte in this cell contains 10% BaTiO_3 powder ($0.1 \mu\text{m}$). The first charge profile is a little different from the following ones, this is originated from an incomplete recovery of intermetallic SnSb phase after lithium is extracted from this host in the first cycle. Different ceramic powders (BaTiO_3 , LiAlO_2 , TiO_2 , and $\gamma\text{-Al}_2\text{O}_3$) have been examined for use as filler. The preliminary results reveal that the kind and the particle size of fillers have a direct influence on the cell performance. The ceramic fillers, especially BaTiO_3 , not only enhance mechanical strength of the electrolyte, but also improve the interfacial stability, so that cycle life of the cells can be improved (Fig. 2).

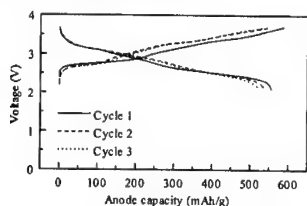


Fig. 1. The initial 3 cycle profiles for a cell with $\text{SnSb}/\text{Li}_{2.6}\text{Co}_{0.4}\text{N}$ composite anode and $\text{LiNi}_{0.8}\text{Co}_{0.2}\text{O}_2$ cathode at 80°C . $i_c = i_d = 0.15 \text{ mA/cm}^2$.

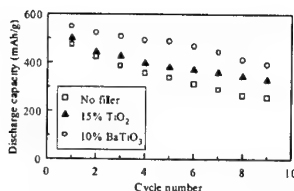


Fig. 2. Cycling behavior of cells at 75°C with polymer electrolytes containing different fillers.

Acknowledgements

This work was financially supported by Genesis Research Institute, INC., Nagoya, Japan.

References

- [1] J. Yang, Y. Takeda, N. Imanishi, and O. Yamamoto, The 1999 Joint Intern. Meeting, Hawaii, Oct. 17-22, 1999, Abstract No. 259.

Elucidation of the Charge-Discharge Mechanism of Lithium/Polymer Electrolyte/Pyrite Batteries.

E. Strauss, D. Golodnitsky, and E. Peled
School of Chemistry, Tel Aviv University, Tel Aviv, 69978, Israel

Much effort has gone into the investigation of the oxidation-reduction of pyrite in the Li/FeS₂ battery systems and several discharge mechanisms have been proposed. It was found that the reduction of FeS₂ in non-aqueous and polymer electrolytes as well as in molten media proceeds as a multi-stage process with the formation of metallic iron and lithium sulfide as the final products. Charge-discharge processes in the Li/LiI-P(EO)_n-Al₂O₃-based CPE/pyrite battery during long-term cycle life have been analyzed with the use of dq/dV curves. Up to seven phases have been identified and found to change during the first 50 - 100 cycles. These phases do not change much over the subsequent 400 cycles. The major phases have been recently identified by EXAFS and NEXAFS measurements. It was proved that reduction of the ferrous disulfide proceeds as a multi-stage process via Li₂FeS₂ to metallic iron. No evidence of FeS was found.

Close inspection of the charge-discharge curves showed that the 1.1 to 1.65 V discharge region is more prolonged than the corresponding charge region and a sudden voltage jump appears (Fig.1). At the end of the discharge the cathode consists of adjacent nanosize lithium sulfide and iron particles that have to interact with each other on charge. We believe that the all-solid-state reaction of iron oxidation, followed by the formation of Li₂FeS₂ starts at the Fe/Li₂S interphase (step 1). The generated Li₂FeS₂ phase (step 2) creates a barrier to the migration of iron atoms on their way to lithium sulfide phase. This may be followed by a potential jump. When high enough overpotential is reached the de-intercalation process starts. The structure of Li₂FeS₂ consists of hexagonal-close-packed layers of sulfur with iron and lithium, equally and randomly filling all the tetrahedral interstices between the more separated pairs of sulfur layers. The remaining lithium atoms fill the octahedral interstices between the alternate, closer sulfur layers. It is believed that removal of lithium and formation of a defect-rich Li_{2-x}FeS₂ (1.2 ≤ x < 2) structure is followed by enhanced electronic conductivity explained as a simple Schottky effect. The "free" ion sites may favor Fe²⁺ migration inside the bulk of the de-intercalated phase and the two reactions (atomic iron oxidation and Li₂FeS₂ de-intercalation)

most likely proceed simultaneously (step 4).

The precise composition of possible intermediates of all the reactions are not yet known with certainty and we are actively pursuing electrochemical, XRD and EXAFS investigations into the mechanism of charge-discharge of the Li/composite polymer electrolyte/pyrite battery.

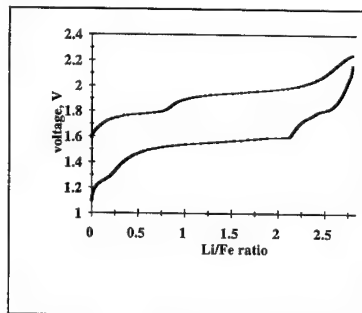


Fig.1 Typical charge-discharge curves of the Li/CPE/FeS₂ battery
 cathode composition: 50% (v/v) FeS₂, 50% (v/v) CPE, cathode thickness 7 μm
 CPE composition: LiI-P(EO)₂₀-EC₁ 9%Al₂O₃
 Operation conditions: T = 135 °C, id = 0.3 mA/cm², ic = 0.05 mA/cm²

Development of a Bipolar Li/Composite Polymer Electrolyte/Pyrite Battery for Electric Vehicles Application

V. Livshits¹, A. Blum¹, E. Strauss¹, G. Ardel¹, D. Golodnitsky^{1,2}, E. Peled¹

¹*School of Chemistry,*

²*Wolfson Applied Materials Research Center*

Tel Aviv University, Tel Aviv, 69978, Israel

Electric vehicles need batteries that are affordable, meet or exceed current safety standards, and satisfy customer expectations for performance.

We are developing a bipolar lithium/composite polymer electrolyte (CPE)/pyrite battery that shows great promise for matching all these requirements. The Li/CPE/FeS₂ battery has many attractive properties. This all-solid-state battery utilizes metallic lithium as its anode and a thin composite polymer electrolyte that acts both as a separator and as the electrolyte. The flexible, multilaminate structure of the polymer electrolyte battery makes possible very high power and energy densities. The use of a solid polymer as the electrolyte is particularly advantageous because it does not leak and emit dangerous gases. The battery operates over a moderate temperature range of 75 -140 °C. At c/10 discharge rate thin-cathode cells operating at 90°C deliver 50% of their 135°C capacity. Pyrite was found to be fully compatible with polymer electrolyte components up to 300°C. Over 500 100% DOD cycles (at c/3 rate) with a capacity fading rate of less than 0.1 %/cycle were carried out in small (1cm² area) laboratory prototype cells with 7 µm-thick cathodes. A single 10cm²-cell went through over 70 reversible cycles. Internal electrochemical overcharge/overdischarge protection mechanisms were shown for the Li/CPE/FeS₂ battery. Up to 100% overcharge and discharge down to 0.3 V are possible in this system with no significant negative effects. The existence of the buffer capacities is a very important battery feature against accidental damage. Overcharge and overdischarge protection mechanism becomes particularly important in the design of high-voltage multi-cell batteries. The bipolar battery design minimizes IR losses between adjacent cells in a cell-stack and provides for uniform current and potential distributions over the active surface area of each cell component. Three-cell 5V bipolar batteries with good performance were assembled and tested. 20mAh with 100% Faradaic efficiency was routinely obtained during discharge (Fig.1). Charge-discharge characteristics of these cells were similar to those of the small 1 cm² cell monopolar prototype.

The long-term projection for a prototype sealed bipolar Li/CPE/FeS₂ battery, with a 45µm-thick cathode is 250Wh/kg specific energy.

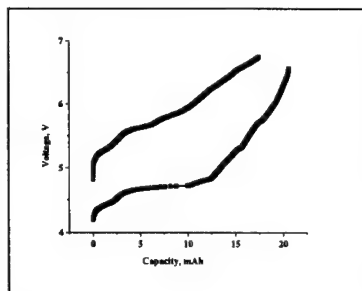


Fig. 1. Charge-discharge curves of three-cell bipolar Li/CPE/FeS₂ battery (cycle 4), T= 135 °C

Near-Room-Temperature Rechargeable Lithium/Pyrite Battery

G. Ardel, D. Golodnitsky, and E. Peled

School of Chemistry, Tel Aviv University, Tel
Aviv 69978, Israel

G. B. Appetecchi, P. Romagnoli, B. Scrosati

Department of Chemistry, University "La
Sapienza", 00185 Rome, Italy

A continuing demand for mobile equipment and the growing interest in the development of electric and hybrid vehicles caused the recent sharp increase in competition for high-energy-density lithium batteries. The balance between ecological and economical objectives is another but no less important factor. The abundance, low cost and the high theoretical specific energy of the Li/FeS₂ couple (1273 Wh/kg based on 4e/ FeS₂) make the natural mineral pyrite a promising cathode material for lithium batteries. The estimated material cost of the Li/composite polymer electrolyte (CPE)/FeS₂ battery is about \$40/kWh (excluding the case), one sixth of that for lithium ion batteries and for other lithium polymer electrolyte batteries (estimated at \$250/kWh). The Li/CPE/pyrite battery with a 10 μm-thick cathode had a reversible capacity of 625 mAh/g (2.8 e/FeS₂), which is about five times that of the Li/Li₂CoO₂ battery.

The low room-temperature ion conductivity of commonly used PEO-based electrolytes (10⁻⁸ to 10⁻⁶ S/cm) has hampered the development of near-ambient-temperature batteries. Hybrid and gel electrolytes consisting of a polymer matrix and organic liquid electrolytes were studied in this work as candidates for Li/pyrite rechargeable battery. Recent progress in the development of rechargeable Li/gel or hybrid electrolyte/pyrite cells is described. The advantages and limitations of the system are evaluated.

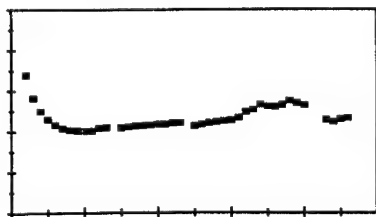
Different types of hybrid and gel polymer electrolytes (HPE and GPE) based on polymers and organic solvents combined with organic or inorganic gelation agents for Li/pyrite battery were studied. Ionic conductivity of 1*10⁻⁴ to 2.5*10⁻³ S/cm at room temperature (RT) was achieved for HPE and 5*10⁻³ S/cm for GPE. At 70 °C tetraglyme-based HPE electrolytes had conductivity of 6 to 8*10⁻³ S/cm, almost one order of magnitude higher than that of "dry" solid polymer electrolytes. R_{SEI} of 6-10 ohm*cm² was stable for about 2000 hours. The first discharge at room temperature showed a single plateau at 1.5 V indicating parallel reactions. At 70 °C two well defined plateaus at

1.7 V and 1.5 V were observed on the first discharge. The specific capacity of the first discharge RT cells varied from 650 to 1000 mAh/g. Reversible specific capacity (Qd) at the second cycle ranged from 250 to 600 mAh/g; the maximal Qd is similar to that of solid-electrolyte batteries at 135 °C. After the initial capacity loss over the first five cycles a stable cycling behavior was observed. (Fig. 1). Most of the capacity loss occurred at high-voltage section of the discharge curve.

Fig. 1 Cycle life of Li/hybrid electrolyte/FeS₂ cell
T= 70°C. Electrolyte composition:
1M LiImide, PEGDME⁵⁰⁰, EC(1%V/V),
Membrane composition (75% porosity):
60% (V/V) PVDF and 40% (V/V) fumed silica
id= ich=0.05mA/cm²

Acknowledgement

The TAU group would like to thank the Israel Ministry of Energy for financial support. The Italian laboratory is grateful to ENEA for financial support under contract 9981.



The Two-Phase Battery Concept: A New Strategy for High Performance Lithium Polymer Batteries.
Pier Paolo Prosini, Maria Carewska, Fabrizio Alessandrini and Stefano Passerini
ENEA, Advanced Energy Technologies
C.R. Casaccia, Via Anguillarese 301, Rome 00060, Italy

A new concept is proposed to realize solid-state high-performance lithium-polymer batteries in which two different polymers are used as ionically conductive matrices in the cathode and in the separator.

The major drawback of PEO-based solid polymer electrolyte (SPE) is the reduced cationic transport at ambient temperature. The low ionic conductivity is due to the high degree of crystallinity of PEO and to the low cation transference number. Ionic conductivities of about 1×10^{-4} S/cm, which would give current density sufficient for high-power application, are obtainable only around 100°C . The problem is especially accentuated in the cathodic compartment where, due to the presence of the other cathodic components, the cross-sectional area of the polymer electrolyte, i.e., the ionic conductor, is reduced [1]. The low ionic conductivity leads to severe transport limitations in the depth of the electrode thus reducing the active material utilization, especially at high discharge currents.

To increase the transport properties into the cathodic compartment, we propose to use two different polymers as ionically conductive matrices in the cathode and in the separator. A low molecular weight polyether is used in the composite cathode to assure high ionic conductivity while a high molecular weight polyether is used in the electrolyte formulation

In this work a composite cathode based on a solid, low molecular weight poly(ethyleneglycol) dimethyl ether (PEG-DME, M.W. 2000), was coupled with a SPE based on poly(ethylenoxide) (PEO, M.W. 4×10^6). The electrochemical stability window, evaluated by a low scan voltammetry, shown that this system has an anodic breakdown voltage higher than 4.0 V vs. Li (fig. 1). The feasibility of two-phase batteries, realized by using different cathodic materials, was evaluated by cycling tests. Batteries based on vanadium oxide showed excellent performance both at moderate (65°C) and high (100°C) temperatures (fig. 2). Cells were cycled at 65°C with good utilization of the active material. About 48% of utilization of active material (corresponding at 140 mAh/g) was attained in 1.7 hour discharges. The performance of the cells cycled at 100°C was very high in terms of specific energy and specific power. Cells were cycled for more than 100 cycles. The initial specific energy was 460 Wh/kg with a power density of 416 W/kg. A capacity fading of about 0.4-0.45 % per cycle affects the cells, reducing the energy density upon cycling.

The excellent performance of such cells allows identifying the poor performance of PEO-based lithium polymer batteries in the reduced ionic transport properties into the cathodic compartment. In fact, the presence of other components in the composite cathode reduces the cross-sectional area of the polymer electrolyte. Especially at high discharge rate, the concentration of lithium in the polymer electrolyte in the composite cathode is easily depleted and the utilization of the active material is reduced. The use of a composite cathodes based on highly ionically conductive matrix allows higher utilization of the active material and higher discharge rate.

Acknowledgements

The work was developed within the ALPE (Advanced Lithium Polymer Electric Vehicle Battery) project, an Italian integrated project devoted to the realization of lithium polymer batteries for electric vehicle applications.

References

1. P.P. Prosini, S. Passerini, R. Vellone, W.H.Smyrl, J. Power Sources 75, 73 (1998)

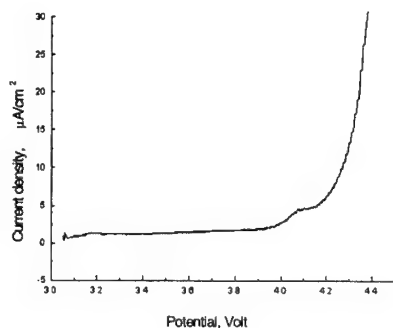
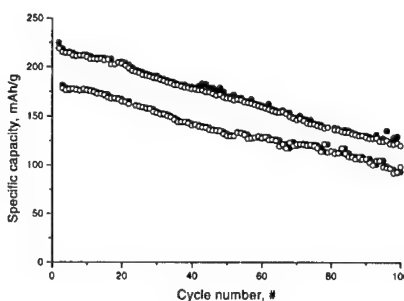


Figure 1. Sweep voltammetry of a PEO-LiClO₄+20% γ -LiAlO₂ electrolyte sandwiched between a lithium disc and a PEG-DME composite carbon electrode. Temperature: 90°C . Scan rate: 0.05 mV/sec

Figure 2. Specific capacity in charge (solid dots) and discharge (empty dots) of two V₂O₅-PEG composite



cathode/polymer electrolyte/lithium cells discharged at different temperatures. Upper curve: Current density was 0.16 mA/cm² for discharge and 0.08 mA/cm² for charge, temperature 65°C , cathodic load (V₂O₅) 3.3 mg/cm². Lower curve: Current density was 0.80 mA/cm² for discharge and 0.20 mA/cm² for charge, temperature 100°C , cathodic load (V₂O₅) 5 mg/cm².

Investigation on Lithium Polymer Electrolyte Batteries
G.B. Appetecchi, F. Alessandrini, M. Carewska, P.P. Prosini, S. Scaccia and S. Passerini
ENEA, ERG-TEA-ECHI CR, Casaccia
Via Anguillarese 301, 00060 Rome, Italy

In this work are reported the tests on lithium polymer batteries using vanadium oxide based composite electrodes operating at moderate temperatures (60-100°C). The work was focused on the fabrication and characterization of polymer-based composite cathodes and electrolytes for use in such batteries. The work was developed within the ALPE (Accumulatori al Litio Per Elettrolizzazione, Lithium Batteries for Electric Vehicles) project, an Italian integrated project, devoted to the realization of lithium polymer batteries for electric vehicle applications.

Battery systems based on the use of a dry-polymer electrolytes in conjunction with a lithium anode and moderate voltage cathode (~3 Volt) are finding a renewed interest in the scientific and industrial communities. The reason resides in the forecasted high energy, power and safety performance that makes this battery system the most reasonable candidate for electric vehicle applications.

Polymer-based lithium electrolytes have been studied since the introduction of polymer electrolytes in 1979¹. However, the use of a polymer electrolyte in a battery requires a careful engineering of the cathode. As an example, electrolytes based on high-molecular weight polymers such as poly(ethylene oxide) (PEO), the most commonly used polymer, are characterized by low ionic conductivity and low density. A careful choice of the cathode composition is then needed to optimize both the energy and the power performance of the device.

ACKNOWLEDGMENT

The authors would like to thank all the participants to the A.L.P.E. project. The financial contribution from MICA (Ministero per l'Industria, il Commercio e l'Artigianato) is kindly acknowledged.

REFERENCES

1. M. Armand, J.M. Chabagno, and M. J. Duclot, in P. Vashishita, J.N. Mundy and G.K. Shenoy (eds.), *Fast Ion Transport in Solids*, Elsevier, New York (1979) p. 131.

Figure 1. Voltage profiles of a $\text{Li/Cu}_{0.1}\text{V}_2\text{O}_5\text{XRG}$ polymer electrolyte cell during constant current ($J=0.1 \text{ mAcm}^{-2}$) cycle tests at 90°C. Voltage limits: 3.4V and 2.0V

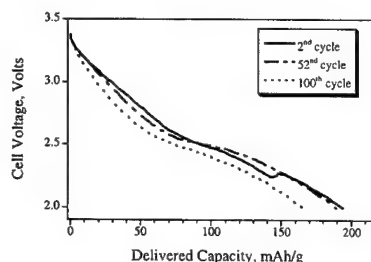
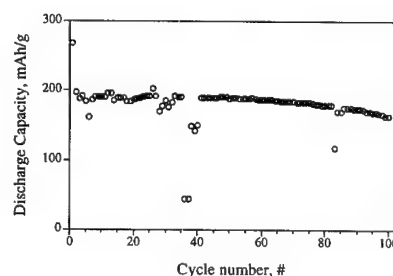


Figure 2. Cycle life performance of a $\text{Li/Cu}_{0.1}\text{V}_2\text{O}_5\text{XRG}$ polymer electrolyte cell during constant current ($J=0.1 \text{ mAcm}^{-2}$) cycle tests at 90°C. Voltage limits: 3.4V and 2.0V.



Cycling performance and interface properties of Li/PEO-Li(CF₃SO₂)₂N-ceramic fillers/LiNi_{0.8}Co_{0.2}O₂

Li Qi, Y. Takeda, N. Imanishi, J. Yang, H.Y. Sun and O. Yamamoto*

Department of Chemistry, Mie University
Kamihama-cho, Tsu, Mie 514-8507, Japan

*Genesis Research Institute, INC. Nagoya, Japan

Lithium polymer batteries are expected to result in the improvement of energy density and applying for versatility in the battery design with a plastic configuration under the relatively low costs. Now, two types of lithium polymer batteries have been developed namely the gel polymer electrolyte type and dry polymer electrolyte type. The dry type has the advantage of better chemical stability and high energy density. The most important technology in this field is to achieve the good cycleability, which is related to the anode/electrolyte and cathode/electrolyte interfaces as well as electrode materials. The reaction of electrolyte with electrode materials can lead to a low conductivity passivation film such as LiF and Li₂O.

It has been reported [1] that the poly(ethylene)oxide(PEO) based polymer electrolyte was improved the mechanical strength and interface properties between the electrolyte and lithium metal electrode by addition of the ceramic fillers like γ -LiAlO₂. In this study, we have prepared the composite polymer electrolyte of PEO-Li(CF₃SO₂)₂N-ceramic fillers(BaTiO₃, TiO₂ and γ -Al₂O₃) and examined the interface resistance of the cells: Li/PEO-composite polymer electrolyte/Li (cell I) and LiNi_{0.8}Co_{0.2}O₂/composite polymer electrolyte/LiNi_{0.8}Co_{0.2}O₂ (cell II), and also, the cycling performance of the cell, Li/composite polymer electrolyte/LiNi_{0.8}Co_{0.2}O₂ has been examined as a function of the fillers.

Figure 1 showed the cycling performance of the cell for electrolyte with different fillers. The cathode capacity and cycling performance depended on the kind of the fillers. In the cell of the composite electrolyte with 10wt% BaTiO₃ showed the highest capacity, better cycling performance, and the high coulombic efficiency of 97%. The excellent cell performance of the cell could be explained by the interface resistance. Figure 2 shows the interface resistance of cell(I) and cell(II). The interface resistance was estimated from impedance analysis of the cell. The interface resistance could be attributed to the passivation film on both anode and cathode interface. The composite polymer electrolyte with 10wt% BaTiO₃ showed the relatively stable and low interfacial resistances on the both Li metal anode /electrolyte interface and the LiNi_{0.8}Co_{0.2}O₂ cathode/electrolyte interface.

Fig1: Cycling performance of Li/PEO-Li(CF₃SO₂)₂N-Fillers/LiNi_{0.8}Co_{0.2}O₂ cell at 80°C, $i_a=i_c=0.2\text{mA/cm}^2$

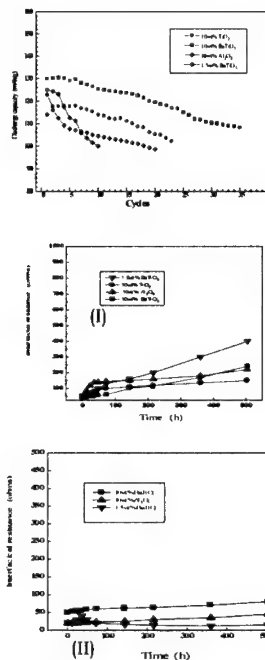


Fig2: Time dependence of the interfacial resistance at 80°C. (I): Li/PEO-Li(CF₃SO₂)₂N-Fillers/Li cell (II): LiNi_{0.8}Co_{0.2}O₂/PEO-Li(CF₃SO₂)₂N-Fillers/LiNi_{0.8}Co_{0.2}O₂ cell

Acknowledgement: This work was financially supported by Genesis Research Institute, INC, Nagaya, Japan

Reference: [1]: G. B. Appetecchi et al., J.Electrochem. Soc., 145, 4133(1998)

Fabrication and electrochemical characteristics of all-solid-state lithium-ion rechargeable batteries composed of LiMn_2O_4 positive and V_2O_5 negative electrodes

M. Baba, N. Kumagai, N. Fujita, K. Ohta, K. Nishidate
Faculty of Engineering, Iwate University, 4-3-5, Ueda,
Morioka 020-8551 Japan

and
H. Groult, D. Devilliers

Pierre & Marie Curie University, 4, Place Jussieu-Batiment
F 75252 Pares Cedex 05-France

Recently, considerable attention has been paid to the investigations of lithium-metal-free batteries¹⁾ and solid-state lithium rechargeable batteries.²⁻⁴⁾ If such a rocking-chair type of battery is constructed with only a thin-film type of electrodes and electrolytes, it will be very compact, light and highly reliable, and therefore find widespread application in many types of portable electronic devices. In this study, we presented the electrochemical characteristics of all-solid-state lithium-ion batteries composed of LiMn_2O_4 and V_2O_5 electrodes for the first time.

A thin film of LiMn_2O_4 was prepared on a stainless steel substrate or the like by an rf-magnetron sputtering method with a typical rf power of 100W and an Ar-gas pressure of 10 mTorr. Next, a thin film of solid electrolyte $\text{Li}_3\text{PO}_4\cdot\text{N}_x$ was deposited on it using the same sputtering method.⁵⁾ Subsequently, a V_2O_5 negative electrode and a V-metal film for a current collector were deposited by the sputtering method. As a result, an all-solid-state lithium-ion battery was fabricated by only the rf-magnetron sputtering throughout the cell preparation process. A typical cell size was 1cm^2 in area and $2\cdot\text{m}$ in thickness as a whole. Main experimental results of the cells described above were obtained as follows.

(1) The charge-discharge characteristics of the LiMn_2O_4 / $\text{Li}_3\text{PO}_4\cdot\text{N}_x$ / V_2O_5 cell operating in the practical voltage range of 3.0 - 1.2V were measured at a current density of $2\cdot\text{A}/\text{cm}^2$. A typical discharge capacity was about $12\cdot\text{Ah}/\text{cm}^2$. In this case, the ratio between charge and discharge capacities was nearly one. This means that any retention which is often seen in solid-state batteries does not occur in the present solid-state cell.

(2) The cyclic performance of the LiMn_2O_4 / $\text{Li}_3\text{PO}_4\cdot\text{N}_x$ / V_2O_5 chair cell was also measured at a current density of $4\cdot\text{A}/\text{cm}^2$. Then, no degradation was observed at least until several tens of charge-discharge cycles.

(3) Next, two cells were prepared separately but simultaneously on one substrate with the same sputtering condition. Then, each of the cells showed almost the same charge-discharge characteristics each other. Furthermore, these two cells were connected in series or in parallel. Then, the total cell voltage in series and the total current in parallel could successfully be obtained as expected. These experimental results indicate that the present solid-state battery is endowed with the superior reliability or reproducibility which is characteristic of solid-state devices.

In summary, we have accomplished the lithium-ion rechargeable battery in which all of the electrodes and the electrolyte were simply made of metal oxides with the dry process of the rf-sputtering method. As a result, a very light, compact and flexible dry cell with good reliability was realized in a completely solid-state and thin-film configuration.

References

- 1) N. Kumagai, H. Kitamoto, M. Baba, S. Durand-Vidal, D. Devilliers and H. Groult, *J. Appl. Electrochem.*, **28**, 41(1998).
- 2) S. D. Jones and J. R. Akridge, *Solid State Ionics*, **53-56**, 628(1992).

3) J. B. Bates, N. J. Dudney, G. R. Gruzalski, R. A. Zuhr, A. Choudhury and C. F. Luck, *J. Power Sources*, **43-44**, 103(1993).

4) M. Baba, N. Kumagai, H. Kobayashi, O. Nakano and K. Nishidate, *Electrochem. & Solid-State Lett.*, **2**, 320(1999).

A Lithium-Ion Polymer Battery Using PVdF-HFP / Polyethylene Composite Gel Electrolyte

X. Liu, H. Kusawake and S. Kuwajima

Office of Research and Development, National Space
Development Agency of Japan;
2-1-1 Sengen, Tsukuba, Ibaraki, 305-8505, Japan

Introduction

Space missions require the use of high specific energy density and high reliability batteries to provide power for various applications. The lithium-ion secondary batteries with high energy density are promising for space application. Moreover, the lithium-ion polymer batteries are also considered for future small satellite use, because it can be fabricated for a flexible thin film without electrolyte leakage. However, the safety of lithium-ion battery is an important problem during operation under abusive usage, even using the gel electrolyte. To improve the safety of lithium-ion battery with gel electrolyte, it is an effective method using gel electrolyte with thermal shut-down function as internal safety device^{1,2)}. We have successfully prepared a PVdF-HFP / polyethylene (PE, with lower melting point: 90°) composite gel electrolyte with thermal shut-down function³⁾. In this work, we discuss the mechanism of thermal shut-down for the composite gel electrolyte, and tried to use it to the lithium-ion secondary cell.

Results and discussion

PVdF-HFP / PE composite gel electrolyte was prepared by casting the THF solution containing the 1.0 mol / dm³ LiClO₄ / PC + EC (or LiPF₆ / GBL+EC), PE and PVdF-HFP. The composition of resulted gel electrolyte is shown as Table 1. When the content of PE is over 23 wt %, the composite gel electrolyte exhibits the ability to rapidly increase the impedance of the electrolyte, around the melting point of PE. For example, the impedance of the composite gel electrolyte with 45 wt % PE can be rise rapidly by about three orders around 90°. Figure 1 shows the SEM observations of PVdF-HFP/PE composite gel electrolyte before and after thermal shut-down. Before thermal shut-down, the ultra-fine PE particles was uniformly dispersed in the PVdF-HFP gel electrolyte. After shut-down, the PE particles are fused and formed a continuous film. The PE continuous film can be shut-down the ion diffusion, which make the electrode reaction stop, and prevent the thermal runaway of the cell. However, the composite gel electrolyte shows a lower ionic conductivity and poor on mechanical strength. Thus, we prepared a three layers film of pure PVdF-HFP gel / composite gel / pure PVdF-HFP gel for assembling a coin-type lithium-ion cell. And the cell is well worked at normal condition as shown in Fig. 2. In this presentation, we will also report about the cell thermal shut-down behavior under higher temperature.

Reference

1. R. C. Laman, M. A. Gee and J. Denovan, J. Electrochem. Soc., 140, L51, 1993.
2. M. Gee and I. Olsen, US Patent 5,534,365, 1996.
3. X. Liu, H. Kusawake and S. Kuwajima, The 40th Battery Symposium in Japan, 3D12, 1999.

Table 1 Composition of the composite gel electrolyte.

Component	Property	wt %
PVdF-HFP	Mw: 3.2E5; mp: 158°	14• 23
Polyethylene	mp: 90°, or 104 - 115°	23• 54
Plasticizer	1 mol dm ⁻³ , LiClO ₄ / PC+EC or LiPF ₆ / EC+GBL	32• 54

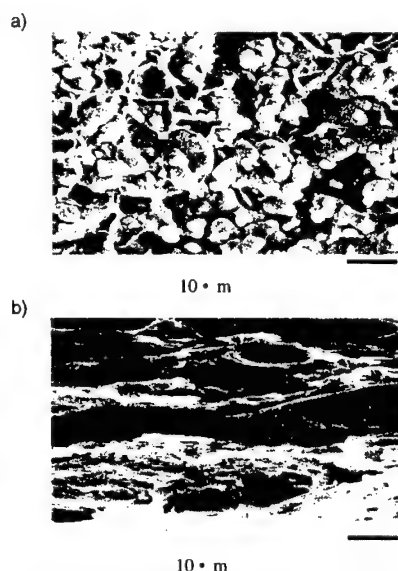


Fig. 1 Scanning electron micrographs of cross-section of the PVdF-HFP/PE composite gel electrolyte. a). before shut-down, b). after shut-down.

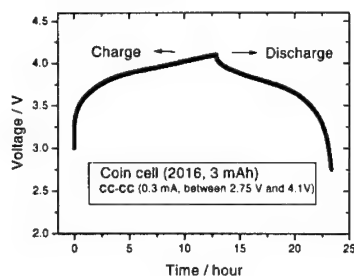


Fig. 2 Typical charge-discharge curves for the coin type lithium ion cell using PVdF-HFP/PE composite gel electrolyte at ambient temperature.

DEVELOPMENT OF SOLID-POLYMER LITHIUM SECONDARY BATTERIES

J. Kuratomi, T. Iguchi, T. Bando, Y. Aihara, T. Ono, and K. Kuwana

Yuasa Corporation,
4-5-1 Ohgi-cho, Odawara 250-0001, Japan

INTRODUCTION

The solid-polymer lithium secondary batteries have been expected to be used for the electric vehicles or load conditioning devices from its safety and high energy density. M. Armand and his coworkers started the studies on the solid-polymer lithium batteries about three decades ago¹⁾. It is well known that one of the difficulties to develop the practical batteries is low ionic conductivity of polymer electrolytes, but problems on the total battery systems composed of all solid materials have not yet been clarified. We have developed 4V-class lithium secondary batteries, whose electrolyte is a solid polymer without including an organic solvent and the anode and the cathode are metal lithium and LiCoO_2 , respectively. Our present achievement is over 300 cycles at charge-discharge test of 1/8C rate. The battery performances have been greatly improved by investigating the solid electrolytes, e.g., polymer structure, lithium salt, the salt concentration, and polymerization method. The characteristics, and present problems of the solid batteries are discussed in this paper.

EXPERIMENTAL PROCEDURE

To obtain the reasonable battery performances for the 4V-class solid-polymer batteries, we adopted the typical LiCoO_2 -Li metal system. The polymer used in this study was a random co-polymer of the ethylene oxide and propylene oxide and the lithium salts tested were lithium imide salts such as $\text{LiN}(\text{CF}_3\text{SO}_2)_2$ (LiTFSI) and $\text{LiN}(\text{CF}_3\text{SO}_2)(\text{C}_4\text{F}_9\text{SO}_2)$, and LiBF_4 . Also the electrolytes having various salt concentrations were prepared. The measurement of the cell impedance was performed by AC impedance method. The deposited components on the lithium were determined by using XPS. The battery cycle ability was obtained by constant current charge-discharge at C/8 at 60 deg.C.. The cut-off voltage was in the ranges between 3.0 and 4.1V.

RESULT AND DISCUSSION

The storage characteristic of the interface resistance is shown in Fig.1 for the batteries including the three different lithium salts. The interface resistance, which corresponds to the equivalent circuit of the interface resistance in the lithium symmetrical cell, increased according to the storage time for the battery systems having the LiBF_4 electrolytes. It can be assumed that the passive layer was formed on the lithium surface due to the decomposition of the anion. This was confirmed by the XPS measurement. On the lithium metal surface, the fluorinated compounds were observed and its concentration was also increased with the storage time in the LiBF_4 batteries. The battery performance was better for the systems composed of the imide salts. Although the similar decomposition was observed in the batteries having imide salts, the existence of the fluorinated components on the anode was much less than that of the LiBF_4 system. It was clearly indicated that imide salt is chemically stable in the battery. The cycle ability decreased significantly in the LiBF_4 system. Generally LiTFSI is electrochemically unstable over 3.6V, i.e. and the corrosion on the aluminum plate is well known.

However, the corrosion of the current collector was not observed in this present LiTFSI system. The cycle ability was achieved over 300 cycles with charge-discharge test with the excellent efficiency of approximately 100%. It was clearly shown that suitable salt concentration is very important for the good battery performances of the cycle ability.

CONCLUSION

To obtain the good battery performance in the secondary batteries, we found that the lithium salt and the suitable salt concentration are important. The present performance is not yet good enough for the practical usage, but it was demonstrated that all solid-polymer lithium-ion batteries are possible.

ACKNOWLEDGMENT

The study was supported by the Energy and Industrial Development Organization (NEDO).

REFERENCES:

1. M.B. Armand, et al., Fast Ion Transport in Solids, Elsevier, New York, 1979, p.131

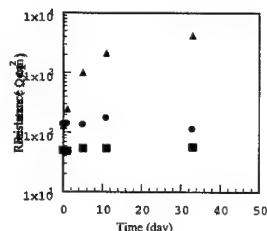


Fig.1 The interface resistance of Li-LiCoO₂ cells are plotted versus storage time: (○) $\text{LiN}(\text{CF}_3\text{SO}_2)_2$, (●) $\text{LiN}(\text{CF}_3\text{SO}_2)(\text{C}_4\text{F}_9\text{SO}_2)$ and (■) LiBF_4

Electrochemical Performance of Gel-type Lithium Polymer Battery

Young-Min CHOI, Jae-II HAN,
Seok-Gwang Doo and Do-Young Seung

Electrochemistry Lab.
Samsung Advanced Institute of Technology
P.O. Box 111, Suwon 440-600, KOREA

Rechargeable lithium batteries, because of their higher energy density, higher voltage, and longer shelf life than competitive system like Ni-metal hydride battery, have attracted much attention over the last decade. Recently, 'rocking-chair' or 'lithium-ion' battery technology was developed to overcome the reversibility and safety problems associated with the lithium metal anode. In this technology, lithium is confined to its ionic state, which is inherently safer than its metallic state. More recently, advances in the miniaturization of new electronic devices such as mobile telephone, lap-top computer and camcorder have required greater innovation in the field of rechargeable lithium battery systems and miniaturization, unpredictable ten years ago. Polymer electrolyte based lithium batteries are actively being developed because of the advantage they offer in comparison to conventional systems containing liquid electrolyte(1, 2). For example, polymer electrolyte based construction allows cell fabrication in a variety of sizes and shapes including spirally wound, rectangular and Z folded geometries. Applications such as cellular phones and smart credit cards require thin flat batteries which are readily fabricated from polymer electrolyte based systems. Also, the excitement in lithium polymer batteries is mainly the reduced thickness and weight reduction of the cell. However, more time will be needed before the polymer battery gains a substantial share in the lithium battery market. The battery is not expected to be an immediate success in replacing the traditional lithium ion battery; however, because of the advantage in safety, the lithium polymer battery will become a key energy source product for the next generation.

The present work is concerned with the electrochemical performance of innovative gel-type lithium polymer battery system. For this purpose, gel-coated electrolyte was prepared by coating acrylonitrile-methyl methacrylate-styrene(AMS) terpolymer on PE(poly ethylene) porous film. The capacity of retaining organic electrolyte solution and mechanical state of the gel polymer was found to be dependent on the AN/MMA/ST molar composition of the AMS terpolymer, as previously reported(3). The gel-type polymer electrolyte supported by PE film were 30 to 50 μm thick films which exhibit good mechanical strength.

The 800mAh-class gel-type lithium polymer battery employing a carbon anode, an AMS-based gel-polymer electrolyte and LiCoO_2 cathode was assembled, and its electrochemical performance was investigated. The gel-type lithium polymer battery showed high rate capability and excellent cell capacity at low temperature. Also, at 1C rate charge-discharge cycling, about 85 % of the initial capacity could be recovered even after 100 cycles. From the electrochemical experiments, it is noted that this gel-polymer electrolyte based cell is very attractive for innovative rechargeable lithium battery system.

ACKNOWLEDGEMENTS

The receipt of research grant under the program 'Development of Material and Cell Technology for Lithium Polymer Battery' from Ministry of Commerce, Industry and Energy, KOREA is gratefully acknowledged.

REFERENCES

1. M. B. Armand, J. M. Chabagno and M. Duclot, in Extended Abstract of Second International Meeting on Solid Electrolytes, St. Andrews, Scotland (1978).
2. K. M. Abraham, *Electrochim. Acta*, **38**, 1233 (1993).
3. D.-W. Kim and Y.-K. Sun, *J. Electrochem. Soc.*, **145**, 1958 (1998).

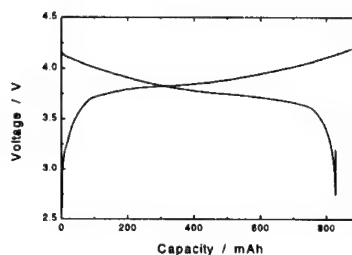


Fig. 1. Charge-discharge curve of 800 mAh-class gel-type cell during the cell formation at 0.1 C rate.

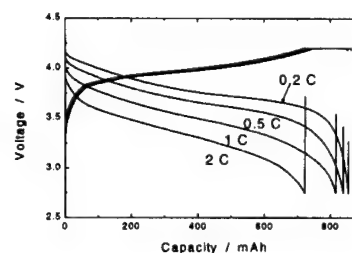


Fig. 2. Charge-discharge curves of 800 mAh-class gel-type cell at various C rate.

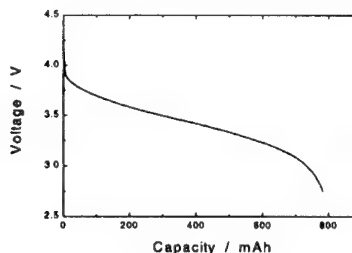


Fig. 3. Discharge curve of 800 mAh-class gel-type cell at -10°C .

ONSET OF DENDRITIC GROWTH IN LITHIUM/POLYMER CELLS

C. Brissot, M. Rosso, J.-N. Chazalviel
Laboratoire de Physique de la Matière Condensée
Ecole Polytechnique - CNRS, 91128, Palaiseau, France
and
S. Lascaud
EDF/DER, BP 1, 77250, Moret sur Loing, France

The all-solid-state lithium battery is considered as one of the promising technologies to fulfil the requirements of the electrical vehicles. In particular, metallic lithium is a good candidate for the anode, since it has a very high theoretical specific capacity. Nonetheless, the formation of dendrites affects the charge efficiency of this type of battery. Our aim is to understand the dendritic growth mechanism in order to prevent or to limit this phenomenon.

In this study, we have studied the onset of dendritic growth in symmetrical lithium/polymer/lithium cells under galvanostatic conditions, at current densities ranging from 10^{-2} to $3 \cdot 10^{-1} \text{ mA cm}^{-2}$, and at temperatures of 70-100°C. The polymer electrolyte consisted of poly(ethylene oxide) ($M_w=3 \cdot 10^5$) and of the lithium salt $\text{LiN}(\text{CF}_3\text{SO}_2)_2$ (abbreviated in LiTFSI), discovered by Armand et al. [1]. The salt concentration in terms of O/Li ratio was 26. We performed experiments in cells consisting of two lithium foils sandwiching a polymer electrolyte layer about 50-100 μm thick.

In the current density range we have investigated, previous *in situ* studies [2] have shown that the dendrites have needle-like morphologies: they appear as bright, metallic filaments. Their cross section is about 10-20 μm which makes them very fragile.

We show in Fig.1 a typical time variation of the cell potential measured at a current density $J = 0.1 \text{ mA cm}^{-2}$. After a rapid increase of the potential, one observes a quasi-stationary behavior for about 3.5 hours. Then a sudden jump is observed (see the arrow in Fig.1), which is attributed to a partial short-circuit of the cell by a dendrite. A rapid degradation of the cell follows.

We have discovered that the time t_{cc} at which the potential jump is observed, follows a power law as a function of J (namely $t_{cc} \sim J^{-2}$), very close to the Sand's law [3]: the Sand's time is the time at which, in a semi-infinite electrolyte, the concentration at the negative electrode would go to zero. However, in our case, for a small inter-electrode distance, and at low current density, the concentration is expected to remain very close to the initial concentration C_0 .

Moreover, experiments performed at different temperatures in the range 70-100°C show that the time t_{cc} increases almost proportionally to the diffusion constant of the ionic species. This again is in agreement with the Sand's behavior.

We think that this surprising result is due to the existence and/or formation of local inhomogeneities at the surface of the electrodes (related either to the geometry of the electrode or to the passivation layer). Due to these inhomogeneities, the concentration distribution tends to become non-uniform. The characteristic time for the onset of this non-uniformity is limited by diffusion, and depends on the current density. A preliminary model describing this effect predicts a Sand-like dependence very close to the observed behavior.

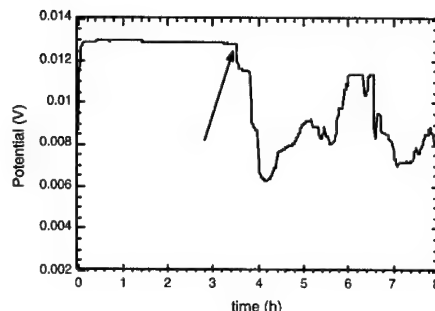


Fig.1 Time evolution of the cell potential ($J = 0.1 \text{ mA cm}^{-2}$). The arrow shows a sudden jump, occurring when a dendrite partially short-circuits the cell.

References

- [1] M. Armand, J. M. Chabagno and M. J. Duclot, in *Fast Transport in Solids*, (Edited by P. Vashishta) 131, North-Holland, New York (1979); M. Armand, W. Gorecki and R. Andréani, in "Second Int. Symp. on Polymer Electrolytes", B. Scrosati, Editor, p. 91, Elsevier Applied Science, London (1990).
- [2] C. Brissot, M. Rosso, J.-N. Chazalviel and S. Lascaud, *J. Power Sources*, 81-82, 925-929 (1999)
- [3] H.J.S. Sand, *Phil. Mag.* 1, 45 (1901)

Abstract No. 376

Influence of Added Plasticizer on Dispersion of Electrode Active Materials and on the Discharge Performance of Plastic Lithium Ion Batteries

Hyungkeun Lee, Tae Hyung Kim, Hyang Mok Lee, and Soonho Ahn
Battery Research Institute, LG Chemical, Taejeon, Korea

Since the introduction of plastic lithium ion battery technology by Bellcore (now Telcordia) [1], poor low temperature performance and low energy densities during high rate discharge (compared to their liquid lithium ion counterpart) has been the most blamed for the very limited success in various portable applications. High intra-electrode resistance as well as transport limitation within the electrodes causes premature voltage drop to a cut-off during discharge, preventing complete drain of charged batteries. In our efforts to solve this problem, we have found that the high electrode resistance and poor electrode utilization is a result of poor dispersion of electrode active particulates. And the amount of plasticizer added during electrode preparation strongly dictates the uniform distribution of carbon black conductive additives. According to Telcordia technology, plasticizer added in the binder renders temporary flexibility to electrode film and easiness in lamination with separator film by lowering melting point of polymer material to make battery structure.

To prepare electrodes we have followed Telcordia description [1] such that LiCoO_2 and MCMB are added into a binder solution along with appropriate conductive agents and plasticizer to cast into electrode films. The materials adopted for this study were Kynar 2801 (Elf Atochem) as a binder, acetone as a casting solvent, and dibutyl phthalate (DBP) as an extractable plasticizer. DBP was removed, after cell fabrication, with ether to make the electrode binder permeable to lithium ions. Half cells were fabricated with electrode films with varied DBP content. Electrolyte was 1M LiPF_6 in EC/EMC solution throughout this study. Examined were electrode physical properties, surface morphology, ac impedance, and charge/discharge behavior.

In general, we have observed that the discharge capacity at high drain rates improves with DBP content in the pristine electrode film as shown in Figure 1. The increased capacity can be attributed to the increase in electrode porosity. The higher DBP amount in the film, which acts as a pore former, the higher void space left behind. Figure 1 also demonstrates a far less voltage drop during discharge at higher DBP contents as indicated by the capacity difference between 3.3V and 3.6V termination. SEM pictures (Figures 2 and 3) exhibit very interesting features on the dispersion of cathodes - one with poor contacts of LiCoO_2 particles with conductive carbon matrix, the other with very intimate inter-mixing. Figure 3 shows the surface of the electrode prepared with a film with 42 vol % of DBP while Figure 2 that with 36%. It can be expected or speculated that surplus amount of plasticizer enhances dispersion of carbon black by saturating micropores in the carbon aggregates and reduces surface energy to bring about more uniform mixing. Or alternatively, excessive amount of DBP expands the volume of binder-carbon black mixture to fill up the electrode void space more easily.

Reference

- [1] Tarascon, J.M., Gozdz, A.S., Schmutz, C., Shokoohi, F.K., and Warren, P.C., *Solid State Ionics*, **86**, 49 (1996)

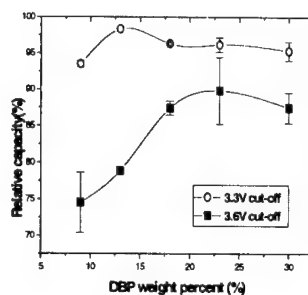


Figure 1. Relative capacities of cathode within various DBP at each cut-off voltage.



Figure 2 and 3. SEM Images of cathodes prepared with 36 and 42 vol% DBP, respectively.

Use of Grafted PVdF-based Polymers in Lithium Rechargeable Batteries

C R Jarvis, W J Macklin, A J Macklin, N. J. Mattingley and E Kronfli^a

AEA Technology Batteries

Culham Science Centre, E1 Culham, Abingdon, Oxfordshire, OX14 3ED, U.K.

^aRMCS, Shrivenham, Swindon, Wiltshire, SN6 8LA, U.K.

Introduction

Many Li-ion batteries and Li-ion polymer batteries contain PVdF-based polymers as electrode binders¹ and gel electrolytes². Whilst PVdF-based polymers show good chemical and electrochemical stability in the Li-ion cell environment, their performance can be improved by use of grafted additives³. Areas that have been considered for development include:

- 1 improvement of the adhesion of the electrodes to current collectors,
- 2 development of a thin conductive layer on current collectors,
- 3 modification of the solubility characteristics of the polymer, and
- 4 modification of polymer properties to increase uptake of electrolyte.

A range of additives have been grafted onto PVdF-based polymers and assessed for these properties. Grafting is achieved by first subjecting the base polymer to irradiation to activate the substrate. The graft monomer material is then brought into contact with the polymer. The degree of grafting is determined by several factors, including contact time with the graft monomer, the extent of substrate pre-activation, the extent to which the graft monomer can penetrate the substrate and reaction temperature.

Results

An improvement in the adhesion of electrodes containing PVdF-based polymers to current collectors has been obtained by use of acrylic acid (AA) or methacrylic acid (MAA) grafted PVdF. For example, peel tests were performed on composite anodes with copper current collectors according to ASTM D1876-72. The results of such tests are given in Table 1. It can be seen that the adhesion of the composite electrode to the copper current collector is significantly improved by use of AA-g-PVdF as electrode binder.

The use of dimethyl acrylamide (DMAM) has been evaluated as graft additive to PVdF to modify the solubility characteristics of PVdF. Homopolymer PVdF is soluble in aprotic polar solvents at room temperature, such as dimethyl acetamide, dimethyl formamide and N-methyl pyrrolidinone⁴. However, homopolymer PVdF grafted with 15 wt% dimethylacrylamide is soluble in acetone. Such modifications to the polymer characteristics increase the options available for mix formulation.

Small 0.5 Ah soft-packaged graphite - LiCoO₂ test cells have been fabricated containing dimethyl acrylamide grafted PVdF in the electrolyte layer. Cells containing such electrolyte films exhibit stable cycle behaviour as illustrated in Figure 1.

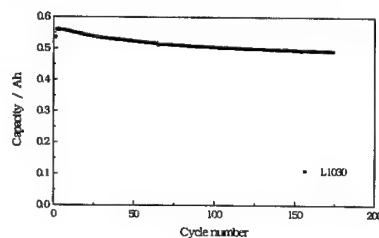
Conclusions

Improvements to the properties of PVdF-based polymers have been demonstrated by the use of grafted additives. In particular, improvements in adhesion and changes to solubility characteristics have been achieved.

Table 1 Effect of use of AA-g-PVdF on adhesion of composite anode to copper current collector

Mean value of 3 samples	Average load N	Maximum Load N	Average strength Nmm ⁻¹
PVdF	0.107	0.525	0.0043
AA-g-PVdF	0.222	0.908	0.0089

Figure 1 Cycle performance of Li-ion polymer cell containing DMAM-g-PVdF polymer electrolyte



References

1. S. Megahead & W Ebner, J. Power Sources, **54**, (1995) 115
2. J.-M Tarascon, A. S.Gozdz, C. Schmutz, F. Shokoohi & P.C. Warren, Solid State Ionics **86/88** (1996) 49
3. E. Konfli & C.R. Jarvis EP 0 793 286 B1
4. Solef - Polyvinylidene fluoride from Solvay, Properties

THE PRODUCTION AND STUDY OF PHYSICAL AND CHEMICAL PROPERTIES OF THIN-FILM CC-ES

V.A. DUSHEIKO, L. P. PASKAL, V. U. BURYAK

Department of Chemistry, Kiev State Trade and Economic University, 19, Kioto St., Kiev, 253156, Ukraine
Kiev Taras Shevchenko University, 252017, Kiev, Vladimirska St. 64, Ukraine

1. Introduction

An active development of solid thin-film lithium polymer batteries (LPB's) is closely associated with solving the problem of highly energy-intensive and environmentally pure power sources useful for both the power industry (to decrease peak loads of electric power stations, electric cars) and low-power electric devices. The main advantage of LPBs is the possibility of putting the battery into a necessary shape, the battery being a part of devices as a construction material.

A success in developing LPBs is intimately bound up with the search for film-forming Composite Cathode-electrolyte systems (CC-ES) consisting of a Li^+ -conducting solid polymer electrolyte (SPE) [1,2] and highly energy-intensive active cathode material dispersed in the SPE.

This work is aimed at the search for and production of such thin-film CC-ES with the use of the TiS_2 -SPE system, determination of its conductivity dependence on the filler content.

2. Experimental

One of the promising to improve operating characteristics of SPEs used at normal temperatures is the employment of non-regular polymers, in particular, co-polymers, as a matrix. This allows physical and chemical properties of the electrolytes under consideration to be optimized for a maximum ionic conductivity to be achieved.

Our preliminary results summarized in Table 1 show that the most suitable electrolyte compositions (for their conductivity and physical and chemical properties) are those with LiClO_4 based on two co-polymers: poly (acrylonitrilestyrene) and poly (acrylonitrilevinylacetate). The two are readily soluble in acetone and formamide, respectively. As a filler in CC-ES titanium disulfide (TiS_2) has been chosen. It is satisfactorily compatible with the above polymers.

Properties of TiS_2 are presented in [3-5].

Table 1. Composition and ionic conductivity of SPE films based on different polymer matrices at $T=20^\circ\text{C}$.

Polymer Matrix	LiClO_4 , % of polymer weight	PC, % of polymer weight	Solvent	Thickness of film, μm	σ , S/cm	Comment
AN-VA poly (acrylonitrilevinylacetate)	20	-	DMF	60	$1.4 \cdot 10^{-5}$	Stable mechanical properties
AN-VF poly (acrylonitrilevinylidene fluoride)	15	-	DMF	40	$3 \cdot 10^{-4}$	Stable mechanical properties
SAN poly (acrylonitrilestyrene)	20	15	Ac	100	$1.2 \cdot 10^{-5}$	Stable mechanical properties

The following co-polymers were used in the work: SANS-poly (acrylonitrilestyrene) and AN-VA-poly (acrylonitrilevinyl acetate).

As a plasticizer and additional donor of Li^+ ions an aprotic electrolyte (EPIEL) was used in the CC-ES. The electrolyte with a high PC content is 1M LiClO_4 in propylene carbonate: dimethoxyethane with a conductivity of $1.2 \cdot 10^{-2}$ S/cm. Its weight composition corresponds to LiClO_4 (9,2%) - PC (69,2%) - DME (21,6%), $d=1,2$ g/cm.

The method of producing CC-ES films comprises the following steps:

1. Preparation of solution of dry LiClO_4 in anhydrous acetone (9% solution for SAN) or dimethylformamide (6% solution for AN-VA).
2. Stirring of the solution with a calculated amount of co-polymers in a magnetic stirrer for 6 to 8 hours until a viscous polymer electrolyte is produced.
3. Milling and drying of TiS_2 powder (at 200°C in vacuum over P_2O_5 for 2 hours).
4. Impregnation of the TiS_2 powder with a solution of aprotic electrolyte - EPIEL for 2 hours.
5. Dispersion of the TiS_2 powder in co-polymer solution for 2 hours in an ultrasound disperser.
6. Applying of liquid CC-ES to a glass substrate in a dry box under argon by casting.
7. Drying of the CC-ES films in a vacuum drier over P_2O_5 for 20 to 48 hours at 30 to 35°C .

It has been found that in introducing more than 40% disperse filler into the polymer electrolyte matrix both composite systems become more electroconductive, and with further increasing titanium disulfide content the conductivity increases by 3 to 4 orders in comparison with the initial SPEs. Within the 62 - 65% filling range CC-ES films based on the two polymer electrolytes possess satisfactory mechanical properties and strength. The composite with more than 65% filling losses elasticity and become brittle.

The transition from purely ionic conductivity characteristic of SPEs to ion-electron one inherent to CC-ESs involves a change in the structure of composite system with increasing the degree of its filling. This results in the formation of a continuous cluster from the filler particles. In other words, a certain part of the disperse filler forms a continuous phase from the particles which are in contact with each other thereby providing the appearance of conducting ways. Studies of the structure of CC-ESs carried out with a scanning electron microscope verify the formation of continuous electron-conducting phases (clusters) of the filler with increasing its concentration in the system.

3. Conclusions.

1. CC-ESs films based on co-polymers of polyacrylonitrile with titanium disulfide have been produced for the first time. A dependence of ion-electron conductivity of CC-ESs on the filler concentration has been established. An optimum TiS_2 content has been shown to be within the 62-65% range of the total mass of composite whose conductivity is $\sim 10^{-2}$ S/cm.

4. References.

1. V.A. Dusheiko, V.V. Mikhailik, N.G. Parkhomenko 40th Meet. Int. Society Electrochemistry, Kyoto, Japan, 1989, №886
2. V.A. Dusheiko, M.S. Lipkin, A.E. Redun Ext. Abstr. 6th IMLB, Münster, Germany, 1992
3. V.A. Dusheiko, M.S. Lipkin - J.P.S., 54, 1995, p.264-267
4. V.G. Syromyatnikov, L.P. Paskal, V.A. Dusheiko Ext. Abstr. 8th IMLB, Nagoya, Japan, 1996
5. V.A. Dusheiko, L.P. Paskal Ext. Abstr. 9th IMLB, Edinburgh, Scotland, 1998

^7Li -Nuclear Magnetic Resonance Observation of Lithium Insertion into Coke Carbon Modified with Mesophase-Pitch

Yuichi Sato, Ken-ichi Tanuma, Toshio Takayama, Koichi Kobayakawa, Takanobu Kawai*, and Akira Yokoyama*

Department of Applied Chemistry, Faculty of Engineering, Kanagawa University, 3-27-1 Rokkakubashi, Kanagawa-ku, Yokohama 221-8686, Japan

*Nippon Carbon Co., Ltd.

1-1 Shin-Urashimacho, Kanagawa-ku, Yokohama 221-0031, Japan.

Introduction : To increase the capacity of carbon electrodes for use in lithium ion secondary batteries, coke carbon was modified with mesophase-pitch carbon by a heat treatment¹⁾. In the present paper, we attempted to investigate the lithium insertion into the modified carbon using solid-state ^7Li -nuclear magnetic resonance (^7Li -NMR) spectroscopy.

Results and Discussion : Modified cokes were obtained by heat-treatment at 800, 1000, and 3000°, where coke carbon itself was at first heated at 3000°C. Figure 1 shows the ^7Li -NMR spectra of the modified cokes charged to 0V(vs. Li/Li^+). The main peaks accompanied by spinning side bands were clearly observed at 43.9, 44.4, and 43.6ppm. The other peaks were observed at ca. 17 ppm as shown in Figs. 1 (b) and (c) for the modified coke heat-treated at 800 and 1000°C. The spinning side bands corresponding to these peaks did not appear. The peak at about 45 ppm indicated that the first-stage $\text{Li-GIC}(\text{LiC}_8)$ is present^{2, 3)}, and the ca. 17 ppm peak indicated that lithium was stored in the modified part showing more ionic character as the modified carbon was charged to 0 V.

The dynamic behavior of the intercalated Li nucleus was evaluated using the spin-lattice relaxation time (T_1). The T_1 values for the modified coke heat-treated at different temperatures are shown in Table 1. The T_1 values of the modified coke heat-treated at 800, 1000, and 3000° showed almost identical values of 1.8 s in the graphite part as they are charged to 0V. However, the values of the modified part of the heat-treated carbon at 800 and 1000° are significantly different compared with that of the graphite part, which are 0.38 s and 0.63 s, respectively. This means that the Li nucleus stored in the modified layer can move more freely compared with that in the graphite part. For the 1000°C heated carbon, T_1 increased about two times from 0.87 s to 1.8 s in the graphite part charged from 0.1 V to 0 V, which suggests Li-GIC changed from the second stage (LiC_{18}) to the first stage and the dynamic behavior of the Li nucleus was restricted as the Li density in this stage increased. On the other hand, T_1 values in the modified part and bulk mesophase-pitch carbon itself(not shown here) heated at 800

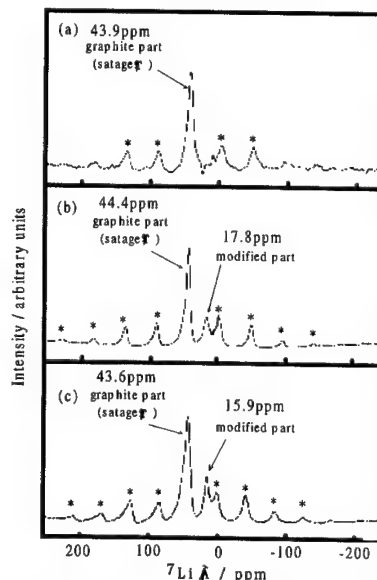


Fig. 1 ^7Li -NMR spectra of modified coke charged to 0V in the second cycle.

(a) HTT 3000°, (b) HTT 1000°, (c) HTT 800°
Ref. is LiCl ($\delta = 0.0$) * ssb (spinning side bands of stage 1)

Table 1 Relaxation time of modified coke.

Sample	T_1 (s)	
	graphite part	modified part
modified coke - HTT 3000° charged to 0V	1.8 * 1	
modified coke - HTT 1000° charged to 0.2V	— * 2	0.48
modified coke - HTT 1000° charged to 0.1V	0.87	— * 3
modified coke - HTT 1000° charged to 0V	1.8	0.38
modified coke - HTT 800° charged to 0V	1.8	0.63

* 1 : Only one peak appeared, and Li in the graphite part and in the modified part could not be distinguished.

* 2 : Li is not present in the graphite part at this potential.

* 3 : Signal is too small to analyze the data although Li is present.

and 1000°C did not change so much charged from 0.2 V or 0.1 V to 0 V. This may suggest modified layer does not form a stage structure.

References

1. Y. Sato, Y. Kikuchi, T. Nakano, G. Okuno, K. Kobayakawa, T. Kawai, and A. Yokoyama, *J. Power Sources*, **81-82**, 182 (1999).
2. J. Conard and H. Estrade, *Mater. Sci. Eng.*, **31**, 173 (1977).
3. K. Zaghib, K. Tatsumi, Y. Sawada, S. Higuchi, H. Abe and T. Ohsaki, *J. Electrochem. Soc.*, **146**, 2784 (1999).

X-ray photoemission studies of surface pre-treated graphite electrodes

R. I. R. Blyth¹, H. Buqa², F. P. Netzer¹, M. G. Ramsey¹,
J. O. Besenhard², P. Golob³, and M. Winter²

¹ Institute für Experimentalphysik,
Karl-Franzens-Universität Graz, A-8010 Graz, Austria

² Institute for Chemical technology of Inorganic
Materials, Graz University of Technology,
Stremayrgasse 16/III, A-8010 Graz, Austria

³ Research Institute for Electron Microscopy, Graz
University of Technology, Steyergasse 17/III, A-8010
Graz, Austria

Graphite anodes in lithium ion cells have to be protected by a film of electrolyte decomposition products, which in ideal cases is lithium permeable, but electronically insulating. This film, known as solid-electrolyte-interphase (SEI), halts the electrolyte decomposition while permitting cell operation, but inevitably involves the consumption of both lithium and electrolyte, leading to a loss in charge called the irreversible capacity, C_{irr} . Minimising C_{irr} while still forming a functioning SEI is clearly advantageous.

One route to efficient SEI formation involves surface treatment of the graphitic materials prior to the employment of the carbon in the electrode. Treatment with oxygen and carbon dioxide at elevated temperatures, for example, has been shown to lower C_{irr} [1]. In this contribution, we investigate the suitability of two different graphitic materials as model materials for surface studies using X-ray photoemission spectroscopy (XPS).

Graphite basically possesses two kinds of surfaces, prismatic (edge) surfaces and basal plane surfaces. Whereas the basal plane surfaces of graphites essentially contain only carbon atoms, the surface chemistry of the prismatic planes includes various, mostly oxygen surface-groups, such as carboxyl- and hydroxyl-groups, for example. With regard to a modification treatment with gaseous reactants at elevated temperatures, the chemical composition of the prismatic surfaces may be changed significantly, i.e., these are the surfaces of interest for XPS analysis. In contrast, the basal planes of single-crystal graphite are, in any case, rather unreactive. With regard to anode performance, again the surface chemistry and morphology of the prismatic surfaces of graphite play a major role in chemical and electrochemical reactivity, interaction with SEI products, etc. [1] Finally, it should be noted that transport of either solvated or unsolvated lithium cations take place via the prismatic planes rather than the basal planes.

The materials investigated were TIMREX[®] SFG 44 (TIMCAL AG) graphite powder and Thorne[®] P100S carbon fibres (Amoco). SEM micrographs show that the SFG 44 powder consists of small platelets, with a relatively small proportion of the surface area consisting of prismatic planes. In contrast the P100 S fibre cross-section shows a radial distribution of graphitic layers, ensuring that the fibre surface is dominated by prismatic planes. Both of these materials were subjected to four different surface pre-treatments: CO₂ and O₂ treatment at

elevated temperatures, [1] and two at present proprietary treatments, P1 and P2.

XPS survey spectra were used to determine the surface elemental composition of the treated and untreated materials. C 1s spectra can be used to determine the chemical state of the surface C groups. We discuss the peak assignments and lineshapes appropriate to the graphitic C 1s photoemission, and the uncertainties involved in using curve fitting to extract surface chemical composition. The peak assignments for C-O bonds were taken from the work of Sherwood et al. [2].

The XPS data show that there is very little variation in the surface elemental composition between SFG 44 graphite powder samples regardless of surface treatment, with C and O percentages essentially constant at around 95 % and 5% respectively. Similarly the SFG 44 C 1s lineshapes show very little change with treatment, with the relative C-O group percentage changes observed being of the order of the uncertainties in the curve fitting procedure.

In contrast the P100S fibre data show wide variation in surface chemistry, depending on the surface treatment followed. Surface elemental composition was found to vary from 70 % carbon for the two proprietary treatments, to 95 % carbon for CO₂ treatment, with significant and sometimes dramatic changes in the C 1s lineshape, showing a wide variation in the relative percentages of different O functional groups. In particular treatment P2 resulted in only 4% graphitic carbon remaining on the surface, with the remaining surface carbon signal being distributed quite widely among several different C-O groups.

We suggest that the SFG 44 XPS signal is dominated by the basal plane, whose chemistry remains essentially unchanged with surface treatment. The P100S data, however, are dominated by the prismatic planes of interest, and therefore we are able to directly observe the surface chemistry, which is thought to be relevant to SEI formation. Further experiments were carried out using SFG 6 powder, with a smaller average particle size than SFG 44 (3µm cf. 22µm) and thus a larger proportion of prismatic surface area. However, even the surface treatment which produced the most dramatically altered surface chemistry for the P100 S fibres, proprietary treatment P2, did not produce a significant change in the SFG 6 C 1s lineshape.

We conclude that the XPS investigations of graphitic carbons are strongly influenced by the texture of the respective material, in particular by the amount of prismatic surfaces exposed to the X-ray-beam.

- [1] M. Winter, H. Buqa, B. Evers, T. Hodal, K.-C. Möller, C. Reisinger, M. V. Santis Alvarez, I. Schneider, G. H. Wroldnigg, F. P. Netzer, R. I. R. Blyth, M. G. Ramsey, P. Golob, F. Hofer, C. Grogger, W. Kern, R. Saf, and J. O. Besenhard, ITE Batt. Lett. 1(2), 129 (1999)
- [2] Y. Xie and P. M. A. Sherwood, Appl. Spectrosc. 44, 797 (1990), and references therein.

Support by the Austrian science fund in the special research program "Electroactive Materials" is acknowledged.

Raman Microscopy as a Quality Control Tool for Electrodes of Lithium-Ion Batteries

Petr Novák and Jan-Christoph Panitz

Paul Scherrer Institute, Laboratory for Electrochemistry,
CH-5232 Villigen PSI, Switzerland

Several tens of millions of lithium-ion cells are manufactured monthly worldwide. For the market success of the final products, fast and reliable component characterization tools are needed, since component quality is crucial. Carbonaceous materials are used in both electrodes of a lithium-ion battery. Raman spectroscopy is well suited for an analysis of the structural properties of carbons. Moreover, even the electroactive oxides used in positive electrodes can readily be characterized by Raman spectroscopy. The surfaces of the electrodes are not homogeneous and typically reveal one or two types of carbon and/or an oxide, a binder, and occasionally an additive, hence a lateral resolution at the electrode surface corresponding to a typical particle size of a few μm must be achieved in order to successfully characterize each component individually. The required resolution can be accomplished with surface mapping techniques based on Raman microscopy. It was the aim of the present work to demonstrate that the Raman mapping technique is suitable for a quality control of battery electrodes.

The spectrum seen in Fig. 1 shows that Raman microscopy is able to differentiate the main components of a commercial cathode. From the well-developed signals in the wavenumber range from 900 to 1200 cm^{-1} , which are assigned to second-order modes of LiCoO_2 , we infer that the manufacturer of this electrode used a well crystallized pigment, while the spectral features due to the carbon matrix indicate that pyrolytic carbon was used as the conductive filler. The arrows point to the bands used a follow-up evaluation performed to illustrate the distribution of LiCoO_2 and pyrolytic carbon, which is shown in Fig. 2 for that particular electrode sheet. On the gray scale employed, lightness is proportional to the ratio R , defined as $R = I(\text{A}_{1g}\text{-mode, LiCoO}_2)/I(\text{2D-band, carbon})$. Therefore, darker shades correspond to spots with low or zero LiCoO_2 content, whereas the light gray zones correspond to areas with higher amounts of LiCoO_2 . Further analysis of the Raman map allows one to calculate the band position and linewidth at each point of the map where signals of LiCoO_2 are present. In this way a fingerprint is obtained for a particular electrode. For example, Fig. 3 shows the distribution of band positions for two different cathodes. For cathode A, the average value of the band position of the A_{1g} -mode is $585.7 \pm 4.0 \text{ cm}^{-1}$ (set of band positions at 87 sites), while cathode B is characterized by an average band position of $587.1 \pm 12.0 \text{ cm}^{-1}$ (set of 163 band positions). Similar calculations can be performed on linewidths and intensity ratios. With this approach, therefore, possibilities open up to correlate a set of Raman fingerprints for each electrode type with the performance of the same electrode in a lithium-ion cell.

We are grateful to Dr. F. Joho and Dr. O. Haas, both of Paul Scherrer Institute, for useful discussions.

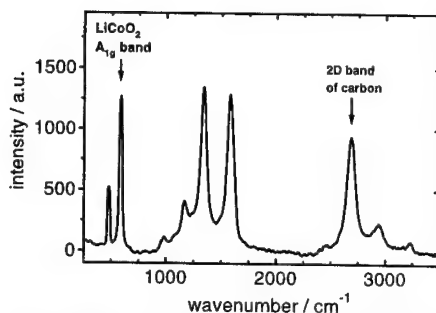


Fig. 1: Raman spectrum for the surface of a typical cathode.

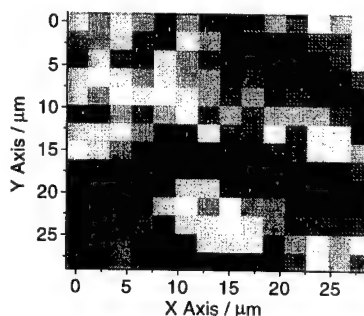


Fig. 2: Map of band intensity ratios R obtained by Raman microscopy for the surface of a typical cathode.

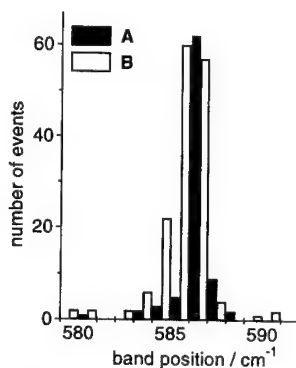


Fig. 3: Distribution of band positions of the A_{1g} -mode of LiCoO_2 recorded for two different cathodes, A and B.

Structural and concentrational changes in lithium polymer electrolytes under current flow: In situ micro-Raman investigation

D. Ostrovskii, P. Jacobsson
Department of Experimental Physics, Chalmers
University of Technology, SE-41296 Göteborg, Sweden

The interest in lithium and lithium ion polymer batteries is motivated by their high applicability in a wide range of devices, such as microelectronics and electric vehicles. During the years a considerable effort have been made to improve the performance of the batteries. The present work mainly concerns the optimization of the individual components (polymer electrolyte (PE), cathode, anode) and the strive for better compatibility between the PE and electrodes. However, despite a large number of studies devoted to the different properties of the components themselves [1-3], there are very few investigations concerning dynamical processes occurring during battery operation [4]. However, it is clear that applied potential will cause not only a current of lithium cations through the PE but, obviously, an opposite flow of negatively charged species will appear as well. Such a situation may result in essential structural changes and concentration redistribution inside the PE membrane, which, in turn, may significantly change the properties of the material. Therefore a knowledge of dynamical properties of the polymer electrolyte becomes extremely important.

To obtain dynamical information about the structural and compositional variations in polymer electrolytes under applied potential, we designed a special chamber, which allows simultaneous control of external (temperature and atmosphere) and electrochemical (applied current/potential) conditions (Fig. 1). In addition, since the diameter of the laser spot in micro-Raman experiments is significantly less than the typical thickness of an investigated membrane (3-10 vs 200-500 μm), it allows determination of concentrational profiles of different components in the system through the membrane crosssection.

In this work we present the results of spectroelectrochemical study of several typical PE systems. Figure 2 shows Raman spectra of a polymer gel electrolyte (LiClO_4 - ethylene carbonate (EC) - polyacrylonitrile (PAN)) recorded at three different positions in the sample: near the two electrodes and in the middle of the membrane. It is clearly seen that while the initial material is highly homogenous (plot A), an essential redistribution of the Li cations through the membrane crosssection appears when an external potential is applied (plot B). We note an intensity increase of the spectral bands at about 730 and 907 cm^{-1} characteristic for Li-solvent complexes [3] (marked with asterisk) and an appearance of a pronounced high frequency shoulder near the spectral band of $\nu_1(\text{ClO}_4^-)$ (marked with arrow), that may be attributed to the creation of solvent shared ion pairs [3]. In addition to these changes, which indeed are expected, we also note an essential decrease of the PAN concentration at the SS side of the sample. It is seen that the characteristic band of C \equiv N stretchings of PAN (around 2220 cm^{-1}) is absent near the SS electrode.

Concentrational and compositional changes occurring in different PE at battery operation will be discussed and analysed.

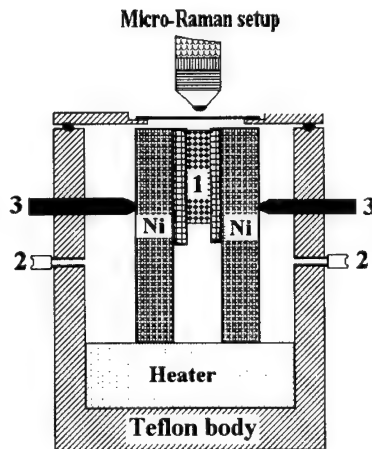


Fig. 1. Schematic presentation of the chamber for in situ spectroelectrochemical investigations. 1 – battery assembly; 2 – purging inlet/outlet; 3 – potentiostat/galvanostat connection.

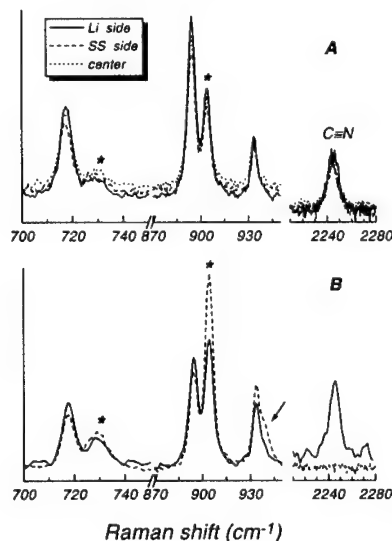


Fig. 2. In situ Raman spectra of the LiClO_4 -EC-PAN polymer gel electrolyte: A – initial membrane, B – during Li current flow.

Current flow direction: Li \rightarrow SS (stainless steel).

This work was supported by MISTRA (Sweden).

1. H Akashi, S L Hsu, W J MacKnight, M Watanabe, N Ogata, *J. Electrochem. Soc.* 142, L205 (1995).
2. D Aurbach, B Markovsky, A Shechter, Y Ein-Eli, H Cohen, *J. Electrochem. Soc.* 143, 3809 (1999).
3. D Ostrovskii, A Brodin, L M Torell, G B Appetecchi, B Scrosati, *J. Chem. Phys.* 109 7618 (1998).
4. I Rey, J-L Brunel, J Grondin, L Servant, J-C Lassegues, *J. Electrochem. Soc.* 145, 3034 (1998).

Abstract No. 383

Studies of Lithium Battery Materials using Cold Neutron Depth Profiling

G.P. Lamaze, H.H. Chen-Mayer and D. Becker
National Institute of Standards and Technology
Chemical Science and Technology Laboratory
Gaithersburg, MD 20899-8395

F. Vereda, A. Gerouki, N. Clay, P. Zerigian, T. Haas and
R.B. Goldner
Electro-Optics Technology Center
Tufts University
Medford, MA 02155

The technique of neutron depth profiling (NDP) permits the analysis of depth profiles in thin films up to a few micrometers for several light elements. The most readily analyzed elements are lithium, nitrogen and boron. Lithium of course is the principal element in the subject of this conference, although many of the materials also contain nitrogen. The lithium depth profiles are based on the measurement of the energy of alpha particles and/or tritons from the ${}^6\text{Li}(n,\alpha){}^3\text{H}$ reaction. Nitrogen depth profiles are based on the measurement of the energy of protons from the ${}^{14}\text{N}(n,p){}^{14}\text{C}$ reaction. Samples are placed in a beam of "cold" neutrons, and the outgoing charged particles are measured by surface barrier detectors, which record both the number and energy of the particles. Comparing the emission intensity with that of a known standard leads to quantitative determination of the lithium and nitrogen concentrations. The emitted charged particles lose energy as they exit the film; this energy loss provides a direct measurement of the depth of the originating lithium nucleus. A great advantage of the NDP technique is that it is non-destructive, which allows repeated observations of the concentrations under different conditions. When combined with other techniques, e.g., activation analysis, ratios to other constituents can be determined.

Figure 1 gives an example of the technique. Two samples of lipon manufactured under different conditions have been profiled. The concentrations in at/cm^3 are presented as a function of depth. Because the alpha particle loses energy at a greater rate than the proton, the resolution for the lithium profile is better than that for nitrogen. One observes that the sample Y245 has a much more uniform distribution of lithium than sample Y239. By integrating the areas under the curves, one obtains the average concentration ratio of lithium to nitrogen. Table I gives measured lithium/nitrogen ratios and the thicknesses of four lipon samples.

The method can also be combined with other techniques to provide other isotope ratios. Figure 2 gives lithium depth distributions for two thin films of LiCoO_2 . After the depth distributions were obtained, the samples were encapsulated in polyethylene "rabbits" for irradiation in the core of the NIST reactor. The total cobalt content concentration was then determined by instrumental neutron activation analysis. Table II gives the lithium/cobalt atom ratios for these and other samples.

The data acquisition method and data analysis techniques are explained. Other examples of profiling of lithium multilayers are given.

Table I

Sample	Atom ratio -Li/N	Thickness, μm
Y243	4.46	0.7
Y232	4.39	1.5
Y239	1.63	0.4
Y245	3.1	0.6

Table II

Sample i.d.	Lithium (at/cm^2)	Cobalt (at/cm^2)	Li/Co Ratio	Ratio Uncertainty (%) (1σ)
Z57a,T	4.9e17	7.0e17	.70	3.5
Z57a,B	2.2e17	7.0e17	.31	3.5
Z57b,T	4.8e17	7.0e17	.68	3.5
Z57b,B	1.9e17	7.0e17	.27	3.5
Z59	9.4e17	7.6e17	1.25	3.5

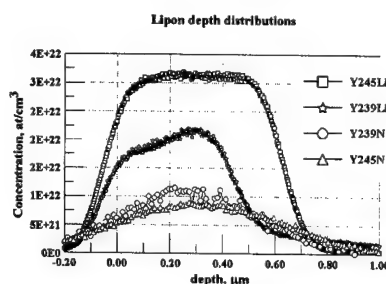


Figure 1. Depth profiles of lithium and nitrogen for two different lipon samples.

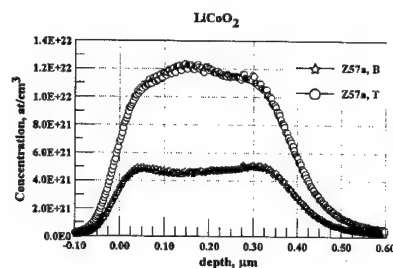


Figure 2. Typical lithium depth profiles of two LiCoO_2 samples.

Application of EELS to characterization of cathode materials for lithium secondary batteries

Y. Shiraishi, I. Nakai, K. Kimoto* and Y. Matsui*

Dept. of Applied Chemistry, Faculty of Science, Science Univ. of Tokyo, Kagurazaka, Shinjuku, Tokyo 162

*National Institute for Research in Inorganic Materials, Namiki, Tsukuba, Ibaraki 305

Introduction

Electron Energy Loss Spectroscopy (EELS) is a comparable technique to XAFS¹⁾. Similar to the XANES region of the XAFS spectrum, ELNES (Energy Loss Near Edge Structure) region of the EELS spectrum, which is a fine structure about the energy loss edge, is closely related to the density of states (DOS) near Fermi energy. The advantage of EELS over XAFS is that the method is suitable for a micro analysis with condensed electron beam and can be applied to an independent particle of submicron size, which is just the case of the cathode materials. EELS measurement is suitable for obtaining low energy region below 1 keV similar to soft-ray XAFS. This technique allows to obtain the information about the O K-edge and L-edge of the transition metals used in the cathode materials. This study demonstrates a performance of EELS and the analytical electron microscope technique for the investigation of the cathode materials.

Experimental

$\text{Li}(\text{Mn}, \text{M})_2\text{O}_4$ (M=Mn, Cr, Co) samples were obtained by a sintering method. These materials were crushed in CCl_4 in an agate mortar, and were spread on carbon supporting films on microgrids. Metallic Fe was evaporated on the microgrids as a standard material for energy calibration of EELS. EELS measurements were carried out by HITACHI HF-3000S transmission electron microscope operating at 300 kV as an acceleration voltage and Gatan parallel EELS spectrometer was used at 0.2 eV per channel as an energy dispersive detector. Electron diffraction pattern and EDX spectrum were taken for each material to characterize the samples. ELNES spectra of Mn-L and O-K absorption edges were obtained from the raw data by energy calibration and subtracting the background.

Result and Discussion

Figures 1(a) and (b) show the white line of the ELNES spectra for MnO after calibration using the zero-loss peak and Fe-L edge peak, respectively. The use of the Fe-L edge, which can be measured simultaneously with the desired core-loss peak of the sample, yielded a better energy axis than that determined by the zero-loss peak which was measured independently. This calibration technique has improved the reproducibility of the chemical shift of the spectrum. The spectra shown below were calibrated with the Fe-L edge. On the other hand, electron diffraction pattern and EDX spectrum were used to help the identification of the sample. Figure 2 shows Mn L-ELNES spectra corresponding to the transition from Mn 2p orbital to the levels near Fermi energy, for several spinel lithium manganates. The white line peak shifts to higher energy side by doping the third cation. This positive shift indicates that the average oxidation state of Mn increased with doping. These results were consistent with the result of XAFS²⁾. Figure 3 shows O K-ELNES spectra of the same materials. Similar to the Mn L spectra, the chemical shift of the white line peak (A) of the O K-edge was also observed by doping the cation. This indicates that the inner shell electrons of both

manganese and oxygen atoms were affected by decrease in the lattice volume when the third cation was doped. Further, the second peak (B) on the higher energy side of the white line appeared for the Cr doped spinel. It is considered that this fine structure (B) could be assigned to the Cr-O bond of the Cr-O_6 octahedron.

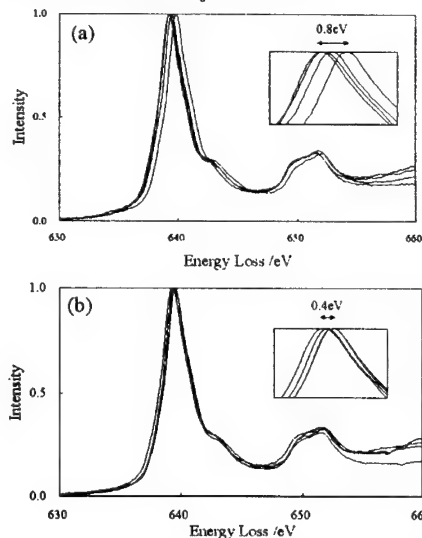


Fig.1. L_{III} peak of Mn L-edge ELNES spectra for several particles of MnO. Energy axis is calibrated by (a) zero-loss peak, (b) Fe core-loss peak.

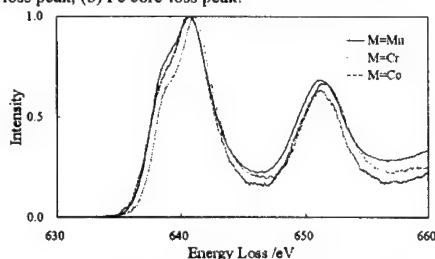


Fig.2. Mn L-ELNES spectra of several spinel compounds $\text{Li}(\text{Mn}, \text{M})_2\text{O}_4$ (M=Mn, Cr, Co).

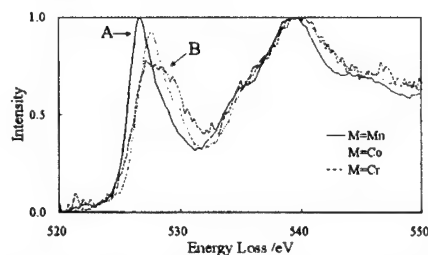


Fig.3. O K-ELNES spectra of the lithium manganates given in Fig.2.

References

- 1) S. Suzuki et al. *J. Phys. Chem. Solids* **57**, 1851 (1996).
- 2) B. Amundsen *J. Phys. Chem. B* **102**, 7939 (1998).

Mechanisms and dynamics of the microcorrosion phenomena in the coin cells of an electrochemical system "CF_{1-x} - lithium"

Valentin N. Mitkin, Tatjana N. Denisova, Vera E. Kerzhentseva, Eugeny A. Shinelev, Viktor V. Moukhlin *)

Recently we noted [1], that the main reason of the corrosion phenomena in the coin «CF_{1-x}» - Li» cells during their storage was not removed moisture at a level of 0.04-0.1 %_{mass} in cathodic composites. Due to slow autocatalytic hydrolysis of C-F bonds the microamounts of HF are generated in the pores of cell's cathode. The most active is HF that located in «open» pores whereas HF from «closed» pores is relatively «calm» during the storage. All components of cell's system «cover-subcover» cathode-separator-electrolyte-Li anode «subcover» «cover» are reacted with HF and other products of microchemical reaction chains. There were observed two separated group of BR2325 cell's behavior under storage - A ([HF] = 0.10-0.5%, OCV = 2.9-3.1 V) and B ([HF] = 0.0-0.04%, OCV = 3.3-3.5 V). This distribution was described in [1]. It has been shown that just [HF] contents in «open» pores of the cathodes determined a future rate of corrosion.

The aim of presented work was the research of main stages and chemical dynamic of corrosion processes and their influences onto life storage of the coin batteries BR2325. Kinetic study of Li, Fe, Cr and Ni migration was made by a standard thermostating of cells (group B) at 40 - 100 °C and chemical analysis of metals in cells.

Microcorrosion products are distributed among internal parts of cell. The typical products of these processes are the solid Fe, Ni, Cr simple and complex fluorides MeF₂, MeF₃, Li₂[MeF₄] which deposited both in the pores of cathodic composite and also onto the boundaries between cathode and subcover (current collector). Part of construction metals migrates through liquid phase as a fluorocomplexes or mixed fluoro- and solvocomplexes to a surface of anode where are reduced to a highly dispersed metal state. The rates of metal deposition and their distribution among all parts of stored cells under various «time-temperature» are shown in tables 1 and 2. Such reactions decreases amount of Li and finally lead to a self-discharge with subsequent shortening of the «CF_{1-x}» - Li» cell's life.

Analyses of all kinetic data are shown, that the rates of metal's migration in cells can be described with zero-order reactions. The temperature dependences of Fe, Ni, Cr and Li migration rate presented in tables 1-3. These data leads to activation energies for Fe, Cr and Ni equal to ca. 14 kcal/mol with a standard deviation ± 15-20 %. Activation energy of Li migration is depends on the stage of process and changed from value of 15 ± 4 in the beginning of heat-treatment to ~7 kcal/g-atom in the middle of reaction and ~1-2 kcal/g-atom in the stationary state of process. We assumes that appointed changes in Li migration rate's behavior are connected with the fact of anodic polymer film slow dissolution at temperature range 70-100 °C. At the same time an activation energy for self-discharge of all «time-temperature» separately tested series of BR2325 cells from B-group is equal 7 ± 1.4 kcal at 25-100 °C. Results of microcorrosion kinetical study are allowed to use this approach for development of improved accelerated method of the BR2325 cell's storage and for other BR-types a self-discharge detection. The mentioned method is also reported this Symposium.

Table 1
Rates of metal migration in group B of BR2325
(n = 3-5 in T-series, S_r = 0.15-0.25, p = 0.95)

T, °C	Rate of Me deposition in components of cell, mg/hr (x10 ⁻⁴)				Selfdischarge of cell, mAh/day
	Fe	Ni	Cr	ΣMe	
RT	4.5-7.2	<0.1	<0.1	5-7	0.04±0.01
40	15	1.5	1	17.5	0.35±0.1

3, Lavrentjeva Pr., Institute of Inorganic Chemistry SB RAS,
Novosibirsk, 630090, RUSSIA
*) 94, B. Khmelitsky Str., JS Novosibirsk Chemical
Concentrates Plant, Novosibirsk, 630110, RUSSIA

70	92	9	6	107	3.19±0.28
100	520	63	61	644	6.96±2.0

Note: T - temperature; RT - room temperature

Table 2
Distribution of metals in components of cells (B)
(n = 3-4 in T-series, S_r = 0.15-0.25, p = 0.95)

Parts of BR2325 cell *)	Rate of metal migration in details of cell design units, -mg/hr (x10 ⁻⁴)				T, °C
	Fe	Ni	Cr	ΣMe	
C	0.9	<0.01	<0.01	0.9	RT
A + S	1.3	<0.05	<0.01	1.3	
CC	1.3-4	<0.1	<0.1	1.2	
FC	28.2	4.2	2.4	34.8	70
A + S	29.6	2.6	2.4	34.6	
CC	34.6	2.3	2.2	39.1	
FC	60.6	10	8.9	79.5	100
A + S	157.2	13.3	13.9	184.4	
CC	306.7	40	38.3	385	

*) - FC - fluorocarbon cathode; A+S - anode + separator;
CC - surface of cathode's subcover

Table 3
Migration of Lithium in BR2325 cells (group B)
(n = 3-5 in T-series, S_r = 0.2-0.35; p = 0.95)

Content Of [H] ⁺ in the cathode mcmol	Rates of Li migration from anode to cathode, W _i (t); mcg/hour			Rate of [F] ⁻ increasing, mg/hr	T, °C
	W _{max} calcd.	W _{min} Plateau	W ₁₈₀ calcd.		
0 - 3	0.17	<0.1	<0.1	<0.1	RT
1 - 3.2	30±7	9±3	13±3	0.6-4.5	55
0 - 21	40±10	5±3	16±4	0.5-2.9	70
0 - 60 *)	108±35	19±7	19±7	3-32	100

*) Acidity after heat storage; **) W₁₈₀ - rate of reaction after 180 hours of storage. Starting acidity is near to 0.

I. V. Mitkin, et al., Proc. Of XIII Ann. Bat. Conf., Calif. State Univ., Long Beach, 13-16.01.1998, pp. 423-428

In Situ Raman Study of a Lithium-Polymer Battery

C. Naudin, J.L. Bruneel, M. Deschamps*, C. Edwards, J. Grondin, S. Lascaud*, J.C. Lassègues and L. Servant

Laboratoire de Physico-Chimie Moléculaire, UMR 5803, Université Bordeaux I, 351 Cours de la Libération, 33405 Talence, France.

*EDF-DER, Les Renardières, BP1, 77250 Moret-sur-Loing, France.

*Bolloré Technologies, ODET BP 607, 29551, Quimper, France.

In a previous work, Confocal Raman Microspectrometry was applied to the study of a symmetric lithium cell $\text{Li}/\text{PEO}/\text{LiTFSI}/\text{Li}$ where PEO is poly(ethylene oxide) and TFSI the $[\text{N}(\text{SO}_2\text{CF}_3)_2]^-$ anion [1]. The salt concentration variations could be measured between the two electrodes when a current was passed through the cell. From these data, it was shown that transport properties of the polymer electrolyte such as salt diffusion coefficient and transport numbers could be derived.

The same experimental approach is applied here to a prototype $\text{Li}/\text{PEO}_{20}\text{LiTFSI}/\text{V}_2\text{O}_5$ battery where the vanadium oxide active material is actually mixed with carbon and polymer binder to make a self-supported cathode film of 20 - 50 μm thickness. The three elements of the battery are interfaced between nickel collectors under vacuum inside a calibrated glass tube as schematised in fig.1. The cell is heated at 80°C and the laser spot is focused onto the edge of the battery along a line of points perpendicular to the electrode/electrolyte interfaces at a depth of about 20 μm for Raman measurements.

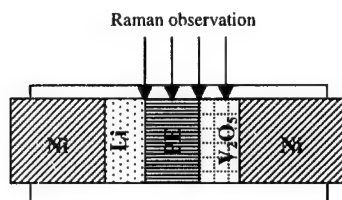


Fig. 1 : Raman Spectroelectrochemical cell made of a glass tube of 8 mm internal diameter and 1 mm thickness, Nickel current collectors (Ni), lithium 100 μm thickness (Li), PEO, 1/20 LiTFSI, 100 μm thickness (PE) and composite cathode V_2O_5 /carbon/electrolyte, 50 μm thickness (V_2O_5).

The geometric configuration of the cell, which resembles industrial designs, allows good electrochemical cyclability of the battery while preserving the cell from moisture for several days. The battery is cycled under galvanostatic

conditions in the potential range 3.2V to 2V. The first discharge, under a current density of $80\mu\text{A}/\text{cm}^2$, gives the expected plateaus in the Potential vs. Lithium intercalation plot (fig.2). As the lithium content in $\text{Li}_x\text{V}_2\text{O}_5$ increases up to $x = 3$, irreversible phase changes occur in the host material [2]. Subsequent charge-discharge cycles are performed under a higher current density of $120\text{-}160\mu\text{A}/\text{cm}^2$.

The battery is submitted to discharge and charge cycles while Raman spectra are continuously recorded along a 120 μm line of selected points (Labram spectrometer, He/Ne laser, x50 ULWD objective). The spatial resolution at a given point is of the order of less than 10 μm . The distance between two points is 5 μm and the time needed to record a spectrum of acceptable quality in the range $250 - 3090\text{ cm}^{-1}$ is of the order of 20 s. As the charge and discharge times are several hours, a very large number of spectra can be recorded at different states of charge of the battery. Information is obtained on the salt concentration variations inside the electrolyte as well as on the redox process at the vanadium oxide insertion compound.

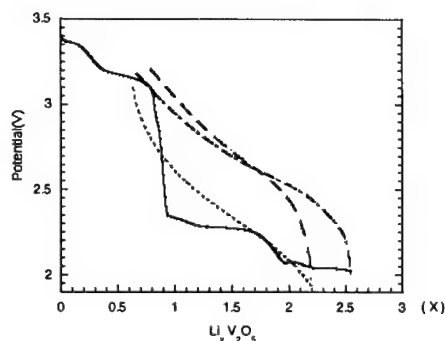


Fig. 2 : Galvanostatic curves of the battery $\text{Li}/\text{PEO}/\text{LiTFSI}/\text{V}_2\text{O}_5$ (—) first discharge ($80\mu\text{A}/\text{cm}^2$), (---) first charge ($60\mu\text{A}/\text{cm}^2$), (.....) second discharge ($160\mu\text{A}/\text{cm}^2$), (-.-) second charge ($120\mu\text{A}/\text{cm}^2$)

References:

- [1] I. Rey, J. L. Bruneel, J. Grondin, L. Servant and J. C. Lassègues, *J. Electrochem. Soc.*, 145 (1998) 3034.
- [2] J.M. Cocciantelli, M. Ménétrier, C. Delmas, J.P. Doumerc, M. Prouhard, M. Broussely and J. Labat, *Solid State Ionics*, 78 (1995) 143.

Quinone-Introduced Conducting Polymers for Supercapacitor Material

Shunzo Suematsu, Ari Manago, Takashi Ishikawa,
and Katsuhiko Naoi

Department of Applied Chemistry,
Tokyo University of Agriculture and Technology
2-24-16 Naka-Cho, Koganei, Tokyo 184-8588, Japan
E-mail: naoi_lab@cc.tuat.ac.jp

As one of the quinone-based conducting polymers with high theoretical specific capacity, we focused on a poly(1,5-diaminoanthraquinone) [poly(DAAQ)] film (theoretical specific capacity: 338 Ah kg^{-1}). [1] We have already demonstrated that poly(DAAQ) has high electronic conductivity in the wide potential range in an acidic aqueous solution and that redox interaction occurs between the π -conjugated system and the quinone group in the polymer. In order to further enhance its specific capacity and its coulombic utilization of the poly(DAAQ) film, we attempted to prepare poly(DAAQ) films complexed with 1,4-benzoquinone (1,4-BQ), 2,6-dichloro-1,4-benzoquinone, or 2,3,5,6-tetrafluoro-1,4-benzoquinone to form various CT complex compounds. Especially, the complex film with 1,4-benzoquinone [a poly(DAAQ)-1,4-BQ film] delivered higher specific capacity (156 Ah kg^{-1}) and higher coulombic utilization (59%) than those for the poly(DAAQ) film itself (50 Ah kg^{-1} , 21%) as shown in Fig.1. The enhancement of specific capacity and the coulombic utilization caused by the introduction of 1,4-BQ to the poly(DAAQ) film was recognized and investigated electrochemically and spectroscopically. The feasibility as a supercapacitor material was discussed.

The enhancement of the heterogenous rate constant (k) of the poly(DAAQ) by the introduction of 1,4-BQ was evaluated by the rotating disk electrode voltammetry. The obtained k for the poly(DAAQ)-1,4-BQ film was $38.8 \text{ cm}^3 \text{ mol}^{-1} \text{ s}^{-1}$, while that for the poly(DAAQ) film was $19.1 \text{ cm}^3 \text{ mol}^{-1} \text{ s}^{-1}$. Such an enhancement of the rate constant can be caused by the promotion of the electron transfer due to the formation of CT complex. The similar behavior was already observed for a polyaniline-1,4-BQ composite film.[2] This promotion of the electron transfer plus the capacity increase mentioned earlier can lead to the enhancement of the energy and power densities when the poly(DAAQ)-

1,4-BQ film is utilized as a supercapacitor material.

FT-IR analysis indicates that there is no direct chemical interaction between the introduced 1,4-BQ and the poly(DAAQ), and that the hydrogen bond between -OH group in 1,4-BQ and $-\text{NH}_3^+$ group in the poly(DAAQ) gives the cross-linked structure. The XRD analysis indicated that the poly(DAAQ)-1,4-BQ film maintained the poly(DAAQ) crystalline structure whose interlattice distance is slightly extended by the incorporation of 1,4-BQ by the formation of the CT complex as shown in Fig.2.

References

- [1] K. Naoi, S. Suematsu and A. Manago, *J. Electrochem. Soc.*, in press.
- [2] E. S. Matveeva, *Synth. Met.*, **83**, 89 (1996).

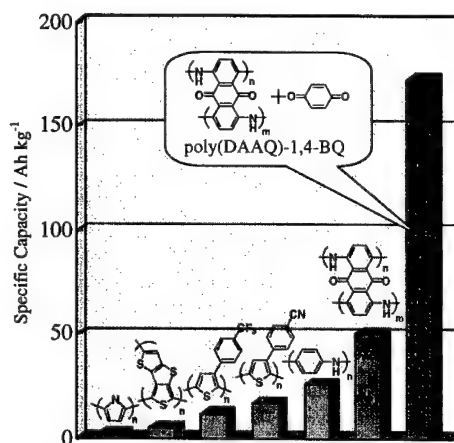


Figure 1. Practical specific capacity of conventional conducting polymers, poly(DAAQ), and poly(DAAQ)-1,4-BQ.

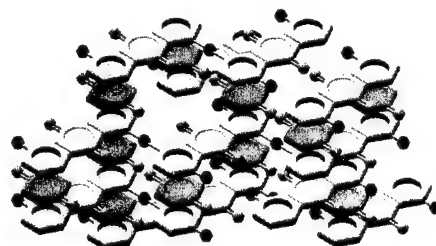


Figure 2. Schematic illustration of the poly(DAAQ)-1,4-BQ film.

New gel electrolytes for batteries and supercapacitor applications [5] G.B. Appetechi, F. Croce, P. Romagnoli, B. Scrosati, U. Heider, R. Oesten, *Electrochem. Commun.* 1 (1999) 83.

J. Chojnacka, J.L. Acosta and E. Morales.

Instituto de Ciencia y Tecnología de Polímeros C.S.I.C.
C/ Juan de la Cierva 3, 28006 Madrid, Spain

Introduction

Gel-type polymer electrolytes are currently receiving a great deal of attention because of their proposed large scale applications in secondary lithium batteries and electrochemical supercapacitors [1,2]. The membranes, in which a liquid electrolyte has been immobilised by incorporation of a matrix polymer, combine the high conductivity liquid solution with the mechanical properties of the host polymer. A variety of polymers, ranging from polyacrylonitrile, poly(vinyl chloride), poly(methyl methacrylate), poly(vinyl sulfone), poly(vinylidene fluoride), etc. have been used as polymer matrices [3,4]. In this work we report on the thermal behaviour, ionic conductivity and electrochemical stability of gel electrolytes based on PAN and a commercially available copolymer of poly(vinylidene fluoride) (PVDF) and hexafluoropropylene (HFP).

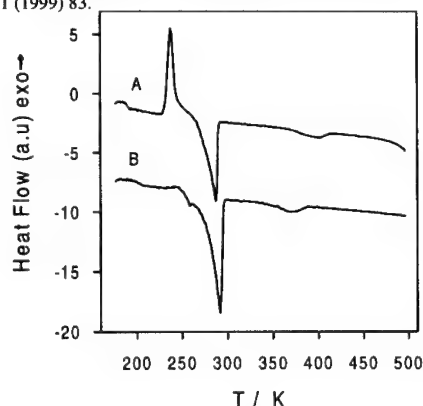
Results and Discussion

The electrolyte membranes were prepared by gelling (160 °C, 5 min) PAN and PVDF-HFP (KF2801) polymer matrixes in a solution of LiCF_3SO_3 in ethylene carbonate- γ -butyrolactone (EC- γ BL) solvent mixture. The composition of the membranes (wt%) was PAN/PVDF-HFP 12.5, LiCF_3SO_3 11, EC 56.3, γ -BL 20.2.

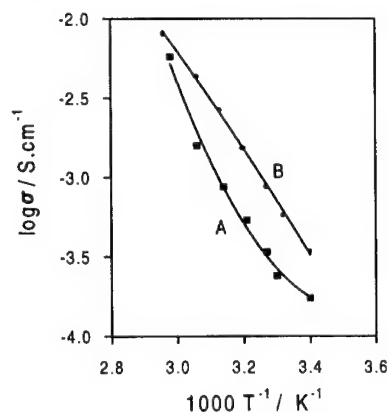
The DSC curves show the melting of EC at 14.3°C (PAN gel) and 16.9°C (PVDF-HFP gel), and a second melting region (PAN gel) and 97.2°C (PVDF-HFP gel). The ionic conductivity of the membranes measured by impedance spectroscopy show slightly higher values for the PVDF-HFP gel, values of the order of $10^{-3} \text{ S}\cdot\text{cm}^{-1}$ measured only at temperatures higher than 45°C for PAN gel membranes and 32°C for the PVDF-HFP ones. Even this values are lower than those reported in the literature [5], the high electrochemical stability (the current onset is detected around 4.7 V vs Li for the PAN-based gel, the PVDF-HFP gel practically being stable up to 5 V vs Li) make this membranes of definite interest for practical applications in lithium batteries and supercapacitors technology.

References

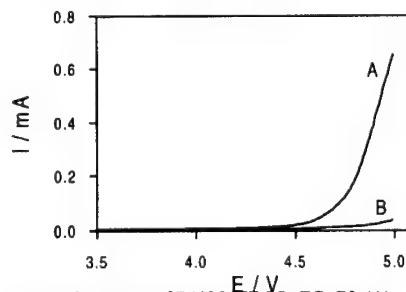
- [1] J.-M. Tarascón, A.S. Gozdz, C. Schmutz, F. Shokoohi, P.C. Warren, *Solid State Ionics* 86-88 (1996) 49.
- [2] X. Lin, T. Osaka, *J. Electrochem. Soc.* 144 (1997) 3066.
- [3] D. Peramunage, D.M. Pasquariello, K.M. Abraham, *J. Electrochem. Soc.* 142 (1995) 1789.
- [4] A.M. Christie, L. Cristie, C.A. Vincent, *J. Power Sources* 74 (1998) 77.



DSC thermograms of PAN: LiCF_3SO_3 :EC: γ BL (A) and KF2801: LiCF_3SO_3 :EC: γ BL (B) gel electrolytes. Heating rate 10 K/min.



Arrhenius plot of ionic conductivity results for PAN: LiCF_3SO_3 :EC: γ BL (A) and KF2801: LiCF_3SO_3 :EC: γ BL (B) gel electrolytes.



Linear voltammetry of PAN: LiCF_3SO_3 :EC: γ BL (A) and KF2801: LiCF_3SO_3 :EC: γ BL (B) gel electrolytes. Scan rate 10 mV/s.

Electric Capacitance of Active Carbon Fiber Electrode in Aqueous Electrolyte Solutions

Yoshiharu Matsuda, Shuichi Ohmura
and Kengou Ohno

Department of Applied Chemistry, Faculty of
Engineering, Kansai University, Yamate-cho, 3-3-
35, Suita, Osaka 564-8680, Japan

Electric double layer capacitors with active carbon electrodes have been used for memory back up electric sources. In the present work the electric capacitance of active carbon fiber electrodes in aqueous solutions of HCl, H_2SO_4 , $LaCl_3$ and some electrolytic salt was measured and the mechanism of the capacitance was discussed.

The active carbon fiber was BW554 by Toyobo and the electrolyte solutions were aqueous solutions of HCl, H_2SO_4 , KCl, $LaCl_3$ etc. A beaker type cell with a test electrode ($1cm^2$ active carbon fiber, 31.9mg) and a counter electrode ($10cm^2$ active carbon fiber, 319.0mg) was used in the electrochemical measurement. Current collectors were platinum plates. Usually charge-discharge cut-off voltage were 0.175 and 0.7 V respectively. The current density was normally $5.0Acm^{-2}$.

The results are shown in Fig.1 and 2.

The capacitance of the carbon fiber positive electrode was around $160 Fg^{-1}$ and that of the negative electrode was $125 Fg^{-1}$ in 2mol/l HCl. Usually the capacitance of the positive electrode was larger than that of negative electrode. The capacitance increased adding $LaCl_3$ in the electrolyte solutions. The current efficiency was around 100% after 10 cycles. The capacitance was influenced with surface functional groups, $-COOH$, $-OH$, $-CHO$, CO , specific adsorption coexisting ions, and pH of the electrolyte solutions.

This study was supported by the Proposed New Industry Creative Type Technology R&D Promotion Program from the New Energy and Industrial Technology Development Organization (NEDO) of Japan.

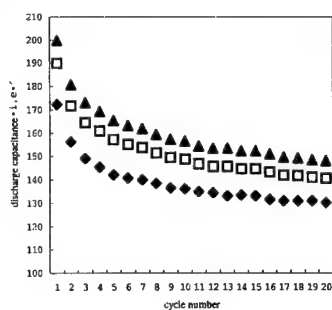
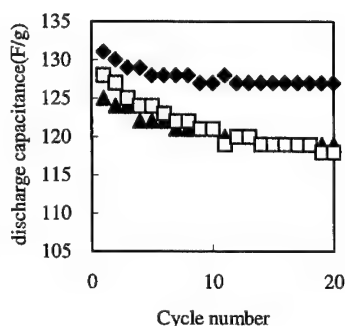


Fig.1 Discharge capacitance of the positive electrode

- $LaCl_3(1.5mol/l) + HCl(1.0mol/l)$
- $LaCl_3(1.0mol/l) + HCl(1.0mol/l)$
- ▲ $LaCl_3(0.5mol/l) + HCl(1.0mol/l)$



NANOTUBULAR MATERIALS FOR SUPERCAPACITORS

*E. Frackowiak, K. Méténier, F. Béguin

*Poznan University of Technology, ul. Piotrowo 3,
60-965 Poznan, Poland

CRMD, CNRS-University, 1B, rue de la Férollerie,
45071 Orléans, France

Carbon nanotubes apart from their technical use in molecular electronic devices, micromechanics, electron field emission, nanowires, are also considered for electrochemical storage of energy.

Our investigation of lithium storage by carbon nanotubes (NTs) in aprotic medium (Li/C cells) proved that they can accumulate extremely large amount of lithium, however, the deinsertion is only partial and involves a high polarization [1]. The shape of the charge/discharge characteristics indicated capacitance properties of the nanotubes. This experience encouraged us to use this nanotubular material as electrodes for building the capacitors [2, 3].

The application of different type of multiwalled nanotubes proved the high ability of this material for the accumulation of charges in the electrode-electrolyte interface. Our target was to investigate the two types of capacitance, i. e. a pure electrostatic attraction of ions in the electrical double layer and pseudocapacitance effects which involve fast faradaic reactions.

Intentionally, we selected extremely various types of nanotubes with open and close central canal, entangled and straight, to elucidate the role of canal and mesopores in charging the double layer.

Multiwalled carbon nanotubes (MWNTs) with an open central hollow have been obtained by the catalytic decomposition of acetylene at 700°C, where cobalt supported on silica was used as catalyst. Nanofilaments of fishbone morphology with an ill defined canal have been elaborated in the same conditions but at 900°C. Both types of catalytic MWNTs have sinuous shape (Fig.1) and the internal diameter varied from 4 to 6 nm whereas the external diameter varied from 15 to 30 nm.

Purification process of MWNTs, by hydrofluoric and nitric acids used for removing silica and cobalt particles, caused a modification of the nanotubes through the formation of oxygenated surface groups confirmed by titration method, XPS and elemental analysis. The amount of oxygen varied from 2 to 10% by weight.

In some cases, an additional oxidative treatment was performed in strong nitric acid at 80°C to enhance the surface functionality of MWNTs.

Completely different nanotubes (straight and rigid) were obtained by chemical vapor deposition CVD of propylene at 800°C within the pores of an alumina template. In this case the wide central canal was remarkable, of the order of 10 nm, but

only a few concentric, non-continuous graphitic layers formed the nanotube walls.

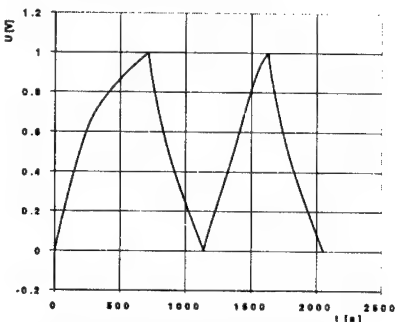


Fig. 1 Purified MWNTs obtained at 900°C

The capacitance properties of the nanotubular materials were studied in two electrode carbon/carbon cells. Electrodes were prepared in the form of pellets of ca. 10 mg with acetylene black (10%) and PVDF (5%). Experiments were performed in 6M KOH using voltammetry and galvanostatic charge/discharge techniques (Fig. 2). Some experiments were also performed in aprotic medium. The values of specific capacitance ranged from 2 to 120 F/g depending on the microtexture and surface functionality.

Fig. 2 Charge/discharge of a supercapacitor from functionalized MWNTs I=1mA; 6M KOH

References



- [1] E. Frackowiak, S. Gautier, H. Gaucher, S. Bonnamy, F. Béguin *Carbon* 37 (1999) 61.
- [2] E. Frackowiak, K. Méténier, R. Pellenq, S. Bonnamy, F. Béguin *Electronic Properties of Novel Materials* ed. H. Kutzmany (1999) pp. 429-432.
- [3] E. Frackowiak, K. Méténier, T. Kyotani, S. Bonnamy, F. Béguin *Ext. Abstr. 24th Bien. Carbon Conf.* (1999) pp. 544-545.

CHARGE/DISCHARGE CHARACTERISTICS OF V_2O_5 - CARBON COMPOSITE FOR SUPERCAPACITOR

Myung-San Kim, Jong-Uk Kim, Bok-Kee Park*
and Hal-Bon Gu
Department of Electrical Engineering, Chonnam
National University
300 Yongbong-dong, Kwangju, 500-757, Korea
*Department of Electrical Engineering, Howon
University
727 Wolhari, Impimyun, Kunsan, Chonbuk,
573-718, Korea

Recently the trend of increasing of portable electric devices demand for global environmental conservation and demands the development of high energy density supercapacitor. Electrical double layer capacitor is an energy storage device that employs the principle of the electrical double layer formed between conductive porous electrode material and electrolyte. The supercapacitor has characteristics of fast charge/discharge, high energy density.[1,2] The supercapacitor is expected to be applied not only to the memory back-up device for various electronic/electrical product (portable computer, VCR, etc.) but to the engine starter of electric vehicles (including hybrid electric vehicles), the actuator of various industrial motors, military devices, artificial satellite, medical appliances, high power pulse laser, and plasma switching device.

The Purpose of this study is to research and develop V_2O_5 -carbon composite electrode for supercapacitor. We performed electrochemical characteristic, impedance spectroscopy, charge/discharge property, power density and cycle life. V_2O_5 -AC composite electrode with 25PVDF/LiClO₄/PC₁₀EC₁₀ polymer electrolyte bring out good capacitor performance below 3V. The discharge capacitance of V_2O_5 -AC (30:70) composite with 70wt.% AC at 1st and 200th cycles was 9.6 and 8.2 F/g respectively. The capacitance of V_2O_5 -AC composite with 70wt.% AC capacitor was larger than that of others. The coulombic efficiency of supercapacitor with 70wt.% AC content showed good capacitance and stability with cycling.

References

- [1] Y. Taksus, Y. Murakami, S. Mioura, H. Ogawa and K. Yahikozawa, Proc. Symp. Electrochemical Capacitors, The Electrochemical Society, 95-29, p.57 1996.
- [2] Y. Murakami, T. Kondo, Y. Shimoda, H. Kaji, X.-G. Zhang and Y. Taksu, J. Alloys and compounds, 239, 111, 1996.

APPLICATION OF CONDUCTING POLYMER COMPOSITE ELECTRODE FOR SUPERCAPASITOR

Kwang-Woo Kang, Jong-Uk Kim and Hal-
Bon Gu
Department of Electrical Engineering, Chonnam
National University
300 Yongbong-dong, Kwangju 500-757, Korea

Recently, miniaturization, lightweight or high effectiveness of electronic equipment by current, power source of this equipment has been required power source of high energy density such as capacitor, secondary battery. Particularly electronic equipment has been required that it is high energy density of energy storage system such as capacitor has short charge time. Electrochemical capacitor used adsorption and desorption reaction of charge in the electric double layer take place at interface between electrolyte and high porosity electrode is energy storage system[1]. Supercapacitor having the advantage that compared with secondary battery, that is short charge time and a remarkable characteristic with dependability. Therefore supercapacitor possible to application for electric vehicle power source or load equalization power source by high capacitance. Supercapacitor has much energy storage per gram than general capacitor and discharged high power density than secondary batteries. The redox reaction on surface of electrode has advantage that it has long cycle life than secondary battery because of high reversibility of charge. As well as the electricity stored in double layer in proportion to surface area of electrode enable to polarization[2]. Particularly carbon suitable as a polarization active material of capacitor because of carbon has high surface area and high chemical stability.

In this paper electrode material synthesized electrochemical polymerization or chemical polymerization the polyaniline(PAn) as conducting polymer in order to development supercapacitor electrode of high energy density or long cycle life and PAn composite electrode produced with activated carbon and composed cell with 1M H₂SO₄ solution or 1M LiClO₄/PC etc. And so investigated of electrochemical properties, impedance properties, charge discharge properties, power density or cycle life.

The discharge capacitance of PAn composite with 15wt% SP270 in 1st and 200th cycles was 42 and 42 F/g at current density of 1mA/cm². The capacitance of PAn composite with 15wt% SP270 was larger than that of PAn electrode without SP270. Also we researched various carbon-conducting polymer electrodes.

References

- [1] F. Uribe, A. Budge, J. Davey, J. Landeros Jr and S. Gottesfeld, Proceedings of The Electrochemical Society Volume 94-23.
- [2] B. E. Conway, V. Birss, J. Wojtowicz, J. Power Source 66 (1997) 1-14.

INDEX OF AUTHORS

Abe, T.	18, 128, 148,	Bando, T.	297, 373	Chandrasekaran, R.	256
Abura, T.	230	Bannerjee, P.	29	Chang, Y.-C.	293, 294
Acosta, J.L.	388	Banov, B.	91	Chazalviel, J.-N.	375
Adachi, K.	340	Bar Tow, D.	24, 60	Chen, C.	332
Ado, K.	220	Barbarelo, J.	320	Chen, C.-L.	10
Adschiri, T.	235	Barnett, B.	126	Chen, J.-S.	312
Afanasjev, V.	98	Barriere, B.	349	Chen, X.	75
Ahn, S.	376	Barusseau, S.	282	Chen, Y.	130
Aihara, Y.	297, 373	Baskevich, A.	70	Chen-Mayer, H.	383
Akiyama, T.	340	Baudrin, E.	11, 117	Cherniy, A.	352
Al Hallaj, S.	357	Beaudoin, B.	93	Chervakov, O.	333, 341
Alain, V.	202	Beaulieu, L.	69	Chevallier, F.	133
Albering, J.H.	72	Becker, D.	383	Chia, F.	313
Aleksey, B.	81	Beguín, F.	129, 133	Cho, B.-W.	44
Alessandrini, F.	347, 368, 369	Bele, M.	191, 273, 57	Cho, W.-I.	44
Alexandrov, A.	98	Belliard, F.	108, 132	Choi, B.K.	302
Alliata, D.	68, 9	Benedek, R.	137	Choi, Y.-M.	374
Amancio, S.	264	Benjelloun, N.	55	Chojnacka, J.	388
Amandi, R.	131	Bergman, R.	31	Chottiner, G.	33
Amatucci, G.	292, 36	Bernard, S.	286	Chouinard, Y.	166
Amezawa, K.	188, 325	Besenhard, J.O.	113, 12, 120, 121, 289,	Chouvin, J.	139
Amine, K.	332		290, 380, 72, 73	Chow, W.	209, 212
Ammundsen, B.	17, 185, 224	Besner, S.	166	Chowdary, B.V.R.	187, 89
Amouzegar, K.	271	Biensan, P.	237, 282, 284, 3, 339	Christensen, L.	42
Andersson, A.M.	82	Bindin, P.	358	Christian, J.	199
Andersson, A.S.	20	Birke, P.	46	Christian, M.	207
Andou, H.	255	Biscazzo, S.	318	Christophe, J.	286
Andreas, B.	76	Blanc, G.	339	Chua, D.	214
Andrukaitis, E.	210, 342	Bloch, D.	189	Chun, J.H.	304
Angell, C.A.	274	Blomgren, G.	211	Chung, H.-T.	267
Angenault, J.	206	Blum, A.	366	Chung, K.Y.	170
Ann, J.-H.	58	Blyth, R.I.R.	380	Chung, S.	298, 314, 32
Anne, M.	192	Bodet, J.-M.	282	Chusid, O.	303, 34, 86
Annie, L.G.L.S.	196, 202	Bodin, F.	276	Clay, N.	383
Antipenko, B.	98	Bodoardo, S.	175	Claye, A.	85
Antonini, A.	135	Boldyrev, Y.Y.	146	Cohen, Y.	179, 179, 180, 34, 86
Aoshima, T.	176	Botte, G.	279	Connor, P.A.	109, 132
Apostolova, R.	159, 180	Bottino, A.	317	Conte, M.	347
Appel, W.K.	290	Bourbon, C.	189	Cook, C.	321
Appetecchi, G.	367, 369	Boyd, S.	278	Coowar, F.	358
Arai, K.	235	Bradhurst, D.H.	152, 58	Corbett, M.	327
Arai, N.	1	Briois, V.	117	Coustier, F.	30
Arakawa, R.	230	Brissot, C.	375	Cressent, A.	93
Arbizzani, C.	53	Brousse, T.	100, 112, 13, 99	Croce, F.	204, 214, 239, 27, 300, 314
Ardel, G.	366, 367	Broussely, M.	3, 339	Croguennec, L.	237
Armand, M.	166, 26	Bruce, P.G.	15, 193, 260	Crosnier, O.	100, 13
Armstrong, A.R.	15, 193, 260	Brundage, M.	6	Cullen, J.	358
Arof, A.K.	356	Bruneel, J.L.	386	D'Epifanio, A.	204
Arrabito, M.	175, 92	Bueno, P.	264	Dahn, J.R.	42, 69, 74
Ashkenazi, V.	34	Bugga, R.	127, 7	Dallek, S.	141
Au, G.	6	Bulhoes, L.	264	Dalton, P.	7
Audry, C.	339	Buqa, H.	12, 120, 121, 380	Daroux, M.	164
Aurbach, D.	159, 178, 179, 180, 303,	Burstein, L.	24	Dass, V.	358
	34, 85, 86	Buryak, V.U.	149, 378	Davidson, I.	234, 345
Aymard, L.	213	Buvat, P.	99	deCastro, S.	263
Azuma, Y.	150	Byers, J.	351	Dedryvère, R.	138
Börjesson, L.	110	Caillon, G.	276	Dees, D.W.	125, 332
Béguin, F.	390	Cairns, E.J.	216	Delmas, C.	19, 200, 237
Baba, M.	371	Calis, G.	291	Denis, S.	11, 138
Bach, S.	143	Carewska, M.	368, 369	Denisova, T.N.	385
Badway, F.	292	Carre, B.	272, 284	Deptula, A.	214
Baffier, N.	143	Catti, M.	195	Deschamps, M.	386
Baik, H.-K.	114, 223	Ceder, G.	251, 252	Desilvestro, H.	224
Balasubramanian, M.	162	Chabre, Y.	165, 208	Desilvestro, J.	17
Ban, S.-H.	172	Chagnes, A.	272	Devau, X.	100
Bandara, K.	315	Chai, C.	363	Devyatkina, E.	217

Author	Abs. No.	Author	Abs. No.	Author	Abs. No.
Di Noto, V.	318	Gedanken, A.	87	Hirata, N.	305
Dobler, B.	280, 281	Gejke, C.	110	Hironaka, K.	354
Dolle, M.	93	Geoffroy, I.	284	Hodal, T.	290
Dominique, G.	196, 202	Geronov, Y.	353	Holl, K.	229
Dominko, R.	191, 273, 57	Gerouki, A.	383	Holmes, C.F.	48
Doo, S.-G.	374	Gerrits, N.	291	Honda, H.	104
Dou, S.X.	152, 58	Giorgetti, M.	30	Hong, J.K.	103
Drews, J.	50	Gitzendanner, R.	351	Horiba, T.	255, 354
Drofenik, J.	191, 273, 57	Gizbar, H.	34, 86	Hou, X.	296
Du Pasquier, A.	36, 292	Gladkich, A.	24	Hsieh, M.-C.	294
Du, C.	130	Globa, N.	248, 333, 70	Huang, B.	29, 321
Duclot, M.	39	Gnanaraj, J.	85	Huang, H.	106, 124, 249, 299
Duncan, M.J.	15, 260	Gofer, Y.	303, 34, 86	Hubbard, H.	311
Dunlap, R.	69	Goldner, R.	383	Huchet, O.	282
Dupin, J.C.	241	Golob, P.	120, 136, 380	Hugener, T.	75
Dupont, L.	208, 93	Golodnitsky, D.	298, 326, 365, 366, 367	Huggins, R.A.	41
Dupré, N.	206	Gonbeau, D.	241	Hussénus, A.	82
Durand, C.	75	Gong, M.S.	302	Hwang, B.-J.	246, 254
Dusheiko, V.A.	149, 378	Gopukumar, S.	116	Ibarra Palos, A.	192
Dygas, J.	310	Gorenstein, A.	263	Ignat'ev, N.	22
Ebner, W.	363	Gorev, A.	98	Iguchi, T.	297, 373
Edstrom, K.	110, 83, 119, 82	Goto, A.	323	Ihm, D.-J.	350, 363
Edwards, C.	386	Gover, R.	265	Ikuta, H.	115, 308
Egashira, M.	144, 232	Gozdz, A.	36	Ilic, D.	229
Eguchi, M.	253	Green, R.	358	Imachi, N.	344
Ehrlich, G.	329, 75	Greenbaum, S.	175, 298, 314, 32	Imanishi, N.	186, 364, 63, 370
Elder, S.	161	Grey, C.	224	Imhof, R.	280, 281
Elkaim, E.	205	Grincourt, Y.	234, 345	Inaba, M.	128, 148, 18
Engel, J.	160	Grogger, C.	121	Inada, T.	40
Enin, A.	98	Grondin, J.	386	Inoue, S.	362
Eriksson, T.	225	Groult, H.	247	Ionescu, M.	152
Esaka, T.	104	Grugeon, S.	93	Irvine, J.T.S.	108, 109, 132
Exnar, I.	280, 281	Gu, H.-B.	245, 266, 316, 391, 392	Ishida, S.	177
Faiers, J.	163	Guo, X.	175, 32	Ishida, T.	111
Fang, L.	89	Gustafsson, T.	197, 225	Ishihara, T.	122, 123
Fantini, M.	263	Guyomard, D.	157, 161, 201	Ishikawa, M.	145, 56
Fauri, M.	318	Gwenaëlle, R.	207	Ishikawa, T.	285, 387
Fay, M.	30	Höwing, J.	197	Islam, M.S.	185
Fehrman, G.	50	Haas, T.	383	Isozaki, Y.	231
Fejeda, T.	215	Hackney, S.A.	125	Itoh, T.	305, 43
Ferrando, W.A.	141	Hajime, M.	338	Ivanova, N.D.	146
Fey, G.T.-K.	10, 254, 293, 294	Hakuta, Y.	235	Iwabe, S.	253
Fischer, J.	85	Hamlen, R.	320, 6	Jacobsson, P.	155, 31, 382
Florjanczyk, Z.	310	Hammond, M.	332	Jak, M.	348
Fowkes, A.J.	15, 193	Hamon, Y.	99	Jannasch, P.	301
Frackowiak, E.	129, 133, 390	Han, J.	130	Jansen, A.N.	125, 332
Fragnaud, P.	100, 13	Han, J.-I.	374	Jarvis, C.	377
Francoise, P.	286	Handa, M.	275	Jean-Marie, B.	286
Franger, S.	143	Haronian, D.	326	Jean-Marie, T.	207
Fransson, L.	110, 119, 82	Harrison, S.	271	Jeong, G.-J.	79, 88
Fujieda, T.	101	Hasegawa, M.	71	Jeong, I.-S.	245
Fujii, M.	186	Hashimoto, T.	340	Jiangang, L.	154, 158
Fujitani, S.	219	Hatazawa, T.	4	Jianjun, X.	154, 158
Fukushima, T.	230	Hatchard, T.	42	Jo, S.I.	304
Funahashi, A.	337	Haupt, W.	280, 281	Johansson, P.	31
Fung, K.-Z.	312	Hayamizu, K.	297	Johnson, B.	278
Furlani, M.	315	Hector, A.	151	Johnson, C.S.	119, 125, 244
Furusaka, M.	134	Heider, U.	178, 22	Joho, F.	76, 9
Gaberscek, M.	191, 273, 57	Hendrickson, M.	23, 6	Jones, D.	224
Gadad, S.	140	Henriksen, G.	332	Jousse, F.	99
Gao, Y.	160, 164, 59	Herranen, M.	83	Jumas, J.-C.	138, 139
Gaoping, C.	154, 158	Herreyre, S.	282, 284, 3	Jung, J.-S.	304
Garche, J.	229	Hetzel, M.	329, 75	Jungnitz, M.	22
Garcia-Alvarado, F.	131	Higobashi, H.	362	Juzkow, M.	47
Garza, L.	132	Hill, I.	210, 342	Kageyama, H.	111, 220, 232, 236
Gaubicher, J.	118, 165, 21, 249	Hinton, A.	324	Kai, T.	354
Gauthier, M.	166	Hirahara, K.	319	Kajiya, A.	40
Gautier, S.	133	Hirano, A.	134	Kakirde, A.	363
Gavelin, P.	301	Hirano, Y.	357	Kalaiselvi, N.	257, 258, 259, 261

Author	Abs. No.	Author	Abs. No.	Author	Abs. No.
Kamaruddin, N.	356	Kong, F.	25	Levi, E.	178, 179, 34
Kaminya, T.	134	Konishi, T.	232	Levi, M.	178, 179
Kamioka, K.	228	Korai, Y.	97	Li, Q.	364
Kamiyama, T.	226	Koseki, M.	354	Li, Z.	59
Karnizori, H.	283	Kosova, N.	217	Lifshits, E.	298
Kanamura, K.	235, 323	Kostecki, R.	25, 68	Lim, M.-R.	184
Kanari, K.	335	Kouguchi, M.	40	Lin, H.-P.	214, 23
Kanasaku, T.	188, 325	Kozlova, S.	217	Lin, S.-W.	269, 270
Kanbe, C.	147	Kozono, Y.	255	Lindner, H.J.	153, 187
Kanda, M.	231, 328	Krause, L.	278	Lindsay, M.J.	152, 58
Kaneko, S.	343	Krok, F.	310	Lippens, P.E.	138, 139
Kang, H.-R.	79	Ksenzhek, O.	70	Liu, D.G.	246
Kang, K.-W.	392	Ku, C.-H.	97	Liu, H.K.	152, 58
Kang, T.	78, 79, 88, 95, 96	Kubo, M.	305	Liu, J.	332
Kanno, R.	134, 220, 226, 265	Kubota, M.	104	Liu, Q.	130
Kargina, I.	234, 345	Kuehner, A.	22	Liu, W.-K.	293
Kasai, M.	255	Kuhn, A.	131	Liu, X.	372
Kaszejna, P.	3	Kumagai, N.	183, 183, 247	Liu, Z.	153
Katayama, K.	150	Kumashiro, Y.	255	Livshits, V.	366
Katayama, Y.	182	Kurashima, K.	275	Ljungbäck, R.	301
Kato, K.	335	Kuratomi, J.	297, 373	Loic, D.	207
Kato, Y.	219, 308	Kurokawa, H.	219	Lu, C.-H.	269, 270
Katsuhito, T.	338	Kusawake, H.	372	Lu, Z.	34
Katsuta, T.	107, 287	Kuwana, K.	373	Möller, K.-C.	12, 290
Kawabata, A.	101	Kuwashima, S.	372	Méténier, K.	390
Kawahara, A.	122, 123	Kylyvnyk, K.	248, 341, 70	Ma, S.	194
Kawai, T.	379	Lada, W.	214	Machnikowski, J.	129
Kawakami, A.	283	Lain, M.	359	Macklin, A.	377
Kawamoto, Y.	226, 265	Lamanna, W.	278	Macklin, B.	358, 377
Kazuma, K.	338	Lamaze, G.	383	MacNeil, D.	42
Kelder, E.	106, 240, 348	Lampe-Onnerud, C.	126	Magistris, A.	317
Kelder, E.M.	291	Landers, R.	263	Magnan, J.-F.	166
Kerr, T.	249	Lantelme, F.	247	Maki, F.	253
Kerzhentseva, V.E.	385	Lanz, M.	9	Makino, K.	182
Kezuka, K.	4	Larcher, D.	69	Maksyuta, I.	333, 341
Kida, Y.	337	Laruelle, S.	11, 117	Manago, A.	387
Kikuchi, M.	105	Lascaud, S.	375, 386	Manivannan, V.	363
Kilroy, W.P.	141	Lasségués, J.C.	386	Manual, A, S.	116, 238, 250, 309
Kim, C.S.	306	Lauriat, J.-P.	205	Manzo, M.	7
Kim, D.-G.	78	Lavi, Y.	326	Marassi, R.	239
Kim, H.	304, 78, 88	Le Cras, F.	189	Mari, C.M.	195
Kim, H.-S.	44	Le Gal La Salle, A.	157, 161, 201	Maria Rosa, P.	207
Kim, J.-S.	61	Le Granvalet-Mancini, M.	140	Marianetti, C.	251
Kim, J.-U.	266, 316, 391, 392	Lee, B.W.	142	Markovsky, B.	159, 180
Kim, K.-B.	170, 171, 172, 173, 174, 184	Lee, C.-W.	37	Marsh, C.	351
Kim, M.-S.	391	Lee, H.	376	Marsh, R.	7
Kim, S.-S.	115	Lee, H.-S.	277	Martin, C.	35
Kim, S.-W.	168, 79	Lee, H.M.	376	Martin-Litas, I.	241
Kim, S.H.	142	Lee, J.	306, 66	Martinet, A.	77
Kim, T.H.	376	Lee, J.-A.	266, 316	Maryvonne, H.	207
Kim, Y.-J.	78, 88, 95, 96, 97	Lee, J.-F.	254	Masquelier, C.	165, 205, 208, 21
Kim, Y.-U.	79	Lee, J.-H.	350	Mastragostino, M.	53
Kim, Y.W.	302	Lee, J.-K.	114, 223	Mathieu, M.	207
Kimoto, K.	384	Lee, J.Y.	153	Matoba, N.	65
Kimura, T.	156	Lee, J.Y.	67	Matsuda, Y.	230, 288, 389
Kinoshita, K.	25, 68, 90	Lee, K.-K.	171, 173, 174	Matsui, S.	362
Kishi, T.	182	Lee, M.-H.	169	Matsui, Y.	384
Kita, F.	283	Lee, N.	35	Matsumura, T.	354
Kiyohara, C.	176	Lee, S.-B.	80	Matsuoka, M.	111, 236
Ko, J.-M.	304	Lee, S.-J.	114, 223	Matsuta, S.	219
Kobayakawa, K.	379	Lee, S.-M.	114, 223	Mattinlgey, N.	377
Kobayashi, H.	111, 220, 236	Lee, Y.-G.	28	Mayes, A.	29, 321
Kobayashi, T.	308	Lee, Y.J.	224	McBreen, J.	162, 164, 277
Koetz, R.	68, 9	Leising, R.A.	330	McGuinn, J.	75
Kokhany, V.	70	Lemordant, D.	272, 284	McLarnon, F.	25
Komaba, S.	183	Lenhof, C.	276	Medjutov, M.	98
Kondo, S.	40	Levasseur, A.	241	Meenakshisundaram, R.	116, 238, 238,
Konfli, E.	377	Levasseur, S.	200		243, 250, 309

Author	Abs. No.	Author	Abs. No.	Author	Abs. No.
Mellander, B.-E.	315	Nishiguchi, H.	122, 123	Pereira-Ramos, J.-P.	143
Menetrier, M.	200	Nishimura, K.	255	Peres, J.-P.	339
Merson, A.	24	Nishiwaki, Y.	222	Periasamy, P.	257, 258, 259, 261
Meshri, D.	333	Nishizawa, M.	43	Perner, A.	229
Michael E., S.	76	Nitta, Y.	71	Persi, L.	204, 239, 27, 300, 314
Michael, M.S.	233	Niu, J.	66	Perton, F.	282, 339
Michael, S.	84	Nobili, F.	239	Pham, P.	278
Michel, B.	286	Nobuyuki, T.	338	Philippe, B.	286
Middaugh, R.	262	Noguchi, H.	194	Piaggio, P.	317
Mihara, T.	111	Nohma, T.	337	Pickering, P.	17, 224
Misztal-Faraj, B.	310	Nomoto, S.	52	Piffard, Y.	157
Mitchell, B.	265	Novák, P.	113	Ping, X.	59
Mitkin, V.N.	98, 385	Novak, P.	9, 76, 113, 381,	Pisniy, V.	248
Mitsuishi, I.	231	Nozaki, K.	335	Plichta, E.	23, 6
Miura, T.	182	Numata, K.	177	Poizot, P.	11, 117
Miyake, H.	71	Numata, T.	147	Polyschuk, Y.	341
Mochida, I.	97	Oesten, R.	178, 22	Portal, R.	201
Mochizuki, S.	111	Ogarkov, V.	98	Potiron, E.	157
Mogi, R.	128	Ogumi, Z.	128, 148, 18	Pouillier, C.	237
Mohamed, N.S.	356	Oh, S.M.	103, 306	Pozin, M.	352, 361
Mohamed, M.	43	Ohmura, S.	389	Prabakaran, S.R.S.	233, 84
Mohd Noor, A.F.	233	Ohno, K.	389	Prakash, J.	37
Molz, M.	320	Ohsaki, T.	328	Prasad, R.	137
Momma, T.	303, 87	Ohzono, H.	71	Preishuber-Pfl, gl, P.	73
Momose, Y.	253	Ohzuku, T.	64, 65	Prem Kumar, T.	116, 261
Montchilov, A.	203, 94	Okada, M.	228	Prosin, P.P.	347, 368, 369
Moon, S.-I.	266	Okada, S.	144, 232	Puglia, F.	351
Moore, G.	161, 201	Okahara, K.	176	Purgin, V.	98
Morais, J.	263	Okuya, M.	343	Pyun, S.-I.	167, 168, 169, 80
Morales, E.	388	Olivier, J.P.	136	Qi, L.	370
Morales, J.	112	Olivier-Fourcade, J.	138, 139	Quartarone, E.	317
Morcrette, M.	208	Olsen, I.	276	Quarton, M.	206
Morgan, D.	251	Onnerud, P.	126	Quine, T.E.	15, 260
Morita, M.	145, 56	Ono, T.	373	R. Sriram	238
Moshkovich, M.	34, 86	Ooms, F.G.B.	240, 291	Radshenko, V.V.	149
Moskovich, M.	179	Osaka, T.	303, 45, 87	Raekelboom, E.	151
Mostafa, M.A.	134	Osman, Z.	356	Raghavan, M.	257, 258, 259, 261
Moukhin, V.V.	98, 385	Ostrovskii, D.	155, 382	Ramesh Babu, B.	257, 258, 259, 261
Mouri, T.	228	Ota, H.	102	Ramsey, M.G.	380
Mui, S.	321	Ota, T.	219	Rao, G.	346
Muniyandi, N.	257, 258, 259, 261	Otomo, T.	134	Rao, G.V.S.	187
Muranaga, T.	362	Ouvrard, G.	190	Ravet, N.	166
Muranaka, Y.	255, 354	Owen, J.	151	Reale, P.	92
Mustarelli, P.	317	Owens, B.	30, 51	Reiche, A.	307
Myung, S.-T.	267	Pérez Vicente, C.	139	Reimer, J.A.	216
N.G. Renganathan	238, 243, 309, 250	Palacin, R.M.	208	Reimers, J.	212
Nadeau, G.	25, 90	Palazzo, M.J.	330	Reisner, D.	341
Nagashima, H.	283	Pan, C.	224	Rendek Jr., L.	33
Nagimny, V.	159, 180	Panero, S.	175, 198, 92	Renganathan, N.G.	116, 257, 258, 259, 261
Nakade, K.	343	Panitz, J.-C.	381, 9	Ribalka, A.	333
Nakagawa, T.	145	Park, B.	78	Ribes, M.	55
Nakai, I.	218, 222, 384	Park, B.-K.	391	Richardson, T.	334
Nakajima, K.	4	Park, C.-K.	363	Robertson, A.D.	15, 193, 260
Nakane, I.	38	Park, C.W.	103	Rodriguez-Carvajal, J.	205, 21
Nakanishi, T.	319	Park, G.-C.	316	Rogalska, E.	310
Nakata, H.	285, 52	Park, H.-C.	304	Roh, K.-S.	350
Naoki, K.	387, 54	Park, J.-K.	28	Romagnoli, P.	367
Narukawa, S.	344, 38	Park, Y.-T.	61	Romanovskaya, L.	333
Natchi, M.	116, 238, 243, 250, 309	Paskal, L.P.	378	Ronci, F.	155, 204
Nathan, M.	326	Pasquali, M.	135	Rosenberg, Y.	60, 62
Naudin, C.	386	Passerini, S.	30, 347, 368, 369, 51	Ross, P.	334
Nazar, L.	118, 124, 165, 21, 249	Pastushkin, T.	70	Rosignol, C.	190
Nazri, G.A.	355	Pavlenko, N.	283	Rosso, M.	375
Nechev, K.	3	Pei, C.C.	233	Rouault, H.	189
Neduzhko, L.	341	Pejovnik, S.	191, 273, 57	Rougier, A.	213
Negishi, A.	335, 336	Peled, E.	24, 298, 326, 365, 366, 367, 60, 62	Rousse, G.	205, 208
Netz, A.	41	Penazzi, N.	175	Rouzaud, J.N.	133
Netzer, F.P.	380	Perego, R.	240	Rowell, J.	118

Author	Abs. No.	Author	Abs. No.	Author	Abs. No.
Roy, B.	119	Shigemura, H.	220	Takamura, T.	105, 107, 287
Rozhkov, V.	98	Shikano, M.	225	Takano, K.	335, 336
Roziere, J.	185, 224	Shim, Y.-J.	350	Takayama, T.	379
Ruffo, R.	195	Shimada, H.	278	Takeda, Y.	14, 186, 364, 370, 63
Ruth Mangani, I.	256	Shin, H.-C.	167	Takei, K.	181
Rykart, B.	76, 9	Shinelev, E.A.	385	Takemitsu, T.	288
S��verine, J.	196	Shiraishi, N.	87	Takeuchi, E.S.	330
Sadoway, D.	29, 321	Shiraishi, Y.	384	Takeuchi, K.J.	330
Saha, S.K.	270	Shirakata, M.	147	Takigawa, Y.	236
Saishou, K.	344	Shizuka, K.	176	Takita, Y.	122, 123
Saito, H.	322	Sin, H.-S.	350	Tamaki, J.	111, 236
Saito, M.	287	Siow, K.S.	296	Tamura, S.	111
Saito, Y.	335, 336	Skarstad, P.	49	Tanaka, T.	1
Sakaebe, H.	197, 220, 225	Skekhtman, A.	360	Taniguchi, S.	340
Sakaguchi, H.	104	Skotheim, T.	353	Tanuma, K.	379
Sakai, H.	183	Slane, S.	23, 329	Tarascon, J.-M.	11, 117, 208, 93
Sakai, T.	101, 162, 215, 225, 227, 362	Slegri, H.	345	Tarascon, J.M.	213
Sakata, H.	283	Smart, M.	127, 7	Tatebayashi, Y.	231
Sakurai, S.	101	Smyrl, W.	30	Tatsumi, K.	101, 134, 215
Sakurai, T.	156	Soavi, F.	53	Teagle, D.	358
Sakurai, Y.	181	Sohn, H.-J.	304, 78, 79, 88, 95, 96	Teeters, D.	140
Salam, F.	46	Soiron, S.	213	Telezhkin, V.	98
Salitra, G.	180	Sokol'sky, G.V.	146	Terada, Y.	221, 222
Salomon, M.	214, 23	Sominski, L.	87	Thackeray, M.M.	2, 119, 125, 137, 244
Sanchez, L.	112	Song, X.	25, 68	Thangadurai, V.	41
Sandner, B.	307	Sonoda, T.	283	Thirunakaran, R.	257, 258, 259, 261
Sano, A.	148	Soo, P.	29, 321	Thomas, J.	119, 197, 225
Santhanam, R.	246	Souquet, J.-L.	39	Thomas, J.O.	20
Santiago, E.	264	Speiss, F.	75	Tikhonov, Jr., K.	361
Santis, M.	121	St-Amant, G.	271	Tikhonov, K.	352
Santos-Pena, J.	112	Staelin, D.	321	Tobishima, S.	181
Sarac, A.S.	268	Staniewicz, R.J.	3	Topart, P.	99
Sarakonsri, T.	125	Staub, R.	50	Torlone, G.	210, 342
Sarradin, J.	55	Stauss, E.	365	Torres, L.	132
Sartori, P.	22	Steiner, R.	17, 224	Toru, I.	338
Sasaki, Y.	275	Stelzer, F.	73	Toshikatsu, T.	338
Sato, T.	102	Storey, C.	234, 345	Tossici, R.	239
Sato, Y.	379	Stramare, S.	41	Totir, D.	33
Satolli, D.	198	Strauss, E.	366	Touboul, M.	11, 117
Sawa, S.	232	Strobel, P.	192	Trapa, P.	29
Sawai, K.	64, 65	Subramanian, V.	116	Tsai, Y.-W.	254
Sayers, B.	324	Sudalaimuthu, R.	309	Tsui, A.	285
Scaccia, S.	369	Suematsu, S.	387	Tsuda, S.	5
Schechter, A.	34, 86	Sugihara, T.	156	Tsutsumi, S.	71
Scherson, D.	33	Sugimoto, K.	297	Tucker, M.C.	216
Schleich, D.M.	13, 99, 100, 112	Suhara, M.	150	Turgeman, R.	34, 86
Schmidt, C.	49	Suib, S.	75	Uchida, I.	357, 43
Schmidt, M.	178, 22	Sukumaran, G.	238, 243, 250	Uchimoto, Y.	242
Schmied, M.	73	Sun, H.Y.	364, 370	Uebou, Y.	111, 236
Schoonman, J.	106, 240, 291, 348	Sun, L.	58	Ueno, M.	319
Schwenzel, J.	41	Sun, X.	162, 164, 277	Ulus, A.	62
Scrosati, B.	155, 175, 198, 204, 239, 27, 300, 314, 35, 367, 92	Surampudi, S.	127, 7	Umegaki, T.	323
Seel, J.A.	74	Suzuki, H.	102	Ungar, G.	313
Sekine, K.	105, 107, 287	Suzuki, J.	105, 107, 287	Urbano, A.	263
Sekino, M.	231, 328	Suzuki, Y.	115	Usami, K.	275, 322
Sekiya, S.	275	Svanberg, C.	31	Usami, T.	102
Selladurai, S.	256	Sverdllov, E.	326	Uvarov, N.	217
Selman, J.R.	357	Sylv��re, S.	196	Vaidyanathan, H.	346
Sergeev, V.	98	Sylvie, B.	286	van Beek, J.R.	331
Servant, L.	386	Sylvie, H.	286	Van der Ven, A.	252
Seung, D.-Y.	234, 374	T. Prem Kumar	243, 250, 309	Van Landschoot, N.	348
Sever Skapin, A.	191	Tabuchi, M.	111, 220, 226, 232, 236	van Schalkwijk, W.	47
Shao-Horn, Y.	262	Taillades, G.	55	Vanessa, L.	202
Shembel, E.	159, 180, 248, 333, 341, 70	Tajima, H.	340	Vasanthi, R.	256
Shi, J.	126	Takada, K.	40	Vaughan, G.	165
Shiao, A.	214	Takahashi, K.	215	Vaughney, J.T.	119, 125
Shiao, H.C.A.	23	Takahashi, M.	181	Venkatachalam, S.	238, 243, 250
		Takami, N.	328	Venkatasesetty, H.V.	295

Author	Abs. No.	Author	Abs. No.	Author	Abs. No.
Verbaere, A.	157	Wilson, A.M.	209	Yokoyama, S.	308
Vereda, F.	383	Winter, M.113, 12, 120, 121, 136, 289,		Yoneda, H.	52
Victoria, O.	81290, 380, 72, 73		Yonemura, M.	226
Videa, M.	274	Wohlfahrt-Mehrens, M.	229	Yonezawa, M.	147
Vinatier, P.	241	Wolf, R.	50	Yonezu, I.	219, 337
Vishnyakov, L.	70	Wolfenstine, J.	214	Yong, T.T.	84
Vittadello, M.	318	Wright, P.V.	313	Yoo, Y.	234
Vladimir, G.	81	Wrodnigg, G.H.113, 12, 289		Yoon, W.-S.170, 171, 172, 173, 174	
von Sacken, U.163, 209, 212		Wunder, S.	299	Yoshida, A.	52
Vukson, S.	7	Wurm, C.	165, 21	Yoshida, M.	105
Wachtler, M.12, 72, 73		Xia, Y.	101, 162, 215, 225	Yoshimoto, N.	145
Wagner, M.R.	73	Xia, Y.	227	Yoshimura, S.	219
Waki, M.	236	Xiao, T.	341	Yoshino, A.	232
Wakihara, M.115, 16, 308		Xing, X.-K.	164	Yoshio, M.122, 123, 162, 194, 215, 227, 228	
Wallez, G.	206	Xu, W.	274	Yoshioka, K.	52
Walsh, F.	352, 361	Yagi, Y.	227	Yufit, V.	60
Wang, D.	59, 59	Yagupolskii, Y.	283	Yun, K.-S.	44
Wang, G.X.	152, 58	Yakimov, V.	98	Yves, P.	196, 202
Wang, H.	299	Yakovleva, M.160, 164		Zaderey, N.248, 333, 70	
Wang, X.	59	Yamada, O.	145	Zaghib, K.	25
Wang, X.	227	Yamaguchi, K.105, 107, 287		Zaghib, K.V.	90
Wang, Y.175, 212, 314, 32		Yamaki, J.-I.	144, 232	Zane, D.	135
Ward, I.	311	Yamamoto, M.	328	Zanghellini, E.	110
Watanabe, H.	344	Yamamoto, N.188, 325		Zerigian, P.	383
Watanabe, M.303, 40		Yamamoto, O.305, 364, 370, 63		Zhang, G.	130
Watanabe, O.	319	Yamamoto, Y.111, 236		Zhang, M.	212
Weaving, J.	358	Yamaura, J.	71	Zhang, S.	285
Weinkauf, A.	307	Yanagida, K.	337	Zhang, Z.	279
Weller, M.	151	Yanai, A.	337	Zhaolin, L.	67
Wen, Z.	305	Yang, J.14, 364, 370, 63		Zheng, T.	36
Weppner, W.	41	Yang, L.	137	Zheng, Y.	313
Wessén, B.	301	Yang, X.-Q.162, 164, 277		Zhiyuan, T.154, 158	
White, R.	279	Yao, T.	242	Zhong, Q.	163
Whitfield, P.	345	Yazami, R.77, 8		Zhonghua, L.	179
Williamson, M.	311	Yo, K.	338	Zhu, J.	87
Willmann, P.237, 272		Yokoyama, A.	379	Zygadlo-Monikowska, E.	310

AD NUMBER		DATE	DTIC ACCESSION NOTICE
1. REPORT IDENTIFYING INFORMATION			REQ 1. Put on 2. Corr. 3. Attache 4. Use 5. Do not DTIC: 1. Assi 2. Reti
A. ORIGINATING AGENCY UNIVERSITY OF ROME, ITALY			
B. REPORT TITLE AND/OR NUMBER 10TH INT'L MEETING ON LITHIUM BATTERIES			
C. MONITOR REPORT NUMBER R+D 8932-CH-02			
D. PREPARED UNDER CONTRACT NUMBER N68171-00-M-5518			
2. DISTRIBUTION STATEMENT APPROVED FOR PUBLIC RELEASE DISTRIBUTION UNLIMITED PROCEEDINGS			EDITIONS ARE OBSOLETE

200000016027